HANDBOOK OF

SUPERCONDUCTIVITY

Edited by

CHARLES P. POOLE, JR.

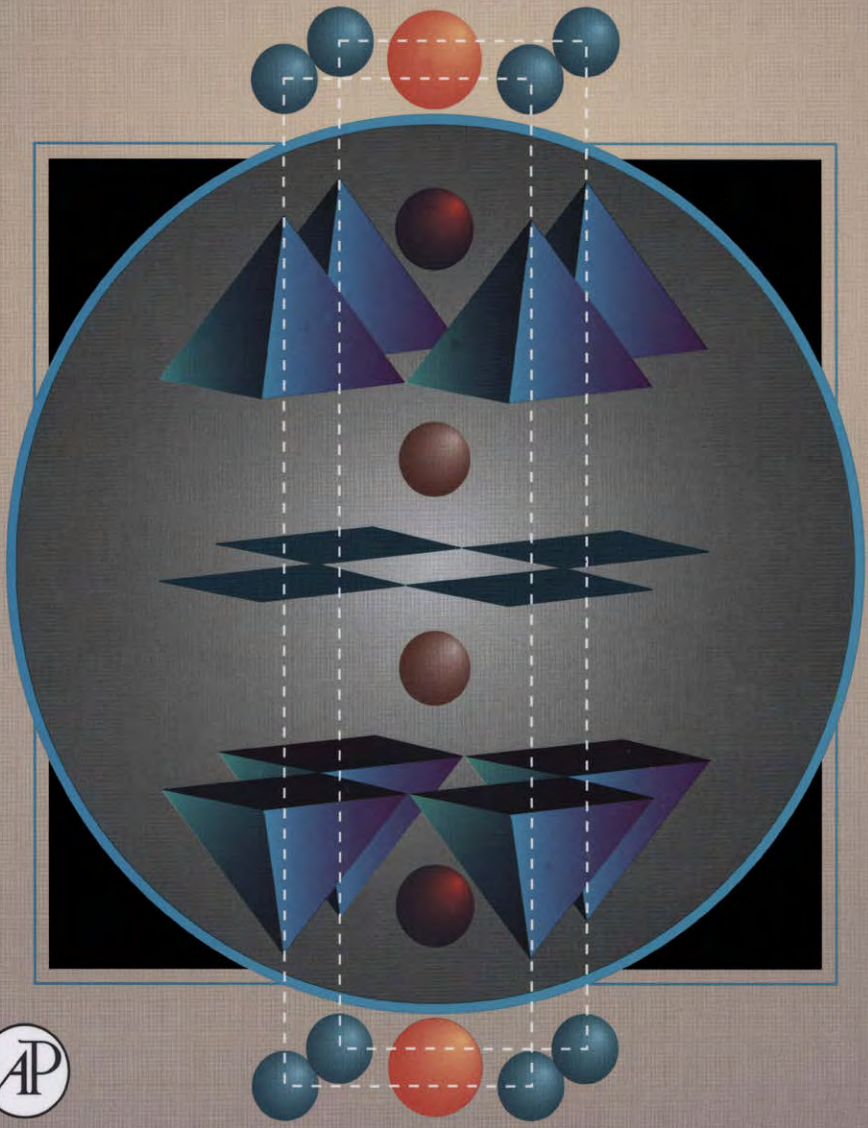

Handbook of Superconductivity

This Page Intentionally Left Blank

Handbook of Superconductivity

Charles P. Poole, Jr.
Department of Physics and Institute of Superconductivity
University of South Carolina

ACADEMIC PRESS

A Harcourt Science and Technology Company

San Diego San Francisco New York Boston
London Sydney Tokyo

ACADEMIC PRESS
A Harcourt Science and Technology Company
525 B Street, Suite 1900, San Diego, CA 92101-4495, USA
http://www.academicpress.com

Academic Press
24–28 Oval Road, London NW1 7DX, UK
http://www.hbuk.co.uk/ap/

ISBN: 0-12-561460-8
Library of Congress Catalog Card Number: 99-60091

Printed in the United States of America

99 00 01 02 03 EB 9 8 7 6 5 4 3 2 1

Contents

Contributors

Numbers in parentheses indicate the pages on which the authors' contributions begin.

Philip B. Allen (478), *Department of Physics and Astronomy, State University of New York, Stony Brook, NY*

Paul C. Canfield (92), *Department of Physics and Ames Laboratory, Iowa State University, Ames, Iowa*

Karin Cenzual (109), *Département de Chimie Minérale, Analytique et Appliquée, Université de Genève, Switzerland*

Philippe Galez (267), *Laboratoire d'Instrumentation et de Matériaux d'Annecy, Université de Savoie, Annecy, France*

Roman Gladyshevskii (109, 267), *Department of Inorganic Chemistry, L'viv State University, Ukraine*

Alan B. Kaiser (510), *Physics Department, Victoria University, Wellington, New Zealand*

Ronald G. Munro (569), *Ceramics Division, National Institute of Standards and Technology, Gaithersburg, Maryland*

Frank J. Owens (251), *Army Armament Research, Engineering and Development Center, Picatinny, New Jersey, and Department of Physics, Hunter College, City University of New York, New York*

Charles P. Poole Jr. (1), *Department of Physics and Institute of Superconductivity, University of South Carolina, Columbia, South Carolina*

Arthur P. Ramirez (96), *Lucent Technologies, Bell Laboratories, Murray Hill, New Jersey*

Ctirad Uher (491), *Department of Physics, University of Michigan, Ann Arbor, Michigan*

Winnie Wong-Ng (625), *Ceramics Division, National Institute of Standards and Technology, Gaithersburg, Maryland*

John F. Zasadzinski (445), *Physics Department, Illinois Institute of Technology, Chicago, Illinois*

Roberta K. Zasadzinski (445), *Physics Department, Illinois Institute of Technology, Chicago, Illinois*

Preface

On April 17, 1986 the brief article "Possible High temperature Superconductivity in the Ba-La-Cu-O System" by J. G. Bednorz and K. A. Müller appeared in the journal *Zeitschrift für Physik*, and the High-T_c era had began. The initial skepticism about the discovery was soon dispelled when several other research groups confirmed the findings, and an enormous world wide research effort began in quest of a room temperature superconductor. Within a year, the critical temperature was raised to 90–93 K (above liquid nitrogen temperature) with the discovery of the yttrium compound, and then in 1988 it increased further to 120 K and 125 K with the successive discoveries the bismuth and thallium cuprates. In 1993, the mercury cuprate went superconducting at 133 K at atmospheric pressure, and at 155 K when subjected to a pressure of 25 GPa. We were past the half-way point to room temperature! During this same period, several new types of compounds were found to exhibit superconductivity, such as the cubic perovskite BaKBiO, alkali metal doped buckmasterfullerenes, and borocarbides.

Some of the exciting things about the high T_c cuprates are the ways in which many of their properties differ from those typical of most classical materials. For example, their Cooper pair charge carriers are formed from positive holes rather than negative electrons; they have layered structures with some two dimensional behaviors; their coherence lengths are approaching interatomic distances; their pairing mechanism seems to be d-wave rather than s-wave; their properties are highly anisotropic, fluctuation effects are prominent, and polycrystalline cuprate materials are composed of micron sized grains. Clarifying and explaining these properties has been one of the principal concerns of all workers in the field.

Prior to Bednorz and Müller's discovery, the field of superconductivity was in a steady state of activity, with the number of annual publications on the subject comprising about 0.6% of the overall physics literature. During the two year period after the discovery the number of publications underwent a dramatic rise to about 3.5% of the total, and then two years after that the rate began a gradual decline, but it is still far above the pre-1986 value. In the early years of the

high-T_c era much of the work was carried out with granular samples, and single crystals were often extensively twinned, especially those of YBaCuO. Most of the initial important research was reported at meetings, and conference proceedings became an important vehicle for disseminating information. Many early reports appeared in letter journals, then longer articles became more frequent, and finally review articles. The year 1988 saw the appearance of the *Journal of Superconductivity*, the review series *Physical Properties of High Temperature Superconductors*, and our book *Copper Oxide Superconductors*, signaling that the field had reached an initial level of maturity. By 1990, several monographs had appeared, several Institutes of Superconductivity had been established, much more definitive measurements on well characterized monocrystals and epitaxial thin films were being reported in the literature, and theoretical explanations were providing more understanding. Experimental and theoretical progress has continued to be made until the present time.

During the past decade, an enormous amount of reliable experimental data have been accumulated on both classical, High T_c, and other types of superconductors. The time is now right to gather together this information into a handbook to make it readily available for researchers. This volume represents an effort to do this for the field of superconductivity as a whole, i.e. for all types of superconductors. The initial draft for this work was a compilation of handbook type material made from the 1995 monograph *Superconductivity*, coauthored by the present editor. This provided definitions, equations, temperature and field dependencies, and much other information routinely needed by researchers. To this was added material from other sources, and tabulations of experimentally determined parameters of various types such as critical temperatures T_c, atom positions, coherence lengths, penetration depths, energy gaps, critical fields B_c, and critical currents J_c, among others. The main conclusions from several models and theories were summarized for easy comparison with measurements. The goal is to provide a ready source containing most of the information that a researcher would be likely to look up during the course of his or her investigations.

This handbook is not just about the copper oxide superconductors, but about all superconductors. The first chapter provides an overview, units and conversion factors, and a lengthy glossary of terms. Chapter 2 summarizes the properties of the normal state, and Chapter 3 does the same for the superconducting state. The fourth chapter presents the results of the main models and theories that are routinely used to explain experimental data. Chapter 5 summarizes the properties of the various types of classical materials as well as those of more recently discovered superconducting systems, and provides an extensive tabulation of their transition temperatures. The crystal structures of these compounds are presented in the sixth chapter. The general features of the atom arrangements in high T_c cuprates are reviewed in Chapter 7, and the details of their individual structures are provided in Chapter 8. The ninth chapter furnishes long tabulations of the various parameters such as B_c and J_c that were mentioned above. The next chapter covers thermal properties such as the

specific heat, thermal conductivity, and entropy transport, as well as thermoelectric and thermomagnetic effects. Chapter 11 surveys electrical properties such as the Hall effect, tunneling, Josephson junctions, and superconducting quantum interference devices (SQUIDS). Chapter 12 covers magnetic properties such as susceptibility, magnetization, critical fields, vortices including their anisotropies and their motion, transport current in a magnetic field, and intermediate states. Chapter 13 examines various mechanical properties like elastic, shear, and bulk moduli, Poisson's ratio, flexural and tensile strength, hardness, and fracture toughness. Finally, the last chapter on compositional phase diagrams presents many ternary and a few quaternary (tetrahedral) phase diagrams for all the basic cuprate systems. Included are several liquidus surface, subsolidus equilibrium, primary crystallization field, and temperature/composition plots.

It is hoped that, *Deo volente*, the data tabulations, and other information gathered together in this volume will have a significant influence on expediting the progress of future research.

Charles P. Poole, Jr.
Columbia, South Carolina

This Page Intentionally Left Blank

Chapter 1

Introduction

Charles P. Poole, Jr.
Department of Physics and Institute of Superconductivity,
University of South Carolina, Columbia, South Carolina

A Introduction

This handbook is concerned with superconductors, materials characterized by certain electrical, magnetic, and other properties, many of which will be explained in the third chapter. In this chapter we will define the two types of superconductors, describe the format and content of the Handbook, make some suggestions for how to use it, and provide the basic units and conversion factors that are commonly used in the field. Much of the material in this handbook has been elaborated upon in greater detail in the 1995 monograph *Superconductivity* [Poole *et al.*], and for many topics that volume will provide more details. The present book, of course, is much more complete in areas such as tabulations of data and descriptions of crystallographic structures. Some topics found here, such as mechanical properties and phase diagrams, were not covered in the earlier work.

ISBN: 0-12-561460-8
$30.00

HANDBOOK OF SUPERCONDUCTIVITY

B

Definition of a Superconductor

A Type I superconductor exhibits two characteristic properties, namely zero dc electrical resistance and perfect diamagnetism, when it is cooled below its critical temperature T_c. Above T_c it is a normal metal, but ordinarily not a very good conductor. The second property of perfect diamagnetism, also called the Meissner effect, means that the magnetic susceptibility has the value $\chi = -1$ in mks or SI units, so a magnetic field (i.e., magnetic flux) cannot exist inside the material. There is a critical magnetic field B_c with the property that at the temperature 0 K applied fields $B_{app} \geq B_c$ drive the material normal. The temperature dependence of the critical field $B_c(T)$ can often be approximated by the expression, where we use the notation $B_c(0) = B_c$,

$$B_c(T) = B_c[1 - (T/T_c)^2]. \tag{1}$$

The Type I superconductors are elements, whereas alloys and compounds are Type II.

A Type II superconductor is also a perfect conductor of electricity, with zero dc resistance, but its magnetic properties are more complex. It totally excludes magnetic flux in the Meissner state when the applied magnetic field is below the lower critical field B_{c1}, as indicated in Fig. 1.1. Flux is only partially excluded when the applied field is in the range from B_{c1} to B_{c2}, and the material becomes normal for applied fields above the upper critical field B_{c2}. Thus, in the region of

Fig. 1.1.

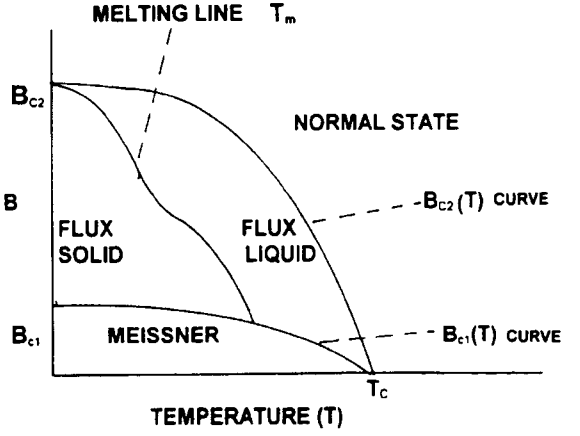

Simplified magnetic phase diagram of a Type II superconductor showing the Meissner region of excluded magnetic flux below the lower critical curve $B_{c1}(T)$, the flux solid and flux liquid phases separated by the melting curve T_m, and the normal state region that lies outside the upper critical field curve $B_{c2}(T)$. [From Owens and Poole (1996), Fig. 3.12.]

higher magnetic fields the diamagnetism is not perfect, but rather of a mixed type that exhibits solid-like properties at lower temperatures and liquid-like properties at higher temperatures, as indicated in the figure. The melting line separates these two regions of magnetic behavior.

These definitions of superconductors have been expressed in terms of properties. In addition, they do not take into account demagnetization effects that cause the diagmagnetism to depend on the shape of the sample and its orientation in an applied field. More fundamentally, a superconductor can be defined as a conductor that has undergone a phase transition to a lower energy state below a transition temperature T_c in which conduction electrons form pairs called Cooper pairs, which carry electrical current without any resistance to the flow, and which are responsible for the perfect diamagnetism and other properties.

C

Form and Content of Handbook

The various chapters of this Handbook cover different aspects of the field of superconductivity. The present chapter provides the units and conversion factors that will be widely referred to throughout the remainder of the text, as well as a glossary of terms. This is followed by chapters that describe the normal state above T_c and the superconducting state below T_c. Then comes a chapter that summarizes the important theories and models that are employed to understand the nature and explain the properties of superconductors. Next we present, in succession, the classical superconductors, the superconducting materials that were discovered during the past decade and a half, and most importantly, the cuprates. The remaining seven chapters present data on the various properties of superconductors. The chapters are self-contained, so any one of them can be referred to without previously reading earlier ones. It is anticipated that the main use of the Handbook will be its consultation by researchers who need information on particular topics or data on particular compounds, although many sections can be read to refresh one's memory about particular aspects of the subject. Of especial interest are the tabulations of critical temperatures in Chapter 5 and the tabulations of data on critical magnetic fields, critical currents, and other properties found in Chapter 9. The glossary in Section E of this chapter contains many definitions of terms.

D

Several Miscellaneous Tables

Table 1.1 provides some of the physical constants and key equations that are commonly encountered in superconductivity research, and lists some conventions

Table I.I.

List of physical constants and important equations.

Fundamental constants	
Avogadro's number	$N_A = 6.0221 \times 10^{23}\ \text{mol}^{-1}$
Boltzmann constant	$k_B = R/N_A = 1.3807 \times 10^{-23}\ \text{J/K}$
Dieletric constant of vacuum	$\varepsilon_0 = 8.8542 \times 10^{-12}\ \text{F/m}$
Electron charge	$e = 1.6022 \times 10^{-19}\ \text{C}$
Fine structure constant	$\alpha = e^2/4\pi\varepsilon_0\hbar c = 7.2974 \times 10^{-3}\left(\frac{1}{\alpha} \sim 137\right)$
Gas constant	$R = N_A k_B = 8.3145\ \text{J/mol K}$
Gravitation constant	$G = 6.6726 \times 10^{-11}\ \text{m}^3/\text{kg s}^2$
Light speed *in vacuo*	$c = 2.9979 \times 10^8\ \text{m/s}$
Permeability of vacuum	$\mu_0 = 4\pi \times 10^{-7}\ \text{N/A}^2 = 1.2566 \times 10^{-6}\ \text{N/A}^2$
Planck constant	$\text{h} = 6.6261 \times 10^{-34}\ \text{Js}\ (4.1357 \times 10^{-15}\ \text{eVs})$
Planck reduced constant	$\hbar = h/2\pi = 1.0546 \times 10^{-34}\ \text{Js}$
Quantum of circulation	$h/m_e = 7.2739 \times 10^{-4}\text{m}^2/\text{s}$
Rydberg (H-atom) energy	$e^2/8\pi\varepsilon_0 a_0 = 2.1799 \times 10^{-18}\ \text{J}\ (13.606\ \text{eV})$
Stefan Boltzmann constant	$\sigma = 5.6705 \times 10^{-8}\ \text{W/m}^2\text{K}^4$
Wien displacement law	$\lambda_{max} T = 2.8978 \times 10^{-3}\ \text{mK}$
Electromagnetic constants	
Bohr magneton	$\mu_B = e\hbar/2m_e = 9.2740 \times 10^{-24}\ \text{J/T}$
Nuclear magneton	$\mu_N = 5.0508 \times 10^{-27}\ \text{J/T}$
Faraday constant	$F = N_A e = 96485\ \text{C/mol}$
Flux quantum, magnetic	$\Phi_0 = h/2e = 2.0678 \times 10^{-15}\ \text{Wb}$
g-factor, electron	$g_e = 2.0023$
Hall resistance	$R_H = h/e^2 = 25{,}813\ \Omega$
Resistance quantum	$R_Q = R_H/4 = 6453.2\ \Omega$
Josephson frequency	$\omega_J = 2\pi(2\ \text{eV/h})\ [1\ \mu\text{V} = 483.60\ \text{MHz}]$
Length constants	
Classical electron radius	$r_e = \alpha^2 a_0 = e^2/4\pi\varepsilon_0 m_e c^2 = 2.8179 \times 10^{-15}\ \text{m}$
Thomson cross section	$\sigma = (8\pi/3)r_e^2 = 6.6525 \times 10^{-29}\ \text{m}^2$
Compton wavelength (electron)	$\lambda_c = h/m_e c = 2.4263 \times 10^{-12}\ \text{m}$
Bohr radius	$a_0 = r_e/\alpha^2 = 4\pi\varepsilon_0\hbar^2/me^2 = 5.2918 \times 10^{-11}\ \text{m}$
Temperature expressions	
Debye temperature	$\Theta_D = \hbar\omega_D/k_B$
Fermi temperature	$T_F = E_F/k_B = \hbar^2 k_F^2/2mk_B$
Supercond. trans. Temp.	$T_c = 0.2834E_g/k_B$
Specific heat ($T \ll \Theta_D$)	$C = \gamma T + AT^3$
Critical current	$J_c(T) = J_c(0)[1 - (T/T_c)^2][1 - (T/T_c)^4]^{1/2}$
Critical field	$B_c(T) = B_c(0)[1 - (T/T_c)^2]$
Critical field slope	$dB_{c2}/dT = -1.83T/K$
Energy gap	$E_g(T) = E_g(0)[1 - (T/T_c)]^{1/2}$
Penetration depth	$\lambda_T = \lambda(0)[1 - (T/T_c)^4]^{-1/2}$
Superelectron density	$n_s(T) = n_s(0)[1 - (T/T_c)^4]$

(*continued*)

Table I.I. *(continued)*

Temperature expressions (0°C = 273.15 K)	
He^4 lambda point	$T_\lambda = 2.174$ K
He^3 boiling point	$T_{BP} = 3.20$ K
He^4 boiling point	$T_{BP} = 4.216$ K
H_2 boiling point	$T_{BP} = 20.28$ K
N_2 boiling point	$T_{BP} = 77.35$ K
O_2 boiling point	$T_{BP} = 90.18$ K

Conversion factors	
Energy:	$1\text{ eV} = 1.6022 \times 10^{-19}\text{ J} = 1.7827 \times 10^{-36}\text{ kg}$ $= 2.4180 \times 10^{14}\text{ Hz} = 806554\text{ m}^{-1}$ $= 1.0735 \times 10^{-9}\text{ u} = 1.1604 \times 10^{4}\text{ K}$
Length:	$1\text{ m} = 100\text{ cm} = 10^{10}$ Å; 1 marathon = 42.352 km
Magnetic field:	$1\text{ T} = 1\text{ Wb/m}^2 = 10^4\text{ G}$
Pressure:	$1\text{ GPa} = 10\text{ kBar} = 7.5 \times 10^6\text{ torr} = 0.987 \times 10^4\text{ atm}$
Temperature:	$1\text{ K} = 1.3807 \times 10^{-23}\text{ J} = 1.5362 \times 10^{-40}\text{ kg} = 2.0837 \times 10^{10}\text{ Hz}$ $= 69.504\text{ m}^{-1} = 9.251 \times 10^{-14}\text{ u} = 8.6174 \times 10^{-5}\text{ eV}$
Multiples:	k (kilo, 10^3); M (mega, 10^6); G (giga, 10^9); T (tera, 10^{12}); P (peta, 10^{15}); E (exa, 10^{18}); Z (zetta, 10^{21}); Y (yotta, 10^{24})
Submultiples:	m (milli, 10^{-3}); μ (micro, 10^{-6}); n (nano, 10^{-9}); p (pico, 10^{-12}); f (femto, 10^{-15}); a (atto, 10^{-18}); z (zepto, 10^{-21}); y (yocto, 10^{-24})

Particle properties

Particle	Mass ($\times 10^{-31}$ kg)	Rest energy ($\times 10^{-19}$ J)	Rest energy (MeV)	Magnetic moment ($\times 10^{-26}$ J/T)
Electron	9.10939	0.81871	0.51100	928.48
Muon	1883.53	169.29	105.66	4.4905
Proton	16726.2	1503.3	938.27	1.4106
Neutron	16749.3	1505.4	939.57	− 0.99624
Atomic constant (1/12 of ^{12}C)	16605.4	1492.4	931.494	

Normal state expressions	
Density of states	$D(E_F) = (1/2\pi^2)(2m^*/\hbar^2)^{3/2}E_F^{1/2}$
Electrical conductivity	$\sigma_0 = ne^2\tau/m$
Hall effect	$R_H = \pm 1/ne$
Magnetic field	$B = \mu_0(H + M) = \mu_0 H(1 + \chi) = \mu H$
Plasma frequency	$\omega_p = (ne^2/\varepsilon_0 m)^{1/2}$
Electronic specific heat	$\gamma = \frac{1}{3}\pi^2 D(E_F)k_B^2 \approx \frac{1}{2}\pi^2 R/T_F$

(continued)

Table 1.1. (*continued*)

Superconducting state expressions	
BCS factors	
Coherence length	$\xi = 2\hbar v_F/\pi E_g$
Density of states	$D_s(E) = D_n(0)/[1 - (\Delta/E)^2]^{1/2}$
Electron-phonon coupling constant	$\lambda - \mu_c^* = V_0 D_n(E_F)$
Energy gap ratio	$E_g/k_B T_c = 2\Delta/k_B T_c = 3.528$
Isotope effect exponent	$(T_c M^\alpha = \text{const})$, $\alpha_{BCS} = \frac{1}{2}$
Specific heat jump	$(C_s - \gamma T_c)/\gamma T_c = 1.43$
Transition temperature	$T_c = 1.13\Theta_D \exp[-1/(\lambda - \mu_c^*)]$
Expressions based on models and theories	
Ampére law	$\nabla \times B = \mu_0 J$
Bean model critical current	$J_c = 2\Delta M/d$ A/m^2
Critical current	$J_c = B_c/\mu_0\lambda$
Josephson equations	$J = J_c \sin\phi; \dfrac{d\phi}{dt} = 2eV/\hbar$
London equations	1st $E = \mu_0\lambda_L^2 dJ/dt$ 2nd $B = -\mu_0\lambda_L^2 \nabla \times J$
Lorentz force	$F/L = J \times \Phi_0$
Penetration depth (London)	$\lambda_L = (m/\mu_0 n e^2)^{1/2}$
Penetration depth (Josephson)	$\lambda_J = [\Phi_0/2\pi\mu_0 J_c(2\lambda + d)]^{1/2}$
Shielding current	$J_{sh} = \nabla \times M$
Vortex expressions	
Critical field, lower	$B_{c1} = \Phi_0 \ln\kappa/4\pi\lambda^2$
Critical field, thermodynamic	$B_c = \Phi_0/2\sqrt{2}\pi\lambda\xi$
Critical field, upper	$B_{c2} = \Phi_0/2\pi\xi^2 \approx 1.83 T_c$
Surface sheath field	$B_{c3} = 1.695 B_{c2}$
Ginzburg–Landau parameter	$\kappa = \lambda/\xi$
Vortex field	$B(r) \approx e^{-r/\lambda}/(r/\lambda)^{1/2}$, $r > \lambda$
Anisotropies and shape dependence	
Characteristic lengths	$\xi_a\lambda_a = \xi_b\lambda_b = \xi_c\lambda_c$
Axial symmetry	$\xi_{ab}/\xi_c = \lambda_c/\lambda_{ab} = (m_c/m_{ab})^{1/2}$
High-temperature superconductors	$\xi_c \ll \xi_{ab} \ll \lambda_{ab} \ll \lambda_c$
Demagnetization factor	$NB_{in} + \mu_0(1 - N)H_{in} = B_{app}$
Normalization	$N_a + N_b + N_c = N_\parallel + 2N_\perp = 1$
Flat disk	$N_\parallel = 1 - \delta$, $N_\perp = \frac{1}{2}\delta$
Long rod	$N_\parallel = \delta$, $N_\perp = \frac{1}{2}(1 - \delta)$
Sphere	$N = \frac{1}{3}$
Susceptibility	$\chi = \chi_{exp}/(1 - N\chi_{exp})$

and conversion factors involving them. In most cases we adopt the SI (Système International d'Unités) or mks (meter–kilometer–second) system of units, and for the convenience of workers who feel more comfortable with cgs (centimeter–gram–second), some expressions will be repeated in cgs notation. There are also other units in common use for particular quantities such as pressure and energy,

and some of the spectroscopies have their own characteristic units, so conversion factors will be given where appropriate.

Table 1.2 lists some of the symbols that appear commonly in the superconductivity literature, together with their meaning and sometimes with the conventional units used for them. Table 1.3 lists most of the elements alphabetically by symbol and gives the transition temperatures of the ones that superconduct. Table 1.4 provides ionic radii of many of the elements in their more important valence states. The chapter ends with a long glossary of terms. A shorter glossary was published in an earlier work [Owens and Poole, 1996].

Table 1.2.

List of symbols that appear commonly in the superconductivity literature. Values and units are given for some of the entries in this table.

A, amp or ampere, unit of electric current, coulomb/second, C/sec
Å, angstrom unit, $1\text{Å} = 0.1$ nm
B, magnetic field symbol, tesla, T
B_c, critical magnetic field (some authors write H_c)
B_{c1}, lower critical field (some authors write H_{c1})
B_{c2}, upper critical field (some authors write H_{c2})
c, speed of light in a vacuum, 2.9979×10^8 m/sec
°C, degrees Celsius (centrigrade), unit of temperature
cm, centimeter
e, charge of an electron, 1.6022×10^{-19} C
E, electric field, V/m
E_g, energy gap ($E_g = 2\Delta$)
F, force, newton, N
h, Planck's constant, 6.6261×10^{-34} J-sec
J, joule, unit of energy
J, electric current density, A/cm^2
J_c, critical current density. A/cm^2
K, kelvin, unit of temperature
k_B, Boltzmann's constant, 1.3807×10^{-23} joule/kelvin
m, meter, unit of length
N_e, number of valence electrons in an atom
R, resistance, ohm, Ω
sec, second
T, tesla, unit of magnetic field B
T_c, critical temperature
V, volt

ξ, coherence length, radius of a vortex core (Greek xi)
κ, Ginzburg Landau parameter, $\kappa = \lambda/\xi$ (Greek kappa)
λ, penetration depth, electron phonon coupling constant (Greek lambda)
λ_L, London penetration depth
χ, susceptibility (Greek chi)
Φ, magnetic flux, with units Tm^2 (Greek phi)
Φ_o, flux quantum, with value $h/2e = 2.0678 \times 10^{-15}$ Tm^2 (Greek phi)

Table 1.3.

Symbols for most of the elements together with their atomic numbers and the transition temperatures T_C of those that superconduct. Most of the radioactive elements are not included.

Ag, silver, 47
Al, aluminum, 13; $T_c = 1.18\,K$
Am, americium, 95; $T_c = 1.0\,K$
Ar, argon, 18
As, antimony, 33
Au, gold, 79
B, boron, 5
Ba, barium, 56
Be, beryllium, 4; $T_c = 0.026\,K$
Bi, bismuth, 83
Br, bromine, 35
C, carbon, 6
Ca, calcium, 20
Cd, cadmium 48; $T_c = 0.5\,K$
Ce, cerium, 58
Cl, chlorine, 17
Co, cobalt, 27
Cr, chromium, 24
Cs, cesium, 55
Cu, copper, 29
Dy, dysprosium, 66
Er, erbium, 68
Eu, europium, 63
F, fluorine, 9
Fe, iron, 26
Ga, gallium, 31; $T_c = 1.1\,K$
Gd, gadolinium, 64
Ge, germanium, 32
H, hydrogen, 1
He, helium, 2
Hf, hafnium, 72, $T_c = 0.1\,K$
Hg, mercury, 80; $T_c = 4.15\,K$
Ho, holmium, 67
I, iodine, 53
In, indium, 49; $T_c = 3.4\,K$
Ir, iridium, 77; $T_c = 0.1\,K$
K, potassium, 19
Kr, krypton, 36
La, lanthanum, 57; $T_c = 6.1\,K$
Li, lithium, 3
Lu, lutetium, 71, $T_c = 0.1\,K$
Mg, magnesium, 12
Mn, manganese, 25
Mo, molybdenum, 42; $T_c = 0.9\,K$
N, nitrogen, 7
Na, sodium, 11
Nb, niobium, 41; $T_c = 9.3\,K$
Nd, neodymium, 60
Ne, neon, 10
Ni, nickel, 28
O, oxygen, 8
Os, osmium, 76; $T_c = 0.7$
P, phosphorus, 15
Pa, protactinium, 91; $T_c = 1.4\,K$
Pb, lead, 82; $T_c = 7.2\,K$
Pd, palladium, 46
Pm, promethium, 61
Pr, praseodymium, 59
Pt, platinum, 78
Re, rhenium, 75, $T_c = 1.7\,K$
Rb, rubidium, 37
Rh, rhodium, 45
Ru, ruthenium, 44, $T_c = 0.5\,K$
S, sulfur, 16
Sb, antimony, 51
Sc, scandium, 21, $T_c = 0.5\,K$
Se, selenium, 34
Si, silicon, 14
Sm, samarium, 62
Sn, tin, 50; $T_c = 3.7\,K$
Sr, strontium, 38
Ta, tantalum, 73; $T_c = 4.5\,K$
Tb, terbium, 65
Tc, technetium, 43; $T_c = 7.8\,K$
Te, tellurium, 52
Th, thorium, 90; $T_c = 1.4\,K$
Ti, titanium, 22; $T_c = 0.4\,K$
Tl, thallium, 81; $T_c = 2.4\,K$
Tm, thulium, 69
U, uranium, 92
V, vanadium, 23; $T_c = 5.4\,K$
W, tungsten (wolfram), 74; $T_c = 0.02\,K$
Xe, xenon, 54
Y, yttrium, 39
Yb, ytterbium, 70
Zn, zinc, 30; $T_c = 0.85\,K$
Zr, zirconium, 40; $T_c = 0.6\,K$

Table I.4.

Ionic radii in angstroms of selected elements for various positive charge states[a] [from Poole *et al.*, 1988, p. 79]

z	Element	+1	+2	+3	+4	+5	+6
			Alkali				
3	Li	0.68					
11	Na	0.97					
19	K	1.33					
37	Rb	1.47					
55	Cs	1.67					
			Alkaline earths				
4	Be	0.44	0.35				
12	Mg	0.82	0.66				
20	Ca	1.18	0.99				
38	Sr		1.12				
56	Ba	1.53	1.34				
			Group III				
5	B	0.35		0.23			
13	Al			0.51			
31	Ga	0.81		0.62			
49	In			0.81			
81	Tl	1.47		0.95			
			Group IV				
6	C				0.16		
14	Si	0.65			0.42		
32	Ge		0.73		0.53		
50	Sn		0.93		0.71		
82	Pb		1.20		0.84		
			Group V				
15	P			0.44		0.35	
33	As			0.58		0.46	
51	Sb	0.89		0.76		0.62	
83	Bi	0.98		0.96		0.74	
			Chalcogenides				
16	S				0.37		0.30
34	Se	0.66			0.50		0.42
52	Te	0.82			0.70		0.56
			First transition series ($3d^n$)				
21	Sc			0.81			
22	Ti	0.96	0.94	0.76	0.68		
23	V		0.88	0.74	0.63	0.59	
24	Cr	0.81	0.89	0.63			0.52
25	Mn		0.80	0.66	0.60		
26	Fe		0.74	0.64			

(*continued*)

Table 1.4. *(continued)*

Ionic radii in angstroms of selected elements for various positive charge states[a] [from Poole *et al.*, 1998, p. 79]

z	Element	+1	+2	+3	+4	+5	+6
27	Co		0.72	0.63			
28	Ni		0.69				
29	Cu	0.96	0.72				
30	Zn	0.88	0.74				
			Second transition series ($4d^n$)				
39	Y			0.8[a]			
40	Zr	1.09			0.79		
41	Nb	1.00			0.74	0.69	
42	Mo	0.93			0.70		0.62
43	Tc						
44	Ru				0.67		
45	Rh			0.68			
46	Pd		0.80		0.65		
47	Ag	1.26	0.89				
48	Cd	1.14	0.97				
			Third transition series ($5d^n$)				
72	Hf				0.78		
73	Ta					0.68	
74	W				0.70		0.62
75	Re				0.72		
76	Os				0.88		0.69
77	Ir				0.68		
78	Pt		0.80		0.65		
79	Au	1.37		0.85			
80	Hg	1.27	1.10				
			Rare earths ($4f^n$)				
57	La	1.39		1.06			
58	Ce	1.27		1.07	0.94		
59	Pr			1.06	0.92		
60	Nd			1.04			
61	Pm			1.06			
62	Sm			1.00			
63	Eu			0.98			
64	Gd			0.62			
65	Tb			0.93	0.81		
66	Dy			0.92			
67	Ho			0.91			
68	Er			0.89			
69	Tm			0.87			
70	Yb			0.86			
71	Lu			0.85			

[a]Anion radii are 1.32 for O^{2-}, 1.33 for F^-, 1.84 for S^{2-}, 1.91 for Se^{2-}, and 2.11 for Te^{2-} (*Handbook of Chemistry and Physics*, p. 187).

E

Glossary of Terms

A-15 compound An A_3B binary compound with a cubic structure, many of which superconduct.
Abrikosov vortex Cylinder or rod of quantized magnetic flux in a Type II superconductor, usually referred to simply as vortex.
ACAR Angular correlation of annihilation radiation, measured in positron annihilation studies.
Acoustic phonon Phonon of low-frequency branch.
Aligned crystal structure Cuprate lacking body-centered operation.
Aligned grains Grains with their magnetizations pointing in more or less the same direction.
Alloy Two or more metals intimately mixed.
Ampère's law $\nabla \times H = \partial D/\partial t + J$.
Angstrom (Å) Unit of length equal to 10^{-10} meters.
Anisotropy Variation of properties along different directions.
Annealing Heating generally followed by gradual cooling.
Antiferromagnetism (AFM) Ordered magnetic state in which spins of identical magnetic atoms are alternately in up and down directions.
Antiparamagnon Antiferromagnetic fluctuation in CuO_2 plane.
Antistokes line Spectral line arising from a Raman scattered photon with a frequency greater than that of the incident photon.
Antivortex Vortex aligned opposite to the applied magnetic field.
Anyon Particle with fractional statistics and symmetry under interchange $(0 < \theta < \pi)$ between the boson case of $\theta = 0$ and the fermion case $\theta = \pi$, corresponding to $\psi(\mathbf{r}_2, \mathbf{r}_1) = e^{i\theta}\psi(\mathbf{r}_1, \mathbf{r}_2)$.
ARPES Angular resolved photoemission spectra.
Array of Josephson junctions An ordered arrangement of coupled Josephson junctions.
Atomic number (of an atom) The number of protons in its nucleus.
Auger effect Radiationless transition whereby a photon generated within an atom ejects an electron from a higher energy level.
Aurivillius phase Layered compound $Bi_2O_2(M_{m-1}R_mO_{3m+1})$ related to the cuprates.
Avalanche or cascade process One involving rapid change or discharge.
Band structure Arrangement of energy bands in k-space.
BCS Superconductivity theory originated by J. Bardeen, L. N. Cooper, and J. R. Schrieffer in 1957.
Bean model Most common critical state model in which the critical current density can equal either 0 or the value J_c.
Bessel function Radial solution of Laplace's equation in cylindrical coordinates. The zero-order modified Bessel function $K_0(r/\lambda)$ describes the radial

dependence of the magnetic field around a vortex for $\kappa \gg 1$, and $K_1(r/\lambda)$ describes the vortex critical current density.

Binary compound One containing two elements.

BIS, Bremsstrahlen isochromat spectroscopy The sample is irradiated with an electron beam and the emitted ultraviolet photons are measured.

Bloch T^5 law for electrical resistivity $\rho = \rho_0 T^5$ for $T \ll \Theta_D$.

Bloch's theorem $\Psi(\mathbf{r} + \mathbf{R}) = e^{i\mathbf{k}\cdot\mathbf{R}}\Psi(\mathbf{r})$ for wavefunctions in periodic lattice.

Bloch wavefunctions $\psi(\mathbf{r})$ obey Bloch's theorem and are linear combinations of atomic states $\phi(\mathbf{r} - \mathbf{R})$ localized on atoms at positions $\mathbf{R}$.

Bogoliubon Quasi-particle excitation.

Bogoliubov transformation A transformation involving raising and lowering operators that is used in solving the BCS Hamiltonian.

Borocarbide A compound containing the elements boron B and carbon C such as RM_2B_2C, where ordinarily M is Ni and R is a rare earth.

Boronitride A compound containing the elements boron B and nitrogen N such as $RM_2B_2N_3$, where ordinarily M is the element Ni and R is a rare earth.

Bose–Einstein condensation Passage of a system of boson particles such as Cooper pairs or helium atoms to their lowest energy state where they exhibit special properties such as superconductivity or superfluidity; also called Bose condensation.

Boson A particle with integer intrinsic spin obeying Bose–Einstein statistics.

Branch imbalance A nonequilibrium state with an imbalance between quasi-particles in two branches of k-space.

Brillouin scattering Light scattering in which the frequency shift of the reflected beam arises from an acoustic branch phonon.

Brillouin zone Unit cell in reciprocal space (k-space).

Buckminsterfullerene Fancy name for a fullerene.

Bucky ball Nickname for a fullerene.

Bundle of flux A group of flux lines (vortices) that undergo motions in unison.

Cascade process See Avalanche.

CDW Charge density wave.

Celsius (centigrade) C Related to Fahrenheit through $C = 5\ (F - 32)/9$.

Ceramic A product made from a clay or a related material.

Chalcogenide One of the four elements oxygen O, sulfur S, selenium Se, and tellurium Te in row 6 of the periodic table.

Charge density wave (CDW) Periodic fluctuation in the density of charge.

Charge imbalance See Branch imbalance.

Charge transfer organics Class of organic superconductors.

Chemical shift A shift in the resonant frequency of a spectral line; terminology common to NMR and Mössbauer spectroscopies.

Chevrel compound Generally a ternary compound $A_jMo_6X_8$, where X is sulfur S, selenium Se, or tellurium Te, A can be almost any element, and j has a value between 1 and 2; many Chevrel compounds superconduct.

Clean superconductor One in which the electron mean free path l exceeds the coherence length ξ.
Clogston–Chandrasekhar limit See Paramagnetic limit.
Coercive field The applied magnetic field needed to restore a magnetized material to the state of zero magnetization.
Coherence length ξ Distance ξ_{GL} over which Ginsburg–Landau order parameter $\phi(r)$ can change without an appreciable energy change; radius of core of a vortex; size $\xi_{Pippard}$ of a Cooper pair.
Collective pinning Restricted motion of many nearby vortices arising from an assembly of weak pinning centers.
Composite Made of separate or disparate elements or parts.
Condensation energy density Energy released by transforming normal electrons to super-electron state, with the value $B_c^2/2\mu_o$.
Conductivity, electrical Ratio $\sigma = J/E$ of the current density J to the applied electric field E that causes it to flow.
Conductivity, thermal Ratio $\kappa = -U/\nabla T$ of the heat current per unit area U to the temperature gradient ∇T that causes it to flow.
Conductor Material of low resistivity, i.e., conducts electricity well.
Cooper pair Paired electrons that constitute the charge carrier of supercurrent.
Coulomb Mks or SI unit of electrical charge.
Coulomb blockade Blockage of single electron jumps in ultrasmall Josephson junctions (nanobridges).
Coulomb integral $\int \psi_A^*(r_m)\psi_B^*(r_n)V(r_{mn})\psi_A(r_m)\psi_B(r_n)d^3r$.
Coulomb staircase Steps on current vs voltage plots of ultrasmall Josephson junctions arising from fluctuations in single-electron tunneling.
Covalent bonding Chemical bonding scheme in which the involved atoms share electrons; commonly found in organic molecules.
Creation operator Quantum mechanical operator that creates a particle.
Critical current density J_c Highest current density that can flow through a superconducting material without driving it normal.
Critical current I_c Highest current that can flow through a particular superconducting wire or tape.
Critical magnetic field B_c Highest field sustained by a Type I superconductor. Type II superconductors have lower B_{c1} and upper B_{c2} critical fields with thermodynamic critical field $B_c = (B_{C1}B_{C2}/\ln\kappa)^{1.2}$.
Critical state Magnetic field penetration and associated super current flow configuration in surface region of superconductor in accordance with a particular model such as the Bean model (q.v.).
Critical surface Surface in B, J, T (magnetic field, current density, temperature) coordinate system below which a material is superconducting.
Critical temperature T_c Temperature below which a material superconducts.
Cryogenic Adjective signifying low temperature.
Cryostat Apparatus for maintaining a low, constant temperature.

Cryotron Type of superconducting switch.
Cubic structure All lengths equal, $a = b = c$; all angles 90°.
Curie law for susceptibility $\chi = C/T$, where $C = n\mu^2/3k_B$ is the Curie constant.
Curie–Weiss law $\chi = C/(T - \Theta)$, where Θ is the Curie–Weiss temperature.
Curie temperature The temperature below which a material becomes ferromagnetic.
Current density J Electric current per unit cross-section, A/cm^2.
D'Alembertian Differential Operator $\Box^2 = \nabla^2 - c^{-2}\partial^2/\partial t^2$.
Debye approximation Assumption of linear dispersion relation $\omega = ck$ in phonon specific heat determination.
Debye temperature $\Theta_D = \hbar\omega_D/k_B$, a measure of the temperature above which all vibrational modes begin to be excited in a solid.
deHaas–van Alphen effect Oscillations in the magnetization exhibited by a sample during magnetic field scanning.
Delocalization Continual wandering throughout a material of electrons that, for example, carry electrical current.
Demagnetization Removal of magnetization.
Demagnetization factor N_i Parameter characterizing shape dependence of magnetization in a material.
Density of states (DOS) Number of states or levels per unit energy, dN/dE, or number of states per frequency interval, $dn/d\omega$.
Depairing Uncoupling of bound electron pair.
Depinning Release of vortices from being pinned.
Dewar Container for holding a low-temperature liquid.
Diamond A cubic form of carbon with each atom at the center of a regular tetrahedron.
Dielectric A material with a dielectric constant $\epsilon > \epsilon_0$.
Dirty superconductor One in which the electron mean free path l is less than the coherence length ξ.
Dispersion relation k-dependence of the frequency $\omega(k)$.
Distribution function Energy dependence of electron density.
Doping Adding a small amount of one atom to replace another, as in the superconductor $(La_{0.9}Sr_{0.1})_2CuO_4$.
Doppler broadening Spread in energy of monochromatic γ-rays arising from positron annihilation.
DOS Density of states.
Drude model Description of electrical and thermal conductivity of a metal in terms of a gas of conduction electrons.
***d*-wave pairing** Cooper pair coupling via d-state wavefunctions.
Eccentricity ϵ Measure of the deviation of an ellipsoid from a spherical shape.
EDAX or EDX Energy dispersive analysis by X-rays; provides small-area atomic composition analysis.
EELS Electron energy loss spectroscopy.

Effective mass of electron Experimentally measured mass m^* that deviates from actual mass m_e.
Electron microscopy (EM) Electron beam plays role of light beam in conventional microscope.
Electron paramagnetic resonance (EPR) Alternate name for electron spin resonance.
Electron–phonon interaction Cooper pair coupling mechanism in classical superconductors.
Electron spin resonance (ESR) Microwave detection of magnetic moments of unpaired (electron) spins.
Eliashberg relation Integral of the product of the electron phonon coupling strength $\alpha(\omega)$, the phonon density of states $D_{ph}(\omega)$, and ω^{-1} for determining the electron–phonon coupling constant λ.
Energy band Set of very closely spaced energy levels.
Energy gap Separation in energy between two energy bands.
Enthalpy $H = U + PV$.
Entropy S Thermodynamic measure of disorder.
Epitaxial film A thin-film single crystal, in the case of the cuprates made with the copper oxide planes parallel to the surface.
Ettingshausen effect Establishment of transverse temperature gradient in a conductor carrying a uniform current and maintained in a constant magnetic field at a constant temperature.
EXAFS Extended X-ray absorption fine structure.
Exchange integral $\int \psi_A^*(r_m)\psi_B^*(r_n)V(r_{mn})\psi_A(r_n)\psi_B(r_m)d^3r$.
Exciton Bound electron–hole pair.
Exclusion of flux Inability of magnetic field lines to enter superconductor cooled below T_c in zero field and then placed in a field.
Expulsion of flux Exit of magnetic field lines from a material when it is cooled below T_c in an applied magnetic field.
Extinction Decrease in intensity of light passing through a medium.
Extrude To thrust out—for example, in forming a material such as a wire to a desired cross-section by forcing it through a die.
Face centered cubic (fcc) Crystal structure in which the unit cell is a cube with atoms at the vertices and in the centers of the faces.
Faraday's law $\nabla \times \mathbf{E} = -\partial \mathbf{B}/\partial t$.
Fermi–Dirac statistics Statistics of indistinguishable particles of half integer spin $S = 1/2, 3/2, \ldots$ obeying the Pauli exclusion principle.
Fermi energy Energy of highest occupied level in k space.
Fermi gas Collection of noninteracting fermions.
Fermi level E_F Uppermost occupied fermion energy level.
Fermi liquid Collection of weakly interacting fermions confined, at absolute zero, to occupy all energy states below the Fermi surface.
Fermion Particle such as an electron with half integer spin obeying Fermi–Dirac statistics.

Fermi surface Energy surface bounding occupied region of k-space.
Ferroelectric Alignment of electric dipole moments in material.
Field cooling (FC) Cooling a superconductor below its transition temperature while maintaining it in a constant magnetic field.
Flux Φ Quantity of magnetic field, $\Phi = \mathbf{B} \cdot \mathbf{A}$, with unit weber $= Tm^2$.
Flux bundle Group of vortices that move in unison.
Flux creep Very slow motion of magnetic flux when vortex pinning forces are strong and dominate over the Lorentz force.
Flux flow Faster motion of magnetic flux when vortex pinning forces are weak and dominated by the Lorentz force.
Flux jumping Sudden and dissipative rearrangement of magnetic flux within superconductor.
Flux line Another name for vortex.
Flux melting Conversion of array of rigidly fixed vortices to array of randomly shifting or wandering vortices.
Fluxoid A quantity of magnetic flux Φ in a vortex with the quantum value $\Phi_0 = h/2e$.
Fluxon Alternate term for fluxoid.
Flux pump Device for inducing a large persistent current into a magnet coil.
Flux quantum $\Phi_0 = h/2e$, amount of magnetic flux in a vortex.
Flux tube A vortex.
Fourier series Expansion of a function in terms of sines and cosines, sin $(n\omega t)$ and cos $(n\omega t)$, or in terms of exponentials exp $(\pm in\omega t)$.
Free electron approximation Assumption that conduction electrons in a metal do not interact with the background positive charges.
Free energy See Gibbs and Helmholtz.
Fullerene Carbon compound closed on itself in which each carbon atom is bonded to three others, applied especially to the 60-atom compound C_{60}.
Gap Separation in energy, especially that between normal and superconducting states.
Gauge Condition on vector and scalar potentials. For Lorentz gauge $\nabla \cdot \mathbf{A} + \partial\phi/c^2\partial t = 0$ and for Coulomb or London–Landau gauge $\nabla \cdot \mathbf{A} = 0$.
Gauss's law $\nabla \cdot \mathbf{D} = \rho$.
Geodesic dome Architectural structure invented by R. Buckminster Fuller.
***g*-factor** Dimensionless proportionality factor for atomic magnetic moment, $\mu = g\mu_B J$; for a free electron $J = S = 1/2$ and $g = 2.0023$.
Giant flux creep Flux creep arising from thermally activated flux motion.
Gibbs free energy $G = H - TS$.
Ginsburg–Landau parameter $\kappa = \lambda/\xi$.
Ginsburg–Landau theory Description of superconductivity by minimizing free energy expressed in terms of complex order parameter $\phi(\mathbf{r}) = |\phi(\mathbf{r})|e^{i\theta}$.
GLAG Ginzburg–Landau theory with Abrikosov and Gorkov extensions.
Glass Intermediate state between solid and liquid, with very long correlation time, used to describe configuration of vortices.

Gorter–Casimir formula $B_c(T) = B_c(0)[1 - (T/T_C)^2]$.
Gorter–Casimir phenomenological theory A two-fluid model of superconductivity.
Grain alignment Arrangement of grains or microcrystals with most atomic planes aligned in the same general direction.
Graphite Form of carbon with atoms arranged in hexagonal sheets.
Green phase Nonsuperconducting impurity phase Y_2BaCuO_5 sometimes admixed with superconducting $YBa_2Cu_3O_7$.
Gyromagnetic ratio Ratio of angular frequency to magnetic field at which a nucleus or electron absorbs radio frequency or microwave energy, respectively.
Hall coefficient $R_H = E_x/J_yB_z$.
Hall effect Establishment of transverse electric field in current carrying conductor located in a transverse magnetic field.
Hall number Dimensionless coefficient V_o/R_He.
Hard superconductor One with pinning forces strong enough to prevent flux motion.
Heavy electron Electron that acts as if it has a large mass.
Heavy electron compound (material) One with heavy (i.e., large effective mass) electrons.
Heavy fermion Synonym for heavy electron compound.
Helmholtz equation $\nabla^2\psi + k^2\psi = 0$, equation that occurs in the London theory with $\psi = \mathbf{A}, \mathbf{B}, \mathbf{J}$, and $k = 1/\lambda_L$.
Helmholtz free energy $F = U - TS$.
Hexagonal close packed (hcc) Crystal structure with hexagonal layers of atoms stacked in the order ABABA....
High-kappa superconductor One with $\kappa = \lambda/\xi \gg 1$.
Hole The absence of an electron in an otherwise full electron band.
Holon Charged boson particle.
HREM, High-resolution electron microscopy Provides resolutions of 0.13–0.16 nm at 400 keV operation.
Hubbard model Theoretical model for superconductivity with a Hamiltonian containing a "hopping amplitude" kinetic energy term t and a Coulomb repulsion term $U > 0$.
Hybrid orbital One formed by linear combination of atomic orbitals.
Hyperfine interaction Coupling together of an electronic and a nuclear spin, $a\mathbf{S} \cdot \mathbf{I}$.
Hysteresis Lack of reversibility, as in magnetization vs applied magnetic field plots.
Infrared (IR) Light beyond the visible range with a frequency less than that of visible light.
Infrared spectroscopy Measurement of infrared light frequencies corresponding to molecular vibrations; can provide band gaps.
Insulator Poor conductor of electricity.
Intercalation Insertion of atoms or ions between atomic layers of materials.

Intermediate state A state of Type I superconductivity involving mixture of normal and superconducting regions, arising because of a nonzero demagnetization factor.
Intermetallic compound An alloy in which the ratio of component atoms is expressed in terms of integers, such as A_2B_3 or A_3B.
Inverse Josephson effect Inducing a dc voltage across an unbiased junction by introduction of an rf current into the junction.
Ioffe–Regel criterion Onset of resistivity saturation at $k_F l \approx 1$.
Ioffe–Regel parameter Product $k_F l$ of Fermi wave number k_F and electron mean free path l.
Ion Electrically charged atom such as Cu^{2+}.
Ionic radius Effective radius of a charged atom (ion) in a solid.
IPS inverse photoelectron spectroscopy.
IR see Infrared.
Irreversibility For example failure of superconductor to retrace its magnetic state when applied magnetic field reverses its direction.
Isomer shift Shift in gamma ray energy in a Mössbauer experiment.
Isotope Two isotopes of an element have the same number of protons and a different number of neutrons in the nucleus.
Isotope effect Shift in the superconducting transition temperature T_c arising from the presence of different isotopes.
Jahn–Teller effect Spontaneous distortion of a high-symmetry atomic or molecular configuration to a lower-energy, less symmetrical arrangement.
Josephson effect Tunneling of Cooper pairs with zero applied voltage.
Josephson equations $d\phi/dt = 2eV/\hbar = \omega_J$ and $J = J_c \sin\phi$.
Josephson frequency $\nu_J = 2eV/h$.
Josephson junction Two superconductors separated by a barrier through which Cooper pairs can tunnel from one side to the other.
Josephson penetration depth $\lambda_J = (\Phi_o/2\pi\mu_o J_C d)^{1/2}$.
Josephson vortex Loops of super current density J encircling magnetic flux in a Josephson junction, having no core, and with $J = 0$ in the center.
Kappa dimensionless ratio $\kappa = \lambda/\xi$.
Kelvin temperature scale Related to Celsius through $K = C + 273.15$.
Kim model A critical state model that assumes a particular magnetic field dependence of the critical current density J_C.
Kondo effect Presence of a minimum in the temperature dependence of the resistivity of certain dilute alloys.
Kosterlitz–Thouless transition Process involving separation or dissociation of vortex–antivortex pairs.
Kramers–Kronig Method of extracting frequency dependence of the complex dielectric constants ϵ' and ϵ'' and the conductivity σ from infrared reflectance measurements.
Landau diamagnetism Involves orbital electronic interaction with applied magnetic field.

Laplace equation $\nabla^2\psi = 0$.
Latent heat L Heat associated with a first-order phase transition; a second-order transition has no latent heat.
Lattice vacancy Missing atom at regular lattice site.
Laves phase Class of metallic AB_2 compounds, some of which superconduct.
Layering scheme Arrangement of atomic layers in the cuprates.
Lenz's law The induced current and accompanying magnetic flux are in directions that oppose the change in flux through a circuit.
Levitation Suspension of a magnet in space above a superconductor.
Lindemann criterion Vortex lattice melts when average root mean square vortex fluctuation exceeds 10% of average vortex separation.
Little–Parks experiment Demonstrates flux quantization via magnetic field dependence of shift in T_C of thin-walled superconducting cylinder.
Lock-in-detector Reduces noise by passing only signals with predetermined frequency and phase.
London equations (1) $\mathbf{E} = \mu_0\lambda_L^2(d\mathbf{J}/dt)$, and (2) $\mathbf{B} = -\mu_0\lambda_L^2\nabla \times \mathbf{J}$.
London (or London–Landau) gauge $\nabla \cdot \mathbf{A} = 0$.
London penetration depth $\lambda_L = (m/\mu_0 n_S e^2)^{1/2}$.
London theory Simple phenomenological approach that gives the London equations and the associated penetration depth λ_L.
Long-range order Regularities extend over the entire lattice.
Lorentz force $F = I \times B = J \times \Phi$, actually a force per unit length.
Lower critical field of Type II superconductor $B_{C1} = \Phi_0 \ln\kappa/4\pi\lambda^2$.
Luttinger liquid Fermi liquid of strongly correlated electrons.
MAGLEV Magnetic levitation.
Magnetic field Magnetic flux per unit area.
Magnetic moment Magnetic analogue of electric dipole moment.
Magnetic resonance imaging (MRI) Application of NMR to produce images of the human body and other things.
Magnetization M Magnetic dipole moment per unit volume.
Magnetometer Device for measuring magnetic fields.
Magnetoresistivity $\boldsymbol{\rho}_m$ The resistivity of a material in the presence of an applied magnetic field B_{app}. The magnetoresistivity is longitudinal when B_{app} is in the current direction I, and transverse when B_{app} is perpendicular to I, as in the Hall effect.
Magnus force Acting on a moving vortex, this force is proportional to $\mathbf{v} \times \Phi_0$.
Mass, effective see Effective mass.
Mass spectrometer Device for determining mass of atom or molecule.
Matthias's rule Mean number of valence electrons is crucial factor in determining T_C.
Matthiessen's rule Conductivities of a conductor add as reciprocals.
Maxwell–Boltzmann Statistics Classical statistics of distinguishable particles, for example, Maxwellian distribution of velocities in a gas.

Maxwell relations Partial derivative relations between various thermodynamic variables.
Mean free path Average root mean square distance of travel between collisions.
Meissner effect Exclusion and expulsion of magnetic field from a superconductor; sometimes called Meissner–Ochsenfeld effect.
Melting line Line of demarcation between vortex solid and vortex liquid states. Melting temperature is temperature along melting line.
Microwaves Electromagnetic radiation between 1 and 1000 GHz.
Miedema empirical method Linear correlations of properties of superconducting alloys with mole fractions of their constituents.
Mixed state Type II superconductor state of partial flux exclusion existing in the applied field range $B_{c1} < B_{app} < B_{c2}$.
Molecular beam epitaxy (MBE) Method of preparing a superconductor by depositing one layer of atoms at a time.
Monte Carlo Computational method based on random variables.
Moseley's law Proportionality of square root of X-ray frequency with atomic number of atom.
Mössbauer effect Recoilless gamma ray emission by nucleus.
Mott insulator Insulating state formed during Mott transition.
Mott transition Abrupt drop of electrical conductivity to zero, interpreted in terms of nearest-neighbor separation.
Multicore wire Comprising many filamentary superconducting wires embedded (in symmetrical configuration) in normally conducting matrix.
Muon Particle with mass $m = 206.77\ m_e$ that acts in most respects like an electron (μ^-) or a positron (μ^+).
Muon spin relaxation (μSR) A technique using muons to determine the magnetic field distribution and penetration depth in a superconductor.
Nanobridge Ultrasmall Josephson junction.
Nanostructure Structure in size range of tens of angstroms.
Néel temperature T_N Temperature below which a material becomes antiferromagnetic.
Nernst effect Establishment of a transverse electric field in a conductor with a longitudinal temperature gradient located in an applied magnetic field with no electric current flow.
Nesting Occurs when two sheets of Fermi surface are parallel and separated by common reciprocal lattice vector; can lead to instabilities.
Neutron Neutral particle found in nucleus of atom.
Nonlocal electrodynamics Current density J at point arises from electric field averaged over region the size of electron mean free path l.
Normal state Synonymous with nonsuperconducting state.
Nuclear magnetic resonance (NMR) Measures interaction of nuclear magnetic moment with applied magnetic field, involving absorption of energy.
Oblate ellipsoid Ellipsoid compressed along its symmetry axis.

Ohm's law $V = IR$, or in normalized form $E = J\rho$.
Optical extinction Reduction of light intensity during transmission through matter.
Optical phonon Phonon of high-frequency branch.
Orbital Angular momentum wavefunction.
Order parameter Complex parameter $\phi(r) = |\phi|e^{i\theta}$ of the Ginzburg–Landau theory whose square $|\phi|^2$ is the super electron density.
Orthorhombic structure One with rectangular unit cell having mutually perpendicular sides unequal in length: $a \neq b \neq c$.
Overlap integral $\int \psi_A^*(r_m)\psi_B(r_n)d^3r$.
Pair breaking Split up of Cooper pair into two electrons sometimes called quasi-particles.
Pairing mechanism Factors responsible for holding together the two electrons of a Cooper pair.
Pairon Alternate name for Cooper pair.
Pancake vortex Vortex aligned along c direction of a cuprate considered as a stacking of two-dimensional pancake-shaped vortices.
Paramagnetic limit (Clogston-Chandrasekhar limit) Magnetic field where Zeeman energy is comparable with energy gap.
Paramagnetism Magnetic state with magnetic moments almost randomly oriented, but with thermal equilibrium configuration in a magnetic field.
PAS Positron annihilation spectroscopy
Peak effect Rise of the critical current density J_C with increasing applied field to a sharp peak just before it vanishes at B_{C2}.
Peierls instability Crystal structure distortion associated with production of charge density wave.
Peltier effect Uniform electric current accompanied by a thermal current in a conductor maintained at constant temperature.
Penetration depth λ Distance externally applied magnetic field B_{app} reaches inside superconductor. See London penetration depth.
Perfect conductor Hypothetical conductor with zero resistivity but susceptibility of normal conductor (i.e., lacks perfect diamagnetism).
Perfect diamagnetism Magnetic susceptibility (mks) $\chi = -1$.
Periodic table Systematic arrangement of elements in tabular form.
Permeability Parameter $\mu = B/H$ determining magnetism of a material.
Perovskite Mineral calcium titanate, $CaTiO_3$; term is also used for a material with the same crystal structure.
Persistent current Current that flows in a superconductor without energy loss for an indefinite period of time.
Phase diagram Displays various regions of magnetic behavior on a plot of applied field vs temperature (B vs T plot).
Phase θ of Ginsburg–Landau order parameter $\phi(\mathbf{r}) = |\phi(\mathbf{r})|e^{i\theta}$.
Phase rule (Gibbs) Degrees of freedom $f = c - \phi + 2$ in a system of c components with ϕ phases in equilibrium.

Phonon localized sound vibration or "particle" of sound
Phonon density of states Number of normal vibrational modes per frequency interval.
Photoconductivity Increase in electrical conductivity produced by shining light on a material. It is called transient when very short-lived and persistent when the photoinduced change lingers for a while after the light is removed.
Photoelectron Electron ejected from material by incidient light or X-rays.
Photoemission spectroscopy (PES) Measures energy distribution of electrons emitted from solids undergoing electromagnetic irradiation.
Photon "Particle" of light $h\nu$.
Photovoltaic effect Inducing voltage in material by light.
Pinning Holding in place or restraining the motion of a vortex.
Pippard coherence length $\xi_o = a\hbar v_F/k_B T_C$, where v_F is the Fermi speed and the dimensionless parameter $a = 0.18$ by BCS.
Pippard nonlocal electrodynamics Current density J at point arises from electric field averaged over region the size of electron mean free path l.
Planck distribution Distribution function for photons.
Plasma Electrically neutral ionized gas.
Plasmon Quantum of plasma oscillation.
Poisson's equation $\nabla^2\psi = -\rho/\epsilon_o$.
Polariton Quantum of coupled phonon–photon transverse wave.
Polaron Combination of an electron and its induced lattice polarization (strain field), found in insulators, especially ionic solids.
Polymer Long-chain organic molecule formed by joining together many individual segments called monomers.
Porosity $P = (1 - \rho/\rho_{Xray})$, where ρ is the density; a measure of the granularity.
Positron Electron with positive charge; antiparticle of an electron.
Prolate ellipsoid Ellipsoid stretched along its symmetry axis.
Proximity effect The penetration of electron pairs from one superconductor into a neighboring conductor or superconductor produces intermediate properties such as an average T_C near the interface.
Puckering Deviation of atomic layer (e.g., CuO_2 layer) from planarity.
***p*-wave pairing** Cooper pair coupling via p-state wavefunctions.
Quadrupole resonance Method for studying molecules with electric quadrupole moments.
Quasiparticle Excitation (electron) from Cooper pair ground state.
Quenching Rapid cooling; rapid reduction of superconducting magnet to normal state; uncoupling of orbital and spin motions.
Raman spectroscopy Determination of infrared vibrational frequencies by measuring frequency shifts of visible light scattered from the sample.
Rare earth One of 14 metallic elements in the periodic table with a partly full $4f$-shell and an atomic number between 57 and 71.
Reciprocal space Momentum or k-space; space of reciprocal lattice.

Reentrant property Property with second occurrence.
Reflectivity Percentage (or fractional amount) of reflected light intensity.
Relaxation time Time for process to reach $1/e = 36.8\%$ of its final value.
Remanent magnetization M_{rem} Value of the magnetization when the applied field passes through zero along a hysteresis loop.
Resistance R Measure of heat dissipation of wire carrying electrical curent; $R = \rho L/A$ for wire of resistivity ρ, length L, and cross-section A.
Resistance per square Same as sheet resistance.
Resistivity ρ Property of a metal that measures its ability to carry an electric current, with the unit ohm-centimeter, $\Omega - \text{cm}$; $\rho = E/J$.
Resonant valence bond (RVB) A theoretical approach to superconductivity.
Rhombal distortion Lowering symmetry from tetragonal to orthorhombic by stretching along diagonal in $a \cdot b$ plane.
Righi–Leduc effect Establishment of a transverse temperature gradient in a conductor carrying a longitudinal thermal current in a transverse magnetic field; thermal analogue of Hall effect.
Rutger's formula Expression for jump in specific heat at T_C.
Scanning electron microscope Electron beam scans the specimen surface.
Schrödinger equation $(\hbar^2/2m)\nabla^2\psi + V\psi = E\psi$, basic equation of quantum mechanics.
Screening length Characterisic distance over which a potential is appreciable in magnitude.
Second sound A type of sound in a superfluid caused by variations in the density of the normal and superfluid components.
Seebeck effect Establishment of a steady-state longitudinal electric field in a conductor with a longitudinal temperature gradient and no current flow; the Seebeck coefficient S is also called thermopower.
SEM, scanning electron microscopy Provides micrographs or highly enlarged pictures of superconductor surfaces.
Semiconductor Material with electrical conductivity between those of a metal and an insulator.
Semion An anyon with phase $\theta = \frac{1}{2}\pi$ that is intermediate between that of a boson ($\theta = 0$) and fermion ($\theta = \pi$); see Anyon.
Shapiro steps Staircase pattern on current–voltage (I–V) characteristic of Josephson junction.
Sheet resistance The resistance $R_{\text{sheet}} = \rho/d$ of a film of thickness d and resistivity ρ.
Shielding current In the absence of applied transport current the current density J in Maxwell's equations, denoted $J_{\text{sh}} = \nabla \times M$, is called shielding current density or magnetization current density.
Short-range order Regularities extend only over limited regions of the lattice.
Shubnikov phase Another name for mixed state.
Silsbee effect Super-current-carrying wire going normal when its encircling B field reaches the critical field value B_C at the surface.

Sine Gordon equation $\Box^2\psi = k^2 \sin\psi$, Klein–Gordon equation with sine function added; used to describe long Josephson junction, where $\Box^2$ is the d'Alembertian operator defined above.
Skin depth $\delta = (2/\omega\mu_0\sigma)^{1/2}$, depth of penetration of electromagnetic waves into conductor.
Skin effect High-frequency electromagnetic waves penetrate only surface layer of a conductor.
Slave boson Operator in a version of the t–J model.
SMES Superconducting magnetic energy storage.
Soft mode (soft phonon) Vibrational mode that decreases in frequency as the transition temperature is approached from above, and reaches a very low value near T_C.
Soft superconductor One in which the pinning forces are not strong enough to prevent flux motion.
Sol–gel Method of preparing a superconductor by evaporating a solution containing the starting materials down to a viscous mass.
Soliton Solitary wave; sine Gordon equation has soliton solutions.
Sommerfeld term γ Coefficient of electronic specific heat $C_e = \gamma T$.
Specific heat Quantity of heat energy that must be added to a material to raise its temperature by 1°C.
Specific heat discontinuity at T_C BCS gives $(C_S - \gamma T_C)/\gamma T_C = 1.43$.
Spin angular momentum Amount of rotational motion associated with an electron or nucleus arising from its intrinsic spin.
Spin density wave (SDW) Periodic fluctuation in the spin density.
Spin–lattice relaxation time The time required for a magnetic moment that absorbs radio-frequency or microwave energy to pass that energy on to the surrounding medium.
Spinel The mineral $MgAl_2O_4$ or a compound having the same structure.
Spinon A neutral spin $\frac{1}{2}$ soliton (solitary oscillation) particle.
SQUID Acronym for Superconducting QUantum Intereference Device, superconducting loop containing Josephson junction(s) that responds to very small changes in magnetic field.
Stacking Arrangement of crystallographic layers one above the next along the c-axis of a cuprate.
Stacking rules Regularities in layering of atomic planes of cuprate structures.
Stewart–McCumber parameter Admittance ratio β_C of Josephson junction circuit.
STM, scanning tunneling microscopy Provides highly enlarged pictures of superconductor surfaces.
Stoichiometry Integer ratios of elements in a chemical compound; the compound A_2B_3 is stoichiometric, whereas $A_{1.9}B_{3.1}$ is not.
Stokes line Spectral line arising from a Raman-scattered photon with a frequency less than that of the incident photon.
Strong coupled BCS Involves large electron–phonon coupling constant, $\lambda > 1$.

Substrate Nonsuperconducting material on which a superconducting thin film is grown.
Superconducting gap Separation in energy between state containing Cooper pairs and higher energy state containing normal unpaired conduction electrons.
Superfluidity Flow of a liquid such as helium below lambda point (2.17 K) without viscous drag and without dissipation of heat.
Susceptibility $\chi = M/H$, magnetization per unit H-field in material.
***s*-wave pairing** Cooper pair coupling via s-state wave functions; implied in traditional presentation of BCS theory.
Ternary compound One containing three elements.
Tesla (T) Unit of magnetic field; $1\ \mathrm{T} = 10^4$ gauss.
Tetragonal crystal structure Having a rectangular unit cell with two of its sides equal in length $a = b$, but not equal to the third dimension c.
Thermal conductivity Coefficient measuring efficiency of thermal current flow, thermal analogue of electrical conductivity.
Thermal current Flow of heat energy.
Thermodynamic critical field $B_C = (B_{C1}B_{C2}/\ln\kappa)^{1/2}$.
Thermoelectric effect Electric field induced in a conductor by the presence of a temperature gradient.
Thermogravimetric analysis (TGA) Monitoring weight of sample during heating or cooling cycle.
Thermopower see Seebeck effect.
Thin film (superconductor) Has thickness less than penetration depth.
Thomson relation Expression $\pi_P = ST$ relating Peltier coefficient π_P, thermopower S, and temperature T.
Tight binding Band structure approximation involving linear combination of (overlapping) atomic orbitals.
***t*–*J* model** Variant of Hubbard model.
Transition element Element with partly filled inner d-shell.
Transport current Electric current impressed from outside.
Transport entropy Entropy carried along by a thermal current.
Trapped flux Magnetic flux retained by superconductor after removing externally applied magnetic field.
Tublene Tube of carbon in which the walls have a graphite structure.
Tunneling current Arises from electrons or Cooper pairs passing through a barrier such as a weak link.
Twinning Growth pattern of an orthorhombic crystal in which some regions have their a and b axes interchanged relative to other regions.
Two-fluid model Interpenetrating fluids of normal electrons and super electrons (Cooper pairs).
Type I superconductor Exhibits perfect diamagnetism below transition temperature T_c and has only one critical magnetic field B_c.

Type II superconductor Totally expels and excludes magnetic flux below lower critical field B_{c1} and partially does so between B_{c1} and upper critical field B_{c2}; all superconductors except elements are Type II.
Ultrasmall Josephson junction The junction size is smaller than typical weak link.
Ultrasound absorption Can provide the width of energy gap in classical superconductors.
Ultraviolet (UV) Light beyond visible range in which the frequency is greater than that of visible light.
Umklapp process three-phonon "flipping over" process involving nonzero reciprocal lattice vector G ($G = 0$ for normal process); a mechanism for thermal conductivity.
Upper critical field of Type II superconductor $B_{C2} = \Phi_o/2\pi\xi^2$.
USO Unconfirmed superconductivity observation.
Vacancy Absence of atom at an atomic site.
Valence electron Outer atomic electron, available for chemical bond.
Van der Waals force Relatively weak force between molecules arising from shifts in their electric charge distributions.
Van Hove singularity Associated with flat energy bands and peak in density of states.
Villars–Phillips model Provides structural and atomic criteria for presence of high T_C.
Vortex Cylinder or tube of magnetic flux containing one quantum of flux Φ_o; found in Type II superconductor located in magnetic field B_{app}.
Vortex fluid Array of vortices capable of motion because of lack of sufficient pinning.
Vortex glass State intermediate between flux liquid and flux solid.
Vortex lattice Regular arrangement of vortices, usually in a hexagonal pattern, sometimes called Abrikosov lattice.
Wannier functions $W(\mathbf{r} - \mathbf{R})$; summations of normalized Bloch wave functions over all the k-states of a band.
Weak coupled BCS Small electron–phonon coupling constant, $\lambda \ll 1$.
Weak link Intermediate case between thick barrier connecting superconductors that prevents interactions and thin barrier with strong coupling.
Weak pinning Vortex pinning force is less than Lorentz force
Wiedermann–Franz law Thermal to electrical conductivity ratio $K_{th}/\sigma T = 3k_B^2/2e^2$.
Woodstock of Physics "Special Panel Discussion on Novel High Temperature Superconductivity" held at the March 1987 New York meeting of the American Physical Society. It introduced high-T_C to the world.
Work function Minimum energy needed to remove an electron from the interior of a solid.
XAFS X-ray absorption fine structure.
XANES X-ray absorption near edge structure.

XAS X-ray absorption spectroscopy.
XPS X-ray photoemission spectroscopy.
Zeeman splitting Splitting of spectral line in a magnetic field.
Zero field cooling (ZFC) Cooling superconductor below its transition temperature in the absence of an applied magnetic field.

References

F. J. Owens and C. P. Poole, Jr., *The New Superconductors*, Plenum Press, New York, 1996.
C. P. Poole, Jr., H. A. Farach, and R. J. Creswick, *Superconductivity*, Academic Press, New York, 1995.
C. P. Poole, Jr., T. Datta and H. A. Farach, *Copper Oxide Superconductors*, Wiley, NY, 1988.

This Page Intentionally Left Blank

Chapter 2

Properties of the Normal Metallic State

Charles P. Poole, Jr.
Department of Physics and Institute of Superconductivity, University of South Carolina, Columbia, South Carolina

A Introduction

The present chapter furnishes background on normal conductors, which provides some perspective on the superconducting state. Material in this chapter constitutes a convenient source for key definitions and formulas referred to later in the Handbook. A standard solid-state physics text such as those by Kittel (1996) and by Ashcroft and Mermin (1976) should be consulted for more details on these

ISBN: 0-12-561460-8
$30.00
HANDBOOK OF SUPERCONDUCTIVITY

normal state properties. Our earlier works *Superconductivity* (1995) and *The Physics Handbook* (1998) also supplement this material.

B

Conduction Electron Transport

The number density n (electrons/cm^3) of conduction electrons in a metallic element such as copper or aluminum of density ρ_m (g/cm^3), atomic mass number A (g/mole), and valence Z is given by

$$n = N_A Z \rho_m / A, \tag{1}$$

where N_A is Avogadro's number. Table 2.1 lists the electron densities of several metals, and we see that they are a thousand times greater than the density of an ideal gas at standard temperature and pressure.

A potential difference applied along a conducting wire produces an electric field E and hence the force $F = -eE = m(dv/dt)$, which accelerates the electrons. They undergo successive periods of acceleration interrupted by collisions, and during the average time τ between collisions they attain a component of velocity along the field direction,

$$v_{av} = -(eE/m)\tau, \tag{2}$$

which is called the drift velocity, The negative sign means that the electrons move in a direction opposite to that of the electric field.

The current density J,

$$J = nev_{av}, \tag{3}$$

can be written, with the aid of Eq. (2), in the form

$$J = (ne^2\tau/m)E = \sigma_o E, \tag{4}$$

and we have for the dc electrical conductivity σ_o and its reciprocal the resistivity ρ

$$\sigma_o = ne^2\tau/m = 1/\rho. \tag{5}$$

The drift velocity v_{av} is much less than the Fermi velocity v_F at which the conduction electrons actually move on the Fermi surface. The mean free path l, or average distance traveled between collisions, is given by

$$l = v_F \tau. \tag{6}$$

Typically, $v_F \approx 10^6$ m/s for good conductors (i.e., 1/300 the speed of light) and it is perhaps one-tenth of this value for A-15 compounds and high-temperature superconductors in their normal states.

Table 2.1.

Characteristics of selected metallic elements [from Poole *et al.* (1995), p. 2]

Z	Element	Valence	Radius (Å)	Xtal type	a (Å)	n_e $\left(\frac{10^{22}}{\text{cm}^3}\right)$	r_s (Å)	ρ, 77 K ($\mu\Omega$ cm)	ρ, 273 K ($\mu\Omega$ cm)	τ, 77 K (fs)	τ, 273 K (fs)	K_{th} $\left(\frac{\text{W}}{cmK}\right)$
11	Na	1	0.97	bcc	4.29	2.65	2.08	0.8	4.2	170	32	1.38
19	K	1	1.33	bcc	5.23	1.40	2.57	1.38	6.1	180	41	1.0
29	Cu	1	0.96	fcc	3.61	8.47	1.41	0.2	1.56	210	27	4.01
47	Ag	1	1.26	fcc	4.09	5.86	1.60	0.3	1.51	200	40	4.28
41	Nb	1	0.67	bcc	3.30	5.56	1.63	3.0	15.2	21	4.2	0.52
20	Ca	2	0.99	fcc	5.58	4.61	1.73		3.43		22	2.06
38	Sr	2	1.12	fcc	6.08	3.55	1.89	7	23	14	4.4	≈0.36
56	Ba	2	1.34	bcc	5.02	3.15	1.96	17	60	6.6	1.9	≈0.19
13	Al	3	0.51	fcc	4.05	18.1	1.10	0.3	2.45	6.5	8.0	2.36
81	Tl	3	0.95	bcc	3.88	10.5	1.31	3.7	15	9.1	2.2	0.5
50	Sn(W)	4	0.71	tetrg	$a = 5.82$ $c = 3.17$	14.8	1.17	2.1	10.6	11	2.3	0.64
82	Pb	4	0.84	fcc	4.95	13.2	1.22	4.7	19.0	5.7	1.4	0.38
51	Sb	5		rhomb	4.51	16.5	1.13	8	39	2.7	0.55	0.18
83	Bi	5		rhomb	4.75	14.1	1.19	35	107	0.72	0.23	0.09

[a] Notation: a. lattice constant; n_e. conduction electron density; $r_s = (3/4\pi n_e)^{1/3}$; ρ, resistivity: τ, Drude relaxation time; K_{th}, thermal conductivity; $L = \rho K_{th}/\text{T}$ is the Lorentz number; γ, electronic specific heat parameter; m^*. effective mass; R_H, Hall constant; Θ_D, Debye temperature; ω_p, plasma frequency in radians per femtosecond (10^{-15}s); IP, first ionization potential; WF, work function; E_F, Fermi energy; T_F, Fermi temperature in kilokelvins; k_F, Fermi wavenumber in mega reciprocal centimeters; and v_F, Fermi velocity in centimeters per microsecond.

The resistivity $\rho(T)$ of a typical metal has a temperature-independent impurity contribution ρ_o and a temperature-dependent phonon contribution $\rho_{ph}(T)$, and these add by Matthiessen's rule,

$$\rho(T) = \rho_o + \rho_{ph}(T), \tag{7}$$

where ρ_o is the controlling factor at very low temperatures. We see from the data in columns 11 and 12 of Table 2.1 that the collision time decreases with the temperature; it has the temperature dependences $\tau \approx T^{-3}$ for $T \ll \Phi_D$ and $\tau \approx T^{-1}$ for $T \gg \Phi_D$, where Φ_D is the Debye temperature. The dominance of scattering in the forward direction for $T \ll \Phi_D$ introduces the additional factor T^2 leading to the Bloch T^5 law $\rho_{ph}(T) = AT^5$. Umklapp processes, phonon drag, and other factors can cause deviations from this T^5 law. We obtain the limiting behaviors

$$\rho(T) \approx \rho_o + AT^5, \quad T \ll \Theta_D \tag{8a}$$

$$\rho(T) \approx \rho_o + A'T, \quad T \gg \Theta_D. \tag{8b}$$

Figure 2.1 shows the temperature dependence of the resistivity of a high purity (low ρ_o) and a lower purity (larger ρ_o) good conductor. Typical resistivities at

L $\left(\frac{\mu\Omega W}{K^2}\right)$	γ $\left(\frac{mJ}{mol\ K^2}\right)$	$\frac{m^*}{m_e}$	$\frac{1}{R_H ne}$	Θ_D (K)	ω_p $\left(\frac{rad}{fs}\right)$	IP (eV)	WF (eV)	E_F (eV)	T_F (kK)	k_f (M cm^{-1})	v_F $\left(\frac{cm}{\mu s}\right)$
0.021	1.5	1.3	−1.1	150	8.98	5.14	2.75	3.24	37.7	92	107
0.022	2.0	1.2	−1.1	100	5.98	4.34	2.3	2.12	24.6	75	86
0.023	0.67	1.3	−1.4	310	3.85	7.72	4.6	7.0	81.6	136	157
0.023	0.67	1.1	−1.2	220		7.57	4.3	5.49	63.8	120	139
0.029	7.8	12		265		6.8	4.3	5.32	61.8	118	137
0.026	2.7	1.8	−0.76	230		6.11	2.9	4.69	54.4	111	128
0.030	3.6	2.0		150		5.69	2.6	3.93	45.7	102	118
0.042	2.7	1.4		110		5.21	2.7	3.64	42.3	98	113
0.021	1.3	1.4	−0.3	394	14.5	5.99	4.3	11.7	136	175	203
0.028	1.5	1.1		96		6.11	3.8	8.15	94.6	146	169
0.025	1.8	1.3		170		7.34	4.4	10.2	118	164	190
0.026	2.9	1.9		88		7.41	4.3	9.47	110	158	183
0.026	0.11	0.38		200		8.64	4.6	10.9	127	170	196
0.035	0.01	0.047		120		7.29	4.2	9.90	115	161	187

room temperature are 1.5 to 2 $\mu\Omega$ cm for very good conductors (e.g., Cu), 10 to 100 for poor conductors, 300 to 10,000 for high-temperature superconducting materials, 10^4 to 10^{15} for semiconductors, and 10^{20} to 10^{28} for insulators. Representative data on the cuprates are provided in Table 2.2.

The resistivity of poor metals at high temperatures tends to saturate to a temperature-independent value when the mean free path l approaches the wavelength $\lambda_F = 2\pi/k_F$ associated with the Fermi wave vector k_F. The Ioffe–Regel criterion for the onset of this saturation is

$$k_F l \approx 1. \tag{9}$$

For the cuprates this criterion is reached beyond 1000 K.

Fig. 2.1.

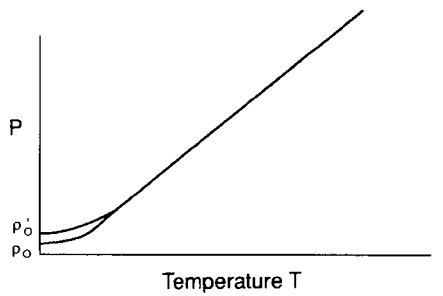

Temperature dependence of the resistivity ρ of a pure (ρ_0) and a less pure conductor. Impurities limit the zero temperature resistivity (ρ_0') in the latter case.

Table 2.2.

Representative normal state resistivities of some cuprates for axial symmetry. The data are from Table 2.2 of Poole *et al.*, (1995). For some compounds, averaged data are shown.

Compound	T (K)	ρ_{ab}(mΩ cm)	ρ_c(mΩ cm)	ρ_c/ρ_{ab}
$(La_{0.925}Sr_{0.075})_2CuO_4$	45	1.7	19	11
	290	5.0		
$(Nd_{0.925}Ce_{0.075})_2CuO_4$	30	0.9	500	550
	290	2.6	1300	500
$YBa_2Cu_3O_{7-\delta}$	100	0.15	13	87
	290	0.33	14	42
$Bi_2Sr_2CuO_6$	25	0.09	14,000	1.6×10^5
	290	0.28	6000	2.2×10^4
$Tl_2Ba_2CuO_6$	110	0.9		
$Tl_2Ba_2CaCu_2O_8$	10	3.5		

The resistivity of the cuprates in the normal state is far greater along the c axis than it is perpendicular to this axis, that is, in the a, b plane, as may be seen from the data in Table 2.2. The angular dependence

$$\rho(\theta) = \rho_{ab} \sin^2 \theta + \rho_c \cos^2 \theta \tag{10}$$

has been reported, where θ is the angle of the current flow direction relative to the c axis. Sometimes the resistivity anisotropy is lower than axial with the ratio $\rho_a/\rho_b \approx 2$ reported for $YBa_2Cu_3O_{7-\delta}$ (Friedmann *et al.*, 1990) and $Bi_2Sr_{2.2}Ca_{0.8}Cu_2O_8$ (Martin *et al.*, 1988).

Good conductors of electricity are generally good conductors of heat, and metals tend to have the same ratio $K_{th}/\sigma T$ involving the thermal and electrical conductivities, K_{th} (Jcm^{-1}sec^{-1}K^{-1}) and $\sigma(\Omega^{-1}\text{cm}^{-1})$, respectively, which is about twice the value predicted by he law of Wiedermann and Franz,

$$K_{th}/\sigma T = 1.5(k_B/e)^2, \tag{11}$$

where the Lorenz number $1.5(k_B/e)^2 = 1.11 \times 10^{-8}\text{W}\Omega/\text{K}^2$ is a universal constant.

C

Frequency-Dependent Electrical Conductivity

A harmonically varying electric field $E = E_o e^{-i\omega t}$ periodically accelerates the conduction electrons in the forward and backward directions to give, for the ac conductivity,

$$\sigma = \frac{\sigma_o}{1 - i\omega\tau}, \tag{12}$$

which reduces to Eq. (5) when the frequency is zero. When $\omega\tau \ll 1$, many collisions occur during each cycle of the E field, and the average electron motion follows the oscillations. When $\omega\tau \gg 1$, then E oscillates more rapidly than collisions occur, the electrical conductivity becomes predominantly imaginary, corresponding to a reactive impedance, and the high-frequency dielectric constant $\epsilon(\omega)$ becomes

$$\epsilon(\omega) = \epsilon_0\left(1 - \frac{\omega_p^2}{\omega^2}\right), \tag{13}$$

where ω_p is the plasma frequency,

$$\omega_p = (ne^2/\epsilon_0 m)^{1/2}, \tag{14}$$

and $\lambda_p = 2\pi c/\omega_p$ is the plasma wavelength. For frequencies $\omega < \omega_p$ the dielectric constant is negative so electromagnetic waves cannot propagate, and above this value ϵ is positive and propagation occurs. This causes metals to be opaque for $\omega < \omega_p$ and transparent for $\omega > \omega_p$. The quantity λ_p varies between 200 and 440 nm for the alkali metals.

D

Brillouin Zones

The positions of the atoms in crystals are expressed in ordinary direct lattice coordinates x, y, z, and the energy bands of conductors and superconductors are expressed in reciprocal space coordinates k_x, k_y, k_z, sometimes called momentum space. The reciprocal space basis vectors **A**, **B**, and **C** are related to their coordinate space counterparts **a**, **b**, and **c** as follows:

$$\mathbf{A} = \frac{2\pi\mathbf{b}\times\mathbf{c}}{\mathbf{a}\cdot(\mathbf{b}\times\mathbf{c})}, \quad \mathbf{B} = \frac{2\pi\mathbf{c}\times\mathbf{a}}{\mathbf{a}\cdot(\mathbf{b}\times\mathbf{c})}, \quad \mathbf{C} = \frac{2\pi\mathbf{a}\times\mathbf{b}}{\mathbf{a}\cdot(\mathbf{b}\times\mathbf{c})}. \tag{15}$$

When **a**, **b**, and **c** are orthogonal to each other, they are inverse in magnitude and parallel in direction to their counterparts **A**, **B**, and **C** in k-space:

$$A = 2\pi/a, \quad B = 2\pi/b, \quad C = 2\pi/c. \tag{16}$$

For orthorhombic structures ($a < b < c$) the $A > B > C$ are all different lengths; for tetragonal crystals ($a = b \neq c$) we have $A = B \neq C$, and for the cubic case ($a = b = c$) the reciprocal space basis vectors $A = B = C$ are all equal in length. The unit cell in reciprocal space, called the (first) Brillouin zone BZ, has the volume $ABC = (2\pi)^3/abc$ for the orthogonal case.

Figure 2.2 sketches the Brillouin zone of the orthorhombic $YBa_2Cu_3O_7$ structure which is not body-centered. The mercury high-temperature superconductors have the same type of Brillouin zone, with the dimensions given in Table

Fig. 2.2.

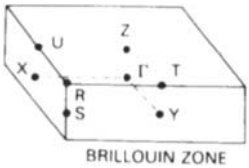

Sketch of the Brillouin zone of orthorhombic $YBa_2Cu_3O_7$ with the symmetry points indicated. [Krakauer *et al.*, 1988.]

Table 2.3.

Dimensions of the unit cell (a, b, c, in nm) and Brillouin zone (A, B, C, in nm^{-1}) of four non-body centered cuprates

Compound	a	b	c	A	B	C
$YBa_2Cu_3O_{7-\delta}$	3.82	3.88	11.7	1.64	1.62	0.537
$HgBa_2CuO_4$	3.88	3.88	9.53	1.62	1.62.	0.659
$HgBa_2CaCu_2O_6$	3.86	3.86	12.66	1.63	1.63	0.496
$HgBa_2Ca_2Cu_3O_8$	3.85	3.85	15.78	1.63	1.63	0.398

2.3. We see from the table that the space unit cells of these four compounds are elongated along c, and their Brillouin zones are compressed along C.

Figure 2.3 shows the Brillouin zone of La_2CuO_4, which is body-centered, and Fig. 2.4 shows how two adjacent La_2CuO_4 unit cells fit together. The thallium and bismuth compounds have the same types of Brillouin zones, but compressed in the k_z direction since their real space unit cells have about the same a and b values, and much larger c values (hence smaller C values) than La_2CuO_4.

Fig. 2.3.

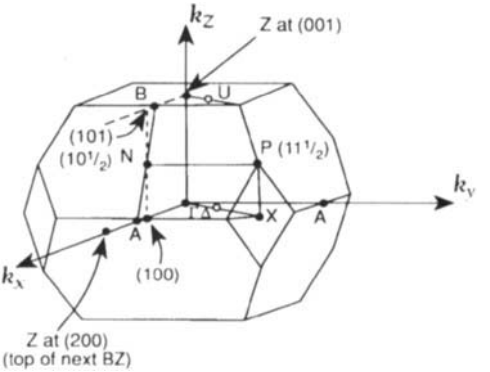

Brillouin zone of body centered tetragonal La_2CuO_4 with the symmetry points indicated. The symbols Δ and U designate general points along [110] directions. [Adapted from Pickett, 1989.]

Fig. 2.4.

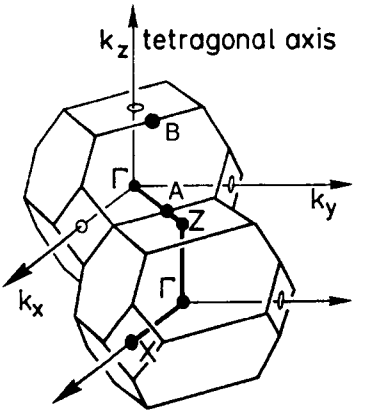

Geometric relationship between adjacent Brillouin zones of La_2CuO_4. Note that the k_x and k_y axes of this figure and those of Fig. 2.3 are rotated by 45° relative to each other. [Kulkarni *et al.*, 1991.]

E

Fermi Surface

Conduction electrons follow Fermi–Dirac statistics with the FD distribution function,

$$f(E) = \frac{1}{\exp[(E-\mu)/k_B T] + 1}, \tag{17}$$

where the chemical potential μ is related to the Fermi temperature T_F by

$$\mu \approx E_F = k_B T_F \tag{18}$$

and T_F is typically about 10^5 K. Equation (17) is plotted in Fig. 2.5a for $T = 0$ and in Fig. 2.5b for $T > 0$. We see from the figures that $f(E)$ is 1 for energies below E_F, it is zero above E_F, and it assumes intermediate values only in a narrow region of width $k_B T$ near the Fermi energy E_F.

The electron kinetic energy

$$E_K = \hbar^2 k^2/2m = (\hbar^2/2m)(k_x^2 + k_y^2 + k_z^2) \tag{19}$$

is quantized in k-space, and at 0 K these k-space levels are doubly occupied by electrons of opposite spin up to the Fermi surface at $E = E_F$,

$$E_F = \hbar^2 k_F^2/2m, \tag{20}$$

as indicated in the figure. Partial occupancy occurs in the narrow region of width $k_B T$ at the Fermi surface shown in Fig. 2.5b, and the levels are empty for higher

Fig. 2.5.

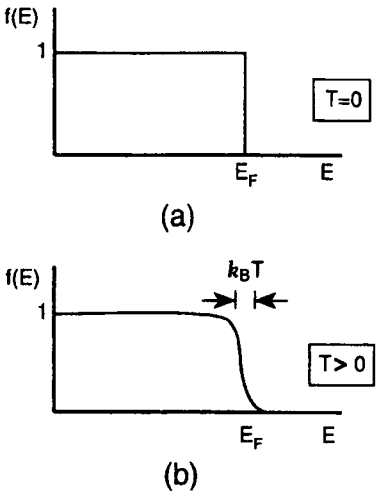

Fermi–Dirac distribution function $f(E)$ for electrons (a) at $T = 0$ K, and (b) above 0 K for the condition $T \ll T_f$. [Poole *et al.*, 1995, p. 9.]

energies. For the isotropic case of a spherical Fermi surface, the electron density n at this surface is

$$n = k_F^3/3\pi^2 = \frac{1}{3\pi^2}(2mE_F/\hbar^2)^{3/2}. \tag{21}$$

The derivative dn/dE with E_F replaced by E provides the density of states $D(E)$ per unit volume,

$$D(E) = \frac{d}{dE}n(E) = \frac{1}{2\pi^2}(2m/\hbar^2)^{3/2}E^{1/2} = D(E_F)[E/E_F]^{1/2}. \tag{22}$$

With the aid of Eqs. (18) and (20), $D(E)$ at the Fermi level can be written in two equivalent ways:

$$D(E_F) = \begin{cases} 3n/2k_BT_F \\ mk_F/\hbar^2\pi^2 \end{cases}. \tag{23}$$

The electron density n and the total electron energy E_T can be expressed in terms of integrals over the density of states multiplied by $f(E)$ from Eq. (17):

$$n = \int D(E)f(E)\,dE \tag{24}$$

$$E_T = \int D(E)f(E)\,E\,dE. \tag{25}$$

The energy dependence of $D(E)f(E)$ in these integrands is given in Fig. 2.6a for $T = 0$ and in Fig. 2.6b for $T > 0$.

Fig. 2.6.

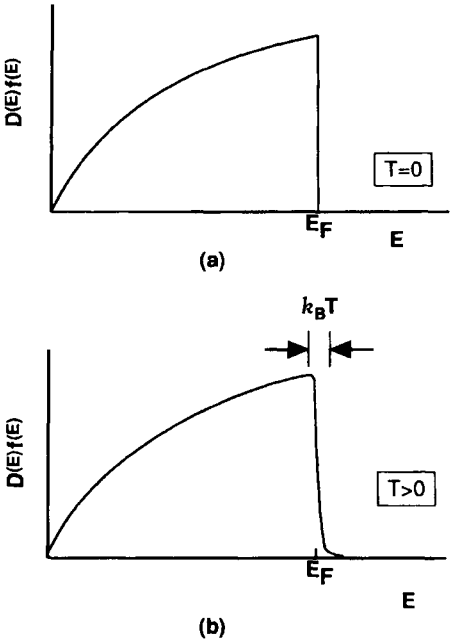

Energy dependence of the occupation by electrons of a free electron energy band (a) at 0 K and (b) for $T > 0$ K for the condition $T \ll T_F$. [Poole *et al.*, 1995, p. 10.]

The kinetic energy near an energy gap may be expressed in terms of an effective mass m^*,

$$E_k = \hbar^2 k^2 / 2m^*, \tag{26}$$

where

$$\frac{1}{m^*} = \frac{1}{\hbar^2} \left| \frac{d^2 E_k}{dk^2} \right| \tag{27}$$

and the density of states, which is proportional to the effective mass m^*,

$$D(E) = m^* k_F / \hbar^2 \pi^2, \tag{28}$$

becomes large near the gap, as indicated in Fig. 2.7.

Fig. 2.7.

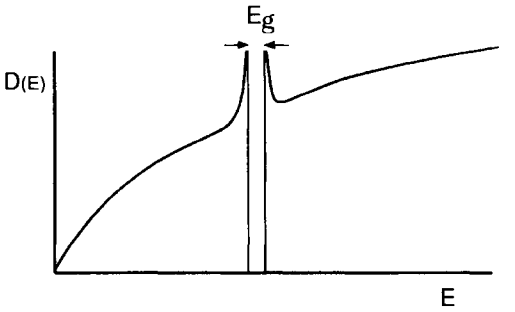

Energy dependence of the density of states *D(E)* in the presence of an energy gap.

F

Electromagnetic Fields

The electromagnetic fields obey Maxwell's two homogeneous equations [Jackson, 1998; Lorrain *et al.*, 1988],

$$\mathbf{V} \cdot \mathbf{B} = 0 \tag{29}$$

$$\mathbf{V} \times \mathbf{E} + \partial \mathbf{B}/\partial \mathbf{t} = 0, \tag{30}$$

as well as the corresponding inhomogeneous ones,

$$\mathbf{V} \cdot \mathbf{D} = \boldsymbol{\rho} \tag{31}$$

$$\mathbf{V} \times \mathbf{H} = \mathbf{J} + \partial \mathbf{D}/\partial \mathbf{t}, \tag{32}$$

where $\boldsymbol{\rho}$ and $\mathbf{J}$, respectively, are the free charge density and the free current density. They are called "free" because they do not arise from the reaction of the medium to applied fields, charges, or currents. The constitutive relations between the $\mathbf{B}$, $\mathbf{H}$ fields and the $\mathbf{E}$, $\mathbf{D}$ fields, respectively, in a medium characterized by a permeability μ and dielectric constant ϵ, are as follows:

$$\mathbf{B} = \mu \mathbf{H} = \mu_0(\mathbf{H} + \mathbf{M}) \tag{33}$$

$$\mathbf{D} = \epsilon \mathbf{E} = \epsilon_0 \mathbf{E} + \mathbf{P}. \tag{34}$$

These, of course, are SI formulas. When cgs units are used we have $\mu_0 = \epsilon_0 = 1$ in free space, and the factor 4π is added in front of M and P in Eqs. (33) and 34). Otherwise, for the SI case μ_0 and ϵ_0 have the values given in Table 1.1.

At the interface of two media of respective permeabilities μ' and μ'' in contact with each other, the $\mathbf{B}'$, $\mathbf{H}'$ fields in one medium are related to $\mathbf{B}''$, $\mathbf{H}''$ in the other medium through the following two boundary conditions:

Fig. 2.8.

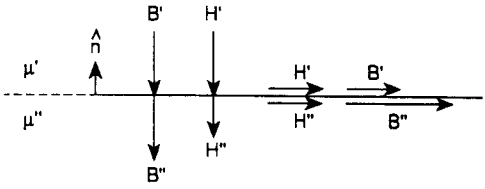

Boundary conditions for the components of the **B** and **H** magnetic field vectors perpendicular to and parallel to the interface between regions that have different values of the permeability. The figure is drawn for the case $\mu'' = 2\mu'$. [Poole *et al.*, 1995, p. 15.]

1. The components of B normal to the interface are continuous across the boundary

$$B'_{\perp} = B''_{\perp}. \tag{35}$$

2. The components of H tangential to the interface are continuous across the boundary

$$H'_{\parallel} = H_{\parallel}, \tag{36}$$

as shown in Fig. 2.8. For a surface current density $\mathbf{K}_{\text{surf}}$ at the interface the second condition (36) becomes

$$\mathbf{n} \times (\mathbf{H}' - \mathbf{H}''_{\parallel}) = \mathbf{K}_{\text{surf}}, \tag{37}$$

where the unit vector $\mathbf{n}$ is defined in the figure, and $\mathbf{K}_{\text{surf}}$, which has the units A/m, flows perpendicular to the field direction. For the analogous electric case the normal components of **D** and the tangential components of **E** are continuous across an interface, and the condition on **D** is modified in accordance with Eq. (31) when there are surface charges present.

The Lorentz force **F** on a charge q moving at the velocity **v** is expressed in terms of the macroscopically measured magnetic and electric fields **B** and **E**, respectively:

$$\mathbf{F} = q(\mathbf{E} + \mathbf{v} \times \mathbf{B}). \tag{38}$$

The field B is sometimes called the magnetic flux density because $B = \Phi/A$ where Φ is the magnetic flux and A is the cross-sectional area perpendicular to B. The magnetic flux inside Type II superconductors is quantized with the value $\Phi_0 = h/2e = 2.0678 \times 10^{-15}\,\text{T m}^2$, where the unit tesla meter squared is called a weber.

References

N. W. Ashcroft and N. D. Mermin, *Solid State Physics*, Saunders, Philadelphia, 1976.

T. A. Friedmann, M. W. Rabin, J. Giapintzakis, J. P. Rice, and D. M. Ginzberg, *Phys. Rev. B* **42**, 6217 (1990).

J. D. Jackson, *Classical Electrodynamics*, 3nd ed., Wiley, New York, 1998.
C. Kittel, *Introduction to Solid State Physics*, 7th Ed., Wiley, New York, 1996.
H. Krakauer, W. E. Pickett, and R. E. Cohen, *J. Supercond.* **1**, 111 (1988).
A. D. Kulkarni, F. W. De Wette, J. Prade, U. Schröder, and W. Kress, *Phys. Rev. B* **43**, 5451 (1991).
P. Lorrain, D. P. Corson, and F. Lorrain, *Electromagnetic Fields and Waves*, W. H. Freeman and Company, New York, 1988.
S. Martin, A. T. Fiory, R. M. Fleming, L. F. Schneemeyer, and J. V. Waszczak, *Phys. Rev. Lett.* **60**, 2194 (1988).
W. E. Pickett, *Rev. Mod. Phys.* **61**, 433 (1989).
C. P. Poole, Jr., H. A. Farach, and R. J. Creswick, *Superconductivity*, Academic Press, New York, 1995.
C. P. Poole, Jr., *The Physics Handbook*, Wiley, New York, 1998.

This Page Intentionally Left Blank

Chapter 3

Superconducting State

Charles P. Poole, Jr.
Department of Physics and Institute of Superconductivity,
University of South Carolina, Colombia, South Carolina

A Introduction

This chapter will provide a short introduction to the nature of the superconducting state, with an emphasis on its two salient properties, namely, zero resistance and perfect diamagnetism. The emphasis will be on Type I superconductors, with Type II mentioned briefly at the end. Much of the material in this chapter was elaborated on in our earlier work (Poole *et al.*, 1995).

ISBN: 0-12-561460-8
$30.00

HANDBOOK OF SUPERCONDUCTIVITY

B

Persistent Current and Surface Resistance

Even though superconductors have, by nature, zero dc resistance, it is still of interest to see how close they come to zero. Ideally an electric current established in a loop of superconducting wire will persist forever. An upper limit on the resistivity ρ is set by the duration of persistent current flow. For a loop of radius $r = 15\,\text{cm}$ and wire radius $a = 1.5\,\text{mm}$ the ratio of the inductance $L = \mu_0 r[\ln(8r/a) - 2]$ to the resistance $R = 2r\rho/a^2$ provides the time constant $\tau = L/R$, and we find

$$\rho\tau \approx 6.6 \times 10^{-10}\ \Omega\ \text{cm sec.} \tag{1}$$

Since the current flows undiminished for well over a year,

$$\tau \gg 3.2 \times 10^{7}\ \text{sec}, \tag{2}$$

the resistivity is far less than the limiting value

$$\rho \ll 2.1 \times 10^{-17}\ \Omega\ \text{cm}. \tag{3}$$

A special case to consider is current flow along a film of thickness d. For the square region of surface with dimensions $a \times a$ shown in Fig. 3.1, the current encounters the resistance $R_s = \rho a/A$, where $A = ad$, to give

$$R_s = \rho/d. \tag{4}$$

This resistance ρ/d is called the sheet resistance, or the resistance per square, because it is for a square section of film independent of the length of the side a. It is analagous to the surface resistance $R_s = \rho/\delta$ of a metal with the skin depth δ. There is a quantum of resistance $h/4e^2$ with the value

$$h/4e^2 = 6.45\ \text{k}\Omega, \tag{5}$$

which is one-fourth of the Hall effect resistance $R_H = h/e^2$. When the sheet resistance in the normal state just above T_c exceeds this value (5), the metal does not become superconducting, as illustrated in Fig. 3.2 for bismuth. The condition

$$R_s < h/4e^2 \tag{6}$$

must be satisfied for the material to superconduct.

Fig. 3.1

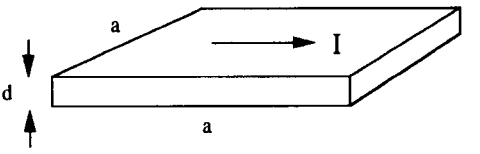

Geometrical arrangement and current flow direction for sheet resistance measurement. [From Poole *et al.* (1995), p. 32.]

Fig. 3.2

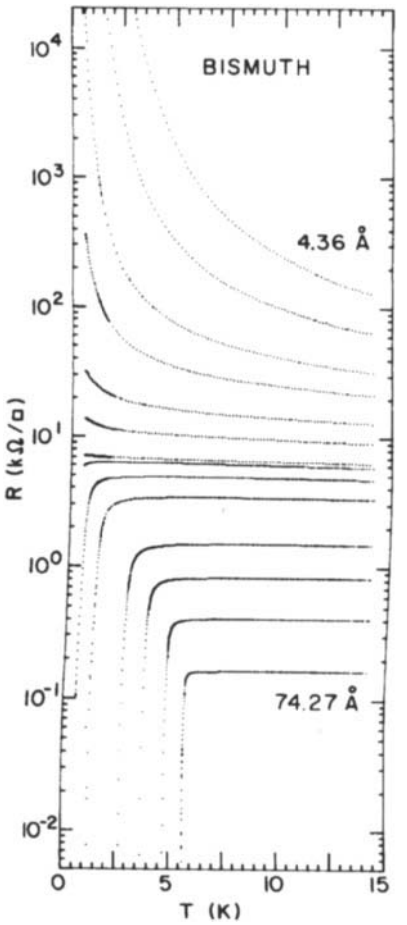

Temperature dependence of the sheet resistance of films of Bi deposited on Ge as a function of the film thickness in the range from 4.36 Å to 74.27 Å. [From Haviland *et al.* (1989).]

C

Fields inside Superconductor

More quantitatively, when an idealized Type I superconducting cylinder of radius R much greater than the penetration depth $\lambda = (m/\mu_0 n_s e^2)^{1/2}$ is placed in an external field $B_{app} = B_0 = \mu_0 H_0$ directed along its axis; then demagnetizing or shielding current J_{sh} is induced to flow in circles around the outside regions of the cylinder. Far inside the cylinder the H field balances the magnetization,

$H_{in} = -M$, and the B field is zero. Near the surface the fields and current exist, and they have the following values inside ($0 \leq r \leq R$):

$$B_{in}(r) \approx B_o \exp[-(R - r)/\lambda] \tag{7}$$

$$H_{in} = H_o \tag{8}$$

$$M(r) \approx -H_o[1 - \exp(R - r)/\lambda] \tag{9}$$

$$J_{sh}(r) \approx -J_o \exp[-(R - r)/\lambda]. \tag{10}$$

These values are plotted in Fig. 3.3, where

$$B_o = \mu_o \lambda J_o \tag{11}$$

The vectors $\mathbf{B}_{in}$ and $\mathbf{J}_{sh} = \nabla \times \mathbf{M}$ are perpendicular to each other, and $B_{in}(r)$ satisfies the expression

$$B_{in}(r) = \mu_o[H_o + M(r)] \tag{12}$$

where $M(r)$ is negative everywhere inside. The superconducting medium can be considered as reacting to the presence of the applied field by generating (a) shielding currents J_{sh} that cancel the interior B field, or (b) a magnetization M that nullifies the interior field B_{in} through Eq. (12), where $\mathbf{J}_{sh} = \nabla \times \mathbf{M}$.

When transport current is caused to flow longitudinally along a Type I superconducting wire in the absence of an applied field, it flows in a surface layer of thickness λ with the radial distance dependence given by Eq. (10). This applied current induces magnetic field lines that encircle the wire outside and an

Fig. 3.3

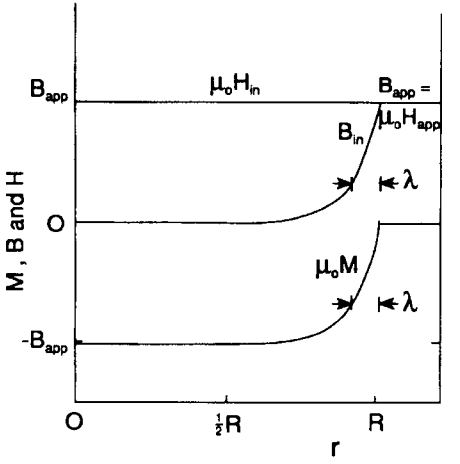

Plot of the fields B and H and of the magnetization $\mu_o M$ inside ($r < R$) and outside ($r > R$) a Type I superconducting cylinder of radius R in an axial applied magnetic field $B_{app} = \mu_o H_o$. [From Poole *et al.* (1995), p. 42.]

internal field B_{in} confined to the surface layer with the distance dependence of Eq. (7).

There is really no fundamental difference between transport current and shielding current. Current impressed from outside into a superconductor is called transport current, and it induces an encircling magnetic field. When an external magnetic field penetrates a superconductor, it is accompanied by induced encircling shielding currents.

D

Temperature Dependencies

The critical field and critical current density are related through the expression

$$B_c(T) = \mu_o \lambda(T) J_c(T), \tag{13}$$

where all three quantities are temperature dependent. At absolute zero we use the notation $B_c(0) = B_c$, etc., and Eq. (13) becomes, in analogy with Eq. (11),

$$B_c = \mu_o \lambda J_c. \tag{14}$$

A particular superconducting wire of radius R has a maximum current called the critical current I_c, and for a Type I superconductor it has the value

$$I_c = 2\pi R \lambda J_c = 2\pi R B_c / \mu_o. \tag{15}$$

The destruction of the superconducting state by exceeding the critical (transport) current I_c is called the Silsbee effect.

The penetration depth $\lambda(T)$ is related to the super electron density n_s(T) through the expression

$$\lambda(T) = \lambda_L(T) = [m/\mu_o n_s(T) e^2]^{1/2}, \tag{16}$$

due to London. In the two-fluid model we have the temperature-dependent expression for the super n_s and normal n_n, electron densities, respectively,

$$n_s(T) + n_n(T) = n, \tag{17}$$

where the total electron density n is independent of temperature, and at $T = 0$ we have $n_n(0) = 0$ and $n_s(0) = n$. The two fluids n_s and n_n interpenetrate but to not interact, and simple theory predicts the following temperature dependences:

$$B_c(T) = B_c(0)[1 - (T/T_c)^2] \tag{18}$$

$$\lambda(T) = \lambda(0)[1 - (T/T_c)^4]^{-1/2} \tag{19}$$

$$J_c(T) = J_c(0)[1 - (T/T_c)^2][1 - (T/T_c)^4]^{1/2} \tag{20}$$

$$n_s(T) = n[1 - (T/T_c)^4] \tag{21}$$

$$n_n(T) = n(T/T_c)^4. \tag{22}$$

These dependences are sketched in Figs. 3.4 to 3.7. Some authors report other exponent values or related expressions for these temperature dependences. The dashed lines show the asymptotic behaviours.

Fig. 3.4

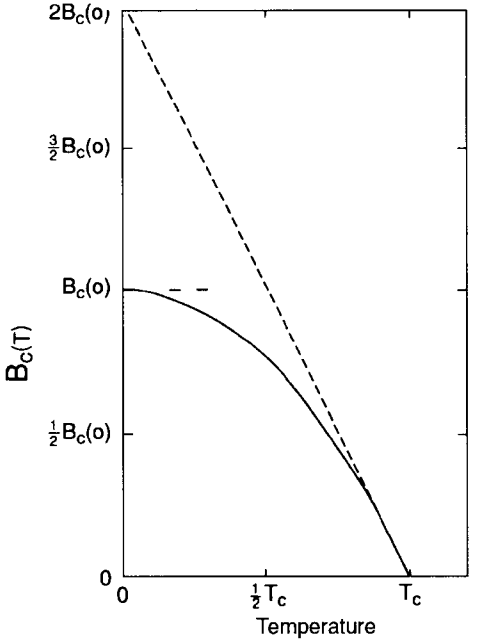

Temperature dependence of the critical field $B_c(T)$ corresponding to Eq. (18). The asymptotic behaviors near $T = 0$ and $T = T_c$ are indicated by dashed lines. [From Poole *et al.* (1995), p. 51.]

Fig. 3.5

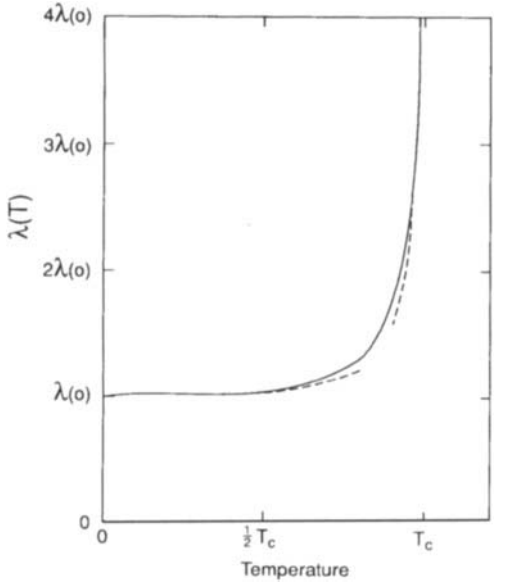

Temperature dependence of the penetration depth $\lambda(T)$ corresponding to Eq. (19). The asymptotic behaviours near $T = 0$ and $T = T_c$ are indicated by dashed lines. [From Poole *et al.* (1995), p. 52.]

Fig. 3.6

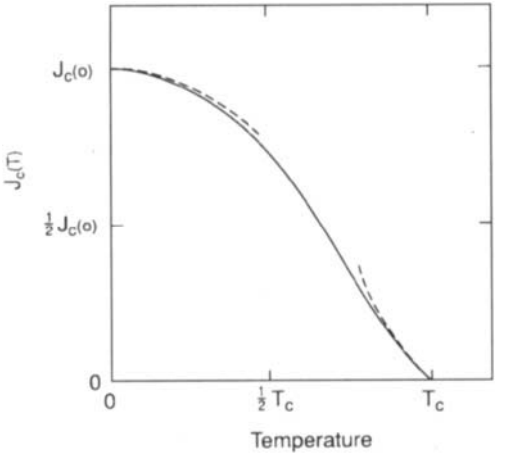

Temperature dependence of the critical current density $J_c(T)$ in accordance with Eq. (20). The asymptotic behaviors near $T = 0$ and $T = T_c$ are indicated by dashed lines. [From Poole *et al.* (1995), p. 52.]

Fig. 3.7

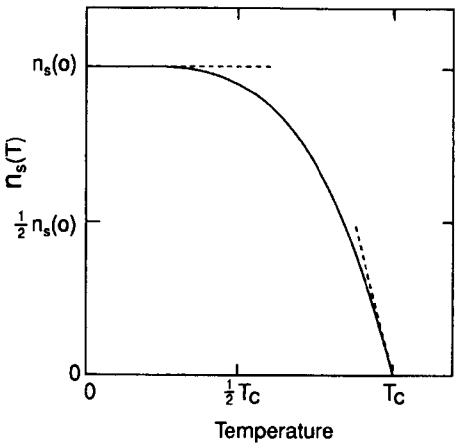

Temperature dependence of density of superconducting electrons n_s as given by Eq. (21). The dashed lines indicate the slopes $dn_s/dT = 0$ at $T = 0$, and $dn_s/dT = -4n/T_c$ at $T = T_c$. [From Poole *et al.* (1995), p. 53.]

The temperature dependencies of Eqs. (18) and (20), respectively, permit us to define a critical surface in the three-dimensional space of applied magnetic field B_{app}, applied transport current J_{Tr}, and temperature T, and this is sketched in Fig. 3.8. This surface constitutes the boundary between the normal and superconducting regions, so the material is superconducting for points (B_{app}, J_{Tr}, T) that lie below it and normal for points above it.

Fig. 3.8

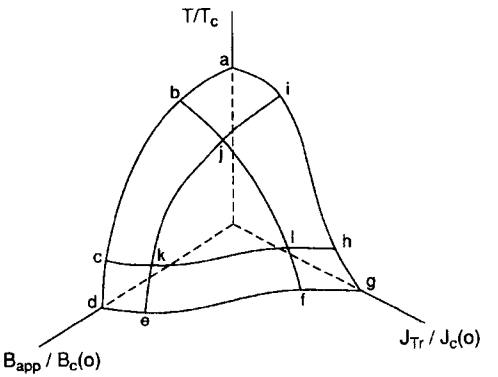

Critical surface of a superconductor. Values of applied field B_{app}, transport current J_{Tr} and temperature T corresponding to points below the critical surface are in the superconducting region, and points above this surface are in the normal region. [From Poole *et al.* (1995), p. 54.]

Fig. 3.9

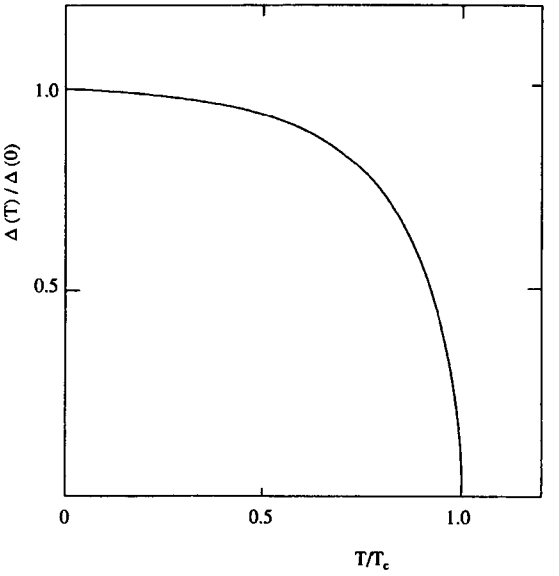

Temperature dependence of the BCS energy gap $\Delta(T)$ normalized relative to the zero temperature gap $\Delta(0)$ as given by Eq. (23), where $\Delta(T) = \frac{1}{2}E_g(T)$. [From Poole *et al.* (1995), p. 167.]

The superconducting energy gap $E_g(T) = 2\Delta(T)$ in the neighborhood of T_c has the simple theory temperature dependence:

$$E_g(T) \approx 3.53\, k_B T_c [1 - (T/T_c)]^{1/2}, \tag{23}$$

sketched in Fig. 3.9 where $\Delta(0) = 1.76\, k_B T_c$.

The temperature dependences of the various quantities presented in this section are predicted by simple theoretical approaches to superconductivity and are sometimes reasonable approximations to experimentally measured values. These expressions all assume an isotropic material.

E

Critical Magnetic Field Slope

The critical magnetic field has the parabolic dependence on the temperature given by Eq. (18), with the following slope near T_c:

$$\frac{dB_c(T)}{dT} = -\frac{2B_c(T)}{T_c}. \tag{24}$$

For typical Type I superconductors this slope varies between -15 and $-50\,\mathrm{mT/K}$. A Type II superconductor has lower B_{c1} and upper B_{c2} critical fields, and typical values of their slopes for a cuprate are

$$\frac{dB_{c1}}{dT} = -\frac{2B_{c1}(0)}{T_c} \approx -1\ \mathrm{mT/K} \tag{25}$$

$$\frac{dB_{c2}}{dT} = -\frac{2B_{c2}(0)}{T_c} \approx -1.83\ \mathrm{T/K}. \tag{26}$$

The latter slope of $-1.83\,\mathrm{T/K}$ comes from the Pauli limiting field approximation

$$B_{\mathrm{Pauli}} = E_g/2\sqrt{2}\mu_B = 1.83\ T_c, \tag{27}$$

obtained by using the BCS expression $E_g = 3.53k_BT_c$. The slopes of Eqs. (25) and (26) near T_c can be quite anisotropic for high-temperature superconductors.

References

D. B. Haviland, Y. Liu and A. M. Goldman, *Phys. Rev. Lett.* **62**, 2180 (1989).

C. P. Poole, Jr., H. A. Farach, and R. J. Creswick, *Superconductivity*, Academic Press, New York, 1995.

Chapter 4

Models and Theories

Charles P. Poole, Jr.
Department of Physics and Institute of Superconductivity,
University of South Carolina, Columbia, South Carolina

A Introduction

Superconductivity was discovered in 1911 by H. Kamerlingh Onnes when he found that the element mercury went resistanceless below the critical temperature $T_c = 4.1$ K, and 25 years were to pass before Meissner and Ochsenfeld (1933) found that superconductors also exclude magnetic flux. Two years later in 1935 the London brothers proposed a simple theory to explain the Meissner effect. In 1950 Ginzburg and Landau advanced a macroscopic theory that described superconductivity in terms of an order parameter, and they provided a derivation

ISBN: 0-12-561460-8
$30.00
HANDBOOK OF SUPERCONDUCTIVITY

of the London equations. That same year Fröhlich (1950) predicted the isotope effect whereby the transition temperature of a superconducting element decreases when its isotopic mass increases, a prediction confirmed forthwith by Maxwell (1950) and also by Reynolds *et al.* (1950). In 1957 Bardeen, Cooper, and Schrieffer proposed a microscopic theory that provides our present theoretical understanding of the nature of superconductivity. They showed that bound electron pairs called Cooper pairs carry the supercurrent, and that there is an energy gap between the normal and superconducting states. The validity of the earlier Ginzburg–Landau theory was not accepted worldwide until Gor'kov showed in 1959 that it is derivable from the BCS theory.

The London equations provided an early simple model for describing experimental results. The Bean model put forward in 1962 lacks theoretical underpinning, but it has been surprisingly successful in describing some magnetic properties of superconductors. There has been a great deal of recent interest in the Hubbard and related models as ways of explaining the essential features of superconductivity from a minimum of assumptions. The present chapter presents some of the results of these models, as well as the results of the more sophisticated theories mentioned earlier. No explanations or justifications of the models and theories will be given, since many books are available to provide this information.

B

London Equations

The 1935 theory of the London brothers provides the first and second London equations, which relate the electric and magnetic fields E and B, respectively, inside a superconductor to the current density J:

$$\mathbf{E} = \mu_0 \lambda_L^2 \frac{d}{dt}\mathbf{J} \tag{1}$$

$$\mathbf{B} = -\mu_0 \lambda_L^2 \mathbf{V} \times \mathbf{J}. \tag{2}$$

The constant of proportionality in these expressions is the London penetration depth λ_L,

$$\lambda_L = (m/\mu_0 n_S e^2)^{1/2}, \tag{3}$$

where n_S is the density of superconducting electrons. These expressions furnish us with the modified Helmholtz equations

$$\mathbf{V}^2\mathbf{B} = \mathbf{B}/\lambda_L^2 \tag{4}$$

$$\mathbf{V}^2\mathbf{J} = \mathbf{J}/\lambda_L^2, \tag{5}$$

which are also satisfied by the vector potential **A**.

C

Ginzburg–Landau Theory

The Ginzburg–Landau (GL, 1950) phenomenological theory provides a good description of many of the properties of both classical and high-temperature superconductors. This theory assumes that in the superconducting state the current is carried by super electrons of mass m^*, charge e^*, and density n^*, where we now know that $m^* = 2m^*$, $e^* = 2e$, and $n_S^* = \frac{1}{2}n_S$ in terms of the free electron values m, e, and n_S, respectively. The order parameter $\phi(\mathbf{r})$ is complex,

$$\phi(\mathbf{r}) = |\phi(\mathbf{r})|e^{i\Theta}, \tag{6}$$

and its square $|\phi|^2$ is identified with the super electron density,

$$n_S^* = |\phi|^2. \tag{7}$$

The parameter ϕ is zero above T_c and increases continuously as the temperature is decreased below T_c, as shown in Fig. 4.1a. Figure 4.1b shows the dependence $\phi(x)$ on the distance x inside the surface of a superconductor.

Below, but close to, T_c the Gibbs free energy per unit volume G_S is expanded in terms of the order parameter and then minimized with respect to ϕ to provide the first GL equation in the London–Landau gauge ($\nabla \cdot \mathbf{A} = 0$):

$$(1/2m^*)[\hbar^2\nabla^2\phi - 2i\hbar e^*\mathbf{A}\cdot\nabla\phi - e^{*2}A^2\phi] - a\phi - b|\phi|^2\phi = 0. \tag{8}$$

Minimization of G_S with respect to the vector potential $\mathbf{A}$ provides the second GL equation:

$$\nabla \times (\nabla \times \mathbf{A}) + \frac{i\hbar e^*}{2m^*}(\phi^*\nabla\phi - \phi\nabla\phi^*) + \frac{e^{*2}}{m^*}\mathbf{A}|\phi|^2 = 0. \tag{9}$$

These two coupled equations determine the properties of the superconducting state.

It is assumed that below but near T_c the parameter a depends linearly on the temperature,

$$a(T) \approx a_o[(T/T_c) - 1], \tag{10}$$

and b is independent of the temperature, where a_o and $b = b_O$ are both positive so $a(T)$ is negative below T_c. Deep inside a superconductor in the absence of a magnetic field, we have the following expression near T_c

$$|\phi|^2 = n_s^* = -a/b = (a_o/b_o)[1 - (T/T_c)], \tag{11}$$

and the overall temperature dependence plotted in Fig. 4.1a. The coherence length ξ, the characteristic length over which ϕ varies in the manner illustrated in Fig. 4.1b, is the first of the two fundamental length scales from the GL theory:

$$\xi^2 = \hbar^2/2m^*|a|. \tag{12}$$

Fig. 4.1.

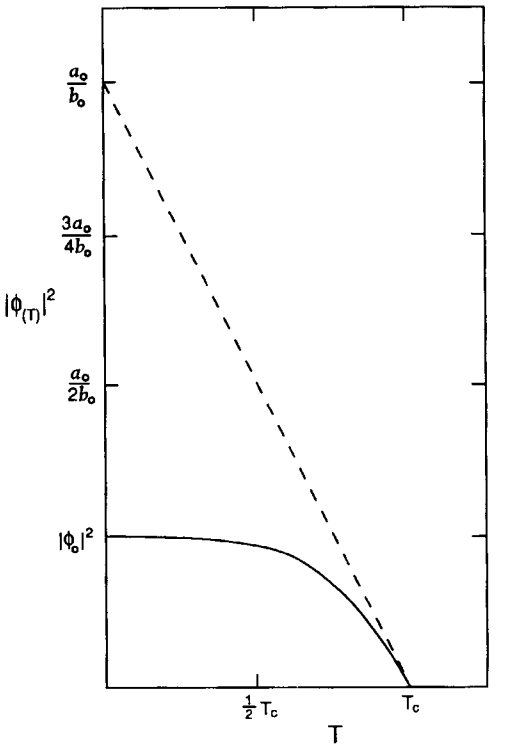

(a) Temperature dependence of the GL order parameter $|\phi|^2$ showing its value $|\phi_o|^2$ at $T = 0$, and the linear behavior (- - -) near T_c that extrapolates to the ordinate value a_o/b_o. This figure was drawn using the assumption $|\phi_o|^2 = \frac{1}{4}a_o/b_o$. [Poole *et al* (1995), p. 123.] (b) Dependence of the GL order parameter $\phi(x)$ on the distance x inside a superconductor. The order parameter is large for $x > \xi$, where ξ is the coherence length. [Poole *et al.* (1995), p. 127.]

The condensation energy of the super electrons, the energy released per unit volume by transforming normal electrons to the superconducting state, is given by

$$E_{\text{cond}} = \tfrac{1}{2}(a^2/b) = B_c^2/2\mu_o. \tag{13}$$

In the presence of an applied magnetic field the line integral of $\mathbf{J}/|\phi|^2$ around a closed path inside the superconductor and the flux Φ enclosed by this path obey the relation

$$(m^*\mu_o/e^*2)\oint (\mathbf{J}/|\phi|^2)\cdot dl + \Phi = n\Phi_o, \tag{14}$$

where n is an integer and the quantum of flux Φ_o has the value

$$\Phi_o = h/e^*. \tag{15}$$

Equation (15) is the quantum condition whereby the sum of the enclosed flux Φ and the line integral of the current density J is quantized.

A parallel magnetic field $B(x)$ and a current density $J(x)$ decay exponentially with the distance x inside the surface of a superconductor in accordance with the expressions

$$B(x) = B_o e^{-x/\lambda} \tag{16a}$$

$$J(x) = J_c e^{-x/\lambda}, \tag{16b}$$

where the London penetration depth λ_L, the second fundamental length scale, is given by

$$\lambda_L^2 = \frac{m^*}{\mu_o e^{*2}|\phi_\infty|^2}, \tag{17}$$

in agreement with Eq. (3).

The ratio $\kappa = \lambda/\xi = 1/\sqrt{2}$ divides superconductors into the two types

$$\kappa \leq 1/\sqrt{2} \quad \text{(Type I)} \tag{18a}$$

$$\kappa \geq 1/\sqrt{2} \quad \text{(Type II)}. \tag{18b}$$

Type II superconductors have lower, thermodynamic, and upper critical fields given by

$$B_{c1} = \frac{\Phi_o \ln \kappa}{4\pi\lambda^2}, \quad B_c = \frac{\Phi_o}{2\sqrt{2}\pi\xi\lambda}, \quad B_{c2} = \frac{\Phi_o}{2\pi\xi^2}, \tag{19}$$

respectively, where $B_{c1}B_{c2} = B_c^2 \ln\kappa$. The Meissner effect is complete for $B_{\text{app}} < B_{c1}$, and as B_{app} is increased above the low critical field B_{c1}, flux penetrates the material in the form of vortices. The magnetization continues to increase until the upper critical field B_{c2} is reached where the vortex cores almost overlap and bulk superconductivity is destroyed. Residual superconductivity may

persist in a thin sheath up to an even higher critical field $B_{c3} = \sqrt{3}B_{c2}$ where the entire sample goes completely normal.

D

Bardeen–Cooper–Schrieffer Theory

In 1957 Bardeen, Cooper, and Schrieffer (BCS) proposed the general microscopic theory of superconductivity that quantitatively predicts many properties of superconductors and is now widely accepted as providing a satisfactory explanation of the phenomenon. There are various levels of approximation in which the BCS theory has been applied, and some of them are commented upon in the next section. The mathematical underpinning of the BCS theory is so complex that it will not be of much benefit to summarize its general formulation, so this section will emphasize predictions that are often compared with experiment. These predictions arise mainly from the homogeneous, isotropic, phonon-mediated, square well, *s*-wave coupling simplification of the BCS theory, and many superconductors, to a greater or lesser extent, have been found to satisfy these predictions. Some of them are as follows:

The isotope effect involves the claim that for a particular element the transition temperature T_c depends on the mass M of the isotope as follows:

$$M^{\alpha}T_c = \text{const.} \tag{20}$$

The weak coupling BCS limit [vide Eqs. (24) to (26)] gives the value $\alpha \approx 1/2$, which has been observed in some superconducting elements, but not in all of them.

A superconductor has an energy gap $E_g = 2\Delta(k)$, which is assumed to be independent of k, and for this assumption the energies in the normal and superconducting states are

$$E(\xi) = \begin{cases} \xi & \text{(normal state)} \\ (\xi^2 + \Delta^2)^{1/2} & \text{(superconducting state)} \end{cases}, \tag{21}$$

where ξ is the energy in the absence of a gap measured relative to the chemical potential μ:

$$\xi = \frac{\hbar^2 k^2}{2m} - \mu. \tag{22}$$

The density of states $D(E)$ given by (with $E = 0$ at the center of the gap)

$$D_s(\mathrm{E}) = \begin{cases} \dfrac{D_n(0)E}{(E^2 - \Delta^2)^{1/2}}, & E > \Delta \\ 0, & -\Delta < E < \Delta \\ \dfrac{-D_n(0)E}{(E^2 - \Delta^2)^{1/2}}, & E < -\Delta \end{cases} \tag{23}$$

is shown plotted in Fig. 2.7, where the normal electron density of states $D_n(E)$ is assumed to have the constant value $D_n(0)$ in the neighborhood of the gap.

Consider a square-well electron–electron potential V_o and an energy gap $\Delta(k)$ that is equal to Δ_o in the neighborhood of the Fermi surface,

$$\Delta(k) = \Delta_o, \quad -\hbar\omega_D \leq \xi(k) \leq \hbar\omega_D, \tag{24}$$

and is zero elsewhere. The Debye frequency ω_D determines the range of ξ because it is assumed that Cooper pair formation is mediated by phonons. The energy gap Δ_o in this approximation is given by

$$\Delta_o = \frac{\hbar\omega_D}{\sinh[1/V_o D_n(0)]}. \tag{25}$$

In the weak coupling (small V_o) limit,

$$V_o D_n(0) \ll 1, \qquad k_B T_c \ll \hbar\omega_D. \tag{26}$$

we obtain the dimensionless ratios

$$\frac{E_g}{k_B T_c} = \frac{2\Delta_o}{k_B T_c} = \frac{2\pi}{e^{\gamma}} = 3.52, \tag{27}$$

where $\gamma = 0.5772\ldots$ is the Euler–Mascheroni constant. This ratio approximates experimental measurements that have been made on many superconductors.

The dimensionless electron–phonon coupling constant λ is related to the phonon density of states $D_{ph}(\omega)$ through the Eliashberg expression:

$$\lambda = 2\int_0^{\infty} \frac{\alpha^2(\omega) D_{ph}(\omega)}{\omega} d\omega. \tag{28}$$

Superconductors are characterized as having weak ($\lambda \ll 1$), intermediate ($\lambda \sim 1$), and strong ($\lambda \gg 1$) coupling. The electron–electron interaction potential V_o for Cooper pair bonding has an attractive electron–phonon part measured by λ and a repulsive screened Coulomb part μ_c^* to give

$$V_o D_n(0) = \lambda - \mu_c^*, \tag{29}$$

and this provides the following approximate expression for the transition temperature:

$$T_c = 1.13\ \theta_D \exp[-1/(\lambda - \mu_c^*)]. \tag{30}$$

A number of related formulas for the dependence of T_c on λ and μ_c^* have appeared in the literature (e.g., McMillan, 1968).

The BCS theory predicts that at T_c there is a jump in the electronic specific heat from its normal state value $C_e = \gamma T$ to its superconducting state value C_s given by

$$\frac{C_s - \gamma T_c}{\gamma T_c} = 1.43. \tag{31}$$

In the free electron approximation the electronic specific heat coefficient γ depends on the Fermi temperature T_F and the gas constant R through the expression

$$\gamma = \pi^2 R/2T_F. \tag{32}$$

Below T_c, the BCS theory predicts that the specific heat $C_s(T)$ depends exponentially on the inverse temperature,

$$C_s(T) = a \exp[-\Delta/k_B T], \tag{33}$$

where $\Delta = 1.76\, k_B T_C$, and a is a constant.

E

Mechanisms for Cooper Pairing

There are three levels of explanation of the nature of superconductivity that are commonly called BCS. One is the general formulation that does not specify particular interactions. The second is the phonon-mediated version of the theory, in which phonons play the role of bringing about the coupling together of two electrons to form Cooper pairs. The third level, which was described in the original formulation of the theory and provided the results summarized in the previous section, further assumes the simplification of an isotropic, homogeneous material with a square-well electron–electron interaction potential involving a phonon coupling mechanism and *s*-wave singlet-state pairing. The superconducting elements, which are almost all Type I, as well as many classical Type II superconductors, are looked upon as phonon-mediated *s*-state types. Pairing mechanisms involving the exchange of particles other than phonons, such as excitons or antiferromagnetic spin fluctuations, have been proposed for nonclassical superconductors. In particular, no consensus exists yet about the pairing mechanism of the cuprates, although *d*-wave pairing seems to be favored (Annett et al., 1996). A handbook is probably not the appropriate forum for elaborating on these matters.

F

Critical State Models

A critical state model postulates that for low applied fields or currents the outer part of the sample is in what is called a critical state, with particular values of current density and magnetic field, and that the interior is shielded from these fields and currents. The magnetic field B and the super current density J are coupled through the Maxwell relation

$$\nabla \times \mathbf{B} = \mu_0 \mathbf{J}, \tag{34}$$

which has the following form in the one-dimensional cases to be discussed here:

$$\frac{d}{dx} B_z(x) = \mu_0 J_y(x), \tag{35}$$

and each model makes an assumption about the magnetic field dependence $J(B)$ consistent with these Maxwell relations. Fields and currents applied simultaneously and then reversed in direction produce modified critical states in the outer parts of the sample. High values of the applied field or currents extend the critical state to fill the entire superconductor. The models do not take into account the existence of a lower critical field B_{c1}, or the difference between the Meissner and the mixed states. They do not explain the nature of superconductivity, but rather provide a convenient description of some experimentally observed phenomena.

Many configurations of $B_z(x)$ and $J_y(x)$ meet requirement (35), and for most models the critical state current density is related to the field by a characteristic equation,

$$J_y(B_z) = J_K / f(B_z), \tag{36}$$

where J_K is independent of the field and is generally the critical current J_c. The characteristic equations of nine critical state models are provided elsewhere (Poole *et al*, 1995). By far the most widely used of these models is the Bean model (Bean, 1962, 1964), which has the simplest characteristic equation:

$$J(B) = J_c. \tag{37}$$

The Kim model (Kim *et al*, 1962, 1963) has also been used occasionally, and it makes the assumption

$$J(B) = \frac{J_c}{1 + |B(x)|/B_K}. \tag{38}$$

Perhaps the most important application of the Bean model is the determination of the critical current density J_c from magnetic hysteresis loops.

G

Bean Model

The Bean model assumes that the current density can only take on the values $\pm J_c$ or 0. A sample of thickness $2a$ has a characteristic field B^*,

$$B^* = \mu_o J_c a, \tag{39}$$

and when the applied field B_o attains this value B^*, the fields and currents reach the center of the sample. We shall examine the one-dimensional case (35) for applied fields below and above B^*.

For low applied fields, $B_o < B^*$, the internal fields and currents only exist near the surface, with a field and current-free region ($-a' < x < a'$) near the center, and the current density given by, from Eq. (37),

$$\begin{aligned} J_y(x) &= J_c, \qquad -a \le x \le -a' \\ J_y(x) &= 0, \qquad -a' \le x \le a' \\ J_y(x) &= -J_c, \qquad a' \le x \le a. \end{aligned} \tag{40}$$

Equation (35) requires that $B_z(x)$ depend linearly on x in the regions where $J_y = \pm J_c$, so we have for the internal magnetic fields

$$\begin{aligned} B_z(x) &= B_o\left[\frac{a'+x}{a'-a}\right], \qquad -a \le x \le -a' \\ B_z(x) &= 0, \qquad -a' \le x \le a' \\ B_z(x) &= B_o\left[\frac{x-a'}{a-a'}\right], \qquad a' \le x \le a. \end{aligned} \tag{41}$$

These formulas match the boundary condition $B_z(0) = B_o$ at the surfaces $x = \pm a$, with the magnitudes of J_c and B_o related by the expression obtained from Eq. (35)

$$J_c = \frac{B_o}{\mu_o(a-a')}. \tag{42}$$

These expressions for $B_z(x)$ and $J_y(x)$ are plotted in Fig 4.2a for a finite value of a′, and in Fig. 4.2b for the case where $B_o = B^*$ and $a' = 0$.

For high applied fields, $B_o > B^*$, the currents and internal fields are present throughout the sample and are given by the expressions

$$\begin{aligned} J_y(x) &= J_c, \qquad -a \le x \le 0 \\ J_y(x) &= -J_c, \qquad 0 \le x \le a \end{aligned} \tag{43}$$

$$\begin{aligned} B_z(x) &= B_o - B^*\left[\frac{a+x}{a}\right], \qquad -a \le x \le 0 \\ B_z(x) &= B_o + B^*\left[\frac{x-a}{a}\right], \qquad 0 \le x \le a. \end{aligned} \tag{44}$$

Fig. 4.2.

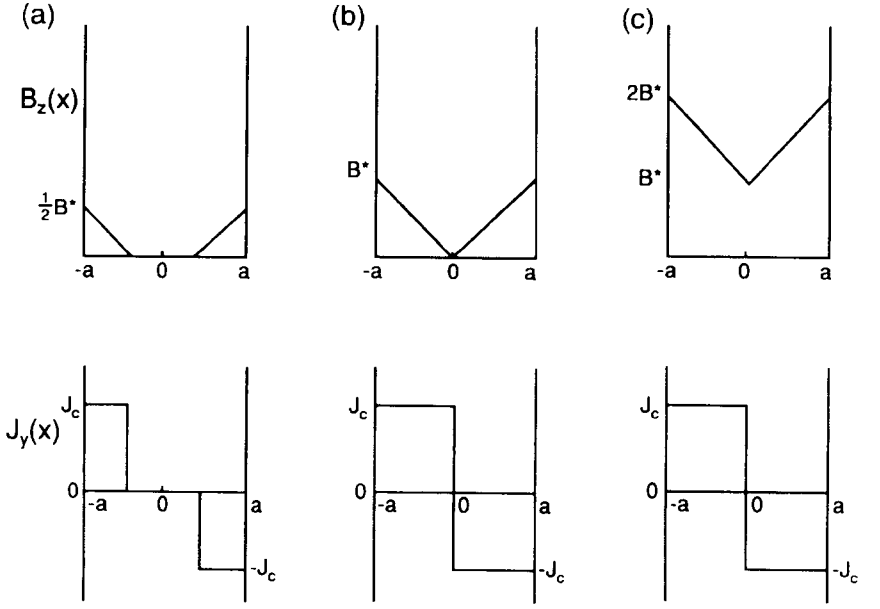

Manner in which the internal magnetic field $B_z(x)$ and the current density $J_y(x)$ depend on the strength of the applied magnetic field B_0 for normalized applied fields given by (a) $B_0/\mu_0 J_c a = 1/2$, (b) $B_0/\mu_0 J_c a = 1$, and (c) $B_0/\mu_0 J_0 a = 2$ for the Bean model. There is a field-free region in the center for case (a) and case (b) is the boundary between having and not having such a region. [Poole *et al.* (1995), p. 373.]

Figure 4.2 shows how the internal field and current density vary with the ratio B_0/B^* (a) for low fields $B_0 < B^*$, (b) for the maximum penetration field $B_c = B^*$, and (c) for high fields $B_0 > B^*$ We can see from the figure that $B_z(x)$ is symmetric about the $x = 0$ point, and $J_y(x)$ is antisymmetric about this point.

If the applied field is zero but the transport current

$$I = 2(a - a')LJ_c \tag{45}$$

is flowing through a wire with a rectangular cross-section of width L much greater than its thickness $2a$, then the internal magnetic field and current density will be as shown in Fig. 4.3a, which is drawn for the case $I = \frac{1}{2}I_c$, where I_c is the critical current:

$$I_c = 2aLJ_c. \tag{46}$$

Figure 4.3b is drawn for the limiting case $I = I_c$, and higher applied transport currents drive the wire normal. The equations for J_y and B_z of the transport current case of Fig. 4.3a are the same as Eqs. (40) and (41), respectively, for the applied field case of Fig. 4.2a, except for some changes in sign, as may be seen by

Fig. 4.3.

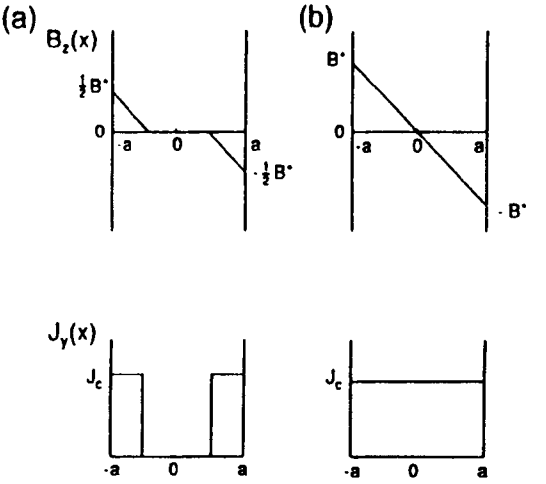

Dependence of the internal magnetic field $B_z(x)$ and the current density $J_y(x)$ on the strength of an applied transport current for the Bean model. Figures are drawn for applied currents I which are (a) less than the critical current $I_c = 2aLJ_c$, and (b) equal to I_c. Higher currents cause the wire to go normal. This figure should be compared to Fig. 4.2. [Poole *et al.* (1995), p. 375.]

comparing the figures. When an applied field and an (applied) transport current are present simultaneously, the situation is more complicated, and Fig. 12-12 of our 1995 book gives an example of this situation.

The critical states of the Bean model can be complicated when fields exceeding B^* are applied and then reversed in direction, as illustrated by Fig. 12-15 of the aforementioned 1995 work. This model provides simple explanations of flux shielding whereby the average field $\langle B_{in} \rangle$ inside the superconductor is lower in magnitude than the applied field B_{app}, and of flux trapping whereby $\langle B_{in} \rangle$ exceeds B_{app}. These two cases are associated with current flow in opposite directions around the material.

H

Reversed Critical States and Hysteresis

Probably the most important application of the Bean model is its use to estimate the magnetization of a sample in a high applied field, $B_{app} > B^*$, and Fig. 4.4 shows typical hysteresis loops for low, medium, and high applied fields. Explicit expressions for the average internal field $\langle B \rangle$ and the magnetization $\mu_0 M$ are

Fig. 4.4.

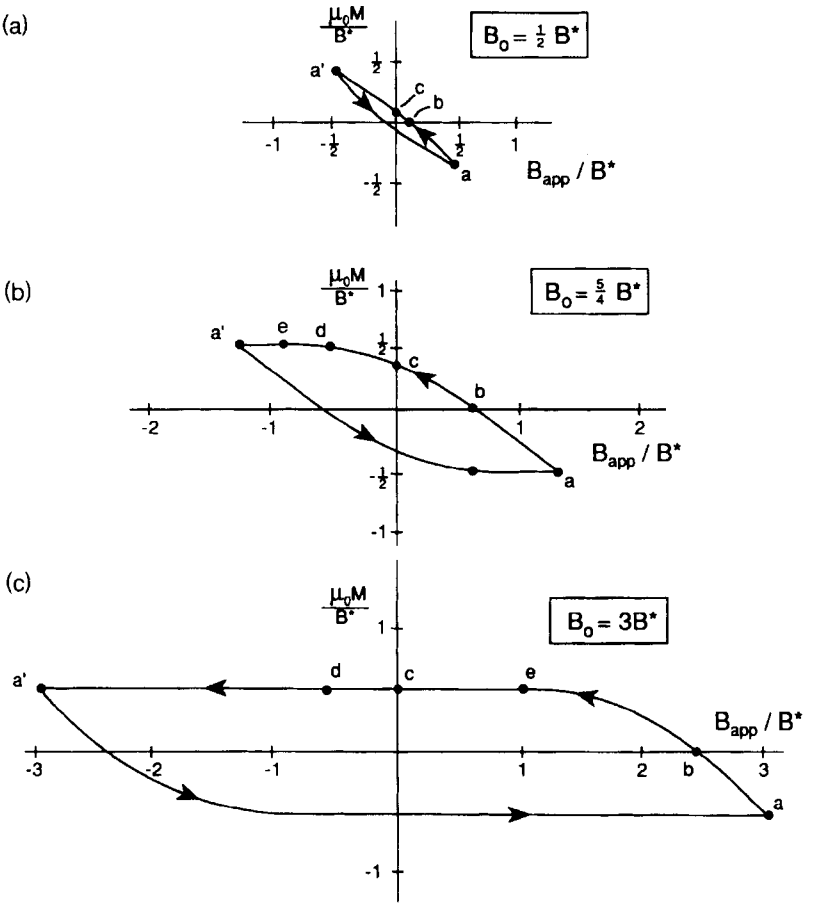

Hysteresis loops of magnetization $\mu_0 M$ vs the applied magnetic field B_{app} cycled over the range $-B_0 \leq B_{app} \leq B_0$ for the three cases (a) $B_0 = \frac{1}{2}B^*$, (b) $B_0 = (5/4)B^*$, and (c) $B_0 = 3B^*$. [Poole *et al.* (1995), p. 388.]

given in Table 12-2 of our earlier work (1995) for the special points a, b, c, d, and e of these loops. A high field hystereisis loop ($B_0 > B^*$) furnishes the difference

$$M_+ - M_- = J_c a \tag{47}$$

between the upper and lower magnetization plateaus of Fig. 4.4c, where

$$\begin{aligned} \mu_o M_+ &= \tfrac{1}{2} B^* \\ \mu_0 M_- &= -\tfrac{1}{2} B^*, \end{aligned} \tag{48}$$

as indicated in the figure. This gives the critical current in terms of the measured magnetization through the high-field Bean model formula

$$J_c = 2(M_+ - M_-)/d = 1.59 \times 10^6 \mu_0 \Delta M/d \quad (\mathrm{A/m^2}), \tag{49}$$

where current is measured in amperes, $\mu_0 \Delta M = \mu_0(M_+ - M_-)$ is in tesla, and d is the diameter of the sample grains in meters. If CGS units are used Eq. (49) becomes

$$J_c = 30(M_+ - M_-)/d \quad (\mathrm{A/cm^2}), \tag{50}$$

where d is now in centimeters.

I Hubbard Models and Band Structure

This section provides background information that is important for Hubbard-type models (Lynn, 1990) and band structure calculations.

The electronic configurations of several atoms that occur commonly in high-temperature superconductors are given in Table 4.1. The notation used is nl^N, where n is the principal quantum number, the orbital quantum number $l = 0$ for an s state, $l = 1$ for a p state, $l = 2$ for a d state, and N is the number of electrons in each l-state. A full l-state contains $2(2l + 1)$ electrons, corresponding to 2, 6, and 10 for s, p, and d states, respectively. The Cu^{2+} ion ($3d^9$) may be looked upon as a filled d-shell ($3d^{10}$) plus one $3d$ hole, and in the cuprates this hole is a $d_{x^2-y^2}$ orbital in the CuO_2 plane.

The various s, p, and d wavefunctions called orbitals have the unnormalized analytical forms given in Table 4.2, and the spacial electronic charge distribution of the d orbitals is sketched in Fig. 4.5, the sign on each lobe being the sign of the wavefunction. Figure 4.6 shows the sigma (σ) bonding between oxygen p_x and p_y orbitals and copper $d_{x^2-y^2}$ orbitals in a cuprate CuO_2 plane.

The orbitals $\phi(r - R)$ used in band structure calculations are normalized

$$\int \phi^*(r - R)\phi(r - R)d^3r \tag{51}$$

for an atom located at position R. The overlap integral $\beta(R - R')$

$$\beta(R - R') = \int \phi^*(r - R)\phi(r - R')d^3r \tag{52}$$

is a measure of the extent to which the orbitals of atoms at positions R and R' overlap. The Coulomb integral $U(R)$,

$$U(R) = \int \phi^*(r - R)V_c(R)\phi(r - R)d^3r, \tag{53}$$

provides the Coulomb repulsion energy associated with orbital $\phi(r - R)$ on an atom at position R.

Table 4.I

Electron configurations of selected atoms commonly used for band structure calculations of superconductors[a] [Poole *et al.* (1995), p. 218]

Atom number	Symbol	Core[b,c]	Atom configuration	No. valence electrons	Ion	Ion configuration	No. electrons
8	O	Be 4	$[2s^2]2p^4$	4	O^{1-}	$2p^5$	5
					O^{2-}	$2p^6$	6
14	Si	Ne 10	$3s^23p^2$	4	Si^{4+}	—	0
19	K	Ar 18	$[3p^6]4s$	1	K^+	—	0
20	Ca	Ar 18	$4s^2$	2	Ca^{2+}	—	0
23	V	Ar 18	$3d^34s^14p^1$	5	V^{3+}	$3d^2$	2
29	Cu	Ar 18	$3d^{10}4s^1$	11	Cu^{1+}	$3d^{10}$	10
					Cu^{2+}	$3d^9$	9
					Cu^{3+}	$3d^8$	8
38	Sr	Kr 36	$5s^2$	2	Sr^{2+}	—	0
39	Y	Kr 36	$4d^15s^2$	3	Y^{3+}	—	0
41	Nb	Kr 36	$4d^35s^15p^1$	5	Nb^{4+}	$4d^1$	1
50	Sn	–46	$5s^25p^2$	4	Sn^{4+}	—	0
56	Ba	Xe 54	$[5p^6]6s^2$	2	Ba^{2+}	—	0
57	La	Xe 54	$5d^16s^2$	3	La^{3+}	—	0
80	Hg	–78	$[5d^{10}]6s^2$	2	Hg^{2+}	$[5d^{10}]$	0
81	Tl	–78	$[5d^{10}[6s^2p^1$	3	Tl^{3+}	$[5d^{10}]$	0
82	Pb	–78	$[5d^{10}]6s^26p^2$	4	Pb^{4+}	$[5d^{10}]$	0
83	Bi	–78	$[5d^{10}]6s^26p^3$	5	Bi^{3+}	$[5d^{10}]6s^2$	2
					Bi^{4+}	$[5d^{10}]6s^1$	1
					Bi^{5+}	$[5d^{10}]$	0

[a]Core electrons listed in square brackets are sometimes included in the basis set.
[b]The core of Sn is Kr plus the fourth transition series ($4d^{10}$) closed shell.
[c]The core of Tl, Pb, and Bi is Xe plus the rare earth ($4f^{14}$) and fifth transition series ($5d^{10}$) closed shells.

The simplest model of correlated electrons is the one-state Hubbard model which, despite its simplicity, exhibits many properties characteristic of superconductors. The Hamiltonian written in terms of creation ($a_\sigma^\dagger$) and annihilation (a_σ) operators of spin σ associated with atoms at positions R' and R has the form

$$H = -t \sum_{R,R',\sigma} [a_\sigma^\dagger(R)a_\sigma(R') + a_\sigma^\dagger(R')a_\sigma(R)] - \mu \sum_{R,\sigma} a_\sigma^\dagger(R)a_\sigma(R) + U \sum_R n_+(R)n_-(R), \tag{54}$$

where the Coulomb repulsion term $U > 0$ is defined by Eq. (53), and the hopping amplitude $t > 0$ is a measure of the contribution from an electron hopping from one site to another. The chemical potential μ takes into account changes in the number of electrons and is zero if there is no doping. The hopping amplitude t may also be written in the form of an integral. This Hamiltonian exhibits an electron–hole symmetry, which is of some importance because most high-temperature superconductors are hole types with a close to half-full band.

Table 4.2

Unnormalized analytical expressions in Cartesian and polar coordinates for the *s*, *p*, and *d* orbitals[a] [C. P. Poole *et al.* (1995), p.219]

Orbital	Cartesian form	Polar form
s	1	1
p_x	$\frac{x}{r}$	$\sin\Theta\cos\phi$
p_y	$\frac{y}{r}$	$\sin\Theta\sin\phi$
p_z	$\frac{z}{r}$	$\cos\Theta$
d_{xy}	$\frac{xy}{r^2}$	$\sin^2\Theta\sin\phi\cos\phi$
d_{yz}	$\frac{yz}{r^2}$	$\sin\Theta\cos\Theta\sin\phi$
d_{zx}	$\frac{zx}{r^2}$	$\sin\Theta\cos\Theta\cos\phi$
$d_{x^2-y^2}$	$\frac{x^2-y^2}{r^2}$	$\sin^2\Theta(\cos^2\phi-\sin^2\phi)$
d_{z^2}	$\frac{3z^2-r^2}{r^2}$	$3\cos^2\Theta-1$

[a] $l = 0$, 1, and 2, respectively.

Fig. 4.5.

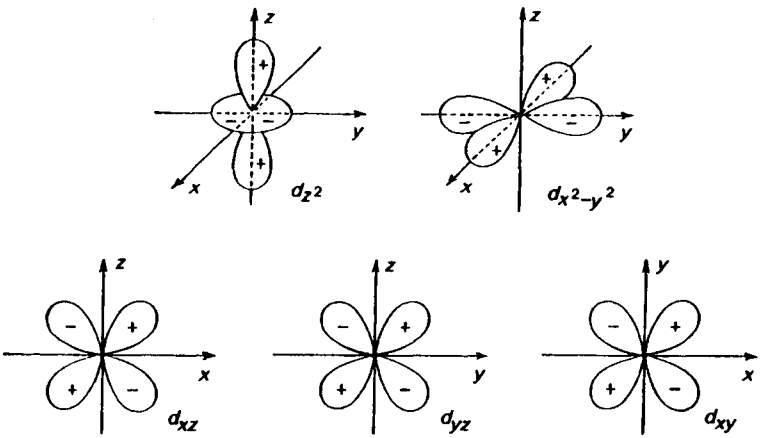

Spatial distribution of electron density for the five *d*-orbitals. The signs (±) on the lobes are for the wavefunction; the sign of the electric charge is the same for each lobe of a particular orbital. [Ballhausen (1962).]

Fig. 4.6.

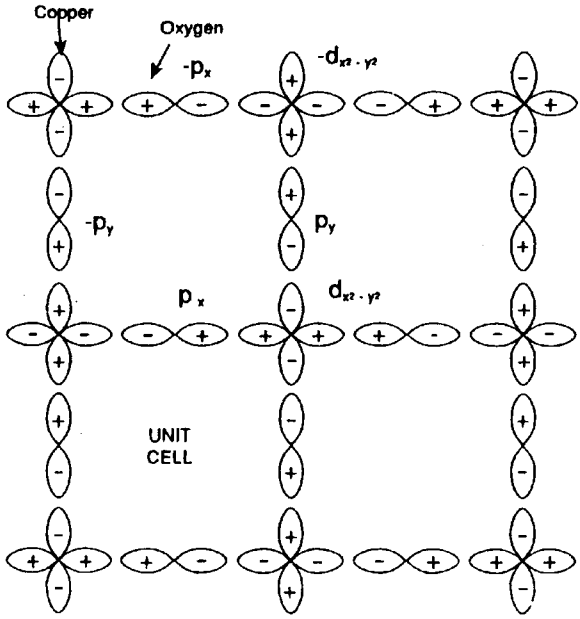

Orbitals used for the three-state model of Cu–O planes. Each copper contributes a $d_{x^2-y^2}$ orbital, and each oxygen contributes either a p_x or a p_y orbital, as shown. The unit cell contains one of each type of ion, and hence one of each type of orbital. The figure shows four unit cells. [Poole *et al.* (1995), p. 230.]

References

J. F. Annett, N. Goldenfeld and A. J. Leggett, *Physical Properties of High Temperature Superconductors*, Vol. 5, D. M. Ginsberg, Ed., World Scientific, Singapore, 1996.

C. J. Ballhausen, *Introduction to Ligand Field Theory*, McGraw-Hill, New York, 1962.

J. Bardeen, L. N. Cooper, and J. R. Schrieffer, *Phys. Rev.* **108**, 1175 (1957).

C. P. Bean, *Phys. Rev. Lett.* **8**, 250 (1962); *Rev. Mod. Phys.* **36**, 31 (1964).

H. Fröhlich, *Phys. Rev.* **79**, 845 (1950).

V. L. Ginzburg and L. Landau, *Zh. Eksp. Teor. Fiz.* **20**, 1064 (1950).

L. P. Gor'kov, *Zh. Eksp. Teor. Fiz*, **36**, 1918 (1959); *Sov. Phys. JETP* **36** 1364 (1959).

Y. B. Kim, C. F. Hempstead, and A. R. Strand, *Phys. Rev. Lett.* **9**, 306 (1962); *Phys. Rev.* **129**, 528 (1963).

F. London and H. London, *Proc. Roy. Soc (London)* **A141**, 71 (1935).

J. W. Lynn, Ed., *High Temperature Superconductivity*, Springer-Verlag, Berlin, (1990); several chapters discuss Hubbard models.

E. Maxwell, *Phys. Rev.* **78**, 477 (1950).

W. L. McMillan, *Phys. Rev.* **167**, 331 (1968).

W. Meissner and R. Ochsenfeld, *Naturwissen.* **21**, 787 (1933).

H. Kamerlingh Onnes, Leiden Comm., *120b, 122b, 124c*, (1911).

C. P. Poole, Jr., H. A. Farach, and R. J. Creswick, M *Superconductivity*, Academic Press, New York, 1995.

C. A. Reynolds, B. Serin, W. H. Wright, and L. B. Nesbitt, *Phys. Rev.* **78**, 487 (1950).

This Page Intentionally Left Blank

Chapter 5

Superconductor Types

Charles P. Poole, Jr.
Department of Physics and Institute of Superconductivity, University of South Carolina, Columbia, South Carolina

Paul C. Canfield
Department of Physics and Ames Laboratory, Iowa State University, Ames, Iowa

Arthur P. Ramirez
Lucent Technologies, Bell Laboratories, Murray Hill, New Jersey

ISBN: 0-12-561460-8
$30.00

HANDBOOK OF SUPERCONDUCTIVITY

A

Introduction

Until the early 1980s, superconductivity studies were carried out with what are called classical materials, consisting of elements, alloys, and compounds. Some categories of compounds produced many superconductors, such as those with the sodium chloride structure, Laves phases, Chevrel types, and A-15 compounds. In addition, there are superconducting materials without isomorphous counterparts. During the few years preceding the advent of superconductivity above 77 K, the heavy electron and organic superconductors had been discovered and were widely investigated. During this same period some work was carried out with noncubic perovskites, precursors for the cuprates, and more recently superconductivity has been found in cubic barium–potassium–bismuth perovskite. Two other compound types, borocarbides and especially fullerenes, have been extensively investigated in recent years.

The present chapter comments on and provides 39 tabulations, summarized in Table 5.1, with systematic listings of T_c values for the main classes of superconducting materials, and the next chapter discusses their structures. The tabulated T_c values were obtained, in almost all cases, from the data furnished by Vonsovsky *et al.* (1982), Phillips (1989), and Chapter 6 of the present Handbook. In some cases these sources quoted somewhat different values of T_c, and when this was the case either one specified value or an average was selected for inclusion here. Our earlier work (Poole *et al.*, 1995) may be consulted for more details. Landolt–Bornstein is the most comprehensive source of T_c values, but their tabulations are not yet completed. The main object in presenting T_c values in the present tabular form that had been adapted in our initial publication of the data (Poole and Farach, 1999) is to make it easy to look them up in a context in which they can be compared with values of related compounds.

B

Elements and Alloys

Superconductivity was discovered in 1911 when the element mercury exhibited zero resistance at $T_c = 4.1$ K, and it has been subsequently found in many elements, alloys and compounds. Figure 5.1 shows how superconducting elements cluster in two regions of the periodic table, with the transition metals on the left and the nontransition metals on the right. Some elements become superconducting only as thin films, under pressure, or after irradiation, as indicated. This figure gives the transition temperature T_c, the Debye temperature θ_D, the electronic specific heat constant γ, the dimensionless electron–phonon coupling constant λ, and the density of states at the Fermi level $D(E_F)$ for the

Table 5.I.

Summary of characteristics of compounds in the transition temperature tables.

Table no.	Compound	Strukturbericht	Compound type	Pearson code	Structure
5.3a	A		Transition elements	—	—
5.3b	A		Nontransition elements	—	—
5.4	AB	B1	NaCl, rock salt	cF8	$Fm\bar{3}m$
5.5	AB	B2	CsCl	cP2	$Pm\bar{3}m$
5.6	AB	$B8_1$	NiAs, nickeline	hP4	$P6_3/mmc$
5.7	AB	B14	FeAs (MnP), westerveldite	oP8	Pnma
5.8	AB	$D8_b$	CrFe, σ phase	tP30	$P4_2/mnm$
5.9	AB		Miscellaneous AB types	—	—
5.10	AB_2	C14	$MgZn_2$, hexagonal Laves phase	hP12	$P6_3/mmc$
		C15	$MgCu_2$, cubic Laves phase	cF24	$Fd\bar{3}m$
5.11	AB_2	C16	$CuAl_2$	tI12	I4/mcm
5.12	AB_2	C1	CaF_2, fluorite	cF12	$Fm\bar{3}m$
5.13	AB_2		Miscellaneous AB_2 types	—	—
5.14	AB_3	A15	Cr_3Si, A15 compound	cP8	$Pm\bar{3}n$
5.15	AB_3	$L1_2$	Cu_3Au	cP4	$Pm\bar{3}m$
5.16	AB_3	A12	αMn	cI58	$I\bar{4}3m$
5.17	AB_3		Miscellaneous AB_3 types	—	—
5.18	AB_n		Miscellaneous AB_n types for $n > 3$	—	—
5.19	A_3B_7	$D10_2$	Fe_3Th_7	hP20	
5.20	A_mB_n		Miscellaneous A_mB_n types for $m, n > 2$	—	—
5.21	ACX		GdCBr	mS12	C2/m
5.22	APd_2X	$L2_1$	$MnCu_2Al$, Heusler	cf16	$Fm\bar{3}m$
5.23	AXB_2		$LuRuB_2$	oP16	Pnma
5.24	$A(X_3B_2)$		$CeCo_3B_2$	hP6	P6/mmm
5.25	AX_4B_4		$CeCo_4B_4$	tP18	$P4_2/nmc$
			$LuRu_4B_4$	tI72	
			$LuRh_4B_4$	oS108	Ccca
5.26	AX_4P_{12}		$LaFe_4P_{12}$, skutterudite	cI34	$Im\bar{3}$
5.27	AMo_6X_8		$PbMo_6S_8$, Chevrel	hR45	$R\bar{3}$
	AMo_6X_6		$Tl_2Fe_6Te_6$, Chevrel	hP14	$P6_3/m$
5.28	$A_2B_3Si_5$		$U_2Mn_3Si_5$	tP40	P4/mnc
			$U_2Co_3Si_5$	oI40	Ibam
5.29	$A_3X_4Y_{13}$		$Yb_3Rh_4Sn_{13}$	cP40	$Pm\bar{3}n$
5.30	$A_4B_5X_{10}$		$Sc_5Co_4Si_{10}$	tP38	P4/mbm
5.31	$A_4X_6Sn_{19}$		$Tb_4Rh_6Sn_{19}$	cF116	$Fm\bar{3}m$
			$Er_4Rh_6Sn_{19}$	tI232	$I4_1/acd$
5.32	$A_nMo_{15}Se_{19}$		α-$Mo_{15}Se_{19}$	hP68	$P6_3/m$
			β-$Mo_{15}Se_{19}$	hR204	R3c
5.33	$A_mB_nC_p$		Miscellaneous $A_mB_nC_p$ types for $m, n, p > 1$, and $A_mB_nC_pD_q$ types	—	—
5.34	AB		Magnet material alloys	—	—
	$A(B_xC_{1-x})O_3$	$E2_1$	Cr_3AsN, tetragonal perovskite	tI20	I4/mcm

(*continued*)

Table 5.1. (*continued*)

Table no.	Compound	Strukturbericht	Compound type	Pearson code	Structure
			$CaTiO_3$, cubic perovskite	cP5	$Pm\bar{3}m$
	AB_2X_4	$H1_1$	$MgAl_2O_4$, spinel	cF56	$Fd\bar{3}m$
5.35	—		Heavy electron compounds	—	—
5.36	AX_2B_2C		$LuNi_2B_2C$, borocarbide	tI12	I4/mmm
5.37	AX_2B_2C		$LuNi_2B_2C$, borocarbide	tI12	I4/mmm
5.38	$A_nB_{3-n}C_{60}$		K_3C_{60}, fullerene	cF252	$Fm\bar{3}m$
5.39	$A_nB_{3-n}C_{60}$		K_3C_{60}, fullerene	cF252	$Fm\bar{3}m$
5.40	$A_nB_{3-n}C_{60}$		K_3C_{60}, fullerene	cF252	$Fm\bar{3}m$

superconducting elements, and Table 5.2 lists these and many other properties. Included in the table are the energy gap ratio $E_g/k_BT_c = 2\Delta/k_BT_c$ which has the value 3.52 in the BCS theory, and the isotope effect exponent α from the expression

$$M^{\alpha}T_c = \text{constant} \tag{1}$$

for different isotopic masses M of the same element, where $\alpha = \frac{1}{2}$ for the simplified phonon BCS theory.

Fig. 5.1.

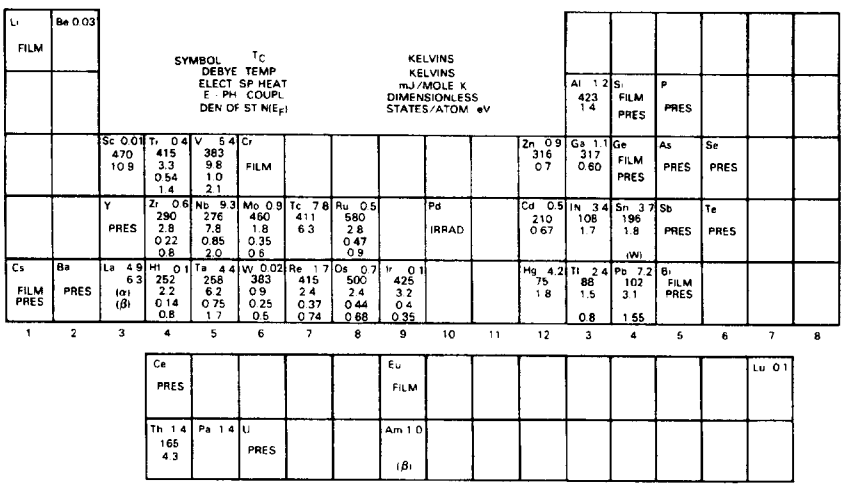

Periodic table showing the superconducting elements, their transition temperatures T_c, and some of their properties. Valence electron values $N_e = 1, 2, 3, \ldots 12, 3, 4, \ldots 8$ of elements in columns are listed at the bottom of the main body of the table [Poole *et al.* (1988) p. 62.]

Table 5.2.

Properties of the superconducting elements (Poole *et al.* 1995 p. 60)

Element	N_e	Crystal Structure	T_c (K)	Θ_D (K)	B_c (mT)	$2B_c/T_c$ (mT/K)	γ $\left(\frac{\text{mJ}}{\text{mol K}^2}\right)$	$\chi \times 10^6$ (cm^3/mol)	λ	μ_c^*	dT_c/dP (K/GPa)	P (GPa)	α	WF (eV)	$E_g = 2\Delta$ (meV)	E_g/kT_c	$D(E_F)$ (states, atom eV)	Z
Be	2	hcp	0.026	940			0.21							5.0				4
Al	3	fcc	1.18	420	10.5	18	1.4							4.3	0.35	3.4		13
Sc	3	hcp	0.5	470			10.9							5.9				21
Ti	4	hcp	0.40	415	5.6		3.3	155	0.38	0.17	0.6	0–1.4		4.33			≈ 1.4	22
V	5	bcc	5.40	383	141.0	52	9.82	300	0.60	0.17	6.3	0–2.5		4.3	1.6	3.4	≈ 2.1	23
Zn	12	hcp	0.85	316	5.4	12	0.66						0.45	4.3	0.26	3.2		30
Ga	3	orthr	1.08	325	5.83	11	0.60							4.0	0.33	3.5		31
Zr	4	hcp	0.61	290	4.7	15	2.77	129	0.41	0.15	15.0	0–2.0	0	4.05			≈ 0.8	40
Nb	5	bcc	9.25	276	206.0	45	7.80	212	0.82	0.15	−2.0	0–2.5		4.3	3.0	3.8	≈ 2.1	41
Mo	6	bcc	0.92	460	9.6	21	1.83	89	0.41	0.10	−1.4	0–2.5	0.37	4.6	0.26	3.4	0.65	42
Tc	7	hcp	7.9	411	141.0	36	6.28	270			−12.5	0–1.5		5.0	2.4	3.6		43
Ru	8	hcp	0.49	580	6.9	28	2.8	39	0.38	0.14	−2.3	0–1.8	0	4.7	0.15	3.5	0.91	44
Cd	12	hcp	0.517	210	2.8	11	0.69						0.5	4.2	0.14	3.2		48
In	3	tetrg	3.41	108	28.2	17	1.67							3.8	1.05	3.6		49
Sn(w)	4	tetrg	3.72	195	30.5	16	1.78						0.47	4.38	1.2	4.4		50
La(α)	3	hcp	4.9	152	80.0	33	9.8				190	0–2.3			1.5	3.5		57
La(β)	3	fcc	6.1	140	110.0	37	11.3				110				1.5			57

(*continued*)

Table 5.2. (*continued*)

Element	N_e	Crystal Structure	T_c (K)	Θ_D (K)	B_c (mT)	$2B_c/T_c$ (mT/K)	γ $\left(\frac{\text{mJ}}{\text{mol K}^2}\right)$	$\chi \times 10^6$ (cm^3/mol)	λ	μ_c^*	dT_c/dP (K/GPa)	P (GPa)	α	WF (eV)	$E_g = 2\Delta$ (meV)	E_g/kT_c	$D(E_F)$ (states, atom eV)	Z
Lu	3	hcp	1.0		<35.0										0.028	3.3		71
Hf	4	hcp	0.13	252	1.27	20	2.2	70	0.14		−2.6	0–1.0			0.044	3.9	0.83	72
Ta	5	bcc	4.47	258	82.9	37	6.15	162	0.75		−2.6				1.4	≈3.5	≈1.7	73
W	6	bcc	1.5	383	0.12	16	0.90	53	0.25					4.5	≈0.006	≈4.5	≈0.5	74
Re	7	hcp	1.70	415	20.0	24	2.35	68	0.37	0.10	−2.3	0–1.8	0.23		0.78	3.4	0.76	75
Os	8	hcp	0.66	500	7.0	21	2.35	13	0.44	0.12	−1.8		0.20		0.29	4.8	0.70	76
Ir	9	fcc	0.11	425	1.6	29	3.2	24	0.35						0.048	5.6		77
Hg(α)	12	trig	4.15	88	41.1	20	1.81						0.50	4.52	1.7	4.6		80
Hg(β)	12	tetrg	3.9	93	33.9	17	1.37											80
Tl	3	hcp	2.38	79	17.8	15	1.47		0.80				0.50	3.7	0.79	3.8		81
Pb	4	fcc	7.20	96	80.3	22	3.1		1.55				0.48	4.3	2.7	4.3		82
Th	4	fcc	1.38	165	16.0	23	4.32								0.41	3.4		90
Pa	5		1.4															91
Am	9	fcc	1.0															95

N_e is as defined in the text; Θ_D, Debye temperature; B_c, critical field; γ, electronic specific heat parameter; χ, susceptibility; λ, electron–phonon coupling constant; μ_c^*, Coulomb pseudopotential; P, pressure; WF, work function; 2Δ, energy gap; and $D(E_F)$, density of states at the Fermi level.

Most of the data in the table come from Roberts (1976), Vonsovsky *et al.* (1982), and *Handbook of Chemistry and Physics*, 70th edition (1989–1990).

Sn is the gray diamond structure form below 13.2°C, and the white tetragonal ω form above; La is the fcc β form above 310°C, and the hcp α form at lower temperatures.

The transition temperature for each transition series reaches a maximum for elements with 5 and 7 valence electrons N_e, as shown in Table 5.3a. Solid solutions of adjacent transition elements qualitatively exhibit the same dependence of T_c on N_e as the elements, with maxima in T_c near $N_e = 4.7$ and 6.7, as indicated in Fig. 5.2. Other properties such as the electronic specific heat factor γ, the magnetic susceptibility χ, the electron–phonon coupling constant λ, and the

Table 5.3a.

Elements of the three transition series. The element that superconducts as a thin film (fl) is so indicated.

$N_e \Rightarrow$	3	4	5	6	7	8	9
structure $\Rightarrow$	hcp	hcp	bcc	bcc	hcp	hcp	fcc
First series							
Element	Sc	Ti	V	Cr	Mn		
T_c	0.5	0.4	5.4	fl	0.04		
Pearson code	hP2	hP2	cI2				
Second series							
Element	Y	Zr	Nb	Mo	Tc	Ru	
T_c	2.5	0.61	**9.25**	0.92	**7.9**	0.49	
Pearson code	hP2	hP2	cI2	cI2	hP2	hP2	
Third series							
Element	La	Hf	Ta	W	Re	Os	Ir
T_c	4.9/6.1	0.13	**4.47**	1.5	**1.7**	0.66	0.11
Pearson code	hP4/cF4	hP2	cI2	cI2	hP2	hP2	cF4

Fig. 5.2.

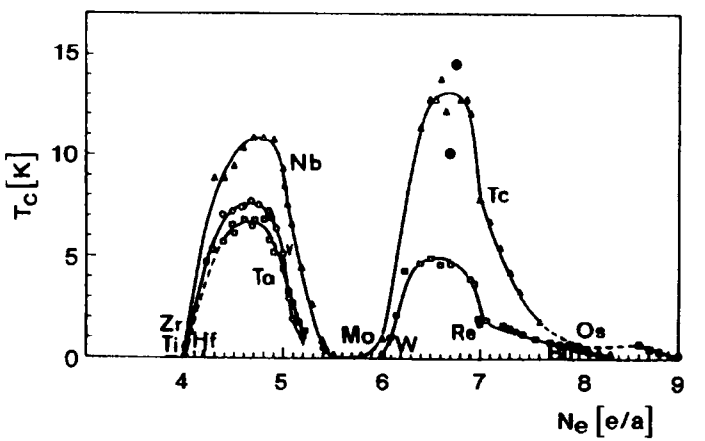

Dependence of the transition temperature on the number of valence electrons N_e in solid solutions of adjacent 3*d* (○), 4*d* (△), and 5*d* (□) elements on the periodic table. Darkened symbols are for pure elements. [Vonsovsky *et al.* (1982), p. 239.]

inverse Debye temperature exhibit similar correlations with N_e. Table 5.3b shows T_c of nontransition elements in the format of Table 5.3a. We use the same values of N_e for the elements that were employed by Phillips (1989).

Miedema (1973, 1974) noted that some physical properties of AB alloys such as the density of states $D(E_F)_{AB} = D_{AB}$ at the Fermi level sometimes depend linearly on the mole fractions f_i of the constituents,

$$D_{AB} = f_A D_A(N_e^A) + f_B D_B(N_e^B), \tag{2}$$

where the individual densities of states D_A and D_B depend on the number of valence electrons N_e^A and N_e^B on atoms A and B, respectively. The properties T_c, γ, λ, and θ_D^{-1} mentioned earlier often approximate expressions similar to Eq. (2).

Table 5.3b.

Some non transition series elements. Elements that superconduct only at high pressure (pr) or as thin films (fl) are so indicated.[a]

$N_e \Rightarrow$	2	3	4	5	6
Second row					
Element		Al	Si	P	
T_c		1.2	fl/pr	pr	
Pearson code		cF4	tI4	oS8	
Third row					
Element	Zn	Ga	Ge	As	Se
T_c	0.9	1.1/6.2	fl/pr	pr	pr
Pearson code	hP2	oS8/mS4	tI4		
Fourth row					
Element	Cd	In	Sn	Sb	Te
T_c	0.5	3.4	**3.7**	pr	pr
Pearson code	hP2	tI2	tI4		
Fifth row					
Element	Hg	Tl	Pb	Bi	
T_c	4.15/3.9	2.4/2.4	**7.2**	fl/pr	
Pearson code	hR3/tI2	hP2/cI2	cF4		

[a] Several other superconducting elements are: (symbol, N_e, T_c, Pearson code)

Am	3	1.0	cF4	Lu	3	1.0	hP2
β-Ca	2	0.5	hP2	Pa	3	1.4	tI2
γ-Ga	3	7.0	oS40	Th	3	1.4	cF4
δ-Ga	3	7.9	hR66	γ-U	3	0.2	cI2

Transition temperatures at high pressure are:

Ge	4	5.4	tI4	11.5 GPa	Si	4	7.1	tI4	13 GPa

C

Description of the Data Tables

The transition temperature T_c is, perhaps, the most important characteristic of a superconductor. This is because it is an index of the goodness of a material and of its suitability for practical applications. For example, we know from simple theory, confirmed by BCS, that the upper critical field B_{c2} and the critical current density J_c are both proportional to T_c. We can also conjecture from the data on elements mentioned in the previous section that T_c might be expected to depend on the number N_e of valence electrons. We have, accordingly, composed a number of tables that present the transition temperatures of compounds of various types by arranging their constituent elements in rows and columns according to the number of their valence electrons. The N_e value is given for each element that is listed. Separate tables are provided for the structures that include many examples of superconductors, such as the A15 compounds and the Chevrel phases. Some classes of materials have more than one structure, such as the Laves phases, and when this occurs an asterisk (*) is used to differentiate them. Some of the tables display data for several structures of the same chemical formula, such as AB_2, and if this is the case the rows and columns are labeled with the structure type when it is the same for every element in a particular row or column. Occasionally, an individual compound has two structural modifications, both of which superconduct, and sometimes this will be indicated.

The tables are arranged in the order of increasing complexity of their chemical formulas, with elements A first, binary compounds A_mB_n second, ternary compounds $A_mB_nC_p$ third, etc. The tables for binary compounds present data in the order AB, AB_2, AB_3, ..., A_mB_n, and analogously for the ternary compounds. The T_c values for additional compounds that remain after presenting the main structure types, such as for miscellaneous AB_2 compounds, are listed in separate tables arranged alphabetically by element A and then by element B. Each table caption provides the compound type and structure(s), and the compounds in the miscellaneous listings are identified by their structure type. The structures are designated by abbreviated Pearson codes, such as cF, where the initial lowercase letter indicates the crystal system and the final capital letter denotes the type of lattice, in accordance with the following notation:

Crystal system: c = cubic, h = hexagonal, t = tetragonal, o = orthorhombic, m = monoclinic; Lattice type: P = primitive, S = side-centered, I = body-centered, F = face-centered, R = rhombohedral

The Pearson code ends with a number, such as cF8, where 8 denotes the number of atoms in the unit cell. The abbreviations bcc, fcc, and hcp are occasionally used for body-centered cubic, face-centered cubic, and hexagonal close-packed, respectively. Chapter 6 provides a more detailed explanation of Pearson codes. Phillips (1989) uses a Pearson code classification for the arrangement of the T_c

tables in the appendix of his book. Sometimes the Strukturbericht symbol (e.g., A15), compound designation (e.g., NaCl) or common name (e.g., Chevrel) are given in table captions.

D

Classical Compounds

Many types of compounds have been found to superconduct, and the main ones were summarized in Table 3.2 of our earlier work (Poole *et al.*, 1995). In this section we will make some comments on the principal classes that were widely studied before the advent of high T_c. Motivated by the results mentioned earlier for the elements, we will examine how the transition temperature T_c correlates with the number N_e of valence electrons in the compounds within each structure type.

Tables 5.4 to 5.7 show that the highest T_c values for four types of AB compounds come at the following electron counts:

fcc NaCl type	$N_e = 4.5$ and 5
bcc CsCl type	$N_e = 6.5$
Hexagonal NiAs type	$N_e = 7.5$ and 8
Orthorhombic FeAs type	$N_e = 6.5$

These were obtained from the expression

$$N_e = f_A N_e^A + f_B N_e^B, \tag{3}$$

Table 5.4.

AB compound, NaCl type (rock salt), cF8.

B ⇒	B	Y	C	Ge	N	O	S	Se
A	3	3	4	4	5	6	6	6
⇓								
La 3					1.4		0.9	1.0
Th 3							0.5	1.7
Ti 4			3.4		5.6	0.14		
Zr 4	3.4		0.25		10.7			
Hf 4	3.1		0.25		8.8			
V 5					8.5			
Nb 5			11.1		16.6	1.4		
Ta 5			10.2		14.0			
Te 6		1.5		0.4				
Mo 6			14.3		14.8			
W 6			10.0					
Re 7			3.4					

LaTe 1.5, PdD 10.7, PdH 9.6, NbW 13.6.

Table 5.5.

AB compound, CsCl type, cP2.

B ⇒	Hg	Sc	Y	La	Lu	Ru	Os	Rh
A	2	3	3	3	3	8	8	9
⇓								
Cu 1		0.5	0.3					
Ag 1			0.3	0.9	0.3			
Au 1		2.0			0.4			
Mg 2	1.4							
Ca 2	1.6							
Ba 2	2.3							
Zn 2			0.3	1.0				
Ti 4						1.1	0.5	
Zr 4								2.4
Hf 4							2.4	
V 5						5.1	1.7	

ZnAu 0.4.

Table 5.6.

AB compound, NiAs type, hP4

B ⇒	C	Sn	Sb	Bi	Te
A	4	4	5	5	6
⇓					
Mo_2 6	5.8				
W_2 6	3.1				
Ir 9					3.0
Rh 9				2.2	
Ni 10				4.3	
Pd 10			1.5		4.5
Pt 10		0.4	2.1	1.8	0.6
Cu 11				1.4	
Au 11		1.3			

Table 5.7.

AB compound, FeAs (MnP) type, oP8.

B ⇒	Ga	In	Ge	Si	Sn	As	Bi
A	3	3	4	4	4	5	5
⇓							
Rh 9			1.0			0.6	2.1
Ir 9			4.7				
Pd 10			<0.3	0.9	0.4		
Pt 10			0.4	0.9			
Au 11	1.2	0.6					

Table 5.8.

A_xB_{1-x} compound, CrFe type (σ phase), tP30, where x lies in the range $0.25 < x < 0.50$. See Phillips (1989, p. 347) and data set CrFe in Chapter 6 for the x values of each compound.

B ⇒	Nb	Ta	Cr	Mo	W	Tc	Re	Fe
A	5	5	6	6	6	7	7	8
⇓								
Al 3	12.0							
V 5							4.5/6.3	
Nb 5							2.5/5.3	
Ta 5							1.4	
Mo 6						12.0	8.6/7.8	
W 6						9.0	5.0	
Re 7		1.4		6.5				6.6
Ru 8			2.1	8.8/7.0	4.7			
Os 8	1.9			5.7	3.8			
Rh 9	4.0	2.4						
Ir 9	2.2/9.8	1.2		6.7	4.5			
Pt 10	4.0	1.0						

where the mole fractions $f_A = f_B = \frac{1}{2}$ for an AB compound. The tetragonal A_xB_{1-x} material called the σ phase has atom concentrations that vary between $A_{0.24}B_{0.76}$ and $A_{0.50}B_{0.50}$, and the transition temperatures of this group are listed in Table 5.8. The CrFe compound type data set in Chapter 6 gives the x values for the compounds listed in the table. Table 5.9 lists T_c values for some additional AB compounds of miscellaneous structures.

Tables 5.10 to 5.13 display T_c data for many AB_2 structure types, and in particular Table 5.10 provides transition temperatures for several dozen Laves phase AB_2 compounds. Some of these have the cubic C15 structure, and others have the hexagonal C14 structure; these structures are described in data sets $MgCu_2$ and $MgZn_2$, respectively, of Chapter 6 and are compared in Fig. 6.8. The highest transition temperature is $T_c = 10.9$ K for the hexagonal compound $ScTc_2$, and the cubic compound HfV_2 with $T_c = 9.3$ K is second, as indicated in the table. High T_c values come for N_e in the range from 4.7 to 6.7.

The A15 intermetallic compounds AB_3 provided the highest transition temperature of the older superconductors at particular electron contents calculated from the expression (3),

$$N_e = (N_e^A + 3N_e^B)/4, \tag{4}$$

with maxima in T_c found at

$$N_e = 4.5, 4.75, 6.25, \text{and } 6.5, \tag{5}$$

as shown by the data in Table 5.14 and Fig. 5.3, respectively. These maxima are near those seen in Fig. 5.2 for alloys of elements and listed above for AB compounds. The A element of these materials either is a transition element or

Table 5.9.

Miscellaneous AB compounds with various structures[a]

B ⇒		B	Ga	Th	C	Si	P	Sb	Bi	O
A		3	3	3	4	4	5	5	5	6
⇓					h					
Li 1	tP								2.5	
Na 1	tP								2.3	
Cu 1	cI									1.7
Ag 1	m								2.8	
Al 3	tI							2.8		
Ga 3	tI							4.2		
In 3	tI							2.0	5.8	
Si 4	oP			2.4						
Sn 4	tP									3.8
Pb 4							7.8			
N 5	hP		5.9							
Nb 5		8.3								1.3
Ta 5		4.0				4.4				
Te 6	mS		0.17							
Mo 6		0.5			9.3					
Tc 7					3.9					
Ru 8					2.0				5.7	
Co 9	m								0.5	
Rh 9	oS		0.4							
Ir 9	oS		0.4							
Pd 10	oS								4.0	
Pt 10	oS		0.4							

[a] Several additional AB compounds with their transition temperature T_c and structure types are:

Compound	T_c (K)	Structure
CdHg	1.8	tI2
CuLa	5.9	oP8
MgZn	0.9	oP
NbRh	3.0	oP

appears in rows III to V of the periodic table, and the B atom is adjacent to niobium in the periodic table.

Tables 5.15 and 5.16, respectively, list transition temperatures for two additional AB_3 classes, namely the cubic $AuCu_3$ and α-Mn compound types, and Tables 5.17 and 5.18 give additional AB_n data. The hexagonal Fe_3Th_7 type has the T_c values of Table 5.19, and miscellaneous binary A_mB_n compounds are listed in Table 5.20.

Transition temperature data for some ternary compounds are presented in Tables 5.21 to 5.33. Transition temperatures for the boride compounds AXB_2, AX_3B_2, and AX_4B_4 are presented in Tables 5.23 to 5.25, and skutterudites AX_4P_{12} are in Table 5.26. Transition temperatures of miscellaneous ternary

Table 5.10.

AB_2 compound, Laves phase, hP12 (designated by *) and cF24.

$B_2 \Rightarrow$	Au	Mg	Al	Sn	Hf	Bi	V	Te	Mo	W	Tc	Re	Ru	Os	Rh	Ir	Pt
A	1	2	3	4	4	5	5	6	6	6	7	7	8	8	9	9	10
⇓																	
K 1						3.6											
Rb 1						4.3											
Cs 1						4.8											
Ca 2															6.4	6.2	
Sr 2															6.2	5.7	0.7
Ba 2															6.0		
Sc 3			1.0								10.9*	4.2*	1.7*	4.6*	6.2	2.2	0.7
Y 3			0.4								8.8*	1.8*	1.5*	4.7*		2.1	1.6
La 3		1.1	3.2										4.4	8.9/5.9*		0.5	
Lu 3			1.0								9.9*		0.9/0.9*	3.5*	1.3	2.9	
Ce 3													6.2				
Th 3											5.3*	5.0*	4.1			5.6	
Zr 4							8.8	7.6*	0.13	2.2	7.6	6.4*	1.8*	3.0*		4.1	
Hf 4							9.3	5.6*	0.07*		5.6	5.2*		2.7*			
Pb 4	1.2																
Bi 5	1.8																
Nb 5				2.6													
Rh 9						2.0											

Table 5.11.

AB_2 compound, $CuAl_2$ type, tI12.

$B_2 \Rightarrow$	Al	In	Tl	Th	Zr	Hf	Pb	Ta	Mo	W
A	3	3	3	3	4	4	4	5	6	6
$\Downarrow$										
Cu 1	1.0			3.4						
Ag 1		2.1		2.2						
Au 1				3.7			3.1			
Al 3				0.1						
B 3								3.1	5.1	3.2
Ga 3						0.21				
Co 9					5.0					
Rh 9					11.3		1.3			
Ir 9					7.6					
Ni 10					1.6					
Pd 10			1.3	0.9			3.0			
Pt 10			1.6							

Table 5.12.

AB_2 compound, CaF_2-type, cF12.

$B_2 \Rightarrow$	Al	Ga	In	Si	Rh
A	3	3	3	4	9
$\Downarrow$					
P 5					1.3
Co 9				1.2	
Pt 10	0.5	1.8			
Au 11	0.1	1.6	0.2		

compounds are listed in Table 5.33. Of especial importance are the Chevrel phases $A_xMo_6X_8$ with $1 \leq x \leq 2$. These are chalcogenides where X is S, Se, Te and the atom A can be almost any element. Table 5.27 provides the transition temperatures for several dozen of these superconductors with $x = 1$ and $x = 1.2$. The Mo_6X_8-group building blocks described in Section F.c of Chapter 6 are mainly responsible for the superconducting properties. Magnetic order and superconductivity often coexist with these compounds.

E

Perovskites

Before the advent of the high-T_c era it was found that superconductivity exists in the mixed valence compound $BaPb_{1-x}Bi_xO_3$, which is structurally a distorted

Table 5.13.

Miscellaneous AB_2 compounds with various structures. Compounds listed with two values of T_c have two different structures.[a]

$B_2 \Rightarrow$		Hg	C	Si	Ge	Bi	S	Se	Mo	W	Re
A		2	4	4	4	5	6	6	6	6	7
⇓			tI					hP			
Na 1	hP	1.6									
Ag 1	m	3.0									
Mg 2		4.0									
Ca 2	tI			1.6							
Sr 2	tI			3.1							
Ba 2	tI				4.9						
B 3									4.7	3.1	2.8
Sc 3	oS				1.3						
Y 3	tI		3.9		3.8						
La 3	tI		1.7	2.5	2.6						
Lu 3	tI		3.3								
Th 3				2.4/3.2							
C 4	hP								7.3	4.5	
Zr 4	oS				0.3						
Hf 4	hP								0.05		
N 5	tI								5.0		
Bi 5											2.2
Nb 5							5.0/6.2	7.1			
Mo 6	hP						<1.2				
Ir 9						2.2					
Pd 10				0.9		4.3					

[a] Several additional AB_2 compounds with their transition temperature T_c and structure types are:

Compound	T_c(K)	Structure
$AsPd_2$	1.7	hP
$BiIn_2$	5.8	hP6
$CoTi_2$	3.4	cF96
$CoZr_2$	6.3	cF96
$CoHf_2$	0.5	cF96
$GeNb_2$	1.9	—
$HgMg_2$	0.5	—
$IrZn_2$	0.8	—
$PbSb_2$	1.3	cP12
$RhSe_2$	6.0	cP12
RhTe2	1.5	cP12
$SePd_2$	2.2	—
$SnPd_2$	0.4	oP12

perovskite (Sleight *et al.*, 1975). Its stoichiometric ($x = 1$) form probably has the valence state $Ba_2Bi^{3+}Bi^{5+}O_6$. The highest T_c of 13 K was obtained for oxygen-deficient mixed crystals. In their original work Bednorz and Müller were seeking higher T_c compounds within the perovskite type or related oxides, and their

Table 5.14.

AB_3 compound, Cr_3Si type (A15), cP8.

$B_3 \Rightarrow$	Ti	Zr	V	Nb	Ta	Cr	Mo
A	4	4	5	5	5	6	6
$\Downarrow$							
Al 3			9.6	19.1			0.6
Ga 3			14.9	20.7			1.0
In 3			13.9	9.2			
Tl 3				9.0			
Si 4			17.0	19.0			1.7
Ge 4			8.2	23.2	8.0	1.2	1.8
Sn 4	5.8	0.9	3.8	17.9	8.4		
Pb 4		0.8		8.0	17.0		
As 5			0.2				
Sb 5	6.5		0.8	2.0	0.7		
Bi 5		3.4		3.1			
Tc 7							15.0
Re 7							15.0
Ru 8						3.4	10.6
Os 8			5.7	1.1		4.7	12.7
Rh 9			0.7	2.6	10.0	0.3	
Ir 9	5.0		1.7	3.2	6.6	0.8	9.1
Pd 10			0.08				
Pt 10	0.5		2.9	10.9	0.4		4.7
Au 11		0.9	3.0	11.5	16.0		

success in 1986 opened up the field of high-T_c superconductivity. The cubic perovskite $Ba_{1-x}K_xBiO_{3-y}$ discovered 2 years later (Cava *et al.*, 1988; Mattheiss *et al.*, 1988) with $T_c \approx 30$ K for $x \approx 0.4$ is the first oxide superconductor without copper with T_c above that of all the A-15 compounds. Another oxide superconductor type is fcc spinel, and $Li_{0.75}Ti_2O_4$ has $T_c = 13.2$ K. Very few spinels superconduct; see data set $MgAl_2O_4$ in Chapter 6. Data for these compounds are provided in Table 5.34. Also included in this table are T_c data for four magnet wire materials.

F

Heavy Electron Systems

Heavy electron superconductors have an effective conduction electron mass m^* that is typically more than 100 electron masses. These are sometimes referred to

Fig. 5.3.

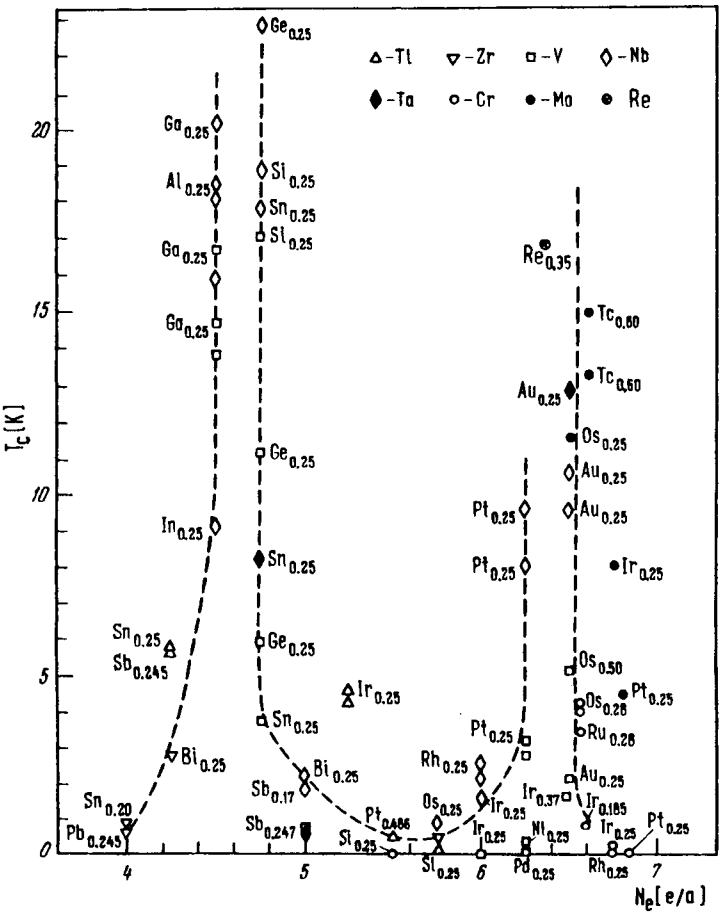

Dependence of the transition temperature T_c on the number of valence electrons N_e in $A_{0.25}B_{0.75}$ compounds with the A15 structure. The B element is specified by the symbol at the top right, and the A element is indicated at the experimental points. (Vonsovsky *et al.* (1982), p. 269.]

by the more pretentious name heavy Fermion superconductors. The large effective mass produces a long penetration depth,

$$\lambda_L = (m^*/\mu_0 n_s e^2)^{1/2}, \tag{6}$$

and a large electron density of states at the Fermi level,

$$D(E_F) = \frac{1}{2\pi^2}(2m^*/\hbar^2)^{3/2}E_F^{1/2}, \tag{7}$$

Table 5.15.

AB_3 compound, Cu_3Au type, cP4.

$B_3 \Rightarrow$	Mg	Hg	Ga	Tl	La	Sn	Pb	Bi	Nb
A	2	2	3	3	3	4	4	5	5
$\Downarrow$									
Na 1							5.6		
Ca 2				2.0					
Sr 2								5.7	
Ga 3					5.8				
In 3	2.2				9.7				
Tl 3					8.9				
Y 3				1.5			4.7		
La 3				1.6		6.0	4.1		
Th 3						3.3	5.6		
Lu 3			2.3						
Sn 4					6.2				
Pb 4									9.6
Zr 4		3.3							
Bi 5				4.2					

$YbAl_3$ 0.9 K.

which in turn leads to a large value for the conduction electron contribution γ to the specific heat since γ is proportional to $D(E_F)$. The specific heat ratio $(C_s - \gamma T_c)/\gamma T_c$, however, remains close to the usual BCS value of 1.43. Heavy electron systems often exhibit two ordering transitions, a superconducting transition at T_c and an antiferromagnetically ordering transition at the Néel temperature T_N, with typical values given in Table 5.35. Many heavy electron superconductors are anisotropic in critical field, electrical resistivity, ultrasonic attenuation, thermal conductivity, NMR relaxation, and other properties.

Table 5.16.

AB_3 compound α-Mn type, cI58.

$B_3 \Rightarrow$	Tc	Re	Os	Pd
A	7	7	8	10
$\Downarrow$				
Al 3		3.4		
Sc 3		2.2		
Ti 4		6.6		
Zr 4	9.7	7.4		
Hf 4		5.9		
Nb 5	10.5	9.7	2.9	2.5
Ta 5		6.8	2.0	
Mo 6		9.9		
W 6		9.0		

Table 5.17.

Miscellaneous AB_3 compounds with various structures. Compounds with two values of T_c have two different structures.[a]

$B_3 \Rightarrow$		Hg	Al	La	Zr	Bi	Nb	Fe	Rh	Ir	Pd
A		2	3	3	4	5	5	8	9	9	10
⇓		hP			tP		tP	oP	hP		oP
Li 1	hP	1.7									
Ca 2	hP	1.6									
Ba 2	tP					5.7					
Zn 2	m					0.9					
Al 3	hP			5.7							
Tl 3	h		0.8			4.2					
La 3									2.6	2.5	
Y 3									1.1	3.5	
Ce 3	hP									3.3	
Th 3										4.7	
C 4	oP							1.3			
Si 4	tP				0.5		0.3				
Ge 4				3.7	0.4						
Sn 4	m					3.8					
P 5							1.8				0.8
As 5	tP						0.3				
Sb 5	tP						0.2				
Nb 5	tI		0.6								
Mo 6	m					3.7					
Fe 8	m					1.0					
Ru 8	oP			4.2							
Co 9	hP			4.1							
Rh 9			0.7			3.2					
Ni 10	oP			6.2		4.1					

[a] Seven additional AB_3 compounds with their transition temperatures T_c and structure types are:

Compound	T_c(K)	Structure
$AuZn_3$	1.3	cP32
$OsMo_3$	7.2	—
PMo_3	5.3	tI32
PW_3	2.3	tI32
RhY_3	0.7	oP16
$SrPb_3$	1.9	tP4
YLa_3	2.5	h

Table 5.18.

Miscellaneous AB_n compounds of several structure types with $n > 3$

Compound	T_c(K)	Structure
$GeAg_4$	0.8	h
$MgBi_4$	1.0	m
$SnAg_4$	0.1	h
$PtPb_4$	2.8	oS20
$PtSn_4$	2.4	oS20
$RhBi_4$	2.7	cI120
$SePd_4$	0.4	tP10
BAu_5	0.7	—
$BaAu_5$	0.7	—
$BiIn_5$	4.1	m
$CaAu_5$	0.4	cF24
$CaHg_5$	1.7	—
$CeIr_5$	1.8	cF24
$LaIr_5$	2.1	hP6
$LaRh_5$	1.6	—
$LuRh_5$	0.5	—
$SnAu_5$	1.1	hR6
$ThIr_5$	3.9	hP6
$ThPt_5$	3.1	hR6
$ThRh_5$	1.1	—
YRh_5	1.6	hP6
CoU_6	2.3	tI28
FeU_6	3.9	tI28
$HgSn_6$	5.1	m
LaB_6	5.7	cP7
MnU_6	2.3	tI28
ThB_6	0.7	cP7
YB_6	7.1	cP7
LuB_{12}	0.5	cF52
$ReMgBe_{12}$	10.1	tI26
ScB_{12}	0.4	cF52
YB_{12}	4.7	cF52
ZrB_{12}	5.8	cF52
$ReBe_{13}$	9.9	tI28
UBe_{13}	0.9	cF112
WBe_{13}	4.1	tI28
$MoBe_{22}$	2.5	cF184
$ReBe_{22}$	9.7	cF184
$TcBe_{22}$	5.7	cF184
WBe_{22}	4.1	cF184

Table 5.19.

A_3B_7 compounds, all hP20 (except the one labeled with an asterisk *).

$B_7 \Rightarrow$	La	Y	Th	Ge	Ru
A_3	3	3	3	4	8
$\Rightarrow$					
B 3					2.6
Fe 8			1.9		
Os 8			1.5		
Co 9			1.8		
Rh 9	2.6	0.3	2.2		
Ir 9	2.2		1.5	0.9*	
Ni 10			2.0		
Pt 10		0.82	1.0		

G

Borocarbides

Paul C. Canfield

The RNi_2B_2C (R = Gd–Lu, Y) series of materials is a recently discovered family of magnetic superconductores. The T_c values for the nonmagnetic rare earths Lu and Y are relatively high, 16.1 K and 15.6 K, respectively. The replacement of Y or Lu with a moment-bearing rare earth leads to a suppression of T_c and the advent of antiferromagnetic ordering below the Néel temperature T_N. It can be seen from Table 5.36 that T_c and T_N values for this series have a ratio T_c/T_N that ranges from 7.3 for R = Tm to 0.60 for R = Dy. $DyNi_2B_2C$ is of especial interest as a rare example of an ordered compound with $T_c < T_N$. Table 5.37 lists T_c values for additional borocarbides.

The crystalline electric field splitting of the Hund's rule J-multiplet leads to extremely anisotropic local moment magnetism for $T \leq 100$ K. These anisotropies also manifest themselves in the B_{c2} vs temperature phase diagrams. In addition, $B_{c2}(T)$ is nonmonotonic in T for R = Ho–Tm because of the effects of local moment ordering. For $HoNi_2B_2C$ there is a local minimum in B_{c2} at $T = 5$ K, while for $ErNi_2B_2C$ there is a local maximum in B_{c2} at $T = 6$ K for $B_{app} \| c$.

The compound $YbNi_2B_2C$ does not order or superconduct for temperatures above 0.3 K, but instead enters a heavy Fermion ground state with a characteristic Kondo temperature of $T_K \approx 10$ K. The electronic specific heat coefficient of $YbNi_2B_2C$ at low temperatures has the value $\gamma = 530$ mJ/K^2 mol.

Table 5.20.

A_mB_n compounds with $m, n > 2$.

Compound	T_c(K)	Structure
Ir_2Y_3	1.6	tI40
$La_2C_{2.7}$	11.0	cI40
Lu_2C_3	15.0	cI40
Mg_2Al_3	0.8	cF
Pt_2Y_3	0.9	—
Rh_2Y_3	1.5	tI40
Ru_2Nb_3	1.2	t
Si_2W_3	2.8	—
Th_2C_3	4.1	cI40
Y_2C_3	11.5	cI40
As_2Pd_5	0.46	—
Rh_2Se_5	1.0	—
Se_2Pd_5	2.3	—
V_2Ga_5	3.6	tP14
C_3Sc_4	8.5	cI28
La_3As_4	0.6	cI28
La_3S_4	8.1	cI28
La_3Se_4	7.8	cI28
La_3Sb_4	0.2	—
La_3Te_4	5.3	cI28
Nb_3Se_4	2.0	hP14
Nb_3Te_4	1.8	hP14
As_3Pd_5	1.9	—
Bi_3In_5	4.2	tI32
Ga_3Zr_5	3.8	hP16
Hg_3Mg_5	0.5	hP16
P_4Rh_5	1.2	oP28
Os_4Al_{13}	5.5	mS34
Th_4D_{15}	7.6	cI76
Sn_5Nb_6	2.8	oI44
Al_5Re_{24}	3.4	cI58
Sc_5Re_{24}	2.2	cI58
Ti_5Re_{24}	6.6	cI58
Mo_6S_8	1.9	hR42
Mo_6Se_8	6.5	hR42
$Mo_6Ga_{30.75}$	9.8	mP148
$S_{15}Rh_{17}$	5.8	cP64
$Mo_{15}Se_{19}$	4.3	hP68

Table 5.21.

ACX compounds, mS12, where C is carbon, X = Y, La, and A is a halogen.

X ⇒	Y	La
A	3	3
⇓		
Cl	2.3	
$Cl_{0.65}Br_{0.35}$	3.6	
$Cl_{0.5}I_{0.5}$		3.7
Br	5.1	6.2
$Br_{0.88}Cl_{0.12}$	4.7	
$Br_{0.85}Cl_{0.15}$		7.2
$Br_{0.9}I_{0.1}$		5.0
$Br_{0.62}I_{0.38}$	7.0	
I	9.7	<2
$I_{0.88}Cl_{0.12}$	10.7	
$I_{0.75}Br_{0.25}$	11.1	
$Na_{0.23}Br$	6.2	

Table 5.22.

APd_2X compounds, $MnCu_2Al$ type (Heusler), cF16.

X ⇒	In	Sn	Pb	Sb	Bi
A	3	4	4	5	5
⇓					
Sc 3		2.2			
Y 3	0.85	5.5	4.8	0.85	<0.07
Lu 3		3.1			
Tm 3		2.8			
Yb 3		2.4			

For $ScAu_2Al$, $T_c = 4.4$, and for $ScAu_2In$, $T_c = 3.0$.

Table 5.23.

AXB_2 boride compound, $LuRuB_2$ type, oP16.

X ⇒	Ru	Os
A	8	8
⇓		
Sc 3		1.3
Y 3	7.8	2.2
Lu 3	10.0	2.7

Table 5.24.

$A(X_3B_2)$ boride compounds and isostructural AX_5 compounds, $CeCo_3B_2$ type, hP6.

$(X_3B_2) \Rightarrow$ A $\Downarrow$	Ru_3B_2	Os_3B_2	Rh_3B_2	Ir_3B_2	Rh_5	Ir_5
La 3			2.8	1.7		2.1
Y 3	2.9				1.6	
Lu 3		4.7				
Th 3	1.8			2.1		3.9

Table 5.25.

AX_4B_4 boride compounds, tP18 (no symbol), tI72 (designated by *) and oS108 (in footnote). See Chapter 6 for details.

$X_4 \Rightarrow$ A $\Downarrow$	Ru 8	Os 8	Rh 9	Ir 9	$Rh_{0.85}Ru_{0.15}$ 8.85
Sc 3	7.2*				
Y 3	1.4*		11.3/10*		9.6*
Lu 3	2.1*		11.8/6.2*		9.2*
Th 3	<1.5*		4.3		
Pr 3					2.4*
Nd 3			5.4		<1.5*
Sm 3			2.5		<1.5*
Eu 3					2.0*
Gd 3					<1.5*
Tb 3					<1.5*
Dy 3					4.1*
Ho 3				2.1	6.5*
Er 3			8.6/7.8*	2.3	8.0*
Tm 3			9.9/5.4*	1.8	8.4*
Yb 3					<1.5*

For side-centered orthorhombic compounds, $T_c = 4.3$ K for $ErRh_4B_4$, $T_c = 5.4$ K for $TmRh_4B_4$, and $T_c = 6.2$ K for $LuRh_4B_4$. For primitive tetragonal: $T_c = 4.6$ for $DyRh_2Ir_2B_4$, $T_c = 6.4$ K for $HoRh_2Ir_2B_4$, $T_c = 11.9$ K for $Lu_{0.75}Th_{0.25}Rh_4B_4$, $T_c = 3.2$ for $Y_{0.5}Lu_{0.5}Ir_4B_4$.

Table 5.26.

AX_4P_{12} phosphide compound, $LaFe_4P_{12}$ (skutterudite), cI34.

$X_4 \Rightarrow$	Fe	Ru
A	8	8
$\Downarrow$		
La 3	4.1	7.2
Ce 3	<0.35	<0.35
Pr 3	<0.35	<0.35
Nd 3	<1.0	<1.0

H

Fullerenes

Arthur P. Ramirez

The C_{60} molecule sketched in Fig. 6.26 was originally discovered in molecular beam experiments. It is one of the most stable molecules in the series of even-numbered fullerenes and the one that most closely approximates a sphere. C_{60} is a truncated icosahedron, that is, a polygon with 60 vertices and 32 faces divided into 20 hexagons and 12 pentagons. The solidification of C_{60} is a multistep process. First, soot is formed by spark erosion in a helium atmosphere. Second, column chromatography is performed to isolate the C_{60} components of the soot. Then, for single crystal production, the black powder is dissolved in a nonpolar solvent such as benzene, which is then allowed to evaporate, leaving behind small (<1 mm) single crystals. For both powder and crystalline samples doping is achieved by exposing C_{60} to alkali vapor in the absence of air.

Solid C_{60} is the third crystalline form of carbon, besides diamond and graphite. The crystal structure is fcc. The diameter of a C_{60} molecule is 7 Å and C atoms are separated by 1.4–1.45 Å, depending on whether the bonds comprise a pentagon or connect pentagons. The separation between the C_{60} molecules on the edge of the fcc cell is 14.2 Å for pure C_{60} and increases to 14.25 Å for K_3C_{60} and to 14.43 Å for Rb_3C_{60}. There are other structural variations among doped C_{60} compounds: A_2C_{60} is fcc, A_4C_{60} is bct, and A_6C_{60} is bcc, where A is an alkali atom. None of these compounds exhibit superconductivity, at least not above 2 K. Other compound families can be formed by intercalating NH_3 and alkaline earths. All of these systems are nearly line compounds at room temperature, meaning that continuous doping is not possible.

Undoped, C_{60} is a semiconductor with a band gap of about 1.5 eV. Because of the curvature of the molecular surface, there is a significant σ–p hybridization, intermediate between that of diamond and graphite. The band widths are typically 0.5 eV and are identified by the parent molecular orbitals. The extra rotational

Table 5.27.

$A_xMo_6X_8$ compound, for $X = S$, Se and $0 \leq x \leq 2$, $PbMo_6S_8$ type (Chevrel), hR45. Columns 2 and 3 are for $x = 1$, columns 4 and 5 are for $x = 1.2$, and the remaining columns are for special cases. $Tl_2Fe_6Te_6$ type hP14 Chevrel compounds are marked with the asterisk (*).

	Case $x = 1.0$		Case $x = 1.2$		Special cases	
$X_8 \Rightarrow$	S	Se	S	Se		
A	6	6	6	6	Compound	T_c
$\Downarrow$						
Li 1	5.5	3.9			Mo_6S_8	1.9
Na 1	8.6				Mo_6Se_8	6.5
K 1	2.9				Mo_6Se_6*	<1
Ag 1	9.5			5.9	Mo_6Se_8*	<1
Ca 2	6.0				Mo_6Te_8	1.7
Hg 2	8.1				$BrMo_6Se_7$	7.1
Sc 3	3.6				$Br_2Mo_6S_6$	13.8
Y 3		6.2	2.1		IMo_6Se_7	7.6
In 3	<0.6	8.1			$I_2Mo_6S_6$	14.0
Tl 3	8.7	12.2			$I_2Mo_6Te_6$	2.6
La 3	7.0	11.4			$Cu_2Mo_6S_8$	10.7
Ce 3	<1.1	<1.1			$Cu_{1.73}Mo_6S_8$[a]	10.9
Pr 3	2.6	9.2			$Cu_2Mo_6Se_8$	5.9
Nd 3	3.5	8.2			$Zn_2Mo_6S_8$	3.6
Sm 3			2.4	6.8	$CdMo_5S_6$	3.5
Eu 3	<1.1			<1.1	$In_2Mo_6Se_6$*	<1
Gd 3	1.4			5.6	$In_2Mo_6Te_6$*	<1
Tb 3			1.4	5.7	$Tl_2Mo_6Se_6$*	5.8
Dy 3			1.7	5.8	$Tl_2Mo_6Te_6$*	<1
Ho 3	1.9		2.0	6.1		
Er 3	<1.1		2.0	6.2		
Tm 3			2.0	6.3		
Yb 3	8.6	5.8	8.7	5.8		
Lu 3			2.0	6.2		
Np 3		5.6				
Pu 3		<2.5				
Am 3		<3.5				
Sn 4	11.8		14.2			
Pb 4	15.0	3.8				
Sb 5	<2					
Bi 5	<2					

* $Tl_2Fe_6Te_6$ type hP14 structure.
[a] hR78 structure.

Table 5.28.

$A_2B_3Si_5$ silica compound, $U_2Mn_3Si_5$ type tP40 (no symbol) and $U_2Co_3Si_5$ type, oI40 (designated by asterisk*).

$B_3 \Rightarrow$	Re	Fe	Rh	Ir
A_2	7	8	9	9
$\Downarrow$				
Sc 3		4.5		
Y 3	1.8	2.4	2.7*	3.0*
La 3			4.4*	
Lu 3		6.1		
Tm 3		1.3		

Table 5.29.

$A_3X_4Y_{13}$ compound, $Yb_3Rh_4Sn_{13}$ type, cP40; stannides $A_3X_4Sn_{13}$ are on the left, and germanides $A_3X_4Ge_{13}$ are on the right.

	$A_3X_4Sn_{13}$ compounds					$A_3X_4Ge_{13}$ compounds				
$X_4 \Rightarrow$	Ru	Os	Rh	Ir	Co	Ru	Os	Rh	Ir	Co
A_3	8	8	9	9	9	8	8	9	9	9
$\Downarrow$										
Ca 2			8.7	7.1	5.9			2.1	1.7	
Sr 2			4.3	5.1						
Sc 3			4.5	1.1				1.9	1.4	
Y 3			3.2			1.7	3.9			
La 3	3.9		3.2	2.6	2.8					
Lu 3				3.2		2.3	3.6	2.3		
Th 3		5.6	1.9	2.6						
Yb 3			8.6		2.5					

$T_c = 4.8$ K for $La_3RuPd_3Sn_{13}$ and $T_c = 2.2$ K for $La_3Rh_4Pb_{13}$, both with structure cP40; $T_c = 3.2$ K for $La_3Rh_4Sn_{13}$, with structure cI320.

Table 5.30.

$A_4X_5Y_{10}$ compounds, $Sc_5Co_4Si_{10}$ type, tP38; silicides $A_4X_5Si_{10}$ are shown on the left and germanides $A_4X_5Ge_{10}$ on the right.

$A_4X_5Si_{10}$ compounds				$A_4X_5Ge_{10}$ compounds			
$X_5 \Rightarrow$	Sc	Y	Lu	$X_5 \Rightarrow$	Sc	Y	Lu
A_4	3	3	3	A_4	3	3	3
$\Downarrow$				$\Downarrow$			
Co 9	4.7			Os 8		9.1	
Rh 9	8.4		4.0	Rh 9		1.4	2.8
Ir 9	8.4	3.1	3.9	Ir 9		2.7	2.6

Table 5.31.

$A_4X_6Sn_{19}$ compound with two structures, $Tb_4Rh_6Sn_{19}$ type, cF116 (no symbol) and $Er_4Rh_6Sn_{19}$ type, tI232 (designated by *).

$X_6 \Rightarrow$ / $A_4 \Downarrow$	Ru 8	Os 8	Co 9	Rh 9	Ir 9
Sc 3		1.5		4.5*	1.1*
Y 3	1.3	2.5		3.2*	2.2
Lu 3	<1.1*	1.8	1.5*	4.0*	3.2*
Tb 3		1.4			
Ho 3		1.4			
Er 3	<1.1*	1.3	<1.1*	1.2*	<1.1*
Tm 3		1.1		2.3*	<1.1*

$Ca_4Rh_6Pb_{19}$ 3.3*; $Sc_4Ir_6Ge_{19}$ 1.4*; $Sc_4Rh_6Ge_{19}$ 1.9*.

degree of freedom of the C_{60} molecule gives rise to unusual structural behavior in the undoped material. This behavior includes orientational ordering at 260 K and glassy dynamics observed below 200 K in thermal conductivity, dielelectric constant, and Young's modulus studies. This behavior is not observed in the doped compounds, and it is also not clear to what extent residual rotational

Table 5.32.

$A_nMo_{15}Se_{19}$ compound with two structures: α-$Mo_{15}Se_{19}$ type, hP68 (no symbol) and β-$Mo_{15}Se_{19}$ type, hR204 (designated by an asterisk *).

A_n	N_e	T_c (K)
Li_2	1	2.6*
Li_3	1	3.5
Na_2	1	<0.5*
Na_3	1	<0.5
K_2	1	2.1*
$Cd_{2.5}$	2	<0.5*
In_2	3	1.4*
In_3	3	3.8
Sn_2	4	<0.5*
In_2	3	<0.5*
K_2In	1.7	1.3

For hP68 structure $T_c < 0.5$ K for X = S and A_n = Na, K, Zn, Cd, In, Tl, Sn, Pb; $T_c < 0.5$ K for $Mo_{15}S_{19}$ and $T_c = 4.3$ K for $Mo_{15}Se_{19}$.
For hR204 structure, $T_c = 4.3$ K for $Mo_{15}Se_{19}$, and $T_c = 3.3$ K for $K_2Mo_{15}S_{19}$.

Table 5.33.

Miscellaneous $A_mB_nC_p$ and $A_mB_nC_pD_q$ compounds with various structures.

	Compound	T_c(K)	Structure
ABC			
	AsHfOs	3.2	hP9
	AsHfRu	4.9	hP9
	AsOsZr	8.0	hP9
	AsRuZr	11.9	hP9
	GeIrLa	1.6	tI12
	GeLaPt	3.5	tI12
	HfIrSi	3.5	oP12
	HfOsP	6.1	hP9
	HfPRu	10.0	hP9
	IrSiTh	6.5	tI12
	IrSiTi	<1.7	oP12
	IrSiY	2.7	oP12
	IrSiZr	2.0	oP12
	LaPtSi	3.3	tI12
	LaRhSi	4.4	cP12
	NbPRh	4.4	oP12
	NbPS	12.5	oI12
	NbReSi	5.1	oI36
	NbRuSi	2.7	oI36
	OsPTi	1.2	hP9
	OsPZr	7.4	hP9
	PRhTa	4.4	oP12
	PRhZr	1.6	oP12
	PRuTi	1.3	hP9
	PRuZr	3.7, 12.9	oP12, hP12
	ReSiTa	4.4	oI36
	RuSiTa	3.2	oI36
ABC_2			
	$BCMo_2$	7.5	oS16
	$BNNb_2$	2.5	oS16
	$BiPbPt_2$	1.3	—
	$BiSbNi_2$	2.0	hP
	$BiSbPt_2$	1.5	hP
	$IrLaSi_2$	2.0	oS16
	$LaRhSi_2$	3.4	oS16
	$LaRuB_2$	7.8	oP16
	$NiRhBi_2$	3.0	hP
	$PdPtBi_2$	3.7	hP
	$ReWC_2$	3.8	cF8
ABC_3			
	$ClrMo_3$	3.2	cF
	$IrLaSi_3$	2.7	tI10
	$LaRhSi_3$	2.7	tI10

Table 5.33. (*continued*)

	Compound	T_c(K)	Structure
	$MoReC_3$	3.8	cF8
	$TaPbS_3$	3.0	—
	$ThIrSi_3$	1.8	tI10
	$ThRhSi_3$	1.8	tI10
AB_2C_2			
	LaB_2C_2	<1.8	tP10
	$LaRh_2Si_2$	3.9	tI10
	$LaRu_2P_2$	4.1	tI10
	LuB_2C_2	2.4	tP10
	$SrRu_2P_2$	<1.8	tI10
	$ThIUr_2Si_2$	2.1	tI10
	UAl_2Ge_2	1.6	cP
	yB_2C_2	3.6	tP10
	YIr_2Si_2	2.6	tI10
	YRh_2Si_2	3.1	tI10
AB_2C_3			
	CAl_2Mo_3	10.0	cP24
	CIr_2W_3	2.1	cF
	CIr_2Mo_3	1.8	cF
	COs_2W_3	2.9	cF
	CPt_2Mo_3	1.1	cF
	CPt_2W_3	1.2	cF
	LaB_2Rh_3	2.8	hP6
	LaB_2Ir_3	1.7	hP6
	$LaSi_2Ru_3$	7.6	hP12
	LuB_2Os_3	4.6	hP6
	OsY_2Ir_3	2.4	hP
	ThB_2Ir_3	2.1	hP6
	ThB_2Ru_3	1.8	hP6
	$ThSi_2Ru_3$	4.0	hP12
	YB_2Ru_3	2.9	hP6
	YSi_2Ru_3	3.5	hP12
AB_2C_4			
	$CuRh_2S_4$	4.4	cF56
	$CrRh_2Se_4$	3.5	cF56
	CuV_2S_4	4.5	cF56
	HfP_2Ru_4	9.5	tP14
	ZrP_2Ni_4	<2.0	tP14
	ZrP_2Ru_4	11.0	tP14
AB_3C_3			
	OV_3Zr_3	7.5	cF112
	$TlMo_3Se_3$	4.0	hP14
	$TlOs_3W_3$	2.1	—

Table 5.33. (*continued*)

	Compound	T_c(K)	Structure
AB_3C_4			
	$NiPd_3As_4$	1.6	hP
	$SbTe_3In_4$	1.5	cF8
	$SeTe_3Nb_4$	4.4	—
AB_3C_9			
	NaW_2O_0	3.0	—
AB_4C_{12}			
	$LaFe_4P_{12}$	4.1	cI34
	$LaRu_4P_{12}$	7.2	cI34
$A_2B_3C_5$			
	$La_2Rh_3Si_5$	4.5	oI40
	$Y_2Ir_3Si_5$	2.8	oI40
	$Y_2Rh_3Si_5$	2.7	oI40
$A_2B_5C_6$			
	$B_2La_5C_6$	6.9	tP52
$A_2B_6C_9$			
	$Ba_{0.67}B_2Pt_3$	5.6	hP12
	$Ca_{0.67}B_2Pt_3$	1.6	hP12
	$Sr_{0.67}B_2Pt_3$	2.8	hP12
$A_3B_4C_{13}$			
	$La_3Rh_4Sn_{13}$	3.2	cI320
$A_mB_nC_pD_q$			
	BNLaNi	<4.2	tP8
	$B_2Ni_2N_{2.9}La_3$	13.0	tI20
	$B_2Br_5C_6La_9$	6.6	oP46

motion hinders superconductivity. The energy scale for rotational motion is much lower than that needed to produce the large T_c's observed.

The superconducting phase has a stoichiometry of three alkali atoms for each C_{60} molecule. The mechanism of doping involves charge transfer from the alkali-atom outer shell onto the C_{60} molecule, populating the t_{1u} molecular conduction band. The alkali atoms do not possess states near the Fermi level and are thus electronically inactive. The highest reported T_c is 40 K for Cs_3C_{60}, although this material is metastable. The more stable forms K_3C_{60} (T_c = 19.5 K) and Rb_3C_{60} (T_c = 29.5 K) have properties listed in Tables 5.38 to 5.40. Ramirez (1994) has reviewed superconducting fullerenes.

Table 5.34.

AB magnet material alloys, $A(B_xC_{1-x})O_3$ tetragonal and cubic perovskites, and AB_2X_4 spinels.

Type	Compound	T_c	Structure
Magnet alloy			
	Nb-Ti, 50 mole %Nb	9.5	—
	Nb-Ti, 67 mole %Nb	10.1	—
	Nb-N	10.5	—
	Nb_3Sn, A15 compound	17.9	cP8
Perovskite			
	$BaPb_{0.8}Bi_{0.2}O_3$, tetragonal	10.0	tI20
	$BaPb_{0.7}Bi_{0.3}O_3$, tetragonal	11.5	tI20
	$Ba_{0.57}K_{0.43}BiO_3$, cubic	30.0	cP5
Spinel			
	$Li_{0.75}Ti_2O_4$	13.2	cF56
	$Li_{1.03}Ti_{1.90}O_4$	12.3	cF56
	CuV_2S_4	4.5	cF56
	$CuRh_2S_4$	4.4	cF56
	$CuRh_2Se_4$	3.5	cF56

Table 5.35.

Properties of several heavy electron superconductors where T_c is the superconducting transition temperature, T_N is the Néel temperature, Θ_D is the Debye temperature, μ_{eff} is the effective magnetic moment, and m^*/m_e is the ratio of the effective mass to the free electron mass.

Compound	$T_c(K)$	$T_N(K)$	$\Theta_D(K)$	μ_{eff}/μ_B	m^*/m_e
$NpBe_{13}$		3.4	−42	2.76	
UBe_{13}	0.85	8.8	−70	3.1	192
UCd_{11}		5.0	−23	3.45	
UPt_3	0.43	5.0	−200	2.9	187
U_2Zn_{17}		9.7	−250	4.5	
$CeCu_2Si_2$	0.6	0.7	−140	2.6	220

Most of the data on the superconducting phase can be understood using existing strong coupling (McMillan) theory. The magnitude of T_c, which is greatest among noncuprate materials, can be understood as arising from the combined effects of (1) a large phonon frequency arising from intramolecular modes; (2) a strong electron–phonon coupling resulting from the curvature of the molecular surface, which leads to strong sp^2 hybridization among the π-orbitals of neighboring carbon atoms; and (3) a large density of states arising from the narrow bands, which is a direct result of the spatial separation between C_{60} molecules.

Table 5.36.

Properties of superconducting borocarbides RNi_2B_2C, where R = Gd–Lu, Y.

R	T_c (K)	B_{c2}(2 K) (kG)	T_N (K)	θ_c (K)	θ_{ab} (K)	θ_{ave} (K)	μ_{eff} (μ_B)	Easy axis ($T \sim T_N$)
Gd	<1.8	—	20, 14	—	—	−1	8.1	iso
Tb	<0.3	—	14.8	−60	16	0	9.8	100
Dy	6.2	4 $B \parallel c$	10.3	−82	25	1	9.8	110
Ho	8.7	5 $B \parallel c$	6, 5.5 5.0	−33	8.5	−1	10.4	110
Er	10.5	15 $B \parallel c$	6.0	−6	−7.5	−7.0	9.4	100
Tm	11.0	18 $B \perp c$	1.5	21	−36	−12	7.5	001
Yb	<0.3	—	<0.3	−63	−191	−130	4.7	001
Lu	16.1	70	—	—	—	—	—	—
Y	15.6	90	—	—	—	—	—	—

θ and μ_B values are taken from anlaysis of low field $M(T)$ data using the Curie–Weiss form $M(T)/B = \chi(T) = C/(T - \theta)$, where $C = N\mu_{eff}^2/3k_B$. θ_c and θ_{ab} values are from $\chi(T)$ data measured with $B \parallel c$ and $B \perp c$, respectively. θ_{ave} and μ_B are taken from a polycrystalline average of the $\chi(T)$ data $\chi_{ave} = (\chi_c + 2\chi_{ab})/3$.

Table 5.37.

Transition temperatures of AX_2B_2C borocarbide compounds, $LuNi_2B_2C$ type, tI12.

$X_2 \Rightarrow$ A ⇓	Rh 9	Ir 9	Ni 10	Pd 10	Pt 10	$Pt_{1.5}Au_{0.6}$ 10.3
Sc 3			15.6			
$Sc_{0.5}Lu_{0.5}$ 3			15.6			
Y 3			15.6	23.0	10.0	11.0
La 3	<4.2	<4.2	<4.2		10.0	11.0
$La_{0.5}Lu_{0.5}$ 3			14.8			
Lu 3			16.1			
$La_{0.5}Th_{0.5}$ 3			3.9			
Th 3			8.0	14.5	6.5	
Pr 3					6.0	6.5
U 3			<2.0			
Gd 3			<1.8			
Tb 3			<0.3			
Dy 3			6.2			
Ho 3			8.7			
Er 3			10.5			
Tm 3			11.0			
Yb 3			<0.3			

Table 5.38.

Solid-state parameters of two alkali metal doped fullerenes.

	K_3C_{60}	Rb_3C_{60}
Lattice properties		
fcc lattice constant a_0 (10 K)	14.25 Å	14.43 Å
Density	1.97 g/cm^3	2.23 g/cm^3
Phonon spectrum—average frequencies		
Librational mode	4 meV	—
*Inter*molecular modes		
radial	25–110 meV	—
tangential	110–200 meV	—
Bulk modulus (undoped C_{60})	18.2 GPa	—
Bulk modulus (A_3C_{60})	27 ± 1.9 GPa	21.9 ± 1.9 GPa
Electronic parameters		
n (electron density at 10 K)	4.24×10^{21} cm^{-3}	4.1×10^{21} cm^{-3}
ω_p	1.56 eV	—
$v_F = (\pi^4/3)^{1/3} k_B^2 n^{2/3} \gamma \hbar$	1.4×10^7 cm/sec	—
ρ_0 (transport—films)	~2 mΩcm	—
ρ_0 (optical)	~0.4 mΩcm	—
ρ_0 (optical)	—	0.8 mΩcm
ρ_0 (mocrowave)	0.41 mΩcm	—
ρ_0 (specific heat, H_{c2})	0.5 mΩcm	—
$N(E_F)$ (thermopower)	14.2 ± 1.1	23.2 ± 0.7
$N(E_F)$(NMR)	14.1 ± 1	23 ± 1
$N(E_F)$(ESR)	10.6 ± 3	—
$N(E_F)$ (χ_{dc})	14 ± 1	19 ± 0.6

I

Charge Transfer Organics

The great majority of organic compounds and polymers are electrical insulators, but a few of them do conduct electricity, such as salts of the compound bis(ethylenedithio)tetrathiafulvalene, which is often called BEDT-TFF. Figure 5.4 gives the structural formulas of this and other organic molecules that play the role of electron donors in conducting and superconducting organics (Ishiguro and Yamaji, 1990). The electrical properties of organic conductors are often highly anisotropic and can exhibit low dimensional behavior. Crystallographic data and transition temperatures of some of these compounds are given at the end of Chapter 6.

Table 5.39.

Superconducting state parameters of two alkali metal doped fullerenes [adapted from A. P. Ramirez, Superconductivity Rev., second issue of Vol. 1, No. 1 (1994)].

	K_3C_{60}	Rb_3C_{60}
T_c	19.5	29.5
λ (penetration depth—μSR)	4800 ± 200 Å	4200 Å
λ (optical)	800 ± 500 Å	800 ± 500 Å
λ (NMR)	6000 Å	4600 Å
ξ_0 (coherence length—χ_{ac})	35 Å	30 Å
ξ_0 (χ_{ac})	29–33 Å	—
$B_{c1}(0)$ (μSR)	4.6 mT	—
$B'_{c1}(0)$ (χ_{dc})	—	−0.28 mT/K
$B'_{c1}0)$ (χ_{dc})	−1.2 mT/K	−0.7 mT/K
$B_{c2}(0)$ (χ_{ac})	26 T	34 T
$B_{c2}(0)$ (χ_{ac})	30–38 T	—
B'_{c2} (χ_{ac})	−3.73 T/K	−3.9 T/K
B'_{c2} (χ_{ac})	-2.14 ± 0.08 T/K	—
B'_{c2} (ρ)	−1.34 T/K	
$\Delta C/T_c$	68 ± 13 mJ/mole K^2	—
$2\Delta_0/k_BT_c$ (NMR)	3.0	4.1
$2\Delta_0/k_BT_c$ (optical)	2.98	3.52
$2\Delta_0/k_BT_c$ (μSR)	—	3.6 ± 0.3
$2\Delta_0/k_BT_c$ (tunneling)	5.3 ± 0.2	5.2 ± 0.3
dT_c/da_0 (chemical subst.)	5.4 K/Å	—
dT_cdV (chemical subst.)	0.088 K/Å^3	
dT_c/dP	−7.8 K/GPa	−9.7 K/GPa
dT_c/dP	−6.3 K/GPa	—

Table 5.40.

$A_nB_{3-n}C_{60}$ alkali doped fullerene compounds, cF252.

	Na_2	K_2	Rb_2	Cs_2
Na	<2			
K	2.5	19.5	27	
Rb	2.5	23	29.5	33
Cs	10.5	24	31	47

Fig. 5.4.

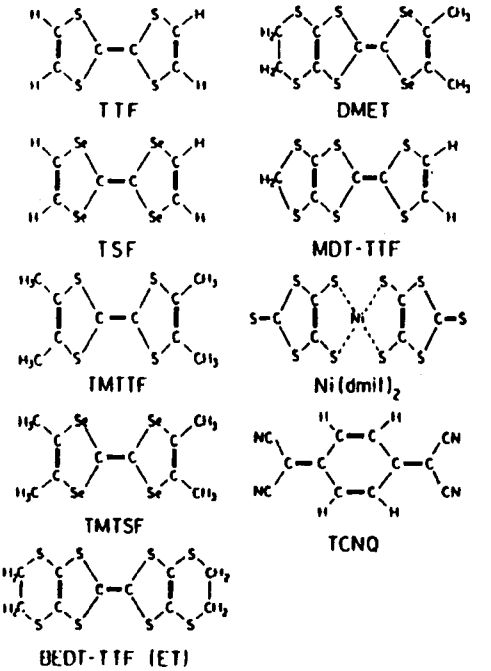

Structures of various molecules that form organic conductors and superconductors. [Ishiguro and Yamaji, 1990, p. 2.]

J

Crystal Chemistry

Villars and Phillips (1998) proposed to explain the combinations of elements in compounds that are favorable for superconductivity at relatively high temperatures by assigning three metallic parameters to each atom, namely an electron number N_e, a size r, and an electronegativity X. These atomic parameters were employed to calculate three Villars–Phillips (VP) coordinates for each compound, namely (a) an average number of valence electrons $N_v = \langle N_e \rangle_{av}$, (b) a spectroscopic electronegativity difference ΔX, and (c) a spectroscopic radius difference ΔR. The text by Phillips (1989; see also Poole *et al.*, 1995, p. 204) tabulates the VP coordinates for more than 60 superconductors with $T_c > 10$ K, and for about 600 additional ones with T_c in the range $1 < T_c < 10$ K. Various classes of superconductors with $T_c > 10$ K are found to have similar Villars–Phillips parameters.

References

R. J. Cava, B. Batlogg, J. J. Krajewski, R. Farrow, L. W. Rupp, Jr., A. E. White, K. Short, W. F. Pick and T. Kometani, *Nature* **332**, 814 (1988).

M. S. Dresselhaus and G. F. Dresselhaus, Eds., *Science of Fullerenes and Carbon Nanotubes*, Academic Press, Boston, 1996.

T. Ishiguro and K. Yamaji, *Organic Superconductors*, Springer-Verlag, Berlin, 1990.

Landolt–Bornstein, Group III: Condensed Matter, Vol. 21, *Superconductors*, Subvol. a (1990), b1 (1993), b2 (1994), c 1997), d (in preparation), and e (in preparation), R. Flükiger and W. Klose, Eds., Springer-Verlag, Berlin.

L. F. Mattheiss, either *Phys. Rev. B* **37**, 3749 (1988) or *Phys. Rev. Lett.* **60**, 2681 (1988).

A. R. Miedema, *J. Phys. (Paris)* **F3**, 1803 (1973); **F4**, 129 (1974).

J. C. Phillips, *Physics of High-T_c Superconductors*, Academic Press, New York, 1989.

C. P. Poole, Jr., T. Datta and H. A. Farach, *Copper Oxide Superconductors*, Wiley, New York, 1988.

C. P. Poole, Jr. and H. A. Farach, J. *Superconductivity* (1999), in press.

C. P. Poole, Jr., H. A. Farach, and R. J. Creswick, *Superconductivity*, Academic Press, New York, 1995.

A. P. Ramirez, *Superconductivity Review, second issue of Vol.* **1**, 1 (1994).

B. W. Roberts, *J. Phys. Chem. Ref. Data* **5**, 581 (1976).

A. W. Sleight, J. L. Gillson, and E. Bierstedt, *Solid State Commun.* **17**, 27 (1975).

P. Villars and J. C. Phillips, *Phys. Rev. B* **37**, 2345 (1988).

S. V. Vonsovsky, Yu. A. Izumov, and E. Z. Kuramev, *Superconductivity in Transition Metals*, Springer-Verlag, Berlin, 1982.

Chapter 6

Crystal Structures of Classical Superconductors

Roman Gladyshevskii
Department of Inorganic Chemistry, L'viv State University, Ukraine
Karin Cenzual
Département de Chimie Minérale, Analytique et Appliquée, Université de Genève, Switzerland

ISBN: 0-12-561460-8
$30.00
HANDBOOK OF SUPERCONDUCTIVITY

A

Introduction

a. Preliminary Remarks

Classical superconductors cover a large spectrum of chemically different compounds, ranging from alloys to chalcogenides and organic compounds, and crystallize with very different structures. The highest superconducting transition temperatures are observed among representatives of structure types such as the K_3C_{60} type with C_{60} fullerene "balls," the simple cubic Cr_3Si ($A15$) and NaCl types, the Pu_2C_3 type with C_2 dumbbells, the layered borocarbide type

$LuNi_2B_2C$, the Chevrel phases with octahedral metal atom clusters, and the perovskite type, precursor of the high-T_c superconducting oxides. When the limit in T_c is decreased, superconducting representatives are found for a relatively large number of different structure types.

The present overviews have, with a few exceptions, been restricted to structure types for which at least one compound has been reported with a critical temperature above the boiling point of helium, 4.2 K. The exceptions concern closely related structures or compounds, as well as heavy-electron compounds. Structure types represented by materials that become superconducting only under high pressure, after irradiation, or in thin films have not been taken into account. The more than 100 structure types presented here are listed in Table 6.1, ordered according to the highest temperature reported for an isotypic compound.

In the text the structures have been grouped at a first level according to the chemical family within which superconducting representatives are found. The chapter has thus been subdivided roughly into structures found among superconducting elements, intermetallics, interstitial compounds, borides and carbides, chalcogenides, and organic compounds. This classification is, however, not absolute, since the same structure type is sometimes adopted by different classes of compounds. Within each section, particular structural features, such as the substructure formed by one of the elements or selected coordination polyhedra, have been emphasized. Also, this subdivision is only approximate, since a structure type may contain both a particular substructure and a defined coordination.

Almost one century has passed since the discovery of superconductivity, and a huge amount of literature on superconductors has been published. The literature search for the preparation of this chapter was simplified by the existence of lists of superconducting compounds, such as those given in the works by B. T. Matthias *et al.* (1963), S. V. Vonsovsky *et al.* (1982), B. W. Roberts (1976), E. M. Savitsky *et al.* (1985), and L. I. Berger and R. W. Roberts (1997). A certain number of books and review articles on particular classes of superconductors were also consulted. Publications with structural data were often found via *TYPIX* (Parthé *et al.*, 1993/94; Cenzual *et al.*, 1995), *Pearson's Handbook* (Villars, 1997), or the *Inorganic Crystal Structures Database* (Kirchhoff *et al.*, 1991); however, the original papers were always examined. No claim is made on completeness; however, we hope that few structure types responding to the criteria defined here have been overlooked.

b. Structure Types and Structural Relationships

Ignoring the chemical nature of the constituents, a particular geometric arrangement of atoms is generally referred to as a *structure type*. Following recommendations of the International Union of Crystallography, to be considered as such, *isotypic* compounds should crystallize with the same space group and comparable

TABLE 6.1

Structure types for which at least one representative with critical temperature above 4.2 K has been reported.

T_c	Compound	Structure type	Strukturbericht	Pearson code	Space group
45.0	$Rb_{2.7}Tl_{2.2}C_{60}$	**K_3C_{60}**		*cF*252	$Fm\bar{3}m$
30	$Ba_{0.6}K_{0.4}BiO_3$	**$CaTiO_3$**	$E2_1$	*cP*5	$Pm\bar{3}m$
23.2	Nb_3Ge	**Cr_3Si**	*A*15	*cP*8	$Pm\bar{3}n$
23.0	YPd_2BC	**$LuNi_2B_2C$**		*tI*12	*I*4/*mmm*
18.0	$NbN_{0.75}C_{0.25}$	**NaCl**	*B*1	*cF*8	$Fm\bar{3}m$
17.0	$Y_{1.4}Th_{0.6}C_{3.1}$	**Pu_2C_3**	$D5_c$	*cI*40	$I\bar{4}3d$
15.2	$Pb_{0.92}Mo_6S_8$	**HT-$Pb_{0.9}Mo_6S_8$**		*hR*45	$R\bar{3}$
15.1	MoN	**LT-$Nb_{1-x}S$**		*hP*16	$P6_3mc$
14.0	$Mo_6S_6I_2$	**Mo_6Se_8**		*hR*42	$R\bar{3}$
13.7	$Tc_{0.82}Mo_{0.18}$	**Mg**	*A*3	*hP*2	$P6_3/mmc$
13.2	$Li_{0.75}Ti_2O_4$	**$MgAl_2O_4$**	$H1_1$	*cF*56	$Fd\bar{3}m$
13	$BaPb_{0.7}Bi_{0.3}O_3$	**Cr_3AsN**		*tI*20	*I*4/*mcm*
13	$La_3Ni_2B_2Ni_{2.91}$	**$La_3Ni_2B_2N_3$**		*tI*20	*I*4/*mmm*
13	$Li_{0.3}Ti_{1.1}S_2$	**4H-$Ti_{1+x}S_2$**		*hP*8	$P6_3mc$
12.9	$Nb_{0.24}Tc_{0.76}$	**Ti_5Re_{24}**	*A*12	*cI*58	$I\bar{4}3m$
12.9	ZrRuP	**ZrNiAl**	*C*22	*hP*9	$P\bar{6}2m$
12.5	κ-$(ET)_2Cu[N(CN)_2]Cl$	**Charge-transfer salt**		*oP*...	*Pnma*
12.5	NbPS	**NbPS**		*oI*12	*Imnm*
12.0	$Mo_{0.30}Tc_{0.70}$	**CrFe**	$D8_b$	*tP*30	$P4_2/mnm$
12.0	$Mo_{0.6}Re_{0.4}$	**W**	*A*2	*cI*2	$Im\bar{3}m$
12	Mo_2C	**ξ-Fe_2N**		*oP*12	*Pbcn*
11.9	$Lu_{0.75}Th_{0.25}Rh_4B_4$	**$CeCo_4B_4$**		*tP*18	$P4_2/nmc$
11.8	$Zr_{0.61}Rh_{0.285}O_{0.105}$	**W_3Fe_3C**	$E9_3$	*cF*112	$Fd\bar{3}m$
11.3	Zr_2Rh	**θ-$CuAl_2$**	*C*16	*tI*12	*I*4/*mcm*
11.2	$Mo_{0.85}Zr_{0.15}B_{2.5}$	**AlB_2**	*C*32	*hP*3	*P*6/*mmm*
11.1	$YCl_{0.75}Br_{0.25}$	**1s-GdCBr**		*mS*12	*C*2/*m*
11.0	$Nb_{0.51}Ir_{0.30}O_{0.19}$	**Hf_5Sn_3Cu**	$D8_8$	*hP*18	$P6_3/mcm$
11	$ZrRu_4P_2$	**$ZrFe_4Si_2$**		*tP*14	$P4_2/mnm$
10.9	$Cu_{2.76}Mo_6S_8$	**HT-$Ni_{2.5}Mo_6S_8$**		*hR*78	$R\bar{3}$
10.9	$ScTc_2$	**$MgZn_2$**	*C*14	*hP*12	$P6_3/mmc$
10.8	$Cu_{1.84}Mo_6S_8$	**LT-$Ni_{0.66}Mo_6Se_8$**		*aP*16	$P\bar{1}$
10.7	$Hf_{0.84}Nb_{0.16}V_2$	**$MgCu_2$**	*C*15	*cF*24	$Fd\bar{3}m$
10.1	$ReMgBe_{12}$	**$ThMn_{12}$**	$D2_b$	*tI*26	*I*4/*mmm*
10.0	$LuRuB_2$	**$LuRuB_2$**		*oP*16	*Pnma*
10.0	Mo_3Al_2C	**Mo_3Al_2C**		*cP*24	$P4_132$
10	YRh_4B_4	**$LuRu_4B_4$**		*tI*72	$I4_1/acd$
9.8	$Mo_6Ga_{30.75}$	**Mo_6Ga_{31}**		*mP*148	$P2_1/c$
9.7	La_3In	**Cu_3Au**	$L1_2$	*cP*4	$Pm\bar{3}m$
9.7	$ReBe_{22}$	**$ZrZn_{22}$**		*cF*184	$Fd\bar{3}m$
9.3	MoC	**WC**	B_h	*hP*2	$P\bar{6}m2$
9.1	$Y_5Os_4Ge_{10}$	**$Sc_5Co_4Si_{10}$**		*tP*38	*P*4/*mbm*
9.0	$Mo_{1.8}Rh_{0.2}BC$	**Mo_2BC**		*oS*16	*Cmcm*
8.9	$MoC_{0.67}$	**η-MoC_{1-x}**		*hP*12	$P6_3/mmc$
8.8	MoIr	**β′-AuCd**	*B*19	*oP*4	*Pmma*

(*continued*)

TABLE 6.1 (*continued*)

T_c	Compound	Structure type	Strukturbericht	Pearson code	Space group
8.7	$Ca_3Rh_4Sn_{13}$	**$Yb_3Rh_4Sn_{13}$**		*cP*40	$Pm\bar{3}n$
8.3	NbB	**α-TlI**	*B*33	*oS*8	*Cmcm*
8.1	La_3S_4	**Th_3P_4**	$D7_3$	*cI*28	$I\bar{4}3d$
7.9	Ga	**δ-Ga**		*hR*66	$R\bar{3}m$
7.8	$Mo_{0.69}Pt_{0.31}$	**LT-Mg_3Cd**	$D0_{19}$	*hP*8	$P6_3/mmc$
7.6	$LaRu_3Si_2$	**$LaRu_3Si_2$**		*hP*12	$P6_3/m$
7.6	Th_4H_{15}	**$Cu_{15}Si_4$**	$D8_6$	*cI*76	$I\bar{4}3d$
7.5	$Ag_{0.72}Ga_{0.28}$	**ξ-(AgZn)**	B_b	*hP*9	$P\bar{3}$
7.2	$LaRu_4P_{12}$	**$LaFe_4P_{12}$**		*cI*34	$Im\bar{3}$
7.2	Pb	**Cu**	*A*1	*cF*4	$Fm\bar{3}m$
7.1	$NbSe_2$	**2H-NbS_2**		*hP*6	$P6_3/mmc$
7.1	Si	**β-Sn**	*A*5	*tI*4	$I4_1/amd$
7.1	YB_6	**CaB_6**	$D2_1$	*cP*7	$Pm\bar{3}m$
7	Ba_6C_{60}	**Cs_6C_{60}**		*cI*132	$Im\bar{3}$
7	Ga	**γ-Ga**		*oS*40	*Cmcm*
7.0	$YCBr_{0.62}I_{0.38}$	**3s-GdCBr**		*mS*12	*C*2/*m*
6.9	$La_5B_2C_6$	**$La_5B_2C_6$**		*tP*52	*P*4
6.6	$Rb_{0.28}WO_3$	**Rb_xWO_3**		*hP*26	$P6_3/mcm$
6.5	ThIrSi	**LaPtSi**		*tI*12	$I4_1md$
6.5	$V_{1.06}Ru_{0.80}Rh_{0.14}$	**CsCl**	*B*2	*cP*2	$Pm\bar{3}m$
6.3	$Cs_{0.3}MoS_2$	**2H-MoS_2**	*C*7	*hP*6	$P6_3/mmc$
6.3	$NbSe_2$	**4H-$NbSe_2$**		*hP*12	$P\bar{6}m2$
6.2	Ga	**β-Ga**		*mS*4	*C*2/*c*
6.2	La_3Ni	**Fe_3C**	$D0_{11}$	*oP*16	*Pnma*
6.2	$LuRh_4B_4$	**$LuRh_4B_4$**		*oS*108	*Ccca*
6.1	$Lu_2Fe_3Si_5$	**$U_2Mn_3Si_5$**		*tP*40	*P*4/*mnc*
6	$La_9B_3C_6Br_5$	**$Ce_9B_3C_6Br_5$**		*oP*46	*Pmmn*
6.0	$RhSe_{1.75}$	**p-FeS_2**	*C*2	*cP*12	$Pa\bar{3}$
5.9	GaN	**2H-ZnS**	*B*4	*hP*4	$P6_3mc$
5.9	LaCu	**FeB**	*B*27	*oP*8	*Pnma*
5.8	$BaBi_3$	**$SrPb_3$**	$L6_0$	*tP*4	*P*4/*mmm*
5.8	In_2Bi	**Ni_2In**	$B8_2$	*hP*6	$P6_3/mmc$
5.8	$MoC_{0.5}$	**NiAs**	$B8_1$	*hP*4	$P6_3/mmc$
5.8	$Rh_{17}S_{15}$	**$Pd_{17}Se_{15}$**		*cP*64	$Pm\bar{3}m$
5.8	$Tl_2Mo_6Se_6$	**$Tl_2Fe_6Te_6$**		*hP*14	$P6_3/m$
5.8	ZrB_{12}	**UB_{12}**	$D2_f$	*CF*52	$Fm\bar{3}m$
5.7	$Ba_{0.2}(NH_3)_yMoS_2$	**3R-MoS_2**		*hR*9	*R*3*m*
5.6	$Ba_{0.67}Pt_3B_2$	**$Ba_{0.67}Pt_3B_2$**		*hP*12	$P6_3/mmc$
5.6	$In_{0.65}Sb_{0.35}$	**Cr_5B_3**	$D8_l$	*tI*32	*I*4/*mcm*
5.5	Os_4Al_{13}	**Os_4Al_{13}**		*mS*34	*C*2/*m*
5.5	YPd_2Sn	**$MnCu_2Al$**	$L2_1$	*cF*16	$Fm\bar{3}m$
5.3	Mo_3P	**Ni_3P**	$D0_e$	*tI*32	$I\bar{4}$
5.1	NbReSi	**TiFeSi**		*oI*36	*Ima*2
5.0	Mo_2N	**β-Mo_2N**		*tI*12	$I4_1/amd$
4.9	$BaGe_2$	**α-$ThSi_2$**	C_c	*tI*12	$I4_1/amd$
4.9	La	**α-Nd**	*A*3′	*hP*4	$P6_3/mmc$

(*continued*)

TABLE 6.1 (*continued*)

T_c	Compound	Structure type	Strukturbericht	Pearson code	Space group
4.9	TaRhP	**TiNiSi**		*oP*12	*Pnma*
4.8	$Nb_{0.95}Ir_{1.05}$	**CuAu**	$L1_0$	*tP*2	*P*4/*mmm*
4.7	IrGe	**FeAs**	*B*14	*oP*8	*Pnma*
4.7	$LuOs_3B_2$	**$CeCo_3B_2$**	$D2_d$	*hP*6	*P*6/*mmm*
4.6	$Nb_{0.85}Ir_{1.15}$	**TaIr**		*oP*12	*Pmma*
4.5	$Sc_4Rh_6Sn_{19}$	**$Er_4Rh_6Sn_{19}$**		*tI*232	$I4_1/acd$
4.4	$La_2Rh_3Si_5$	**$U_2Co_3Si_5$**		*oI*40	*Ibam*
4.4	LaRhSi	**ZrSO**		*cP*12	$P2_13$
4.3	$Mo_{15}Se_{19}$	**α-$Mo_{15}Se_{19}$**		*hP*68	$P6_3/m$
4.3	$Mo_{15}Se_{19}$	**β-$Mo_{15}Se_{19}$**		*hR*204	$R\bar{3}c$
4.3	$PdBi_2$	**$MoSi_2$**	$C11_b$	*tI*6	*I*4/*mmm*
4.2	Hg	**α-Hg**	*A*10	*hR*3	$R\bar{3}m$
4.1	$LaRu_2P_2$	**$CeAl_2Ga_2$**	$D1_3$	*tI*10	*I*4/*mmm*
3.9	Hg	**In**	*A*6	*tI*2	*I*4/*mmm*
3.9	YC_2	**CaC_2**	$C11_a$	*tI*6	*I*4/*mmm*
3.6	YB_2C_2	**YB_2C_2**		*tP*10	$P4_2/mmc$
3.3	$Ca_4Rh_6Pb_{19}$	**$Tb_4Rh_6Sn_{19}$**		*cF*116	$Fm\bar{3}m$
3.2	$La_3Rh_4Sn_{13}$	**$La_3Rh_4Sn_{13}$**		*cI*320	$I4_132$
1.1	Ga	**α-Ga**	*A*11	*oS*8	*Cmca*
1.0	UBe_{13}	**$NaZn_{13}$**	$D2_3$	*cF*112	$Fm\bar{3}c$
...	$BaMo_6S_8$	**LT-$BaMo_6S_8$**		*aP*15	$P\bar{1}$
...	LuNiBC	**LuNiBC**		*tP*8	*P*4/*nmm*

unit cells. The atoms should in addition occupy the same Wyckoff positions (see later definition) with similar numerical values for the coordinates. As a consequence, the atomic environment (coordination) of all atoms should be similar in both structures and the same general description can be applied to all representatives of the structure type. In a strict definition, the composition is also taken into consideration and different substitution variants are considered as distinct types. Within this review, differently ordered or partly ordered derivatives have, however, generally been considered together when the overall symmetry remains the same (e.g. $CaCu_5$ and $CeCo_3B_2$). The same is true for structures with localized or delocalized atoms, in particular since only a complete structure determination can tell the exact position of the atoms. For certain families, such as the intercalation compounds, no distinction has been made between structures with and without interstitial atoms, which, from a formal point of view, crystallize with different structure types. The concept of structure type is very useful among inorganic structures, where the number of isotypic compounds may be very high; however, no attempt was made to try to apply similar classification criteria to the few organic salts presented here. Structure types are generally named after the compound for which this particular atom arrangement was reported for the first time.

Some 10,000 structure types are known for inorganic compounds and the comparison of different types often reveals similar geometrical features. Structure types may, for instance, be related to each other by simple relations such as deformation, substitution, or filling up of vacancies. A deformation may cause a lowering of the symmetry; for example, the orthorhombic FeAs type is a deformation derivative of the hexagonal NiAs type. Partial substitution of one element by another in a particular ratio commonly leads to an ordered atom distribution. The resulting structure may respect the original symmetry, as is the case for α-Mn and Ti_5Re_{24}, or break some of the symmetry elements present in the parent type. For example, on replacing half of the nonmetal atoms in α-$ThSi_2$ to obtain the LaPtSi type, one of the mirror planes is lost. A particular case of substitution occurs when a pair of atoms replaces one atom. An example of such a relationship is found between Sc_4C_3 with single carbon atoms (Th_3P_4 antitype) and Pu_2C_3 with carbon atom dumbbells. Several structure types present vacancies large enough to host additional atoms. In the Chevrel phases, for example, the large cavities in the Mo_6Se_8 type are occupied by cations. The superconducting nitrides and carbides crystallizing with NaCl-type structures are generally considered as interstitial compounds, whereas the layered structures found with chalcogenides are known to form a large number of intercalation derivatives, sometimes hosting very thick layers of molecules between the chalcogenide slabs. Structural units with common geometric features are often recognized in different structures; for example, $CaTiO_3$ and $LaFe_4P_{12}$ both contain frameworks of corner-sharing octahedra. When two structures can be decomposed into the same kind of subunit, arranged in different ways, they are considered as stacking variants. The types FeB and α-TlI represent two different ways to stack a several-angstrom thick structural slab of interconnected trigonal prisms. Two or more kinds of subunit may be present in different proportions in several structures, and a series of intergrowth structures may be considered. This is the case for some of the superconducting borocarbides and boronitrides, which are conveniently decomposed into two different kinds of slab. Finally, larger units may be packed in the same way as smaller units; for example, in one of the fulleride structures fullerene molecules and alkaline-earth cations adopt the same arrangement as the single atoms in intermetallic Cr_3Si.

c. Atom Coordinations

The stability of a structure is deduced from its overall band structure, but at the very local level, each individual atom in a structure will try to accommodate itself to satisfy a series of criteria. These criteria represent a combination of constraints due to covalent bonding, local electroneutrality, and space-filling. An atom connected to the surrounding atoms by covalent bonds will have a well-defined coordination that can suffer relatively little distortion. On the other extreme, a highly ionized atom has less demand on the shape of the cavity in which it is

located. For alloys, optimal space filling is generally the dominating criterion and the *coordination number*, that is, the number of nearest neighbors, increases with the atomic radius. Small atoms in large interstices are often delocalized over several off-centered positions.

Crystal structures rapidly become complex, and a description emphasizing particular coordination polyhedra helps in visualizing and memorizing a structure and finding relations between different structures. Examples of coordination polyhedra that are commonly observed in crystal structures of inorganic compounds are presented in Fig. 6.1. It may be noted that it is not always easy to decide how many atoms belong to the first coordination sphere. There is also a certain amount of subjectivity in the labeling of the polyhedron. For instance, a distorted polyhedron built up by eight atoms can be considered as a bicapped trigonal prism, but also as a square antiprism. In the same way, an octahedron elongated or compressed along one of its 4-fold axes is still called an octahedron, whereas if the deformation takes place along one of the 3-fold axes, it is generally referred to as a trigonal antiprism. Straight trigonal prisms are frequent in intermetallic compounds, such as borides, and silicides. In this case, the first coordination sphere often includes atoms capping the rectangular faces, sometimes located at a shorter distance from the central atom than the prism-forming atoms. For a better visualization of the structure, the capping atoms are, however, generally omitted in the description. The largest atom coordination presented here, the 16-vertex Frank–Kasper polyhedron, is conveniently decomposed into a truncated tetrahedron (a polyhedron, obtained by cutting the 4 vertices of a tetrahedron, with 12 vertices and 4 hexagonal and 4 triangular faces) and a tetrahedron formed by atoms capping the 4 hexagonal faces of this. Coordination numbers exceeding 20 are found in some intermetallic compounds combining atoms of very different sizes.

d. Definitions and Conventions

A crystallographic data set contains information about the cell parameters (the edge lengths and the angles of the unit cell), the coordinates of the atoms in the asymmetric unit (a representative triplet $x\ y\ z$ for each atom site), and the space group symbol. The *International Tables for Crystallography (Volume A)* (Hahn, 1983) defines how to choose the unit cell with respect to the symmetry operations in each of the 230 possible space groups. By consulting the lists of equivalent triplets in the *International Tables for Crystallography*, the coordinates of any atom in the structure can be derived from this condensed information. Distinction is made between atom sites in general position (site symmetry 1) and atom sites in special position, that is, situated on one or several symmetry elements. Within each space group the general and the special positions are defined by the so-called *Wyckoff letters*, which are lowercase letters starting from *a* for the highest site symmetry. The Wyckoff letter is generally preceded by the corre-

Fig. 6.1.

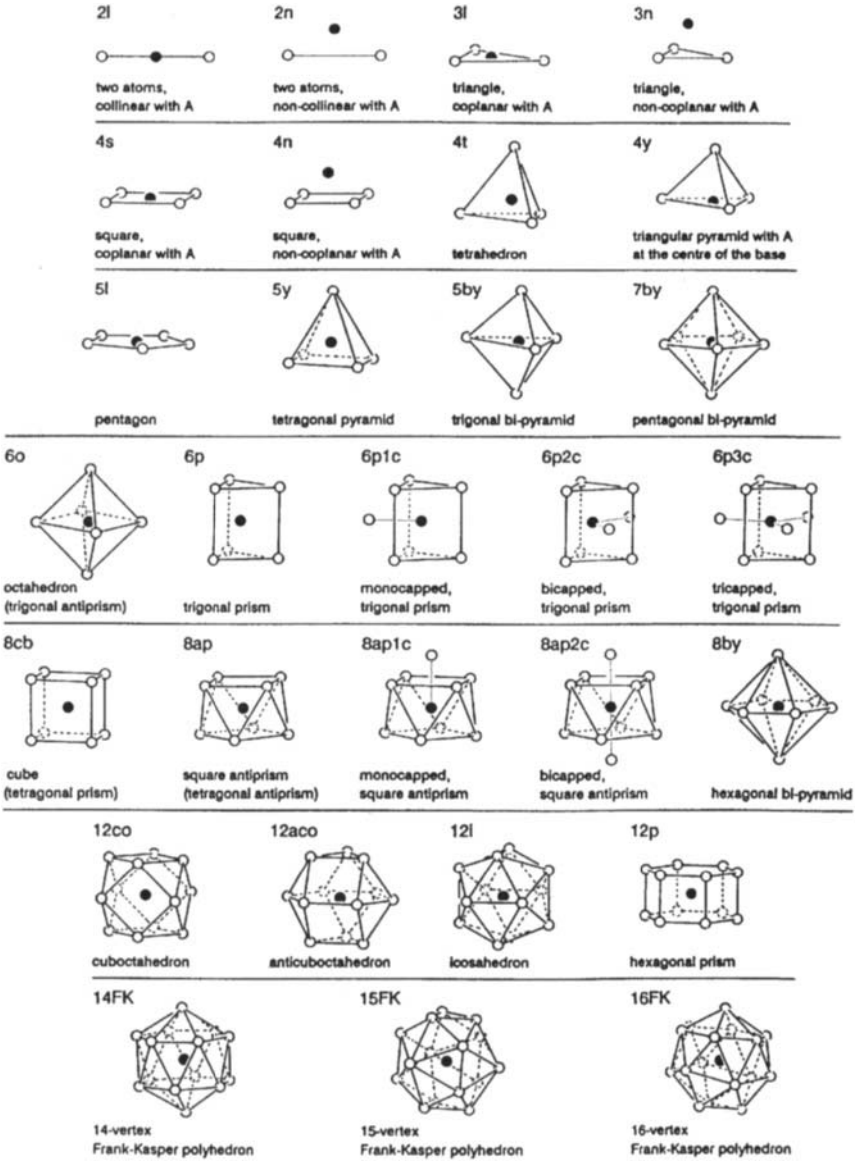

Coordination polyhedra commonly observed in structures of inorganic compounds.

sponding *site multiplicity*, the number of symmetry-related atoms in the unit cell belonging to this site, to define together the *Wyckoff position*. The multiplicity of a special position is always a fraction of the multiplicity of the general position. For atoms in special positions, all or part of the coordinates are fixed, either to particular values (e.g., 0 $\frac{1}{2}$ 0), or with respect to each other (e.g., x $2x$ z). As an example, the atom site given as Cu(2) in 4(*c*) with the triplet 0.175 $\frac{1}{4}$ 0.061 in space group *Pnma* (No. 62 in the *International Tables for Crystallography*) designates four atoms in the unit cell with the following fractional coordinates: $Cu(2)_1$ at 0.175 $\frac{1}{4}$ 0.061, $Cu(2)_2$ at 0.325 $\frac{3}{4}$ 0.561, $Cu(2)_3$ at 0.825 $\frac{3}{4}$ 0.939, and $Cu(2)_4$ at 0.675 $\frac{1}{4}$ 0.439. The atom site given as W in 6(*c*) with the triplet 0 0 0.176 in space group $R\bar{3}m$ (No. 166, hexagonal axes) defines the positions of six atoms in the unit cell: W_1 at 0 0 0.176, W_2 at 0 0 0.824, W_3 at $\frac{2}{3}$ $\frac{1}{3}$ 0.509, W_4 at $\frac{2}{3}$ $\frac{1}{3}$ 0.157, W_5 at $\frac{1}{3}$ $\frac{2}{3}$ 0.843, W_6 at $\frac{1}{3}$ $\frac{2}{3}$ 0.491, considering the translations characteristic of a rhombohedral lattice.

However, even when the symmetry elements are located in agreement with the *International Tables for Crystallography*, there exists more than one way to present the same crystal structure. In order to facilitate the recognition of isotypic compounds, a standardization procedure was developed in Geneva (Parthé and Gelato, 1984, 1985; Parthé *et al.*, 1993). This procedure applies a series of criteria for the choice of the space group setting (e.g., setting *Pnma* is preferred to *Pmnb* with interchanged axes), the cell parameters (important for monoclinic and triclinic symmetry), the origin of the cell (considering space-group-permitted origin shifts), and the representative triplets. All complete crystallographic data sets given in Section J have been standardized.

One of the more common classification schemes applied to structures of intermetallic compounds uses the so-called *Pearson code*. Two letters and a number compose this code, for example, *hP*12. The lowercase letter indicates the crystal system: *a*, anorthic (triclinic); *m*, monoclinic; *o*, orthorhombic; *t*, tetragonal; *h*, hexagonal and trigonal; *c*, cubic. The uppercase letter stands for the Bravais lattice: *P*, primitive (a lattice point at 0 0 0); *S*, side-face centered (for instance, *C*-centered—0 0 0, $\frac{1}{2}$ $\frac{1}{2}$ 0); *R*, rhombohedral (0 0 0 $\frac{2}{3}$ $\frac{1}{3}$ $\frac{1}{3}$, $\frac{1}{3}$ $\frac{2}{3}$ $\frac{2}{3}$); *F*, face-centered (0 0 0, 0 $\frac{1}{2}$ $\frac{1}{2}$, $\frac{1}{2}$ 0 $\frac{1}{2}$, $\frac{1}{2}$ $\frac{1}{2}$ 0); or *I*, body-centered (0 0 0 and $\frac{1}{2}$ $\frac{1}{2}$ $\frac{1}{2}$). The number corresponds to the number of atoms in the unit cell. For structures with vacancies we have replaced this number by the sum of multiplicities of all partly and fully occupied atom sites, when full occupation is not impeded by impossibly short distances.

Since the atoms in isotypic compounds must occupy the same Wyckoff positions, the so-called *Wyckoff sequence*, the sequence of Wyckoff letters of all atom sites in the structure, becomes an important feature for the recognition of isotypic structures. The two different layered structure types, 2H-MoS_2 and 2H-NbS_2, for example, have similar unit cells and are described in the same space group, $P6_3/mmc$. Structures crystallizing with one or the other modification may be identified from the Wyckoff sequence, which is *fc* for the former type and *fb* for the latter. It must be emphasized that Wyckoff sequences can only be

compared for standardized data, since it is often possible to "move" an atom from one Wyckoff position to another by shifting the whole structure by a space-group-permitted origin shift (e.g., by 0 0 $\frac{1}{2}$ in many space groups). The letters in the Wyckoff sequence are written in inverse alphabetic order. When several atom sites occupy the same Wyckoff position, the corresponding letter is followed by the number of times the particular position is present, written as a superscript (e.g., g^2db).

e. Strukturbericht Notation for Structure Types

Strukturberichte is the German-speaking predecessor of the *Structure Reports*, which were published yearly for the *International Union of Crystallography* until 1990. The usefulness of grouping compounds crystallizing with similar atom arrangements appeared early and a coding system for structure types was already being used in the first volume of *Strukturberichte*, edited in 1931. The notation starts with an uppercase letter, giving information about the ideal composition, or the family of compounds. The letter *A* was assigned to element types, e.g., *A*1 to Cu, *A*2 to W, *A*3 to Mg. The number following the letter is here a simple ordering number, assigned to chronology of discovery. Historical reasons are behind the fact that the structure type Cr_3Si, well-known among binary superconductors, is referred to as *A*15. The code was indeed originally assigned to the so-called β-modification of elementary W, which was later shown to be an oxide. The letter *B* was chosen for the ideal element ratio 1 : 1, *C* for the ratio 1 : 2, *D* for other binary compounds, etc., whereas *L* was reserved for alloy structures. In the second volume of *Strukturberichte* the notation was slightly modified and subscripts were introduced to allow for a finer subdivision. A certain number of already-known structure types changed codes, e.g., the code of cubic perovskite was modified from *G*5 to $E2_1$, and that of Cu_3Au from *L*12 to $L1_2$. However, it rapidly became clear that the number of existing structures and their complexity were far beyond the limits of such a simple classification system. The coding was not continued in *Structure Reports*, but a few authors went on extending the list of codes for some time, in particular for intermetallic compounds. These more recent codes may be recognized by subscripts containing lowercase letters. It may be noticed that, because of the difficulty of recognizing isotypic structures described in different settings, two or more codes have in some cases been assigned to the same atom arrangement. After a closer comparison of the crystal structures, the codes *B*31 (MnP) and B_d (NiSi), for instance, turned out to be synonyms of *B*14, defined on FeAs. In the literature, different substitution variants are often grouped under the same notation and, for example, the binary χ phases are often referred to as *A*12 (elementary α-Mn). In a similar way, interstitial compounds are often referred to by the Strukturbericht notation defined on the parent type. A list of Strukturbericht notations defined on structure types treated here is given in Table 6.2.

TABLE 6.2

Strukturbericht notations for structure types.

Strukturbericht	Structure type	Strukturbericht	Structure type
*A*1	**Cu**	*C*14	**$MgZn_2$**
*A*2	**W**	*C*15	**$MgCu_2$**
*A*3	**Mg**	*C*16	**θ-$CuAl_2$**
*A*3′	**α-Nd**	*C*22	Fe_2P (**ZrNiAl**)
*A*5	**β-Sn**	*C*32	**AlB_2**
*A*6	**In**	C_c	**α-$ThSi_2$**
*A*10	**α-Hg**	$D0_2$	$CoAs_3$ (**$LaFe_4P_{12}$**)
*A*11	**α-Ga**	$D0_3$	BiF_3 (**$MnCu_2Al$**)
*A*12	α-Mn (**Ti_5Re_{24}**)	$D0_{11}$	**Fe_3C**
*A*13	β-Mn (**Mo_4Al_2C**)	$D0_{19}$	**LT-Mg_3Cd**
*A*15	**Cr_3Si**	$D0_e$	**Ni_3P**
A_a	α-Pa (**In**)	$D1_3$	$BaAl_4$ (**$CeAl_2Ga_2$**)
A_b	β-U (**CrFe**)	$D2_1$	**CaB_6**
*B*1	**NaCl**	$D2_3$	**$NaZn_{13}$**
*B*2	**CsCl**	$D2_b$	**$ThMn_{12}$**
*B*4	**2H-ZnS**	$D2_d$	$CaCu_5$ (**$CeCo_3B_2$**)
$B8_1$	**NiAs**	$D2_f$	**UB_{12}**
$B8_2$	**Ni_2In**	$D5_c$	**Pu_2C_3**
*B*14	**FeAs**	$D7_3$	**Th_3P_4**
*B*15	**FeB**[a]	$D8_6$	**$Cu_{15}Si_4$**
*B*19	**β′-AuCd**	$D8_8$	Mn_5Si_3 (**Hf_5Sn_3Cu**)
*B*27	**FeB**	$D8_b$	**CrFe**
*B*31	MnP[b]	$D8_l$	**Cr_5B_3**
*B*33	**α-TlI**	$E2_1$	**$CaTiO_3$**
B_b	**ξ-(AgZn)**	$E9_3$	**W_3Fe_3C**
B_f	CrB[c]	$H1_1$	**$MgAl_2O_4$**
B_h	**WC**	$L1_0$	**CuAu**
*C*2	**p-FeS_2**	$L1_2$	**Cu_3Au**
*C*7	**2H-MoS_2**	$L2_1$	**$MnCu_2Al$**
$C11_a$	**CaC_2**	$L6_0$	**$SrPb_3$**
$C11_b$	**$MoSi_2$**	*L*′3	ε-$FeN_{0.5}$ (**NiAs**)

[a]Superseded structure proposal; see *B*27.
[b]Isotypic with FeAs, *B*14.
[c]Isotypic with α-TlI, *B*33.

B

Elements

a. Close-Packed Element Structures

At ambient temperature and pressure the metal elements, which represent some 80% of all chemical elements, crystallize with a small number of different

structure types. The majority of them adopt structures that can be assimilated to the packing of solid spheres. Balls on a flat surface will arrange themselves so that six of these surround each ball. Most metal atoms do likewise, forming so-called close-packed layers. One such layer is shown in the upper part of Fig. 6.2. To achieve an optimal space filling, identical layers are stacked in a way that the atoms of one layer are placed over the triangular voids of the other layer. Since there are twice as many voids as atoms, there are two possibilities for placing the second layer. If we fix one atom from the first layer at 0 0 z_1 referring to a hexagonal unit cell, we can stack the next layer so that there is an atom at $\frac{1}{3}\ \frac{2}{3}\ z_2$, or shift the layer slightly along the long diagonal of the cell so that there is an atom at $\frac{2}{3}\ \frac{1}{3}\ z_2$. These three possibilities for placing a layer are generally referred to as *A*, *B*, and *C*. Any stacking sequence of close-packed layers is in principle possible, but only the simplest ones are found among the element structures.

By shifting consecutive layers alternatively forwards and backwards along the long diagonal of the hexagonal cell indicated at the top of Fig. 6.2, the atom arrangement shown on the lower left, corresponding to the structure type defined on **Mg**, is obtained. The overall symmetry is hexagonal and the unit cell contains two atoms. The structure may be described by placing one atom at 0 0 0 and the other at $\frac{1}{3}\ \frac{2}{3}\ \frac{1}{2}$; however, in agreement with the *International Tables for Crystallography*, space group $P6_3/mmc$, the origin of the cell is shifted so that the two atoms have the coordinates $\frac{1}{3}\ \frac{2}{3}\ \frac{1}{4}$ and $\frac{2}{3}\ \frac{1}{3}\ \frac{3}{4}$. The stacking mode where a layer is sandwiched between two layers shifted in the same direction (e.g., *ABA*, *CBC*) is

Fig. 6.2.

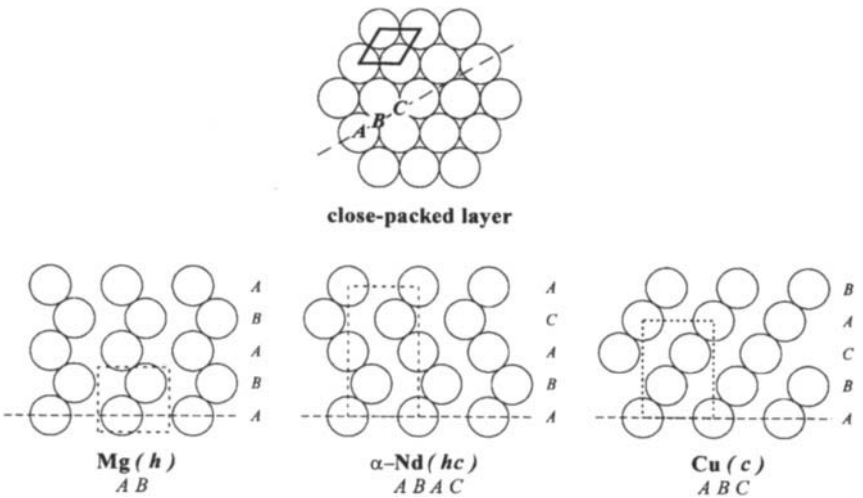

Close-packed layer, letters *A*, *B*, and *C* indicate the three possible stacking positions; atoms in the (1 1 0) cross-section of the close-packed element structures **Mg**, **α-Nd**, and **Cu** (referring to hexagonal setting).

called hexagonal, abbreviated *h*. The Mg type is often referred to as *hexagonal close-packed*, h.c.p. Derived structures are sometimes preceded by the specification 2H, where the digit indicates the number of layers in the translation unit and H stands for hexagonal.

If, in contrast, consecutive layers are always shifted in the same direction along the diagonal of the hexagonal cell, the translation unit in the stacking direction will correspond to three layers, as sketched at the lower right of Fig. 6.2. The overall symmetry of this structure type, defined on **Cu**, is cubic. The conventional unit cell is face-centered with atoms located at the vertices of the cube and the centers of the cube faces. Figure 6.3 shows a portion of such an atom arrangement corresponding to several unit cells. One of the corners of the large cube has been cut to evidence the close-packed layers perpendicular to [1 1 1]. Note that, in agreement with the cubic symmetry, similar layers are found also perpendicular to the other body diagonals i.e., [−1 1 1], [1 −1 1], and [1 1 −1]. The structure type is also referred to as *face-centered cubic* (f.c.c.), *cubic close-packed* (c.c.p.), or 3C. A close-packed layer sandwiched between two layers shifted in opposite directions (e.g., *ABC*, *BAC*) is considered to be *c*-stacked. It may be noted that in the more general case, where the interatomic distances within and between the layers are not identical, the overall symmetry is trigonal with an *R* (rhombohedral) lattice (atoms at 0 0 0, $\frac{2}{3}$ $\frac{1}{3}$ $\frac{1}{3}$, and $\frac{1}{3}$ $\frac{2}{3}$ $\frac{2}{3}$ in the triple hexagonal cell). The overall stacking is then referred to as 3R.

A third variant of stacking of close-packed layers, shown at the lower center position of Fig. 6.2, is labeled after **α-Nd**. This stacking is a combination of the

Fig. 6.3.

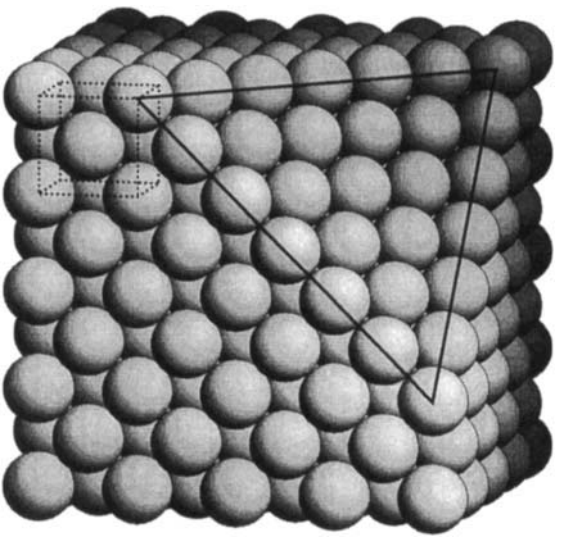

Cubic close-packed, i.e., f.c.c., atom arrangement (**Cu** type). One corner of a large cube is cut to emphasize the close-packed layers perpendicular to the body diagonal.

two modes described previously, since consecutive layers are alternately shifted in the same and in opposite directions (*ABAC*). The overall stacking is consequently called *hc*. The resulting structure is hexagonal and the translation unit in the stacking direction corresponds to four layers. The type is sometimes referred to as d.h.c.p. (*double hexagonal close-packed*).

Since the stacking is defined by the relative shift along the diagonal of the hexagonal cell, structures with close-packed layers are conventionally represented by the atoms in the cross-section (1 1 0). Cross-sections of the three structures just described are presented in Fig. 6.2. Note that a projection of all atoms in the structure onto the same plane would contain twice as many circles. Independently of the stacking sequence, each atom has, in addition to six atoms in the close-packed layer, three near neighbors in each of the adjacent layers. In the case of a *c*-stacked layer, the twelve atoms form the cuboctahedron sketched in Fig. 6.1. For an *h*-stacked layer the top and bottom triangles have the same orientation and the polyhedron is called an anticuboctahedron, also sketched in Fig. 6.1.

The highest superconducting transition temperature observed for an element in close-packed arrangement is reported for technetium, which crystallizes with a Mg-type structure. The transition temperature was earlier reported as 11.2 K, but is now generally accepted to be 7.9 K, the actual value depending strongly on the purity. Isotypic Re and α-Tl are superconducting at lower temperatures. Relatively high critical temperatures for Cu-type stacking are reached by Pb (7.2 K) and β-La (6.1 K). Superconductivity is also observed for another modification of the latter element, α-La with an α-Nd-type structure (4.9 K).

b. Other Element Structures

Another very simple structure type, defined in **W** (also called α-Fe) is adopted by all alkaline metal elements and a certain number of transition elements. The cubic, body-centered unit cell contains two atoms, located at the origin and the center (0 0 0, $\frac{1}{2}$ $\frac{1}{2}$ $\frac{1}{2}$), corresponding to Fig. 6.4a with $a_1 = a_2 = a_3$. Eight atoms forming a cube surround each atom. The type is generally referred to as b.c.c., but it should be noted that the term *body-centered cubic* may also be applied to any crystal structure that has a body-centered cubic translation lattice: for example, $La_3Rh_4Sn_{13}$, the cubic unit cell of which contains 320 atoms. The same remark is also valid for the term f.c.c., designating the Cu type. Figure 6.4 illustrates the close relationship that exists between a cubic body-centered (left) and a cubic close-packed (right) atom arrangement. The projections along one of the cell edges show identical square-mesh patterns; however, the ratios of the translation units perpendicular to and in the plane of projection are different. It is thus possible to go from the b.c.c. W type to the f.c.c. Cu type by extending the structure by a factor of $\sqrt{2}$ along one of the 4-fold axes.

Fig. 6.4.

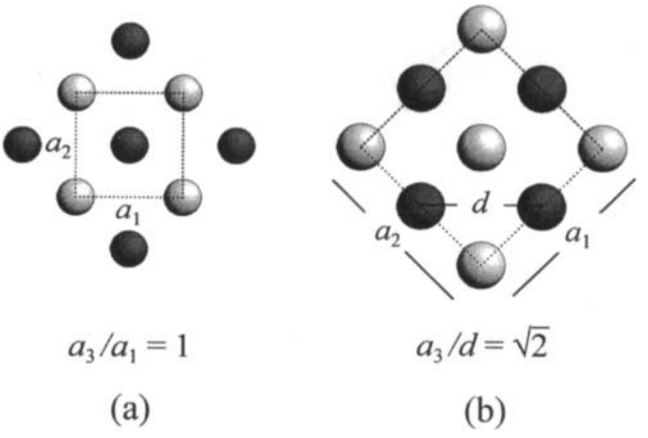

Structures of Nb (**W** type, b.c.c.) (a) and β-La (**Cu** type, f.c.c.) (b) in projections along [0 0 1]. Dark shading: $z = \frac{1}{2}$; light shading: $z = 1$. For both structures $a_1 = a_2$.

The superconducting transition temperature of the W-type element Nb, 9.3 K, is the highest observed for an element at ambient pressure. Isotypic V and Ta, with the same number of valence electrons, become superconducting around 5 K. β-Zr may be stabilized by the presence of, for example, Rh, and then undergoes a transition to a superconducting state at 6.5 K. A comparison of critical temperatures reported for different elements early revealed a correlation between T_c and the valence electron concentration. The critical temperatures of the transition elements and their solid solutions as a function of the number of valence electrons show well-defined maxima around 4.65 and 6.5 electrons per atom. It has been pointed out that the same values characterize the borders of the stability domain of the W-type atom arrangement, in competition with the hexagonal Mg type on both sides.

The nonmetals tend to complete their electron octet by forming covalent bonds. As expected, no superconductivity is observed for nonmetals at ambient pressure. Near the zigzag Zintl line, which draws a rough border between metals and nonmetals in the periodic table, structures related to the metal element structures, but with a tendency toward partly localized bonding, are formed. Mercury occupies a particular position in the history of superconductivity, since the phenomenon was discovered during low-temperature studies of this element, for which the superconducting transition takes place at 4.2 K. The structure of **α-Hg** may be considered as a deformation variant of the cubic close-packed Cu type. The rhombohedral unit cell contains one atom, but it is usual to represent the structure referred to its triple hexagonal cell (c-axis along the body diagonal of the rhombohedral cell). The c/a ratio of the hexagonal cell of α-Hg is 1.93, i.e., significantly lower than $\sqrt{6} = 2.45$, corresponding to the Cu type described in a similar hexagonal cell. As a consequence, the distances between atoms in

neighboring layers are shorter than the interatomic distances within the layers. The 12 atoms of the original cuboctahedron in the Cu type are subdivided into 6 atoms at a shorter distance, forming a trigonal antiprism, and 6 atoms at a longer distance.

The tetragonal structure of **In** represents a different deformation variant of the Cu type. The originally close-packed structure is here extended along one of the 4-fold axes. Described in a tetragonal face-centered cell similar to the cubic cell of Cu, the c/a ratio is 1.08. However, following crystallographic conventions, tetragonal face-centered cells are reduced to body-centered cells and the structure is correctly described in a tetragonal cell with one atom at the origin and one atom at the center. The c/a ratio of the body-centered cell, 1.52, should here be compared with $\sqrt{2} = 1.41$ to estimate the deformation. The 12 atoms of the original cuboctahedron are subdivided into 4 atoms at a shorter distance, forming a square, and 8 atoms at a longer distance. Indium itself becomes superconducting at 3.4 K, but the highest T_c for this structure type is observed for a second modification of mercury. The cell parameter ratio of β-Hg is significantly lower than unity and the coordination polyhedron is reduced to a compressed tetragonal prism, with two additional atoms capping the square faces. This structure is better seen as a deformation derivative of W and may be classified under the corresponding branch of the structure type, defined on α-Pa.

The semiconducting, gray α-modification of tin crystallizes with the cubic diamond structure, where each atom is covalently bonded to four others situated at the corners of a tetrahedron. White **β-Sn** has metallic character and becomes superconducting at 3.7 K. This structure is tetragonal, with four atoms in the unit cell. The coordination number is 6 and the six-vertex polyhedron can be described as a distorted octahedron formed by a heavily compressed tetrahedron and two additional atoms at a slightly longer distance. The elements Si and Ge from the same group IVB crystallize with this structure type at high pressure. The quenched samples show superconducting transition temperatures of up to 7.1 K at 13.6 GPa for Si. Equiatomic mixtures of elements from the surrounding columns IIIB and VB of the periodic table, like GaSb and InSb, adopt the same structure type within certain ranges of pressure and become superconducting at 4.2 and 2.1 K, respectively.

Gallium presents several superconducting structural modifications. The structure of the orthorhombic ambient-pressure modification **α-Ga** contains strongly puckered close-packed layers. Each atom has seven nearest neighbors, one in either the over- or underlying layer and six within the same layer. The distance to the atom in the neighboring layer is shorter (2.48 Å) than that to the other atoms, so that Ga–Ga pairs are sometimes considered. This structure modification becomes superconducting at a modest temperature of 1.1 K, whereas critical temperatures increasing from 6.2 to 7.9 K are observed for the metastable modifications β, γ, and δ. In monoclinic **β-Ga** the atoms are arranged in infinite zigzag chains with interatomic distances of 2.68 Å. Six additional atoms are located around each atom at distances ranging from 2.77 to 2.92 Å. The

relatively complex structures of orthorhombic **γ-Ga** and rhombohedral **δ-Ga** contain six and five crystallographically independent atom sites, respectively, with different coordinations and nearest neighbors distributed over a range of distances between 2.57 and 3.19 Å.

The α-Mn and β-U types are discussed in the section on intermetallic compounds, referring to their substitution derivatives, Ti_5Re_{24} and CrFe.

C

Intermetallic Compounds

a. Close-Packed Structures

When the difference in atom size or electronegativity is not excessive, binary alloys form close-packed structures following the principles described for the elements. Partial or complete ordering is often observed around particular compositions such as 1 : 1, 2 : 1, or 3 : 1. The degree of ordering decreases with increasing temperature and an order–disorder phase transition is sometimes observed. Common atom distributions found within close-packed layers of compositions 1 : 1 and 3 : 1, respectively, are shown in Fig. 6.5. The first ordering pattern (left) is observed in the structure types **β′-AuCd**, **CuAu** and **TaIr**. The close-packed layers in orthorhombic β′-AuCd are arranged in *h* stacking, which means that it is an ordered substitution derivative of the Mg type. Tetragonal CuAu is an ordered substitution derivative of Cu (*c* stacking), whereas orthorhombic TaIr represents a new kind of stacking, *hcc*, also written as hc_2. For all three structure types the highest superconducting transition temperatures are reported for Ir-based alloys: MoIr (8.8 K), $Nb_{0.95}Ir_{1.05}$ (4.8 K), and $Nb_{0.85}Ir_{1.15}$ (4.6 K). The second pattern, shown on the right in Fig. 6.5, is found in hexagonal **LT-Mg_3Cd** and cubic **Cu_3Au** (Fig. 6.6). It corresponds to a homogenous distribution of the atoms of the minority element, which tend to be as distant as possible from each other. The close-packed layers in LT-Mg_3Cd are arranged in *h* stacking, those in Cu_3Au in *c* stacking. The former structure type is represented here by slightly off-stoichiometric $Mo_{0.69}Pt_{0.31}$ (7.8 K) and stoichiometric La_3Al (5.8 K). The Cu_3Au type is widespread among both superconducting and nonsuperconducting phases. Relatively high transition temperatures are observed for phases containing La or Pb, two elements that crystallize with the parent Cu element structure, the highest value being reported for La_3In (9.7 K). T_c as a function of the valence electron concentration shows an oscillatory dependence.

The **$SrPb_3$** type is a deformation variant of the Cu_3Au type. A slight elongation or compression of the Cu_3Au structure in the direction of one of the 4-fold axes results in a lowering of the symmetry to tetragonal. $BaBi_3$, which becomes superconducting at 5.8 K, crystallizes with this type. It may be noted

Fig. 6.5.

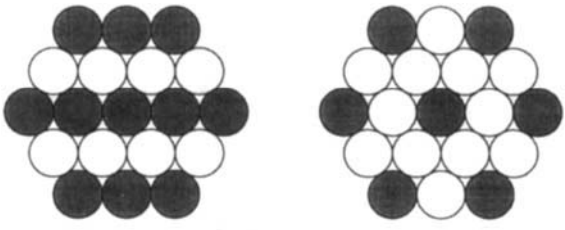

Atom distributions commonly observed in close-packed layers of element ratios 1 : 1 (*left*) and 3 : 1 (*right*), respectively.

Fig. 6.6.

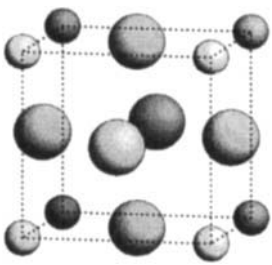

Structure of La_3In (**Cu_3Au** type), content of one unit cell. Large spheres: La; small spheres: In.

that structures isotypic with CuAu are often described with a pseudocubic cell containing four atoms, similar to the cell of $SrPb_3$, and the space group is given as $P4/mmm$. However, for this particular atom ordering, atoms of the same kind occupy positions 0 0 0 and $\frac{1}{2}$ $\frac{1}{2}$ 0, which means that the tetragonal cell is in fact C-centered. Tetragonal C-centered cells are conventionally reduced to primitive cells with half cell volume, which leads to the description with two atoms in the unit cell given in Section J.

b. CsCl Type and Related Structures

The cubic **CsCl** type, shown in Fig. 6.7a, is an ordered substitution derivative of the W type. The structure is easily visualized as being built up by $CsCl_8$ cubes sharing all faces. The two atom positions are equivalent, and from a geometric point of view the structure can also be described as a 3D array of face-sharing $ClCs_8$ cubes. CsCl is a "universal" structure type, adopted by compounds ranging from pure alloys to ionic salts. Relatively few superconductors are

Fig. 6.7.

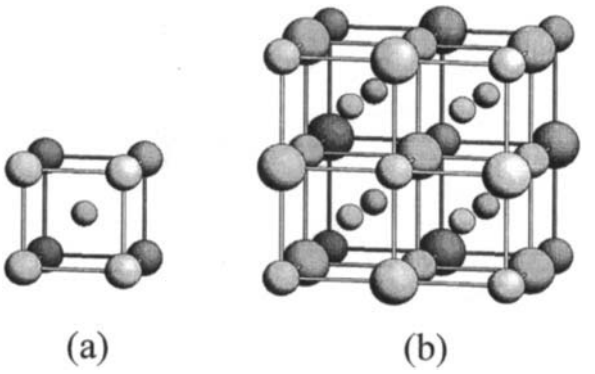

Structures of VRu (**CsCl** type) (a) and YPd_2Sn (**$MnCu_2Al$** type) (b), content of one unit cell each. Large spheres: Y; medium spheres: V, Sn; small spheres: Ru, Pd.

reported with this type, which is generally considered to be unfavorable for superconductivity. As an exception to the rule, $V_{1.09}Ru_{0.91}$ becomes superconducting at 5.2 K. At the equiatomic composition VRu, approximately one-third of the sample was found to adopt a tetragonally distorted structure. The temperature range for the phase transformation appears to be very broad and is shifted toward higher temperatures for a higher Ru content. A partial substitution of Ru by Rh increases the superconducting transition temperature to 6.5 K.

Substitution variants of the W type with an ideal element ratio of 2 : 1 are defined on so-called **ξ-(AgZn)** and **$MoSi_2$**. The former has trigonal and the latter tetragonal symmetry. Only one superconducting phase isotypic with ξ-(AgZn) has been reported so far, $Ag_{0.72}Ga_{0.28}$ ($T_c = 7.5$ K). Both β-$PdBi_2$ and $MgHg_2$ crystallize with the $MoSi_2$ type; however, the c/a ratios of the two structures differ significantly: 3.9 for the former and 2.3 for the latter. As seen earlier, it is possible to pass gradually from a W-type to a Cu-type structure by an extension along one of the 4-fold axes. For an ideal W-type atom arrangement the unit cell of $MoSi_2$ corresponds to three body-centered cubes and the c/a ratio is equal to 3. For a Cu-type arrangement, the corresponding ratio is close to 4.2. For both configurations, the only refinable coordinate has a value close to $\frac{1}{3}$. The structure type branch more closely related to the Cu type is identified on Zr_2Cu, whereas $MoSi_2$ itself represents the substitution variant derived from W. The former variant is observed for AB_2 compounds where B is larger than A, the latter when A is larger than B.

A ternary substitution variant of the W and CsCl (Fig. 6.7a) types with an 8-fold cubic cell is known under the name **$MnCu_2Al$**. In this structure cubes formed by Cu atoms are centered by Mn or Al atoms in an ordered way. Seen from another point of view (Fig. 6.7b), cubes formed by four Mn and four Al atoms are centered by Cu atoms. YPd_2Sn becomes superconducting at 5.5 K, $ScAu_2Al$ at 4.4 K.

c. Laves Phases

Alloys with atoms of slightly different sizes sometimes adopt another class of close-packed structures, the so-called *tetrahedrally close-packed* or Frank–Kasper phases, which contain only tetrahedral voids between the atoms. Geometric considerations have shown that the coordinations are here restricted to four different kinds: the 12-, 14-, 15-, and 16-vertex Frank–Kasper polyhedra. In the structures of hexagonal **$MgZn_2$** and cubic **$MgCu_2$**, the Mg atom centers a 16-vertex Frank–Kasper polyhedron (also called Friauf polyhedron). The 12 atoms forming the truncated tetrahedron are all Zn or Cu atoms, whereas the tetrahedron is formed by Mg atoms capping the hexagonal faces of the former. The whole structure can be visualized as a framework of face-sharing truncated tetrahedra centered by Mg atoms. The Mg atoms alone build up a tetrahedral sublattice, similar to the one found in hexagonal diamond in the case of $MgZn_2$, cubic diamond in the case of $MgCu_2$. The transition metal atoms form small, empty tetrahedra. It is seen in Fig. 6.8 that in $MgZn_2$ the tetrahedra share both faces and vertices, in $MgCu_2$ only vertices.

$MgZn_2$ and $MgCu_2$ represent two different ways to stack the same kind of structural slab containing three atom layers (see comparison with the $CeCo_3B_2$ type in Fig. 6.11). The central atom layer is a puckered close-packed layer of composition Mg_2T. The outer layers are identical to each other, but shifted, and constitute the common interfaces in the structure. The atoms in these layers form a so-called Kagome net, a tessellation of hexagons and triangles, which can be derived from a close-packed layer by removing one-quarter of the atoms. As for the simple close-packed layers, three stacking positions are possible. $MgZn_2$

Fig. 6.8.

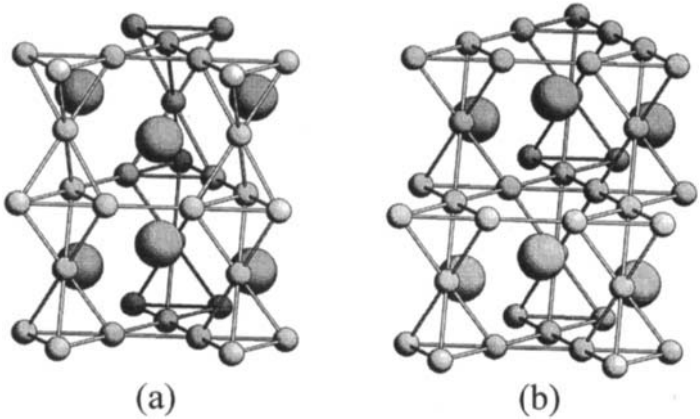

Structures of LT-$LaOs_2$ (**$MgZn_2$** type, hexagonal Laves phase) (a) and HT-$LaOs_2$ (**$MgCu_2$** type, cubic Laves phase) (b), emphasizing the framework of interconnected Os_4 tetrahedra. Large spheres: La; small spheres: Os.

represents the variant 2H, and $MgCu_2$ the variant 3R, which, like Cu, has an overall cubic symmetry. The simple Laves phases are extremely common among intermetallic compounds of composition close to 1 : 2, and more than 10 other stacking variants are known, most of them observed for pseudobinary compounds.

High superconducting transition temperatures are reported for the binary $MgCu_2$-type phases ZrV_2 (8.8 K) and HfV_2 (9.3 K). Both compounds exhibit a temperature-induced structural instability and undergo a phase transition at low temperature. The two low-temperature structures are, however, different, and the diffraction diagrams revealed a rhombohedral cell for ZrV_2, but an orthorhombic cell for HfV_2. A maximum in T_c is observed for the solid solution $Hf_{1-x}Nb_xV_2$ at the composition $Hf_{0.84}Nb_{0.16}V_2$. $LaRu_2$ ($T_c = 4.4$ K) represents a third kind of structural deformation, where a body-centered tetragonal cell is observed below 30 K. The highest critical temperature reported for a $MgZn_2$-type phase is 10.9 K ($ScTc_2$). $LaOs_2$ is superconducting in both modifications, with $T_c = 8.9$ K for the $MgCu_2$-type structure and 5.9 K for the $MgZn_2$-type structure.

d. A15 Phases

The *A*15 phases, with superconducting transition temperatures exceeding 20 K, are the best-known family of intermetallic superconductors. The structure type was earlier referred to as β-W, but is now generally called **Cr_3Si**, sometimes α-UH_3. The structure is tetrahedrally close-packed, cubic, space group $Pm\bar{3}n$. The Si atoms in Cr_3Si are located at the origin and the center of the cell, forming a body-centered sublattice. The Cr atoms are situated, two by two, in the faces of the cell. The resulting polyhedron around the Si atoms is an icosahedron, a polyhedron with 12 vertices, 20 triangular faces, and 5-fold axes passing through opposite vertices. The whole structure can be described as a framework of $SiCr_{12}$ icosahedra sharing faces and edges (Fig. 6.9b). The Cr atoms form infinite nonintersecting straight chains parallel to each of the cell edges, emphasized in Fig. 6.9a, with interatomic distances equal to $a/2$. Deviations from the ideal composition A_3B correspond to a partial substitution on one or the other site by the other element. An excess of *B* element atoms breaks the infinite -*A*- chains and has generally a negative effect on T_c. Typical *A* elements are Ti, V, Nb, Ta, Cr, Mo, and W. The highest superconducting transition temperatures are observed for phases where *B* is a nonmetal such as Al, Ga, Si, Ge, or Sn. Such compounds show narrow homogeneity domains, extending only on the *A*-rich side. The critical temperature depends strongly on the composition and, for example, for Nb-based compounds a variation of 1 at % corresponds to a change of 2.5 K in T_c. The maximum value of T_c corresponds to the stoichiometric composition and a high degree of ordering on the two atom sites. Unfortunately, the *A*15 structure is often in competition with other structure types at this composition and the 3 : 1 ratio cannot always be obtained. Sputtering

Fig. 6.9.

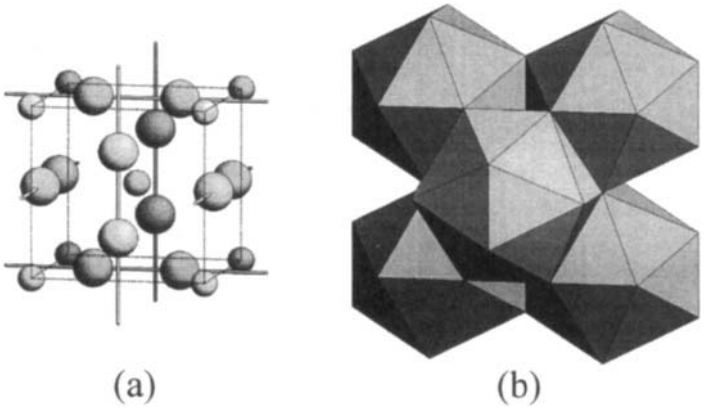

Structure of Nb_3Ge (**Cr_3Si** type, *A*15), emphasizing the infinite linear chains of Nb atoms (a) and the framework of $GeNb_{12}$ icosahedra (b). Large spheres: Nb; small spheres: Ge.

techniques have in some cases allowed confirmation of the expected high values for the stoichiometric composition. For instance, a superconducting transition temperature of 23.2 K is reported for Nb_3Ge sputtered thin films. Stoichiometric Nb_3Sn ($T_c = 17.9$ K) transforms to a tetragonal structure at 43 K. The amplitude of the discontinuity in heat capacity was found to be proportional to the fraction of tetragonal phase in the sample. V_3Si ($T_c = 17.0$ K) undergoes a similar phase transition at 21 K. Another category of isotypic phases, called *atypical A*15 phases, are formed where *B* is a late transition metal. These compounds have broader homogeneity domains, and the maximum in T_c vs the composition is not always observed for the element ratio 3 : 1. For both categories, gradual substitution by a third element on one or both sites has confirmed that there is a close correlation between the critical temperature and the valence electron concentration, and the plot of T_c vs the number of electrons per atom show well-defined maxima around 4.6 and 6.4 electrons. The former corresponds to compounds where *B* is (mainly) a nonmetal, the latter to compounds with (mainly) transition or noble metal elements on the *B* site.

e. Other Tetrahedrally Close-Packed and Related Structures

The tetragonal structure type **CrFe** is better known under the name σ phase. The ideal composition and the homogeneity range vary greatly from one system to another. It is interesting to note that this structure type, with 12-, 14-, and 15-vertex Frank–Kasper coordination polyhedra, is also formed by an element modification, β-U. In the binary ordered variant Nb_2Al, the 12-vertex polyhedra, i.e., the icosahedra, are centered by Al atoms in sites conventionally labeled *A* and

D. A high degree of mixed occupation is observed for most σ phases, with a slight preference for elements to the left of Mn in the periodic table, i.e., generally the larger atoms, to occupy the sites of higher coordination. The atoms at $z = 0$ and $\frac{1}{2}$ form symmetry-related nets, which can be seen in Fig. 6.10a. The atoms from site *E* are located between the hexagons of the nets, centering bicapped hexagonal antiprisms. The Cr_3Si structure can be decomposed into atom nets containing similar fragments (Fig. 6.10b).

The cubic structure of α-Mn is not tetrahedrally close-packed, but contains similar coordination polyhedra. In particular, the site at the origin and the one located on the body diagonal (Wyckoff position 8(*c*) in space group $I4\bar{3}m$) center 16-vertex Frank–Kasper polyhedra, like the large atoms in the Laves phases. A series of binary so-called χ phases are known, and the ordered substitution variant where the atoms of the minority element occupy selectively the sites inside the 16-vertex polyhedra is defined on $\mathbf{Ti_5Re_{24}}$. The highest superconducting transition temperature is observed in the system Nb–Tc.

A series of Be-rich compounds exhibit superconductivity at temperatures reaching 9.7 K in the case of $ReBe_{22}$. Like the large atoms in the Laves phases and α-Mn, the Zr atoms in the $\mathbf{ZrZn_{22}}$ type center 16-vertex Friauf polyhedra. All 16 vertices are occupied by atoms of the same element. The Zn atoms are distributed over four crystallographically independent sites and three different kinds of polyhedra are observed: icosahedron, bicapped pentagonal prism, and bicapped hexagonal prism.

Fig. 6.10.

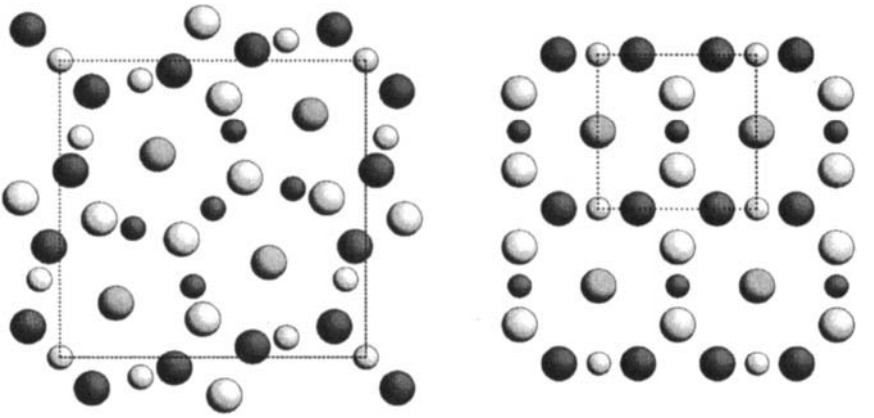

Structures of Nb_2Al (**CrFe** type) (a) and Nb_3Ge (**Cr_3Si** type) (b) in projections along [0 0 1]. Large spheres: Nb; small spheres: Al, Ge. Dark shading: $z = \frac{1}{2}$; medium shading: $z \sim \frac{1}{4}, \frac{3}{4}$; light shading: $z = 1$.

f. $CaCu_5$ Type and Related Structures

Kagome nets (6363 mesh), similar to those observed in the Laves phases, are found in another well-known alloy structure type, hexagonal $CaCu_5$. The nets are formed by Cu atoms and stacked upon each other without shift in the plane of the layer. The Ca atoms are located between the hexagons, the remaining Cu atoms between the triangles. The Cu atoms form a 3D framework of empty tetrahedra sharing faces and vertices. **$CeCo_3B_2$** is an ordered substitution derivative that crystallizes in the same space group, but with a considerably reduced c/a ratio. The B atoms substitute exclusively on the sites located between the Kagome nets and center trigonal prisms formed by transition metal atoms. In Fig. 6.11 the structure is compared with the hexagonal Laves phase, $MgZn_2$. Binary $ThIr_5$ becomes superconducting at 3.9 K, ternary $LuOs_3B_2$ at 4.7 K.

Different deformation derivatives of $CeCo_3B_2$ are known, among which is hexagonal **$LaRu_3Si_2$** with distorted $SiRu_6$ trigonal prisms. The unit cell is doubled along [0 0 1] with respect to $CeCo_3B_2$. The structure variant is formed by a series of Ru-based silicides, of which only the compounds containing Y, La, or Th are superconducting.

The structure of superconducting **$Ba_{0.67}Pt_3B_2$** was reported as a hexagonal deformation derivative of $CeCo_3B_2$ with a disordered arrangement of vacancies on the Ba site. A rhombohedral structure with an ordered arrangement of vacancies and a 9-fold unit cell was later refined for $Ba_2Ni_9B_6$ and isotypism cannot be excluded. Among the series of Pt-based borides with Ca, Sr and Ba, $Ba_{0.67}Pt_3B_2$ exhibits the highest superconducting transition temperature (5.6 K).

Fig. 6.11.

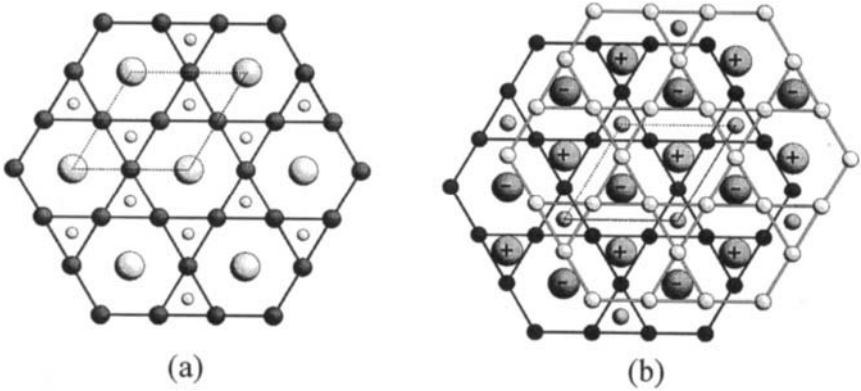

Structures of $LuOs_3B_2$ (**$CeCo_3B_2$** type) (a) and $LaOs_2$ (**$MgZn_2$** type) (b) in projections along [0 0 1]. Large spheres: Lu, La; medium spheres: Os; small spheres: B. For $LuOs_3B_2$, dark shading: $z = \frac{1}{2}$, light shading: $z = 1$; for $LaOs_2$ dark shading: $z = \frac{1}{4}$, medium shading: $z \sim 0, \frac{1}{2}$, light shading: $z = \frac{3}{4}$; plus and minus signs indicate displacements along [0 0 1] of atoms at $z \sim \frac{1}{2}$. Solid lines connect atoms forming Kagome nets.

A certain number of different structure types derived from $CaCu_5$ are known where the large atoms centering the hexagonal prismatic voids between the Kagome nets are replaced by a pair of the smaller atoms. The axes of the substituting "dumbbells" are parallel to the *c*-axis of the original hexagonal cell. The replacement of half of the large atoms by atom pairs changes the composition from 1 : 5 to 1 : 12. One of the possible ordering variants for this element ratio is found for tetragonal **$ThMn_{12}$**. Superconducting transition temperatures of 4.1 and 9.9 K were reported for so-called WBe_{13} and ReB_{13} with an unknown tetragonal structure. A $ThMn_{12}$-type structure was later identified in the W-Be system. Transition temperatures of 8.6 and 9.2 K were reported for two other Be compounds, "$OsBe_4$" and "$OsBe_5$", with unknown structure.

g. Structures with Atoms in Square-Antiprismatic Coordination

The Cu atoms in **θ-$CuAl_2$** are surrounded by eight Al atoms forming a square antiprism, a polyhedron with two parallel square faces rotated by 45° with respect to each other, and eight triangular faces. The antiprisms share their square faces to form infinite columns, but also edges to form a 3D framework. Part of the framework is drawn in Fig. 6.12. The structure is tetragonal and the translation unit along the 4-fold axis contains two $CuAl_8$ antiprisms. The minority atoms are arranged in infinite straight chains, with interatomic distances equal to $c/2$. A closer analysis reveals two sets of hexagon-mesh (honeycomb) Al atom layers that are perpendicular to the diagonals of the square faces and intersect with each other without common atoms. For $c/a = \sqrt{(2/3)}$ and $x(\mathrm{Al}) = 1/6$ the hexagons are regular. Among the numerous isotypic compounds, the c/a ratio decreases with increasing valence electron concentration to reach a minimum value for ~3.3 electrons per atom, and then increases again. The *x*-parameter shows a similar variation. The highest superconducting transition temperatures are reported for Zr_2Rh (11.3 K) and Zr_2Ir (7.6 K), with the same number of valence electrons. Superconductors with lower T_c are found among *Th* alloys, as well as among borides and plumbides where Pb is the majority element.

One-antiprism-thick θ-$CuAl_2$ type slabs may be recognized in the structure type **Cr_5B_3**, which is described in the same tetragonal space group $I4/mcm$. The superconductors In_5Bi_3 and $In_{0.65}Sb_{0.35}$ ($T_c \sim 5$ K) are generally considered to belong to a different branch of the structure type since their c/a ratios differ significantly from that of Cr_5B_3 (1.5, compared to 1.9 for Cr_5B_3). Two-thirds of the B atoms in Cr_5B_3 form dumbbells, whereas no short distances are observed between the nonmetal atoms in the bismuthide or antimonide. In In_5Bi_3 an indium atom is located above each of the square faces of the antiprism so that the actual coordination number of the central Bi site is 10. The $CuAl_2$-type slabs alternate with slabs containing pairs of face-sharing bicapped trigonal prisms, formed by In atoms and centered by atoms from the second Bi site. A bicapped

Fig. 6.12.

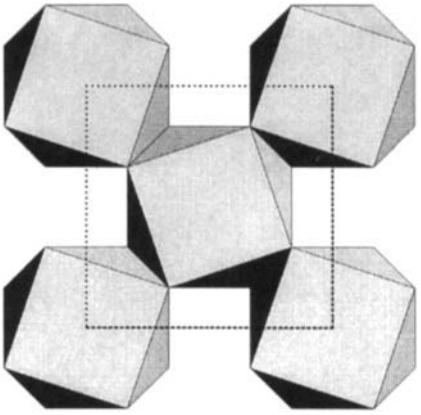

Structure of $ZrRh_2$ (**θ-$CuAl_2$** type) in a projection along [0 0 1], emphasizing the framework of $ZrRh_8$ square antiprisms.

trigonal prism is formed by eight atoms and little distortion is necessary to convert it into a square antiprism.

$CeAl_2Ga_2$, also known under the name $ThCr_2Si_2$, is a substitution variant of the tetragonal body-centered $BaAl_4$ type. The ordering of Al and Ga atoms respects all symmetry elements present in the binary structure. In the description of $CeAl_2Ga_2$ the stress is often put on the square antiprisms surrounding the Ga site (Si site in $ThCr_2Si_2$). A large square of Ce atoms on one side and a smaller square of Al atoms on the other side form the antiprisms, which are emphasized in the drawing of the structure in Fig. 6.13. Considering also the atoms located above the square faces, the site is in fact coordinated by an (Al_4Ga) and a Ce_5 square pyramid. The Al atoms center a Ga_4 tetrahedron and a Ce_4 tetrahedron. In a different ordering variant of $BaAl_4$, $CaBe_2Ge_2$ (tetragonal primitive), the atom distribution is such that both Be and Ge atoms occupy square pyramidal and tetrahedral sites. The Be atoms center Ge_5 square pyramids and the Ge atoms center Be_5 square pyramids. A superconducting transition temperature of 4.1 K is observed for the phosphide $LaRu_2P_2$, crystallizing with a $CeAl_2Ga_2$-type structure. The values reported for isotypic silicides with rhodium and iridium do not exceed 4 K.

Orthorhombic **$U_2Co_3Si_5$** represents another ordered substitution variant of $BaAl_4$. The Co atoms occupy half of the square pyramidal and one-quarter of the tetrahedral sites, both kinds of polyhedra being built up exclusively by Si atoms. The resulting orthorhombic cell is related to that of $BaAl_4$ ($CeAl_2Ga_2$) by the relations: $a = c(BaAl_4)$, $b = 2\sqrt{2}\, a(BaAl_4)$ and $c = \sqrt{2}\, a(BaAl_4)$. The superconducting transition temperature of isotypic $La_2Rh_3Si_5$ reaches 4.4 K.

The structure of **$U_2Mn_3Si_5$** contains $U_2Co_3Si_5$-type columns of rhombic cross-section, intergrown with columns of $Si(U_4Mn_4)$ square antiprisms sharing

Fig. 6.13.

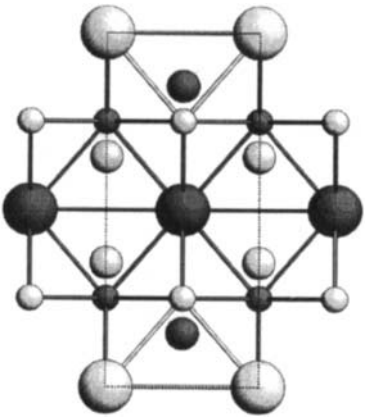

Structure of $\mathbf{CeAl_2Ga_2}$ in a projection along [1 0 0]. Large spheres: Ce; medium spheres: Ga; small spheres: Al. Dark shading: $x = \frac{1}{2}$; light shading: $x = 1$. Solid lines connect atoms forming square antiprisms around the Ga atoms.

square faces. The columns run parallel to the *c*-axis of the tetragonal cell. The Fe-based silicides with Sc, Y, Tm, and Lu are superconductors, with a maximum value of 6.1 K measured for $Lu_2Fe_3Si_5$. The Fe atoms are arranged in square clusters and isolated linear chains with interatomic distances only slightly longer than in elementary Fe. $Tm_2Fe_3Si_5$ becomes superconducting at 1.3 K, but reenters the normal state at 1.1 K.

Infinite columns of $Co(Sc_4Si_4)$ square antiprisms are found in tetragonal $\mathbf{Sc_5Co_4Si_{10}}$. The cross-section of the column, in which a $CeAl_2Ga_2$-type arrangement is found, also includes a Sc atom capping the Si_4 face and a Si atom capping the Sc_4 face. The columns form a framework in which it is also possible to recognize structural features characteristic of Cu_3Au and AlB_2 (see later discussion). $Sc_5Rh_4Si_{10}$, $Sc_5Ir_4Si_{10}$, and $Y_5Os_4Ge_{10}$ become superconducting at 8–9 K; a few other silicides and germanides with Sc, Y, and Lu do so at lower temperatures.

h. Structures with Atoms in Trigonal Prismatic Coordination

Trigonal prismatic coordination is common in intermetallic compounds combining atoms of different sizes. One, two, or the three square faces of the prisms are often capped by additional atoms, which belong to the first coordination sphere, but are generally ignored in the structural description.

When close-packed layers are stacked upon each other without shift, trigonal prismatic voids are created between the layers. There are two voids per atom, and the filling of all interstices is realized in the type $\mathbf{AlB_2}$, projected in

Fig. 6.14a. This simple hexagonal structure type with three atoms in the unit cell corresponds to a compact arrangement of BAl_6 trigonal prisms. The boron atoms form planar infinite hexagon-mesh nets. The Al atoms center straight hexagonal prisms, with all faces capped by atoms from the same site (12 B + 8 Al). A few borides, based on Nb or Mo, have been reported to be superconducting at the

Fig. 6.14.

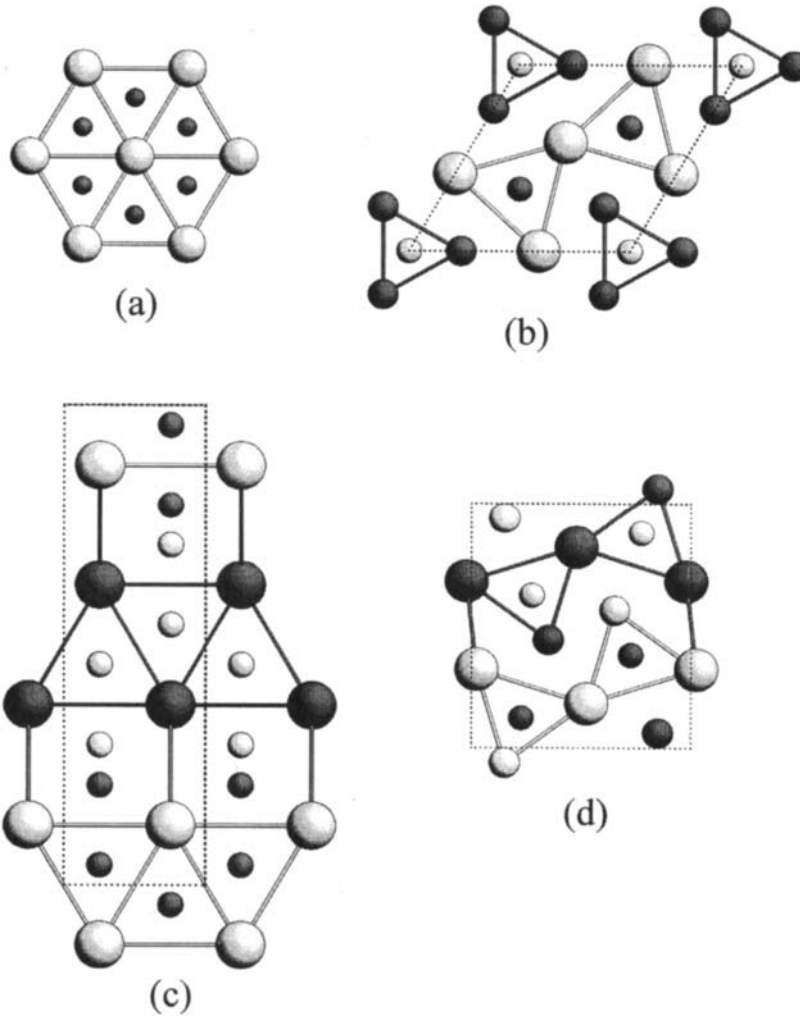

Structures of MoB_2 (**AlB_2** type) (a), HT-ZrRuP (**ZrNiAl** type) (b), α-**$ThSi_2$ 2** (c), and LT-ZrRuP (**TiNiSi** type) (d) in projections along [0 0 1], [0 0 1], [1 0 0], and [0 1 0], respectively. Large spheres: Mo, Zr, Th; medium spheres: Ru; small spheres: B, P, Si. For MoB_2, HT-ZrRuP, and α-$ThSi_2$, dark shading: $z, x = 0$, light shading: $z, x = 1$; for LT-ZrRuP, dark shading: $y = \frac{1}{4}$, light shading: $y = \frac{3}{4}$. Solid lines connect atoms forming trigonal prisms.

boron-rich boundary of the homogeneity range. In **Ni_2In**, the same kind of atom (Ni) that forms the trigonal prisms is found also at half of the prism-centering sites. The ordered atom distribution leads to a doubling of the *c*-parameter with respect to AlB_2. Isotypic indium antimonide and indium bismuthide both become superconducting at $T_c = 5.8\,K$.

β-$ThSi_2$ ($T_c = 2.4\,K$) crystallizes with an AlB_2-type structure. A stacking variant is adopted by the α-modification of the same compound. Slabs of fused trigonal prisms, cut parallel to the (1−10) plane of AlB_2, are in **α-$ThSi_2$** rotated by 90° and stacked upon each other so that the mutually perpendicular prisms form consecutive slabs share square faces. The resulting structure, shown in Fig. 6.14c, is tetragonal, space group $I4_1/amd$. Like the B atoms in AlB_2, each Si atom is bonded to three others, forming a coplanar triangle. The triangles are, however, rotated with respect to each other and form a 3D framework. α-$ThSi_2$ itself is superconducting ($T_c = 3.2\,K$) and the transition temperature can be increased to 4.6 K by replacing part of the Th atoms by Y atoms. The optimal amount of substitution reduces the valence electron concentration to a value close to 3.9 electrons per atom. Superconductivity is also reported for silicides and germanides of alkaline-earth metals prepared at high pressure ($T_c = 4.9\,K$ for $BaGe_2$). An ordered substitution variant is known for **LaPtSi**, where every second Si atom is replaced by a transition metal atom. The ordering of the atoms lowers the symmetry to space group $I4_1md$. The highest superconducting transition temperature observed for this structure type, 6.5 K, is reported for ThIrSi.

Similar slabs of trigonal prisms sharing the triangular and two of the rectangular faces are found in orthorhombic **α-TlI** where I_6 prisms are centered by Tl atoms. The slabs have no common atoms, which leads to the equiatomic composition. The type is often referred to as CrB, where the B atoms center prisms formed by the metal atoms. Isotypic NbB becomes superconducting at 8.3 K. α-TlI is the end member of a family of stacking variants where slightly tilted, infinite columns of prisms sharing rectangular faces are arranged in layers that can be stacked upon each other in two different ways. In α-TlI consecutive slabs are stacked so that the prism columns share triangular faces. In the other end member, orthorhombic **FeB**, the same slabs are stacked so that the prism columns share edges and form a 3D framework. Many intermediate stacking variants are known, but superconductivity is reported only for the end members. LaCu (Cu inside La_6 prisms) is isotypic with FeB and becomes superconducting at 5.9 K.

If the structure of FeB is cut into slabs in such a way that the trigonal prisms no longer share rectangular faces, the composition becomes 3 : 1. Such slabs, inside which the prisms share edges and single comers, are found in the orthorhombic **Fe_3C** type. The decomposition into slabs is, however, a purely geometric operation with the aim of emphasizing structural relationships, and the structure presents no layered character. The "slabs" are interconnected via Fe atoms that cap CFe_6 prisms in a neighboring slab. The highest T_c, 6.2 K, is reported for La_3Ni.

In **Ni_3P**, distorted trigonal prisms, formed by the metal atoms and centered by the P atoms, share only vertices. The true coordination number of the P atoms is 9, considering also the Ni atoms capping the prism faces. Type-defining Ni_3P is not superconducting, but isotypic Mo_3P superconducts below 5.3 K. The structure of Ni_3P is often described as being built up of tetrahedron star columns. A *tetrahedron star* is an empty tetrahedron, the faces of which are capped by four atoms forming a larger tetrahedron. When arranged in columns, the two concentric tetrahedra are deformed so that two rhombs, perpendicular to the column axis, are formed. In Ni_3P such columns are isolated, neighboring columns being shifted with respect to each other. The same motif is found in Cr_3Si where similar columns share atoms. The mutually perpendicular Cr_2Si_2 rhombs situated at $z = 0$ and $z = \frac{1}{2}$ (column axis at $\frac{1}{2}$ 0 z, for instance) can be recognized in Fig. 6.10b. By further condensation, the Al sublattice in θ-$CuAl_2$ is obtained.

A superconducting transition temperature of 5.5 K is reported for the binary aluminide **Os_4Al_{13}**. The structure is monoclinic with 34 atoms in a side-face centered cell, distributed over nine atom sites. Single and double columns of base-sharing $OsAl_6$ prisms, can be distinguished. All rectangular faces are capped by one or even two Al atoms, leading to the coordination numbers 10 and 11 for the two Os sites.

The hexagonal structure of Fe_2P contains columns of base-sharing Fe_6 trigonal prisms centered by P atoms. Part of the columns share edges to form a framework with large channels, inside which are located single columns, shifted by $c/2$. Several ordered atom arrangements with the same space group and unit cell are known for ternary compounds. Among these, the **ZrNiAl** type (Fig. 6.14b) is presented here because of a series of isotypic superconducting pnictides. In ZrRuP ($T_c = 12.9$ K) the prism framework is made of Zr atoms and the isolated prism columns of Ru atoms. All prisms are centered by P atoms. Interatomic distances of 2.63 Å are observed within the Ru_3 triangular clusters. For both phosphides and arsenides the superconducting transition temperatures are higher for Zr than for Hf or Ti, and higher for Ru than for Os. The hexagonal ZrNiAl-type phase exists predominantly as an HT-modification. Below ~1273 K HfRuAs crystallizes with a TiFeSi-type structure and samples annealed below this temperature exhibit no superconductivity above 1 K. However, the isotypic silicides NbReSi and TaReSi become superconducting at 5.1 and 4.4 K, respectively. The **TiFeSi** type is an orthorhombic deformation derivative of hexagonal ZrNiAl with $a = 2c$(ZrNiAl), $b = \sqrt{3}a$(ZrNiAl), $c = a$(ZrNiAl), and the Si atoms in the Fe_6 prisms significantly displaced from the prism center. HT-ZrRuP undergoes a phase transition at 1523 K to another orthorhombic structure, the **TiNiSi** type. Also, this modification is superconducting, but at a lower temperature (3.8 compared to 12.9 K). The TiNiSi type is an ordered substitution variant of Co_2P, a structural branch and antitype of $PbCl_2$, which implies no lowering of the symmetry with respect to the binary type. The Si atoms center trigonal prisms formed by four Ti and two Ni atoms. As can be seen from Fig. 6.14d, the prisms share trigonal faces and edges to form a

puckered layer-like arrangement. Here, too, metal atoms cap the prisms and the decomposition into slabs is a mere help to recognize particular structural features.

One more superconductor was identified in the metal-rich part of the Zr–Ru–P system. $ZrRu_4P_2$ has a superconducting transition temperature of 11 K and crystallizes with a tetragonal structure type first identified on a silicide, $\mathbf{ZrFe_4Si_2}$. Four Ru and two Zr atoms form a trigonal prism around the P atoms in $ZrRu_4P_2$. The prisms are capped by one Zr and two Ru atoms. The late transition metal atoms are arranged in tetrahedra that share edges to form infinite chains parallel to the *c*-axis. Neighboring chains are interconnected via metal-to-metal distances of the same magnitude as within the chains.

The **NiAs** type corresponds to the filling of all octahedral interstices in a hexagonal close-packed arrangement of As atoms and can be considered as the hexagonal counterpart to the NaCl type (see Section D on interstitial compounds). The same simple type can, however, alternatively be described as a stacking of directly superposed close-packed Ni layers, with every second trigonal prismatic interstice filled by an As atom. The Ni atoms form a framework similar to the Al sublattice in AlB_2, but, because of the ordered arrangement of the trigonal prismatic voids, the unit cell is doubled along [0 0 1] with respect to AlB_2. Which description is the most appropriate depends on the c/a ratio. For $c/a = \sqrt{8/3} = 1.63$ the atoms in the *h*-stacked layers have interatomic distances of the same length within and between the layers, whereas for $c/a = 2$ the same is true for the directly superposed layers. The **FeAs** type (also called MnP type) is an orthorhombic deformation variant of the NiAs type with relatively important distortions in both sublattices. For the NiAs type, superconducting compounds are antimonides, bismuthides, and tellurides with group VIII metals, as well as interstitial carbides. IrGe, which crystallizes with the FeAs type, becomes superconducting at 4.7 K.

i. $Yb_3Rh_4Sn_{13}$ Type and Related Structures

Interesting properties, among which is superconductivity, are observed for a series of stannides of approximate composition $R_3Rh_4Sn_{13}$. Four different structure types have been identified, usually referred to as phases I, I′, II, and II′. Phase I, refined on $\mathbf{Yb_3Rh_4Sn_{13}}$, is cubic with a cell parameter of approximately 9.7 Å. The Sn atoms on the two crystallographically independent sites have different chemical behavior. The Sn(2) atoms in Wyckoff position 2(*a*) (space group $Pm\bar{3}n$) may be considered as divalent cations, whereas the atoms from site Sn(1) make up a complex polyanion. Consequently, the chemical formula is often written as $SnYb_3Rh_4Sn_{12}$. Sn_6 trigonal prisms centered by Rh atoms share corners to form a 3D framework, shown in Fig. 6.15. The *R* atoms occupy cuboctahedral and the Sn cations icosahedral voids in the framework. The *R* atoms and the Sn(2) atoms form a Cr_3Si-type sublattice. Rhodium may be replaced by other late transition elements, and isotypic superconductors

Fig. 6.15.

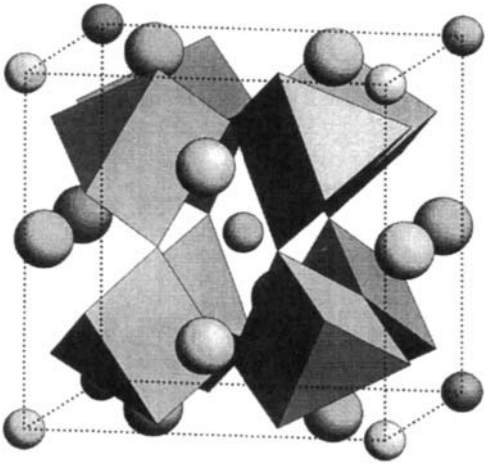

Structure of $\mathbf{Yb_3Rh_4Sn_{13}}$, emphasizing the framework of corner-linked $RhSn_6$ trigonal prisms. Large spheres: Yb; medium spheres: Sn(2).

are also found among germanides and plumbides. The highest superconducting transition temperature, 8.7 K, is observed for $Ca_3Rh_4Sn_{13}$. Phase I′, defined on $\mathbf{La_3Rh_4Sn_{13}}$ ($T_c = 3.2$ K), is a deformation variant of phase I with a body-centered cubic cell and a doubled cell parameter. The distortion implies a complex change in the relative orientation of the Rh-centered trigonal prisms, which remain almost undistorted.

Phase II has a slightly different composition, varying between $R_4T_6M_{19}$ and $R_5T_6M_{18}$, corresponding to a mixed M/R occupation of one of the cation sites. The refined composition of the type-defining compound $\mathbf{Er_4Rh_6Sn_{19}}$ is $Er_{4.32}Rh_6Sn_{18.68}$. As in phase I and phase I′, the main part of the Sn atoms form a framework of corner-sharing trigonal prisms centered by Rh atoms, with Rh–Sn distances ranging from 2.64 to 2.74 Å. The structure is tetragonal body-centered with an a-parameter corresponding to the face diagonal of the cubic cell of $Yb_3Rh_4Sn_{13}$, and a c-parameter twice as large. Phase II′, refined on $\mathbf{Tb_4Rh_6Sn_{19}}$ and sometimes referred to as phase III, has a cubic face-centered cell with the cube edge equal to the a-parameter of phase II. It is considered to be a disordered microtwinned pseudocubic version of phase II.

j. Other Structures of Intermetallic Compounds

As in LaPtSi, the transition metal and silicon atoms in cubic LaIrSi ($T_c = 2.3$ K) form a 3D framework where each atom is connected to three atoms of the other kind. This structure type, defined on **ZrSO**, is an ordered substitution derivative of cubic $SrSi_2$ with a lowering of the symmetry from space group $P4_132$ to

$P2_13$. The superconducting transition temperature of isotypic LaRhSi exceeds by little the 4.2 K mark fixed here.

The cubic structure of **$LaFe_4P_{12}$** contains a framework of corner-sharing octahedra, formed by P atoms and centered by Fe atoms. Instead of being straight as in idealized perovskite (see Fig. 6.23), the octahedra are tilted so that one-quarter of the original cuboctahedral voids are enlarged, at the expense of the remaining voids. The resulting large, icosahedral voids are filled by the La atoms and the cell edge is twice that of perovskite. The unstuffed structure is known under the name skutterudite, a mineral of composition $CoAs_3$. Phosphides are formed with the early rare-earth metals and transition metals from the subgroup of iron. $LaFe_4P_{12}$ becomes superconducting at 4.1 K and $LaRu_4P_{12}$ at 7.2 K.

A superconducting transition temperature of 9.8 K was observed relatively early in the Mo–Ga system, at the approximate composition $MoGa_4$. The crystal structure turned out to be one of the most complicated ever found for a superconducting inorganic compound, with monoclinic symmetry and 38 independent atom sites in the unit cell. The Mo atoms are surrounded by a Ga_{10} polyhedron, which is a combination of half an icosahedron and half a cube: a capped pentagon on one side and a square on the other. A small deviation from the ideal composition **Mo_6Ga_{31}** was observed. The complexity of this structure is in contradiction with the long accepted idea that high superconducting temperatures are associated with high symmetry and simple crystal structures.

D

Interstitial Carbides, Nitrides, Oxides, and Hydrides

a. NaCl Type

A close-packed atom arrangement is by definition dense, but interstices large enough to host small interstitial atoms exist. Independently of the stacking mode, there are one octahedral and two tetrahedral interstices per atom. Figure 6.16 shows where these are located in the (1 1 0) plane bisecting the hexagonal cell of the h.c.p. Mg type and of the c.c.p. Cu type in hexagonal setting. It may be noted that for a layer in *h* stacking, the octahedra surrounding neighboring voids share faces. Within some families of compounds it is not possible to fill both these interstices simultaneously.

Close-packed atom arrangements with filled-up interstices are found among two very different classes of compounds. On one side there are a large number of ionocovalent compounds where the close-packed layers are formed by anions and the interstices filled by cations. On the other side one finds alloys where the close-packed layers are formed by metal atoms and the interstices are filled by small atoms such as, carbon, nitrogen, or hydrogen. The former are antitypes with respect to the latter ("cations" and "anions" interchanged). For evident

Fig. 6.16.

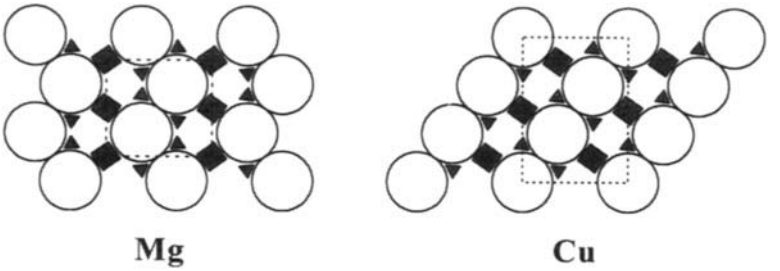

Atoms in the (1 1 0) cross-section of h.c.p. **Mg** and c.c.p. **Cu** (referring to hexagonal setting). Squares indicate octahedral voids, triangles tetrahedral voids in the close-packed atom arrangements.

reasons, some structure types were first identified in an ionocovalent compound, others in an alloy.

When all octahedral interstices in a cubic close-packed arrangement of anions are filled, the well-known **NaCl**, rock salt, type is obtained. From a geometric point of view the two atom sites in this cubic face-centered structure, shown in Fig. 6.17, are equivalent and can be interchanged. This means that the anions also have octahedral coordination. Because of the difference in size, however, it is reasonable to distinguish between the interstitial atoms and the atoms forming the framework. Carbides with transition metals from group V or VI and nitrides with transition metals from group IV or V exhibit superconductivity at temperatures that must be considered high on the scale for classical superconductors. α-MoC becomes superconducting at 14.3 K and isoelectronic δ-NbN at 16.0 K. A critical temperature of 18.0 K is reached for the mixed carbide–nitride $NbN_{0.75}C_{0.25}$ with a valence electron concentration of 4.9 electrons per atom. The superconducting transition temperature strongly depends on the nonmetal content and tends to reach its maximum for an ordered structure at the stoichiometric composition. Partial vacancies are, however, frequent in both sublattices, and an equiatomic composition generally corresponds to equal amounts, typically a few percent, of defects of both kinds. Stoichiometric VN undergoes a phase transition at 205 K to a tetragonal structure, characterized by distortions toward the formation of tetrahedral V_4 clusters. No phase transition is observed for off-stoichiometric concentrations in the same system. Band structure calculations, in combination with electron density studies, have revealed a mixing of different kinds of chemical bonding. In addition to covalent interactions, there is a metallic bonding contribution, as well as a considerable charge transfer from the metal to the nonmetal site.

A NaCl-type atom arrangement is also adopted by the hydride β-PdH. In this case too, T_c varies strongly with the content of interstitial atoms and reaches its maximum value, 9.6 K, for the stoichiometric composition. Higher critical

Fig. 6.17.

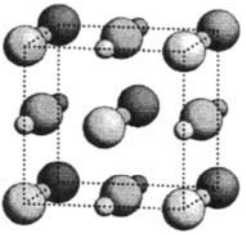

Structure of MoC (**NaCl** type), content of one unit cell. Large spheres: Mo; small spheres: C.

temperatures are reported for hydrides where Pd has been partly substituted by Cu (16.6 K), Ag (15.6 K) or Au (13.6 K). The increase in T_c observed in palladium hydrides is explained as a consequence of the suppression of spin fluctuations in Pd.

b. Other Structures with Close-Packed Metal Atom Layers

Light atoms such as C or N in alloys are practically "invisible" in ordinary X-ray diffraction experiments where the diffraction patterns are dominated by contributions from the metal atoms. Early reports on carbides and nitrides were sometimes limited to information about the metal atom sublattice and the expansion of the cell, which confirms the incorporation of nonmetal atoms. It is thus not surprising to find a great deal of confusion in the literature about the exact structure and composition of different interstitial compounds.

A partly ordered arrangement of nonmetal atoms in a cubic close-packed arrangement of Mo atoms is proposed for β-$Mo_2N_{0.75}$ (**β-Mo_2N** type). The type is characterized by the occupation of half of the available octahedral voids. The structure is tetragonal body-centered and the nitride exhibits superconductivity below 5.0 K.

The orthorhombic **ξ-Fe_2N** type represents an ordered arrangement of interstitial atoms in octahedral voids between close-packed layers in *h* stacking. The N atoms occupy selectively half of the octahedral voids in every interlayer. The highest superconducting transition temperature reported for isotypic α-Mo_2C (12 K) is almost as high as for the NaCl-type compound α-MoC formed in the same system (14.3 K). β-Mo_2C (5.8 K) crystallizes with a deficient NiAs-type structure (discussed in the section on intermetallic compounds), where the C atoms are statistically distributed over all octahedral sites. The chemical formula is in this case better written as $MoC_{0.5}$.

A superconducting transition temperature of 15.1 K is reported for a high-pressure high-temperature modification of molybdenum nitride, δ-MoN. The structure is isotypic with **LT-$Nb_{1-x}S$**, a hexagonal deformation variant of the NiAs type, with a doubling of the translation unit in the (0 0 1) plane. The N

atoms in δ-MoN occupy trigonal prismatic voids between directly superposed close-packed metal atoms layers that are distorted toward the formation of triangular clusters. Intra- and intercluster distances of 2.70 and 3.04 Å respectively, are observed.

A different ordering of nonmetal atoms occupying the trigonal prismatic voids in a similar metal atom framework is found in the hexagonal **WC** type. As in the NiAs type, every second void is occupied; however, the C atoms in WC are distributed so that infinite columns of base-sharing CW_6 prisms are formed. The hexagonal unit cell contains only two atoms and, as in CsCl or NaCl, the two sites are crystallographically equivalent and can be interchanged. This means that the C atoms also form a framework of fused trigonal prisms. γ-MoC is reported to crystallize with this structure type and to exhibit superconductivity below 9.3 K. According to some authors, the phase with directly superposed Mo atom layers reported in the Mo–C system is oxygen-stabilized.

Another modification of molybdenum carbide, hexagonal **η-MoC_{1-x}**, becomes superconducting at 8.9 K. The close-packed metal atom layers are arranged in hc_2 stacking and the C atoms occupy the octahedral voids to the limiting composition $MoC_{0.67}$.

The structure type defined on **2H-ZnS** is usually referred to by its mineral name wurtzite. As in NiAs with the same element ratio, close-packed anion layers are arranged in h stacking. However, the octahedral voids remain empty and the Zn atoms occupy half of the tetrahedral voids in every interlayer. The ZnS_4 tetrahedra share corners to form a 3D framework. A large number of stacking variants have been identified for the same compound, or for SiC, both valence compounds with complete electron octets. A superconducting transition temperature of 5.9 K is reported for isotypic GaN.

c. Other Interstitial Structures

Superconductivity has been reported also for compounds with more complicated structures where C atoms, as in the NaCl type and other structures discussed previously are found inside octahedra formed by transition metal atoms. An example of such a compound is **Mo_3Al_2C**, which becomes superconducting at 10.0 K. The structure is a ternary, filled-up substitution derivative of the β-Mn element type. The cubic element structure contains two crystallographically different atom sites, one centering an icosahedron, the other a larger, 14-vertex polyhedron. In the ternary carbide the Al atoms selectively occupy the former site and the Mo atoms the latter. The C atoms center octahedral voids formed exclusively by Mo atoms, without breaking any of the symmetry elements present in the element structure.

The so-called Nowotny phases are Mn_5Si_3-type compounds stabilized by nonmetal atoms located in octahedral voids. In hexagonal Mn_5Si_3 the atoms from one of the Mn sites are arranged in infinite chains parallel to [0 0 1] with interatomic distances equal to $c/2$, the shortest metal–metal distances in the

structure. The atoms from the other Mn site form columns of face-linked octahedra, susceptible to host interstitial atoms. The Si atoms center trigonal prisms formed by Mn atoms. A structure where all octahedral voids are filled is defined on the intermetallic compound **Hf_5CuSn_3** with $CuHf_6$ octahedra. In carbides and related compounds, the octahedral site is only partly occupied. In superconducting $Mo_{4.8}Si_3C_{0.6}$ the Mo–Mo distances within the chains are 2.52 Å. An isotypic O-stabilized phase, identified in a sample of nominal composition $Nb_{0.51}Itr_{0.30}O_{0.19}$, was found to become superconducting at 11.0 K.

Certain superconducting compounds crystallizing with a Ti_2Ni-type structure are also stabilized by oxygen. Also for this structure type, many alloys originally reported as binary were later shown to contain small amounts of a nonmetal. The cubic face-centered cell of Ti_2Ni contains 96 atoms and the Ti atoms occupy two crystallographically independent sites. The atoms from the site of lowest multiplicity form tetrahedra. This site may in some cases be occupied by atoms of the other element, resulting in a different ordered substitution derivative, defined on NiCd. The atoms from the other Ti site form relatively large empty octahedra. The structure type was in fact first identified on its filled-up form, on the so-called η-carbide, **W_3Fe_3C**, with C atoms inside W_6 octahedra. Superconductivity is reported for several O-stabilized Ti_2Ni-type alloys formed by Zr or Ti and a group VIII transition metal. A maximum value of 11.8 K is observed for a sample of nominal composition $Zr_{0.61}Rh_{0.285}O_{0.105}$. The full occupation of the octahedral site in Zr_3V_3O was confirmed by neutron diffraction experiments.

Unlike the superconducting Pd hydride, which crystallizes with the NaCl-type structure, Th_4H_{15} ($T_c = 7.6$ K) is stable at room temperature. The structure type was first identified on its antitype version, the silicide **$Cu_{15}Si_4$**. The Th atoms in Th_4H_{15} are located on infinite nonintersecting lines parallel to the body diagonals. Four atoms, one from each of four neighboring chains, together form a tetrahedron. The metal atom substructure is identical to the one formed by the metal atoms in Pu_2C_3 and Sc_4C_3, the latter crystallizing with a Th_4P_3-antitype structure. One-fifth of the H atoms center the Th_4 tetrahedra just mentioned, whereas the atoms from the other H site form triangles (d(D–D)= 2.25 Å). Each Th atom is surrounded by 12 H atoms.

E

Borides, Carbides, and Borocarbides with Nonmetal Polymers

a. Layered Carbohalides

The compound GdCBr crystallizes with two structural modifications of layered character, **1s-GdCBr** and **3s-GdCBr**, shown in Fig. 6.18. Both structures contain C_2 dumbbells, octahedrally surrounded by Gd atoms. The C–C distance

Fig. 6.18.

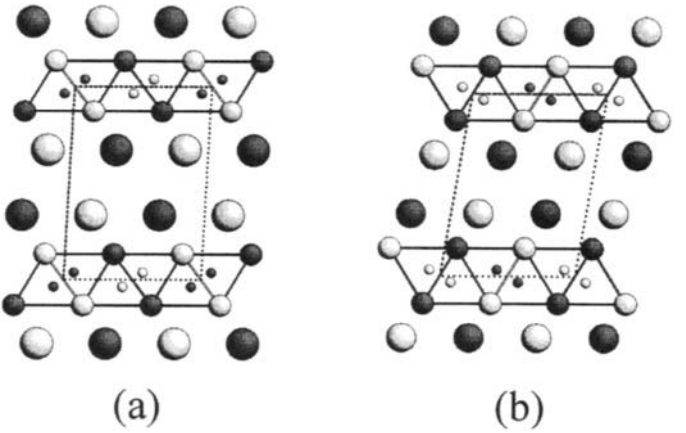

Structures of YCI (**1s-GdCBr** type) (a) and **3s-GdCBr** (b) in projections along [0 1 0]. Large spheres: I, Br; medium spheres: Y, Gd; small spheres: C. Dark shading: $y = \frac{1}{2}$; light shading: $y = 1$. Solid lines connect atoms forming octahedra around the C_2 dumbbells.

(1.3 Å) approximately corresponds to a double bond. The $(C_2)Gd_6$ octahedra share edges to form infinite sheets, which are separated by double layers of bromine ions. The Gd and Br atoms form approximately close-packed layers, which are arranged in simple hexagonal stacking in the variant called 1s. In the variant 3s a stacking sequence with a three times larger translation unit, corresponding to the stacking code h_2c_2, is found. The structures where each metal atom octahedron is centered by a single atom can be described in space groups $P\bar{3}m1$ and $R\bar{3}m$, respectively, and are known for two structural modifications of Ta_2CS_2. The replacement of the atoms centering the octahedra by atom dumbbells, all parallel and oriented along 4-fold axes of the octahedra, lowers the symmetry to monoclinic. The structures of the two modifications of GdCBr are isopointal (same space group and Wyckoff sequence), but the unit cells can be distinguished from the value of the monoclinic angle. The infinite stacking of condensed RC_2R layers corresponds to the tetragonal structure of CaC_2, described later.

At first sight, the chemical bonding can be approximated by the formula $(R^{3+})_2(C_2)^{4-}(X^-)_2$, but the compounds are conducting in two dimensions because of a mixing of $C_2^{-\pi^*}$ antibonding and *R-d* states. Band structure calculations have revealed a very flat band (localization) with a significant $C_2^{-\pi^*}$ contribution at the Fermi level, corresponding to a maximum density of states. The Fermi level also crosses bands with a large slope (delocalization). Such a situation is considered to be favorable for superconductivity (Simon, 1997). Superconducting properties are observed for compounds with nonmagnetic rare-earth elements such as Y and La. Substitution of one halogen by

another modifies the cell dimensions and alters the degree of covalence of the *R–C* bonds. T_c increases from 2.3 K for YCCl to 5.1 K for YCBr, reaches a maximum of 11.1 K for $YCBr_{0.25}I_{0.75}$, and then decreases to 9.7 K for YCI. The structure changes from 1s to 3s, and back to 1s, during the progressive substitution. The variation of T_c appears to be independent of the actual stacking of the slabs, which seems to indicate that superconductivity takes its origin in the YC_2Y slabs. The incorporation of Na atoms into YCBr increases the translation unit along the stacking direction and produces a transition from the 3s- to the 1s-modification. As expected, the interstitial atoms were found to occupy the octahedral sites between the two bromine layers (partial occupation of Wyckoff position 2(*d*) 0 $\frac{1}{2}$ $\frac{1}{2}$ in space group *C*2/*m*).

Superconductivity at 6 K is reported for the compound $La_9B_3C_6Br_5$. The orthorhombic crystal structure, defined on $\mathbf{Ce_9B_3C_6Br_5}$, contains C–B–C units with an angle of 148° at the central atom. As in the carbohalides discussed earlier, nonmetal atom layers are sandwiched between two *R* atom layers to form slabs, separated by halogen atom layers. However, the *R* atom layers differ significantly from the close-packed layers found in the carbohalides. The B atoms center R_6 trigonal prisms and the C atoms R_5 square pyramids, which are fused to the trigonal prisms via common rectangular faces and share edges with each other. The resulting $R_3(CBC)_2R_3$ slabs are corrugated and separated by single Br layers.

b. $CeCo_4B_4$ Type and Stacking Variants

Superconductivity is observed at the composition RT_4B_4 in several ternary rare-earth–transition metal boride systems. A series of different structure types have been identified for this general composition, all characterized by the presence of boron dimers, empty transition metal atom tetrahedra, and single rare-earth metal atoms. In the structure types defined on $\mathbf{CeCo_4B_4}$, $\mathbf{LuRu_4B_4}$ and $\mathbf{LuRh_4B_4}$, shown in Fig. 6.19, T_4 tetrahedra and *R* atoms are arranged as the Na and Cl atoms in the simple NaCl type (compare Fig. 6.17). The main difference between the three structures concerns the relative orientation of the T_4 tetrahedra. A structural slab may be considered where tetrahedra and *R* atoms alternately occupy the points of a 2D square-mesh lattice. Neighboring tetrahedra within the slab are rotated by 90° with respect to each other. When two slabs are stacked upon each other, an *R* atom is always placed over a tetrahedron and vice versa. For convenience we will label the corners of the square mesh *A* (0 0), α (1 0), *B* (1 1), and β (0 1). The translation unit of the square-mesh lattice itself, *a*(mesh), is identical to the thickness of the slab. In the starting layer, points *A* and *B* are occupied by tetrahedra, points α and β by *R* atoms. The tetrahedra at *A* and *B* are rotated by 90° with respect to each other. A tetrahedron in the same orientation as the one placed at *A* in the starting layer, may in the second layer be found either in position α or in position β. In the third layer a similarly oriented

Fig. 6.19.

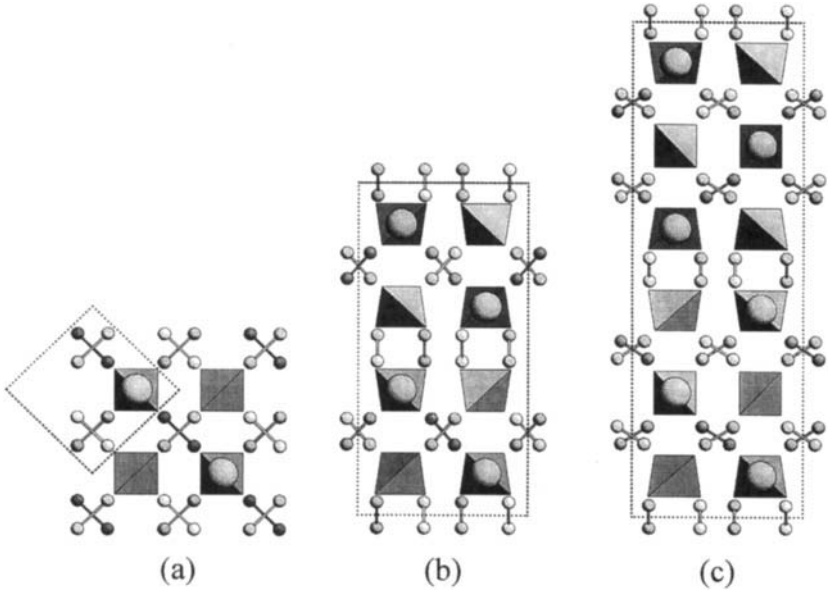

Structures of $ErRh_4B_4$ (**$CeCo_4B_4$** type) (a), **$LuRu_4B_4$** (b), and **$LuRh_4B_4$** (c) in projections along [0 0 1], [1 0 0], and [1 0 0], respectively, emphasizing the arrangement of R atoms, T_4 tetrahedra, and B_2 dumbbells. Note that R atoms are sometimes hidden by overlying T_4 tetrahedra.

tetrahedron may occupy position A, as in the first layer, or be placed in position B. The stacking mode $A\alpha$ is observed in $CeCo_4B_4$. The resulting structure is tetragonal primitive with $a \sim \sqrt{2}a$(mesh) and $c \sim 2a$(mesh). The boron dumbbells are located across the slab interface. When the slabs are stacked together, distances of the same magnitude as those observed within the tetrahedra appear between tetrahedra in the same orientation, so that infinite 2D frameworks result.

The slabs in $LuRu_4B_4$ are stacked according to the sequence $A\alpha B\beta$. The structure is tetragonal body-centered with the arrangement of the mutually rotated tetrahedra along [0 0 1] described by a 4-fold screw axis (space group $I4_1/acd$). The cell parameters are related to the translation units of the square-mesh lattice according to $a \sim 2a$(mesh), $c \sim 4a$(mesh). The general characteristics of the structure are otherwise similar to those described for $CeCo_4B_4$, with the difference that the interconnections of the T_4 tetrahedra lead to the formation of two independent interpenetrating 3D frameworks.

The stacking mode observed in $LuRh_4B_4$, $A\alpha A\beta B\beta$ is a combination of the former two. This structure is orthorhombic and the cell parameters of the conventional C-centered cell may be derived from the translation unit of the square-mesh lattice by the following relations: $a \sim c \sim 2a$(mesh),

$b \sim 6a$(mesh). The $CeCo_4B_4$ type is formed by RT_4B_4 compounds with Co or Rh, less often Ir. Superconducting transition temperatures above 10 K are observed for isotypic YRh_4B_4 and $LuRh_4B_4$. A few Rh-based compounds, such as $LuRh_4B_4$, form the three stacking variants under different conditions. The three modifications become superconducting at 11.8, 9.2 (stabilized by Ru), and 6.2 K, respectively.

c. Other Structures with Nonmetal Atom Dumbbells

The structure of **CaC_2** may be considered as a substitution derivative of the NaCl type with single anions replaced by C_2 dumbbells. The dumbbells are all parallel to [0 0 1] of the tetragonal body-centered cell. The structure is isopointal (same space group and Wyckoff sequence) with the $MoSi_2$ type, discussed in the section on intermetallic compounds. However, the presence of atom dumbbells in one structure, but not the other, excludes isotypism. The structure type is formed by most rare-earth elements; however, superconductivity is observed only for nonmagnetic ions. The C–C distance within the acetylene ion increases with increasing valence of the cation, e.g., from 1.19 for CaC_2 to 1.29 for YC_2 and 1.32 Å for UC_2. Of these three compounds, only YC_2 is a superconductor ($T_c = 3.9$ K).

Of the many R_2C_3 compounds crystallizing with the **Pu_2C_3** type, three truly binary compounds show superconducting transition temperatures above 10 K. The carbon atoms are arranged in dimers, with C–C distances ranging from 1.2 to 1.4 Å which can be assimilated to a multiple bond. The cubic body-centered unit cell contains 16 metal atoms and 12 carbon dumb-bells. As shown in Fig. 6.20, the dumbbells are parallel to the cell axes. The lanthanide atoms

Fig. 6.20.

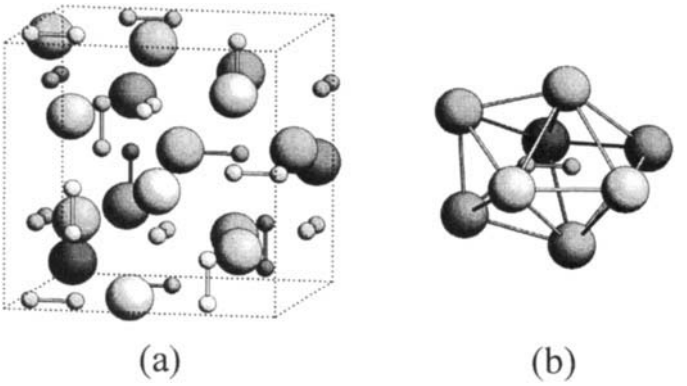

Structure of Lu_2C_3 (**Pu_2C_3** type), content of one unit cell (a) and Lu_8 dodecahedron around a C_2 dumbbell (b). Large spheres: Lu; small spheres: C.

were found to be in the trivalent state, except cerium, for which an average value of 3.4+ was determined. Each carbon atom has short distances to six surrounding rare-earth metal atoms forming a distorted octahedron. The other carbon atom of the dumbbell centers an octahedron edge that is significantly longer than the other edges. This crystallographically equivalent carbon atom is surrounded by an identical distorted octahedron, perpendicular to the preceding one. The two octahedra interpenetrate each other and the C_2 dumbbell is surrounded by a total of eight *R* atoms.

In most binary systems the Pu_2C_3-type phase presents a certain homogeneity range that presumably corresponds to the substitution of a certain proportion of C_2 dumbbells by single C atoms. If all dumbbells are replaced by single atoms, the composition becomes R_4C_3 and the structure that of the Th_3P_4 antitype. This structure has been reported for nonsuperconducting Sc_4C_3, whereas a superconducting transition temperature of 8.5 K is observed at the approximate composition $Sc_{13}C_{10}$. The structure of the superconducting phase may correspond to a small replacement of single atoms by dumbbells, but additional lines in the diffraction pattern could not be indexed. The superconducting properties of the Pu_2C_3-type phases are very sensitive to variations in the carbon content, the highest values being recorded at the C-rich boundary. They can be further enhanced by alloying and the highest critical temperature, 17.0 K, is known for the nominal composition $Y_{1.4}Th_{0.6}C_{3.1}$. In this case the cubic structure is formed by synthesis at high pressure and high temperature, whereas the product obtained by arc melting contains a tetragonal phase that is not superconducting.

The **$LuRuB_2$** type is also characterized by nonmetal dimers. In contrast to the RT_4B_4 borides, where the boron dimers are well separated from each other, they are here arranged in infinite zigzag chains where B–B distances of 1.74 Å alternate with distances of 1.92 Å. The angles are close to 120° and the chains may be considered as cut from the hexagon-mesh boron nets found, for example, in AlB_2 and $CeCo_3B_2$. Each boron atom centers a trigonal prism formed by three Lu and three Ru atoms. The B–B dimer distances occur when the prisms share rectangular faces. Relatively short distances are observed between the metal atoms, in particular between the Lu atoms (3.10 Å). Ruthenium may be replaced by osmium, and lutetium by other trivalent rare-earth elements. Superconductivity is observed for compounds with nonmagnetic lanthanide elements, the highest critical temperature, 10.0 K, being reached by the type-defining compound itself.

A superconducting transition temperature near 7 K was measured for the carbon-rich phase **$La_5B_2C_6$**, with 52 atoms in the tetragonal unit cell. The orthorhombic structure is virtually isotypic with that of nonsuperconducting $Ce_5B_2C_6$. Double square-mesh NaCl-type *RC* slabs may be considered in the structure, however, every fifth C atom is replaced by a C_2 dumbbell, changing the composition of the slab to R_5C_6. The dimers are approximately perpendicular to the NaCl-type slabs, but slightly tilted away from the 4-fold axes with a certain degree of disorder. Four partly occupied carbon sites were refined for $Ce_5B_2C_6$,

eight for $La_5B_2C_6$. The "single" carbon atoms of neighboring slabs are interconnected via the boron atoms and form approximately linear CBC units (d(C–B) ~ 2.0 Å). A limited homogeneity range with respect to the carbon content probably corresponds to different proportions of single C atoms and C_2 dumbbells. The superconducting transition temperature was found to decrease smoothly on both sides of the composition $La_5(CBC)_2C_2$.

d. $LuNi_2B_2C$ Type and Members of the Same Structure Series

A short time after the discovery of the high-T_c superconducting oxides, the more than 30-year-old record held by Nb_3Ge thin films was reached also by classical superconductors. A few ternary borocarbides (e.g., Mo_2BC) were known to be superconducting below 10 K. However, the discovery that by doping "YNi_2B_3" with small amounts of carbon, T_c could be increased to 13.5 K, and the almost simultaneous report on superconducting samples in the Y–Pd–B–C system with critical temperatures above 20 K, stimulated an intensive search for superconducting borocarbides in 1994. The identification of $La_3Ni_2B_2N_3$ with a closely related structure and a superconducting transition temperature of 12 K extended the interest to boronitrides. The crystal structures of this family of superconductors are strongly reminiscent of those of the high-T_c superconducting oxides.

The structure type defined on **$LuNi_2B_2C$**, shown on the left side of Fig. 6.2l, is a filled-up derivative of the tetragonal $CeAl_2Ga_2$ type. More than 400 intermetallic compounds, among which several ternary borides, crystallize with this well-known type, discussed in the section on intermetallic compounds. The insertion of carbon into the rare-earth metal atom layers is accompanied by an increase of the translation unit along the 4-fold axis. Like the structures of the high-T_c superconductors, the tetragonal structure of $LuNi_2B_2C$ can be decomposed into atom layers with square mesh. The stacking along the c-axis corresponds to the sequence –B–Ni_2–B–LuC–. The distances between the Ni atoms within the square mesh (2.45 Å) are slightly shorter than in metallic nickel. There is a considerable amount of covalent bonding extending in three dimensions, in particular between nickel and boron and between boron and carbon atoms. The short interatomic distances between the latter elements (1.47 Å) suggest double bonds. The Ni atoms center B_4 tetrahedra that share edges to form slabs, which may be considered as characteristic of the PbO antitype or of the CaF_2 (fluorite) type. These Ni_2B_2 slabs are held together by linear BCB units to form a relatively rigid, porous 3D framework that can accept rare-earth metal atoms of different sizes. Band calculations have shown that the Fermi level coincides with a sharp peak in the density of states, with contributions mainly from the d orbitals of nickel, but also from the BCB units.

The $LuNi_2B_2C$ type is formed by all lanthanide nickel borocarbides. The variation of the cell parameters with the radius of the rare-earth metal atom shows

Fig. 6.21.

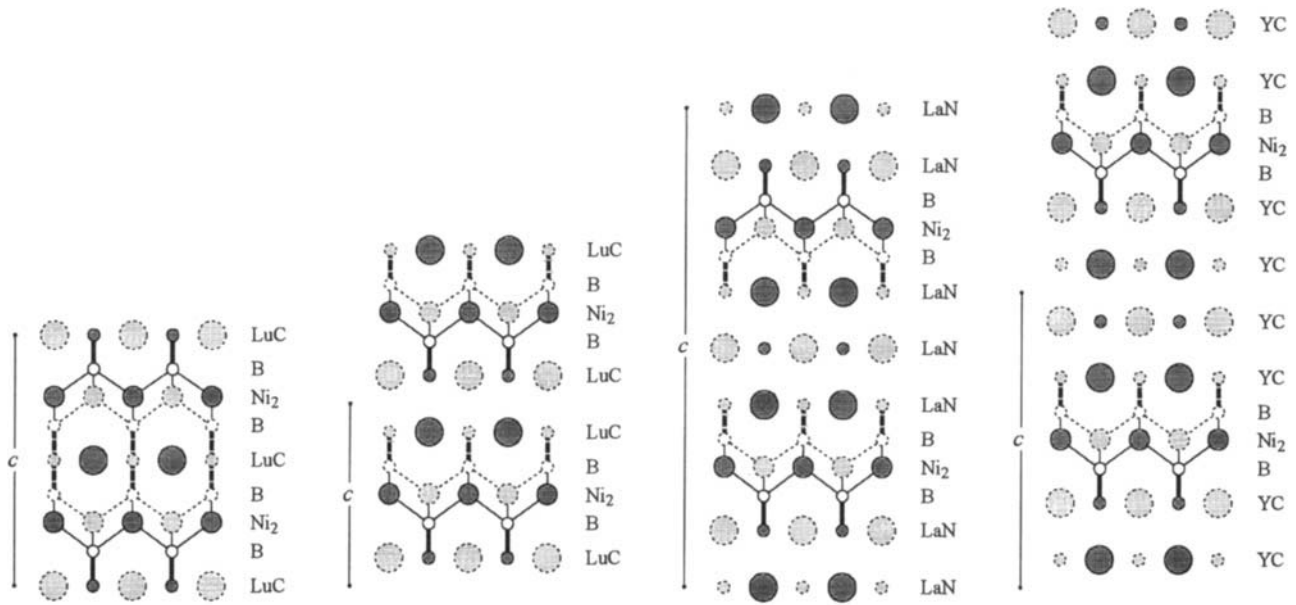

Schematic drawings of members of the structure series $R_nT_2B_2C_n$ ($n = 1, 2, 3$, and 4) formed by borocarbides and boronitrides, with Pearson codes. Shading indicates relative heights. Thick lines connect nonmetal atoms, thin lines Ni and B atoms.

an approximately linear increase of a but a decrease of c, corresponding to an overall increase of the cell volume. The apparently contradictory behavior observed for the c-parameter is explained by the relative rigidity of the Ni–B–C skeleton. When a larger rare-earth metal atom is inserted into the framework, the R-C distances become longer and the translation parameter of the square-mesh RC layer, i.e., the a-parameter, is increased. Structural refinements have revealed that the C–B, as well as the Ni–B, distances remain approximately constant for the whole series of lanthanides and that, in order to keep the latter unchanged when the a-parameter is increased, the tetrahedral angle in the NiB_4 unit is progressively decreased. The tetrahedra are distorted so that the thickness of the Ni_2B_2 slab is reduced, and consequently also the c-parameter.

Superconductivity is observed for lanthanide nickel borocarbides where the R atoms are not too large. A critical temperature of 16.6 K is reached by $LuNi_2B_2C$, the structure of which contains less distorted NiB_4 tetrahedra than the isotypic compounds. As observed for the RT_4B_4 borides and the Chevrel phases, some magnetic elements also form superconductors. $HoNi_2B_2C$, for instance, orders antiferromagnetically at 8 K and becomes superconducting at a slightly lower temperature. The pair-breaking effect is believed to be diminished by the fact that the magnetic system is electronically well isolated from the superconducting system. $GdNi_2B_2C$, on the contrary, orders magnetically at 19 K, and shows no superconductivity. When Ni is doped by small amounts of Co or Cu, the superconductivity is rapidly destroyed.

Superconducting transition temperatures above 20 K are observed for multiphase samples in the system Y–Pd–B–C. The samples are readily reproduced, but there is controversy over the exact composition and structure of the contributing phase. It is most commonly believed to be an off-stoichiometric, possibly boron-deficient variant of the $LuNi_2B_2C$-type structure. By progressively replacing platinum by gold, nearly single-phase samples could be obtained for nominal compositions with a slight excess of transition metal ($R(Pt,Au)_{2.1}B_2C$), for which the diffraction patterns indicated a $LuNi_2B_2C$ type structure. Transition temperatures above 20 K have also been reported for multiphase samples in the Th–Pd–B–C system, where two superconducting phases were found to coexist.

The square-mesh atom layers found in the structure of $LuNi_2B_2C$ can be combined in different proportions. $LuNi_2B_2C$ may be considered as the first member of a homologous structure series of the general formula $R_nT_2B_2C_n$, of which several members with higher values of n have been reported since the discovery of $LuNi_2B_2C$ ($n = 1$). Consecutive RC layers are stacked upon each other like in the NaCl type, revealing another analogy with high-T_c superconducting cuprates. The first four members of this structure series are shown in Fig. 6.21. Thicker NaCl-type slabs are expected to accentuate the 2D character of the superconductor. For odd values of n the unit cell is tetragonal body-centered (space group of highest symmetry $I4/mmm$); for even values it is tetragonal

primitive ($P4/nmm$). In contrast to the high-T_c superconductors, few planar defects or intergrowths are observed on HREM images.

The structure of the second member of the $R_nT_2B_2C_n$ series was identified on **LuNiBC** ($n = 2$), i.e., in the same system as $LuNi_2B_2C$. The structure type was later found also for the quaternary boronitride LaNiBN. The nonmetal atoms form BC (or BN) dimers, but the insertion of an additional LuC layer destroyed the strong connection between the slabs of edge-linked NiB_4 tetrahedra. The structure is a substitution variant of a structure type known for ternary carbides, the $ScCoC_2$ type. It may also be considered as a filled-up derivative of the universal type PbClF, of which several branches are known. None of the isotypic compounds is superconducting, and band calculations performed on LuNiBC have shown that the Fermi level is located in a well-defined valley.

A structure with three NaCl-type layers has been reported for another boronitride, $\mathbf{La_3Ni_2B_2N_3}$ ($n = 3$), which becomes superconducting at 13 K. The structure contains BN units and single nitrogen atoms inside La_6 octahedra. Vacancies on the latter nitrogen site, situated in the central NaCl-type layer, are probably responsible for minor variations in T_c.

A member of the same structure series with $n = 4$ was deduced from HREM images for nonsuperconducting Y_2NiBC_2 (Li *et al.*, 1995). The authors claim that a larger cell must be used for the indexation of the electron diffraction pattern. A different structure, where the two central *R*C layers are replaced by two *R* layers separated by a layer containing carbon atoms, was proposed for the same composition but another rare-earth element, Lu_2NiBC_2 (Zandbergen *et al.*, 1994a). The true symmetry of this phase was stated to be monoclinic. An intergrowth structure with B–Ni_2–B slabs separated by alternately one and two YC layers was reported for $Y_3Ni_4B_4C_3$.

e. Structures with Nonmetal Polymers

Only a few binary borides are known to be superconducting, among these YB_6 ($T_c = 7.1$ K), which crystallizes with the cubic $\mathbf{CaB_6}$ type. The primitive unit cell contains seven atoms. The B atoms form octahedra, centered at $\frac{1}{2}\ \frac{1}{2}\ \frac{1}{2}$, which are interconnected via interatomic distances of the same length as those within the octahedra to form a 3D framework with large voids. Each B atom is bonded to five others, which form a surrounding square pyramid. The coordination polyhedron around the cation is made from 24 boron atoms, all located at the same distance from the central atom.

The cubic face-centered $\mathbf{UB_{12}}$ type contains empty B_{12} cuboctahedra in a cubic close-packed arrangement. The cations are situated between the cuboctahedra so that polyhedra and cations form a NaCl-type arrangement. The B_{12} cuboctahedra are interconnected via exo bonds to form a 3D framework with BB_5 square pyramids, similar to those found in CaB_6. This structure type is also

present in the Y–B system, but the superconducting transition temperature is slightly lower (4.7 K) than for YB_6. The highest value observed for this type, 5.8 K, is reported for ZrB_{12}. When Zr is partly substituted by Sc, the compound undergoes a phase transition to a nonsuperconducting rhombohedral modification.

Superconducting properties were detected for the ternary borocarbide **Mo_2BC** (Fig. 6.22) as early as the sixties. As in the structure of LuNiBC, discussed previously, T_2B_2 layers are separated by double NaCl-type layers containing the carbon atoms. However, the stacking sequence within the T_2B_2 slabs is here T–B–B–T (as compared with B–T_2–B for LuNiBC). The square-mesh layers are further shifted so that orthorhombic symmetry results. The B atoms center Mo_6 trigonal prisms, which share triangular and rectangular faces to form infinite slabs, inside which the atom arrangement is characteristic of that observed in AlB_2. The distances between boron atoms through the rectangular faces of the prisms are short (1.79 Å) and infinite boron zigzag chains are observed. Little distorted Mo_6 octahedra surround the carbon atoms in the NaCl-type layers. No bonding distances occur between boron and carbon atoms and HREM studies have confirmed the intergrowth character of the structure. Attempts to increase the superconducting transition temperature by partly substituting Mo by different other metals (Zr, Hf, Nb, Ta, W, Rh) were successful only for substitutions by the electron-rich Rh, T_c reaching a maximum (9.0 K) for a Rh : Mo ratio of 0.2 : 1.8. For phases with the same valence electron concentration, T_c increases with increasing cell volume. The same structure type was later found for a ternary boronitride, Nb_2BN.

All lanthanide elements have been reported to form compounds that crystallize with the tetragonal **YB_2C_2** structure type. Only YB_2C_2 and LuB_2C_2, however, become superconducting at 3.6 and 2.4 K, respectively. The structure of YB_2C_2, which is richer in nonmetal elements than the borocarbides discussed earlier, contains planar BC nets with four- and eight-membered rings. Consecutive BC nets are rotated by 90° with respect to each other. The rare-earth metal atoms are situated between two eight-membered rings. The a-parameter, which is determined mainly by the B–C bonds, remains approximately constant

Fig. 6.22.

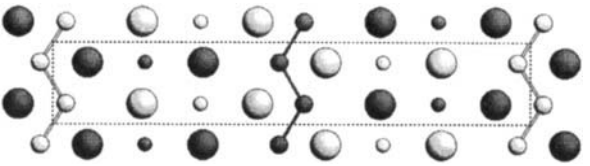

Structure of **Mo_2BC** in a projection along [1 0 0]. Large spheres: Mo; medium spheres: B; small spheres: C. Dark shading: $x = \frac{1}{2}$; light shading: $x = 1$. Solid lines connect nonmetal atoms forming infinite zigzag chains.

for all isotypic compounds, whereas the c-parameter increases linearly with the radius of the trivalent rare-earth metal ion.

F

Chalcogenides

a. Perovskite, Bronze, and Spinel

For a long time Oxides were not considered to be promising materials for superconducting properties. The series of heavy metal oxides reported with perovskite-type structures are generally seen as the precursors of the high-T_c superconducting cuprates.

The cubic unit cell of idealized perovskite, **$CaTiO_3$**, contains five atoms. A Ca atom is located at the center of the cube, a Ti atom at the origin, and O atoms at the centers of the edges. TiO_6 octahedra share vertices to form a 3D framework, the cuboctahedral voids of which are centered by Ca atoms (Fig. 6.23). The structure can alternatively be seen as built up of close-packed mixed CaO_3 layers in c stacking. The Ti atoms selectively occupy all octahedral voids in the resulting framework that are surrounded exclusively by O atoms. Numerous related structures with different distortions of the octahedron framework and/or off-centered cation sites are known. Three different deformation variants are described in the chapter on the crystal structures of high-T_c superconducting cuprates.

At room temperature, $BaBiO_3$ crystallizes with a monoclinically distorted perovskite-type structure. As bismuth is progressively substituted by lead, the structure of $BaPb_xBi_{1-x}O_3$ undergoes a transformation from monoclinic to

Fig. 6.23.

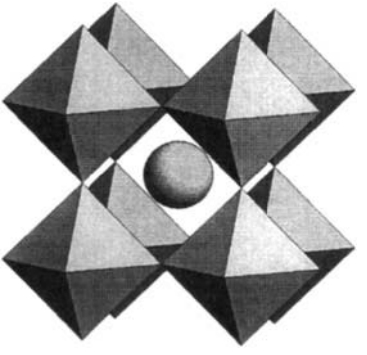

Structure of **$CaTiO_3$**, perovskite, emphasizing the framework of corner-linked TiO_6 octahedra. Large sphere: Ca atom.

orthorhombic ($x \sim 0.25$), and then to a different monoclinic structure ($x \sim 0.8$). For values of x between 0.7 and 0.8 a two-phase region is observed where the orthorhombic phase coexists with a tetragonal phase. The superconducting transition at 10–13 K is attributed to the tetragonal, quenched high-temperature phase, stable above 425 K. The atom arrangement observed for this phase had earlier been identified on the antitype **Cr_3AsN**. The $(Pb,Bi)O_6$ octahedra in $BaPb_{0.7}Bi_{0.3}O_3$ are slightly tilted and the cell is doubled in one direction with respect to cubic perovskite. The maximum value of T_c is observed at the Pb-poor phase boundary. Substitution by up to ~50% potassium on the barium site in the same $BaBiO_3$ causes different changes in the crystal structure. From monoclinic, $Ba_{1-x}K_xBiO_3$ becomes first orthorhombic ($x \sim 0.1$), then cubic ($x \sim 0.37$). $Ba_{0.6}K_{0.4}BiO_3$, which crystallizes with the undistorted cubic perovskite-type structure, exhibits superconductivity at 30 K.

The basic feature of hexagonal tungsten bronzes, defined on **Rb_xWO_3**, is also a framework of corner-linked TO_6 octahedra. The W atoms make a Kagome net when projected along [0 0 1]. The octahedra are slightly tilted, which is generally expressed by the splitting of one O site. The alkaline metal atoms are found in the large channels formed by rings of six octahedra. Rb and Cs atoms are located approximately midway between the two O_6 hexagons, whereas the smaller K atoms are displaced toward one or the other. The superconducting properties are strongly enhanced when some of the cations are removed by acid etching. For Rb_xWO_3 the superconducting transition temperature could be increased from 2.2 to 6.6 K this way.

The oxygen atoms in cubic spinel, **$MgAl_2O_4$**, form a cubic close-packed arrangement. Half of the octahedral voids are filled by Al atoms and one-eighth of the tetrahedral ones by Mg atoms. The AlO_6 octahedra share edges to form infinite chains parallel to the face diagonals. Chains in layers alternating along the cell edges are mutually perpendicular and interconnected via common octahedron edges to form a complex 3D framework described in space group $Fd\bar{3}m$. The MgO_4 tetrahedra share single corners with the octahedron framework. Superconductivity up to 13.2 K is reported for the spinel $Li_{1-x}Ti_2O_4$. The maximum value is observed for $x = 0.25$, whereas on further removal of Li atoms the diffraction peaks become broad and superconductivity is destroyed. In $Li_{1+x}Ti_{2-x}O_4$ ($x \leq 0.33$) solid solutions, Ti and excess Li atoms are randomly distributed on the octahedral site. A metal-to-insulator transition takes place at $x = 0.15$. $CuRh_2S_4$ and the corresponding selenide are superconducting below 4.4 and 3.5 K, respectively. Like the lithium titanate, these chalcogenides have essentially a *normal* spinel structure, which means that the atoms of the minority element occupy the tetrahedral site.

b. Layered Structures and Intercalation Compounds

Mo, Nb, and Ta form a series of polytypic disulfides and diselenides of layered character. The sulfur or selenium atoms are arranged in close-packed layers that

are directly superposed two by two. The metal atoms occupy half of the trigonal prismatic voids between the directly superposed layers. The slabs consisting of a metal atom layer sandwiched between two close-packed chalcogen layers can then be stacked upon each other with the same possibilities (*A*, *B*, or *C*) as single close-packed layers. The simple polytypes discussed here, **2H-MoS_2**, **2H-NbS_2**, **3R-MoS_2**, and **4H-$NbSe_2$**, are compared in Fig. 6.24. The former two contain slabs in *h* stacking, whereas the latter two contain slabs in *c* and *hc* stacking, respectively. An additional reason for polytypism arises from the possibility for the metal atoms in consecutive slabs to occupy different trigonal prismatic voids. This is illustrated by the structure types defined on 2H-MoS_2 and 2H-NbS_2, which both contain TS_2 slabs in *h* stacking, but have different arrangements of metal atoms. The slabs are held together only by van der Waals interactions, which provides a pronounced layer character to the structures. Some of the compounds show a certain homogeneity range extending on the metal-rich side of the 1 : 2 element ratio, where the excess atoms occupy part of the octahedral sites between the slabs. Binary MoS_2 is a semiconductor, whereas binary $NbSe_2$ becomes superconducting around 7 K.

Alkali and alkaline-earth metals dissolved in liquid ammonia react with MoS_2 to form intercalation compounds of the general formula A_xMoS_2. K, Rb, and Cs intercalates ($T_c \sim 6$ K) have well-defined compositions, whereas Na and Li intercalates ($T_c \sim 4$ K) present a significant homogeneity range. The limiting metal composition for divalent cations is slightly lower than for monovalent ones. The refinement of the structure of $Cs_{0.34}NbS_2$ has shown that the Cs atoms are located at the octahedral sites between the slabs. A large number of molecules, such as amides, pyridines, or alkylamines, can be intercalated between the slabs of TaS_2 or NbS_2 to form intercalates where the "interlayer spacing"

Fig. 6.24.

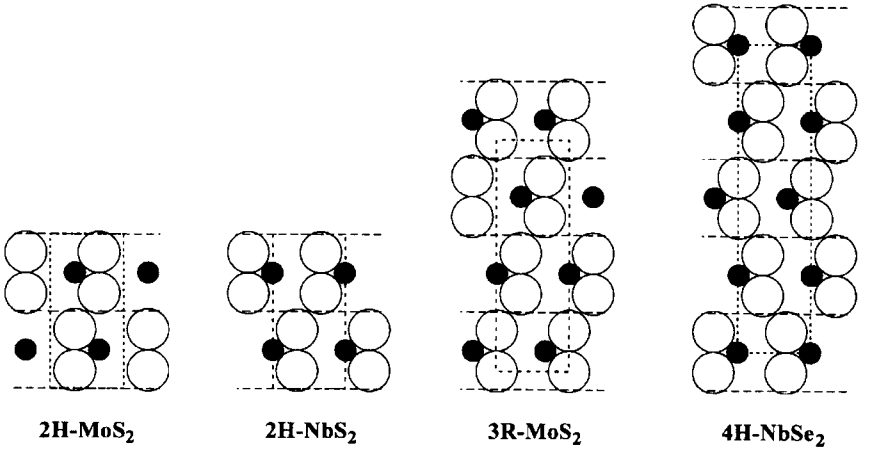

Stacking sequences in four-layered chalcogenide structures. Only the atoms in the (1 1 0) cross-section are shown. Large white circles: S, Se; small black circles: Mo, Nb.

exceeds by far the thickness of the chalcogenide slab itself. The increase of the chain length from ammonia to octylamine was found to decrease the superconducting transition temperature of the TaS_2 intercalate linearly from 4.2 to 1.8 K.

Differing from the group VA elements Nb and Ta, Ti atoms prefer octahedral coordination. In the **4H-$Ti_{1+x}S_2$** polytype presented here, the close-packed layers formed by the sulfur atoms are arranged in *hc* stacking. The titanium atoms preferentially occupy the octahedral voids in every second interlayer, the excess metal atoms being distributed over the remaining octahedral sites. The Li atoms in 4H-$Li_{0.3}Ti_{1.1}S_2$ (T_c = 13 K) are believed to substitute for Ti on one or both octahedral sites. The structure is not considered to be an intercalate in the proper sense, since the parent type is not a truly layered structure.

A superconducting transition temperature of 5.3 K is reported for the compound "$LaNb_2Se_5$," an example of a so-called *misfit layer compound*, which crystallizes with a composite layered structure containing $NbSe_2$ slabs, similar to those discussed earlier and NaCl-type LaSe slabs. The thickness of the latter corresponds to two square-mesh atom layers. The translation unit in the plane perpendicular to the stacking direction is 3.437 Å for the $NbSe_2$ slabs (*a* of the hexagonal subcell), but 6.019 Å for the LaSe slab (*a* of a NaCl-type face-centered cubic cell). The ratio is an irrational number and the composite structure is made up of two "independent" substructures with incommensurate translation vectors in one direction. The stacking sequence corresponds to two $NbSe_2$ slabs, stacked as in 2H-NbS_2, followed by one LaSe slab. In order to take into account the particular features of the structure, the chemical formula is generally written as $(LaSe)_{1.14}(NbSe_2)_2$. The layered character is due to the van der Waals bonding between the two consecutive $NbSe_2$ slabs. The cell parameters are listed with the data set of 2H-NbS_2 (Section J).

c. Chevrel Phases and Related Structures

Among the best-known families of superconductors are the so-called Chevrel phases, a family of Mo-based chalcogenides, which show critical temperatures of up to 15.2 K. Their crystal structures contain Mo_6X_8 (X = S, Se or Te) clusters where a Mo_6 octahedron is surrounded by eight chalcogen atoms, located above the octahedron faces and forming a concentric cube.

The Mo_6X_8 units are arranged so that their centers form a distorted cubic lattice. The rotation of the clusters by about 27° around the 3-fold axes leads to clear trigonal (rhombohedral) symmetry, even if the cell angle is close to 90°. This atom arrangement leaves relatively large interstices, susceptible to host interstitial atoms. The projection of the structure of the filled-up derivative **HT-$Pb_{0.9}Mo_6S_8$** along the edge of the rhombohedral cell is shown in Fig. 6.25. The list of known filled-up derivatives is impressive, with interstitial

atoms ranging from alkaline, alkaline-earth, or rare-earth elements to transition metals and nonmetals such as lead or tin. Eight chalcogen atoms forming a distorted cube surround the void at the origin of the cell. Large *M* atoms such as alkaline-earth metal or Pb atoms center these voids, whereas smaller *M* atoms, such as Ni or Cu, are displaced from the 3-fold axis. The angle of the rhombohedral cell increases with the degree of delocalization of the *M* atoms. Compounds with localized *M* atoms show angles ranging from 88 to 92°, whereas the cell angle of $Cu_{3.36}Mo_6S_8$ reaches 95.6°.

The *M* atoms transfer their electrons to the Mo_6 cluster, which, in agreement with the bond-valence rules, is progressively contracted when the oxidation state or the concentration of the element *M* is increased. The shortest intercluster distances are ~3.2 Å, providing a certain linear-chain character to the Mo substructure.

Many Chevrel phases show a phase transition to a triclinic structure, corresponding to a distortion of the cluster, and, in the case of small *M* atoms, to a partial ordering of these. For certain compounds with transition elements such as Fe, the phase transition takes place above room temperature. The fact that, contrary to what is observed for many other families of superconductors, the application of high pressure has a negative influence on the superconductivity is explained as a consequence of the "freezing-in" of the rhombohedral-to-triclinic phase transition. Data sets are given here for the following types: **Mo_6Se_8**,

Fig. 6.25.

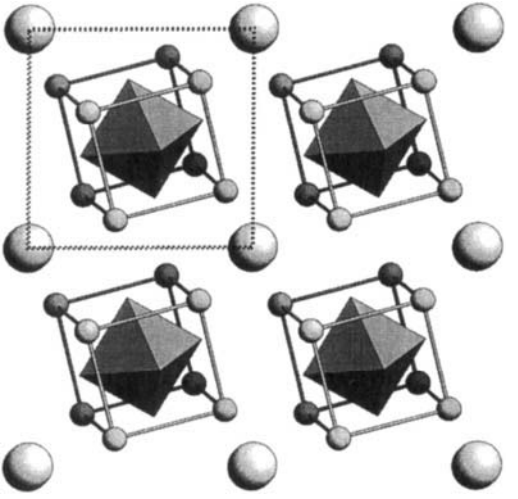

Structure of the Chevrel phase **HT-$Pb_{0.9}Mo_6S_8$** in a projection along [0 0 1] of the rhombohedral cell, emphasizing the arrangement of Pb atoms and Mo_6 octahedral clusters surrounded by S_8 cubes. Large spheres: Pb; small spheres: S.

rhombohedral HT-$Pb_{0.9}Mo_6S_8$ and **HT-$Ni_{2.5}Mo_6S_8$**, triclinic **LT-$BaMo_6S_8$** and **LT-$Ni_{0.66}Mo_6Se_8$**.

Band structure calculations have shown that the Fermi level is situated in a narrow region of bands with mainly Mo-4*d* character. For $M_xMo_6S_8$ a forbidden energy gap is present in the band structure just above the Fermi level and the conduction band is filled for an electron concentration of 24 electrons per Mo_6 cluster. For the corresponding selenides and tellurides this limiting number is lower. As a consequence, the homogeneity ranges of the latter two are systematically shifted toward a lower *M* content, with respect to the sulfides.

Binary Mo_6S_8 is difficult to synthesize, but may be obtained by removing the *M* atoms from one of its filled-up derivatives. Mo_6Se_8 and Mo_6Te_8 both exist as stable compounds, but few filled-up derivatives are known for the latter. The chalcogens form solid solutions and can in part also be replaced by halogen atoms. Partial substitution of Mo by other transition elements has also been reported. Of the three binary compounds, only Mo_6Se_8 has a superconducting transition temperature exceeding 4.2 K, but substitution of two of the eight S atoms in Mo_6S_8 by I atoms (22 electrons per cluster) leads to $T_c = 14.0$ K. Solid solutions S–Se or Se–Te show lower transition temperatures than pure Mo_6Se_8.

The filled-up derivatives are generally subdivided into three categories, as a function of the position of the interstitial element in the periodic table. The highest superconducting transition temperatures within each of the three categories are reached by $YbMo_6S_8$ (8.6 K), $Cu_{1.84}Mo_6S_8$ (10.8 K), and $PbMo_6S_8$ (15.2 K). For $Cu_{1.84}Mo_6S_8$ the superconducting material is claimed to be the triclinic low-temperature phase. At the limiting composition $Cu_4Mo_6S_8$, the phase undergoes no structural transition and is semiconducting, in agreement with a valence electron concentration of 24 electrons per cluster. For compounds containing rare-earth elements, the superconducting transition temperature was found to increase with increasing cell volume.

It may be noted that, for some of the "compounds" listed in the table for HT-$Pb_{0.9}Mo_6S_8$ in Section J, the Mo:*X* ratio differs from 6:8. None of the structure refinements of Chevrel phases has given any indication for significant vacancies on the anion site or for the presence of additional Mo atoms in interstices. Several samples were reported as also containing MoS_2 or Mo_2S_3.

The Chevrel phases are members of a family counting some 50 structure types based on octahedral metal atom clusters with anions situated above the faces of the octahedra. Structures with additional anions between the clusters are observed at higher *X*:*T* ratios. On the other side in the phase diagram, structures with condensed clusters, where two or several transition metal atom octahedra share faces, are found. The general formula of a condensed cluster can be written as $T_{3n+3}X_{3n+5}$, where *n* is the number of fused octahedra.

Combinations of simple Mo_6Se_8 and double Mo_9Se_{11} clusters are found in $Mo_{15}Se_{19}$. In both structural modifications known for this compound, the arrangement of the clusters can be assimilated to close packing. In hexagonal

α-$Mo_{15}Se_{19}$ close-packed slabs of alternately single and double clusters adopt an *hc* stacking, the double clusters being always in stacking position *h*. In rhombohedral **β-$Mo_{15}Se_{19}$** similar alternating slabs are arranged in *c* stacking. These structures can also host a certain number of cations in the interstices, but the highest critical temperature, 4.3 K, is reported for the two modifications of the binary compound.

A superconducting transition temperature close to 6 K was reported for a sample of nominal composition $Tl_2Mo_6Se_6$. The significantly lower values observed by the same authors for other samples of the same composition are in agreement with the critical temperature of about 3 K reported elsewhere. The presence of infinite columns of condensed T_6 octahedra provides a 1D character to this hexagonal structure, first determined on **$Ti_2Fe_6Te_6$**. None of the sulfides, selenides, or tellurides reported with the same structure was found to be superconducting above 1 K.

d. Other Chalcogenide Structures

The antitype of cubic **Th_3P_4** has already been mentioned for nonsuperconducting Sc_4C_3, together with the related Pu_2C_3 type, where single C atoms are replaced by C_2 dumbbells. A Th_3P_4-type atom arrangement with anions and cations distributed as in the type-defining phosphide is adopted by a series of R_2S_3 sesquisulfides of early trivalent rare-earth elements. The metal atoms center 8-vertex dodecahedra and the nonmetal atoms distorted octahedra. Since the C_2 dumbbells in Pu_2C_3 occupy the same positions as the Th atoms here, the dodecahedron found around a Th atom can be seen in Fig. 6.20b. It can be decomposed into two concentric and mutually rotated tetrahedra, one elongated and the other flat. The composition R_2X_3 of the semiconducting compounds corresponds to one-ninth of vacancies on the cation site. Progressive filling of the site has no significant influence on the cell parameter, but changes the electric properties. Transition temperatures ranging from 5.3 K for La_3Te_4 to 8.1 K for La_3S_4 are reported for lanthanum chalcogenides with fully occupied cation sites. La_3S_4 and La_3Se_4 undergo a phase transition to a tetragonal structure at 90 and 62 K, respectively.

Close-to-equiatomic **$Pd_{17}Se_{15}$** crystallizes with a cubic structure and 64 atoms in the unit cell. The Pd atoms are found in octahedral and approximately square coordination. There are no short Se–Se distances. The isotypic Rh-based sulfide $Rh_{17}S_{15}$ becomes superconducting at 5.8 K.

The structure of pyrite, cubic **p-FeS_2**, can be derived from that of NaCl by replacing single anions by anion pairs. The existence of such pairs in a structure with divalent Fe is in agreement with generalized valence rules, according to which the compound can be written as $Fe^{2+}(S_2)^{2-}$. The S_2 pairs are present in four different orientations, parallel to the four body diagonals of the cubic cell. This distinguishes the pyrite type from the tetragonal CaC_2 type, discussed

earlier, which can be derived from the NaCl type in a similar way, but where the atom pairs are all parallel. FeS_6 octahedra share single comers to form a 3D framework. The cubic pyrite-type phase $Rh_{1-x}Se_2$ exists in the homogeneity range $0.02 \leq x \leq 0.24$. At $x = 0.25$, an ordered arrangement of metal atoms and vacancies is observed, defined as the rhombohedral Rh_3Se_8 type. Superconductivity is reported for the pyrite-type phase with a maximum value of 6.0 K for the nominal composition $RhSe_{1.75}$. Critical temperatures up to 4.3 K have sometimes been assigned to the rhombohedral phase; however, according to other authors, this ordered Rh-deficient phase is semiconducting.

In the orthorhombic structure of **NbPS**, each Nb atom centers a trigonal prism formed by four P and two S atoms and capped by two additional S atoms. Neighboring trigonal prisms share P_4 faces, with a distance of 2.93 Å between the Nb atoms centering the prisms. The P atoms also form pairs, arranged in infinite chains with alternating interatomic distances of 2.22 and 2.51 Å.

G

Heavy-Electron Compounds

Heavy-electron, also called heavy-fermion, compounds are characterized by exceptionally large effective electron masses. Among the various interesting properties exhibited by this class of compounds is superconductivity, sometimes combined with magnetic order. Heavy-electron compounds contain elements with *f* electrons, such as Ce, Yb, or U. From a structural point of view they do not present any particular features, but crystallize with structure types formed also by other compounds. The superconducting transition temperatures do not reach the value of 4.2 K, but because of their exceptional properties, the structures of the best-known representatives will be briefly mentioned here.

The first heavy-electron superconductor, $CeCu_2Si_2$, was reported in 1979 (Steglich *et al.*, 1979). It crystallizes with a tetragonal $CeAl_2Ga_2$ (also called $ThCr_2Si_2$) type structure. This structure type, an ordered substitution derivative of $BaAl_4$, is discussed earlier under structures with atoms in square-antiprismatic coordination (Section C). The compound exhibits superconductivity up to 0.6 K in samples containing an excess of Cu forming impurity phases. Structural refinements have shown slightly shorter Ce–Si distances in the superconducting phase at the Cu-rich boundary than in the nonsuperconducting phase observed in Cu-poor samples, indicating a slightly lower *f* occupation in the former. In isotypic URu_2Si_2 superconductivity coexists with long-range antiferromagnetic order ($T_c = 1.2$ K, $T_N = 17.5$ K).

The highest superconducting transition temperature reported up to now for a heavy-electron compound, 2.0 K, is observed for UPd_2Al_3. This compound crystallizes with a $CeCo_3B_2$-type structure, a type that is also presented in the

section on intermetallic compounds. Hexagonal $CeCo_3B_2$ is an ordered substitution derivative of $CaCu_5$, implying no lowering of the symmetry. A structural branch, defined on $PrNi_2Al_3$, is sometimes considered, where the transition metal atoms occupy the sites that are occupied by the nonmetal, boron atoms in $CeCo_3B_2$. UPd_2Al_3 belongs to this branch, for which the c/a ratio is considerably higher than for the boride, ~0.8 compared with ~0.6. The shortest U–U distance is equal to the cell parameter c, 4.19 Å. The compound orders antiferromagnetically at 14.4 K. The isotypic heavy-electron compound UNi_2Al_3 shows a slightly shorter U–U distance, 4.02 Å, and lower transition temperatures ($T_c = 1.1$ K, $T_N = 4.6$ K).

UPt_3 contains close-packed UPt_3 layers in h stacking, characteristic of the hexagonal LT-Mg_3Cd type, discussed under intermetallic compounds with close-packed structures (Section C).

The cubic **$NaZn_{13}$** type, the face-centered unit cell of which contains 112 atoms, is adopted by the heavy-electron compound UBe_{13}. The Na atoms and distorted Zn_{12} icosahedra centered by a Zn atom form a CsCl-type arrangement. The Na atoms are coordinated by 24 Zn atoms forming a snub cube, a polyhedron obtained by cutting the eight vertices of a cube. The compound becomes superconducting close to 1 K. Upon doping UBe_{13} by a small amount of Th, T_c decreases drastically, but reaches a new maximum (~0.6 K) for the approximate composition $U_{0.97}Th_{0.03}Be_{13}$.

H

Organic Compounds

a. Fullerides

The discovery of buckminsterfullerene, or pristine, with its large pseudospherical units, marked the starting point for research on carbon polymers and related compounds in many different fields. Among other interesting properties, fullerenes doped with alkaline or alkaline-earth metal atoms are superconducting, with critical temperatures exceeding 30 K.

The fullerene molecule contains 60 carbon atoms forming 12 pentagons and 20 hexagons, fused into a pseudosphere. From a structural point of view the "balls" behave like single metal atoms and adopt close-packed arrangements, preferentially a face-centered cubic arrangement, similar to the one found in elementary Cu. At room temperature the molecules are orientationally disordered, but below 249 K a preferred orientation is adopted and the space group is lowered from $Fm\bar{3}m$ to $Pa\bar{3}$.

Up to about 10 metal atoms per fullerene unit can be inserted into this basic structure, which contains one octahedral and two tetrahedral voids per C_{60} molecule. At the composition A_3C_{60} both the octahedral and the tetrahedral

sites are occupied by single atoms. The resulting arrangement of metal atoms and fullerene molecules, illustrated in Fig. 6.26 for $\mathbf{K_3C_{60}}$, corresponds to the simple structure of BiF_3, of which $MnCu_2Al$, described in the section on intermetallic compounds, is an ordered substitution derivative. Sr and Yb atoms were found to occupy off-centered positions in the octahedral voids. In substituted fullerides such as Na_2CsC_{60}, the larger metal atoms preferentially occupy the octahedral sites, whereas in Na_2KC_{60} a disordered arrangement of cations was found. In "stuffed" $Na_2Cs(NH_3)_4C_{60}$, part of the Na atoms are surrounded by four ammonium molecules forming a tetrahedron. These complex cations occupy the octahedral sites, whereas the remaining Na and Cs atoms are randomly distributed over the tetrahedral sites. An ordered vacancy derivative is reported for $Yb_{2.75}C_{60}$, where part of the tetrahedral sites remain empty so that the cell is doubled in all directions and the overall symmetry lowered to orthorhombic. Only the tetrahedral voids were found to be occupied in Na_2C_{60}.

For metal-to-fullerene ratios exceeding 3 : 1, two slightly different solutions are adopted by different cations. In Na_6C_{60} and Ca_5C_{60} the octahedral voids are occupied by up to four metal atoms each, forming a tetrahedron. In the Na-richest compound $Na_{9.7}C_{60}$ this tetrahedron is extended to a cube, with Na–Na distances of 3.2 Å. For metal atoms such as K, Rb, Cs, Sr, or Ba, the arrangement of the fullerene molecules changes from face-centered cubic (Cu type) to body-centered cubic (W type). As described previously for the structures of the elements, this change can be achieved by extending the cubic close-packed

Fig. 6.26.

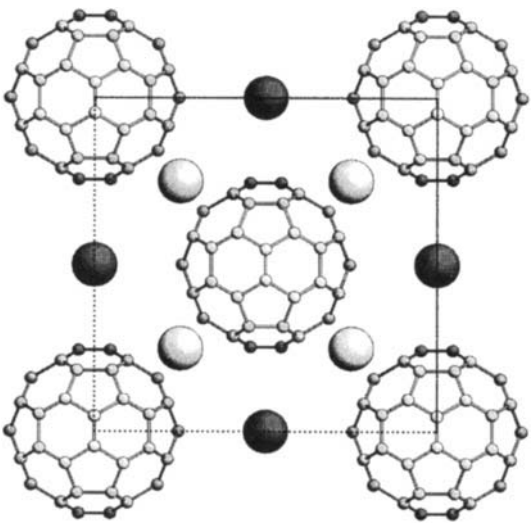

Structure of $\mathbf{K_3C_{60}}$ in a partial projection along [0 0 1]. Dark shading and fullerene molecules: $z = 0$; light shading: $z = \frac{1}{4}$.

structure in the plane perpendicular to one of its 4-fold axes. Such packing is less dense and contains six tetrahedral voids per molecule. In the cubic body-centered structure of $\mathbf{Cs_6C_{60}}$ all these voids are occupied by metal atoms, which form a pattern where all faces of the cubic cell contain a square of atoms. At the metal-to-molecule ratio 4 : 1, an ordered arrangement of metal atoms and vacancies is found, with a square of metal atoms on two and a pair of atoms on the other four faces of the cell. The symmetry of this structure is tetragonal and the c/a ratio slightly lower than unity. For the ratio 3 : 1, one-half of the tetrahedral voids are empty and all faces of the cell contain two metal atoms. The structure is cubic primitive and the arrangement of metal atoms and fullerene molecules identical to the one formed by the atoms in the Cr_3Si ($A15$) type.

Different kinds of rotational disorder are reported for the fullerene molecules in different compounds, the exact situation being not always clear. The rotational disorder in Li_2CsC_{60} is considered to be spherical. K_3C_{60} presents a merohedral disorder, where the C_{60} molecules are randomly distributed over two orientations. In both orientations, related by a 90° rotation, eight of the 20 hexagonal faces are perpendicular to 3-fold axes. In LT-Na_2CsC_{60} and Na_2RbC_{60} a preferred orientation is adopted, where the molecules are rotated by 98° around the body diagonals. The ordered atom arrangement is described in $Pa\bar{3}$, the same space group as found for the LT-modification of C_{60}. In the "$A15$-type" structure the molecules located at 0 0 0 and $\frac{1}{2}$ $\frac{1}{2}$ $\frac{1}{2}$ are rotated by 90° with respect to each other.

The alkaline metal atoms fully donate their electrons to the C_{60} unit. Superconductivity is observed for a metal-to-fullerene ratio close to 3 : 1, with critical temperatures near 30 K measured for $Na_2Cs(NH_3)_4C_{60}$, Rb_3C_{60}, Rb_2CsC_{60}, and Cs_2RbC_{60}. A maximum value of 45.0 K is reported for nominal $Rb_{2.7}Tl_{2.2}C_{60}$. For the alkaline-earth metals the charge transfer is not complete and superconductivity is found for a higher metal-to-fullerene ratio, e.g., Ca_5C_{60} (8.4 K), Sr_6C_{60} (4 K) and Ba_6C_{60} (7 K). T_c increases monotonically with increasing cell parameter for both the f.c.c. and the b.c.c. packing.

b. ET and Other Charge-Transfer Salts

A large number of crystal structures of **charge-transfer salts** containing the molecule bis(ethylenedithio)tetrathiafulvalene, abbreviated BEDT-TTF or simply ET, have been determined. The ET molecule, shown in Fig. 6.27, is rather flat because of the presence of an extended π-electron system, but deviations are always observed, in particular in the ethylene end groups. ET salts contain slabs of ET molecules separated by anion layers, as illustrated by the structure of β-$(ET)_2I_3$ in Fig. 6.28.

The structures of the β-$(ET)_2X_3$ family of compounds are triclinic with one donor-molecule layer per translation unit. All molecules are parallel and the linear anions, which can be I_3^-, IBr_2^-, or AuI_2^-, are located at inversion centers.

Fig. 6.27.

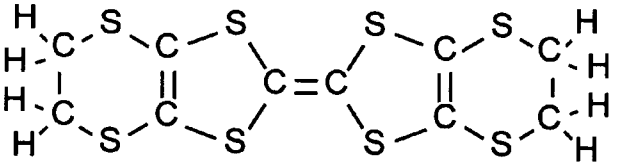

ET (BEDT - TTF)

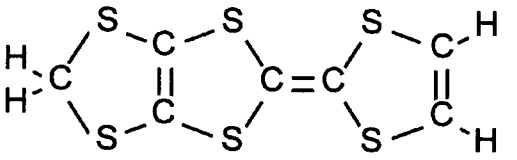

MDT - TTF

Bis(ethylenedithio)tetrathiafulvalene (ET) and methylenedithiotetrathiafulvalene (MDT-TTF) molecules.

β-$(ET)_2I_3$ undergoes a phase transition at 175 K to an incommensurate modulated structure. Both the I_3 units and the ET molecules retain their orientation but are displaced from the original positions in the HT-modification. Applied pressure suppresses the onset of the modulated structure and an ordered, so-called β^* phase with a superconducting transition temperature of 8 K is formed. Among the β phases, higher values of T_c are observed for larger anions.

In κ-$(ET)_2Cu(NCS)_2$ ($T_c = 10.4$ K) the donor molecules form face-to-face dimers, where the two molecules are rotated by 90° with respect to each other. There are two dimers per cell, related by a 2-fold screw axis. The ET molecule layer is essentially centrosymmetric, but the overall symmetry is lower. The Cu atoms and the linear NCS^- anions form infinite branched zigzag chains where the Cu atoms are coordinated to two N and one terminal S atom in an approximately trigonal planar configuration. The presence of twisted dimers is a common feature to all κ phases. In the superconducting compounds, the central C=C bond of one molecule is located above a five-membered ring of the neighboring layer. Superconducting transition temperatures up to 12.5 K are reached for κ-$(ET)_2Cu[N(CN)_2]X$ halides with anion layers similar to those observed in κ-$(ET)_2Cu(NCS)_2$. However, in the former structure a network of S–S interactions extends in two dimensions within the donor layers, whereas in the latter similar contacts lead to the formation of infinite ribbons.

Fig. 6.28.

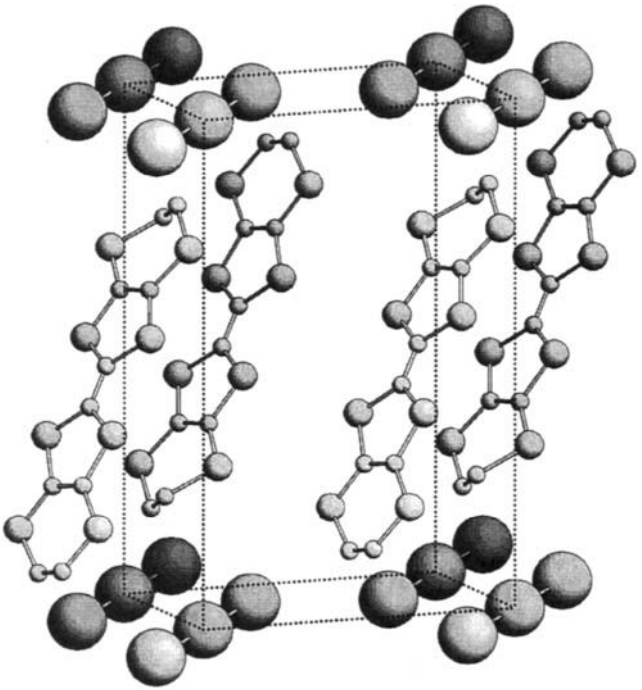

Structure of β-$(ET)_2I_3$. Large spheres: I; medium spheres: S; small spheres: C; H atoms not shown.

The structure of θ-$(ET)_2(I_3)_{1-x}(AuI_2)_x$ ($T_c = 3.6\,K$ for $x < 0.02$) is orthorhombic and centrosymmetric. The ET molecules within each layer are approximately parallel to each other, but tilted from the intersecting plane, the molecules of alternating layers being tilted in opposite directions. The molecular packing within the slabs is similar to that found in the α phases, which, however, have triclinic symmetry. The anions are located in mirror planes between the layers. The unit cell is enlarged and the symmetry lowered to monoclinic when an ordered arrangement of I_3^- anions is taken into account.

The crystal structure of $(ET)_4Hg_{3-\delta}X_8$ ($X = Cl$) is built up of two substructures, one formed by the ET molecules and the halogen atoms and the other by the Hg atoms, with incommensurate translation units in one direction. The halogen atoms form infinite channels, inside which the mercury atoms are arranged with their own translation period. As in the κ phases, the ET molecules form face-to-face dimers. λ-$(Se\text{-}ET)_2GaCl_4$, containing bis(ethylenedithio)tetraselenafulvalene molecules, becomes superconducting at 9.5 K. The slabs of seleno-substituted molecules are separated by tetrahedral $GaCl_4$ acceptors.

A number of salts with the asymmetric MDT-TTF molecule (methylenedithiotetrathiafulvalene), shown in Fig. 6.27, have been synthesized. Among

these, κ-(MDT-TTF)$_2$AuI$_2$ is found to become superconducting at 4.5 K. The orthorhombic structure contains donor molecule layers with dimers that are rotated with respect to each other, similar to those found in the κ phases of the ET salts. There are, however, two layers in the translation unit, related by a mirror plane.

I Crystallographic Data Sets

a. Criteria for Selection

Complete crystallographic data sets, including atom coordinates, are given for 111 compounds, representative for structure types found among classical superconductors. As a general rule for selection, at least one compound with a superconducting transition temperature exceeding 4.2 K should have been reported for the structure type. Whenever one or more isotypic superconductors are known, the set of atom coordinates is followed by a table listing cell parameters and superconducting transition temperatures for selected isotypic compounds. Compounds becoming superconducting at temperatures lower than 4.2 K, including particular nonsuperconducting materials, have also been considered in these tables. However, a lower limit around 1 or 2 K has sometimes been fixed, without special indication.

Preference has been given, when possible, to recent literature references and to references where the cell parameters and the critical temperature are determined for the same sample. The historical aspect has thus not been emphasized, which means that the original publications stating for the first time the existence of a particular phase or its superconductivity may not be mentioned. As a further consequence, the superconducting transition temperatures listed here do not always correspond to the highest values reported in the literature. Differences that were too large were, however, avoided. For systems with a strong dependence on the chemical composition, an effort was made to select a close-to-optimal composition, but also to respect the correspondence between composition and cell parameters. Transition temperatures determined for high pressure or on thin films were considered only occasionally.

The cell parameters listed in each table were taken from the first reference indicated on the same line and the critical temperature, if not from the first, then from the second reference. One or two literature references reporting structure refinements, marked with an asterisk, are sometimes added. The term structure refinement is here understood in a broad sense, depending on the class of compound and the structure type. In some cases publications with additional data are mentioned in remarks, without any claim on completeness. To avoid differences due to small variations in experimental conditions used by different

authors, cell parameters for series of isotypic compounds were sometimes preferably taken from the same reference.

b. Presentation and Notation

The general presentation of a data set is explained in Fig. 6.29 and the few abbreviations used here are listed in Table 6.3. The Pearson code and the Wyckoff sequence are defined in Section A, where the use of the *International Tables for Crystallography* is also briefly explained. In a few particular cases a slightly different presentation has been chosen. This is the case for the structures

Fig. 6.29.

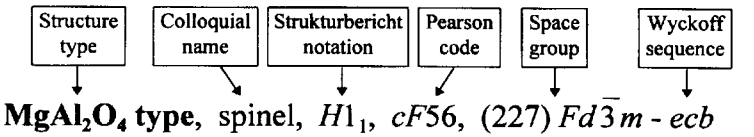

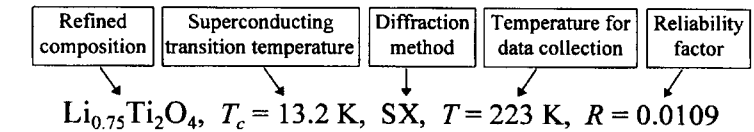

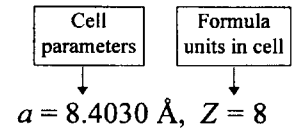

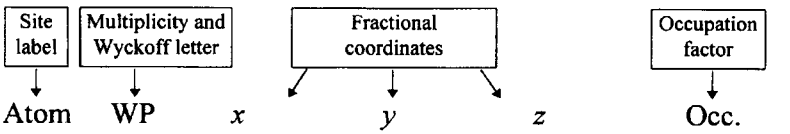

Atom	WP	x	y	z	Occ.
Li	8(*b*)	3/8	3/8	3/8	0.75
Ti	16(*c*)	0	0	0	
O	32(*e*)	0.23685	0.23685	0.23685	

Extract from the tables with explanation of items. For some tables reference is made to figures in which the structure type is presented.

TABLE 6.3

Notations used in the data sets.

Bravais lattice	*aP*	anorthic (triclinic) primitive (lattice point at 0 0 0)
	mP	monoclinic primitive (0 0 0)
	mS	monoclinic side-centered (0 0 0, $\frac{1}{2}$, $\frac{1}{2}$ 0 for *C*-centered)
	oP	orthorhombic primitive (0 0 0)
	oS	orthorhombic side-centered (0 0 0, $\frac{1}{2}$ $\frac{1}{2}$ 0 for *C*-centered)
	oF	orthorhombic face-centered (0 0 0, 0 $\frac{1}{2}$ $\frac{1}{2}$, $\frac{1}{2}$ 0 $\frac{1}{2}$, $\frac{1}{2}$ $\frac{1}{2}$ 0)
	oI	orthorhombic body-centered (0 0 0, $\frac{1}{2}$ $\frac{1}{2}$ $\frac{1}{2}$)
	tP	tetragonal primitive (0 0 0)
	tI	tetragonal body-centered (0 0 0, $\frac{1}{2}$ $\frac{1}{2}$ $\frac{1}{2}$)
	hP	hexagonal primitive (0 0 0)
	hR	hexagonal rhombohedral (0 0 0, $\frac{2}{3}$ $\frac{1}{3}$ $\frac{1}{3}$, $\frac{1}{3}$ $\frac{2}{3}$ $\frac{2}{3}$)
	cP	cubic primitive (0 0 0)
	cF	cubic face-centered (0 0 0, 0 $\frac{1}{2}$ $\frac{1}{2}$, $\frac{1}{2}$ 0 $\frac{1}{2}$, $\frac{1}{2}$ $\frac{1}{2}$ 0)
	cI	cubic body-centered (0 0 0, $\frac{1}{2}$ $\frac{1}{2}$ $\frac{1}{2}$)
Diffraction data	SX	single-crystal X-ray
	PX	powder X-ray
	PN	powder neutron
Reliability factor	*R*	single-crystal conventional
	R_w	single-crystal weighted
	R_B	powder Bragg
	R_{wp}	powder weighted profile
Other	n.o.	superconductivity not observed
	HT	high temperature
	LT	low temperature
	RT	room temperature
	WP	Wyckoff position
	*	reference containing structure refinement

of the fullerides, which have been subdivided into structures with fullerene molecules in f.c.c. and b.c.c. packing, respectively. The Chevrel phases with interstitial atoms are represented by four complete data sets. Compounds with rhombohedral and triclinic structures are listed separately, with T_c indicated only in the former, when relevant. A table with information about the space group and cell parameters of charge-transfer salts is presented at the end of this section, but no complete data set with atom coordinates was selected.

The data sets are subdivided into element, binary, ternary, and quaternary structure types. Within each category they are listed according to the coefficients in the name of the representative compound, indicated as the first item in each data set. Structure types with the same coefficients are ordered alphabetically. The structure type names are written with bold-faced characters in the text and in

Tables 6.1 and 6.2. References for type-defining compounds can be found in *TYPIX* (Parthé *et al.*, 1993/1994; Cenzual *et al.*, 1995), a compilation of standardized data for inorganic compounds defining structure types, accompanied by a brief crystal chemical characterization.

J

Tabulated Data

a. Element Structure Types

Cu type, c.c.p., f.c.c., *A*1, *cF*4, (225) $Fm\bar{3}m$–*a*
La, $T_c = 6.06$ K, PX
$a = 5.290$ Å, $Z = 4$, Figs. 6.2, 6.3, 6.4b, 6.16 (Heiniger *et al.*, 1973)

Atom	WP	*x*	*y*	*z*
La	4(*a*)	0	0	0

Compound	*a*(Å)	T_c(K)	Ref.
La	5.290	6.06[a]	1
Th	5.0861	1.38	2, 3
Al	4.0495[b]	1.175	4, 3
Pb	4.9508	**7.22**	5, 6

[a] $T_c = 11.93$ K at 14 GPa (Maple *et al.*, 1969).
[b] Value taken from figure.
References: 1, Heiniger *et al.* (1973); 2, Harris and Raynor (1964); 3, Roberts (1976); 4, Bandyopadhyay and Gupta (1978); 5, Klug (1946); 6, Claeson (1966).

α-Ga type, *A*11, *oS*8, *Cmca–f*
Ga, $T_c = 1.083$ K, SX, $R = 0.143$
$a = 4.523$, $b = 7.661$, $c = 4.524$ Å, $Z = 8$ (Sharma and Donohue, 1962; Roberts, 1976)

Atom	WP	*x*	*y*	*z*
Ga	8(*f*)	0	0.1549	0.0810

β-Ga type, *mS*4, (15) *C*2/*c–e*
Ga, $T_c = 6.2$ K, PX, $T = 248$ K, $R = 0.08$
$a = 2.766$, $b = 8.053$, $c = 3.332$ Å, $\beta = 92.03°$, $Z = 4$ (Bosio *et al.*, 1969; Roberts, 1976)

Atom	WP	*x*	*y*	*z*
Ga	4(*e*)	0	0.131	$\frac{1}{4}$

γ-Ga type, *oS*40, (63) $Cmcm$–g^3fc^2
Ga, $T_c = 7$ K, SX, $T = 220$ K, $R = 0.057$
$a = 10.593$, $b = 13.523$, $c = 5.203$ Å, $Z = 40$ (Bosio *et al.*, 1972; Roberts, 1976)

Atom	WP	x	y	z
Ga(1)	8(*g*)	0.2206	0.0504	$\frac{1}{4}$
Ga(2)	8(*g*)	0.2282	0.3612	$\frac{1}{4}$
Ga(3)	8(*g*)	0.3744	0.2062	$\frac{1}{4}$
Ga(4)	8(*f*)	0	0.1053	0.0000
Ga(5)	4(*c*)	0	0.2853	$\frac{1}{4}$
Ga(6)	4(*c*)	0	0.5009	$\frac{1}{4}$

δ-Ga type, *hR*66, (166) $R\bar{3}m$–h^3ea
Ga, $T_c = 7.85$ K, SX, $T = 191$ K, $R = 0.09$
$a = 9.087$, $c = 17.02$ Å, $Z = 66$ (Bosio *et al.*, 1973; Roberts, 1976)

Atom	WP	x	y	z
Ga(1)	18(*h*)	0.434	0.566	0.2437
Ga(2)	18(*h*)	0.507	0.493	0.3971
Ga(3)	18(*h*)	0.566	0.434	0.1562
Ga(4)	9(*e*)	$\frac{1}{2}$	0	0
Ga(5)	3(*a*)	0	0	0

α-Hg type, *A*10, *hR*3, (166) $R\bar{3}m$–a
Hg, $T_c = 4.154$ K, PX, $T = 5$ K
$a = 3.4574$, $c = 6.6634$ Å, $Z = 3$ (Barrett, 1957; Roberts, 1976)

Atom	WP	x	y	z
Hg	3(*a*)	0	0	0

In type, *A*6, *tI*2, (139) $I4/mmm$–a
branch α-Pa, A_a
In, $T_c = 3.408$ K, PX
$a = 3.2530$, $c = 4.9455$ Å, $Z = 2$ (Smith and Schneider, 1964; Roberts, 1976)

Atom	WP	x	y	z
In	2(*a*)	0	0	0

Compound	a(Å)	c(Å)	T_c(K)	Ref.
Hg	3.995	2.825[a]	**3.949**	1, 2
In	3.2530	4.9455	3.408	3, 2

[a]At 77 K.
References: 1, Donohue (1974); 2, Roberts (1976); 3, Smith and Schneider (1964).

Mg type, h.c.p., *A3*, *hP2*, (194) $P6_3/mmc$–c
Tc, $T_c = 7.9$ K, PX, $T = 4.2$ K
$a = 2.7364$, $c = 4.3908$ Å, $Z = 2$, Figs. 6.2, 6.16 (Marples and Koch, 1972; Giorgi and Szklarz, 1970a)

Atom	WP	x	y	z
Tc	2(c)	$\frac{1}{3}$	$\frac{2}{3}$	$\frac{1}{4}$

Compound[a]	a(Å)	c(Å)	T_c(K)	Ref.
Tc	2.740	4.399	7.92	1
$Tc_{0.94}Nb_{0.06}$	2.757	4.432	12.8	2
$Tc_{0.82}Mo_{0.18}$	2.752	4.443	**13.7**	3
$Tc_{0.82}W_{0.18}$	2.755	4.449	11.3	1
Re	2.7550[b]	4.4437[b]	1.697	4, 5
$Re_{0.88}W_{0.12}$	2.7575[b]	4.4590[b]	7.5	4, 6
Tl	3.463	5.539	2.38	7, 5

[a]Data for $Tc_{1-x}T_x$ (T = Ru, Os, Rh, Pd, Sn; $T_c < T_c$(Tc)) reported in Alekseyevskiy *et al.* (1975).
[b]Value taken from figure.
References: 1, Giorgi (1985); 2, Giorgi and Szklarz (1970a); 3, Stewart and Giorgi (1978); 4, Savitskiy *et al.* (1969); 5, Roberts (1976); 6, Chu *et al.* (1971); 7, Staun Olsen *et al.* (1994).

α-Nd type, d.h.c.p., *A3′*, *hP4*, (194) $P6_3/mmc$–ca
La, $T_c = 4.88$ K, PX
$a = 3.770$, $c = 12.159$ Å, $Z = 4$, Fig. 6.2 (Spedding *et al.*, 1956; Maple *et al.*, 1969)

Atom	WP	x	y	z
La(1)	2(c)	$\frac{1}{3}$	$\frac{2}{3}$	$\frac{1}{4}$
La(2)	2(a)	0	0	0

β-Sn type, white tin, *A5*, *tI4*, (141) $I4_1/amd$–b
Si, $T_c = 7.1$ K, PX, $p = 13$ GPa
$a = 4.686$, $c = 2.585$ Å, $Z = 4$ (Jamieson, 1963; Roberts, 1976)

Atom	WP	x	y	z[a]
Si	4(b)	0	$\frac{1}{4}$	$\frac{3}{8}$

[a]Origin at center ($2/m$).

(*continued*)

Compound	a(Å)	c(Å)	T_c(K)	Ref.
Si	4.686	2.585[a]	**7.1**[a]	1, 2
Ge	4.884	2.692[a]	5.35[b]	1, 2
Sn	5.8316[c]	3.1815[c]	3.722	3, 2
GaSb	5.1785	2.8494[d]	4.24[e]	4, 5
InSb	5.810	3.136[f]	2.1[g]	6, 7

[a]At 13 GPa.
[b]At 11.5 GPa.
[c]Average value.
[d]At 23.3 GPa.
[e]Prepared at 12 GPa, pressure released at 77 K.
[f]At 4.3 GPa.
[g]Prepared above 2.25 GPa, pressure released at 77 K.
References: 1, Jamieson (1963); 2, Roberts (1976); 3, Donohue (1974); 4, Weir *et al.* (1987); 5, McWhan *et al.* (1965); 6, Yu *et al.* (1978); 7, Geller *et al.* (1963).

W type, b.c.c., *A2*, *cI2*, (229) $Im\bar{3}m$–*a*
Nb, $T_c = 9.25$ K, PX, $T = 293$ K
$a = 3.304$ Å, $Z = 2$, Fig. 6.4a (Pialoux *et al.*, 1982; Roberts, 1976)

Atom	WP	x	y	z
Nb	2(*a*)	0	0	0

Compound	a(Å)	T_c(K)	Ref.
Zr	3.610	...	1
$Zr_{0.92}Rh_{0.08}$	3.510	6.5	1
$Zr_{0.90}Pt_{0.10}$	...	7.5	2
V	3.0321[a]	5.40	3, 4
Nb	3.3008[a]	9.25	3, 4
$Nb_{0.7}Zr_{0.3}$	3.376	11	5, 6
Ta	3.3019[a]	4.47	3, 4
Mo	3.150[a]	0.915	7, 4
$Mo_{0.6}Re_{0.4}$	3.124	**12.0**	8
$Mo_{0.84}Rh_{0.16}$	3.131[a]	8	9, 6
W	3.165	1.5	10
$W_{0.50}Tc_{0.50}$	3.118	8.1	10
$W_{0.65}Re_{0.35}$	3.139	6.75	8
Tl	3.871[b]	2.36	11, 12

[a]Value taken from figure.
[b]At 523 K.
References: 1, Yorda *et al.* (1988); 2, Raub (1964); 3, Smirnov and Finkel' (1966); 4, Roberts (1976); 5, Doi *et al.* (1966); 6, Matthias *et al.* (1963); 7, Pawar (1967); 8, Stewart and Giorgi (1978); 9, Haworth and Hume-Rothery (1959); 10, Giorgi (1985); 11, Ponyatovskii and Zakharov (1962); 12, Claeson (1966).

b. Binary Structure Types

1. *AB* Types

ξ-(AgZn) type, B_b, *hP*9, (147) $P\bar{3}$–*gda*
$Ag_{0.72}Ga_{0.28}$, $T_c = 7.5\,K$[a], PX, $T = 293\,K$, $R = 0.059$
$a = 7.7677$, $c = 2.8778\,Å$, $Z = 9$ (Stratton and Kitchingman, 1964; Alekseevskii, 1966)

Atom	WP	*x*	*y*	*z*
Ag	6(*g*)	0.350	0.032	0.250
Ga(1)[b]	2(*d*)	$\frac{1}{3}$	$\frac{2}{3}$	0.250
Ga(2)	1(*a*)	0	0	0

[a]Superconducting phase not identified with certainty.
[b]Ga(1) = $Ga_{0.76}Ag_{0.24}$.

β′-AuCd type, *B*19, *oP*4, (51) *Pmma–fe*
$Nb_{0.85}Rh_{1.15}$, $T_c = 3.00\,K$, PX
$a = 4.510$, $b = 2.813$, $c = 4.808\,Å$, $Z = 2$, Fig. 6.5 (Ritter *et al.*, 1964; Savitskii *et al.*, 1985)

Atom	WP	*x*	*y*	*z*
Nb[a]	2(*e*)	$\frac{1}{4}$	0	0.182
Rh	2(*f*)	$\frac{1}{4}$	$\frac{1}{2}$	0.672

[a]Nb = $Nb_{0.85}Rh_{0.15}$.

Compound	*a*(Å)	*b*(Å)	*c*(Å)	T_c(K)	Ref.
$Nb_{0.85}Rh_{1.15}$	4.510	2.813	4.808	3.00	1*, 2
MoIr	4.429	2.752	4.804	**8.8**	3, 2

References: 1, Ritter *et al.* (1964); 2, Savitskii *et al.* (1985); 3, Giessen *et al.* (1966).

CrFe type, σ phase, $D8_b$, *tP*30, (136) $P4_2/mnm$–ji^2ga
substitution derivative of β-U, A_b
$Mo_{0.45}Re_{0.55}$, $T_c = 6.47\,K$, PX
$a = 9.6010$, $c = 4.9850\,Å$, $Z = 30$, Fig. 6.10a (Wilson, 1963; Koch and Scarbrough, 1971)

Atom[a]	WP	*x*	*y*	*z*
E	8(*j*)	0.3177	0.3177	0.2524
D	8(*i*)	0.0653	0.2624	0
C	8(*i*)	0.1316	0.5368	0
B	4(*g*)	0.3981	0.6019	0
A	2(*a*)	0	0	0

[a]Atom coordinates determined for σ-CrFe (Bergman and Shoemaker, 1954); *A* = Re, *B* = $Mo_{0.75}Re_{0.25}$, *C* = $Mo_{0.50}Re_{0.50}$, *D* = $Re_{0.81}Mo_{0.19}$, *E* = $Mo_{0.62}Re_{0.38}$.

(*continued*)

Compound	a(Å)	c(Å)	T_c(K)	Ref.
$V_{0.24}Re_{0.76}$	9.44	4.89	4.52	1*, 2
$Nb_{0.40}Re_{0.60}$	9.77	5.14	2.5	3, 4*
$Nb_{0.60}Os_{0.40}$	9.85	5.06	1.85	3, 4*
$Nb_{0.60}Rh_{0.40}$	9.80	5.07	4.04	3
$Nb_{0.60}Ir_{0.40}$	9.842	5.045	2.20	5, 4*
$Nb_{0.62}Pt_{0.38}$	9.91	5.13	4.01	3
$Ta_{0.40}Re_{0.60}$	9.77	5.09	1.4	3
$Ta_{0.60}Rh_{0.40}$	9.80	5.09	2.35	3
$Mo_{0.30}Tc_{0.70}$	9.5091	4.9448	**12.0**[a]	6, 7
$Mo_{0.35}Re_{0.65}$	9.57	4.97	8.6	3, 8*
$Mo_{0.63}Ru_{0.37}$	9.5652	4.9362	8.8	9
$Mo_{0.62}Os_{0.38}$	9.60	4.93	5.65	3, 4*
$Mo_{0.74}Ir_{0.26}$[b]	9.63	4.96	6.7	3, 4*
$W_{0.25}Tc_{0.75}$	9.478	4.950	9.0	10
$W_{0.50}Re_{0.50}$	9.63	5.01	5.03	3
$W_{0.60}Ru_{0.40}$	9.57	4.96	4.67	3
$W_{0.66}Os_{0.34}$	9.63	4.98	3.81	3
$W_{0.72}Ir_{0.28}$	9.67	5.00	4.46	3

[a]Value taken from figure.
[b]Nominal composition of sample also containing $A15$ phase.
References: 1, Eremenko *et al.* (1983); 2, Roberts (1976); 3, Bucher *et al.* (1961); 4, Spooner and Wilson (1964); 5, Koch and Scarbrough (1971); 6, Darby and Zegler (1962); 7, Compton *et al.* (1961); 8, Wilson (1963); 9, Rasmussen and Lundtoft (1987); 10, Giorgi (1985).

CsCl type, $B2$, $cP2$, (221) $Pm\bar{3}m$–ba
VRu, $T_c = 5.1\,K$[a], PX, $T = 300\,K$
$a = 2.986$ Å, $Z = 1$, Fig. 6.7a (Marezio *et al.*, 1971; Susz *et al.*, 1979)

Atom	WP	x	y	z
V	1(a)	0	0	0
Ru	1(b)	$\frac{1}{2}$	$\frac{1}{2}$	$\frac{1}{2}$

[a]For composition $V_{1.09}Ru_{0.91}$.

Compound	a(Å)	T_c(K)	Ref.
$Zr_{1.02}Rh_{0.98}$	3.264	2.4	1
HfOs	3.239	2.4	2, 3
$V_{1.02}Ru_{0.98}$[a]	2.990	5.1[b]	4, 5
$V_{1.06}Ru_{0.80}Rh_{0.14}$	...	**6.50**	5
$V_{1.10}Os_{0.90}$	3.01[c]	1.7	5

[a]Transforms to a tetragonal structure below room temperature, $a = 2.928$, $c = 3.118$ Å at 110 K.
[b]For composition $V_{1.09}Ru_{0.91}$.
[c]Value taken from figure.
References: 1, Jorda *et al.* (1988); 2, Dwight (1959); 3, Savitskii *et al.* (1985); 4, Marezio *et al.* (1971); 5, Susz *et al.* (1979).

CuAu type, $L1_0$, $tP2$, (123) $P4/mmm$–da
$Nb_{0.95}Ir_{1.05}$, $T_c = 4.75$ K, PX
$a = 2.848$, $c = 3.863$ Å, $Z = 1$, Fig. 6.5 (Giessen and Grant, 1964; Savitskii *et al.*, 1985)

Atom	WP	x	y	z
Nb[a]	1(a)	0	0	0
Ir	1(d)	$\frac{1}{2}$	$\frac{1}{2}$	$\frac{1}{2}$

[a]Nb = $Nb_{0.95}Ir_{0.05}$.

Compound	a(Å)	c(Å)	T_c(K)	Ref.
$Nb_{0.96}Rh_{1.04}$	2.842	3.809	3.76	1, 2
$Nb_{0.95}Ir_{1.05}$	2.848	3.863	**4.75**	1, 2

References: 1, Giessen and Grant (1964); 2, Savitskii *et al.* (1985).

FeAs type, westerveldite, $B14$ ($B31^a$), $oP8$, (62) $Pnma$–c^2
IrGe, $T_c = 4.7$ K, PX
$a = 5.611$, $b = 3.490$, $c = 6.281$ Å, $Z = 4$ (Pfisterer and Schubert, 1950; Matthias *et al.*, 1963)

Atom	WP	x	y	z
Ir	4(c)	0.010	$\frac{1}{4}$	0.192
Ge	4(c)	0.185	$\frac{1}{4}$	0.590

[a]Defined on isotypic MnP.

Compound	a(Å)	b(Å)	c(Å)	T_c(K)	Ref.
AuGa	6.267	3.421	6.397	1.17	1*, 2
PdSi	5.599	3.381	6.133	0.93	1*, 3
PtSi	5.595	3.603	5.932	0.88	1*, 3
RhGe	5.70	3.25	6.48	0.96	4*, 3
IrGe	5.611	3.490	6.281	**4.7**	1*, 5
PdGe	5.782	3.481	6.259	< 0.30	1*, 2
PtGe	5.733	3.701	6.088	0.40	1*, 3
PdSn	6.13	3.87	6.32	0.41	1*, 3

References: 1, Pfisterer and Schubert (1950); 2, Savitskii *et al.* (1985); 3, Raub *et al.* (1963); 4, Geller (1955); 5, Matthias *et al.* (1963).

FeB type, $B27$ ($B15^a$), $oP8$, (62) $Pnma$–c^2
CeCu, SX, $R = 0.110$
$a = 7.30$, $b = 4.30$, $c = 6.36$ Å, $Z = 4$ (Larson and Cromer, 1961)

Atom	WP	x	y	z
Ce	4(c)	0.1670	$\frac{1}{4}$	0.6469
Cu	4(c)	0.0413	$\frac{1}{4}$	0.1034

[a]Defined on superseded structure proposal.

(*continued*)

Compound	a(Å)	b(Å)	c(Å)	T_c(K)	Ref.
LaCu	7.543	4.616	5.724	**5.85**	1, 2
CeCu	7.30	4.30	6.36	...	3*

References; 1, Cirafici and Palenzona (1977); 2, Smith and Luo (1967); 3, Larson and Cromer (1961).

η-MoC_{1-x} type, *hP*12, (194) $P6_3/mmc$–f^2ba
$MoC_{0.67}$, $T_c = 8.9$ K, PX
$a = 3.01$, $c = 14.61$ Å, $Z = 6$ (Nowotny *et al.*, 1954; Morton *et al.*, 1971)

Atom	WP	x	y	z	Occ.
Mo(1)	4(*f*)	$\frac{1}{3}$	$\frac{2}{3}$	0.5833	
Mo(2)	2(*b*)	0	0	$\frac{1}{4}$	
C(1)	4(*f*)	$\frac{1}{3}$	$\frac{2}{3}$	0.1667	0.67[a]
C(2)	2(*a*)	0	0	0	0.67[a]

[a]Partial occupancy stated in Parthé and Yvon (1970).

NaCl type, rock salt, *B*1, *cF*8, (225) $Fm\bar{3}m$–ba
$NbN_{0.98}$, $T_c = 16.0$ K, PN, $R = 0.037$
$a = 4.394$ Å, $Z = 4$, Fig. 6.17 (Christensen, 1977a; Matthias *et al.*, 1963)

Atom	WP	x	y	z	Occ,
Nb	4(*a*)	0	0	0	
N	4(*b*)	$\frac{1}{2}$	$\frac{1}{2}$	$\frac{1}{2}$	0.98

Compound	a(Å)	T_c(K)	Ref.
ZrB	4.65	3.4	1
HfB	4.62	3.1	1
$TiC_{0.94}$	4.32965	n.o.	2*
$VC_{0.84}$[a]	4.159	n.o.	3
$NbC_{0.98}$	4.4704	11.1	4, 5
$Nb_{0.80}W_{0.20}C$	4.447[b]	13.6[b]	4
TaC	4.4548	10.1	4
$TaC_{0.60}N_{0.40}$	...	11.3	6
MoC	4.2777	14.3	4
WC	4.266	10.0	4
$TiN_{0.99}$	4.24129	5.6	2*, 5
ZrN	4.585	10.7	7*, 8
HfN	4.512	8.83	9, 8, 10*
$VN_{1.00}$	4.13711[c]	8.5	11*, 8
$NbN_{0.98}$	4.394	16.0[d]	12*, 5
$NbN_{0.75}C_{0.25}$	4.419	**18.0**	9

(*continued*)

PdH	4.08	9.62[e]	13, 14*
PdD	...	10.7	13

[a]Maximum carbon content $VC_{0.88}$ for samples prepared by usual techniques (Toth *et al.*, 1965).
[b]Value taken from figure.
[c]Stoichiometric compound transforms to a tetragonal structure at 205 K, space group $P\bar{4}2m$, $a = 4.1314$, $c = 4.1198$ Å at 45 K (Kubel *et al.*, 1988)*.
[d]$T_c = 17.3$ K reported for thin film (Keskar *et al.*, 1971).
[e]$T_c = 16.6$, 15.6 and 13.6 K reported for $Pd_{0.55}Cu_{0.45}H_{0.7}$, $Pd_{0.70}Ag_{0.30}H_{0.8}$ and $Pd_{0.84}Au_{0.16}H_{0.9}$ (Stritzker, 1974).
References: 1, Shulishova and Shcherbak (1967); 2, Dunand *et al.* (1985); 3, Samsonow and Morosow (1971); 4, Willens *et al.* (1967); 5, Matthias *et al.* (1963); 6, Toth *et al.* (1965); 7, Christensen (1975); 8, Roberts (1976); 9, Pessall *et al.* (1968); 10, Christensen (1990); 11, Kubel *et al.* (1987); 12, Christensen (1977a); 13, Savitskii *et al.* (1985); 14, Khodyrev *et al.* (1978).

LT-$Nb_{1-x}S$ type, $hP16$, (186) $P6_3mc$–c^2ba
MoN[a], $T_c = 15.1$ K, PX, $R = 0.06$
$a = 5.745$, $c = 5.622$ Å, $Z = 8$ (Bezinge *et al.*, 1987)

Atom	WP	x	y	z
Mo(1)	6(c)	0.490	0.510	0.000
Mo(2)	2(a)	0	0	0.000
N(1)	6(c)	0.8333	0.1667	0.25
N(2)	2(b)	$\frac{1}{3}$	$\frac{2}{3}$	0.25

[a]Prepared at 6 GPa.

NiAs type, nickeline, $B8_1$, $hP4$, (194) $P6_3/mmc$–ca
branch ε-$FeN_{0.5}$, $L'3$
NiBi, $T_c = 4.25$ K, PX
$a = 4.070$, $c = 5.35$ Å, $Z = 2$ (Hägg and Funke, 1929; Zhuravlev *et al.*, 1962)

Atom	WP	x	y	z
Ni	2(a)	0	0	0
Bi	2(c)	$\frac{1}{3}$	$\frac{2}{3}$	$\frac{1}{4}$

Compound	a(Å)	c(Å)	T_c(K)	Ref.
$MoC_{0.5}$	3.00	4.77	**5.8**	1
$WC_{0.5}$	3.00	4.72	3.05	2
PdSb	4.078	5.593	1.5	3
PtSb	4.138	5.483	2.1	3
RhBi	4.094	5.663[a]	2.2	3
NiBi	4.070	5.35[a]	4.25	4, 3
PtBi	4.324	5.501	1.21	3

(*continued*)

IrTe	3.930	5.386	3.0	5, 6
PdTe[b]	4.150	5.670	4.5	7

[a]Bismuth-poor boundary.
[b]Two-phase sample.
References: 1, Morton *et al.* (1971); 2, Morton *et al.* (1972); 3, Zhuravlev *et al.* (1962); 4, Hägg and Funke (1929); 5, Groeneveld Meijer (1955); 6, Raub *et al.* (1965); 7, Kjekshus and Pearson (1965).

TaIr type, *oP*12, (51) *Pmma–jife*
$Ta_{0.86}Ir_{1.14}$[a], PX
$a = 13.661$, $b = 2.830$, $c = 4.803$ Å, $Z = 6$, Fig. 6.5 (Ferguson *et al.*, 1963)

Atom[b]	WP	x	y	z
Ta(1)	4(*j*)	0.583	$\frac{1}{2}$	0.32
Ta(2)	2(*f*)	$\frac{1}{4}$	$\frac{1}{2}$	0.04
Ir(1)	4(*i*)	0.083	0	0.18
Ir(2)	2(*e*)	$\frac{1}{4}$	0	0.54

[a]Nominal composition.
[b]Site occupation not refined.

Compound	a(Å)	b(Å)	c(Å)	T_c(K)	Ref.
$Nb_{0.85}Ir_{1.15}$	13.619	2.823	4.818	**4.6**	1, 2
$Ta_{0.86}Ir_{1.14}$	13.661	2.830	4.803	n.o.	3*, 2

References: 1, Giessen and Grant (1964); 2, Savitskii *et al.* (1985); 3, Ferguson *et al.* (1963).

4H-$Ti_{1+x}S_2$ type, *hP*8, (1986) $P6_3mc$–b^3a
$Ti_{1.23}S_2$, SX, $R = 0.026$
$a = 3.4198$, $c = 11.444$ Å, $Z = 2$ (Norrby and Franzen, 1970)

Atom	WP	x	y	z	Occ.
Ti(1)	2(*b*)	$\frac{1}{3}$	$\frac{2}{3}$	0.10910	0.227
Ti(2)	2(*b*)	$\frac{1}{3}$	$\frac{2}{3}$	0.37461	
S(1)	2(*b*)	$\frac{1}{3}$	$\frac{2}{3}$	0.74750	
S(2)	2(*a*)	0	0	0.00000	

Compound	a(Å)	c(Å)	T_c(K)	Ref.
$Ti_{1.23}S_2$	3.4198	11.444	...	1*
$Li_{0.3}Ti_{1.1}S_2$	3.439	11.511	**13**	2

References: 1, Norrby and Franzen (1970); 2, Barz *et al.* (1972).

α-TlI type, *B*33 (B_f[a]), *oS*8, (63) *Cmcm*–c^2
TaB, $T_c = 4.0$ K, PX
$a = 3.276$, $b = 8.669$, $c = 3.157$ Å, $Z = 4$ (Kiessling, 1949; Shulishova and Shcherbak, 1967)

Atom	WP	x	y	z
Ta	4(*c*)	0	0.354	$\frac{1}{4}$
B	4(*c*)	0	0.060	$\frac{1}{4}$

[a]Defined on isotypic CrB.

Compound	a(Å)	b(Å)	c(Å)	T_c(K)	Ref.
TaB	3.276	8.669	3.157	4.0	1*, 2
NbB	3.297	8.72	3.166	**8.25**	3, 4

References: 1, Kiessling (1949); 2, Shulishova and Shcherbak (1967); 3, Nowotny *et al.* (1959); 4, Matthias *et al.* (1963).

WC type, B_h, *hP*2, (187) $P\bar{6}m2$–*da*
MoC, $T_c = 9.26$ K, PX
$a = 2.898$, $c = 2.809$ Å, $Z = 1$ (Schuster *et al.*, 1976; Roberts, 1976)

Atom	WP	x	y	z
Mo	1(*a*)	0	0	0
C	1(*d*)	$\frac{1}{3}$	$\frac{2}{3}$	$\frac{1}{2}$

2H-ZnS type, wurtzite, *B*4, *hP*4, (186) $P6_3mc$–b^2
GaN, $T_c = 5.85$ K, SX, $R = 0.026$
$a = 3.190$, $c = 5.189$ Å, $Z = 2$ (Schulz and Thiermann, 1977; Alekseevskii *et al.*, 1963)

Atom	WP	x	y	z
Ga	2(*b*)	$\frac{1}{3}$	$\frac{2}{3}$	0.000
N	2(*b*)	$\frac{1}{3}$	$\frac{2}{3}$	0.377

2. AB_2 Types

AlB_2 type, *C*32, *hP*3, (191) *P*6/*mmm*–*da*
NbB_2[a], PX
$a = 3.111$, $c = 3.263$ Å, $Z = 1$, Fig. 6.14a (Cooper *et al.*, 1970)

Atom[b]	WP	x	y	z
Nb	1(*a*)	0	0	0
B	2(*d*)	$\frac{1}{3}$	$\frac{2}{3}$	$\frac{1}{2}$

[a]Nominal composition.
[b]Site occupation not refined.

(*continued*)

Compound[a]	a(Å)	c(Å)	T_c(K)	Ref.
NbB_2	3.111	3.263	n.o.	1
$NbB_{2.5}$[b]	3.098	3.308	6.4	1
$Nb_{0.95}Sc_{0.05}C_{2.5}$	3.096	3.316	6.6	1
$Nb_{0.95}Y_{0.05}B_{2.5}$[c]	3.093	3.312	9.3	1
$Nb_{0.90}Th_{0.10}B_{2.5}$[c]	3.106	3.303	7.0	1
MoB_2	3.041	3.065	n.o.	1
$MoB_{2.5}$[d]	3.047	3.119	8.1	1
$Mo_{0.90}Sc_{0.10}B_{2.5}$	3.049	3.162	9.0	1
$Mo_{0.95}Y_{0.05}B_{2.5}$[e]	3.040	3.074	8.6	1
$Mo_{0.85}Zr_{0.15}B_{2.5}$[f]	3.052	3.193	**11.2**	1
$Mo_{0.90}Hf_{0.10}B_{2.5}$	3.053	3.157	8.7	1
$Mo_{0.85}Nb_{0.15}B_{2.5}$	3.048	3.153	8.5	1
$ThSi_{1.5}$	3.985	4.220	2.41[g]	2, 3

[a]For borides nominal composition of sample.
[b]Data for $Nb_{1-x}T_xB_{2.5}$(T = Ti, Zr, Hf, V, Mo, Ru; $T_c < T_c(NbB_{2.5})$) reported in Cooper *et al.* (1970).
[c]Multiphase sample containing also RB_4 and RB_6.
[d]Splat-melted; data for $Mo_{1-x}T_xB_{2.5}$ (T = Ti, V, Ta, Au, Al; $T_c < T_c(MoB_{2.5})$) reported in Cooper *et al.* (1970).
[e]Multiphase sample containing also Mo_2B_5.
[f]Splat-melted.
[g]For nominal composition $ThSi_2$.
References: 1, Cooper *et al.* (1970); 2, Jacobsen *et al.* (1956); 3, Hardy and Hulm (1954).

CaC_2 type, $C11_a$, *tI*6, (139) *I*4/*mmm*–*ea*
YC_2, $T_c = 3.88$ K, PN, RT, $R_{wp} = 0.115$
$a = 3.663$, $c = 6.171$ Å, $Z = 2$ (Jones *et al.*, 1984; Giorgi *et al.*, 1968)

Atom	WP	x	y	z	Occ.
Y	2(*a*)	0	0	0	
C	4(*e*)	0	0	0.3957	

Compound	a(Å)	c(Å)	T_c(K)	Ref.
YC_2	3.6614	6.1725	**3.88**	1, 2*, 3*
LaC_2	3.934	6.572	1.61	2*, 4, 5*
LuC_2	3.563	5.964	3.33	2*, 4

References: 1, Giorgi *et al.* (1968); 2, Atoji (1961); 3, Jones *et al.* (1984); 4, Roberts (1976); 5, Jones *et al.* (1991).

θ-$CuAl_2$ type, *C*16, *tI*12, (140) *I*4/*mcm*–*ha*
$ZrRh_2$, $T_c = 11.3$ K, PX
$a = 6.496$, $c = 5.605$ Å, $Z = 4$, Fig. 6.12 (Havinga *et al.*, 1972a; Jorda *et al.*, 1988)

Atom	WP	x	y	z
Zr	4(*a*)	0	0	$\frac{1}{4}$
Rh	8(*h*)	0.1667	0.6667	0

Compound	a(Å)	c(Å)	T_c(K)	Ref.
Th_2Cu	7.324	5.816	3.44	1*, 2
Th_2Ag	7.591	5.844	2.19	1*, 2
Th_2Au	7.462	5.989	3.65	1*, 2
Zr_2Co	6.364	5.518	5.0	1*, 2
Zr_2Rh	6.490	5.605	**11.3**	3, 1*
Zr_2Ir	6.51	5.62	7.6	4, 5
Zr_2Ni	6.483	5.267	1.58	1*, 2
Mo_2B	5.547	4.739	5.07	1*, 2
W_2B	5.568	4.744	3.22	1*, 2
$AgIn_2$	6.881	5.620	2.11	1*, 2
$PdTl_2$	6.712	5.748	1.32	1*, 2
$PtTl_2$	6.822	5.565	1.58	1*, 2
$RhPb_{1.9}$	6.674	5.831	1.32	1*, 2
$PdPb_2$	6.865	5.844	3.01	1*, 2
$AuPb_2$	7.338	5.658	3.10	1*, 2

References: 1, Havinga *et al.* (1972a); 2, Havinga *et al.* (1972b); 3, Jorda *et al.* (1988); 4, Eremenko *et al.* (1983); 5, Savitskii *et al.* (1985).

ζ-Fe_2N type, *oP*12, (60) *Pbcn*–*dc*
Mo_2C[a], $T_c = 7.3$ K, PN, RT, $R_B = 0.050$
$a = 4.735$, $b = 6.025$, $c = 5.210$ Å, $Z = 4$ (Epicier *et al.*, 1988*; Morton *et al.*, 1971)

Atom	WP	x	y	z
Mo	8(*d*)	0.245	0.375	0.0833
C	4(*c*)	0	0.125	$\frac{1}{4}$

[a]Partly disordered arrangement of C atoms and vacancies and existence of orthorhombic superstructure reported in Christensen (1977b)*.

Compound	a(Å)	b(Å)	c(Å)	T_c(K)	Ref.
Mo_2C	4.73	6.02	5.20	**7.3**[a]	1, 2*, 3*
W_2C	4.72	5.98	5.17	3.90	4

[a]$T_c = 12$ K reported in Roberts (1976).
References: 1, Morton *et al.* (1971); 2, Parthé and Sadagopan (1963); 3, Epicier *et al.* (1988); 4, Morton *et al.* (1972).

p-FeS_2 type, pyrite, *C*2, *cP*12, (205) $Pa\bar{3}$–*ca*
$Rh_{0.98}Se_2$, $T_c = 6.0$ K,[a], PN, $T = 295$ K, $R = 0.02$
$a = 6.0153$ Å, $Z = 4$ (Kjekshus *et al.*, 1979; Matthias, 1955)

Atom	WP	*x*	*y*	*z*	Occ.
Rh	4(*a*)	0	0	0	0.98
Se	8(*c*)	0.3800	0.3800	0.3800	

[a]For composition $RhSe_{1.75}$.

Compound	*a*(Å)	T_c(K)	Ref.
$PdSb_2$	6.459	1.25	1
$Rh_{0.98}Se_2$	6.0153	**6.0**[a]	2*, 3, 4*
$RhTe_2$	6.4481	1.51	5*, 3

[a]For composition $RhSe_{1.75}$.
References: 1, Matthias *et al.* (1963); 2, Kjekshus *et al.* (1979); 3, Matthias (1955); 4, Geller and Cetlin (1955); 5, Kjekshus *et al.* (1978)

$MgCu_2$ type, cubic Laves phase, *C*15, *cF*24, (227) $Fd\bar{3}m$–*cb*
HfV_2, $T_c = 9.27$ K, PX
$a = 7.396$ Å, $Z = 8$, Fig. 6.8b (Takei *et al.*, 1985)

Atom	WP	*x*	*y*	*z*[a]
Hf	8(*b*)	$\frac{3}{8}$	$\frac{3}{8}$	$\frac{3}{8}$
V	16(*c*)	0	0	0

[a]Origin at center ($\bar{3}m$).

Compound	*a*(Å)	T_c(K)	Ref.
ZrV_2	7.450[a]	8.8	1, 2
HfV_2	7.396[b]	9.27	3
$Hf_{0.84}Nb_{0.16}V_2$	7.390	**10.67**	3
$LaRu_2$	7.704[c]	4.416[d]	4
$CeRu_2$	7.536[d]	6.221	4
$Ce_{0.90}La_{0.10}Ru_2$	7.554[d]	7.194	4
$ThRu_2$	7.653[d]	4.1[d]	5
$LaOs_2$	7.743	8.9	6, 7
$CaRh_2$	7.525	6.4	8, 2
$SrRh_2$	7.706	6.2	8, 2
$BaRh_2$	7.852	6.0	8, 2
$CaIr_2$	7.545	6.15	8, 2
$SrIr_2$	7.700	5.7	8, 2
$ScIr_{2.5}$	7.343	2.46	9
YIr_2	7.500	2.18	10
$LuIr_3$	7.434	2.89	9
$ThIr_2$	7.664[d]	5.75[d]	5
$ZrIr_2$	7.359	4.10	11

(*continued*)

$LaAl_2$	8.13	3.23	12
KBi_2	9.501	3.58	13, 14
$RbBi_2$	9.609	4.25	14
$CsBi_2$	9.726	4.75	15

[a]Value taken from figure; transforms to a rhombohedral structure at 121 K, $a = 5.341$, $c = 12.453$ Å (values taken from figure) at 4 K (Lawson, 1978).
[b]Transforms to an orthorhombic structure at 118 K, $a = 5.240$, $b = 5.147$, $c = 7.467$ Å (values taken from figure) at 4 K (Lawson, 1978).
[c]Value taken from figure; transforms to a tetragonal structure at 30 K, $a = 5.419$, $c = 7.773$ Å at 6 K (Lawson *et al.*, 1974).
[d]Value taken from figure.
References: 1, Finkel' and Pushkarev (1980); 2, Matthias *et al.* (1963); 3, Takei *et al.* (1985); 4, Shelton *et al.* (1977); 5, Houghton *et al.* (1982); 6, Cannon *et al.* (1973); 7, Lawson *et al.*; 8, Wood and Compton (1958); 9, Geballe *et al.* (1965); 10, Compton and Matthias (1959); 11, Matthias *et al.* (1961); 12, Smith and Luo (1967); 13, Zintl and Harder (1932); 14, Zhuravlev *et al.* (1958); 15, Zhuravlev (1958).

$MgZn_2$ type, hexagonal Laves phase, *C*14, *hP*12, (194) $P6_3/mmc$–*hfa*
$ScRe_2$, $T_c = 4.2$ K, PX
$a = 5.271$, $c = 8.592$ Å, $Z = 4$, Figs. 6.8a, 6.11b (Kripyakevich *et al.*, 1963; Phillips, 1989)

Atom	WP	x	y	z
Sc	4(*f*)	$\frac{1}{3}$	$\frac{2}{3}$	0.5625
Re(1)	6(*h*)	0.1667	0.3334	$\frac{1}{4}$
Re(2)	2(*a*)	0	0	0

Compound	a(Å)	c(Å)	T_c(K)	Ref.
$Zr_{0.95}V_{1.37}Nb_{0.68}$	5.316	8.562	4.30	1, 2
$ScTc_2$	5.224	8.570	**10.9**	3
YTc_2	5.371	8.862	8.8	3
$LuTc_2$	5.310	8.736	9.9	3
$ThTc_2$	5.393	9.223	5.3	4
$ZrTc_2$	5.2185	8.6527	7.6	4
$HfTc_2$	5.2001	8.6175	5.6	4
$ScRe_2$	5.271	8.592	4.2	5, 6
YRe_2	5.396	8.819	1.83	7
$ThRe_2$	5.4927	9.1010	5.0	4
$ZrRe_2$	5.267	8.632	6.4	4
$HfRe_2$	5.254	8.600	5.2	4
$ScRu_2$	5.119	8.542	1.67	7
YRu_2	5.256	8.792	1.52	7
$ZrRu_2$	5.144	8.504	1.84	8

(*continued*)

$ScOs_2$	5.179	8.484	4.6	7
YOs_2	5.307	8.786	4.7	7
$LaOs_2$[a]	5.419	9.083	5.9	9, 10
$LuOs_2$	5.254	8.661	3.49	7
$ZrOs_2$	5.219	8.538	3.00	8
$HfOs_2$	5.184	8.468	2.69	7

[a]Prepared at 7.0 GPa.
References: 1, Raevskaya *et al.* (1968); 2, Roberts (1976); 3, Szklarz and Giorgi (1981); 4, Giorgi and Szklarz (1970b); 5, Kripyakevich *et al.* (1963); 6, Phillips (1989); 7, Compton and Matthias (1959); 8, Matthias *et al.* (1961); 9, Cannon *et al.* (1973); 10, Lawson *et al.* (1973).

β-Mo_2N type, *tI*12, (141) $I4_1/amd$–*eb*
$Mo_2N_{0.75}$, $T_c = 5.0$ K,[a] PX
$a = 4.200$ $c = 8.010$ Å, $Z = 4$ (Evans and Jack, 1957; Roberts, 1976)

Atom	WP	*x*	*y*	*z*[b]	Occ.
Mo	8(*e*)	0	$\frac{1}{4}$	0.117	
N	4(*b*)	0	$\frac{1}{4}$	$\frac{3}{8}$	0.75

[a]For nominal composition Mo_2N.
[b]Origin at center (2/*m*).

2H-MoS_2 type, 2H-molybdenite, *C*7, *hP*6, (194) $P6_3/mmc$–*fc*
MoS_2, SX
$a = 3.15$, $c = 12.30$ Å, $Z = 2$, Fig. 6.24 (Dickinson and Pauling, 1923)

Atom	WP	*x*	*y*	*z*
Mo	2(*c*)	$\frac{1}{3}$	$\frac{2}{3}$	$\frac{1}{4}$
S	4(*f*)	$\frac{1}{3}$	$\frac{2}{3}$	0.621
$\square_{oct.}$	2(*a*)	0	0	0

Compound	*a*(Å)	*c*(Å)	T_c(K)	Ref.
MoS_2	3.1603	12.2943	< 1.2	1, 2
$Sr_{0.2}(NH_3)_yTaS_2$	...	18.30	2.8	3
$Li_x(NH_3)_yMoS_2$[a]	...	19.039[b]	3.7	1
Na_xMoS_2[c]	...	14.998[d]	4.15	1
$K_{0.4}MoS_2$	3.2036	16.5804	6.1	1
$Rb_{0.3}MoS_2$	3.2039	17.1937	6.25	1
$Cs_{0.3}MoS_2$	...	19.606	**6.30**	1
Ca_xMoS_2[e]	...	...[f]	5.25	4
$Sr_{0.2}(NH_3)_yMoS_2$	...	18.70[g]	5.0	3
$Sr_{0.2}(NH_3)_yWS_2$	...	18.70	3.5	3

(*continued*)

$Yb_{0.4}(NH_3)_yWS_2$	...	18.60	2.2	3
$Sr_{0.2}(NH_3)_yMoSe_2$	...	19.30	5.0	3

[a] $0.4 \leq x \leq 1.0$; chemical analysis detected no intercalated NH_3, however, NH_3 molecules are presumed to be present.
[b] Probably not hexagonal.
[c] $0.3 \leq x \leq 0.6$.
[d] Tetragonal cell, $a = 14.081$, $c = 14.967$ Å, reported in Somoano *et al.* (1975).
[e] $0.05 \leq x \leq 0.07$.
[f] Orthorhombic, $a = 8.894$, $b = 9.869$, $c = 18.640$ Å.
[g] Tetragonal cell reported for Sr_xMoS_2 ($0.06 \leq x \leq 0.10$), $a = 10.396$, $c = 18.620$ Å, $T_c = 5.6$ K, (Somoano *et al.*, 1975).
References: 1, Somoano *et al.* (1973); 2, Dickinson and Pauling (1923); 3, Subba Rao *et al.* (1974); 4, Somoano *et al.* (1975).

3R-MoS_2 type, 3R-molybdenite, *hR*9, (160) $R3m$-a^3
NbS_2, $T_c = 5.0$ K, SX, $R = 0.055$
$a = 3.3303$, $c = 17.918$ Å, $Z = 3$, Fig. 6.24 (Morosin, 1974; Hulliger, 1968)

Atom	WP	x	y	z
Nb	3(*a*)	0	0	0.4201
S(1)	3(*a*)	0	0	0.0000
S(2)	3(*a*)	0	0	0.1737
$\square_{oct.}$	3(*a*)	0	0	0.59

Compound	*a*(Å)	*c*(Å)	T_c(K)	Ref.
NbS_2	3.3303	17.918	5.0[a]	1*, 2
MoS_2	3.1620	18.3670	< 1.2	3, 4*
$K_{0.4}MoS_2$	3.2072	24.7915	5.5	3
$Ca_{0.2}(NH_3)_yMoS_2$	...	27.69	3.6	5
$Sr_{0.5}(NH_3)_yMoS_2$[b]	...	27.90	5.2	5
$Ba_{0.2}(NH_3)_yMoS_2$	...	28.08	**5.7**	5
$Yb_{0.2}(NH_3)_yMoS_2$[c]	...	27.63	2.4	5

[a] According to Meerschaut *et al.* (1990), 3R-NbS_2 is not superconducting.
[b] Composition $Sr_{0.19}(NH_3)_{0.54}MoS_2$ from chemical analysis.
[c] Composition $Yb_{0.10}(NH_3)_{0.15}MoS_2$ from chemical analysis.
References: 1, Morosin (1974); 2, Hulliger (1968); 3, Somoano *et al.* (1973); 4, Takéuchi and Nowacki (1964); 5, Subba Rao *et al.* (1974).

$MoSi_2$ type, $C11_b$, *tI*6, (139) *I*4/*mmm*–*ea*
branch Zr_2Cu
$PdBi_2$, $T_c = 4.25$ K, PX
$a = 3.362$, $c = 12.983$ Å, $Z = 2$ (Zhuravlev, 1957)

Atom	WP	x	y	z
Pd	2(*a*)	0	0	0
Bi	4(*e*)	0	0	0.363

Compound	a(Å)	c(Å)	T_c(K)	Ref.
$MgHg_2$	3.838	8.799	4.0	1
$PdBi_2$	3.362	12.983	**4.25**	2*

References: 1, Claeson and Luo (1966); 2, Zhuravlev (1957).

2H-NbS_2 type, *hP*6, (194) $P6_3/mmc$–*fb*
$NbSe_2$, $T_c = 7.13$ K, SX, $T = 298$ K, $R = 0.030$
$a = 3.4446$, $c = 12.5444$ Å, $Z = 2$, Fig. 6.24 (Marezio *et al.*, 1972; Roeske *et al.*, 1977)

Atom	WP	x	y	z
Nb	2(*b*)	0	0	$\frac{1}{4}$
Se	4(*f*)	$\frac{1}{3}$	$\frac{2}{3}$	0.1172
$\square_{oct.}$	2(*a*)	0	0	0

Compound[a]	a(Å)	c(Å)	T_c(K)	Ref.
NbS_2	3.31	11.89	6.2	1*, 2
$Rb_{0.33}NbS_2$	3.3425	18.075	2.0	3
$Cs_{0.34}NbS_2$	3.3452	18.424	3.0	3*
$(pyr)_{0.5}NbS_2$[b]	3.34	23.68	4.0	4
$NbSe_2$[c]	3.4446	12.5444	**7.13**	5*, 6
$(NH_3)TaS_2$	3.324	18.14	4.2	4
$LiOH_{aq} + TaS_2$	3.330	17.84	4.5	4
$NaOH_{aq} + TaS_2$	3.326	23.72	4.8	4
$KOH_{aq} + TaS_2$	3.328	18.04	5.3	4
$RbOH_{aq} + TaS_2$	3.325	18.20	4.3	4
$CsOH_{aq} + TaS_2$	3.330	18.56	3.8	4

[a]Data for intercalates of TaS_2 with amides, alkylamines, substituted pyridines, etc. ($T_c \leq 5$ K), most with unknown polytype, reported in Gamble *et al.* (1971a, b); $T_c = 5.3$ K, reported for misfit layer compound $(LaSe)_{1.14}(NbSe_2)_2$, LaSe substructure refined in space group *C*1, $a = 6.019$, $b = 5.998$, $c = 36.540$ Å, $\alpha = \beta = \gamma = 90°$, $NbSe_2$ substructure in $Cmc2_1$, $a = 3.4372$, $b = 6.004$, $c = 36.531$ Å (Roesky *et al.*, 1993).
[b]pyr = pyridine.
[c]Transform to a hexagonal superstructure at ~40 K, $a = 6.880$, $c = 12.482$ Å at 15 K (Marezio *et al.*, 1972)*.
References: 1, Jellinek *et al.* (1960); 2, van Maaren and Schaeffer (1966); 3, Chen *et al.* (1993); 4, Gamble *et al.* (1971a); 5, Marezio *et al.* (1972); 6, Roeske *et al.* (1977).

4H-$NbSe_2$ type, $hP12$, (187) $P\bar{6}m2$–ih^2g^2fa
$NbSe_2$, $T_c = 6.3$ K, SX, $R = 0.144$
$a = 3.44$, $c = 25.24$ Å, $Z = 4$, Fig. 6.24 (Brown and Beerntsen, 1965; Revolinsky *et al.*, 1965)

Atom	WP	x	y	z
Nb(1)	2(g)	0	0	0.250
Nb(2)	1(f)	$\frac{2}{3}$	$\frac{1}{3}$	$\frac{1}{2}$
Nb(3)	1(a)	0	0	0
Se(1)	2(i)	$\frac{2}{3}$	$\frac{1}{3}$	0.066
Se(2)	2(h)	$\frac{1}{3}$	$\frac{2}{3}$	0.185
Se(3)	2(h)	$\frac{1}{3}$	$\frac{2}{3}$	0.318
Se(4)	2(g)	0	0	0.432
$\square_{oct.}$	2(g)	0	0	0.125
$\square_{oct.}$	2(i)	$\frac{2}{3}$	$\frac{1}{3}$	0.375

Compound	a(Å)	c(Å)	T_c(K)	Ref.
$NbSe_2$	3.451	25.24	**6.3**	1, 2*, 3*
$Nb_{1.05}Se_2$	3.446	25.16	5.9	1

References: 1, Revolinsky *et al.* (1965); 2, Kadijk *et al.* (1964); 3, Brown and Beerntsen (1965).

Ni_2In type, $B8_2$, $hP6$, (194) $P6_3/mmc$–dca
In_2Bi, $T_c = 5.8$ K, SX, $T = 293$ K, $R = 0.097$
$a = 5.495$, $c = 6.579$ Å, $Z = 2$ (Kubiak, 1977; Degtyareva *et al.*, 1981)

Atom	WP	x	y	z
In(1)	2(d)	$\frac{1}{3}$	$\frac{2}{3}$	$\frac{3}{4}$
In(2)	2(a)	0	0	0
Bi	2(c)	$\frac{1}{3}$	$\frac{2}{3}$	$\frac{1}{4}$

Compound	a(Å)	c(Å)	T_c(K)	Ref.
$In_{0.80}Sb_{0.20}$[a]	5.364	6.408	5.8	1
In_2Bi	5.496	6.579	**5.8**[b]	1, 2*

[a]Prepared at 5.5 GPa.
[b]$T_c = 6.0$ K for sample prepared at 7.5 GPa.
References: 1, Degtyareva *et al.* (1981); Kubiak (1977).

α-$ThSi_2$ type, C_c, $tI12$, (141) $I4_1/amd$–ea
$ThSi_2$, $T_c = 3.2$ K, SX
$a = 4.134$, $c = 14.375$ Å, $Z = 4$, Fig. 6.14c (Brauer and Mitius, 1942; Cooper *et al.*, 1970)

Atom	WP	x	y	z[a]
Th	4(a)	0	$\frac{3}{4}$	$\frac{1}{8}$
Si	8(e)	0	$\frac{1}{4}$	0.2915

[a]Origin at center ($2/m$).

(*continued*)

Compound	a(Å)	c(Å)	T_c(K)	Ref.
$CaSi_2$[a]	4.283	13.53	1.58	1*, 2
$SrSi_2$[a]	4.438	13.83	3.1	3*, 4
$LaSi_2$	4.326	13.84	2.5	2*
$ThSi_2$	4.134	14.375	3.2	5*, 6
$Th_{0.6}Y_{0.4}Si_2$	...	...	4.6	6
$BaGe_2$[a]	4.769	14.737	**4.93**	7*, 4
YGe_2	4.060	13.683	3.80	8, 6

[a]Prepared at 4 GPa.
References: 1, Evers *et al.* (1982); 2, Nakano and Yamanaka (1994); 3, Evers *et al.* (1983); 4, Evers *et al.* (1980a); 5, Brauer and Mitius (1942); 6, Cooper *et al.* (1970); 7, Evers *et al.* (1980b); 8, Schob and Parthé (1964).

3. AB_3 Types

Cr_3Si type, $A15$, $cP8$, (223) $Pm\bar{3}n$–ca
Mo_3Os, $T_c = 11.68$ K, PX, $R_B = 0.0066$
$a = 4.9689$ Å, $Z = 2$, Figs 6.9a, b, 6.10b (van Reuth and Waterstrat, 1968; Blaugher *et al.*, 1969)

Atom	WP	x	y	z
Mo[a]	6(c)	$\frac{1}{4}$	0	$\frac{1}{2}$
Os[b]	2(a)	0	0	0

[a]$Mo = Mo_{0.953}Os_{0.047}$.
[b]$Os = Os_{0.858}No_{0.142}$.

Compound	a(Å)	T_c(K)	Ref.
$Ti_{0.73}Ir_{0.27}$	5.000[a]	5.0[a]	1, 2*
$Ti_{0.75}Sb_{0.25}$	5.2228	6.54	3
$V_{0.50}Os_{0.50}$	4.809	5.7	4
V_3Pt	4.8166	2.86	2*, 5
$V_{0.76}Au_{0.24}$	4.880[a]	2.96	6, 2*
V_3Al[b]	4.829	9.6	7
V_3Ga	4.817	14.9	8*
$V_{0.75}Si_{0.25}$	4.7250[c]	17.0[a]	9
$V_{0.76}Ge_{0.24}$	4.7830	6.2[d]	10, 11
$V_{0.81}Sn_{0.19}$	4.98	3.8	12, 11
Nb_3Rh	5.1317	2.64	13
Nb_3Pt	5.1547	10.9	13, 2*
Nb_3Au	5.2027	11.5	13, 2*
Nb_3Al	5.180	19.1	14, 15, 16*
$Nb_3Al_{0.75}Ge_{0.25}$	5.174	20.52	17, 18*
$Nb_{0.76}Ga_{0.24}$	5.168	**20.7**	19
Nb_3In[e]	5.303	9.2	20

(*continued*)

$Nb_{0.82}Si_{0.18}$	5.15	4.4[f]	21
$Nb_{0.77}Ge_{0.23}$	5.156	17[g]	22, 23*
$Nb_{0.75}Sn_{0.25}$	5.289[h]	17.9	24
$Nb_{0.83}Sb_{0.17}$	5.265	1.95	25
Nb_3Bi[i]	5.320	3.05	26
Ta_3Sn	5.2801	8.35	27
$Cr_{0.72}Ru_{0.28}$	4.679	3.42	28, 2*
$Cr_{0.72}Os_{0.28}$	4.682	4.68	29, 2*
$Mo_{0.40}Tc_{0.60}$	4.9350	13.5	30
$Mo_{0.7}Re_{0.3}$[j]	4.980	15	31
$Mo_{0.75}Os_{0.25}$	4.969	12.70	29, 2*
$Mo_{0.78}Ir_{0.22}$	4.975	8.55	29, 2*, 32*
$Mo_{0.82}Pt_{0.18}$	4.989	4.65	33, 2*
$Mo_{0.77}Si_{0.23}$	4.900	1.70	29, 34*
$Mo_{0.77}Ge_{0.23}$	4.937	1.80	29

[a]Value taken from figure.
[b]Film prepared by cocondensation.
[c]Transforms to a tetragonal structure at 21 K, $a = 4.7150$, $c = 4.7275$ Å at 10 K (values taken from figure) (Chaddah and Simmons, 1983).
[d]$T_c \approx 11.2$ K reported for sputtered film (Somekh and Evetts, 1977),
[e]Prepared at 4–7 GPa.
[f]$T_c = 14.0$ K reported for sputtered film (Somekh and Evetts, 1977).
[g]T_c up to 23.2 K reported for sputtered films (Gavaler, 1973; Testardi *et al.*, 1974; Krevet *et al.*, 1980).
[h]Transforms to a tetragonal structure at 43 K, $a = 5.298$, $c = 5.252$ Å at 10 K (values taken from figure) (Mailfert *et al.*, 1967).
[i]Prepared above 3.2 GPa.
[j]Sputtered film.

References: 1, Junod *et al.* (1976); 2, van Reuth and Waterstrat (1968); 3, Ramakrishnan and Chandra (1984); 4, Susz *et al.* (1979); 5, Blaugher *et al.* (1969); 6, Flükiger *et al.* (1975); 7, Hartsough and Hammond (1971); 8, Flükiger *et al.* (1976); 9, Jorda and Muller (1982); 10, Luo *et al.* (1970); 11, Flükiger (1981); 12, Morton *et al.* (1979); 13, Zegler (1965); 14, Jorda *et al.* (1980); 15, Flükiger *et al.* (1981); 16, Sweedler and Cox (1975); 17, Arrhenius *et al.* (1968); 18, Christensen *et al.* (1991); 19, Jorda *et al.* (1977); 20, Banus *et al.* (1962); 21, Waterstrat *et al.* (1979); 22, Jorda *et al.* (1978); 23, Rasmussen and Hazell (1979); 24, Junod *et al.* (1978); 25, Junod *et al.* (1970); 26, Killpatrick (1964); 27, Courtney *et al.* (1965); 28, Flükiger *et al.* (1970); 29, Flükiger *et al.* (1974); 30, Marples and Koch (1972); 31, Gavaler *et al.* (1972); 32, Koksbang *et al.* (1989); 33, Flükiger *et al.* (1973); 34, Christensen (1983).

Cu_3Au type, $L1_2$, $cP4$, (221) $Pm\bar{3}m$–ca
La_3In, $T_c = 9.7$ K, PX
$a = 5.070$ Å, $Z = 1$ Figs. 6.5, 6.6 (Garde *et al.*, 1993)

Atom	WP	x	y	z
La	3(*c*)	0	$\frac{1}{2}$	$\frac{1}{2}$
In	1(*a*)	0	0	0

(*continued*)

Compound	a(Å)	T_c(K)	Ref.
$ZrHg_3$	4.368	3.28	1
$LuGa_3$	4.191	2.30	1
$CaTl_3$	4.796	2.04	1
YTl_3	4.678	1.52	1
$LaTl_3$	4.799	1.63	1
$LaSn_3$	4.771	6.02	1
$ThSn_3$	4.714	3.33	1
$NaPb_3$	4.888	5.62	1
YPb_3	4.813	4.72	1
$LaPb_3$	4.905	4.10	1
$ThPb_3$	4.853	5.55	1
$SrBi_3$	5.035	5.70	1
La_3Ga	5.610	5.8	2
La_3In	5.070	**9.7**	2
La_3Tl	5.06	8.86	3
La_3Sn	5.102	6.2	2
$Tl_{0.74}Bi_{0.26}$	4.677	4.15	4

References: 1, Havinga *et al.* (1970); 2, Garde *et al.* (1993); 3, Heiniger *et al.* (1973); 4, Rong-Yao (1986).

Fe_3C type, cementite, $D0_{11}$, $oP16$, (62) $Pnma$–dc^2
Gd_3Co, SX, $R = 0.099$
$a = 7.05$, $b = 9.54$, $c = 6.32$ Å, $Z = 4$ (Strydom and Alberts, 1970)

Atom	WP	x	y	z
Gd(1)	8(d)	0.1758	0.0651	0.1738
Gd(2)	4(c)	0.0416	$\frac{1}{4}$	0.6372
Co	4(c)	0.3880	$\frac{1}{4}$	0.4512

Compound	a(Å)	b(Å)	c(Å)	T_c(K)	Ref.
La_3Ru	7.465	10.016	6.570	4.2	1
La_3Co	7.282	10.020	6.594	4.0	1
La_3Ir	7.458	10.096	6.662	n.o.	1
La_3Ni	7.189	10.160	6.650	**6.2**	1
La_3Ge	7.416	9.954	6.497	3.7	1
Gd_3Co	7.05	9.54	6.32	...	2*

References: 1, Garde *et al.* (1993); 2, Strydom and Alberts (1970).

LT-Mg_3Cd type, $D0_{19}$, $hP8$, (194) $P6_3/mmc$–hd
La_3Al, $T_c = 5.8$ K, PX
$a = 7.192$, $c = 5.528$ Å, $Z = 2$, Fig. 6.5 (Garde *et al.*, 1993)

Atom	WP	x	y	z
La	6(h)	0.1667	0.3333	$\frac{1}{4}$
Al	2(d)	$\frac{1}{3}$	$\frac{2}{3}$	$\frac{3}{4}$

Compound	a(Å)	c(Å)	T_c(K)	Ref.
La_3Al	7.192	5.528	5.8	1
$Mo_{0.69}Pt_{0.31}$	5.612	4.502	**7.8**	2
UPt_3	5.7534	4.9011	0.5	3, 4

References: 1, Garde *et al.* (1993); 2, Flükiger *et al.* (1973); 3, Trinkl *et al.* (1996); 4, Wüchner *et al.* (1993).

Ni_3P type, $D0_e$, $tI32$, (82) $I\bar{4}$–g^4
Ni_3P, SX, $R = 0.083$
$a = 8.954$, $c = 4.386$ Å, $Z = 8$ (Rundqvist *et al.*, 1962)

Atom	WP	x	y	z
Ni(1)	8(g)	0.0775	0.1117	0.2609
Ni(2)	8(g)	0.1351	0.4679	0.0235
Ni(3)	8(g)	0.3311	0.2800	0.2476
P	8(g)	0.2862	0.0487	0.0193

Compound	a(Å)	c(Å)	T_c(K)	Ref.
Mo_3P	9.729	4.923	**5.31**	1, 2
W_3P	9.890	4.808	2.26	2
Ni_3P	8.954	4.386	...	3*

References: 1, Schönberg (1954); 2, Blaugher *et al.* (1965); 3, Rundqvist *et al.* (1962).

$SrPb_3$ type, $L6_0$, $tP4$, (123) $P4/mmm$–eca
$BaBi_3$, $T_c = 5.69$ K, PX, RT
$a = 5.188$, $c = 5.157$ Å, $Z = 1$ (Zhuravlev and Melik-Adamyan, 1961)

Atom	WP	x	y	z
Ba	1(a)	0	0	0
Bi(1)	2(e)	0	$\frac{1}{2}$	$\frac{1}{2}$
Bi(2)	1(c)	$\frac{1}{2}$	$\frac{1}{2}$	0

Compound	a(Å)	c(Å)	T_c(K)	Ref.
$BaBi_3$	5.19	5.16	**5.80**	1, 2
$SrPb_3$	4.962	5.025	1.85	1

References: 1, Havinga *et al.* (1970); 2, Zhuravlev and Melik-Adamyan (1961).

4. AB_n Types ($n \geq 4$)

CaB_6 type, $D2_1$, $cP7$, (221) $Pm\bar{3}m$–fa
LaB_6, $T_c = 5.7$ K, SX, $R = 0.0115$
$a = 4.1571$ Å, $Z = 1$ (Korsukova *et al.*, 1986; Matthias *et al.*, 1968)

Atom	WP	x	y	z
La	1(a)	0	0	0
B[a]	6(f)	0.19948	$\frac{1}{2}$	$\frac{1}{2}$

[a]Refined occupancy 0.982(5), however, occurence of vacancies could not be established with certainty.

Compound	a(Å)	T_c(K)	Ref.
YB_6	4.156[a]	**7.1**	1, 2
LaB_6	4.1571	5.7	3*, 2
ThB_6	4.113	0.74	4, 2

[a]Value taken from figure.
References: 1, Dutchak *et al.* (1972); 2, Matthias *et al.* (1968); 3, Korsukova *et al.* (1986); 4, Cannon and Farnsworth (1983).

$ThMn_{12}$ type, $D2_b$, $tI26$, (139) $I4/mmm$–$jifa$
$MoBe_{12}$, SX, $T_c = 295$ K, $R = 0.012$
$a = 7.251$, $c = 4.234$ Å, $Z = 2$ (Collins and Mahar, 1984; Alekseevskii and Mikhailov, 1963)

Atom	WP	x	y	z
Mo	2(a)	0	0	0
Be(1)	8(j)	0.2895	$\frac{1}{2}$	0
Be(2)	8(i)	0.3505	0	0
Be(3)	8(f)	$\frac{1}{4}$	$\frac{1}{4}$	$\frac{1}{4}$

Compound[a]	a(Å)	c(Å)	T_c(K)	Ref.
$MoBe_{12}$	7.251	4.234	n.o.	1*, 2
WBe_{12}	7.362	4.216	4.1[b]	3, 2
$ReBe_{13}$[c]	...	...	9.9	4
$ReMgBe_{12}$[c]	...	...	**10.1**	4

[a]$T_c = 8.6$ and 9.2 K reported for compositions $OsBe_4$ and $OsBe_5$ (unknown structure) (Alekseevskii and Zakosarenko, 1973).
[b]Nominal composition WBe_{13}, tetragonal, $a = 10.14$, $c = 4.23$ Å (unknown structure).
[c]Nominal composition of sample.
References: 1, Collins and Mahar (1984); 2, Alekseevskii and Mikhailov (1963); 3, von Batchelder and Raeuchle (1957); 4, Alekseevskii and Zakosarenko (1973).

UB_{12} type, $D2_f$, $cF52$, (225) $Fm\bar{3}m$-*ia*
ZrB_{12}, $T_c = 5.82$ K, PN, $R_B = 0.028$
$a = 7.388$ Å, $Z = 4$ (Kennard and Davis, 1983; Matthias *et al.*, 1968)

Atom	WP	x	y	z
Zr	4(*a*)	0	0	0
B	48(*i*)	$\frac{1}{2}$	0.1710	0.1710

Compound	a(Å)	T_c(K)	Ref.
ScB_{12}	7.402[a]	0.39	1*, 2
YB_{12}	7.501	4.7	3, 2
LuB_{12}	7.464	0.48	3, 2
ZrB_{12}	7.388[b]	**5.82**	4*, 2

[a]Tetragonal distortion ($a = 5.22$, $c = 7.35$ Å) reported in Hamada *et al.* (1993).
[b]$Zr_{1-x}Sc_xB_{12}$ ($0.1 \leq x \leq 0.9$) transforms to a rhombohedral structure near room temperature, space group $R\bar{3}m$, $a = 5.2278$. $c = 25.6752$ Å for $x = 0.50$ (not superconducting) (Hamada *et al.*, 1993*).
References: 1, Bruskov *et al.* (1988); 2, Matthias *et al.* (1968); 3, Paderno *et al.* (1971); 4, Kennard and Davis (1983).

$NaZn_{13}$ type, $D2_3$, $cF112$, (226) $Fm\bar{3}c$-*iba*
UBe_{13}, $T_c = 0.96$ K[a], SX, RT, $R = 0.022$
$a = 10.268$ Å, $Z = 8$ (McElfresh *et al.*, 1990; Smith *et al.*, 1985)

Atom	WP	x	y	z
U	8(*a*)	$\frac{1}{4}$	$\frac{1}{4}$	$\frac{1}{4}$
Be(1)	8(*b*)	0	0	0
Be(2)	96(*i*)	0	0.1151	0.1765

[a]Value taken from figure.

Compound	a(Å)	T_c(K)	Ref.
$ThBe_{13}$	10.41727[a]	n.o.	1*
UBe_{13}	10.2550	0.96[b]	2, 1*, 3*
$U_{0.9692}Th_{0.0308}Be_{13}$	10.2591	0.62[b]	2

[a]At 250 K.
[b]Value taken from figure.
References: 1, Goldman *et al.* (1985); 2, Smith *et al.* (1985); 3, McElfresh *et al.* (1990).

$ZrZn_{22}$ type, *cF*184, (227) $Fd\bar{3}m$–*gfdca*
$ReBe_{22}$, $T_c = 9.7$ K, SX, $R = 0.036$
$a = 11.561$ Å, $Z = 8$ (Sands *et al.*, 1962; Giorgi *et al.*, 1982)

Atom	WP	x	y	z[a]
Re	8(*a*)	$\frac{1}{8}$	$\frac{1}{8}$	$\frac{1}{8}$
Be(1)	96(*g*)	0.0598	0.0598	0.3235
Be(2)	48(*f*)	0.4894	$\frac{1}{8}$	$\frac{1}{8}$
Be(3)	16(*d*)	$\frac{1}{2}$	$\frac{1}{2}$	$\frac{1}{2}$
Be(4)	16(*c*)	0	0	0

[a]Origin at center ($\bar{3}m$).

Compound	a(Å)	T_c(K)	Ref.
$MoBe_{22}$	11.634	2.52	1, 2
WBe_{22}	11.631	4.14	1, 2
$TcBe_{22}$	11.566	5.7	2
$ReBe_{22}$	11.560	**9.7**	2, 3*

References: 1, Kripyakevich and Gladyshevskii (1963); 2, Giorgi *et al.* (1982); 3, Sands *et al.* (1962).

5. A_mB_n Types ($m, n \geq 2$)

Pu_2C_3 type, $D5_c$, *cI*40, (220) $I\bar{4}3d$–*dc*
Lu_2C_3[a], $T_c = 15$ K, PX, $R = 0.064$
$a = 8.0354$ Å, $Z = 8$, Fig. 6.20a, b (Novokshonov, 1980; Novokshonov *et al.*, 1980)

Atom	WP	x	y	z
Lu	16(*c*)	0.0499	0.0499	0.0499
C	24(*d*)	0.2915	0	$\frac{1}{4}$

[a]Prepared at 3–9 GPa.

Compound[a]	a(Å)	T_c(K)	Ref.
Sc_4C_3	7.2067[b]	< 1	1*, 2, 3*
$Sc_{13}C_{10}$	8.531[c]	8.5	2
Y_2C_3[d]	8.2378	11.5	4, 5*
$Y_{1.4}Th_{0.6}C_{3.1}$[e]	8.362	**17.0**	6
$Y_{1.8}Ti_{0.2}C_{3.1}$[e]	8.2382	14.5	6
$Y_{1.8}Zr_{0.2}C_{2.9}$[e]	8.2360	13.0	6
$Y_{1.8}Cr_{0.2}C_{2.9}$[e]	8.2384	12.4	6
$Y_{1.8}Mo_{0.2}C_{2.9}$[e]	8.239	13.8	6
$Y_{1.8}W_{0.2}C_{3.1}$[e]	8.240	14.8	6
$La_2C_{2.70}$	8.8095	11.0	7, 8*, 9*
$La_{1.6}Th_{0.4}C_{3.2}$	8.7717	14.3	7
Lu_2C_3[f]	8.0361[b]	15[g]	5*, 8
$Th_2C_{2.90}$[h]	8.5520	4.1	7

(*continued*)

$Th_{1.6}Sc_{0.4}C_3$ [i]	8.531	6.8	9
$Th_{1.6}Ho_{0.4}C_3$ [i]	8.526	5.5	9
$Th_{1.6}Er_{0.4}C_3$ [i]	8.523	8.2	9
$Th_{1.4}Lu_{0.6}C_3$ [i]	8.461	11.7	9

[a]Data for R_2C_3 (R = Ce–Nd, Sm, Gd–Yb) reported in Spedding *et al.* (1958); Atoji and Williams (1961*); Atoji and Tsunoda (1971*); Atoji (1978*); Novokshonov (1980*). Data for R_2C_3 (R = U–Am) reported in Zachariasen (1952*); Austin (1959*); Mitchell and Lam (1970); Green *et al.* (1970*).
[b]At carbon-rich boundary.
[c]Additional diffraction lines could not be indexed.
[d]Prepared at 1.5–2.5 GPa; data for $Y_{2-x}T_xC_{3\pm y}$ (T = U, V, Nb, Ru, Au, Si, Ge, Sn, Pb, Bi; $T_c < T_c(Y_2C_3)$) reported in Krupka *et al.* (1969b).
[e]Prepared at 1.5–2.5 GPa.
[f]Prepared at 3–9 GPa.
[g]No similar value reported elsewhere.
[h]Prepared at 3.5 GPa; data for $Th_{2-x}R_xC_{3\pm y}$ (R = Ce–Nd, Gd–Dy; $T_c < T_c(Th_2C_{2.90})$) reported in Krupka *et al.* (1973)
[i]Prepared at 3–4 GPa.
References: 1, Krikorian *et al.* (1969a); 2, Krikorian *et al.* (1969b); 3, Rassaerts *et al.* (1967); 4, Krupka *et al.* (1969a); 5, Novokshonov (1980); 6, Krupka *et al.* (1969b); 7, Giorgi *et al.* (1970); 8, Novokshonov *et al.* (1980): 9, Krupka *et al.* (1973).

Th_3P_4 type, $D7_3$, $cI28$, (220) $I\bar{4}3d$–ca
La_3Se_4, T_c = 7.80 K, SX
a = 9.055 Å, Z = 4 (Holtzberg *et al.*, 1965; Bucher *et al.*, 1975)

Atom	WP	x	y	z
La	12(a)	$\frac{3}{8}$	0	$\frac{1}{4}$
Se	16(c)	0.075	0.075	0.075

Compound	a(Å)	T_c(K)	Ref.
La_3S_4 [a]	8.730	**8.06**	1
La_3Se_4 [b]	9.060	7.80	1, 2*
La_3Te_4	9.630	5.30	1

[a]Transforms to a tetragonal structure at 90 K, a = 8.648, c = 8.730 Å at 4.2 K (Dernier *et al.*, 1975).
[b]Transforms to a tetragonal structure at 60 K, a = 8.971, c = 9.055 Å at 4.2 K (Dernier *et al.*, 1975).
References: 1, Bucher *et al.* (1975); 2, Holtzberg *et al.* (1965).

Cr_5B_3 type, $D8_l$, $tI32$, (140) $I4/mcm$–$lhca$
branch In_5Bi_3
In_5Bi_3, T_c = 4.2 K, SX, T = 293 K, R = 0.066
a = 8.544, c = 12.680 Å, Z = 4 (Kubiak, 1977; Degtyareva *et al.*, 1981)

Atom	WP	x	y	z
In(1)	16(l)	0.1446	0.6446	0.1649
In(2)	4(c)	0	0	0
Bi(1)	8(h)	0.6559	0.1559	0
Bi(2)	4(a)	0	0	$\frac{1}{4}$

(*continued*)

Compound	a(Å)	c(Å)	T_c(K)	Ref.
$In_{0.65}Sb_{0.35}$[a]	8.34	12.34	**5.6**	1
In_5Bi_3	8.544	12.68	4.2[b]	1, 2*

[a]Prepared at 5.5 GPa.
[b]$T_c = 6.4$ K for $In_{0.60}Bi_{0.40}$ prepared at 5.0 GPa.
References: 1, Degtyareva *et al.* (1981); 2, Kubiak (1977).

Os_4Al_{13}, *mS*34, (12) $C2/m$–i^8d
Os_4Al_{13}, $T_c = 5.5$ K, SX, $R = 0.103$
$a = 17.64$, $b = 4.228$, $c = 7.773$ Å, $\beta = 115.15°$, $Z = 2$ (Edshammar, 1964; Muller *et al.*, 1968)

Atom	WP	x	y	z
Os(1)	4(i)	0.0081	0	0.3053
Os(2)	4(i)	0.7060	0	0.2085
Al(1)	4(i)	0.086	0	0.068
Al(2)	4(i)	0.132	0	0.662
Al(3)	4(i)	0.210	0	0.413
Al(4)	4(i)	0.257	0	0.113
Al(5)	4(i)	0.413	0	0.132
Al(6)	4(i)	0.591	0	0.306
Al(7)	2(d)	0	$\frac{1}{2}$	$\frac{1}{2}$

$Cu_{15}Si_4$ antitype, $D8_6$, *cI*76, (220) $I\bar{4}3d$–*eca*
Th_4D_{15}, $T_c = 7.63$ K[a], PN, RT, $R_p = 0.0368$
$a = 9.110$ Å, $Z = 4$ (Mueller *et al.*, 1977; Dietrich *et al.*, 1974).

Atom	WP	x	y	z
Th	16(c)	0.2066	0.2066	0.2066
D(1)	48(e)	0.0345	0.3794	0.1548
D(2)	12(a)	$\frac{3}{8}$	0	$\frac{1}{4}$

[a]For hydride; $T_c = 8.46$ K at 2.8 GPa (values taken from figure).

Ti_5Re_{24} type, χ phase, *cI*58, (217) $I\bar{4}3m - g^2ca$
substitution derivative of α-Mn, *A*12
Ti_5Re_{24}, $T_c = 6.6$ K, PX
$a = 9.609$ Å, $Z = 2$ (Trzebiatowski and Niemiec, 1955; Matthias *et al.*, 1961)

Atom	WP	x	y	z
Ti(1)	8(c)	0.317	0.317	0.317
Ti(2)	2(a)	0	0	0
Re(1)	24(g)	0.089	0.089	0.278
Re(2)	24(g)	0.356	0.356	0.042

Compound	a(Å)	T_c(K)	Ref.
$Zr_{0.14}Tc_{0.86}$	9.636	9.7	1
$Nb_{0.24}Tc_{0.76}$	9.592	**12.9**	2

(*continued*)

Sc_5Re_{24}	9.65	2.2	3, 4
Ti_5Re_{24}	9.587	6.6	5, 6*
$Zr_{0.14}Re_{0.86}$	9.698	7.4	5
$Hf_{0.14}Re_{0.86}$	9.6801	5.86	7, 8
$Nb_{0.18}Re_{0.82}$	9.641	9.7	5, 9*
$Ta_{0.25}Re_{0.75}$	9.650[a]	6.78	10, 8
$Ta_{0.19}Nb_{0.10}Re_{0.71}$	...	9.8	11
$Mo_{0.25}Re_{0.75}$	9.593	9.26	12, 8
$W_{0.25}Re_{0.75}$	9.594	9.00	13, 8
Al_5Re_{24}	9.58	3.35	14, 15
$Nb_{0.50}Os_{0.50}$	9.760	2.86	16
$Nb_{0.60}Pd_{0.40}$	9.77	2.47	16

[a]Value taken from figure.

References: 1, Compton *et al.* (1961); 2, Giorgi and Szklarz (1970a); 3, Kripyakevich *et al.* (1963); 4, Phillips (1989); 5, Matthias *et al.* (1961); 6, Trzebiatowski and Niemiec (1955); 7, Taylor *et al.* (1963); 8, Matthias *et al.* (1963); 9, Steadman and Nuttall (1964); 10, Brophy *et al.* (1960); 11, Tylkina *et al.* (1973); 12, Knapton (1958/1959); 13, Kuz'ma *et al.* (1968); 14, Kripyakevich and Kuz'ma (1962); 15, Roberts (1976); 16, Bucher *et al.* (1961).

Mo_6Se_8 type, Chevrel phase, *hR*42, (148) $R\bar{3}$–f^2c

Mo_6Se_8, $T_c = 6.5$ K, SX, $R = 0.045$

$a = 9.545$, $c = 11.210$ Å, $Z = 3$ (Bars *et al.*, 1973a; Tarascon *et al.*, 1984b)

Atom	WP	x	y	z
Mo	18(f)	0.17099	0.15205	0.10597
Se(1)	18(f)	0.03792	0.32762	0.08291
Se(2)	6(c)	0	0	0.28627

Compound	a(Å)	c(Å)	T_c(K)	Ref.
Mo_6S_8	9.183	10.909	1.85	1, 2*
$Mo_2Re_4S_8$	9.338	10.424	...	3
$Mo_6S_6Br_2$	9.545	10.357	13.8	4*, 5
$Mo_6S_6I_2$	9.639	10.437	**14.0**	5
Mo_6Se_8	9.545	11.210	6.5	6*, 1
$Mo_{5.25}Nb_{0.75}Se_8$	9.60	11.16	6.2	7
$Mo_{1.5}Re_{4.5}Se_8$	9.674	10.752	...	8*
$Mo_4Ru_2Se_8$	9.680	10.850	...	8*
$Mo_6Se_5Cl_3$	9.64	11.05	5.7	7
Mo_6Se_7Br	9.65[a]	11.01[a]	7.1	5
Mo_6Se_7I	9.80[a]	10.88[a]	7.6	5
Mo_6Te_8	10.212	11.681	< 1.3	9
$Mo_{5.25}Nb_{0.75}Te_8$	10.21	11.70	< 1.7	7
$Mo_{5.25}Ta_{0.75}Te_8$	10.21	11.70	< 1.7	7
$Mo_4Re_2Te_8$	10.225	11.508	3.55	3

(*continued*)

Mo_5RuTe_8	10.242	11.505	3.21	9
$Mo_{4.66}Rh_{1.33}Te_8$	10.25	11.53	< 1.7	7
$Mo_6Te_6Cl_2$	10.19	11.68	...	7
$Mo_6Te_5Br_3$	10.20	11.66	...	7
$Mo_6Te_6I_2$	10.31[a]	11.35[a]	2.6	5

[a]Value taken from figure.

References: 1, Tarascon *et al.* (1984b); 2, Chevrel *et al.* (1974); 3, Perrin *et al.* (1978); 4, Perrin *et al.* (1979); 5, Sergent *et al.* (1977); 6, Bars *et al.* (1973a); 7, Perrin *et al.* (1980); 8, Hönle *et al.* (1983); 9, Berry *et al.* (1988).

Mo_6Ga_{31} type, $mP148$, (14) $P2_1/c$–$e^{36}ca$
$Mo_6Ga_{30.75}$[a], $T_c = 9.8$ K, SX, $R = 0.06$
$a = 9.517$, $b = 16.067$, $c = 16.995$ Å, $\beta = 95.09°$, $Z = 4$ (Yvon, 1974; Matthias *et al.*, 1961)

Atom	WP	x	y	z	Occ.
Mo(1)	4(*e*)	0.0622	0.3819	0.2381	
Mo(2)	4(*e*)	0.1701	0.1489	0.0394	
Mo(3)	4(*e*)	0.1848	0.6131	0.0403	
Mo(4)	4(*e*)	0.3000	0.1109	0.3434	
Mo(5)	4(*e*)	0.5753	0.3839	0.3591	
Mo(6)	4(*e*)	0.6908	0.1585	0.1605	
Ga(1)	4(*e*)	0.0180	0.7456	0.0122	
Ga(2)	4(*e*)	0.0492	0.1218	0.3923	
Ga(3)	4(*e*)	0.0707	0.8804	0.3983	
Ga(4)	4(*e*)	0.0740	0.6328	0.4049	
Ga(5)	4(*e*)	0.0894	0.3791	0.3927	
Ga(6)	4(*e*)	0.1066	0.7566	0.2875	
Ga(7)	4(*e*)	0.1093	0.0033	0.2909	
Ga(8)	4(*e*)	0.1561	0.2416	0.2959	
Ga(9)	4(*e*)	0.1563	0.5204	0.3035	
Ga(10)	4(*e*)	0.1669	0.8845	0.1836	
Ga(11)	4(*e*)	0.1778	0.2859	0.1337	
Ga(12)	4(*e*)	0.2014	0.4729	0.1319	
Ga(13)	4(*e*)	0.2046	0.1210	0.1914	
Ga(14)	4(*e*)	0.2223	0.6351	0.1927	
Ga(15)	4(*e*)	0.2683	0.0051	0.0800	
Ga(16)	4(*e*)	0.2766	0.2008	0.4806	
Ga(17)	4(*e*)	0.2812	0.7562	0.0913	
Ga(18)	4(*e*)	0.3008	0.0028	0.4582	0.9
Ga(19)	4(*e*)	0.3420	0.3841	0.2600	
Ga(20)	4(*e*)	0.3727	0.3844	0.4529	
Ga(21)	4(*e*)	0.4314	0.1959	0.0981	
Ga(22)	4(*e*)	0.4357	0.2488	0.3619	
Ga(23)	4(*e*)	0.4359	0.3846	0.0978	
Ga(24)	4(*e*)	0.4974	0.1309	0.2514	
Ga(25)	4(*e*)	0.5408	0.0850	0.4265	0.9
Ga(26)	4(*e*)	0.5604	0.0203	0.1359	
Ga(27)	4(*e*)	0.5956	0.4702	0.2187	
Ga(28)	4(*e*)	0.5986	0.2955	0.2252	
Ga(29)	4(*e*)	0.6541	0.1224	0.0110	

(*continued*)

Ga(30)	4(*e*)	0.6729	0.2971	0.0659	
Ga(31)	2(*c*)	0	0	$\frac{1}{2}$	
Ga(32)	2(*a*)	0	0	0	0.9

[a]Earlier referred to as $MoGa_4$ or $MoGa_5$.

$Pd_{17}Se_{15}$ type, palladseite, *cP*64, (221) $Pm\bar{3}m$–*mjifeca*
$Rh_{17}S_{15}$, $T_c = 5.8$ K, SX, $R = 0.12$
$a = 9.911$ Å, $Z = 2$ (Geller, 1962; Raub *et al.*, 1963)

Atom	WP	*x*	*y*	*z*
Rh(1)	24(*m*)	0.1436	0.1436	0.3565
Rh(2)	6(*f*)	0.2612	$\frac{1}{2}$	$\frac{1}{2}$
Rh(3)	3(*c*)	0	$\frac{1}{2}$	$\frac{1}{2}$
Rh(4)	1(*a*)	0	0	0
S(1)	12(*j*)	$\frac{1}{2}$	0.2690	0.2690
S(2)	12(*i*)	0	0.3304	0.3304
S(3)	6(*e*)	0.2357	0	0

α-$Mo_{15}Se_{19}$ type, *hP*68, (176) $P6_3/m$–i^4h^2fe
filled-up derivative $In_3Mo_{15}Se_{19}$
$In_{2.87}Mo_{15}Se_{19}$, $T_c = 3.8$ K, SX, $R = 0.07$
$a = 9.804$, $c = 19.49$ Å, $Z = 2$ (Grüttner *et al.*, 1979; Tarascon *et al.*, 1985)

Atom	WP	*x*	*y*	*z*	Occ.
In(1)	6(*h*)	0.0458	0.2127	$\frac{1}{4}$	0.29
In(2)	4(*f*)	$\frac{1}{3}$	$\frac{2}{3}$	0.1288	
Mo(1)	12(*i*)	0.1647	0.0142	0.0571	
Mo(2)	12(*i*)	0.5035	0.3185	0.1334	
Mo(3)	6(*h*)	0.5127	0.1692	$\frac{1}{4}$	
Se(1)	12(*i*)	0.2858	0.3198	0.0509	
Se(2)	12(*i*)	0.3794	0.0091	0.1393	
Se(3)	6(*h*)	0.3543	0.3136	$\frac{1}{4}$	
Se(4)	4(*f*)	$\frac{1}{3}$	$\frac{2}{3}$	0.5297	
Se(5)	4(*e*)	0	0	0.1617	

Compound[a]	*a*(Å)	*c*(Å)	T_c(K)	Ref.
$Mo_{15}S_{19}$	9.218	18.077	< 0.5	1
$Mo_{15}Se_{19}$	9.462	19.61	**4.3**	2, 3*
$Li_3Mo_{15}Se_{19}$	9.724	19.47	3.5	2
$Na_3Mo_{15}Se_{19}$	9.712	19.68	< 0.5	2
$K_2InMo_{15}Se_{19}$	9.790	19.59	1.3	2

(*continued*)

$In_3Mo_{15}Se_{19}$	9.793	19.44	3.8	2, 4
$Tl_{3.3}Mo_{15}Se_{19}$	9.853	19.41	< 0.5	2
$Sn_{2.6}Mo_{15}Se_{19}$	9.890	19.57	< 0.5	2
$Pb_{2.3}Mo_{15}Se_{19}$	9.611	19.59	< 0.5	2

[a]Data for $A_xMo_{15}S_{19}$ (A = Na, K, Zn, Cd, In, Tl, Sn; T_c < 0.5 K) reported in Tarascon and Hull (1986).
References: 1, Tarascon and Hull (1986); 2, Tarascon *et al.* (1985); 3, Davis and Robinson (1990); 4, Grüttner *et al.* (1979).

β-$Mo_{15}Se_{19}$ type, *hR*204, (167) $R\bar{3}c$-$f^4e^2c^2$
filled-up derivative $In_2Mo_{15}Se_{19}$
$In_2Mo_{15}Se_{19}$, T_c = 1.5 K, SX, R = 0.055
a = 9.688, c = 59.10 Å, Z = 6 (Potel *et al.*, 1981, 1984)

Atom	WP	x	y	z
In	12(c)	0	0	0.11425
Mo(1)	36(f)	0.15307	0.16491	0.21066
Mo(2)	36(f)	0.16911	0.14921	0.01977
Mo(3)	18(e)	0.15973	0	$\frac{1}{4}$
Se(1)	36(f)	0.04005	0.32681	0.01663
Se(2)	36(f)	0.32380	0.02960	0.21427
Se(3)	18(e)	0.69019	0	$\frac{1}{4}$
Se(4)	12(c)	0	0	0.05457
Se(5)	12(c)	0	0	0.17609

Compound	a(Å)	c(Å)	T_c(K)	Ref.
$Mo_{15}Se_{19}$	9.478	58.76	**4.3**	1, 2*
$K_2Mo_{15}S_{19}$	...	...	3.32	3
$Li_2Mo_{15}Se_{19}$	9.637	58.16	2.6	1
$Na_2Mo_{15}Se_{19}$	9.611	58.51	< 0.5	1
$K_2Mo_{15}Se_{19}$	9.727	58.17	2.1	1
$Ba_2Mo_{15}Se_{19}$	9.811	57.57	...	4*
$Ag_3Mo_{15}Se_{19}$[a]	9.910	57.070	...	3*
$Cd_{2.5}Mo_{15}Se_{19}$	9.970	56.70	< 0.5	1
$In_2Mo_{15}Se_{19}$	9.687	58.15	1.4	1, 5*
$Sn_2Mo_{15}Se_{19}$	9.676	58.98	< 0.5	1
$Pb_2Mo_{15}Se_{19}$	9.683	57.78	< 0.5	1

[a]The Ag atoms are displaced from the 3-fold axis to three partly occupied tetrahedral sites.
References: 1, Tarascon *et al.* (1985); 2, Gougeon *et al.* (1991); 3, Potel *et al.*, 1984; 4, Gougeon *et al.* (1989); 5, Potel *et al.* (1981).

6. A_mC_{60} Types

K_3C_{60} type, f.c.c., *cF*252, (225) $Fm\bar{3}m$–I^2jca
filled-up derivative of C_{60}, fullerene
K_3C_{60}, $T_c = 19.3$ K, PX[a], RT, $R_{wp} = 0.08$
$a = 14.24$ Å, $Z = 4$, Fig. 6.26 (Stephens *et al.*, 1991)

Atom	WP	x	y	z	Occ.
K(1)	8(*c*)	$\frac{1}{4}$	$\frac{1}{4}$	$\frac{1}{4}$	
K(2)	4(*a*)	0	0	0	
C(1)	192(*l*)	0.051	0.316	0.160	0.5
C(2)	192(*l*)	0.084	0.096	0.287	0.5
C(3)	96(*j*)	0	0.046	0.255	0.5

[a]Synchrotron radiation.

Fullerides wtih C_{60} molecules in (approximate) f.c.c. arrangement.

Compound	Space Group	a(Å)	b(Å)	c(Å)	T_c(K)	Ref.
C_{60}	$Fm\bar{3}$	14.161[a]			n.o.	1, 2
KC_{60}	*Pmnn*	9.109	9.953	14.321[b]	n.o.	3*
RbC_{60}	*Pmnn*	9.138	10.107	14.233[c]	n.o.	3*
Na_2C_{60}	$Pa\bar{3}$	14.189			< 2	4*
Li_2CsC_{60}	$Fm\bar{3}m$	14.0746			n.o.[d]	5*
Na_3C_{60}	$Fm\bar{3}m$	14.191			< 2[e]	4*
Na_2KC_{60}	f.c.c.	14.025			2.5	1
Na_2RbC_{60}	$Pa\bar{3}$	14.028			2.5	1, 6
Na_2CsC_{60}	$Fm\bar{3}m$	14.132[f]			10.5	7, 6
$Na_2Cs(NH_3)_4C_{60}$	$Fm\bar{3}$	14.473			29.6	7*
K_3C_{60}	$Fm\bar{3}m$	14.240			19.3	1, 8*
K_2RbC_{60}	f.c.c.	14.243			23	1
K_2CsC_{60}	f.c.c.	14.292			24	1
$K_3(NH_3)C_{60}$	*Fmmm*	13.687	14.895	14.971	n.o.	9*
Rb_3C_{60}	$Fm\bar{3}m$	14.384			29	1, 10*
Rb_2KC_{60}	f.c.c.	14.323			27	1
Rb_2CsC_{60}	f.c.c.	14.431			31.30	1, 11
Cs_2RbC_{60}	f.c.c.	14.555			33	1
$Sr_{0.08}C_{60}$[g]	$Fm\bar{3}$	14.144			n.o.	12*
$Yb_{2.75}C_{60}$	*Pbca*	27.8733	27.9804	27.8743	6	13*
Ca_5C_{60}	$Fm\bar{3}m$	14.01			8.4	14*
Na_6C_{60}	$Fm\bar{3}m$	14.380			< 2	4*

(*continued*)

$Na_{9.7}C_{60}$[h]	$Fm\bar{3}$	14.59	< 2	15*
$K_3Tl_{4.5}C_{60}$[i]	f.c.c.	14.7	25.6	16
$Rb_{2.7}Tl_{2.2}C_{60}$[j]	f.c.c.	14.46	**45.0**[k]	16

[a]Order–disorder phase transition takes place at 249 K, LT-modification refined in space group $Pa\bar{3}$, $a = 14.0408$ Å at 5 K (David *et al.*, 1991*).
[b]Polymer structure; order–disorder phase transition takes places at 423 K, for HT-modification $a = 14.07$ Å at 473 K, space group $Fm\bar{3}m$; slow cooling to room temperature produced disproportionation to C_{60} and K_3C_{60}; monoclinic structure observed after rapid quenching, $C2/m$, $a = 17.092$, $b = 9.771$, $c = 19.209$ Å, $\beta = 124.06°$ at 19 K (Zhu *et al.*, 1995*).
[c]Polymer structure.
[d]$T_c = 12$ K reported for sample containing 1% Li_2CsC_{60} in Tanigaki *et al.* (1992).
[e]Disproportionation to Na_2C_{60} and Na_6C_{60} observed below 250 K (Rosseinsky *et al.*, 1992).
[f]Order–disorder phase transition takes place at 299 K, LT-modification refined in space group $Pa\bar{3}$, $a = 14.0458$ Å at 1.6 K (Prassides *et al.*, 1994*).
[g]Sample of nominal composition Sr_3C_{60} containing also 66.2% of "*A*15-type" phase.
[h]Composition from chemical analysis.
[i]Nominal composition of sample, prepared from mixture C_{60}/C_{70}, also containing body-centered tetragonal phase.
[j]Nominal composition of sample also containing body-centered tetragonal phase.
[k]No similar value reported elsewhere.
References: 1, Tanigaki *et al.* (1992); 2, David *et al.* (1991); 3, Stephens *et al.* (1994); 4, Rosseinsky *et al.* (1992); 5, Hirosawa *et al.* (1994); 6, Prassides *et al.* (1994); 7, Zhou *et al.* (1993); 8, Stephens *et al.* (1991); 9, Rosseinsky *et al.* (1993); 10, Fischer *et al.* (1995); 11, Fleming *et al.* (1991a); 12, Kortan *et al.* (1994); 13, Özdas *et al.* (1995); 14, Kortan *et al.* (1992a); 15, Yildirim *et al.* (1992); 16, Iqbal *et al.* (1991).

Cs_6C_{60} type, *cI*132, (204) $Im\bar{3}$–h^2ge
Ba_6C_{60}, $T_c = 7$ K, PX, $R_B = 0.096$
$a = 11.171$ Å, $Z = 2$ (Kortan *et al.*, 1992b)

Atom	WP	x	y	z
Ba	12(*e*)	0.2207	0	$\frac{1}{2}$
C(1)	48(*h*)	0.0635	0.2301	0.2057
C(2)	48(*h*)	0.1029	0.1262	0.2693
C(3)	24(*g*)	0	0.0635	0.3087

Fullerides with C_{60} molecules in (approximate) b.c.c. arrangement.

Compound	Space Group	a(Å)	c(Å)	T_c(K)	Ref.
Sr_3C_{60}[a]	$Pm\bar{3}$	11.140		n.o.	1*
Ba_3C_{60}	$Pm\bar{3}n$	11.343		n.o.	2*

(*continued*)

K_4C_{60}	$I4/mmm$	11.886	10.774	n.o.	3
Rb_4C_{60}	$I4/mmm$	11.962	11.022	n.o.	3
Cs_4C_{60}	$I4/mmm$	12.057	11.443	n.o.	3
K_6C_{60}	$Im\bar{3}$	11.385		n.o.	3
Rb_6C_{60}	$Im\bar{3}$	11.548		n.o.	3
Cs_6C_{60}	$Im\bar{3}$	11.79		n.o.	4*
Sr_6C_{60}	$Im\bar{3}$	10.975		4	1*
Ba_6C_{60}	$Im\bar{3}$	11.171		**7**	5*

[a]Multi-phase sample also containing 33.8% of f.c.c. $Sr_{2.08}C_{60}$.
References: 1, Kortan *et al.* (1994); 2, Kortan *et al.* (1993); 3, Fleming *et al.* (1991b); 4, Zhou *et al.* (1991); 5, Kortan *et al.* (1992b).

c. Ternary Structure Types

1. *ABC* Types

1s-GdCBr type, $mS12$, (12) $C2/m$–i^3
YCl, $T_c = 9.7$ K, SX, $T = 293$ K, $R = 0.075$
$a = 7.174$, $b = 3.866$, $c = 10.412$ Å, $\beta = 92.98°$, $Z = 4$, Fig. 6.18a (Mattausch *et al.*, 1994; Simon *et al.*, 1996)

Atom	WP	x	y	z
Y	4(i)	0.1470	0	0.1316
C	4(i)	0.429	0	0.037
I	4(i)	0.1707	0	0.6676

Compound	a(Å)	b(Å)	c(Å)	β(°)	T_c(K)	Ref.
YCCl	6.830	3.712	9.332	95.01	2.30	1
$YCCl_{0.65}Br_{0.35}$	6.866	3.731	9.568	94.82	3.55	1
$Na_{0.23}YCBr$[a]	7.061	3.724	10.464	92.96	6.2	2*
LaCBr	7.451	4.056	10.026	94.31	6.2	3
$LaCBr_{0.85}Cl_{0.15}$	7.421	4.045	10.013	94.70	7.2	3
$LaCBr_{0.90}I_{0.10}$	7.508	4.051	10.287	93.77	5.0	3
GdCBr	7.025	3.8361	9.868	94.47	n.o.	4*, 5
YCI	7.217	3.879	10.435	93.55	9.7	1, 6*
$YCI_{0.88}Cl_{0.12}$	7.172	3.857	10.452	93.79	10.70	1
$YCI_{0.75}Br_{0.25}$	7.154	3.851	10.388	93.92	**11.10**	1*
LaCI	7.673	4.130	10.843	92.99	< 2	3
$LaCI_{0.5}Cl_{0.5}$	7.570	4.086	10.644	93.69	3.7	3

[a]Filled-up derivative.
References; 1, Simon *et al.* (1996); 2, Bäcker *et al.* (1996); 3, Ahn *et al.* (1997); 4, Schwanitz-Schüller and Simon (1985); 5, Simon *et al.* (1991); 6, Mattausch *et al.* (1994).

3s-GdCBr type, $mS12$, (12) $C2/m$–i^3
YCBr, $T_c = 5.03$ K, PN, $R_{wp} = 0.055$
$a = 6.990$, $b = 3.765$, $c = 9.949$ Å, $\beta = 100.1°$, $Z = 4$, Fig. 6.18b (Simon *et al.*, 1996)

Atom	WP	x	y	z
Y	4(i)	0.4040	0	0.1485
C	4(i)	0.0861	0	0.0361
Br	4(i)	0.2099	0	0.6667

Compound	a(Å)	b(Å)	c(Å)	β(°)	T_c(K)	Ref.
YCBr	6.958	3.767	9.932	99.97	5.05	1*
$YCBr_{0.88}Cl_{0.12}$	6.941	3.761	9.898	99.94	4.70	1
$YCBr_{0.62}I_{0.38}$	7.054	3.808	10.321	100.06	**7.00**	1
GdCBr	7.066	3.827	9.967	99.95	n.o.	2*, 3
TbCBr	7.015	3.801	9.948	100.05	n.o.	2, 3

References: 1, Simon *et al.* (1996); 2, Mattausch *et al.* (1992); 3, Simon *et al.* (1991).

LaPtSi type, $tI12$, (109) $I4_1md$–a^3
substitution derivative of α-$ThSi_2$, C_c
LaPtSi, $T_c = 3.3$ K, SX, $R = 0.052$
$a = 4.2490$, $c = 14.539$ Å, $Z = 4$ (Klepp and Parthé, 1982a; Evers *et al.*, 1984)

Atom	WP	x	y	z
La	4(a)	0	0	0.581
Pt	4(a)	0	0	0.1660
Si	4(a)	0	0	0.000

Compound	a(Å)	c(Å)	T_c(K)	Ref.
LaPtSi	4.245	14.54	3.3	1, 2*
$ThRh_{0.96}Si_{1.04}$	4.128[a]	14.28[a]	6.45	3
ThIrSi	4.142[a]	14.27[a]	**6.50**	3
LaIrGe	4.3166	14.430	1.64	4, 5
LaPtGe	4.266	14.96	3.4	1

[a]Value taken from figure.
References: 1, Evers *et al.* (1984); 2, Klepp and Parthé (1982a); 3, Lejay *et al.* (1983); 4, Hovestreydt *et al.* (1982); 5, Subba Rao *et al.* (1985).

NbPS type, *oI*12, (71) *Immm–jig*
NbPS[a], $T_c = 12.5$ K, PX, $T = 298$ K, $R = 0.093$
$a = 3.438$, $b = 4.725$, $c = 11.88$ Å, $Z = 4$ (Donohue and Bierstedt, 1969)

Atom	WP	x	y	z
Nb	4(*j*)	$\frac{1}{2}$	0	0.1232
P	4(*g*)	0	0.265	0
S	4(*i*)	0	0	0.288

[a]Prepared at 6.5 GPa.

TiFeSi type, *oI*36, (46) *Ima2–c*^{2}*b*^{4}*a*
TiFeSi, SX, $R = 0.094$
$a = 6.997$, $b = 10.830$, $c = 6.287$ Å, $Z = 12$ (Jeitschko, 1970)

Atom	WP	x	y	z
Ti(1)	4(*b*)	$\frac{1}{4}$	0.2207	0.0206
Ti(2)	4(*b*)	$\frac{1}{4}$	0.4979	0.1677
Ti(3)	4(*b*)	$\frac{1}{4}$	0.7996	0.0463
Fe(1)	8(*c*)	0.5295	0.1236	0.3699
Fe(2)	4(*a*)	0	0	0.0000
Si(1)	8(*c*)	0.5060	0.3325	0.2452
Si(2)	4(*b*)	$\frac{1}{4}$	0.0253	0.2554

Compound	a(Å)	b(Å)	c(Å)	T_c(K)	Ref.
NbReSi	7.070	11.442	6.606	**5.1**	1
TaReSi	7.002	11.614	6.605	4.4	1
TiFeSi	6.997	10.830	6.287	...	2*
NbRuSi	7.123	11.413	6.535	2.65	1
TaRuSi	7.222	11.111	6.482	3.15	1

References: 1, Subba Rao *et al.* (1985); 2, Jeitschko (1970).

TiNiSi type, *oP*12, (62) *Pnma–c*^{3}
substitution derivative of Co_2P
ZrRuP, $T_c = 3.82$ K, SX, $R = 0.036$
$a = 6.4169$, $b = 3.8623$, $c = 7.3215$ Å, $Z = 4$, Fig. 6.14d (Müller *et al.*, 1983)

Atom	WP	x	y	z
Zr	4(*c*)	0.0225	$\frac{1}{4}$	0.6804
Ru	4(*c*)	0.1508	$\frac{1}{4}$	0.0606
P	4(*c*)	0.2744	$\frac{1}{4}$	0.3778

(*continued*)

Compound	a(Å)	b(Å)	c(Å)	T_c(K)	Ref.
YIrSi	6.789	4.188	7.462	2.70	1
TiIrSi	6.2578	3.8581	7.2006	< 1.7	1
ZrIrSi	6.5578	3.9537	7.3762	2.04	1
HfIrSi	6.4710	3.9380	7.3763	3.50	1*
ZrRuP	6.4169	3.8623	7.3215	3.82	2*
NbRuP	6.318	3.719	7.173	< 1.1	2
TaRuP	6.288	3.713	7.164	< 1.1	2
ZrRhP	6.483	3.787	7.393	1.55	2
NbRhP	6.306	3.737	7.187	4.42	2
TaRhP	6.253	3.736	7.180	**4.86**	2

References: 1, Xian-Zhong *et al.* (1985); 2, Müller *et al.* (1983).

ZrNiAl type, *hP9*, (189) $P\bar{6}2m$–*gfda*
substitution derivative of Fe_2P, *C*22
ZrRuP, $T_c = 12.93$ K, PX, $R_B = 0.10$
$a = 6.459$, $c = 3.778$ Å, $Z = 3$, Fig. 6.14b (Barz *et al.*, 1980; Meisner and Ku, 1983)

Atom	WP	x	y	z
Zr	3(*f*)	0.585	0	0
Ru	3(*g*)	0.235	0	$\frac{1}{2}$
P(1)	2(*d*)	$\frac{1}{3}$	$\frac{2}{3}$	$\frac{1}{2}$
P(2)	1(*a*)	0	0	0

Compound	a(Å)	c(Å)	T_c(K)	Ref.
TiRuP	6.303	3.567	1.3	1*, 2*
ZrRuP	6.459	3.778	**12.93**[a]	2*, 1*
HfRuP	6.414	3.753	10.8	2, 1*
TiOsP	6.285	3.625	<0.35	2, 1
ZrOsP	6.460	3.842	7.4	2, 1
HfOsP	6.417	3.792	6.10	2, 1
ZrRuAs	6.586	3.891	11.90	1
HfRuAs	6.568	3.842	4.93	1
ZrOsAs	6.602	3.794	8.0	1
HfOsAs	6.569	3.808	3.2	1

[a] $T_c = 13.3$ K determined for sample containing ~83% of the phase.
References: 1, Meisner and Ku (1983); 2, Barz *et al.* (1980).

ZrSO type, $cP12$, (198) $P2_13$–a^3
LaIrSi, $T_c = 2.3$ K, PX, $R = 0.12$
$a = 6.337$ Å, $Z = 4$ (Chevalier *et al.*, 1982a)

Atom	WP	x	y	z
La	4(a)	0.365	0.365	0.365
Ir	4(a)	0.077	0.077	0.077
Si	4(a)	0.674	0.674	0.674

Compound	a(Å)	T_c(K)	Ref.
LaRhSi	6.296	**4.35**	1
LaIrSi	6.337	2.3	1*, 2*

References: 1, Chevalier *et al.* (1982a); 2, Klepp and Parthé (1982b).

2. ABC_n Types ($n \geq 2$)

$LuRuB_2$ type, $oP16$, (62) $Pnma$–dc^2
$LuRuB_2$, $T_c = 9.99$ K, SX, $R = 0.085$
$a = 5.809$, $b = 5.229$, $c = 6.284$ Å, $Z = 4$ (Shelton *et al.*, 1980; Ku and Shelton, 1980)

Atom	WP	x	y	z
Lu	4(c)	0.0105	$\frac{1}{4}$	0.6648
Ru	4(c)	0.1816	$\frac{1}{4}$	0.1824
B	8(d)	0.358	0.084	0.464

Compound[a]	a(Å)	b(Å)	c(Å)	T_c(K)	Ref.
$YRuB_2$	5.918	5.297	6.377	7.80	1, 2
$Y_{0.8}Sc_{0.2}RuB_2$	...	...	...	8.10	2
$LuRuB_2$	5.809	5.229	6.284	**9.99**	1*, 2
$ScOsB_2$	5.647	5.178	6.184	1.34	1, 2
$YOsB_2$	5.905	5.299	6.391	2.22	1, 2
$LuOsB_2$	5.809	5.231	6.318	2.66	1, 2

[a]Data for $RRuB_2$ and $ROsB_2$ (R = Tb–Tm) reported in Shelton *et al.* (1980); data for $PuTB_2$ (T = Tc, Re, Ru, Os) reported in Rogl *et al.* (1987).
References: 1, Shelton *et al.* (1980); 2, Ku and Shelton (1980).

$MnCu_2Al$ type, Heusler phase, $L2_1$, $cF16$, (225) $Fm\bar{3}m$–cba
substitution derivative of BiF_3, $D0_3$
YPd_2Sn[a], $T_c = 5.5$ K, SX
$a = 6.718$ Å, $Z = 4$, Fig. 6.7b (Jorda *et al.*, 1985)

Atom	WP	x	y	z
Y	4(b)	$\frac{1}{2}$	$\frac{1}{2}$	$\frac{1}{2}$
Pd	8(c)	$\frac{1}{4}$	$\frac{1}{4}$	$\frac{1}{4}$
Sn	4(a)	0	0	0

[a]Sample of nominal composition $Y_{0.24}Pd_{0.52}Sn_{0.24}$.

Compound[a]	a(Å)	T(K)	Ref.
$ScAu_2Al$	6.535	4.40	1, 2
$ScAu_2In$	6.692	3.02	1, 2
$ScPd_2Sn$	6.503	2.15	3
YPd_2In	6.723	0.85	4
YPd_2Sn[b]	6.718	**5.5**	5
YPd_2Pb	6.790	4.76	4
YPd_2Sb	6.691	0.85	4
YPd_2Bi	6.825	<0.07	4
$TmPd_2Sn$	6.670	2.82	3
$YbPd_2Sn$	6.658	2.42	3
$LuPd_2Sn$	6.645	3.05	3

[a]Data for RPd_2Sn (R = Tb–Er; superconductivity not observed) reported in Malik *et al.* (1985).
[b]Sample of nominal composition $Y_{0.24}Pd_{0.52}Sn_{0.24}$.
References: 1, Dwight and Kimball (1987); 2, Savitskii *et al.* (1985); 3, Malik *et al.* (1985); 4, Ishikawa *et al.* (1982); 5, Jorda *et al.* (1985).

Mo_2BC type, $oS16$, (63) $Cmcm$–c^4
Mo_2BC, $T_c = 5.4$ K, SX, $R = 0.035$
$a = 3.086$, $b = 17.35$, $c = 3.047$ Å, $Z = 4$, Fig. 6.22 (Smith *et al.*, 1969)

Atom	WP	x	y	z
Mo(1)	4(c)	0	0.1861	$\frac{1}{4}$
Mo(2)	4(c)	0	0.4279	$\frac{1}{4}$
B	4(c)	0	0.0269	$\frac{1}{4}$
C	4(c)	0	0.3080	$\frac{1}{4}$

(*continued*)

Compound	a(Å)	b(Å)	c(Å)	T_c(K)	Ref.
Mo_2BC[a]	3.084[b]	17.355[b]	3.045[b]	7.5	1, 2*, 3*
$Mo_{1.18}Rh_{0.2}BC$	3.083[b]	17.323[b]	3.042[b]	**9.0**[b]	4
$Nb_2BN_{0.98}$	3.172	17.841	3.114	2.5	5*

[a]Data for $Mo_{2-x}T_xBC$ (T = Zr, Hf, Nb, Ta, W; $T_c < T_c(Mo_2BC)$) reported in Lejay *et al.* (1981a, b).
[b]Value taken from figure.
References: 1, Lejay *et al.* (1981b); 2, Jeitschko *et al.* (1963b); 3, Smith *et al.* (1969); 4, Lejay *et al.* (1981a); 5, Rogl *et al.* (1988).

$CaTiO_3$ type, perovskite, $E2_1$, $cP5$, (221) $Pm\bar{3}m$–dba
$Ba_{0.57}K_{0.43}BiO_3$, $T_c = 30$ K, PN, $T = 10$ K, $R_{wp} = 0.0857$
$a = 4.2742$ Å, $Z = 1$, Fig. 6.23 (Pei *et al.*, 1990)

Atom	WP	x	y	z
Ba[a]	1(b)	$\frac{1}{2}$	$\frac{1}{2}$	$\frac{1}{2}$
Bi	1(a)	0	0	0
O	3(d)	$\frac{1}{2}$	0	0

[a]$Ba = Ba_{0.57}K_{0.43}$.

Cr_3AsN antitype, $tI20$, (140) $I4/mcm$–$hcba$
deformation derivative of $CaTiO_3$, perovskite, $E2_1$
$BaPb_{0.8}Bi_{0.2}O_3$, $T_c = 10$ K[a], PN, $T = 10$ K, $R_{wp} = 0.0795$[b]
$a = 6.0217$, $c = 8.6110$ Å, $Z = 4$ (Marx *et al.*, 1992)

Atom	WP	x	y	z
Ba	4(b)	0	$\frac{1}{2}$	$\frac{1}{4}$
Pb[c]	4(c)	0	0	0
O(1)	8(h)	0.2134	0.7134	0
O(2)	4(a)	0	0	$\frac{1}{4}$

[a]Value taken from figure.
[b]Sample contained 42% of nonsuperconducting orthorhombic modification.
[c]$Pb = Pb_{0.8}Bi_{0.2}$.

Compound	a(Å)	c(Å)	T_c(K)	Ref.
$BaPb_{0.75}Sb_{0.25}O_3$	6.028	8.511	3.5	1
$BaPb_{0.7}Bi_{0.3}O_3$	6.0576	8.6182	**11.5**[a]	2*
$BaPb_{0.5}Bi_{0.25}Tl_{0.25}O_{2.91}$[b]	6.0564	8.5947	9	3*

[a]Value taken from figure; $T_c = 13$ K reported in Sleight *et al.* (1975).
[b]Site O(2) split into 16(j) 0.0375 0 $\frac{1}{4}$.
References: 1, Cava *et al.* (1989); 2, Marx *et al.* (1992); 3, Iqbal *et al.* (1990).

Rb_xWO_3 type, hexagonal bronze, *hP*26, (193) $P6_3/mcm$–*kjgb*
$Rb_{0.28}WO_3$, $T_c = 2.90$ K, SX, $R = 0.047$
$a = 7.3875$, $c = 7.5589$ Å, $Z = 6$ (Labbé *et al.* 1978; Wanlass and Sienko, 1975)

Atom	WP	*x*	*y*	*z*	Occ.
Rb	2(*b*)	0	0	0	0.85
W	6(*g*)	0.48053	0	$\frac{1}{4}$	
O(1)	12(*k*)	0.4769	0	0.0009	0.5
O(2)	12(*j*)	0.2149	0.4224	$\frac{1}{4}$	

Compound	*a*(Å)	*c*(Å)	T_c(K)	Ref.
WO_3	7.3244	7.6628	...	1*
$K_{0.20}WO_3$	7.3869	7.5101[a]	5.70[b]	2*, 3
$Rb_{0.28}WO_3$	7.3875	7.5589	**6.55**[b]	4*, 3
$Cs_{0.20}WO_3$	7.4203	7.5674	4.76[b]	2*, 3, 5*

[a]Splitting of K site reported for $K_{0.33}WO_3$ in Kudo *et al.* (1991*); structure refined in space group $P6_322$ in Pye and Dickens (1979*), $P6_3$ in Schultz *et al.* (1986a*).
[b]For acid-etched sample.
References: 1, Oi *et al.* (1992); 2, Kihlborg and Hussain (1979); 3, Remeika *et al.* (1967); 4, Labbé *et al.* (1978); 5, Oi *et al.* (1993).

3. AB_2C_n Types ($n \geq 2$)

$CeAl_2Ga_2$ type, *tI*10, (193) $I4/mmm$–*eda*
substitution derivative of $BaAl_4$, $D1_3$
$LaRu_2P_{1.89}$, $T_c = 4.1$ K, SX, $R = 0.028$
$a = 4.031$, $c = 10.675$ Å, $Z = 2$, Fig. 6.13 (Jeitschko *et al.*, 1987)

Atom	WP	*x*	*y*	*z*	Occ.
La[a]	2(*a*)	0	0	0	
Ru	4(*d*)	0	$\frac{1}{2}$	$\frac{1}{4}$	
P	4(*e*)	0	0	0.3593	0.947

[a]Refined occupancy 0.997(2).

Compound[a]	*a*(Å)	*c*(Å)	T_c(K)	Ref.
URu_2Si_2	4.126	9.568	1.2	1*, 2
$CeCu_2Si_2$[b]	4.1012	9.925	0.67	3, 4*
$SrRu_2P_2$	4.032	11.122	<1.8	5*
$LaRu_2P_2$	4.031	10.675	**4.1**	5*

[a]Data for RRu_2P_2 (R = Ca, Ba, Y, Ce–Nd, Sm–Yb; $T_c < 1.8$ K for R = Ca, Ba, Y) reported in Jeitschko *et al.* (1987).
[b]Sample of nominal composition $Ce_{0.193}Cu_{0.42}Si_{0.387}$.
References: 1, Cordier *et al.* (1985); 2, Wüchner *et al.* (1993); 3, Ishikawa and Braun (1983); 4, Neumann *et al.* (1988); 5, Jeitschko *et al.* (1987).

YB_2C_2 type, *tP*10, (131) $P4_2/mmc$–*mke*
LaB_2C_2[a], SX, $R = 0.038$
$a = 3.8218$, $c = 7.9237$ Å, $Z = 2$ (Bauer and Bars, 1980)

Atom	WP	x	y	z
La	2(*e*)	0	0	$\frac{1}{4}$
B	4(*k*)	0.226	$\frac{1}{2}$	$\frac{1}{2}$
C	4(*m*)	0.173	$\frac{1}{2}$	0

[a]Original description in space group $P\bar{4}2c$ does not take into consideration all symmetry elements (Cenzual *et al.*, 1991).

Compound[a]	a(Å)	c(Å)	T_c(K)	Ref.
YB_2C_2	3.780	7.111	**3.6**	1, 2*
LaB_2C_2	3.823	7.927	<1.8	1, 3*
DyB_2C_2	3.779	7.119	n.o.	1, 4*
LuB_2C_2	3.762	6.890	2.4	1

[a]Data for RB_2C_2 (R = Ce–Nd, Sm-Tb, Ho–Yb; superconductivity not observed or not investigated) reported in Fishel and Eick (1969) and Sakai *et al.* (1982).
References: 1, Sakai *et al.* (1982); 2, Bauer and Nowotny (1971); 3, Bauer and Bars (1980); 4, Bauer and Debuigne (1972).

$Ba_{0.67}Pt_3B_2$ type, *hP*12, (194) $P6_3/mmc$–*hfa*
$Ba_{0.67}Pt_3B_2$[a], $T_c = 5.60$ K, PX, $R_B = 0.077$
$a = 6.161$, $c = 5.268$ Å, $Z = 2$ (Shelton, 1978)

Atom	WP	x	y	z	Occ.
Ba	2(*a*)	0	0	0	0.67
Pt	6(*h*)	0.512	0.024	$\frac{1}{4}$	
B	4(*f*)	$\frac{1}{3}$	$\frac{2}{3}$	0.033	

[a]Possibly isotypic with $Ba_2Ni_9B_6$ with ordered vacancies, space group $R\bar{3}c$, $a = 10.029$, $c = 14.533$ Å (Jung and Quentmeier, 1980*).

Compound	a(Å)	c(Å)	T_c(K)	Ref.
$Ca_{0.67}Pt_3B_2$	5.989	5.127	1.57	1
$Sr_{0.67}Pt_3B_2$	6.092	5.184	2.78	1
$Ba_{0.67}Pt_3B_2$	6.161	5.268	**5.60**	1*

Reference: 1, Shelton (1978).

$CeCo_3B_2$ type, *hP*6, (191) $P6/mmm$–gca
substitution derivative of $CaCu_5$, $D2_d$
branch $PrNi_2Al_3$
$LuOs_3B_2$, $T_c = 4.67$ K, PX
$a = 5.455$, $c = 3.064$ Å, $Z = 1$, Fig. 6.11a (Lee *et al.*, 1987)

Atom	WP	x	y	z
Lu	1(*a*)	0	0	0
Os	3(*g*)	$\frac{1}{2}$	0	$\frac{1}{2}$
B	2(*c*)	$\frac{1}{3}$	$\frac{2}{3}$	0

Compound[a]	a(Å)	c(Å)	T_c(K)	Ref.
$LaIr_5$	5.399	4.203	2.13	1, 2
$ThIr_5$	5.315	4.288	3.93	2
UNi_2Al_3	5.207	4.018	1.1	3, 4
UPd_2Al_3	5.365	4.186	2.0	5, 4
$LaRh_3B_2$	5.480	3.137	2.82	6
$LaIr_3B_2$	5.543	3.116	1.65	6
$LuOs_3B_2$	5.457	3.052	**4.67**	6, 7
$ThRu_3B_2$	5.526	3.070	1.79	6
$ThIr_3B_2$	5.449	3.230	2.09	6

[a]Data for RRu_3B_2 (R = Y, La, Ce–Nd, Sm, Gd–Lu, U), UOs_3B_2, RRh_3B_2 (R = Ce–Nd, Sm–Gd) and UIr_3B_2 ($T_c < 1.2$ K) reported in Ku *et al.* (1980); $T_c = 6.00$ K reported for YOs_3B_2 (unknown structure) in Ku and Shelton (1980).
References: 1, Vorob'ev and Mel'nikova (1974); 2, Geballe *et al.* (1965); 3, Geibel *et al.* (1991b); 4, Geibel *et al.* (1993); 5, Geibel *et al.* (1991a); 6, Ku *et al.* (1980); 7, Lee *et al.* (1987).

$LaRu_3Si_2$ type, *hP*12, (176) $P6_3/m$–hfb
deformation derivative of $CeCo_3B_2$
$LaRu_3Si_2$, $T_c = 7.60$ K, PX
$a = 5.676$, $c = 7.120$ Å, $Z = 2$ (Vandenberg and Barz, 1980; Barz, 1980)

Atom	WP	x	y	z
La	2(*b*)	0	0	0
Ru	6(*h*)	0.01	0.490	$\frac{1}{4}$
Si	4(*f*)	$\frac{1}{3}$	$\frac{2}{3}$	0.0

Compound[a]	a(Å)	c(Å)	T_c(K)	Ref.
YRu_3Si_2	5.543	7.152	3.51[b]	1, 2
$LaRu_3Si_2$	5.676	7.120	**7.60**[b]	1*, 2
$ThRu_3Si_2$	5.608	7.201	3.98[b]	1, 2

[a]Data for RRu_3Si_2 (R = Sc, Ce–Nd, Sm–Lu, U; $T_c < 1$ K) reported in Barz (1980).
[b]Ru-rich sample containing also free Ru.
References: 1, Vandenberg and Barz (1980); 2, Barz (1980).

Mo_3Al_2C type, *cP*24, (213) $P4_132$–*dca*
filled-up substitution derivative of β-Mn, *A*13
Mo_3Al_2C, $T_c = 10.0$ K, PX
$a = 6.866$ Å, $Z = 4$ (Jeitschko *et al.*, 1963a; Johnston *et al.*, 1964)

Atom	WP	*x*	*y*	*z*
Mo	12(*d*)	$\frac{1}{8}$	0.206	0.456
Al	8(*c*)	0.061	0.061	0.061
C	4(*a*)	$\frac{3}{8}$	$\frac{3}{8}$	$\frac{3}{8}$

$MgAl_2O_4$ type, spinel, $H1_1$, *cF*56, (227) $Fd\bar{3}m$–*ecb*
$Li_{0.75}Ti_2O_4$, $T_c = 13.2$ K, SX, $T = 223$ K, $R = 0.0109$
$a = 8.4030$ Å, $Z = 8$ (Moshopoulou *et al.*, 1994)

Atom	WP	*x*	*y*	*z*[a]	Occ.
Li	8(*b*)	$\frac{3}{8}$	$\frac{3}{8}$	$\frac{3}{8}$	0.75
Ti	16(*c*)	0	0	0	
O	32(*e*)	0.23685	0.23685	0.23685	

[a]Origin at center ($\bar{3}m$).

Compound	*a*(Å)	T_c(K)	Ref.
$Li_{0.75}Ti_2O_4$	8.4030	**13.2**	1*
$Li_{1.03}Ti_{1.90}O_4$	8.40099	12.3	2*
CuV_2S_4	9.82	4.45	3
$CuRh_2S_4$	9.790	4.35	4, 5*
$CuRh_2Se_4$	10.263	3.50	4, 5*

References: 1, Moshopoulou *et al.* (1994); 2, Dalton *et al.* (1994); 3, van Maaren *et al.* (1967); 4, Robbins *et al.* (1967); 5, Riedel *et al.* (1976).

$ZrFe_4Si_2$ type, *tP*14, (136) $P4_2/mnm$–*ifa*
$ZrNi_4P_2$, SX, $R = 0.028$
$a = 6.934$, $c = 3.565$ Å, $Z = 2$ (Pivan *et al.*, 1989)

Atom	WP	*x*	*y*	*z*
Zr	2(*a*)	0	0	0
Ni	8(*i*)	0.1648	0.5851	0
P	4(*f*)	0.2819	0.2819	0

Compound	*a*(Å)	*c*(Å)	T_c(K)	Ref.
$ZrNi_4P_2$	6.944	3.576	<2	1, 2*
$ZrRu_4P_2$	6.992	3.699	**11**	1
$HfRu_4P_2$	...	...	9.5	1

References: 1, Shirotani *et al.* (1997); 2, Pivan *et al.* (1989).

4. AB_3C_n Types ($n \geq 3$)

W_3Fe_3C type, η-carbide, $E9_3$, $cF112$, (227) $Fd\bar{3}m$–*fedc*
filled-up derivative of NiCd and Ti_2Ni
Zr_3V_3O, $T_c = 7.5$ K, PN
$a = 12.1703$ Å, $Z = 16$ (Rotella *et al.*, 1983; Matthias *et al.*, 1963)

Atom	WP	x	y	z[a]
Zr	48(*f*)	0.43541	$\frac{1}{8}$	$\frac{1}{8}$
V(1)	32(*e*)	0.2078	0.2078	0.2078
V(2)	16(*c*)	0	0	0
O	16(*d*)	$\frac{1}{2}$	$\frac{1}{2}$	$\frac{1}{2}$

[a]Origin at center ($\bar{3}m$).

Compound	a(Å)	T_c(K)	Ref.
Ti_2Co	11.30	3.44	1
$Ti_{0.573}Rh_{0.287}O_{0.14}$	11.588	3.37	1
$Ti_{0.573}Ir_{0.287}O_{0.14}$	11.620	5.5	1
Zr_3V_3O	12.160	7.5	1, 2*
$Zr_{0.61}Rh_{0.285}O_{0.105}$	12.408	**11.8**	1
$Zr_{0.65}Ir_{0.265}O_{0.085}$	12.430	2.30	1
$Zr_{0.61}Pd_{0.285}O_{0.105}$	12.470	2.09	1

References: 1, Matthias *et al.* (1963); 2, Rotella *et al.* (1983).

Hf_5Sn_3Cu type, Nowotny phase, $hP18$, (193) $P6_3/mcm$–g^2db
filled-up derivative of Mn_5Si_3, $D8_8$
$Mo_{4.8}Si_3C_{0.6}$, $T_c = 7.6$ K, PN, $R_B = 0.04$
$a = 7.286$, $c = 5.046$ Å, $Z = 2$ (Parthé *et al.* 1965; Sadagapan and Gatos, 1966)

Atom	WP	x	y	z	Occ.
Mo(1)	6(*g*)	0.240	0	$\frac{1}{4}$	
Mo(2)	4(*d*)	$\frac{1}{3}$	$\frac{2}{3}$	0	0.9
Si	6(*g*)	0.60	0	$\frac{1}{4}$	
C	2(*b*)	0	0	0	0.6

Compound	a(Å)	c(Å)	T_c(K)	Ref.
Zr_5Ga_3	8.020	5.678	3.8	1, 2
$Mo_{4.8}Si_3C_{0.6}$	7.286	5.046	7.6	3*, 4
$Nb_{0.51}Ir_{0.30}O_{0.19}$[a]	7.869	5.094	**11.0**	5

[a]Nominal composition of sample.
References: 1, Boller and Parthé (1963); 2, Chapnik (1985); 3, Parthé *et al.* (1965); 4, Sadagapan and Gatos (1966); 5, Horyn *et al.* (1978).

5. AB_4C_n Types ($n \geq 4$)

$CeCo_4B_4$ type, $tP18$, (137) $P4_2/nmc\text{-}g^2b$
$ErRh_4B_4$, $T_c = 8.55$ K, SX, $T = 290$ K, $R = 0.049$
$a = 5.292$, $c = 7.379$ Å, $Z = 2$, Fig. 6.19a (Watanabe *et al.*, 1984; Matthias *et al.*, 1977)

Atom	WP	x	y	z^a
Er	2(*b*)	$\frac{3}{4}$	$\frac{1}{4}$	$\frac{1}{4}$
Rh	8(*g*)	$\frac{1}{4}$	0.5011	0.3953
B	8(*g*)	$\frac{1}{4}$	0.0772	0.0971

[a]Origin at $\bar{1}$.

Compound[a]	a(Å)	c(Å)	T_c(K)	Ref.
$Sc_{0.65}Th_{0.35}Rh_4B_4$	5.317	7.422	8.74[b]	1, 2
YRh_4B_4	5.308	7.403	11.34	1*, 2, 3*
$NdRh_4B_4$	5.333	7.468	5.36	1, 2
$SmRh_4B_4$	5.312	7.430	2.51	1, 2, 3*
$GdRh_4B_4$	5.309	7.417	...	1
$TbRh_4B_4$	5.303	7.404	...	1
$DyRh_4B_4$	5.302	7.395	...	1
$DyRh_2Ir_2B_4$	...	...	4.64	4
$HoRh_4B_4$	5.293	7.379	...	1
$HoRh_2Ir_2B_4$	...	...	6.41	4
$ErRh_4B_4$	5.292	7.374	8.55	1, 5*, 2
$TmRh_4B_4$	5.287	7.359	9.86	1, 2
$LuRh_4B_4$	5.294	7.359	11.76	1, 2
$Lu_{0.75}Th_{0.25}Rh_4B_4$	...	...	**11.93**	2
$ThRh_4B_4$	5.356	7.538	4.34	1, 2, 3*
$Y_{0.5}Lu_{0.5}Ir_4B_4$	5.408	7.280	3.21	4
$Ho_{1.1}Ir_4B_{3.6}$	...	...	2.12	4
$ErIr_4B_4$	5.408	7.278	2.34	4
$TmIr_4B_4$	5.404	7.281	1.75	4

[a]Data for RCo_4B_4 (R = Y, Ce, Gd–Tm, Lu) reported in Kuz'ma and Bilonizhko (1972*).
[b]For composition $Sc_{0.75}Th_{0.25}Rh_4B_4$.
References: 1, Vandenberg and Matthias (1977); 2, Matthias *et al.* (1977); 3, Yvon and Grüttner (1980); 4, Ku *et al.* (1979b); 5, Watanabe *et al.* (1984).

$LuRh_4B_4$ type, *oS*108, (68) *Ccca*–i^6fa
$LuRh_4B_4$, $T_c = 6.2$ K, SX, $R = 0.05$
$a = 7.410$, $b = 22.26$, $c = 7.440$ Å, $Z = 12$, Fig. 6.19c (Yvon and Johnston, 1982; Johnston and Braun, 1982)

Atom	WP	x	y	z^a
Lu(1)	8(*f*)	0	0.5824	$\frac{1}{4}$
Lu(2)	4(*a*)	0	$\frac{1}{4}$	$\frac{1}{4}$
Rh(1)	16(*i*)	0.1180	0.0417	0.0955
Rh(2)	16(*i*)	0.1530	0.1245	0.3670
Rh(3)	16(*i*)	0.3531	0.2065	0.1272
B(1)	16(*i*)	0.13	0.147	0.07
B(2)	16(*i*)	0.19	0.023	0.40
B(3)	16(*i*)	0.36	0.318	0.09

[a]Origin at $\bar{1}$.

Compound	a(Å)	b(Å)	c(Å)	T_c(K)	Ref.
$ErRh_4B_4$	7.444	22.30	7.465	4.3	1, 2
$TmRh_4B_4$	7.432	22.28	7.455	5.4	1, 2
$YbRh_4B_4$	7.424	22.26	7.458	n.o.	1, 2
$LuRh_4B_4$	7.410	22.26	7.440	**6.2**	1*, 2

References: 1, Yvon and Johnston (1982); 2, Johnston and Braun (1982).

$LuRu_4B_4$ type, *tI*72, (142) $I4_1/acd$–g^2b
$LuRu_4B_4$, $T_c = 2.06$ K, PX, $R_B = 0.065$
$a = 7.419$, $c = 14.955$ Å, $Z = 8$, Fig. 6.19b (Johnston, 1977; Ku *et al.*, 1979a)

Atom	WP	x	y	z^a
Lu	8(*b*)	0	$\frac{1}{4}$	$\frac{1}{8}$
Ru	32(*g*)	0.350	0.138	0.1875
B	32(*g*)	0.139	0.068	0.289

[a]Origin at $\bar{1}$.

Compound[a]	a(Å)	c(Å)	T_c(K)	Ref.
$ScRu_4B_4$	7.346	14.895	7.23	1
YRu_4B_4	7.454	14.994	1.4	2, 1, 3*
$LuRu_4B_4$	7.419	14.955	2.06	2*, 1
$ThRu_4B_4$	7.540	15.143	<1.5	2
URu_4B_4	7.459	14.986	...	4*
UOs_4B_4	7.512	15.053	...	4
YRh_4B_4	...	...	**10**	2
$Y(Rh_{0.85}Ru_{0.15})_4B_4$	7.484	14.895	9.56	2, 5*, 3*
$Pr(Rh_{0.85}Ru_{0.15})_4B_4$	7.543	14.995	2.41	2

(*continued*)

$Nd(Rh_{0.85}Ru_{0.15})_4B_4$	7.537	14.969	<1.5	2
$Sm(Rh_{0.85}Ru_{0.15})_4B_4$	7.516	14.945	<1.5	2
$Eu(Rh_{0.85}Ru_{0.15})_4B_4$	7.505	14.932	2.0	2
$Gd(Rh_{0.85}Ru_{0.15})_4B_4$	7.502	14.916	<1.5	2
$Tb(Rh_{0.85}Ru_{0.15})_4B_4$	7.490	14.898	<1.5	2
$Dy(Rh_{0.85}Ru_{0.15})_4B_4$	7.479	14.885	4.08	2
$Ho(Rh_{0.85}Ru_{0.15})_4B_4$	7.476	14.872	6.45	2
$ErRh_4B_4$	7.461	14.804	7.80	6*, 7
$Er(Rh_{0.85}Ru_{0.15})_4B_4$	7.468	14.862	8.02	2
$Tm(Rh_{0.85}Ru_{0.15})_4B_4$	7.458	14.853	8.38	2
$Yb(Rh_{0.85}Ru_{0.15})_4B_4$	7.449	14.851	<1.5	2
$Lu(Rh_{0.85}Ru_{0.15})_4B_4$	7.445	14.837	9.16	2

[a]Data for RRu_4B_4 (R = Ce–Nd, Sm–Yb; T_c < 1.5 K for R = Ce, Pr, Sm, Eu, Tm, Yb) reported in Johnston (1977).
References: 1, Ku *et al.* (1979a); 2, Johnston (1977); 3, Shelton *et al.* (1983); 4, Rogl (1980); 5, Yvon and Grüttner (1980); 6, Watanabe *et al.* (1986); 7, Iwasaki *et al.* (1986).

$LaFe_4P_{12}$ type, *cI*34, (204) $Im\bar{3}$–*gca*
filled-up derivative of $CoAs_3$, skutterudite, $D0_2$
$LaFe_4P_{12}$, T_c = 4.08 K, SX, R = 0.028
a = 7.8316 Å, Z = 2 (Jeitschko and Braun, 1977; Meisner, 1981)

Atom	WP	x	y	z
La	2(*a*)	0	0	0
Fe	8(*c*)	$\frac{1}{4}$	$\frac{1}{4}$	$\frac{1}{4}$
P	24(*g*)	0	0.1504	0.3539

Compound[a]	a(Å)	T_c(K)	Ref.
$LaFe_4P_{12}$	7.8316	4.08	1*, 2
$CeFe_4P_{12}$	7.7920	<0.35	1, 2
$PrFe_4P_{12}$	7.8149	<0.35	1, 2
$NdFe_4P_{12}$	7.8079	<1.0	1, 2
$SmFe_4P_{12}$	7.8029	...	1
$EuFe_4P_{12}$	7.8055	...	1
$LaRu_4P_{12}$	8.0561	**7.20**	1, 2
$CeRu_4P_{12}$	8.0376	<0.35	1, 2
$PrRu_4P_{12}$	8.0420	<0.35	1, 2
$NdRu_4P_{12}$	8.0364	<1.0	1, 2
$EuRu_4P_{12}$	8.0406	...	1

[a]Data for ROs_4P_{12} (R = La, Ce–Nd) reported in Jeitschko and Braun (1977).
References: 1, Jeitschko and Braun (1977); 2, Meisner (1981).

6. $A_xB_6C_8$ Types

LT-$BaMo_6S_8$ type, Chevrel phase, $aP15$, (2) $P\bar{1}$–i^7a
$BaMo_6S_8$, SX, $T = 173$ K, $R = 0.070$
$a = 6.5896$, $b = 6.6500$, $c = 6.6899$ Å, $\alpha = 88.731$, $\beta = 88.818$, $\gamma = 88.059°$, $Z = 1$ (Kubel and Yvon, 1990)

Atom	WP	x	y	z
Ba	1(a)	0	0	0
Mo(1)	2(i)	0.23750	0.56443	0.41916
Mo(2)	2(i)	0.41765	0.23305	0.56528
Mo(3)	2(i)	0.56678	0.41669	0.23264
S(1)	2(i)	0.1240	0.3924	0.7369
S(2)	2(i)	0.2556	0.2469	0.2524
S(3)	2(i)	0.3915	0.7359	0.1247
S(4)	2(i)	0.7376	0.1224	0.3878

For a list of triclinic Chevrel phases, see LT-$Ni_{0.66}Mo_6Se_8$.
For superconducting transition temperatures of Chevrel phases, see HT-$Pb_{0.9}Mo_6S_8$.

HT-$Ni_{2.5}Mo_6S_8$ type, Chevrel phase, $hR78$, (148) $R\bar{3}$–f^4c
$Cu_{2.76}Mo_6S_8$, $T_c = 10.9$ K[a], SX, $R = 0.03$
$a = 9.713$, $c = 10.213$ Å, $Z = 3$ (Yvon *et al.*, 1977; Flükiger *et al.*, 1977)

Atom	WP	x	y	z	Occ.
Cu(1)	18(f)	0.15378	0.05862	0.00161	0.24
Cu(2)	18(f)	0.23611	0.14694	0.10334	0.22
Mo	18(f)	0.15080	0.16564	0.39103	
S(1)	18(f)	0.05620	0.35913	0.07637	
S(2)	6(c)	0	0	0.20195	

[a]For sample containing two LT modifications.
For a list of rhombohedral Chevrel phases and superconducting transition temperatures, see HT-$Pb_{0.9}Mo_6S_8$.

LT-$Ni_{0.66}Mo_6Se_8$ type, Chevrel phase, $aP16$, (2) $P\bar{1}$–i^8
$Cu_{1.84}Mo_6S_8$, $T_c = 10.8$ K, SX, $T = 250$ K, $R = 0.08$
$a = 6.479$, $b = 6.559$, $c = 6.569$ Å, $\alpha = 96.89$, $\beta = 95.74$, $\gamma = 93.44°$, $Z = 1$ (Yvon *et al.*, 1979; Flükiger *et al.*, 1977)

Atom	WP	x	y	z	Occ.
Cu	2(i)	0.3407	0.0912	0.0576	0.92
Mo(1)	2(i)	0.0442	0.4013	0.2194	
Mo(2)	2(i)	0.0943	0.7792	0.4629	
Mo(3)	2(i)	0.2796	0.4567	0.5936	
S(1)	2(i)	0.1266	0.2845	0.8595	
S(2)	2(i)	0.2282	0.1261	0.3828	
S(3)	2(i)	0.3627	0.6186	0.2826	
S(4)	2(i)	0.7044	0.1995	0.1958	

(*continued*)

Compound	T(K)	Wyckoff sequence	a(Å) α(°)	b(Å) β(°)	c(Å) γ(°)	Ref.
$CaMo_6S_8$	27		6.4912 89.461	6.4977 89.555	6.5060 88.393	1
$SrMo_6S_8$	20	i^7a	6.481 89.246	6.572 89.304	6.611 88.169	2*
$BaMo_6S_8$	19	i^7a	6.6976 87.929	6.6545 88.978	6.5685 88.887	3*, 4*
$EuMo_6S_8$	40	i^7a	6.4692 89.179	6.5651 89.184	6.5986 88.009	4*
$Cr_{1.73}Mo_6S_8$	RT	i^8	6.522 94.68	6.497 90.70	6.449 97.91	5*
$Fe_2Mo_6S_8$	RT	i^8	6.502 95.94	6.466 97.37	6.481 91.33	6*
$Cu_{1.84}Mo_6S_8$[a]	250	i^8	6.479 96.89	6.569 93.44	6.559 95.74	7*
$AgMo_6S_8$	140	i^7a	6.4592 91.77	6.4469 91.57	6.4590 91.72	8*
$InMo_6S_8$	100		6.492 93.55	6.534 91.34	6.500 94.40	9
$PbMo_6S_8$	10		6.5759 88.516	6.5383 89.604	6.4948 89.298	10
$Li_4Mo_6Se_8$[b]	RT		6.908 95.828	6.938 91.645	6.980 96.794	11
$Ti_{1.2}Mo_6Se_8$	RT		6.69 91.22	6.79 98.52	6.76 94.21	12
$V_{1.2}Mo_6Se_8$	RT		6.73 91.56	6.75 98.12	6.69 94.29	12
$Cr_{1.2}Mo_6Se_8$	RT		6.75 92.20	6.75 98.02	6.70 94.17	12
$Mn_{1.2}Mo_6Se_8$	RT		6.82 92.21	6.67 97.01	6.74 91.57	12
$Fe_{1.2}Mo_6Se_8$	RT		6.80 91.08	6.66 96.03	6.66 93.19	12
$Ni_{0.66}Mo_6Se_8$[c]	RT	i^8	6.727 90.61	6.582 92.17	6.751 90.98	13*
$Ni_{0.85}Mo_6Te_8$	RT	i^8	7.028 91.23	7.100 95.73	7.102 90.82	14*

[a]Homogeneity range $Cu_xMo_6S_8$, $1.75 \leq x \leq 1.85$ ($9.9 \leq T_c \leq 11.0$ K), two other LT modifications (unknown structure) were observed for $x = 1.2$ ($T_c = 5.6$ K) and $3.1 \leq x \leq 3.3$ ($6.4 \leq T_c \leq 4.0$ K); two LT modifications (unknown structures) are reported for $Cu_xMo_6Se_8$ at $x \sim 1.7$ ($T_c = 5.7$) and $x \sim 2.5$ ($T_c = 2.0$ K) (Flükiger and Baillif, 1982).

[b]Homogeneity range $Li_xMo_6Se_8$, $3.6 < x \leq 4$ at room temperature, a second triclinic single-phase region was observed for $2.5 < x < 2.6$; $Li_xMo_6S_8$ is reported to be triclinic for $x > 3.95$ at rooom temperature (McKinnon and Dahn, 1985).

[c]Homogeneity range $Ni_xMo_6Se_8$, $0.6 < x < 1.2$ (Sergent and Chevrel, 1973).

References: 1, Kubel and Yvon (1989); 2, Koppelhuber-Bitschnau *et al.* (1990); 3, Jorgensen and Hinks (1986); 4, Kubel and Yvon (1990); 5, Harbrecht and Mahne (1992); 6, Yvon *et al.* (1980); 7, Yvon *et al.* (1979); 8, Shamrai *et al.* (1990); 9, Tarascon *et al.* (1984b); 10, Jorgensen *et al.* (1987); 11, Dahn *et al.* (1985); 12, Sergent and Chevrel (1973); 13, Bars *et al.* (1973b); 14, Hönle and Yvon (1987).

For superconducting transition temperatures of Chevrel phases see HT-$Pb_{0.9}Mo_6S_8$.

HT-$Pb_{0.9}Mo_6S_8$ type, Chevrel phase, *hR*45, (148) $R\bar{3}$-f^2ca
$Pb_{0.92}Mo_6S_8$, $T_c = 15.2\,K^a$, SX, $R = 0.057$
$a = 9.212$, $c = 11.437$ Å, $Z = 3$, Fig. 6.25 (Guillevic *et al.*, 1976b; Marezio *et al.*, 1973)

Atom	WP	x	y	z	Occ.
Pb	3(*a*)	0	0	0	0.92
Mo	18(*f*)	0.16015	0.17456	0.40182	
S(1)	18(*f*)	0.04182	0.34136	0.08347	
S(2)	6(*c*)	0	0	0.24363	

[a]Highest reported value.

For a structure with off-centered cations, see HT-$Ni_{2.5}Mo_6S_8$.
For structures of triclinic Chevrel phases, see LT-$BaMo_6S_8$ and LT-$Ni_{0.66}Mo_6Se_8$.

Compound	Wyckoff sequence	a(Å)	c(Å)	T_c(K)	Ref.
$LiMo_6S_8$[a]	f^3c	9.308	10.757	5.5	1, 2*, 3*
$NaMo_6S_8$		9.231	11.321	8.6[b]	4, 5
KMo_6S_8		9.24	11.57	...	6
$MgMo_6S_7$		9.490	10.550	3.5	7, 8
$CaMo_6S_8$	f^2ca	9.1832	11.3561	6[c]	9*, 10
$SrMo_6S_8$	f^2ca	9.2000	11.5645	...[d]	11*, 12*
$BaMo_6S_8$	f^2ca	9.2881	11.8004	...[e]	12*, 13*
$ScMo_6S_8$		...	...	3.6	8
$Y_{1.2}Mo_6S_8$		9.08	11.25	2.10[f]	14
$LaMo_6S_8$	f^2ca	9.120	11.554	6.95	15*, 14
$CeMo_6S_8$		9.10	11.45	<1.1	14
$PrMo_6S_8$		9.10	11.44	2.55	14
$NdMo_6S_8$		9.10	11.42	3.5	14
$Sm_{1.2}Mo_6S_8$		9.09	11.37	2.4	14
$EuMo_6S_8$	f^2ca	9.1801	11.5635	<1.1[g]	12*, 16*, 14
$GdMo_6S_8$	f^2ca	9.071	11.349	1.4	15*, 14
$Tb_{1.2}Mo_6S_8$		9.09	11.30	1.4	14
$Dy_{1.2}Mo_6S_8$		9.09	11.27	1.7	14
$HoMo_6S_8$	f^2ca	9.0674	11.2933	1.91	17*, 15*
$ErMo_6S_8$	f^2ca	9.071	11.271	<1.1	15*, 14
$Tm_{1.2}Mo_6S_8$		9.10	11.20	1.95	14
$YbMo_6S_8$	f^2ca	9.1509	11.3917	8.6	18*, 14
$Lu_{1.2}Mo_6S_8$		9.08	11.15	1.95	14
$Th_{1.2}Mo_6S_8$		9.05	11.37	n.o.	19
$U_{1.2}Mo_6S_8$		9.05	11.32	n.o.	19
$NbMo_6S_8$		9.08	11.34	n.o.	20
$MnMo_6S_7$		9.480	10.522	...	7
$Fe_{1.32}Mo_6S_8$	f^4c	9.563	10.273	...	21*
$Co_{1.60}Mo_6S_8$	f^4c	9.581	10.143	...	21*
$Ni_{1.40}Mo_6S_8$	f^4c	9.478	10.210	...	21*
$Pd_{1.6}Mo_6S_8$		9.30	10.68	...	5
$Cu_{1.73}Mo_6S_8$	f^4c	9.524	10.336	10.9[h]	22*, 8
$Cu_{3.66}Mo_6S_8$	f^4c	9.773	10.255	6.4	23*, 5
$AgMo_6S_8$	f^2ca	9.308	10.873	9.5	24*
$Zn_2Mo_6S_8$		9.533	10.282	3.6	25
$CdMo_5S_8$		9.440	10.720	3.5	7, 8

(*continued*)

$Hg_{0.9}Mo_6S_8$		9.406	10.759	8.1	27
$Al_3Mo_6S_8$		9.68	10.02	n.o.	20
$Ga_2Mo_6S_8$		9.60	10.12	n.o.	20
$InMo_6S_8$	f^3c	9.464	10.697	<0.6	27, 28*
$TlMo_6S_8$		9.17	11.689	8.7	27
$Sn_{0.9}Mo_6S_8$		9.150	11.421	14	1
$PbMo_6S_8$	f^2ca	9.183	11.497	**15.2**	1, 28*, 29*
$SbMo_6S_8$		9.122	11.282	<2	30
$BiMo_6S_8$		9.194	11.325	<2	30
$LiMo_6Se_8$[i]		9.69	11.194	3.9	1
$NaMo_6Se_8$		9.566	11.722	...	25
$Ca_{1.2}Mo_6Se_8$		9.50	11.83	...	5
$Sr_{1.2}Mo_6Se_8$		9.51	12.07	...	5
YMo_6Se_8		9.44	11.72	6.21	31
$LaMo_6Se_8$	f^2ca	9.49	12.00	11.39	31, 15*
$CeMo_6Se_8$		9.46	11.98	<1.1	31
$PrMo_6Se_8$		9.45	11.96	9.16	31
$NdMo_6Se_8$		9.44	11.95	8.22	31
$Sm_{1.2}Mo_6Se_8$		9.42	11.85	6.83	31
$Eu_{1.2}Mo_6Se_8$		9.51	12.04	<1.1	31
$Gd_{1.2}Mo_6Se_8$		9.43	11.84	5.59	31
$Tb_{1.2}Mo_6Se_8$		9.43	11.83	5.70	31
$Dy_{1.2}Mo_6Se_8$		9.43	11.82	5.77	31
$Ho_{1.2}Mo_6Se_8$		9.44	11.77	6.10	31
$Er_{1.2}Mo_6Se_8$		9.44	11.75	6.17	31
$Tm_{1.2}Mo_6Se_8$		9.43	11.71	6.33	31
$YbMo_6Se_8$		9.47	11.94	5.80	31
$Lu_{1.2}Mo_6Se_8$		9.44	11.62	6.20	31
$NpMo_6Se_8$		9.449	11.907	5.6	32
$PuMo_6Se_8$		9.476	11.908	<2.5	32
$AmMo_6Se_8$		9.449	11.906	<3.5	32
$Co_{1.4}Mo_6Se_8$		9.70[j]	11.07[j]	...	33
$Ni_{1.6}Mo_6Se_8$		9.66[j]	11.30[j]	...	33
$Cu_2Mo_6Se_8$	f^4c	9.981	10.741	5.9	15*, 5
$Ag_{1.2}Mo_6Se_8$	f^4c	9.65	11.30	5.9	34, 5, 15*
$Zn_2Mo_6Se_8$		10.053	10.824	...	25
$Cd_2Mo_6Se_8$		10.250	10.840	...	25
$InMo_6Se_8$	f^2ca	9.585	11.782	8.1	27, 35*
$TlMo_6Se_8$		9.526	12.177	12.2	27
$Sn_{0.8}Mo_6Se_8$	f^2ca	9.492	11.887	4.2	1, 15*
$Pb_{0.9}Mo_6Se_8$	f^2ca	9.525	11.956	4.12	1, 29*
$Li_{3.5}Mo_6Te_8$		10.204	11.681	...	36
$Fe_2Mo_6Te_8$		10.24	11.57	...	28
$Co_{0.66}Mo_6Te_8$		10.18	11.58	...	28
$Ni_{0.85}Mo_6Te_8$		10.457	11.866[k]	...	37

[a]Wyckoff sequence f^4c reported for $Li_{3.3}Mo_6S_8$ and $Li_4Mo_6S_8$.
[b]For nominal composition $Na_2Mo_6S_8$.
[c]$T_c = 9.5$ K reported for $Ca_{0.94}Mo_6S_8$ (Geantet *et al.*, 1987).
[d]Becomes superconducting above 1.1 GPa.
[e]$T_c = 14$ K obtained at 2.5 GPa (Jorgensen *et al.*, 1987).
[f]$T_c = 3.0$ reported in Marezio *et al.* (1973).

(*continued*)

[g]T_c = 11.8 K obtained at high pressure (Jorgensen *et al.*, 1987).
[h]T_c = 11.8 K reported for $Cu_2Mo_6S_8$ at 0.5 GPa (Shelton *et al.*, 1975).
[i]Wyckoff sequence f^4c reported for $Li_{3.2}Mo_6Se_8$ (Cava *et al.*, 1984*).
[j]Value taken from figure.
[k]At 1073 K.

References: 1, Tarascon *et al.* (1984a); 2, Ritter *et al.* (1992); 3, Cava *et al.* (1984); 4, Gocke *et al.* (1987); 5, Fischer (1978); 6, Potel *et al.* (1979); 7, Chevrel *et al.* (1971); 8, Marezio *et al.* (1973); 9, Kubel and Yvon (1988); 10, Geantet *et al.* (1987); 11, Koppelhuber-Bitschnau *et al.* (1990); 12, Kubel and Yvon (1987); 13, Jorgensen and Hinks (1986); 14, Fischer *et al.* (1993); 15, Yvon (1979); 16, Peña *et al.* (1986); 17, Peña *et al.* (1985); 18, Peña *et al.* (1984); 19, Sergent *et al.* (1978); 20, Umarji *et al.* (1980); 21, Guillevic *et al.* (1976a); 22, Shamrai *et al.* (1987); 23, Yvon *et al.* (1977); 24, Shamrai *et al.* (1990); 25, Gocke *et al.* (1987); 26, Tarascon *et al.* (1983); 27, Tarascon *et al.* (1984b); 28, Chevrel and Sergent (1982); 29, Guillevic *et al.* (1976b); 30, Chevreau and Johnson (1986); 31, Shelton *et al.* (1976); 32, de Novion *et al.* (1981b); 33, Sergent and Chevrel (1973); 34, Sergent and Chevrel (1972); 35, Lipka and Yvon (1980); 36, Mironov *et al.* (1987); 37, Hönle and Yvon (1987).

7. $A_2B_mC_n$ Types ($m, n \geq 2$)

$U_2Co_3Si_5$ type, *oI*40, (72) *Ibam*-j^3gba
$La_2Rh_3Si_5$, T_c = 4.4 K, SX, R = 0.029
a = 9.944, b = 11.886, c = 5.855 Å, Z = 4 (Venturini *et al.*, 1989; Chevalier *et al.*, 1982b)

Atom	WP	x	y	z
La	8(j)	0.2660	0.3691	0
Rh(1)	8(j)	0.1067	0.1381	0
Rh(2)	4(b)	$\frac{1}{2}$	0	$\frac{1}{4}$
Si(1)	8(j)	0.3478	0.1063	0
Si(2)	8(g)	0	0.2755	$\frac{1}{4}$
Si(3)	4(a)	0	0	$\frac{1}{4}$

Compound[a]	a(Å)	b(Å)	c(Å)	T_c(K)	Ref.
$Y_2Rh_3Si_5$	9.78	11.69	5.672	2.7	1
$La_2Rh_3Si_5$	9.90	11.84	5.828	**4.4**	1, 2*
$Dy_2Rh_3Si_5$	9.80	11.67	5.685	n.o.	1*
$Y_2Ir_3Si_5$	9.877	11.693	5.714	3.05	3

[a]Data for $R_2Rh_3Si_5$ (R = Nd, Sm, Gd–Er; superconductivity not observed) reported in Chevalier *et al.* (1982b).
References: 1, Chevalier *et al.* (1982b); 2, Venturini *et al.* (1989); 3, Hirjak *et al.* (1985).

$U_2Mn_3Si_5$ type, *tP*40, (128) *P*4/*mnc*-h^3ged
$Lu_2Fe_3Si_5$, T_c = 6.1 K, SX, R = 0.054
a = 10.346, c = 5.3875 Å, Z = 4 (Chabot, 1984; Braun, 1980)

Atom	WP	x	y	z
Lu	8(h)	0.2625	0.4306	0
Fe(1)	8(h)	0.1428	0.1228	0
Fe(2)	4(d)	0	$\frac{1}{2}$	$\frac{1}{4}$

(*continued*)

Si(1)	8(*h*)	0.0231	0.3188	0
Si(2)	8(*g*)	0.1786	0.6786	$\frac{1}{4}$
Si(3)	4(*e*)	0	0	0.249

Compound[a]	*a*(Å)	*c*(Å)	T_c(K)	Ref.
$Y_2Re_3Si_5$	10.88	5.533	1.76	1, 2
$Sc_2Fe_3Si_5$	10.225	5.275	4.52	3
$Y_2Fe_3Si_5$	10.43	5.47	2.4	3
$Tm_2Fe_3Si_5$	10.37[b]	5.42[b]	1.3	3, 2
$Lu_2Fe_3Si_5$	10.34	5.375	**6.1**	3, 4*

[a]Data for $R_2Fe_3Si_5$ (R = Sm, Gd–Er, Yb; superconductivity not observed) reported in Braun (1980).
[b]Value taken from figure.
References: 1, Bodak *et al.* (1978); 2, Johnston and Braun (1982); 3, Braun (1980); 4, Chabot (1984).

$Tl_2Fe_6Te_6$ type, *hP*14, (176) $P6_3/m$–h^2c
$Tl_2Mo_6Se_6$, $T_c = 5.84$ K, SX, $R = 0.049$
$a = 8.918$, $c = 4.482$ Å, $Z = 1$ (Hönle *et al.*, 1980; Armici *et al.*, 1980)

Atom	WP	*x*	*y*	*z*
Tl	2(*c*)	$\frac{1}{3}$	$\frac{2}{3}$	$\frac{1}{4}$
Mo	6(*h*)	0.1530	0.1857	$\frac{1}{4}$
Se	6(*h*)	0.3658	0.0656	$\frac{1}{4}$

Compound[a]	*a*(Å)	*c*(Å)	T_c(K)	Ref.
$K_2Mo_6S_6$	8.7203	4.4076	···	1*
$Rb_2Mo_6S_6$	8.9589	4.4114	···	1*
$Cs_2Mo_6S_6$	9.2698	4.4191	···	1*
Mo_6Se_6	8.35	4.44	< 1	2, 3
$In_2Mo_6Se_6$	8.835	4.492	< 1	4*, 3
$Tl_2Mo_6Se_6$	8.918	4.482	**5.84**[b]	4*, 5, 6*
$In_2Mo_6Te_6$	9.326	4.590	< 1	4*, 3
$Tl_2Mo_6Te_6$	9.428	4.583	< 1	4*, 3

[a]Data for $A_2Mo_6Se_6$ (A = Li, Na, K, Rb, Cs, Ba, Ag; $T_c < 1.2$ K, A = Ba not investigated) and $A_2Mo_6Te_6$ (A = Na, K, Rb, Cs, Ba; $T_c < 1.2$ K, A = Ba not investigated) reported in Chevrel *et al.* (1985); Tarascon *et al.* (1984c).
[b]Midpoint, for other samples $T_c = 2.6$–3.2 K; $T_c \approx 3$ K reported in Tarascon *et al.* (1984c).
References: 1, Huster *et al.* (1983); 2, Chevrel *et al.* (1985); 3, Tarascon *et al.* (1984c); 4, Hönle *et al.* (1980); 5, Armici *et al.* (1980); 6, Potel *et al.* (1980).

$La_5B_2C_6$ type, *tP*52, (75) $P4\text{–}d^{18}b^2a^2$
deformation derivative of $Ce_5B_2C_6$[a]
$La_5B_2C_6$, $T_c = 6.9$ K, SX, $R = 0.079$
$a = 8.585$, $c = 12.313$ Å, $Z = 4$ (Bauer and Bars, 1983; Bauer and Politis, 1982)

Atom	WP	x	y	z	Occ.
La(1)	4(*d*)	0.0996	0.2961	0.2333	
La(2)	4(*d*)	0.2042	0.4013	0.5090	
La(3)	4(*d*)	0.2991	0.0978	0.7227	
La(4)	4(*d*)	0.4022	0.2004	0.0220	
La(5)	1(*b*)	$\frac{1}{2}$	$\frac{1}{2}$	0.2715	
La(6)	1(*b*)	$\frac{1}{2}$	$\frac{1}{2}$	0.7623	
La(7)	1(*a*)	0	0	0.0000	
La(8)	1(*a*)	0	0	0.4932	
B(1)	4(*d*)	0.179	0.374	0.8715	
B(2)	4(*d*)	0.385	0.194	0.3315	
C(1)	4(*d*)	0.019	0.038	0.6825	0.25
C(2)	4(*d*)	0.019	0.038	0.7865	0.25
C(3)	4(*d*)	0.038	0.019	0.2045	0.25
C(4)	4(*d*)	0.038	0.019	0.2855	0.25
C(5)	4(*d*)	0.092	0.304	0.0365	
C(6)	4(*d*)	0.202	0.402	0.7085	
C(7)	4(*d*)	0.315	0.114	0.4785	
C(8)	4(*d*)	0.405	0.218	0.1715	
C(9)	4(*d*)	0.462	0.481	0.0585	0.25
C(10)	4(*d*)	0.462	0.481	0.9735	0.25
C(11)	4(*d*)	0.481	0.462	0.4755	0.25
C(12)	4(*d*)	0.481	0.462	0.5565	0.25

[a]Different number of split sites considered.

Compound	a(Å)	c(Å)	T_c(K)	Ref.
$La_5B_2C_6$	8.585	12.313	**6.9**	1*, 2
$Ce_5B_2C_6$	8.418	12.077	...	3*
$Ho_5B_2C_6$	7.981	11.561	...	4

References: 1, Bauer and Bars (1983); 2, Bauer and Politis (1982); 3, Bauer and Bars (1982); 4, Bauer *et al.* (1985).

8. $A_lB_mC_n$ Types (l, m, $n \geq 3$)

$La_3Rh_4Sn_{13}$ type, phase I′, *cI*320, (214) $I4_132\text{–}i^4h^2g^2eba$
$La_3Rh_4Sn_{13}$, $T_c = 3.2$ K, PX[a], $R_B = 0.0848$
$a = 19.4918$ Å, $Z = 16$ (Bordet *et al.*, 1991; Espinosa *et al.*, 1982)

Atom	WP	x	y	z
La(1)	24 (*h*)	$\frac{1}{8}$	0.2495	0.0005
La(2)	24 (*g*)	$\frac{1}{8}$	0.2495	0.4995
Rh(1)	24 (*h*)	$\frac{1}{8}$	0.625	0.625
Rh(2)	24 (*g*)	$\frac{1}{8}$	0.125	0.375

(*continued*)

Rh(3)	8 (*b*)	$\frac{7}{8}$	$\frac{7}{8}$	$\frac{7}{8}$
Rh(4)	8 (*a*)	$\frac{1}{8}$	$\frac{1}{8}$	$\frac{1}{8}$
Sn(1)	48 (*i*)	0.0003	0.1432	0.4257
Sn(2)	48 (*i*)	0.001	0.1532	0.0773
Sn(3)	48 (*i*)	0.0924	0.2497	0.329
Sn(4)	48 (*i*)	0.251	0.3281	0.4039
Sn(5)	16 (*e*)	0.0011	0.0011	0.0011

[a]Synchrotron radiation.

$Yb_3Rh_4Sn_{13}$ type[a], phase I, *cP*40, (223) $Pm\bar{3}n$–*keca*
$Yb_{2.80}Rh_4Sn_{13.20}$, $T_c = 8.6$ K, SX, $R = 0.015$
$a = 9.676$ Å, $Z = 2$, Fig. 6.15 (Hodeau *et al.*, 1980; Espinosa *et al.*, 1982)

Atom	WP	*x*	*y*	*z*
Yb[b]	6(*c*)	$\frac{1}{4}$	0	$\frac{1}{2}$
Rh	8(*e*)	$\frac{1}{4}$	$\frac{1}{4}$	$\frac{1}{4}$
Sn(1)	24(*k*)	0	0.15333	0.30570
Sn(2)[c]	2(*a*)	0	0	0

[a]Sometimes referred to as $Pr_3Rh_4Sn_{13}$ type, however, $Pr_3Rh_4Sn_{13}$ was later found to crystallize with phase I′ ($La_3Rh_4Sn_{13}$) type structure; splitting of site in Wyckoff position 24(*k*) reported for $Y_3Co_4Ge_{13}$ (Bruskov *et al.*, 1986).
[b]Yb = $Yb_{0.915}Sn_{0.085}$.
[c]Sn(2) = $Sn_{0.943}Yb_{0.057}$.

Compound	*a*(Å)	T_c(K)	Ref.
$Y_3Ru_4Ge_{13}$	8.962	1.7	1*
$Lu_3Rh_4Ge_{13}$	8.912[a]	2.3	1
$Y_3Os_4Ge_{13}$	8.985	3.9	1
$Lu_3Os_4Ge_{13}$	8.938[a]	3.6	1
$Ca_3Rh_4Ge_{13}$	9.025	2.1	2
$Ca_3Ir_4Ge_{13}$	9.055	1.7	2
$La_3Ru_4Sn_{13}$[b]	9.772	3.9	3
$La_3RuPd_3Sn_{13}$[c]	9.780	4.8	3
$Th_3Os_4Sn_{13}$	9.721	5.6	4
$Ca_3Co_4Sn_{13}$	9.584	5.9	4
$La_3Co_4Sn_{13}$	9.641	2.8	4
$Yb_3Co_4Sn_{13}$	9.563	2.5	4
$Ca_3Rh_4Sn_{13}$	9.702	**8.7**	4, 5*
$Sr_3Rh_4Sn_{13}$	9.800	4.3	4, 5*
$Yb_3Rh_4Sn_{13}$	9.675	8.6	4, 6*, 5*
$Th_3Rh_4Sn_{13}$	9.692	1.9	4, 5*
$Ca_3Ir_4Sn_{13}$	9.718	7.1	4,
$Sr_3Ir_4Sn_{13}$	9.807	5.1	4
$La_3Ir_4Sn_{13}$	9.755	2.6	4
$Th_3Ir_4Sn_{13}$	9.695	2.6	4
$La_3Rh_4Pb_{13}$	10.031	2.2	2

(*continued*)

[a]Value taken from figure.
[b]Composition $LaRu_{1.5}Sn_{4.5}$ from chemical analysis; structure with site Sn(2) occupied by La reported for $LaRuSn_3$ in Eisenmann and Schäfer (1986).
[c]Ru/Pd ratio from nominal composition; composition $LaRu_{1.1}Pd_{0.1}Sn_{4.3}$ from chemical analysis.
References: 1, Segre *et al.* (1981); 2, Venturini *et al.* (1986); 3, Espinosa *et al.* (1980); 4, Espinosa *et al.* (1982); 5, Miraglia *et al.* (1986); 6, Hodeau *et al.* (1980).

$Sc_5Co_4Si_{10}$ type, *tP*38, (127) $P4/mbm\text{-}ji^2h^2ga$
$Sc_5Co_4Si_{10}$, $T_c = 4.53$ K, SX, $R = 0.04$
$a = 12.01$, $c = 3.936$ Å, $Z = 2$ (Braun *et al.*, 1980; Yang *et al.*, 1986)

Atom	WP	x	y	z
Sc(1)	4(*h*)	0.1756	0.6756	$\frac{1}{2}$
Sc(2)	4(*h*)	0.6118	0.1118	$\frac{1}{2}$
Sc(3)	2(*a*)	0	0	0
Co	8(*i*)	0.2460	0.0240	0
Si(1)	8(*j*)	0.1638	0.0031	$\frac{1}{2}$
Si(2)	8(*i*)	0.1575	0.1985	0
Si(3)	4(*g*)	0.0679	0.5679	0

Compound[a]	a(Å)	c(Å)	T_c(K)	Ref.
$Sc_5Co_4Si_{10}$	12.01	3.936	4.53	1*, 2
$Sc_5Rh_4Si_{10}$	12.325	4.032	8.27	1, 2
$Sc_5Ir_4Si_{10}$	12.316	4.076	8.29	1, 2
$Y_5Ir_4Si_{10}$	12.599	4.234	3.10	2
$Lu_5Rh_4Si_{10}$	12.502	4.137	3.95	2
$Lu_5Ir_4Si_{10}$	12.475	4.171	3.91	2
$Y_5Os_4Ge_{10}$	13.006	4.297	**9.06**	1, 2
$Y_5Rh_4Ge_{10}$	12.953	4.272	1.35	2
$Y_5Ir_4Ge_{10}$	12.927	4.308	2.76	1, 2
$Lu_5Rh_4Ge_{10}$	12.850	4.208	2.79	2
$Lu_5Ir_4Ge_{10}$	12.831	4.252	2.60	2

[a]Data for $R_5Rh_4Si_{10}$ and $R_5Ir_4Ge_{10}$ (R = Gd–Yb; $T_c < 1.4$ K) reported in Venturini *et al.* (1984); $T_c = 9.7$ and 10.5 K reported for phases of approximate compositions $Y_4Os_4Si_{13}$ and $Y_5Os_4Si_{15}$ (unknown structures) in Gueramian *et al.* (1988).
References: 1, Braun *et al.* (1980); 2, Yang *et al.* (1986).

$Er_4Rh_6Sn_{19}$ type, phase II, *tI*232, (142) $I4_1/acd$–g^5f^2edb
$Er_{4.32}Rh_6Sn_{18.68}$, $T_c = 0.97$ K, SX, $R = 0.033$
$a = 13.73$, $c = 27.42$ Å, $Z = 8$ (Hodeau *et al.*, 1984)

Atom	WP	x	y	z^a
Er	32(*g*)	0.13343	0.11235	0.30658
Rh(1)	32(*g*)	0.25609	0.25120	0.1251
Rh(2)	16(*d*)	0	$\frac{1}{4}$	0.25255
Sn(1)	32(*g*)	0.0047	0.07420	0.03777
Sn(2)	32(*g*)	0.08725	0.16149	0.41909
Sn(3)	32(*g*)	0.17422	0.25919	0.03792
Sn(4)	16(*f*)	0.1765	0.4265	$\frac{1}{8}$
Sn(5)	16(*f*)	0.3266	0.5766	$\frac{1}{8}$
Sn(6)	16(*e*)	0.2889	0	$\frac{1}{4}$
Sn(7)[b]	8(*b*)	0	$\frac{1}{4}$	$\frac{1}{8}$

[a]Origin at $\bar{1}$.
[b]$Sn(7) = Sn_{0.68}Er_{0.32}$.

Compound[a]	a(Å)	c(Å)	T_c(K)	Ref.
$Er_4Ru_6Sn_{19}$	13.730	27.354	<1.1	1, 2
$Lu_4Ru_6Sn_{19}$	13.692	27.263	<1.1	1, 2
$Er_4Co_6Sn_{19}$	13.529	26.932	<1.1	1, 2
$Lu_4Co_6Sn_{19}$	...	...	1.5	2
$Sc_4Rh_6Sn_{19}$	13.565	27.034	**4.5**	1, 2
$Y_4Rh_6Sn_{19}$	13.772	27.456	3.2	1, 2
$Ho_4Rh_6Sn_{19}$	13.747	27.388	...	1
$Er_4Rh_6Sn_{19}$	13.725	27.365	1.2[b]	1, 2, 3*
$Tm_4Rh_6Sn_{19}$	13.706	27.320	2.3[b]	1, 2
$Lu_4Rh_6Sn_{19}$	13.693	27.289	4.0	1, 2
$Sc_4Ir_6Sn_{19}$	13.574	27.057	1.1	1, 2
$Er_4Ir_6Sn_{19}$	13.756	27.402	<1.1	1, 2
$Tm_4Ir_6Sn_{19}$	13.727	27.371	<1.1	1, 2
$Yb_4Ir_6Sn_{19}$	13.757	27.444	...	1
$Lu_4Ir_6Sn_{19}$	13.708	27.325	3.2	1, 2

[a]Idealized composition.
[b]Multiphase sample.
References: 1, Cooper (1980); 2, Espinosa *et al.* (1982); 3, Hodeau *et al.* (1984).

$Tb_4Rh_6Sn_{19}$ type, phase II′ (III), *cF*116, (225) $Fm\bar{3}m$–kf^2eca
$Tb_{4.6}Rh_6Sn_{18.4}$, SX, RT, $R = 0.082$[a]
$a = 13.772$ Å, $Z = 4$ (Miraglia *et al.*, 1987)

Atom	WP	x	y	z	Occ.
Tb(1)	32(f)	0.3629	0.3629	0.3629	0.5
Tb(2)[b]	4(a)	0	0	0	
Rh	24(e)	0.2553	0	0	
Sn(1)	96(k)	0.1745	0.1745	0.0131	0.5
Sn(2)	32(f)	0.4124	0.4124	0.4124	0.5
Sn(3)	8(c)	$\frac{1}{4}$	$\frac{1}{4}$	$\frac{1}{4}$	

[a]Refinement considering triple microtwinning of phase II gave $R = 0.074$; refinement in space group $F\bar{4}3m$ reported in Vandenberg (1980).
[b]Tb(2) = $Tb_{0.6}Sn_{0.4}$.

Compound[a]	a(Å)	T_c(K)	Ref.
$Sc_4Rh_6Ge_{19}$	12.605	1.9	1
$Sc_4Ir_6Ge_{19}$	12.629	1.4	1
$Y_4Ru_6Sn_{19}$[b]	13.772	1.3	2
$Sc_4Os_6Sn_{19}$	13.606	1.5	3
$Y_4Os_6Sn_{19}$	13.801	2.5	2
$Tb_4Os_6Sn_{19}$	13.813	1.4	3
$Ho_4Os_6Sn_{19}$	13.774	1.4	3
$Er_4Os_6Sn_{19}$	13.760	1.25	2
$Tm_4Os_6Sn_{19}$	13.744	1.1	3
$Lu_4Os_6Sn_{19}$	13.720	1.8	3
$Tb_4Rh_6Sn_{19}$	13.774	n.o.	3, 4*
$Y_4Ir_6Sn_{19}$	13.773	2.2	3
$Ca_4Rh_6Pb_{19}$	14.23	**3.3**	1

[a]Idealized composition.
[b]Composition $YRu_{1.1}Sn_{3.1}$ from chemical analysis.
References: 1, Venturini *et al.* (1986); 2, Espinosa *et al.* (1980); 3, Espinosa *et al.* (1982); 4, Miraglia *et al.* (1987).

d. Quaternary Structure Types

LuNiBC type, *tP*8, (129) $P4/nmm$–c^3a
LuNiBC, SX, $T = 296$ K, $R = 0.028$
$a = 3.4985$, $c = 7.7556$ Å, $Z = 2$, Fig. 6.21 (Siegrist *et al.*, 1994b)

Atom	WP	x	y	z[a]
Lu	2(*c*)	$\frac{1}{4}$	$\frac{1}{4}$	0.66202
Ni	2(*a*)	$\frac{3}{4}$	$\frac{1}{4}$	0
B	2(*c*)	$\frac{1}{4}$	$\frac{1}{4}$	0.1511
C	2(*c*)	$\frac{1}{4}$	$\frac{1}{4}$	0.3477

[a]Origin at center (2/*m*).

Compound	a(Å)	c(Å)	T_c(K)	Ref.
YNiBC	3.5660	7.5625	...[a]	1
HoNiBC	3.5631	7.5486[b]	n.o.	2*
LuNiBC	3.4985	7.7556	n.o.	3*
LaNiBN	3.725	7.590	<4.2	4, 5*

[a]$T_c = 3.0$ K reported for sample containing also YNi_2B_2C ($T_c = 11.0$ K) and $Y_3Ni_4B_4C_3$, $a = 3.55190$, $c = 25.6454$ Å (superconducting phase not identified).
[b]Magnetic structure at 2.1 K determined.
References: 1, Kitô *et al.* (1997); 2, Huang *et al.* (1996); 3, Siegrist *et al.* (1994b); 4, Cava *et al.* (1994f); 5, Zandbergen *et al.* (1994b).

$LuNi_2B_2C$ type, *tI*12, $I4/mmm$–$edba$
$LuNi_2B_2C$, $T_c = 16.6$ K, SX, $R = 0.025$
$a = 3.4639$, $c = 10.6313$ Å, $Z = 2$, Fig. 6.21 (Siegrist *et al.*, 1994a; Cava *et al.*, 1994e)

Atom	WP	x	y	z
Lu	2(*b*)	0	0	$\frac{1}{2}$
Ni	4(*d*)	0	$\frac{1}{2}$	$\frac{1}{4}$
B	4(*e*)	0	0	0.1382
C	2(*a*)	0	0	0

Compound[a]	a(Å)	c(Å)	T_c(K)	Ref.
$GdCo_2B_2C$	3.548	10.271	...	1
$LaRh_2B_2C$	3.9019	10.2460	<4.2	2*
$GdRh_{1.87}B_2C$	3.7491	10.4122	...	3*
$LaIr_2B_2C$	3.8965	10.454	<4.2	2*
$ScNi_2B_2C$	...	...	15.6	4
$Sc_{0.5}Lu_{0.5}Ni_2B_2C$	3.441	10.66	15.6	4

(*continued*)

YNi_2B_2C	3.533	10.566	15.6	2*, 5, 6*
$La_{0.5}Lu_{0.5}Ni_2B_2C$	3.577	10.44	14.8	4
$La_{0.5}Th_{0.5}Ni_2B_2C$	3.746	9.929	3.9	4
$HoNi_2B_2C$	3.527	10.560[b]	8.0	2*, 5, 7*
$ErNi_2B_2C$	3.509	10.582	10.5	2*, 5
$TmNi_2B_2C$	3.494	10.613	11.0	2*, 5
$YbNi_2B_2C$	3.483	10.633	...	2*
$LuNi_2B_2C$	3.472	10.658	16.6	2*, 5, 8*
$ThNi_2B_2C$	3.683	10.22	8.0	4
UNi_2B_2C	3.486	10.70	<2	4
YPd_2BC	3.75	10.7	**23.0**[c]	9, 10
$ThPd_2B_2C$	3.84	10.67	14.5[d]	11, 12
YPt_2B_2C	3.79	10.71	10	13
$YPt_{1.5}Au_{0.6}B_2C$	...	...	11	14
$LaPt_2B_2C$	3.8681	10.705	10	15*, 2*
$LaPt_{1.5}Au_{0.6}B_2C$	3.8729	10.7401	11	16, 14
$PrPt_2B_2C$	...	...	6	15
$PrPt_{1.5}Au_{0.6}B_2C$	3.8358	10.7442	6.5	16, 14
$ThPt_2B_2C$	3.83	10.86	6.5	11

[a]Data for RNi_2B_2C (R = La, Ce–Nd, Sm–Dy; $T_c < 4.2$ K) reported in Siegrist *et al.* (1994a*); Cava *et al.* (1994e); Gupta *et al.* (1995). Data for YT_2B_2C (T = Os, Co, Rh, Ir; $T_c < 4.2$ K) reported in Nagarajan *et al.* (1995). Data for LaT_2B_2C (T = Rh, Ir; $T_c < 1.4$ K) reported in Cava *et al.* (1994c*).
[b]Magnetic structure at 5.1 and 2.2 K reported in Huang *et al.* (1995b*); substitution of 0.75% of Ni by Co destroyed superconductivity, magnetic structure at 2 K reported in Huang *et al.* (1996*).
[c]T_c~23 K reported for multiphase samples of compositions $YPd_4BC_{0.2}$ or $YPd_5B_3C_{0.3}$, sometimes showing second signal at ~ 10 K (superconducting phase not identified with certainty) (Nagarajan *et al.*, 1994; Hossain *et al.*, 1994; Cava *et al.*, 1994d).
[d]Second signal at 21.5 K observed for sample of nominal composition $ThPd_3B_3C$ (superconducting phase not identified).
References: 1, Mulder *et al.* (1995); 2, Siegrist *et al.* (1994a); 3, Ye *et al.* (1996); 4, Lai *et al.* (1995); 5, Cava *et al.* (1994e); 6, Chakoumakos and Paranthaman (1994); 7, Huang *et al.* (1995b); 8, Siegrist *et al.* (1994b); 9, Zandbergen *et al.* (1994c); 10, Cava *et al.* (1994d); 11, Sarrao *et al.* (1994); 12, Zandbergen *et al.* (1994d); 13, Yang *et al.* (1995); 14, Buchgeister *et al.* (1995); 15, Cava *et al.* (1994b); 16, Cava *et al.* (1994a).

$La_3Ni_2B_2N_3$ type, *tI*20, (139) $I4/mmm$–e^3dba
$La_3Ni_2B_2N_{2.91}$, T_c = 13 K[a], PN, RT, R_{wp} = 0.0697
a = 3.72512, c = 20.5172 Å, Z = 2, Fig. 6.21 (Huang *et al.*, 1995a; Cava *et al.*, 1994f)[b]

Atom	WP	x	y	z	Occ.
La(1)	4(e)	0	0	0.3705	
La(2)	2(a)	0	0	0	
Ni	4(d)	0	$\frac{1}{2}$	$\frac{1}{4}$	
B	4(e)	0	0	0.1946	
N(1)	4(e)	0	0	0.1246	
N(2)	2(b)	0	0	$\frac{1}{2}$	0.91

[a]T_c varies from 12 to 13 K with nitrogen content.
[b]Alternative refinement in Zandbergen *et al.* (1994b) and Zandbergen and Cava (1995).

$Ce_9B_3C_6Br_5$ type, *oP*46, (59) $Pmmn$–$e^{10}b^2a$
$La_9B_3C_6Br_5$, $T_c = 6$ K, SX, $R = 0.053$
$a = 3.853$, $b = 33.19$, $c = 7.906$ Å, $Z = 2$ (Mattausch *et al.*, 1996)

Atom	WP	x	y	z^a
La(1)	4(*e*)	$\frac{1}{4}$	0.1946	0.0457
La(2)	4(*e*)	$\frac{1}{4}$	0.5093	0.8027
La(3)	4(*e*)	$\frac{1}{4}$	0.5959	0.0887
La(4)	4(*e*)	$\frac{1}{4}$	0.6330	0.6497
La(5)	2(*a*)	$\frac{1}{4}$	$\frac{1}{4}$	0.4536
B(1)	4(*e*)	$\frac{1}{4}$	0.079	0.144
B(2)	2(*b*)	$\frac{1}{4}$	$\frac{3}{4}$	0.774
C(1)	4(*e*)	$\frac{1}{4}$	0.0434	0.023
C(2)	4(*e*)	$\frac{1}{4}$	0.1253	0.137
C(3)	4(*e*)	$\frac{1}{4}$	0.7060	0.726
Br(1)	4(*e*)	$\frac{1}{4}$	0.1520	0.6724
Br(2)	4(*e*)	$\frac{1}{4}$	0.5481	0.4272
Br(3)	2(*b*)	$\frac{1}{4}$	$\frac{3}{4}$	0.2142

[a]Origin at $\bar{1}$.

Compound	a(Å)	b(Å)	c(Å)	T_c(K)	Ref.
$La_9B_3C_6Br_5$	3.853	33.19	7.906	**6**	1*
$Ce_9B_3C_6Br_5$	3.804	32.935	7.816	n.o.	1*
$La_9B_3C_6I_5$	3.9481	33.857	8.218	...	1

[a]Reference: 1, Mattausch *et al.* (1996).

e. Charge-Transfer Salts

Compound	Space group	a(Å) α(°)	b(Å) β(°)	c(Å) γ(°)	T_c(K)	Ref.
α-$(ET)_2I_3$	$P\bar{1}$	9.211 96.95	10.850 97.97	17.488 90.75	8	1*, 2
β-$(ET)_2AuI_2$	$P\bar{1}$	6.603 94.95	9.015 96.19	15.403 110.66	4.97	3*
β-$(ET)_2I_3$	$P\bar{1}$	6.615 94.38	9.100 95.59	15.286[a] 109.78	1.40	4*, 5*
β-$(ET)_2IBr_2$	$P\bar{1}$	6.593 93.79	8.975 94.97	15.093 110.54	2.7	6*
β^*-$(ET)_2I_3$	$P\bar{1}$	6.449 94.79	8.986 96.57	15.034[b] 111.29	8[c]	7*, 2
γ-$(ET)_3(I_3)_{2.5}$	$Pbnm$	13.76	14.73	33.61	2.5	8*
ε-$(ET)_2I_3(I_8)_{0.5}$	$P2_1/b$	13.974 67.3	17.40 90	18.77 90	2.5	9*

(*continued*)

θ-$(ET)_2I_3$[d]	*Pnma*	10.076	33.853	4.994[e]	3.6	10*
κ-$(ET)_2I_3$	$P2_1/c$	16.387	8.466	12.832	3.6	11*
		90	108.56	90		
κ-$(ET)_2Cu(NCS)_2$	$P2_1$	16.248	8.440	13.124	10.4	12*
		90	110.30	90		
κ-$(ET)_2Cu[N(CN)_2]Cl$	*Pnma*	12.977	29.979	8.480	**12.5**[f]	13, 14*
κ-$(ET)_2Cu[N(CN)_2]Br$	*Pnma*	12.942	30.016	8.539	12.5	15*, 14
κ-$(ET)_2Cu[N(CN)_2]CN$	mon.	15.987	8.647	12.887	10.7	16, 17
		90	110.88	90		
κ-$(ET)_2Ag(CN)_2(H_2O)$	$P2_1$	12.593	8.642	16.080	5.0	18*, 2
		90	109.33	90		
$(ET)_4Hg_3Cl_8$	$I2/c$	11.062	8.754	35.92[g]	5.3[h]	19*, 2
		90	91.01	90		
$(ET)_4Hg_{2.89}Br_8$	$I2/c$	11.219	8.706	37.105[g]	4.3[i]	20*
		90	90.97	90		
λ-$(Se\text{-}ET)_2GaCl_4$	$P\bar{1}$	16.156	18.934	6.595	9.5	21, 22*
		96.06	96.76	115.77		
κ-$(MDT\text{-}TTF)_2AuI_2$	*Pbnm*	10.797	7.789	28.991	4.5	23*, 2

[a]Transforms to an incommensurate modulated structure at 175 K at ambient pressure (Williams *et al.*, 1992).
[b]At 4.5 K and 0.15 GPa.
[c]At 0.05 GPa.
[d]Trace amounts of AuI_2^- anions.
[e]Average structure, superstructure reported in space group $P2_1/c$, $a = 9.928$, $b = 10.076$, $c = 34.220$ Å, $\beta = 98.39°$ Kobayashi *et al.*, 1986a).
[f]At 0.03 GPa.
[g]Incommensurate composite structure, data given here describe ET–halogen substructure.
[h]At 2.9 GPa.
[i]$T_c = 6.7$ at 0.35 GPa (Williams *et al.*, 1992).
References: 1, Bender *et al.* (1984); 2, Williams *et al.* (1992); 3, Wang *et al.* (1985); 4, Williams *et al.* (1984a); 5, Shibaeva *et al.* (1984); 6, Williams *et al.* (1984b); 7, Schultz *et al.* (1986b); 8, Shibaeva *et al.* (1985); 9, Shibaeva *et al.* (1986); 10, Kobayashi *et al.* (1986b); 11, Kobayashi *et al.* (1987); 12, Urayama *et al.* (1988); 13, Williams *et al.* (1990b); 14, Williams *et al.* (1990a); 15, Kini *et al.* (1990); 16, Komatsu *et al.* (1991); 17, Mori (1994); 18, Kurmoo *et al.* (1988); 19, Shibaeva and Rozenberg (1988); 20, Lyubovskaya *et al.* (1987); 21, Kobayashi *et al.* (1993a); 22, Kobayashi *et al.* (1993b); 23, Papavassiliou *et al.* (1988).

References

K. Ahn, Hj. Mattausch, and A. Simon, *Z. anorg. allg. Chem.* **623**, 619–622 (1997).
N. E. Alekseevskii, *Sov. Phys. JETP* **22**, 114–116 (1966).
N. E. Alekseevskii and N. N. Mikhailov, *Sov. Phys. JETP* **16**, 1493–1495 (1963).
N. E. Alekseevskii and V. M. Zakosarenko, *Sov. Phys. Doklady* **18**, 45–47 (1973).
N. E. Alekseevskii, G. V. Samsonov, and O. I. Shulishova, *Sov. Phys. JETP* **17**, 950–952 (1963).
N. Ye. Alekseyevskiy, O. A. Balakhovskiy, and I. V. Kirillov, *Phys. Met. Metall.* **40**, 1, 38–42 (1975).
J. C. Armici, M. Decroux, Ø. Fischer, M. Potel, R. Chevrel, and M. Sergent, *Solid State Commun.* **33**, 607–611 (1980).

G. Arrhenius, E. Corenzwit, R. Fitzgerald, G. W. Hull, Jr., H. L. Luo, B. T. Matthias, and W. H. Zachariasen, *Proc. Natl. Acad. Sci. USA* **61**, 621–628 (1968).
M. Atoji, *J. Chem. Phys.* **35**, 1950–1960 (1961).
M. Atoji, *J. Solid State Chem.* **26**, 51–57 (1978).
M. Atoji and Y. Tsunoda, *J. Chem. Phys.* **54**, 3510–3513 (1971).
M. Atoji and D. E. Williams, *J. Chem. Phys.* **35**, 1960–1966 (1961).
M. Atoji, K. Gschneidner, Jr., A. H. Daane, R. E. Rundle, and F. H. Spedding, *J. Am. Chem. Soc.* **80**, 1804–1808 (1958).
A. E. Austin, *Acta Crystallogr.* **12**, 159–161 (1959).
M. Bäcker, A. Simon, R. K. Kremer, H.-J. Mattausch, R. Dronskowski, and J. Rouxel, *Angew. Chem. Int. Ed. Engl.* **35**, 752–753 (1996).
J. Bandyopadhyay and K. P. Gupta, *Cryogenics* **18**, 54–55 (1978).
M. D. Banus, T. B. Reed, H. C. Gatos, M. C. Lavine, and J. A. Kafalas, *J. Phys. Chem. Solids* **23**, 971–973 (1962).
C. S. Barrett, *Acta Crystallogr.* **10**, 58–60 (1957).
O. Bars, J. Guillevic, and D. Grandjean, *J. Solid State Chem.* **6**, 48–57 (1973a).
O. Bars, J. Guillevic, and D. Grandjean, *J. Solid State Chem.* **6**, 335–339 (1973b).
H. Barz, *Mater. Res. Bull.* **15**, 1489–1491 (1980).
H. E. Barz, A. S. Cooper, E. Corenzwit, M. Marezio, B. T. Matthias, and P. H. Schmidt, *Science* **175**, 884–885 (1972).
H. Barz, H. C. Ku, G. P. Meisner, Z. Fisk, and B. T. Matthias, *Proc. Natl. Acad. Sci. USA* **77**, 3132–3134 (1980).
J. Bauer and O. Bars, *Acta Crystallogr. B* **36**, 1540–1544 (1980).
J. Bauer and O. Bars, *J. Less-Common Met.* **83**, 17–27 (1982).
J. Bauer and O. Bars *J. Less-Common Met.* **95**, 267–274 (1983).
J. Bauer and J. Debuigne, *C. R. Acad. Sci. C* **274**, 1271–1274 (1972).
J. Bauer and H. Nowotny. *Monatsh. Chem.* **102**, 1129–1145 (1971).
J. Bauer and C. Politis, *J. Less-Common Met.* **88**, L1–L2 (1982).
J. Bauer and O. P. Vennegès, and J. L. Vergneau, *J. Less-Common Met.* **110**, 295–298 (1985).
K. Bender, I. Hennig, D. Schweitzer, K. Dietz, H. Endres, and H. J. Keller, *Mol. Cryst. Liq. Cryst.* **108**, 359–371 (1984).
L. I. Berger and B. W. Roberts, in *CRC Handbook of Chemistry and Physics* 78th ed. (D. R. Lide, Ed.), pp. **12**–60 to **12**–86. CRC Press, Boca Raton, 1997.
G. Bergman and D. P. Shoemaker, *Acta Crystallogr.* **7**, 857–865 (1954).
F. J. Berry, E. M. Forgan, and C. D. Gibbs, *Solid State Commun.* **66**, 667–670 (1988).
A. Bezinge, K. Yvon, J. Muller, W. Lengauer, and P. Ettmayer, *Solid State Commun.* **63**, 141–145 (1987).
R. D. Blaugher, J. K. Hulm, and P. N. Yocom, *J. Phys. Chem. Solids* **26**, 2037–2039 (1965).
R. D. Blaugher, R. E. Hein, J. E. Cox, and R. M. Waterstrat, *J. Low Temp. Phys.* **1**, 539–561 (1969).
O. I. Bodak, V. K. Pecharskii, and E. I. Gladyshevskii, *Inorg. Mater.* **14**, 188–192 (1978).
H. Boller and E. Parthé, *Monatsh. Chem.* **94**, 225–226 (1963).
P. Bordet, D. E. Cox, G. P. Espinosa, J. L. Hodeau, and M. Marezio, *Solid State Commun.* **78**, 359–366 (1991).
L. Bosio, A. Defrain, H. Curien, and A. Rimsky, *Acta Crystallogr. B* **25**, 995 (1969).
L. Bosio, H. Curien, M. Dupont, and A. Rimsky, *Acta Crystallogr. B* **28**, 1974–1975 (1972).
L. Bosio, H. Curien, M. Dupont, and A. Rimsky, *Acta Crystallogr. B* **29**, 367–368 (1973).
G. Brauer and A. Mitius, *Z. anorg. allg. Chem.* **249**, 325–412 (1942).
H. F. Braun, *Phys. Lett. A* **75**, 386–388 (1980).
H. F. Braun, K. Yvon, and R. M. Braun, *Acta Crystallogr. B* **36**, 2397–2399 (1980).
J. H. Brophy, P. Schwarzkopf, and J. Wulff, *Trans. Metall. Soc. AIME* **218**, 910–914 (1960).
B. E. Brown and D. J. Beerntsen, *Acta Crystallogr.* **18**, 31–36 (1965).
V. A. Bruskov, V. K. Pecharskii, and O. I. Bodak, *Inorg. Mater.* **22**, 1289–1292 (1986).

V. A. Bruskov, L. V. Zavalii, and Yu. B. Kuz'ma, *Inorg. Mater.* **24**, 420–421 (1988).
E. Bucher, F. Heiniger, and J. Müller, *Helvetica Phys. Acta* **34**, 843–858 (1961).
E. Bucher, K. Andres, F. J. Di Salvo, J. P. Maita, A. C. Gossard, A. S. Cooper, and G. W. Hull, Jr., *Phys. Rev. B* **11**, 500–513 (1975).
M. Buchgeister, G. Fuchs, J. Klosowski, U. Wiesner, and J. Zawadzki, *Physica C* **255**, 19–29 (1995).
J. F. Cannon and P. B. Farnsworth, *J. Less-Common Met.* **92**, 359–368 (1983).
J. F. Cannon, D. L. Robertson, H. T. Hall, and A. C. Lawson, *J. Less-Common Met.* **31**, 174–176 (1973).
R. J. Cava, A. Santoro, and J. M. Tarascon, *J. Solid State Chem.* **54**, 193–203 (1984).
R. J. Cava, B. Batlogg, G. P. Espinosa, A. P. Ramirez, J. J. Krajewski, W. F. Peck, Jr., L. W. Rupp, Jr., and A. S. Coooper, *Nature* **339**, 291–293 (1989).
R. J. Cava, B. Batlogg, J. J. Krajewski, W. F. Peck, Jr., T. Siegrist, R. M. Fleming, S. Carter, H. Takagi, R. J. Felder, R. B. van Dover, and L. W. Rupp, Jr., *Physica C* **226**, 170–174 (1994a).
R. J. Cava, B. Batlogg, T. Siegrist, J. J. Krajewski, W. F. Peck, Jr., S. Carter, R. J. Felder, H. Takagi, and R. B. van Dover, *Phys. Rev. B* **49**, 12384–12387 (1994b).
R. J. Cava, T. Siegrist, B. Batlogg, H. Takagi, H. Eisaki, S. A. Carter, J. J. Krajewski, and W. F. Peck, Jr., *Phys. Rev. B* **50**, 12966–12968 (1994c).
R. J. Cava, H. Takagi, B. Batlogg, H. W. Zandbergen, J. J. Krajewski, W. F. Peck, Jr., R. B. van Dover, R. J. Felder, T. Siegrist, K. Mizuhashi, J. O. Lee, H. Eisaki, S. A. Carter, and S. Uchida, *Nature* **367**, 146–148 (1994d).
R. J. Cava, H. Takagi, H. W. Zandbergen, J. J. Krajewski, W. F. Peck, Jr., T. Siegrist, B. Batlogg, R. B. van Dover, R. J. Felder, K. Mizuhashi, J. O. Lee, H. Eisaki, and S. Uchida, *Nature* **367**, 252–253 (1994e).
R. J. Cava, H. W. Zandbergen, B. Batlogg, H. Eisaki, H. Takagi, J. J. Krajewski, W. F. Peck, Jr., E. M. Gyorgy, and S. Uchida, *Nature* **372**, 245–247 (1994f).
K. Cenzual, L. Gelato, M. Penzo, and E. Parthé, *Acta Crystallogr. B* **47**, 433–439 (1991).
K. Cenzual, R. Gladyshevskii, and E. Parthé, *TYPIX 1995 Database of Inorganic Structure Types, User's Guide*, Gmelin-Institut für Anorganische Chemie, Frankfurt, 1995.
B. Chabot, *J. Less-Common Met.* **102**, L23–L25 (1984).
P. Chaddah and R. O. Simmons, *Phys. Rev. B* **27**, 119–124 (1983).
B. C. Chakoumakos and M. Paranthaman, *Physica C* **227**, 143–150 (1994).
I. M. Chapnik, *J. Mater. Sci. Lett.* **4**, 370–372 (1985).
B.-H. Chen, B. Eichhorn, J.-L. Peng, and R. L. Greene, *J. Solid State Chem.* **103**, 307–313 (1993).
B. Chevalier, P. Lejay, A. Cole, M. Vlasse, and J. Etourneau, *Solid State Commun.* **41**, 801–804 (1982a).
B. Chevalier, P. Lejay, J. Etourneau, M. Vlasse, and P. Hagenmuller, *Mater. Res. Bull.* **17**, 1211–1220 (1982b).
N. Chevreau and D. C. Johnson, *J. Solid State Chem.* **61**, 347–353 (1986).
R. Chevrel and M. Sergent, in *Superconductivity in Ternary Compounds I. Topics in Current Physics 32* (Ø. Fischer and M. B. Maple, Eds.), pp. 25–86. Springer-Verlag, Berlin, 1982.
R. Chevrel, M. Sergent, and J. Prigent, *J. Solid State Chem.* **3**, 515–519 (1971).
R. Chevrel, M. Sergent, and J. Prigent, *Mater. Res. Bull.* **9**, 1487–1498 (1974).
R. Chevrel, P. Gougeon, M. Potel, and M. Sergent, *J. Solid State Chem.* **57**, 25–33 (1985).
A. N. Christensen, *Acta Chem. Scand. A*, **29**, 563–564 (1975).
A. N. Christensen, *Acta Chem. Scand. A*, **31**, 77–78 (1977a).
A. N. Christensen, *Acta Chem. Scand. A*, **31**, 509–511 (1977b).
A. N. Christensen, *Acta Chem. Scand. A*, **37**, 519–522 (1983).
A. N. Christensen, *Acta Chem. Scand.* **44**, 851–852 (1990).
K. N. Christensen, S. E. Rasmussen, and J. Thygesen, *J. Appl. Crystallogr.* **24**, 108–110 (1991).
C. W. Chu, W. L. McMillan, and H. L. Luo, *Phys. Rev. B* **3**, 3757–3762 (1971).
S. Cirafici and A. Palenzona, *J. Less-Common Met.* **53**, 199–203 (1977).
T. Claeson, *Phys. Rev. B* **147**, 340–347 (1966).
T. Claeson and H. L. Luo, *J. Phys. Chem. Solids* **27**, 1081–1085 (1966).
D. M. Collins and M. C. Mahar, *Acta Crystallogr. C* **40**, 914–915 (1984).

V. B. Compton and B. T. Matthias, *Acta Crystallogr.* **12**, 651–654 (1959).
V. B. Compton, E. Corenzwit, J. P. Maita, B. T. Matthias, and F. J. Morin, *Phys. Rev.* **123**, 1567–1568 (1961).
A. S. Cooper, *Mater. Res. Bull.* **15**, 799–805 (1980).
A. S. Cooper, E. Corenzwit, L. D. Longinotti, B. T. Matthias, and W. H. Zachariasen, *Proc. Natl. Acad. Sci.* **67**, 313–319 (1970).
G. Cordier, E. Czech, H. Schäfer, and P. Woll, *J. Less-Common Met.* **110**, 327–330 (1985).
T. H. Courtney, G. W. Pearsall and J. Wulff, *J. Appl. Phys.* **36**, 3256–3260 (1965).
J. R. Dahn, W. R. McKinnon, and S. T. Coleman, *Phys. Rev. B* **31**, 484–489 (1985).
M. Dalton, I. Gameson, A. R. Armstrong, and P. P. Edwards, *Physica C* **221**, 149–156 (1994).
J.B. Darby, Jr., and S. T. Zegler, *J. Phys. Chem. Solids* **23**, 1825–1827 (1962).
W. I. F. David, R. M. Ibberson, J. C. Matthewman, K. Prassides, T. J. S. Dennis, J. P. Hare, H. W. Kroto, R. Taylor, and D. R. M. Walton, *Nature* **353**, 147–149 (1991).
B. D. Davis and W. R. Robinson, *J. Solid State Chem.* **85**, 332–336 (1990).
C. H. de Novion, D. Damien, and H. Hubert, *J. Solid State Chem.* **39**, 360–367 (1981).
V. F. Degtyareva, S. A. Ivakhnenko, E. G. Ponyatovskii, and V. I. Rashchupkin, *Sov. Phys. Solid State* **23**, 951–954 (1981).
P. D. Dernier, E. Bucher, and L. D. Longinotti, *J. Solid State Chem.* **15**, 203–207 (1975).
R. G. Dickinson and L. Pauling, *J. Am. Chem. Soc.* **45**, 1466–1471 (1923).
M. Dietrich, W. Gey, H. Rietschel, and C. B. Satterthwaite, *Solid State Commun.* **15**, 941–943 (1974).
T. Doi, H. Ishida, and T. Umezawa, *Nippon Kinzoku Gakkaishi* **30**, 139–145 (1966).
J. Donohue, *The Structures of the Elements*. Wiley, New York, 1974.
P. C. Donohue and P. E. Bierstedt, *Inorg. Chem.* **8**, 2690–2694 (1969).
A. Dunand, H. D. Flack, and K. Yvon, *Phys. Rev. B* **31**, 2299–2315 (1985).
Ya. I. Dutchak, Ya. I. Fedyshin, and Yu. B. Paderno, *Inorg. Mater.* **8**, 1877–1880 (1972).
A. E. Dwight, *Trans Metall. Soc. AIME* **215**, 283–286 (1959).
A. E. Dwight and C. W. Kimball, *J. Less-Common Met.* **127**, 179–182 (1987).
L.-E. Edshammar, *Acta Chem. Scand.* **18**, 2294–2302 (1964).
B. Eisenmann and H. Schäfer, *J. Less-Common Met.* **123**, 89–94 (1986).
T. Epicier, J. Dubois, C. Esnouf, G. Fantozzi, and P. Convert, *Acta Metall.* **36**, 1903–1921 (1988).
V. N. Eremenko, E. L. Semenova, and T. D. Shtepa, *Russ. Metall.* **5**, 210–213 (1980).
V. N. Eremenko, A. M. Kharkova, and T.Ya. Velikanova, *Dopov. Akad. Nauk Ukr. RSR A* **1**, 77–80 (1983).
G. P. Espinosa, A. S. Cooper, H. Barz, and J. P. Remeika, *Mater. Res. Bull.* **15**, 1635–1641 (1980).
G. P. Espinosa, A. S. Cooper, and H. Barz, *Mater. Res. Bull.* **17**, 963–969 (1982).
D. A. Evans and K.H. Jack, *Acta Crystallogr.* **10**, 833–834 (1957).
J. Evers, G. Oehlinger, and H. R. Ott, *J. Less-Common Met.* **69**, 389–391 (1980a).
J. Evers, G. Oehlinger, and A. Weiss, *Z. Naturforsch. B* **35**, 397–398 (1980b).
J. Evers, G. Oehlinger, and A. Weiss, *Z. Naturforsch. B* **37**, 1487–1488 (1982).
J. Evers, G. Oehlinger, and A. Weiss, *Z. Naturforsch. B* **38**, 899–900 (1983).
J. Evers, G. Oehlinger, A. Weiss, and C. Probst, *Solid State Commun.* **50**, 61–62 (1984).
W. H. Ferguson, Jr., B. C. Giessen, and N. J. Grant, *Trans, Metall. Soc. AIME* **227**, 1401–1406 (1963).
V. A. Finkel' and E. A. Pushkarev, *Sov. Phys. JETP* **51**, 422–424 (1980).
N. A. Fischel and H. A. Eick, *J. Inorg. Nucl. Chem* **31**, 891–893 (1969).
Ø. Fischer, *Appl. Phys.* **16**, 1–28 (1978).
Ø. Fischer, A. Treyvaud, R. Chevrel, and M. Sergent, *Solid State Commun.* **88**, 867–870 (1993).
J. E. Fischer, G. Bendele, R. Dinnebier, P. W. Stephens, C. L. Lin, N. Bykovetz, and Q. Zhu, *J. Phys. Chem. Solids* **56**, 1445–1457 (1995).
R. M. Fleming, A. P. Ramirez, M. J. Rosseinsky, D. W. Murphy, R. C. Haddon, S. M. Zahurak, and A. V. Makhija, *Nature* **352**, 787–788 (1991a).

R. M. Fleming, M. J. Rosseinsky, A. P. Ramirez, D. W. Murphy, J. C. Tully, R. C. Haddon, T. Siegrist, R. Tycko, S. H. Glarum, P. Marsh, G. Dabbagh, S. M. Zahurak, A. V. Makhija, and C. Hampton, *Nature* **352**, 701–703 (1991b).

R. Flükiger, in *Superconductor Materials Science* (S. Foner and B. B. Schwartz, Eds.), pp. 511–604. Plenum, New York, 1981.

R. Flükiger and R. Baillif, in *Superconductivity in Ternary Compounds I, Vol. 32, Topics in Current Physics* (Ø. Fischer and M. B. Maple, Eds.), pp. 113–141. Springer-Verlag, Berlin, 1982.

R. Flükiger, F. Heiniger, A. Junod, J. Muller, P. Spitzli, and J. L. Staudenmann, *J. Phys. Chem. Solids* **32**, 459–463 (1970).

R. Flükiger, K. Yvon, Ch. Susz, R. Roggen, A. Paoli, and J. Muller, *J. Less-Common Met.* **32**, 207–225 (1973).

R. Flükiger, A. Paoli, and J. Muller, *Solid State Commun.* **14**, 443–447 (1974).

R. Flükiger, Ch. Susz, F. Heiniger, and J. Muller, *J. Less-Common Met.* **40**, 103–119 (1975).

R. Flükiger, J.-L. Staudenmann, and P. Fischer, *J. Less-Common Met.* **50**, 253–273 (1976).

R. Flükiger, A. Junod, R. Baillif, P. Spitzli, A. Treyvaud, A. Paoli, H. Devantay, and J. Muller, *Solid State Commun.* **23**, 699–702 (1977).

R. Flükiger, J. L. Jorda, A. Junod, and P. Fischer, *Appl. Phys. Commun.* **1**, 9–30 (1981).

F. R. Gamble, J. H. Osiecki, M. Cais, R. Pisharody, F. J. DiSalvo, and T. H. Geballe, *Science* **174**, 493–497 (1971a).

F. R. Gamble, J. H. Osiecki, and F. J. DiSalvo, *J. Chem. Phys.* **55**, 3525–3530 (1971b).

C. S. Garde, J. Ray, and G. Chandra, *J. Alloys Comp.* **198**, 165–172 (1993).

J. R. Gavaler, *Appl. Phys. Lett.* **23**, 480–482 (1973).

J. R. Gavaler, M. A. Janocko, and C. K. Jones, *Appl. Phys. Lett.* **21**, 179–180 (1972).

C. Geantet, J. Padiou, O. Peña, M. Sergent, and R. Horyn, *Solid State Commun.* **64**, 1363–1368 (1987).

T. H. Geballe, B. T. Matthias, V. B. Compton, E. Corenzwit, G. W. Hull, Jr., and L. D. Longinotti, *Phys. Rev.* **137**, A119–A127 (1965).

C. Geibel, C. Schank, S. Thies, H. Kitazawa, C. D. Bredl, A. Böhm, M. Rau, A. Grauel, R. Caspary, R. Helfrich, U. Ahlheim, G. Weber, and F. Steglich, *Z. Phys. B* **84**, 1–2 (1991a).

C. Geibel, S. Thies, D. Kaczorowski, A. Mehner, A. Grauel, B. Seidel, U. Ahlheim, R. Helfrich, K. Petersen, C. D. Bredl, and F. Steglich, *Z. Phys. B* **83**, 305–306 (1991b).

C. Geibel, A. Böhm, R. Caspary, K. Gloos, A. Grauel, P. Hellmann, R. Modler, C. Schank, G. Weber, and F. Steglich, *Physica B* **186/188**, 188–194 (1993).

S. Geller, *Acta Crystallogr.* **8**, 15–21 (1955).

S. Geller, *Acta Crystallogr.* **15**, 1198–1201 (1962).

S. Geller and B. B. Cetlin, *Acta Crystallogr.* **8**, 272–274 (1955).

S. Geller, D. B. McWhan and G. W. Hull, Jr., *Science.* **140**, 62–63 (1963).

B. C. Giessen and N. J. Grant, *Acta Crystallogr.* **17**, 615–616 (1964).

B. C. Giessen, U. Jaehnigen, and N. J. Grant, *J. Less-Common Met.* **10**, 147–150 (1966).

A. L. Giorgi, *Physica B* **135**, 420–422 (1985).

A. L. Giorgi and E. G. Szklarz, *J. Less-Common Met.* **20**, 173–175 (1970a).

A. L. Giorgi and E. G. Szklarz, *J. Less-Common Met.* **22**, 246–248 (1970b).

A. L. Giorgi, E. G. Szklarz, M. C. Krupka, T. C. Wallace, and N. H. Krikorian, *J. Less-Common Met.* **14**, 247 (1968).

A. L. Giorgi, E. G. Szklarz, N. H. Krikorian, and M. C. Krupka, *J. Less-Common Met.* **22**, 131–135 (1970).

A. L. Giorgi, G. R. Stewart, and E. G. Szklarz, in *Superconductivity in d- and f-Band Metals, Proc. 4th Conf.* (W. Buckel and W. Weber, Eds.), pp. 455–458. Kernforschungszentrum, Karlsruhe, 1982.

E. Gocke, W. Schramm, P. Dolscheid, and R. Schöllhorn, *J. Solid State Chem.* **70**, 71–81 (1987).

A. I. Goldman, S. M. Shapiro, D. E. Cox, J. L. Smith, and Z. Fisk, *Phys. Rev. B* **32**, 6042–6044 (1985).

P. Gougeon, M. Potel, and M. Sergent, *Acta Crystallogr. C* **45**, 1285–1287 (1989).

P. Gougeon, M. Potel, and M. Sergent, *Acta Crystallogr. C* **47**, 1791–1794 (1991).

J. L. Green, G. P. Arnold, J. A. Leary, and N. G. Nereson, *J. Nucl. Mater.* **34**. 281–289 (1970).

W. O. J. Groeneveld Meijer, *Am. Mineral.* **40**, 646–657 (1955).
A. Grüttner, K. Yvon, R. Chevrel, M. Potel, M. Sergent, and B. Seeber, *Acta Crystallogr. B* **35**, 285–292 (1979).
M. Gueramian, B. Chabot, K. Yvon, L. Schellenberg, and H. F. Braun, *J. Less-Common Met.* **142**, 169–176 (1988).
J. Guillevic, O. Bars, and D. Grandjean, *Acta Crystallogr. B* **32**, 1338–1342 (1976a).
J. Guillevic, H. Lestrat, and D. Grandjean, *Acta Crystallogr. B* **32**, 1342–1345 (1976b).
L. C. Gupta, R. Nagarajan, Z. Hossain, C. Mazumdar, S. K. Dhar, C. Godart, C. Levy-Clement, B. D. Padalia, and R. Vijayraghavan, *J. Mag. Mag. Mater.* **140/144**, 2053–2054 (1995).
G. Hägg and G. Funke, *Z. Physikal. Chem. Abt. B* **6**, 272–283 (1929).
T. Hahn (Ed.), *International Tables for Crystallography A*. Reidel, Dordrecht (distributor Kluwer, Dordrecht), 1983.
K. Hamada, M. Wakata, N. Sugii, K. Matsuura, K. Kubo, and H. Yamauchi, *Phys. Rev. B* **48**, 6892–6898 (1993).
B. Harbrecht and S. Mahne, *J. Alloys Comp.* **178**, 467–475 (1992).
G. F. Hardy and J. K. Hulm, *Phys. Rev.* **93**, 1004–1016 (1954).
I. R. Harris and G. V. Raynor, *J. Less-Common Met.* **7**, 11–16 (1964).
L. D. Hartsough and R. H. Hammond, *Solid State Commun.* **9**, 885–889 (1971).
E. E. Havinga, H. Damsma, and M. H. van Maaren, *J. Phys. Chem. Solids* **31**, 2653–2662 (1970).
E. E. Havinga, H. Damsma, and P. Hokkeling, *J. Less-Common Met.* **27**, 169–186 (1972a).
E. E. Havinga, H. Damsma, and J. M. Kanis, *J. Less-Common Met.* **27**, 281–291 (1972b).
C. W. Haworth and W. Hume-Rothery, *J. Inst. Met.* **87**, 265–272 (1958/1959).
F. Heiniger, E. Bucher, J. P. Maita, and P. Descouts, *Phys. Rev. B* **8**, 3194–3205 (1973).
M. Hirjak, P. Lejay, B. Chevalier, J. Etourneau, and P. Hagenmuller, *J. Less-Common Met.* **105**, 139–148 (1985).
I. Hirosawa, K. Prassides, J. Mizuki, K. Tanigaki, M. Gevaert, A. Lappas, and J. K. Cockcroft, *Science* **264**, 1294–1297 (1994).
J. L. Hodeau, J. Chenevas, M. Marezio, and J. P. Remeika, *Solid State Commun.* **36**, 839–845 (1980).
J. L. Hodeau, M. Marezio, and J. P. Remeika, *Acta Crystallogr. B* **40**, 26–38 (1984).
F. Holtzberg, Y. Okaya and N. Stemple, *Abstr. ACA Meeting*, Gatlinburg, Tennessee, 46 (1965).
W. Hönle and K. Yvon, *J. Solid State Chem.* **70**, 235–240 (1987).
W. Hönle, H. G. von Schnering, A. Lipka, and K. Yvon, *J. Less-Common Met.* **71**, 135–145 (1980).
W. Hönle, H. D. Flack, and K. Yvon, *J. Solid State Chem.* **49**, 157–165 (1983).
R. Horyn, L. Folcik-Kokot, and N. Iliev, *J. Less-Common Met.* **57**, P69–P74 (1978).
Z. Hossain, L. C. Gupta, C. Mazumdar, R. Nagarajan, S. K. Dhar, C. Godart, C. Levy-Clement, B. D. Padalia, and R. Vijayaraghavan, *Solid State Commun.* **92**, 341–344 (1994).
J. S. Houghton, M. Dewess, A. C. Lawson, and J. L. Smith, *J. Less-Common Met.* **83**, L47–L49 (1982).
E. Hovestreydt, N. Engel, K. Klepp, B. Chabot, and E. Parthé, *J. Less-Common Met.* **85**, 247–274 (1982).
Q. Huang, B. C. Chakoumakos, A. Santoro, R. J. Cava, J. J. Krajewski, and W. F. Peck Jr., *Physica C* **244**, 101–105 (1995a).
Q. Huang, A. Santoro, T. E. Grigereit, J. W. Lynn, R. J. Cava, J. J. Krajewski, and W. F. Peck, Jr., *Phys. Rev. B* **51**, 3701–3708 (1995b).
Q. Huang, J. W. Lynn, A. Santoro, B. C. Chakoumakos, R. J. Cava, J. J. Krajewski, and W. F. Peck, Jr., *Physica C* **271**, 311–318 (1996).
F. Hulliger, in *Structure and Bonding 4* (C. K. Jørgensen, J. B. Neilands, R. S. Nyholm, D. Reinen, and R. J. P. Williams, Eds.), pp. 83–229. Springer-Verlag, Berlin, 1968.
J. Huster, G. Schippers, and W. Bronger, *J. Less-Common Met.* **91**, 333–337 (1983).
Z. Iqbal, G. H. Kwei, B. L. Ramakrishna, and E. W. Ong, *Physica C* **167**, 369–374 (1990).
Z. Iqbal, R. H. Baughman, B. L. Ramakrishna, S. Khare, N. S. Murthy, H. J. Bornemann, and D. E. Morris, *Science*, **254**, 826–829 (1991).

M. Ishikawa, J.-L. Jorda, and A. Junod, in *Superconductivity in d- and f-Band Metals, Proc. 4th Conf.* (W. Buckel and W. Weber, Eds.), pp. 141–144. Kernforschungszentrum, Karlsruhe, 1982.
M. Ishikawa, H. F. Braun, and J. L. Jorda, *Phys. Rev. B* **27**, 3092–3095 (1983).
H. Iwasaki, M. Ikebe, and Y. Muto, *Phys. Rev. B* **33**, 4669–4679 (1986).
E. L. Jacobsen, R. D. Freeman, A. G. Tharp, and A. W. Searcy, *J. Am. Chem. Soc.* **78**, 4850–4852 (1956).
J. C. Jamieson, *Science* **139**, 762–764 (1963).
W. Jeitschko, *Acta Crystallogr. B* **26**, 815–822 (1970).
W. Jeitschko, and D. Braun, *Acta Crystallogr. B* **33**, 3401–3406 (1977).
W. Jeitschko, H. Nowotny, and F. Benesovsky, *Monatsh, Chem.* **94**, 247–251 (1963a).
W. Jeitschko, H. Nowotny, and F. Benesovsky, *Monatsh, Chem.* **94**, 565–568 (1963b).
W. Jeitschko, R. Glaum, and L. Boonk, *J. Solid State Chem.* **69**, 93–100 (1987).
F. Jellinek, G. Brauer, and H. Müller, *Nature* **185**, 376–377 (1960).
D. C. Johnston, *Solid State Commun.* **24**, 699–702 (1977).
D. C. Johnston and H. F. Braun, in *Superconductivity in Ternary Compounds II, Vol. 34, Topics in Current Physics* (M. B. Maple and Ø. Fischer, Eds.), pp. 11–55. Springer-Verlag, Berlin, 1982.
J. Johnston, L. Toth, K. Kennedy, and E. R. Parker, *Solid State Commun.* **2**, 123 (1964).
D. W. Jones, I. J. McColm, R. Steadman, and J. Yerkess, *J. Solid State Chem.* **53**, 376–381 (1984).
D. W. Jones, I. J. McColm, and J. Yerkess, *J. Solid State Chem.* **92**, 301–311 (1991).
J. L. Jorda and J. Muller, *J. Less-Common Met.* **84**, 39–48 (1982).
J.-L. Jorda, R. Flükiger, and J. Muller, *J. Less-Common Met.* **55**, 249–264 (1977).
J. L. Jorda, R. Flükiger, and J. Müller, *J. Less-Common Met.* **62**, 25–37 (1978).
J. L. Jorda, R. Flükiger, and J. Muller, *J. Less-Common Met.* **75**, 227–239 (1980).
J. L. Jorda, M. Ishikawa, and J. Muller, *J. Less-Common Met.* **107**, 321–330 (1985).
J. L. Jorda, T. Graf, L. Schellenberg, J. Muller, K. Cenzual, J. C. Gachon, and J. Hertz, *J. Less-Common Met.* **136**, 313–328 (1988).
J. D. Jorgensen and D. G. Hinks, *Phys. B* **136**, 485–488 (1986).
J. D. Jorgensen, D. G. Hinks, and G. P. Felcher, *Phys. Rev. B* **35**, 5365–5368 (1987).
W. Jung and D. Quentmeier, *Z. Kristallogr.* **151**, 172–174 (1980).
A. Junod, F. Heiniger, J. Muller, and P. Spitzli, *Helvetica Phys. Acta* **43**, 59–66 (1970).
A. Junod, R. Flükiger, and J. Muller, *J. Phys. Chem. Solids* **37**, 27–31 (1976).
A. Junod, J. Muller, H. Rietschel, and E. Schneider, *J. Phys. Chem. Solids* **39**, 317–328 (1978).
F. Kadijk, R. Huisman, and F. Jellinek, *Recl. Trav. Chim. Pays Bas* **83**, 768–775 (1964).
C. H. L. Kennard and L. Davis, *J. Solid State Chem.* **47**, 103–106 (1983).
K. S. Keskar, T. Yamashita, and Y. Onodera, *Jpn. J. Appl. Phys.* **10**, 370–374 (1971).
Yu. P. Khodyrev, R. V. Baranova, R. M. Imamov, and S. A. Semiletov, *Sov. Phys. Crystallogr.* **23**, 592–594 (1978).
R. Kiessling, *Acta Chem. Scand.* **3**, 603–615 (1949).
L. Kihlborg and A. Hussain, *Mater. Res. Bull.* **14**, 667–674 (1979).
D. H. Killpatrick, *J. Phys. Chem. Solids* **25**, 1213–1216 (1964).
A. M. Kini, U. Geiser, H. H. Wang, K. D. Carlson, J. M. Williams, W. K. Kwok, K. G. Vandervoort, J. E. Thompson, D. L. Stupka, D. Jung, and M.-H. Whangbo, *Inorg. Chem.* **29**, 2555–2557 (1990).
A. Kirchhoff, A. Pebler, E. Warkentin, G. Bergerhoff and P. Luksch, *ICSD Inorganic Crystal Structure Database (release 97/2), User Manual.* Fachinformationszentrum, Karlsruhe, Gmelin-Institut für Anorganische Chemie, Frankfurt and Institut für Anorganische Chemie der Universität Bonn (1991).
H. Kitô, S. Ikeda, S. Takekawa, H. Abe, and H. Kitazawa, *Physica C* **291**, 332–340 (1997).
A. Kjekshus and W. B. Pearson, *Can. J. Phys.* **43**, 438–449 (1965).
A. Kjekshus, T. Rakke, and A. F. Andresen, *Acta Chem. Scand. A* **32**, 209-217 (1978).
A. Kjekshus, T. Rakke, and A. F. Andresen, *Acta Chem. Scand. A* **33**, 719–725 (1979).
K. Klepp and E. Parthé, *Acta Crystallogr. B* **38**, 1105–1108 (1982a).
K. Klepp and E. Parthé, *Acta Crystallogr. B* **38**, 1541–1544 (1982b).
H. P. Klug, *J. Am. Chem. Soc.* **68**, 1493–1494 (1946).

A. G. Knapton, *J. Inst. Met.* **87**, 62–64 (1958/1959).
A. Kobayashi, R. Kato, H. Kobayashi, S. Moriyama, Y. Nishio, K. Kajita, and W. Sasaki, *Chem. Lett.*, 2017–2020 (1986a).
H. Kobayashi, R. Kato, A. Kobayashi, Y. Nishio, K. Kajita, and W. Sasaki, *Chem. Lett.*, 833–836 (1986b).
A. Kobayashi, R. Kato, H. Kobayashi, S. Moriyama, Y. Nishio, K. Kajita, and W. Sasaki, *Chem. Lett.* 459–462 (1987).
H. Kobayashi, T. Udagawa, H. Tomita, K. Bun, T. Naito, and A. Kobayashi, *Chem. Lett.* 1559–1562 (1993a).
A. Kobayashi, T. Udagawa, H. Tomita, T. Naito, and H. Kobayashi, *Chem. Lett.* 2179–2182 (1993b).
C. C. Koch and J. O. Scarbrough, *Phys. Rev. B* **3**, 742–748 (1971).
R. Koksbang, S. E. Rasmussen, and R. G. Hazell, *J. Appl. Crystallogr.* **22**, 23–25 (1989).
T. Komatsu, T. Nakamura, N. Matsukawa, H. Yamochi, G. Saito, H. Ito, T. Ishiguro, M. Kusunoki, and K.-I. Sakaguchi, *Solid State Commun.* **80**, 843–847 (1991).
B. Koppelhuber-Bitschnau, F. A. Mautner, and K. Yvon, *Monatsh. Chem.* **121**, 505–509 (1990).
M. M. Korsukova, V. N. Gurin, T. Lundström, and L.-E. Tergenius, *J. Less-Common Met.* **117**, 73–81 (1986).
A. R. Kortan, N. Kopylov, S. Glarum, E. M. Gyorgy, A. P. Ramirez, R. M. Fleming, F. A. Thiel, and R. C. Haddon, *Nature* **355**, 529–532 (1992a).
A. R. Kortan, N. Kopylov, S. Glarum, E. M. Gyorgy, A. P. Ramirez, R. M. Fleming, O. Zhou, F. A. Thiel, P. L. Trevor, and R. C. Haddon, *Nature* **360**, 566–568 (1992b).
A. R. Kortan, N. Kopylov, R. M. Fleming, O. Zhou, F. A. Thiel, R. C. Haddon, and K. M. Rabe, *Phys. Rev. B* **47**, 13070–13073 (1993).
A. R. Kortan, N. Kopylov, E. Özdas, A. P. Ramirez, R. M. Fleming, and R. C. Haddon, *Chem. Phys. Lett.* **223**, 501–505 (1994).
B. Krevet, W. Schauer, F. Wüchner, and K. Schulze, *Appl. Phys. Lett.* **36**, 704–706 (1980).
N. H. Krikorian, A. L. Bowman, M. C. Krupka, and G. P. Arnold, *High-Temp. Sci.* **1**, 360–366 (1969a).
N. H. Krikorian, A. L. Giorgi, E. G. Szklarz, M. C. Krupka, and B. T. Matthias, *J. Less-Common Met.* **19**, 253–257 (1969b).
P. I. Kripyakevich and E. I. Gladyshevskii, *Sov. Phys. Crystallogr.* **8**, 349–351 (1963).
P. I. Kripyakevich and Yu. B. Kuz'ma, *Sov. Phys. Crystallogr.* **7**, 240 (1962).
P. I. Kripyakevich, Yu. B. Kuz'ma, and V. S. Protasov, *Dop. Akad. Nauk Ukr. RSR* **4**, 492–495 (1963).
M. C. Krupka, A. L. Giorgi, N. H. Krikorian, and E. G. Szklarz, *J. Less-Common Met.* **17**, 91–98 (1969a).
M. C. Krupka, A. L. Giorgi, N. H. Krikorian, and E. G. Szklarz, *J. Less-Common Met.* **19**, 113–119 (1969b).
M. C. Krupka, A. L. Giorgi, and E. G. Szklarz, *J. Less-Common Met.* **30**, 217–223 (1973).
H. C. Ku and R. N. Shelton, *Mater. Res. Bull.* **15**, 1441–1444 (1980).
H. C. Ku, D. C. Johnston, B. T. Matthias, H. Barz, G. Burri, and L. Rinderer, *Mater. Res. Bull.* **14**, 1591–1599 (1979a).
H. C. Ku, B. T. Matthias, and H. Barz, *Solid State Commun.* **32**, 937–944 (1979b).
H. C. Ku, G. P. Meisner, F. Acker, and D. C. Johnston, *Solid State Commun.* **35**, 91–96 (1980).
F. Kubel and K. Yvon, *Acta Crystallogr. C* **43**, 1655–1659 (1987).
F. Kubel and K. Yvon, *J. Solid State Chem.* **73**, 188–191 (1988).
F. Kubel and K. Yvon, *Solid State Commun.* **72**, 1219–1221 (1989).
F. Kubel and K. Yvon, *Acta Crystallogr. C* **46**, 181-186 (1990).
F. Kubel, H. D. Flack, and K. Yvon, *Phys. Rev. B* **36**, 1415–1419 (1987).
F. Kubel, W. Lengauer, K. Yvon, K. Knorr, and A. Junod, *Phys. Rev. B* **38**, 12908–12912 (1988).
R. Kubiak, *Z. anorg. allg. Chem.* **431**, 261–267 (1977).
T. Kudo, J. Oi, A. Kishimoto, and M. Hiratani, *Mater. Res. Bull.* **26**, 779–787 (1991).
M. Kurmoo, D. R. Talham, K. L. Pritchard, P. Day, A. M. Stringer, and J. A. K. Howard, *Synth. Met.* **27**, A177–A182 (1988).

Yu. B. Kuz'ma and N. S. Bilorizhko, *Sov. Phys. Crystallogr.* **16**, 897–898 (1972).
Yu. B. Kuz'ma, V. I. Lakh, B. I. Stadnyk, and Yu. V. Voroshilov, *Sov. Powder Metall. Met. Ceram.* **7**, 462–466 (1968).
Ph. Labbé, M. Goreaud, B. Raveau, and J. C. Monier, *Acta Crystallogr. B* **34**, 1433–1438 (1978).
C. C. Lai, M. S. Lin, Y. B. You, and H. C. Ku, *Phys. Rev. B* **51**, 420–423 (1995).
A. C. Larson and D. T. Cromer, *Acta Crystallogr.* **14**, 545–546 (1961).
A. C. Lawson, *Phys. Rev. B* **17**, 1136–1138 (1978).
A. C. Lawson, J. F. Cannon, D. L. Robertson, and H. T. Hall, *J. Less-Common Met.* **32**, 173–174 (1973).
A. C. Lawson, K. Baberschke, and U. Engel, *Phys. Lett. A* **48**, 107–108 (1974).
W. H. Lee, S. Appl, and R. N. Shelton, *J. Low Temp. Phys.* **68**, 147–157 (1987).
P. Lejay, B. Chevalier, J. Etourneau, and P. Hagenmuller, *J. Less-Common Met.* **82**, 193–200 (1981a).
P. Lejay, B. Chevalier, J. Etourneau, and P. Hagenmuller, *Synth. Met.* **4**, 139–145 (1981b).
P. Lejay, B. Chevalier, J. Etourneau, J. M. Tarascon, and P. Hagenmuller, *Mater. Res. Bull.* **18**, 67–71 (1983).
R. Li, X. Chaoshui, Z. Hong, L. Bin, and Y. Li, *J. Alloys Comp.* **223**, 53–55 (1995).
A. Lipka and K. Yvon, *Acta Crystallogr. B* **36**, 2123–2126 (1980).
H. L. Luo, E. Vielhaber, and E. Corenzwit, *Z. Phys.* **230**, 443–448 (1970).
R. N. Lyubovskaya, E. I. Zhilyaeva, S. I. Pesotskii, R. B. Lyubovskii, L. O. Atovmyan, O. A. D'yachenko, and T. G. Takhirov, *JETP Lett.* **46**, 188–191 (1987).
R. Mailfert, B. W. Betterman, and J. J. Hanak, *Phys. Lett. A* **24**, 315–316 (1967).
S. K. Malik, A. M. Umarji, and G. K. Shenoy, *Phys. Rev. B* **31**, 6971–6975 (1985).
M. B. Maple, J. Witting, and K. S. Kim, *Phys. Rev. Lett.* **23**, 1375–1377 (1969).
M. Marezio, P. D. Dernier, and C. W. Chu, *Phys. Rev. B* **4**, 2825–2826 (1971).
M. Marezio, P. D. Dernier, A. Menth, and G. W. Hull, Jr., *J. Solid State Chem.* **4**, 425–429 (1972).
M. Marezio, P. D. Dernier, J. P. Remeika, E. Corenzwit, and B. T. Matthias, *Mater. Res. Bull.* **8**, 657–668 (1973).
J. A. C. Marples and C. C. Koch, *Phys. Lett. A* **41**, 307–308 (1972).
D. T. Marx, P. G. Radaelli, J. D. Jorgensen, R. L. Hitterman, D. G. Hinks, S. Pei, and B. Dabrowski, *Phys. Rev. B* **46**, 1144–1156 (1992).
Hj. Mattausch, R. K. Kremer, R. Eger, and A. Simon, *Z. anorg. allg. Chem.* **609**, 7–11 (1992).
Hj. Mattausch, H. Borrmann, and A. Simon, *Z. Kristallogr.* **209**, 281 (1994).
Hj. Mattausch, A. Simon, C. Felser, and R. Dronskowski, *Angew. Chem. Int. Ed. Engl.* **35**, 1685–1687 (1996).
B. T. Matthias, *Phys. Rev.* **97**, 74–76 (1955).
B. T. Matthias, V. B. Compton, and E. Corenzwit, *J. Phys. Chem. Solids* **19**, 130–133 (1961).
B. T. Matthias, T. H. Geballe, and V. B. Compton, *Rev. Mod. Phys.* **35**, 1–22 (1963).
B. T. Matthias, T. H. Geballe, K. Andres, E. Corenzwit, G. W. Hull, and J. P. Maita, *Science* **159**, 530 (1968).
B. T. Matthias, E. Corenzwit, J. M. Vandenberg, and H. E. Barz, *Proc. Natl. Acad. Sci. USA* **74**, 1334–1335 (1977).
M. W. McElfresh, J. H. Hall, R. R. Ryan, J. L. Smith, and Z. Fisk, *Acta Crystallogr. C* **46**, 1579–1580 (1990).
W. R. McKinnon and J. R. Dahn, *Phys. Rev. B* **31**, 3084–3087 (1985).
D. B. McWhan, G. W. Hull, Jr., T. R. R. McDonald, and E. Gregory, *Science* **147**, 1441–1442 (1965).
A. Meerschaut, L. Guemas, C. Auriel and J. Rouxel, *Eur. J. Solid State Inorg. Chem.* **27**, 557–570 (1990).
G. P. Meisner, *Phys. B* **108**, 763–764 (1981).
G. P. Meisner and H. C. Ku, *Appl. Phys. A* **31**, 201–212 (1983).
S. Miraglia, J. L. Hodeau, M. Marezio, C. Laviron, M. Ghedira, and G. P. Espinosa, *J. Solid State Chem.* **63**, 358–368 (1986).
S. Miraglia, J. L. Hodeau, F. de Bergevin, M. Marezio, and G. P. Espinosa, *Acta Crystallogr. B* **43**, 76–83 (1987).

Yu. V. Mironov, P. P. Samoilov, V. E. Fedorov, V. I. Lisoivan, and S. A. Gromilov, *Russ. J. Inorg. Chem.* **32**, 622–624 (1987).
A. W. Mitchell and D. J. Lam, *J. Nucl. Mater.* **36**, 110–112 (1970).
H. Mori, *Int. J. Mod. Phys. B* **8**, 1–45 (1994).
B. Morosin, *Acta Crystallogr. B* **30**, 551–552 (1974).
N. Morton, B. W. James, G. H. Wostenholm, D. G. Pomfret, M. R. Davies, and J. L. Dykins, *J. Less-Common Met.* **25**, 97–106 (1971).
N. Morton, B. W. James, G. H. Wostenholm, and D. C. B. Hepburn, *J. Less-Common Met.* **29**, 423–426 (1972).
N. Morton, B. W. James, G. H. Wostenholm, and N. A. Howard, *J. Less-Common Met.* **64**, 69–75 (1979).
E. Moshopoulou, P. Bordet, A. Sulpice, and J. J. Capponi, *Physica C* **235/240**, 747–748 (1994).
M. H. Mueller, R. A. Beyerlein, J. D. Jorgensen, T. O. Brun, C. B. Satterthwaite, and R. Caton, *J. Appl. Crystallogr.* **10**, 79–83 (1977).
F. M. Mulder, J. H. V. J. Brabers, R. Coehoorn, R. C. Thiel, K. H. J. Buschow, and F. R. de Boer, *J. Less-Common Met.* **217**, 118–122 (1995).
J. Muller, F. Heiniger, and J.-L. Staudenmann, *Helvetica Phys. Acta* **41**, 1052–1057 (1968).
R. Müller, R. N. Shelton, J. W. Richardson, Jr., and R. A. Jacobson, *J. Less-Common Met.* **92**, 177–183 (1983).
R. Nagarajan, C. Mazumdar, Z. Hossain, S. K. Dhar, K. V. Gopalakrishnan, L. C. Gupta, C. Godart, B. D. Padalia, and R. Vijayaraghavan, *Phys. Rev. Lett.* **72**, 274–277 (1994).
R. Nagarajan, L. C. Gupta, C. Mazumdar, Z. Hossain, S. K. Dhar, C. Godart, B. D. Padalia, and R. Vijayaraghavan, *J. Alloys Comp.* **225**, 571–577 (1995).
H. Nakano and S. Yamanaka, *J. Solid State Chem.* **108**, 260–266 (1994).
K. U. Neumann, H. Capellmann, and K. R. A. Ziebeck, *Z. Phys. B* **72**, 247–251 (1988).
L.-J. Norrby and H. F. Franzen, *J. Solid State Chem.* **2**, 36–41 (1970).
V. I. Novokshonov, *Russ. J. Inorg. Chem.* **25**, 375–378 (1980).
V. I. Novokshonov, E. P. Khlybov and V. V. Evdokimova, *Russ. J. Metall.* **3**, 167–169 (1980).
H. Nowotny, E. Parthé, R. Kieffer, and F. Benesovsky, *Monatsh. Chem.* **85**, 255–272 (1954).
H. Nowotny, F. Benesovsky, and R. Kieffer, *Z. Metallk.* **50**, 417–423 (1959).
J. Oi, A. Kishimoto, T. Kudo, and M. Hiratani, *J. Solid State Chem.* **96**, 13–19 (1992).
J. Oi, A. Kishimoto, and T. Kudo, *J. Solid State Chem.* **103**, 176–185 (1993).
E. Özdas, A. R. Kortan, N. Kopylov, A. P. Ramirez, T. Siegrist, K. M. Rabe, H. E. Bair, S. Schuppler, and P. H. Citrin, *Nature* **375**, 126–129 (1995).
Yu. B. Paderno, V. V. Odintsov, I. I. Timofeeva, and L. A. Klochkov, *High Temperature* **9**, 175–177 (1971).
G. C. Papavassiliou, G. A. Mousdis, J. S. Zambounis, A. Terzis, A. Hountas, B. Hilti, C. W. Mayer, and J. Pfeiffer, *Synth. Met.* **27**, B379–B383 (1988).
E. Parthé and L. M. Gelato, *Acta Crystallogr. A* **40**, 169–183 (1984).
E. Parthé and L. M. Gelato, *Acta Crystallogr. A* **41**, 142–151 (1985).
E. Parthé and V. Sadagopan, *Acta Crystallogr.* **16**, 202–205 (1963).
E. Parthé and K. Yvon, *Acta Crystallogr. B* **26**, 153–163 (1970).
E. Parthé, W. Jeitschko, and V. Sadagopan, *Acta Crystallogr.* **19**, 1031–1037 (1965).
E. Parthé, K. Cenzual, and R. E. Gladyshevskii, *J. Alloys Comp.* **197**, 291–301 (1993).
E. Parthé, L. Gelato, B. Chabot, M. Penzo, K. Cenzual, and R. Gladyshevskii, *TYPIX Standardized Data and Crystal Chemical Characterization of Inorganic Structure Types, Gmelin Handbook of Inorganic and Organometallic Chemistry*, Vols. 1–4. Springer-Verlag, Heidelberg, 1993/1994.
R. R. Pawar, *Curr. Sci. India* **36**, 428 (1967).
S. Pei, J. D. Jorgensen, B. Dabrowski, D. G. Hinks, D. R. Richards, A. W. Mitchell, J. M. Newsam, S. K. Sinha, D. Vaknin, and A. J. Jacobson, *Phys. Rev. B* **41**, 4126–4141 (1990).
O. Peña, P. Gougeon, M. Sergent, and R. Horyn, *J. Less-Common Met.* **99**, 225–232 (1984).
O. Peña, R. Horyn, M. Potel, J. Padiou, and M. Sergent, *J. Less-Common Met.* **105**, 105–117 (1985).

O. Peña, R. Horyn, C. Geantet, P. Gougeon, J. Padiou, and M. Sergent, *J. Solid State Chem.* **63**, 62–69 (1986).
A. Perrin, M. Sergent, and Ø. Fischer, *Mater. Res. Bull.* **13**, 259–264 (1978).
C. Perrin, R. Chevrel, M. Sergent, and Ø. Fischer, *Máter. Res. Bull.* **14**, 1505–1515 (1979).
A. Perrin, R. Chevrel, M. Sergent, and Ø. Fischer, *J. Solid State Chem.* **33**, 43–47 (1980).
N. Pessall, R. E. Gold, and H. A. Johansen, *J. Phys. Chem. Solids* **29**, 19–38 (1968).
H. Pfisterer and K. Schubert, *Z. Metallk.* **41**, 358–367 (1950).
J. C. Phillips, *Physics of High-T_c Superconductors*. Academic Press, Boston, 1989.
A. Pialoux, M. L. Joyeux, and G. Cizeron, *J. Less-Common Met.* **87**, 1–19 (1982).
J. Y. Pivan, R. Guerin, E. H. El Ghadraoui, and M. Rafiq, *J. Less-Common Met.* **153**, 285–292 (1989).
E. G. Ponyatovskii and A. I. Zakharov, *Sov. Phys. Crystallogr.* **7**, 367–369 (1962).
M. Potel, R. Chevrel, M. Sergent, M. Decroux, and Ø. Fischer, *C. R. Acad. Sc. C* **288**, 429–432 (1979).
M. Potel, R. Chevrel, and M. Sergent, *Acta Crystallogr. B* **36**, 1545–1548 (1980).
M. Potel, R. Chevrel, and M. Sergent, *Acta Crystallogr. B* **37**, 1007–1010 (1981).
M. Potel, P. Gougeon, R. Chevrel, and M. Sergent, *Rev. Chim. Min.* **21**, 509–536 (1984).
K. Prassides, C. Christides, I. M. Thomas, J. Mizuki, K. Tanigaki, I. Hirosawa, and T. W. Ebbesen, *Science* **263**, 950–954 (1994).
M. F. Pye and P. G. Dickens, *Mater. Res. Bull.* **14**, 1397–1402 (1979).
M. V. Raevskaya, I. G. Sokolova, E. M. Sokolovskaya, G. N. Ronami, S. M. Kuznetsova, and V. A. Aleshina, *Moscow Univ. Chem. Bull.* **23**, 41–42 (1968).
S. Ramakhrisnan and G. Chandra, *Phys. Lett. A* **100**, 441–444 (1984).
S. E. Rasmussen and R. G. Hazell, *Acta Crystallogr. B* **35**, 1677–1679 (1979).
S. E. Rasmussen and B. Lundtoft, *Powder Diffr.* **2**, 29–30 (1987).
H. Rassaerts, H. Nowotny, G. Vinek, and F. Benesovsky, *Monatsh. Chem.* **98**, 460–468 (1967).
Ch. Raub, *Z. Metallk.* **55**, 195–199 (1964).
Ch. J. Raub, W. H. Zachariasen, T. H. Geballe, and B. T. Matthias, *J. Phys. Chem. Solids* **24**, 1093–1100 (1963).
Ch. J. Raub, V. B. Compton, T. H. Geballe, B. T. Matthias, J. P. Maita, and G. W. Hull, Jr., *J. Phys. Chem. Solids* **26**, 2051–2057 (1965).
J. P. Remeika, T. H. Geballe, B. T. Matthias, A. S. Cooper, G. W. Hull, and E. M. Kelly, *Phys. Lett. A* **24**, 565–566 (1967).
E. Revolinsky, G. A. Spiering, and D. J. Beerntsen, *J. Phys. Chem. Solids* **26**, 1029–1034 (1965).
E. Riedel, J. Pickardt, and J. Söchtig, *Z. anorg. allg. Chem.* **419**, 63–66 (1976).
D. L. Ritter, B. C. Giessen, and N. J. Grant, *Trans. Metall. Soc. AIME* **230**, 1259–1267 (1964).
C. Ritter, E. Gocke, C. Fischer, and R. Schöllhorn, *Mater. Res. Bull.* **27**, 1217–1225 (1992).
M. Robbins, R. H. Willens, and R. C. Miller, *Solid State Commun.* **5**, 933–934 (1967).
B. W. Roberts, *J. Phys. Chem. Ref. Data* **5**, 581–821 (1976).
F. Roeske, Jr., H. R. Shanks, and D. K. Finnermore, *Phys. Rev. B* **16**, 3929–3935 (1977).
R. Roesky, A. Meerschaut, J. Rouxel, and J. Chen, *Z. anorg. allg. Chem.* **619**, 117–122 (1993).
P. Rogl, *Monatsh. Chem.* **111**, 517–527 (1980).
P. Rogl, P. E. Potter, and H. R. Haines, *J. Nucl. Mater.* **149**, 283–288 (1987).
P. Rogl, H. Klesnar, and P. Fischer, *J. Am. Ceram. Soc.* **71**, C450–C452 (1988).
W. Rong-Yao, *J. Mater. Sci. Lett.* **5**, 87–88 (1986).
M. J. Rosseinsky, D. W. Murphy, R. M. Fleming, R. Tycko, A. P. Ramirez, T. Siegrist, G. Dabbagh, and S. E. Barrett, *Nature* **356**, 416–418 (1992).
M. J. Rosseinsky, D. W. Murphy, R. M. Fleming, and O. Zhou, *Nature* **364**, 425–427 (1993).
F. J. Rotella, H. E. Flotow, D. M. Gruen, and J. D. Jorgensen, *J. Chem. Phys.* **79**, 4522–4531 (1983).
S. Rundqvist, E. Hassler, and L. Lundvik, *Acta Chem. Scand.* **16**, 242–243 (1962).
V. Sadagapan and H. C. Gatos, *J. Phys. Chem. Solids* **27**, 235–238 (1966).
T. Sakai, G.-Y. Adachi, and J. Shiokawa, *J. Less-Common Met.* **84**, 107–114 (1982).
G. W. Samsonow and W. W. Morosow, *Monatsh. Chem.* ***102***, 1667–1678 (1971).

D. E. Sands, Q. C. Johnson, A. Zalkin, O. H. Krikorian, and K. L. Kromholtz, *Acta Crystallogr.* **15**, 832–834 (1962).
J. L. Sarrao, M. C. de Andrade, J. Herrmann, S. H. Han, Z. Fisk, M. B. Maple, and R. J. Cava, *Physica C* **229**, 65–69 (1994).
E. M. Savitskii, Yu. V. Efimov, Ch. Raub, and H. Khan, *Superconductivity in Alloys of Nobel Metals* (in Russian). Metallurgiya, Moscow, 1985.
E. M. Savitskiy, M. A. Tylkina, and O.Kh. Khamidov, *Russ. Metall.* **4**, 130–135 (1969).
O. Schob and E. Parthé, *Monatsh. Chem.* **95**, 1466–1472 (1964).
N. Schönberg, *Acta Chem. Scand.* **8**, 226–239 (1954).
A. J. Schultz, H. Horiuchi, and H. B. Krause, *Acta Crystallogr. C* **42**, 641–644 (1986a).
A. J. Schultz, H. H. Wang, J. M. Williams, and A. Filhol, *J. Am. Chem. Soc.* **108**, 7853–7855 (1986b).
H. Schulz and K. H. Thiermann, *Solid State Commun.* **23**, 815–819 (1977).
J. Schuster, E. Rudy, and H. Nowotny, *Monatsh. Chem.* **107**, 1167–1176 (1976).
U. Schwanitz-Schüller and A. Simon, *Z. Naturforsch. B* **40**, 710–716 (1985).
C. U. Segre, H. F. Braun and K. Yvon, in *Ternary Superconductors. Proc. Int. Conf.* (G. K. Shenoy, B. D. Dunlap, and F. Y. Fradin, Eds.), pp. 243–246. Elsevier North Holland, New York, 1981.
M. Sergent and R. Chevrel, *C. R. Acad. Sci. C* **274**, 1965–1967 (1972).
M. Sergent and R. Chevrel, *J. Solid State Chem.* **6**, 433–437 (1973).
M. Sergent, Ø. Fischer, M. Decroux, C. Perrin, and R. Chevrel, *J. Solid State Chem.* **22**, 87–92 (1977).
M. Sergent, R. Chevrel, C. Rossel, and Ø. Fischer, *J. Less-Common Met.* **58**, 179–193 (1978).
V. F. Shamrai, G. M. Leitus, and A. V. Tandid, *Sov. Phys. Crystallogr.* **32**, 671–673 (1987).
V. F. Shamrai, G. M. Leitus, and S. G. Zhukov, *Sov. Phys. Crystallogr.* **35**, 197–200 (1990).
B. D. Sharma and J. Donohue, *Z. Kristallogr.* **117**, 293–300 (1962).
R. N. Shelton, *J. Less-Common Met.* **62**, 191–196 (1978).
R. N. Shelton, A. C. Lawson, and D. C. Johnston, *Mater. Res. Bull.* **10**, 297–302 (1975).
R. N. Shelton, R. W. McCallum, and H. Adrian, *Phys. Lett. A* **56**, 213–214 (1976).
R. N. Shelton, A. C. Lawson, and K. Baberschke, *Solid State Commun.* **24**, 465–468 (1977).
R. N. Shelton, B. A. Karcher, D. R. Powell, R. A. Jacobson, and H. C. Ku, *Mater. Res. Bull.* **15**, 1445–1452 (1980).
R. N. Shelton, H. E. Horng, A. J. Bevolo, J. W. Richardson, R. A. Jacobson, S. D. Bader, and H. C. Hamaker, *Phys. Rev. B* **27**, 6703–6712 (1983).
R. P. Shibaeva and L. P. Rozenberg, *Sov. Phys. Crystallogr.* **33**, 834–837 (1988).
R. P. Shibaeva, V. F. Kaminskii, and V. K. Bel'skii, *Sov. Phys. Crystallogr.* **29**, 638–640 (1984).
R. P. Shibaeva, V. F. Kaminskii, and E. B. Yagubskii, *Mol. Cryst. Liq. Cryst.* **119**, 361–373 (1985).
R. P. Shibaeva, R. M. Lobkovskaya, E. B. Yagubskii, and E. E. Kostyuchenko, *Sov. Phys. Crystallogr.* **31**, 267–271 (1986).
I. Shirotani, G. Iwasaki, I. Kaneko, C. Sekine, S. Todo, and T. Yagi, *Solid State Commun.* **104**, 217–221 (1997).
O. I. Shulishova and I. A. Shcherbak, *Inorg. Mater.* **3**, 1304–1306 (1967).
T. Siegrist, R. J. Cava, J. J. Krajewski and W. F. Peck, Jr., *J. Alloys Comp.* **216**, 135–139 (1994a).
T. Siegrist, H. W. Zandbergen, R. J. Cava, J. J. Krajewski, and W. F. Peck, Jr., *Nature* **367**, 254–256 (1994b).
A. Simon, *Angew. Chem. Int. Ed. Engl.* **36**, 1788–1806 (1997).
A. Simon, Hj. Mattausch, R. Eger, and R. K. Kremer, *Angew. Chem. Int. Ed. Engl.* **30**, 1188–1189 (1991).
A. Simon, A. Yoshiasa, M. Bäcker, R. W. Henn, C. Felser, R. K. Kremer, and Hj. Mattausch, *Z. anorg. allg. Chem.* **622**, 123–137 (1996).
A. W. Sleight, J. L. Gillson, and P. E. Bierstedt, *Solid State Commun.* **17**, 27–28 (1975).
Yu. M. Smirnov and V. A. Finkel', *Sov. Phys. JETP* **22**, 750–753 (1966).
T. F. Smith and H. L. Luo, *J. Phys. Chem. Solids* **28**, 569–576 (1967).
J. F. Smith and V. L. Schneider, *J. Less-Common Met.* **7**, 17–22 (1964).
G. S. Smith, A. G. Tharp and Q. Johnson, *Acta Crystallogr. B* **25**, 698–701 (1969).

J. L. Smith, Z. Fisk, J. O. Willis, A. L. Giorgi, R. B. Roof, H. R. Ott, H. Rudigier, and E. Felder, *Physica B* **135**, 3–8 (1985).
R. B. Somoano, V. Hadek, and A. Rembaum, *J. Chem. Phys.* **58**, 697–701 (1973).
R. B. Somoano, V. Hadek, A. Rembaum, S. Samson, and J. A. Woollam, *J. Chem. Phys.* **62**, 1068–1073 (1975).
R. E. Somekh and J. E. Evetts, *Solid State Commun.* **24**, 733–737 (1977).
F. H. Spedding, A. H. Daane, and K. W. Herrmann, *Acta Crystallogr.* **9**, 559–563 (1956).
F. H. Spedding, K. Gschneidner, Jr., and A. H. Daane, *J. Am. Chem. Soc.* **80**, 4499–4503 (1958).
F. J. Spooner and C. G. Wilson, *Acta Crystallogr.* **17**, 1533–1538 (1964).
J. Staun Olsen, L. Gerward, S. Steenstrup, and E. Johnson, *J. Appl. Crystallogr.* **27**, 1002–1005 (1994).
R. Steadman and P. M. Nuttall, *Acta Crystallogr.* **17**, 62–63 (1964).
F. Steglich, J. Aarts, C. D. Bredl, W. Lieke, D. Meschede, W. Franz, and H. Schäfer, *Phys. Rev. Lett.* **43**, 1892–1896 (1979).
P. W. Stephens, L. Mihaly, P. L. Lee, R. L. Whetten, S.-M. Huang, R. Kaner, F. Deiderich, and K. Holczer, *Nature* **351**, 632–634 (1991).
P. W. Stephens, G. Bortel, G. Falgel, M. Tegze, A. Jánossy, S. Pekker, G. Oszlanyl, and L. Forró, *Nature* **370**, 636–639 (1994).
G. R. Stewart and A. L. Giorgi, *Solid State Commun.* **28**, 969–972 (1978).
R. P. Stratton and W. J. Kitchingman, *Acta Crystallogr.* **17**, 1471 (1964).
B. Stritzker, *Z. Phys.* **268**, 261–264 (1974).
O. A. W. Strydom and L. Alberts, *J. Less-Common Met.* **22**, 511–515 (1970).
G. V. Subba Rao, M. W. Shafer, S. Kawarazaki, and A. M. Toxen, *J. Solid State Chem.* **9**, 323–329 (1974).
G. V. Subba Rao, K. Wagner, G. Balakrishnan, J. Janaki, W. Paulus, R. Schöllhorn, V. S. Subramanian, and U. Poppe, *Bull. Mater. Sci. India* **7**, 215–228 (1985).
C. Susz, R. Flükiger, J. L. Jorda, J. Muller, and R. M. Waterstrat, *J. Less-Common Met.* **63**, P45–P52 (1979).
A. R. Sweedler and D. E. Cox, *Phys. Rev. B* **12**, 147–156 (1975).
E. G. Szklarz and A. L. Giorgi, *J. Less-Common Met.* **81**, 349–351 (1981).
H. Takei, M. Yamawaki, A. Oota, and S. Noguchi, *J. Phys. F* **15**, 2333–2338 (1985).
Y. Takéuchi and W. Nowacki, *Schweiz. Mineral. Petrogr. Mitt.* **44**, 105–120 (1964).
K. Tanigaki, I. Hirosawa, T. W. Ebbesen, J. Mizuki, Y. Shimakawa, Y. Kubo, J. S. Tsai, and S. Kuroshima, *Nature* **356**, 419–421 (1992).
J. M. Tarascon and G. W. Hull, *Mater. Res. Bull.* **21**, 859–869 (1986).
J. M. Tarascon, J. V. Waszczak, G. W. Hull, Jr., F. J. DiSalvo, and L. D. Blitzer, *Solid State Commun.* **47**, 973–979 (1983).
J. M. Tarascon, F. J. DiSalvo, D. W. Murphy, G. W. Hull, E. A. Rietman, and J. V. Waszczak, *J. Solid State Chem.* **54**, 204–212 (1984a).
J. M. Tarascon, F. J. DiSalvo, D. W. Murphy, G. Hull, and J. V. Waszczak, *Phys. Rev. B* **29**, 172–180 (1984b).
J. M. Tarascon, G. W. Hull, and F. J. DiSalvo, *Mater. Res. Bull.* **19**, 915–924 (1984c).
J. M. Tarascon, G. W. Hull, and J. V. Waszczak, *Mater. Res. Bull.* **20**, 935–946 (1985).
A. Taylor, B. J. Kagle, and N. J. Doyle, *J. Less-Common Met.* **5**, 26–40 (1963).
L. R. Testardi, J. H. Wernick, and W. A. Royer, *Solid State Commun.* **15**, 1–4 (1974).
L. E. Toth, V. F. Zackay, M. Wells, J. Olson, and E. R. Parker, *Acta Metall.* **13**, 379–385 (1965).
W. Trinkl, S. Corsépius, and G. R. Stewart, *J. Alloys Comp.* **240**, 96–100 (1996).
W. Trzebiatowski and J. Niemiec, *Rocz. Chem.* **29**, 277–283 (1955).
M. A. Tylkina, E. M. Savitskiy, and V. E. Alyushin, *Russ. Metall.* **4**, 159–162 (1973).
A. M. Umarji, G. V. Subba Rao, M. P. Janawadkar, and T. S. Radhakrishnan, *J. Phys. Chem. Solids* **41**, 421–429 (1980).
H. Urayama, H. Yamochi, G. Saito, S. Sato, A. Kawamoto, J. Tanaka, T. Mori, Y. Maruyama, and H. Inokuchi, *Chem. Lett.* 463–466 (1988).

M. H. van Maaren and G. M. Schaeffer, *Phys. Lett.* **20**, 131 (1966).
N. H. van Maaren, G. M. Schaeffer, and F. K. Lotgering, *Phys. Lett. A* **25**, 238–239 (1967).
E. C. van Reuth and R. M. Waterstrat, *Acta Crystallogr. B* **24**, 186–196 (1968).
J. M. Vandenberg, *Mater. Res. Bull.* **15**, 835–847 (1980).
J. M. Vandenberg and H. Barz, *Mater. Res. Bull.* **15**, 1493–1498 (1980).
J. M. Vandenberg and B. T. Matthias, *Proc. Natl. Acad. Sci. USA* **74**, 1336–1337 (1977).
G. Venturini, M. Méot-Meyer, E. McRae, J. F. Marêché, and B. Roques, *Mater. Res. Bull.* **19**, 1647–1652 (1984).
G. Venturini, M. Kamta, E. McRae, J. F. Marêché, B. Malaman, and B. Roques, *Mater. Res. Bull.* **21**, 1203–1208 (1986).
G. Venturini, B. Malaman, and B. Roques, *J. Less-Common Met.* **152**, 51–66 (1989).
P. Villars, *Pearson's Handbook*, Vols. 1, 2. ASM International, Materials Park, OH 44073, 1997.
F. W. von Batchelder and R. F. Raeuchle, *Acta Crystallogr.* **10**, 648–649 (1957).
S. V. Vonsovsky, Yu. A. Izyumov, and E. Z. Kurmaev, *Superconductivity of Transition Metals, Springer Series in Solid-State Sciences*, Vol. 27. Springer-Verlag, Berlin, 1982.
V. D. Vorob'ev and V. A. Mel'nikova, *Sov. Phys. Crystallogr.* **19**, 397 (1974).
H. H. Wang, M. A. Beno, U. Geiser, M. A. Firestone, K. S. Webb, L. Nunez, G. W. Crabtree, K. D. Carlson, J. M. Williams, L. J. Azevedo, J. F. Kwak, and J. E. Schirber, *Inorg. Chem.* **24**, 2465–2466 (1985).
D. R. Wanlass and M. J. Sienko, *J. Solid State Chem.* **12**, 362–369 (1975).
Y. Watanabe, H. Iwasaki, and H. Takei, *Acta Crystallogr. C* **40**, 1644–1646 (1984).
Y. Watanabe, H. Iwasaki, H. Iwasaki, and Y. Muto, *Acta Crystallogr. C* **42**, 1469–1472 (1986).
R. M. Waterstrat, F. Haenssler, and J. Müller, *J. Appl. Phys.* **50**, 4763–4766 (1979).
S. T. Weir, Y. K. Vohra, and A. L. Ruoff, *Phys. Rev. B* **36**, 4543–4546 (1987).
R. H. Willens, E. Buehler, and B. T. Matthias, *Phys. Rev.* **159**, 327–330 (1967).
J. M. Williams, T. J. Emge, H. H. Wang, M. A. Beno. P. T. Copps, L. N. Hall, K. D. Carlson, and G. W. Crabtree, *Inorg. Chem.* **23**, 2558–2560 (1984a).
J. M. Williams, H. H. Wang, M. A. Beno, T. J. Emge, L. M. Sowa, P. T. Copps, F. Behroozi, L. N. Hall, K. D. Carlson, and G. W. Crabtree, *Inorg. Chem.* **23**, 3839–3841 (1984b).
J. M. Williams, A. M. Kini, U. Geiser, H. H. Wang, K. D. Carlson, W. K. Kwok, K. G. Vandervoort, J. E. Thompson, D. L. Stupka, D. Jung, and M.-H. Whangbo, in *Organic Superconductivity* (V. Z. Kresin and W. A. Little, Eds.), pp. 39–50. Plenum, New York, 1990a.
J. M. Williams, A. M. Kini, H. H. Wang. K. D. Carlson, U. Geiser, L. K. Montgomery, G. J. Pyrka, D. M. Watkins, J. M. Kommers, S. J. Boryschuk, A. V. Strieby Crouch, W. K. Kwok, J. E. Schirber, D. L. Overmyer, D. Jung and M.-H. Whangbo, *Inorg. Chem.* **29** 3272–3274 (1990b).
J. M. Williams, J. R. Ferraro, R. J. Thorn, K. D. Carlson, U. Geiser, H. H. Wang, A. M. Kini, and M.-H. Whangbo, *Organic Superconductors (Including Fullerenes)*. Prentice Hall, Englewood Cliffs, NJ, 1992.
C. G. Wilson, *Acta Crystallogr.* **16**, 724–730 (1963).
E. A. Wood and V. B. Compton, *Acta Crystallogr.* **11**, 429–433 (1958).
S. Wüchner, N. Keller, J. L. Tholence, and J. Flouquet, *Solid State Commun.* **85**, 355–360 (1993).
W. Xian-Zhong, B. Chevalier, J. Etourneau, and P. Hagenmuller, *Mater. Res. Bull.* **20**, 517–523 (1985).
H. D. Yang, R. N. Shelton, and H. F. Braun, *Phys. Rev. B* **33**, 5062–5065 (1986).
F. Yang, N. Tang, J. Wang, W. Qin, Z.-X. Li, and J. Luo, *J. Phys. Condens. Matter.* **7**, 2369–2373 (1995).
J. Ye, T. Shishido., T. Kimura, T. Matsumoto, and T. Fukuda, *Acta Crystallogr. C* **52**, 2652–2655 (1996).
T. Yildirim, O, Zhou, J. E. Fischer, N. Bykovetz, R. A. Strongin, M. A. Cichy, A. B. Smith III, C. L. Lin, and R. Jelinek, *Nature* **360**, 568–571 (1992).
S.-C. Yu, I. L. Spain, and E. F. Skelton, *J. Appl. Phys.* **49**, 4741–4745 (1978).
K. Yvon, *Acta Crystallogr. B* **30**, 853–861 (1974).
K. Yvon, in *Current Topics in Materials Science 3* (E. Kaldis, Ed.), pp. 53–129. North-Holland, Amsterdam, 1979.

K. Yvon and A. Grüttner, in *Superconductivity in d- and f-Band Metals* (H. Suhl and M. B. Maple, Eds.), pp. 515–519. Academic Press, New York, 1980.
K. Yvon and D. C. Johnston, *Acta Crystallogr. B* **38**, 247–250 (1982).
K. Yvon, A. Paoli, R. Flükiger, and R. Chevrel, *Acta Crystallogr. B.* **33**, 3066–3072 (1977).
K. Yvon, R. Baillif, and R. Flükiger, *Acta Crystallogr. B* **35**, 2859–2863 (1979).
K. Yvon, R. Chevrel, and M. Sergent, *Acta Crystallogr. B* **36**, 685–687 (1980).
W. H. Zachariasen, *Acta Crystallogr.* **5**, 17–19 (1952).
H. W. Zandbergen and R. J. Cava, *Nature* **374**, 682 (1995).
H. W. Zandbergen, R. J. Cava, J. J. Krajewski, and W. F. Peck, Jr., *J. Solid State Chem.* **110**, 196–199 (1994a).
H. W. Zandbergen, J. Jansen, R. J. Cava, J. J. Krajewski, and W. F. Peck, Jr., *Nature* **372**, 759–761 (1994b).
H. W. Zandbergen, W. G. Sloof, R. J. Cava, J. J. Krajewski, and W. F. Peck, Jr., *Physica C* **226**, 365–376 (1994c).
H. W. Zandbergen, E. J. van Zwet, J. C. Sarrac, M. C. de Andrade, J. Hermann, S. H. Han, Z. Fisk, M. B. Maple, and R. J. Cava, *Physica C* **229**, 29–34 (1994d).
S. T. Zegler, *Phys. Rev.* **137** A1438–A1440 (1965).
O. Zhou, J. E. Fischer, N. Coustel, S. Kycia, Q. Zhu, A. R. McGhie, W. J. Romanow, J. P. McCauley, Jr., A. B. Smith III, and D. E. Cox, *Nature* **351**, 462–464 (1991).
O. Zhou, R. M. Fleming, D. W. Murphy, M. J. Rosseinsky, A. P. Ramirez, R. B. van Dover, and R. C. Haddon, *Nature* **362**, 433–435 (1993).
Q. Zhu, D. E. Cox, and J. E. Fischer, *Phys. Rev. B* **51**, 3966–3969 (1995).
N. N. Zhuravlev, *Sov. Phys. JETP* **5**, 1064–1072 (1957).
N. N. Zhuravlev, *Sov. Phys. JETP* **7**, 571–573 (1958).
N. N. Zhuravlev and V. P. Melik-Adamyan, *Sov. Phys. Crystallogr.* **6**, 99–100 (1961).
N. N. Zhuravlev, T. A. Mingazin, and G. S. Zhdanov, *Sov. Phys. JETP* **7**, 566–571 (1958).
N. N. Zhuravlev, G. S. Zhdanov, and Ye. M. Smirnova, *Phys. Met. Metallogr.* **13**, 55–61 (1962).
E. Zintl and A. Harder, *Z. Phys. Chem. B* **16**, 206–212 (1932).

Chapter 7

Cuprates

Charles P. Poole Jr
Department of Physics and Astronomy and Institute of Superconductivity, University of South Carolina, Columbia, South Carolina

Frank J. Owens
Army Armament Research, Engineering, and Development Center, Picatinny, New Jersey, and Department of Physics, Hunter College, City University of New York, New York

A Introduction

The previous two chapters discussed the classical and the more recently discovered types of superconductor, meaning all major classes of superconductors except the cuprates, and now we turn to examine this last group. The present chapter emphasizes overall characteristics of cuprates, and the next chapter provides crystallographic data on specific compounds. The general features arise from the layered structure involving the alternation between conduction slabs and binding slabs, with each slab consisting of one or more individual layers of atoms. We begin the chapter by delineating this arrangement. Then we

ISBN: 0-12-561460-8
$30.00
HANDBOOK OF SUPERCONDUCTIVITY

TABLE 7.1

Crystallographic characteristics of the main families of the cuprates, where Z is the number of atoms in the unit cell, A denotes aligned, and S staggered CuO_2 layers. Lattice constants a_0 and c_0 are in angstrom units. For orthorhombic compounds $a_0 = \frac{1}{2}(a + b)$ and $\%\text{Anis} = 200(b - a)/(b + a)$.

Compound	Symbol	Space group	Pearson code	Type	Z	a_0	c_0	%Anis	T_c
$La_{1.85}Sr_{0.15}CuO_4$	0201	I4/mmm	iT14	S	2	3.779	13.23	0	37.5
$La_{1.85}Sr_{0.15}CuO_4$	0201	Bmab	oS28	S	4	$3.782\sqrt{2}$	13.18	0.57	37.5
$YBa_2Cu_3O_6$	1212	P4/mmm	tP12	A	1	3.857	11.79	0	—
$YBa_2Cu_3O_7$	1212	Pmmm	oP13	A	1	3.853	11.68	1.68	91
$TlBa_2CaCu_2O_7$	1212	P4/mmm	tP13	A	1	3.847	12.72	0	80
$TlBa_2Ca_2Cu_3O_9$	1223	P4/mmm	tP17	A	1	3.808	15.23	0	120
$TlBa_2Ca_3Cu_4O_{11}$	1234	P4/mmm	tP21	A	1	3.848	19.00	0	114
$HgBa_2CuO_4$	1201	P4/mmm	tP8	A	1	3.881	9.53	0	95
$HgBa_2CaCu_2O_6$	1212	P4/mmm	tP12	A	1	3.858	12.66	0	114
$HgBa_2Ca_2Cu_3O_8$	1223	P4/mmm	tP16	A	1	3.850	15.78	0	133
$HgBa_2Ca_3Cu_4O_{10}$	1234	P4/mmm	tP20	A	1	3.853	18.97	0	125
$HgBa_2Ca_4Cu_5O_{12}$	1245	P4/mmm	tP24	A	1	3.852	22.10	0	101
$HgBa_2Ca_5Cu_6O_{14}$	1256	P4/mmm	tP28	A	1	3.852	25.33	0	114
$Bi_2Sr_2CuO_6$	2201	Amaa	oS44	S	4	$3.796\sqrt{2}$	24.62	0.22	9
$Bi_2Sr_2CaCu_2O_8$	2212	A2aa	oS60	S	4	$3.829\sqrt{2}$	30.86	0.018	92
$Bi_2Sr_2Ca_2Cu_3O_{10}$	2223	A2aa	oS76	S	4	$3.83\sqrt{2}$	37.07	0.23	110
$Tl_2Ba_2CuO_6$	2201	I4/mmm	tI122	S	2	3.866	23.24	0	90
$Tl_2Ba_2CaCu_2O_8$	2212	I4/mmm	tI30	S	2	3.855	29.32	0	110
$Tl_2Ba_2Ca_2Cu_3O_{10}$	2223	I4/mmm	tI38	S	2	3.850	35.88	0	125
$Tl_2Ba_2Ca_3Cu_4O_{12}$	2234	I4/mmm	tI46	S	2	3.849	40.05	0	109
$YBa_2Cu_4O_8$	—	Ammm	oS30	—	2	3.8	27.24	0.80	80

describe the roles of the conduction and binding slabs and differentiate particular types of cuprates. We end with some comments on infinite layer phases. Table 7.1 summarizes the crystallographic characteristics of the compounds discussed here.

Many authors use the notation "conduction and binding layers," with each layer comprising "individual planes of atoms." Our notation "conduction and binding slabs" consisting of "layers of atoms" is consistent with that used in the next chapter.

B

Multislab Structure

All of the cuprates have the same ordered arrangement of slabs parallel to each other, and stacked along the c axis. This multislab structure is summarized in a general way in Fig. 7.1, and sketched with actual atom positions for the thallium

Fig. 7.1.

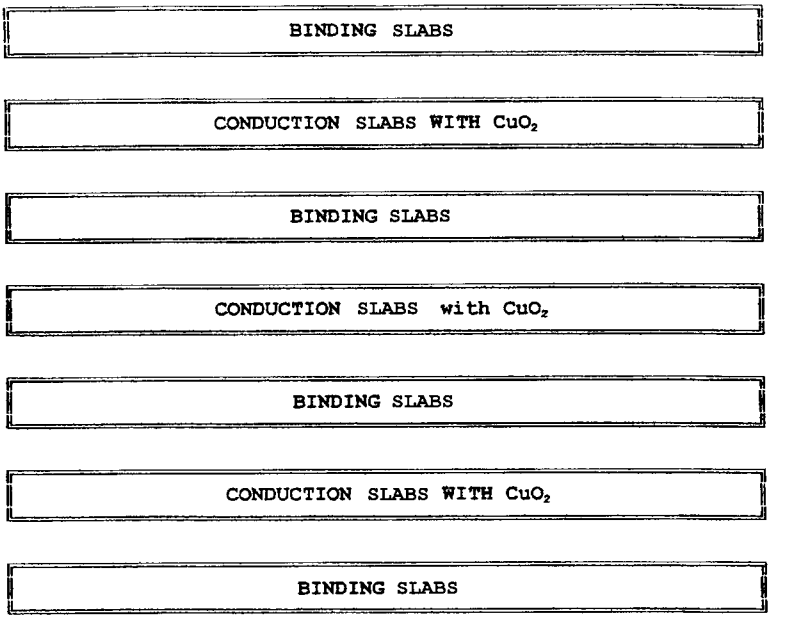

Layering scheme of the cuprate superconductors. Figure 7.4 shows details of the conduction slabs for different sequences of copper oxide layers, and Figs. 7.5 and 7.6 present details of the binding slabs for several cuprates. [Owens and Poole, 1996, p. 99.]

series of compounds in Fig. 7.2. Both figures show that there are alternating conduction slabs where the super current flows and binding slabs that hold together the conduction slabs. The conduction slabs consist of copper oxide (CuO_2) layers with each copper ion Cu^{2+} surrounded by four oxygen ions O^{2-} and each oxygen bonded to two coppers, as illustrated in Fig. 7.3. The conduction slabs have one, two, three, or more CuO_2 layers, and for $n > 1$ the layers are held in place within the slab by calcium Ca^{2+} ions located between them, as shown in Fig. 7.4, with the exception of $YBa_2Cu_3O_7$, in which the intervening cations are yttrium, Y^{3+}, instead of calcium. The ease of current flow along the CuO_2 layers of the slabs, compared to flow in the perpendicular direction, helps to explain the anisotropic properties of the cuprates.

Each particular cuprate compound has its own specific binding slab, consisting mainly of layers of metal oxides (MO). Figure 7.5 gives the layer sequences within these slabs for compounds in which the layers are odd in number, and Fig. 7.6 sketches the even cases. The odd case is called aligned because the copper ions of all the conduction slabs are arranged one above the other along the c axis. In other words, the CuO_2 layers of successive conduction slabs stack in alignment. The barium ions are also aligned above one another along c, and to emphasize this they are all listed in Fig. 7.5 as BaO groups. In

Fig. 7.2.

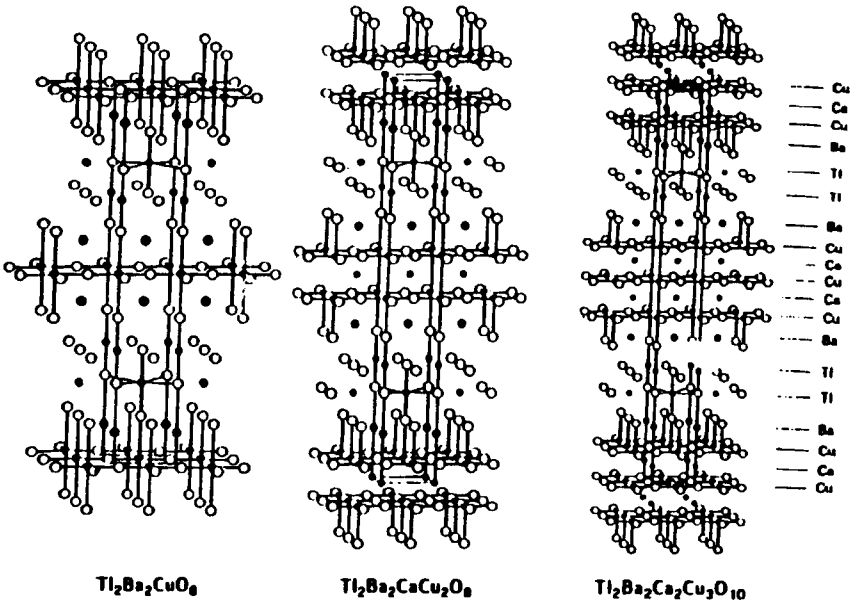

Crystal structures of the $Tl_2Ba_2Ca_{n-1}Cu_nO_{2n+4}$ compounds with $n = 1, 2, 3$, arranged to display the layering schemes. The $Bi_2Sr_2Ca_{n-1}Cu_nO_{2n+4}$ compounds have the same respective structures. [Courtesy of C. C. Torardi; see Poole *et al.* 1988, p. 106.]

Fig. 7.3.

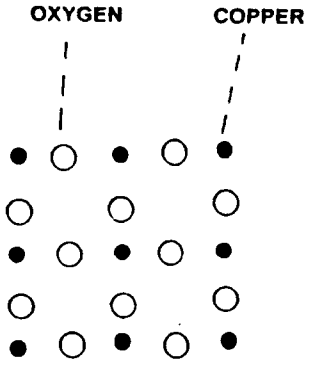

Arrangement of copper and oxygen ions in a CuO_2 layer of a conduction slab. [Owens and Poole, 1996, p. 99.]

Fig. 7.4.

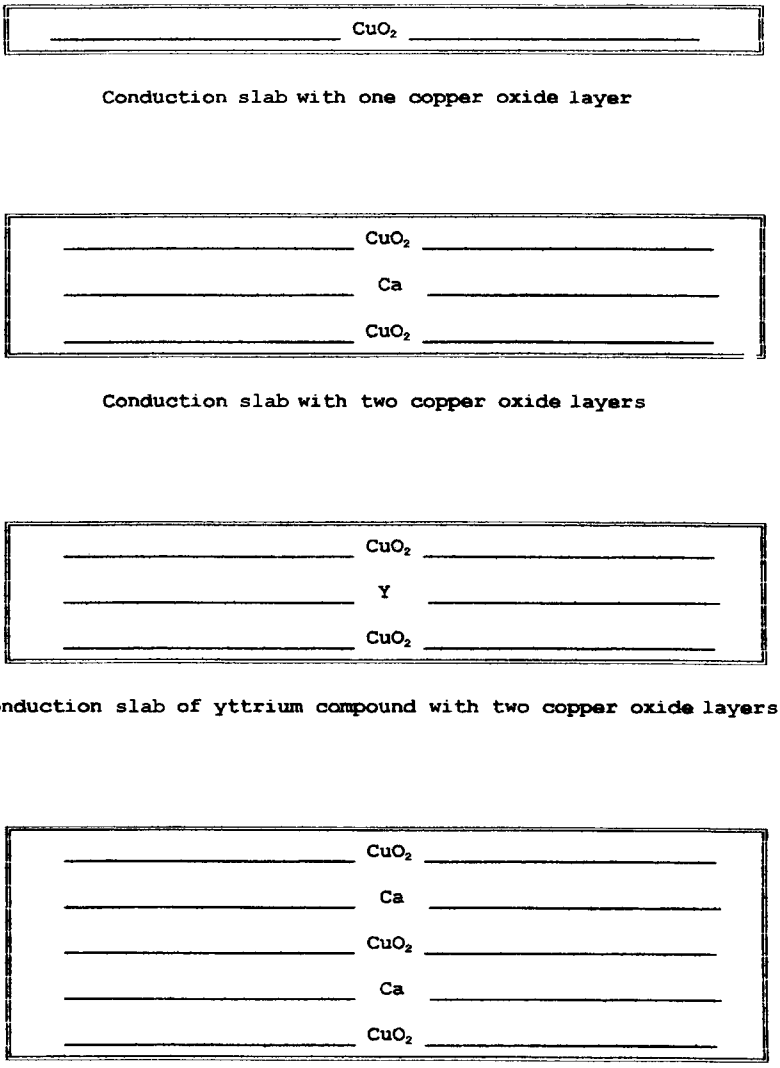

Conduction slabs of the various cuprate superconductors showing sequences of CuO_2 and Ca (or Y) layers in the conduction slabs of Fig. 7.1. [Owens and Poole, 1996, p. 100.]

contrast to this, in the even case, each binding slab has half MO and half OM groups for each metal ion M. Thus, the even thallium compounds $Tl_2Ba_2Ca_{n-1}Cu_nO_{2n+4}$ have BaO, OTl, TlO, and OBa arrangements within the binding slab sketched at the bottom of Fig. 7.6. Within the individual conduction

Fig. 7.5.

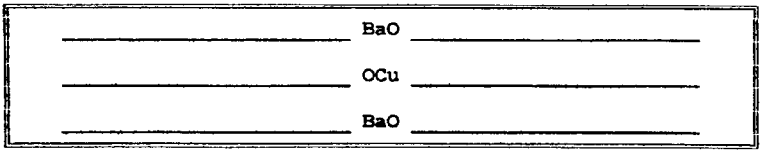

Yttrium Superconductor $YBa_2Cu_3O_7$

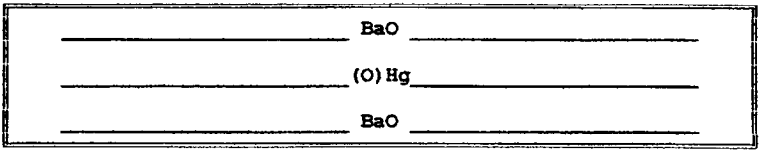

Mercury Superconductor $HgBa_2Ca_{n-1}Cu_nO_{2n+2}$

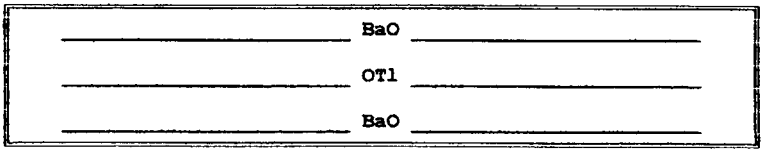

Thallium Superconductor $TlBa_2Ca_{n-1}Cu_nO_{2n+3}$

Sequences of MO layers in the binding slabs of aligned compounds, where M stands for various metal ions. The parentheses around the oxygen atom O in the middle panel indicate partial occupancy.

slabs of even compounds all of the Cu ions are still one above the other as in Fig. 7.4, but now successive conduction slabs of the even compounds are staggered with respect to each other, with the copper ions of a particular conduction slab at *xy* sites occupied by oxygens of the adjacent conduction slabs above and below, as can be seen easily in Fig. 7.2. This staggering or alternation in alignment of conduction slabs occurs because the even compounds are structurally body-centered (BC), as we explain in the next section.

Fig. 7.6.

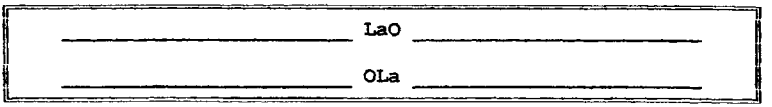

Lanthanum Superconductor La_2CuO_4

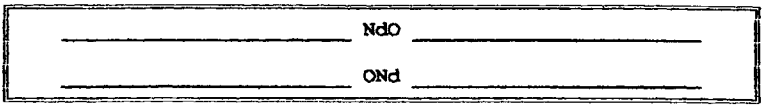

Neodymium (electron) Superconductor Nd_2CuO_4

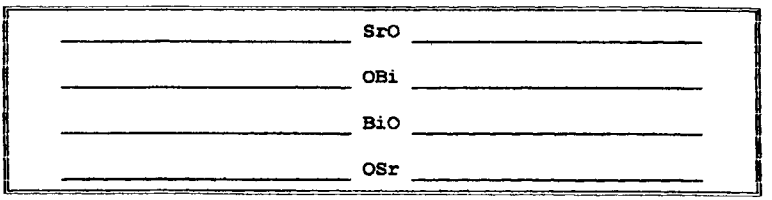

Bismuth Superconductor $Bi_2Sr_2Ca_{n-1}Cu_nO_{2n+4}$

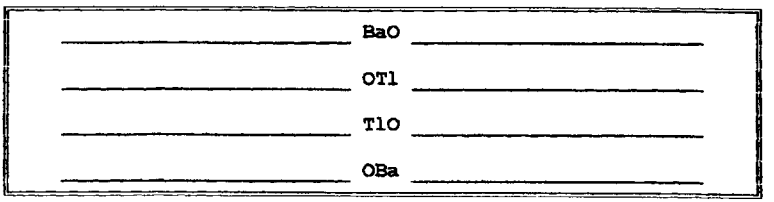

Thallium Superconductor $Tl_2Ba_2Ca_{n-1}Cu_nO_{2n+4}$

Sequences of MO layers in the binding slabs of body-centered compounds, where M stands for various metal ions indicated on the figure.

C

Aligned and Body-Centered Types

Each atom in a high-temperature superconductor occupies an edge (E) site on the edge (0, 0, z), a face (F) site on the midline of a face (0, $\frac{1}{2}$, z) or ($\frac{1}{2}$, 0, z), or a centered (C) site at the center vertical axis ($\frac{1}{2}$, $\frac{1}{2}$, z) of the unit cell. The atoms in a particular horizontal layer can be designated by the notation [E F C], where, for example, a copper oxide layer with copper at edge sites and the oxygens at face

Fig. 7.7.

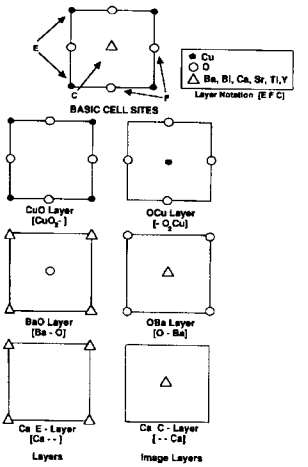

Types of atom positions in the layers of a high-temperature superconductor structure, using the edge, face, center notation [E F C]. Typical occupancies are given in the upper right. [Poole *et al.* 1995, p. 181.]

Fig. 7.8.

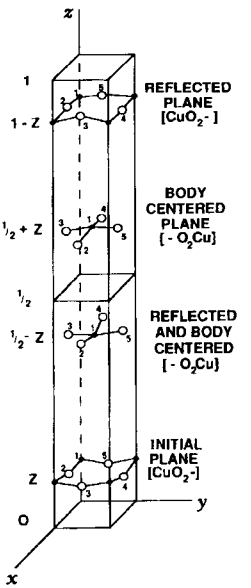

Body-centered tetragonal unit cell containing four puckered CuO_2 groups showing how the initial group (bottom) is replicated by reflecting in the horizontal reflection plane σ_h at $z = \frac{1}{2}$, by the body centering operation, and by both. [Poole *et al.* 1995, p. 188.]

sites is designated [Cu O_2 —]. The complementary layer [— O_2 Cu] has copper in the centered sites. Figure 7.7 illustrates the notation for several commonly occurring layers.

All of the cuprates under discussion have a horizontal reflection plane, σ_h at the center of the unit cell, and σ_h planes at the top and bottom of the cell. This means that each atom in the lower half of the unit cell ($z < \frac{1}{2}$) at the position x, y, z has a counterpart in the upper half of the cell ($z > \frac{1}{2}$) at the position

$$x \Rightarrow x, \qquad y \Rightarrow y, \qquad z \Rightarrow 1 - z \tag{1}$$

Atoms exactly on the σ_h symmetry planes only occur once since they cannot be reflected. Figure 7.8 shows a layer at a height z reflected to the height $1 - z$. This symmetry operation preserves the structure of the layer, i.e., a [Ba — O] layer reflects to [Ba — O] under σ_h.

The even-type cuprates have, in addition to the σ_h plane, the body centering operation, whereby every atom at a position x, y, z generates another atom at the following position:

$$x \Rightarrow x \pm \tfrac{1}{2}, y \Rightarrow y \pm \tfrac{1}{2}, z \Rightarrow z \pm \tfrac{1}{2}. \tag{2}$$

Thus, a layer at the height z forms an image layer at the height $z \pm \frac{1}{2}$ in which the edge atoms become centered, the centered ones become edge types, and each face atom moves to another face site. The signs in these operations are selected so that the generated points and layers remain within the unit cell. Thus, if z is less than $\frac{1}{2}$, the plus sign must be selected, viz. $z \Rightarrow z + \frac{1}{2}$, etc. The body centering operation converts [Cu O_2 —] and [— O_2 Cu] conduction layers into each other. Figure 7.8 illustrates these symmetry features, whereby for both aligned and body-centered compounds an initial [Cu O_2 —] layer at a vertical position $z < \frac{1}{2}$ has a reflection layer [Cu O_2 —] at the height $1 - z$. Body-centered compounds generate two additional layers, namely, a [— O_2 Cu] layer at the height $\frac{1}{2} + z$ and another [— O_2 Cu] layer at the height $\frac{1}{2} - z$, in which the Cu ions are out of alignment because of the interchange of edge and center positions,

Fig. 7.9.

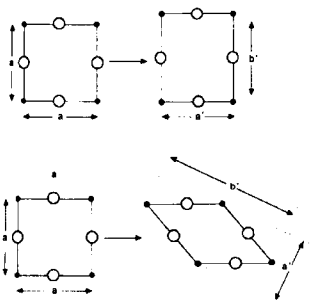

Rectangular (top) and rhombal (bottom) type distortions of a tetragonal unit cell of width a to an orthorhombic cell of dimensions a', b'. [Poole et al. 1995, p. 177.]

TABLE 7.2

Superconducting transition temperatures of the cuprates containing $n = 1, 2$ and 3 copper oxide layers in their conduction slabs. Some compounds have aligned (alig) and others have body-centered (BC) crystallographic structures

Compound	Type	Formula	$n = 1$	$n = 2$	$n = 3$
Bismuth	BC	$Bi_2Sr_2Ca_{n-1}Cu_nO_{2n+4}$	9	92	110
Thallium	Alig	$TlBa_2Ca_{n-1}Cu_nO_{2n+3}$	9	80	120
Thallium	BC	$Tl_2Ba_2Ca_{n-1}Cu_nO_{2n+4}$	90	110	125
Mercury	Alig	$HgBa_2Ca_{n-1}Cu_nO_{2n+2+\delta}$	95	114	133

as shown. The aligned compounds have one formula unit per unit cell, and the body-centered ones have two formula units per unit cell. Table 7.2 identifies the cuprates of each type and gives their transition temperatures. We see from this table that increasing the number of n of CuO_2 layers in the conduction slabs raises T_c, but unfortunately T_c begins to decrease for further increases in this number beyond 3. Some cuprates are tetragonal and others are orthorhombic because of either rectangular or rhombic distortion, as illustrated in Fig. 7.9. Rhombic distortion increases the a, b lattice parameters by $\sqrt{2}$ and doubles the number of formula units per unit cell.

Consider an aligned cuprate with n atoms per formula unit, which also means n atoms per unit cell. If its structure is tetragonal it is probably in space group $P4/mmm$ (#123, D^1_{4h}) with the Pearson code of tPn, and if it has undergone a rectangular distortion to orthorhombic it is in space group $Pmmm$ (#47, D^1_{2h}) with the Pearson code oPn. A rhombic distortion could produce the orthorhombic space group $Cmmm$ (#65, D^{19}_{2h}) with the Pearson code oS2n. A body-centered cuprate with n atoms per formula unit has $2n$ atoms in the unit cell. If it is tetragonal it is in space group $I4/mmm$ (#139, D^{17}_{4h}) with the Pearson code tI2n. A rhombic distortion could bring it to the orthorhombic space group Azaa

TABLE 7.3

Ionic radii for some selected elements. See Table VI-2 of our earlier work (1988) for a more extensive list

Small	Cu^{2+}	0.72 Å	Bi^{5+}	0.74 Å
Small–medium	Cu^{+}	0.96 Å	Y^{3+}	0.89 Å
	Bi^{3+}	0.96 Å	Tl^{3+}	0.95 Å
	Ca^{2+}	0.99 Å		
	Nd^{3+}	0.995 Å		
Medium–large	Hg^{2+}	1.10 Å	La^{3+}	1.06 Å
	Sr^{2+}	1.12 Å		
	Pb^{2+}	1.20 Å	Ag^{+}	1.26 Å
Large	K^{+}	1.33 Å	O^{2-}	1.32 Å
	Na^{2+}	1.34 Å	F^{-}	1.33 Å

Fig. 7.10.

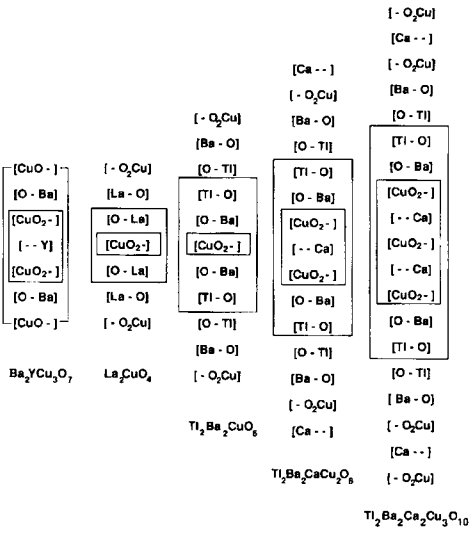

Unit cells of various high-temperature superconductors showing the layering schemes. Conduction slabs are enclosed in small, inner boxes, and the groupings of slabs that make up a formula unit are enclosed in larger boxes. The Bi–Sr compounds $Bi_2Sr_2Ca_{n-1}Cu_nO_{2n+4}$ have the same layering schemes as their Tl–Ba counterparts shown in this figure. [Poole *et al.*, 1995, p. 195.]

(#37, C_{2v}^{13}) with the Pearson Code oS4n. Chapter 8 describes these various structures for the cuprates, and the Pearson code notation is explained in Sections 5,C and 6,A,d.

The atoms are distributed in the slabs in a manner that permits efficient stacking of layers one above the other. The size of an ion determines how it can substitute in a crystal structure, and Table 7.3 lists the ionic sizes of some elements that appear commonly in the cuprates. Steric effects prevent large atoms such as Ba (1.34 Å) and O (1.32 Å) from overcrowding a slab, and from aligning directly on top of each other in adjacent layers. Stacking occurs in accordance with two empirical rules:

1. Metal ions can occupy either edge or centered sites, and in adjacent layers they alternate between E and C sites.
2. Oxygens can be found on any type of site, but can occupy only one type in a particular layer, and in adjacent layers they must be on different types of sites.

Figure 7.10 illustrates these rules for several cuprates using the [E C F] notation explained in Fig. 7.7. Puckering or symmetry lowering from tetragonal to orthorhombic can provide more room for the atoms. The side-centered $YBa_2Cu_4O_8$ and intergrowth $YBa_2Cu_7O_{15}$ compounds do not follow these rules, as will be explained later.

D

Role of the Binding Slab

These binding slabs sketched in Figs. 7.2, 7.5, and 7.6 are sometimes called charge reservoir slabs because they contain the source of charge that brings about the hole (h^+) doping of the conduction layers through the interaction

$$Cu^{2+} \rightarrow Cu^{3+} + e^- \tag{3}$$

which can also be written in hole notation as

$$h^+ + Cu^{2+} \rightarrow Cu^{3+}. \tag{4}$$

In normal-state cuprates, holes carry the electric current, and hence in the superconducting state the Cooper pairs are positively charged. This is in contrast to classical superconductors, in which the electrical transport is via negative electrons.

Holes can arise from an oxygen deficiency, as in the compound $YBa_2Cu_3O_{7-\delta}$, where the subscript $7-\delta$ designates the oxygen content, and in a typical superconducting compound we have $YBa_2Cu_3O_{6.9}$ with $\delta = 0.1$. Another way to achieve the hole doping is to replace some of the positively charged ions of the binding slab with other positive ions of lower charge. For example, the compound $(La_{1-x}Sr_x)_2CuO_4$ has the fraction x of La^{3+} replaced by Sr^{2+}, and a comparison of the reactions

$$La \Rightarrow La^{3+} + 3e^- \tag{5}$$

$$Sr \Rightarrow Sr^{2+} + 2e^- \tag{6}$$

shows that this leads to hole doping.

E

Particular Cuprate Superconductors

We see from Table 7.1 that the 123 compound $YBa_2Cu_3O_{7-\delta}$ and the mercury family compounds $HgBa_2Ca_{n-1}Cu_nO_{2n+2+\delta}$ with $n = 1$ to 6, often referred to as Hg-1201 to Hg-1256, respectively, are aligned types. There is also a set of aligned thallium compounds with the formula $TlBa_2Ca_{n-1}Cu_nO_{2n+3}$ designated by 1201 to 1245, but they are less often studied. The 123 yttrium compound differs from the other cuprates by having Y instead of Ca in its conduction slab, and in having -Cu–O–Cu–O- chains along its b axis as a structural component of its binding slab. These chains may contribute to carrying some current. We notice from the figures that the copper atoms are all stacked one above the other on edge (E) sites, as expected for an aligned-type superconductor. The families

of isostructural bismuth and thallium compounds, $Bi_2Sr_2Ca_{n-1}Cu_nO_{2n+4}$ and $Tl_2Ba_2Ca_{n-1}Cu_nO_{2n+4}$, as well as $(La_{1-x}Sr_x)_2CuO_4$ and $(Nd_{0.9}Ce_{0.1})_2CuO_4$, are body-centered. The superconducting BC, compounds are designated by Bi-2212, Bi-2223, and Tl-2201 to Tl-2234, as indicated in the table. The general stacking rules mentioned in Section C are satisfied by these compounds, namely, that the metal ions in adjacent layers alternate between edge (E) and centered (C) sites,

Fig. 7.11.

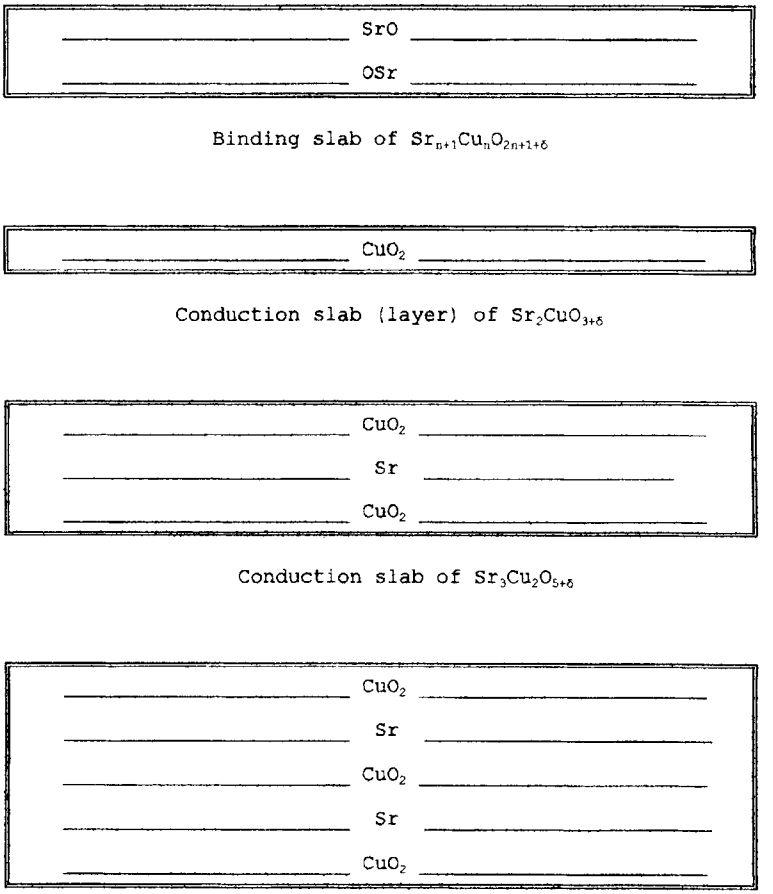

Binding slab (top) followed by, in succession, conduction slabs of the first three infinite layer phase compounds, namely $Sr_2CuO_{3+\delta}$, $Sr_3Cu_2O_{5+\delta}$, and $Sr_4Cu_3O_{7+\delta}$. The figures are drawn assuming $\delta = 0$. [Owens and Poole, 1996, p. 117.]

and adjacent layers never have oxygens on the same types of sites. The aligned and body-centered compounds all have about the same a and b lattice parameters.

In addition to the aligned and body-centered varieties, there exist some other types of cuprate superconductors. The $YBa_2Cu_4O_8$ compound, sometimes referred to as a 124 type, is side-centered since for each atom at the position (x, y, z) there is another identical atom at the position (x, $y + \frac{1}{2}$, $z + \frac{1}{2}$), and hence the stacking rules of Section B do not apply. The compound $Y_2Ba_4Cu_7O_{15}$ may be considered as an intergrowth of the 123 and 124 compounds $YBa_2Cu_3O_7$ and $YBa_2Cu_4O_8$. The body-centered compound M_2CuO_4 has three structural variations. The two common types called the T-phase (M = La) and the T′ phase (M = Nd) correspond to the superconductors $(La_{1-x}Sr_x)_2CuO_4$ and $(Nd_{0.9}Ce_{0.1})_2CuO_4$, and the third variety, called the T* phase, is a hybrid structure adopted by the compound $(Nd_{1-x-y}Sr_xCe_y)_4Cu_2O_{8-\delta}$. The upper half of its unit cell is T type and lower half is T′ type. The structures of these compounds are described in the next chapter. In Chapter 8 the T, T′ and T* phases are designated by the codes 0201, 0021 and 0222, respectively.

Fig. 7.12.

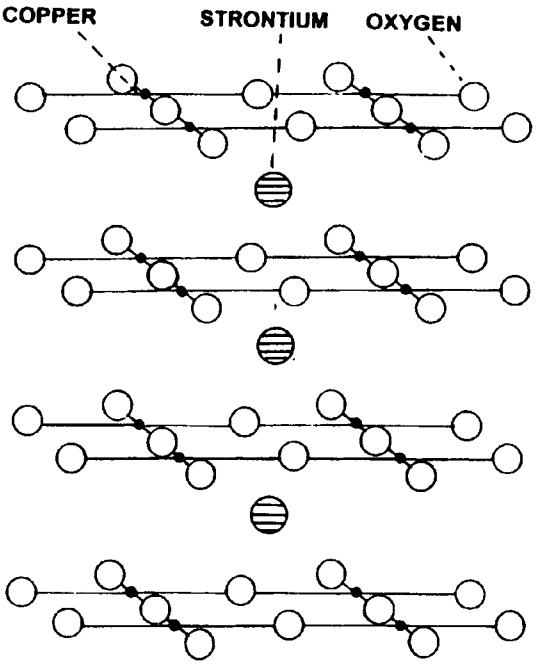

Crystal structure of the infinite layer phase $SrCuO_2$. [Owens and Poole, 1996, p. 118.]

F

Infinite-Layer and Related Phases

In 1993 superconductivity was discovered in the body centered series of compounds with the general formula $Sr_{n+1}Cu_nO_{2n+1+\delta}$. These are among the simplest of the copper oxide superconductors since they contain only two metallic elements strontium and copper. Like the cuprates they are layered compounds with the simple scheme presented in Fig. 7-11. The binding slabs resemble those of La_2CuO_4 but with Sr in place of La. The conduction slabs are the same as the cuprate ones sketched in Fig. 7-4, but with strontium atoms between the CuO_2 layers, instead of calcium or yttrium. The n = 1, 2, 3 compounds $Sr_2CuO_{3.1}$ [0201], $Sr_3Cu_2O_{5+\delta}$ [0212] and $Sr_4Cu_3O_8$ [0223] have T_c values of 70 K, 100 K and 100 K, respectively. There is also a 0234 compound with $T_C = 70$ K which contains some Ca in place of Sr. If the binding layers of $Sr_{n+1}Cu_nO_{2n+1+\delta}$ are replaced by Sr layers then one obtains $SrCuO_2$ which is called an infinite layer compound with the structure presented in Fig. 7-12. Structurally all of its atoms form a macroscopic conduction layer. This material, denoted by the code 0011, can be made an electron doped superconductor by replacing some of the divalent Sr^{2+} with trivalent La^{3+}, which has the effect of putting electron carriers in the copper oxide layers, and $Sr_{0.9}La_{0.1}CuO_2$ has a transition temperature of 42 K. These various structures are described in the next chapter.

References

F. J. Owens and C. P. Poole, Jr., *The New Superconductors*, Plenum, New York, 1996.

C. P. Poole, Jr., T. Datta and H. A. Farach, *Copper Oxide Superconductors*, Wiley, New York, 1988.

C. P. Poole,, Jr., H. A. Farach and R. J. Cheswick, *Superconductivity*, Wiley, New York, 1995.

C. C. Torardi, M. A. Subramanian, J.C. Calabrese, J. Gopalakrishnan, M. K. Morrisey, T. R. Askew, R.B. Flippen, U. Chowdhry and A. W. Sleight, Science 240, 631 (1988).

This Page Intentionally Left Blank

Chapter 8

Crystal Structures of High-T_c Superconducting Cuprates

Roman Gladyshevskii
Département de Physique de la Matière Condensée, Université de Genève, Geneva, Switzerland

Philippe Galez
Laboratoire d'Instrumentation et de Matériaux d'Annecy, Université de Savoie, Annecy, France

ISBN: 0-12-561460-8
$30.00

HANDBOOK OF SUPERCONDUCTIVITY

A

Introduction

Knowledge of crystal chemistry is essential for understanding and influencing the synthesis and properties of materials. Intense studies of the crystal structures of high-T_c superconducting oxides, reflected in an exceptionally high number of publications, have greatly contributed to the development of these materials. The efforts invested since the discovery of superconductivity in the La–Ba–Cu–O system by Bednorz and Müller in 1986 have led to the synthesis of hundreds of different superconducting cuprates, some of them suitable for applications. It appeared early that these compounds have common structural features, such as a pronounced layered character, and can be grouped not only into chemical but also into structural families. Multiple cation substitutions, variable oxygen contents, and distortions make the crystal structures appear complicated, but the main features are simple. All structures of superconducting cuprates known up to now are based on the stacking of a limited number of different kinds of atom layer, one of these always being a square-mesh layer containing copper and oxygen atoms.

This work is a critical compilation of crystallographic data of structures found among high-T_c superconducting cuprates, reported up to January 1997. After a brief description of the structure of perovskite, four kinds of atom layer are defined, and stacking rules for these layers are formulated. Based on these, a high-T_c superconductor family tree is generated, and the space groups for undistorted structures are derived. Cation coordinations, interatomic distances, and structural peculiarities of the main chemical families are then discussed. Finally, representative crystallographic data sets with drawings, followed by tables for selected compounds, are given.

The term "structure type" is commonly used for structures of inorganic compounds to denote a specific geometrical arrangement of atoms. Following the definition proposed in Parthé *et al.* (1993/1994),[1] two structures with similar atom arrangements crystallize with different structure types, if a slight distortion or a change in the ordering of the atoms leads to a description in a different space group, or if additional, fully or partly occupied, atom sites are present in one of the structures. In the case of high-T_c superconducting cuprates, a strict application of this definition would result in an artificially large number of "structure types," since in some cases the structure of the same compound has been refined in different space groups or with different Wyckoff sites occupied. For this reason, in the present work, the term "structure type" is used to denote the ideal, undistorted, generally tetragonal structure with the a-parameter similar to that of cubic perovskite. These structure types will be referred to by generalized chemical formulas where the cations are represented by the letters A, B, C, and D.

The data sets contain complete crystallographic data for selected high-T_c superconducting cuprates, lists of cell parameters, and critical temperatures for related compounds. They are ordered according to a classification scheme based on the widely used four-digit code, which gives a general view of the structural relationships. It is our hope that this work may be a help in finding systematic trends in the physical properties related to the structural features and thereby provide hints for the preparation of new compounds.

B

Perovskite-Type Structures

It was noticed at an early stage that the structures of high-T_c superconducting cuprates are related to that of perovskite. The first structural studies of the mineral perovskite, $CaTiO_3$, revealed a cubic cell with $a \approx 3.8$ Å (Barth, 1925; Levi and Natta, 1925). The proposed structure with five atoms in the unit cell respects the

[1] Two structures are considered isotypic if they have the same stoichiometry, the same space group, the same Wyckoff sites with the same or similar positional coordinates, and the same or similar values of the unit cell axial ratios and cell angles.

symmetry of space group $Pm\bar{3}m$, calcium atoms being situated at the corners of the cube, a titanium atom at the center of the cube, and oxygen atoms at the centers of the cube faces (Fig. 8.1). The Ca site is surrounded by 12 equidistant oxygen atoms that form a cuboctahedron, and the Ti site is located between six oxygen atoms forming a perfect octahedron. The TiO_6 octahedra share corners to form a three-dimensional framework. Two kinds of layer, of composition CaO and TiO_2, respectively, may be considered. These layers are stacked along [0 0 1] and build up the structure completely (note that for a cubic structure, similar layers may also be considered perpendicular to [1 0 0] or [0 1 0]).

The cubic structure of perovskite, denoted $E2_1$ (originally G5) in the Strukturbericht notation (see chapter on classical superconductors), represents only an average structure for the mineral $CaTiO_3$, the real structure being a distortion to orthorhombic or monoclinic. The name perovskite is, however, used to designate not only the mineral, but also the simple cubic structure and, in a larger sense, all distorted variants of this. Such structures are formed by a large range of $M(1)^{2+}M(2)^{4+}O_3$ and $M(1)^{+}M(2)^{2+}F_3$ ($r_{M(1)} > r_{M(2)}$) compounds, where the $M(2)$ cations center the corner-sharing octahedra. Only a few compounds, such as $SrTiO_3$ (room-temperature modification) and $BaTiO_3$ (high-temperature modification), crystallize with the truly cubic structure. Owing to its ferroelectric properties, $BaTiO_3$ is one of the most studied materials. Upon cooling, it undergoes successive phase transitions: At 393 K the structure becomes tetragonal, at 278 K orthorhombic (see data sets) and at 183 K rhombohedral (Megaw, 1947; Kwei *et al.*, 1993). The structures of the superconducting pervoskites $Ba_{1-x}K_xBiO_3$ and $BaPb_{1-x}Bi_xO_3$ are discussed in the chapter on classical superconductors.

Fig. 8.1.

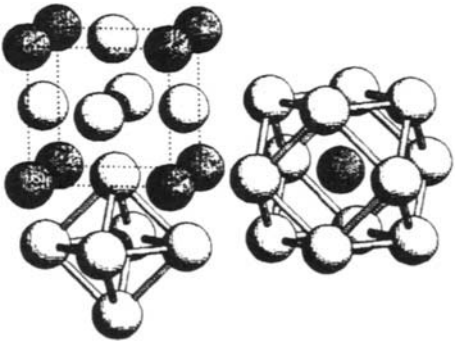

The average structure of perovskite $CaTiO_3$ ($Pm\bar{3}m$). The unit cell is indicated with dotted lines; a CaO_{12} cuboctahedron and a TiO_6 octahedron are presented (see also data set for cubic $BaTiO_3$ in Section H,b).

C

Atom Layers and Stacking Rules

The crystal structures of the high-T_c superconducting cuprates have essentially a layered character, confirmed by the anisotropy of their properties, and are conveniently described as a stacking of atom layers. Basically four kinds of atom layer can be considered, two of which are identical to those found in the perovskites. The translation period within the undistorted layers remains that of the ideal structure of perovskite (~ 3.85 Å for cuprates), whereas the periodicity in the third direction depends on the number and kind of atom layers in the stacking unit, the average interlayer distance being ~ 2.0 Å.

a. Definition of Atom Layer

To understand the structures of high-T_c superconducting cuprates it is convenient to distinguish four kinds of layers, which have different "functions" in the structure. The notations used here will allow a direct correspondence with the conventional four-digit codes, described later on. The layers are presented in Fig. 8.2.

DO_2 (*conducting* layers): Superconductivity is believed to take place in these layers, which are present as CuO_2 layers in all superconducting cuprates. They consist of a regular square mesh of copper atoms with oxygen atoms centering the square edges. In the (nonsuperconducting) perovskites discussed earlier, the corresponding layers have the composition TiO_2.

C (*separating* layers typically Ca or Y): The structure of pervoskite does not contain this kind of layer, which consists of a simple regular square mesh of metal atoms. The insertion of a *C* layer into perovskite will "split" the TiO_6 octahedron into two TiO_5 square pyramids, the basal planes of which will be separated by the new layer. Consecutive *C* layers in superconducting cuprates are always intercalated by O_2 layers, where the oxygen atoms are arranged as in the *D*O_2 layers, that is, centering the edges of the square lattice.

*B*O (*bridging* layers typically BaO, LaO or SrO): These layers are located next to a *D*O_2 layer and contain the apical oxygen atom of the octahedron or square pyramid coordinating the copper atom. They are present in perovskite (CaO or BaO above) and in all basic structures as defined here (see Section C,c). They consist of a regular square mesh of metal atoms with oxygen atoms centering the squares.

*A*O (*additional* layers typically BiO, HgO or TlO): In contrast to the *C* and the *B*O layers, these layers are never in direct contact with the *D*O_2 layers, but

separated from these by a *bridging* BO layer. They can have different oxygen contents, leading to compositions ranging from A to AO_2. In all cases the cations are arranged in a regular square mesh, whereas the oxygen atoms may occupy different positions: A, none; AO, centering the squares; AO', centering square edges in one direction; AO_2, centering square edges in two directions; AO'', centering square edges with partial occupancy. For simplicity, unless specified, *additional* layers will hereafter be represented by AO layers.

It may be noted that from a geometrical point of view the BO layer is identical to the AO layer (as well as C and DO_2 to A and AO_2, respectively), but

Fig. 8.2.

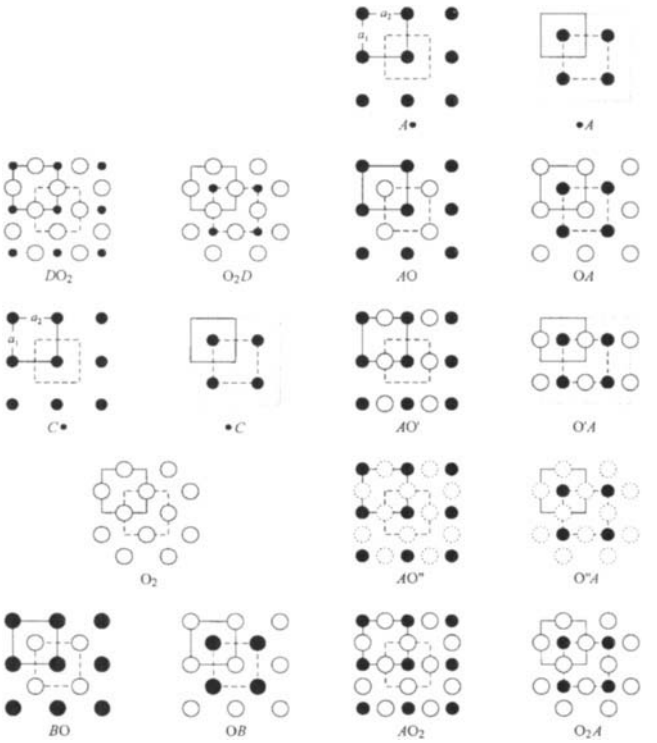

Schematic drawings of the atom layers building up the structures of high-T_c superconducting cuprates. Except for the O_2 layer, each layer is shown twice. For layers with labels starting (e.g., DO_2) and ending (e.g., O_2D) with D, C, B, or A, solid lines delimit two-dimensional cells with the cation (shaded circles) located at the corner (0 0) and at the center ($\frac{1}{2}$ $\frac{1}{2}$) of the square, respectively. Cells shifted by $\frac{1}{2}$ $\frac{1}{2}$ (dashed lines) are indicated to emphasize the equivalence. Open circles represent oxygen atoms. All atom layers (except AO') are described in plane group *p4mm*.

that the former acquires its specificity from the position in the structure, next to a DO_2 layer. All layers have a square lattice, except the AO' layer, where the presence of oxygen atoms along only one of the cell edges leads to a rectangular lattice (see Section E,a).

b. Stacking Rules

In the structures of most high-T_c superconducting cuprates, the atom layers just defined are stacked on top of each other, so that the cation sites in neighboring layers are shifted by $\frac{1}{2}\ \frac{1}{2}$ with respect to each other. There are, however, two notable exceptions, $Ba_2YCu_4O_8$ and $Ba_4Y_2Cu_7O_{14.94}$, for which the cation positions in consecutive *additional* AO' (CuO) layers are shifted by $0\ \frac{1}{2}$. As a consequence of these systematic shifts, the translation period in the stacking direction must contain an even number of layers. This means that for an odd number of layers in what we define as the stacking unit, the translation period in the stacking direction has to be doubled. As shown in Fig. 8.2, a shift by $\frac{1}{2}\ \frac{1}{2}$ respects the 4-fold symmetry, and therefore undistorted structures that do not contain AO' layers will have tetragonal symmetry (see Section E,b). It may be noted that the presence of an O_2 layer between consecutive C layers does not modify the relative shift of the cation sites.

Not all stacking combinations are possible. Stacking rules that are respected in all structures of superconducting cuprates are illustrated in Fig. 8.3 and may be formulated as follows for each kind of layer. They lead to a limited number of coordinations characteristic of the different cation sites.

1. *Conducting* DO_2 layers (i.e. CuO_2 layers) cannot be stacked directly upon each other. They can have as closest neighbors either two BO layers, one BO and one C layer, or two C layers. In the first case the D atom will be surrounded by six oxygen atoms forming an octahedron, in the second case by five oxygen atoms forming a square pyramid, and in the third case by four oxygen atoms, belonging to the DO_2 layer itself, forming a square. Copper atoms are always present in this layer at the D position, but may exceptionally be partly replaced by a $3d$-transition metal.
2. *Separating* C layers may be inserted between two DO_2 layers. Consecutive C layers, sandwiched between DO_2 layers, are always intercalated by O_2 layers. In all cases, the coordination polyhedron formed by the oxygen atoms around the C atom is a tetragonal prism. The C layers are generally built up by Ca or Y, and sometimes by La or rare-earth metal atoms.
3. Since, by definition, a BO layer must be in direct contact with a DO_2 layer, one, or at most two, *bridging* BO layers can be placed between two DO_2 layers. When AO layers are present, a single BO layer makes the bridge to the neighboring DO_2 layer. When a BO layer is surrounded by two DO_2 layers, as in perovskite, the B atom is coordinated by 12 oxygen atoms

Fig. 8.3.

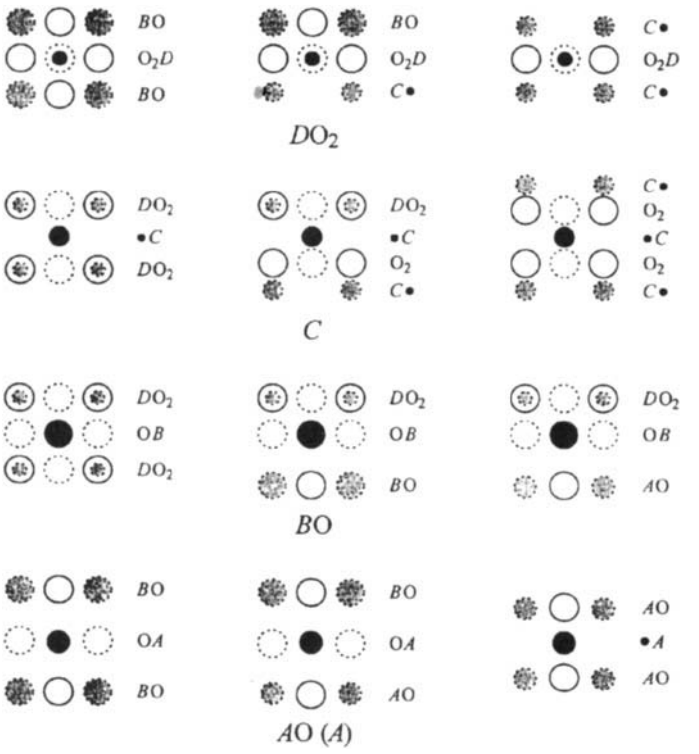

Possible stacking combinations for DO_2, C, BO and AO (A) layers, corresponding to stacking rules 1, 2, 3, and 4 (Section C,b), respectively.

located at the corners of a cuboctahedron. In all other cases, the coordination is reduced, generally to nine oxygen atoms forming a monocapped square antiprism, but other coordinations may also occur, depending on the exact type of neighboring *additional* layer. Typical *B* atoms are large, ionized, and spherical like Ba, Sr, and La.

4. Several *additional* *A*O layers can be stacked on each other to form slabs that are always delimited by a *B*O layer on each side. The coordination of the *A* cation depends on the actual composition and geometry of the *additional* layers. Considering, for example, an *additional* layer stacked between two *A*O layers, the coordination of the cation in a central layer of type *A*O will be octahedral, in a layer of type *A* linear, and in a layer of type *A*O′ square planar. Cations in *additional* layers are usually main group elements, such as Tl, Pb, Bi, or C, but can also be Cu or Hg, the cations of the latter elements preferring low coordination numbers.

In summary DO_2 are CuO_2, C layers are Ca (or Y), BO layers are BaO, LaO or SrO and AO layers are BiO, HgO or TlO in most common cuprates.

c Basic Structures

Any basic structure, as defined here, must contain at least one DO_2 layer and one BO layer, like the structure of perovskite. It derives from the stacking rules just formulated, that AO and BO layers are never in direct contact with C layers, nor are AO layers in contact with DO_2 layers. Two kinds of thicker structural slab may thus be considered, one built up of DO_2 (and C) layers, the other by BO (and AO) layers. The former is sometimes referred to as "conduction" and the latter as "charge reservoir" slab. The stacking unit of a basic structure will contain one slab of each kind.

Slabs formed by DO_2 and C layers: In its simplest version, the slab will contain a single DO_2 layer. When there is more than one DO_2 layer ($\boldsymbol{n}$ of them), then together with $\boldsymbol{m}$ C layers a slab of composition $C_mD_nO_{2m+2}$ is formed. Since the outside layers of the slab must always be DO_2 layers, when consecutive DO_2 layers are separated by single C layers the formula of the slab becomes $C_{n-1}D_nO_{2n}$. A grouping of $\boldsymbol{p}$ consecutive C layers, intercalated by O_2 layers and sandwiched between two DO_2 layers, is described by the formula $C_pD_2O_{2p+2}$. Following the definition used here, groupings between two DO_2 layers in a basic structure contain a constant number ($\boldsymbol{p}$) of C layers. The general formula for the slab, considering groupings of $\boldsymbol{p}$ C and $(\boldsymbol{p}-1)O_2$ layers, intercalated between $\boldsymbol{n}$ consecutive DO_2 layers, becomes $C_{p(n-1)}D_nO_{2p(n-1)+2}$. The stacking sequence inside the slab can be written as

$$DO_2-(\boldsymbol{n}-1)\{C-(\boldsymbol{p}-1)[O_2-C]-DO_2\}.$$

Slabs formed by BO and AO layers: In the simplest case, the slab is reduced to the expression B_lO_l, where $\boldsymbol{l}$ can only take the values 1 or 2. When there is more than one, $\boldsymbol{k}$ AO layers are stacked directly upon each other, between two BO layers, to form a slab of composition $A_kB_2O_{k+2}$. Note that the total number of oxygen atoms in the *additional* layers may differ from $\boldsymbol{k}$ and consequently the oxygen content of the slab may show large variations.

In a basic structure, conduction $C_mD_nO_{2m+2}$ and charge reservoir $A_kB_lO_{k+l}$ slabs alternate, so that the general formula can be written as

$$A_kB_lC_mD_nO_{k+l+2m+2}.$$

The outer *conducting* DO_2 layers of the former slab are in direct contact with the *bridging* BO layers of the latter. As a consequence of the definition of a basic structure and of the stacking rules formulated earlier, the following relations are

observed between the number of atom layers of different kinds in the stacking unit:

1. $n \geq 1$ (DO_2 layers must always be present)
2. $m + l \geq n$ (DO_2 layers cannot be stacked directly upon each other)
3. $m = p(n - 1)$ (a constant number of C layers is required between consecutive DO_2 layers)
4. $l = 1$ or 2 (if $k \neq 0$ then $l = 2$) (imposed by the specificity of the BO layers)

If $p = 1$ (single C layers between consecutive DO_2 layers), the general formula can be simplified to

$$A_k B_l C_{n-1} D_n O_{k+l+2n}.$$

As stated previously, the number of cation-containing layers in the translation period must be even, in order to compensate for the relative shift of the cation sites in consecutive layers. This means that when $N = k + l + m + n$ is even, the conventional cell of the undistorted structure will contain one stacking unit, that is, one formula unit ($Z = 1$), whereas when N is odd, it will contain two stacking units ($Z = 2$). In the first case the tetragonal cell of a structure without AO' layers will be primitive (P), and in the second case body-centered (I) because of the shift of $\frac{1}{2}\ \frac{1}{2}$ observed within the plane for layers separated by half a translation period along [0 0 1]. The symmetry of basic structures will be further discussed in Section E,b.

d. Limiting Structures

In contrast to the basic structures, limiting structures, as defined here, do not contain any BO, and consequently no AO layers. Such structures, where DO_2 layers alternate with groupings of p C layers intercalated by O_2 layers, have the general formula

$$C_p DO_{2p}.$$

The structure where DO_2 layers alternate with single C layers ($p = 1$) is known for the so-called infinite-layer compound (e.g., (Sr,La)CuO_2). Depending on the parity of p, the translation period of the limiting structures contains either one (p odd) or two (p even) stacking units.

Well-known structures are in some cases obtained when one or two of the layers just described are combined. The stacking sequence -C–O_2-, for example, corresponds to the fluorite-type (CaF_2) structure, whereas a simple stacking of AO (or BO) layers leads to the rock-salt-type (NaCl) structure. These "limiting" structures do not contain *conducting* DO_2 layers and hence do not superconduct; they will therefore not be considered in the following.

e. Intergrowth of Basic Structures

As shown earlier, the stacking unit of a basic structure contains one $C_mD_nO_{2m+2}$ and one $A_kB_lO_{k+l}$ slab. Other structures are known, where the "stacking unit" contains several slabs with different indices, slabs of DO_2 and C layers alternating with slabs of BO and AO layers. Such structures are generally considered as an intergrowth of stacking units of different basic structures. The general formula for intergrowth structures can be written as

$$A_{\Sigma k}B_{\Sigma l}C_{\Sigma m}D_{\Sigma n}O_{\Sigma k+\Sigma l+2\Sigma m+2q}.$$

where q is the number of intergrown stacking units. Since all but one of the intergrowth structures refined so far are built up from the stacking units of two different basic structures, only structures with $q = 2$ will be considered in the present work. Note that structures where the "stacking unit" contains more than two slabs because of a different ordering of the chemical elements are here considered as superstructures of the basic structures and will be discussed together with these.

f. Four-Digit Codes

Basic structures are commonly referred to by a four-digit code that is derived from the general formula, $A_kB_lC_mD_nO_{k+l+2m+2}$, considering the numbers of cation-containing layers of each kind in the stacking unit:

klmn.

The structures of $LaCuO_{2.95}$ ($A_0B_1C_0D_1O_3$) and $Tl_{1.64}Ba_2Ca_3Cu_4O_{12}$ ($A_2B_2C_3D_4O_{12}$), for example, are denoted as **0101** and **2234**, respectively. The code generally reflects the cation ratios in the compound; however, partial vacancies are ignored and in some cases the same chemical element may be present in different layers (e.g., Cu in both DO_2 and AO' layers). Mixed occupation of one or several cation sites is also common. The oxygen content is not considered in the code and cannot be derived with certainty from it, in particular since no distinction is made between different types of *additional* layer.

In order to be able to distinguish different chemical families, the four-digit code is sometimes preceded by the chemical symbol of the cations in the *additional* layers. For the thallium-based compound mentioned earlier, the code can, for instance, be written as Tl-**2234**. Note that, in the literature, some compounds are denoted by codes that correspond to coefficients in the conventional chemical formula, but do not take into account the distribution of the cations among the different kinds of layer. For example, $Ba_2YCu_3O_7$ is often abbreviated as 123 or Y-123 ($YBa_2Cu_3O_7$), but is more properly classified as **1212** or Cu-**1212** ($CuBa_2YCu_2O_7$).

The four-digit code can also be extended to the limiting structures with the general formula C_pDO_{2p}. For these phases the number of DO_2 layers in the stacking unit equal 1, so that the code takes the general expression **00*p*1**. Following this scheme, $(Nd,Ce)_2CuO_{3.92}$, for example, is denoted as **0021**. The code for an intergrowth structure contains the four-digit codes of the basic structures it derived from, for example, **1201/2201** for $CBi_2Sr_4Cu_2O_{11}$ ($CSr_2CuO_5/Bi_2Sr_2CuO_6$).

D

High-T_c Superconductor Family Tree

A family tree, in which all basic structures of high-T_c superconducting cuprates find their place, can be built by applying three structural operations to the ideal structure of perovskite. These consist in inserting, one by one, the layers described earlier, respecting the stacking rules.

a. Structural Operations

As explained previously, the structure of perovskite contains one DO_2 (TiO_2) and one BO (CaO) layer, which corresponds to the generalized formula $B_1D_1O_3$ and the four-digit code **0101**. All basic structures of superconducting cuprates can be generated from the ideal structure of perovskite by applying one or a combination of three different structural operations, which consist in adding one of the following:

1. An *additional* AO (or a *bridging* BO) layer
2. A *conducting* DO_2 and a *separating* C layer
3. A *separating* C and an O_2 layer

Each operation may be performed several times. Note that an AO layer can only be added into a stacking unit that already contains two *bridging* BO layers. In a similar way, the structural operation (3) can only be applied to structures that already contain two or more *conducting* DO_2 layers in the stacking unit.

b. Application of the Three Structural Operations

Figure 8.4 shows how operation (1), adding an AO or a BO layer, can be stepwise applied to the structure with formula $B_1C_1D_2O_5$ (**0112**, e.g., $BaY(Cu,Fe)_2O_5$). In the initial structure, two DO_2 layers are separated by a single C layer, the resulting CDO_2 slabs being connected via single BO layers. As in perovskite, the B atom is

Fig. 8.4.

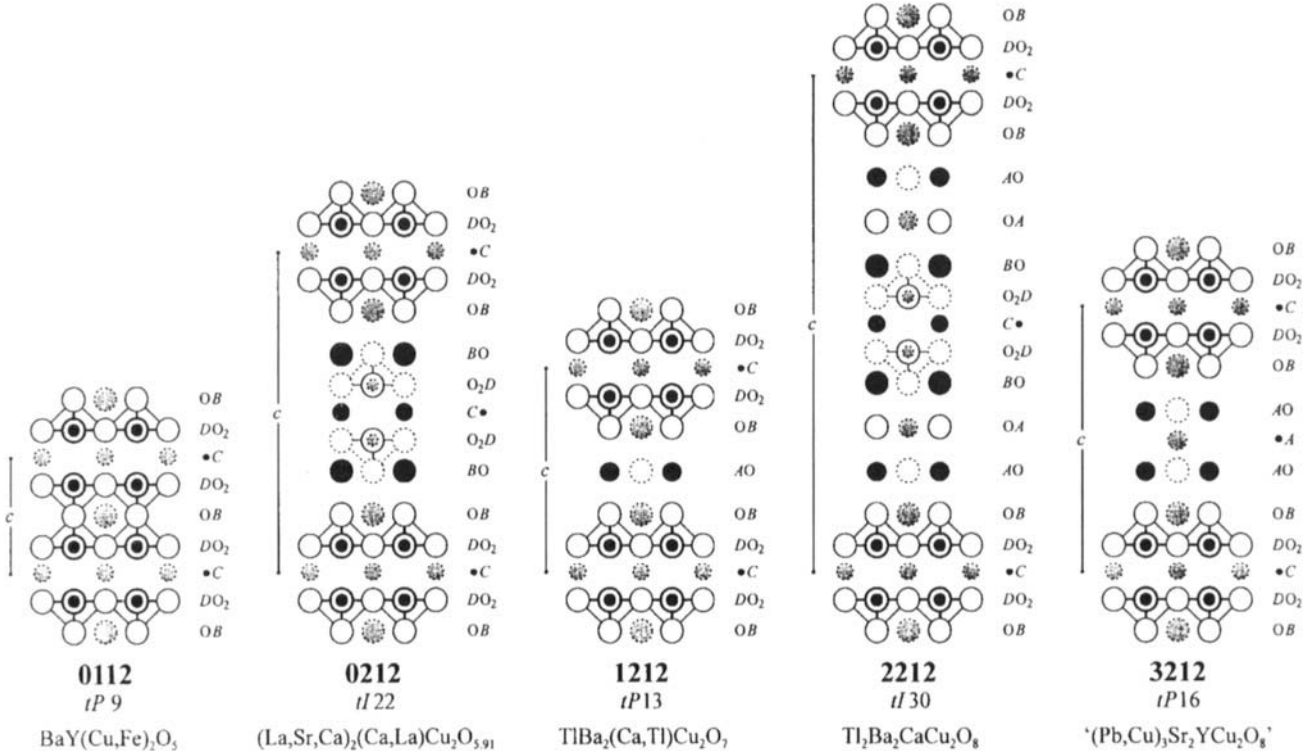

Structures obtained by stepwise adding a *bridging BO* or an *additional AO* (*A*) layer, starting from the **0112** structure. The Pearson code corresponds to the ideal composition. The real structure of $(Pb,Cu)_3Sr_2YCu_2O_8$ is orthorhombic.

12-fold coordinated. The metal atoms from the DO_2 layers are 5-fold coordinated, the surrounding oxygen atoms forming square pyramids. The C atom is located at the center of a tetragonal prism formed by eight oxygen atoms. When a second *bridging* BO layer is inserted between the BO and DO_2 layers, a structure with the formula $B_2C_1D_2O_6$ (**0212**, $(La,Sr,Ca)_2(Ca,La)Cu_2O_{5.91}$) is obtained. The tetragonal cell of the resulting structure contains two stacking units and the two neighboring BO layers form a rock-salt-type atom arrangement. The coordination numbers of the C and D atoms remain the same as in **0112**, whereas the B atom is here 9-fold coordinated. An *additional* AO layer can now be inserted between the two consecutive BO layers, leading to the formula $A_1B_2C_1D_2O_7$ (**1212**, $TlBa_2(Ca,Tl)Cu_2O_7$). The coordination numbers of the C and D cations remain the same as in **0212**, whereas the coordination of the B and A cations will depend on the actual composition of the *additional* layer. When the operation consisting in adding an AO layer is repeated, other members of the structure series with formula $A_kB_2C_1D_2O_{k+6}$ are generated ($k = 0$ and 1 for the **0212** and **1212**, respectively). In Fig. 8.4 schematic drawings of the structures of the members with $k = 2$ and 3, **2212** ($Tl_2Ba_2CaCu_2O_8$) and **3212** ($(Pb,Cu)_3Sr_2YCu_2O_8$), respectively, are also shown. For **2212**, the cations in both AO layers belong to the same crystallographic site and have octahedral environment. In the example chosen to illustrate the formula **3212**, the inner *additional* layer is built up from cations only. In this structure the cations in the outer AO layers are 5-fold coordinates, whereas those in the inner A layer have two neighboring oxygen atoms in linear coordination.

The operation (2), consisting in adding a DO_2 and a C layer, is illustrated in Fig. 8.5 on Hg-based superconductors. The stacking unit of $A_1B_2DO_4$ (**1201**, $HgBa_2CuO_{4.18}$), chosen as starting point, contains one DO_2 layer and one A layer surrounded by a BO layer on each side. Simultaneous insertion of a *conducting* DO_2 and a *separating* C layer produces a structure with the formula $A_1B_2C_1D_2O_6$ (**1212**, $HgBa_2CaCu_2O_{6.26}$). The environments of the A and B cations in **1212** are the same as in **1201** (2- and 8-fold coordination, respectively), whereas the coordination number of the metal atoms in the DO_2 layers is reduced from six to five ("splitting" of the octahedron). The C atom is located inside a tetragonal prism. The structures of the members of the structure series $A_1B_2C_{n-1}D_nO_{2n+2}$ with $\boldsymbol{n} = 3$ and 4, **1223** ($HgBa_2Ca_2Cu_3O_{8.44}$) and **1234** ($(Hg,Pb)Ba_2Ca_3Cu_4O_{10.14}$), respectively, are also shown ($\boldsymbol{n} = 1$ and 2 for **1201** and **1212**, respectively). In the case where there are three or more *conducting* DO_2 layers in the stacking unit, the metal atoms of the external DO_2 layers are 5-fold coordinated, whereas those of the internal DO_2 layers have four neighboring oxygen atoms in square planar coordination.

The structure with formula $B_2C_1D_2O_6$ (**0212**), as shown in Fig. 8.6, contains CD_2O_4 slabs where two DO_2 layers are separated by a single C layer and B_2O_2 slabs formed by two BO layers. The structural operation (3) is illustrated in the same figure with schematic drawings of the three first members ($\boldsymbol{m} = 1$, 2 and 3) of the structure series with the formula $B_2C_mD_2O_{2m+4}$. If a

Fig. 8.5.

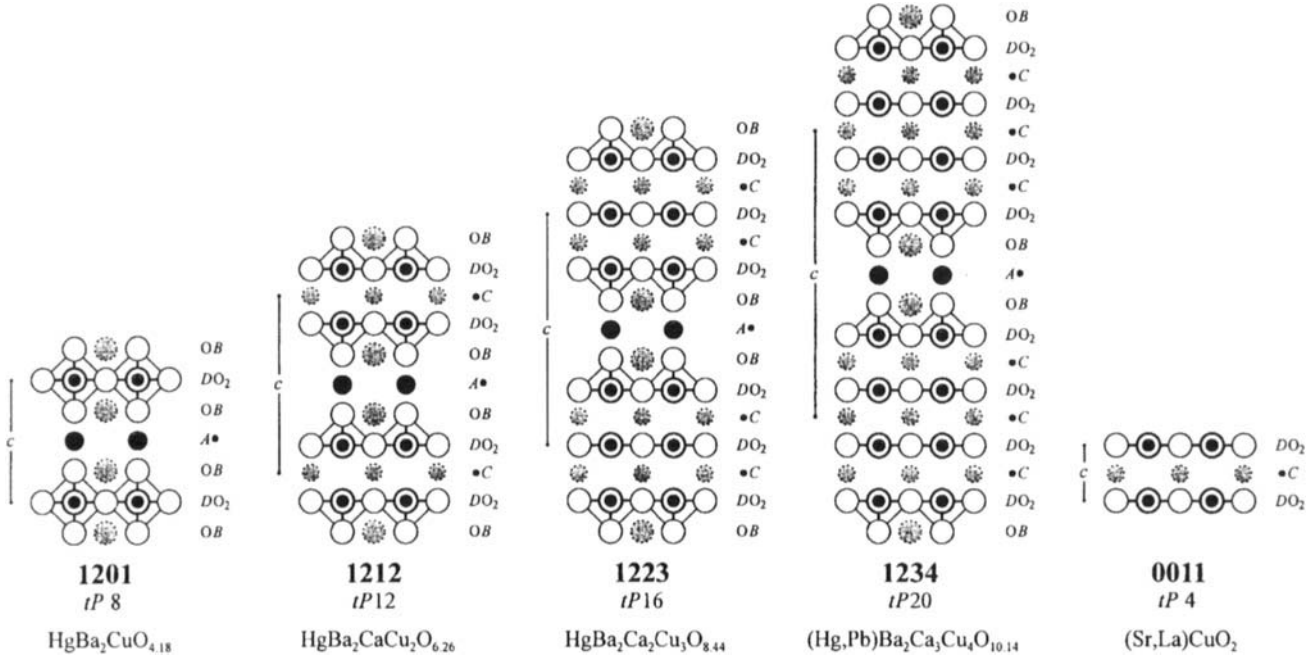

Structures obtained by stepwise adding a *conducting* DO_2 and a *separating* C layer, starting from the **1201** structure with an A layer. The end member of the structure series, **0011**, is also shown. The Pearson code corresponds to the ideal composition.

Fig. 8.6.

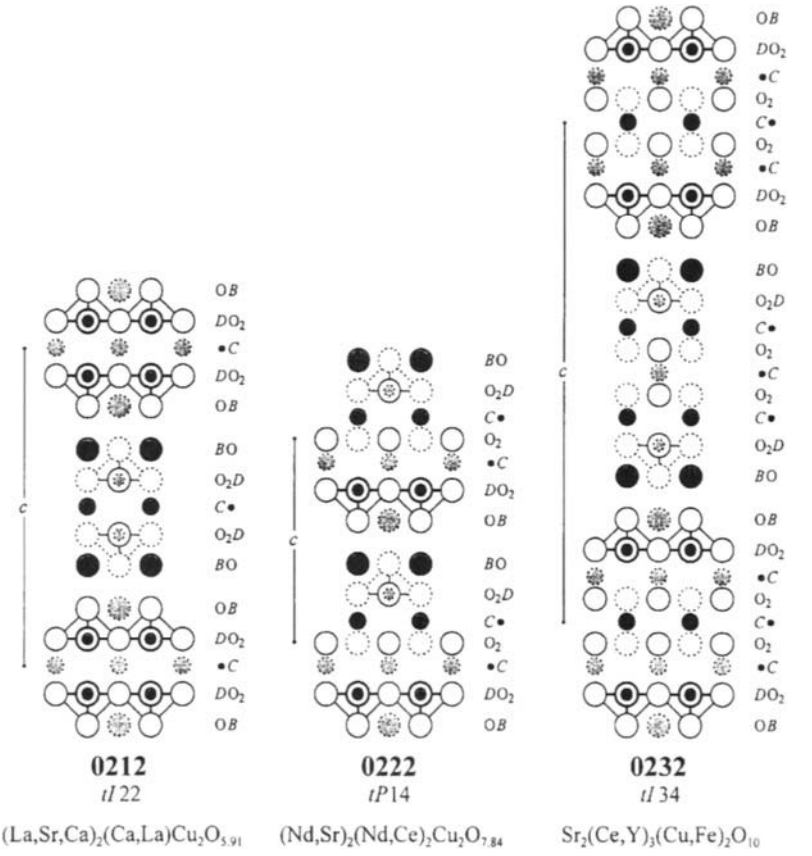

Structures obtained by stepwise adding a *separating C* and an O_2 layer, starting from the **0212** structure. The Pearson code corresponds to the ideal composition.

second *separating C* layer is inserted between the *C* layer and one of the DO_2 layers in **0212**, adding simultaneously an O_2 layer, a structure with the formula $B_2C_2D_2O_8$ (**0222**, $(Nd,Sr)_2(Nd,Ce)_2Cu_2O_{7.84}$) is obtained. The coordination of the metal atoms is unchanged through this structural operation, that is, the *B*, *C*, and *D* cations remain 9-, 8-, and 5-fold coordinated, respectively. If the operation is repeated, a structure with the formula $B_2C_3D_2O_{10}$ (**0232**, $Sr_2(Ce,Y)_3(Cu,Fe)_2O_{10}$) is built (two stacking units in the translation period as in **0212**), again leaving the cation coordination unchanged. Note that independently of the number of *separating C* layers, the *C* atoms remain 8-fold coordinated, since the oxygen atoms in the O_2 layer are arranged as in the DO_2 layers.

C and O_2 layers can also be added to structures that contain $\boldsymbol{n}$ DO_2 and $\boldsymbol{p}(\boldsymbol{n}-1)$ *C* layers ($\boldsymbol{n} \geq 2$). For a basic structure, the number of *C* layers between

consecutive DO_2 layers ($\boldsymbol{p}$) must be constant and, hence, ($\boldsymbol{n}-1$) C and ($\boldsymbol{n}-1$) O_2 layers must be added simultaneously. When, for example, this operation is performed on $A_1B_2C_2D_3O_9$ (**1223**), a structure with the formula $A_1B_2C_4D_3O_{13}$ (**1243**, hypothetical) is obtained. Inserting pairs of C and O_2 layers into the structure of the so-called infinite-layer compound $C_1D_1O_2$ (**0011**, (Sr,La)CuO_2, Fig. 8.5), gives a structure with the formula $C_2D_1O_4$ (**0021**, $(Nd,Ce)_2CuO_{3.92}$).

c. Generation of the Family Tree

Starting from the ideal structure of perovskite, or from the tetragonally distorted structure of the cuprate $LaCuO_{2.95}$ (**0101**), and performing, one by one, the structural operations defined in Section D,a, one can generate the high-T_c superconductor family tree shown in Fig. 8.7. The four-digit codes representing structures with one and two stacking units in the translation period are placed within open and shaded rectangles, respectively. Horizontal lines correspond to the structural operation which consists in adding a *bridging* BO or an *additional* AO layer. When AO layers are progressively added, the members of structure series with the formulas $A_kB_2C_{cst}D_{cst}O_{k+cst}$ are generated. The end points of the vectors (infinite number of AO layers) correspond to a rock-salt-type (NaCl) atom arrangement. The simultaneous insertion of a *conducting* DO_2 and a *separating* C layer is represented by vertical lines. Repeating the operation generates members of structure series with the formulas $A_{cst}B_{cst}C_{n-1}D_nO_{2n+cst}$. The end member of each series is the structure of the infinite-layer compound (**0011**, (Sr,La)CuO_2). Diagonal lines represent the structural operation consisting in adding a *separating* C layer and an O_2 layer. The structure series grouping the structures produced along one of these lines can be described by the formulas $A_{cst}B_{cst}C_mD_{cst}O_{2m+cst}$. Infinite adding of layers leads in this case to the structure of fluorite (CaF_2). This last operation is also applied, at the bottom of the figure, to the limiting structure **0011**. Only a certain number of basic structures are indicated in the diagram; however, structures with higher numbers in the four-digit code, such as **1256** and **5222**, are also known.

It follows from the diagram that, for example, the structure of **1232** ($(Bi,Cu)Sr_2(Ce,Nd)_3Cu_2O_{11}$) can be obtained from **0101** ($LaCuO_{2.95}$) in 10 different ways, one of which corresponds to the following path:

$$\mathbf{0101} \rightarrow \mathbf{0201} \rightarrow \mathbf{1201} \rightarrow \mathbf{1212} \rightarrow \mathbf{1222} \rightarrow \mathbf{1232}.$$

The simultaneous adding of one DO_2 layer and $\boldsymbol{p}$ C ($\boldsymbol{p} > 1$) layers, which would correspond to vertical lines ending with the structures **0021** ($\boldsymbol{p} = 2$, $(Nd,Ce)_2CuO_{3.92}$), **0031** ($\boldsymbol{p} = 3$, hypothetical), etc., is not illustrated in the diagram.

Fig. 8.7.

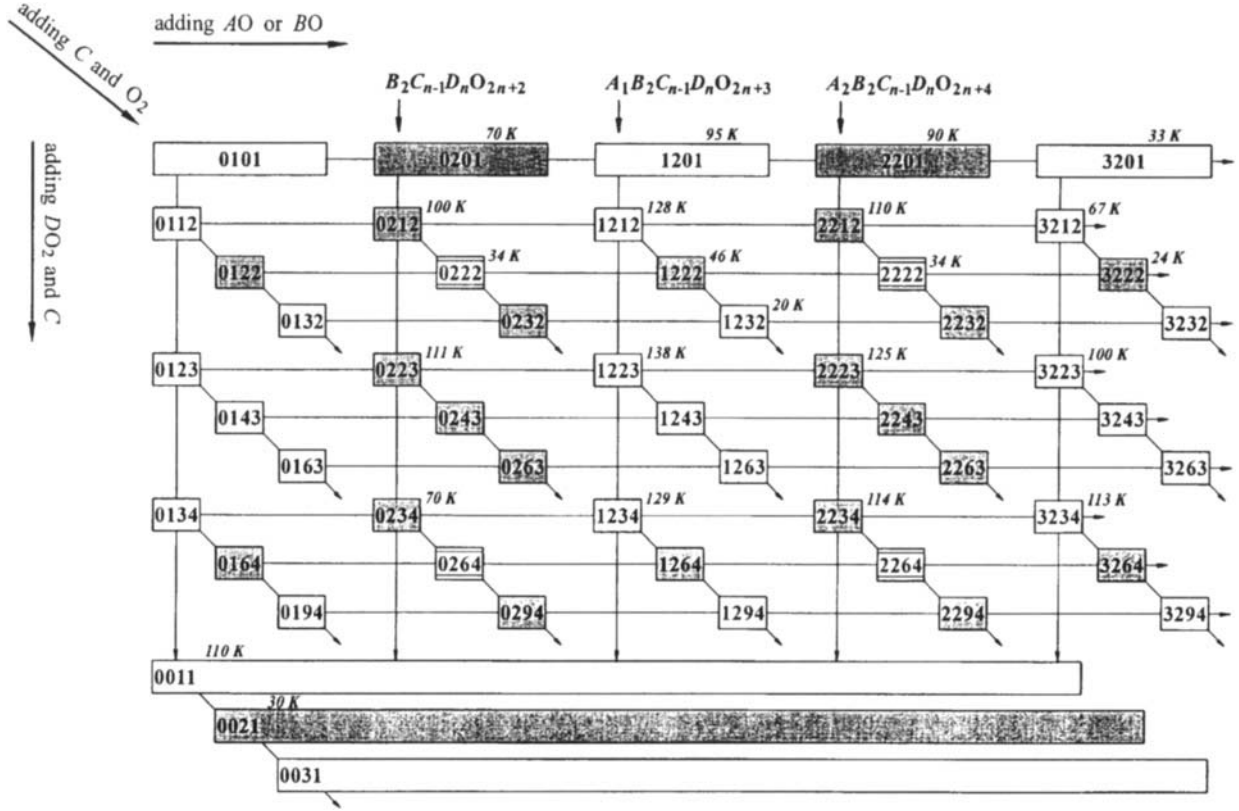

High-T_c superconductor family tree. Horizontal, vertical and diagonal lines correspond to the structural operations (1), (2) and (3) (Section D,a), respectively. Four-digit codes placed within open and shaded rectangles identify structures with a primitive (one stacking unit in the translation period, space group $P4/mmm$ (single frame) or $P4/nmm$ (double frame)) and a body-centered (two stacking units, $I4/mmm$) tetragonal cell, respectively. Four-digit codes for which superconducting representatives are known are followed by the highest transition temperature quoted in this work.

E

Symmetry

Undistorted basic structures are described in a limited number of space groups, most of them tetragonal. In the following section, the symmetry of the individual atom layers is discussed. It is then shown how the space group for ideal basic, limiting, and intergrowth structures may be derived from the four-digit code. Distortions to, for example, orthorhombic are common in the real structures. We will clarify the relationships between the space groups of the undistorted parent types and space groups of lower symmetry, which have been used in the literature to refine structures of high-T_c superconducting cuprates.

a. Plane Groups for Individual Atom Layers

All atom layers defined in Section C,a and shown in Fig. 8.2 except AO', can be described in the square plane group $p4mm$, with cell parameters $a = b \approx 3.85$ Å. There are 4-fold rotation points at the origin and the center of the cell, and mirror lines along the cell axes ([0 1], [1 0]) and the cell diagonals ([1 1], [1 $\bar{1}$]). The cation sites are located at 4-fold rotation points (site symmetry $4mm$), either at 0 0 or at $\frac{1}{2}$ $\frac{1}{2}$. The oxygen atoms occupy the following positions:

1. Either $\frac{1}{2}$ $\frac{1}{2}$ or 0 0 for AO and BO layers
2. $\frac{1}{2}$ 0 and 0 $\frac{1}{2}$ for AO_2, DO_2 and O_2 layers
3. $\frac{1}{2}$ $\frac{1}{2}$ (or 0 0), $\frac{1}{2}$ 0 and 0 $\frac{1}{2}$, with partial occupancy, for AO'' layers

Some structures contain distorted layers, in particular distorted *additional* layers, which can generally be described in the rectangular plane groups $p2mm$ or $c2mm$, as shown in Fig. 8.8. In the latter case the cell vectors correspond to the diagonals of the small cell ($a' \approx b' \approx 5.4$ Å) and the number of atoms in the cell doubles. The AO' layer, shown in Fig. 8.2, is also described in the rectangular plane group $p2mm$. The cell parameter ratio $b/a > 1$, if, by convention, the oxygen atoms are located along [0 1].

b. Space Groups for Basic Structures

When the lattice of perovskite is distorted so that $a = b < c$, all 3-fold axes are suppressed and of the three mutually perpendicular 4-fold rotation axes, only the axis along [0 0 1] remains. Such a $B_1D_1O_3$ structure (**0101**, $LaCuO_{2.95}$), containing two layers in the translation unit like the cubic perovskite structure, is described in the tetragonal space group $P4/mmm$, which is a maximal nonisomorphic subgroup of $Pm\bar{3}m$. The cation sites are located at the intersec-

Fig. 8.8.

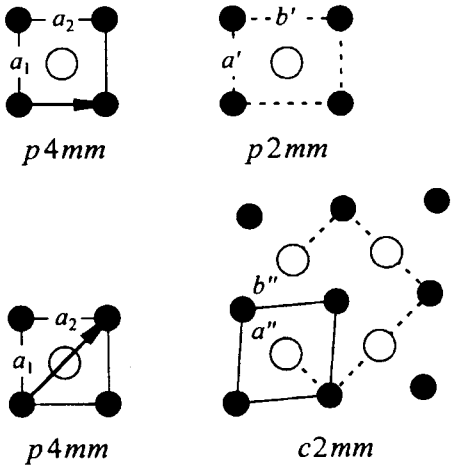

Rectangular and rhombal distortions of a primitive square cell (plane group $p4mm$) leading to a primitive rectangular ($p2mm$) and a 2-fold centered rectangular ($c2mm$) cell, respectively.

tions of the 4-fold rotation axes and the mirror planes perpendicular to these (site symmetry $4/mmm$). The tetragonal structure of $BaTiO_3$ presents similar distortions, the space group being, however, $P4mm$, because of additional deformations leading to puckered layers.

When the atom layers described in the square planar group $p4mm$ are added to the **0101** structure, the symmetry remains tetragonal if the 4-fold rotation points of the new layers coincide with the 4-fold rotation axes of the initial structure. This is the case for an ideal basic structure, even if the cation sites in neighboring layers are never stacked directly on top of each other, but are shifted by a vector $\frac{1}{2}\ \frac{1}{2}$ in the plane, that is, from one 4-fold rotation axis to another. The space group of the resulting, undistorted structure will preserve the 4-fold rotation axes parallel to the stacking direction, as well as the mirror planes perpendicular to the cell axes [0 1 0] and [1 0 0], and to the diagonals of these.

As explained previously, the translation period of the resulting structure must contain an even number of shifts by $\frac{1}{2}\ \frac{1}{2}$, and therefore an even number of cation-containing layers (see Section C,c). If the sum of the numbers in the four-digit code ($N = \boldsymbol{k} + \boldsymbol{l} + \boldsymbol{m} + \boldsymbol{n}$) is even, the unit cell is primitive and the translation period contains one stacking unit. If, on the other hand, it is odd, the unit cell is body-centered and contains two stacking units. Thus, depending on the number of layers in the stacking unit, the tetragonal Bravais lattice for an ideal basic structure $A_kB_lC_mD_nO_{k+l+2m+2}$, containing no AO' layers, will be either primitive (P) or body-centered (I).

Each $A_kB_lO_{k+l}$ and $C_mD_nO_{2m+2}$ slab has, in addition to the 4-fold rotation axes and the mirror planes containing these, a symmetry plane (mirror plane m or

diagonal glide plane n), situated halfway between its external layers. When the number of layers in the slab, $(k + l)$ or $(m + n)$, is even, the symmetry plane is located between two cation-containing layers, that is, between two AO or two BO ($k = 0$) layers for a $A_kB_lO_{k+l}$ slab, and between two C layers, coinciding with an inner O_2 layer, for a $C_mD_nO_{2m+2}$ slab. Because of the shift by $\frac{1}{2}\,\frac{1}{2}$ of the cation sites in consecutive layers, the plane is in this case a diagonal glide plane n. In contrast, when the number of layers in the slab is odd, the symmetry plane coincides with an atom layer. This may be an inner AO or BO ($k = 0$) layer for the $A_kB_lO_{k+l}$ slab and a C (n even) or an inner DO_2 (n odd) layer for the $C_mD_nO_{2m+2}$ slab. The plane is here a simple mirror plane m. Combining the two kinds of slab, three cases may occur:

1. Both $(k + l)$ and $(m + n)$ are even: The combination of the two glide planes n results in space group $P4/nmm$ with one stacking unit in the translation period. The **0222** structure, shown in Fig. 8.9 is an example of this category.
2. Both $(k + l)$ and $(m + n)$ are odd: The two mirror planes m give space group $P4/mmm$ with one stacking unit in the translation period. This case is illustrated in Fig. 8.9 by the **1223** structure.
3. $(k + l)$ and $(m + n)$ are of different parity: One mirror plane m and one diagonal glide plane n lead to space group $I4/mmm$ with two stacking units in the translation period. The **2201** structure is representative for this category.

These cases are summarized in Table 8.1, which has been subdivided to consider the different parity of the individual indices. It results from the stacking rules described earlier that k and l cannot be odd simultaneously (if $l = 1$, $k = 0$). The same is true for m and n, since $m = p(n-1)$.

The ideal basic structures can thus be described in one of the following tetragonal space groups: $P4/mmm$ (or cubic $Pm\bar{3}m$ in the particular case of idealized perovskite), $P4/nmm$, or $I4/mmm$. Indeed, the crystal structures of the majority of the high-T_c superconducting cuprates known up to now have been refined in one of these groups. However, space groups of lower symmetry have been used to describe and refine some crystal structures with significant distortions. The group–maximal nonisomorphic subgroup relationships that lead from one of the space groups listed previously to space groups used in data sets given in Section H,b are indicated in Table 8.2. The lowering of symmetry observed for the real structures may be caused by any of the following:

1. Displacements of the atoms from the ideal positions
2. An ordered arrangement of different cations within layers of the same kind
3. An ordered arrangement of vacancies
4. The insertion of extra atoms

Fig. 8.9.

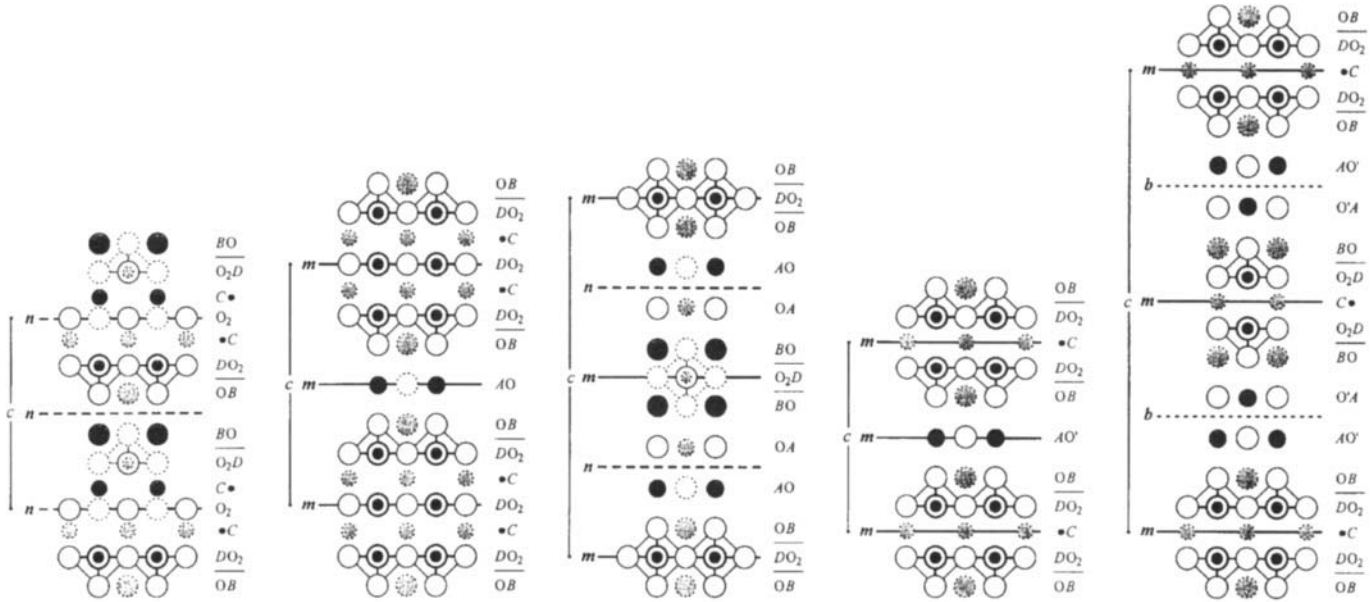

Examples of cuprate structures with different symmetries. The symmetry planes (*m*, mirror; *n*, diagonal glide; *b*, axial glide plane) perpendicular to the stacking direction ([0 0 1]) are indicated; the Pearson code and the space group are given.

Table 8.1.

Space groups for undistorted basic structures of high-T_c superconducting cuprates as derived from the parity of the numbers k, l, m, and n in the four-digit code.

		$(k+l)$ even		$(k+l)$ odd	
		k odd, l odd impossible	k even, l even ($l=2$)	k even, l odd ($k=0$, $l=1$)	k odd, l even ($l=2$)
$(m+n)$ even	m odd, n odd impossible	×	×	×	×
	m even, n even (p even)	×	*P4/nmm*	*I4/mmm*	*I4/mmm*
$(m+n)$ odd	m even, n odd	×	*I4/mmm*	*P4/mmm*	*P4/mmm*
	m odd, n even (p odd)	×	*I4/mmm*	*P4/mmm*	*P4/mmm*

Table 8.2.

Group–maximal nonisomorphic subgroup relationships[a] for basic structures of superconducting cuprates. Standard settings according to the International Tables for Crystallography (Hahn, 1983) are given within parentheses. Space group symbols within square brackets are not represented among the data sets reported here but complete the transformation paths.

Space group of ideal structure	Path to space group of distorted basic structure		
$[Pm\bar{3}m]$	**I** → *P4/mmm*		
	I → $[R\bar{3}m]$	**IIb** → $R\bar{3}c$	
P4/mmm	**I** → *Pmmm*		
	I → *Cmmm*	**IIa** → *Pman* (*Pmna*)	
		IIb → *Imam* (*Imma*)	**I** → *I2cm* (*Ima2*)
	IIb → *P4/mbm*		
P4/nmm	**I** → *Cmma*		
I4/mmm	**I** → *I4mm*		
	I → *Fmmm*	**IIa** → *Bmab* (*Cmca*)	
		IIa → *Amaa* (*Cccm*)	**I** → *A2aa* (*Ccc2*)
		IIa → [*Bbmb* (*Cccm*)]	**IIa** → *Pnan* (*Pnna*)
	IIa → $[P4_2/mmc]$	**IIb** → $P4_2/ncm$	

[a] **I**, *translationengleiche* (t) subgroup (all translations are retained but certain point symmetry operations are lost); **II**, *klassengleiche* (k) subgroup (**IIa**, the unit cell is retained but the space group is different; **IIb**, the unit cell is larger owing to the loss of some of the integral translations and the space group is different).

These lead, in a majority of cases, to structures that are described in orthorhombic space groups with cell vectors $\mathbf{a} + \mathbf{b}$, $-\mathbf{a} + \mathbf{b}$ and $\mathbf{c}$ ($a' \approx b' \approx 5.4$ Å), where **a**, **b**, and **c** are the cell vectors of the ideal structures. Note that the orthorhombic structure of $BaTiO_3$ (space group *Cm2m*) presents distortions resulting in a similar cell. Owing to positional or occupational commensurate modulations, superstructures with large unit cells are sometimes observed. Incommensurately modulated structures are also known.

As stated previously, the symmetry considerations up to now do not apply to structures containing AO' layers. The oxygen atoms in these layers center the square edges only in one direction, breaking the 4-fold symmetry. Among the basic structures of superconducting cuprates, there are two well-known examples, $Ba_2YCu_3O_7$ (**1212**, $CuBa_2YCu_2O_7$) and $Ba_2YCu_4O_8$ (**2212**, $Cu_2Ba_2YCu_2O_8$), where the undistorted structures are orthorhombic. Both structures contain *additional* CuO layers, the copper atoms of which center mutually parallel squares of oxygen atoms perpendicular to the layer. The replacement of a single AO layer by a AO' layer, as in $Ba_2YCu_3O_7$, does not alter the general stacking scheme, but the 4-fold rotation axis is reduced to a 2-fold one. The resulting orthorhombic structure, shown in Fig. 8.9, is described in space group *Pmmm*, which is a direct subgroup of *P4/mmm* ($(\boldsymbol{k} + \boldsymbol{l})$ odd, $(\boldsymbol{m} + \boldsymbol{n})$ odd). The cell parameter b is slightly larger than a, because of the presence of oxygen atoms along [0 1 0] in the AO' layer. The structure can be derived from the structure of $Ba_2YCu_3O_{6.26}$ with the same four-digit code (**1212**), space group *P4/mmm*, where one-third of the copper atoms form A layers, considering an ordered arrangement of extra oxygen atoms in the *additional* layer.

In the case of $Ba_2YCu_4O_8$ (**2212**), the two consecutive AO' layers are shifted by 0 $\frac{1}{2}$ with respect to each other if, by convention, the oxygen atoms in the AO' layers are located along [0 1 0]. Such a shift corresponds to an axial glide plane b, situated between the two layers, that is, halfway between the BO layers delimiting the $A_2B_2O_4$ slab. Combined with the mirror plane m coinciding with the central C layer of the CD_2O_4 slab, this leads to space group *Ammm* (standard setting *Cmmm*). There are two stacking units in the translation period along c and the cell parameter ratio $b/a > 1$ (Fig. 8.9).

c. Space Groups for Limiting Structures

Like the majority of the basic structures, the limiting structures with the general formula C_pDO_{2p} are described in tetragonal space groups. When $\boldsymbol{p}$ is odd, the translation period contains two mirror planes m. The first one coincides with the DO_2 layer and the other one with the inner C layer. This combination yields space group *P4/mmm* with one stacking unit in the translation period (**0011**, (Sr,La)CuO_2). When $\boldsymbol{p}$ is even, the mirror planes through the DO_2 layers alternate with diagonal glide planes n, which coincide with the O_2 layer situated between

the internal C layers. The resulting space group is $I4/mmm$ with two stacking units in the translation period (**0021**, $(Nd,Ce)_2CuO_{3.92}$).

d. Space Groups for Intergrowth Structures

As for the basic structures, the 4-fold rotation axes and the mirror planes containing these are preserved in the intergrowth structures, as long as there are no AO' layers. When the total number of cation-containing layers in all stacking units forming an intergrowth structure, that is, the sum of the numbers in all four-digit codes, is even, the tetragonal Bravais lattice is primitive; otherwise, it is body-centered. Three cases may be distinguished:

1. The $A_{k_1}B_{l_1}O_{k_1+l_1}$ and $A_{k_2}B_{l_2}O_{k_2+l_2}$ slabs are identical, that is, $\boldsymbol{k_1 = k_2}$ and $\boldsymbol{l_1 = l_2}$
2. The $C_{m_1}D_{n_1}O_{2m_1+2}$ and $C_{m_2}D_{n_2}O_{2m_2+2}$ slabs are identical, that is, $\boldsymbol{m_1 = m_2}$ and $\boldsymbol{n_1 = n_2}$
3. The corresponding slabs in the two stacking units are different

In cases (1) and (2), only the symmetry planes in the corresponding slabs that are different will remain. As for the basic structures, the space group is either $P4/mmm$, $P4/nmm$, or $I4/mmm$, depending in case (1) on the parity of $(\boldsymbol{m_1 + n_1})$ and $(\boldsymbol{m_2 + n_2})$ and in case (2) on the parity of $(\boldsymbol{k_1 + l_1})$ and $(\boldsymbol{k_2 + l_2})$. This is summarized in Table 8.3 and illustrated for case (2) by the idealized structure of $CBi_2Sr_4Cu_2O_{11}$ (**1201/2201**) in Fig. 8.10.

Table 8.3.

Space groups for undistorted intergrowth structures of high-T_c superconducting cuprates with identical $A_{k_1}B_{l_1}O_{k_1+l_1}$ and $A_{k_2}B_{l_2}O_{k_2+l_2}$ (or $C_{m_1}D_{n_1}O_{2m_1+2}$ and $C_{m_2}D_{n_2}O_{2m_2+2}$) slabs as derived from the parity of $(\boldsymbol{m_1 + n_2})$ and $(\boldsymbol{m_2 + n_2})$ [or $(\boldsymbol{k_1 + l_1})$ and $(\boldsymbol{k_2 + l_2})$].

	$\boldsymbol{k_1 = k_2, l_1 = l_2}$ $[\boldsymbol{m_1 = m_2, n_1 = n_2}]$	
	$(\boldsymbol{m_1 + n_1})$ even $[(\boldsymbol{k_1 + l_1})$ even$]$	$(\boldsymbol{m_1 + n_1})$ odd $[(\boldsymbol{k_1 + l_1})$ odd$]$
$(\boldsymbol{m_2 + n_2})$ even $[(\boldsymbol{k_2 + l_2})$ even$]$	$P4/nmm$	$I4/mmm$
$(\boldsymbol{m_2 + n_2})$ odd $[(\boldsymbol{k_2 + l_2})$ odd$]$	$I4/mmm$	$P4/mmm$

Fig. 8.10.

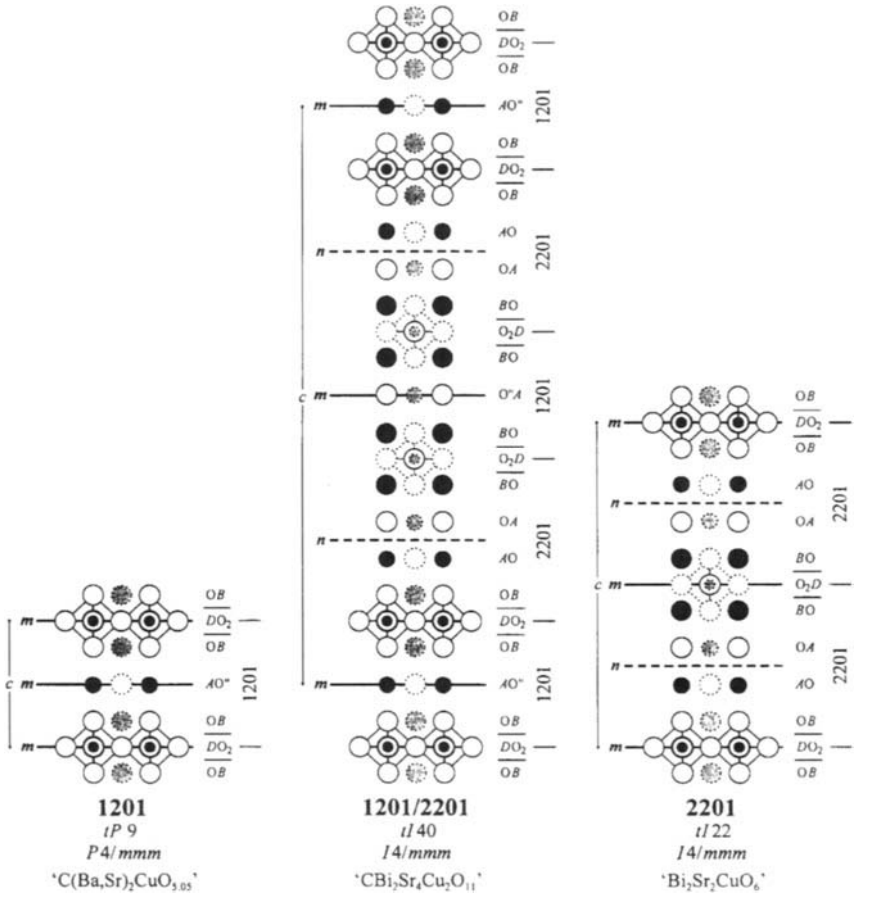

The **1201/2201** structure, an example of an intergrowth of two basic structures. The interfaces and symmetry planes (*m*, mirror; *n*, diagonal glide plane) perpendicular to the stacking direction ([0 0 1]) are indicated; the Pearson code and the space group are given. The real structures of the examples chosen here have lower symmetry.

In case (3) all symmetry planes perpendicular to the 4-fold rotation axes present in the basic structures are lost and the space group is either *P*4*mm* or *I*4*mm*, depending on the sum of the numbers in the two four-digit codes.

Note that if the site occupations in the two slabs with identical indices are different, the symmetry plane perpendicular to the stacking direction is lost. As stated previously, structures where the $A_{k_1}B_{l_1}O_{k_1+l_1}$ and $A_{k_2}B_{l_2}O_{k_2+l_2}$ slabs and/or the $C_{m_1}D_{n_1}O_{2m_1+2}$ and $C_{m_2}D_{n_2}O_{2m_2+2}$ slabs differ only in the chemical composition are here considered as superstructures resulting from cation ordering (e.g., **1201**, (C,Tl,Pb)Sr_2CuO_5) and not as intergrowth structures.

Table 8.4.

Group–maximal nonisomorphic subgroup relationships for intergrowth structures of superconducting cuprates (for notations, see Table 8.2).

Space group of ideal structure	Path to space group of distorted intergrowth structure	
[*P*4/*mmm*]	**I** → [*Cmmm*]	**IIa** → *Pbmm* (*Pmma*)
*I*4/*mmm*	**I** → [*Fmmm*]	**IIa** → *Abmm* (*Cmma*)

The majority of the intergrowth structures known up to now are described in subgroups of the space groups derived for the ideal structures. Group–maximal nonisomorphic subgroup relationships are presented in Table 8.4.

Intergrowth of $Ba_2YCu_3O_7$ (**1212**) and $Ba_2YCu_4O_8$ (**2212**), crystallizing in the orthorhombic space groups *Pmmm* and *Ammm*, respectively, is known for the compound $Ba_4Y_2Cu_7O_{14.94}$ (**1212/2212**, $CuBa_2YCu_2O_{6.94}/Cu_2Ba_2YCu_2O_8$). The total number of layers in the four slabs is odd, that is, there are two stacking units from each parent structure in the translation period. Since the basic structures contain identical CD_2O_4 (YCu_2O_4) slabs, the axial glide planes *b*, situated between the two consecutive AO' (CuO) layers in the $A_2B_2O_4$ slab from **2212**, and the mirror planes *m*, coinciding with the AO' layers in the AB_2O_3 slab from **1212**, remain from the basic structures and alternate along [0 0 1]. The space group of the resulting structure is *Ammm* and the cell parameter ratio $b/a > 1$ (oxygen atoms in the AO' layers located along [0 1 0]).

F

Ideal and Real Cation Coordinations

The ideal coordination of the cation derives from the stacking of the layers, the cation in each layer being surrounded by oxygen atoms from the same and/or the directly neighboring layers (see Fig. 8.3). The real coordinations are often distorted to better accommodate a particular cation. The strongest covalent bonding is generally observed within the DO_2 (CuO_2) layers and within the coordination polyhedra of the *A* cations.

a. Coordination Polyhedra

Figure 8.11 shows ideal coordination polyhedra represented in high-T_c superconducting cuprates. The coordination number of the *D* (Cu) atoms can be 6, 5, or 4. Six oxygen neighbors form an octahedron (6o), as in perovskite. This coordination of the *D* atoms is observed only in cuprates ***kl*01** with a single

Fig. 8.11.

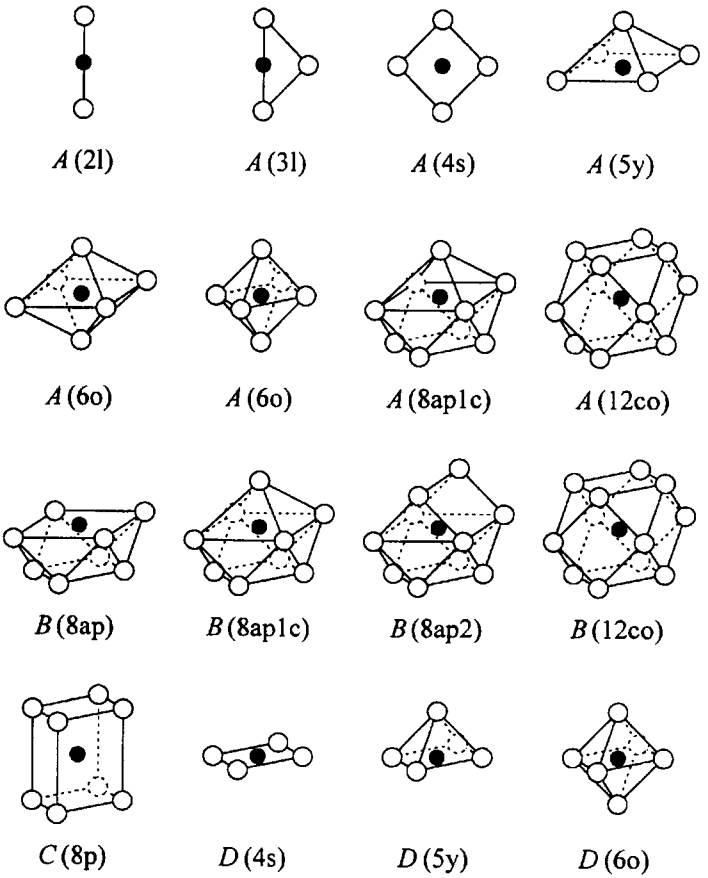

Commonly observed coordination polyhedra built up of oxygen atoms around the *A*, *B*, *C*, and *D* cations: 21, two collinear atoms; 31, triangle; 4s, square; 5y, square pyramid; 6o, octahedron; 8ap, square antiprism; 8aplc, monocapped square antiprism; 8ap2, square antiprism with two additional atoms; 12co, cuboctahedron; and 8p, tetragonal prism.

conducting DO_2 layer in the stacking unit (e.g., **1201**, $Tl_{0.92}(Ba,La)_2CuO_{4.86}$). Coordination number five, a square pyramid (5y), is present when there are two or more DO_2 layers (**1212**, $TlBa_2(Ca,Tl)Cu_2O_7$). In the latter case the 5-fold coordinated *D* atoms are located in the external DO_2 layers, whereas the *D* atoms in the internal layers are 4-fold coordinated, the oxygen atoms forming a square (4s) (**1223**, $(Tl,Pb)Sr_2(Ca,Tl,Pb)_2Cu_3O_9$) (see also Fig. 8.5). In all cases four oxygen atoms are situated in the DO_2 layer, the apical oxygen atom, when present, belonging to the neighboring *B*O layer.

In all structures of superconducting cuprates, only one type of coordination polyhedron is observed for the *C* atoms, that is, a tetragonal prism (8p). The

oxygen atoms forming the tetragonal prism may belong to two neighboring DO_2 layers (**0212**, $(La,Sr,Ca)_2(Ca,La)Cu_2O_{5.91}$), one DO_2 and one O_2 layer (**0222**, $(Nd,Sr)_2(Nd,Ce)_2Cu_2O_{7.84}$), or two O_2 layers (**0232**, $Sr_2(Ce,Y)_3(Cu,Fe)_2O_{10}$) (see also Fig. 8.6).

The coordination number of the *B* atoms in perovskite and cuprates containing one *bridging* *B*O layer in the stacking unit is 12, the surrounding oxygen atoms forming a cuboctahedron (12co) (**0112**, $BaY(Cu,Fe)_2O_5$). Four oxygen atoms are located in the *B*O layer, and the other eight in the two neighboring DO_2 layers. When a second *B*O layer is added, the coordination number of the *B* atoms is reduced to 9, the nine oxygen atoms forming a monocapped square antiprism (8ap1c) (**0212**). In the real structures the *B*O layers are often puckered so that the *B* atoms are located closer to the center of the polyhedron. This coordination is also observed when an *A*O layer with oxygen atoms centering all squares of the cation square mesh is present (**1212**, $TlBa_2(Ca,Tl)Cu_2O_7$) (see also Fig. 8.4). Depending on the number and the arrangement of the oxygen atoms in the neighboring *additional* layer, the coordination number of the *B* cation varies: 8 (square antiprism, 8ap) for an *A* layer (**1212**, $CuBa_2YCu_2O_{6.26}$), 10 (two capping atoms on one side, 8ap2) for an AO' layer (**1212**, $CuBa_2YCu_2O_7$), and 12 (cuboctahedron) for an AO_2 layer (**4212**, $(Ti,Gd,Ca)_4Ba_2(Gd,Ca)Cu_2O_{12}$). The *B* sites are occupied by Ba, Sr, or rare-earth elements in ionized states, with little localized bonding and consequently few requirements on the shape of the coordination polyhedron.

Depending on the exact type of *additional* layers present (*A*, *A*O, AO', AO'', or AO_2), a wide range of different coordinations are found. In contrast to the *B* metal atoms, the elements found on the *A* sites, generally nonmetals, have characteristic coordination polyhedra, with a large proportion of covalent bonding. Five types of ideal coordination polyhedra are observed: two collinear atoms (2l), a triangle (3l), a square (4s), a square pyramid (5y), and an octahedron (6o). Linear coordination is typical for Hg or Cu. In this case the *additional* layer contains no oxygen atoms (type *A*), and the neighboring layers are either *B*O (**1201**, $HgBa_2CuO_{4.18}$) or *A*O (**3212**, $(Pb,Cu)_3Sr_2YCu_2O_8$). Trigonal coordination is characteristic of carbon atoms (**1201**, $C(Ba,Sr)_2CuO_{5.05}$), the structures containing planar carbonate units, perpendicular to the AO'' layers. Square coordination is observed for copper atoms in AO' layers, the two neighboring layers being *A*O and/or *B*O (**1212**, $CuBa_2YCu_2O_7$). To achieve square pyramidal coordination, sometimes found for lead atoms (**3212**, $(Pb,Cu)_3Sr_2YCu_2O_8$), one of the surrounding layers must contain no oxygen atoms (type *A*). Bi, Pb, and Tl preferentially form *A*O layers, which would lead to 6-fold, octahedral coordination. The real coordination polyhedra are, however, often strongly distorted because of the presence of lone-electron pairs, and the cations displaced from the centers of the original octahedra (**2212**, $(Bi,Pb)_2Sr_2(Y,Ca)Cu_2O_8$). The presence of AO_2 layers will give rise to higher coordination numbers, suitable for metal atoms. When the structure contains four *additional* layers in the stacking sequence -AO_2–*A*O–*A*O–AO_2-, for instance, the cations of the

internal layers have monocapped square antiprismatic coordination (8ap1c, **4212**, $(Ti,Gd,Ca)_4Ba_2(Gd,Ca)Cu_2O_{12}$). In $(Ti,Sm,Ca)_5Ba_2(Ca,Sm)Cu_2O_{14}$ (**5212**), where the number of *additional* layers is five, AO_2 layers alternating with AO layers, the cations from the AO layers are 12-fold coordinated (cuboctahedron, 12co), yielding a local perovskite-like atom arrangement.

b. Interatomic Distances

Displacements of the atoms from their ideal positions distort the coordination polyhedra, and the interatomic distances from the cations to the surrounding oxygen atoms exhibit a wide range of values.

The atoms in the *conducting* DO_2 layers are tightly bonded, and the in-plane Cu–O distances vary little from one superconducting cuprate to another. Usual distances range from 1.92 to 1.94 Å, the shortest distance (1.89 Å) being reported for **0201** $(La,Sr)_2CuO_4$) and the longest one (1.98 Å) for **1201** $(C(Ba,Sr)_2CuO_{5.05})$ and **0011** $((Sr,La)CuO_2)$. This relatively rigid atom layer determines the values of the cell parameters a and b, a slight puckering being possible. When there are two or more DO_2 layers, the copper atoms from the outside DO_2 layers are slightly moved from the center of the square base toward the center of the pyramid. The distances from the copper atoms to the oxygen atoms located in the BO layers, that is, the apical atoms of the square pyramid or octahedron, are considerably longer (2.10–2.82 Å), in agreement with the Jahn–Teller effect. The large variations observed for this Cu–O distance depend on the size of the B atom and the chemical nature of the A cations. For structures with *bridging* SrO layers, the distances from the copper atoms to the apical oxygen atoms are in general shorter than for structures containing BaO layers. When *additional* layers are present, the same apical oxygen atoms are usually tightly bonded to the A cations, situated on the other side of the BO layer. For example, in structures of Hg-based compounds, because of the bonding between the oxygen atoms from the BO layers and the mercury atoms (and because of the presence of barium atoms in the BO layers), the apical Cu–O distances are very long (2.70–2.82 Å).

For structures with only one *separating* C layer between two consecutive DO_2 layers, the tetragonal prisms around the C atoms are almost regular. The C–O interatomic distances range from 2.39 to 2.61 Å. In general, yttrium atoms have shorter C–O distances than calcium atoms. For structures with two or more C layers between consecutive DO_2 layers, the distances from the C atom to the oxygen atoms in the O_2 layers are slightly shorter (2.26–2.39 Å).

For distorted perovskite-type structures (one BO layer) the interatomic distances from the B atoms to the vertices of the surrounding cuboctahedra range from 2.50 to 3.01 Å. For structures with two *bridging* BO layers, where only half of the cuboctahedron (square antiprism) remains, there are four distances of similar length to the oxygen atoms in the DO_2 layer (2.58–2.97 Å, depending on

the *B* cation) and four distances of similar length to the oxygen atoms within the *B*O layer (2.73–2.88 Å). The distances to the capping oxygen atoms in the neighboring *bridging* or *additional* layer vary from 2.28 to 2.37 Å and from 2.61 to 3.19 Å, respectively.

The *A*–O interatomic distances, like the coordination polyhedra of the *A* atoms, depend on the chemical nature of the cation. As in the previous cases, they are of the same magnitude as those commonly observed for the corresponding cations (e.g., Hg^{2+}, Cu^{2+}, C^{4+}, Bi^{3+}, Pb^{2+}, Tl^{3+}) in other oxides. The distances between the mercury and oxygen atoms along the stacking direction vary from 1.92 to 2.01 Å. The corresponding distances for copper atoms in the same 2-fold linear coordination range from 1.81 to 1.89 Å. Copper atoms in 4-fold coordination have two distances of 1.94 Å to oxygen atoms within the *A*O′ layer and two shorter distances (~1.84 Å) to oxygen atoms from neighboring *A*O′ and/or *B*O layers. Carbon atoms usually show three similar *A*–O distances of 1.23–1.29 Å. The displacement of the atoms in the *A*O layers containing Pb are such that the square pyramids are strongly distorted with three short distances (including one to an oxygen atom in the neighboring *B*O layer) of 2.14–2.48 Å and two long distances of 2.95–3.23 Å. The resulting coordination polyhedron can be described as a tetrahedron with one of the vertices occupied by a lone electron pair (ψ-tetrahedron). In a similar way, the ideal octahedra around thallium and bismuth atoms are transformed into tetrahedra and ψ-tetrahedra, respectively. The interatomic distances from thallium atoms to the two oxygen atoms in the neighboring *A*O and/or *B*O layers vary from 1.82 to 2.20 Å, whereas the distances to the four oxygen atoms within *A*O layer range from 2.30 to 2.56 (two short) and from 2.77 to 3.16 Å (two long distances). Bismuth atoms are not bonded to the oxygen atoms in the neighboring *A*O (BiO) layer, the distance to the oxygen atoms in *B*O layer being 1.96–2.08 Å. Within the *A*O layer there are usually two short (2.02–2.61 Å) and two long interatomic distances, or three short (2.10–2.70 Å) and one long distance.

G

Chemical Families

Chemical families of high-T_c superconducting cuprates are usually denoted by the cation in the *additional* layers. This allows one to emphasize structural features (including distortions) common to a particular group of compounds. Cuprates containing halogens and so-called ladder compounds will also be briefly discussed. References are specified for first reports, whereas other references for compounds mentioned here can be found with the data sets in Section H,b. Compounds with structures containing four and more *additional* layers and mainly metal atoms, such as Ti, on the *A* sites are known, but so far no superconductivity has been reported.

a. Rare-Earth–Alkaline-Earth Cuprates

The structures of the compounds considered in this section contain no *additional* layers, whereas rate-earth–alkaline-earth superconducting cuprates with A or AO' layers are treated in the next section.

The first **0101** cuprate, $LaCuO_3$, was prepared by Demazeau *et al.* (1972) at high pressure. It crystallizes with a trigonal structure based on an R Bravais lattice, a distorted variant of the cubic perovskite-type structure. Copper is in the oxidation state Cu^{3+} and the compound is not superconducting. Decreasing the oxygen content produces vacancies in the CuO_2 layers. Other members of the structure series with the general formula $BC_mD_nO_{2m+3}$ (pervoskite is the first member with $\boldsymbol{n} = 1$ and $\boldsymbol{m} = 0$), reported so far, were prepared with a mixture of Cu and Fe or Co on the D site, none of them being superconducting.

The structure series with the general formula $B_2C_{n-1}Cu_nO_{2n+2}$ includes structures with two *bridging* layers in the stacking unit. La_2CuO_4 (Longo and Raccah, 1973; Grande *et al.*, 1977), $LaSrCuO_4$ (Goodenough *et al.*, 1973), and $La_{2-x}Ba_xCuO_4$ ($x = 0$–0.2) (Michel and Raveau, 1984) crystallize with a body-centered tetragonal K_2NiF_4-type structure (Balz, 1953) or with an orthorhombically distorted variant ($\boldsymbol{n} = 1$, **0201**). The discovery of superconductivity in the La–Ba–Cu–O system ($T_c = 30$ K) by Bednorz and Müller (1986) started the era of high-temperature superconductivity. Superconductivity for **0201** compounds can be achieved not only by partial substitution of trivalent La by a divalent alkaline-earth element, but also by insertion of additional oxygen. At low temperature and/or for a low content of alkaline-earth element, the crystal structures of these compounds are distorted (primitive tetragonal or orthorhombic), while at high temperature and/or for a higher Ba(Sr) content the structures remain of the K_2NiF_4 type.

The second member of the structure series ($\boldsymbol{n} = 2$, **0212**) was first prepared by Nguyen *et al.* (1980) for $La_{2-x}M_{1+x}Cu_2O_{6-\delta}$ (M = Sr or Ca, $x = 0$–0.14). Superconductivity is known only for Ca-containing compounds and was discovered by Cava *et al.* (1990a) for $La_{1.6}Sr_{0.4}CaCu_2O_6$ ($T_c = 60$ K).

Members with $\boldsymbol{n} = 3$ (**0223**) and $\boldsymbol{n} = 4$ (**0234**), with superconducting transition temperatures of about 90 and 70 K for the nominal compositions $Sr_{0.6}Ca_{0.33}CuO_{2.10}$ and $Sr_{0.65}Ca_{0.3}CuO_{2.10}$ (synthesized at high pressure), respectively, were first reported by Adachi *et al.* (1993). Later on it was shown that **0223** compounds may also be prepared without calcium.

A superconducting ($T_c = 28$ K) **0222** compound was reported by Akimitsu *et al.* (1988) in the Nd–Sr–Ce–Cu–O system (nominal composition $Nd_2Sr_{0.5}Ce_{0.5}Cu_{1.2}O_y$). In contrast to the structures belonging to the series mentioned above, where the CuO_2 layers are separated by a single C layer with mainly alkaline-earth metal atoms, here the CuO_2 layers are separated by double C layers with La or rare-earth metal atoms. A **0232** compound with three *separating* layers between consecutive DO_2 layers has also been reported.

An infinite-layer compound (**0011**) was first prepared by Siegrist *et al.* (1988b) by stabilizing calcium cuprate by Sr ($Ca_{0.86}Sr_{0.14}CuO_2$), whereas the first superconductor, $Sr_{0.86}Nd_{0.14}CuO_2$ ($T_c = 40$ K), was reported by Smith *et al.* (1991). A nonsuperconducting **0021** compound, Nd_2CuO_4, was prepared by Müller-Buschbaum (and Wollschläger, 1975), superconductivity ($T_c = 24$ K) being reported by Tokura *et al.* (1989b) for the partly substituted derivative $Nd_{1.84}Ce_{0.16}CuO_{3.93}$.

b. Ba–Y Cuprates

Superconductivity in the Ba–Y–Cu–O system was discovered by Wu *et al.* (1987) for $Ba_{0.8}Y_{1.2}CuO_{4-\delta}$, the first compound that showed superconductivity above the temperature of liquid nitrogen and later identified as $Ba_2YCu_3O_{7-\delta}$ (**1212**) ($T_c = 93$ K for $\delta = 0.07$). For $\delta = 0$–0.6, the compound crystallizes with an orthorhombic structure. At $\delta = 0.6$, the structure becomes tetragonal and superconductivity is suppressed. On decreasing the oxygen content, the arrangement of the oxygen atoms in the *additional* CuO layer becomes disordered. The square planar coordination of the copper atoms (chains of corner-linked CuO_4 squares) is transformed to defect octahedral (random vacancies in the basal plane) and then reduced to 2-fold linear.

Another compound in the Ba–Y–Cu–O system, $Ba_2YCu_4O_8$ (**2212**), was identified as planar defects in $Ba_2YCu_3O_{7-\delta}$ by Zandbergen *et al.* (1988b) and was prepared as bulk material ($T_c = 81$ K) by Karpinski *et al.* (1988b). The **1212** and **2212** compounds can be described by the general formula $Cu_kBa_2YCu_2O_{k+6}$ ($k = 1$ and 2, respectively). In the structure of the latter, edge-linked CuO_4 squares form zigzag chains and, in contrast to the **1212** compounds, the oxygen content is fixed. A third superconducting compound in the same system, $Ba_4Y_2Cu_7O_{15-\delta}$ ($T_c = 92$ K), was observed by Zandbergen *et al.* (1988b) and further studied by Karpinski *et al.* (1988a). The structure consists of an intergrowth of **1212** and **2212** stacking units. Cu-**1222** compounds with a mixture of rare-earth elements (one of which is Ce) in the *separating* layers have also been reported.

c. Bi-Based Cuprates

A superconducting Bi-based material was found for the first time in the Bi–Sr–Cu–O system by Michel *et al.* (1987). A sample of nominal composition $Bi_2Sr_2Cu_2O_{7+\delta}$ was reported to have a transition temperature of up to 22 K, the superconducting compound being later identified as **2201**. Maeda *et al.* (1988) obtained a critical temperature above 105 K in the Bi–Sr–Ca–Cu–O system for the nominal composition $BiSrCaCu_2O_y$. The structures of Bi-based superconducting cuprates form a series with the general formula

$Bi_2B_2C_{n-1}Cu_nO_{2n+4}$ with mainly Sr and Ca on the *B* and *C* sites, respectively. The **2201** ($n = 1$) and **2212** ($n = 2$) compounds have considerable homogeneity ranges, and the **2223** ($n = 3$) compound is generally prepared with a partial substitution of Bi by Pb. The superconducting transition temperature increases with an increasing number of *conducting* CuO_2 layers up to 110 K (**2223**). Bi-**2222**, which is not a member of this structure series, has also been reported.

In all structures of Bi-based superconductors, the bismuth and oxygen atoms in the *additional* BiO layers are displaced from the ideal positions on the 4-fold rotation axes, along [1 1 0] of the tetragonal cell. The displacements occur in a progressive manner, resulting in the formation of voids large enough to accommodate extra oxygen atoms and incommensurate modulations. The translation period of the modulation depends on partial substitutions and on the oxygen content, but for particular compositions the structures can be conveniently described in large supercells. The Bi sites have ψ-tetrahedral coordination, typical for Bi^{3+}, the lone electron pairs being located between consecutive BiO layers that are hence only weakly bonded. The asymmetry of the BiO layer is probably the reason that phases with a single "pure" BiO layer are not known. A **1232** compound, containing a mixture of Bi and Cu in the *additional* *A*O layer and three *separating* *C* layers, has also been reported.

d. Tl- and Ga-Based Cuprates

The first Tl-based superconducting material was reported in the Tl–Ba–Cu–O system by Kondoh *et al.* (1988). A critical temperature of 19 K was measured for a sample of nominal composition $Tl_{1.2}Ba_{0.8}CuO_y$. Independently, Sheng and Hermann (1988a) reported critical temperatures up to 90 K for the nominal compositions $Tl_2Ba_2Cu_3O_{8+\delta}$, $TlBaCu_3O_{5.5+\delta}$, and $Tl_{1.5}Ba_2Cu_3O_{7.3+\delta}$, the superconducting compound being later identified as **2201**. A short time later, the same authors (Sheng and Hermann, 1988b) succeeded in preparing superconductors with $T_c = 120$ K in the Tl–Ba–Ca–Cu–O system for the nominal compositions $Tl_2BaCa_{1.5}Cu_3O_{8.5+\delta}$ and $Tl_{1.86}BaCaCu_3O_{7.8+\delta}$. At present, Tl-based cuprates constitute one of the largest chemical families of high-T_c superconductors, forming two distinct structure series with the general formulas $TlB_2C_{n-1}Cu_nO_{2n+3}$ and $Tl_2B_2C_{n-1}Cu_nO_{2n+4}$, respectively. The *B* atoms in compounds with single *additional* TlO layers are usually Ba and/or Sr (Tl being partly substituted by Pb or Bi in Sr-containing cuprates), whereas Sr-containing compounds with two TlO layers have not been reported so far. For both structure series, the *C* sites are mainly occupied by Ca, with small amounts of Tl. With an increasing number of *conducting* CuO_2 layers, the superconducting transition temperature progressively increases, reaching a maximum value for **1223**, **1234** ($\sim$120 K) and **2223** (125 K), and then decreases. Apart from the compounds that are members of these two structure series, other compounds, such as **1222** and **2222**, have also been reported.

A common feature of the structures of Tl-based superconductors is the displacement of the thallium and oxygen atoms in the *additional* TlO layers from the ideal positions on the 4-fold rotation axes. The resulting tetrahedral coordination of the thallium atoms is typical for Tl^{3+}. Vacancies may occur on the O sites in the *additional* layers.

Ga-based compounds were first reported by Vaughey *et al.* (1991) ($GaLaSrCuO_5$, **1201**) and Roth *et al.* (1991) ($Ga_{0.97}Sr_2YCu_2O_7$, **1212**), whereas the first superconductor ($T_c = 35$ K), a **1212** compound ($GaSr_2Er_{0.6}Ca_{0.4}Cu_2O_7$), was prepared by Cava *et al.* (1991). The structures of the Ga-based cuprates known so far contain a single *additional* GaO layer and are described by the general formula $GaB_2C_{n-1}Cu_nO_{2n+3}$. The *B* sites are occupied by Sr (or a mixture of Sr and La), superconductivity occurring when Ca is present on the *C* sites. As in the corresponding structures of Tl-based cuprates, the *A* cations are surrounded by oxygen atoms forming tetrahedra; however, the GaO_4 tetrahedra are arranged in chains along [1 1 0] of the tetragonal cell, lowering the symmetry to orthorhombic.

e. Pb-Based Cuprates

Bi- and Tl-based superconductors are often prepared with a partial substitution of Bi and Tl by Pb. In the latter case, the substitution can reach 50 at.%. Structures containing only Pb on the *A* sites in the *additional* layers are not known so far; however, a large number of compounds where Pb is the majority element on the *A* site are known and form a distinct family of Pb-based superconducting cuprates. Superconductivity was discovered in the Pb–Sr–Y–Ca–Cu–O system by Cava *et al.* (1988), a critical temperature of 68 K being measured for a sample of nominal composition $Pb_2Sr_2Y_{0.5}Ca_{0.5}Cu_3O_8$ (**3212**). For structures with a single *separating C* layer between consecutive DO_2 layers, the series with one, two, or three *additional* layers are described by the general formulas $(Pb,M)_kB_2C_{n-1}Cu_nO_{k+2n+2}$ ($\boldsymbol{k} = 1$, 2 or 3). The majority of the compounds contain trivalent cations (e.g., Y^{3+}) in the *separating C* layers and become superconducting when part of them are substituted by divalent cations (Ca^{2+}). The structures with two *separating C* layers between the DO_2 layers can be grouped into a series with the general formula $(Pb,M)_kB_2C_2Cu_2O_{k+8}$. Note that the general formulas given here consider *A*O layers but the total number of oxygen atoms in the *additional* layers may differ from $\boldsymbol{k}$.

In most Pb-based cuprates, copper atoms are also present in the *additional* layers, whereas for compounds with one *additional A*O layer, mixtures of lead (Pb^{4+}) and other elements (alkaline-earth, Sc, Cd) on the *A* site have also been reported. In compounds with three *additional* layers, the lead and copper atoms are always ordered, giving the stacking sequence PbO–Cu–PbO (oxidation states Pb^{2+} and Cu^{+}). Ordering can also occur in compounds with two *additional* layers.

f. Hg-Based Cuprates

Superconductivity for Hg-based materials was discovered in the Hg–Ba–Cu–O system ($HgBa_2CuO_{4.10}$, **1201**) by Putilin *et al.* (1993a), the critical temperature reaching 94 K. Later, Schilling *et al.* (1993) reported two high-T_c superconducting compounds in the Hg–Ba–Ca–Cu–O system, $HgBa_2CaCu_2O_{6+\delta}$ (**1212**) and $HgBa_2Ca_2Cu_3O_{8+\delta}$ (**1223**). The critical temperature of 133 K, attributed to Hg-**1223**, is the highest value reported so far at ambient pressure and can be increased to 157 K by applying high pressure (23.5 GPa). Hg-based superconducting cuprates form a series with the general formula $HgB_2C_{n-1}Cu_nO_{2n+2+\delta}$ (Fig. 8.12) with mainly Ba and Ca on the *B* and *C* sites, respectively. On increasing the number of CuO_2 layers, T_c progressively increases, reaching a maximum value for **1223**, and then decreases, as can be seen from Fig. 8.13.

For the members of this series, an extra O site in the *additional* layer is partly occupied and vacancies have often been reported also for the Hg site. The superconducting transition temperature depends on the oxygen content, each compound having an optimal value for δ, which increases with the number of *conducting* CuO_2 layers. Apart from the compounds that are members of the series mentioned earlier, a **2212** compound has also been reported.

g. C-Based Cuprates

The first cuprate containing carbonate groups (oxycarbonate), CSr_2CuO_5 (**1201**), was reported by von Schnering *et al.* (see Müller-Buschbaum, 1989), whereas superconductivity ($T_c = 26$ K) was discovered by Kinoshita and Yamada (1992a)

Fig. 8.12.

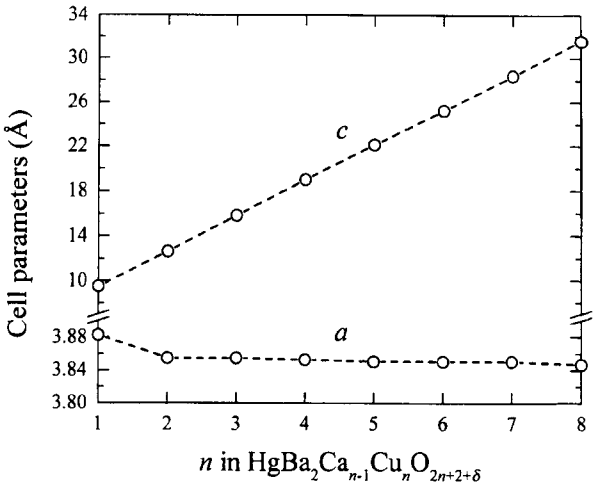

Cell parameters vs number of CuO_2 layers for Hg-based cuprates (Scott *et al.*, 1994).

Fig. 8.13.

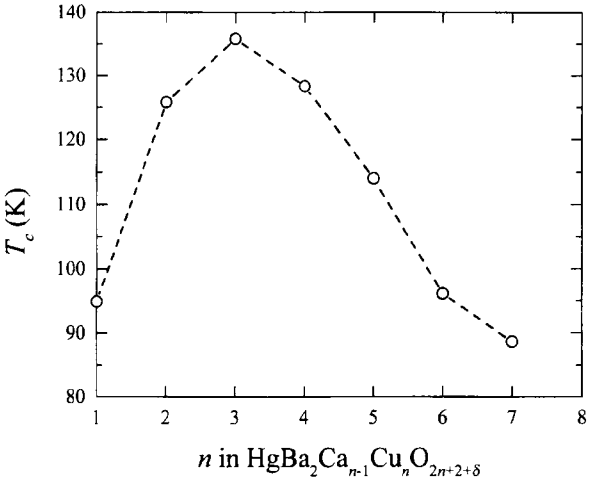

Superconducting transition temperature vs number of CuO_2 layers for Hg-based cuprates ($T_c < 90$ K for $n = 8$; Scott *et al.*, 1994).

in the C–Ba–Sr–Cu–O system ($C_{0.9}Ba_{1.1}Sr_{0.9}Cu_{1.1}O_{4.9+\delta}$). Carbon-based superconducting cuprates with a single *additional A* layer form a series with the general formula $(C,M)B_2C_{n-1}Cu_nO_{2n+3}$. In most compounds carbon is mixed with copper; however, partial substitutions of C by B, or even N, have also been reported. The oxygen atoms in the *additional* AO'' layer are displaced from the ideal positions on the cell edges (tetragonal cell) toward the carbon atoms to achieve triangular coordination of the carbon site. Depending on the C/Cu cation ratio in the *additional* layer and the orientation of the CO_3 triangles, different superstructures have been observed. Apart from the compounds with a single *additional* layer, superconducting oxycarbonates ($T_c = 91$–113 K) with two carbon-containing layers in the stacking unit have been reported (Kawashima *et al.*, 1994b,c). In the proposed structural models the (C,Cu)-containing layers are separated by a single BaO layer which is here also considered as an *additional* layer, these compounds thus having the four-digit codes **3223**, **3234**, and **3245**.

Boron-, phosphorus-, and sulfur-based superconducting cuprates also form structure series with a single *additional* layer. The phosphorus and sulfur atoms are 4-fold coordinated, located at the center of tetrahedra formed by oxygen atoms.

h. Cuprates with Halogens

During the past few years a number of compounds with partial substitution of oxygen by halogen (fluorine or chlorine), as well as compounds with "interstitial" halogen atoms (bromine or iodine), have been reported. The

majority of these compounds were prepared by high-pressure synthesis (4–6 GPa) giving only small amount of the final product, generally insufficient for a complete structure determination. In the present work, crystallographic parameters for such compounds are given only when the classification has been deduced.

Substitution of oxygen has been intensively studied for cuprates without *additional* layers, such as **0201** and **0212**. Substitution of O^{2-} by F^- (Cl^-) takes place in the *bridging* BO layers, making it possible to decrease the average oxidation state of the B cation and in some cases significantly increasing the critical temperature [e.g., $Ca_{1.9}Na_{0.1}CuO_2Cl_2$, $T_c = 26$ K (Argyriou *et al.*, 1995) and $Sr_{2.3}Ca_{0.7}Cu_2O_{4.76}Cl_{1.24}$, $T_c = 80$ K (Jin *et al.*, 1995)]. In the case where complete substitution has taken place in the *bridging* layers, an extra layer of halogen atoms can be inserted between consecutive BO layers, without changing the relative shifts of these, leading to a local fluorite-type atom arrangement [$Sr_2CuO_2F_{2.57}$, $T_c = 46$ K (Al-Mamouri *et al.*, 1994) and $Sr_2CaCu_2O_{4.6}F_{2.0}$, $T_c = 99$ K (Kawashima *et al.*, 1994a)].

According to some reports, bromine and iodine atoms can be incorporated into basic structures, forming an extra *additional* layer [$(Bi_2I)Sr_2Ca_2Cu_3O_y$ (**3223**), $T_c = 100$ K (Xiang *et al.*, 1991)].

i. Ladder Compounds

Compounds with the general formula $Sr_{n-1}Cu_{n+1}O_{2n}$ ($n = 3, 5, 7, \ldots, \infty$) were first reported by Hiroi *et al.* (1991). They are generally referred to as ladder compounds and can only be prepared at high pressure. Their structures contain $Cu_{n+1}O_{2n}$ layers separated by charge-compensating layers of strontium atoms (Fig. 8.14). In the former, zigzag chains of edge-linked CuO_4 squares share corners with m chains of corner-linked CuO_4 squares, leading to an alternative general formula:

$$(m+1)\mathrm{Sr} + \mathrm{Cu_2O_3} + m\,\mathrm{CuO_2} \rightarrow \mathrm{Sr}_{m+1}\mathrm{Cu}_{m+2}\mathrm{O}_{2m+3} \qquad (m = 0, 1, 2, \ldots, \infty).$$

In the limiting case where m is infinitely large, square-mesh DO_2 layers are formed and the infinite-layer compound (**0011**) is obtained.

Superconductivity at high pressure ($T_c = 12$ K at 3 GPa) has been observed by Uehara *et al.* (1996) for $Ca_{13.6}Sr_{0.4}Cu_{24}O_{41.84}$, which crystallizes with an orthorhombic, $(Sr_8Ca_6)Cu_{24}O_{41}$ (McCarron *et al.*, 1988) or $(Ca_8La_6)Cu_{24}O_{41}$ (Siegrist *et al.*, 1988a) type structure. In this structure Cu_2O_3 layers, similar to those found in the ladder compounds ($m = 0$), alternate with a new kind of CuO_2 layer, consisting of single straight chains of edge-linked CuO_4 squares. The squares of the Cu_2O_3 layer are rotated by 45° with respect to those of the CuO_2 layer and the translation periods approximately coincide for a ratio of multiples

Fig. 8.14.

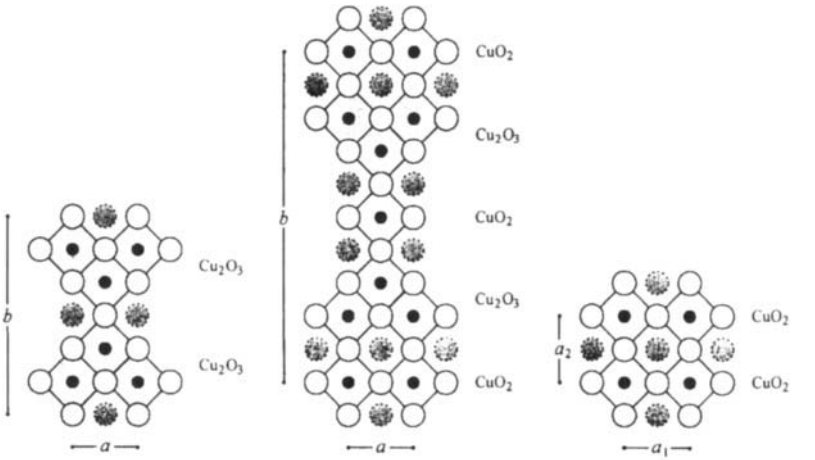

Ladder compounds $Sr_{m+1}Cu_{m+2}O_{2m+3}$ with layers built up of zigzag chains of edge-linked CuO_4 squares (shaded) and m chains of corner-linked CuO_4 squares running along [1 0 0]. Large shaded circles represent Sr atoms located between the layers. The Pearson code is given.

close to $\sqrt{2}/2$ (e.g., 7/10). As for the ladder compounds, the Cu-containing layers are separated by a layer of cations (C):

$$7\ C + 7\ Cu_2O_3 + 7\ C + 10\ CuO_2 \rightarrow C_{14}Cu_{24}O_{41}.$$

H

Crystallographic Data Sets

Next are given complete crystallographic data sets for 69 structures, followed by information on some 351 related compounds. Crystallographic data from studies on single crystals and powders by X-ray, neutron diffraction, and transmission electron microscopy, as well as hypothetical models, have been considered.

a. Conventions Used

Because of the difficulties in growing single crystals suitable for diffraction studies, the majority of the structural investigations reported in the literature on high-T_c superconductors were performed on powdered samples. Neutron

diffraction data allow a precise determination of the positional and occupational parameters of the oxygen sites, whereas, in some cases, X-ray diffraction data are more reliable for the refinement of the metal-atom distribution on the cation sites. Crystallographic data sets included in the present work refer to complete structural refinements carried out on superconducting cuprates that are widely recognized and contain the main structural features. Structures with short in-plane cell parameters corresponding to the perovskite cell (~3.85 Å) or its diagonal (~5.4 Å) are given in the data sets, whereas superstructures reported in the literature are mentioned in remarks. When no structural refinement on a superconducting cuprate was available, or when no superconducting representatives were known so far, a crystallographic data set for a related nonsuperconducting cuprate was chosen. Several data sets, presenting deformations typical for particular chemical families or different kinds of *additional* layer (A, AO, AO', AO'' or AO_2), are sometimes given for the same four-digit code.

Each data set is preceded by a framed header containing the four-digit code (see Section C,f) and a chemical formula of the compound for which complete data are given, where the elements are ordered according to the four-digit code. The first line lists the generalized formula of the structure type (see Introduction), the Pearson code (Bravais lattice and number of atoms in the unit cell, ignoring extra, partly occupied oxygen sites), the number and Hermann–Mauguin symbol of the space group, and the Wyckoff sequence (Wyckoff letters of occupied atom sites, Wyckoff letters of extra, partly occupied, oxygen sites in *additional A* layers being placed within parentheses) for the ideal structure. On the second line, the sequence of layers in the stacking unit is indicated. The next two lines contain the refined composition of the representative compound, its superconducting transition temperature (T_c), a code for the diffraction method used, the temperature (T) for the data collection, the reliability factor of the structural refinement, the literature reference, the number and Hermann–Mauguin symbol of the space group, the cell parameters (a, b, c), and the number of formula units in the cell (Z). The refined composition as given here, multiplied by Z, gives the actual number of atoms in the unit cell. By default, the superconducting transition temperature is given as onset of the diamagnetic signal (n.s., nonsuperconducting). The diffraction data can be single-crystal neutron (SN), single-crystal X-ray (SX), powder neutron (PN), or powder X-ray (PX). Preference has been given to crystallographic parameters refined on data collected at room temperature (RT). The reliability factor reported here is either conventional (R) or weighted (R_w) for refinements on a single crystal, Bragg (R_B) or weighted profile (R_{wp}) for refinements on powder. The space group is given in a setting with the c axis parallel to the stacking direction, the Hermann–Mauguin symbol for the standard setting as defined in the International Tables for Crystallography (Hahn, 1983) being added within parentheses when different. Note that the space group used for the refinement of the real, often considerably distorted structure, may differ from the space group of the structure type (see Tables 8.2 and 8.4). In this case the cell transformation from the ideal structure (new axes and, when relevant, a

translation of the origin) is indicated on the following line. For each atom site there are given a site label, the site multiplicity and the Wyckoff letter (WP), the point symmetry (PS), the fractional atom coordinates (x, y, z), and the occupation parameter (Occ.). The last is only indicated if smaller than unity, which corresponds to a number of atoms per cell equal to the site multiplicity. Atom sites for which a mixed occupation was reported are labeled by the chemical symbol of the majority element, the different elements on the site being specified in a remark. Displacement (temperature) parameters are omitted here, but were taken into account in the selection of the data sets. The cation sites are ordered in the same way as the layers in the stacking unit and start from the *additional*,

Table 8.5.

Coordinates of equivalent positions in space group (123) $P4/mmm$ (D^1_{4h}) (Hahn, 1983).

Wyckoff position	Point symmetry	Coordinates of equivalent positions
1(*a*)	$4/mmm$	$0\,0\,0$
1(*b*)	$4/mmm$	$0\,0\,\frac{1}{2}$
1(*c*)	$4/mmm$	$\frac{1}{2}\,\frac{1}{2}\,0$
1(*d*)	$4/mmm$	$\frac{1}{2}\,\frac{1}{2}\,\frac{1}{2}$
2(*e*)	$mmm.$	$0\,\frac{1}{2}\,\frac{1}{2}$, $\frac{1}{2}\,0\,\frac{1}{2}$
2(*f*)	$mmm.$	$0\,\frac{1}{2}\,0$, $\frac{1}{2}\,0\,0$
2(*g*)	$4mm$	$0\,0\,z$, $0\,0\,\bar{z}$
2(*h*)	$4mm$	$\frac{1}{2}\,\frac{1}{2}\,z$, $\frac{1}{2}\,\frac{1}{2}\,\bar{z}$
4(*i*)	$2mm.$	$0\,\frac{1}{2}\,z$, $0\,\frac{1}{2}\,\bar{z}$, $\frac{1}{2}\,0\,z$, $\frac{1}{2}\,0\,\bar{z}$
4(*j*)	$m.2m$	$x\,x\,0$, $\bar{x}\,\bar{x}\,0$, $x\,\bar{x}\,0$, $\bar{x}\,x\,0$
4(*k*)	$m.2m$	$x\,x\,\frac{1}{2}$, $\bar{x}\,\bar{x}\,\frac{1}{2}$, $x\,\bar{x}\,\frac{1}{2}$, $\bar{x}\,x\,\frac{1}{2}$
4(*l*)	$m2m.$	$x\,0\,0$, $\bar{x}\,0\,0$, $0\,x\,0$, $0\,\bar{x}\,0$
4(*m*)	$m2m.$	$x\,0\,\frac{1}{2}$, $\bar{x}\,0\,\frac{1}{2}$, $0\,x\,\frac{1}{2}$, $0\,\bar{x}\,\frac{1}{2}$
4(*n*)	$m2m.$	$x\,\frac{1}{2}\,0$, $\bar{x}\,\frac{1}{2}\,0$, $\frac{1}{2}\,x\,0$, $\frac{1}{2}\,\bar{x}\,0$
4(*o*)	$m2m.$	$x\,\frac{1}{2}\,\frac{1}{2}$, $\bar{x}\,\frac{1}{2}\,\frac{1}{2}$, $\frac{1}{2}\,x\,\frac{1}{2}$, $\frac{1}{2}\,\bar{x}\,\frac{1}{2}$
8(*p*)	$m..$	$x\,y\,0$, $\bar{x}\,\bar{y}\,0$, $\bar{x}\,y\,0$, $x\,\bar{y}\,0$, $\bar{y}\,x\,0$, $y\,\bar{x}\,0$, $y\,x\,0$, $\bar{y}\,\bar{x}\,0$
8(*q*)	$m..$	$x\,y\,\frac{1}{2}$, $\bar{x}\,\bar{y}\,\frac{1}{2}$, $\bar{x}\,y\,\frac{1}{2}$, $x\,\bar{y}\,\frac{1}{2}$, $\bar{y}\,x\,\frac{1}{2}$, $y\,\bar{x}\,\frac{1}{2}$, $y\,x\,\frac{1}{2}$, $\bar{y}\,\bar{x}\,\frac{1}{2}$
8(*r*)	$..m$	$x\,x\,z$, $\bar{x}\,\bar{x}\,z$, $x\,x\,\bar{z}$, $\bar{x}\,\bar{x}\,\bar{z}$, $\bar{x}\,x\,z$, $x\,\bar{x}\,z$, $\bar{x}\,x\,\bar{z}$, $x\,\bar{x}\,\bar{z}$
8(*s*)	$.m.$	$x\,0\,z$, $\bar{x}\,0\,z$, $x\,0\,\bar{z}$, $\bar{x}\,0\,\bar{z}$, $0\,x\,z$, $0\,\bar{x}\,z$, $0\,x\,\bar{z}$, $0\,\bar{x}\,\bar{z}$
8(*t*)	$.m.$	$x\,\frac{1}{2}\,z$, $\bar{x}\,\frac{1}{2}\,z$, $x\,\frac{1}{2}\,\bar{z}$, $\bar{x}\,\frac{1}{2}\,\bar{z}$, $\frac{1}{2}\,x\,z$, $\frac{1}{2}\,\bar{x}\,z$, $\frac{1}{2}\,x\,\bar{z}$, $\frac{1}{2}\,\bar{x}\,\bar{z}$
16(*u*)	1	$x\,y\,z$, $\bar{x}\,\bar{y}\,z$, $x\,y\,\bar{z}$, $\bar{x}\,\bar{y}\,\bar{z}$, $\bar{x}\,y\,z$, $x\,\bar{y}\,z$, $\bar{x}\,y\,\bar{z}$, $x\,\bar{y}\,\bar{z}$, $\bar{y}\,x\,z$, $y\,\bar{x}\,z$, $\bar{y}\,x\,\bar{z}$, $y\,\bar{x}\,\bar{z}$, $y\,x\,z$, $\bar{y}\,\bar{x}\,z$, $y\,x\,\bar{z}$, $\bar{y}\,\bar{x}\,\bar{z}$

Table 8.6.

Coordinates of equivalent positions in space group (139) $I4/mmm$ (D_{4h}^{17}) (Hahn, 1983). Positions related by I-translation $[(\frac{1}{2}\ \frac{1}{2}\ \frac{1}{2})+]$ are given within square brackets.

Wyckoff position	Point symmetry	Coordinates of equivalent positions
2(*a*)	$4/mmm$	$0\,0\,0$, $[\frac{1}{2}\ \frac{1}{2}\ \frac{1}{2}]$
2(*b*)	$4/mmm$	$0\,0\,\frac{1}{2}$, $[\frac{1}{2}\ \frac{1}{2}\ 0]$
4(*c*)	$mmm.$	$0\ \frac{1}{2}\ 0$, $\frac{1}{2}\ 0\ 0$, $[\frac{1}{2}\ 0\ \frac{1}{2}$, $0\ \frac{1}{2}\ \frac{1}{2}]$
4(*d*)	$\bar{4}m2$	$0\ \frac{1}{2}\ \frac{1}{4}$, $\frac{1}{2}\ 0\ \frac{1}{4}$, $[\frac{1}{2}\ 0\ \frac{3}{4}$, $0\ \frac{1}{2}\ \frac{3}{4}]$
4(*e*)	$4mm$	$0\,0\,z$, $0\,0\,\bar{z}$, $[\frac{1}{2}\ \frac{1}{2}\ \frac{1}{2}+z$, $\frac{1}{2}\ \frac{1}{2}\ \frac{1}{2}-z]$
8(*f*)	$..2/m$	$\frac{1}{4}\ \frac{1}{4}\ \frac{1}{4}$, $\frac{3}{4}\ \frac{3}{4}\ \frac{1}{4}$, $\frac{1}{4}\ \frac{1}{4}\ \frac{3}{4}$, $\frac{3}{4}\ \frac{3}{4}\ \frac{3}{4}$, $[\frac{3}{4}\ \frac{3}{4}\ \frac{3}{4}$, $\frac{1}{4}\ \frac{1}{4}\ \frac{3}{4}$, $\frac{3}{4}\ \frac{1}{4}\ \frac{1}{4}$, $\frac{1}{4}\ \frac{3}{4}\ \frac{1}{4}]$
8(*g*)	$2mm.$	$0\ \frac{1}{2}\ z$, $0\ \frac{1}{2}\ \bar{z}$, $\frac{1}{2}\ 0\ z$, $\frac{1}{2}\ 0\ \bar{z}$, $[\frac{1}{2}\ 0\ \frac{1}{2}+z$, $\frac{1}{2}\ 0\ \frac{1}{2}-z$, $0\ \frac{1}{2}\ \frac{1}{2}+z$, $0\ \frac{1}{2}\ \frac{1}{2}-z]$
8(*h*)	$m.2m$	$x\,x\,0$, $\bar{x}\,\bar{x}\,0$, $x\,\bar{x}\,0$, $\bar{x}\,x\,0$, $[\frac{1}{2}+x\ \frac{1}{2}+x\ \frac{1}{2}$, $\frac{1}{2}-x\ \frac{1}{2}-x\ \frac{1}{2}$, $\frac{1}{2}+x\ \frac{1}{2}-x\ \frac{1}{2}$, $\frac{1}{2}-x\ \frac{1}{2}+x\ \frac{1}{2}]$
8(*i*)	$m2m.$	$x\,0\,0$, $\bar{x}\,0\,0$, $0\,x\,0$, $0\,\bar{x}\,0$, $[\frac{1}{2}+x\ \frac{1}{2}\ \frac{1}{2}$, $\frac{1}{2}-x\ \frac{1}{2}\ \frac{1}{2}$, $\frac{1}{2}\ \frac{1}{2}+x\ \frac{1}{2}$, $\frac{1}{2}\ \frac{1}{2}-x\ \frac{1}{2}]$
8(*j*)	$m2m.$	$x\ \frac{1}{2}\ 0$, $\bar{x}\ \frac{1}{2}\ 0$, $\frac{1}{2}\ x\ 0$, $\frac{1}{2}\ \bar{x}\ 0$, $[\frac{1}{2}+x\ 0\ \frac{1}{2}$, $\frac{1}{2}-x\ 0\ \frac{1}{2}$, $0\ \frac{1}{2}+x\ \frac{1}{2}$, $0\ \frac{1}{2}-x\ \frac{1}{2}]$
16(*k*)	$..2$	$x\ \frac{1}{2}+x\ \frac{1}{4}$, $\bar{x}\ \frac{1}{2}-x\ \frac{1}{4}$, $\frac{1}{2}+x\,x\ \frac{1}{4}$, $\frac{1}{2}-x\,\bar{x}\ \frac{1}{4}$, $x\ \frac{1}{2}-x\ \frac{1}{4}$, $\bar{x}\ \frac{1}{2}+x\ \frac{1}{4}$, $\frac{1}{2}+x\,\bar{x}\ \frac{1}{4}$, $\frac{1}{2}-x\,x\ \frac{1}{4}$, $[\frac{1}{2}+x\,x\ \frac{3}{4}$, $\frac{1}{2}-x\,\bar{x}\ \frac{3}{4}$, $x\ \frac{1}{2}+x\ \frac{3}{4}$, $\bar{x}\ \frac{1}{2}-x\ \frac{3}{4}$, $\frac{1}{2}+x\,\bar{x}\ \frac{3}{4}$, $\frac{1}{2}-x\,x\ \frac{3}{4}$, $x\ \frac{1}{2}-x\ \frac{3}{4}$, $\bar{x}\ \frac{1}{2}+x\ \frac{3}{4}]$
16(*l*)	$m..$	$x\,y\,0$, $\bar{x}\,\bar{y}\,0$, $\bar{x}\,y\,0$, $x\,\bar{y}\,0$, $\bar{y}\,x\,0$, $y\,\bar{x}\,0$, $y\,x\,0$, $\bar{y}\,\bar{x}\,0$, $[\frac{1}{2}+x\ \frac{1}{2}+y\ \frac{1}{2}$, $\frac{1}{2}-x\ \frac{1}{2}-y\ \frac{1}{2}$, $\frac{1}{2}-x\ \frac{1}{2}+y\ \frac{1}{2}$, $\frac{1}{2}+x\ \frac{1}{2}-y\ \frac{1}{2}$, $\frac{1}{2}-y\ \frac{1}{2}+x\ \frac{1}{2}$, $\frac{1}{2}+y\ \frac{1}{2}+x\ \frac{1}{2}$, $\frac{1}{2}-y\ \frac{1}{2}-x\ \frac{1}{2}]$
16(*m*)	$..m$	$x\,x\,z$, $\bar{x}\,\bar{x}\,z$, $\bar{x}\,x\,z$, $x\,\bar{x}\,z$, $x\,x\,\bar{z}$, $\bar{x}\,\bar{x}\,\bar{z}$, $\bar{x}\,x\,\bar{z}$, $x\,\bar{x}\,\bar{z}$, $[\frac{1}{2}+x\ \frac{1}{2}+x\ \frac{1}{2}+z$, $\frac{1}{2}-x\ \frac{1}{2}-x\ \frac{1}{2}+z$, $\frac{1}{2}-x\ \frac{1}{2}+x\ \frac{1}{2}+z$, $\frac{1}{2}+x\ \frac{1}{2}-x\ \frac{1}{2}+z$, $\frac{1}{2}+x\ \frac{1}{2}+x\ \frac{1}{2}-z$, $\frac{1}{2}-x\ \frac{1}{2}-x\ \frac{1}{2}-z$, $\frac{1}{2}-x\ \frac{1}{2}+x\ \frac{1}{2}-z$, $\frac{1}{2}+x\ \frac{1}{2}-x\ \frac{1}{2}-z]$
16(*n*)	$.m.$	$0\,x\,z$, $0\,\bar{x}\,z$, $0\,x\,\bar{z}$, $0\,\bar{x}\,\bar{z}$, $x\,0\,z$, $\bar{x}\,0\,z$, $x\,0\,\bar{z}$, $\bar{x}\,0\,\bar{z}$, $[\frac{1}{2}\ \frac{1}{2}+x\ \frac{1}{2}+z$, $\frac{1}{2}\ \frac{1}{2}-x\ \frac{1}{2}+z$, $\frac{1}{2}\ \frac{1}{2}+x\ \frac{1}{2}-z$, $\frac{1}{2}\ \frac{1}{2}-x\ \frac{1}{2}-z$, $\frac{1}{2}+x\ \frac{1}{2}\ \frac{1}{2}+z$, $\frac{1}{2}-x\ \frac{1}{2}\ \frac{1}{2}+z$, $\frac{1}{2}+x\ \frac{1}{2}\ \frac{1}{2}-z$, $\frac{1}{2}-x\ \frac{1}{2}\ \frac{1}{2}-z]$
32(*o*)	1	$x\,y\,z$, $\bar{x}\,\bar{y}\,z$, $x\,y\,\bar{z}$, $\bar{x}\,\bar{y}\,\bar{z}$, $\bar{x}\,y\,z$, $x\,\bar{y}\,z$, $\bar{x}\,y\,\bar{z}$, $x\,\bar{y}\,\bar{z}$, $\bar{y}\,x\,z$, $y\,\bar{x}\,z$, $\bar{y}\,x\,\bar{z}$, $y\,\bar{x}\,\bar{z}$, $y\,x\,z$, $\bar{y}\,\bar{x}\,z$, $y\,x\,\bar{z}$, $\bar{y}\,\bar{x}\,\bar{z}$, $[\frac{1}{2}+x\ \frac{1}{2}+y\ \frac{1}{2}+z$, $\frac{1}{2}-x\ \frac{1}{2}-y\ \frac{1}{2}+z$, $\frac{1}{2}+x\ \frac{1}{2}+y\ \frac{1}{2}-z$, $\frac{1}{2}-x\ \frac{1}{2}-y\ \frac{1}{2}-z$, $\frac{1}{2}-x\ \frac{1}{2}+y\ \frac{1}{2}+z$, $\frac{1}{2}+x\ \frac{1}{2}-y\ \frac{1}{2}+z$, $\frac{1}{2}-x\ \frac{1}{2}+y\ \frac{1}{2}-z$, $\frac{1}{2}+x\ \frac{1}{2}-y\ \frac{1}{2}-z$, $\frac{1}{2}-y\ \frac{1}{2}+x\ \frac{1}{2}+z$, $\frac{1}{2}+y\ \frac{1}{2}-x\ \frac{1}{2}+z$, $\frac{1}{2}-y\ \frac{1}{2}+x\ \frac{1}{2}-z$, $\frac{1}{2}+y\ \frac{1}{2}-x\ \frac{1}{2}-z$, $\frac{1}{2}+y\ \frac{1}{2}+x\ \frac{1}{2}+z$, $\frac{1}{2}-y\ \frac{1}{2}-x\ \frac{1}{2}+z$, $\frac{1}{2}+y\ \frac{1}{2}-x\ \frac{1}{2}-z$, $\frac{1}{2}-y\ \frac{1}{2}+x\ \frac{1}{2}-z]$

bridging, or *conducting* layers (*A*, *B*, *D*, *C*). They are followed by the anion sites listed in the same order. The atom coordinates have been chosen so that the *z* values increase for consecutive layers and, therefore, some coordinate triplets do not correspond to the first ones given in the International Tables for Crystallography (Hahn, 1983). The equivalent coordinate triplets of the general and all special Wyckoff positions in space groups *P*4/*mmm* and *I*4/*mmm* are listed in Tables 8.5 and 8.6, respectively. All crystallographic data sets presented here were checked for the presence of overlooked symmetry elements or excessively short interatomic distances, and corrected when relevant. The notations used in the data sets are summarized in Table 8.7.

At least one structure drawing is given for each four-digit code. The drawings include the complete sequence of atom layers in the unit cell (indicated by dotted lines) along the stacking direction. The in-plane periods of each layer are limited to the translation period of the structure type (~ 3.85 Å). The Cu sites in the *conducting* and *additional* layers and the O sites surrounding them are displayed as octahedra, square pyramids, squares, or linear units. Other cation and anion sites are shown as small, shaded and larger, non-shaded spheres, respectively. Oxygen atoms from extra sites in an *additional A* layer are marked by dots. The correspondence between the crystallographic data and the schematic drawings is explained in Figs. 8.15 and 8.16 on the data sets of two cuprates, crystallizing in space groups *P*4/*mmm* and *I*4/*mmm*, respectively. In order to facilitate the comparison of drawings of different structures, the origin of the cell has in some cases been shifted by $\frac{1}{2}\ \frac{1}{2}\ 0$ with respect to the data in the corresponding table.

The complete data sets are accompanied by tables listing information on the composition (refined or nominal), space group (when different from the one used in the data set), cell parameters, superconducting transition temperature and literature references for selected compounds. Both the data sets and the tables are followed by remarks concerning high-pressure synthesis, determination of the chemical composition (by default refined), possible superstructures, or determination of the critical temperature (by default onset of diamagnetic signal). In some cases, figures illustrating the influence of composition, temperature, or pressure on the cell parameters and on the superconducting transition temperature are presented. When relevant, condensed information about related structure models proposed in the literature is added, literature references being here given to the first structural refinements and reports on superconductivity.

b. Data Sets

The data sets are ordered according to the four-digit codes. Starting from perovskite, **0101**, the three structural operations indicated in Fig. 8.7 are applied one after the other. At first a DO_2 and a *C* layer are inserted (vertical lines). To the

Table 8.7.

Notation used in the data sets.

Generalized formula		$A_kB_lC_mD_nO_{k+l+2m+2}$
Pearson code		Bravais lattice and number of atoms in the cell
Bravais lattice	*cP*	cubic primitive
	tI	tetragonal body-centered
	tP	tetragonal primitive
	oS	orthorhombic side-centered
	oP	orthorhombic primitive
Space group		(number in the International Tables for Crystallography)
		Hermann–Mauguin symbol
		(Hermann–Mauguin symbol for standard setting if different)
Wyckoff sequence		Wyckoff letters of the atom sites in the ideal structure, superscripts indicate how many times a letter occurs
Cell	*a*, *b*, *c*	cell parameters
	Z	number of formula units in the cell
Superconductivity	T_c	superconducting transition temperature
	n.s.	non-superconducting
Diffraction data	SN	single-crystal neutron
	SX	single-crystal X-ray
	PN	powder neutron
	PX	powder X-ray
Reliability factor	*R*	single-crystal conventional
	R_w	single-crystal weighted
	R_B	powder Bragg
	R_{wp}	powder weighted profile
Other	*T*	temperature for the data collection
	RT	room temperature
	TG	thermogravimetry
Column headings	Atom	site label
	WP	Wyckoff position: site multiplicity (Wyckoff letter)
	PS	point symmetry
	x, *y*, *z*	fractional atom coordinates
	Occ.	occupation parameter
	Ref.	literature reference

0112 structure obtained this way *C* layers (accompanied by O_2 layers) are added, one by one (diagonal lines). Another DO_2 and *C* layer is then added to perovskite and further *C* layers, one by one, to the new structure. These operations are repeated, after which a second *BO* layer is inserted into the structure of perovskite (horizontal line). The procedure is now started over again, adding a new pair of DO_2 and *C* layers to **0201**. The four-digit codes indicated in Fig. 8.7 are thus treated following the diagonals, column by column, starting from the upper left-hand side corner.

Fig. 8.15.

1212, $AB_2CD_2O_{6+\delta}$, $HgBa_2CaCu_2O_{6.26}$, (123) $P4/mmm$, $a = 3.85766$, $c = 12.6562$ Å, $Z = 1$

Data in the table

Atom	WP	PS	x	y	z
Hg	1(*a*)	4/*mmm*	0	0	0
Ba	2(*h*)	4*mm*	½	½	0.2197
Cu	2(*g*)	4*mm*	0	0	0.3754
Ca	1(*d*)	4/*mmm*	½	½	½
O(1) [a]	1(*c*)	4/*mmm*	½	½	0
O(2)	2(*g*)	4*mm*	0	0	0.159
O(3)	4(*i*)	2*mm* .	0	½	0.389

[a] occupancy 0.26

Atom positions in the cell

Atom	x	y	z
Hg^{I}	0	0	0
Ba^{I}	½	½	0.2197
Ba^{II}	½	½	0.7803
Cu^{I}	0	0	0.3754
Cu^{II}	0	0	0.6246
Ca^{I}	½	½	½
$O(1)^{I}$ [a]	½	½	0
$O(2)^{I}$	0	0	0.159
$O(2)^{II}$	0	0	0.841
$O(3)^{I}$	0	½	0.389
$O(3)^{II}$	0	½	0.611
$O(3)^{III}$	½	0	0.389
$O(3)^{IV}$	½	0	0.611

[a] occupancy 0.26

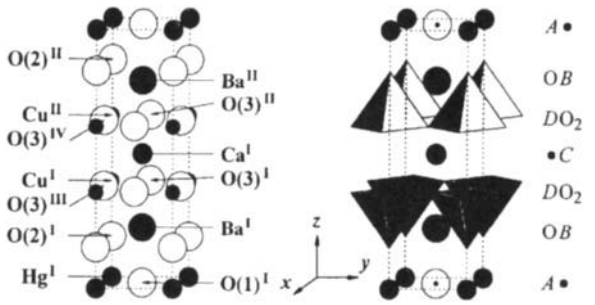

Example for a crystallographic data set in primitive space group $P4/mmm$ showing the correspondence between the data in the table and the schematic drawing. For the derivation of the atom positions in the cell, see Table 8.5. Positions related by cell translations are not included in the table and are not labeled on the drawing.

Fig. 8.16.

2212, $A_2B_2CD_2O_8$, $Tl_2Ba_2CaCu_2O_8$, (139) $I4/mmm$, $a = 3.8550$, $c = 29.318$ Å, $Z = 2$

Data in the table

Atom	WP	PS	x	y	z
Tl	4(*e*)	4*mm*	0	0	0.28641
Ba	4(*e*)	4*mm*	½	½	0.37821
Cu	4(*e*)	4*mm*	0	0	0.4460
Ca	2(*a*)	4/*mmm*	½	½	½
O(1) [a]	16(*n*)	. *m* .	0.396	½	0.2815
O(2)	4(*e*)	4*mm*	0	0	0.3539
O(3)	8(*g*)	2*mm* .	0	½	0.4469

[a] occupancy 0.25

Atom positions in the cell

Atom	x	y	z
Tl I	0	0	0.28641
Tl II	0	0	0.71359
Tl III	½	½	0.78641
Tl IV	½	½	0.21359
Ba I	½	½	0.37821
Ba II	½	½	0.62179
Ba III	0	0	0.87821
Ba IV	0	0	0.12179
Cu I	0	0	0.4460
Cu II	0	0	0.5540
Cu III	½	½	0.9460
Cu IV	½	½	0.0540
Ca I	½	½	½
Ca II	0	0	0
O(1) I *a*	0.396	½	0.2815
O(1) II *b*	0.396	½	0.7185
O(1) III *c*	0.896	0	0.7815
O(1) IV *d*	0.896	0	0.2185
O(2) I	0	0	0.3539
O(2) II	0	0	0.6461
O(2) III	½	½	0.8539
O(2) IV	½	½	0.1461
O(3) I	0	½	0.4469
O(3) II	0	½	0.5531
O(3) III	½	0	0.4469
O(3) IV	½	0	0.5531
O(3) V	½	0	0.9469
O(3) VI	½	0	0.0531
O(3) VII	0	½	0.9469
O(3) VIII	0	½	0.0531

[a] or 0.604 ½ 0.2815, or ½ 0.396 0.2815, or ½ 0.604 0.2815
[b] or 0.604 ½ 0.7185, or ½ 0.396 0.7185, or ½ 0.604 0.7185
[c] or 0.104 0 0.7815, or 0 0.896 0.7815, or 0 0.104 0.7815
[d] or 0.104 0 0.2185, or 0 0.896 0.2185, or 0 0.104 0.2185

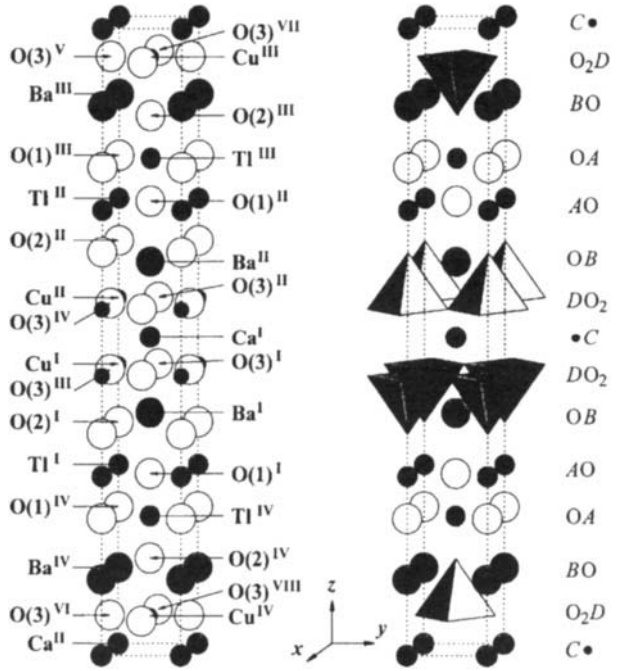

Example for a crystallographic data set in body-centered space group $I4/mmm$ showing the correspondence between the data in the table and the schematic drawing. For the derivation of the atom positions in the cell, see Table 8.6. Positions related by cell translations are not included in the table and are not labeled

perovskite $Ba_1Ti_1O_3$

$BaTiO_3$, *cP*5, n.s., PX, $T = 403$ K (Megaw, 1947)
(221) $Pm\bar{3}m$, $a = 4.0092$ Å,[a] $Z = 1$

Atom	WP	PS	x	y	z	Occ.
Ba	1(*a*)	$m\bar{3}m$	0	0	0	
Ti	1(*b*)	$m\bar{3}m$	$\frac{1}{2}$	$\frac{1}{2}$	$\frac{1}{2}$	
O	3(*c*)	4/*mm*.*m*	$\frac{1}{2}$	$\frac{1}{2}$	0	

[a] Modification stable above 393 K.

perovskite $Ba_1Ti_1O_3$

$BaTiO_3$, *tP*5, n.s., SX, $T = 298$ K, $R_w = 0.013$ (Buttner and Maslen, 1992)
(99) *P*4*mm*, $a = 3.9998$, $c = 4.0180$ Å,[a] $Z = 1$

Atom	WP	PS	x	y	z	Occ.
Ba	1(*a*)	4*mm*	0	0	0.0	
Ti	1(*b*)	4*mm*	$\frac{1}{2}$	$\frac{1}{2}$	0.482	
O(1)	1(*b*)	4*mm*	$\frac{1}{2}$	$\frac{1}{2}$	0.016	
O(2)	2(*c*)	2*mm*.	0	$\frac{1}{2}$	0.515	

[a] Modification stable between 278 and 393 K.

perovskite $Ba_1Ti_1O_3$

$BaTiO_3$, *oS*10, n.s., PN, $T = 270$ K, $R_{wp} = 0.0483$ (Kwei *et al.*, 1993)
(38) *Cm*2*m* (*Amm*2), $a = 5.6751$, $b = 5.6901$, $c = 3.9874$ Å,[a] $Z = 2$

Atom	WP	PS	x	y	z	Occ.
Ba	2(*a*)	*m*2*m*	0	0.0	0	
Ti	2(*b*)	*m*2*m*	$\frac{1}{2}$	0.0169	$\frac{1}{2}$	
O(1)	2(*a*)	*m*2*m*	$\frac{1}{2}$	−0.0090	0	
O(2)	4(*e*)	. . *m*	0.2560	0.2360	$\frac{1}{2}$	

[a] Modification stable between 183 and 278 K.

0011

Infinite layer compounds. The structural information is given toward the end of this chapter.

0021

T′ compound. The structural information is given toward the end of this chapter. Related compounds are the T phase (0201) and the T* phase (0222) which is a hybrid of the T and T′ phases. See Section 7-E and Poole *et al.*, 1995, p. 189.

0101 $La_1Cu_1O_3$

***BDO*$_3$**, *cP5*, (221) $Pm\bar{3}m$–*cba*
-O_2*D*–*BO*-
$LaCuO_3$,[a] n.s., SX, $R_w = 0.020$ (Weigl and Range, 1993)
(167) $R\bar{3}c$, $a = 5.4409$ Å, $\alpha = 60.80°$, $Z = 2$
$\mathbf{a}_1 + \mathbf{a}_2$, $\mathbf{a}_2 + \mathbf{a}_3$, $\mathbf{a}_1 + \mathbf{a}_3$

Atom	WP	PS	*x*	*y*	*z*	Occ.
La	2(*a*)	32	$\frac{1}{4}$	$\frac{1}{4}$	$\frac{1}{4}$	
Cu	2(*b*)	$\bar{3}$.	$\frac{1}{2}$	$\frac{1}{2}$	$\frac{1}{2}$	
O	6(*e*)	.2	0.7031	0.7969	$\frac{1}{4}$	

[a] Prepared at 4 GPa.

Compound	*a* (Å)	*c* (Å)[a]	T_c (K)	Ref.
$LaCuO_3$[b]	5.501	13.217	n.s.	1
$La_{0.90}Sr_{0.10}CuO_3$[c]	5.495	13.209	n.s.	2
$La_{0.90}Y_{0.10}CuO_3$[c]	5.404	13.23	n.s.	3

[a] Hexagonal setting.
[b] Prepared at 6.5 GPa.
[c] Prepared at 7 GPa; nominal composition.
References: 1, Demazeau *et al.* (1972); 2, Darracq *et al.* (1995b); 3, Darracq *et al.* (1994).

0101 $La_1Cu_1O_{2.95}$

***BDO*$_3$**, *tP5*, *P4/mmm–edca* [*cP5*, (221) $Pm\bar{3}m$–*cba*]
-O_2*D*–*BO*-
$LaCuO_{2.95}$,[a] n.s., PX,[b] RT, $R = 0.0812$ (Bringley *et al.*, 1993)
(123) *P4/mmm*,[c] $a = 3.81897$, $c = 3.97258$ Å, $Z = 1$ Fig. 1

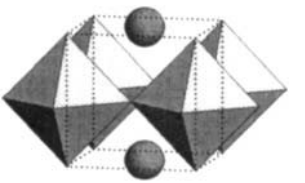

Atom	WP	PS	*x*	*y*	*z*	Occ.
La	1(*a*)	4/*mmm*	0	0	0	
Cu	1(*d*)	4/*mmm*	$\frac{1}{2}$	$\frac{1}{2}$	$\frac{1}{2}$	
O(1)	4(*n*)	*m*2*m*.	0.593	$\frac{1}{2}$	0	0.25
O(2)	8(*s*)	.*m*.	0	0.585	0.560	0.244[d]

[a] Prepared under 0.1 GPaO_2.
[b] Synchrotron radiation.
[c] Reported space group *P4/m* does not take into consideration all symmetry elements.
[d] Value taken from TG analysis.

Compound	*a* (Å)	*c* (Å)	T_c (K)	Ref.
$LaCuO_{2.95}$[a]	3.81897	3.97258	n.s.	1
$La_{0.90}Sr_{0.10}CuO_{2.92}$[b]	3.805	3.966	n.s.	2
$La_{0.90}Y_{0.10}CuO_{2.86}$[c]	3.812	3.967	n.s.	2

[a] Prepared under 0.1 GPaO_2; oxygen content from TG analysis.
[b] Prepared at 3 GPa; nominal composition.
[c] Prepared at 4 GPa; nominal composition.
References: 1, Bringley *et al.* (1993); 2, Darracq *et al.* (1995a).

Stoichiometric $LaCuO_3$ can be prepared at high pressure (4–6.5 GPa; Demazeau *et al.*, 1972; Webb *et al.*, 1989; Weigl and Range, 1993) and crystallizes with a trigonal; $LaAlO_3$-type structure (Geller and Bala, 1956; de Rango *et al.*, 1964), a deformation derivative of perovskite. The oxygen atoms are displaced from the ideal perovskite positions so that the CuO_6 octahedra are tilted and the CuO_2 layers puckered.

Preparation at a lower pressure (0.02–0.1 GPa; Bringley *et al.*, 1990; Karppinen *et al.*, 1996) results in oxygen-deficient $LaCuO_{3-\delta}$ with a tetragonal ($0 < \delta \leq 0.2$, "$PbTiO_3$"-type structure, $P4/mmm$; Náray-Szabó, 1943), monoclinic ($0.2 < \delta \leq 0.4$, $P2/m$, $a = 8.62884$, $b = 3.83076$, $c = 8.65148$ Å, $\beta = 90.2166°$ for $\delta = 0.33$; La Placa *et al.*, 1995) or orthorhombic ($0.4 < \delta \leq 0.5$, $a = 5.5491$, $b = 10.4782$, $c = 3.87956$ Å for $\delta = 0.47$; Bringley *et al.*, 1990) structure. The CuO_6 octahedra in the tetragonal structure are elongated along [0 0 1]. The monoclinic and orthorhombic structures result from an ordering of the oxygen vacancies and contain no infinite CuO_2 square-mesh layers.

0112 $Ba_1Y_1(Cu_{0.50}Fe_{0.50})_2O_5$

***BCD*$_2$O$_5$**, *tP*9, (123) *P*4/*mmm*–*ihcba*
-O_2*D*–*C*–O_2*D*–*B*O-
$BaYCuFeO_5$, n.s., PN, $T = 298$ K, $R_B = 0.093$ (Ruiz-Aragón *et al.*, 1994)
(123) *P*4/*mmm*, $a = 3.8736$, $c = 7.6637$ Å,
$Z = 1$ Fig. 2

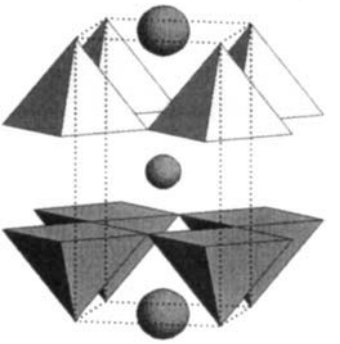

Atom	WP	PS	*x*	*y*	*z*	Occ.
Ba	1(*a*)	4/*mmm*	0	0	0	
Cu[a]	2(*h*)	4*mm*	$\frac{1}{2}$	$\frac{1}{2}$	0.2679	
Y	1(*b*)	4/*mmm*	0	0	$\frac{1}{2}$	
O(1)	1(*c*)	4/*mmm*	$\frac{1}{2}$	$\frac{1}{2}$	0	
O(2)	4(*i*)	2*mm*.	0	$\frac{1}{2}$	0.3153	

[a] $Cu = Cu_{0.5}Fe_{0.5}$.

Compound	*a* (Å)	*c* (Å)	T_c (K)	Ref.
$BaYCuFeO_5$	3.8736	7.6637	n.s.	1
$BaYCu_{0.5}Fe_{0.5}CoO_5$	3.8785	7.5441	n.s.	2
$BaYCuCoO_5$	3.8679	7.5674	n.s.	3

References: 1, Ruiz-Aragón *et al.* (1994); 2, Barbey *et al.* (1995); 3, Huang *et al.* (1994b).

The **0112** compounds known so far contain mixtures of copper and iron (and/or cobalt) atoms in the DO_2 layers. $BaYCuFeO_5$ was first reported in Er-

Rakho *et al.* (1988) and its structural refinement was carried out in space group *P4mm* ($a = 3.867$, $c = 7.656$ Å at $T = 500$ K) with two cation sites in the DO_2 layers, describing a partial ordering of copper and iron atoms. Splitting of the *D* site (Cu and Fe site separation) in space group *P4/mmm* was proposed in Caignaert *et al.* (1995).

0122 $Ba_1(Nd_{0.50}Ce_{0.45})_2(Cu_{0.45}Fe_{0.55})_2O_7$

***BC*$_2$*D*$_2$O$_7$**, *tI*24, (139) *I*4/*mmm*–*ge*^{2}*dba*
-DO_2–•*C*–O_2–*C*•–O_2*D*–*B*O-
$BaNdCe_{0.9}Cu_{0.9}Fe_{1.1}O_7$, n.s., PX, $R_B = 0.046$ (Michel *et al.*, 1991a)
(139) *I*4/*mmm*, $a = 3.9025$, $c = 20.8955$ Å, $Z = 2$
Fig. 3

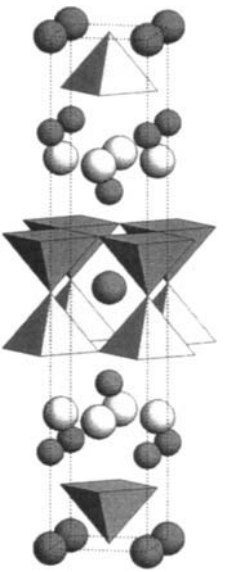

Atom	WP	PS	*x*	*y*	*z*	Occ.
Ba	2(*a*)	4/*mmm*	0	0	0	
Cu[a]	4(*e*)	4*mm*	$\frac{1}{2}$	$\frac{1}{2}$	0.0976	
Nd[b]	4(*e*)	4*mm*	0	0	0.1876	0.95[c]
O(1)	2(*b*)	4/*mmm*	$\frac{1}{2}$	$\frac{1}{2}$	0	
O(2)	8(*g*)	2*mm*.	0	$\frac{1}{2}$	0.1124	
O(3)[d]	4(*d*)	$\bar{4}m2$	0	$\frac{1}{2}$	$\frac{1}{4}$	

[a] Cu = $Cu_{0.45}Fe_{0.55}$.
[b] Nd = $Nd_{0.5263}Ce_{0.4737}$.
[c] Value taken from nominal composition.
[d] Site may be partly vacant.

(*continued*)

Compound	a (Å)	c (Å)	T_c (K)	Ref.
$BaNdCe_{0.9}Cu_{0.9}Fe_{1.1}O_7$	3.9025	20.8955	n.s.	1
$SrY_2CuFeO_{6.5}$	[a]		n.s.	2

[a] 4-fold superstructure (*Ibam*, $a = 5.4149$, $b = 10.7244$, $c = 20.2799$ Å).
References: 1, Michel *et al.* (1991a); 2, Kim *et al.* (1991).

0122 compounds are known only with mixtures of Cu and Fe on the *D* site. Pure samples of $BaNdCe_{0.9}Cu_{0.9}Fe_{1.1}O_{7-\delta}$ were obtained for rare-earth element deficient compositions (Michel *et al.*, 1991a). A possible ordering of Cu and Fe, or Nd and Ce, was not considered in the structural refinement. The oxygen vacancies ($\delta \leq 0.05$) were suggested to be located in the O_2 layer between the two *separating* (Nd,Ce) layers. The superstructure observed for $SrY_2CuFeO_{6.5}$ results from an ordering of oxygen vacancies in the corresponding layer (Kim *et al.*, 1991).

0132 $Sr_1(Y_{0.55}Ce_{0.45})_3(Cu_{0.50}Fe_{0.50})_2O_9$

***BC*$_3$*D*$_2$O$_9$**, *tP*15, (123) *P*4/*mmm*–*i*^{2}*hgdca*
-O_2*D*–*C*-·–O_2-·*C*–O_2–*C*·–O_2*D*–*B*O-
$SrY_{1.65}Ce_{1.35}CuFeO_9$, n.s., PX, $R_B = 0.051$ (Li *et al.*, 1992b)
(123) *P*4/*mmm*, $a = 3.830$, $c = 12.960$ Å, $Z = 1$ Fig. 4

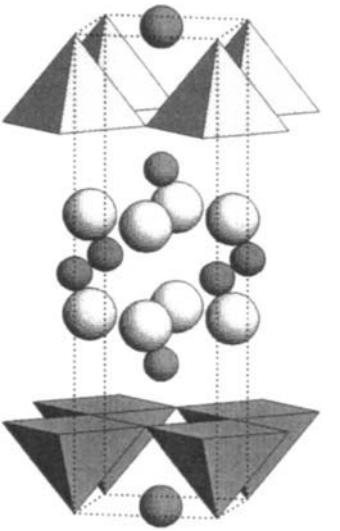

Atom	WP	PS	x	y	z	Occ.
Sr	1(*a*)	4/*mmm*	0	0	0	
Cu[a]	2(*h*)	4*mm*	$\frac{1}{2}$	$\frac{1}{2}$	0.157	
Y(1)[b]	2(*g*)	4*mm*	0	0	0.2955	
Y(2)[b]	1(*d*)	4/*mmm*	$\frac{1}{2}$	$\frac{1}{2}$	$\frac{1}{2}$	
O(1)	1(*c*)	4/*mmm*	$\frac{1}{2}$	$\frac{1}{2}$	0	
O(2)	4(*i*)	2*mm*.	0	$\frac{1}{2}$	0.186	
O(3)	4(*i*)	2*mm*.	0	$\frac{1}{2}$	0.395	

[a] $Cu = Cu_{0.5}Fe_{0.5}$.
[b] $Y(1) = Y(2) = Y_{0.55}Ce_{0.45}$.

0201 $(La_{0.92}Sr_{0.08})_2Cu_1O_4$

***B*$_2$*DO*$_4$**, *tI*14, (139) $I4/mmm$-e^2ca
-O_2*D*–*BO*–*OB*-
$La_{1.85}Sr_{0.15}CuO_4$ (T_c = 37.5 K), PN, T = 300 K,
R_B = 0.0371 (Cava *et al.*, 1987c)
(139) $I4/mmm$, a = 3.7793, c = 13.2260 Å,[a] Z = 2 Fig. 5

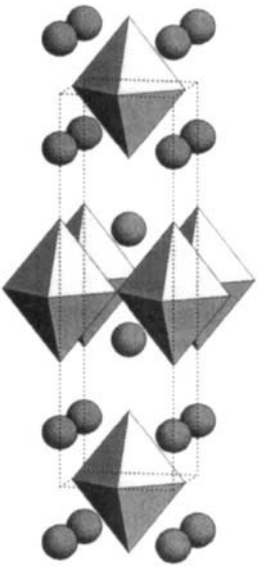

Atom	WP	PS	x	y	z	Occ.
La[b]	1(*e*)	4*mm*	0	0	0.36046	
Cu	2(*a*)	4/*mmm*	$\frac{1}{2}$	$\frac{1}{2}$	$\frac{1}{2}$	
O(1)	4(*e*)	4*mm*	$\frac{1}{2}$	$\frac{1}{2}$	0.3176	
O(2)	4(*c*)	*mmm*.	0	$\frac{1}{2}$	$\frac{1}{2}$	

[a] Modification stable above 200 K.
[b] La = $La_{0.925}Sr_{0.075}$.

Compound	a (Å)	c (Å)	T_c (K)	Ref.
$Ba_{1.2}Sr_{0.8}CuO_{3.26}$	3.8988	12.815[a]	50	1
$Sr_2CuO_{3+\delta}$[b]	3.764	12.548[c]	70[d]	2
$Sr_{1.81}Cu_{0.905}O_{3.4}$	3.7907	12.417	n.s.	3
$Sr_{1.3}La_{0.7}Cu(O,F)_{4+\delta}$[e]	3.9368	13.075	55	4
$Sr_{1.3}Nd_{0.7}Cu(O,F)_{4+\delta}$[e]	3.9288	12.9630	44	5
$Sr_2CuO_2Cl_2$	3.9716	15.6126	n.s.	6
$Ca_{1.85}K_{0.15}CuO_2Cl_2$[f]	3.856[g]	15.27[g]	24	7
$Ca_{1.9}Na_{0.1}CuO_2Cl_2$[h]	3.8495	15.1729	26	8
$La_{1.945}Rb_{0.055}CuO_4$	3.7858	13.2759	22	9
$La_{1.8}Na_{0.2}CuO_4$	3.7796	13.1871	30[i]	10
$La_{1.85}Ba_{0.15}CuO_4$	3.7873	13.2883	33	11
$La_{1.85}Sr_{0.15}CuO_4$	3.7793	13.2260	37.5	12

(*continued*)

$La_{1.85}Ca_{0.15}CuO_4$[e]	3.7791	13.166	20[j]	13
$La_{1.95}Bi_{0.05}CuO_{4.08}$[k]	3.799[g]	13.22[g]	35	14

[a] Additional reflections indicate 4-fold superstructure (monoclinic, $a = 15.60$, $b = 3.899$, $c = 13.395$ Å, $\beta = 106.9°$).
[b] Prepared at 6 GPa; nominal composition, $\delta = 0.1$ from chemical analysis.
[c] 32-fold superstructure ($P4/mbm$, $a = 21.2900$, $c = 12.5611$ Å) in Shimakawa *et al.* (1994b).
[d] $T_c = 94$ K in Han *et al.* (1994); according to Shaked *et al.* (1995), superconductivity should be attributed to impurity phases $Sr_3Cu_2O_{5+\delta}$ (**0212**) and/or $Sr_4Cu_3O_{7+\delta}$ (**0223**).
[e] Nominal composition.
[f] Prepared at 5 GPa; nominal composition.
[g] Value taken from figure.
[h] Prepared at 6 GPa.
[i] $T_c = 36$ K for $La_{1.59}Na_{0.41}CuO_{4-\delta}$ (Markert *et al.*, 1988).
[j] From resistivity measurements (midpoint), value taken from figure.
[k] Nominal composition, oxygen content from TG analysis.
References: 1, Hodges *et al.* (1996); 2, Hiroi *et al.* (1993b); 3, Lobo *et al.* (1990); 4, Chen *et al.* (1995); 5, Yang *et al.* (1996); 6, Miller *et al.* (1990); 7, Tatsuki *et al.* (1995); 8, Argyriou *et al.* (1995); 9, Keane *et al.* (1994); 10, Torardi *et al.* (1989); 11, Jorgensen *et al.* (1987b); 12, Cava *et al.* (1987c); 13, Oh-ishi *et al.* (1988); 14, Kato *et al.* (1996).

0201 $(La_{0.92}Sr_{0.08})_2Cu_1O_4$

***B*$_2$*DO*$_4$**, *tI*14, (139) $I4/mmm$-e^2ca
-O_2*D*–*BO*–*OB*-
$La_{1.85}Sr_{0.15}CuO_4$, $T_c = 37.5$ K, PN, $T = 10$ K, $R_B = 0.0341$ (Cava *et al.*, 1987c)
(64) *Bmab* (*Cmca*), $a = 5.3240$, $b = 5.3547$, $c = 13.1832$ Å,[a] $Z = 4$
$\mathbf{a}_1 + \mathbf{a}_2$, $-\mathbf{a}_1 + \mathbf{a}_2$, $\mathbf{c}$

Atom	WP	PS	x	y	z	Occ.
La[b]	8(*f*)	*m*..	0	−0.004964	0.36077	
Cu	4(*a*)	2/*m*..	$\frac{1}{2}$	0	$\frac{1}{2}$	
O(1)	8(*f*)	*m*..	$\frac{1}{2}$	−0.0255	0.31740	
O(2)	8(*e*)	..2	$\frac{1}{4}$	$\frac{1}{4}$	0.50573	

[a] Modification stable below 200 K.
[b] La = $La_{0.925}Sr_{0.075}$.

0201 $(La_{0.93}Ba_{0.07})_2Cu_1O_4$

***B*$_2$*DO*$_4$**, *tI*14, (139) $I4/mmm$-e^2ca
-O_2*D*–*BO*–*OB*-
$La_{1.855}Ba_{0.145}CuO_4$, $T_c = 30$ K,[a] PN, $T = 30$ K, $R_B = 0.0230$ (Takayama-Muromachi *et al.*, 1993)
(138) $P4_2/ncm$ (origin at 2/*m*), $a = 5.34294$, $c = 13.2432$ Å,[b] $Z = 4$
$\mathbf{a}_1 + \mathbf{a}_2$, $-\mathbf{a}_1 + \mathbf{a}_2$, $\mathbf{c}$

(*continued*)

Atom	WP	PS	x	y	z	Occ.
La[c]	8(*i*)	..*m*	0.0036	0.0036	0.36074	
Cu	4(*d*)	..2/*m*	$\frac{1}{2}$	0	$\frac{1}{2}$	
O(1)	8(*i*)	..*m*	0.4826	0.0174	0.31791	
O(2)	4(*e*)	2.*mm*	$\frac{1}{4}$	$\frac{1}{4}$	0.5074	
O(3)	4(*a*)	2.22	$\frac{1}{4}$	$\frac{3}{4}$	$\frac{1}{2}$	

[a] Value taken from figure.
[b] Modification stable below 60 K.
[c] La = $La_{0.9275}Ba_{0.0725}$.

0201 $La_2Cu_1O_{4.08}$

***B*$_2$*DO*$_4$**, *tI*14, (139) *I*4/*mmm*–e^2ca
-O_2*D*–*BO*–*OB*-
$La_2CuO_{4.081}$,[a] T_c = 42 K, PN, RT, R_{wp} = 0.0643 (Radaelli *et al.*, 1993a)
(69) *Fmmm*, a = 5.33794, b = 5.4106, c = 13.2155 Å,[b] Z = 4
$\mathbf{a}_1 + \mathbf{a}_2$, $-\mathbf{a}_1 + \mathbf{a}_2$, **c**

Atom	WP	PS	x	y	z	Occ.
La	8(*i*)	*mm*2	0	0	0.3601	
Cu	4(*a*)	*mmm*	$\frac{1}{2}$	0	$\frac{1}{2}$	
O(1)	16(*m*)	*m*..	$\frac{1}{2}$	0.029	0.3180	0.4225
O(2)	32(*p*)	1	0.546	0.124	0.313	0.045
O(3)	8(*e*)	..2/*m*	$\frac{1}{4}$	$\frac{1}{4}$	$\frac{1}{2}$	
O(4)	8(*f*)	222	$\frac{1}{4}$	$\frac{1}{4}$	$\frac{1}{4}$	0.0155

[a] Electrochemically oxidized; oxygen content $La_2CuO_{4.12}$ from TG analysis.
[b] Average structure; additional reflections indicate superstructure.

Compound	a (Å)	b (Å)	c (Å)	T_c (K)	Ref.
$Sr_2CuO_2F_{2.57}$	5.394	5.513	13.468	46	1
$La_2CuO_{4.081}$[a]	5.33794	5.4106	13.2155[b]	42	2

[a] Electrochemically oxidized; oxygen content $La_2CuO_{4.12}$ from TG analysis.
[b] Additional reflections indicate superstructure.
References: 1, Al-Mamouri *et al.* (1994); 2, Radaelli *et al.* (1993a).

0201 compounds are usually referred to as T phases. Superconductivity in the La–Ba–Cu–O system was first reported by Bednorz and Müller (1986) with a critical temperature close to 30 K. The superconducting compound was later identified as $La_{2-x}Ba_xCuO_4$ (Takagi *et al.*, 1987), and the first structural refinement was carried out by Jorgensen *et al.* (1987b). Superconductivity (T_c = 36 K) in the La–Sr–Cu–O system was reported by Cava *et al.* (1987d) for the composition $La_{1.8}Sr_{0.2}CuO_4$. At room temperature both the Ba- and Sr-containing compounds crystallize with a tetragonal, K_2NiF_4-type structure (*I*4/*mmm*) (Balz, 1953). At low temperature ($T \sim 200$ K for $La_{1.85}Sr_{0.15}CuO_4$) they undergo a structural phase transition from tetragonal to orthorhombic (*Bmab*, La_2CuO_4 type, Grande *et al.*, 1977), caused by a tilting of the CuO_6

Fig. 8.17.

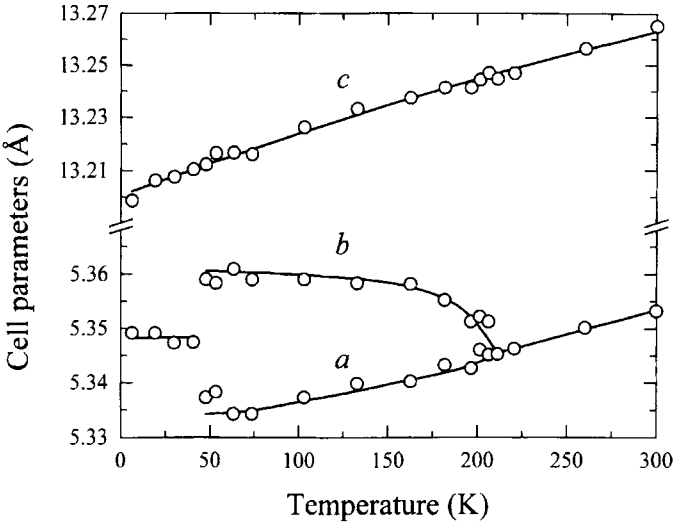

Cell parameters vs temperature for $La_{1.882}Ba_{0.118}CuO_4$ (for the high-temperature tetragonal modification $\sqrt{2}a$ is plotted) (Suzuki and Fujita, 1989).

Fig. 8.18.

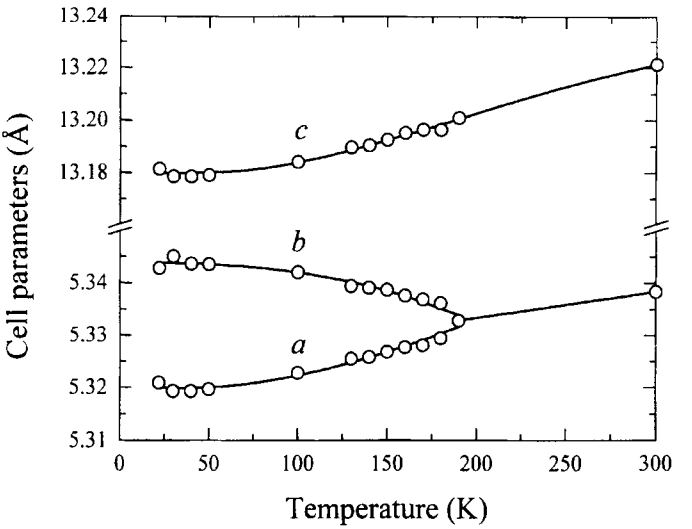

Cell parameters vs temperature for $La_{1.85}Sr_{0.15}CuO_4$ (for the tetragonal modification $\sqrt{2}a$ is plotted) (Day *et al.*, 1987).

Fig. 8.19.

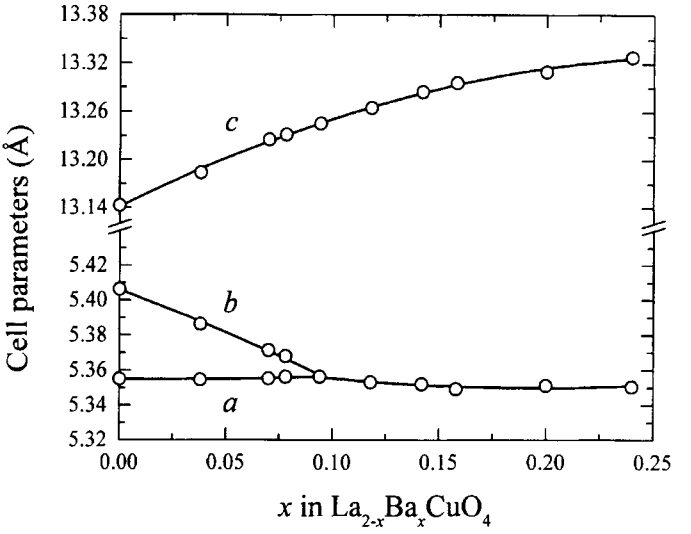

Cell parameters vs Ba content for $La_{2-x}Ba_xCuO_4$ (for the tetragonal modification $\sqrt{2}a$ is plotted) (Suzuki and Fujita, 1989).

Fig. 8.20.

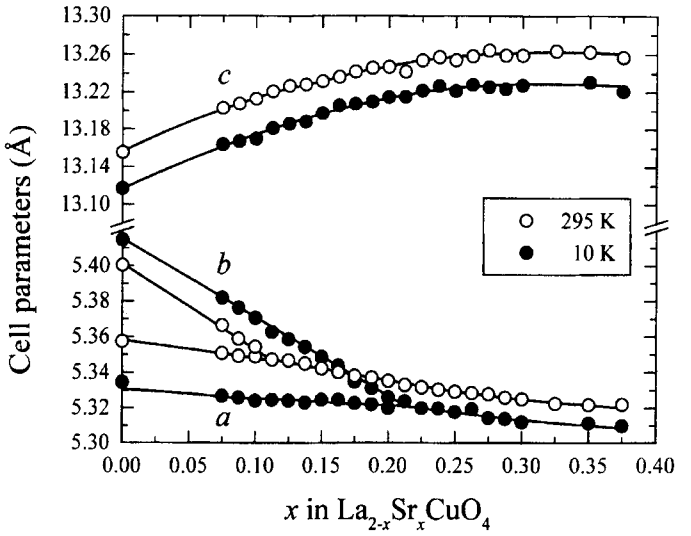

Cell parameters vs Sr content for $La_{2-x}Sr_xCuO_4$ (for the tetragonal modification $\sqrt{2}a$ is plotted) (Radaelli *et al.*, 1994a).

octahedra. A similar transformation is observed on decreasing the Ba or Sr content ($x \sim 0.1$ for $La_{2-x}Sr_xCuO_4$ at 295 K). Upon further cooling, the compounds undergo a second structural transition, $La_{2-x}Ba_xCuO_4$ ($T \sim 50$ K for $x = 0.1$) to another tetragonal ($P4_2/ncm$) (Axe *et al.*, 1989) and $La_{1.885}Sr_{0.115}CuO_4$ to another orthorhombic modification ($Pccn$) (Koyama *et al.*, 1995). For $La_{1.6-x}Nd_{0.4}Sr_xCuO_4$ three successive structural transformations were reported to take place upon cooling, following the sequence $I4/mmm$–$Bmab$–$Pccn$–$P4_2/ncm$ (Crawford *et al.*, 1991). The cell parameters of $La_{2-x}M_xCuO_4$ vs the temperature and the Ba(Sr)-content are presented in Figs. 8.17, 8.18, 8.19 and 8.20, respectively. The superconducting transition temperature of $La_{2-x}Ba_xCuO_4$ as a function of the Ba content shows two maxima, with an intermediate suppression of the superconductivity at $x = 0.125$ (Fig. 8.21). For the Sr-containing compound, T_c vs the Sr content is shown in Fig. 8.22, suppression of the superconductivity being reported to occur at $x = 0.115$ (Kumagai *et al.*, 1994).

Structural refinements on $Sr_2CuO_{3+\delta}$ showed oxygen vacancies in the CuO_2 layers (Shimakawa *et al.*, 1994b). Studies of $Ba_{1.2}Sr_{0.8}CuO_{3+\delta}$ led to similar conclusions, and a monoclinic superstructure with an ordered arrangement of vacancies was proposed (Hodges *et al.*, 1996). Note that a Cu-free compound, Sr_2RuO_4, crystallizing with a K_2NiF_4-type structure and superconducting below 1 K, has also been reported ($I4/mmm$, $a = 3.87$, $c = 12.74$ Å, $T_c = 0.93$ K) (Maeno *et al.*, 1994).

Fig. 8.21.

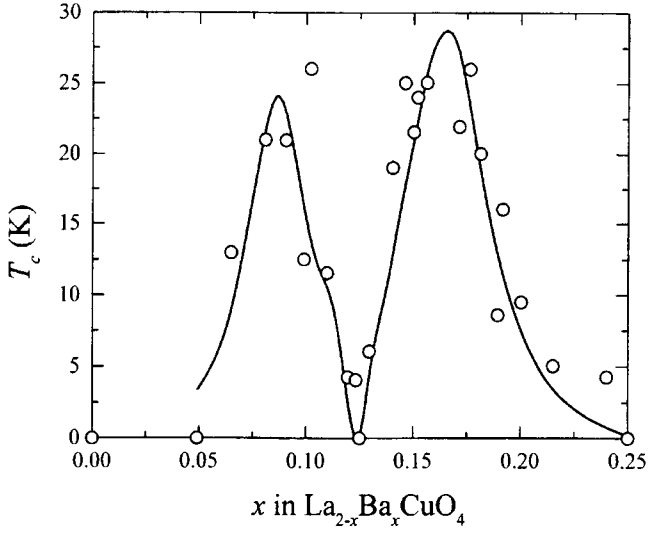

Superconducting transition temperature vs Ba content for $La_{2-x}Ba_xCuO_4$ (Axe *et al.*, 1989).

Fig. 8.22.

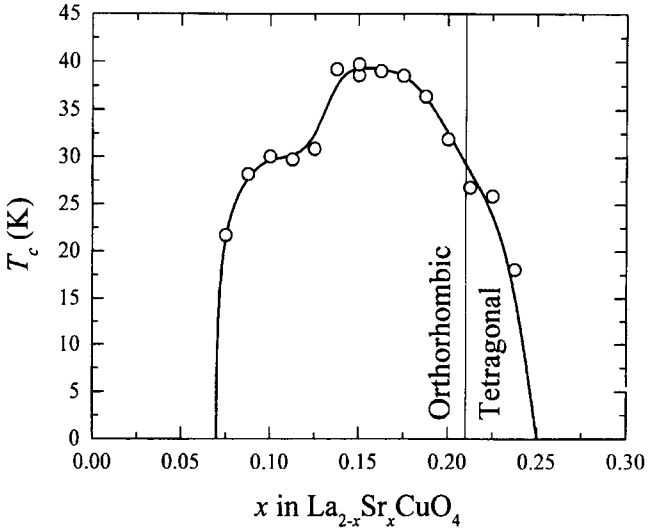

Superconducting transition temperature vs Sr content for $La_{2-x}Sr_xCuO_4$ (Radaelli *et al.*, 1994a).

Superconductors can be obtained not only by doping La_2CuO_4 with alkaline-earth cations, but also by introducing excess oxygen. The compound $La_2CuO_{4+\delta}$ with $\delta < 0.02$ (at 300 K) crystallizes in space group *Bmab*. In Chaillout *et al.* (1990) the structure of the oxygen-rich compound with $\delta > 0.04$ is also described in space group *Bmab* with two extra O sites, located in and between the *bridging* layers, respectively (16(*g*) 0.533 0.105 0.315 and 8(*e*) $\frac{1}{4}$ $\frac{1}{4}$ 0.258, occupancy 0.040 and 0.024), the original O site being partly vacant (occupancy 0.922). Approximately the same structure was also refined in space group *Fmmm* (Radaelli *et al.*, 1993a) (filled-up variant of the "La_2CuO_4" type; Longo and Raccah, 1973).

0212 $(La_{0.71}Sr_{0.20}Ca_{0.09})_2(Ca_{0.81}La_{0.19})_1Cu_2O_{5.91}$

***B*$_2$*CD*$_2$**O**$_6$**, *tI*22, (139) *I*4/*mmm*–*ge*^{3}*b*
-O$_2$*D*–*C*–O$_2$*D*–*BO*–*OB*-
$La_{1.6}Sr_{0.4}CaCu_2O_{5.908}$, [a] $T_c = 55$ K, PN, RT, $R_B = 0.0627$
(Cava *et al.*, 1990b)
(139) *I*4/*mmm*, $a = 3.8208$, $c = 19.5993$ Å, $Z = 2$ Fig. 6

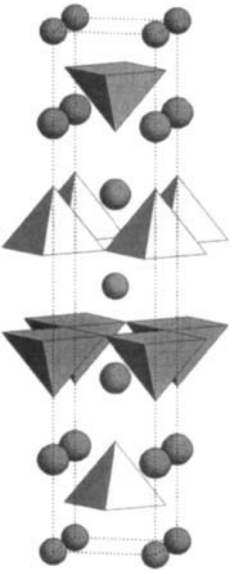

Atom	WP	PS	*x*	*y*	*z*	Occ.
La[b]	4(*e*)	4*mm*	0	0	0.32334	
Cu	4(*e*)	4*mm*	$\frac{1}{2}$	$\frac{1}{2}$	0.41344	
Ca[c]	2(*b*)	4/*mmm*	0	0	$\frac{1}{2}$	
O(1)	4(*e*)	4*mm*	$\frac{1}{2}$	$\frac{1}{2}$	0.2964	0.954
O(2)[d]	8(*g*)	2*mm*.	0	$\frac{1}{2}$	0.41789	

[a] Oxygen content $La_{1.6}Sr_{0.4}CaCu_2O_{5.94}$ from TG analysis.
[b] La = $La_{0.706}Sr_{0.2}Ca_{0.094}$.
[c] Ca = $Ca_{0.812}La_{0.188}$.
[d] Full occupation confirmed.

Compound	*a* (Å)	*c* (Å)	T_c (K)	Ref.
$Sr_3Cu_2O_{5+\delta}$[a]	3.902	21.085	100	1
$Sr_2CaCu_2O_{5.5}$[b]	3.821	20.74	77	2
$Sr_2CaCu_2O_{4.6}F_{2.0}$[b]	3.843	19.88	99	3
$Sr_{2.3}Ca_{0.7}Cu_2O_{4.76}Cl_{1.24}$[c]	3.8679	22.161	80	4
$Sr_2Ca_{0.8}Nd_{0.2}Cu_2O_5F$[d]	3.8606	20.1130	85	5
$Ca_3Cu_2O_4Cl_2$	3.861	21.349	n.s.	6
$La_{1.85}Sr_{1.15}Cu_2O_{6.25}$	3.8530	20.0833	n.s.	7
$La_{1.2}Sr_{1.3}Pb_{0.4}Bi_{0.2}Cu_{1.9}O_{5.78}$[e]	3.867	20.01	75	8

(*continued*)

$La_{1.6}Sr_{0.4}CaCu_2O_{5.908}$	3.8208	19.5993	55	9
$La_{1.82}Ca_{1.18}Cu_2O_{6.014}$[f]	3.81604	19.4214	50[g]	10

[a] Prepared at 6 GPa; nominal composition.
[b] Prepared at 5.5 GPa; nominal composition.
[c] Prepared at 5 GPa.
[d] Prepared at 6 GPa.
[e] Nominal composition, oxygen content from chemical analysis.
[f] Prepared at 0.2 GPa.
[g] Value taken from figure.
References: 1, Hiroi *et al.* (1993b); 2, Kawashima and Takayama-Muromachi (1996); 3, Kawashima *et al.* (1996); 4, Jin *et al.* (1995); 5, Isobe *et al.* (1996a); 6, Huang *et al.* (1990); 7, Lightfoot *et al.* (1990b); 8, Seling *et al.* (1995); 9, Cava *et al.* (1990b); 10, Kinoshita *et al.* (1992).

0212 compounds are sometimes referred to as 326 or 2126 phases and were first reported for $La_{2-x}M_{1+x}Cu_2O_{6-\delta}$ (M = Sr or Ca), with a complete structure determination published by Nguyen *et al.* (1980). $La_{2-x}Sr_{1+x}Cu_2O_6$ and stoichiometric $La_2CaCu_2O_6$ are not superconducting, but superconductivity occurs after partial substitution of La by Sr or Ca in the latter and postannealing at high oxygen pressure (Cava *et al.*, 1990a; Kinoshita and Yamada, 1992b). The high-pressure treatment is believed to increase the ordering of cations (Kinoshita *et al.*, 1991; Shaked *et al.*, 1993), superconductivity being suppressed for a high degree of disorder, in particular when strontium atoms are present also in the *separating* layer. A partly occupied O site (2(*a*) $\frac{1}{2}\ \frac{1}{2}\ \frac{1}{2}$) in the *separating* layer is often reported and can be related to the substitution of Ca by Sr or La (occupancy 0.28 for Ca-free $La_{1.85}Sr_{1.15}Cu_2O_{6.25}$; Lightfoot *et al.*, 1990b). Note that a full occupation of this site would give a $Sr_3Ti_2O_7$-type structure (Ruddlesden and Popper, 1958).

0222 $(Nd_{0.59}Sr_{0.41})_2(Nd_{0.73}Ce_{0.27})_2Cu_2O_{7.84}$

***B*$_2$*C*$_2$*D*$_2$O$_8$**, *tP*14, (129) *P*4/*nmm*–*fc*^{4}*b*
-*D*O$_2$–·*C*–O$_2$–*C*·–O$_2$*D*–*B*O–O*B*-
$Nd_{2.64}Sr_{0.82}Ce_{0.54}Cu_2O_{7.840}$, T_c = 22 K, PN, RT,
R_B = 0.0332 (Izumi *et al.*, 1989c)
(129) *P*4/*nmm* (origin at 2/*m*), a = 3.8564,
c = 12.4846 Å, Z = 1 Fig. 7

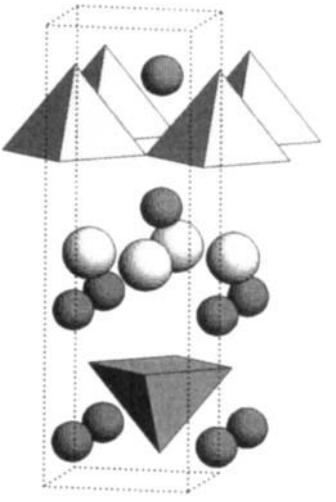

(*continued*)

Atom	WP	PS	x	y	z	Occ.
Nd(1)[a]	2(*c*)	4*mm*	$\frac{1}{4}$	$\frac{1}{4}$	0.1107	
Cu	2(*c*)	4*mm*	$\frac{3}{4}$	$\frac{3}{4}$	0.2490	
Nd(2)[b]	2(*c*)	4*mm*	$\frac{1}{4}$	$\frac{1}{4}$	0.3965	
O(1)	8(*j*)	. . *m*	0.796	0.796	0.0709	0.230
O(2)	4(*f*)	2*mm*.	$\frac{1}{4}$	$\frac{3}{4}$	0.2622	
O(3)	2(*b*)	$\bar{4}m2$	$\frac{1}{4}$	$\frac{3}{4}$	$\frac{1}{2}$	

[a] $Nd(1) = Nd_{0.59}Sr_{0.41}$.
[b] $Nd(2) = Nd_{0.73}Ce_{0.27}$.

Compound	a (Å)	c (Å)	T_c (K)	Ref.
$Sr_2Nd_2Cu_2O_6Cl_2$[a]	3.956	13.880	n.s.	1
$Sr_{1.5}Bi_{0.5}Y_{1.15}Ce_{0.85}Cu_2O_8$	3.822	12.659	30	2
$La_{1.5}Sr_{0.5}Sm_{2.0}Cu_2O_{7.9}$	3.8588	12.5725	20[b]	3
$La_{1.8}Sr_{0.4}Eu_{1.8}Cu_2O_8$[c]	. . .	. . .	34	4
$La_{1.8}Sr_{0.4}Gd_{1.8}Cu_2O_8$	3.85344	12.53367	13[d]	5
$La_{2.5}Dy_{1.5}Cu_2O_{7.5}F_{1.0}$	[e]		n.s.	6
$Nd_{2.64}Sr_{0.82}Ce_{0.54}Cu_2O_{7.840}$	3.8564	12.4846	22	7

[a] Nominal composition.
[b] $T_c = 37$ K for $La_{1.64}Sr_{0.36}Sm_{2.0}Cu_2O_8$ (nominal composition) prepared under 0.3 GPa O_2 (Hundley *et al.*, 1989).
[c] Prepared under 0.3 GPa O_2; nominal composition.
[d] $T_c = 33$ K for sample prepared under 0.3 GPa O_2 (Fisk *et al.*, 1989).
[e] Space group *Cmma*, $a = 5.4609$, $b = 5.5089$ and $c = 12.4842$ Å.
References: 1, Fuller and Greenblatt (1991); 2, Chen *et al.* (1993a); 3, Tokura *et al.* (1989c); 4, Fisk *et al.* (1989); 5, Kwei *et al.* (1990); 6, Lightfoot *et al.* (1990a); 7, Izumi *et al.* (1989c).

0222 compounds are usually referred to as T* phases. Superconductivity was first reported in the Nd–Sr–Ce–Cu–O system (Akimitsu *et al.*, 1988). The superconducting compound was identified as $Nd_{2.64}Ce_{0.54}Sr_{0.82}Cu_2O_y$ and a structural model was proposed by Takayama-Muromachi *et al.* (1988a). The rare-earth metal and strontium atoms occupy two cation sites, with coordination numbers 9 and 8, which correspond to the *B* site in the **0201** structure (T phase) and the *C* site in **0021** (T′), respectively. The **0222** structure may thus be described as an intergrowth of these two structures. The first refinement was reported by Sawa *et al.* (1989b), who stated that the Nd site in the *bridging BO* layers was occupied by a statistical mixture of Nd, Sr, and Ce. Partial ordering of R^{3+} and Sr^{2+} was shown by Izumi *et al.* (1989c) and confirmed by a refinement on $La_{1.8}Sr_{0.4}Gd_{1.8}Cu_2O_8$ ($(La_{0.8}Sr_{0.2})_2(Gd_{0.9}La_{0.1})_2Cu_2O_8$) by Kwei *et al.* (1990). The cell parameters and the critical temperature vs the Sm content in $La_{3.6-x}Sr_{0.4}Sm_xCu_2O_8$ are presented in Figs. 8.23 and 8.24, respectively. Partial oxygen pressure during the synthesis was shown to have a positive effect on the critical temperature (Tokura *et al.*, 1989c).

Fig. 8.23.

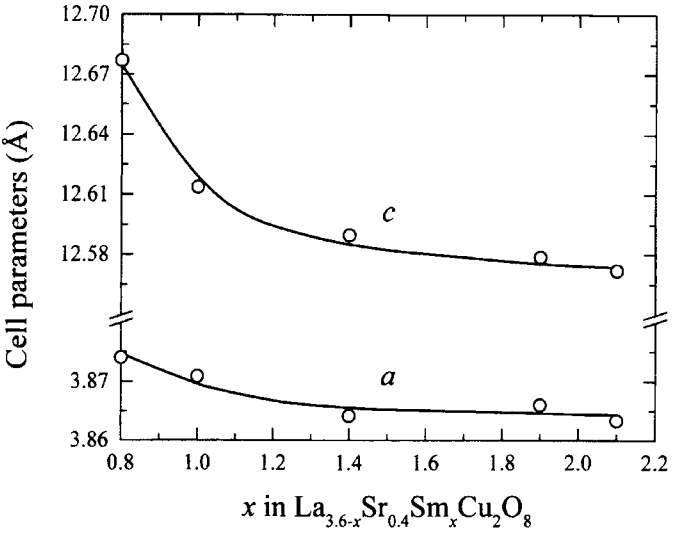

Cell parameters vs Sm content for $La_{3.6-x}Sr_{0.4}Sm_xCu_2O_8$ (T* phase; Fisk *et al.*, 1989).

Fig. 8.24.

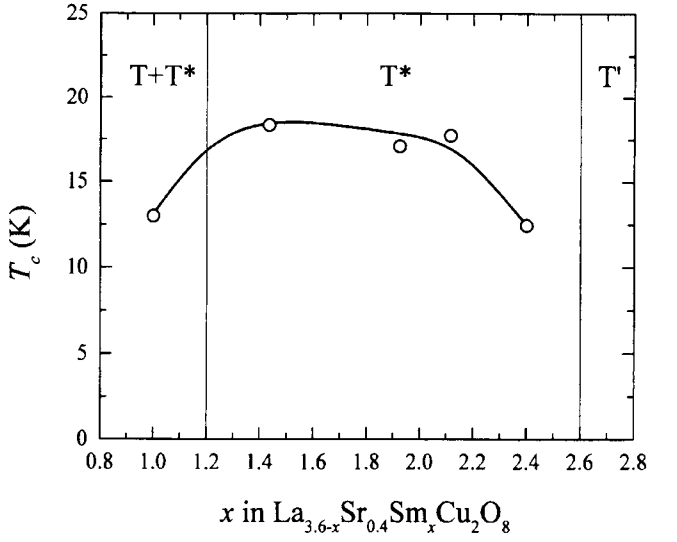

Superconducting transition temperature vs Sm content for $La_{3.6-x}Sr_{0.4}Sm_xCu_2O_8$ (Fisk *et al.*, 1989; Tan *et al.*, 1991).

0223 $(Sr_{0.90}Ca_{0.10})_2(Ca_{0.50}Sr_{0.50})_2Cu_3(O_{0.85}Cl_{0.15})_8$

***B*$_2$*C*$_2$*D*$_3$O$_8$**, *tI*30, (139) *I*4/*mmm*–*ge*^{4}*ca*
-O$_2$*D*–*C*•–O$_2$*D*–*C*•–O$_2$*D*–*B*O–O*B*-
$Sr_{2.8}Ca_{1.2}Cu_3O_{6.8}Cl_{1.2}$,[a] $T_c = 46$ K (Wu *et al.*, 1996a)
(139) *I*4/*mmm*, $a = 3.877$, $c = 28.65$ Å, $Z = 2$ Fig. 8

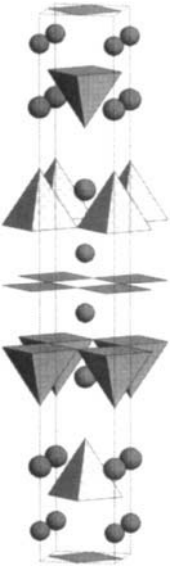

Atom	WP	PS	*x*	*y*	*z*	Occ.
Sr[b]	4(*e*)	4*mm*	0	0	0.3284	
Cu(1)	4(*e*)	4*mm*	$\frac{1}{2}$	$\frac{1}{2}$	0.3881	
Ca[c]	4(*e*)	4*mm*	0	0	0.4448	
Cu(2)	2(*a*)	4/*mmm*	$\frac{1}{2}$	$\frac{1}{2}$	$\frac{1}{2}$	
Cl[d]	4(*e*)	4*mm*	$\frac{1}{2}$	$\frac{1}{2}$	0.2828	
O(1)	8(*g*)	2*mm*.	0	$\frac{1}{2}$	0.3881	
O(2)	4(*c*)	*mmm*.	0	$\frac{1}{2}$	$\frac{1}{2}$	

[a] Prepared at 5 GPa; sample also contained **0212** compound.
[b] Sr = $Sr_{0.9}Ca_{0.1}$.
[c] Ca = $Ca_{0.5}Sr_{0.5}$.
[d] Cl = $Cl_{0.6}O_{0.4}$.

Compound	*a* (Å)	*c* (Å)	T_c (K)	Ref.
$Sr_4Cu_3O_8$[a]	3.8730	27.39	100	1, 2
$Sr_2CaCu_2O_{5.5}$[b]	3.863	27.22	109	3
$Sr_2Ca_2Cu_3O_{6.2}F_{3.2}$[b]	3.840	26.17	111	4
$Sr_{2.8}Ca_{1.2}Cu_3O_{6.8}Cl_{1.2}$[c]	3.877	28.65	46	5

[a] Prepared at 5.7 GPa; sample also contained **0212** compound.
[b] Prepared at 5.5 GPa; nominal composition.
[c] Prepared at 5 GPa; sample also contained **0212** compound.
References: 1, Shaked *et al.* (1995); 2, Hiroi and Takano (1994); 3, Kawashima and Takayama-Muromachi (1996); 4, Kawashima *et al.* (1996); 5, Wu *et al.* (1996a).

A **0223** compound was first reported in the Sr–Ca–Cu–O system for the nominal composition $Sr_{0.6}Ca_{0.333}CuO_{2.10}$ ($a = 3.86$, $c = 27.2$ Å, $T_c = 90$ K; Adachi *et al.*, 1993). All compounds known so far were prepared at high pressure. The isotypic compound without calcium, $Sr_4Cu_3O_8$, was also obtained (Hiroi *et al.*, 1993b; Shaked *et al.*, 1995); however, the only structural refinement was carried out on a compound with oxygen partly substituted by chlorine. Note that $PbBaSrYCu_3O_{7+\delta}$ is sometimes referred to as **0223** (Rouillon *et al.*, 1989, 1992a), but that according to the classification criteria proposed here it corresponds to the **2212** structure.

0232 $Sr_2(Ce_{0.53}Y_{0.47})_3(Cu_{0.50}Fe_{0.50})_2O_{10}$

***B*$_2$*C*$_3$*D*$_2$**O**$_{10}$**, *tI*34, (139) *I*4/*mmm*-g^2e^4a
-O_2*D*–*C*•–O_2–•*C*–O_2–*C*•–O_2*D*–*BO*–*OB*-
$Sr_2Ce_{1.599}Y_{1.401}CuFeO_{10}$, n.s., PX, $R_B = 0.066$
(Tang *et al.*, 1993)
(139) *I*4/*mmm*, $a = 3.828$, $c = 30.560$ Å, $Z = 2$ Fig. 9

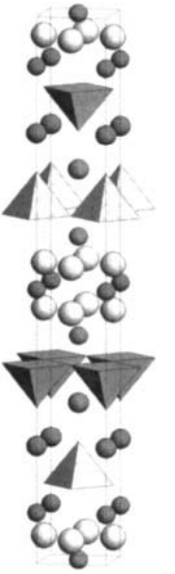

Atom	WP	PS	x	y	z	Occ.
Sr	4(*e*)	4*mm*	0	0	0.287	
Cu[a]	4(*e*)	4*mm*	$\frac{1}{2}$	$\frac{1}{2}$	0.356	
Ce(1)[b]	4(*e*)	4*mm*	0	0	0.409	
Ce(2)[b]	2(*a*)	4/*mmm*	$\frac{1}{2}$	$\frac{1}{2}$	$\frac{1}{2}$	
O(1)	4(*e*)	4*mm*	$\frac{1}{2}$	$\frac{1}{2}$	0.284	
O(2)	8(*g*)	2*mm*.	0	$\frac{1}{2}$	0.364	
O(3)	8(*g*)	2*mm*.	0	$\frac{1}{2}$	0.458	

[a] $Cu = Cu_{0.5}Fe_{0.5}$.
[b] $Ce(1) = Ce(2) = Ce_{0.533}Y_{0.467}$.

0234 $Sr_2Ca_3Cu_4O_{10}$

***B*$_2$*C*$_3$*D*$_4$**O$_{10}$**, *tI*38, (139) $I4/mmm$–g^2e^5b
-O_2D–C-–O_2D–C-–O_2D–C-–O_2D–BO–OB-
$Sr_2Ca_3Cu_4O_{10}$,[a] $T_c = 70\,K$[b] (Adachi *et al.*, 1993)
(139) $I4/mmm$,[c] $a = 3.86$, $c = 34.0$ Å, $Z = 2$ Fig. 10

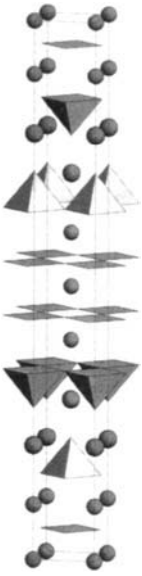

Atom	WP	PS	x	y	z	Occ.
Sr	4(*e*)	4*mm*	0	0	0.29	
Cu(1)	4(*e*)	4*mm*	$\frac{1}{2}$	$\frac{1}{2}$	0.35	
Ca(1)	4(*e*)	4*mm*	0	0	0.40	
Cu(2)	4(*e*)	4*mm*	$\frac{1}{2}$	$\frac{1}{2}$	0.45	
Ca(2)	2(*b*)	4/*mmm*	0	0	$\frac{1}{2}$	
O(1)	4(*e*)	4*mm*	$\frac{1}{2}$	$\frac{1}{2}$	0.28	
O(2)	8(*g*)	2*mm*.	0	$\frac{1}{2}$	0.35	
O(3)	8(*g*)	2*mm*.	0	$\frac{1}{2}$	0.45	

[a] Prepared at 5 GPa; nominal composition $Sr_{0.65}Ca_{0.3}CuO_{2.10}$; sample also contained infinite-layer compound; $a = 3.901$, $c = 33.82$ Å and $T_c = 83\,K$ for $Sr_3CaCu_{2.8}O_{7.5}$ (nominal composition) prepared at 5.5 GPa (Kawashima and Takayama-Muromachi, 1996).
[b] Value taken from figure.
[c] Atom coordinates for ideal structure derived from drawing.

1201 $(Tl_{0.92})_1(Ba_{0.60}La_{0.40})_2Cu_1O_{4.86}$

***AB*$_2$*DO*$_5$**, *tP*9, (123) *P*4/*mmm*–*hgecba*
-*DO*$_2$–*OB*–*A*O–*OB*-
$Tl_{0.920}Ba_{1.2}La_{0.8}CuO_{4.864}$, $T_c = 52$ K, PN, $T = 305$ K,
$R_{wp} = 0.0369$ (Subramanian *et al.*, 1990c)
(123) *P*4/*mmm*, $a = 3.8479$, $c = 9.0909$ Å, $Z = 1$ Fig. 11

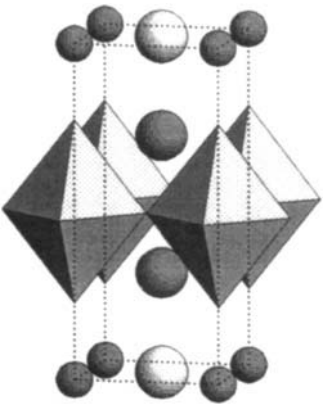

Atom	WP	PS	x	y	z	Occ.
Tl	4(*l*)	*m*2*m*.	0.0801	0	0	0.230
Ba[a]	2(*h*)	4*mm*	$\frac{1}{2}$	$\frac{1}{2}$	0.2942	
Cu	1(*b*)	4/*mmm*	0	0	$\frac{1}{2}$	
O(1)	4(*n*)	*m*2*m*.	0.4281	$\frac{1}{2}$	0	0.216
O(2)	2(*g*)	4*mm*	0	0	0.2250	
O(3)	2(*e*)	*mmm*.	0	$\frac{1}{2}$	$\frac{1}{2}$	

[a] Ba = $Ba_{0.6}La_{0.4}$.

Compound	a (Å)	c (Å)	T_c (K)	Ref.
$TlBa_2CuO_5$[a]	3.869	9.694	n.s.[b]	1
$TlBaSrCuO_{5-\delta}$[c]	3.805	9.120	43[d]	2
$Tl_{0.920}Ba_{1.2}La_{0.8}CuO_{4.864}$	3.8479	9.0909	52	3
$TlBa_2CuO_{4.7}F_{0.3}$	3.836	9.590	75	4
$TlSr_2CuO_5$	3.7344	9.007[e]	n.s.	5
$Tl_{0.8}Pr_{0.6}Sr_{1.6}CuO_5$	3.741	8.875	40	6
$Tl_{0.5}Cr_{0.5}Sr_2CuO_5$	3.795	8.880[f]	50	7
$Tl_{0.5}Pb_{0.5}Sr_2CuO_5$	3.7405	9.0097	n.s.[g]	8
$Tl_{0.5}Pb_{0.5}Sr_{1.5}Nd_{0.5}CuO_{5.07}$	3.76[h]	8.88[h]	40	9
$TlSrLaCuO_5$	3.765	8.838	46	10
$Pb_{0.5}SrLaCu_{1.5}O_{5.03}$[i]	3.77305	8.6876	35	11–14

[a] Composition $Tl_{1.2}Ba_2Cu_{0.7}O_{4.8}$ from microprobe analysis.
[b] $a = 3.859$, $c = 9.261$ Å and $T_c = 9.5$ K (from resistivity measurements, zero resistivity) for sample prepared under reducing conditions (Gopalakrishnan, 1991).
[c] Prepared under reducing conditions; nominal composition.
[d] From resistivity measurements (zero resistivity).
[e] Space group *Pmmm*, $a = 3.661$, $b = 3.793$, and $c = 8.99$ Å reported for oxygen-deficient compound (Ganguli and Subramanian, 1991); 2-fold superstructure (*Pmmm*, $a = 3.6607$, $b = 7.5709$, $c = 8.9672$ Å) reported for $TlSr_2CuO_{4.515}$ (Ohshima *et al.*, 1994).
[f] 8-fold superstructure (*A*2*mm*, $a = 3.7803$, $b = 15.2573$, $c = 17.6737$ Å) reported for $Tl_{0.75}Cr_{0.25}Sr_2CuO_{4.975}$ (Michel *et al.*, 1996).
[g] $T_c = 60$ K in Pan and Greenblatt (1991).

[h] Value taken from figure.
[i] Oxygen content from chemical analysis.
References: 1, Parkin *et al.* (1988c); 2, Gopalakrishnan *et al.* (1991); 3, Subramanian *et al.* (1990c); 4, Subramanian (1994); 5, Kim *et al.* (1989); 6, Bourgault *et al.* (1989); 7, Sheng *et al.* (1992); 8, Kaneko *et al.* (1991); 9, Ohshima *et al.* (1993); 10, Subramanian (1990); 11, Khasanova *et al.* (1996a); 12, Nakahigashi *et al.* (1990); 13, Adachi *et al.* (1990b); 14, Sasakura *et al.* (1990).

1201 $Ga_1(Sr_{0.50}La_{0.50})_2Cu_1O_5$

AB_2DO_5, *tP*9, (123) *P*4/*mmm*–*hgecba*
-DO_2–OB–AO–OB-
$GaSrLaCuO_5$, n.s., SX, RT, $R_w = 0.077$ (Roth *et al.*, 1992)
(46) *I*2*cm* (*Ima*2), $a = 5.369$, $b = 5.510$, $c = 16.51$ Å, $Z = 4$
$\mathbf{a}_1 + \mathbf{a}_2$, $-\mathbf{a}_1 + \mathbf{a}_2$, 2**c**; origin shift 0 $\frac{1}{4}$ $\frac{1}{4}$

Atom	WP	PS	x	y	z	Occ.
Ga	4(*b*)	. . *m*	0.038	−0.065	$\frac{1}{4}$	
Sr[a]	8(*c*)	1	0.5	0.0164	0.3932	
Cu	4(*a*)	2. .	−0.001	0	$\frac{1}{2}$	
O(1)	4(*b*)	. . *m*	0.381	−0.141	$\frac{1}{4}$	
O(2)	8(*c*)	1	−0.01	0.063	0.354	
O(3)	8(*c*)	1	0.25	0.25	0.49	

[a] $Sr = Sr_{0.5}La_{0.5}$.

1201 $Hg_1Ba_2Cu_1O_{4.18}$

$AB_2DO_{4+\delta}$, *tP*8, (123) *P*4/*mmm*–*hge*(*c*)*ba*
-DO_2–OB–A·–OB-
$HgBa_2CuO_{4.18}$, $T_c = 95$ K, PN, $T = 296$ K, $R_{wp} = 0.0687$ (Huang *et al.*, 1995)
(123) *P*4/*mmm*, $a = 3.88051$, $c = 9.5288$ Å, $Z = 1$

Atom	WP	PS	x	y	z	Occ.
Hg	1(*a*)	4/*mmm*	0	0	0	
Ba	2(*h*)	4*mm*	$\frac{1}{2}$	$\frac{1}{2}$	0.2981	
Cu	1(*b*)	4/*mmm*	0	0	$\frac{1}{2}$	
O(1)	1(*c*)	4/*mmm*	$\frac{1}{2}$	$\frac{1}{2}$	0	0.18
O(2)	2(*g*)	4*mm*	0	0	0.2076	
O(3)	2(*e*)	*mmm*.	0	$\frac{1}{2}$	$\frac{1}{2}$	

Compound	a (Å)	c (Å)	T_c (K)	Ref.
$HgBa_2CuO_{4.10}$	3.8766	9.5073	94	1
$Hg_{0.85}Ce_{0.15}Ba_2CuO_{4.15}$	3.8801	9.495	90	2
$Hg_{0.8}W_{0.2}Ba_2CuO_{4.4}$[a]	3.8713	9.416	45	3
$Hg_{0.8}Mo_{0.2}Ba_2CuO_{4.4}$[a]	3.8819	9.378	74	3
$Hg_{0.7}Tl_{0.3}Ba_2CuO_{4+\delta}$	3.885[b]	9.53[b]	41[b]	4
$Hg_{0.743}S_{0.184}Ba_2CuO_{4.486}$	3.8986	9.2466	62[c]	5
$Hg_{0.4}Pr_{0.65}Sr_{1.95}CuO_{4+\delta}$	[d]		n.s.	6
$Hg_{0.50}Cr_{0.50}Sr_2CuO_{4.88}$	3.85000	8.6961	60	7

(*continued*)

$Hg_{0.66}V_{0.34}Sr_{1.8}La_{0.2}CuO_{4.82}$	3.8170	8.7564	41[b]	8
$Hg_{0.5}Pb_{0.5}Sr_{1.2}La_{0.8}CuO_5$	3.7908	8.6915	32	9
$Hg_{0.5}Bi_{0.5}Sr_{1.5}La_{0.5}CuO_5$	3.7769	8.8252	27	10

[a] Nominal composition.
[b] Value taken from figure.
[c] $T_c = 77$ K for sample annealed under reducing conditions.
[d] 2-fold superstructure (primitive orthorhombic, $a = 7.606$, $b = 3.6827$, $c = 8.881$ Å).
References: 1, Putilin *et al.* (1993a); 2, Letouzé *et al.* (1996); 3, Maignan *et al.* (1995a); 4, Nakajima *et al.* (1996); 5, Loureiro *et al.* (1996b); 6, Goutenoire *et al.* (1993a); 7, Chmaissem *et al.* (1995); 8, Mandal *et al.* (1996); 9, Liu *et al.* (1993b); 10, Pelloquin *et al.* (1996a).

1201 $C_1(Ba_{0.50}Sr_{0.50})_2Cu_1O_{5.05}$

AB_2DO_5, *tP*9, (123) *P4/mmm–hgfeba*
-DO_2–OB–AO''–OB-
$CBaSrCuO_{5.05}$, n.s., PN, RT, $R_B = 0.0670$ (Chaillout *et al.*, 1992)
(127) *P4/mbm*, $a = 5.5899$, $c = 7.7153$ Å, $Z = 2$
$\mathbf{a}_1 + \mathbf{a}_2$, $-\mathbf{a} + \mathbf{a}_2$, $\mathbf{c}$

Atom	WP	PS	x	y	z	Occ.
C	2(*d*)	*m.mm*	0	$\frac{1}{2}$	0	
Sr	4(*e*)	4..	0	0	0.2577	0.5
Ba	4(*e*)	4..	0	0	0.2885	0.5
Cu	2(*c*)	*m.mm*	0	$\frac{1}{2}$	$\frac{1}{2}$	
O(1)	8(*k*)	..*m*	0.1566	0.3434	0.0447	0.2625
O(2)	8(*k*)	..*m*	0.0860	0.4140	0.1229	0.25
O(3)	8(*k*)	..*m*	0.0328	0.4672	0.1714	0.25
O(4)	8(*k*)	..*m*	0.2491	0.2509	0.4813	0.5

Compound	Space group	a (Å)	c (Å)	T_c (K)	Ref.
$BBaLaCuO_5$	*P4/mmm*	3.94[a]	7.50[a]	n.s.	1
$CBaSrCuO_{5.05}$	*P4/mbm*	5.5899	7.7153	n.s.	2
$C_{0.9}Ba_{1.1}Sr_{0.9}Cu_{1.1}O_{4.9+\delta}$	$P42_12$	5.5639	7.8567	26	3, 4
CSr_2CuO_5	*P4/mmm*	3.9033	7.4925[b]	n.s.	5
$C_{0.85}B_{0.15}Sr_2CuO_5$	$I\bar{4}$	7.7881	14.9681	32	6
$C_{0.7}B_{0.3}Sr_2CuO_5$[c]	*P4/mmm*	3.86	7.40	50	7
$CSr_{1.6}K_{0.4}CuO_5$[d]	*P4/mmm*	3.8907	7.522[e]	23	8

[a] Value taken from figure.
[b] 8-fold superstructure ($I\bar{4}$, $a = 7.8045$, $c = 14.993$ Å) in Miyazaki *et al.* (1992a).
[c] Prepared at 5 GPa.
[d] Prepared at 4 GPa; nominal composition.
[e] Additional reflections indicate superstructure (2*a*, 2*a*, 2*c*).
References: 1, Li *et al.* (1993); 2, Chaillout *et al.* (1992); 3, Kinoshita and Yamada (1992a); 4, Izumi *et al.* (1992); 5, Babu *et al.* (1991); 6, Uehara *et al.* (1993a); 7, Uehara *et al.* (1994b); 8, Kazakov *et al.* (1995).

1201 $(C_{0.50}Tl_{0.25}Pb_{0.25})_1Sr_2Cu_1O_5$

***AB*$_2$*DO*$_5$**, *tP*9, (123) *P*4/*mmm*–*hgfeba* (*hgecba*)
-*DO*$_2$–*OB*–*AO*″(*AO*)–*OB*-
$CTl_{0.5}Pb_{0.5}Sr_4Cu_2O_{10}$, $T_c = 60$ K,[a] PX, $R_B = 0.0655$ (Huvé *et al.*, 1993b)
(123) *P*4/*mmm*, $a = 3.8244$, $c = 16.516$ Å, $Z = 1$
a$_1$, **a**$_2$, **2c**

Atom	WP	PS	x	y	z	Occ.
C	1(*a*)	4/*mmm*	0	0	0	
Sr(1)	2(*h*)	4*mm*	$\frac{1}{2}$	$\frac{1}{2}$	0.1275	
Cu	2(*g*)	4*mm*	0	0	0.2346	
Sr(2)	2(*h*)	4*mm*	$\frac{1}{2}$	$\frac{1}{2}$	0.3404	
Tl[b]	4(*m*)	*m*2*m*.	0.083	0	$\frac{1}{2}$	0.25
O(1)	4(*l*)	*m*2*m*.	0.316	0	0	0.25
O(2)	8(*s*)	.*m*.	0.162	0	0.086	0.25
O(3)	4(*i*)	2*mm*.	0	$\frac{1}{2}$	0.223	
O(4)	2(*g*)	4*mm*	0	0	0.379	
O(5)	4(*o*)	*m*2*m*.	0.330	$\frac{1}{2}$	$\frac{1}{2}$	0.25

[a] $T_c = 70$ K for sample annealed under reducing conditions.
[b] Tl = $Tl_{0.5}Pb_{0.5}$.

Compound	a (Å)	c (Å)	T_c (K)	Ref.
$CTlBa_2Sr_2Cu_2O_{10}$	[a]		62	1
$CTl_{0.8}Hg_{0.2}Ba_2Sr_2Cu_2O_y$	[b]		60[c]	2
$CHgBa_2Sr_2Cu_2O_{9+\delta}$	3.88	16.94[d]	66	3
$CTl_{0.8}Mo_{0.2}Sr_4Cu_2O_{10}$	3.8251	16.429	80	4
$CTl_{0.5}Pb_{0.5}Sr_4Cu_2O_{10}$	3.8244	16.516	60[e]	5
$CTl_{0.5}Bi_{0.5}Sr_4Cu_2O_{10}$	3.8309	16.518	54	6
$CPb_{0.7}Hg_{0.3}Sr_4Cu_2O_{10}$	3.8242	16.4681	70	7
$C_{0.955}Bi_{0.5}Hg_{0.545}Sr_4Cu_2O_{9.72}$	3.8265	16.4742[f]	17	8
$CHg_{0.57}V_{0.43}Sr_4Cu_2O_{9.6}$	3.8505	16.240	76	9
$CHg_{0.46}Cr_{0.54}Sr_4Cu_2O_{9.88}$	3.8747	16.1555	37	10
$CHg_{0.52}Mo_{0.48}Sr_4Cu_2O_{9.21}$	3.8448	16.3173	74	10

[a] 8-fold superstructure (*Ammm* or *Amm*2, $a = 3.839$, $b = 31.003$, $c = 16.930$ Å); incommensurate modulation ($\mathbf{q} \approx \mathbf{b}^*/6$ to $\mathbf{b}^*/7.4$) and $T_c = 73$ K in Matsui *et al.* (1993).
[b] Orthorhombic, $a = 3.85$, $b = 3.87$ and $c = 16.95$ Å (values taken from figure).
[c] From resistivity measurements (zero resistivity), value taken from figure.
[d] Additional reflections indicate superstructure (orthorhombic, $a = 5.49$, $b = 24.71$, $c = 16.94$ Å).
[e] $T_c = 70$ K for sample annealed under reducing conditions.
[f] Additional reflections indicate superstructure (a, 8a, c).
References: 1, Goutenoire *et al.* (1993b); 2, Noda *et al.* (1995); 3, Uehara *et al.* (1994a); 4, Letouzé *et al.* (1995); 5, Huvé *et al.* (1993b); 6, Maignan *et al.* (1993c); 7, Martin *et al.* (1994); 8, Pelloquin *et al.* (1994); 9, Maignan *et al.* (1995b); 10, Pelloquin *et al.* (1995).

Stoichiometric $TlBa_2CuO_5$ is nonsuperconducting (Parkin *et al.*, 1988c); however, superconductivity may be induced by partial substitution of Ba^{2+} by La^{3+} ($TlBa_{1.2}La_{0.8}CuO_5$, $T_c = 40$ K) (Manako *et al.*, 1989) (Figs. 8.25 and 8.26). The structure is tetragonal (*P*4/*mmm*), whereas that of the Sr analogue,

Fig. 8.25.

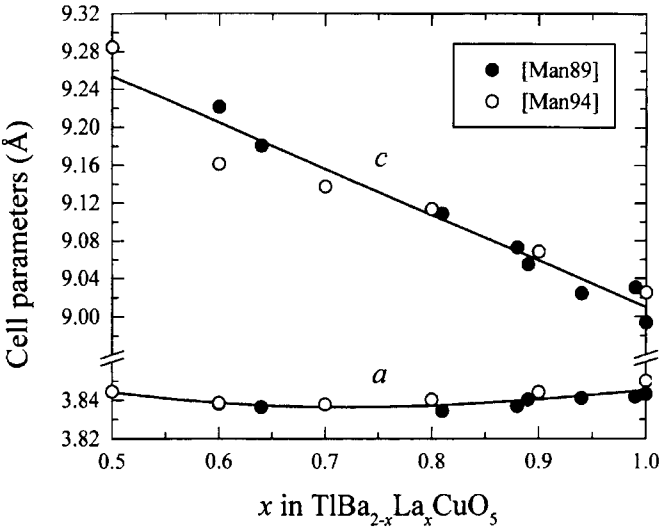

Cell parameters vs La content for $TlBa_{2-x}La_xCuO_5$ (Manako *et al.*, 1989; Manako and Kubo, 1994).

Fig. 8.26.

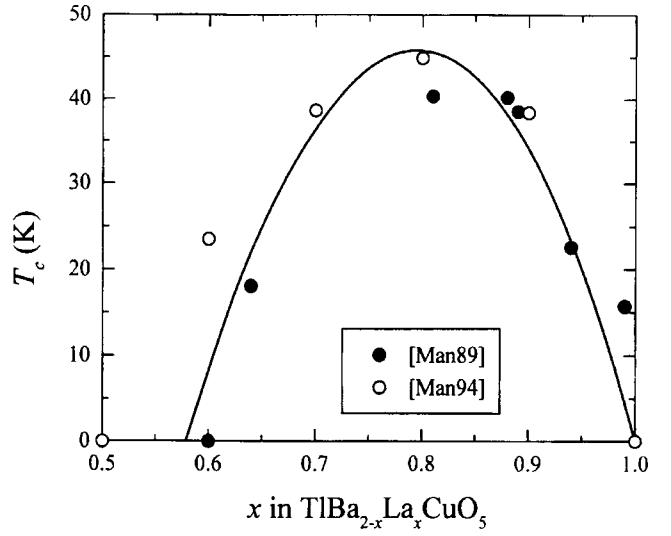

Superconducting transition temperature vs La content for $TlBa_{2-x}La_xCuO_5$ (Manako *et al.*, 1989; Manako and Kubo, 1994).

$TlSr_2CuO_{5-\delta}$, is reported to be either tetragonal (Kim *et al.*, 1989) or orthorhombic (*Pmmm*) (Ganguli and Subramanian, 1991), depending on the oxygen content. The latter compound can be stabilized by partial substitution of Tl by Pb and becomes superconducting when Sr is partly replaced by La or a rare-earth element (Subramanian, 1990). Upon substituting Tl by Pb, the oxygen content of oxygen-deficient $(Tl_{1-x}Pb_x)Sr_2CuO_{5-\delta}$ is increased and the compound undergoes a structural transformation from the orthorhombic to the tetragonal modification at $x = 0.12$ (Kaneko *et al.*, 1991). Ohshima *et al.* (1993) found the cell to be orthorhombic for $\delta = 0.69$, but tetragonal for $\delta \leq 0.42$ ($x = 0.5$). A superstructure with doubling of the *b*-parameter and an ordered arrangement of oxygen vacancies in the CuO_2 layer was reported for $TlSr_2CuO_{4.515}$ (Ohshima *et al.*, 1994).

A superconducting (Pb,Cu)-**1201** compound, with nominal composition $Pb_{0.6}SrLaCu_{1.5}O_y$ ($T_c = 28$ K), was first reported by Adachi *et al.* (1990b). Two partly occupied cation sites in the *additional* layer were considered in the structural refinement on $Pb_{0.5}SrLaCu_{1.5}O_{5+\delta}$ ($(Pb_{0.5}Cu_{0.5})(Sr_{0.5}La_{0.5})_2CuO_{5+\delta}$, Pb in 1(*a*) 0 0 0 and Cu in 4(*l*) 0.104 0 0, occupancy 0.5 and 0.125) (Khasanova *et al.*, 1996a). In addition, distinct sites were refined for La and Sr, and the O site in the *bridging* layers was split.

The Ga-**1201** compounds known so far are not superconducting and contain a mixture of Sr and La (or rare-earth elements) in the *bridging* layers. Their structures are orthorhombic because of the arrangement of the GaO_4 tetrahedra in chains.

$HgBa_2CuO_{4.10}$, with $T_c = 94$ K, crystallizes in the tetragonal space group *P*4/*mmm* (Putilin *et al.*, 1993a). In Wagner *et al.* (1993) partial substitution of Hg by Cu (7 at.%) was proposed to be accompanied by the presence of extra O sites (4(*i*) 0 $\frac{1}{2}$ 0.043 and 1(*c*) $\frac{1}{2}$ $\frac{1}{2}$ 0, occupancy 0.09 and 0.059). According to Alexandre *et al.* (1995), the Cu content on the Hg site cannot exceed 10 at.%. Like many other high-T_c superconducting cuprates, $HgBa_2CuO_{4+\delta}$ can be overdoped, the compound becoming nonsuperconducting for $\delta = 0.23$ (Loureiro *et al.*, 1995).

The crystal structure of CSr_2CuO_5 was first refined in space group *P*4/*mmm* (Babu *et al.*, 1991). Miyazaki *et al.* (1992a) used an 8-fold supercell to account for an ordered arrangement of mutually perpendicular CO_3 triangular groups. Partial substitution of Sr by Ba (25 at.%) was first reported by Armstrong and Edwards (1992), who refined the average structure. A 2-fold supercell (*P*4/*mbm*, $\sqrt{2}a$, *c*) was adopted for the refinement of the structure of $CSrBaCuO_{5+\delta}$ by Chaillout *et al.* (1992) and Miyazaki *et al.* (1993). A similar 2-fold supercell, but space group $P42_12$ was proposed for $C_{0.89}Ba_{1.11}Sr_{0.89}Cu_{1.11}O_{4.99}$ (Izumi *et al.*, 1992). Superconductivity ($T_c = 26$ K) was first reported for the compound $C_{0.9}Ba_{1.1}Sr_{0.9}Cu_{1.1}O_{4.9+\delta}$, prepared under 5 MPa O_2 (Kinoshita and Yamada, 1992a).

Carbon-based **1201** compounds with 50% of the carbon atoms substituted by, for example, Tl, Pb, Bi, Hg, Mo, Cr, and/or V crystallize with a 2-fold

superstructure where the translation period along [0 0 1] contains one slab with carbonate groups and one slab with the mentioned cations in the *additional* layer. Larger supercells, resulting from a crystallographic shear in the (1 0 0) or (1 1 0) planes by **c**/2, are often observed. The cell parameters *a* and *b* of such so-called (1 0 0)- or (1 1 0)-collapsed oxycarbonate structures depend on the periodicity of the crystallographic shear planes, whereas the *c*-parameter corresponds to two stacking units (Maignan *et al.*, 1995b).

1212 $Cu_1Ba_2Y_1Cu_2O_7$

$AB_2CD_2O_7$, *oP*13, (47) *Pmmm–tsrq²hea*
-DO_2–C–DO_2–OB–AO′–OB-
$Ba_2YCu_3O_7$, $T_c = 91$ K,[a] PN, $T = 300$ K, $R_B = 0.0715$
(Capponi *et al.*, 1987)
(47) *Pmmm*, $a = 3.8206$, $b = 3.8851$, $c = 11.6757$ Å,
$Z = 1$ Fig. 12

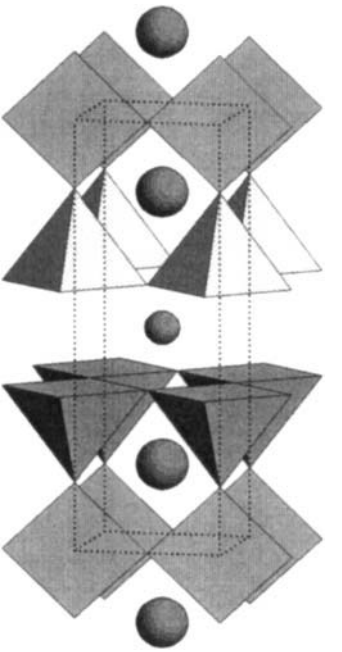

Atom	WP	PS	*x*	*y*	*z*	Occ.
Cu(1)	1(*a*)	*mmm*	0	0	0	
Ba	2(*t*)	*mm*2	$\frac{1}{2}$	$\frac{1}{2}$	0.1841	
Cu(2)	2(*q*)	*mm*2	0	0	0.3549	
Y	1(*h*)	*mmm*	$\frac{1}{2}$	$\frac{1}{2}$	$\frac{1}{2}$	
O(1)	1(*e*)	*mmm*	0	$\frac{1}{2}$	0	
O(2)	2(*q*)	*mm*2	0	0	0.1581	
O(3)	2(*r*)	*mm*2	0	$\frac{1}{2}$	0.3777	
O(4)	2(*s*)	*mm*2	$\frac{1}{2}$	0	0.3779	

[a] Value taken from Cava *et al.* (1987b).

(*continued*)

Compound	a (Å)	b (Å)	c (Å)	T_c (K)	Ref.
$Ba_2LaCu_{2.94}O_7$	3.8829	3.9342	11.810	89	1
Ba_2PrCu_3Oy[a]	3.88	3.93	11.84	80	2
$Ba_2NdCu_3O_7$	3.8590	3.9112	11.7412	91[b]	3
$Ba_2SmCu_3O_7$	3.8440	3.9018	11.7248	93.8[c]	4
$Ba_2EuCu_3O_7$	3.8384	3.8973	11.7069	94.5[c]	4
$Ba_2GdCu_3O_7$	3.8350	3.8947	11.6992	94.7[c]	4
$BaSrGdCu_3O_{6.94}$[d]	3.804	3.863	11.588	82.6[b]	5
$Ba_2DyCu_3O_{6.90}$	3.84215	3.88721	11.67772	92	6, 7
$BaSrDyCu_3O_{6.93}$[d]	3.816	3.838	11.542	83[b]	8
$Ba_2HoCu_3O_{6.96}$	3.8205	3.8851	11.6822	93.4[c]	9
$BaSrHoCu_3O_{6.94}$[d]	3.789	3.851	11.546	79[b]	10
$Ba_2ErCu_3O_7$	3.8128	3.8781	11.6644	93.2[c]	11
$BaSrErCu_3O_{6.94}$[d]	3.791	3.847	11.560	78[b]	10
$Ba_2TmCu_3O_7$	3.8087	3.8746	11.6655	90.5[c]	12
$BaSrTmCu_3O_{6.94}$[d]	3.821	3.836	11.550	70[b]	10
$Ba_2YbCu_3O_7$	3.8018	3.8710	11.6576	90.0[c]	13
$Ba_2YCu_3O_7$	3.8206	3.8851	11.6757	91	14, 15
$Ba_2YCu_{2.89}Al_{0.11}O_7$	3.851	3.859	11.677	82[e]	16
$Ba_2YCu_{2.82}Zn_{0.18}O_{6.9}$[f]	3.835[e]	3.880[e]	11.67[e]	45[e]	17
$Ba_2YCu_{2.91}Fe_{0.09}O_{7-\delta}$[a]	3.852	3.861	11.686	85	18
$Ba_2YCu_{2.75}Ni_{0.25}O_7$	3.8191	3.8857	11.6571	63.9	19
$BaSrYCu_3O_{6.94}$[d]	3.791	3.845	11.542	79[b]	10

[a] Nominal composition.
[b] From resistivity measurements (zero resistivity).
[c] From resistivity measurements (midpoint).
[d] Nominal composition, oxygen content from chemical analysis.
[e] Value taken from figure.
[f] Nominal composition, oxygen content from TG analysis.

References: 1, Yoshizaki *et al.* (1987); 2, Zou *et al.* (1997); 3, Takita *et al.* (1988); 4, Asano *et al.* (1987c); 5, Wang *et al.* (1995); 6, Currie and Weller (1993); 7, Guillaume *et al.* (1994); 8, Wang *et al.* (1992b); 9, Asano *et al.* (1987b); 10, Wang *et al.* (1992a); 11, Ishigaki *et al.* (1987a); 12, Ishigaki *et al.* (1987b); 13, Asano *et al.* (1987a); 14, Capponi *et al.* (1987); 15, Cava *et al.* (1987b); 16, Siegrist *et al.* (1987a); 17, Westerholt *et al.* (1989); 18, Xu *et al.* (1989); 19, Tarascon *et al.* (1987).

1212 $Cu_1Ba_2Y_1Cu_2O_{6.26}$

$AB_2CD_2O_{6+\delta}$, *tP*12, (123) *P*4/*mmm*–*ihg*^{2}(*f*)*da*
-DO_2–*C*–DO_2–O*B*–*A*.
$Ba_2YCu_3O_{6.26}$, n.s., SN, $T = 298$ K, $R_w = 0.047$
(Renault *et al.*, 1987)
(123) *P*4/*mmm*, $a = 3.8573$, $c = 11.7913$ Å, $Z = 1$ Fig. 13

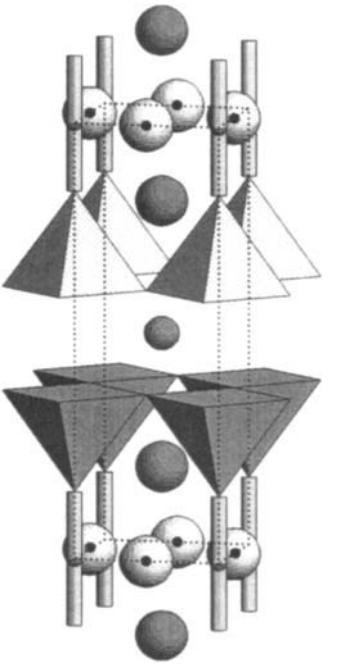

Atom	WP	PS	*x*	*y*	*z*	Occ.
Cu(1)	1(*a*)	4/*mmm*	0	0	0	
Ba	2(*h*)	4*mm*	$\frac{1}{2}$	$\frac{1}{2}$	0.1940	
Cu(2)	2(*g*)	4*mm*	0	0	0.3598	
Y	1(*d*)	4/*mmm*	$\frac{1}{2}$	$\frac{1}{2}$	$\frac{1}{2}$	
O(1)	2(*f*)	*mmm*.	0	$\frac{1}{2}$	0	0.13
O(2)	2(*g*)	4*mm*	0	0	0.1533	
O(3)	4(*i*)	2*mm*.	0	$\frac{1}{2}$	0.3793	

Compound	*a* (Å)	*c* (Å)	T_c (K)	Ref.
$BaSrLaCu_3O_{6.94}$[a]	3.877	11.728	57[b]	1
$Ba_{1.5}La_{1.5}Cu_3O_{7.20}$	3.9069	11.6925	n.s.	2
$Ba_{1.5}LaCa_{0.5}Cu_3O_{7.01}$	3.8742	11.7138	78	3
$Ba_{1.25}La_{1.25}Ca_{0.5}Cu_3O_{7.137}$	3.873	11.622	79.2	4
$Ba_2PrCu_{2.907}O_{6.16}$	3.9060	11.824	n.s.	5
$BaSrPrCu_3O_{6.94}$[a]	3.859	11.551	n.s.	1
$Ba_2NdCu_3O_{6.24}$	3.9015	11.8539	n.s.	6
$BaSrNdCu_3O_{6.94}$[a]	3.870	11.622	74[b]	1
$Ba_{1.75}Nd_{1.25}Cu_3O_{7.16}$	3.8923	11.7145	40[c]	7
$Ba_{1.6}NdCa_{0.4}Cu_3O_{6.96}$	3.8752	11.6963	65[c]	8
$BaSrSmCu_3O_{6.94}$[a]	3.851	11.591	80[b]	1
$Ba_{1.8}Sm_{1.2}Cu_3O_{7.2}$	3.8730	11.6763	43[d]	9

(*continued*)

$BaSrEuCu_3O_{6.94}$[a]	3.844	11.579	80[b]	1
$Ba_{1.8}Eu_{1.2}Cu_3O_{7.18}$[e]	3.873	11.631	28[b]	10
$BaSrGdCu_3O_7$[e]	3.835	11.554	86[b]	11
$Ba_2DyCu_3O_{6.25}$	3.8675	11.811	n.s.	12
$BaSrDyCu_3O_{6.94}$[a]	3.828	11.533	80[b]	13
$Ba_2HoCu_3O_6$	3.8650	11.824	n.s.	12
$Ba_2ErCu_3O_{6.18}$	3.8648	11.857	n.s.	14
$Ba_2YCu_3O_{6.26}$	3.8573	11.7913	n.s.	15
$Ba_2YCu_{2.55}Zn_{0.45}O_{6.9}$[e]	3.850[c]	11.67[c]	n.s.	16
$Ba_2YCu_{2.7}Fe_{0.3}O_{7.15}$[f]	3.8655	11.674	35[c]	17
$Ba_2Y_{0.73}Ca_{0.27}Cu_{2.70}Co_{0.30}O_7$	3.8646	11.7257	84	18
$Ba_2YCu_{2.55}Ni_{0.45}O_{6.9}$[e]	3.865[c]	11.63[c]	50[d]	16
$Sr_2YCu_3O_y$[g]	3.7949	11.4102	60	19
$TaBa_2LaCu_2O_8$	3.9674	12.052	n.s.	20
$NbBa_2LaCu_2O_8$	3.9679	12.001[h]	n.s.	21
$RuSr_2SmCu_2O_8$	3.852	11.56	n.s.	22

[a] Nominal composition; oxygen content from chemical analysis.

[b] From resistivity measurements (zero resistivity).

[c] Value taken from figure.

[d] From resistivity measurements (zero resistivity); value taken from figure.

[e] Nominal composition, oxygen content from TG analysis.

[f] Nominal composition.

[g] Prepared at 7 GPa; nominal composition.

[h] Additional reflections indicate superstructure (*P4/mbm* or *P4bm*, $\sqrt{2}a$, *c*); 4-fold superstructure (*I4/mcm*, $a = 5.6107$, $c = 23.9863$ Å) in Rey *et al.* (1990).

References: 1, Wang *et al.* (1992a); 2, Izumi *et al.* (1988); 3, Skakle and West (1994); 4, Goldschmidt *et al.* (1993); 5, Lowe-Ma and Vanderah (1992); 6, Shaked *et al.* (1990); 7, Kramer *et al.* (1994); 8, Skakle and West (1996); 9, Asano *et al.* (1988); 10, Li *et al.* (1988); 11, Wang and Bäuerle (1991); 12, Onoda *et al.* (1987); 13, Wang *et al.* (1992b); 14, Mirmelstein *et al.* (1992); 15, Renault *et al.* (1987); 16, Westerholt *et al.* (1989); 17, Xu *et al.* (1989); 18, Suard *et al.* (1993); 19, Okai (1990); 20, Murayama *et al.* (1988); 21, Kopnin *et al.* (1996); 22, Bauernfeind *et al.* (1995).

1212 $Tl_1Ba_2(Ca_{0.87}Tl_{0.13})_1Cu_2O_7$

$AB_2CD_2O_7$, *tP*13, (123) *P*4/*mmm*–*ihg*^{2}*dca*
-*D*O_2–·*C*–*D*O_2–*O*B–*A*O–*O*B-
$Tl_{1.13}Ba_2Ca_{0.87}Cu_2O_7$, $T_c = 80$ K, SX, $R_w = 0.032$
(Kolesnikov *et al.*, 1989)
(123) *P*4/*mmm*, $a = 3.8472$, $c = 12.721$ Å, $Z = 1$ Fig. 14

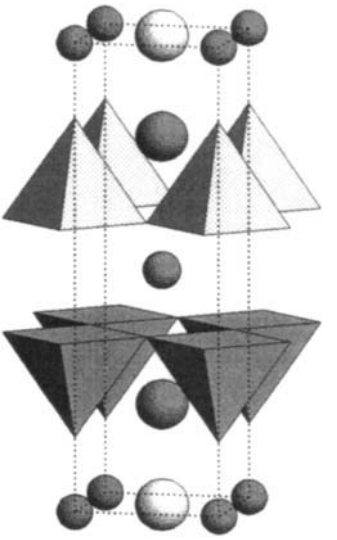

Atom	WP	PS	x	y	z	Occ.
Tl	4(*l*)	*m*2*m*.	0.0877	0	0	0.25
Ba	2(*h*)	4*mm*	$\frac{1}{2}$	$\frac{1}{2}$	0.21550	
Cu	2(*g*)	4*mm*	0	0	0.3740	
Ca[a]	1(*d*)	4/*mmm*	$\frac{1}{2}$	$\frac{1}{2}$	$\frac{1}{2}$	
O(1)	1(*c*)	4/*mmm*	$\frac{1}{2}$	$\frac{1}{2}$	0	
O(2)	2(*g*)	4*mm*	0	0	0.1582	
O(3)	4(*i*)	2*mm*.	0	$\frac{1}{2}$	0.3797	

[a] $Ca = Ca_{0.87}Tl_{0.13}$.

Compound	a (Å)	c (Å)	T_c (K)	Ref.
$Tl_{1.13}Ba_2Ca_{0.87}Cu_2O_7$	3.8472	12.721	80	1
$TlBa_{1.7}La_{0.3}CaCu_2O_7$[a]	3.843	12.72	100	2
$TlBa_2Ca_{0.8}Nd_{0.2}Cu_2O_7$	3.85638	12.6534	100	3
$TlBa_2Ca_{0.8}Y_{0.2}Cu_2O_7$[a]	3.86[b]	12.70[b]	100	4
$TlBa_2YCu_2O_7$	3.86873	12.4732	n.s.	5
$TlBaSrYCu_2O_7$	3.8421	12.2064	n.s.	6
$TlSr_2CaCu_2O_7$	3.794	12.133	20	7
$Tl_{1.15}Sr_2Ca_{0.82}Cu_2O_{6.85}$	3.79395	12.1281	60	8
$Tl_{0.97}Cr_{0.10}Sr_2Ca_{0.93}Cu_2O_7$	3.8155	12.0222	100[c]	9
$Tl_{0.5}Pb_{0.5}Sr_2CaCu_2O_7$[a]	3.806	12.147	90	10, 11
$Tl_{0.5}Pb_{0.5}Sr_2Ca_{0.75}Y_{0.25}Cu_2O_7$[a]	3.819[b]	12.13[b]	105	12
$Tl_{0.67}Bi_{0.33}Sr_2CaCu_2O_7$	3.7922	12.0661	86	13
$Tl_{0.55}Bi_{0.45}Sr_2CaCu_2O_7$	3.7988	12.076	94.9	14
$Tl_{0.5}Bi_{0.5}Sr_2CaCu_2O_7$[a]	3.796	12.113	90[c]	15
$TlSr_{1.5}La_{0.5}CaCu_2O_7$[a]	3.800	12.050	92	16
$TlSr_{1.65}Ce_{0.35}CaCu_2O_{7-\delta}$[a]	3.812[b]	12.038[b]	62	17

(*continued*)

$TlSr_2Ca_{0.5}La_{0.5}Cu_2O_y$[a]	...	...	90	18
$TlSr_2Pr_{0.6}Ca_{0.4}Cu_2O_7$[a]	3.82	12.11	74	19
$TlSr_{2.4}Nd_{0.6}Cu_2O_7$	3.842	12.129	95	20
$Tl_{0.97}Sr_2Lu_{0.60}Ca_{0.40}Cu_2O_{6.94}$	3.79601	12.0251	82	8
$TlSr_2YCu_2O_7$	3.8157	11.9963	n.s.	6
$Pb_{0.5}Sr_{2.5}Ca_{0.5}Y_{0.5}Cu_2O_7$	3.8166	11.907	70	21
$Pb_{0.5}Sr_2CaY_{0.5}Cu_2O_{6.78}$	3.8123	11.916	50[c]	22
$Pb_{0.5}Mg_{0.5}Sr_2Ca_{0.5}Y_{0.5}Cu_2O_{7-\delta}$[a]	3.8249	11.9237	40[c]	23
$Pb_{0.7}Sc_{0.3}Sr_2Ca_{0.5}Y_{0.5}Cu_2O_7$[a]	3.8265	11.9303	38	23
$Pb_{0.5}Cd_{0.5}Sr_2Ca_{0.5}Y_{0.5}Cu_2O_7$	3.8055	11.9410	76	24
$Pb_{0.75}Sr_2Ca_{0.7}Y_{0.3}Cu_{2.25}O_{7-\delta}$[a]	3.8159	11.8758	55	25
$Pb_{0.65}Sr_2Ca_{0.3}Y_{0.7}Cu_{2.35}O_{7.05}$	3.81813	11.8657	25	26
$Pb_{0.5}Sr_2Ca_{0.5}Y_{0.5}Cu_{2.5}O_{7-\delta}$[a]	3.818	11.882	65	27
$Bi_{0.33}Cd_{0.67}Sr_2YCu_2O_7$[a]	3.802	11.96	40	28
$Bi_{0.3}Sr_2YCu_{2.7}O_{7.94}$[d]	3.8157	11.661	20[e]	29
$Ce_{0.5}Cd_{0.5}Sr_2YCu_2O_7$[a]	3.808	12.10	30	28

[a] Nominal composition.
[b] Value taken from figure.
[c] From resistivity measurements (zero resistivity).
[d] Oxygen content $Bi_{0.3}Sr_2YCu_{2.7}O_{7.125}$ from chemical analysis.
[e] From resistivity measurements (zero resistivity); $T_c = 68$ K for $Bi_{0.5}Sr_2Y_{0.8}Cu_{2.7}O_{6.95}$ (Ehmann *et al.*, 1992).

References: 1, Kolesnikov *et al.* (1989); 2, Badri and Varadaraju (1995); 3, Michel *et al.* (1991b); 4, Nakajima *et al.* (1990); 5, Manako *et al.* (1988); 6, Huvé *et al.* (1993a); 7, Martin *et al.* (1989b); 8, Shimakawa *et al.* (1995); 9, Li *et al.* (1995b); 10, Ganguli *et al.* (1988); 11, Subramanian *et al.* (1988e); 12, Vijayaraghavan *et al.* (1991); 13, Ledésert *et al.* (1994); 14, Wahlbeck *et al.* (1996); 15, Li and Greenblatt (1989); 16, Subramanian *et al.* (1990b); 17, Lee and Wang (1995); 18, Rao *et al.* (1989); 19, Sundaresan *et al.* (1995); 20, Manivannan *et al.* (1993); 21, Rouillon *et al.* (1990c); 22, Rouillon *et al.* (1990b); 23, Maignan *et al.* (1993a); 24, Min *et al.* (1994); 25, Liu *et al.* (1991); 26, Maeda *et al.* (1991a); 27, Tang *et al.* (1991); 28, Beales *et al.* (1993); 29, Wang *et al.* (1994).

1212 $(Ga_{0.97})_1Sr_2Y_1Cu_2O_7$

$AB_2CD_2O_7$, *tP*13, (123) *P*4/*mmm*–*ihg*^{2}*dca*
-DO_2–*C*–DO_2–*OB*–*AO*–*OB*-
$Ga_{0.97}Sr_2YCu_2O_7$, n.s., SX, RT, $R_w = 0.0528$ (Roth *et al.*, 1991)
(46) *I*2*cm* (*Ima*2), $a = 5.396$, $b = 5.484$, $c = 22.793$ Å, $Z = 4$
$\mathbf{a}_1 + \mathbf{a}_2, -\mathbf{a}_1 + \mathbf{a}_2, 2\mathbf{c}$; origin shift 0 $\frac{1}{4}$ $\frac{1}{4}$

Atom	WP	PS	*x*	*y*	*z*	Occ.
Ga	4(*b*)	..*m*	−0.044	−0.0691	$\frac{1}{4}$	0.97
Sr	8(*c*)	1	0.501	0.0163	0.3493	
Cu	8(*c*)	1	−0.001	0.0005	0.4269	
Y	4(*a*)	2..	0.5	0	$\frac{1}{2}$	
O(1)	4(*b*)	..*m*	0.596	−0.122	$\frac{1}{4}$	
O(2)	8(*c*)	1	0.002	0.044	0.3233	
O(3)	8(*c*)	1	0.240	0.749	0.4346	
O(4)	8(*c*)	1	0.234	0.249	0.4372	

(*continued*)

Compound	a (Å)	b (Å)	c (Å)	T_c (K)	Ref.
$GaSr_2Tm_{0.6}Ca_{0.4}Cu_2O_7$[a]	5.369	5.458	22.787	51	1
$Ga_{0.97}Sr_2YCu_2O_7$	5.396	5.484	22.793	n.s.	2
$GaSr_2Y_{0.6}Ca_{0.4}Cu_2O_7$	5.3821	5.4717	22.805	41[b]	3

[a] Prepared at 2 GPa; nominal composition.
[b] $T_c = 73$ K for $GaSr_2Y_{0.7}Ca_{0.3}Cu_2O_7$ (Dabrowski *et al.*, 1992).
References: 1, Ono and Tsutsumi (1996); 2, Roth *et al.* (1991); 3, Babu and Greaves (1995).

1212 $Hg_1Ba_2Ca_1Cu_2O_{6.26}$

$AB_2CD_2O_{6+\delta}$, *tP*12, (123) *P*4/*mmm*–*ihg*^{2}*d*(*c*)*a*
-*DO*$_2$–•*C*–*DO*$_2$–*OB*–*A*•–*OB*-
$HgBa_2CaCu_2O_{6.26}$,[a] $T_c = 114$ K, PX, $R_B = 0.0689$ (Putilin *et al.*, 1993b)
(123) *P*4/*mmm*, $a = 3.85766$, $c = 12.6562$ Å, $Z = 1$

Atom	WP	PS	x	y	z	Occ.
Hg	1(*a*)	4/*mmm*	0	0	0	
Ba	2(*h*)	4*mm*	$\frac{1}{2}$	$\frac{1}{2}$	0.2197	
Cu	2(*g*)	4*mm*	0	0	0.3754	
Ca	1(*d*)	4/*mmm*	$\frac{1}{2}$	$\frac{1}{2}$	$\frac{1}{2}$	
O(1)	1(*c*)	4/*mmm*	$\frac{1}{2}$	$\frac{1}{2}$	0	0.26
O(2)	2(*g*)	4*mm*	0	0	0.159	
O(3)	4(*i*)	2*mm*.	0	$\frac{1}{2}$	0.389	

[a] Prepared at 4 GPa.

Compound	a (Å)	c (Å)	T_c (K)	Ref.
$Hg_{0.96}Ba_2CaCu_2O_{6.24}$	3.8552	12.6651	126	1
$Hg_{0.8}Ti_{0.2}Ba_2CaCu_2O_{6.2}$[a]	3.8568	12.581	127	2
$Hg_{0.8}V_{0.2}Ba_2CaCu_2O_{6.3}$[a]	3.8692	12.500	128	2
$Hg_{0.8}Cr_{0.2}Ba_2CaCu_2O_6$[a]	3.8753	12.488	115	2
$Hg_{0.8}W_{0.2}Ba_2CaCu_2O_{6.4}$[a]	3.8607	12.661	118	2
$Hg_{0.8}Mo_{0.2}Ba_2CaCu_2O_{6.4}$[a]	3.8602	12.576	127	2
$Hg_{0.85}Re_{0.15}Ba_2CaCu_2O_{6+\delta}$[a]	...	...	112	3
$Hg_{0.91}Ba_2Ca_{0.86}Sr_{0.14}Cu_2O_{6.11}$	3.8584	12.6646	120[b]	4
$Hg_{0.4}Pr_{0.6}Sr_{2.7}Pr_{0.3}Cu_2O_{6+\delta}$[a]	[c]		85	5
$Hg_{0.75}Nb_{0.25}Sr_2Ca_{0.4}Nd_{0.6}Cu_2O_{6+\delta}$[a]	3.839	11.988	39[d]	6
$Hg_{0.520}V_{0.480}Sr_2Ca_{0.36}Y_{0.64}Cu_2O_{6.81}$	3.8415	11.8514	110[e]	7
$Hg_{0.8}Mo_{0.2}Sr_2Ca_{0.65}Y_{0.35}Cu_2O_{6+\delta}$[a]	3.820	11.930	75[d]	8
$Hg_{0.62}Re_{0.38}Sr_2CaCu_2O_{7.15}$[f]	3.8152	12.0621	90	9
$Hg_{0.5}Tl_{0.5}Sr_2Ca_{0.7}Y_{0.3}Cu_2O_{6+\delta}$[a]	3.8	12.0	92	10
$Hg_{0.29}Pb_{0.60}Sr_2Ca_{0.43}Y_{0.48}Cu_{2.20}O_7$[a]	3.8166	11.9484	90[g]	11
$Hg_{0.67}Bi_{0.33}Sr_2Ca_{0.33}Y_{0.67}Cu_2O_{6.68}$	3.80960	12.0157	100	12
$Hg_{0.5}Bi_{0.5}Sr_2Ca_{0.65}Nd_{0.35}Cu_2O_{6+\delta}$[a]	3.8093	12.0654	94	13

[a] Nominal composition.
[b] $T_c = 124$ K for sample annealed under O_2.
[c] Space group *Pmmm*, $a = b = 3.8335$ and $c = 12.264$ Å; additional reflections indicate superstructure (*B*-centered orthorhombic, 2*a*, *b*, 2*c*).
[d] From resistivity measurements (zero resistivity).

[e] From resistivity measurements (onset).
[f] Prepared at 6 GPa.
[g] T_c given for $Hg_{0.5}Pb_{0.5}Sr_2Ca_{0.7}Y_{0.3}Cu_2O_{6+\delta}$.
References: 1, Radaelli *et al.* (1993b); 2, Maignan *et al.* (1995a); 3, Wolters *et al.* (1996); 4, Hur *et al.* (1994); 5, Hervieu *et al.* (1993); 6, Tang *et al.* (1995b); 7, Chmaissem and Sheng (1996); 8, Tang *et al.* (1995a); 9, Chmaissem *et al.* (1996); 10, Liu *et al.* (1993a); 11, Liu *et al.* (1994); 12, Chmaissem *et al.* (1994); 13, Pelloquin *et al.* (1993b).

1212 $(C_{0.47}Cu_{0.42})_1(Sr_{0.88}Ca_{0.12})_2(Y_{0.50}Ca_{0.26}Sr_{0.24})_1Cu_2O_{6.79}$

$AB_2CD_2O_7$, *tP*13, (123) *P4/mmm–ihg²fda*
-DO_2–·C–DO_2–OB–AO″–OB-
$C_{0.47}Sr_2Ca_{0.5}Y_{0.5}Cu_{2.42}O_{6.79}$,[a] $T_c = 22$ K,[b] PN, RT, $R_B = 0.0509$ (Miyazaki *et al.*, 1994)
(47) *Pmmm*, $a = 3.8319$, $b = 3.8501$, $c = 11.1144$ Å,[c] $Z = 1$
a_1, a_2, c

Atom	WP	PS	x	y	z	Occ.
C[d]	1(*a*)	*mmm*	0	0	0	0.89
Sr[e]	2(*t*)	*mm2*	$\frac{1}{2}$	$\frac{1}{2}$	0.189	
Cu	2(*q*)	*mm2*	0	0	0.356	
Y[f]	1(*h*)	*mmm*	$\frac{1}{2}$	$\frac{1}{2}$	$\frac{1}{2}$	
O(1)	2(*i*)	*2mm*	0.365	0	0	0.235[g]
O(2)	1(*e*)	*mmm*	0	$\frac{1}{2}$	0	0.32
O(3)	4(*w*)	*.m.*	0.75	0	0.068	0.235[g]
O(4)	2(*q*)	*mm2*	0	0	0.157	0.53[h]
O(5)	2(*r*)	*mm2*	0	$\frac{1}{2}$	0.354	0.58
O(6)	2(*r*)	*mm2*	0	$\frac{1}{2}$	0.394	0.42
O(7)	2(*s*)	*mm2*	$\frac{1}{2}$	0	0.349	0.58
O(8)	2(*s*)	*mm2*	$\frac{1}{2}$	0	0.368	0.42

[a] Carbon and oxygen content $C_{0.51}Sr_2Ca_{0.5}Y_{0.5}Cu_{2.42}O_{6.92}$ from chemical analysis.
[b] Value taken from figure.
[c] Average structure; additional reflections indicate superstructure.
[d] $C = C_{0.53}Cu_{0.47}$.
[e] $Sr = Sr_{0.88}Ca_{0.12}$.
[f] $Y = Y_{0.50}Ca_{0.26}Sr_{0.24}$.
[g] Value taken from carbon content (refined value 0.24).
[h] Value taken from occupancy of site O(3) considering occ. O(4) + 2 × occ. O(3) = 1 (refined value 0.70).

(*continued*)

Compound	Space group	a (Å)	b (Å)	c (Å)	T_c (K)	Ref.
$Bo_{.5}Ba_{1.2}Sr_{0.8}YCu_{2.5}O_7$[a]	*P4/mmm*	3.877[b]		11.33[b]	51	1
$Bo_{.5}Ba_{1.5}Sr_{0.5}Y_{0.85}Ca_{0.15}Cu_{2.5}O_7$[a]	tetr.	3.865[b]		11.45[b]	55	2
$C_{0.35}N_{0.15}Ba_2Y_{0.5}Ca_{0.5}Cu_{2.5}O_7$[a]	orth.	3.879	3.885	11.536[c]	82	3
$C_{0.75}Sr_{2.1}Ca_{0.9}Cu_2O_y$[d]	tetr.	3.851		10.941[e]	92	4
$C_{0.55}Ba_{0.45}Sr_{2.5}Ca_{0.5}Cu_2O_7$[f]	tetr.	3.86		10.62	105	5
$C_{0.7}Sr_2Ca_{0.7}Y_{0.3}Cu_{2.3}O_7$[a]	*Pmmm*	3.838[b]	3.858[b]	10.97[b]	40[g]	6
$C_{0.47}Sr_2Ca_{0.5}Y_{0.5}Cu_{2.42}O_{6.79}$[h]	*Pmmm*	3.8319	3.8501	11.1144[i]	22[b]	6
$S_{0.22}Ba_{1.5}Sr_{0.6}Y_{0.74}Ca_{0.16}Cu_{2.78}O_7$[a]	...	3.85[b]		11.60[b]	78	7
$S_{0.22}Sr_{2.1}Y_{0.74}Ca_{0.16}Cu_{2.78}O_{7.12}$	*Pmmm*	3.8254	3.8436	11.2572	45	8

[a] Nominal composition.
[b] Value taken from figure.
[c] Additional reflections indicate superstructure ($2a$, b, $2c$).
[d] Prepared at 6 GPa; nominal composition.
[e] Additional reflections indicate superstructure ($4a$, a, $2c$).
[f] Prepared at 5 GPa; nominal composition.
[g] From resistivity measurements (zero resistivity); value taken from figure.
[h] Carbon and oxygen content $C_{0.51}Sr_2Ca_{0.5}Y_{0.5}Cu_{2.42}O_{6.92}$ from chemical analysis.
[i] Additional reflections indicate superstructure.
References: 1, Zhu *et al.* (1993); 2, Slater and Greaves (1993); 3, Maignan *et al.* (1993b); 4, Yamaura *et al.* (1994); 5, Uehara *et al.* (1994b); 6, Miyazaki *et al.* (1994); 7, Slater *et al.* (1993b); 8, Slater *et al.* (1993a).

The first identified superconducting Cu-**1212** compound, $Ba_2YCu_3O_{7-\delta}$ ($\delta = 0.1$, $T_c = 91$ K), was found to crystallize in an orthorhombic cell with $a = 3.8218$, $b = 3.8913$, and $c = 11.677$ Å (Cava *et al.*, 1987b). Structural models were proposed by Hazen *et al.* (1987), Grant *et al.* (1987), and Beyers *et al.* (1987), who, however, chose noncentrosymmetric, tetragonal or orthorhombic, space groups. For the superconducting, orthorhombic modification, space group *Pmmm* was adopted by LePage *et al.* (1987), Siegrist *et al.* (1987b), Izumi *et al.* (1987a), Beno *et al.* (1987), Beech *et al.* (1987), Greedan *et al.* (1987), and Capponi *et al.* (1987). An ordered arrangement of the oxygen atoms in the *additional* layer, resulting in the formation of chains of corner-sharing CuO_4 squares, was proposed in the latter four articles. For the tetragonal modification space group *P4/mmm* was reported in LePage *et al.* (1987) and Izumi *et al.* (1987b). The orthorhombic structure exists in the range $\delta = 0$–0.6 ($Ba_2YCu_3O_y$, $y = 6.4$–7) (Fig. 8.27), the highest critical temperature, $T_c = 93$ K, being observed for the oxygen content $Ba_2YCu_3O_{6.93}$ (Fig. 8.28), which corresponds to an occupancy of 0.93 for the O site in the *additional* AO' layer ($1(e)$ 0 $\frac{1}{2}$ 0). Partial occupancy of the O position, which in space group *P4/mmm* is related to the former by symmetry ($1(b)$ $\frac{1}{2}$ 0 0), is generally reported (<0.20). The occupancy of this site increases on decreasing the overall oxygen content, and a transition to the tetragonal structure takes place near $\delta = 0.6$ (sample quenched from 873 K), suppressing the superconductivity. It should be noted that the orthorhombic structure may be retained (and the superconductivity preserved) to a lower oxygen content ($\delta = 0.8$), by removing the oxygen atoms at lower

Fig. 8.27.

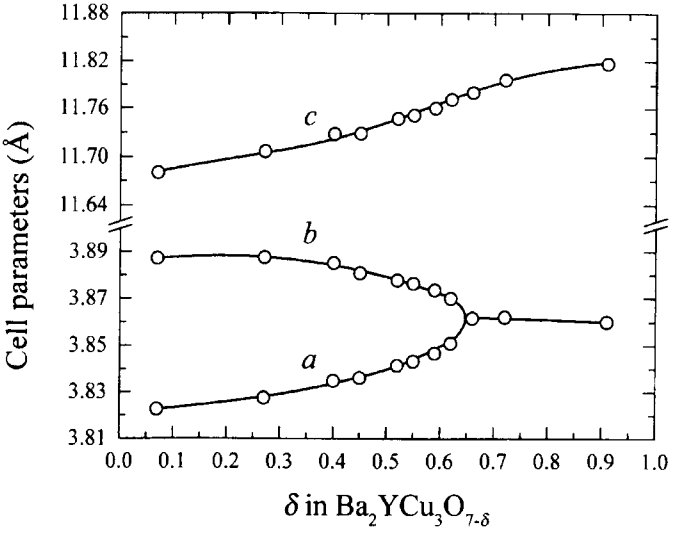

Cell parameters vs δ for $Ba_2YCu_3O_{7-\delta}$ (Jorgensen *et al.*, 1990).

Fig. 8.28.

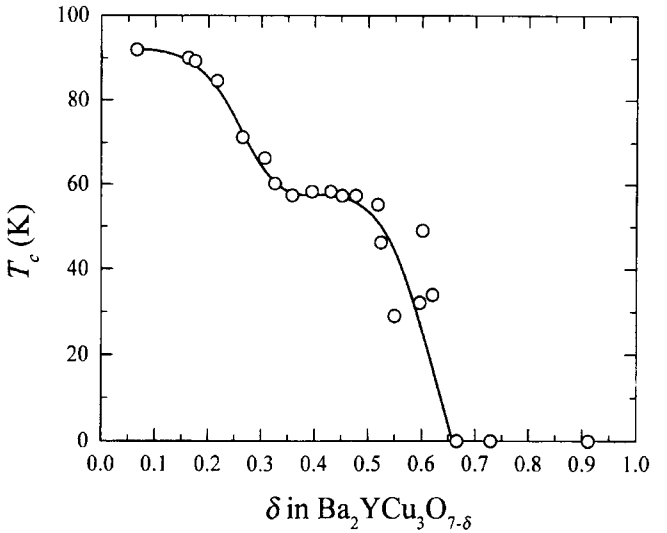

Superconducting transition temperature vs δ for $Ba_2YCu_3O_{7-\delta}$ (Jorgensen *et al.*, 1990).

temperatures (633–793 K) by a Zr-gettered annealing technique (Cava *et al.*, 1987a). For the orthorhombic, as well as for the tetragonal structure, partial vacancies on the Cu site in the *additional* layer (occupancy >0.90) were reported to have a negative effect on the superconducting transition temperature (Collin *et al.*, 1988; Inoue *et al.*, 1987). Several refinements of the orthorhombic structure were carried out considering split sites in the *additional* layer (e.g., Cu in 2(*i*) 0.045 0 0 (Raudsepp *et al.*, 1987) or O in 2(*k*) 0.0356 $\frac{1}{2}$ 0 (François *et al.*, 1988). The cell parameters and the oxygen content of $Ba_2YCu_3O_{7-\delta}$ vs the temperature are shown in Figs. 8.29 and 8.30, respectively.

Under certain preparation conditions, a superstructure with a doubling of the *a*-parameter, usually referred to as ortho II, was observed for $\delta = 0.35$–0.60 ($Ba_2YCu_3O_y$, $y = 6.65$–6.40; Chaillout *et al.*, 1987; Schwarz *et al.*, 1993). It results from an ordering of the oxygen vacancies in the *additional* layer; however, the correlation length is relatively short (e.g., 10.2*a*, 45*b*, 1.66*c*; Schleger *et al.*, 1995b). A structural refinement in a 2-fold supercell, space group *Pmmm*, was carried out by Simon *et al.* (1993) and Grybos *et al.* (1995). The structure is characterized by an ordered arrangement of CuO and Cu chains, and the cation sites in the *bridging*, *separating*, and *conducting* layers, as well as the O site in the *bridging* layers, are displaced from the ideal positions (Burlet *et al.*, 1992). The formation of the superstructure is generally associated with a T_c plateau at about 60 K (Cava *et al.*, 1987a). For a higher oxygen content ($\delta \sim 0.3$) a different superstructure, referred to as ortho III, with a tripling of the *a*-parameter (two CuO chains alternating with one Cu chain) and an even shorter correlation length than ortho II, was observed (Schleger *et al.*, 1995a; Plakhty *et al.*, 1995).

Fig. 8.29.

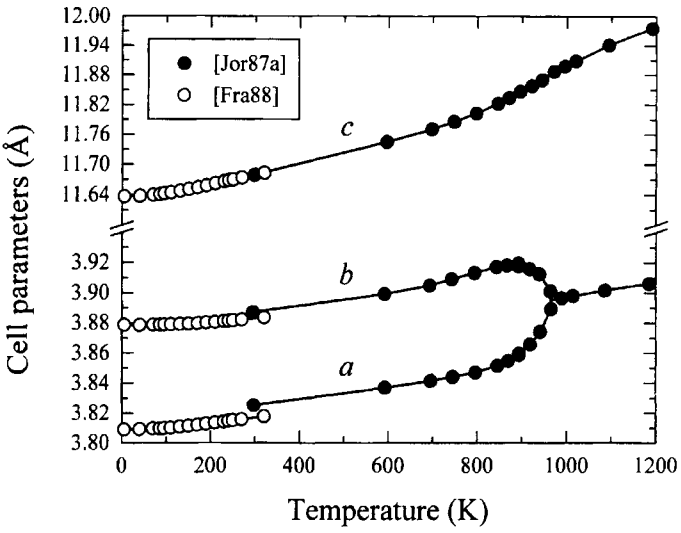

Cell parameters vs temperature for $Ba_2YCu_3O_{7-\delta}$ (Jorgensen *et al.*, 1987a; François *et al.*, 1988).

Fig. 8.30.

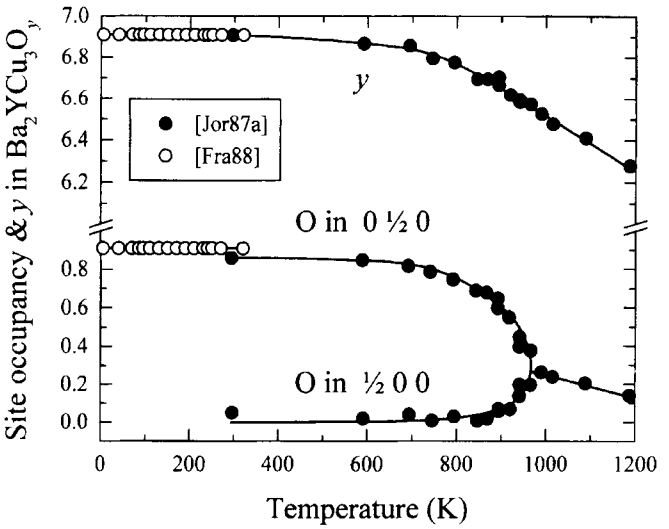

Occupancy of the O sites in the *additional* layer and oxygen content per formula unit vs temperature for $Ba_2YCu_3O_y$ (Jorgensen *et al.*, 1987a; François *et al.*, 1988).

Numerous examples for complete or partial substitutions on all cation sites have been tested (e.g., rare-earth elements or Ca for Y, Sr for Ba, transition elements for Cu). Substitution of Cu by Fe, Ni, or Zn rapidly leads to a suppression of the superconductivity. On the contrary, when Y is partly or completely substituted by a rare-earth element, T_c remains approximately the same. Note that superconductivity for $Ba_2PrCu_3O_y$ was reported relatively recently (T_c up to 90 K; Blackstead *et al.*, 1995; Zou *et al.*, 1997). $Ba_{2-x}R_{1+x}Cu_3O_y$ compounds with R = La, Nd, Sm, Eu, and Gd show considerable homogeneity ranges with respect to the partial substitution of Ba by these elements (Segre *et al.*, 1987; Zhang *et al.*, 1987), the solubility limit decreasing with increasing atomic number of R. In the fully oxygenated compounds, a transformation from the basic orthorhombic to the tetragonal structure, accompanied by a decrease of the critical temperature, is observed on increasing x (Figs. 8.31 and 8.32). $BaSr\mathit{R}Cu_3O_{7-\delta}$ compounds with δ = 0–0.07, prepared at 0.6–0.8 GPa, crystallize with either the tetragonal (R = La, Pr, Nd, Sm, Eu, Gd, or Dy) or the orthorhombic (R = Gd, Dy, Y, Ho, Er, or Tm) structure. The only Ba-free superconducting compound known so far, $Sr_2YCu_3O_y$, was prepared at 7 GPa (Okai, 1990).

A superconducting Tl-**1212** compound (T_c = 88 K) was first reported for the composition $(Tl_{0.75}Bi_{0.25})_{1.33}Sr_{1.33}Ca_{1.33}Cu_2O_{6.67+\delta}$, and a structural model was proposed in space group $P4/mmm$ (a = 3.800, c = 12.072 Å; Haldar *et al.*, 1988). For $Tl_{1.169}Ba_2Ca_{0.831}Cu_2O_{6.747}$ the occupancy of the O site in the *additional* layers was refined to 0.747 and part of the thallium and barium atoms were found to be displaced towards the oxygen vacancies (Morosin *et al.*,

Fig. 8.31.

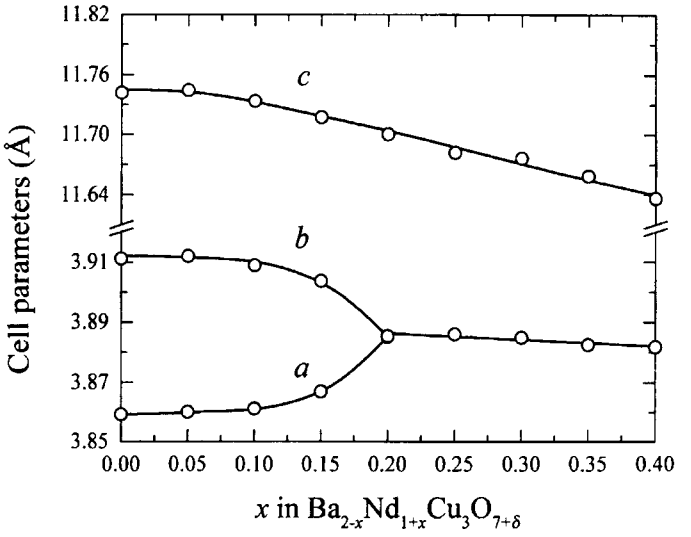

Cell parameters vs x for $Ba_{2-x}Nd_{1+x}Cu_3O_{7+\delta}$ ($\delta = 0$ for $0 \leq x < 0.2$) (Takita *et al.*, 1988).

Fig. 8.32.

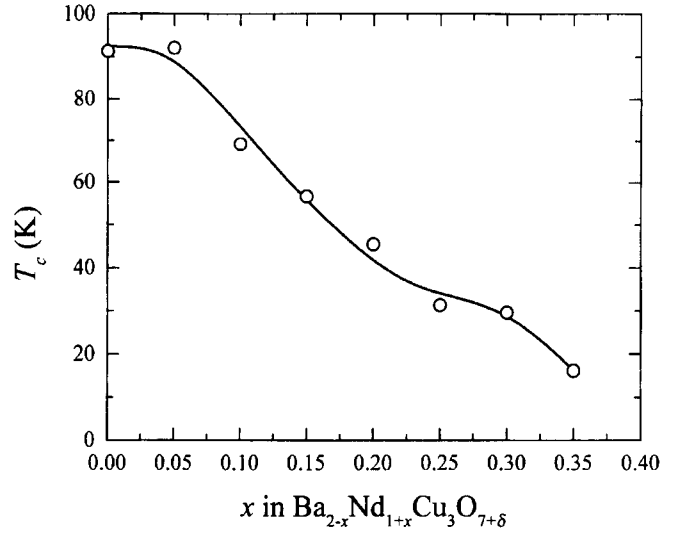

Superconducting transition temperature (zero resistivity) vs x for $Ba_{2-x}Nd_{1+x}Cu_3O_{7+\delta}$ ($\delta = 0$ for $0 \leq x < 0.2$) (Takita *et al.*, 1988).

1988). The cell parameters and the critical temperature of $TlBa_{2-x}La_xCaCu_2O_7$ vs the La content are presented in Figs. 8.33 and 8.34, respectively. For the refinement on $Tl_{0.5}Pb_{0.5}Sr_2CaCu_2O_7$, the oxygen atoms in the TlO layer were displaced along the diagonals of the square face of the tetragonal cell (4(*j*) 0.42 0.42 0) (Martin *et al.*, 1989b). A similar structure was reported for (Tl,Bi)-**1212** by Ledésert *et al.* (1994), whereas in Parise *et al.* (1989a) the same atoms were displaced along the short translation vectors (4(*n*) 0.408 $\frac{1}{2}$ 0). In the latter refinement, the Tl site was also split. For $Tl_{0.464}Pb_{0.500}Sr_2CaCu_2O_{6.963}$ both the thallium and the oxygen atoms in the *additional* layer were found to be moved from the ideal positions and partial vacancies were detected on the Tl site (occupancy 0.964) (Ogborne and Weller, 1994a). In all the refinements discussed earlier, the displacements of the atoms in the TlO layer result in tetrahedral coordination of the thallium atoms.

A Pb-based **1212** compound was first reported for the composition $Pb_{0.705}Sr_2Y_{0.73}Ca_{0.27}Cu_{2.295}O_7$ (Lee *et al.*, 1989). A structural refinement in space group *P4/mmm* ($a = 3.8207$, $c = 11.826$ Å) considered two partly occupied cation sites in the *additional* layer, one occupied by the lead and the other by the copper atoms (Pb in 1(*a*) 0 0 0 and Cu in 4(*l*) 0.221 0 0, occupancy 0.705 and 0.074) and splitting of the O site in the same layer (4(*n*) 0.324 $\frac{1}{2}$ 0). Superconductivity ($T_c = 25$ K) was detected for reduced $Pb_{0.65}Sr_2Y_{0.7}Ca_{0.3}Cu_{2.35}O_{7.05}$ (Maeda *et al.*, 1991a). The extra oxygen atoms in nonsuperconducting $Pb_{0.65}Sr_2Y_{0.7}Ca_{0.3}Cu_{2.35}O_{7.11}$ were found to be located in the *additional* layer (2(*f*) 0 $\frac{1}{2}$ 0).

Fig. 8.33.

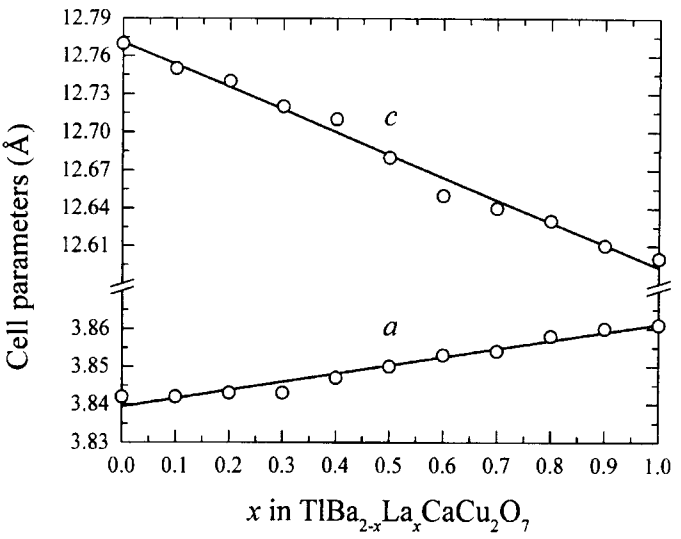

Cell parameters vs La content for $TlBa_{2-x}La_xCaCu_2O_7$ (Badri and Varadaraju, 1995).

Fig. 8.34.

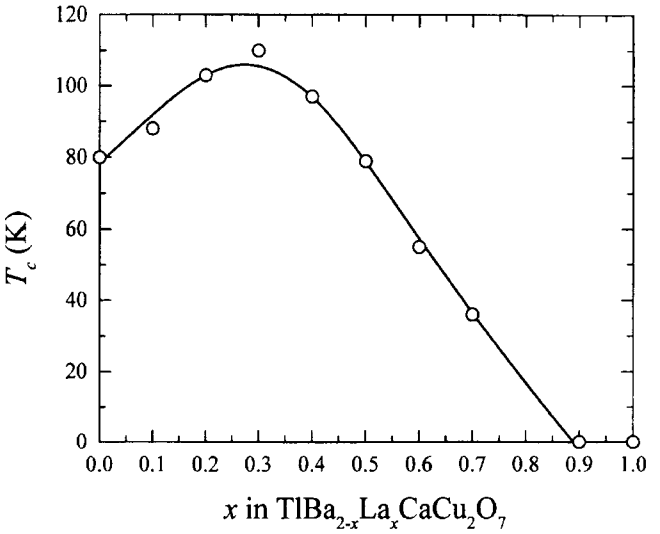

Superconducting transition temperature (zero resistivity) vs La content for $TlBa_{2-x}La_xCaCu_2O_7$ (Badri and Varadaraju, 1995).

A superconducting Ga-**1212** compound ($T_c = 35$ K) was first reported for the nominal composition $GaSr_2Er_{0.6}Ca_{0.4}Cu_2O_7$ (Cava *et al.*, 1991). The crystal structure, like that of Ga-**1201**, is orthorhombic because of the arrangement of GaO_4 tetrahedra in chains.

Nonsuperconducting Hg-**1212** compounds were reported for the composition $HgBa_2RCu_2O_7$ (R = La, Nd, Eu, Gd, Dy, and Y; Putilin *et al.*, 1991). They crystallize with a tetragonal structure ($P4/mmm$, $a = 3.8905$, $c = 12.546$ Å for $HgBa_2Eu_{0.76}Ca_{0.24}Cu_2O_7$). After the discovery of superconductivity in the Hg–Ba–Ca–Cu–O system (Schilling *et al.*, 1993), the structures of Hg-based compounds with T_c up to 128 K were refined by many research groups, who reported similar results. In particular, it was noted that a partly occupied O site is generally present in the *additional* layer, but its occupancy does not exceed 0.40. The critical temperature depends on the oxygen content, the maximum value being reached for $\delta = 0.24$–0.27 (Radaelli *et al.*, 1993b; Loureiro *et al.*, 1993).

The first synthesis of a carbon-containing Cu-**1212** compound was reported by Karen and Kjekshus (1991). A structural refinement carried out in space group $Pmmm$ ($a = 3.8278$, $b = 3.8506$, $c = 11.1854$ Å) showed that carbon had partly substituted for copper in the *additional* layers, yielding the overall composition $C_{0.4}Sr_{2.14}Y_{0.86}Cu_{2.6}O_7$ (Miyazaki *et al.*, 1992c). Superstructures with ordered arrangements of rows of CO_3 triangles and chains of corner-linked CuO_4 squares ($2a$, b, $2c$ and $3a$, b, $2c$) were proposed by Miyazaki *et al.* (1992c) and Ohnishi *et al.* (1993). A critical temperature of 63 K was reported for the composition $C_{0.6}Sr_{2.05}Y_{0.475}Ca_{0.475}Cu_{2.4}O_y$, for which a 4-fold superstructure with a *B*-

centered orthorhombic cell was suggested (Akimitsu *et al.*, 1992). Two different superstructures in space group *Bm2m* were refined for $(C_{0.25}Cu_{0.75})Sr_2YCu_2O_7$ and $(C_{0.5}Cu_{0.5})Ba_2YCu_2O_7$, respectively ($a = 15.311$, $b = 3.851$, $c = 22.371$ Å and $a = 7.7704$, $b = 3.8876$, $c = 22.9812$ Å; Domengès *et al.*, 1993, 1994), the latter being identical to the one mentioned earlier. More superstructures with similar ordered arrangements of carbon and copper atoms in the *additional* layer can be derived from the average structure. One short cell parameter (*b*) remains the same while the other is multiplied by a factor that depends on the C/Cu ratio.

1222 $Cu_1(Ba_{0.63}Nd_{0.37})_2(Nd_{0.67}Ce_{0.33})_2Cu_2O_{8.91}$

***AB*$_2$*C*$_2$*D*$_2$O$_9$**, *tI*32, (139) *I*4/*mmm*–*ge*^{4}*dca*
-O$_2$*D*–*C*–O$_2$–*C*–*D*O$_2$–*OB*–*AO*″–*OB*-
$Ba_{1.266}Nd_{2.084}Ce_{0.65}Cu_3O_{8.912}$, $T_c = 37$ K,[a] PN, RT,
$R_B = 0.0385$ (Izumi *et al.*, 1989a)
(139) *I*4/*mmm*, $a = 3.8747$, $c = 28.599$ Å, $Z = 2$ Fig. 15

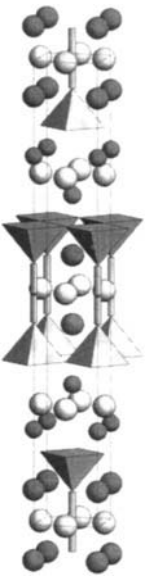

Atom	WP	PS	*x*	*y*	*z*	Occ.
Cu(1)	8(*h*)	*m*.2*m*	0.0527	0.0527	0	0.25
Ba[b]	4(*e*)	4*mm*	$\frac{1}{2}$	$\frac{1}{2}$	0.0756	
Cu(2)	4(*e*)	4*mm*	0	0	0.1418	
Nd[c]	4(*e*)	4*mm*	$\frac{1}{2}$	$\frac{1}{2}$	0.2044	
O(1)	16(*l*)	*m*..	0.060	0.440	0	0.114
O(2)	16(*m*)	..*m*	0.054	0.054	0.0639	0.25
O(3)	8(*g*)	2*mm*.	0	$\frac{1}{2}$	0.1475	
O(4)	4(*d*)	$\bar{4}$*m*2	0	$\frac{1}{2}$	$\frac{1}{4}$	

[a] Value taken from figure.
[b] Ba = $Ba_{0.633}Nd_{0.367}$.
[c] Nd = $Nd_{0.675}Ce_{0.325}$.

(*continued*)

Compound	a (Å)	c (Å)	T_c (K)	Ref.
$TiSr_2Nd_{1.5}Ce_{0.5}Cu_2O_y$[a]	3.873	28.36	n.s.	1
$TaSr_2Nd_{1.5}Ce_{0.5}Cu_2O_y$[a]	3.881	28.93	n.s.	1
$NbSr_2Pr_{1.5}Ce_{0.5}Cu_2O_{10}$	3.8870	28.752	n.s.	2
$NbSr_2Nd_{1.5}Ce_{0.5}Cu_2O_{10-\delta}$[a]	3.885	28.864	28	3
$NbSr_2Sm_{1.5}Ce_{0.5}Cu_2O_{10}$	3.8709	28.791	28	2
$NbSr_2Eu_{1.5}Ce_{0.5}Cu_2O_{10}$	3.8687	28.774	28	2
$NbSr_2Gd_{1.5}Ce_{0.5}Cu_2O_y$[a]	3.8669	28.742	13[b]	4
$Ba_{1.266}Nd_{2.084}Ce_{0.65}Cu_3O_{8.912}$	3.8747	28.599	37[c]	5
$Ba_{1.34}Eu_2Ce_{0.66}Cu_3O_{8.54}$	3.85044	28.4598	33	6
$Ba_{0.67}Sr_{0.67}La_{0.67}Gd_{1.33}Ce_{0.67}Cu_3O_{9.415}$[a]	3.842	28.349	38	7
$Ba_{1.33}La_{0.67}Gd_{1.33}Ce_{0.67}Cu_3O_{10-\delta}$[a]	3.858	28.489	25	7
$Ba_{1.33}LaGdCe_{0.67}Cu_3O_{10-\delta}$[a]	3.833	28.298	40	7
$Sr_{1.7}Sm_{1.6}Ce_{0.7}Cu_3O_{8+\delta}$[a]	3.8562	28.18	30	8
$Sr_{1.8}Eu_{1.6}Ce_{0.6}Cu_3O_{8.6}$	3.84048	28.0748	36	8
$Al_{0.25}Sr_{1.33}Eu_{2.17}Ce_{0.5}Cu_{2.75}O_{8+\delta}$[a]	3.846[c]	27.95[c]	18	9
$Fe_{0.25}Sr_{1.33}Eu_{2.17}Ce_{0.5}Cu_{2.75}O_{8+\delta}$[a]	3.836[c]	28.20[c]	26	9
$Co_{0.25}Sr_{1.33}Eu_{2.17}Ce_{0.5}Cu_{2.75}O_{8+\delta}$[a]	3.839[c]	28.22[c]	36	9
$RuSr_2Gd_{1.5}Ce_{0.5}Cu_2O_{10}$[a]	3.836	28.58	42[d]	10
$C_{0.35}Sr_2Y_{1.46}Ce_{0.54}Cu_{2.65}O_9$	[e]		18	11

[a] Nominal composition.
[b] From resistivity measurements (zero resistivity).
[c] Value taken from figure.
[d] T_c given for $RuSr_2Gd_{1.4}Ce_{0.6}Cu_2O_{10}$ (value taken from figure).
[e] Space group *Immm*, $a = 3.8272$, $b = 3.8313$, and $c = 27.7077$ Å.

References: 1, Li *et al.* (1991); 2, Goodwin *et al.* (1992); 3, Cava *et al.* (1992); 4, Wang *et al.* (1993); 5, Izumi *et al.* (1989a); 6, Sawa *et al.* (1989a); 7, Wada *et al.* (1990a); 8, Kopnin *et al.* (1994); 9, Ichinose *et al.* (1992); 10, Bauernfeind *et al.* (1995); 11, Miyazaki *et al.* (1992b).

1222 $Tl_1Ba_2(Eu_{0.75}Ce_{0.25})_2Cu_2O_9$

***AB*$_2$*C*$_2$*D*$_2$O$_9$**, *tI*32, (139) *I*4/*mmm*–*ge*^{4}*dba*
-O$_2$*D*–*C*–O$_2$–·*C*–*D*O$_2$–*OB*–*AO*–*OB*-
$TlBa_2Eu_{1.5}Ce_{0.5}Cu_2O_9$, $T_c = 40$ K, PX, RT, $R_B = 0.0944$
(Liu *et al.*, 1992a)
(139) *I*4/*mmm*, $a = 3.8782$, $c = 30.423$ Å, $Z = 2$ Fig. 16

Atom	WP	PS	*x*	*y*	*z*	Occ.
Tl	8(*i*)	*m*2*m*.	0.082	0	0	0.25
Ba	4(*e*)	4*mm*	$\frac{1}{2}$	$\frac{1}{2}$	0.0872	
Cu	4(*e*)	4*mm*	0	0	0.1520	
Eu[a]	4(*e*)	4*mm*	$\frac{1}{2}$	$\frac{1}{2}$	0.2087	
O(1)	2(*b*)	4/*mmm*	$\frac{1}{2}$	$\frac{1}{2}$	0	
O(2)	4(*e*)	4*mm*	0	0	0.0831	
O(3)	8(*g*)	2*mm*.	0	$\frac{1}{2}$	0.1554	
O(4)	4(*d*)	$\bar{4}$*m*2	0	$\frac{1}{2}$	$\frac{1}{4}$	

[a] Eu = $Eu_{0.75}Ce_{0.25}$.

Compound	*a* (Å)	*c* (Å)	T_c (K)	Ref.
$TlBa_2Eu_{1.5}Ce_{0.5}Cu_2O_9$	3.8782	30.423	40	1
$Tl_{0.7}Hg_{0.3}Sr_2Pr_2Cu_2O_9$	3.8642	29.568	n.s.	2
$TlSr_2Nd_{1.5}Ce_{0.5}Cu_2O_9$[a]	3.851	29.64	30	3
$Tl_{0.8}Ti_{0.2}Sr_2Nd_{1.5}Ce_{0.5}Cu_2O_9$[a]	3.847	29.43	27[b]	4
$Tl_{0.8}Nb_{0.2}Sr_2Nd_{1.5}Ce_{0.5}Cu_2O_9$[a]	3.852	29.45	20[b]	4
$Tl_{0.7}Pb_{0.3}Sr_2Nd_{1.5}Ce_{0.5}Cu_2O_9$[a]	3.853	29.61	20[b]	5
$Tl_{0.5}Pb_{0.5}Sr_2Eu_{1.8}Ce_{0.2}Cu_2O_9$[a]	3.91	29.98	40	6
$Tl_{0.5}Pb_{0.5}Sr_2Gd_{1.6}Ce_{0.4}Cu_2O_9$	3.8429	29.5097	46	7
$Ga_{0.5}Sr_{1.5}Eu_2Ce_{0.5}Cu_{2.5}O_9$[a]	3.840	28.14	28	8
$Ga_{0.8}Sr_2Y_{1.4}Ce_{0.6}Cu_{2.2}O_{9-\delta}$[a]	3.812	28.16	14	9
$Pb_{0.5}Sr_{1.75}Eu_{1.75}Ce_{0.5}Cu_{2.5}O_9$	3.83795	29.0116	25	10, 11

(*continued*)

$Pb_{0.5}Cd_{0.5}Sr_{1.8}Eu_{0.2}Gd_{1.4}Ce_{0.6}Cu_2O_9$	3.8250	29.2235	23[b]	12
$Pb_{0.5}Sr_{1.75}Nd_{0.25}Ho_{1.38}Ce_{0.62}Cu_{2.5}O_{8.64}$	3.82496	28.9862	10[c]	13
$Hg_{0.4}Pr_{0.6}Sr_{2.3}Pr_{1.7}Cu_2O_9$[a]	3.8603	29.614	n.s.	2
$Hg_{0.5}Pb_{0.5Sr_2}Gd_{1.5}Ce_{0.5}Cu_2O_y$[a]	3.846	29.418	38[c]	14

[a] Nominal composition.

[b] From resistivity measurements (zero resistivity).

[c] From resistivity measurements (onset).

References: 1, Liu *et al.* (1992a); 2, Hervieu *et al.* (1995b); 3, Chen *et al.* (1993d); 4, Chen *et al.* (1992a); 5, Chen *et al.* (1992b); 6, Iqbal *et al.* (1991); 7, Vijayaraghavan *et al.* (1993); 8, Adachi *et al.* (1992); 9, Li *et al.* (1992a); 10, Maeda *et al.* (1991b); 11, Maeda *et al.* (1990); 12, Luo *et al.* (1996); 13, Maeda *et al.* (1992); 14, Tang *et al.* (1995c).

A superconducting Cu-**1222** compound ($T_c = 33$ K) was first reported for the composition $Ba_{1.34}Eu_2Ce_{0.66}Cu_3O_{8.54}$ (Sawa *et al.*, 1989a). The structural refinement, carried out in space group $I4/mmm$ with all atom sites in ideal positions, revealed vacancies on the Cu site in the *additional* layer (occupancy 0.85). For the refinement of the structure of $Sr_{1.8}Y_{1.5}CeCu_{2.7}O_{8.6}$ $((Cu_{0.7}Ce_{0.3})$-$(Sr_{0.9}Y_{0.1})_2(Y_{0.65}Ce_{0.35})_2Cu_2O_{8.6})$, the cation site in the *additional* layer was split (from 2(*a*) 0 0 0 into 8(*i*) 0.052 0 0) (Kopnin *et al.*, 1994). The structure of Nb-**1222** compounds, first reported by Cava *et al.* (1992), is characterized by full occupation of the O site in the *additional* layer, yielding an oxygen content of $NbSr_2R_2Cu_2O_{10}$ (Goodwin *et al.*, 1992).

Tl-**1222** compounds were first reported for the compositions $Tl_{1.32}Ba_{1.68}Pr_2Cu_2O_9$ and $Tl_{1.3}Sr_{1.6}Pr_2Cu_2O_9$ (Martin *et al.*, 1989a). Structural refinements were carried out in space group $I4/mmm$ ($a = 3.900$, $c = 30.273$ Å and $a = 3.8635$, $c = 29.535$ Å). In both structures the Tl site, partly vacant in the Sr-containing compound, was found to be located in the ideal position (2(*a*) 0 0 0). Superconductivity ($T_c = 40$ K) was observed for $Tl_{0.5}Pb_{0.5}Sr_2Eu_{1.8}Ce_{0.2}Cu_2O_9$ (Iqbal *et al.*, 1991) and a short time later for Pb-free $TlBa_2Eu_{1.5}Ce_{0.5}Cu_2O_9$ (Liu *et al.*, 1992a). The first Pb-based **1222** compound, $PbSr_{1.6}Pr_{2.4}Cu_{2.6}O_y$, was reported by Adachi *et al.* (1990a). A critical temperature of 25 K was measured for a sample of composition $Pb_{0.5}Sr_{1.75}Eu_{1.75}Ce_{0.5}Cu_{2.5}O_9$ (Maeda *et al.*, 1990). The structural refinement considered splitting of both the cation and the oxygen site in the *additional* layer (cation in 8(*i*) 0.070 0 0 and O in 8(*j*) 0.18 $\frac{1}{2}$ 0) (Maeda *et al.*, 1991b). For $Pb_{0.5}Sr_{1.75}Nd_{0.25}Ho_{1.38}Ce_{0.62}Cu_{2.5}O_{8.64}$ an extra O site with very low occupancy (4(*c*) 0 $\frac{1}{2}$ 0, occupancy 0.015) was detected in the *additional* layer (Maeda *et al.*, 1992).

1223 $(Tl_{0.50}Pb_{0.50})_1Sr_2(Ca_{0.94}Tl_{0.03}Pb_{0.03})_2Cu_3O_9$

$AB_2C_2D_3O_9$, *tP*17, (123) *P*4/*mmm*–*ih*^{2}*g*^{2}*ecba*
-DO_2–·*C*–DO_2–·*C*–DO_2–*OB*–*AO*–*OB*-
$Tl_{0.56}Pb_{0.56}Sr_2Ca_{1.88}Cu_3O_9$, T_c = 120 K, SX, RT,
R_w = 0.047 (Subramanian *et al.*, 1988e)
(123) *P*4/*mmm*, *a* = 3.808, *c* = 15.232 Å, *Z* = 1 Fig. 17

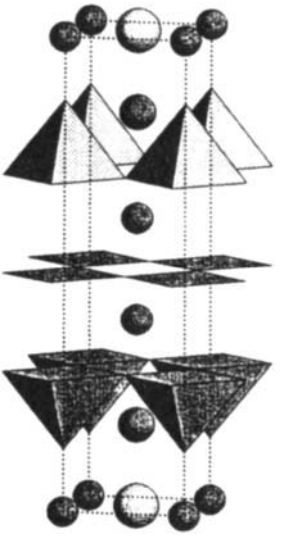

Atom	WP	PS	*x*	*y*	*z*	Occ.
Tl[a]	4(*l*)	*m*2*m*.	0.067	0	0	0.25
Sr	2(*h*)	4*mm*	$\frac{1}{2}$	$\frac{1}{2}$	0.1709	
Cu(1)	2(*g*)	4*mm*	0	0	0.2868	
Ca[b]	2(*h*)	4*mm*	$\frac{1}{2}$	$\frac{1}{2}$	0.3928	
Cu(2)	1(*b*)	4/*mmm*	0	0	$\frac{1}{2}$	
O(1)	4(*n*)	*m*2*m*.	0.40	$\frac{1}{2}$	0	0.25
O(2)	2(*g*)	4*mm*	0	0	0.1311	
O(3)	4(*i*)	2*mm*.	0	$\frac{1}{2}$	0.2924	
O(4)	2(*e*)	*mmm*.	0	$\frac{1}{2}$	$\frac{1}{2}$	

[a] Tl = $Tl_{0.5}Pb_{0.5}$.
[b] Ca = $Ca_{0.94}Tl_{0.03}Pb_{0.03}$.

Compound	*a* (Å)	*c* (Å)	T_c (K)	Ref.
$Tl_{1.1}Ba_{1.88}Ca_{1.9}Cu_3O_9$	3.853	15.913	110	1
$TlSr_2Ca_2Cu_3O_y$[a]	3.815	15.306	106	2
$Tl_{1.16}Sr_{1.28}Ba_{0.72}Ca_{1.84}Cu_3O_9$	3.8274	15.524	90[b]	3
$Tl_{0.6}V_{0.5}Sr_2Ca_2Cu_3O_y$[a]	3.824	15.16	110	4
$Tl_{0.8}In_{0.2}Sr_{1.6}Ba_{0.4}Ca_2Cu_3O_{9-\delta}$[a]	3.8327	15.4713	103	5
$Tl_{0.56}Pb_{0.56}Sr_2Ca_{1.88}Cu_3O_9$	3.808	15.232	122	6
$Tl_{0.668}Pb_{0.404}Sr_{1.604}Ca_{2.324}Cu_3O_9$	3.81516	15.2798	118.2	7
$Tl_{0.660}Pb_{0.2}Bi_{0.2}Sr_{1.586}Ba_{0.212}Ca_{2.142}Cu_3O_9$	3.81798	15.3223	119.5	8
$Tl_{0.5}Bi_{0.5}Sr_2Ca_2Cu_3O_9$[a]	3.815[c]	15.31[c]	120	9
$Tl_{0.68}Bi_{0.17}Sr_{1.6}Ba_{0.4}Ca_2Cu_3O_9$	3.8211	15.4235[d]	113	10
$AlSr_2Ca_2Cu_3O_{9.5}$[e]	3.836	14.405	78	11
$Pb_{0.5}Sr_{2.51}Ca_{1.74}Cu_{3.25}O_9$[f]	3.831	15.30[g]	104	12
$Ge_{0.5}Sr_2Ca_{1.8}Y_{0.2}Cu_{3.5}O_{9.3}$[h]	3.8313	14.533	77	13

(continued)

$BSr_2Ca_2Cu_3O_9$[h]	3.821	13.854	75	14
$B_{0.6}C_{0.4}Sr_{2.7}Ca_{1.3}Cu_3O_9$[e]	3.87	13.98	115	15
$C_{0.5}Ba_2Ca_2Cu_{3.5}O_9$[i]	3.862	14.825[j]	120	16
$P_{0.5}Sr_2Ca_{1.8}Y_{0.2}Cu_{3.5}O_{9.45}$[e]	3.845	14.29[j]	74	17
$S_{0.5}Sr_2Ca_3Cu_{4.5}O_{12.1}$[h]	3.850[c]	14.5[c,k]	100	18

[a] Nominal composition.
[b] $T_c = 110$ K for sample annealed under reducing conditions.
[c] Value taken from figure.
[d] Superstructure (orthorhombic, 4*a*, 2*a*, 4*c*) reported for $Tl_{0.75}Bi_{0.25}Sr_{1.6}Ba_{0.4}Ca_2Cu_3O_9$ (Lee *et al.*, 1996).
[e] Prepared at 5 GPa; nominal composition.
[f] Prepared at 6 GPa.
[g] Additional reflections indicate incommensurate modulation ($\mathbf{q} \approx \mathbf{a}^*/3.1$).
[h] Prepared at 6 GPa; nominal composition.
[i] Prepared at 8 GPa; nominal composition.
[j] Additional reflections indicate superstructure (2*a*, *a*, 2*c*).
[k] Additional reflections indicate superstructure (2*a*, *a*, 2*c* or 2*a*, *a*, *c*).
References: Subramanian *et al.* (1988b); 2, Morgan *et al.* (1993); 3, Martin *et al.* (1993b); 4, Li *et al.* (1994); 5, Hur *et al.* (1996); 6, Subramanian *et al.* (1988e); 7, Marcos and Attfield (1996); 8, Gladyshevskii *et al.* (1996); 9, Subramanian *et al.* (1990a); 10, Hur *et al.* (1995); 11, Matveev and Takayama-Muromachi (1995); 12, Wu *et al.* (1996c); 13, Matveev *et al.* (1996); 14, Kawashima *et al.* (1995); 15, Uehara *et al.* (1994b); 16, Chaillout *et al.* (1996); 17, Isobe *et al.* (1996b); 18, Takayama-Muromachi *et al.* (1995b).

1223 $Ga_1Sr_2Ca_2Cu_3O_9$

$AB_2C_2D_3O_9$, *tP*17, (123) *P*4/*mmm*–*ih*^{2}*g*^{2}*ecba*
-DO_2–·*C*–DO_2–·*C*–DO_2–*OB*–*AO*–*OB*-
$GaSr_2Ca_2Cu_3O_9$,[a] $T_c = 73$ K, PN, RT, $R_B = 0.0263$ (Khasanova *et al.*, 1996b)
(74) *Imam* (*Imma*), $a = 5.4041$, $b = 5.4615$, $c = 29.355$ Å, $Z = 4$
$\mathbf{a}_1 + \mathbf{a}_2$, $-\mathbf{a}_1 + \mathbf{a}_2$, 2**c**; origin shift 0 $\frac{1}{4}$ $\frac{1}{4}$

Atom	WP	PS	*x*	*y*	*z*	Occ.
Ga	8(*i*)	..*m*	0.059	−0.073	$\frac{1}{4}$	0.5
Sr	8(*h*)	*m*..	$\frac{1}{2}$	0.013	0.3288	
Cu(1)	8(*h*)	*m*..	0	0.0039	0.3865	
Ca	8(*h*)	*m*..	$\frac{1}{2}$	−0.001	0.4434	
Cu(2)	4(*a*)	2/*m*..	0	0	$\frac{1}{2}$	
O(1)	8(*i*)	..*m*	0.399	−0.112	$\frac{1}{4}$	0.5
O(2)	16(*j*)	1	−0.047	0.020	0.3060	0.5
O(3)	8(*g*)	..2	$\frac{1}{4}$	$\frac{3}{4}$	0.3898	
O(4)	8(*g*)	..2	$\frac{1}{4}$	$\frac{1}{4}$	0.3928	
O(5)	8(*g*)	..2	$\frac{1}{4}$	$\frac{1}{4}$	0.5008	

[a] Prepared at 6 GPa.

1223 $Hg_1Ba_2Ca_2Cu_3O_{8.44}$

$AB_2C_2D_3O_{8+\delta}$, *tP*16, (123) *P*4/*mmm*–*ih*^{2}*g*^{2}*e*(*c*)*ba*
-*DO*$_2$–·*C*–*DO*$_2$–·*C*–*DO*$_2$–*OB*–*A*·–*OB*-
$HgBa_2Ca_2Cu_3O_{8.44}$,[a] T_c = 133 K, PN, RT, R_{wp} = 0.0815 (Chmaissem *et al.*, 1993)
(123) *P*4/*mmm*, *a* = 3.8502, *c* = 15.7829 Å, *Z* = 1

Atom	WP	PS	*x*	*y*	*z*	Occ.
Hg	1(*a*)	4/*mmm*	0	0	0	
Ba[b]	2(*h*)	4*mm*	$\frac{1}{2}$	$\frac{1}{2}$	0.1773	
Cu(1)	2(*g*)	4*mm*	0	0	0.2979	
Ca	2(*h*)	4*mm*	$\frac{1}{2}$	$\frac{1}{2}$	0.3954	
Cu(2)	1(*b*)	4/*mmm*	0	0	$\frac{1}{2}$	
O(1)	1(*c*)	4/*mmm*	$\frac{1}{2}$	$\frac{1}{2}$	0	0.44
O(2)	2(*g*)	4*mm*	0	0	0.1236	
O(3)	4(*i*)	2*mm*.	0	$\frac{1}{2}$	0.2994	
O(4)	2(*e*)	*mmm*.	0	$\frac{1}{2}$	$\frac{1}{2}$	

[a] Prepared at 1.8 GPa.
[b] Two Ba sites (2(*h*) $\frac{1}{2}$ $\frac{1}{2}$ 0.1865 and 2(*h*) $\frac{1}{2}$ $\frac{1}{2}$ 0.1613, occupancy 0.59 and 0.41) proposed in second refinement.

Compound	*a* (Å)	*c* (Å)	T_c (K)	Ref.
$HgBa_2Ca_2Cu_3O_{8.44}$[a]	3.8502	15.7829	133	1
$Hg_{0.6}Ti_{0.4}Ba_2Ca_2Cu_3O_{8.4}$[b]	3.8507	15.707	134	2
$Hg_{0.8}V_{0.2}Ba_2Ca_2Cu_3O_{8.3}$[b]	3.8629	15.652	127	2
$Hg_{0.8}Cr_{0.2}Ba_2Ca_2Cu_3O_{8.1}$[b]	3.8631	15.625	110	2
$Hg_{0.8}Mo_{0.2}Ba_2Ca_2Cu_3O_{8.4}$[b]	3.8537	15.731	134	2
$Hg_{0.9}Re_{0.1}Ba_2Ca_2Cu_3O_y$[b]	...	...	134	3
$Hg_{0.6}Tl_{0.4}Ba_2Ca_2Cu_3O_{8.33}$	3.8489	15.816	138[c]	4
$Hg_{0.618}Pb_{0.382}Ba_2Ca_2Cu_3O_{8.450}$	3.8457	15.8252	130[d]	5
$Hg_{0.8}Bi_{0.2}Ba_2Ca_2Cu_3O_{8.2}$[b]	3.8504	15.813	130	6
$Hg_{0.69}Au_{0.17}Ba_2Ca_2Cu_3O_{8.30}$[a]	3.8464	15.739	131	7
$Hg_{0.68}Re_{0.32}Sr_2Ca_2Cu_3O_{8.90}$[e]	3.8265	15.2126[f]	120	8

[a] Prepared at 1.8 GPa.
[b] Nominal composition.
[c] T_c given for $Hg_{0.8}Tl_{0.2}Ba_2Ca_2Cu_3O_{8+\delta}$.
[d] From resistivity measurements (zero resistivity).
[e] Prepared at 6 GPa.
[f] Superstructure (*Fmmm*, *Fmm*2 or *F*222, 2*a*, 4*a*, 2*c*) reported for $Hg_{0.75}Re_{0.25}Sr_2Ca_2Cu_3O_y$ (nominal composition) (Yamaura *et al.*, 1995).
References: 1. Chmaissem *et al.* (1993); 2, Maignan *et al.* (1995a); 3, Wolters *et al.* (1996); 4, Dai *et al.* (1995); 5, Wu *et al.* (1996b); 6, Michel *et al.* (1995); 7, Bordet *et al.* (1996); 8, Chmaissem *et al.* (1996).

A superconducting Tl-**1223** compound ($T_c = 110$ K) was identified for the composition $TlBa_2Ca_2Cu_3O_9$. A structure model was proposed in space group $P4/mmm$ ($a = 3.8429$, $c = 15.871$ Å) (Parkin *et al.*, 1988b) and the first refinement was carried out by Martin *et al.* (1988). For $Tl_{1.1}Ba_{1.88}Ca_{1.9}Cu_3O_9$, the Tl site was found to be displaced from the ideal position along the short translation vectors (from 1(*a*) 0 0 0 into 4(*l*) 0.085 0 0), vacancies were detected on the Ba site (occupancy 0.94), and a small amount of Tl was found on the Ca site (5 at.%) (Subramanian *et al.*, 1988b). For $TlBa_2Ca_2Cu_3O_{8.62}$ two partly occupied Tl sites in the *additional* layer were considered (Morosin *et al.*, 1991c). The two sites, one in the ideal position on the 4-fold rotation axis and the other one off-centered (4(*l*) 0.1138 0 0), were associated with oxidation states Tl^+ and Tl^{3+}, respectively. In addition, vacancies were detected on the O site (occupancy 0.62) in the same layer. A superconducting Sr analogue, with 50% of the thallium atoms substituted by Pb, was reported in Subramanian *et al.* (1988e). Aranda *et al.* (1994) found the Tl and O sites in the *additional* layer, as well as the O site in the *bridging* layers, to be off-centered in the [1 1 0] direction (Tl in 4(*j*) 0.0451 0.0451 0, O in 4(*j*) 0.553 0.553 0 and 8(*r*) 0.049 0.049 0.1321). The refinement also showed partial substitution of Sr by Ca (21.1 at.%).

A superconducting (C,Cu)-**1223** compound ($T_c = 67$ K) was first reported for the composition $C_{0.5}Ba_2Ca_2Cu_{3.5}O_9$ ($a = 3.859$, $c = 14.766$ Å) (Kawashima *et al.*, 1994a). By applying a thermal treatment under reducing conditions the superconducting transition temperature was raised to 120 K (Chaillout *et al.*, 1996). No structural refinements are available; however, models have been proposed. In particular, two possible models for a superstructure (2*a*, *a*, 2*c*) with an ordered arrangement of the carbonate groups were discussed by Chaillout *et al.* (1996). A boron-containing **1223** oxycarbonate without Cu in the *additional* layer has also been reported (Uehara *et al.*, 1994b).

A superconducting Ga-**1223** compound ($T_c = 70$ K), $GaSr_2Ca_2Cu_3O_9$, was first reported by Takayama-Muromachi and Isobe (1994), who proposed space group $I2cm$ ($a = 5.391$, $b = 5.454$, $c = 29.371$ Å). A 2-fold superstructure (*a*, 2*b*, *c*) with two kinds of chains, built up from differently oriented corner-sharing GaO_4 tetrahedra, was proposed by Ramirez-Castellanos *et al.* (1995).

A superconducting Hg-**1223** compound ($T_c = 133$ K), $HgBa_2Ca_2Cu_3O_{8+\delta}$, was first reported by Schilling *et al.* (1993) and a tetragonal structure was proposed ($a = 3.93$, $c = 16.1$ Å). The first refinement was carried out by Chmaissem *et al.* (1993). Takahashi *et al.* (1993), Chu *et al.* (1993), and Nuñes-Regueiro *et al.* (1993) observed a significant increase of the superconducting transition temperature at high pressure: $T_c = 150$ K at 11 GPa, 153 K at 15 GPa, and 157 K at 23.5 GPa. The cell parameters of Hg-based compounds vs the pressure are shown in Fig. 8.35. Finger *et al.* (1994) refined a substantial amount of Cu on the Hg site (10–18 at.%) and detected two partly occupied O sites, the occupancies of which were found to depend on the Cu/Hg ratio in the *additional* layer (2(*f*) 0 $\frac{1}{2}$ 0 and 4(*n*) 0.36 $\frac{1}{2}$ 0, occupancy ≥ 0.10 and < 0.0625). Samples with three different oxygen contents were studied by Wagner

Fig. 8.35.

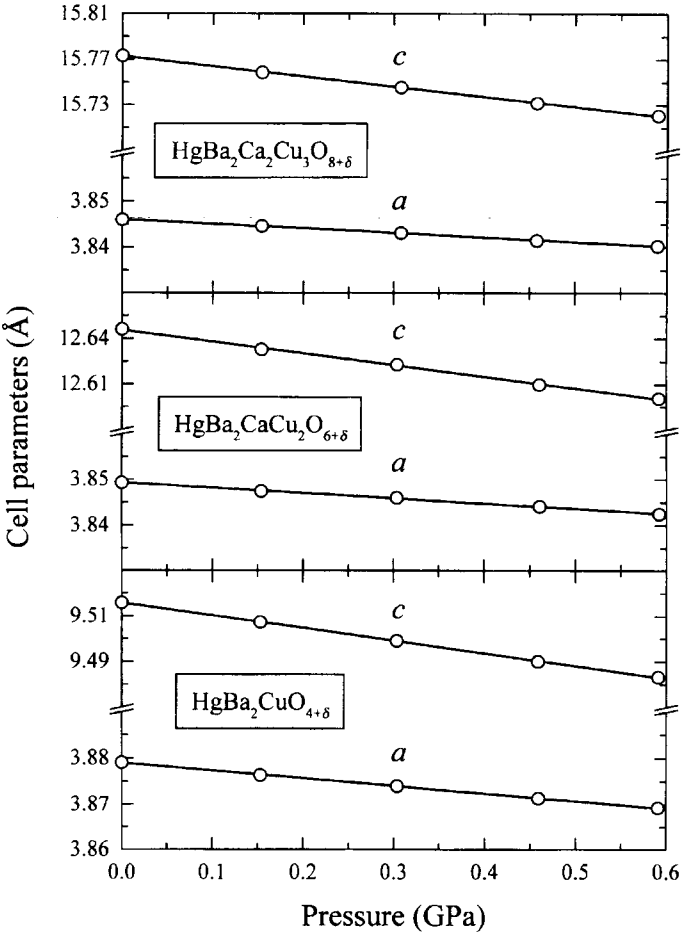

Cell parameters vs pressure for **1201**, **1212**, and **1223** in the Hg–Ba–Ca–Cu–O system (Hunter *et al.*, 1994).

et al. (1995). Vacancies were detected on the Hg site (occupancy 0.90–0.95) and two partly occupied O sites in the *additional* layer were reported also here: one in 2(*f*) with an occupancy of 0.08–0.09, the other in 1(*c*). The occupancy of the second site (0.18, 0.13, and 0.10) could be correlated to the critical temperature (135, 107, and 94 K).

1232 $(Bi_{0.50}Cu_{0.50})_1Sr_2(Ce_{0.67}Nd_{0.33})_3Cu_2O_{11}$

$AB_2C_3D_2O_{11}$, *tP*19, (123) *P*4/*mmm*–$i^2h^2g^2cba$
-DO_2–·*C*–O_2–*C*·–O_2–·*C*–DO_2–*OB*–*AO*–*OB*-
$Bi_{0.5}Sr_2Ce_2NdCu_{2.5}O_{11}$, T_c = 15 K, PX, R_B = 0.077
(Chen *et al.*, 1993b,c)
(123) *P*4/*mmm*, a = 3.848, c = 17.246 Å, Z = 1 Fig. 18

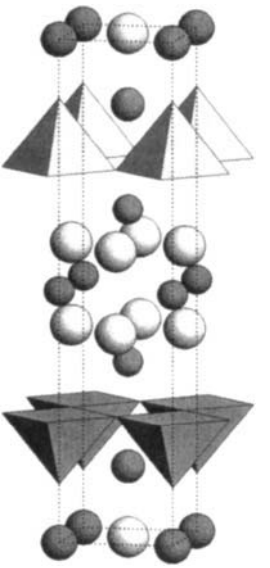

Atom	WP	PS	x	y	z	Occ
Bi[a]	4(*j*)	*m*.2*m*	0.065	0.065	0	0.25
Sr	2(*h*)	4*mm*	$\frac{1}{2}$	$\frac{1}{2}$	0.141	
Cu	2(*g*)	4*mm*	0	0	0.245	
Ce(1)[b]	2(*h*)	4*mm*	$\frac{1}{2}$	$\frac{1}{2}$	0.3485	
Ce(2)[b]	1(*b*)	4/*mmm*	0	0	$\frac{1}{2}$	
O(1)	1(*c*)	4/*mmm*	$\frac{1}{2}$	$\frac{1}{2}$	0	
O(2)	2(*g*)	4*mm*	0	0	0.116	
O(3)	4(*i*)	2*mm*.	0	$\frac{1}{2}$	0.256	
O(4)	4(*i*)	2*mm*.	0	$\frac{1}{2}$	0.4175	

[a] Bi = $Bi_{0.5}Cu_{0.5}$.
[b] Ce(1) = Ce(2) = $Ce_{0.6667}Nd_{0.3333}$.

Compound	a (Å)	c (Å)	T_c (K)	Ref.
$Tl_{0.596}Sr_2Ce_2HoCu_{2.2}O_{11}$	3.8221	17.2855	n.s.	1
$Pb_{0.5}Sr_2Ce_2HoCu_{2.5}O_{11.122}$	3.82615	17.2028	n.s.	1
$Bi_{0.5}Sr_2Ce_2NdCu_{2.5}O_{11}$	3.848	17.246	15	2, 3
$Bi_{0.5}Sr_2Ce_2GdCu_{2.5}O_{11-\delta}$[a]	3.847	17.198	20	2, 3
$Sr_2Ce_2HoCu_3O_{11}$[a]	3.824	17.22	n.s.	4

[a] Nominal composition.
References: 1, Wada *et al.* (1991a); 2, Wada *et al.* (1991b); 3, Chen *et al.* (1993b); 4, Chen *et al.* (1993c); 5, Wada *et al.* (1990b).

Nonsuperconducting **1232** compounds were reported for the composition $M_xSr_2Ce_2HoCu_{3-x}O_{11}$, where Cu could be partly substituted by Pb, Fe, or Al

(Wada *et al.*, 1990b). A structural refinement on $Pb_{0.5}Sr_2Ce_2HoCu_{2.5}O_{11}$ ($(Cu_{0.5}Pb_{0.5})Sr_2(Ce_{0.67}Ho_{0.33})_3Cu_2O_{11}$) in space group $P4/mmm$ ($a = 3.82246$, $c = 17.2082$ Å) indicated that the atoms in the *additional* layer were displaced from the ideal positions along the short translation vectors (cation from 1(*a*) 0 0 0 into 4(*l*) 0.072 0 0 and O from 1(*c*) $\frac{1}{2}$ $\frac{1}{2}$ 0 into 4(*n*) 0.32 $\frac{1}{2}$ 0). Wada *et al.* (1991b) detected an extra O site in the *additional* layer (2(*f*) 0 $\frac{1}{2}$ 0, occupancy 0.061). The only superconducting **1232** compounds known so far are $Bi_{0.5}Sr_2Ce_2RCu_{2.5}O_{11}$ with R = Nd or Gd (Chen *et al.* 1993c).

1234 $Tl_1Ba_2(Ca_{0.98})_3Cu_4O_{11}$

$AB_2C_3D_4O_{11}$, *tP*21, (123) $P4/mmm$-$i^2h^2g^3dca$
-*DO*$_2$-·*C*-*DO*$_2$-·*C*-*DO*$_2$-·*C*-*DO*$_2$-*OB*-*AO*-*OB*-
$Tl_{0.996}Ba_2Ca_{2.96}Cu_4O_{11}$, $T_c = 114$ K, PX, RT, $R_B = 0.044$
(Ogborne and Weller, 1994c)
(123) $P4/mmm$, $a = 3.84809$, $c = 19.0005$ Å, $Z = 1$ Fig. 19

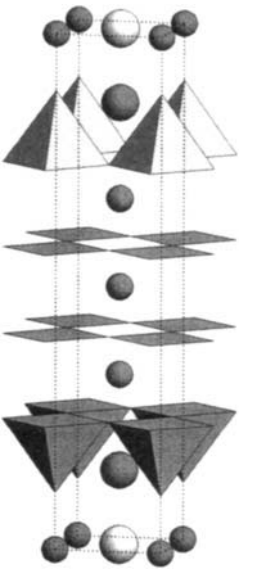

Atom	WP	PS	*x*	*y*	*z*	Occ.
Tl	4(*l*)	*m*2*m*.	0.086	0	0	0.249
Ba	2(*h*)	4*mm*	$\frac{1}{2}$	$\frac{1}{2}$	0.1437	
Cu(1)	2(*g*)	4*mm*	0	0	0.2487	
Ca(1)	2(*h*)	4*mm*	$\frac{1}{2}$	$\frac{1}{2}$	0.3292	0.98
Cu(2)	2(*g*)	4*mm*	0	0	0.4158	
Ca(2)	1(*d*)	4/*mmm*	$\frac{1}{2}$	$\frac{1}{2}$	$\frac{1}{2}$	
O(1)	1(*c*)	4/*mmm*	$\frac{1}{2}$	$\frac{1}{2}$	0	
O(2)	2(*g*)	4*mm*	0	0	0.1099	
O(3)	4(*i*)	2*mm*.	0	$\frac{1}{2}$	0.2515	
O(4)	4(*i*)	2*mm*.	0	$\frac{1}{2}$	0.4156	

1234 $(Hg_{0.73}Pb_{0.18})_1Ba_2Ca_3Cu_4O_{10.14}$

***AB*$_2$*C*$_3$*D*$_4$O$_{10+\delta}$**, *tP*20, (123) *P*4/*mmm*-$i^2h^2g^3d(c)a$
-*DO*$_2$-·*C*-*DO*$_2$-·*C*-*DO*$_2$-·*C*-*DO*$_2$-*OB*-*A*·-*OB*-
$Hg_{0.7336}Pb_{0.1834}Ba_2Ca_3Cu_4O_{10.14}$,[a] T_c = 129 K, SX, R_w = 0.0239 (Schwer *et al.*, 1995a)
(123) *P*4/*mmm*, a = 3.8530, c = 18.968 Å, Z = 1

Atom[b]	WP	PS	x	y	z	Occ.
Hg[c]	1(*a*)	4/*mmm*	0	0	0	0.917
Ba[d]	2(*h*)	4*mm*	$\frac{1}{2}$	$\frac{1}{2}$	0.14375	
Cu(1)	2(*g*)	4*mm*	0	0	0.24840	
Ca(1)	2(*h*)	4*mm*	$\frac{1}{2}$	$\frac{1}{2}$	0.32976	
Cu(2)	2(*g*)	4*mm*	0	0	0.41592	
Ca(2)	1(*d*)	4/*mmm*	$\frac{1}{2}$	$\frac{1}{2}$	$\frac{1}{2}$	
O(1)	1(*c*)	4/*mmm*	$\frac{1}{2}$	$\frac{1}{2}$	0	0.14
O(2)	2(*g*)	4*mm*	0	0	0.1059	
O(3)	4(*i*)	2*mm*.	0	$\frac{1}{2}$	0.2507	
O(4)	4(*i*)	2*mm*.	0	$\frac{1}{2}$	0.4167	

[a] Prepared at 1 GPa.
[b] Sites with occupancy 0.019 (Hg in 2(*g*) 0 0 0.1654, Ba in 2(*h*) $\frac{1}{2}$ $\frac{1}{2}$ 0.0266 and 2(*h*) $\frac{1}{2}$ $\frac{1}{2}$ 0.3102) ignored here.
[c] Hg = $Hg_{0.8}Pb_{0.2}$.
[d] Refined occupancy 0.962.

Compound	a (Å)	c (Å)	T_c (K)	Ref.
$Hg_{0.84}Ba_2Ca_3Cu_4O_{10.4}$	3.8495	19.003	125	1
$Hg_{0.7336}Pb_{0.1834}Ba_2Ca_3Cu_4O_{10.14}$[a]	3.8530	18.968	129	2

[a] Prepared at 1 GPa.
References: 1, Paranthaman and Chakoumakos (1996); 2, Schwer *et al.* (1995a).

1234 $(C_{0.32}Cu_{0.68})_1Ba_2Ca_3Cu_4O_{11.06}$

***AB*$_2$*C*$_3$*D*$_4$O$_{11}$**, *tP*21, (123) *P*4/*mmm*-$i^2h^2g^3fda$
-*DO*$_2$-·*C*-*DO*$_2$-·*C*-*DO*$_2$-·*C*-*DO*$_2$-*OB*-*AO*″-*OB*-
$C_{0.32}Ba_2Ca_3Cu_{4.68}O_{11.06}$,[a] T_c = 117 K, PN, RT, R_{wp} = 0.1068[b] (Shimakawa *et al.*, 1994a)
(123) *P*4/*mmm*, a = 3.86192, c = 17.9512 Å,[c] Z = 1

Atom	WP	PS	x	y	z	Occ.
Cu(1)[d]	1(*a*)	4/*mmm*	0	0	0	
Ba	2(*h*)	4*mm*	$\frac{1}{2}$	$\frac{1}{2}$	0.1219	
Cu(2)	2(*g*)	4*mm*	0	0	0.2332	
Ca(1)	2(*h*)	4*mm*	$\frac{1}{2}$	$\frac{1}{2}$	0.3187	
Cu(3)	2(*g*)	4*mm*	0	0	0.4117	
Ca(2)	1(*d*)	4/*mmm*	$\frac{1}{2}$	$\frac{1}{2}$	$\frac{1}{2}$	
O(1)	2(*f*)	*mmm*.	0	$\frac{1}{2}$	0	0.37
O(2)	4(*l*)	*m*2*m*.	0	0.318	0	0.08
O(3)	2(*g*)	4*mm*	0	0	0.1000	0.68

(*continued*)

O(4)	8(*s*)	.*m*.	0	0.159	0.0593	0.08
O(5)	4(*i*)	2*mm*.	0	$\frac{1}{2}$	0.2376	
O(6)	4(*i*)	2*mm*.	0	$\frac{1}{2}$	0.4130	

[a] Prepared at 5 GPa.
[b] Multiphase refinement; sample also contained small amounts of Ag and Ag_2O.
[c] Average structure; additional reflections indicate superstructure (2*a*, *a*, 2*c*).
[d] $Cu(1) = Cu_{0.68}C_{0.32}$.

Compound	*a* (Å)	*c* (Å)	T_c (K)	Ref.
$AlSr_2Ca_3Cu_4O_{11}$[a]	3.839	17.72	110	1
$GaSr_2Ca_3Cu_4O_{10.8}$[b]	[c]		93[d]	2
$Ba_2Ca_3Cu_{4.6}O_{10.8}$[e]	3.8526	17.974[f]	116	3
$C_{0.32}Ba_2Ca_3Cu_{4.68}O_{11.06}$[e]	3.86192	17.9512[g]	117	4
$BSr_2Ca_3Cu_4O_{11}$[b]	3.8359	17.082	110	5
$P_{0.5}Sr_2Ca_{1.9}Y_{0.1}Cu_{3.5}O_{9.3}$[h]	3.851	17.49[g]	84	6
$S_{0.5}Sr_2Ca_3Cu_{4.5}O_{12}$[b]	3.854[i]	17.5[i,j]	100	7

[a] Prepared at 5.5 GPa; nominal composition.
[b] Prepared at 6 GPa; nominal composition.
[c] Space group *I*2*cm*, $a = 5.417$, $b = 5.462$, and $c = 35.78$ Å.
[d] $T_c = 107$ K for $GaSr_2Ca_3Cu_4O_{11.1}$.
[e] Prepared at 5 GPa.
[f] Additional reflections indicate superstructure (2*a*, 2*a*, 2*c*).
[g] Additional reflections indicate superstructure (2*a*, *a*, 2*c*).
[h] Prepared at 5 GPa; nominal composition.
[i] Value taken from figure.
[j] Additional reflections indicate superstructure (2*a*, *a*, 2*c* or 2*a*, *a*, *c*).
References: 1, Isobe *et al.* (1994); 2, Takayama-Muromachi and Isobe (1994); 3, Akimoto *et al.* (1995); 4, Shimakawa *et al.* (1994a); 5, Takayama-Muromachi *et al.* (1995a); 6, Isobe *et al.* (1996b); 7, Takayama-Muromachi *et al.* (1995b).

A superconducting Tl-**1234** compound ($T_c = 122$ K) with a tetragonal structure ($a = 3.85$, $c = 19.1$ Å) was first reported for the composition $TlBa_2Ca_3Cu_4O_{11}$ (Ihara *et al.*, 1988).

A superconducting Hg-**1234** compound ($T_c = 126$ K) was first reported for $HgBa_2Ca_3Cu_4O_{10+\delta}$ and a tetragonal structure was proposed ($a = 3.8540$, $c = 19.006$ Å) (Antipov *et al.*, 1993). Structural refinements indicated vacancies on the Hg site (occupancy 0.79 or 0.84) and a relatively high occupancy of the extra O site in the *additional* layer (occupancy 0.60 or 0.40) (Loureiro *et al.*, 1996a; Paranthaman and Chakoumakos, 1996). For $Hg_{0.7336}Pb_{0.1834}Ba_2Ca_3Cu_4O_{10.14}$ extra cation sites with very low occupancy, corresponding to a small fraction of intergrowth of **1234** with **1223** and **1245**, were refined (Schwer *et al.*, 1995a).

A critical temperature of 117 K was reported for the first (C,Cu)-**1234** compound (*P*4/*mmm*, $a = 3.855$, $c = 17.930$ Å) and an orthorhombic superstructure (2*a*, *a*, 2*c*) was proposed (Kawashima *et al.*, 1994a). The superstructure, also observed by Alario-Franco *et al.* (1994a) and Matsui *et al.* (1994), is caused by the ordering of carbon and copper atoms in the *additional* layer. In the

refinement of the average structure of $C_{0.32}Ba_2Ca_3Cu_{4.68}O_{11.06}$, two pairs of O sites were considered in the *additional* and *bridging* layers, corresponding to an occupation of the cation site in the *additional* layer by C and Cu, respectively (Shimakawa *et al.*, 1994a). A superconducting, carbon-free **1234** compound ($T_c = 117.1$ K) was reported for the nominal composition $Ag_{1-x}Ba_2Ca_3Cu_{4+x}O_{11-\delta}$ (Ihara *et al.*, 1994a). The average structure was described in space group $P4/mmm$ ($a = 3.8635$, $c = 18.111$ Å), but body-centered tetragonal superstructures ($2a$, $2c$) with ordered arrangements of copper and silver atoms were suggested for $x = 0.25$ and $x = 0.75$. Wu *et al.* (1994b) and Matsuhata *et al.* (1994) stated that the amount of Ag in the compound was negligible and explained the superstructure by the ordering of vacancies on the Cu site in the *additional* layer. Cu-**1234** compounds, with structural features similar to those described earlier, were reported by Jin *et al.* (1994), Wu *et al.* (1994a), Ihara *et al.* (1994b), and Alario-Franco *et al.* (1994b). In the last article, the superstructure was shown to be orthorhombic ($2a$, a, $2c$), but the same authors later detected small amounts of carbon in their samples (Alario-Franco *et al.*, 1994a). In the refinement of the average structure of $Ba_2Ca_3Cu_{4.6}O_{10.8}$, not only the Cu site, but also the O sites in the *additional* and *bridging* layers were found to be partly vacant (Akimoto *et al.*, 1995). The orthorhombic space group $A2mm$ (or monoclinic Am or $A2/m$) was proposed for the description of a 4-fold superstructure by Matsuhata *et al.* (1995).

1245 $Hg_1Ba_2Ca_4Cu_5O_{12.32}$

$AB_2C_4D_5O_{12+\delta}$, *tP*24, (123) $P4/mmm$–$i^2h^3g^3e(c)ba$
-DO_2–·C–DO_2–·C–DO_2–·C–DO_2–·C–DO_2–OB–A·–OB-
$HgBa_2Ca_4Cu_5O_{12.32}$,[a] $T_c = 101$ K, PN, RT, $R_{wp} = 0.0640$[b]
(Huang *et al.*, 1994a)
(123) $P4/mmm$, $a = 3.85151$, $c = 22.1049$ Å, $Z = 1$
Fig. 20

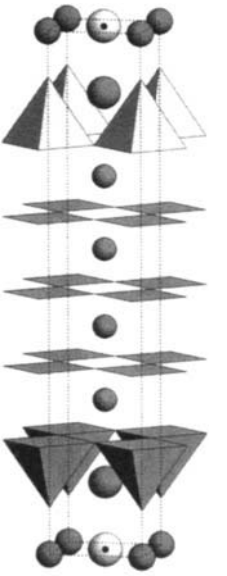

(*continued*)

Atom	WP	PS	x	y	z	Occ.
Hg	1(*a*)	4/*mmm*	0	0	0	
Ba	2(*h*)	4*mm*	$\frac{1}{2}$	$\frac{1}{2}$	0.1269	
Cu(1)	2(*g*)	4*mm*	0	0	0.2144	
Ca(1)	2(*h*)	4*mm*	$\frac{1}{2}$	$\frac{1}{2}$	0.2854	
Cu(2)	2(*g*)	4*mm*	0	0	0.3551	
Ca(2)	2(*h*)	4*mm*	$\frac{1}{2}$	$\frac{1}{2}$	0.4254	
Cu(3)	1(*b*)	4/*mmm*	0	0	$\frac{1}{2}$	
O(1)	1(*c*)	4/*mmm*	$\frac{1}{2}$	$\frac{1}{2}$	0	0.32
O(2)	2(*g*)	4*mm*	0	0	0.0867	
O(3)	4(*i*)	2*mm*.	0	$\frac{1}{2}$	0.2149	
O(4)	4(*i*)	2*mm*.	0	$\frac{1}{2}$	0.3562	
O(5)	2(*e*)	*mmm*.	0	$\frac{1}{2}$	$\frac{1}{2}$	

[a] Prepared at 1.8 GPa.
[b] Multiphase refinement; sample also contained 20% Hg-**1256** and 2% CaO.

Compound	a (Å)	c (Å)	T_c (K)	Ref.
$AlSr_2Ca_4Cu_5O_{13}$[a]	3.845	20.87	83	1
$HgBa_2Ca_4Cu_5O_{12.32}$[b]	3.85151	22.1049	101	2
$Hg_{0.623}Pb_{0.344}Ba_2Ca_4Cu_5O_{12.52}$[c]	3.8529	22.172	116	3
$Hg_{0.7}Au_{0.3}Ba_2Ca_4Cu_5O_{12+\delta}$[d]	3.849	22.061	110	4
$BSr_2Ca_4Cu_5O_{13}$[e]	3.837	20.22	85	5

[a] Prepared at 5.5 GPa; nominal composition.
[b] Prepared at 1.8 GPa.
[c] Prepared at 1 GPa.
[d] Prepared at 1.8 GPa; nominal composition.
[e] Prepared at 6 GPa; nominal composition.
References: 1, Isobe *et al.* (1994); 2, Huang *et al.* (1994a); 3, Schwer *et al.* (1995b); 4, Bordet *et al.* (1996); 5, Kawashima *et al.* (1995).

A critical temperature of 112 K was reached for Hg-**1245** after optimization (Loureiro *et al.*, 1994). For $Hg_{0.623}Pb_{0.344}Ba_2Ca_4Cu_5O_{12.52}$, two distinct cation sites were refined in the *additional* layer (Hg in 1(*a*) 0 0 0 and Pb in 8(*p*) 0.044 0.087 0, occupancy 0.579 and 0.043) (Schwer *et al.*, 1995b). Extra Hg and Ba sites with low occupancy were introduced into the structural model to take into account an intergrowth with **1234** and **1256**.

1256 $Hg_1Ba_2Ca_5Cu_6O_{14.40}$

***AB*$_2$*C*$_5$*D*$_6$O$_{14+\delta}$**, *tP*28, (123) *P*4/*mmm*–$i^3h^3g^4d(c)a$
-DO_2–•*C*–DO_2–•*C*–DO_2–•*C*–
DO_2–•*C*–DO_2–•*C*–DO_2–*OB*–*A*•–*OB*-
$HgBa_2Ca_5Cu_6O_{14.4}$,[a] T_c = 114 K, PN, RT, R_{wp} = 0.0640[b]
(Huang *et al.*, 1994a)
(123) *P*4/*mmm*, a = 3.8515, c = 25.3313 Å, Z = 1
Fig. 21

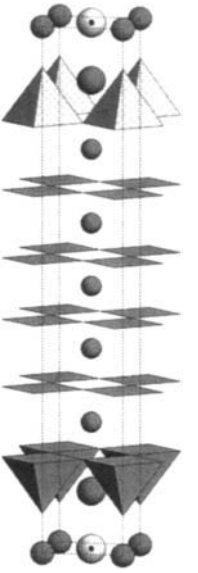

Atom	WP	PS	x	y	z	Occ.
Hg	1(*a*)	4/*mmm*	0	0	0	
Ba	2(*h*)	4*mm*	$\frac{1}{2}$	$\frac{1}{2}$	0.109	
Cu(1)	2(*g*)	4*mm*	0	0	0.184	
Ca(1)	2(*h*)	4*mm*	$\frac{1}{2}$	$\frac{1}{2}$	0.240	
Cu(2)	2(*g*)	4*mm*	0	0	0.314	
Ca(2)	2(*h*)	4*mm*	$\frac{1}{2}$	$\frac{1}{2}$	0.380	
Cu(3)	2(*g*)	4*mm*	0	0	0.437	
Ca(3)	1(*d*)	4/*mmm*	$\frac{1}{2}$	$\frac{1}{2}$	$\frac{1}{2}$	
O(1)	1(*c*)	4/*mmm*	$\frac{1}{2}$	$\frac{1}{2}$	0	0.4
O(2)	2(*g*)	4*mm*	0	0	0.075	
O(3)	4(*i*)	2*mm*.	0	$\frac{1}{2}$	0.180	
O(4)	4(*i*)	2*mm*.	0	$\frac{1}{2}$	0.312	
O(5)	4(*i*)	2*mm*.	0	$\frac{1}{2}$	0.441	

[a] Prepared at 1.8 GPa.
[b] Multiphase refinement; sample also contained 78% Hg-**1245** and 2% CaO.

2201 $Tl_2Ba_2Cu_1O_6$

$A_2B_2DO_6$, *tI*22, (139) *I*4/*mmm*–e^4cb
-*D*O_2–O*B*–*A*O–O*A*–*B*O-
$Tl_2Ba_2CuO_6$, $T_c = 90$ K, SX, RT, $R_w = 0.022$
(Torardi *et al.*, 1988a)
(139) *I*4/*mmm*, $a = 3.866$, $c = 23.239$ Å, $Z = 2$ Fig. 22

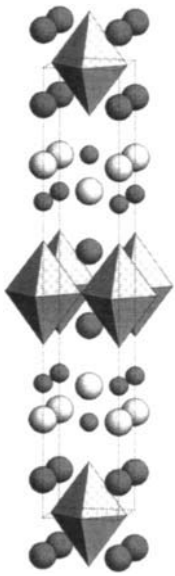

Atom	WP	PS	*x*	*y*	*z*	Occ.
Tl	4(*e*)	4*mm*	0	0	0.29735	
Ba	4(*e*)	4*mm*	$\frac{1}{2}$	$\frac{1}{2}$	0.41699	
Cu	2(*b*)	4/*mmm*	0	0	$\frac{1}{2}$	
O(1)	16(*n*)	.*m*.	0.405	$\frac{1}{2}$	0.2829	0.25
O(2)	4(*e*)	4*mm*	0	0	0.3832	
O(3)	4(*c*)	*mmm*.	0	$\frac{1}{2}$	$\frac{1}{2}$	

Compound	*a* (Å)	*c* (Å)	T_c (K)	Ref.
$Tl_2Ba_2CuO_6$	3.866	23.239	90	1
$Tl_{1.75}Cd_{0.25}Ba_2CuO_6$	3.851	23.313	90[a]	2
$TlHgBa_2CuO_6$	3.856	23.29	n.s.	3

[a] T_c given for $Tl_{1.8}Cd_{0.2}Ba_2CuO_6$ (nominal composition).
References: 1, Torardi *et al.* (1988a); 2, Parise *et al.* (1989b); 3, Nakajima *et al.* (1996).

2201 $Tl_2Ba_2Cu_1O_{6.10}$

$A_2B_2DO_6$, *tI*22, (139) *I*4/*mmm*–e^4cb
-*D*O_2–O*B*–*A*O–O*A*–*B*O-
$Tl_2Ba_2CuO_{6.10}$, $T_c = 90$ K, PN, $T = 4$ K, $R_B = 0.049$ (Parise *et al.*, 1989c)
(69) *Fmmm*, $a = 5.4604$, $b = 5.4848$, $c = 23.2038$ Å, $Z = 4$
$\mathbf{a}_1 + \mathbf{a}_2$, $-\mathbf{a}_1 + \mathbf{a}_2$, $\mathbf{c}$

(*continued*)

Atom	WP	PS	x	y	z	Occ.
Tl	16(*m*)	*m*..	0	−0.025	0.2976	0.5
Ba	8(*i*)	*mm*2	$\frac{1}{2}$	0	0.4172	
Cu	4(*b*)	*mmm*	0	0	$\frac{1}{2}$	
O(1)[a]	8(*f*)	222	$\frac{1}{4}$	$\frac{1}{4}$	$\frac{1}{4}$	0.07
O(2)	16(*m*)	*m*..	$\frac{1}{2}$	−0.059	0.2895	0.49
O(3)	8(*i*)	*mm*2	0	0	0.3837	
O(4)	8(*e*)	..2/*m*	$\frac{1}{4}$	$\frac{1}{4}$	$\frac{1}{2}$	

[a] Extra O site located between the TlO layers.

2201 $Bi_2Sr_2Cu_1O_6$

***A*$_2$*B*$_2$*DO*$_6$**, *tI*22, (139) *I*4/*mmm*–e^4cb
-*D*O_2–*OB*–*A*O–*OA*–*B*O-
$Bi_2Sr_2CuO_6$, T_c = 9 K, SX, RT, R_w = 0.130 (Torardi *et al.*, 1988a)
(66) *Amaa* (*Cccm*), a = 5.362, b = 5.374, c = 24.622 Å,[a] Z = 4
$\mathbf{a}_1 + \mathbf{a}_2$, $-\mathbf{a}_1 + \mathbf{a}_2$, **c**; origin shift 0 $\frac{1}{4}$ $\frac{1}{4}$

Atom	WP	PS	x	y	z	Occ.
Bi	8(*l*)	*m*..	0	0.2758	0.0660	
Sr	8(*l*)	*m*..	$\frac{1}{2}$	0.2479	0.1790	
Cu	4(*e*)	2/*m*..	0	$\frac{1}{4}$	$\frac{1}{4}$	
O(1)	8(*l*)	*m*..	$\frac{1}{2}$	0.334	0.064	
O(2)	8(*l*)	*m*..	0	0.226	0.145	
O(3)	8(*h*)	..2	$\frac{1}{4}$	0	0.254	

[a] Average structure, additional reflections indicate superstructure (5*a*, *b*, 3*c*).

Compound	a (Å)	b (Å)	c (Å)	T_c (K)	Ref.
$Bi_2Sr_2CuO_6$[a]	5.375	5.378	24.377[b]	9.5	1
$Bi_2Sr_{1.6}La_{0.4}CuO_{6.30}$	5.388	5.398	24.399	29.5[c]	2

[a] Refined composition $Bi_{1.86}Sr_{1.56}Cu_{0.83}O_{5.98}$.
[b] Space group *A*2*aa*.
[c] From resistivity measurements (midpoint); T_c = 30.9 K for sample annealed under reducing conditions.
References: 1, Rajagopal *et al.* (1993); 2, Schlögl *et al.* (1993).

2201 $(Bi_{0.90}Pb_{0.10})_2(Sr_{0.85}Bi_{0.06}Pb_{0.01})_2Cu_1O_6$

***A*$_2$*B*$_2$*DO*$_6$**, *tI*22, (139) *I*4/*mmm*–e^4cb
-*D*O_2–*OB*–*A*O–*OA*–*B*O-
$Bi_{1.924}Pb_{0.216}Sr_{1.700}CuO_6$,[a] T_c = 18 K, SX, T = 293 K, R_w = 0.053 (Torardi *et al.*, 1991)
(52) *Pnan* (*Pnna*), a = 5.2757, b = 5.3797, c = 24.558 Å, Z = 4
$\mathbf{a}_1 + \mathbf{a}_2$, $-\mathbf{a}_1 + \mathbf{a}_2$, **c**; origin shift 0 $\frac{1}{4}$ $\frac{1}{4}$

(*continued*)

Atom	WP	PS	x	y	z	Occ.
Bi[b]	8(e)	1	0.9829	0.2681	0.06311	
Sr[c]	8(e)	1	0.9604	0.7530	0.1772	0.92
Cu	4(d)	2..	0.4640	$\frac{3}{4}$	$\frac{1}{4}$	
O(1)	8(e)	1	0.9153	0.6643	0.0716	
O(2)	8(e)	1	0.4662	0.7667	0.1454	
O(3)	8(e)	1	0.7071	0.9998	0.2523	

[a] Cation content $Bi_{1.78}Pb_{0.20}Sr_{1.70}CuO_6$ from microprobe analysis.
[b] $Bi = Bi_{0.899}Pb_{0.101}$.
[c] $Sr = Sr_{0.9239}Bi_{0.0684}Pb_{0.0077}$.

Compound	a (Å)	b (Å)	c (Å)	T_c (K)	Ref.
$BiPbBaLaCuO_6$	5.4028	5.4745	24.515[a]	n.s.	1
$Bi_{1.924}Pb_{0.216}Sr_{1.700}CuO_6$[b]	5.2757	5.3797	24.558	18	2
$Bi_{1.8}Pb_{0.2}Sr_{1.8}La_{0.2}CuO_{6.36}$	5.396	5.374	24.374	21	3

[a] Space group *Fmmm*.
[b] Cation content $Bi_{1.78}Pb_{0.20}Sr_{1.70}CuO_6$ from microprobe analysis.
References: 1, Pham *et al.* (1993); 2, Torardi *et al.* (1991); 3, Rajagopal *et al.* (1993).

Superconductivity in the Tl–Ba–Cu–O system was first reported by Kondoh *et al.* (1988) and Sheng and Hermann (1988a). Tl-**2201** crystallizes with two structural modifications, one tetragonal and the other orthorhombic, and is superconducting with T_c up to 90 K for an optimal oxygen content. The first structural refinement on tetragonal $Tl_2Ba_2CuO_6$ (*I*4/*mmm*) was reported with the Tl site on the 4-fold rotation axis (Torardi *et al.*, 1988a). In more recent articles the Tl site was found to be displaced [16(n) 0.0406 0 0.29696 (Liu *et al.*, 1992b), 32(o) 0.039 0.017 0.29735 (Opagiste *et al.*, 1993a)], and a partial substitution up to 7 at.% Tl by Cu was detected. The presence of an extra O site (8(g) 0 $\frac{1}{2}$ 0.267) with an occupancy ranging from 0.005 (T_c = 73 K) to 0.028 (nonsuperconducting), located between the *additional* TlO layers, was suggested by Shimakawa *et al.* (1990). Orthorhombic Tl-**2201** (a = 5.4451, b = 5.4961, c = 23.153 Å, nonsuperconducting) was first reported by Huang *et al.* (1988), who proposed space group *Fmmm*. The crystal structure was also refined in subgroups of *Fmmm*, in order to take into account distortions in the *additional* layers [*A*2*aa* (Hewat *et al.*, 1988); *Abma* (Parise *et al.*, 1988; Ström *et al.*, 1994)]. Note that in the latter refinements no O site between the TlO layers was considered. It is generally agreed that the tetragonal structure is favored for Tl-deficient compositions, whereas the orthorhombic structure is formed for higher Tl contents (Shimakawa, 1993) (Fig. 8.36). To a minor extent, the transition from the tetragonal to the orthorhombic modification also depends on the oxygen content, a high oxygen content favoring the orthorhombic structure (Jorda *et al.*, 1993; Ström *et al.*, 1994). Stoichiometric compounds (with respect to the Tl content) could be obtained by high-pressure synthesis for both structural modifications (Opagiste *et al.*, 1993b; Jorda *et al.*, 1994).

Fig. 8.36.

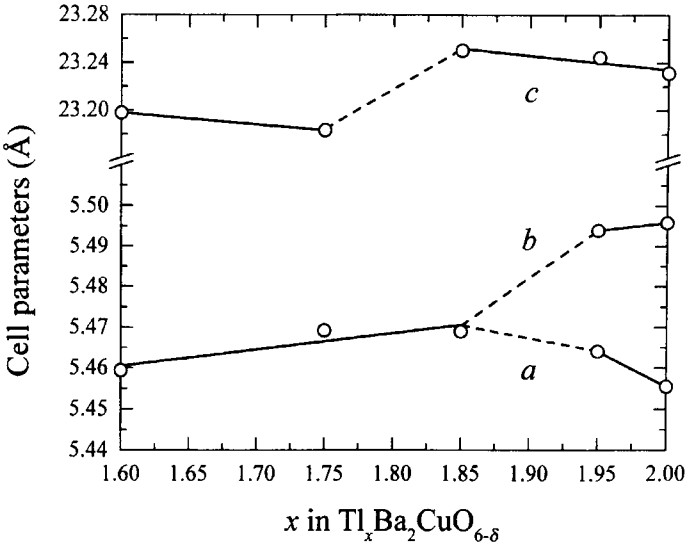

Cell parameters vs Tl content for $Tl_xBa_2CuO_{6-\delta}$ (nominal composition; $T_c = 76$ K for $x = 1.85$ and 1.95, $T_c = 60$ K for $x = 2.00$; for the tetragonal modification $\sqrt{2}a$ is plotted) (Ström *et al.*, 1994).

The Bi–Sr–Cu–O system contains two distinct phases with the approximate composition $Bi_{2+x}Sr_{2-x}CuO_{6+\delta}$. The structure of the semiconducting compound $Bi_2Sr_2CuO_6$ was found to be monoclinic (Roth *et al.*, 1990) and was refined in space group $C2/m$ ($a = 24.451$, $b = 5.425$, $c = 21.954$ Å, $\beta = 105.41°$) (Darriet *et al.*, 1993). It contains stepped CuO_2 layers, the monoclinic angle resulting from a periodic crystallographic shear. The structure of the superconducting, nonstoichiometric, Bi-rich compound contains infinite CuO_2 layers. Superconductivity in the Bi–Sr–Cu–O system ($T_c = 22$ K) was first reported for a sample of nominal composition $Bi_2Sr_2Cu_2O_{7+\delta}$ (Michel *et al.*, 1987). An orthorhombic subcell ($a = 26.6$, $b = 5.32$, $c = 48.8$ Å) was found and a giant supercell was proposed. Later on, a pseudotetragonal cell ($a = b = 5.38$, $c = 24.6$ Å) was reported for the composition $BiSrCuO_y$ ($T_c = 8$ K) (Akimitsu *et al.*, 1987), but the authors suggested a monoclinic superstructure with a 5-fold periodicity along [1 0 2]. The compound was identified as $Bi_2Sr_2CuO_6$ with some Sr deficiency and the structure was refined in space group $I4/mmm$ (Torrance *et al.*, 1988). Von Schnering *et al.* (1988) chose space group *Amaa* and obtained composition $Bi_2Sr_2CuO_{6.4}$. The Bi site was found to be displaced from the ideal position and two O sites (one partly occupied) were found in the *additional* layers. Torardi *et al.* (1988a) considered only one O site in the BiO layers, but detected a slight monoclinic distortion and a large supercell was proposed. Similar results were obtained by Rajagopal *et al.* (1993); however, they preferred the noncentrosym-

metric space group $A2aa$, also used for the structural refinement on Ca-containing Bi-**2201** (Imai *et al.*, 1988). A refinement in the monoclinic space group $A2$ ($a = 26.908$, $b = 5.380$, $c = 26.856$ Å, $\beta = 113.55°$) gave the composition $Bi_{10}Sr_{10}Cu_5O_{29}$, because of oxygen vacancies in the *additional* layers (Onoda and Sato, 1988). The same authors also reported Sr deficiency, based on microprobe analysis. Zandbergen *et al.* (1988a, 1990b) explained the modulation in the structures of Bi-based superconducting cuprates by the difference between the translation periods of the BiO and CuO_2 layers, which is reduced by cooperative displacements of the atoms from the ideal positions and by the incorporation of extra oxygen atoms into the former layers. A refinement of the incommensurate structure in superspace group $P^{A2/a}_{-1\ 1}$ ($a = 5.3791$, $b = 5.3811$, $c = 24.589$ Å, $\beta = 89.93°$, $\mathbf{q} = 0.2030\mathbf{a}^* + 0.467\mathbf{c}^*$) was carried out by Leligny *et al.* (1992). Beskrovnyi *et al.* (1994) used space group $A2/a$ to refine the average structure, the 5-fold superstructure being described in $A2$.

Studies on the substitution of Sr by La in $Bi_2Sr_{2-x}La_xCuO_{6+\delta}$ showed that single-phase samples can be prepared for $0.3 < x \leq 1$ (Schlögl *et al.*, 1993) ($0.2 \leq x \leq 0.8$; Khasanova and Antipov, 1995). An increase of the La content causes a reduction of the c-parameter, accompanied by an expansion of the two short cell parameters (Fig. 8.37), the structure remaining incommensurately modulated. The oxygen content increases linearly with x ($\delta = 0.5$ for $x = 1$), but the superconducting properties are suppressed at $x > 0.7$ (Schlögl *et al.*,

Fig. 8.37.

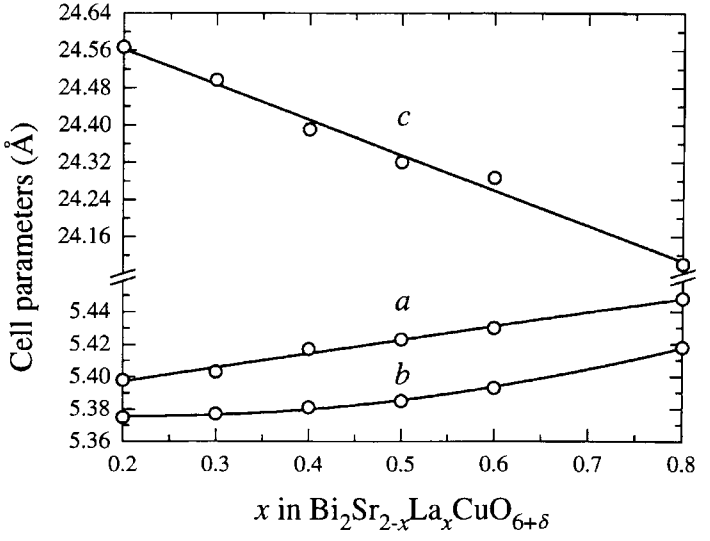

Cell parameters vs La content for $Bi_2Sr_{2-x}La_xCuO_{6+\delta}$ ($0.25 \leq \delta \leq 0.42$) (Khasanova and Antipov, 1995).

Fig. 8.38.

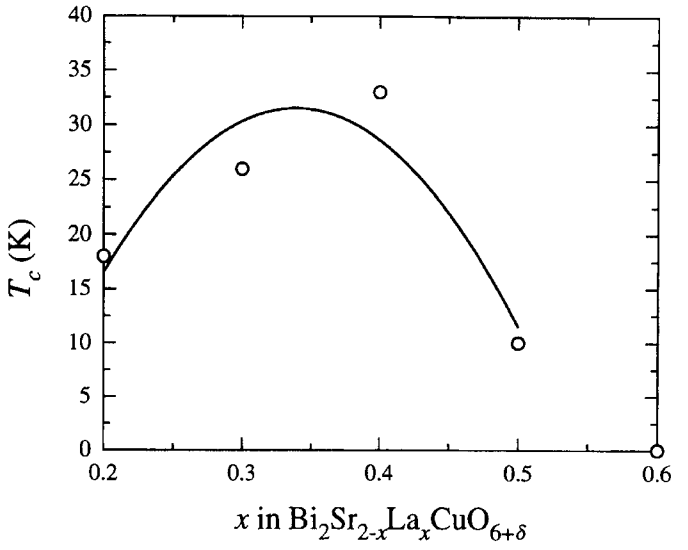

Superconducting transition temperature (from resistivity measurements, onset) vs La content for $Bi_2Sr_{2-x}La_xCuO_{6+\delta}$ ($0.25 \leq \delta \leq 0.42$) (Khasanova and Antipov, 1995).

1993) [$x \geq 0.6$ (Khasanova and Antipov, 1995), Fig. 8.38], the critical temperature having passed through a maximum at $x = 0.4$.

Partial substitution of Bi by Pb in $Bi_{2-x}Pb_xSr_2CuO_6$ can reach $x = 0.25$ (Torardi *et al.*, 1991). The crystal structure of this and other (Bi,Pb)-**2201** compounds is primitive orthorhombic (*Pnan*) and, contrary to the structures of the Pb-free Bi-**2201** compounds, does not show any modulation. Superconducting $Bi_{2-x}Pb_xSr_{2-y}La_yCuO_6$ compounds with $y \leq 0.8$ were identified in the region $x \approx y + 0.2$ (Tarascon *et al.*, 1990).

2212 $Cu_2Ba_2Y_1Cu_2O_8$

$A_2B_2DC_2O_8$, *oS*30, (65) *Ammm–j^2i^5d*
-DO_2–·–C–DO_2–OB–AO'–O'A–BO-
$Ba_2YCu_4O_8$, $T_c = 80$ K, PN, $T = 293$ K, $R_B = 0.080$
(Fischer *et al.*, 1989)
(65) *Ammm* (*Cmmm*), $a = 3.8411$, $b = 3.8718$,
$c = 27.240$ Å, $Z = 2$ Fig. 23

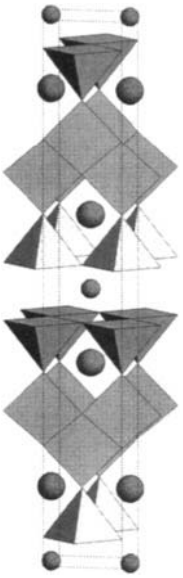

Atom[a]	WP	PS	x	y	z	Occ.
Cu(1)	4(*i*)	*mm*2	0	0	0.2873	
Ba	4(*j*)	*mm*2	$\frac{1}{2}$	$\frac{1}{2}$	0.3644	
Cu(2)	4(*i*)	*mm*2	0	0	0.4386	
Y	2(*d*)	*mmm*	$\frac{1}{2}$	$\frac{1}{2}$	$\frac{1}{2}$	
O(1)[b]	4(*i*)	*mm*2	0	$\frac{1}{2}$	0.2813	
O(2)	4(*i*)	*mm*2	0	0	0.3546	
O(3)	4(*j*)	*mm*2	$\frac{1}{2}$	0	0.4476	
O(4)	4(*i*)	*mm*2	0	$\frac{1}{2}$	0.4472	

[a] O site with occupancy 0.032 (4(*j*) $\frac{1}{2}$ 0 0.246) ignored here.
[b] Full occupation confirmed.

(*continued*)

Compound	a (Å)	b (Å)	c (Å)	T_c (K)	Ref.
$Ba_2NdCu_4O_8$[a]	...	...	27.3	57	1
$Ba_2SmCu_4O_8$[a]	3.872	3.886	27.308	69.3	1
$Ba_2EuCu_4O_8$[a]	3.8650	3.8837	27.279	68.9	1
$Ba_2GdCu_4O_8$[a]	3.863	3.881	27.259	73.4	1
$Ba_2DyCu_4O_8$	3.8463	3.8726	27.237	78	2
$Ba_2HoCu_4O_8$	3.8411	3.8694	27.231	80[b]	3
$Ba_2ErCu_4O_8$	3.8357	3.8668	27.221	83[b]	3
$Ba_2TmCu_4O_8$	3.8305	3.8645	27.212	82[b]	3
$Ba_2YbCu_4O_8$	3.8213	3.859	27.109	79[c]	4
$Ba_2YCu_4O_8$	3.8411	3.8718	27.240	80	5
$Ba_2Y_{0.9}Ca_{0.1}Cu_4O_8$[a]	3.841	3.864	27.21	91	6
$Ba_2Y_{0.6}Pr_{0.4}Cu_4O_8$	3.8614	3.8807	27.260	65[d]	7

[a] Nominal composition.
[b] From resistivity measurements (midpoint).
[c] Value taken from figure.
[d] From resistivity measurements; value taken from figure.
References: 1, Morris *et al.* (1989); 2, Hazen *et al.* (1989); 3, Mori *et al.* (1994); 4, Hijar *et al.* (1995); 5, Fischer *et al.* (1989); 6, Miyatake *et al.* (1989); 7, Berastegui *et al.* (1992).

2212 $Tl_2Ba_2Ca_1Cu_2O_8$

$A_2B_2CD_2O_8$, *tI*30, (139) *I4/mmm–ge*^{5}*a*
-DO$_2$*–C–DO*$_2$*–OB–AO–OA–BO-*
$Tl_2Ba_2CaCu_2O_8$, $T_c = 110$ K, SX, RT, $R_w = 0.018$
(Subramanian *et al.*, 1988a)
(139) *I4/mmm* $a = 3.8550$, $c = 29.318$ Å, $Z = 2$ Fig. 24

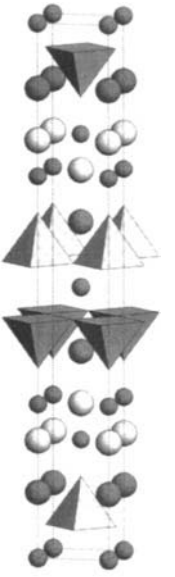

(continued)

Atom	WP	PS	x	y	z	Occ.
Tl	4(*e*)	4*mm*	0	0	0.28641	
Ba	4(*e*)	4*mm*	$\frac{1}{2}$	$\frac{1}{2}$	0.37821	
Cu	4(*e*)	4*mm*	0	0	0.4460	
Ca	2(*a*)	4/*mmm*	$\frac{1}{2}$	$\frac{1}{2}$	$\frac{1}{2}$	
O(1)	16(*n*)	.*m*.	0.396	$\frac{1}{2}$	0.2815	0.25
O(2)	4(*e*)	4*mm*	0	0	0.3539	
O(3)	8(*g*)	2*mm*.	0	$\frac{1}{2}$	0.4469	

Compound	a (Å)	c (Å)	T_c (K)	Ref.
$Tl_2Ba_2CaCu_2O_8$	3.8550	29.318	110	1
$Hg_{1.5}Ba_2Pr_{1.3}Cu_{2.2}O_{8-\delta}$	3.9236	28.993	n.s.	2
$Hg_2Ba_2YCu_2O_{7.55}$[a]	3.8606	28.915	n.s.	3
$Hg_2Ba_2Y_{0.5}Ca_{0.5}Cu_2O_{8-\delta}$[b]	...	...	45	3
$Hg_{1.4}Tl_{0.6}Ba_2Y_{0.6}Ca_{0.4}Cu_2O_{7.78}$[c]	3.86[d]	29.05[d]	84	4

[a] Prepared at 1.8 GPa.
[b] Prepared at 1.8 GPa; nominal composition,
[c] Prepared at 5 GPa; nominal composition, oxygen content from chemical analysis.
[d] Value taken from figure.
References: 1, Subramanian *et al.* (1988a); 2, Martin *et al.* (1995); 3, Radaelli *et al.* (1994b); 4, Tokiwa-Yamamoto *et al.* (1996).

2212 $(Pb_{0.50}Cu_{0.50})_2(Ba_{0.50}Sr_{0.50})_2(Y_{0.80}Ca_{0.20})_1Cu_2O_7$

***A*$_2$*B*$_2$*CD*$_2$**O**$_{6+\delta}$, *tI*26, (139) *I*4/*mmm*-*ge*^{4}(*e*)*a*
-DO_2-·-*C*-DO_2-*OB*-*A*·(*AO*)-·-*A*(*OA*)-*BO*-
PbBaSrY$_{0.8}$Ca$_{0.2}$Cu$_3$O$_7$, T_c = 39 K,[a] PN, RT, R_B = 0.0645
(Ishigaki *et al.*, 1994)
(107) *I*4*mm*, a = 3.83673, c = 27.5098 Å, Z = 2 Fig. 25
a$_1$, **a**$_2$, **c**

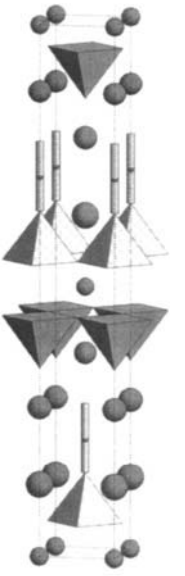

(*continued*)

Atom	WP	PS	x	y	z	Occ.
Pb	2(*a*)	4*mm*	0	0	0.2804	
Sr[b]	2(*a*)	4*mm*	$\frac{1}{2}$	$\frac{1}{2}$	0.3751	
Cu(1)	2(*a*)	4*mm*	0	0	0.4423	
Y[c]	2(*a*)	4*mm*	$\frac{1}{2}$	$\frac{1}{2}$	0.5	
Cu(2)	2(*a*)	4*mm*	0	0	0.5626	
Ba[d]	2(*a*)	4*mm*	$\frac{1}{2}$	$\frac{1}{2}$	0.6340	
Cu(3)	2(*a*)	4*mm*	0	0	0.7154	
O(1)	8(*d*)	.*m*.	0.382	$\frac{1}{2}$	0.2810	0.25
O(2)	2(*a*)	4*mm*	0	0	0.3537	
O(3)	4(*b*)	2*mm*.	0	$\frac{1}{2}$	0.4510	
O(4)	4(*b*)	2*mm*.	0	$\frac{1}{2}$	0.5564	
O(5)	2(*a*)	4*mm*	0	0	0.6501	

[a] From resistivity measurements.
[b] Sr = $Sr_{0.65}Ba_{0.35}$.
[c] Y = $Y_{0.8}Ca_{0.2}$.
[d] Ba = $Ba_{0.65}Sr_{0.35}$.

Compound	a (Å)	c (Å)	T_c (K)	Ref.
$PbBaSrY_{0.8}Ca_{0.2}Cu_3O_7$	3.83673	27.5098	39[a]	1
$PbBaSrY_{0.8}Ca_{0.2}Cu_3O_{8.35}$	3.84413	27.8036	n.s.	1

[a] From resistivity measurements.
Reference: 1, Ishigaki *et al.* (1994).

2212 $(Bi_{0.93})_2(Sr_{0.88}Bi_{0.04})_2(Ca_{0.96}Bi_{0.04})_1Cu_2O_8$

$A_2B_2CD_2O_8$, *tI*30, (139) *I*4/*mmm*–*ge*^{5}*a*
-*D*O_2–·*C*–*D*O_2–*OB*–*A*O–O*A*–*B*O-
$Bi_{1.98}Sr_{1.75}Ca_{0.96}Cu_2O_8$,[a] T_c = 92 K, PN,[b] R_B = 0.060 (Gao *et al.*, 1993; Petricek *et al.*, 1990)
(37) *A*2*aa* (*Ccc*2), a = 5.4150, b = 5.4149, c = 30.861 Å,[c] Z = 4
$\mathbf{a}_1 + \mathbf{a}_2$, $-\mathbf{a}_1 + \mathbf{a}_2$, $\mathbf{c}$; origin shift 0 $\frac{1}{4}$ $\frac{1}{4}$

Atom	WP	PS	x	y	z	Occ.
Bi	8(*d*)	1	0.004	0.2333	0.0523	0.93
Sr[d]	8(*d*)	1	0.5	0.2527	0.1408	0.915
Cu	8(*d*)	1	0.0	0.2502	0.1966	
Ca[e]	4(*c*)	2..	0.5	$\frac{1}{4}$	$\frac{1}{4}$	
O(1)	8(*d*)	1	0.53	0.151	0.0571	
O(2)	8(*d*)	1	0.01	0.277	0.1163	
O(3)	8(*d*)	1	0.25	0.5	0.1980	
O(4)	8(*d*)	1	0.25	0.0	0.1983	

[a] Composition $Bi_{2.08}Sr_{1.82}Ca_{0.80}Cu_2O_8$ from SX refinement; extra 0.14 O atoms per formula unit found from refinement in 4D superspace group $M^{A2aa}_{-1\,1\,1}$, $\mathbf{q} = 0.2095\mathbf{a}^*$ (located in the BiO layers).
[b] Coordinates from combined PN and SX refinement.
[c] Average structure, additional reflections indicate incommensurate modulation ($\mathbf{q} = \mathbf{a}^*/4.773$).
[d] Sr = $Sr_{0.956}Bi_{0.044}$.
[e] Ca = $Ca_{0.96}Bi_{0.04}$.

(continued)

Compound	a (Å)	b (Å)	c (Å)	T_c (K)	Ref.
$Bi_{1.98}Sr_{1.75}Ca_{0.96}Cu_2O_8$	5.4150	5.4149	30.861[a]	92	1
$Bi_{1.6}Pb_{0.4}Sr_2CaCu_2O_{8+\delta}$[b]	5.363[c]	5.404[c]	30.69[c,d]	95	2
$Bi_{1.97}Pb_{0.08}Sr_{1.83}Ca_{0.72}Er_{0.56}Cu_2O_{8+\delta}$[b]	5.44	5.44	30.360	82	3
$Bi_{1.79}Pb_{0.11}Sr_{1.78}Ca_{0.74}Yb_{0.44}Cu_2O_{8+\delta}$[b]	5.41	5.41	30.554	60	3
$Bi_2Sr_{1.5}Ca_{1.25}Y_{0.25}Cu_2O_{8.25}$[b]	5.405[c]	5.403[c]	30.48[c,e]	86[f]	4
$Bi_2Sr_2YCu_2O_{8.5}$[b]	5.428	5.465	30.175[g]	n.s.	5

[a] Additional reflections indicate incommensurate modulation ($\mathbf{q} = \mathbf{a}^*/4.773$).
[b] Nominal composition.
[c] Value taken from figure.
[d] Additional reflections indicate incommensurate modulation ($\mathbf{q} \approx \mathbf{a}^*/5.8$).
[e] Space group *Amaa*.
[f] From resistivity measurements (midpoint).
[g] Additional reflections indicate superstructure (8*a*, *b*, *c*).
References: 1, Gao *et al.* (1993); 2, Fukushima *et al.* (1989); 3, Ilyushin *et al.* (1993); 4, Manthiram and Goodenough (1988); 5, Tamegai *et al.* (1988).

2212 $(Bi_{0.60}Pb_{0.40})_2Sr_2(Y_{0.60}Ca_{0.40})_1Cu_2O_8$

$A_2B_2CD_2O_8$, *tI*30, (139) *I*4/*mmm*-*ge*[5]*a*
-*DO*$_2$–·*C*–*DO*$_2$–*OB*–*AO*–*OA*–*BO*-
$Bi_{1.2}Pb_{0.8}Sr_2Y_{0.6}Ca_{0.4}Cu_2O_8$, $T_c = 75$ K,[a] SX, $R = 0.065$ (Calestani *et al.*, 1992)
(52) *Pnan* (*Pnna*), $a = 5.374$, $b = 5.421$, $c = 30.397$ Å, $Z = 4$
$\mathbf{a}_1 + \mathbf{a}_2$, $-\mathbf{a}_1 + \mathbf{a}_2$, $\mathbf{c}$; origin shift 0 $\frac{1}{4}$ $\frac{1}{4}$

Atom	WP	PS	x	y	z	Occ.
Bi[b]	8(*e*)	1	−0.0100	0.2335	0.0492	
Sr	8(*e*)	1	0.4715	0.2508	0.1371	
Cu	8(*e*)	1	−0.0257	0.2502	0.1958	
Y[c]	4(*d*)	2..	0.4764	$\frac{1}{4}$	$\frac{1}{4}$	
O(1)	8(*e*)	1	0.616	0.152	0.053	
O(2)	8(*e*)	1	−0.042	0.275	0.117	
O(3)	8(*e*)	1	0.224	0.019	0.199	
O(4)	8(*e*)	1	0.228	0.484	0.202	

[a] T_c (from resistivity measurements, value taken from figure) given for $Bi_{1.2}Pb_{0.8}Sr_2Y_{0.4}Ca_{0.6}Cu_2O_8$ (nominal composition).
[b] Bi = $Bi_{0.6}Pb_{0.4}$.
[c] Y = $Y_{0.6}Ca_{0.4}$.

Compound	a (Å)	b (Å)	c (Å)	T_c (K)	Ref.
$Bi_{1.2}Pb_{0.8}Sr_2YCu_2O_8$	5.388	5.423	30.367	n.s.	1
$Bi_{1.2}Pb_{0.8}Sr_2Y_{0.4}Ca_{0.6}Cu_2O_8$[a]	5.362[b]	5.412[b]	30.50[b]	75[b,c]	1

[a] Nominal composition.
[b] Value taken from figure.
[c] From resistivity measurements.
Reference: 1, Calestani *et al.* (1992).

$Ba_2YCu_4O_8$ (Cu-**2212**) was first considered as planar defects in $Ba_2YCu_3O_{7-\delta}$ and structural models (space group *Ammm*) based on the insertion

of an extra AO' (CuO) layer into the structure of Cu-**1212** were proposed (Zandbergen *et al.*, 1988b,c; Marshall *et al.*, 1988). The first refinement was carried out on diffraction data from a superconducting film ($T_c = 80$ K) (Marsh *et al.*, 1988). Bulk synthesis of $Ba_2RCu_4O_8$ compounds were reported for R = Y (Karpinski *et al.*, 1988b) and R = Y, Nd, Sm–Gd, Dy–Tm (Morris *et al.*, 1989). Subsequent structural refinements (Hazen *et al.*, 1989; Fischer *et al.*, 1989) confirmed the structure proposed by Marsh *et al.* (1988). In contrast to the Cu-**1212** compounds, Cu-**2212** compounds do not display a variable oxygen content. A significant enhancement of the superconducting transition temperature was observed at high pressure ($T_c = 108$ K at 12 GPa) (Van Eenige *et al.*, 1990).

Superconductivity in the Tl–Ba–Ca–Cu–O system was first reported by Sheng and Hermann (1988b). A Tl-**2212** compound, $Tl_2Ba_2CaCu_2O_{8+\delta}$, was identified by Hazen *et al.* (1988a), and its structure was refined by Subramanian *et al.* (1988a). In the majority of the structural studies reported up to now, the Ca site was found to be occupied by mixture of Ca and Tl (12–28 at.% Tl), whereas the reduced scattering of the Tl site was attributed to either a partial substitution of Tl by Ca (10–11 at.%) (Maignan *et al.*, 1988; Kikuchi *et al.*, 1989; Johansson *et al.*, 1994) or Cu (9 at.%) (Onoda *et al.*, 1988); or simply to vacancies (occupancy 0.87–0.94) (Morosin *et al.*, 1991a; Ogborne *et al.*, 1992b; Molchanov *et al.*, 1994). Vacancies on the O site in the *additional* layers were detected by Ogborne *et al.* (1992b) and Johansson *et al.* (1994) (occupancy 0.94–0.95 or 0.84–0.88), whereas a displacement of the Tl site from the ideal position (32(*o*) 0.013 0.041 0.28635) was considered by Molchanov *et al.* (1994).

A (Pb,Cu)-**2212** compound was first reported for the composition $PbBaYSrCu_3O_8$ (Rouillon *et al.*, 1989). Ca-free, reduced ($PbSrBaYCu_3O_7$) and oxidized ($PbSrBaYCu_3O_{8.2}$) compounds were also prepared, and structural models were proposed (Tokiwa *et al.*, 1989). Superconductivity was observed for reduced, Ca-containing $PbSrBaY_{0.7}Ca_{0.3}Cu_3O_7$ ($T_c = 55$ K) (Tokiwa *et al.*, 1990a). The first structural refinement, carried out on the reduced, Ca-free compound (Rouillon *et al.*, 1992a), was later confirmed by a refinement on a Ca-containing compound (Ishigaki *et al.*, 1994). In the latter article, the structure of oxidized $PbSrBaY_{0.8}Ca_{0.2}Cu_3O_{8.35}$ was also reported. An ordered arrangement of PbO and Cu layers was observed for the reduced compounds, whereas a close to statistical occupation of the cation sites in the *additional* layers (45 at.% Pb and 55 at.% Cu, and vice versa) and four partly occupied O sites were found for the oxidized compound.

Superconductivity in the Bi–Sr–Ca–Cu–O system was first reported for a sample of composition $BiSrCaCu_2O_y$, which contained two superconducting phases ($T_c = 75$ and 105 K) (Maeda *et al.*, 1988). Studies on a sample of composition $BiSrCaCuO_{7-\delta}$ gave similar results (Chu *et al.*, 1988). The superconducting compound with the lower critical temperature was identified as Bi-**2212** (Tarascon *et al.*, 1988), and an orthorhombic subcell ($a = 5.439$, $b = 5.410$, $c = 30.78$ Å) and a 5-fold superstructure (5*a*, *b*, *c*) were proposed (Hazen *et al.*, 1988b). The first refinements were carried out in space group

I4/mmm ($a = 3.814$, $c = 30.52$ Å) (Tarascon *et al.*, 1988; Torrance *et al.*, 1988), *Fmmm* (Sunshine *et al.*, 1988; Kajitani *et al.*, 1988; Bordet *et al.*, 1988a) or *Amma* (Subramanian *et al.*, 1988c,d; von Schnering *et al.*, 1988; Imai *et al.*, 1988), the structure showing an incommensurate modulation in the direction [1 0 0] of the orthorhombic cell ([1 1 0] for the tetragonal cell) with a translation period of approximately 5 times *a*. The main differences between the proposed structures concern the positions of the oxygen atoms in the *additional* layers, the earliest models containing oxygen atoms between Bi layers, based on the similarity with the Aurivillius phases, known since 1950 (Aurivillius, 1950). In the model described in the noncentrosymmetric space group *A2aa* by Bordet *et al.* (1988b), the oxygen atoms were significantly displaced from the ideal position in order to approach Bi–O distances of ~2.2 Å.

Partial substitution of Ca site by Bi was reported by Sunshine *et al.* (1988) and Imai *et al.* (1988) (20 and 6 at.%, respectively), whereas a considerable homogeneity range with respect to the Sr/Ca ratio has been mentioned in almost all articles. The translation period of the modulation vector, expressed as a multiple of the *a*-parameter of the orthorhombic cell, was shown to be approximately constant within the Sr–Ca homogeneity range (Niu *et al.*, 1989). The same translation period progressively decreased to ~4, when Ca was substituted by a trivalent rare-earth element, the orthorhombicity (b/a) being increased at the same time (from $x = 0.5$ for $Bi_2Sr_2Ca_{1-x}Y_xCu_2O_{8+\delta}$, Figs. 8.39 and 8.40).

Refinements of the incommensurate structure of Bi-**2212** were carried out in 4D superspace group $M^{Amaa}_{-1\,1\,1}$ by Gao *et al.* (1988) and Yamamoto *et al.* (1990),

Fig. 8.39.

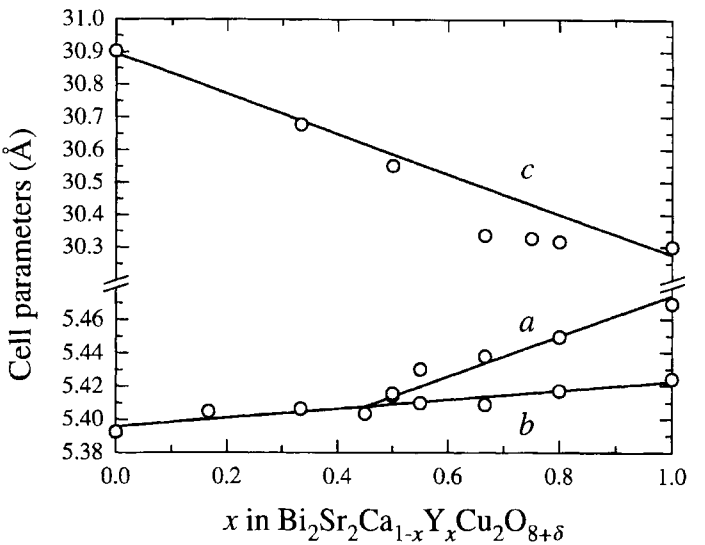

Cell parameters vs Y content for $Bi_2Sr_2Ca_{1-x}Y_xCu_2O_{8+\delta}$ (Niu *et al.*, 1989).

Fig. 8.40.

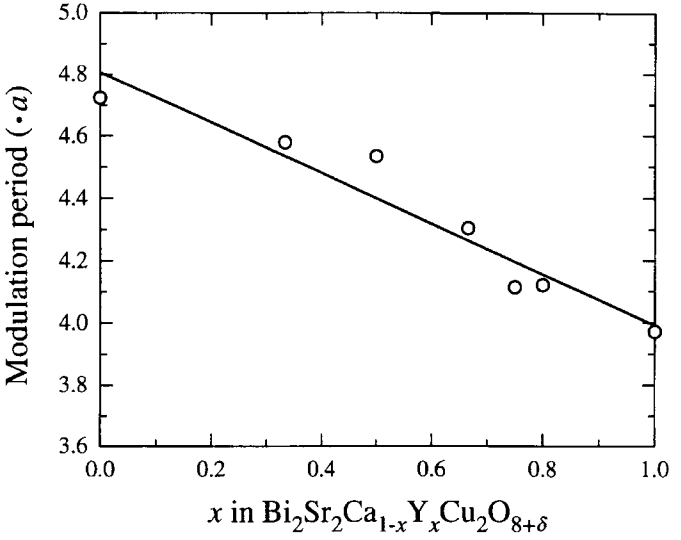

Translation period of the modulation vector vs Y content for $Bi_2Sr_2Ca_{1-x}Y_xCu_2O_{8+\delta}$ (Niu *et al.*, 1989).

whereas the noncentrosymmetric group $M^{A2aa}_{-1\,1\,1}$ was preferred in Petricek *et al.* (1990) and Gao *et al.* (1993). In the last two articles, a saw-shaped function was used to describe the displacements of the oxygen atoms in the *additional* layers and extra O atoms were found. Several refinements in supercells were performed, approximating the modulation period to an integer multiple of a. The apparently truly commensurate structure of the Fe-containing compound $Bi_{10}Sr_{15}Fe_{10}O_{46}$ was refined in a 5-fold supercell (*B*222, $a = 27.245$, $b = 5.4617$, $c = 31.696$ Å), considering one extra oxygen atom per formula unit in the BiO layers (LePage *et al.*, 1989). Calestani *et al.* (1989) and Levin *et al.* (1994) refined the structure of a cuprate in a primitive cell (*Pnnn*) of the same volume, whereas Beskrovnyi *et al.* (1990a,b) used a 19-fold supercell, approximating the translation period of the modulation vector to $4.75a$. In the last three articles, extra O sites and vacancies on some Sr sites were reported. A monoclinic variant of Bi-**2212** with a 9-fold supercell ($Bi_{2.09}Sr_{1.90}Ca_{1.00}Cu_2O_{8.22}$, *Cc*, $a = 37.754$, $b = 5.4109$, $c = 41.070$ Å, $\beta = 103.58°$) was refined by Gladyshevskii and Flükiger (1996), the monoclinic symmetry corresponding to a systematic shift of the modulation waves of consecutive *additional* layers by $\pi/9$.

Studies on the substitution of Bi by Pb showed that the periodicity of the structural modulation increases with increasing Pb content and becomes infinite (no modulation) for a high Pb content (Fukushima *et al.*, 1989). Modulation-free structures with the composition $Bi_{2-x}Pb_xSr_2Y_{1-y}Ca_yCu_2O_z$ were reported to exist

Fig. 8.41.

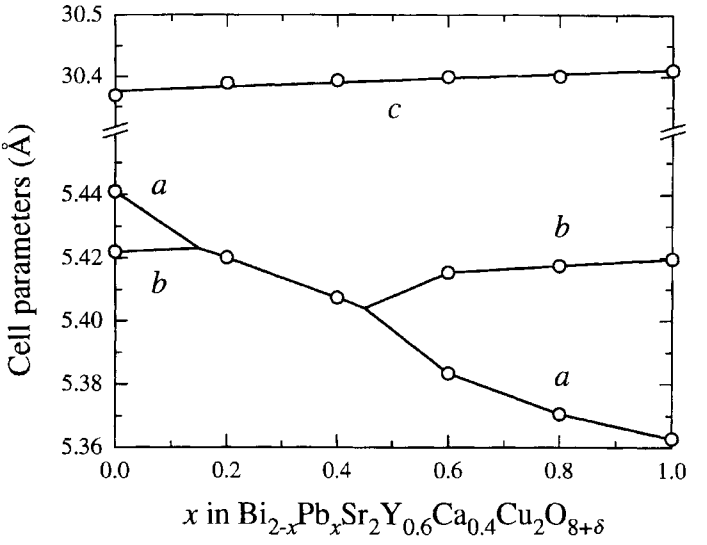

Cell parameters vs Pb content for $Bi_{2-x}Pb_xSr_2Y_{0.6}Ca_{0.4}Cu_2O_{8+\delta}$ (Calestani *et al.*, 1992).

in the region $x = (1 - y/2) \pm 0.2$ (for $0 \leq y \leq 0.8$) (Calestani *et al.*, 1992). The structures, refined in space group *Pnan*, revealed large orthorhombic distortions (Fig. 8.41) and an arrangement of the BiO ribbons different from that observed for Pb-free Bi-**2212**, the BiO chains in consecutive *additional* layers being here directly "superimposed," whereas in the structure of Pb-free Bi-**2212** they are mutually shifted by **a**/2.

2222 $Bi_2Sr_2(Gd_{0.85}Ce_{0.15})_2Cu_2O_{10}$

$A_2B_2C_2D_2O_{10}$, *tP*18, (129) *P4/nmm–fc*^{6}*b*
-O_2*D*–*C*–O_2–*C*–*DO*$_2$–*OB*–*AO*–*OA*–*BO*-
$Bi_2Sr_2Gd_{1.7}Ce_{0.3}Cu_2O_{10}$,[a] $T_c = 25$ K, PX, $R_B = 0.0780$
(Tokura *et al.*, 1989a)
(67) *Cmma*, $a = 5.4445$, $b = 5.4573$, $c = 17.913$ Å,
$Z = 2$ Fig. 26
$\mathbf{a}_1 + \mathbf{a}_2$, $-\mathbf{a}_1 + \mathbf{a}_2$, **c**; origin shift $\frac{1}{4}\ \frac{1}{4}\ 0$

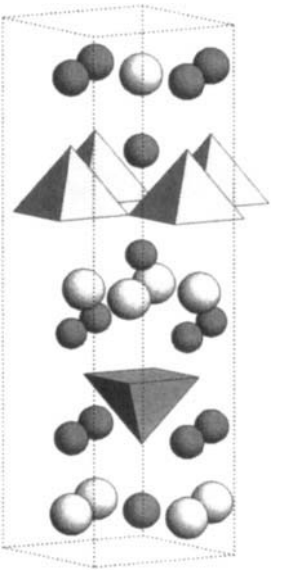

Atom	WP	PS	*x*	*y*	*z*	Occ.
Bi	4(*g*)	*mm*2	0	$\frac{1}{4}$	0.0854	
Sr	4(*g*)	*mm*2	$\frac{1}{2}$	$\frac{1}{4}$	0.234	
Cu	4(*g*)	*mm*2	0	$\frac{1}{4}$	0.336	
Gd[b]	4(*g*)	*mm*2	$\frac{1}{2}$	$\frac{1}{4}$	0.4311	
O(1)	4(*g*)	*mm*2	$\frac{1}{2}$	$\frac{1}{4}$	0.090	
O(2)	4(*g*)	*mm*2	0	$\frac{1}{4}$	0.212	
O(3)	8(*l*)	..2	$\frac{1}{4}$	0	0.341	
O(4)	4(*b*)	222	$\frac{1}{4}$	0	$\frac{1}{2}$	

[a] Oxygen content $Bi_2Sr_2Gd_{1.7}Ce_{0.3}Cu_2O_{10.24}$ from chemical analysis (extra oxygen atoms probably located in the BiO layers).
[b] Gd = $Gd_{0.85}Ce_{0.15}$.

Compound	*a* (Å)	*c* (Å)[a]	T_c (K)	Ref.
$Tl_2Ba_2Eu_{1.8}Ce_{0.2}Cu_2O_{10+\delta}$	3.888	17.281	n.s.	1
$Pb_{0.95}Ba_{0.77}Sr_{1.23}PrCeCu_3O_9$	[b]		n.s.	2
$Bi_2Sr_2Pr_{1.64}Ce_{0.36}Cu_2O_{10.27}$[c]	3.885	17.87	n.s.	3
$Bi_2Sr_2Nd_{1.64}Ce_{0.36}Cu_2O_{10.23}$[c]	3.881	17.93	14	3
$Bi_2Sr_2Sm_{1.64}Ce_{0.36}Cu_2O_{10.24}$[c]	3.863	17.90	16	3
$Bi_2Sr_2Eu_{1.64}Ce_{0.36}Cu_2O_{10.26}$[c]	3.854	17.88	27	3
$Bi_{1.2}Pb_{0.8}Sr_2Eu_{1.8}Th_{0.2}Cu_2O_y$	[d]		15	4
$Bi_2Sr_2Gd_{1.64}Ce_{0.36}Cu_2O_{10.24}$[c]	3.851	17.88	34	3
$Bi_2Sr_2Tb_{1.64}Ce_{0.36}Cu_2O_{10.26}$[c]	3.847	17.83	n.s.	3
$Bi_2Sr_2Dy_{1.64}Ce_{0.36}Cu_2O_{10.26}$[c]	3.844	17.87	27	3
$Bi_2Sr_2Ho_{1.64}Ce_{0.36}Cu_2O_{10.22}$[c]	3.840	17.86	24	3
$Bi_2Sr_2Er_{1.64}Ce_{0.36}Cu_2O_{10.21}$[c]	3.837	17.84	n.s.[e]	3

(*continued*)

$Bi_2Sr_2Tm_{1.64}Ce_{0.36}Cu_2O_{10.20}$[c]	3.827	17.84	n.s.[e]	3
$Bi_2Sr_2Y_{1.64}Ce_{0.36}Cu_2O_{10.22}$[c]	3.836	17.85	20	3
$Hg_{1.5}Ba_2Pr_{2.3}Cu_{2.2}O_{10-\delta}$	3.9072	17.2192	n.s.	5

[a] Space group $P4/nmm$.
[b] Space group $Cmm2$, $a = 5.4703$, $b = 5.4816$, and $c = 16.4017$ Å.
[c] Nominal composition, oxygen content from chemical analysis.
[d] Orthorhombic; $a = 5.430$, $b = 5.466$, and $c = 18.00$ Å.
[e] Superconductivity not observed above 5 K.
References: 1, Tokura *et al.* (1989a); 2, Rouillon *et al.* (1992b); 3, Arima *et al.* (1990); 4, Sasakura and Yoshida (1996); 5, Huvé *et al.* (1995).

Bi and Tl-**2222** were first reported by Tokura *et al.* (1989a). $Tl_2Ba_2Eu_{1.8}Ce_{0.2}Cu_2O_{10+\delta}$ crystallizes with a tetragonal structure ($P4/nmm$) and is not superconducting. The average structure of $Bi_2Sr_2Gd_{1.7}Ce_{0.3}Cu_2O_{10+\delta}$ is the same; however, distortions similar to those described for Bi-**2212** lead to an orthorhombic structure. Extra oxygen atoms ($\delta = 0.24$) were postulated to reside in the BiO layers. A series of nonsuperconducting $PbBa_{0.7}Sr_{1.3}CeRCu_3O_9$ compounds $((Pb_{0.5}Cu_{0.5})_2(Ba_{0.35}Sr_{0.65})_2(Ce_{0.5}R_{0.5})_2Cu_2O_9$, R = Sm, Eu, Gd, Dy, Ho, Er and Tm) were reported by Tokiwa *et al.* (1990b). A structural refinement on $Pb_{0.95}Ba_{0.77}Sr_{1.23}PrCeCu_3O_9$ in space group $Cmm2$ showed an ordered arrangement of PbO and Cu layers (Rouillon *et al.*, 1992b).

2223 $(Tl_{0.85}Ca_{0.15})_2Ba_2(Ca_{0.88}Tl_{0.12})_2Cu_3O_{10}$

$A_2B_2C_2D_3O_{10}$, *tI*38, (139) $I4/mmm$-ge^6cb
$-DO_2-\cdot C-DO_2-\cdot C-DO_2-OB-AO-OA-BO-$
$Tl_{1.94}Ba_2Ca_{2.06}Cu_3O_{10}$, $T_c = 125$ K, SX, RT, $R_w = 0.074$
(Torardi *et al.*, 1988b)
(139) $I4/mmm$, $a = 3.8503$, $c = 35.88$ Å, $Z = 2$ Fig. 27

(*continued*)

Atom	WP	PS	x	y	z	Occ.
Tl[a]	4(*e*)	4*mm*	0	0	0.2799	
Ba	4(*e*)	4*mm*	$\frac{1}{2}$	$\frac{1}{2}$	0.3552	
Cu(1)	4(*e*)	4*mm*	0	0	0.4104	
Ca[b]	4(*e*)	4*mm*	$\frac{1}{2}$	$\frac{1}{2}$	0.4537	
Cu(2)	2(*b*)	4/*mmm*	0	0	$\frac{1}{2}$	
O(1)	4(*e*)	4*mm*	$\frac{1}{2}$	$\frac{1}{2}$	0.2719	
O(2)	4(*e*)	4*mm*	0	0	0.3412	
O(3)	8(*g*)	2*mm*.	0	$\frac{1}{2}$	0.4125	
O(4)	4(*c*)	*mmm*.	0	$\frac{1}{2}$	$\frac{1}{2}$	

[a] Tl = $Tl_{0.85}Ca_{0.15}$; site may be partly vacant.
[b] Ca = $Ca_{0.88}Tl_{0.12}$.

Compound	a (Å)	c (Å)	T_c (K)	Ref.
$Tl_{1.94}Ba_2Ca_{2.06}Cu_3O_{10}$	3.8503	35.88	125	1
$Hg_{1.4}Tl_{0.6}Ba_2Ca_2Cu_3O_y$[a]	3.840	35.69	45	2

[a] Prepared at 5 GPa; nominal composition.
References: 1, Torardi *et al.* (1988b); 2, Tatsuki *et al.* (1996).

2223 $(Bi_{0.86}Pb_{0.14})_2Sr_2Ca_2Cu_3O_{10.24}$

$A_2B_2C_2D_3O_{10}$, *tI*38, (139) *I*4/*mmm*–*ge*^{6}*cb*
-DO_2–·*C*–DO_2–·*C*–DO_2–*OB*–*A*O–O*A*–*B*O-
$Bi_{1.72}Pb_{0.28}Sr_2Ca_2Cu_3O_{10.24}$,[a] T_c = 110 K,[b] PN, RT, R_{wp} = 0.0643 (Miehe *et al.*, 1990)
(37) *A*2*aa* (*Ccc*2), a = 5.4029, b = 5.4154, c = 37.074 Å,[c] Z = 4
$\mathbf{a}_1 + \mathbf{a}_2$, $-\mathbf{a}_1 + \mathbf{a}_2$, $\mathbf{c}$; origin shift 0 $\frac{1}{4}$ $\frac{1}{4}$

Atom	WP	PS	x	y	z	Occ.
Bi[d,e]	8(*d*)	1	−0.036	0.233	0.0411	
Sr[e]	8(*d*)	1	0.490	0.255	0.1148	
Cu(1)	8(*d*)	1	0.000	0.246	0.1619	
Ca[e]	8(*d*)	1	0.468	0.257	0.2072	
Cu(2)[e]	4(*c*)	2..	0.000	$\frac{1}{4}$	$\frac{1}{4}$	
O(1)[e]	8(*d*)	1	0.425	0.139	0.0434	
O(2)[f]	8(*d*)	1	0.230	0.544	0.0372	0.12
O(3)	8(*d*)	1	0.047	0.253	0.0956	
O(4)	8(*d*)	1	0.274	0.498	0.1637	
O(5)	8(*d*)	1	0.252	−0.006	0.1650	
O(6)	8(*d*)	1	0.230	0.002	0.2486	

[a] Composition $Bi_{1.89}Pb_{0.31}Sr_{2.00}Ca_{1.91}Cu_{3.00}O_{10.25}$ from microprobe and chemical analysis.
[b] Value for $Bi_{1.84}Pb_{0.34}Sr_{1.91}Ca_{2.03}Cu_{3.06}O_y$ (nominal composition) taken from Koyama *et al.* (1988).
[c] Average structure, additional reflections indicate incommensurate modulation ($\mathbf{q} \approx \mathbf{a}^*/7.2$).
[d] Bi = $Bi_{0.86}Pb_{0.14}$.
[e] Refined occupancies: Bi, 0.96; Sr, 0.97; Ca, 1.11; Cu(2), 1.04; and O(1), 0.98.
[f] Extra O site located in the BiO layers.

(*continued*)

Compound	a (Å)	b (Å)	c (Å)	T_c (K)	Ref.
$Bi_{1.72}Pb_{0.28}Sr_2Ca_2Cu_3O_{10.24}$	5.4029	5.4154	37.074[a]	110[b]	1, 2
$Bi_{1.7}Pb_{0.3}Sr_{1.7}Ca_{2.3}Cu_3O_y$[c]	5.4146	5.4146	37.135	110	3
$Bi_{1.76}Pb_{0.24}Sr_2Ca_{1.6}Sb_{0.4}Cu_3O_{10}$	5.411	5.411	37.22[d]	111	4
$Bi_2PbSr_{1.7}Ba_{0.3}Ca_2Cu_3O_y$[e]	5.390[f]	5.420[f]	37.18[f]	109.6	5

[a] Additional reflections indicate incommensurate modulation ($\mathbf{q} \approx \mathbf{a}^*/7.2$).
[b] Value for $Bi_{1.84}Pb_{0.34}Sr_{1.91}Ca_{2.03}Cu_{3.06}O_y$ (nominal composition).
[c] Nominal composition.
[d] Space group *Amaa*; additional reflections indicate incommensurate modulations ($\mathbf{q} = \mathbf{a}^*/4.97$ and $\mathbf{a}^*/6.67$).
[e] Nominal composition, composition $Bi_{1.50}Pb_{0.52}Sr_{1.63}Ba_{0.29}Ca_{2.04}Cu_{3.00}O_y$ from ICP analysis.
[f] Value taken from figure.
References: 1, Miehe *et al.* (1990); 2, Koyama *et al.* (1988); 3, Sasry and West (1994); 4, Kijima and Gronsky (1992); 5, Kim *et al.* (1992).

Superconductivity in the Tl–Ba–Ca–Cu–O system was first reported by Sheng and Hermann (1988b). The Tl-**2223** compound was identified by Politis and Luo (1988) and Parkin *et al.* (1988a), and the first structural refinement indicated partial disorder of Tl and Ca (Torardi *et al.*, 1988b). The Ca site was also found to be partly occupied by thallium atoms (3–7 at.%) in Hervieu *et al.* (1998b), Morosin *et al.* (1991b), and Sinclair *et al.* (1994). Vacancies on the Tl site (occupancy 0.88–0.94) were considered in Hervieu *et al.* (1988b), Morosin *et al.* (1991b), and Ogborne *et al.* (1992a), whereas partial substitution of Tl by Cu (14 at.%) was reported by Sinclair *et al.* (1994). The O site in the *additional* layers was found to be displaced from the ideal position in Ogborne *et al.* (1992a) and Morosin *et al.* (1991b) (16(*n*) 0.6112 $\frac{1}{2}$ 0.2753, occupancy 0.234), whereas both the Tl and the O site in the *additional* layers were split in Sinclair *et al.* (1994) (Tl in 16(*m*) 0.0276 0.0276 0.27921 and O in 16(*m*) 0.5819 0.5819 0.2756, occupancy 0.215 and 0.25).

The compound with the superconducting transition temperature of 105 K (Maeda *et al.*, 1988) was identified as Bi-**2223** (Zandbergen *et al.*, 1988d; Takayama-Muromachi *et al.*, 1988b; Ikeda *et al.*, 1988a) and can be stabilized by Pb (Hetherington *et al.*, 1988; Endo *et al.*, 1988). A pseudotetragonal subcell ($a = b = 5.41$, $c = 37.09$ Å) and an incommensurate modulation with a translation period of $\sim 8.7a$ were reported for $Bi_{1.73}Pb_{0.35}Sr_{1.89}Ca_{1.86}Cu_3O_{9.91}$ (Ikeda *et al.*, 1988b). The orthorhombic space groups *Fmmm* (Hetherington *et al.*, 1988), *Amaa* (Kijima *et al.*, 1989; Carrilo-Cabrera and Göpel, 1989), and *A2aa* (Carrilo-Cabrera and Göpel, 1989; Miehe *et al.*, 1990) were used to describe the structure of (Bi,Pb)-**2223**. The structural refinement in Kijima *et al.* (1989) showed that Pb mainly substitutes for Bi, but also for Sr and Ca (*A*, *B*, and *C* site, respectively). An extra O site in the *additional* BiO layers, corresponding to the excess oxygen, was found by Miehe *et al.* (1990).

2234 $(Tl_{0.82})_2Ba_2Ca_3Cu_4O_{12}$

$A_2B_2C_3D_4O_{12}$, *tI*46, (139) $I4/mmm$-g^2e^7a
-DO_2-·-C-DO_2-·-C-DO_2-·-C-DO_2-OB-AO-OA-BO-
$Tl_{1.64}Ba_2Ca_3Cu_4O_{12}$, $T_c = 109$ K, PX, $R_B = 0.1396$
(Ogborne and Weller, 1992)
(139) $I4/mmm$, $a = 3.84877$, $c = 42.0494$ Å, $Z = 2$ Fig. 28

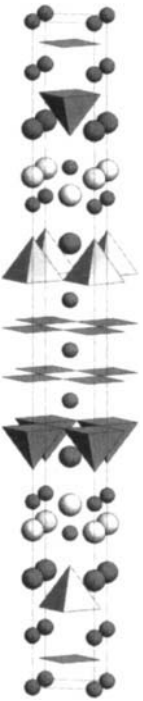

Atom	WP	PS	x	y	z	Occ.
Tl	4(*e*)	4*mm*0	0	0.2757	0.82	
Ba	4(*e*)	4*mm*	$\frac{1}{2}$	$\frac{1}{2}$	0.3387	
Cu(1)	4(*e*)	4*mm*	0	0	0.3866	
Ca(1)	4(*e*)	4*mm*	$\frac{1}{2}$	$\frac{1}{2}$	0.4236	
Cu(2)	4(*e*)	4*mm*	0	0	0.4636	
Ca(2)	2(*a*)	4/*mmm*	$\frac{1}{2}$	$\frac{1}{2}$	$\frac{1}{2}$	
O(1)	16(*n*)	.*m*.	0.394	$\frac{1}{2}$	0.2664	0.25
O(2)	4(*e*)	4*mm*	0	0	0.3234	
O(3)	8(*g*)	2*mm*.	0	$\frac{1}{2}$	0.3874	
O(4)	8(*g*)	2*mm*.	0	$\frac{1}{2}$	0.4626	

Compound	a (Å)	c (Å)	T_c (K)	Ref.
$Tl_{1.64}Ba_2Ca_3Cu_4O_{12}$	3.84877	42.0494	109	1
$Hg_{1.4}Tl_{0.6}Ba_2Ca_3Cu_4O_y$ [a]	3.845	42.06	114	2

[a] Prepared at 5 GPa; nominal composition.
References: 1, Ogborne and Weller (1992); 2, Tatsuki *et al.* (1996).

A superconducting Tl-**2234** compound ($T_c = 114$ K) was first reported by Hervieu *et al.* (1988a) for the composition $Tl_2Ba_2Ca_3Cu_4O_{12}$, and a structural model was proposed in space group $I4/mmm$ ($a = 3.852$, $c = 42.00$ Å). Partial disorder of Tl and Ca, corresponding to 40 at.% Ca on the Tl site and 10–15 at.% Tl on the Ca sites, was reported by Ogborne and Weller (1994b). The Tl and the O site in the *additional* layers were found to be partly vacant (occupancy 0.93–0.94 and 0.95–1.00), and the occupancy of the latter was found to depend on the annealing conditions. The superconducting transition temperature decreased to 106 K for the reduced compound.

3201 $(Pb_{0.67}Cu_{0.28})_3(Sr_{0.50}La_{0.50})_2Cu_1O_6$

$A_3B_2DO_6$, *tP*12, (123) $P4/mmm$-h^2g^2eda
-O_2D-*B*O-O*A*-*A*-O*A*-*B*O-
$Pb_2SrLaCu_{1.84}O_6$, $T_c = 33$ K, PN, $T = 292$ K,
$R_{wp} = 0.0631$ (Benschop *et al.*, 1994)
(53) *Pman* (*Pmna*), $a = 5.3380$, $b = 5.4293$,
$c = 12.6270$ Å, $Z = 2$ Fig. 29
$\mathbf{a}_1 + \mathbf{a}_2$, $-\mathbf{a}_1 + \mathbf{a}_2$, $\mathbf{c}$

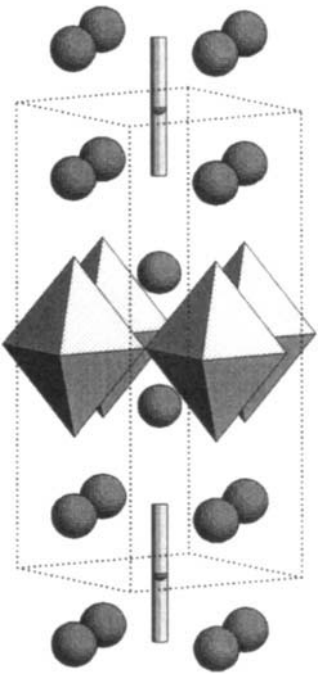

Atom	WP	PS	x	y	z	Occ.
Cu(1)	2(*a*)	2/*m*..	0	0	0	0.840
Pb	4(*h*)	*m*..	0	0.5	0.1381	
Sr[a]	4(*h*)	*m*..	0	−0.0095	0.3576	
Cu(2)	2(*c*)	2/*m*..	0	$\frac{1}{2}$	$\frac{1}{2}$	
O(1)	4(*h*)	*m*..	0	0.043	0.1475	
O(2)	4(*h*)	*m*..	0	0.5420	0.3065	
O(3)	4(*g*)	..2	$\frac{1}{4}$	$\frac{1}{4}$	0.5	

[a] $Sr = Sr_{0.5}La_{0.5}$.

A superconducting **3201** compound ($T_c = 31$ K) was first reported for $Pb_2Sr_{0.8}La_{1.2}Cu_2O_{6+\delta}$ and a structural model was proposed in space group $P22_12$ ($a = 5.333$, $b = 5.421$, $c = 12.609$ Å) (Zandbergen *et al.*, 1989). It was shown that with increasing oxygen content another compound is formed and that a miscibility gap exists between the reduced, superconducting compound ($\delta \approx 0$) and the oxidized, semiconducting compound ($\delta \approx 1.4$) (Zandbergen *et al.*, 1990a). The latter crystallizes with an orthorhombic subcell ($a = 5.421$, $b = 5.421$, $c = 12.652$ Å) and an incommensurate modulation along [0 1 0] with a translation period of $\sim 3.8b$. Extra oxygen atoms are located in the central *additional* (Cu) layer. The first structural refinement on the reduced compound ($Pb_2SrLaCu_2O_6$) was carried out in space group *Pman* ($a = 5.3119$, $b = 5.4140$, $c = 12.6292$ Å) (Benschop *et al.*, 1991). The proposed displacements of the oxygen atoms in the PbO layers result in four Pb–O contact distances. Space group *Pmmm* was adopted for the refinement of the average structure of oxidized $Pb_2SrLaCu_2O_{7.5}$ ($a = 3.8365$, $b = 3.8615$, $c = 12.672$ Å) and the incommensurate modulation with a translation period of 3.1–3.6 was confirmed in Benschop *et al.* (1994). The structure of a (Pb,Cu)-**3201** compound prepared by a polymerized complex method, was claimed to be tetragonal for $1.7 \leq \delta \leq 2$ (Kato *et al.*, 1995).

An iodine-intercalated (Bi,I)-**3201** compound, $(Bi_2I)Sr_2CuO_y$ ($a = 5.40$, $c = 15.76$ Å, $T_c = 22$ K), was reported by Xiang *et al.* (1991).

3212 $(Pb_{0.67}Cu_{0.33})_3Sr_2Y_1Cu_2O_8$

***A*$_3$*B*$_2$*CD*$_2$**O**$_8$**, *tP*16, (123) *P*4/*mmm*–*ih*^{3}*g*^{2}*ba*
-O$_2$*D*–*C*–•O$_2$*D*–*B*O–O*A*–*A*•–O*A*–*B*O-
$Pb_2Sr_2YCu_3O_8$, n.s., PN, RT, $R_B = 0.0624$ (Cava *et al.*, 1989)
(65) *Cmmm*, $a = 5.3933$, $b = 5.4311$, $c = 15.7334$, $Z = 2$ Fig. 30
$\mathbf{a}_1 + \mathbf{a}_2$, $-\mathbf{a}_1 + \mathbf{a}_2$, **c**

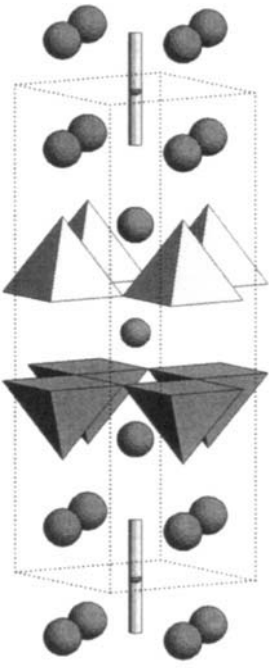

(*continued*)

Atom	WP	PS	x	y	z	Occ.
Cu(1)	2(*a*)	*mmm*	0	0	0	
Pb	4(*l*)	*mm*2	$\frac{1}{2}$	0	0.1117	
Sr	4(*k*)	*mm*2	0	0	0.2793	
Cu(2)	4(*l*)	*mm*2	$\frac{1}{2}$	0	0.3938	
Y	2(*d*)	*mmm*	0	0	$\frac{1}{2}$	
O(1)	16(*r*)	1	0.051	0.074	0.1151	0.25
O(2)	4(*l*)	*mm*2	$\frac{1}{2}$	0	0.2486	
O(3)	8(*m*)	..2	$\frac{1}{4}$	$\frac{1}{4}$	0.4082	

Compound	a (Å)	b (Å)	c (Å)	T_c (K)	Ref.
$Pb_2Sr_{2.24}Nd_{0.76}Cu_3O_8$	5.435	5.463	15.817	n.s.	1
$Pb_2Sr_2YCu_3O_8$	5.3933	5.4311	15.7334	n.s.	2
$Pb_2Sr_2YCu_3O_{9.47}$	3.838	3.870	15.845[a]	n.s.	3, 4
$Pb_2Sr_2Y_{0.73}Ca_{0.27}Cu_3O_{7.8}$	5.3835	5.4091	15.784[b]	67	5

[a] Space group *Pmmm*; additional reflections indicate superstructure (4*a*, 2*b*, *c*).
[b] Space group *Pman*.
References: 1, Cava *et al.* (1988); 2, Cava *et al.* (1989); 3, Marezio *et al.* (1990); 4, Marezio (1991); 5, Chaillout *et al.* (1991).

3212 $(Sn_{0.67}La_{0.24}Ba_{0.09})_3(Ba_{0.86}La_{0.14})_2La_1Cu_2O_{11}$

***A*$_3$*B*$_2$*CD*$_2$O$_{11}$**, *tP*19, (123) *P*4/*mmm*–i^2h^3gcba
-O_2D–*C*–·O_2D–*B*O–O_2A–*A*O–O_2A–*B*O-
$Sn_2La_2Ba_2Cu_2O_{11}$, n.s., PN, $R_B = 0.103$ (Anderson *et al.*, 1992)
(123) *P*4/*mmm*, $a = 3.9893$, $c = 16.232$ Å,[a] $Z = 1$
Fig. 31

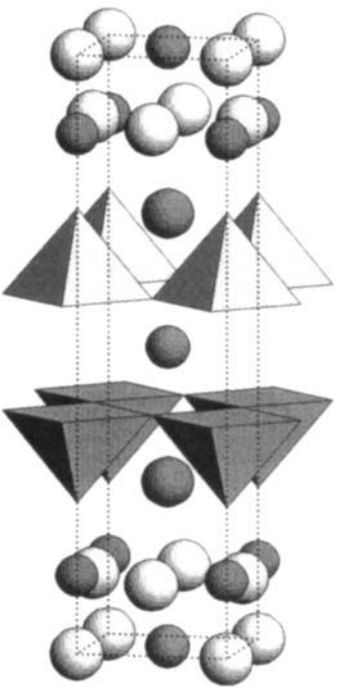

(*continued*)

Atom	WP	PS	x	y	z	Occ.
La(1)[b]	1(*a*)	4/*mmm*	0	0	0	
Sn	2(*h*)	4*mm*	$\frac{1}{2}$	$\frac{1}{2}$	0.1307	
Ba[c]	2(*g*)	4*mm*	0	0	0.2756	
Cu	2(*h*)	4*mm*	$\frac{1}{2}$	$\frac{1}{2}$	0.3903	
La(2)	1(*b*)	4/*mmm*	0	0	$\frac{1}{2}$	
O(1)	1(*c*)	4/*mmm*	$\frac{1}{2}$	$\frac{1}{2}$	0	
O(2)	8(*s*)	.*m*.	0	0.4106	0.1189	0.5
O(3)	2(*h*)	4*mm*	$\frac{1}{2}$	$\frac{1}{2}$	0.2534	
O(4)	8(*s*)	.*m*.	0	0.4830	0.4033	0.5

[a] Average structure, additional reflections indicate superstructure ($\sqrt{2}a$, $\sqrt{2}a$, 6*c*).
[b] La(1) = $La_{0.72}Ba_{0.28}$.
[c] Ba = $Ba_{0.86}La_{0.14}$.

Compound	a (Å)	c (Å)	T_c (K)	Ref.
$Ti_2Nd_2Ba_2Cu_2O_{11}$	3.90951	15.744	n.s.	1
$Ti_2Tb_2Ba_2Cu_2O_{11}$	3.8769	15.7322	n.s.	2
$Sn_2La_2Ba_2Cu_2O_{11}$	3.9893	16.232[a]	n.s.	3

[a] Additional reflections indicate superstructure ($\sqrt{2}a$, $\sqrt{2}a$, 6*c*).
[b] References: 1, Jennings and Greaves (1994); 2, Palacín *et al.* (1995); 3, Anderson *et al.* (1992).

The superconducting (Pb,Cu)-**3212** compound $Pb_2Sr_2Y_{0.5}Ca_{0.5}Cu_3O_8$ ($T_c = 68$ K) was reported by Cava *et al.* (1988), the structure being refined on nonsuperconducting $Pb_2Sr_{2.24}Nd_{0.76}Cu_3O_8$ in space group *Cmmm*. Subramanian *et al.* (1989) described the average structure of $Pb_2Sr_2Y_{0.75}Ca_{0.25}Cu_3O_8$ in space group *P*4/*mmm* ($a = 3.813$, $c = 15.76$ Å) with the O site in the PbO layers displaced from the ideal position (from 2(*g*) 0 0 0.11 into 8(*s*) 0.12 0 0.116). The structure of $Pb_2Sr_2YCu_3O_8$ was also refined in space group *Cmmm* (Cava *et al.*, 1989); however, weak reflections that violate the *C*-centering are observed for most compounds. Space group $P22_12$ was used by Fu *et al.* (1989) to refine the structure of the same compound, whereas other authors reported refinements in the monoclinic space group $P2_1/m$ (Fujishita *et al.*, 1990, 1993). In the structure of superconducting $Pb_2Sr_2Y_{0.73}Ca_{0.27}Cu_3O_{7.8}$, refined in space group *Pman*, the lead atoms are 4-fold coordinated by oxygen atoms (Chaillout *et al.*, 1991), whereas in the structure proposed by Cava *et al.* (1989) the lead atoms have three closest neighbors, forming ψ-tetrahedra. Like (Pb,Cu)-**3201**, $Pb_2Sr_2Y_{1-x}Ca_xCu_3O_{8+\delta}$ can be oxidized, and a miscibility gap was observed between $\delta = 0$ and 1. The average structure of oxidized, nonsuperconducting $Pb_2Sr_2YCu_3O_{9.47}$ was reported in space group *Pmmm* (Marezio *et al.*, 1990; Marezio, 1991), the proposed superstructure (4*a*, 2*b*, *c*) corresponding to an ordered arrangement of O sites in the *additional* layers. Superconductivity up to 70 K was reported for Ca-free samples of composition $Pb_2Sr_2RCu_3O_8$ (R = Y, Nd, Eu, Dy, Ho, Er, Yb, and Lu) prepared under appropriate conditions (Prasad *et al.*, 1990; Xue *et al.*, 1993).

A superconducting iodine-intercalated (Bi,I)-**3212** compound with T_c = 80 K (57 K in Koike *et al.*, 1993), $(Bi_2I)Sr_2CaCu_2O_y$ (a = 5.40, c = 19.02 Å), was reported by Xiang *et al.* (1991).

Besides Pb-based cuprates, nonsuperconducting compounds containing Sn or Ti and a rare-earth element in the *additional* layers have been reported to crystallize with a **3212** structure. For the structural refinement on $Ti_2Nd_2Ba_2Cu_2O_{11}$ partial disorder of Ti and Cu was considered (Jennings and Greaves, 1994), whereas for $Ti_2Tb_2Ba_2Cu_2O_{11}$ ($(Ti_2Tb)Ba_2TbCu_2O_{11}$) no disorder was detected (Palacín *et al.*, 1995).

3222 $(Pb_{0.67}Cu_{0.33})_3Sr_2(Ce_{0.50}Pr_{0.50})_2Cu_2O_{10}$

***A*$_3$*B*$_2$*C*$_2$*D*$_2$O$_{10}$**, *tI*38, (139) *I*4/*mmm*–*ge*^{6}*da*
-*D*O$_2$–·*C*–O$_2$–*C*·–O$_2$*D*–*B*O–O*A*–*A*·–O*A*–*B*O-
$Pb_2Sr_2CePrCu_3O_{10}$, n.s., PN, R_B = 0.081 (Rouillon *et al.*, 1993)
(69) *Fmmm*, a = 5.4512, b = 5.4799, c = 37.0107 Å, Z = 4
Fig. 32
$\mathbf{a}_1 + \mathbf{a}_2$, $-\mathbf{a}_1 + \mathbf{a}_2$, **c**

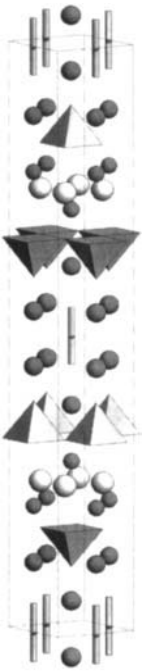

(*continued*)

Atom	WP	PS	x	y	z	Occ.
Cu(1)[a]	4(*a*)	*mmm*	0	0	0	
Pb[a]	8(*i*)	*mm*2	$\frac{1}{2}$	0	0.0475	
Sr[a]	8(*i*)	*mm*2	0	0	0.1184	
Cu(2)	8(*i*)	*mm*2	$\frac{1}{2}$	0	0.1665	
Ce[b]	8(*i*)	*mm*2	0	0	0.2146	
O(1)[c]	32(*p*)	1	0.0608	0.0693	0.0491	0.25
O(2)	8(*i*)	*mm*2	$\frac{1}{2}$	0	0.1050	
O(3)	16(*j*)	..2	$\frac{1}{4}$	$\frac{1}{4}$	0.1717	
O(4)	8(*f*)	222	$\frac{1}{4}$	$\frac{1}{4}$	$\frac{1}{4}$	

[a] Full occupation confirmed.
[b] Ce = $Ce_{0.50}Pr_{0.50}$.
[c] Full occupation confirmed (ignoring site splitting).

Compound	a (Å)	b (Å)	c (Å)	T_c (K)	Ref.
$Pb_2Sr_2CePrCu_3O_{10}$	5.4512	5.4799	37.0107	n.s.	1
$Pb_2Sr_2CeNdCu_3O_{10.2}$	5.442	5.462	36.90	n.s.	2
$Pb_2Sr_2Ce_{0.67}Sm_{1.33}Cu_3O_{9.8}$	5.4299	5.4583	36.93	n.s.	3
$Pb_2Sr_2Ce_{0.67}Eu_{1.33}Cu_3O_{10+\delta}$[a]	5.423	5.452	36.96	24[b]	3

[a] Nominal composition.
[b] Superconducting fraction < 3%.
References: 1, Rouillon *et al.* (1993); 2, Rouillon *et al.* (1990a); 3, Kharlanov *et al.* (1990).

3222 $(Ti_{0.67}Nd_{0.27}Ba_{0.06})_3(Ba_{0.92}Nd_{0.08})_2(Ce_{0.50}Nd_{0.50})_2Cu_2O_{13}$

$A_3B_2C_2D_2O_{13}$, *tI*44, (139) $I4/mmm$-g^2e^5dba
-DO_2–•C–O_2–C•–O_2D–BO–O_2A–AO–O_2A–BO-
$Ti_2Nd_2Ba_2CeCu_2O_{13}$, n.s., PN, RT, $R_B = 0.1129$
(Den *et al.*, 1995)
(139) $I4/mmm$, $a = 3.89978$, $c = 36.9624$ Å, $Z = 2$ Fig. 33

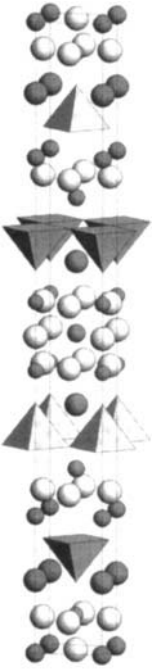

(*continued*)

Atom	WP	PS	x	y	z	Occ.
Nd[a]	2(*a*)	4/*mmm*	0	0	0	
Ti	4(*e*)	4*mm*	$\frac{1}{2}$	$\frac{1}{2}$	0.05459	
Ba[b]	4(*e*)	4*mm*	0	0	0.11362	
Cu	4(*e*)	4*mm*	$\frac{1}{2}$	$\frac{1}{2}$	0.16751	
Ce[c]	4(*e*)	4*mm*	0	0	0.21500	
O(1)	2(*b*)	4/*mmm*	$\frac{1}{2}$	$\frac{1}{2}$	0	
O(2)	8(*g*)	2*mm*.	0	$\frac{1}{2}$	0.04959	
O(3)	4(*e*)	4*mm*	$\frac{1}{2}$	$\frac{1}{2}$	0.10445	
O(4)	8(*g*)	2*mm*.	0	$\frac{1}{2}$	0.17293	
O(5)	4(*d*)	$\bar{4}m2$	0	$\frac{1}{2}$	$\frac{1}{4}$	

[a] $Nd = Nd_{0.83}Ba_{0.17}$.
[b] $Ba = Ba_{0.92}Nd_{0.08}$.
[c] $Ce = Ce_{0.5}Nd_{0.5}$.

Compound	a (Å)	c (Å)	T_c (K)	Ref.
$Ti_2Nd_2Ba_2CeCu_2O_{13}$	3.89978	36.9624	n.s.	1
$Ti_2Gd_2Ba_2CeCu_2O_{13}$	3.881	36.972	n.s.	2

References: 1, Den *et al.* (1995); 2, Li (1995).

(Pb,Cu)-**3222** compounds were first reported for the composition $Pb_2Sr_2CeRCu_3O_{10+\delta}$ ($(Pb_2Cu)Sr_2(Ce_{0.5}R_{0.5})_2Cu_2O_{10+\delta}$, R = La, Pr, Nd and Sm) (Rouillon *et al.*, 1990a). The crystal structure was refined on the Nd-containing compound in space group *Fmmm*. $Pb_2Sr_2Ce_{0.67}R_{1.33}Cu_3O_{10+\delta}$ compounds with R = La, Pr, Nd, Sm–Tm were reported by Kharlanov *et al.* (1990), who claimed superconductivity for the Eu-containing sample. Splitting of the Pb and O sites in the PbO layers was considered in the structural refinement carried out on the Sm-containing compound (Pb in 16(*n*) 0.547 0 0.0487 and O in 16(*m*) 0 0.15 0.052). Further splitting of the O site was proposed by Rouillon *et al.* (1993).

Superconductivity up to 12 K was observed for a bromine-intercalated (Bi,Br)-**3222** compound, $(Bi_2Br_{0.12})Sr_2Ce_{0.36}Gd_{1.64}Cu_2O_{10+\delta}$ (Koike *et al.*, 1994).

Like the Ti-based **3212** compounds, the **3222** compounds with Ti and rare-earth elements in the *additional* layers are nonsuperconducting.

4212 $(Ti_{0.50}Gd_{0.29}Ca_{0.21})_4Ba_2(Gd_{0.85}Ca_{0.15})_1Cu_2O_{12}$

$A_4B_2CD_2O_{12}$, $tI42$, (139) $I4/mmm$–g^2e^6b
-OD_2–·C–O_2D–BO–O_2A–AO–OA–AO_2–OB-
$Ti_2Gd_2Ba_2CaCu_2O_{12}$, n.s., PX, $R_B = 0.0885$ (Fukuoka *et al.*, 1994)
(139) $I4/mmm$, $a = 3.89385$, $c = 35.4859$ Å, $Z = 2$
Fig. 34

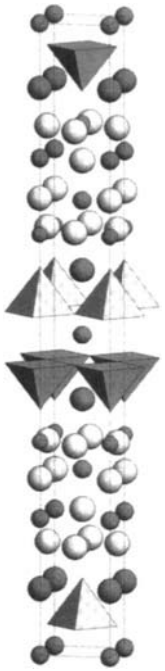

Atom[a]	WP	PS	x	y	z	Occ.
Gd(1)[b]	4(*e*)	4*mm*	0	0	0.2861	
Ti	4(*e*)	4*mm*	$\frac{1}{2}$	$\frac{1}{2}$	0.3350	
Ba	4(*e*)	4*mm*	0	0	0.3970	
Cu	4(*e*)	4*mm*	$\frac{1}{2}$	$\frac{1}{2}$	0.4526	
Gd(2)[c]	2(*b*)	4/*mmm*	0	0	$\frac{1}{2}$	
O(1)	4(*e*)	4*mm*	$\frac{1}{2}$	$\frac{1}{2}$	0.277	
O(2)	8(*g*)	2*mm*.	0	$\frac{1}{2}$	0.330	
O(3)	4(*e*)	4*mm*	$\frac{1}{2}$	$\frac{1}{2}$	0.386	
O(4)	8(*g*)	2*mm*.	0	$\frac{1}{2}$	0.459	

[a] O site reported with full occupation in Table 1, but not drawn in Fig. 1 and stated to be absent in the text (2(*a*) $\frac{1}{2}$ $\frac{1}{2}$ $\frac{1}{2}$), ignored here.
[b] Gd(1) = $Gd_{0.575}Ca_{0.425}$.
[c] Gd(2) = $Gd_{0.85}Ca_{0.15}$.

Compound	a (Å)	c (Å)	T_c (K)	Ref.
$Ti_2Sm_2Ba_2CaCu_2O_{12}$	3.8980	35.622	n.s.	1
$Ti_2Gd_2Ba_2CaCu_2O_{12}$	3.89385	35.4859	n.s.	2
$Mn_2Eu_3Ba_2Cu_2O_{12}$	3.8826	35.266	n.s.	3

References: 1, Zhu *et al.* (1995c); 2, Fukuoka *et al.* (1994); 3, Hervieu *et al.* (1995a).

4222 $(Ti_{0.50}Ca_{0.25}Nd_{0.20}Ba_{0.05})_4(Ba_{0.91}Nd_{0.09})_2(Ce_{0.50}Nd_{0.50})_2Cu_2O_{14}$

$A_4B_2C_2D_2O_{14}$, *tP*24, (129) *P*4/*nmm*–f^2c^7b
-DO_2–·*C*–O_2–*C*·–O_2*D*–*B*O–O_2*A*–*A*O–O*A*–AO_2–O*B*-
$Ti_2Nd_2CaBa_2CeCu_2O_{14}$, n.s., PN, RT, $R_B = 0.0966$
(Den *et al.*, 1995)
(129) *P*4/*nmm* (origin at 2/*m*), $a = 3.89722$,
$c = 20.6041$ Å, $Z = 1$ Fig. 35

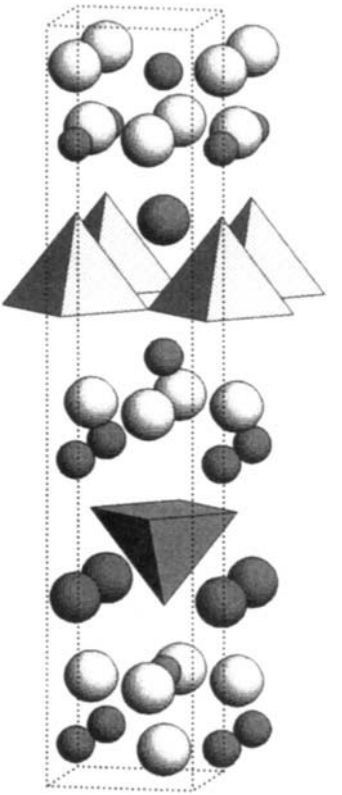

Atom	WP	PS	*x*	*y*	*z*	Occ.
Ca[a]	2(*c*)	4*mm*	$\frac{1}{4}$	$\frac{1}{4}$	0.06310	
Ti	2(*c*)	4*mm*	$\frac{3}{4}$	$\frac{3}{4}$	0.1480	
Ba[b]	2(*c*)	4*mm*	$\frac{1}{4}$	$\frac{1}{4}$	0.25677	
Cu	2(*c*)	4*mm*	$\frac{3}{4}$	$\frac{3}{4}$	0.35226	
Ce[c]	2(*c*)	4*mm*	$\frac{1}{4}$	$\frac{1}{4}$	0.43697	
O(1)	2(*c*)	4*mm*	$\frac{3}{4}$	$\frac{3}{4}$	0.04584	
O(2)	4(*f*)	2*mm*.	$\frac{1}{4}$	$\frac{3}{4}$	0.14001	
O(3)	2(*c*)	4*mm*	$\frac{3}{4}$	$\frac{3}{4}$	0.23690	
O(4)	4(*f*)	2*mm*.	$\frac{1}{4}$	$\frac{3}{4}$	0.36128	
O(5)	2(*b*)	$\bar{4}m2$	$\frac{1}{4}$	$\frac{3}{4}$	$\frac{1}{2}$	

[a] $Ca = Ca_{0.500}Nd_{0.407}Ba_{0.093}$.
[b] $Ba = Ba_{0.907}Nd_{0.093}$.
[c] $Ce = Ce_{0.5}Nd_{0.5}$.

(*continued*)

Compound	a (Å)	c (Å)	T_c (K)	Ref.
$Ti_2Nd_2CaBa_2CeCu_2O_{14}$	3.89722	20.6041	n.s.	1
$Ti_2Sm_2Ca_{1.1}Ba_2Ce_{0.9}Cu_2O_{13.90}$	3.8884	20.488	n.s.	2
$Ti_2Gd_{2.25}CaBa_2Ce_{0.75}Cu_2O_{14}$	3.8839	20.463	n.s.	3

References: 1, Den *et al.* (1995); 2, Zhu *et al.* (1995c); 3, Li *et al.* (1995a).

5212 $(Ti_{0.60}Sm_{0.34}Ca_{0.06})_5Ba_2(Ca_{0.70}Sm_{0.3})_1Cu_2O_{14}$

$A_5B_2CD_2O_{14}$, *tP*24, (123) $P4/mmm$–$i^2h^2g^4fda$
-DO_2–·C–DO_2–OB–AO_2–OA–AO_2–OA–AO_2–OB-
$Ti_3Sm_2Ba_2CaCu_2O_{14}$, n.s., PX, $R_B = 0.076$ (Zhu *et al.*, 1995b)
(123) $P4/mmm$, $a = 3.8885$, $c = 19.577$ Å, $Z = 1$ Fig. 36

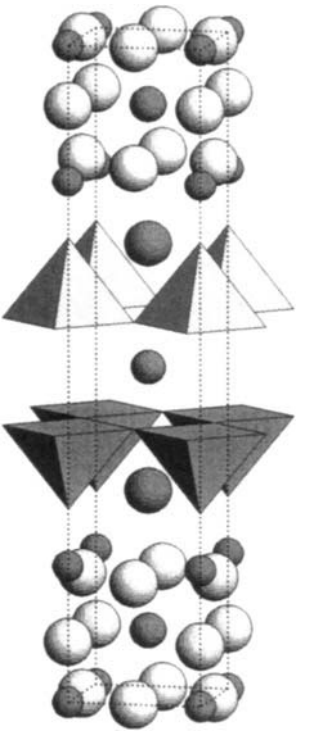

Atom	WP	PS	x	y	z	Occ.
Ti(1)	1(*a*)	4/*mmm*	0	0	0	
Sm[a]	2(*h*)	4*mm*	$\frac{1}{2}$	$\frac{1}{2}$	0.0986	
Ti(2)	2(*g*)	4*mm*	0	0	0.2059	
Ba	2(*h*)	4*mm*	$\frac{1}{2}$	$\frac{1}{2}$	0.3121	
Cu	2(*g*)	4*mm*	0	0	0.4102	
Ca[b]	1(*d*)	4/*mmm*	$\frac{1}{2}$	$\frac{1}{2}$	$\frac{1}{2}$	
O(1)	2(*f*)	*mmm*.	0	$\frac{1}{2}$	0	
O(2)	2(*g*)	4*mm*	0	0	0.091	
O(3)	4(*i*)	2*mm*.	0	$\frac{1}{2}$	0.183	
O(4)	2(*g*)	4*mm*	0	0	0.293	
O(5)	4(*i*)	2*mm*.	0	$\frac{1}{2}$	0.419	

[a] $Sm = Sm_{0.852}Ca_{0.148}$.
[b] $Ca = Ca_{0.704}Sm_{0.296}$.

5222 $(Ti_{0.40}Sm_{0.40}Ga_{0.20})_5Ba_2(Sm_{0.55}Ce_{0.45})_2Cu_2O_{16}$

$A_5B_2C_2D_2O_{16}$, *tI*54, (139) $I4/mmm$–g^2e^7dca
-O_2*D*–*C*-·–O_2–·*C*–*D*O_2–O*B*–*A*O_2–O*A*–*A*O_2–O*A*–*A*O_2–O*B*-
$Ti_2Sm_{3.1}GaBa_2Ce_{0.9}Cu_2O_{16}$, n.s., PX, $R_B = 0.082$ (Zhu *et al.*, 1995a)
(139) $I4/mmm$, $a = 3.8864$, $c = 44.761$ Å, $Z = 2$ Fig. 37

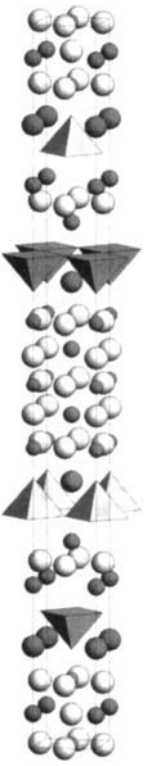

Atom	WP	PS	x	y	z	Occ.
Ga	2(*a*)	4/*mmm*	0	0	0	
Sm(1)	4(*e*)	4*mm*	$\frac{1}{2}$	$\frac{1}{2}$	0.0457	
Ti	4(*e*)	4*mm*	0	0	0.0883	
Ba	4(*e*)	4*mm*	$\frac{1}{2}$	$\frac{1}{2}$	0.1383	
Cu	4(*e*)	4*mm*	0	0	0.1805	
Sm(2)[a]	4(*e*)	4*mm*	$\frac{1}{2}$	$\frac{1}{2}$	0.2217	
O(1)	4(*c*)	*mmm*.	0	$\frac{1}{2}$	0	
O(2)	4(*e*)	4*mm*	0	0	0.0405	
O(3)	8(*g*)	2*mm*.	0	$\frac{1}{2}$	0.0857	
O(4)	4(*e*)	4*mm*	0	0	0.1290	
O(5)	8(*g*)	2*mm*.	0	$\frac{1}{2}$	0.1810	
O(6)	4(*d*)	$\bar{4}m2$	0	$\frac{1}{2}$	$\frac{1}{4}$	

[a] Sm(2) = $Sm_{0.55}Ce_{0.45}$.

1. Other Basic Structures

3223, **3234**, **3245**: Superconducting oxycarbonates with two (C,Cu)O layers were reported by Kawashima *et al.* (1994b,c). In the proposed structural models, the two (C,Cu)O layers are separated by a BaO layer that in the present classification is also considered as an *additional* layer. Superconducting transition temperatures of 91, 113, and 110 K were measured for the nominal compositions $CBa_{2.5}Ca_{2.5}Cu_4O_{11.6}$ (**3223**), $C_{0.6}Ba_2Ca_4Cu_{5.5}O_{13.2}$ (**3234**), and $C_{0.5}Ba_2Ca_4Cu_{5.5}O_{13}$ (**3245**), respectively. An iodine-intercalated (Bi,I)-**3223** compound, $(Bi_2I)Sr_2Ca_2Cu_3O_y$ ($a = 5.40$, $c = 22.01$ Å, $T_c = 100$ K) was reported by Xiang *et al.* (1991).

3232, **3242**, **3252**: A series of nonsuperconducting cuprates with the general formula $(Pb_2Cu)Sr_2(Y_{1-x}Ce_x)_mCu_2O_{6+2m+\delta}$, where $m = 3$ (**3232**), 4 (**3242**) and 5 (**3252**), was described by Tokiwa *et al.* (1991).

0011 $(Sr_{0.9}La_{0.1})_1Cu_1O_2$

***CDO*$_2$**, *tP*4, (123) *P*4/*mmm*–*fda*
-DO_2–·*C*-
$Sr_{0.9}La_{0.1}CuO_2$,[a] $T_c = 42$ K, PN, RT, $R_{wp} = 0.160$
(Jorgensen *et al.*, 1993)
(123) *P*4/*mmm*, $a = 3.95068$, $c = 3.40902$ Å, $Z = 1$
Fig. 38

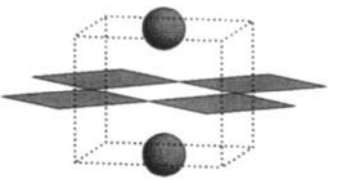

Atom	WP	PS	*x*	*y*	*z*	Occ.
Cu	1(*a*)	4/*mmm*	0	0	0	
Sr[b]	1(*d*)	4/*mmm*	$\frac{1}{2}$	$\frac{1}{2}$	$\frac{1}{2}$	
O	2(*f*)	*mmm*.	0	$\frac{1}{2}$	0	

[a] Prepared at 5 GPa.
[b] Sr = $Sr_{0.9}La_{0.1}$; full occupation confirmed.

(*continued*)

Compound	a (Å)	c (Å)	T_c (K)	Ref.
$Sr_{0.8}Ba_{0.2}CuO_2$[a]	...	...	90	1
$Sr_{0.63}Ca_{0.27}CuO_2$[a]	3.902	3.350	110	2
$Sr_{0.14}Ca_{0.86}CuO_2$	3.8611	3.1995	n.s.	3
$Sr_{0.6375}Ca_{0.2125}Nd_{0.15}CuO_2$[b]	3.9196	3.3505	34	4
$Sr_{0.9}La_{0.1}CuO_2$[c]	3.947[d]	3.412[d]	43	5
$Sr_{0.85}Pr_{0.15}CuO_2$[e]	3.942	3.393	39	6
$Sr_{0.84}Nd_{0.16}CuO_2$[e]	3.944[d]	3.383[d]	40	6
$Sr_{0.92}Sm_{0.08}CuO_2$[c]	3.942[d]	3.399[d]	44	7
$Sr_{0.92}Gd_{0.08}CuO_2$[c]	3.941[d]	3.393[d]	44	7
$CaCuO_2$[f]	3.8556	3.1805	n.s.[g]	8, 9

[a] Prepared at 6 GPa; nominal composition.
[b] Prepared at 2 GPa.
[c] Prepared at 3 GPa; nominal composition.
[d] Value taken from figure.
[e] Prepared at 2.5 GPa; nominal composition.
[f] Prepared at 1 GPa; cation content $Ca_{0.98-0.99}CuO_2$ from microprobe analysis.
[g] Onset of diamagnetic signal (79 K) not confirmed by resistivity measurements.
References: 1, Takano *et al.* (1991); 2, Azuma *et al.* (1992); 3, Siegrist *et al.* (1988b); 4, Alonso and Lapertot (1995); 5, Er *et al.* (1991); 6, Smith *et al.* (1991); 7, Ikeda *et al.* (1993); 8, Karpinski *et al.* (1994); 9, Karpinski (1997).

0011 compounds are usually referred to as infinite-layer compounds. The first crystal structure was reported for the composition $Ca_{0.86}Sr_{0.14}CuO_2$, the refinement being carried out in space group $P4/mmm$ (Siegrist *et al.*, 1988b).

Fig. 8.42.

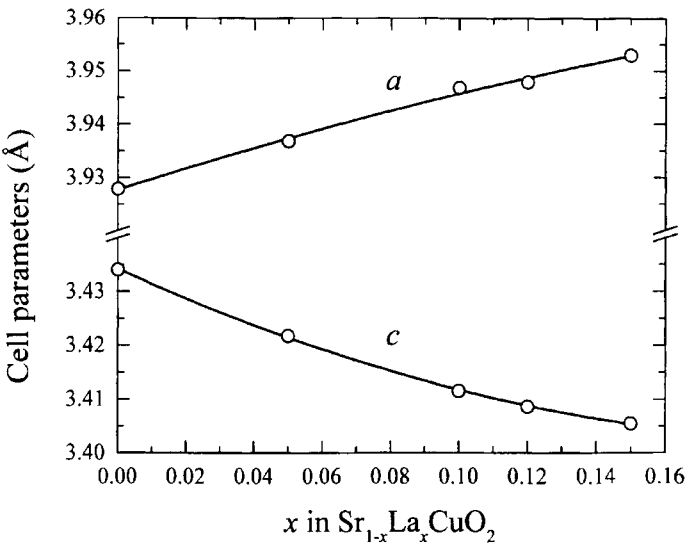

Cell parameters vs La content for $Sr_{1-x}La_xCuO_2$ ($T_c = 42.4$ K for $x = 0.05$–0.12) (Er *et al.*, 1992).

Superconductivity was observed for the electron-doped compounds $Sr_{0.84}Nd_{0.16}CuO_2$ and $Sr_{0.85}Pr_{0.15}CuO_2$ (Smith *et al.*, 1991). For the structural refinement on $Sr_{0.9}La_{0.1}CuO_2$ (compound first prepared by Er *et al.* (1991), a model with oxygen atoms in the *separating* layer ($1(b)$ 0 0 $\frac{1}{2}$) was tested and rejected (Jorgensen *et al.*, 1993). The cell parameters of $Sr_{1-x}La_xCuO_2$ vs the La content are presented in Fig. 8.42. $Sr_{1-x}Ca_xCuO_2$ is not superconducting; however, superconductivity was claimed for hole-doped $(Sr_{0.7}Ca_{0.3})_{1-x}CuO_2$ (Azuma *et al.*, 1992; Hiroi *et al.*, 1993a), as well as for its structural analogue in the Sr–Ba–Cu–O system (Takano *et al.*, 1991). Superconductivity observed for samples of nominal composition $(Sr_{0.7}Ca_{0.3})_{1.1}CuO_2$ (prepared at 5.7 GPa) was stated to be due to the presence of $Sr_3Cu_2O_{5+\delta}$ (**0212**) and $Sr_4Cu_3O_{7+\delta}$ (**0223**) impurities (Shaked *et al.*, 1995).

0021 $(Nd_{0.92}Ce_{0.08})_2Cu_1O_{3.92}$

C_2DO_4, *tI*14, (139) *I*4/*mmm*–*edca*
-DO_2–·C–O_2–C·-
$Nd_{1.845}Ce_{0.155}CuO_{3.922}$, $T_c = 20$ K, PN, RT, $R_B = 0.0247$
(Izumi *et al.*, 1989b)
(139) *I*4/*mmm*, $a = 3.9469$, $c = 12.0776$ Å,[a] $Z = 2$ Fig. 39

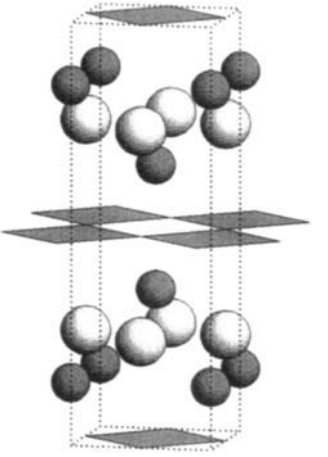

Atom	WP	PS	x	y	z	Occ.
Cu	2(*a*)	4/*mmm*	0	0	0	
Nd[b]	4(*e*)	4*mm*	$\frac{1}{2}$	$\frac{1}{2}$	0.1475	
O(1)	4(*c*)	*mmm*.	0	$\frac{1}{2}$	0	0.992
O(2)	4(*d*)	$\bar{4}m2$	0	$\frac{1}{2}$	$\frac{1}{4}$	0.969

[a] Additional reflections indicate a small fraction of superstructure ($2\sqrt{2}a$, $2\sqrt{2}a$, c).
[b] Nd = $Nd_{0.9225}Ce_{0.0775}$.

(*continued*)

Compound	a (Å)	c (Å)	T_c (K)	Ref.
$Pr_{1.85}Ce_{0.15}CuO_{4-\delta}$	3.9620	12.151	22[a]	1, 2
$Pr_{1.85}Th_{0.15}CuO_{4-\delta}$[b]	...	...	23	3
$Nd_{1.85}Ce_{0.15}CuO_{4-\delta}$	3.9450	12.078	24	1, 2
$Nd_{1.85}Th_{0.15}CuO_{4-\delta}$[b]	...	...	20	4
$Nd_2CuO_{3.6}F_{0.4}$[c]	3.961	12.13	21[d]	5
$Sm_{1.85}Ce_{0.15}CuO_{4-\delta}$	3.9191	11.904	18[a]	1, 2
$Eu_{1.85}Ce_{0.15}CuO_{4-\delta}$	3.9077	11.8409	13[a]	1, 2
$Gd_{1.85}Ce_{0.15}CuO_{4-\delta}$	3.9010	11.832	n.s.	1, 2
$Tm_{1.83}Ca_{0.17}CuO_{3.99}$[e]	3.831	11.642	30	6

[a] Value taken from figure.
[b] Nominal composition.
[c] Nominal composition, oxygen and fluorine content $Nd_2CuO_{3.74}F_{0.28}$ from chemical analysis.
[d] From resistivity measurements (onset), $T_c = 27$ K for $Nd_2CuO_{3.7}F_{0.3}$ (nominal composition).
[e] Prepared at 6 GPa.
References: 1, Uzumaki *et al.* (1991); 2, Xue *et al.* (1990); 3, Markert *et al.* (1989); 4, Markert and Maple (1989); 5, James *et al.* (1989); 6, Zhu *et al.* (1994).

0021 compounds are usually referred to as T′ phases. R_2CuO_4 compounds with R = Pr, Nd, Sm, and Eu crystallize with a Nd_2CuO_4-type structure ($I4/mmm$) (Müller-Buschbaum, 1975). The structure of Gd_2CuO_4 shows orthorhombic distortions ($Acam$, $a = b = 5.500$, $c = 11.871$ Å), caused by the rotation of the CuO_4 squares (Braden *et al.*, 1994; Galez and Collin, 1990). Different superstructures ($\sqrt{2}a$, $\sqrt{2}a$, c; $2\sqrt{2}a$, $\sqrt{2}a$, c, and $2\sqrt{2}a$, $2\sqrt{2}a$, $2c$, referring to

Fig. 8.43.

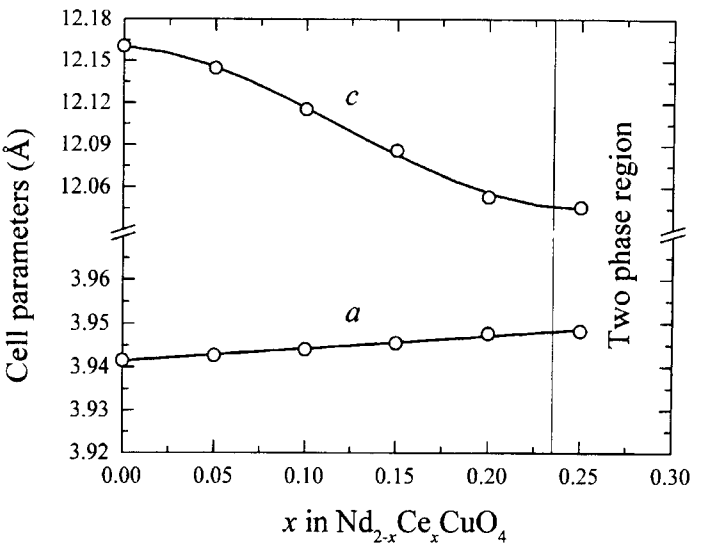

Cell parameters vs Ce content for $Nd_{2-x}Ce_xCuO_4$ (Tarascon *et al.*, 1989).

the tetragonal cell) were proposed by Bordet *et al.* (1992) for compounds with R = Y, Tb, Dy, Ho, Er, and Tm, synthesized at high pressure, first reported by Okada *et al.* (1990). Superconductivity could be induced by partly substituting Pr, Nd, Sm, or Eu by Ce or Th and annealing under reducing conditions (Tokura *et al.*, 1989b; Markert *et al.*, 1989). An O site with occupancy 0.06 was refined in the *separating* layers of oxidized $Nd_{2-x}Ce_xCuO_4$ (Schultz *et al.*, 1996). The cell parameters of $Nd_{2-x}Ce_xCuO_4$ vs the Ce content are presented in Fig. 8.43. As can be seen from Fig. 8.44, the compound is superconducting within a narrow doping range. An 8-fold pseudotetragonal supercell (possibly monoclinic or triclinic), corresponding to a partial ordering of the oxygen vacancies and of the two rare-earth metals, was reported for $Nd_{2-x}Ce_xCuO_4$ (Izumi *et al.*, 1989b). An 8-fold orthorhombic superstructure ($Cmc2_1$), caused by puckering and in-plane distortions of the CuO_2 layers, was suggested by Billinge and Egami (1993).

Fig. 8.44.

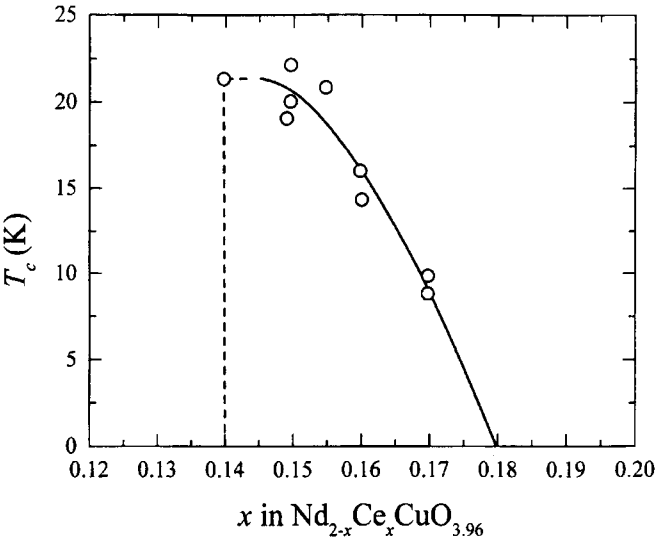

Superconducting transition temperature vs Ce content for $Nd_{2-x}Ce_xCuO_{3.96}$ (Takagi *et al.*, 1989).

0021/0222 $(Ca_{0.90}Gd_{0.10})_2Cu_1(O_{0.50}Cl_{0.50})_4/Ca_2Gd_2Cu_2(O_{0.77}Cl_{0.23})_8$

$B_4C_2D_3O_{12}$, *tI*42, (139) $I4/mmm$–ge^6dca
-O_2D–BO–OB–DO_2–•C–O_2–C•–O_2D–BO–OB-
$Ca_{3.80}Gd_{2.20}Cu_3O_{8.16}Cl_{3.84}$, n.s., PX, $R_B = 0.089$ (Pelloquin *et al.*, 1996b)
(139) $I4/mmm$, $a = 3.8865$, $c = 41.827$ Å, $Z = 2$ Fig. 40

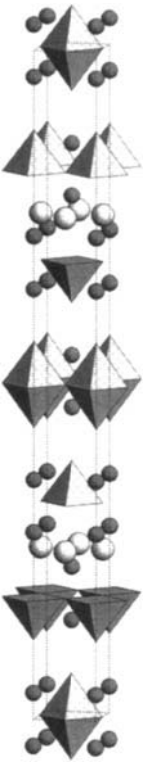

Atom[a]	WP	PS	x	y	z	Occ.
Cu(1)	2(*a*)	4/*mmm*	0	0	0	
Ca(1)[b]	4(*e*)	4*mm*	$\frac{1}{2}$	$\frac{1}{2}$	0.0389	
Ca(2)	4(*e*)	4*mm*	0	0	0.1428	
Cu(2)	4(*e*)	4*mm*	$\frac{1}{2}$	$\frac{1}{2}$	0.1779	
Gd	4(*e*)	4*mm*	0	0	0.2219	
O(1)	4(*c*)	*mmm*.	0	$\frac{1}{2}$	0	
Cl(1)	4(*e*)	4*mm*	0	0	0.0644	
Cl(2)[c]	4(*e*)	4*mm*	$\frac{1}{2}$	$\frac{1}{2}$	0.1176	
O(2)	8(*g*)	2*mm*.	0	$\frac{1}{2}$	0.181	
O(3)	4(*d*)	$\bar{4}m2$	0	$\frac{1}{2}$	$\frac{1}{4}$	

[a] Atom sites listed in the order *D*, *B*, *B*, *D*, *C*.
[b] $Ca(1) = Ca_{0.90}Gd_{0.10}$.
[c] $Cl(2) = Cl_{0.92}O_{0.08}$.

1201/2201 $C_1Sr_2Cu_1O_5/Bi_2Sr_2Cu_1O_6$

***A*$_3$*B*$_4$*D*$_2$O$_{11}$**, *tI*40, (139) *I*4/*mmm*–*ge*^{7}*ca*
-*DO*$_2$–*OB*–*AO*″–*OB*–*DO*$_2$–*OB*–*AO*–*OA*–*BO*-
$CBi_2Sr_4Cu_2O_{11}$, $T_c = 30$ K, PX, $R = 0.13$ (Pelloquin *et al.*, 1993a)
(67) *Abmm* (*Cmma*), $a = 5.466$, $b = 5.460$, $c = 39.500$ Å,[a] $Z = 4$
Fig. 41
$\mathbf{a}_1 + \mathbf{a}_2$, $-\mathbf{a}_1 + \mathbf{a}_2$, **c**; origin shift $\frac{1}{4}$ 0 $\frac{1}{4}$

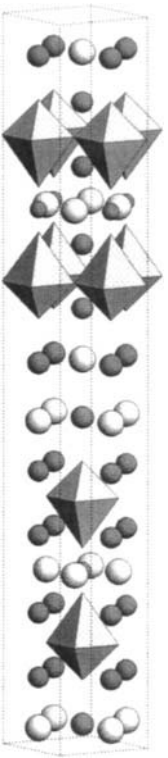

Atom[b]	WP	PS	*x*	*y*	*z*	Occ.
C	4(*g*)	2*mm*	0.25	0	$\frac{1}{4}$	
Sr(1)	8(*m*)	.*m*.	0.75	0	0.303	
Cu	8(*m*)	.*m*.	0.25	0	0.345	
Sr(2)	8(*m*)	.*m*.	0.75	0	0.391	
Bi	8(*m*)	.*m*.	0.25	0	0.460	
O(1)	4(*e*)	..2/*m*	0	$\frac{1}{4}$	$\frac{1}{4}$	0.5
O(2)	4(*f*)	..2/*m*	$\frac{1}{2}$	$\frac{1}{4}$	$\frac{1}{4}$	0.5
O(3)	8(*m*)	.*m*.	0.25	0	0.28	
O(4)	8(*j*)	..2	0	$\frac{1}{4}$	0.35	
O(5)	8(*k*)	..2	$\frac{1}{2}$	$\frac{1}{4}$	0.35	
O(6)	8(*m*)	.*m*.	0.25	0	0.40	
O(7)	8(*m*)	.*m*.	0.75	0	0.46	

[a] Average structure; additional reflections indicate incommensurate modulation ($\mathbf{q} \approx \mathbf{b}^*/8.85$ to $\mathbf{b}^*/9$).
[b] O site with occupancy 0.5 (8(*n*) 0.082 0.168 $\frac{1}{4}$) ignored here (presumed to replace sites O(1) and O(2) in second refinement).

(*continued*)

Compound	a (Å)	c (Å)[a]	T_c (K)	Ref.
$HgTl_2Ba_4Cu_2O_{10}$	3.8584	42.2031	50	1
$CBi_2Sr_4Cu_2O_{11}$	[b]		30	2
$CBi_{1.5}Pb_{0.5}Sr_4Cu_2O_{11}$	3.8409	39.444[c]	41[d]	3

[a] Space group *I4/mmm*.
[b] Space group *Abmm*, $a = 5.466$, $b = 5.460$ and $c = 39.500$ Å; additional reflections indicate incommensurate modulation ($\mathbf{q} \approx \mathbf{b}^*/8.85$ to $\mathbf{b}^*/9$).
[c] Additional reflections indicate superstructure ($\sqrt{2}a$, $\sqrt{2}a$, c).
[d] T_c given for $CBi_{1.6}Pb_{0.4}Sr_4Cu_2O_{11}$.
References: 1, Martin *et al.* (1993a); 2, Pelloquin *et al.* (1993a); 3, Uehara *et al.* (1993b).

1212/2212 $Cu_1Ba_2Y_1Cu_2O_{6.94}/Cu_2Ba_2Y_1Cu_2O_8$

***A*$_3$*B*$_4$*C*$_2$*D*$_4$O$_{15}$**, *oS*56, (65) *Ammm*-j^5i^8ba
-*D*O$_2$-·*C*-*D*O$_2$-O*B*-*A*O′-O*B*-*D*O$_2$-·*C*-*D*O$_2$-O*B*-*A*O′-O′*A*-*B*O-
$Ba_4Y_2Cu_7O_{14.94}$, $T_c = 91.5$ K, SX, $R_w = 0.0282$ (Schwer *et al.*, 1993)
(65) *Ammm* (*Cmmm*), $a = 3.831$, $b = 3.881$, $c = 50.68$ Å, $Z = 2$ Fig. 42

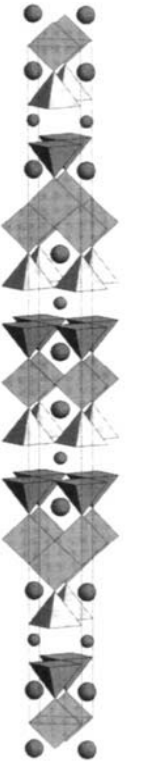

(*continued*)

Atom	WP	PS	x	y	z	Occ.
Cu(1)[a]	2(*a*)	*mmm*	0	0	0	
Ba(1)	4(*j*)	*mm*2	$\frac{1}{2}$	$\frac{1}{2}$	0.04250	
Cu(2)	4(*i*)	*mm*2	0	0	0.08198	
Y	4(*j*)	*mm*2	$\frac{1}{2}$	$\frac{1}{2}$	0.11528	
Cu(3)	4(*i*)	*mm*2	0	0	0.14858	
Ba(2)	4(*j*)	*mm*2	$\frac{1}{2}$	$\frac{1}{2}$	0.18794	
Cu(4)	4(*i*)	*mm*2	0	0	0.23009	
O(1)	2(*b*)	*mmm*	0	$\frac{1}{2}$	0	0.94
O(2)[a]	4(*i*)	*mm*2	0	0	0.0366	
O(3)	4(*j*)	*mm*2	$\frac{1}{2}$	0	0.0872	
O(4)	4(*i*)	*mm*2	0	$\frac{1}{2}$	0.0874	
O(5)	4(*j*)	*mm*2	$\frac{1}{2}$	0	0.1436	
O(6)	4(*i*)	*mm*2	0	$\frac{1}{2}$	0.1435	
O(7)	4(*i*)	*mm*2	0	0	0.1940	
O(8)	4(*i*)	*mm*2	0	$\frac{1}{2}$	0.2328	

[a] Full occupation confirmed.

Compound	a (Å)	b (Å)	c (Å)	T_c (K)	Ref.
$Ba_4Nd_2Cu_7O_{14.85}$	3.89385	3.90132	50.75013	40	1
$Ba_4Dy_2Cu_7O_{14.3}$	3.85649	3.87713	50.666	69	1
$Ba_4Ho_2Cu_7O_{14.36}$	3.84999	3.87100	50.77142	71	1
$Ba_4Er_2Cu_7O_{14.96}$	3.83501	3.87292	50.53369	79	1
$Ba_4Y_2Cu_7O_{14.94}$	3.831	3.881	50.68	91.5	2

References: 1, Currie *et al.* (1994); 2, Schwer *et al.* (1993).

$Ba_4Y_2Cu_7O_{15-\delta}$ was first considered as planar defects in $Ba_2YCu_3O_{7-\delta}$. A structural model based on the replacement of every second AO' (CuO) layer in the structure of Cu-**1212** by two AO' layers was proposed by Zandbergen *et al.* (1988b). Single crystals were obtained during studies on the crystallization of Cu-**1212** at high oxygen pressure (Karpinski *et al.*, 1988a) and a structural refinement was reported by Bordet *et al.* (1988c). The proposed structure (*Ammm*) is an intergrowth of orthorhombic Cu-**1212** and Cu-**2212**, with a variable oxygen content in the *additional* layer of the stacking unit of the former type. When δ differs significantly from zero, the oxygen atoms in this layer are distributed over two sites (2(*b*) 0 $\frac{1}{2}$ 0 and 2(*d*) $\frac{1}{2}$ 0 0), as in tetragonal Cu-**1212**. The superconducting transition temperature and the orthorhombicity were found to increase with increasing oxygen content ($T_c = 92$ K for $\delta = 0$) (Tallon *et al.*, 1990) (Figs. 8.45 and 8.46). A critical temperature as high as 95 K was reported for $Ba_4Y_2Cu_7O_y$ by Genoud *et al.* (1991) and associated with an oxygen content $y = 15.15$–15.32. According to Schwer *et al.* (1993), the oxygen content cannot be raised above $y = 15$ and the high values of T_c observed for some samples should rather be correlated to a partial substitution of copper by carbon or vacancies on the cation site in the *additional* layer of the Cu-**1212** stacking unit.

Fig. 8.45.

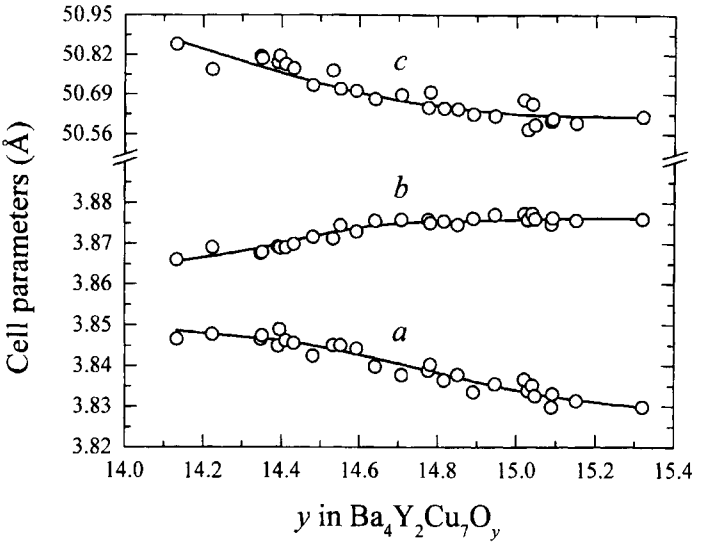

Cell parameters vs oxygen content for $Ba_4Y_2Cu_7O_y$ (Genoud *et al.*, 1992).

Fig. 8.46.

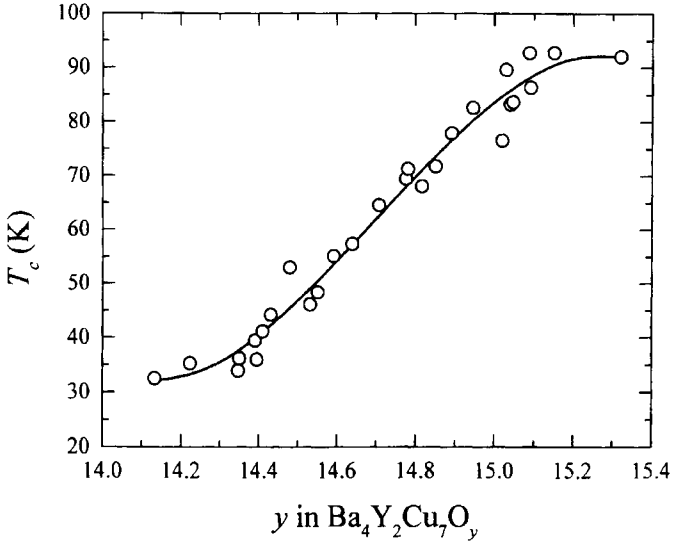

Superconducting transition temperature vs oxygen content for $Ba_4Y_2Cu_7O_y$ (Genoud *et al.*, 1992).

2201/2212 $Bi_2Sr_2Cu_1O_6/Bi_2Sr_2Ca_1Cu_2O_8$

$A_4B_4CD_3O_{14}$, *tP*26, (123) *P*4/*mmm*–*ih*^{5}*g*^{4}*fba*
-*DO*$_2$–*OB*–*AO*–*OA*–*BO*–*O*$_2$*D*–*C*•–*O*$_2$*D*–*BO*–*OA*–*AO*–*OB*-
$Bi_4Sr_4CaCu_3O_{14}$, $T_c = 84$ K, SX, $R_w = 0.072$ (Shepelev *et al.*, 1993)
(51) *Pbmm* (*Pmma*), $a = 5.411$, $b = 5.417$, $c = 27.75$ Å,[a] $Z = 2$
Fig. 43
$\mathbf{a}_1 + \mathbf{a}_2$, $-\mathbf{a}_1 + \mathbf{a}_2$, $\mathbf{c}$; origin shift $\frac{1}{4}\ \frac{1}{4}\ 0$

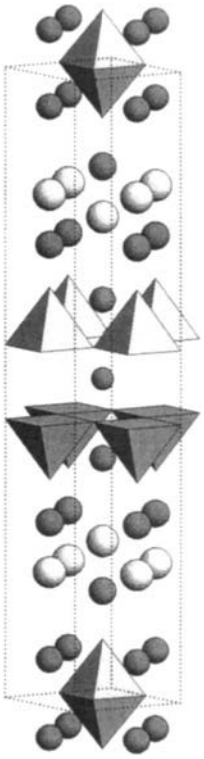

Atom[b]	WP	PS	*x*	*y*	*z*	Occ.
Cu(1)	2(*e*)	2*mm*	0.259	$\frac{1}{4}$	0	
Sr(1)	4(*k*)	.*m*.	0.231	$\frac{3}{4}$	0.0612	
Bi(1)	8(*l*)	1	0.222	0.196	0.1626	0.5
Bi(2)	8(*l*)	1	0.247	0.703	0.2796	0.5
Sr(2)	4(*k*)	.*m*.	0.236	$\frac{1}{4}$	0.3745	
Cu(2)	4(*k*)	.*m*.	0.255	$\frac{3}{4}$	0.4375	
Ca	2(*f*)	2*mm*	0.268	$\frac{1}{4}$	$\frac{1}{2}$	
O(1)	2(*a*)	..2/*m*	0	0	0	
O(2)	2(*c*)	..2/*m*	$\frac{1}{2}$	0	0	
O(3)	4(*k*)	.*m*.	0.240	$\frac{1}{4}$	0.087	
O(4)	8(*l*)	1	0.051	−0.055	0.200	0.5
O(5)	8(*l*)	1	0.401	0.000	0.243	0.5
O(6)	4(*k*)	.*m*.	0.194	$\frac{3}{4}$	0.347	
O(7)	4(*g*)	..2	0	0	0.438	
O(8)	4(*h*)	..2	$\frac{1}{2}$	0	0.445	

[a] Average structure; additional reflections indicate incommensurate modulation ($\mathbf{q} \approx \mathbf{b}^*/4.7$).
[b] Atom sites listed in the order *D*, *B*, *A*, *A*, *B*, *D*, *C*.

2. Other Intergrowth Structures

1201/1212: The structure of nonsuperconducting $B_2Sr_3Nd_2Cu_3O_{12}$ was refined in space group $P4/nnc$ ($a = 7.7671$, $c = 35.8294$ Å) (Amamoto *et al.*, 1994). It is an intergrowth of B-**1201** and B-**1212** stacking units.

1212/1222: The structure of nonsuperconducting $Ga_{1.78}Sr_{3.16}Nd_{3.84}Cu_{4.22}O_{16}$ was reported to be an intergrowth of Ga-**1212** and Ga-**1222** stacking units ($a = 5.458$, $b = 5.535$, $c = 51.300$ Å) (Ono *et al.*, 1995).

1201/1201/2201: The structure of superconducting $C_2Bi_2Sr_6Cu_3O_{16}$ ($T_c = 40$ K) was refined in space group $Fmmm$ ($a = 5.469$, $b = 5.483$, $c = 54.26$ Å) (Pelloquin *et al.*, 1993c). It is an intergrowth of two C-**1201** (CSr_2CuO_5) and one Bi-**2201** ($Bi_2Sr_2CuO_6$) stacking units. A critical temperature of 54 K was observed for the Pb-containing compound $C_2(Bi_{1-x}Pb_x)_2Sr_6Cu_3O_{16}$ ($a = 3.88$, $c = 54.516$ Å) (Uehara *et al.*, 1993b).

ladder $Sr_2Cu_3O_5$

$Sr_2Cu_3O_5$, *oS*20, n.s., PN, $R_B = 0.0263$ (Kazakov *et al.*, 1997)
(65) *Cmmm*, $a = 3.9375$, $b = 19.4342$, $c = 3.4654$ Å, $Z = 2$
Fig. 44

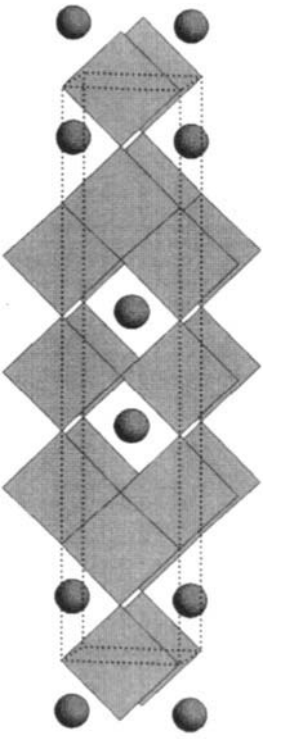

(*continued*)

Atom	WP	PS	x	y	z	Occ.
Cu(1)	2(*a*)	*mmm*	0	0	0	
Sr	4(*j*)	*m2m*	$\frac{1}{2}$	0.1005	$\frac{1}{2}$	
Cu(2)	4(*i*)	*m2m*	0	0.1987	0	
O(1)	2(*b*)	*mmm*	$\frac{1}{2}$	0	0	
O(2)	4(*i*)	*m2m*	0	0.1011	0	
O(3)	4(*i*)	*m2m*	$\frac{1}{2}$	0.2031	0	

ladder $(Ca_{0.57}La_{0.43})_{14}Cu_{24}O_{41}$

$Ca_8La_6Cu_{24}O_{41}$, *oS*316, n.s., SX, $R_w = 0.044$ (Siegrist *et al.*, 1988a)
(66) *Cccm*, $a = 11.305$, $b = 12.610$, $c = 27.608$ Å, $Z = 4$ Fig. 45a,b

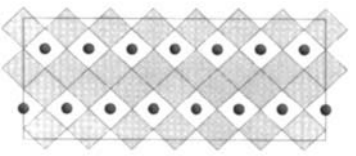

(a) $0.11 < y < 0.27$

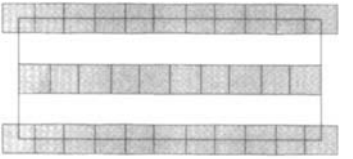

(b) $y \sim 0$

Atom	WP	PS	x	y	z	Occ.
Ca(1)[a]	8(*l*)	..*m*	0.2482	0.1168	0	
Ca(2)[a]	16(*m*)	1	0.2514	0.1166	0.14256	
Ca(3)[a]	16(*m*)	1	0.2489	0.1166	0.28566	
Ca(4)[a]	16(*m*)	1	0.2504	0.1166	0.42879	
Cu(1)	16(*m*)	1	0.0833	0.2492	0.07139	
Cu(2)	16(*m*)	1	0.0831	0.2549	0.21447	
Cu(3)	16(*m*)	1	0.0829	0.2452	0.35747	
Cu(4)	8(*l*)	..*m*	0.0835	0.2544	$\frac{1}{2}$	
Cu(5)	4(*c*)	..2/*m*	0	0	0	
Cu(6)	8(*i*)	..2	0	0	0.1010	
Cu(7)	8(*i*)	..2	0	0	0.1987	
Cu(8)	8(*j*)	..2	0	$\frac{1}{2}$	0.0476	
Cu(9)	8(*j*)	..2	0	$\frac{1}{2}$	0.1490	
Cu(10)	4(*b*)	222	0	$\frac{1}{2}$	$\frac{1}{4}$	
O(1)	8(*l*)	..*m*	0.0864	0.2662	0	
O(2)	16(*m*)	1	0.0839	0.2404	0.1433	
O(3)	16(*m*)	1	0.0834	0.2458	0.2866	
O(4)	16(*m*)	1	0.0851	0.2425	0.4288	
O(5)	8(*k*)	..2	$\frac{1}{4}$	$\frac{1}{4}$	0.0706	
O(6)	8(*k*)	..2	$\frac{1}{4}$	$\frac{1}{4}$	0.2147	
O(7)	8(*k*)	..2	$\frac{1}{4}$	$\frac{1}{4}$	0.3578	
O(8)	4(*f*)	..2/*m*	$\frac{1}{4}$	$\frac{1}{4}$	$\frac{1}{2}$	
O(9)	16(*m*)	1	0.1181	0.0176	0.0535	
O(10)	8(*g*)	2..	0.1184	0	$\frac{1}{4}$	
O(11)	16(*m*)	1	0.1211	0.0298	0.3516	
O(12)	16(*m*)	1	0.1196	0.4957	0.1037	
O(13)	16(*m*)	1	0.1203	0.4790	0.1965	
O(14)	8(*l*)	..*m*	0.1208	0.4721	$\frac{1}{2}$	

[a] $Ca = Ca_{0.5714}La_{0.4286}$.

(continued)

Compound	a (Å)	b (Å)	c (Å)	T_c (K)	Ref.
$Ca_{13.6}Sr_{0.4}Cu_{24}O_{41.84}$[a]	11.14	12.44	27.02	9[b]	1
$Ca_8La_6Cu_{24}O_{41}$	11.305	12.610	27.608	n.s.	2

[a] Prepared at 0.2 GPa.
[b] T_c measured at 3.5 GPa.
References: 1, Uehara *et al.* (1996); 2, Siegrist *et al.* (1988a).

I Conclusions

The present review provides up-to-date information on the crystal structures of high-T_c superconducting cuprates. The classification is based on widely accepted concepts with some personal notes, including the derivation of stacking rules and space groups of ideal structures, and the generation of a high-T_c superconductor family tree.

The compilation contains crystallographic data for more than 400 high-T_c superconductors and related compounds, reported up to 1997, referring to more than 550 scientific publications. Some 1500 articles dealing with crystal structures were studied, which, however, represent only a small part of the abundant literature in the field of high-T_c superconductivity. Hence we cannot be assured that no information was overlooked, in particular concerning thin films and compounds prepared at high pressure. Review articles and monographs were consulted, but all data reported here were taken from the original publications.

Acknowledgment

We thank Dr. Karin Cenzual for useful discussions and critical reading of the manuscript.

References

S. Adachi, O. Inoue, S. Kawashima, H. Adachi, Y. Ichikawa, K. Setsune, and K. Wasa, *Physica C* **168** 1–7 (1990a).
S. Adachi, K. Setsune, and K. Wasa, *Jpn. J. Appl. Phys.* **29**, L890–L892 (1990b).
S. Adachi, A. Nara, and H. Yamauchi, *Physica C* **201**, 403–406 (1992).
S. Adachi, H. Yamauchi, S. Tanaka, and N. Môri, *Physica C* **212**, 164–168 (1993).
J. Akimitsu, A. Yamazaki, H. Sawa, and H. Fujiki, *Jpn. J. Appl. Phys.* **26**, L2080–L2081 (1987).
J. Akimitsu, S. Suzuki, M. Watanabe, and H. Sawa, *Jpn. J. Appl. Phys.* **27**, L1859–L1860 (1988).
J. Akimitsu, M. Uehara, M. Ogawa, H. Nakata, K. Tomimoto, Y. Miyazaki, H. Yamane, T. Hirai, K. Kinoshita, and Y. Matsui, *Physica C* **201**, 320–324 (1992).
J. Akimoto, Y. Oosawa, K. Tokiwa, M. Hirabayashi, and H. Ihara, *Physica C* **242**, 360–364 (1995).
M. A. Alario-Franco, P. Bordet, J. J. Capponi, C. Chaillout, J. Chenavas, T. Fournier, M. Marezio, S. de Brion, B. Souletie, A. Sulpice, J. L. Tholence, C. Colliex, R. Argoud, J. L. Baldonedo, M. F. Gorius, and M. Perroux, *Physica C* **235–240**, 975–976 (1994a).

M. A. Alario-Franco, C. Chaillout, J. J. Capponi, J.-L. Tholence, and B. Souletie, *Physica C* **222**, 52–56 (1994b).
E. T. Alexandre, S. M. Loureiro, E. V. Antipov, P. Bordet, S. de Brion, J. J. Capponi, and M. Marezio, *Physica C* **245**, 207–211 (1995).
M. Al-Mamouri, P. P. Edwards, C. Greaves, and M. Slaski, *Nature* **369**, 382–384 (1994).
J. A. Alonso and G. Lapertot, *Physica C* **250**, 93–100 (1995).
Y. Amamoto, H. Yamane, T. Oku, Y. Miyazaki, and T. Hirai, *Physica C* **227**, 245–253 (1994).
M. T. Anderson, K. R. Poeppelmeier, J.-P. Zhang, H.-J. Fan, and L. D. Marks, *Chem. Mater.* **4**, 1305–1313 (1992).
E. V. Antipov, S. M. Loureiro, C. Chaillout, J. J. Capponi, P. Bordet, J. L. Tholence, S. N. Putilin, and M. Marezio, *Physica C* **215**, 1–10 (1993).
M. A. G. Aranda, D. C. Sinclair, and J. P. Attfield, *Physica C* **221**, 304–310 (1994).
D. N. Argyriou, J. D. Jorgensen, R. L. Hitterman, Z. Hiroi, N. Kobayashi, and M. Takano, *Phys. Rev. B* **51**, 8434–8437 (1995).
T. Arima, Y. Tokura, H. Takagi, S. Uchida, R. Beyers, and J. B. Torrance, *Physica C* **168**, 79–84 (1990).
A. R. Armstrong and P. P. Edwards, *J. Solid State Chem.* **98**, 432–436 (1992).
H. Asano, T. Ishigaki, and K. Takita, *Jpn. J. Appl. Phys.* **26**, L1064–L1065 (1987a).
H. Asano, K. Takita, T. Ishigaki, H. Akinaga, H. Katoh, K. Masuda, F. Izumi, and N. Watanabe, *Jpn. J. Appl. Phys.* **26**, L1341–L1343 (1987b).
H. Asano, K. Takita, H. Katoh, H. Akinaga, T. Ishigaki, M. Nishino, M. Imai, and K. Masuda, *Jpn. J. Appl. Phys.* **26**, L1410–L1412 (1987c).
H. Asano, Y. Yokoyama, M. Nishino, H. Katoh, H. Akinaga, and K. Takita, *Mod. Phys. Lett. B* **2**, 583–588 (1988).
B. Aurivillius, *Arkiv Kemi* **1**, 463–480 (1950).
J. D. Axe, A. H. Moudden, D. Hohlwein, D. E. Cox, K. M. Mohanty, A. R. Moodenbaugh, and Y. Xu, *Phys. Rev. Lett.* **62**, 2751–2754 (1989).
M. Azuma, Z. Hiroi, M. Takano, Y. Bando, and Y. Takeda, *Nature* **356**, 775–776 (1992).
T. G. N. Babu and C. Greaves, *J. Superconduct.* **8**, 21–25 (1995).
T. G. N. Babu, D. J. Fish, and C. Greaves, *J. Mater. Chem.* **1**, 677–679 (1991).
V. Badri and U. V. Varadaraju, *Solid State Commun.* **93**, 1003–1007 (1995).
D. Balz, *Naturwissenschaften* **40**, 241 (1953).
L. Barbey, N. Nguyen, A. Ducouret, V. Caignaert, J. M. Grenèche, and B. Raveau, *J. Solid State Chem.* **115**, 514–520 (1995).
T. Barth, *Norsk Geol. Tidsskr.* **8**, 201–219 (1925).
L. Bauernfeind, W. Widder, and H. F. Braun, *Physica C* **254**, 151–158 (1995).
T. P. Beales, C. Dineen, S. R. Hall, M. R. Harrison, and J. M. Parberry, *Physica C* **207**, 1–8 (1993).
J. G. Bednorz and K. A. Müller, *Z. Phys. B* **64**, 189–193 (1986).
F. Beech, S. Miraglia, A. Santoro, and R. S. Roth, *Phys. Rev. B* **35**, 8778–8781 (1987).
M. A. Beno, L. Soderholm, D. W. Capone II, D. G. Hinks, J. D. Jorgensen, J. D. Grace, I. K. Schuller, C. U. Segre, and K. Zhang, *Appl. Phys. Lett.* **51**, 57–59 (1987).
F. J. M. Benschop, W. T. Fu, and W. J. A. Maaskant, *Physica C* **184**, 311–315 (1991).
F. J. M. Benschop, R. B. Helmholdt, and W. J. A. Maaskant, *Physica C* **227**, 129–142 (1994).
P. Berastegui, L.-G. Johansson, M. Käll, and L. Börjesson, *Physica C* **204**, 147–154 (1992).
A. I. Beskrovnyi, M. Dlouhá, Z. Jirák, and S. Vratislav, *Physica C* **171**, 19–24 (1990a).
A. I. Beskrovnyi, M. Dlouhá, Z. Jirák, S. Vratislav, and E. Pollert, *Physica C* **166**, 79–86 (1990b).
A. I. Beskrovnyi, S. Durčok, J, Hejtmánek, Z. Jirák, E. Pollert, and I. G. Shelkova, *Physica C* **222**, 375–385 (1994).
R. Beyers, G. Lim, E. M. Engler, R. J. Savoy, T. M. Shaw, T. R. Dinger, W. J. Gallagher, and R. L. Sandstrom, *Appl. Phys. Lett.* **50**, 1918–1920 (1987).
S. J. L. Billinge and T. Egami, *Phys. Rev. B* **47**, 14386–14405 (1993).

H. A. Blackstead, D. B. Chrisey, J. D. Dow, J. S. Horwitz, A. E. Klunzinger, and D. B. Pulling, *Phys. Lett. A* **207**, 109–112 (1995).

P. Bordet, J. J. Capponi, C. Chaillout, J. Chenavas, A. W. Hewat, E. A. Hewat, J. L. Hodeau, M. Marezio, J. L. Tholence, and D. Tranqui, *Physica C* **153–155**, 623–624 (1988a).

P. Bordet, J. J. Capponi, C. Chaillout, J. Chenavas, A. W. Hewat, E. A. Hewat, J. L. Hodeau, M. Marezio, J. L. Tholence, and D. Tranqui, *Physica C* **156**, 189–192 (1988b).

P. Bordet, C. Chaillout, J. Chenavas, J. L. Hodeau, M. Marezio, J. Karpinski, and E. Kaldis, *Nature* **334**, 596–598 (1988c).

P. Bordet, J. J. Capponi, C. Chaillout, D. Chateigner, J. Chenavas, Th. Fournier, J. L. Hodeau, M. Marezio, M. Perroux, G. Thomas, and A. Varela, *Physica C* **193**, 178–188 (1992).

P. Bordet, S. Le Floch, J. J. Capponi, C. Chaillout, M. F. Gorius, M. Marezio, J. L. Tholence, and P. G. Radaelli, *Physica C* **262**, 151–158 (1996).

D. Bourgault, C. Martin, C. Michel, M. Hervieu, J. Provost, and B. Raveau, *J. Solid State Chem.* **78**, 326–328 (1989).

M. Braden, W. Paulus, A. Cousson, P. Vigoureux, G. Heger, A. Goukassov, P. Bourges, and D. Petitgrand, *Europhys. Lett.* **25**, 625–630 (1994).

J. F. Bringley, B. A. Scott, S. J. La Placa, R. F. Boehme, T. M. Shaw, M. W. McElfresh, S. S. Trail, and D. E. Cox, *Nature* **347**, 263–265 (1990).

J. F. Bringley, B. A. Scott, S. J. La Placa, T. R. McGuire, F. Mehran, M. W. McElfresh, and D. E. Cox, *Phys. Rev. B* **47**, 15269–15275 (1993).

P. Burlet, V. P. Plakthy, C. Marin, and J. Y. Henry, *Phys. Lett. A* **167**, 401–404 (1992).

R. H. Buttner and E. N. Maslen, *Acta Cryst. B* **48**, 764–769 (1992).

V. Caignaert, I. Mirebeau, F. Bourée, N. Nguyen, A. Ducouret, J.-M. Grenèche, and B. Raveau, *J. Solid State Chem.* **114**, 24–35 (1995).

G. Calestani, C. Rizzoli, M. G. Francesconi, and G. D. Andreetti, *Physica C* **161**, 598–606 (1989).

G. Calestani, M. G. Francesconi, G. Salsi, and G. D. Andreetti, *Physica C* **197**, 283–298 (1992).

J. J. Capponi, C. Chaillout, A. W. Hewat, P. Lejay, M. Marezio, N. Nguyen, B. Ravaeu, J. L. Soubeyroux, J. L. Tholence, and R. Tournier, *Europhys. Lett.* **3**, 1301–1307 (1987).

W. Carrilo-Cabrera and W. Göpel, *Physica C* **161**, 373–389 (1989).

R. J. Cava, B. Batlogg, C. H. Chen, E. A. Rietman, S. Zahurak, and D. Werder, *Phys. Rev. B* **36**, 5719–5722 (1987a).

R. J. Cava, B. Batlogg, R. B. van Dover, D. W. Murphy, S. Sunshine, T. Siegrist, J. P. Remeika, E. A. Rietman, S. Zahurak, and G. P. Espinosa, *Phys. Rev. Lett.* **58**, 1676–1679 (1987b).

R. J. Cava, A. Santoro, D. W. Johnson, Jr., and W. W. Rhodes, *Phys. Rev. B* **35**, 6716–6720 (1987c).

R. J. Cava, R. B. van Dover, B. Batlogg, and E. A. Rietman, *Phys. Rev. Lett.* **58**, 408–410 (1987d).

R. J. Cava, B. Batlogg, J. J. Krajewski, L. W. Rupp, L. F. Schneemeyer, T. Siegrist, R. B. Van Dover, P. Marsh, W. F. Peck, Jr., P. K. Gallagher, S. H. Glarum, J. H. Marshall, R. C. Farrow, J. V. Waszczak, R. Hull, and P. Trevor, *Nature* **336**, 211–214 (1988).

R. J. Cava, M. Marezio, J. J. Krajewski, W. F. Peck, Jr., A Santoro, and F. Beech, *Physica C* **157**, 272–278 (1989).

R. J. Cava, B. Batlogg, R. B. van Dover, J. J. Krajewski, J. V. Waszczak, R. M. Fleming, W. F. Peck, Jr., L. W. Rupp, Jr., P. Marsh, A. C. W. P. James, and L. F. Schneemeyer, *Nature* **345**, 602–604 (1990a).

R. J. Cava, A. Santoro, J. J. Krejewski, R. M. Fleming, J. V. Waszczak, W. F. Peck, Jr., and P. Marsh, *Physica C* **172**, 138–142 (1990b).

R. J. Cava, R. B. Van Dover, B. Batlogg, J. J. Krajewski, L. F. Schneemeyer, T. Siegrist, B. Hessen, S. H. Chen, W. F. Peck, Jr., and L. W. Rupp, Jr., *Physica C* **185–189**, 180–183 (1991).

R. J. Cava, J. J. Krajewski, H. Takagi, H. W. Zandbergen, R. B. Van Dover, W. F. Peck, Jr., and B. Hessen, *Physica C* **191**, 237–242 (1992).

C. Chaillout, M. A. Alario-Franco, J. J. Capponi, J. Chenavas, J. L. Hodeau, and M. Marezio, *Phys. Rev. B* **36**, 7118–7120 (1987).

C. Chaillout, J. Chenavas, S. W. Cheong, Z. Fisk, M. Marezio, B. Morosin, and J. E. Schirber, *Physica C* **170**, 87–94 (1990).
C. Chaillout, O. Chmaissem, J. J. Capponi, T. Fournier, G. J. McIntyre, and M. Marezio, *Physica C* **175**, 293–300 (1991).
C. Chaillout, Q. Huang, R. J. Cava, J. Chenavas, A. Santoro, P. Bordet, J. L. Hodeau, J. J. Krajewski, J. P. Levy, M. Marezio, and W. F. Peck, Jr., *Physica C* **195**, 335–344 (1992).
C. Chaillout, S. Le Floch, E. Gautier, P. Bordet, C. Acha, Y. Feng, A. Sulpice, J. L. Tholence, and M. Marezio, *Physica C* **266**, 215–222 (1996).
Z. Y. Chen, Z. Z. Sheng, Y. Q. Tang, Y. F. Li, and D. O. Pederson, *Mod. Phys. Lett. B* **6**, 1019–1023 (1992a).
Z. Y. Chen, Y. Q. Tang, Y. F. Li, D. O. Pederson, and Z. Z. Sheng, *Mat. Res. Bull.* **27**, 1049–1055 (1992b).
X. H. Chen, H. Chen, L. Z. Cao, Z. J. Chen, and G. E. Zhou, *Physica C* **217**, 342–346 (1993a).
X. Chen, Z. Ding, Y. Qian, Zh. Chen, Z. Chen, and L. Cao, *Physica C* **216**, 458–462 (1993b).
X. Chen, Z. Ding, Y. Qian, Z. Chen, Zh. Chen, and L. Cao, *Phys. Rev. B* **48**, 9799–9802 (1993c).
Z. Y. Chen, Z. Z. Sheng, Y. Q. Tang, Y. F. Li, D. O. Pederson, K. Goretta, P. Kostic, and D. L. Shi, *Physica C* **212**, 206–210 (1993d).
X. Chen, J. Liang, W. Tang, C. Wang, and G. Rao, *Phys. Rev. B* **52**, 16233–16236 (1995).
O. Chmaissem and Z. Z. Sheng, *Z. Phys. B* **99**, 179–184 (1996).
O. Chmaissem, Q. Huang, E. V. Antipov, S. N. Putilin, M. Marezio, S. M. Loureiro, J. J. Capponi, J. L. Tholence, and A. Santoro, *Physica C* **217**, 265–272 (1993).
O. Chmaissem, L. Wessels, and Z. Z. Sheng, *Physica C* **228**, 190–194 (1994).
O. Chmaissem, D. N. Argyriou, D. G. Hinks, J. D. Jorgensen, B. G. Storey, H. Zhang, L. D. Marks, Y. Y. Wang, V. P. Dravid, and B. Dabrowski, *Phys. Rev. B* **52**, 15636–15643 (1995).
O. Chmaissem, J. D. Jorgensen, K. Yamaura, Z. Hiroi, M. Takano, J. Shimoyama, and K. Kishio, *Phys. Rev. B* **53**, 14647–14655 (1996).
C. W. Chu, J. Bechtold, L. Gao, P. H. Hor, Z. J. Huang, R. L. Meng, Y. Y. Sun, Y. Q. Wang, and Y. Y. Xue, *Phys. Rev. Lett.* **60**, 941–943 (1988).
C. W. Chu, L. Gao, F. Chen, Z. J. Huang, R. L. Meng, and Y. Y. Xue, *Nature* **365**, 323–325 (1993).
G. Collin, A. C. Audier, and R. Comes, *J. Phys. France* **49**, 383–387 (1988).
M. K. Crawford, R. L. Harlow, E. M. McCarron, W. E. Farneth, J. D. Axe, H. Chou, and Q. Huang, *Phys. Rev. B* **44**, 7749–7752 (1991).
D. B. Currie and M. T. Weller, *Physica C* **214**, 204–213 (1993).
D. B. Currie, M. T. Weller, P. C. Lanchester, and R. Walia, *Physica C* **224**, 43–50 (1994).
B. Dabrowski, P. Radaelli, D. G. Hinks, A. W. Mitchell, J. T. Vaughey, D. A. Groenke, and K. R. Poeppelmeier, *Physica C* **193**, 63–67 (1992).
P. Dai, B. C. Chakoumakos, G. F. Sun, K. W. Wong, Y. Xin, and D. F. Lu, *Physica C* **243**, 201–206 (1995).
S. Darracq, G. Demazeau, F. Tresse, A. Largeteau, and K. A. Müller, *Eur. J. Solid State Inorg. Chem.* **31**, 301–312 (1994).
S. Darracq, G. Demazeau, and A. Largeteau, *Solid State Commun.* **94**, 629–634 (1995a).
S. Darracq, S. G. Kang, J. H. Choy, and G. Demazeau, *J. Solid State Chem.* **114**, 88–94 (1995b).
J. Darriet, F. Weill, B. Darriet, X. F. Zhang, and J. Etourneau, *Solid State Commun.* **86**, 227–230 (1993).
P. Day, M. Rosseinsky, K. Prassides, W. I. F. David, O. Moze, and A. Soper, *J. Phys. C* **20**, L429–L434 (1987).
G. Demazeau, C. Parent, M. Pouchard, and P. Hagenmuller, *Mat. Res. Bull.* **7**, 913–920 (1972).
T. Den, T. Kobayashi, F. Izumi, T. Kamiyama, Y. Shimakawa, J. D. Jorgensen, F. J. Rotella, and R. L. Hitterman, *Physica C* **255**, 37–52 (1995).
C. de Rango, G. Tsoucaris, and C. Zelwer, *C. R. Acad. Sci. Paris* **259**, 1537–1539 (1964).
B. Domengès, M. Hervieu, and B. Raveau, *Physica C* **207**, 65–78 (1993).
B. Domengès, Ph. Boullay, M. Hervieu, and B. Raveau, *J. Solid State Chem.* **108**, 219–229 (1994).

A. Ehmann, S. Kemmler-Sack, S. Lösch, M. Schlichenmaier, W. Wischert, P. Zoller, T. Nissel, and R. P. Huebener, *Physica C* **198**, 1–6 (1992).
U. Endo, S. Koyama, and T. Kawai, *Jpn. J. Appl. Phys.* **27**, L1476–L1479 (1988).
G. Er, Y. Miyamoto, F. Kanamaru, and S. Kikkawa, *Physica C* **181**, 206–208 (1991).
G. Er, S. Kikkawa, F. Kanamaru, Y. Miyamoto, S. Tanaka, M. Sera, M. Sato, Z. Hiroi, M. Takano, and Y. Bando, *Physica C* **196**, 271–275 (1992).
L. Er-Rakho, C. Michel, Ph. Lacorre, and B. Raveau, *J. Solid State Chem.* **73**, 531–535 (1988).
L. W. Finger, R. M. Hazen, R. T. Downs, R. L. Meng, and C. W. Chu, *Physica C* **226**, 216–221 (1994).
P. Fischer, J. Karpinski, E. Kaldis, E. Jilek, and S. Rusiecki, *Solid State Commun.* **69**, 531–533 (1989).
Z. Fisk, S.-W. Cheong, J. D. Thompson, M. F. Hundley, R. B. Schwarz, G. H. Kwei, and J. E. Schirber, *Physica C* **162–164**, 1681–1686 (1989).
M. François, A. Junod, K. Yvon, A. W. Hewat, J. J. Capponi, P. Strobel, M. Marezio, and P. Fischer, *Solid State Commun.* **66**, 1117–1125 (1988).
W. T. Fu, H. W. Zandbergen, W. G. Haije, and L. J. De Jongh, *Physica C* **159**, 210–214 (1989).
H. Fujishita, S. Yamagata, and M. Sato, *J. Phys. Soc. Jap.* **60**, 913–920 (1991).
H. Fujishita, M. Sato, Y. Morii, and S. Funahashi, *Physica C* **210**, 529–535 (1993).
A. Fukuoka, S. Adachi, T. Sugano, X.-J. Wu, and H. Yamauchi, *Physica C* **231**, 372–376 (1994).
N. Fukushima, H. Niu, S. Nakamura, S. Takeno, M. Hayashi, and K. Ando, *Physica C* **159**, 777–783 (1989).
R. L. Fuller and M. Greenblatt, *J. Solid State Chem.* **92**, 386–400 (1991).
Ph. Galez and G. Collin, *J. Phys. France* **51**, 579–586 (1990).
A. K. Ganguli and M. A. Subramanian, *J. Solid State Chem.* **93**, 250–255 (1991).
A. K. Ganguli, K. S. Nanjundaswamy, and C. N. R. Rao, *Physica C* **156**, 788–790 (1988).
Y. Gao, P. Lee, P. Coppens, M. A. Subramanian, and A. W. Sleight, *Science* **241**, 954–956 (1988).
Y. Gao, P. Coppens, D. E. Cox, and A. R. Moodenbaugh, *Acta Cryst. A* **49**, 141–148 (1993).
S. Geller and V. B. Bala, *Acta Cryst.* **9**, 1019–1025 (1956).
J.-Y. Genoud, T. Graf, A. Junod, D. Sanchez, G. Triscone, and J. Muller, *Physica C* **177**, 315–329 (1991).
J.-Y. Genoud, T. Graf, G. Triscone, A. Junod, and J. Muller, *Physica C* **192**, 137–146 (1992).
R. E. Gladyshevskii and R. Flükiger, *Acta Cryst. B* **52**, 38–53 (1996).
R. E. Gladyshevskii, Ph. Galez, K. Lebbou, J. Allemand, R. Abraham, M. Couach, R. Flükiger, J.-L. Jorda, and M. Th. Cohen-Adad, *Physica C* **267**, 93–105 (1996).
D. Goldschmidt, G. M. Reisner, Y. Direktovitch, A. Knizhnik, E. Gartstein, G. Kimmel, and Y. Eckstein, *Phys. Rev. B* **48**, 532–542 (1993).
J. B. Goodenough, G. Demazeau, M. Pouchard, and P. Hagenmuller, *J. Solid State Chem.* **8**, 325–330 (1973).
T. J. Goodwin, H. B. Radousky, and R. N. Shelton, *Physica C* **204**, 212–224 (1992).
I. K. Gopalakrishnan, J. V. Yakhmi, and R. M. Iyer, *Physica C* **175**, 183–186 (1991).
F. Goutenoire, P. Daniel, M. Hervieu, G. van Tendeloo, C. Michel, A. Maignan, and B. Raveau, *Physica C* **216**, 243–249 (1993a).
F. Goutenoire, M. Hervieu, A. Maignan, C. Michel, C. Martin, and B. Raveau, *Physica C* **210**, 359–366 (1993b).
B. Grande, H. Müller-Buschbaum, and M. Schweizer, *Z. Anorg. Allg. Chem.* **428**, 120–124 (1977).
P. M. Grant, R. B. Beyers, E. M. Engler, G. Lim, S. S. P. Parkin, M. L. Ramirez, V. Y. Lee, A. Nazzal, J. E. Vazquez, and R. J. Savoy, *Phys. Rev. B* **35**, 7242–7244 (1987).
J. E. Greedan, A. H. O'Reilly, and C. V. Stager, *Phys. Rev. B* **35**, 8770–8773 (1987).
J. Grybos, D. Hohlwein, and F. Kubanek, *Physica C* **244**, 349–356 (1995).
M. Guillaume, P. Allenspach, W. Henggeler, J. Mesot, B. Roessli, U. Staub, P. Fischer, A. Furrer, and V. Trounov, *J. Phys. Cond. Matt.* **6**, 7963–7976 (1994).
T. Hahn (Ed.), *International Tables for Crystallography*, Vol. A. Reidel, Dordrecht (distributor Kluwer, Dordrecht), 1983.

P. Haldar, S. Sridhar, A. Roig-Janicki, W. Kennedy, D. H. Wu, C. Zahopoulos, and B. C. Giessen, *J. Superconduct.* **1**, 211–218 (1988).
P. D. Han, L. Chang, and D. A. Payne, *Physica C* **228**, 129–136 (1994).
R. M. Hazen, L. W. Finger, R. J. Angel, C. T. Prewitt, N. L. Ross, H. K. Mao, C. G. Hadidiacos, P. H. Hor, R. L. Meng, and C. W. Chu, *Phys. Rev. B* **35**, 7238–7241 (1987).
R. M. Hazen, L. W. Finger, R. J. Angel, C. T. Prewitt, N. L. Ross, C. G. Hadidiacos, P. J. Heaney, D. R. Veblen, Z. Z. Sheng, A. El Ali, and A. M. Hermann, *Phys. Rev. Lett.* **60**, 1657–1660 (1988a).
R. M. Hazen, C. T. Prewitt, R. J. Angel, N. L. Ross, L. W. Finger, C. G. Hadidiacos, D. R. Veblen, P. J. Heaney, P. H. Hor, R. L. Meng, Y. Y. Sun, Y. Q. Wang, Y. Y. Xue, Z. J. Huang, L. Gao, J. Bechtold, and C. W. Chu, *Phys. Rev. Lett.* **60**, 1174–1177 (1988b).
R. M. Hazen, L. W. Finger, and D. E. Morris, *Appl. Phys. Lett.* **54**, 1057–1059 (1989).
M. Hervieu, A. Maignan, C. Martin, C. Michel, J. Provost, and B. Raveau, *Mod. Phys. Lett. B* **2**, 1103–1109 (1988a).
M. Hervieu, C. Michel, A. Maignan, C. Martin, and B. Raveau, *J. Solid State Chem.* **74**, 428–432 (1988b).
M. Hervieu, G. Van Tendeloo, A. Maignan, C. Michel, F. Goutenoire, and B. Raveau, *Physica C* **216**, 264–272 (1993).
M. Hervieu, C. Michel, R. Genouel, A. Maignan, and B. Raveau, *J. Solid State Chem.* **115**, 1–6 (1995a).
M. Hervieu, G. Van Tendeloo, C. Michel, C. Martin, A. Maignan, and B. Raveau, *J. Solid State Chem.* **115**, 525–531 (1995b).
C. J. D. Hetherington, R. Ramesh, M. A. O'Keefe, R. Kilaas, G. Thomas, S. M. Green, and H. L. Luo, *Appl. Phys. Lett.* **53**, 1016–1018 (1988).
A. W. Hewat, P. Bordet, J. J. Capponi, C. Chaillout, J. Chenavas, M. Godinho, E. A. Hewat, J. L. Hodeau, and M. Marezio, *Physica C* **156**, 369–374 (1988).
C. A. Hijar, C. L. Stern, K. R. Poeppelmeier, K. Rogacki, Z. Chen, and B. Dabrowski, *Physica C* **252**, 13–21 (1995).
Z. Hiroi and M. Takano, *Physica C* **235–240**, 29–32 (1994).
Z. Hiroi, M. Azuma, M. Takano, and Y. Bando, *J. Solid State Chem.* **95**, 230–238 (1991).
Z. Hiroi, M. Azuma, M. Takano, and Y. Takeda, *Physica C* **208**, 286–296 (1993a).
Z. Hiroi, M. Takano, M. Azuma, and Y. Takeda, *Nature* **364**, 315–317 (1993b).
J. P. Hodges, P. R. Slater, P. P. Edwards, C. Greaves, M. Slaski, G. Van Tendeloo, and S. Amelinckx, *Physica C* **260**, 249–256 (1996).
T. C. Huang, V. Y. Lee, R. Karimi, R. Beyers, and S. S. P. Parkin, *Mat. Res. Bull.* **23**, 1307–1314 (1988).
J. Huang, R.-D. Hoffmann, and A. W. Sleight, *Mat. Res. Bull.* **25**, 1085–1090 (1990).
Q. Huang, O. Chmaissem, J. J. Capponi, C. Chaillout, M. Marezio, J. L. Tholence, and A. Santoro, *Physica C* **227**, 1–9 (1994a).
Q. Huang, P. Karen, V. L. Karen, A. Kjekshus, J. W. Lynn, A. D. Mighell, I. Natali Sora, N. Rosov, and A. Santoro, *J. Solid State Chem.* **108**, 80–86 (1994b).
Q. Huang, J. W. Lynn, Q. Xiong, and W. Chu, *Phys. Rev. B* **52**, 462–470 (1995).
M. F. Hundley, J. D. Thompson, S.-W. Cheong, Z. Fisk, R. B. Schwarz, and J. E. Schirber, *Phys. Rev. B* **40**, 5251–5254 (1989).
B. A. Hunter, J. D. Jorgensen, J. L. Wagner, P. G. Radaelli, D. G. Hinks, H. Shaked, R. L. Hitterman, and R. B. Von Dreele, *Physica C* **221**, 1–10 (1994).
N. H. Hur, N. H. Kim, S. H. Kim, Y. K. Park, and J. C. Park, *Physica C* **231**, 227–232 (1994).
N. H. Hur, B. C. Chakoumakos, M. Paranthaman, J. R. Thompson, and D. K. Christen, *Physica C* **253**, 109–114 (1995).
N. H. Hur, M. Paranthaman, J. R. Thompson, and D. K. Christen, *Physica C* **268**, 266–270 (1996).
M. Huvé, C. Martin, C. Michel, A. Maignan, M. Hervieu, and B. Raveau, *J. Phys. Chem. Solids* **54**, 145–152 (1993a).
M. Huvé, C. Michel, A. Maignan, M. Hervieu, C. Martin, and B. Raveau, *Physica C* **205**, 219–224 (1993b).

M. Huvé, C. Martin, A. Maignan, C. Michel, G. Van Tendeloo, M. Hervieu, and B. Raveau, *J. Solid State Chem.* **114**, 230–235 (1995).

A. Ichinose, T. Wada, Y. Yaegashi, A. Nara, H. Yamauchi, and S. Tanaka, *Physica C* **192**, 1–7 (1992).

H. Ihara, R. Sugise, M. Hirabayashi, N. Terada, M. Jo, K. Hayashi, A. Negishi, M. Tokumoto, Y. Kimura, and T. Shimomura, *Nature* **334**, 510–511 (1988).

H. Ihara, K. Tokiwa, H. Ozawa, M. Hirabayashi, H. Matuhata, A. Negishi, and Y. S. Song, *Jpn. J. Appl. Phys.* **33**, L300–L303 (1994a).

H. Ihara, K. Tokiwa, H. Ozawa, M. Hirabayashi, A. Negishi, H. Matuhata, and Y. S. Song, *Jpn. J. Appl. Phys.* **33**, L503–L506 (1994b).

S. Ikeda, H. Ichinose, T. Kimura, T. Matsumoto, H. Maeda, Y. Ishida, and K. Ogawa, *Jpn. J. Appl. Phys.* **27**, L999–L1002 (1988a).

Y. Ikeda, M. Takano, Z. Hiroi, K. Oda, H. Kitaguchi, J. Takada, Y. Miura, Y. Takeda, O. Yamamoto, and H. Mazaki, *Jpn. J. Appl. Phys.* **27**, L2067–L2070 (1988b).

N. Ikeda, Z. Hiroi, M. Azuma, M. Takano, Y. Bando, and Y. Takeda, *Physica C* **210**, 367–372 (1993).

A. S. Ilyushin, L. Shi, L. I. Leonyuk, B. M. Mustafa, I. A. Nikanorova, S. V. Red'ko, Y. Jia, A. G. Vetkin, G. Zhou, and I. V. Zubov, *J. Mater. Res.* **8**, 1791–1797 (1993).

K. Imai, I. Nakai, T. Kawashima, S. Sueno, and A. Ono, *Jpn. J. Appl. Phys.* **27**, L1661–L1664 (1988).

Z. Inoue, S. Sasaki, N. Iyi, and S. Takekawa, *Jpn. J. Appl. Phys.* **26**, L1365–L1367 (1987).

Z. Iqbal, A. P. B. Sinha, D. E. Morris, J. C. Barry, G. J. Auchterlonie, and B. L. Ramakrishna, *J. Appl. Phys.* **70**, 2234–2237 (1991).

T. Ishigaki, H. Asano, and K. Takita, *Jpn. J. Appl. Phys.* **26**, L987–L988 (1987a).

T. Ishigaki, H. Asano, and K. Takita, *Jpn. J. Appl. Phys.* **26**, L1226–L1227 (1987b).

T. Ishigaki, A. Tokiwa-Yamamoto, F. Izumi, T. Kamiyama, H. Asano, and Y. Syono, *Physica C* **231**, 357–366 (1994).

M. Isobe, T. Kawashima, K. Kosuda, Y. Matsui, and E. Takayama-Muromachi, *Physica C* **234**, 120–126 (1994).

M. Isobe, J.-Q. Li, Y. Matsui, F. Izumi, Y. Kanke, and E. Takayama- Muromachi, *Physica C* **269**, 5–14 (1996a).

M. Isobe, Y. Matsui, and E. Takayama-Muromachi, *Physica C* **273**, 72–82 (1996b).

F. Izumi, H. Asano, and T. Ishigaki, *Jpn. J. Appl. Phys.* **26**, L617–L618 (1987a).

F. Izumi, H. Asano, T. Ishigaki, E. Takayama-Muromachi, Y. Uchida, N. Watanabe, and T. Nishikawa, *Jpn. J. Appl. Phys.* **26**, L649–L651 (1987b).

F. Izumi, E. Takayama-Muromachi, M. Kobayashi, Y. Uchida, H. Asano, T. Ishigaki, and N. Watanabe, *Jpn. J. Appl. Phys.* **27**, L824–L826 (1988).

F. Izumi, H. Kito, H. Sawa, J. Akimitsu, and H. Asano, *Physica C* **160**, 235–242 (1989a).

F. Izumi, Y. Matsui, H. Takagi, S. Uchida, Y. Tokura, and H. Asano, *Physica C* **158**, 433–439 (1989b).

F. Izumi, E. Takayama-Muromachi, A. Fujimori, T. Kamiyama, H. Asano, J. Akimitsu, and H. Sawa, *Physica C* **158**, 440–448 (1989c).

F. Izumi, K. Kinoshita, Y. Matsui, K. Yanagisawa, T. Ishigaki, T. Kamiyama, T. Yamada, and H. Asano, *Physica C* **196**, 227–235 (1992).

A. C. W. P. James, S. M. Zahurak, and D. W. Murphy, *Nature* **338**, 240–241 (1989).

R. A. Jennings and C. Greaves, *Physica C* **235–240**, 989–990 (1994).

C.-Q. Jin, S. Adachi, X.-J. Wu, H. Yamauchi, and S. Tanaka, *Physica C* **223**, 238–242 (1994).

C.-Q. Jin, X.-J. Wu, P. Laffez, T. Tatsuki, T. Tamura, S. Adachi, H. Yamauchi, N. Koshizuka, and S. Tanaka, *Nature* **375**, 301–303 (1995).

L.-G. Johansson, C. Ström, S. Eriksson, and I. Bryntse, *Physica C* **220**, 295–302 (1994).

J. L. Jorda, T. K. Jondo, R. Abraham, M. T. Cohen-Adad, C. Opagiste, M. Couach, A. Khoder, and F. Sibieude, *Physica C* **205**, 122–185 (1993).

J. L. Jorda, T. K. Jondo, R. Abraham, M. T. Cohen-Adad, C. Opagiste, M. Couach, A. F. Khoder, and G. Triscone, *J. Alloys Comp.* **215**, 135–140 (1994).
J. D. Jorgensen, M. A. Beno, D. G. Hinks, L. Soderholm, K. J. Volin, R. L. Hitterman, J. D. Grace, I. K. Schuller, C. U. Segre, K. Zhang, and M. S. Kleefisch, *Phys. Rev. B* **36**, 3608–3616 (1987a).
J. D. Jorgensen, H.-B. Schüttler, D. G. Hinks, D. W. Capone II, K. Zhang, M. B. Brodsky, and D. J. Scalapino, *Phys. Rev. Lett.* **58**, 1024–1027 (1987b).
J. D. Jorgensen, B. W. Veal, A. P. Paulikas, L. J. Nowicki, G. W. Crabtree, H. Claus, and W. K. Kwok, *Phys. Rev. B* **41**, 1863–1877 (1990).
J. D. Jorgensen, P. G. Radaelli, D. G. Hinks, J. L. Wagner, S. Kikkawa, G. Er, and F. Kanamaru, *Phys. Rev. B* **47**, 14654–14656 (1993).
T. Kajitani, K. Kusaba, M. Kikuchi, N. Kobayashi, Y. Syono, T. B. Williams, and M. Hirabayashi, *Jpn. J. Appl. Phys.* **27**, L587–L590 (1988).
T. Kaneko, T. Wada, A. Ichinose, H. Yamauchi, and S. Tanaka, *Physica C* **177**, 153–158 (1991).
P. Karen and A. Kjekshus, *Solid State Chem.* **94**, 298–305 (1991).
J. Karpinski, personal communication (1997).
J. Karpinski, C. Beeli, E. Kaldis, A. Wisard, and E. Jilek, *Physica C* **153–155**, 830–831 (1988a).
J. Karpinski, E. Kaldis, E. Jilek, S. Rusiecki, and B. Bucher, *Nature* **336**, 660–662 (1988b).
J. Karpinski, H. Schwer, I. Mangelschots, K. Conder, A. Morawski, T. Lada, and A. Paszewin, *Physica C* **234**, 10–18 (1994).
M. Karppinen, H. Yamauchi, H. Suematsu, and O. Fukunaga, *Physica C* **264**, 268–274 (1996).
M. Kato, T. Miyajima, A. Sakuma, T. Noji, Y. Koike, A. Fujiwara, and Y. Saito, *Physica C* **244**, 263–270 (1995).
M. Kato, H. Chizawa, Y. Ono, and Y. Koike, *Physica C* **256**, 253–260 (1996).
T. Kawashima and E. Takayama-Muromachi, *Physica C* **267**, 106–112 (1996).
T. Kawashima, Y. Matsui, and E. Takayama-Muromachi, *Physica C* **224**, 69–74 (1994a).
T. Kawashima, Y. Matsui, and E. Takayama-Muromachi, *Physica C* **227**, 95–101 (1994b).
T. Kawashima, Y. Matsui, and E. Takayama-Muromachi, *Physica C* **233**, 143–148 (1994c).
T. Kawashima, Y. Matsui, and E. Takayama-Muromachi, *Physica C* **254**, 131–136 (1995).
T. Kawashima, Y. Matsui, and E. Takayama-Muromachi, *Physica C* **257**, 313–320 (1996).
S. M. Kazakov, E. V. Antipov, C. Chaillout, J. J. Capponi, M. Brunner, J. L. Tholence, and M. Marezio, *Physica C* **253**, 401–406 (1995).
S. M. Kazakov, S. Pachot, E. M. Kopnin, S. N. Putilin, E. V. Antipov, C. Chaillout, J. J. Capponi, P. G. Radaelli, and M. Marezio, *Physica C* **276**, 139–146 (1997).
P. M. Keane, D. G. Hinks, U. Geiser, and J. M. Williams, *Physica C* **226**, 353–359 (1994).
A. L. Kharlanov, E. V. Antipov, L. M. Kovba, L. G. Akselrud, I. G. Muttik, A. A. Gippius, and V. V. Moshchalkov, *Physica C* **169**, 469–475 (1990).
N. R. Khasanova and E. V. Antipov, *Physica C* **246**, 241–252 (1995).
N. R. Khasanova, F. Izumi, M. Shida, B. C. Chakoumakos, E. Ohshima, M. Kikuchi, and Y. Syono, *Physica C* **269**, 115–123 (1996a).
N. R. Khasanova, F. Izumi, E. Takayama-Muromachi, and A. W. Hewat, *Physica C* **258**, 227–235 (1996b).
N. Kijima, H. Endo, J. Tsuchiya, A. Sumiyama, M. Mizuno, and Y. Oguri, *Jpn. J. Appl. Phys.* **28**, L787–L790 (1989).
N. Kijima and R. Gronsky, *Jpn. J. Appl. Phys.* **31**, L82–L85 (1992).
M. Kikuchi, T. Kajitani, T. Suzuki, S. Nakajima, K. Hiraga, N. Kobayashi, H. Iwasaki, Y. Syono, and Y. Muto, *Jpn. J. Appl. Phys.* **28**, L382–L385 (1989).
J. S. Kim, J. S. Swinnea, and H. Steinfink, *J. Less-Comm. Met.* **156**, 347–355 (1989).
J. S. Kim, J. Y. Lee, J. S. Swinnea, H. Steinfink, W. M. Reiff, P. Lightfoot, S. Pei, and J. D. Jorgensen, *J. Solid State Chem.* **90**, 331–343 (1991).
S. H. Kim, H. S. Kim, S. H. Lee, and K. H. Kim, *Solid State Commun.* **83**, 127–131 (1992).
K. Kinoshita and T. Yamada, *Nature* **357**, 313–315 (1992a).

K. Kinoshita and T. Yamada, *Phys. Rev. B* **46**, 9116–9122 (1992b).
K. Kinoshita, H. Shibata, and T. Yamada, *Physica C* **176**, 433–440 (1991).
K. Kinoshita, F. Izumi, T. Yamada, and H. Asano, *Phys. Rev. B* **45**, 5558–5562 (1992).
Y. Koike, K. Sasaki, A. Fujiwara, M. Mochida, T. Noji, and Y. Saito, *Physica C* **208**, 363–370 (1993).
Y. Koike, T. Hisaki, K. Sasaki, A. Fujiwara, T. Noji, and Y. Saito, *Physica C* **224**, 31–37 (1994).
N. N. Kolesnikov, V. E. Korotkov, M. P. Kulakov, G. A. Lagvenov, V. N. Molchanov, L. A. Muradyan, V. I. Simonov, R. A. Tanazyan, R. P. Shibaeva, and I. F. Shchegolev, *Physica C* **162–164**, 1663–1664 (1989).
S. Kondoh, Y. Ando, M. Onoda, M. Sato, and J. Akimitsu, *Solid State Commun.* **65**, 1329–1331 (1988).
E. M. Kopnin, A. L. Kharlanov, I. Bryntse, and E. V. Antipov, *Physica C* **219**, 47–56 (1994).
E. M. Kopnin, M. V. Lobanov, A. M. Abakumov, S. V. Lubarskii, O. I. Lebedev, E. V. Antipov, and J. J. Capponi, *Physica C* **241**, 63–68 (1996).
S. Koyama, U. Endo, and T. Kawai, *Jpn. J. Appl. Phys.* **27**, L1861–L1863 (1988).
Y. Koyama, Y. Wakabayashi, K. Ito, and Y. Inoue, *Phys. Rev. B* **51**, 9045–9051 (1995).
M. J. Kramer, S. I. Yoo, R. W. McCallum, W. B. Yelon, H. Xie, and P. Allenspach, *Physica C* **219**, 145–155 (1994).
K. Kumagai, K. Kawano, I. Watanabe, K. Nishiyama, and K. Nagamine, *J. Superconduct.* **7**, 63–67 (1994).
G. H. Kwei, R. B. Von Dreele, S.-W. Cheong, Z. Fisk, and J. D. Thompson, *Phys. Rev. B* **41**, 1889–1893 (1990).
G. H. Kwei, A. C. Lawson, S. J. L. Billinge, and S.-W. Cheong, *J. Phys. Chem.* **97**, 2368–2377 (1993).
S. J. La Placa, J. F. Bringley, B. A. Scott, and D. E. Cox, *J. Solid State Chem.* **118**, 170–175 (1995).
M. Ledésert, A. Maignan, J. Chardon, C. Martin, Ph. Labbé, M. Hervieu, and B. Raveau, *Physica C* **232**, 387–395 (1994).
J. Y. Lee, J. S. Swinnea, and H. Steinfink, *J. Mater. Res.* **4**, 763–766 (1989).
W. H. Lee and D. C. Wang, *Physica C* **253**, 156–164 (1995).
E. Lee, S. Wu, W. Zhou, and W. Y. Liang, *J. Appl. Phys.* **80**, 326–330 (1996).
H. Leligny, S. Durčok, P. Labbe, L. Ledesert, and B. Raveau, *Acta Cryst. B* **48**, 407–418 (1992).
Y. LePage, W. R. McKinnon, J. M. Tarascon, L. H. Greene, G. W. Hull, and D. M. Hwang, *Phys. Rev. B* **35**, 7245–7248 (1987).
Y. LePage, W. R. McKinnon, J.-M. Tarascon, and P. Barboux, *Phys. Rev. B* **40**, 6810–6816 (1989).
F. Letouzé, C. Martin, A. Maignan, C. Michel, M. Hervieu, and B. Raveau, *Physica C* **254**, 33–43 (1995).
F. Letouzé, M. Huvé, C. Martin, A. Maignan, C. Michel, M. Hervieu, and B. Raveau, *Mat. Res. Bull.* **31**, 657–663 (1996).
G. R. Levi and G. Natta, *Rend. Acc. Naz. Lincei* **2**, 1–8 (1925).
A. A. Levin, Yu. I. Smolin, and Yu. F. Shepelev, *J. Phys. Cond. Matt.* **6**, 3539–3551 (1994).
R. Li, *J. Solid State Chem.* **114**, 57–60 (1995).
S. Li and M. Greenblatt, *Physica C* **157**, 365–369 (1989).
S. Li, E. A. Hayri, K. V. Ramanujachary, and M. Greenblatt, *Phys. Rev. B* **38**, 2450–2454 (1988).
R. Li, Y. Zhu, C. Xu, Z. Chen, Y. Qian, and C. Fan, *J. Solid State Chem.* **94**, 206–209 (1991).
R. Li, R. K. Kremer, and J. Maier, *Physica C* **200**, 344–348 (1992a).
R. Li, K. Tang, Y. Qian, and Z. Chen, *Mat. Res. Bull.* **27**, 349–355 (1992b).
R. Li, R. K. Kremer, and J. Maier, *Physica C* **213**, 26–32 (1993).
Y. F. Li, Z. Z. Sheng, S. Sengupta, K. C. Goretta, and P. E. D. Morgan, *Physica C* **232**, 184–188 (1994).
R. Li, D. Chen, and Y. Li, *Physica C* **247**, 62–66 (1995a).
Y. F. Li, O. Chmaissem, and Z. Z. Sheng, *Physica C* **248**, 42–48 (1995b).
P. Lightfoot, S. Pei, J. D. Jorgensen, X.-X. Tang, A. Manthiram, and J. B. Goodenough, *Physica C* **169**, 15–22 (1990a).

P. Lightfoot, S. Pei, J. D. Jorgensen, X.-X. Tang, A. Manthiram, and J. B. Goodenough, *Physica C* **169**, 464–468 (1990b).

R. S. Liu, S. F. Hu, I. Gameson, P. P. Edwards, A. Maignan, T. Rouillon, D. Groult, and B. Raveau, *J. Solid State Chem.* **93**, 276–282 (1991).

R. S. Liu, M. Hervieu, C. Michel, A. Maignan, C. Martin, B. Raveau, and P. P. Edwards, *Physica C* **197**, 131–135 (1992a).

R. S. Liu, S. D. Hughes, R. J. Angel, T. P. Hackwell, A. P. Mackenzie, and P. P. Edwards, *Physica C* **198**, 203–208 (1992b).

R. S. Liu, S. F. Hu, D. A. Jefferson, P. P. Edwards, and P. D. Hunneyball, *Physica C* **205**, 206–211 (1993a).

R. S. Liu, D. S. Shy, S. F. Hu, and D. A. Jefferson, *Physica C* **216**, 237–242 (1993b).

R. S. Liu, S. F. Hu, D. H. Chen, D. S. Shy, and D. A. Jefferson, *Physica C* **222**, 13–18 (1994).

R. C. Lobo, F. J. Berry, and C. Greaves, *J. Solid State Chem.* **88**, 513–519 (1990).

J. M. Longo and P. M. Raccah, *J. Solid State Chem.* **6**, 526–531 (1973).

S. M. Loureiro, E. V. Antipov, J. L. Tholence, J. J. Capponi, O. Chmaissem, Q. Huang, and M. Marezio, *Physica C* **217**, 253–264 (1993).

S. M. Loureiro, E. V. Antipov, E. T. Alexandre, E. Kopnin, M. F. Gorius, B. Souletie, M. Perroux, R. Argoud, O. Gheorghe, J. L. Tholence, and J. J. Capponi, *Physica C* **235–240**, 905–906 (1994).

S. M. Loureiro, E. T. Alexandre, E. V. Antipov, J. J. Capponi, S. de Brion, B. Souletie, J. L. Tholence, M. Marezio, Q. Huang, and A. Santoro, *Physica C* **243**, 1–9 (1995).

S. M. Loureiro, E. V. Antipov, E. M. Kopnin, M. Brunner, J. J. Capponi, and M. Marezio, *Physica C* **257**, 117–124 (1996a).

S. M. Loureiro, P. G. Radaelli, E. V. Antipov, J. J. Capponi, B. Souletie, M. Brunner, and M. Marezio, *J. Solid State Chem.* **121**, 66–73 (1996b).

C. K. Lowe-Ma and T. A. Vanderah, *Physica C* **201**, 233–248 (1992).

H. M. Luo, B. Qu, Z. Y. Chen, Y. T. Qian, and W. C. Yu, *Physica C* **270**, 249–252 (1996).

H. Maeda, Y. Tanaka, M. Fukutomi, and T. Asano, *Jpn. J. Appl. Phys.* **27**, L209–L210 (1988).

T. Maeda, K. Sakuyama, S. Koriyama, A. Ichinose, H. Yamauchi, and S. Tanaka, *Physica C* **169**, 133–136 (1990).

T. Maeda, K. Sakuyama, F. Izumi, H. Yamauchi, H. Asano, and S. Tanaka, *Physica C* **175**, 393–400 (1991a).

T. Maeda, K. Sakuyama, N. Sakai, H. Yamauchi, and S. Tanaka, *Physica C* **177**, 337–344 (1991b).

T. Maeda, N. Sakai, F. Izumi, T. Wada, H. Yamauchi, H. Asano, and S. Tanaka, *Physica C* **193**, 73–80 (1992).

Y. Maeno, H. Hashimoto, K. Yoshida, S. Nishizaki, T. Fujita, J. G. Bednorz, and F. Lichtenberg, *Nature* **372**, 532–534 (1994).

A. Maignan, C. Michel, M. Hervieu, C. Martin, D. Groult, and B. Raveau, *Mod. Phys. Lett. B* **2**, 681–687 (1988).

A. Maignan, D. Groult, R. S. Liu, T. Rouillon, P. Daniel, C. Michel, M. Hervieu, and B. Raveau, *J. Solid State Chem.* **102**, 31–39 (1993a).

A. Maignan, M. Hervieu, C. Michel, and B. Raveau, *Physica C* **208**, 116–120 (1993b).

A. Maignan, M. Huvé, C. Michel, M. Hervieu, C. Martin, and B. Raveau, *Physica C* **208**, 149–154 (1993c).

A. Maignan, D. Pelloquin, S. Malo, C. Michel, M. Hervieu, and B. Raveau, *Physica C* **243**, 233–242 (1995a).

A. Maignan, D. Pelloquin, S. Malo, C. Michel, M. Hervieu, and B. Raveau, *Physica C* **249**, 220–233 (1995b).

T. Manako and Y. Kubo, *Phys. Rev. B* **50**, 6402–6407 (1994).

T. Manako, Y. Shimakawa, Y. Kubo, T. Satoh, and H. Igarashi, *Physica C* **156**, 315–318 (1988).

T. Manako, Y. Shimakawa, Y. Kubo, T. Satoh, and H. Igarashi, *Physica C* **158**, 143–147 (1989).

J. B. Mandal, B. Bandyopadhyay, F. Fauth, T. Chattopadhyay, and B. Glosh, *Physica C* **264**, 145–153 (1996).

V. Manivannan, N. Rangavittal, J. Gopalakrishnan, and C. N. R. Rao, *Physica C* **208**, 253–258 (1993).
A. Manthiram and J. B. Goodenough, *Appl. Phys. Lett.* **53**, 420–422 (1988).
M. D. Marcos and J. P. Attfield, *Physica C* **270**, 267–273 (1996).
M. Marezio, *Acta Cryst. A* **47**, 640–654 (1991).
M. Marezio, A. Santoro, J. J. Capponi, E. A. Hewat, R. J. Cava, and F. Beech, *Physica C* **169**, 401–412 (1990).
J. T. Markert and M. B. Maple, *Solid State Commun.* **70**, 145–147 (1989).
J. T. Markert, C. L. Seaman, H. Zhou, and M. B. Maple, *Solid State Commun.* **66**, 387–391 (1988).
J. T. Markert, E. A. Early, T. Bjørnholm, S. Ghamaty, B. W. Lee, J. J. Neumeier, R. D. Price, C. L. Seaman, and M. B. Maple, *Physica C* **158**, 178–182 (1989).
P. Marsh, R. M. Fleming, M. L. Mandich, A. M. DeSantolo, J. Kwo, M. Hong, and L. J. Martinez-Miranda, *Nature* **334**, 141–143 (1988).
A. F. Marshall, R. W. Barton, K. Char, A. Kapitulnik, B. Oh, R. H. Hammond, and S. S. Laderman, *Phys. Rev. B* **37**, 9353–9358 (1988).
C. Martin, C. Michel, A. Maignan, M. Hervieu, and B. Raveau, *C. R. Acad. Sci. Paris* **307**, 27–32 (1988).
C. Martin, D. Bourgault, M. Hervieu, C. Michel, J. Provost, and B. Raveau, *Mod. Phys. Lett. B* **3**, 993–1000 (1989a).
C. Martin, J. Provost, D. Bourgault, B. Domengès, C. Michel, M. Hervieu, and B. Raveau, *Physica C* **157**, 460–468 (1989b).
C. Martin, M. Huve, G. Van Tendeloo, A. Maignan, C. Michel, M. Hervieu, and B. Raveau, *Physica C* **212**, 274–278 (1993a).
C. Martin, A. Maignan, M. Huve, Ph. Labbe, M. Ledésert, H. Leligny, and B. Raveau, *Physica C* **217**, 106–112 (1993b).
C. Martin, M. Hervieu, M. Huvé, C. Michel, A. Maignan, G. Van Tendeloo, and B. Raveau, *Physica C* **222**, 19–26 (1994).
C. Martin, M. Hervieu, G. Van Tendeloo, F. Goutenoire, C. Michel, A. Maignan, and B. Raveau, *Solid State Commun.* **93**, 53–56 (1995).
H. Matsuhata, H. Ihara, A. Iyo, K. Tokiwa, and H. Ozawa, *Physica C* **242**, 326–332 (1995).
Y. Matsui, M. Ogawa, M. Uehara, H. Nakata, and J. Akimitsu, *Physica C* **217**, 287–293 (1993).
Y. Matsui, T. Kawashima, and E. Takayama-Muromachi, *Physica C* **235–240**, 166–169 (1994).
A. T. Matveev and E. Takayama-Muromachi, *Physica C* **254**, 26–32 (1995).
A. T. Matveev, J. Ramirez-Castellanos, Y. Matsui, and E. Takayama-Muromachi, *Physica C* **262**, 279–284 (1996).
E. M. McCarron III, M. A. Subramanian, J. C. Calabrese, and R. L. Harlow, *Mat. Res. Bull.* **23**, 1355–1365 (1988).
H. D. Megaw, *Proc. R. Soc. London A* **189**, 261–283 (1947).
C. Michel and B. Raveau, *Rev. Chim. Min.* **21**, 407–425 (1984).
C. Michel, M. Hervieu, M. M. Borel, A. Grandin, F. Deslandes, J. Provost, and B. Raveau, *Z. Phys. B* **68**, 421–423 (1987).
C. Michel, M. Hervieu, and B. Raveau, *J. Solid State Chem.* **92**, 339–351 (1991a).
C. Michel, E. Suard, V. Caignaert, C. Martin, A. Maignan, M. Hervieu, and B. Raveau, *Physica C* **178**, 29–36 (1991b).
C. Michel, M. Hervieu, A. Maignan, D. Pelloquin, V. Badri, and B. Raveau, *Physica C* **241**, 1–9 (1995).
C. Michel, F. Letouzé, C. Martin, M. Hervieu, and B. Raveau, *Physica C* **262**, 159–167 (1996).
G. Miehe, T. Vogt, H. Fuess, and M. Wilhelm, *Physica C* **171**, 339–343 (1990).
L. L. Miller, X. L. Wang, S. X. Wang, C. Stassis, D. C. Johnston, J. Faber, Jr., and C.-K. Loong, *Phys. Rev. B* **41**, 1921–1925 (1990).
J. R. Min, J. K. Liang, X. L. Chen, C. Wang, C. Dong, and G. H. Rao, *Physica C* **230**, 389–396 (1994).
A. Mirmelstein, A. Podelsnyak, V. Voronin, S. Lebedev, B. Goshchitskii, P. Allenspach, J. Mesot, U. Staub, M. Guillaume, P. Fischer, and A. Furrer, *Physica C* **200**, 337–343 (1992).

T. Miyatake, S. Gotoh, N. Koshizuka, and S. Tanaka, *Nature* **341**, 41–42 (1989).
Y. Miyazaki, H. Yamane, T. Kajitani, T. Oku, K. Hiraga, Y. Morii, K. Fuchizaki, S. Funahashi, and T. Hirai, *Physica C* **191**, 434–440 (1992a).
Y. Miyazaki, H. Yamane, N. Kobayashi, T. Hirai, H. Nakata, K. Tominoto, and J. Akimitsu, *Physica C* **202**, 162–166 (1992b).
Y. Miyazaki, H. Yamane, N. Ohnishi, T. Kajitani, K. Hiraga, Y. Morii, S. Funahashi, and T. Hirai, *Physica C* **198**, 7–13 (1992c).
Y. Miyazaki, H. Yamane, T. Kajitani, Y. Morii, S. Funahashi, K. Hiraga, and T. Hirai, *Physica C* **215**, 159–166 (1993).
Y. Miyazaki, H. Yamane, T. Kajitani, N. Kobayashi, K. Hiraga, Y. Morii, S. Funahashi, and T. Hirai, *Physica C* **230**, 89–96 (1994).
V. N. Molchanov, R. A. Tamazyan, V. I. Simonov, M. K. Blomberg, M. J. Merisalo, and V. S. Mironov, *Physica C* **229**, 331–345 (1994).
P. E. D. Morgan, T. J. Doi, and R. M. Housley, *Physica C* **213**, 438–443 (1993).
K. Mori, Y. Kawaguchi, T. Ishigaki, S. Katano, S. Funahashi, and Y. Hamaguchi, *Physica C* **219**, 176–182 (1994).
B. Morosin, D. S. Ginley, P. F. Hlava, M. J. Carr, R. J. Baughman, J. E. Schirber, E. L. Venturini, and J. F. Kwak, *Physica C* **152**, 413–423 (1988).
B. Morosin, D. S. Ginley, E. L. Venturini, R. J. Baughman, and C. P. Tigges, *Physica C* **172**, 413–422 (1991a).
B. Morosin, E. L. Venturini, and D. S. Ginley, *Physica C* **175**, 241–249 (1991b).
B. Morosin, E. L. Venturini, and D. S. Ginley, *Physica C* **183**, 90–98 (1991c).
D. E. Morris, J. H. Nickel, J. Y. T. Wei, N. G. Asmar, J. S. Scott, U. M. Scheven, C. T. Hultgren, A. G. Markelz, J. E. Post, P. J. Heaney, D. R. Veblen, and R. M. Hazen, *Phys. Rev. B* **39**, 7347–7350 (1989).
H. Müller-Buschbaum and W. Wollschläger, *Angew. Chem. Int. Ed. Engl.* **28**, 1472–1493 (1989).
H. Müller-Buschbaum and W. Wollschläger, *Z. Anorg. Allg. Chem.* **414**, 76–80 (1975).
N. Murayama, E. Sudo, K. Kani, A. Tsuzuki, S. Kawakami, M. Awano, and Y. Torii, *Jpn. J. Appl. Phys.* **27**, L1623–L1625 (1988).
K. Nakahigashi, H. Sasakura, K. Watari, and S. Minamigawa, *Jpn. J. Appl. Phys.* **29**, L1856–L1858 (1990).
S. Nakajima, M. Kikuchi, Y. Syono, N. Kobayashi, and Y. Muto, *Physica C* **168**, 57–62 (1990).
S. Nakajima, T. Oku, K. Nagase, and Y. Syono, *Physica C* **262**, 1–6 (1996).
S. v. Náray-Szabó, *Naturwissenschaften* **31**, 466 (1943).
N. Nguyen, L. Er-Rakho, C. Michel, J. Choisnet, and B. Raveau, *Mat. Res. Bull.* **15**, 891–897 (1980).
H. Niu, N. Fukushima, S. Takeno, S. Nakamura, and K. Ando, *Jpn. J. Appl. Phys.* **28**, L784–L786 (1989).
T. Noda, M. Ogawa, J. Akimitsu, M. Kikuchi, E. Ohshima, and Y. Syono, *Physica C* **242**, 12–16 (1995).
M. Nuñes-Regueiro, J.-L. Tholence, E. V. Antipov, J.-J. Cappponi, and M. Marezio, *Science* **262**, 97–99 (1993).
D. M. Ogborne and M. T. Weller, *Physica C* **201**, 53–57 (1992).
D. M. Ogborne and M. T. Weller, *Physica C* **220**, 389–395 (1994a).
D. M. Ogborne and M. T. Weller, *Physica C* **223**, 283–290 (1994b).
D. M. Ogborne and M. T. Weller, *Physica C* **230**, 153–158 (1994c).
D. M. Ogborne, M. T. Weller, and P. C. Lanchester, *Physica C* **200**, 167–174 (1992a).
D. M. Ogborne, M. T. Weller, and P. C. Lanchester, *Physica C* **200**, 207–214 (1992b).
K. Oh-ishi, M. Kikuchi, Y. Syono, N. Kobayashi, T. Sasaoka, T. Matsuhira, Y. Muto, and H. Yamauchi, *Jpn. J. Appl. Phys.* **27**, L1449–L1452 (1988).
N. Ohnishi, Y. Miyazaki, H. Yamane, T. Kajitani, T. Hirai, and K. Hiraga, *Physica C* **207**, 175–184 (1993).
E. Ohshima, M. Kikuchi, M. Nagoshi, R. Suzuki, S. Nakajima, K. Nagase, and Y. Syono, *Physica C* **214**, 182–186 (1993).

E. Ohshima, M. Kikuchi, F. Izumi, K. Hiraga, T. Oku, S. Nakajima, N. Ohnishi, Y. Morii, S. Funahashi, and Y. Syono, *Physica C* **221**, 261–268 (1994).
H. Okada, M. Takano, and Y. Takeda, *Physica C* **166**, 111–114 (1990).
B. Okai, *Jpn. J. Appl. Phys.* **29**, L2180–L2182 (1990).
A. Ono and M. Tsutsumi, *Physica C* **271**, 325–330 (1996).
A. Ono, L. L. He, S. Horiushi, and A. Watanabe, *Physica C* **247**, 91–95 (1995).
M. Onoda and M. Sato, *Solid State Commun.* **67**, 799–804 (1988).
M. Onoda, S. Shamoto, M. Sato, and S. Hosoya, *Jpn. J. Appl. Phys.* **26**, L876–L878 (1987).
M. Onoda, S. Kondoh, K. Fukuda, and M. Sato, *Jpn. J. Appl. Phys.* **27**, L1234–L1236 (1988).
C. Opagiste, M. Couach, A. F. Khoder, R. Abraham, T. K. Jondo, J.-L. Jorda, M. Th. Cohen-Adad, A. Junod, G. Triscone, and J. Muller, *J. Alloys Comp.* **195**, 47–52 (1993a).
C. Opagiste, G. Triscone, M. Couach, T. K. Jondo, J.-L. Jorda, A. Junod, A. F. Khoder, and J. Muller, *Physica C* **213**, 17–25 (1993b).
M. R. Palacn, F. Krumeich, M. T. Caldés, and P. Gómez- Romero, *J. Solid State Chem.* **117**, 213–216 (1995).
M.-H. Pan and M. Greenblatt, *Physica C* **176**, 80–86 (1991).
M. Paranthaman and B. C. Chakoumakos, *J. Solid State Chem.* **122**, 221–230 (1996).
J. B. Parise, J. Gopalakrishnan, M. A. Subramanian, and A. W. Sleight, *J. Solid State Chem.* **76**, 432–436 (1988).
J. B. Parise, P. L. Gai, M. A. Subramanian, J. Gopalakrishnan, and A. W. Sleight, *Physica C* **159**, 245–254 (1989a).
J. B. Parise, N. Herron, M. K. Crawford, and P. L. Gai, *Physica C* **159**, 255–266 (1989b).
J. B. Parise, C. C. Torardi, M. A. Subramanian, J. Gopalakrishnan, A. W. Sleight, and E. Prince, *Physica C* **159**, 239–244 (1989c).
S. S. P. Parkin, V. Y. Lee, E. M. Engler, A. I. Nazzal, T. C. Huang, G. Gorman, R. Savoy, and R. Beyers, *Phys. Lett.* **60**, 2539–2542 (1988a).
S. S. P. Parkin, V. Y. Lee, A. I. Nazzal, R. Savoy, R. Beyers, and S. J. La Placa, *Phys. Rev. Lett.* **61**, 750–753 (1988b).
S. S. P. Parkin, V. Y. Lee, A. I. Nazzal, R. Savoy, T. C. Huang, G. Gorman, and R. Beyers, *Phys. Rev. B* **38**, 6531–6537 (1988c).
E. Parthé, L. Gelato, B. Chabot, M. Penzo, K. Cenzual and R. Gladyshevskii, *TYPIX Standardized Data and Crystal Chemical Characterization of Inorganic Structure Types*, *Gmelin Handbook of Inorganic and Organometallic Chemistry*, Vols. 1–4. Springer-Verlag, Heidelberg, 1993, 1994.
D. Pelloquin, M. Caldès, A. Maignan, C. Michel, M. Hervieu, and B. Raveau, *Physica C* **208**, 121–129 (1993a).
D. Pelloquin, M. Hervieu, C. Michel, G. Van Tendeloo, A. Maignan, and B. Raveau, *Physica C* **216**, 257–263 (1993b).
D. Pelloquin, A. Maignan, M. Caldès, M. Hervieu, C. Michel, and B. Raveau, *Physica C* **212**, 199–205 (1993c).
D. Pelloquin, M. Hervieu, C. Michel, A. Maignan, and B. Raveau, *Physica C* **227**, 215–224 (1994).
D. Pelloquin, M. Hervieu, S. Malo, C. Michel, A. Maignan, and B. Raveau, *Physica C* **246**, 1–10 (1995).
D. Pelloquin, C. Michel, M. Hervieu, F. Studer, and B. Raveau, *Physica C* **257**, 195–209 (1996a).
D. Pelloquin, A. Sundaresan, M. Hervieu, C. Michel, and B. Raveau, *J. Solid State Chem.* **127**, 315–324 (1996b).
V. Petricek, Y. Gao, P. Lee, and P. Coppens, *Phys. Rev. B* **42**, 387–392 (1990).
A. Q. Pham, C. Michel, M. Hervieu, A. Maignan, and B. Raveau, *J. Phys. Chem. Solids* **54**, 65–71 (1993).
V. Plakhty, P. Burlet, and J. Y. Henry, *Phys. Lett. A* **198**, 256–260 (1995).
C. Politis and H. L. Luo, *Mod. Phys. Lett. B* **2**, 793–798 (1988).

R. Prasad, N. C. Soni, K. Adhikary, S. K. Malik, and C. V. Tomy, *Solid State Commun.* **76**, 667–669 (1990).
S. N. Putilin, I. Bryntse, and E. V. Antipov, *Mat. Res. Bull.* **26**, 1299–1307 (1991).
S. N. Putilin, E. V. Antipov, O. Chmaissem, and M. Marezio, *Nature* **362**, 226–228 (1993a).
S. N. Putilin, E. V. Antipov, and M. Marezio, *Physica C* **212**, 266–270 (1993b).
P. G. Radaelli, J. D. Jorgensen, A. V. Schultz, B. A. Hunter, J. L. Wagner, F. C. Chou, and D. C. Johnston, *Phys. Rev. B* **48**, 499–510 (1993a).
P. G. Radaelli, J. L. Wagner, B. A. Hunter, M. A. Beno, G. S. Knapp, J. D. Jorgensen, and D. G. Hinks, *Physica C* **216**, 29–35 (1993b).
P. G. Radaelli, D. G. Hinks, A. W. Mitchell, B. A. Hunter, J. L. Wagner, B. Dabrowski, K. G. Vandervoort, H. K. Viswanathan, and J. D. Jorgensen, *Phys. Rev. B* **49**, 4163–4175 (1994a).
P. G. Radaelli, M. Marezio, M. Perroux, S. de Brion, J. L. Tholence, Q. Huang, and A. Santoro, *Science* **265**, 380–383 (1994b).
H. Rajagopal, A. Sequeira, J. V. Yakhmi, P. V. P. S. S. Sastry, and R. M. Iyer, *Jpn. J. Appl. Phys.* **32**, 1595–1600 (1993).
J. Ramirez-Castellanos, Y. Matsui, E. Takayama-Muromachi, and M. Isobe, *Physica C* **251**, 279–284 (1995).
C. N. R. Rao, A. K. Ganguli, and R. Vijayaraghavan, *Phys. Rev. B* **40**, 2565–2567 (1989).
M. Raudsepp, F. C. Hawthorne, X. Z. Zhou, I. Maartense, A. H. Morrish, and Y. L. Luo, *Can. J. Phys.* **65**, 1145–1148 (1987).
A. Renault, G. J. McIntyre, G. Collin, J.-P. Pouget, and R. Comes, *J. Phys. France* **48**, 1407–1412 (1987).
M.-J. Rey, Ph. Dehaudt, J. Joubert, and A. W. Hewat, *Physica C* **167**, 162–167 (1990).
R. S. Roth, C. J. Rawn, and L. A. Bendersky, *J. Mater. Res.* **5**, 46–52 (1990).
G. Roth, P. Adelmann, G. Heger, R. Knitter, and Th. Wolf, *J. Phys. I* **1**, 721–741 (1991).
G. Roth, P. Adelmann, R. Knitter, S. Massing, and Th. Wolf, *J. Solid State Chem.* **99**, 376–387 (1992).
T. Rouillon, R. Retoux, D. Groult, C. Michel, M. Hervieu, J. Provost, and B. Raveau, *J. Solid State Chem.* **78**, 322–325 (1989).
T. Rouillon, D. Groult, M. Hervieu, C. Michel, and B. Raveau, *Physica C* **167**, 107–111 (1990a).
T. Rouillon, A. Maignan, M. Hervieu, C. Michel, D. Groult, and B. Raveau, *Physica C* **171**, 7–13 (1990b).
T. Rouillon, J. Provost, M. Hervieu, D. Groult, C. Michel, and B. Raveau, *J. Solid State Chem.* **84**, 375–385 (1990c).
T. Rouillon, V. Caignaert, M. Hervieu, C. Michel, D. Groult, and B. Raveau, *J. Solid State Chem.* **97**, 56–64 (1992a).
T. Rouillon, V. Caignaert, C. Michel, M. Hervieu, D. Groult, and B. Raveau, *J. Solid State Chem.* **97**, 19–28 (1992b).
T. Rouillon, M. Hervieu, B. Domengès, and B. Raveau, *J. Solid State Chem.* **103**, 63–74 (1993).
S. N. Ruddlesden and P. Popper, *Acta Cryst.* **11**, 54–55 (1958).
M. J. Ruiz-Aragón, U. Amador, E. Morán, and N. H. Andersen, *Physica C* **235–240**, 1609–1610 (1994).
H. Sasakura and K. Yoshida, *Physica C* **267**, 19–23 (1996).
H. Sasakura, K. Nakahigashi, A. Hirose, H. Teraoka, S. Minamigawa, K. Inada, S. Noguchi, and K. Okuda, *Jpn. J. Appl. Phys.* **29**, L1628–L1631 (1990).
P. V. P. S. S. Sastry and A. R. West, *J. Mater. Chem.* **4**, 647–649 (1994).
H. Sawa, K. Obara, J. Akimitsu, Y. Matsui, and S. Horiuchi, *J. Phys. Soc. Jap.* **58**, 2252–2255 (1989a).
H. Sawa, S. Suzuki, M. Watanabe, J. Akimitsu, H. Matsubara, H. Watabe, S. Uchida, K. Kokusho, H. Asano, F. Izumi, and E. Takayama-Muromachi, *Nature* **337**, 347–348 (1989b).
A. Schilling, M. Contoni, J. D. Guo, and H. R. Ott, *Nature* **363**, 56–58 (1993).
P. Schleger, H. Casalta, R. A. Hadfield, H. F. Poulsen, M. von Zimmermann, N. H. Andersen, J. R. Schneider, R. Liang, P. Dosanjh, and W. N. Hardy, *Physica C* **241**, 103–110 (1995a).

P. Schleger, R. A. Hadfield, H. Casalta, N. H. Andersen, H. F. Poulsen, M. von Zimmermann, J. R. Schneider, R. Liang, P. Dosanjh, and W. N. Hardy, *Phys. Rev. Lett.* **74**, 1446–1449 (1995b).
A. E. Schlögl, J. J. Neumeier, J. Diederichs, C. Allgeiger, J. S. Schilling, and W. Yelon, *Physica C* **216**, 417–431 (1993).
A. J. Schultz, J. D. Jorgensen, J. L. Peng, and R. L. Green, *Phys. Rev. B* **53**, 5157–5159 (1996).
W. Schwarz, O. Blaschko, G. Collin, and F. Marucco, *Phys. Rev. B* **48**, 6513–6518 (1993).
H. Schwer, E. Kaldis, J. Karpinski, and C. Rossel, *Physica C* **211**, 165–178 (1993).
H. Schwer, J. Karpinski, K. Conder, L. Lesne, C. Rossel, A. Morawski, T. Lada, and A. Paszewin, *Physica C* **243**, 10–18 (1995a).
H. Schwer, J. Karpinski, L. Lesne, C. Rossel, A. Morawski, T. Lada, and A. Paszewin, *Physica C* **254**, 7–14 (1995b).
B. A. Scott, E. Y. Suard, C. C. Tsuei, D. B. Mitzi, T. R. McGuire, B.-H. Chen, and D. Walker, *Physica C* **230**, 239–245 (1994).
C. U. Segre, B. Dabrowski, D. G. Hinks, K. Zhang, J. D. Jorgensen, M. A. Beno, and I. K. Schuller, *Nature* **329**, 227–229 (1987).
B. Seling, C. Schinzer, A. Ehmann, S. Kemmler-Sack, G. Filoti, M. Rosenberg, J. Linhart, and W. Reimers, *Physica C* **251**, 238–246 (1995).
H. Shaked, B. W. Veal, J. Faber, Jr., R. L. Hitterman, U. Balachandran, G. Tomlins, H. Shi, L. Morss, and A. P. Paulikas, *Phys. Rev. B* **41**, 4173–4180 (1990).
H. Shaked, J. D. Jorgensen, B. A. Hunter, R. L. Hitterman, K. Kinoshita, F. Izumi, and T. Kamiyama, *Phys. Rev. B* **48**, 12941–12950 (1993).
H. Shaked, Y. Shimakawa, B. A. Hunter, R. L. Hitterman, J. D. Jorgensen, P. D. Han, and D. A. Payne, *Phys. Rev. B* **51**, 11784–11790 (1995).
Z. Z. Sheng and A. M. Hermann, *Nature* **332**, 55–58 (1988a).
Z. Z. Sheng and A. M. Hermann, *Nature* **332**, 138–139 (1988b).
Z. Z. Sheng, Y. F. Li, Y. Q. Tang, Z. Y. Chen, and D. O. Pederson, *Solid State Commun.* **83**, 205–208 (1992).
Yu. F. Shepelev, A. A. Levin, Yu. I. Smolin, A. A. Bush, and B. N. Romanov, *Physica C* **215**, 371–374 (1993).
Y. Shimakawa, *Physica C* **204**, 247–261 (1993).
Y. Shimakawa, Y. Kubo, T. Manako, H. Igarashi, F. Izumi, and H. Asano, *Phys. Rev. B* **42**, 10165–10171 (1990).
Y. Shimakawa, J. D. Jorgensen, D. G. Hinks, H. Shaked, R. L. Hitterman, F. Izumi, T. Kawashima, E. Takayama-Muromachi, and T. Kamiyama, *Phys. Rev. B* **50**, 16008–16014 (1994a).
Y. Shimakawa, J. D. Jorgensen, J. F. Mitchell, B. A. Hunter, H. Shaked, D. G. Hinks, R. L. Hitterman, Z. Hiroi, and M. Takano, *Physica C* **228**, 73–80 (1994b).
Y. Shimakawa, J. D. Jorgensen, H. Shaked, R. L. Hitterman, T. Kondo, T. Manako, and Y. Kubo, *Phys. Rev. B* **51**, 568–575 (1995).
T. Siegrist, L. F. Schneemeyer, J. V. Waszczak, N. P. Singh, R. L. Opila, B. Batlogg, L. W. Rupp, and D. W. Murphy, *Phys. Rev. B* **36**, 8365–8368 (1987a).
T. Siegrist, S. Sunshine, D. W. Murphy, R. J. Cava, and S. M. Zahurak, *Phys. Rev. B* **35**, 7137–7139 (1987b).
T. Siegrist, L. F. Schneemeyer, S. A. Sunshine, and J. V. Waszczak, *Mat. Res. Bull.* **23**, 1429–1438 (1988a).
T. Siegrist, S. M. Zahurak, D. W. Murphy, and R. S. Roth, *Nature* **334**, 231–232 (1988b).
A. Simon, K. Trübenbach, and H. Borrmann, *J. Solid State Chem.* **106**, 128–133 (1993).
D. C. Sinclair, M. A. G. Aranda, P. Attfield, and J. Rodríguez-Carvajal, *Physica C* **225**, 307–316 (1994).
J. M. S. Skakle and A. R. West, *Physica C* **227**, 336–342 (1994).
J. M. S. Skakle and A. R. West, *Physica C* **261**, 105–116 (1996).
P. R. Slater and C. Greaves, *Physica C* **215**, 191–194 (1993).
P. R. Slater, C. Greaves, M. Slaski, and C. M. Muirhead, *Physica C* **208**, 193–196 (1993a).
P. R. Slater, C. Greaves, M. Slaski, and C. M. Muirhead, *Physica C* **213**, 14–16 (1993b).

M. G. Smith, A. Manthiram, J. Zhou, J. B. Goodenough, and J. T. Markert, *Nature* **351**, 549–551 (1991).
C. Ström, S.-G. Eriksson, L.-G. Johansson, A. Simon, H. J. Mattausch, and R. K. Kremer, *J. Solid State Chem.* **109**, 321–332 (1994).
E. Suard, V. Caignaert, A. Maignan, F. Bourée, and B. Raveau, *Physica C* **210**, 164–172 (1993).
M. A. Subramanian, *Mat. Res. Bull.* **25**, 191–197 (1990).
M. A. Subramanian, *Mat. Res. Bull.* **29**, 119–125 (1994).
M. A. Subramanian, J. C. Calabrese, C. C. Torardi, J. Gopalakrishnan, T. R. Askew, R. B. Flippen, K. J. Morrissey, U. Chowdhry, and A. W. Sleight, *Nature* **332**, 420–422 (1988a).
M. A. Subramanian, J. B. Parise, J. C. Calabrese, C. C. Torardi, J. Gopalakrishnan, and A. W. Sleight, *J. Solid State Chem.* **77**, 192–195 (1988b).
M. A. Subramanian, C. C. Torardi, J. C. Calabrese, J. Gopalakrishnan, K. J. Morrissey, T. R. Askew, R. B. Flippen, U. Chowdhry, and A. W. Sleight, *Science* **239**, 1015–1017 (1988c).
M. A. Subramanian, C. C. Torardi, J. Gopalakrishnan, J. C. Calabrese, K. J. Morrissey, T. R. Askew, R. B. Flippen, U. Chowdhry, and A. W. Sleight, *Physica C* **153–155**, 608–612 (1988d).
M. A. Subramanian, C. C. Torardi, J. Gopalakrishnan, P. L. Gai, J. C. Calabrese, T. R. Askew, R. B. Flippen, and A. W. Sleight, *Science* **242**, 249–252 (1988e).
M. A. Subramanian, J. Gopalakrishnan, C. C. Torardi, P. L. Gai, E. D. Boyes, T. R. Askew, R. B. Flippen, W. E. Farneth, and A. W. Sleight, *Physica C* **157**, 124–130 (1989).
M. A. Subramanian, P. L. Gai, and A. W. Sleight, *Mat. Res. Bull.* **25**, 101–106 (1990a).
M. A. Subramanian, P. L. Gai, and M.-H. Whangbo, *Mat. Res. Bull.* **25**, 899–907 (1990b).
M. A. Subramanian, G. H. Kwei, J. B. Parise, J. A. Goldstone, and R. B. Von Dreele, *Physica C* **166**, 19–24 (1990c).
A. Sundaresan, A. D. Chinchure, K. Ghosh, S. Ramakrishnan, V. R. Marathe, L. C. Gupta, M. Sharon, and S. S. Shah, *Phys. Rev. B* **51**, 3893–3898 (1995).
S. A. Sunshine, T. Siegrist, L. F. Schneemeyer, D. W. Murphy, R. J. Cava, B. Batlogg, R. V. van Dover, R. M. Fleming, S. H. Glarum, S. Nakahara, R. Farrow, J. J. Krajewski, S. M. Zahurak, J. V. Waszczak, J. H. Marshall, P. Marsh, L. W. Rupp, Jr., and W. F. Peck, *Phys. Rev. B* **38**, 893–896 (1988).
T. Suzuki and T. Fujita, *Physica C* **159**, 111–116 (1989).
H. Takagi, S. Uchida, K. Kitazawa, and S. Tanaka, *Jpn. J. Appl. Phys.* **26**, L123–L124 (1987).
H. Takagi, S. Uchida, and Y. Tokura, *Phys. Rev. Lett.* **62**, 1197–1200 (1989).
H. Takahashi, A. Tokiwa-Yamamoto, N. Môri, S. Adachi, H. Yamauchi, and S. Tanaka, *Physica C* **218**, 1–4 (1993).
M. Takano, M. Azuma, Z. Hiroi, Y. Bando, and Y. Takeda, *Physica C* **176**, 441–444 (1991).
E. Takayama-Muromachi and M. Isobe, *Jpn. J. Appl. Phys.* **33**, L1399–L1402 (1994).
E. Takayama-Muromachi, Y. Matsui, Y. Uchida, F. Izumi, M. Onoda, and K. Kato, *Jpn. J. Appl. Phys.* **27**, L2283–L2286 (1988a).
E. Takayama-Muromachi, Y. Uchida, Y. Matsui, M. Onoda, and K. Kato, *Jpn. J. Appl. Phys.* **27**, L556–L558 (1988b).
E. Takayama-Muromachi, F. Izumi, and T. Kamiyama, *Physica C* **215**, 329–342 (1993).
E. Takayama-Muromachi, Y. Matsui, and K. Kosuda, *Physica C* **241**, 137–141 (1995a).
E. Takayama-Muromachi, Y. Matsui, and J. Ramirez-Castellanos, *Physica C* **252**, 221–228 (1995b).
K. Takita, H. Katoh, H. Akinaga, M. Nishino, T. Ishigaki, and H. Asano, *Jpn. J. Appl. Phys.* **27**, L57–L60 (1988).
J. L. Tallon, D. M. Pooke, R. G. Buckley, M. R. Presland, and F. J. Blunt, *Phys. Rev. B* **41**, 7220–7223 (1990).
T. Tamegai, A. Watanabe, K. Koga, I. Oguro, and Y. Iye, *Jpn. J. Appl. Phys.* **27**, L1074–L1076 (1988).
Z. Tan, J. I. Budnick, S. Luo, W. Q. Chen, S.-W. Cheong, A. S. Cooper, P. C. Canfield, and Z. Fisk, *Phys. Rev. B* **44**, 7008–7017 (1991).
X. X. Tang, D. E. Morris, and A. P. B. Sinha, *Phys. Rev. B* **43**, 7936–7941 (1991).
K. Tang, Y. Qian, R. Li, Z. Chen, B. Lu, and Y. Jia, *Physica C* **205**, 406–411 (1993).

K. Tang, Y. Qian, Z. Chen, L. Yang, L. Wang, and Y. Zhang, *Physica C* **242**, 216–220 (1995a).
K.-B. Tang, Y.-T. Qian, Z.-Y. Chen, L. Yang, and Y.-H. Zhang, *Physica C* **248**, 11–14 (1995b).
K. Tang, X. Xu, Y. Qian, Z. Chen, L. Yang, and Y. Zhang, *Physica C* **249**, 1–4 (1995c).
J. M. Tarascon, L. H. Greene, B. G. Bagley, W. R. McKinnon, P. Barboux, and G. W. Hull, in *Novel Superconductivity* (S. A. Wolf and V. Z. Kresin, Eds.), pp. 705–724. Plenum Press, New York, 1987.
J. M. Tarascon, Y. LePage, P. Barboux, B. G. Bagley, L. H. Greene, W. R. McKinnon, G. W. Hull, M. Giroud, and D. M. Hwang, *Phys. Rev. B* **37**, 9382–9389 (1988).
J.-M. Tarascon, E. Wang, L. H. Greene, B. G. Bagley, G. W. Hull, S. M. D'Egidio, P. F. Miceli, Z. Z. Wang, T. W. Jing, J. Clayhold, D. Brawner, and N. P. Ong, *Phys. Rev. B* **40**, 4494–4502 (1989).
J. M. Tarascon, W. R. McKinnon, Y. LePage, K. Remschnig, R. Ramesh, R. Jones, G. Pleizier, and G. W. Hull, *Physica C* **172**, 13–22 (1990).
T. Tatsuki, S. Adachi, M. Itoh, T. Tamura, X.-J. Wu, C.-Q. Jin, N. Koshizuka, and K. Tanabe, *Physica C* **255**, 61–64 (1995).
T. Tatsuki, A. Tokiwa-Yamamoto, A. Fukuoka, T. Tamura, X.-J. Wu, Y. Moriwaki, R. Usami, S. Adachi, K. Tanabe, and S. Tanaka, *Jpn. J. Appl. Phys.* **35**, L205–L208 (1996).
A. Tokiwa, T. Oku, M. Nagoshi, M. Kikuchi, K. Hiraga, and Y. Syono, *Physica C* **161**, 459–467 (1989).
A. Tokiwa, M. Nagoshi, T. Oku, N. Kobayashi, M. Kikuchi, K. Hiraga, and Y. Syono, *Physica C* **168**, 285–290 (1990a).
A. Tokiwa, T. Oku, M. Nagoshi, D. Shindo, M. Kikuchi, T. Oikawa, K. Hiraga, and Y. Syono, *Physica C* **172**, 155–165 (1990b).
A. Tokiwa, T. Oku, M. Nagoshi, and Y. Syono, *Physica C* **181**, 311–319 (1991).
A. Tokiwa-Yamamoto, T. Tatsuki, S. Adachi, and K. Tanabe, *Physica C* **268**, 191–196 (1996).
Y. Tokura, T. Arima, H. Takagi, S. Uchida, T. Ishigaki, H. Asano, R. Beyers, A. I. Nazzal, P. Lacorre, and J. B. Torrance, *Nature* **342**, 890–893 (1989a).
Y. Tokura, H. Takagi, and S. Uchida, *Nature* **337**, 345–347 (1989b).
Y. Tokura, H. Takagi, H. Watabe, H. Matsubara, S. Uchida, K. Hiraga, T. Oku, T. Mochiku, and H. Asano, *Phys. Rev. B* **40**, 2568–2571 (1989c).
C. C. Torardi, M. A. Subramanian, J. C. Calabrese, J. Gopalakrishnan, E. M. McCarron, K. J. Morrissey, T. R. Askew, R. B. Flippen, U. Chowdhry, and A. W. Sleight, *Phys. Rev. B* **38**, 225–231 (1988a).
C. C. Torardi, M. A. Subramanian, J. C. Calabrese, J. Gopalakrishnan, K. J. Morrissey, T. R. Askew, R. B. Flippen, U. Chowdhry, and A. W. Sleight, *Science* **240**, 631–634 (1988b).
C. C. Torardi, M. A. Subramanian, J. Gopalakrishnan, and A. W. Sleight, *Physica C* **158**, 465–470 (1989).
C. C. Torardi, E. M. McCarron, P. L. Gai, J. B. Parise, J. Ghoroghchian, D. B. Kang, M.-H. Whangbo, and J. C. Barry, *Physica C* **176**, 347–356 (1991).
J. B. Torrance, Y. Tokura, S. J. LaPlaca, T. C. Huang, R. J. Savoy, and A. I. Nazzal, *Solid State Commun.* **66**, 703–706 (1988).
M. Uehara, H. Nakata, and J. Akimitsu, *Physica C* **216**, 453–457 (1993a).
M. Uehara, H. Nakata, J. Akimitsu, T. Den, T. Kobayashi, and Y. Matsui, *Physica C* **213**, 51–56 (1993b).
M. Uehara, S. Sahoda, H. Nakata, J. Akimitsu, and Y. Matsui, *Physica C* **222**, 27–32 (1994a).
M. Uehara, M. Uoshima, S. Ishiyama, H. Nakata, J. Akimitsu, Y. Matsui, T. Arima, Y. Tokura, and N. Mori, *Physica C* **229**, 310–314 (1994b).
M. Uehara, T. Nagata, J. Akimitsu, H. Takahashi, N. Môri, and K. Kinoshita, *J. Phys. Soc. Jap.* **65**, 2764–2767 (1996).
T. Uzumaki, N. Kamehara, and K. Niwa, *Jpn. J. Appl. Phys.* **30**, L981–984 (1991).
E. N. Van Eenige, R. Griessen, R. J. Wijngaarden, J. Karpinski, E. Kaldis, S. Rusiecki, and E. Jilek, *Physica C* **168**, 482–488 (1990).
J. T. Vaughey, J. B. Wiley, and K. R. Poeppelmeier, *Z. Anorg. Allg. Chem.* **598/599**, 327–338 (1991).
R. Vijayaraghavan, N. Rangavittal, G. U. Kulkarni, E. Grantscharova, T. N. Guru Row, and C. N. R. Rao, *Physica C* **179**, 183–190 (1991).

R. Vijayaraghavan, C. Michel, A. Maignan, M. Hervieu, C. Martin, B. Raveau, and C. N. R. Rao, *Physica C* **206**, 81–89 (1993).

H. G. von Schnering, L. Walz, M. Schwarz, W. Becker, M. Hartweg, T. Popp, B. Hettich, P. Müller, and G. Kämpf, *Angew. Chem. Int. Ed. Engl.* **27**, 574–576 (1988).

T. Wada, A. Ichinose, Y. Yaegashi, H. Yamauchi, and S. Tanaka, *Phys. Rev. B* **41**, 1984–1989 (1990a).

T. Wada, A. Ichinose, H. Yamauchi, and S. Tanaka, *Phys. Rev. B* **171**, , 344–347 (1990b).

T. Wada, K. Hamada, A. Ichinose, T. Kaneko, H. Yamauchi, and S. Tanaka, *Physica C* **175**, 529–533 (1991a).

T. Wada, A. Ichinose, F. Izumi, A. Nara, H. Yamauchi, H. Asano, and S. Tanaka, *Physica C* **179**, 455–460 (1991b).

J. L. Wagner, P. G. Radaelli, D. G. Hinks, J. D. Jorgensen, J. F. Mitchell, B. Dabrowski, G. S. Knapp, and M. A. Beno, *Physica C* **210**, 447–454 (1993).

J. L. Wagner, B. A. Hunter, D. G. Hinks, and J. D. Jorgensen, *Phys. Rev. B* **51**, 15407–15414 (1995).

P. G. Wahlbeck, D. E. Peterson, J. O. Willis, E. J. Peterson, J. Y. Coulter, D. S. Phillips, and K. V. Salazar, *Physica C* **256**, 358–364 (1996).

X. Z. Wang and B. Bäuerle, *Physica C* **176**, 507–510 (1991).

X. Z. Wang, B. Hellebrand, and D. Bäuerle, *Physica C* **200**, 12–16 (1992a).

X. Z. Wang, P. L. Steger, M. Reissner, and W. Steiner, *Physica C* **196**, 247–251 (1992b).

S. Wang, Y. Qian, R. Li, Z. Chen, N. Wang, L. Cao, G. Zhou, and Y. Zhang, *Physica C* **210**, 463–465 (1993).

J. Wang, S. Takano, M. Wakata, R. Usami, K. Hamada, A. Fukuoka, and H. Yamauchi, *Physica C* **219**, 33–38 (1994).

X. Z. Wang, B. Hellebrand, D. Bäuerle, M. Strecker, G. Wortmann, and W. Lang, *Physica C* **242**, 55–62 (1995).

A. W. Webb, E. F. Skelton, S. B. Qadri, E. R. Carpenter, Jr., M. S. Osofsky, R. J. Soulen, and V. Letourneau, *Phys. Lett. A* **137**, 205–206 (1989).

C. Weigl and K.-J. Range, *J. Alloys Comp.* **200**, L1–L2 (1993).

K. Westerholt, H. J. Wüller, H. Bach, and P. Stauche, *Phys. Rev. B* **39**, 11680–11689 (1989).

Ch. Wolters, K. M. Amm, Y. R. Sun, and J. Schwartz, *Physica C* **267**, 164–172 (1996).

M. K. Wu, J. R. Ashburn, C. J. Torng, P. H. Hor, R. L. Meng, L. Gao, Z. J. Huang, Y. Q. Wang, and C. W. Chu, *Phys. Rev. Lett.* **58**, 908–910 (1987).

X.-J. Wu, S. Adachi, C.-Q. Jin, H. Yamauchi, and S. Tanaka, *Physica C* **223**, 243–248 (1994a).

X.-J. Wu, C.-Q. Jin, S. Adachi, and H. Yamauchi, *Physica C* **224**, 175–178 (1994b).

X.-J. Wu, C.-Q. Jin, P. Laffez, T. Tatsuki, T. Tamura, S. Adachi, H. Yamauchi, and N. Koshizuka, *Physica C* **258**, 143–152 (1996a).

X. S. Wu, H. M. Shao, S. S. Jiang, C. Gou, D. F. Chen, D. W. Wang, and Z. H. Wu, *Physica C* **261**, 189–195 (1996b).

X.-J. Wu, T. Tamura, S. Adachi, T. Tatsuki, and K. Tanabe, *Physica C* **266**, 261–270 (1996c).

X.-D. Xiang, A. Zettl, W. A. Vareka, J. L. Corkill, T. W. Barbee III, and M. L. Cohen, *Phys. Rev. B* **43**, 11496–11499 (1991).

Y. Xu, M. Suenaga, J. Tafto, R. L. Sabatini, A. R. Moodenbaugh, and P. Zolliker, *Phys. Rev. B* **39**, 6667–6680 (1989).

Y. Y. Xue, P. H. Hor, R. L. Meng, Y. K. Tao, Y. Y. Sun, Z. J. Huang, L. Gao, and C. W. Chu, *Physica C* **165**, 357–363 (1990).

J. S. Xue, J. E. Greedan, and M. Maric, *J. Solid State Chem.* **102**, 501–518 (1993).

A. Yamamoto, M. Onoda, E. Takayama-Muromachi, F. Izumi, T. Ishigaki, and H. Asano, *Phys. Rev. B* **42**, 4228–4239 (1990).

K. Yamaura, Z. Hiroi, and M. Takano, *Physica C* **229**, 183–187 (1994).

K. Yamaura, J. Shimoyama, S. Hahakura, Z. Hiroi, M. Takano, and K. Kishio, *Physica C* **246**, 351–356 (1995).

J. Yang, J. Liang, G. Rao, Y. Qin, Y. Shi, and W. Tang, *Physica C* **270**, 35–40 (1996).

R. Yoshizaki, H. Sawada, T. Iwazumi, Y. Saito, Y. Abe, H. Ikeda, K. Imai, and I. Nakai, *Jpn. J. Appl. Phys.* **26**, L1703–L1706 (1987).
H. W. Zandbergen, W. A. Groen, F. C. Mijlhoff, G. van Tendeloo, and S. Amelinckx, *Physica C* **156**, 325–354 (1988a).
H. W. Zandbergen, R. Gronsky, and G. Thomas, *Phys. Status Solidi (a)* **105**, 207–218 (1988b).
H. W. Zandbergen, R. Gronsky, K. Wang, and G. Thomas, *Nature* **331**, 596–599 (1988c).
H. W. Zandbergen, Y. K. Huang, M. J. V. Menken, J. N. Li, K. Kadowaki, A. A. Menovsky, G. van Tendeloo, and S. Amelinckx, *Nature* **332**, 620–623 (1988d).
H. W. Zandbergen, W. T. Fu, J. M. van Ruitenbeek, L. J. de Jongh, G. van Tendeloo, and S. Amelinckx, *Physica C* **159**, 81–86 (1989).
H. W. Zandbergen, W. T. Fu, and J. M. van Ruitenbeek, *Physica C* **166**, 502–512 (1990a).
H. W. Zandbergen, W. A. Groen, A. Smit, and G. van Tendeloo, *Physica C* **168**, 426–449 (1990b).
K. Zhang, B. Dabrowski, C. U. Segre, D. G. Hinks, I. K. Schuller, J. D. Jorgensen, and M. Slaski, *J. Phys. C* **20**, L935–L940 (1987).
W. J. Zhu, J. J. Yue, Y. Z. Huang, and Z. X. Zhao, *Physica C* **205**, 118–122 (1993).
W. J. Zhu, Y. S. Yao, X. J. Zhou, B. Yin, C. Dong, Y. Z. Huang, and Z. X. Zhao, *Physica C* **230**, 385–388 (1994).
W. J. Zhu, L. Q. Chen, Y. Z. Huang, and Z. X. Zhao, *Mat. Res. Bull.* **30**, 247–250 (1995a).
W. J. Zhu, Y. Z. Huang, T. S. Ning, and Z. X. Zhao, *Mat. Res. Bull.* **30**, 243–246 (1995b).
W. J. Zhu, F. Wu, Y. Z. Huang, and Z. X. Zhao, *J. Alloys Comp.* **226**, 102–106 (1995c).
Z. Zou, K. Oka, T. Ito, and Y. Nishihara, *Jpn. J. Appl. Phys.* **36**, L18–L20 (1997).

This Page Intentionally Left Blank

Chapter 9

Characteristic Parameters

Charles P. Poole, Jr.
Department of Physics and Institute of Superconductivity, University of South Carolina, Columbia, South Carolina

John F. Zasadzinski and Roberta K. Zasadzinski
Physics Department, Illinois Institute of Technology, Chicago, Illinois

Philip B. Allen
Department of Physics and Astronomy, State University of New York, Stony Brook, New York

ISBN: 0-12-561460-8
$30.00

HANDBOOK OF SUPERCONDUCTIVITY

A

Introduction

The main purpose of the present chapter is to present tabulations of data for the important parameters of superconductors, such as coherence length ξ, penetration depth λ, energy gap $E_g = 2\Delta$, critical fields B_c, B_{c1} and B_{c2}, critical current density J_c, and electron–phonon coupling constant λ. Characteristic temperatures T_c are tabulated in Chap. 5 Tables 5-1 to 5-40. These various quantities are related to each other through simple phonon BCS and high kappa ($\kappa = \lambda/\xi$) expressions. These will be reviewed in the next section, and then we will proceed to provide various tabulations in succeeding sections. The materials will tend to appear in the tables in the order: elements, binary compounds and alloys, Laves phases (AB_2), Chevrel compounds, $A15$ compounds (A_3B), miscellaneous materials, heavy electrons (heavy fermions), perovskites, borocarbides, organics, (buckminster)fullerenes, then lanthanum, yttrium-type, bismuth, thallium, and mercury-type cuprates. When more than one reference is given for table entries the values may be composites or averages. Values from Poole *et al.* (1988, 1995) are generally averages.

B

Relationships between Parameters

In Section D of Chapter 4 we summarized the pedictions of the simple, isotropic, phonon mediated BCS theory that are good approximations for many Type II superconducting materials, and in Sections C and D of Chapter 12 we review the high-κ expressions for vortices that relate the various critical fields to the characteristic lengths ξ and λ. In our earlier work [Poole *et al.* 1995, Chap. 10, Sect. 18] we defined an "ideal Type II superconductor" as a material, all of whose parameters satisfy these simple relationships. Therefore if any two of the characteristic parameters of a Type II superconductor are specified, then the remainder can be estimated. We will assume that the transition temperature T_c and the Ginzburg–Landau parameter κ are known and show how to calculate the remaining properties for an isotropic superconductor, where MKS units are, of course, used throughout this section.

The energy gap is given by the BCS relation

$$E_g = 3.528 k_B T_c. \tag{1}$$

The upper critical field B_{c2} can be equated to the Pauli limiting field (paramagnetic limit or Clogston–Chandrasekhar limit) given by

$$B_{c2} = B_{pauli} = E_g/2\sqrt{2}\mu_B, \tag{2}$$

and applying Eq. (1) we obtain

$$B_{c2} = 1.83T_c. \tag{3}$$

The high-κ vortex expression from Eq. (12-9),

$$B_{c2} = \frac{\Phi_0}{2\pi\xi^2}, \tag{4}$$

where $\Phi_0 = h/2e$ is the quantum of flux, provides the coherence length

$$\xi = (\Phi_0/2\pi B_{c2})^{1/2}, \tag{5}$$

and from the definition $\kappa = \lambda/\xi$ of the Ginzburg–Landau parameter κ, we obtain the penetration depth λ:

$$\lambda = \kappa\xi. \tag{6}$$

Equations (12-8) and (12-10), respectively, which are

$$B_{c1} = \frac{\Phi_0 \ln \kappa}{4\pi\lambda^2} \tag{7}$$

$$B_c = \frac{\Phi_0}{2\sqrt{2}\pi\lambda\xi}, \tag{8}$$

provide the thermodynamic and lower critical fields

$$B_c = B_{c2}/\sqrt{2}\kappa \tag{9}$$

$$B_{c1} = B_c \ln \kappa/\sqrt{2}\kappa. \tag{10}$$

The critical current density J_c at 0 K is close to the depairing current density, estimated from Eq. (12-13),

$$J_c = \alpha B_c/\mu_0\lambda. \tag{11}$$

where $\alpha \sim 1$. A better approximation to the upper limit of J_c is given by the Ginzburg–Landau expression

$$J_{cmax} = \left|\frac{2(1-t)}{3}\right|^{3/2}\left|\frac{10B_c}{4\pi\lambda\mu_0}\right|, \tag{12}$$

where $t = T/T_c$. The "ideal" relationships of Eqs. (1)–(10) are fairly good first approximations to the experimentally determined values of many typical Type II superconductors. In contrast to this most measured supercurrent densities are far less than the theoretical limiting values (11) and (12).

Table 9.I.

Coherence lengths ξ and penetration depths λ for various isotropic superconductors. Values for the critical temperature T_c and the dimensionless Ginzburg–Landau parameter $\kappa = \lambda/\xi$ are given, when known. References are identified by first author and year.

Material	T_c	ξ	λ	κ	Comments	Reference
	(K)	(nm)	(nm)	(λ/ξ)		
Zn	0.535		29		Ultrasonic	Almond (1975)
Cd	0.56	760	110	0.14		Meservey (1969)
Cd	0.875		42		Ultrasonic	Almond (1975)
Al*			46–51		10% anisotropy	Doezema (1986)
Al*	1.18	1550	45	0.03		Donnelly (1989), Poole (1995)
In*	3.41	360	40	0.11		Poole (1995)
Sn*	3.72	180	42	0.23		Poole (1995)
Pb*		96	30.5	0.32		Gasparovic (1970)
Pb*	7.20	87	39	0.48		Donnelly (1989), Poole (1995)
Nb*	9.25	39	52	1.3		Donnelly (1989), Poole (1995)
PbIn	7	30	150	5		Donnelly (1989)
PbBi	8.3	20	200	10		Donnelly (1989)
NbTi	9.6	3.8	130	27	Polycrystal	Hampshire (1998)
			200–400		Filament diameter 50–500 nm; see J_c table	Cave (1989)
	9.5	4	300	75		Donnelly (1989)
NbN	16	5	200	40		Donnelly (1989)
$Nb_{0.74}Ge_{0.26}$	3.4	6.5	802	76	Amorphous film	Berghuis (1993)
$Nb_{0.65}Ge_{0.35}$	2.9	7.2	913	77	Amorphous film	Berghuis (1993)
$PbMo_6S_8$ Chevrel	14	2.2	215	98	Polycrystal	Hampshire (1998)
$SnMo_6S_8$ Chevrel	14	3.3	240	73	Polycrystal	Hampshire (1998)
V_3Ga *A*15	15.3	2–3	90	≈36		Donnelly (1989)
V_3Si *A*15	16.3	3	60	20		Donnelly (1989)
	17		145			Gross-Alltag (1991)
Nb_3Sn *A*15	16	2.8	93	33	Polycrystal	Hampshire (1998)

Nb_3Sn $A15$	18.0	3	65	22		Donnelly (1989)
Nb_3Ge $A15$	23.2	3	90	30		Orlando (1991)
Mo_4Si	7.2	4.7	500	65	Thin film	Wördenweber (1989)
UBe_{13}	0.88	7	400	60	Heavy electron compound	Alekseevskii (1986), Signore (1995)
	0.86		1050		Heavy electron, c-magnetization	Gross-Alltag (1991)
UPt_3	0.5		1900		Heavy electron, c-magnetization	Gross-Alltag (1991)
	< 1	11.1	600	54	Heavy electron material	Kleiman (1992)
					$\lambda \approx (T_c - T)^{\beta}$ near T_c with $\beta \approx 1$	Koziol (1991)
YNi_2B_2C	15	8.1	103	12.7	Mass enhancement $m^*/m_0 = 9.4$; see B_c table	Cywinski (1994)
Ba_xC_{60}	6.8	11.6			see B_c table	Baenitz (1995), Lüders (1997)
K_3C_{60}	17.8	4.4			ξ_{GL} given, $\xi_0 = 15$	Heinze (1996), Holczer (1991)
	19.4	2.8	240	92		Gärtner (1992)
K_2CsC_{60}	24	3.4				Heinze (1996)
	23	4.0	200	50		Baenitz (1998)
Rb_3C_{60}	30.7	2.6			ξ_{GL} given, $\xi_0 = 5.0$	Heinze (1996)
	28.5	2.2	157	76		Gärtner (1992)
	30.7	3.2	186	58		Baenitz (1998)
	29.6	2.0	247	124		Sparn (1992)
Rb_2CsC_{60}	32.5	2.5				Heinze (1996)
$(La_{0.925}Sr_{0.075})_2CuO_4$	37	2.0	200	100		Poole (1998)
$YBa_2Cu_3O_{7-\delta}$		2.1			$\xi(0) = 2.1$, $\xi_0 = 2.5$ nm	Kes (1989)
	91	1.65	156	95	Polycrystal	Hampshire (1998)
$Bi_2Sr_2CaCu_2O_x$	89	1.8	250	139	Polycrystal	Hampshire (1988)
$BaPb_{0.75}Bi_{0.25}O_3$		7				Takagi (1990)
$HgBa_2Ca_2Cu_3O_x$	129	2.3		100		Gao (1993), Schilling (1994)
—					λ and the pairing state	Annett (1990)

* To obtain perspective on the accuracy of reported ξ and λ values see Poole *et al.* (1995), p. 271.

C

Coherence Lengths and Penetration Depths

In the Ginzburg–Landau theory the coherence length ξ is given by

$$\xi = \hbar/(2m^*|a|)^{1/2}, \tag{13}$$

where $m^* = 2m_e$ is twice the electron mass, and a is the coefficient of the quadratic term $a\phi\phi^*$ in the GL free energy $G_s(\phi)$ of the superconducting state with the temperature dependence

$$a(T) \approx a_0[t - 1] \tag{14}$$

in the neighborhood of T below T_c, where $t = T/T_c$ is the reduced temperature and $a(T)$ is negative below T_c. The BCS theory provides the approximation

$$\xi_0 \approx \hbar v_F/\pi\Delta(0) \tag{15}$$

for the coherence length ξ_0 at absolute zero temperature in terms of the Fermi velocity v_F, where $E_g = 2\Delta$ is the energy gap. In the Pippard approximation the coherence length of a superconducting metal depends on the electron mean free path l through the expression

$$1/\xi = 1/\xi_0 + 1/l. \tag{16}$$

Since the mean free path of an ordinary conductor such as copper becomes very long when the impurity level is low, the limit $l \gg \xi_0$ in Eq. (16) is called the clean limit with $\xi \approx \xi_0$. In like manner, $l < \xi_0$ is called the dirty limit with $\xi < \xi_0$, and the case $\xi \ll \xi_0$ with $\xi \sim l$ is called the extremely dirty limit. Table 9.1 provides coherence lengths for a number of isotropic superconductors.

The London theory gives for the penetration depth

$$\lambda_L = (m/\mu_0 n_s e^2)^{1/2}, \tag{17}$$

an expression which also appears naturally in the GL theory, where n_s is the density of superconducting charge carriers, that is, Cooper pairs. The penetration depth has the value $\lambda(0) = \lambda_0$ at absolute zero and becomes very large in the neighborhood of T_c, with the following temperature dependence predicted by the two-fluid model:

$$\lambda(T) = \lambda_0(1 - t^4)^{-1/2}. \tag{18}$$

Figure 9.1 compares this temperature dependence (dashed line) with three limiting cases of the BCS theory, namely the pure sample in the local limit $\lambda_L(T)$, the pure sample in the extreme anomalous limit $\lambda_\infty(T)$, and the dirty local limit $\lambda_{eff}(T)$. The book by Tinkham (1996, p. 103) should be consulted for the definitions of these limits. Tables 9.1 and 9.2 list some alternative temperature dependences.

Table 9.2.

Coherence lengths ξ and penetration depths λ perpendicular to (ξ_{ab}, λ_{ab}), and parallel to (ξ_c, λ_c) the c-axis for various anisotropic superconductors. Values for the critical temperature T_c and the anisotropy ratio $\Gamma = (m_c/m_{ab})^{1/2} = \xi_{ab}/\xi_c = \lambda_c/\lambda_{ab}$ are given, when known. References are identified by first author and year.

Material	T_c (K)	ξ_{ab} (nm)	ξ_c (nm)	λ_{ab} (nm)	λ_c (nm)	Γ^a (ξ_{ab}/ξ_c, λ_c/λ_{ab})	Comments ($t = T/T_c$)	Reference
$NbSe_2$	7.7	2.3	69	230	3.2			Salamon (1989)
				496	124			Finley (1980)
$K_{0.33}(H_2O)_{0.66}TaS_2$		30	0.9	3,400	71,000		Intercalated compound	Gygax (1982)
Nb_3S_4		2.9	0.57				Bibersacher (1980)	
C_8KHg	1.88	200	10			20	Effect of pressure	Iye (1982)
C_8RbHg	1.41	200	10			20		Iye (1982)
UPt_3	0.46			782	707		Heavy electron compound	Broholm (1990)
YNi_2B_2C	15	6.0	5.5				Thin film c-axis oriented	Arisawa (1995)
$(BEDT\text{-}TTF)_2Cu(NCS)_2$					2×10^5	≈ 250	Josephson λ	Mansky (1994)
$K\text{-}(ET)_2Cu[NCS]_2$	9			980				Harshman (1990)
	10					> 200		Farrell (1990)
$K\text{-}(ET)_2Cu[N(CN)]_2Bl$	11.4			650				Lang (1992)
	11.6	3.7	0.4			9.3		Kwok (1990)
$(TMSF)_2ClO_4$	1.1	54–60	6				$\xi_a = 60$, $\xi_b = 54$ nm	Murata (1982)
$La_{2-x}Ca_{1+x}Cu_2O_{6-x}$		3.3	1.2			2.8	Monocrystal	Watanabe (1991)
$(La_{1-x}Sr_x)_2CuO_4$		3.2	0.055			58	Values are for $x = 0.08$.	Suzuki (1991)
		3.2	0.3			11	Values are for $x = 0.3$	Suzuki (1991)
$(La_{0.9}Sr_{0.1})_2CuO_4$		4.6	3.0	290	450	1.5	Magnetic measurements	Cobb (1994)
$(La_{0.91}Sr_{0.09})_2CuO_4$	30	3.3		283				Wu (1993)
$(La_{0.925}Sr_{0.075})_2CuO_4$		3.2	0.27			12	Monocrystal thin films	Suzuki (1989)
$(Nd_{0.925}Ce_{0.075})_2CuO_4$	21.5			80	≈ 100	≈ 1.3		Suzuki (1989)
$(Nd_{0.9}Ce_{0.1})_2CuO_4$						≈ 2.5		O and Markert (1993)
$YBa_2Cu_3O_{6.9}$	83			142	> 700	> 5	$\lambda(t) = \lambda(0)[1 - t^4]^{-1/2}$	Harshman (1989)
$YBa_2Cu_3O_{7-\delta}$	66			260				Lee (1991)

(*continued*)

Table 9.2. (*continued*)

Material	T_c (K)	ξ_{ab} (nm)	ξ_c (nm)	λ_{ab} (nm)	λ_c (nm)	Γ^a (ξ_{ab}/ξ_c, λ_c/λ_{ab})	Comments ($t = T/T_c$)	Reference
				140	610		Oriented powder	Scheidt (1989)
		1.6	0.3				Demagnetization	Welp (1989)
		2.8	0.08				Film, pulsed fields	Staghun (1989)
$YBa_2Cu_3O_{7-\delta}$		1.5	0.3			5	Fluctuation conductivity and magnetoresistance	Pagnon (1991)
	90	2.5	0.8			3.3		Chaudhari (1987)
	89	3.4	0.7	36	125	5		Worthington (1987)
	92.4	4.3	0.7	27	180	6.4		Gallagher (1988)
	92	1.2	0.3	89	550	≈ 5		Salamon (1989)
	90	1.3	0.2	130	450	≈ 5		Krusin-Elbaum (1989)
				140	1040		Co and Zn doping studied also	Porch (1993)
		2.65	0.09			29	Magnetoresistance	Gob (1994)
		12.9	4.0	800	2600	3	Microwave measurements at 86.5 K; $\lambda_{ab}(0) = 180$ nm	Jiang (1993, 1994)
				130	650′	5	$\lambda(t) = \lambda(0)[1 - t^4]^{-1/2}$	Pumpin (1990a,b)
				140	610	4.4	BCS temperature-dependent, oriented grains; see B_c table	Scheidt (1989)
				139	700	5	Polycrystals	Schilling (1990)
$YBa_2Cu_4O_8$				198	990	5	Polycrystals	Schilling (1990)
$EuBa_2Cu_3O_{7-\delta}$	95	2.7	0.6			4.5		Hikita (1987)

$EuBa_2Cu_3O_{7-\delta}$	94	3.5	0.38			9.2		Tajima (1988)
$TmBa_2Cu_3O_{7-\delta}$	86	7.4	0.9			8.2		Noel (1987)
							$\lambda_a:\lambda_b:\lambda_c = 1:1.7:4.4$; see B_c table	Moshchalkov (1990)
$Y_{0.8}Pr_{0.2}Cu_3O_{7+\delta}$	73	2.4	0.78			3.1		Jia (1992)
$Pb_2Sr_2(YCa)Cu_3O_{8+\delta}$	75			258	643	2.5	Temperature dependence	Reedyk (1991)
$Bi_2Sr_2CaCu_2O_8$	109			500				Maeda (1992)
		1.42					Thin film; Nernst, Seebeck and Hall measurements	Ri (1994)
$Bi_2Sr_2CaCu_2O_8$	80				200		$\lambda(T) = \lambda(0)[1 - t^4]^{-1/2}$, muon spin rotation	Grebinnik (1990)
$Bi_2Sr_2Ca_2Cu_3O_{10}$	109	2.9	0.09			31		Matsubara (1992)
	111	1.0	0.02			50		Li (1992)
		2.9	0.57					Babic (1995)
$Bi_{3.9}Sr_{3.3}Ca_{1.3}(Cu_{0.961}Fe_{0.039})_3O_x$						10^3	$\Gamma = \lambda_c/\lambda_{ab}$	vom Hedt (1995)
$(Bi,Pb)_2Sr_2CaCu_2O_8$	91	2.0			178			Zhang (1992)
$(Bi,Pb)_2Sr_2Ca_2Cu_3O_{10-\delta}$	103	2.04	0.037			55		Lee (1991)
$Tl_2Ba_2CaCu_2O_{8-\delta}$	100			182				Ning (1992)
$Tl_2Ba_2Ca_2Cu_3O_{10}$	123			173	480	2.8	Magnetization measurement	Thompson (1990)
$Tl_2Ba_2Ca_2Cu_3O_{10}$	100					$\geqslant 300$		Thompson (1993)
$Tl_2Ba_2CaCu_2O_{10}$	103			182	1960	10.7	$\lambda(T) = \lambda(0)[1 + aT + bT^2 + cT^3]$	Ning (1992)
$Tl_2Ba_2Ca_2Cu_3O_{10}$	100			175	2350	13.4		Ning (1992)
TlBaCaCuO		2.8	0.08			33	Oriented film; see B_c table	Staguhn (1989)
$HgBa_2CuO_{4+\delta}$	93	2.1		117				Thompson (1993)
$HgBa_2Ca_2Cu_3O_{8+\delta}$	133	1.3		130	3500	27		Schilling (1994)
		1.5	0.19			$\geqslant 64$		Schilling (1994)

[a] Values of $\Gamma = \xi_{ab}/\xi_c = \lambda_c/\lambda_{ab}$ are listed as approximate when the ratios ξ_{ab}/ξ_c and λ_c/λ_{ab} do not agree.

Fig. 9.1.

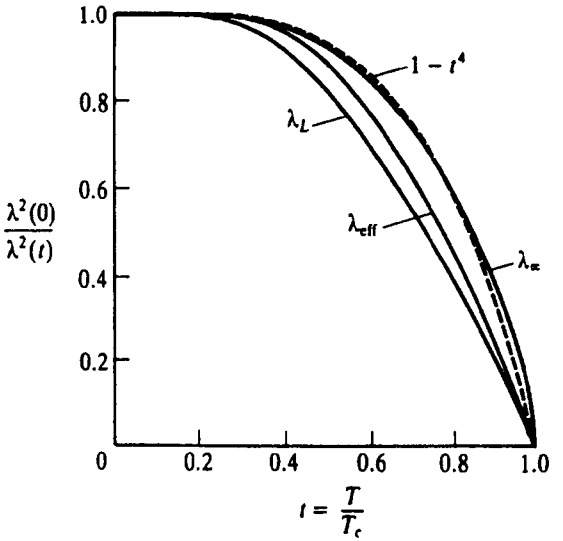

Comparison of the predicted temperature dependence of $1/\lambda^2$ for the two-fluid model (- - - -) and three limiting cases of the BCS theory (——), as explained in the text. (From Tinkham, 1996, p. 104.)

Until now we have not taken anisotropy into account. The tetragonal cuprates are axially symmetric, and the orthorhombic ones are very close to axial, with coherence lengths that are related to their respective penetration depths through the expression

$$\xi_c \ll \xi_{ab} \ll \lambda_{ab} \ll \lambda_c, \tag{19}$$

with the anisotropy factor Γ given by

$$\Gamma = (m_c/m_{ab})^{1/2} = \xi_{ab}/\xi_c = \lambda_c/\lambda_{ab}, \tag{20}$$

where m_{ab} and m_c are effective masses. The validity of this expression (19) for many anisotropic materials is clear from the experimental values listed in Table 9.2.

References for Sections A–C

N. E. Alekseevskii, V. I. Nizhankovskii, V. N. Narozhnyi, E. P. Khlybov, and A. V. Mitin, *J. Low Temp. Phys.* **64**, 87 (1986).

D. P. Almond, M. J. Lea, and E. R. Dobbs, *Proc. Roy. Soc. Lond. A* **343**, 537 (1975).

J. F. Annett, N. D. Golden and S. R. Renn, in *Physical Properties of High Temperature Superconductors II* (D. M. Ginsberg, Ed.). World Scientific, Singapore 1990.

S. Arisawa, T. Hatano, K. Hirata, T. Mochiku, H. Kitaguchi, H. Fujii, H. Kumakura, K. Kadowaki, K. Nakamura, and K. Togano, *Adv. Supercond. VII*, Proc. 7th Intern. Symp. on Supercond. (ISS' 94), E. Babic *et al.*, Fizika *4*, 549 (1995) Vol. 2. p. 271, Springer-Verlag, Tokyo, 1995.

W. Biberacher and H. Schwenk, *Solid State Commun.* **33**, 385 (1980).
M. Baenitz, M. Heinze, K. Lüders, H. Werner, R. Schögl, M. Weiden, G. Sparn, and F. Steglich, *Solid State Commun.* **96**, 539 (1995).
M. Baenitz and K. Lüders, *Festkörperprobleme, Adv. Solid State Phys., Vieweg* (1998).
P. Berghuis and P. H. Kes, *Phys. Rev. B* **47**, 262 (1993).
E. Babic *et al.*, Fizika **4**, 549 (1995).
C. Broholm, G. Aeppli, R. N. Kleiman, D. R. Harshman, D. J. Bishop, E. Bucher, D. Ll. Williams, E. J. Ansaldo, and R. H. Heffner, *Phys. Rev. Lett.* **65**, 2062 (1990).
J. R. Cave, *Cryogenics* **29**(3A), suppl., 304 (1989).
P. Chaudhari, R. T. Collins, P. Freitas, R. J. Gambino, J. R. Kirtley, R. H. Koch, R. B. Laibowitz, F. K. LeGoues, T. R. Mcguire, T. Penney, Z. Schlesinger, A. P. Segmüller, S. Foner, and E. J. McNiff, Jr., *Phys. Rev. B* **36**, 8903 (1987).
J. L. Cobb and J. T. Markert, *Physica C* **226**, 235 (1994).
R. Cywinski, Z. P. Han, R. Bewley, R. Cubitt, M. T. Wylie, E. M. Forgan, S. L. Lee, M. Warden, and S. H. Kilcoyne, *Physica C* **233**, 273 (1994).
R. E. Doezema, S. C. Whitmore, and J. N. Huffaker, *Phys. Rev. B* **34**, 4614 (1986).
R. J. Donnelly, Chapter 7 in *A Physics Desk Reference* (H. L. Anderson, Ed.). American Institute of Physics Press, 1989.
D. E. Farrell, C. J. Allen, R. C. Haddon, and S. V. Chichester, *Phys. Rev. B* **42**, 8694 (1990).
J. J. Finley and B. S. Deaver, Jr., *Solid State Commun.* **36**, 493 (1980).
W. J. Gallagher, *J. Appl. Phys.* **63**, 4216 (1988).
L. Gao, Z. J. Huang, R. L. Menag, J. G. Lin, F. Chen, L. Beauvais, Y. Y. Sun, Y. Y. Xue, and C. W. Chu, *Physica C* **213**, 261 (1993).
S. Gärtner, *Festkörperprobleme, Adv. Solid State Phys.*, Vol. 32 (1992).
R. F. Gasparovic and W. L. McLean, *Phys. Rev. B* **2**, 2519 (1970).
W. Gob, W. Lang, W. Kula, and R. Sobolewski, *Physica C* **235–240**, 1535 (1994).
V. G. Grebinnik, V. N. Duginov, V. A. Zhukov, S. Kapusta, A. B. Lazarev, V. G. Olshevsky, V. Yu. Pomjakushin, S. N. Shilov, I. I. Gurevich, B. F. Kirillov, B. A. Nikolsky, A. V. Pirogov, A. N. Ponomarev, V. A. Suetin, S. Safrata, J. Sebek, J. Burianek, and V. Valvoda, *Hyperfine Interactions* **61**, 1081 (1990).
F. Gross-Alltag, B. S. Chandrasekhar, D. Einzel, P. J. Hirschfeld, and K. Andres, *Z. Phys. B* **82**, 243 (1991).
S. Gygax, W. Biberacher, A. Lerf, and M. Denhoff, *Helvetica Physica Acta* **55**, 755 (1982).
D. P. Hampshire, *Physica C* **296**, 153 (1998).
D. R. Harshman, L. F. Schneemeyer, J. V. Waszczak, G. Aeppli, R. J. Cava, B. Batlogg, L. W. Rupp, E. J. Ansaldo, and D. Ll. Williams, *Phys. Rev. B* **39**, 851 (1989).
D. R. Harshman, R. N. Kleiman, R. C. Haddon, S. V. Chichester-Hicks, M. L. Kaplan, L. W. Rupp, Jr., T. Pfiz, D. Ll. Williams, and D. B. Mitzi, *Phys. Rev. Lett.* **64**, 1293 (1990).
M. Heinze, M. Baenitz, K. Lüders, H. Werner, and R. Schlögl, *Synthetic Metals 77*, **23** (1996).
M. Hikita and M. Suzuki, *Phys. Rev. B* **39**, 4756 (1987).
K. Holczer, O. Klein, G. Grüner, J. D. Thompson, F. Deiderich, and R. L. Whetten, *Phys. Rev. Lett.* **67**, 271 (1991).
Y. Iye and S. Tanuma, *Solid State Commun.* **44**, 1 (1982).
Y. X. Jia, J. Z. Liu, M. D. Lan, P. Klavins, R. N. Shelton, and H. B. Radousky, *Phys. Rev. B* **45**, 10609 (1992).
H. Jiang, T. Yuan, H. How, A. Widom, C. Vittoria, and A. Drehman, *J. Appl. Phys.* **73**, 5865 (1993).
H. Jiang, T. Yuan, H. How, A. Widom, C. Vittoria, D. Chrisey, J. Horwitz, and A. Drehman, *Phys. Rev. B* **49**, 9924 (1994).
P. H. Kes, A. Pruymboom, J. van den Berg, and J. A. Mydosh, *Cryogenics* **29**, 228 (1989).
R. N. Kleiman, C. Broholm, G. Aeppli, E. Bucher, N. Stucheli, D. J. Bishop, K. N. Clausen, K. Mortensen, J. S. Pedersen, and B. Howard, *Phys. Rev. Lett.* **69**, 3120 (1992).
Z. Koziol, A. Bakker, A. de Visser, and J. J. M. Franse, *Physica C* **185–189**, 2633 (1991).

L. Krusin-Elbaum, A. P. Malozemoff, Y. Yeshurun, D. C. Cronemeyer, and F. Holtzberg, *Phys. Rev. B* **39**, 2936 (1989).
W. K. Kwok, U. Welp, K. D. Carlson, G. W. Crabtree, K. G. Vandervoot, H. H. Wang, A. M. Kini, J. M. Williams, D. L. Stupka, L. K. Montgomery, and J. E. Thompson, *Phys. Rev. B* **42**, 8686 (1990).
M. Lang, N. Toyota, T. Sasaki, and H. Sato, *Phys. Rev. Lett.* **69**, 1443 (1992); *Phys. Rev. B* **46**, 5822 (1992).
W. C. Lee and D. M. Ginsberg, *Phys. Rev. B* **44**, 2815 (1991).
Q. Li, M. Suenaga, T. Hikata, and K. Sato, *Phys. Rev. B* **46**, 5857 (1992).
K. Lüders and M. Baenitz, Proc. 192nd Meeting Electrochem. Soc., Paris, Sept. 1997.
A. Maeda, T. Shibauchi, N. Kondo, K. Uchinokura, and M. Kobayashi, *Phys. Rev. B* **46**, 14234 (1992).
P. A. Mansky, P. M. Chaikin, and R. C. Hadden, *Phys. Rev. B* **50**, 15929 (1994).
I. Matsubara, H. Tanigawa, T. Ogura, H. Yamashita, M. Kinoshita, and T. Kawai, *Phys. Rev. B* **45**, 7414 (1992).
R. Meservey and B. B. Schwartz. *Superconductivity.* Vol. 1, Chapter 3. Dekker, New York, 1969.
V. V. Moshchalkov, A. A. Zhukov, O. V. Petrenko, A. A. Gippius, V. I. Voronkova, and V. K. Yanovskii, *International Seminar on High Temperature Superconductivity*, p. 514. World Scientific, Singapore, 1990.
K. Murata, H. Anzai, K. Kajimura, T. Ishiguro, and G. Saito, *Molecular Crystals and Liquid Crystals* **79**, 639 (1982).
H. Ning, H. Duan, P. D. Kirven, A. M. Hermann, and T. Datta, *J. Supercond.* **5**, 503 (1992).
H. Noel, P. Gougeon, J. Padiou, J. C. Levet, M. Potel, O. Laborde, and P. Monceau, *Solid State Commun.* **63**, 915 (1987).
B. H. O and J. T. Markert, *Phys. Rev. B* **47**, 8373 (1993).
T. P. Orlando and K. A. Delin, *Foundations of Applied Superconductivity* Addison-Wesley, MA, 1991.
V. Pagnon, C. Villard, C. Ayache, and J. C. Villegier, *Phys. B* **169**, 645 (1991).
A. Porch, J. R. Cooper, D. N. Zheng, J. R. Waldram, A. M. Campbell, and P. A. Freeman, *Physica C* **214**, 350 (1993).
C. P. Poole, Jr., T. Datta, and H. A. Farach, *Copper Oxide Superconductors.* Wiley, New York, 1988.
C. P. Poole, Jr., H. A. Farach, and R. Creswick, *Superconductivity.* Academic Press, New York, 1995.
B. Pumpin, H. Keller, W. Kundig, W. Odermatt, I. M. Savic, J. W. Schneider, H. Simmler, P. Zimmermann, E. Kaldis, S. Rusiecki, Y. Maeno, and C. Rossel, *Phys. Rev. B* **42**, 8019 (1990a).
B. Pumpin, H. Keller, W. Kundig, I. M. Savic, J. W. Schneider, H. Simmler, P. Zimmerman, E. Kaldis, S. Rusiecki, C. Rossel, and E. M. Forgan, *J. Less-Common Metals* **164–165**, 994 (1990).
M. Reedyk, C. V. Stager, T. Timusk, J. S. Xue, and J. E. Greedan, *Phys. Rev. B* **44**, 4539 (1991).
H.-C. Ri, R. Gross, F. Gollnik, A. Beck, R. P. Huebener, P. Wagner, and H. Adrian, *Phys. Rev. B* **50**, 3312 (1994).
M. B. Salamon, in *Physical Properities of High Temperature Superconductors* (D. M. Ginsberg, Ed.), Vol. 1, Chapter 2. World Scientific, Singapore, 1989.
E.-W. Scheidt, C. Hucho, K. Luders, and V. Muller, *Solid State Commun.* **71**, 505 (1989).
A. Schilling, F. Hulliger, and H. R. Ott, *Physica C* **168**, 272 (1990).
A. Schilling, O. Jeandupeux, S. Büchi, H. R. Ott, and C. Rossel, *Physica C* **235–240**, 229 (1994).
P. J. C. Signore, B. Andraka, G. R. Stewart, and M. W. Meisel, *Phys. Rev. B* **52**, 10315 (1995).
G. Sparn, J. D. Thompson, R. L. Whetten, S.-M. Huang, R. B. Kaner, F. Diederich, G. Grüner, and K. Holczer, *Phys. Rev. Lett.* **68**, 1228 (1992).
W. Staguhn, K. Nakao, N. Miura, M. von Ortenberg, S. Hatta, Y. Ichikawa, and K. Wasa, *J. Phys. Soc. Jpn.* **58**, 2877 (1989).
M. Suzuki, *Jpn. J. Appl. Phys.* **28**, 1541 (1989).
M. Suzuki and M. Hikita, *Phys. Rev. B* **44**, 249 (1991).
Y. Tajima, M. Hikita, T. Ishii, H. Fuke, K. Sugiyama, M. Date, A. Yamagishi, A. Katsui, Y. Hidaka, T. Iwata, and S. Tsurumi, *Phys. Rev. B* **37**, 7956 (1988).
T. Takagi, Y.-M. Chiang, and A. Roshko, *J. Appl. Phys.* **68**, 5750 (1990).

J. R. Thompson, D. K. Christen, H. A. Deeds, Y. C. Kim, J. Brynestad, S. T. Sekula, and J. Budal, *Phys. Rev. B* **41**, 7293 (1990).
J. R. Thompson, J. G. Ossandon, D. K. Christen, B. C. Chakoumakos, Y. R. Sun, M. Paranthaman, and J. Brynestad, *Phys. Rev. B* **48**, 14031 (1993).
M. Tinkham, *Introduction to Superconductivity*, McGraw Hill, New York, 1996.
B. vom Hedt, R. Noetzel, W. Lisseck, H. Bach, K. Westerholt, and B. Freitag, *Phys. Rev. B* **51**, 3993 (1995).
T. Watanabe, T. Ishii, K. Kinoshita, and A. Matsuda, *Physica C* **185–189**, 1235 (1991).
R. Wördenweber and P. H. Kes, *Cryogenics* **29**, 321 (1989).
T. K. Worthington, W. J. Gallagher, and T. R. Dinger, *Phys. Rev. Lett.* **59**, 1160 (1987).
D. H. Wu, J. Mao, S. M. Mao, J. L. Peng, X. X. Xi, T. Vehkatesan, R. L. Greene, and S. M. Anlage, *Phys. Rev. Lett.* **70**, 85 (1993).
H. Zhang, J. W. Lynn, and D. E. Morris, *Phys. Rev. B* **45**, 10022 (1992).

D

Superconducting Gap Parameters

John F. Zasadzinski and Roberta K. Zasadzinski

Below the transition temperature of a superconductor, an energy gap $\Delta = \frac{1}{2}E_g$ develops in the electronic density of states that is exhibited in a number of experimental probes, including specific heat, optical reflectivity, and ultrasonic attenuation. The most direct probe of the gap is from tunneling spectroscopy. Specifically, the tunneling conductance, dI/dV vs. V, in normal metal–insulator–superconductor (NIS) junctions is proportional to the electronic density of states in the superconductor. Table 9.3 presents energy gaps which have been determined by tunneling. One exception is the fullerene Rb_3C_{60} where the energy gap was determined by muon spin rotation. The text by E.L. Wolf (1985) provides a thorough description of the tunneling experiment and includes a comprehensive list of gap values of low-T_c superconductors.

For high-T_c cuprates and other oxides, there are lengthy reviews (Hasegawa *et al.*, 1992; Ekino and Akimitsu, 1992) and general articles (Zasadzinski *et al.*, 1996) that cover most of the important phases and describe the problems associated with tunneling in these exotic materials. Energy gaps of individual compounds can vary considerably among different tunneling experiments and an attempt has been made to select the best values. There is considerable evidence that the gap in high-T_c cuprates is highly anisotropic within the a–b plane and is most likely of $d_{x^2-y^2}$ symmetry. Thus, the energy gap is decribed by

$$\Delta(\mathbf{k}) = {}^1\!/_2\Delta_0(\cos k_x a - \cos k_y a), \tag{21}$$

where k_x, k_y are the components of the wave vector within the plane. This symmetry has nodal regions where the gap is zero. The parameters listed for high-T_c cuprates are the maximum values Δ_0 of the gap. For electron-doped cuprates such as $(Nd_{1-x}Ce_x)_2CuO_4$ which have relatively low T_c, the experimental

Table 9.3.

Energy gaps $\Delta_0 = E_g/2$ for various superconductors.

Material	T_c (K)	Δ(meV)	Source
s,p elements			
Al	1.18	0.179	Wolf (1985)
Cd	0.42	0.072	Wolf (1985)
Zn	0.85	0.13	Wolf (1985)
Ga	1.08	0.169	Wolf (1985)
Am–Ga	8.56	1.66	Wolf (1985)
Sn	3.72	0.593	Wolf (1985)
In	3.41	0.541	Wolf (1985)
Tl	2.38	0.369	Wolf (1985)
Pb	7.196	1.33	Wolf (1985)
Am–Pb	7.2	1.442	Wolf (1985)
Am–Hg	3.90	0.739	Wolf (1985)
Hg (α phase)	4.15	0.824	Wolf (1985)
s,p alloys and unusual phases			
$Tl_{0.9}Bi_{0.1}$	2.3	0.355	Wolf (1985)
$Pb_{0.4}Tl_{0.6}$	4.6	0.805	Wolf (1985)
$Pb_{0.6}Tl_{0.4}$	5.9	1.08	Wolf (1985)
$Pb_{0.8}Tl_{0.2}$	6.8	1.28	Wolf (1985)
$Pb_{0.9}Bi_{0.1}$	7.65	1.539	Wolf (1985)
$Pb_{0.8}Bi_{0.2}$	7.95	1.610	Wolf (1985)
$Pb_{0.7}Bi_{0.3}$	8.45	1.769	Wolf (1985)
$Pb_{0.65}Bi_{0.35}$	8.95	1.843	Wolf (1985)
d-band elements			
Re	1.70	0.263	Wolf (1985)
Ta	4.49	0.720	Wolf (1985)
V	5.40	0.814	Wolf (1985)
Nb	9.25	1.55	Wolf (1985)
d-band alloys and compounds			
$Nb_{0.6}Ti_{0.6}$	9.8	1.73	Wolf (1985)
$Nb_{0.8}Zr_{0.2}$	11.0	1.94	Wolf (1985)
NbN	14.0	2.56	Kihlstrom *et al.* (1985)
VN	8.7	1.5	Zhao *et al.* (1984)
V_3Si (A15)	17	2.78	Wolf (1985)
Nb_3Sn (A15)	18.3	3.39	Wolf (1985)
Nb_3Sn (A15)	17.5	3.30	Wolf (1985)
Nb_3Al (A15)	16.4	3.04	Wolf (1985)
Nb_3Ge(A15)	23	4.16	Wolf (1985)
Ternary compounds			
$ErRh_4B_4$	8.5	1.45	Wolf (1985)
$Cu_{1.8}Mo_6S_8$	12.5	2.3	Pobell (1981)
$PbMo_6S_8$	12	2.4	Pobell (1981)
Heavy fermions			
UBe_{13}	0.80	0.145	Moreland *et al.* (1994)
UPt_3	0.44	0.075[a]	De Wilde *et al.* (1994)
$CeCu_2Si_2$	0.630	0.080	De Wilde *et al.* (1994)
URu_2Si_2	1	0.170	De Wilde *et al.* (1994)
f-band elements			
Th	1.38	0.206	Wolf (1985)

(*continued*)

Table 9.3. (*continued*)

Material	T_c (K)	Δ(meV)	Source
La(α)	4.88	0.8	Wolf (1985)
La(dhcp)	4.95	0.8	Wolf (1985)
Organics			
$(BEDT\text{-}TTF)_2Cu(NCS)_2$	11	2.4	Bando *et al.* (1990)
β-$(BEDT\text{-}TTF)_2I_3$	1.35	0.465	Nowak *et al.* (1987)
β-$(BEDT\text{-}TTF)_2IAuI$	4.1	0.707	Nowak *et al.* (1987)
β-$(BEDT\text{-}TTF)_2AuI_2$	3.8	2.6	Hawley *et al.* (1986)
Fullerenes			
Rb_3C_{60}	29.4	4.6	Kiefl *et al.* (1993)
Oxide superconductors, noncuprate			
$Li_{0.9}Mo_6O_{17}$	1.5	0.23	Ekino and Akimitsu (1992)
$LiTi_2O_4$	11	1.8	Ekino and Akimitsu (1992)
$Ba_{1-x}Pb_xBiO_3$	11	1.6	Ekino and Akimitsu (1992)
$Ba_{1-x}K_xBiO_3$	28	4.5	Huang *et al.* (1990)
Copper oxide superconductors			
$Nd_{2-x}Ce_xCuO_4$ [b]	22	3.7	Huang *et al.* (1990)
$Pr_{2-x}Th_xCuO_4$ [b]	22	3.6	Zasadzinski *et al.* (1996)
$Sr_{1-x}Nd_xCuO_2$ [b,c]	35	6.0	Zasadzinski *et al.* (1996)
$La_{2-x}Sr_xCuO_4$	36	7	Hasegawa *et al.* (1992)
$YBa_2Cu_3O_7$	92	20	Hasegawa *et al.* (1992)
$YBa_2Cu_3O_{7-x}$	60	9	Hasegawa *et al.* (1992)
$Bi_2Sr_2CuO_6$	10	3.5	Hasegawa *et al.* (1992)
$Bi_2Sr_2CaCu_2O_8$	95	38	Miyakawa *et al.* (1998)
$Bi_2Sr_2CaCu_2O_{8+x}$ [d]	86	28	Hasegawa *et al.* (1992)
$Bi_2Sr_2CaCu_2O_{8+x}$ [d]	62	18	Miyakawa *et al.* (1998)
$Bi_2Sr_2Ca_2Cu_3O_{10}$	105	33	Hasegawa *et al.* (1992)
$Tl_2Ba_2CuO_6$	90	22	Zasadzinski *et al.* (1996)
$Tl_2Ba_2CaCu_2O_8$	114	30	Hasegawa *et al.* (1992)
$HgBa_2CuO_4$	94	24	Hasegawa *et al.* (1992)
$HgBa_2CuO_4$	97	33	Wei *et al.* (1996)
$HgBa_2CaCu_2O_6$	124	50	Wei *et al.* (1996)
$HgBa_2Ca_2Cu_3O_8$	135	75	Wei *et al.* (1996)

[a] Not s-wave; may have gap nodes. [b] Electron-doped. [c] Infinite-layer compound. [d] Overdoped.

evidence is more toward a conventional, s-wave, symmetric gap that is isotropic in momentum space. All noncuprate superconductors measured to date appear to be s-wave, with the possible exception of the heavy fermion compound UPt_3, which displays evidence of gap nodes.

Table 9.3 lists the energy gaps Δ_0 for various superconductors.

References for Section D

H. Bando, S. Kashiwaya, H. Tokumoto, H. Anzai, N. Kinoshita, and K. Kajimura, *J. Vac. Sci. Technol. A* **8** (1), 479 (1990).

Y. De Wilde, J. Heil, A. G. M. Jansen, P. Wyder, R. Deltour, W. Assmus, A. Menovsky, W. Sun, and L. Taillerfer, *Phys. Rev. Lett.* **72**, 2278 (1994).
T. Ekino and J. Akimitsu, in *Studies of High Temperature Superconductors, Vol. 9* (Anant Narlikar Ed.) Nova Science, 1992.
T. Hasegawa, H. Ikuta, and K. Kitazawa, in *Physical Properties of High Temperature Superconductors III*, (D. M. Ginsberg Ed.) World Scientific, Singapore, 1992.
M. E. Hawley, K. E. Gray, B. D. Terris, H. H. Wang, K. D. Carlson and Jack M. Williams, *Phys. Rev. Lett.*, **57**, 629 (1986).
Q. Huang, J. F. Zasadzinski, N. Tralshawala, K. E. Gray, D. G. Hinks, J. L.Peng and R. L. Greene, *Nature* **347**, 369 (1990).
R. F. Kiefl, W. A. MacFarlane, K. H. Chow, S. Dunsiger, T. L. Duty, T. M. S. Johnston, J. W. Scneider, J. Sonier, L. Brard, R. M. Strongin, J. E. Fischer, and A. B. Smith III, *Phys. Rev. Lett.*, **70**, 3987 (1993).
K. E. Kihlstrom, R.W. Simon, and S.A. Wolf, in *Materials and Mechanisms of Superconductivity* (K. A. Gschneidner, Jr. and Edward L. Wolf Eds.) North Holland, Amsterdam, 1985.
N. Miyakawa, P. Guptasarma, J. F. Zasadzinski, D. G. Hinks, K. E. Gray, *Phys. Rev. Lett.*, **80**, 157 (1998).
J. Moreland, A. F. Clark, R. J. Soulen, Jr., and J. L. Smith, *Physica B* **194–196**, 1727 (1994).
A. Nowack, U. Poppe, M. Weger, D. Schweitzer, and H. Schwenk, *Z. Phys. B- Condensed Matter* **68**, 41 (1987).
F. Pobell, in *Ternary Superconductors* (G. K. Shenoy, B. D. Dunlap and F. Y. Fradin, Eds.) North Holland, New York, 1981.
J. Y. T. Wei, C. C. Tsuei, P. J. M. van Bentum, Q. Xiong, C. W. Chu, and M. K. Wu, *Phys. Rev. B* **57** 3650 (1998).
E. L. Wolf, *Principles of Electron Tunneling Spectroscopy.* (Oxford Univ. Press, New York, 1985).
J. F. Zasadzinski, L. Ozyuzer, Z. Yusof, J. Chen, K. E. Gray, R. Mogilevsky, D. G. Hinks, J. L. Cobb, and J. T. Market, in *Spectroscopic Studies of High T_c Cuprates*, (I. Bozovic, D. van der Marel Eds.) SPIE, Bellingham, 1996.
B. R. Zhao, B. R. Zhao, L. Chen, H. L. Luo, M. D. Jack, and D. P. Mullin, *Phys. Rev. B* **29**, 6198 (1984).

E

Critical Magnetic Fields

There are various ways to determine the lower and upper critical magnetic fields, B_{c1} and B_{c2}, respectively, and Table 9.4 lists measured values for many superconductors. Also listed in the table are values of the two negative slopes

$$B'_{c1} = -\frac{dB_{c1}}{dT} \tag{22a}$$

$$B'_{c2} = -\frac{dB_{c2}}{dT}, \tag{22b}$$

evaluated at the transition temperature $T = T_c$. Measured values of the upper critical field slope B'_{c2} from Eq. (22b) are often in the neighborhood of the Pauli coefficient 1.83 of Eq. (3),

$$B'_{c2} \approx -1.83\ T/K. \tag{23}$$

Table 9.4.

Lower (B_{c1}, mT), and upper (B_{c2}, T) critical magnetic fields for various superconductors. Values for the critical temperature T_c and the critical field derivatives at T_c, namely $-B'_{c1} = dB_{c1}/dT$ and $-B'_{c2} = dB_{c2}/dT$, are also given. Elements that superconduct only at high pressure, after irradiation, or as thin films are not listed. References are identified by first author and year. D/P denotes average of values tabulated in Donnelly (1989) and Poole *et al.* (1995).

Material	T_c (K)	B_{c1} (mT)	B_{c2} (T)	$-B'_{c1}$ (mT/K)	$-B'_{c2}$ (T/K)	Comments	Reference
Ir	0.11	1.6				Type I superconductor; value is B_c	D/P
Hf	0.13	1.3				Type I superconductor; value is B_c	D/P
Ti	0.40	5.6				Type I superconductor; value is B_c	D/P
Ru	0.49	6.9				Type I superconductor; value is B_c	D/P
Cd	0.52	2.8				Type I superconductor; value is B_c	D/P
Zr	0.61	4.7				Type I superconductor; value is B_c	D/P
Os	0.66	7.0				Type I superconductor; value is B_c	D/P
Zn	0.85	5.4				Type I superconductor; value is B_c	D/P
Ga	1.08	5.8				Type I superconductor; value is B_c	D/P
Al	1.18	10.5				Type I superconductor; value is B_c	Delin (1996)
Th	1.38	16				Type I superconductor; value is B_c	D/P
W	1.5	0.115				Type I superconductor; value is B_c	D/P
Re	1.7	20				Type I superconductor; value is B_c	D/P
Tl	2.38	17.8				Type I superconductor; value is B_c	D/P
In	3.41	22.5				Type I rf measured; value is B_c	Bruynseraede (1971), Delin (1996)
Sn	3.72	30.5				Type I superconductor; value is B_c	Delin (1996)
β-Hg	3.9	33.9				Type I superconductor; value is B_c	D/P
α-Hg	4.15	41				Type I superconductor; value is B_c	D/P
Ta	4.47	83				Type I superconductor; value is B_c	D/P
α-La	4.88	80				Type I superconductor; value is B_c	D/P
V	5.40	141				Type I superconductor; value is B_c	D/P
	5.35	140				Type I superconductor; value is B_c	Däumer (1982)

(*continued*)

Table 9.4. (*continued*)

Material	T_c (K)	B_{c1} (mT)	B_{c2} (T)	$-B'_{c1}$ (mT/K)	$-B'_{c2}$ (T/K)	Comments	Reference
	2.83	900				10% Cr-doped solid solution	Däumer (1982)
	2.11	640				10% Mn-doped solid solution	Däumer (1982)
	4.08	1470				10% Nb-doped solid solution	Däumer (1982)
	2.85	960				10% Mo-doped solid solution	Däumer (1982)
	3.59	1370				10% Ta-doped solid solution	Däumer (1982)
	3.84	980				10% W-doped solid solution	Däumer (1982)
β-La	6.1	110				10% W-doped solid solution	D/P
Tc	7.9	141				10% W-doped solid solution	D/P
Mo	8.0				4.5		Koepke (1976)
Pb		75				rf measurement	Bruynseraede (1971)
	7.20	80				10% W-doped solid solution	Delin (1996)
Nb		158				Wire 10% W-doped solid solution	Ghamati (1985)
	9.25	198				10% W-doped solid solution	Delin (1996)
	9.3	248	≈ 0.4			Cold-drawn wire	Roberts (1976)
$Cr_{0.7}Re_{0.3}$	3.2		2			bcc α phase	Damaschke (1986)
In, Pb doped	3.7	30	0.04			Alloy	Roberts (1976)
Nb, Mo doped	7.8	49	0.4			Alloy	Roberts (1976)
Nb, Jp doped	9.5	60	2			Alloy	Roberts (1976)
Nb, Ta doped	8.8	173	0.445			Alloy	Roberts (1976)
CTa	≈ 10	22	0.46			NaCl structure	Roberts (1976)
NbN	16		15			NaCl structure	Donnelly (1989)
	15		22–25			Tape; see J_c table	Suzuki (1989)
	16.3		12			Thin film; see J_c table	Boffa (1996)
	16		35			NbN on carbon fibers	Dietrich (1985)
NbN	16		28			Film measured at 1.3 K; see J_c table	Gavaler (1983)
	16		22			Neutron irradiation	Gregshammer (1988)
	16		25			B_{app} parallel to film plane	Suzuki (1992)

	16		30	B_{app} perpendicular to film plane	Suzuki (1992)
	16	9	15		Orlando (1991), Roberts (1976)
NbTi			17–18	Alloy	Radhakrishnan (1987)
			12	Polycrystalline, magnetostriction	Wyder (1995)
			11.3	NbTi/Cu wire 1.5 m long	ten Haken (1994)
	9.2		12	Monofilament	Chovanec (1973)
	9.6		14		Hampshire (1998)
PbBi	8.3		0.5		Delin (1996)
PbIn	7		0.2		Delin (1996)
Nb/NbZr multilayer				Consult references	Kuwasawa (1990, 1996)
$NbSe_2$	7.2		17.4		Roberts (1976)
Ti–Nb–Si alloy	5.1		2	Ductile alloy	Inoue (1980)
Nb–Hf/Cu–Sn-Ga			25	Multifilimentary	Ekin (1981)
$In_{0.92}Pb_{0.08}$		27			Bruynseraede (1971)
$Be_{32.5}Mo_5Zr_{62.5}$	3.05		4.2	2.5 Amorphous alloy	Goebbels (1981)
$Be_{32.5}Nb_{2.5}Zr_{65}$	3.26		4.82	2.63 Amorphous alloy, NMR	Freyhardt (1980)
$Be_{32.5}Nb_5Zr_{62.5}$	3.46		5.27	2.88 Amorphous alloy, NMR	Freyhardt (1980), Goebbels (1981)
$Be_{32.5}Nb_7Zr_{60.5}$	3.58		5.70	2.90 Amorphous alloy, NMR	Freyhardt (1980), Goebbels (1981)
Mo_2Rh_2B	3.5		≈ 7	2.3 Ribbons approx. 17 μm × 150 μm	Zöltzer (1985)
$(Mo_{0.55}Ru_{0.45})_4P$	5.43		4.7	Value at 4 K	Häussler (1996)
$NbC_{1-y}N_y$	15–17		21	(Nb carbonitride) see J_c table	Dietrich (1983), Schmaderer (1983)
				Measured at 4.2 K	
			> 20	Coating on carbon fibers; see J_c table	Dietrich (1987)
HfV_2 Laves	9.2	187	21.7		Vonsovsky (1982)
$(Hf_{0.5}Zr_{0.5})V_2$ Laves	10.1	197	28.3		Vonsovsky (1982)
ZrV_2 Laves	8.5	219	16.5		Vonsovsky (1982)
V_2(HfZr) Laves			22	Measured at 4.2 K	Inoue (1985)
			28	Measured in pulsed fields at 2.0 K	Inoue (1985)
$Al_{0.5}SnMo_5S_6$ Chevrel	14.4		56		Donnelly (1989)
$Cu_xMo_6S_8$ Chevrel	10			2.3 Sputtered sample	Alterovitz (1978)

(*continued*)

Table 9.4. (*continued*)

Material	T_c (K)	B_{c1} (mT)	B_{c2} (T)	$-B'_{c1}$ (mT/K)	$-B'_{c2}$ (T/K)	Comments	Reference
$HoMo_6S_8$ Chevrel	0.685		0.32			Monocrystal, magnetic transitions at 0.75 and 0.70 K	Burlet (1987)
$LaMo_6S_8$ Chevrel	7		8				Sulkowski (1984)
	≈ 6.5		5.4				Vonsovsky (1982)
$PbMo_{6.35}S_8$ Chevrel	12.6		54				Donnelly (1990)
$PbMo_6S_8$ Chevrel						$B_{irr} = 39$ T at 4.2 K	Ramsbottom (1997)
	13		55				Ali (1995), Hampshire (1998)
			~ 55			Powder	Cattani (1991)
			> 50				Seeber (1989)
	13		45			Sputtered film, B_{c2} estimated	Alterovitz (1979)
$PbMo_6Se_8$ Chevrel	3.8		3.8				Vonsovsky (1982)
$Pb_{1-x}Gd_xMo_6S_8$ Chevrel	15		60			Chevrel	Ali (1996)
$SnMo_6S_8$ Chevrel	14		31				
	11.8		34				Vonsovsky (1982)
Mo_3Si	7.2				2.1	$\kappa \approx 65$	Wördenweber (1988)
Cr_3Ir *A*15	0.75	16.8	1.05				Roberts (1976)
Nb_3Al *A*15	17.8		> 26.9			Multifilimentary composite wire; $B_{c2} = 26.9$ T at 1.8 K and 24.6 T at 4.2 K	Fukuda (1997)
	18.7		32.5				Donnelly (1989)
	17		23.2			Wire, measured at 4.2 K	Saito (1990a,b)
	15		17–21			Multifilamentary wire	Dew-Hughes (1981)
	15.7		20.2			Powder metallurgy; see J_c table	Watanabe (1990)
Nb_3Ga *A*15	20.2		34.1				Donnelly (1989)
Nb_3Ge *A*15	23		39				Donnelly (1989)
	21		30			Nb_3Ge layers on Al_2O_3 slices	Fröhlich (1989)
	20		33			B_{c2} measurement at 4.2 K, sputtered films	Suzuki (1992)
	3.4				1.96	7.9 μm film	Wördenweber (1986)

α-$Nb_{0.74}Ge_{0.26}$	3.4		5.46		Amorphous film, $B_c = 42.4$ mT	Berghuis (1993)
Nb_3Sn *A*15			24.7		Prepared from Nb_6Sn_5; see J_c table. Tape measured at 4.2 K	Tachikawa (1996, 1997)
			17.4		Unalloyed wire	Kohno (1992)
			20.8		Alloyed wire	Kohno (1992)
	17.8		23.4		Wire	Saito (1992a,b)
			21.4		2 wt% Ti; see J_c table	Schaper (1987)
	17.7		27.8		Measured at 4.2 K, 4 at % Ta, multifilamentary wires	Foner (1987)
	17		24	2.2	10^4 filaments in bronze matrix	Rupp (1981)
	17.8		28	2.1	Film on sapphire	Bormann (1985)
	18		33	2.6	Film on sapphire, with 1.5 at. % Ga	Bormann (1985)
		45.6			Monocrystal	Ghamati (1985)
	18.2	35	23			Roberts (1976)
	16		42			Hampshire (1998)
			26.5		Wires with Ta, Ti and Ni + Zn additives; see J_c table	Drost (1985), see Suenaga (1984)
			31.5		Measured at 4.2 K, with 1 to 1.5 at. % Ga	Bormann (1985)
			19		$B_{c2} = B_{c2}(0)[1 - (T/T_c)^2]$	Finnemore (1983)
	17.5		24	1.9	Superconducting layers	Kozlenkova (1992)
$Nb_3Al_{0.5}Ga_{0.5}$ *A*15	19		31			Donnelly (1989)
$Nb_3Al_{0.57}Ga_{0.23}$	20.1		44			Donnelly (1989)
$(NbTa)_3Sn$			26		Filamentary conductor	Springer (1983)
Nb_3(Al, Si, Bi)	18		21			Muller (1991), Schaper (1989)
V_3Ga *A*15	15		23			Donnelly (1989)
V_3Ge *A*15	6.8		≈ 5			Roberts (1976)
V_3Si A15	16	55	23			Roberts (1976)
			18		For B along (100) direction at 1.5 K, de Haas van Alphen effect	Mueller (1992)
Cu–Nb composite	8.8		1.1			Reddy (1986)
$CeCu_2$	~ 0.17			5	Heavy electron, pressure to 8.3 GPa	Vargoz (1997)

(*continued*)

Table 9.4. (*continued*)

Material	T_c (K)	B_{c1} (mT)	B_{c2} (T)	$-B'_{c1}$ (mT/K)	$-B'_{c2}$ (T/K)	Comments	Reference
$CeCu_2Ge_2$	0.64		2			Heavy electron, pressure of 101 kbar	Jaccaard (1992)
$CeCu_2Si_2$	0.72		1.5			Heavy electron, $B-T$ phase diagram	Hunt (1990)
UBe_{13}		4.4	10			Heavy electron, $\kappa \approx 100$	Mayer (1986)
	0.88		≈ 10		31	Heavy electron, B_{c2} estimated from figs.	Signore (1995)
	0.9		6			Heavy electron	Maple (1984)
$U_{0.97}Th_{0.03}Be_{13}$	0.35	4.0				Heavy electron	Rauchschwalbe (1987)
UPt_3	0.46		1.9			Heavy electron	Schenström (1989)
$Ba_{1-x}K_xBiO_3$ cubic	24					$B_{irr} = 24$ T at 0.4 K	Goll (1996)
$ReNi_2B_2C$	15.3		6			Thin film	Andreone (1997)
YNi_2B_2C	15.7		10.5			Torque method	Goll (1997)
			10.6			Single crystal, de Haas-van Alphen	Heinecke (1995)
	15	37	6			See $\xi\lambda$ table	Cywinski (1994)
K_3C_{60}	17.8		17		1.4	Fullerene	Baenitz (1994, 1995)
	19.5		30		2.8	Fullerene	Foner (1992)
	19	13	32			Fullerene	Poole (1995)
K_2CsC_{60}	23	17	21			Fullerene, $\kappa = 50$	Baenitz (1998)
Rb_3C_{60}		< 0.5				Fullerene	Kraus (1996)
	28.4		55		3.85	Fullerene	Fouer (1992)
	30.7	15	31			Fullerene, $\kappa = 60$	Baenitz (1998)
	29.5		44		2.15	Fullerene, $B_{PL} = 54$	Baenitz (1993)
	29.6	12	57				Poole (1995)
Rb_2CsC_{60}	32.5		50		2.3	Fullerene	Baenitz (1994, 1995)
Ba doped C_{60}	6.8				0.35	Fullerene	Baenitz (1995)
$Nd_{1.82}Ce_{0.18}CuO_{4-\delta}$			~ 3			Single crystal film	Harus (1996), Ponomarev (1996)
$YBa_2Cu_3O_{7-\delta}$			35			At 77.3 K	Watanabe (1989)
			180			At 0 K	Watanabe (1989)
			340			Film, $B_{c2}(0)$ measured	Bykov (1995)

		75			6% Gd substituted for Y, monocrystal	Gupta (1990)
	85	2.5			Low value due to porosity	Ferguson (1988)
	59		~55		Pulsed fields up to 40 T	Kapustin (1994)
			105		Thin film, measured at 4.2 K with $B \perp c$	Basovich (1992)
			68.5			Collocott (1988)
			200		Sintered samples	van Bentum (1989)
					Thermodynamic critical field	Ziese (1994)
					$B_c \sim [1-(T/T_c)]^2$ for $T \geqslant 20$ K	
			59		Films by MOCVD, B_{c2} measured at 77 K; activ. energy $U(B) = 1.98$ eV at 21 T	Matsuno (1991, 1992)
	60		15	0.35		Donglu (1988)
	90		98	1.49		Donglu (1988)
					$B_{c2}(T) = B_{c2}(0)(1-t^2)/(1+t^2)$	Golosovsky (1994)
$TmBa_2Cu_3O_{7-\delta}$				2.2	Single crystal; see $\xi\lambda$ table	Moshchalkov (1990)
$Bi_2Sr_{1.7}CaCu_2O_8$			55			Collocott (1988)
$Bi_2Sr_2CaCu_2O_8$	86		36		Polycrystal, B_{c2} value at 65 K	Ries (1992), Welp (1989a)
$Bi_2Sr_2Ca_2Cu_3O_{10}$	110		58			Li (1988)
$CuBa_2Ca_3Cu_4O_x$	117				$B_{irr} = 9.5$ T at 70 K	Iyo (1997)
					$B_{irr} = 3.7$ T at 77 K	
					$B_{int} \sim 2130[1-(T/T_c)]^{5.91}$	
$Bi_{1.6}Pb_{0.3}Te_{0.1}Sr_2Ca_3Cu_4O_y$			201		Composition is nominal	Vlakhov (1994)
$Tl_2Ba_2Ca_2Cu_3O_y$(Tl-2223)					$B_{irr} = 22.0$ T for $B \| ab$ plane	Nabatame (1992)
					$B_{irr} = 0.89$ T for $B \perp ab$ plane	
Tl ceramics	114		$\approx 10^3$		Pulsed magnetic field	Kapustin (1992)

Table 9.5.

Lower (B_{c1}, mT), and upper (B_{c2}, T) critical magnetic fields perpendicular to (B_{c1}^{ab}, B_{c2}^{ab}), and parallel to (B_{c1}^{c}, B_{c2}^{c}) the c axis for various superconductors. Values for the critical temperature T_c and the upper critical field derivatives at T_c, namely $-B_{c2}^{ab'} = \mathrm{d}B_{c2}^{ab}/dT$ and $-B_{c2}^{c'} = dB_{c2}^{c}/dT$ for the perpendicular and parallel cases, respectively, are also given. References are identified by first author and year.

Material	T_c (K)	B_{c1}^{ab} (mT)	B_{c1}^{c} (mT)	B_{c2}^{ab} (T)	B_{c2}^{c} (T)	$-B_{c2}^{ab'}$ (T/K)	$-B_{c2}^{c'}$ (T/K)	Comments	Reference
Nb	9.3			0.57	0.31			B_{c2}^{c} is value meas. $\perp$ film B_{c}^{ab} is value meas. $\parallel$ film	Oya (1989)
UPd_2Al_2						5.8	4.9	Thin film, temperature, and angular dependence	Hessert (1997)
Nb_3S_4	3.65			0.5	2.1			zig-zag Nb-Nb-Nb- chains	Biberacher (1980)
$CeCu_2Si_2$	0.63			2.0	2.4			Heavy electron	Assmus (1984)
UPd_2Al_3	1.91			3.5	4.1	6.5	5.6	Heavy electron	Hessert (1995)
YNi_2B_2C	15			7	8.3			Meas at 4.2 K	Arisawa (1995)
β-$(ET)_2I_3$	1.5	7	36	1.74	0.08			ab values are averages of measurements along a and b	Ishiguro (1990)
β-$(ET)_2I_3$				25	2.7			Organic, at 1.6 kbar	Ishiguro (1990)
β-$(ET)_2IBr_2$	2.3	390	1600	3.48	1.5			ab values are averages of measurements along a and b	Ishiguro (1990)
β-$(ET)_2AuI_2$	4.2	400	2050	≈ 6.35	≈ 0.8			Organic material	Ishiguro (1990)
K-$(ET)_2Cu[N(CN)_2]Br$	11.6					20	2.2	Organic material	Kwok (1990)
(TMTSF)2ClO4	1.06	0.055	0.24					$B_{c1}^{b} = 0.055$	Schwenk (1984)
$(Sm_{0.925}Ce_{0.075})_2CuO_4$	11.4			28.2	5.2	3.6	0.1	Electron type material	Dalichaouch (1990)
$(La_{0.925}Ca_{0.075})_2CuO_4$	≈ 14			> 20	> 13	4	0.3		Hidaka (1987)
$(La_{0.925}Ca_{0.075})_2CuO_4$	30				32		1.5		Li (1993)
$(La_{0.925}Ca_{0.075})_2CuO_4$	≈ 34	7	30						Naito (1990)
$YBa_2Cu_3O_{6.5}$	62	2.5	8.3	380	87	8.7	2.0		Vandervoort (1991)
$YBa_2Cu_3O_{6.9}$		23	95					Monocrystal	Moschalkov (1991)
$YBa_2Cu_3O_{6.94}$	91.2		32		115		1.8		Ossandon (1992)
$YBa_2Cu_3O_{7-\delta}$	87			145	72			Films on (100) $SrTiO_3$	Topchishvili (1991)

				≈100				Thin film measured at 4.2 K	Basovich (1992)
	92.4	⩽ 5	500	240	34	3.8	0.54	$B_c = 1.93$	Gallagher (1988); see also Worthington (1987)
		24	95						Salamon (1989), Malozemoff (1989)
				110	40	3.4	1.0		Nakao (1993)
	90	18	53						Krushin-Elbaum (1989)
		11.3	34					See $\xi\lambda$ table	Scheidt (1989)
	92					10.5	1.9		Welp (1989a,b)
$DyBa_2Cu_3O_7$				100				Measured at 4.2 K	Hampshire (1988)
$EuBa_2Cu_3O_7$	95			190	45	3.0	0.7		Hikita (1987)
	94.8			245	28	3.8	0.41		Tajima (1988)
$Y_{0.8}Pr_{0.2}Ba_2Cu_3O_{6.9}$	73			174	56	3.4	1.1		Jia (1992)
$Bi_{2.1}Sr_{2.1}Ca_{0.9}Cu_{2.0}O_{8+\delta}$	85			542	71.5			Monocrystal	Li (1988)
	80					8.5	0.56	Oriented thin film	Kang (1988)
	90	85							Maeda (1992)
$Bi_2Sr_2CaCu_2O_{8+\delta}$	≈ 86	6.3						Microwave absorption	Misra (1992)
$(Bi,Pb)_2Sr_2CaCu_2O_8$	91				≈89		1.4	$B_c = 0.65$	Zhang (1992)
$Bi_2Sr_2Ca_2Cu_3O_8$	109					16	0.5		Matsubara (1992)
	110			50	1000			$B_{irrev} = 24$ T	Matushita (1993)
$Bi_{1.7}Pb_{0.7}Sr_2Ca_2Cu_3O_{10}$				39	198			Ag-clad tape	Babic (1995)
$Pb_2Sr_2(Y,Ca)Cu_2O_8$	76	9.5	50.5	590	96	11	1.75	Monocrystal	Reedyk (1992)
TlBaCaCuO						20	0.6	Thin film, pulsed fields; see $\xi\lambda$ table	Staguhn (1989)
$HgBa_2Ca_2Cu_3O_{8+\delta}$	131		45		190		2.0		Schilling (1994)

The upper critical field slope (22b) is of especial interest for materials such as the cuprates in which it is often not feasible to reach high enough applied fields to experimentally determine B_{c2} directly.

The thermodynamic critical field B_c is not usually measured directly, but can be calculated from the expressions

$$B_c = \frac{\sqrt{2}\kappa B_{c1}}{\ln \kappa} = \frac{B_{c2}}{\sqrt{2}\kappa} = \frac{(B_{c1}B_{c2})^{1/2}}{(\ln \kappa)^{1/2}} \tag{24}$$

if the Ginzburg–Landau parameter κ is known. We also have the quotient relation

$$B_{c2}/B_{c1} = 2\kappa^2/\ln \kappa, \tag{25}$$

and of course we know that $\kappa = \lambda/\xi$. The lower, thermodynamic, and upper critical fields in the isotropic high κ approximation ($\kappa \gg 1$ so $B_{c1} \ll B_c \ll B_{c2}$) are related to the coherence length ξ and penetration depth λ through Eqs. (7), (8), and (4), respectively. Equations (4) and (7) can be used to estimate ξ and λ, respectively, when B_{c2} and B_{c1} are known.

Many superconductors are anisotropic, and Table 9.5 lists critical fields for axially symmetric materials. Also listed are the upper critical field slopes (22b) for the perpendicular ($-B_{c2}^{ab'}$) and parallel ($-B_{c2}^{c'}$) cases. We see from the data that the slope $-B_{c2}^{ab'}$ for the cuprates tends to exceed the Pauli limit value 1.83 T/K of Eq. (23), and $-B_{c2}^{c'}$ tends to be less than this value. This occurs because ordinarily $B_{c2}^{ab} > B_{c2}^{c}$.

References for Section E

S. Ali, H. D. Ramsbottom, D. N. Zheng, and D. P. Hampshire, *Appl. Supercond. 1995, Proc. of EuCAS 1995, Second European Conf. on Appl. Supercond.* **1**, 583 (1995); publ. IOP, Bristol.

S. Ali, Univ. Durham, UK (Dissertation, 1996).

S. A. Alterovitz and J. A. Woollam, Solid State Commun. **25**, 141 (1978); *Cryogenics* **19**, 167 (1979).

A. Andreone, F. Fontana, M. Iavarone, M. Salluzzo, and R. Vaglio, *J. Low Temp. Phys.* **107**, 527 (1997).

S. Arisma et al., Adv. Supercond. VII, Vol. 2, Springer, 1995.

W. Assmus, M. Herrmann, U. Rauchschwalbe, S. Riegel, W. Lieke, H. Spille, S. Horn, G. Weber, F. Steglich, and G. Cordier, *Phys. Rev. Lett.* **52**, 469 (1984).

E. Babic et al., Fizika **4**, 549 (1995).

M. Baenitz, E. Straube, S. Gärtner, H. Werner, R. Schlögl, and K. Lüders, *Fullerene Sci. & Tech.* **1**, 177 (1993).

M. Baenitz, M. Heinze, K. Luders, H. Werner, and R. Schlogl, *Solid State Commun.* **91**, 337 (1994); M. Baenitz, M. Heinze, E. Straube, H. Werner, R. Schlögl, V. Thommen, H.-J. Güntherodt, and K. Lüders, *Physica C* **228**, 181 (1994).

M. Baenitz, M. Heinze, K. Luders, H. Werner, and R. Schlogl, *Physics and Chemistry of Fullerenes and Derivatives. Proc. Intern. Winterschool on Electronic Properties of Novel Materials*, p. 436. World Scientific, Singapore, 1995.

M. Baenitz and K. Lüders, submitted for publication.

A. J. Basovich, S. V. Gaponov, E. B. Kluenkov, P. P. Kolokolchikov, U. B. Kudasov, I. M. Markevtsev, A. I. Pavlovskii, V. V. Platonov, O. M. Tatsenko, and S. A. Voronov, *Phys. Lett. A* **163**, 322 (1992).

P. Berghuis and P. H. Kes, *Phys. Rev. B* **47**, 262 (1993).

W. Biberacher and H. Schwenk, Solid State Commun. **33**, 385 (1980).

V. Boffa, U. Gambardella, V. Marotta, A. Morone, F. Murtas, S. Orlando, and G. P. Parisi, *Appl Surf. Sci.* **106**, 361 (1996).
R. Bormann, D.-Y. Yu, R. H. Hammond, T. H. Geballe, S. Foner, and E. J. McNiff, Jr., *IEEE Trans. Magnetics* **MAG-21**, 1140 (1985).
Y. Bruynseraede, D. Gorle, D. Leroy, and P. Morignot, *Physica* **54**, 137 (1971).
P. Burlet, A. Dinia, S. Quezel, W. A. C. Erkelens, J. Rossat-Mignod, R. Horyn, O. Pena, C. Geantet, M. Sergent, and J. L. Genicon, *Physica B & C* **148B + C**, 99 (1987).
A. I. Bykov, M. I. Dolotenko, C. M. Fowler, B. L. Freeman, J. D. Goettee, J. C. King, N. P. Kolokolchikov, Yu. B. Kudasov, W. Lewis, B. R. Marshall, B. J. Papatheofanis, V. V. Platonov, P. J. Rodriguez, O. M. Tatsenko, L. R. Veeser, and W. D. Zerwekh, *Physica B* **211**, 248 (1995).
D. Cattani, J. Cors, M. Decroux, and O. Fischer, *IEEE Trans. Magnetics* **27**, 950 (1991).
F. Chovanec and V. Klabik, *Ceskoslovensky Casopis pro Fyziku, A* **23**, 515 (1973).
S. J. Collocott, C. Andrikidis, R. Driver, and G. K. White, *Intern. J. Modern Physics B* **2**, 1387 (1988).
R. Cywinski, Z. P. Han, R. Bewley, R. Cubitt, M. T. Wylie, E. M. Forgan, S. L. Lee, M. Warden, and S. H. Kilcoyne, *Physica C* **233**, 273 (1994).
Y. Dalichaouch, B. W. Lee, C. L. Seaman, J. T. Markert, and M. B. Maple, *Phys. Rev. Lett.* **64**, 599 (1990).
B. Damaschke and W. Felsch, *Z. Phys. Cond. Master B* **63**, 179 (1986).
W. Däumer, A. Kettschau, H. R. Khan, K. Lüders, Ch. J. Raub, H. Riesemeier, and G. Roth, *Phys. Stat. Sol. (b)* **112**, K67 (1982).
K. A. Delin and T. P. Orlando, "Superconductivity," in *CRC Handbook of Engineering*, (R. C. Dorf, Ed.), p. 1274. CRC Press, Boca Raton, FL, 1996.
D. Dew-Hughes, *IEEE Trans. Magnetics* **MAG-17**, 561 (1981).
M. Dietrich, C.-H. Dustmann, F. Schmaderer, and G. Wahl, *IEEE Trans. Magnetics* **MAG-19**, 406 (1983).
M. Dietrich, *IEEE Trans. Magnetics* **MAG-21**, 455 (1985).
M. Dietrich, E. Fitzer, and T. Stumm, *High Temperatures — High Pressures* **19**, 89 (1987).
Shi Donglu, *J. Appl. Phys.* **64**, 4624 (1988).
R. J. Donnelly, Chapter 7 in *A Physicist's Desk Reference* (H. L. Anderson, Ed.). Amer. Inst. of Phys. Press, New York, 1989.
E. Drost, W. Specking, and R. Flukiger, *IEEE Trans. Magnetics* **MAG-21**, 281 (1985).
J. W. Ekin, H. Sekine, and T. Tachikawa, *J. Appl. Phys.* **52**, 6252 (1981).
G. Ferguson, K. O'Grady, A. Briggs, and I. A. Denton, presented at Critical Currents in High T_c Superconductors, Birmingham, UK, 16 May 1988.
D. K. Finnemore, J. E. Ostenson, E. D. Gibson, J. D. Verhoeven, and T. B. Doyle, *J. Appl. Phys.* **54**, 1476 (1983).
S. Foner, E. J. McNiff, D. Heiman, S.-M. Huang, and R. B. Kaner, *Phys. Rev. B* **46**, 14936 (1992).
S. Foner, E. J. McNiff, Jr., G. M. Ozeryansky, and R. E. Schwall, *IEEE Trans. Magnetics* **23**, 984 (1987).
H. C. Freyhardt, J. Goebbels, K. Luders, J. Reichelt, *Physica Status Solidi B* **102**, K137 (1980).
K. Fröhlich, D. Machajdík, A. Zat'ko, A. Rosová, and S. Takács, *Czech. J. Phys. B* **39**, 196 (1989).
K. Fukuda, G. Iwaki, F. Hosono, S. Sakai, Y. Iijima, T. Takeuchi, K. Inoue, N. Kobayashi, K. Watanabe, and S. Awaji, *IEEE Trans. Appl. Supercond.* **7**, 1572 (1997).
W. J. Gallagher, *J. Appl. Phys.* **63**, 4216 (1988).
J. R. Gavaler, J. Greggi, R. Wilmer, and J. W. Ekin, *IEEE Trans. Magnetics* **MAG-19**, 418 (1983).
S. Ghamati, H. Suhl, W. Vernon, and G. Webb, *IEEE Trans. Magnetics* **MAG-21**, 831 (1985).
J. Goebbels, K. Lüders, H. C. Freyhardt, and J. Reichelt, *Physica B* **108**, 1223 (1981).
G. Goll, A. G. M. Jansen, and J. Marcus, *Czech. J. Phys* **46**, 849 (1996).
G. Goll, L. Nguyen, E. Steep, A. G. M. Jansen, P. Wyder, and K. Winzer, *Physica B* **230**, 868 (1997).
M. Golosovsky, M. Tsindlekht, H. Chayet, and D. Davidov, *Phys. Rev. B* **50** 470 (1994).
P. Gregshammer, H. W. Weber, R. T. Kampwirth and K. E. Gray, *J. Appl. Phys.* **64**, 1301 (1988).
A. Gupta, P. Esquinazi, and H. F. Braun, *Physica B* **165**, 1443 (1990).
D. P. Hampshire, J. Seuntjens, L. D. Cooley, and D. C. Larbalestier, *Appl. Phys. Lett.* **53**, 814 (1988).

D. P. Hampshire, *Physica C* **296**, 153 (1998).
G. I. Harus, A. N. Ignatenkov, N. K. Lerinman, A. I. Ponomarev, L. D. Sabirzyanova, N. G. Shelushinina, N. A. Babushkina and L. M. Belova, *Pis'ma Zhurnal Eksperimental'noi i Teoreticheskoi Fiziki* **64**, 407 (1996).
R. Häussler, G. Goll, Yu. G. Naidyuk, and H. von Löhneysen, *Physica B* **218**, 197 (1996).
M. Heinecke and K. Winzer, *Z. Physik B* **98** 147 (1995).
J. Hessert, M. Huth, M. Jourdan, H. Adrian, C. T. Rieck, and K. Scharnberg, *Physica B* **230–232**, 373 (1997).
Y. Hidaka, Y. Enomoto, M. Suzuki, M. Oda, and T. Murakami, *Jpn. J. Appl. Phys.* **26**, L377 (1987).
M. Hikita, Y. Tajima, A. Katsui, Y. Hidaka, T. Iwata, and S. Tsurumi, *Phys. Rev. B* **36**, 7199 (1987).
M. Hunt, P. Meeson, P.-A. Probst, P. Reinders, M. Springford, W. Assmus, and W. Sun, *Physica B* **165–166**, 337 (1990).
A. Inoue, H. M. Kimura, T. Masumoto, C. Suryanarayana, and A. Hoshi, *J. Appl. Phys.* **51**, 5475 (1980).
K. Inoue, T. Kuroda, and K. Tachikawa, *IEEE Trans. Magnetics* **MAG-21**, 467 (1985).
T. Ishiguro and K. Yamaji, *Organic Superconductors*. Springer-Verlag, Berlin, 1990.
A. Iyo, K. Tokiwa, N. Terada, M. Tokumoto, M. Hirabayashi, and H. Ihara, *Adv. Cryogenic Engrg. Materials* **42**, 623 (1997).
D. Jaccard, K. Behnia, and J. Sierro, *Phys. Lett. A* **163**, 475 (1992).
Y. X. Jia, J. Z. Liu, M. D. Lan, P. Klavins, R. N. Shelton, and H. B. Radousky, *Phys. Rev. B* **45**, 10609 (1992).
P. P. Juschitz and E. Schachinger, *Physica B* **194–196**, 1811 (1994).
J. H. Kang, R. T. Kampwirth, and K. E. Gray, *Applied Phys. Lett.* **52**, 2080 (1988).
G. A. Kapustin, B. B. Tolkachev, Yu. A. Cherushev, and L. D. Shustov, *Physica C* **190**, 549 (1992).
G. Kapustin, B. Tolkachev, Yu. Cherushev, V. Shapiro, G. Fuchs, A. Gladun, and M. Ritschel, *Proc. 7th Intern. Workshop on Critical Currents in Supercond. (7th IWCC)*. World Scientific, Singapore, 1994.
R. Koepke and G. Bergmann, *Solid State Commun.* **19**, 435 (1976).
O. Kohno, T. Saito, N. Sadakata, M. Sugimoto, K. Goto, and K. Watanabe, *Science Reports of Research Institutes, Tohoku University, Series A (Physics, Chemistry, and Metallurgy)* **37**, 84 (1992).
N. I. Kozlenkova, Yu. V. Konovalov, A. I. Skvortsov, A. K. Shikov, Yu. V. Bobkov, and E. Yu. Klimenko, *Superconductivity* **5**, 1309 (1992).
M. Kraus, H. Sindlinger, H. Werner, R. Schlogl, V. Thommen, H. P. Lang, H.-J. Guntherodt, and K. Lüders, *J. Phys. Chem. Solids* **57**, 999 (1996).
L. Krushin-Elbaum, A. P. Malozemoff, Y. Yeshurun, D. C. Cronemeyer, and F. Holtzberg, *Phys. Rev. B* **39**, 2936 (1989).
Y. Kuwasawa, U. Hayano, T. Tosaka, S. Nakano, and S. Matuda, *Physica C* **165**, 173 (1990).
Y. Kuwasawa, T. Nojima, S. Hwang, B. J. Yuan, and J. P. Whitehead, *Physica B* **222**, 92 (1996).
W. K. Kwok, U. Welp, K. D. Carlson, G. W. Crabtree, K. G. Vandervoort, H. H. Wang, A. M. Kini, J. M. Williams, D. L. Stupka, L. K. Montgomery, and J. E. Thompson, *Phys. Rev. B* **42**, 8686 (1990).
J. N. Li, K. Kadowaki, M. J. V. Menken, Y. K. Huang, K. Bakker, A. A. Menovsky and J. J. M. Franse, *Appl. Phys. A* **47**, 209 (1988).
Q. Li, M. Suenaga, T. Kimura, and K. Kishio, *Phys. Rev. B* **47**, 11384 (1993).
K. Lüders and M. Baenitz, Proc. 192nd Meeting Electrochem. Soc. Paris, Aug. 31–Sept. 5 (1997).
A. Maeda, T. Shibauchi, N. Kondo, K. Uchinokura, and M. Kobayashi, *Phys. Rev. B* **46**, 14234 (1992).
A. P. Malozemoff, Chapter 3 in *Physical Properties of High Temperature Superconductors*, Vol. 1 (D. M. Ginsberg, Ed.) World Scientific, Singapore, 1989.
M. B. Maple, J. W. Chen, S. E. Lambert, Z. Fisk, J. L. Smith, and H. R. Ott, cited in G. R. Stewart, *Rev. Mod. Phys.* **56** 755 (1984).
I. Matsubara, H. Tanigawa, T. Ogura, H. Yamashita, M. Kinoshita, and T. Kawai, *Phys. Rev. B* **45**, 7414 (1992).
S. Matsuno, F. Uchikawa, K. Yoshizaki, N. Kobayashi, K. Watanabe, Y. Muto, and M. Tanaka, *IEEE Trans. Magnetics* **27**, 1398 (1991).

S. Matsuno, F. Uchikawa, K. Yoshizaki, N. Kobayashi, K. Watanabe, Y. Muto, and Y. Nakabayashi, *Science Reports of Research Institutes, Tohoku University, Series A (Physics, Chemistry, and Metallurgy)* **37**, 183 (1992).

H. M. Mayer, U. Rauchschwalbe, C. D. Bredl, F. Steglich, H. Rietschel, H. Schmidt, H. Wuhl, and J. Beuers, *Phys. Rev. B* **33**, 3168 (1986).

S. K. Misra and M. Kahrizi, *Physica* **C195**, 71 (1992).

V. V. Moshchalkov, A. A. Zhukov, D. K. Petrov, V. I. Voronkova, V. K. Yanovskii, *Physica C* **166**, 185 (1990a); V. V. Moshchalkov, A. A. Zhukov, O. V. Petrenko, A. A. Gippius, V. I. Voronkova, and V. K. Yanovskii, *Intern. Seminar High Temp. Supercond.*, Dubna, Russia, p. 514. World Scientific, Singapore, 1990b.

V. V. Moshchalkov, J. Y. Henry, C. Marin, J. Rossat-Mignod, and J. F. Jacquot, *Phys. C* **175**, 407 (1991).

F. M. Mueller, D. H. Lowndes, Y. K. Chang, A. J. Arko, and R. S. List, *Phys. Rev. Lett.* **68**, 3928 (1992).

D. Muller, M. Kehlenbeck, W. Schaper, and H. C. Freyhardt, *Supercond. Sci. & Tech.* **4**, 365 (1991).

T. Nabatame, K. Watanbe, S. Awaji, Y. Saito, K. Aihra, T. Kamo, and Shin-Pei Matsuda, *Jpn. J. Appl. Phys.* **31**, L1041 (1992).

M. Naito, A. Matsuda, K. Kitazawa, S. Kambe, I. Tanaka, and H. Kojima, *Phys. Rev. B* **41**, 4823 (1990).

K. Nakao, N. Miura, K. Tatsuhara, H. Takeya, and H. Takei, *Phys. Rev. Lett.* **63**, 97 (1993).

T. P. Orlando and K. A. Delin, *Foundations of Applied Superconductivity*, Addison-Wesley, Reading, MA, 1991.

J. G. Ossandon, J. R. Thompson, D. K. Christen, B. C. Sales, Y. Sun, and K. W. Lay, *Phys. Rev. B* **46**, 3050 (1992a).

J. G. Ossandon, J. R. Thompson, D. K. Christen, B. C. Sales, H. R. Kerchner, J. O. Thomson, Y. R. Sun, K. W. Lay, and J. E. Tkaczyk, *Phys. Rev. B* **45**, 12534 (1992b)

G. Oya, T. Komukai, and Y. Sawada, *J. Materials Research* **4**, 283 (1989).

A. I. Ponomarev, N. A. Babushkina, L. M. Belova, A. N. Ingatenkov, G. I. Harus, N. K. Lerinman, L. D. Sabirayanova, and N. G. Shelushinina, *J. Low Temp. Phys.* **105**, 939 (1996).

C. P. Poole, Jr., H. A. Farach, and R. J. Creswick, *Superconductivity.* Academic Press, New York, 1995.

T. S. Radhakrishnan, *Pramana* **28**, 555 (1987).

H. D. Ramsbottom and D. P. Hampshire, *Physica C* **274**, 295 (1997).

U. Rauchschwalbe, F. Steglich, G. R. Stewart, A. L. Giorgi, P. Fulde and K. Maki, *Europhys. Lett.* **3**, 751 (1987).

Y. S. Reddy, M. M. Krishna, and R. G. Sharma, *J. Low Temp. Phys.* **65**, 261 (1986).

M. Reedyk, C. V. Stager, T. Timusk, J. S. Xue, and J. E. Greedan, *Phys. Rev. B* **45**, 10057 (1992).

G. Ries, H. W. Neumüller, and W. Schmidt, *Supercond. Sci. Technol.* **5**, S81 (1992).

B. W. Roberts, *J. Phys. Chem. Ref. Data* **5**, 581 (1976).

G. Rupp, E. J. McNiff, Jr. and S. Foner, *IEEE Trans. Magnetics* **MAG-17**, 370 (1981).

S. Saito, K. Ikeda, S. Ikeda, A. Nagata, and K. Noto, *Materials Trans., JIM* **31**, 415 (1990a).

S. Saito, K. Ikeda, S. Ikeda, A. Nagata, and K. Noto, *11th Intern. Conf. Magnet Technology (MT-11)*, p. 974. Elsevier Applied Science, 1990b.

S. Saito and S. Hanada, *J. Appl. Phys.* **72**, 4984 (1992a).

S. Saito, T. Wachi, K. Adachi, and S. Hanada, *J. Jpn. Inst. Metals* **56**, 960 (1992b).

M. B. Salamon, in *Physical Properties of High Temperature Superconductors* (D. M. Ginsberg, Ed.), Vol. 1, Chapter 2. World Scientific, Singapore, 1989.

W. Schaper. J. Wecker, K. Mrowiec, R. Bormann, and H. C. Freyhardt, *J. Appl. Phys.* **62**, 1937 (1987).

W. Schaper, M. Kehlenbeck, I. Zimmermann, and H. C. Freyhardt, *IEEE Trans. Magnetics* **25**, 1988 (1989).

E.-W. Scheidt, C. Hucho, K. Luders, and V. Muller, *Solid State Commun.* **71**, 505 (1989).

A. Schenström, M.-F. Xu, Y. Hong, D. Bein, M. Levy, B. K. Sarma, S. Adenwalla, Z. Zhao, T. Tokuyasu, D. W. Hess, J. B. Ketteron, J. A. Sauls, and D. G. Hinks, *Phys. Rev. Lett.* **62**, 332 (1989).

A. Schilling, O. Jeandupeux, S. Büchi, H. R. Ott, and C. Rossel, *Physica C*, **235**, 229 (1994).

F. Schmaderer, G. Wahl, C. H. Dustmann, and M. Dietrich, *Proc. 4th European Conf. Chemical Vapour Deposition*, p. 148 (J. Bloem, G. Verspui, and L. R. Wolff, Eds.) Philips Centre Manuf. Technol., Eindhoven, The Netherlands, 1983.

H. S. Schwenk and K. Andres, *Solid State Commun.* **49**, 723 (1984).
B. Seeber, P. Herrmann, J. Zuccone, D. Cattani, J. Cors, M. Decroux, O. Fischer, E. Kny, and J. A. A. J. Perenboom, *Proc. MRS Intern. Meeting on Advanced Materials*, Vol. 6, *Supercond.*, p. 83 (1989).
P. J. C. Signore, B. Andraka, G. R. Stewart, and M. W. Meisel, *Phys. Rev. B* **52** 10315 (1995).
E. Springer, M. Wilhelm, H. H. Weisse, and G. Rupp, *Adv. Cryogenic Materials* Vol. 30, *Proc. Fifth Intern. Cryogenic Materials Conf.*, p. 747 (1983).
W. Staguhn, K. Nakao, N. Miura, M. von Ortenberg, S. Hatta, Y. Ichikawa, and K. Wasa, *J. Phys. Soc. Jpn.* **58**, 2877 (1989).
M. Suenaga, K. Tsuchiya, and N. Higuchi, *Appl. Phys. Lett.* **44**, 919 (1984).
C. Sulkowski and J. Szymaszek, *Phys. Stat. Sol. (a)* **83**, K191 (1984).
M. Suzuki and T. Anayama, *Sci. Rep. Ritu, A* **37**, No. 1 (1992).
M. Suzuki, T. Kiboshi, T. Anayama, and A. Nagata, *Proc. MRS Intern. Meeting Adv. Mater.*, Vol. 6, *Supercond.*, p. 77 Mater. Res. Soc., Pittsburgh, 1989; M. Suzuki and M. Hikita, *Jpn. J. Appl. Phys.* **28**, L1368 (1989).
K. Tachikawa, M. Natsuume, Y, Kuroda, and H. Tomori, *Cryogenics* **36**, 113 (1996).
K. Tachikawa, Y. Kuroda, H. Tomori, and M. Ueda, *IEEE Trans. Appl. Supercond.* **7**, 1355 (1997).
Y. Tajima, M. Hikita, T. Ishii, H. Fuke, K. Sugiyama, M. Date, A. Yamagishi, A. Katsui, Y. Hidaka, T. Iwata, and S. Tsurumi, *Phys. Rev. B* **37**, 7956 (1988).
B. ten Haken, E. Krooshoop and H. H. J. ten Kate, *Cryogenics* **34**, suppl. issue, 583 (1994).
L. S. Topchishvili, I. A. Baglaenko, B. V. Brodksii, T. Sh. Berdzenishvili, Yu N. Berozashvili, D. Sh. Lordkipanidze, T. S. Shengeliya, and V. Sh. Edilashvili, *Superconductivity: Physics, Chemistry, Technology* **4**, 479 (1991).
P. J. M. van Bentum, H. van Kempen, J. A. A. J. Perenboom, L. W. M. Schreurs, P. A. A. Teunissen, and H. J. L. van der Steen, *Physica B* **155**, 160 (1989).
K. G. Vandervoort, U. Welp, J. E. Kessler, H. Claus, G. W. Crabtree, W. K. Kwok, A. Umezawa, B. W. Veal, J. W. Downey, A. P. Paulikas, and J. Z. Liu, *Phys. Rev. B* **43**, 13042 (1991).
E. Vargoz, P. Link, D. Jaccard, T. Le Bihan, and S. Heathman, *Physica B* **229**, 225 (1997).
E. S. Vlakhov, K. A. Nenkov, M. Ciszek, A. Zaleski, and Y. B. Dimitriev, *Physica C* **225**, 149 (1994).
S. V. Vonsovsky, Yu. A. Izyumov, and E. Z. Kurmaev, *Superconductivity in Transition Metals*. Springer, New York, 1982.
K. Watanabe, H. Yamane, H. Kurosawa, T. Hirai, N. Kobayashi, H. Iwasaki, K. Noto, and Y. Muto, *Appl. Phys. Lett.* **54**, 575 (1989).
K. Watanabe, K. Noto, Y. Kamisada, E. Suzuki, and Y. Muto, *11th Intern. Conf. Magnet Tech. (MT-11)*, p. 968. Elsevier Appl. Sci., London, 1990.
U. Welp, W. K. Kwok, G. W. Crabtree, K. G. Vandervoort, and Z. J. Liu, *Phys. Rev. Lett.* **62**, 1908 (1989a); *Phys. Rev. B* **40**, 5263 (1989b).
R. Wördenweber and P. H. Kes, Intern. Conf. Critical Currents in High-Temperature Superconductors, Snowmass Village, Colorado, USA, 16–19 August 1988.
R. Wördenweber and P. H. Kes, *Phys. Rev. B* **34**, 494 (1986).
T. K. Worthington, W. J. Gallagher, and T. R. Dinger, *Phys. Rev. Lett* **59**, 1160 (1987).
U. Wyder, P. J. E. M. van der Linden, H. P. van der Meulen, A. Gerber, V. H. M. Duyn, J. A. A. J. Perenboom, A. de Visser, and J. J. M. Franse, *Physica B* **211**, 265 (1995).
L. Zhang, J. Z. Liu, and R. N. Shelton, *Phys. Rev. B* **45**, 4978 (1992).
M. Ziese and P. Esquinazi, *Zeit. Phys. B* **94**, 265 (1994).
K. Zöltzer and H. C. Freyhardt, *J. Appl. Phys.* **58**, 1910 (1985).

Table 9.6.

Critical current density J_c for various superconductors. Values for the temperature T_{meas} and the field B_{app} of measurement are also given. References are identified by first author and year.

Material	J_c (A/cm^2)	B_{app} (tesla)	T_{meas} (K)	Comments	Reference
Melt textured high-T_c materiels		0.02 to 1	77	$J_c \sim [1-(T/T_c)]^{\alpha}/B^{\beta}$, where $\alpha \leqslant 7$, $\beta \sim 0.5$	Fisher (1994)
Cu–Nb composite	2.5×10^5	Self field	4.2	$T_c = 8.8$ K	Reddy (1986)
NbTi	3.4×10^5	5	4.2	Superconducting composite	Li (1983)
	3×10^5	5		Filament diameters 5 to 9 μm	Kanithi (1989)
	3×10^5	0.5	4.2	Filament diameter 50–500 nm; see $\xi\lambda$ table	Cave (1989)
	1.41×10^6	1		Wire enclosed by CuNi alloy, 0.072 μm filament diameter, J_c is less for 0.061 μm filament diameter	Kumano (1990)
	1.07×10^6	1		0.4 μm filament, artificial pinning control	Miura (1992)
	4.44×10^5	3		0.4 μm filament, artificial pinning control	Miura (1992)
	5.2×10^5	5	4.2	47 wt% Ti, filaments are aligned	Cooley (1991)
	2.85×10^5	5		48 wt%Ti, 210 filament, 1.6 mm diameter wire	Chernyi (1997)
	3.5×10^5	5	4.2	Industrial wires	Chernoplekov (1992)
	3.36×10^5	3		Wire, 54 wt% Ti	Inoue (1995)
	4.6×10^5	5	4.2	Artificial pinning center wire, 47 wt%Ti	Heussner (1997)
NbN	2×10^4	0		Josephson junction 1.5 μm^2 area	Tarutani (1984)

(*continued*)

Table 9.6. (*continued*)

Material	J_c (A/cm^2)	B_{app} (tesla)	T_{meas} (K)	Comments	Reference
	6.5×10^4	15	4.2	Tape, parallel field, see B_c table; $T_c = 15.6$ K	Suzuki (1989)
	1×10^4	20	4.2	Tape, parallel field, see B_c table; $T_c = 15.6$ K	Suzuki (1989)
	$> 10^7$			Extrapolated value, thin film; see B_c table	Boffa (1996)
	8×10^5	0	4.2	Film; see B_c table	Gavaler (1983)
Nb carbonitride	$1–5 \times 10^5$	13		Layers 50–80 nm thick; see B_c table	Dietrich (1987)
	10^6	0	4.2	$T_c = 15 - 17$ K; see B_c table, $NbC_{1-y}N_y$	Dietrich (1983)
	10^4	13	4.2	$T_c = 15 - 17$ K; see B_c table, $NbC_{1-y}N_y$	Dietrich (1983)
	10^6	0	4.2	Film	Brunet (1979)
	3×10^4	14	4.2	Film	Brunet (1979)
	10^3	18	4.2	Film	Brunet (1979)
NbN/AlN/NbN	5.4×10^4			Tunnel junction	Zhen (1997)
Nb, $Nb_{0.5}Zr_{0.5}$ multilayer	1.2×10^5	0	20	Anisotropy effects	Kuwasawa (1990, 1991)
V_2(Hf,Zr) Laves	1×10^4	17	4.2	Multifilamentary wire	Inoue (1985)
	2×10^4	20	1.8	Multifilamentary wire	Inoue (1985)
$M_xMo_6S_8$Chevrel	2×10^4	8	4.2		Alekseevskii (1977)
$PbMo_6S_8$ Chevrel	1.8×10^4	14	4.2	Tape	Hamasaki (1985)
	1.6×10^4	20	4.2	Hot isostatic-pressed wire	Yamasaki (1992, 1988)
	9.5×10^3	23	4.2	Hot isostatic-pressed wire	Yamasaki (1992, 1988)
	4.8×10^3	26	4.2	Hot isostatic-pressed wire	Yamasaki (1992, 1988)
	4×10^4	10	4.2	Calculated by Kramers' scaling law	Ramsbottom (1997)
	10^4	17	4.2	Monofilamentary wire	Hamasaki (1989)
	1.8×10^3	27	4.2	Monofilamentary wire	Hamasaki (1989)

$SnMo_6S_8$ and $Pb_{0.6}Sn_{0.4}Mo_6S_8$	Range 10^5 to 5×10^3	9	4.2	Monofilament Chevrel wires	Gupta (1995)
$Pb_{0.6}Sn_{0.4}Mo_6S_8$ Chevrel	$> 10^5$	10	4.2	Coils of 1 meter wire	Cheggour (1995)
	5×10^4	15	4.2	Coils of 1 meter wire	Cheggour (1995)
$Pb_{1.2}Mo_6S_{7.8}$ Chevrel	1.3×10^4	23		Wire	Kubo (1989)
$Pb_{1.2}Mo_{6.4}S_8$Chevrel	3.5×10^4	14	1.7		Alekseevskii (1982)
Pb–Mo–S Chevrel	$> 10^6$	0			Hamasaki (1982)
Pb–Mo–S Chevrel	5×10^4	8			Hamasaki (1982)
Chevrel	5.4×10^4	20	1.9	Wire with Nb as antidiffusion barrier	Cheggour (1997)
	3.1×10^4	24	1.9	Wire with Nb as antidiffusion barrier	Cheggour (1997)
V_3Ga, *A*15	2×10^6	10	4.2	Multifilamentary wire	Francavilla (1979)
	1.6×10^6	9	4.2	Single core wire	Sharma (1981)
	1×10^5	20	4.2		Sharma (1987)
Nb_3Al, *A*15	$> 10^4$	23		Tapes with Ge doping for Al	Kumakura (1990)
	4.86×10^4	20	1.8	Composite wire; see B_c table	Fukuda (1997)
	1.95×10^4	20	4.2	Composite wire; see B_c table	Fukuda (1997)
	1.13×10^5	12		Wire	Ayai (1997)
	10^4	18.8		Wire, $T_c = 17\,K$	Saito (1990)
	10^4	16	4.2	Wire, $T_c = 15.7\,K$	Watanabe (1990)
	10^4	17.5	4.2	Wire, powder metallurgy	Watanabe (1987)
Nb_3Ge, *A*15	10^3	Self field	19	Sapphire substrate, $T_c = 22.4\,K$	Oya (1979)
	2×10^4	20	4.2	Nb_3Ge deposited on 0.1 mm thick tapes	Nakagawa (1987)
Nb_3Sn, *A*15	2×10^{10}	5	4.2	Fast neutron irradiated wires	Brown (1978)
	10^5	15		2 at.% Ti in Nb core	Tachikawa (1981)
	3×10^4	15		B_{app} parallel to tape surface	Yoshida (1983)
	6.7×10^4	20	1.8	Bronze processed multifilamentary wires	Suenaga (1984)
	3.7×10^4	20	4.2	Bronze processed multifilamentary wires	Suenaga (1984)
	4×10^4	12		Al-stabilized strand	Takahashi (1985)

(*continued*)

Table 9.6. (*continued*)

Material	J_c (A/cm^2)	B_{app} (tesla)	T_{meas} (K)	Comments	Reference
	6×10^4	18		Studies of Ta, Ti, Ni + Zn addition; see B_c table	Drost (1985)
	10^4	19		Multifilamentary wire with 7.5% Ta	Flukiger (1985)
	1.2×10^4	16		2 wt% Ti; see B_c table	Schaper (1987)
	4.5×10^3	18		2 wt% Ti; see B_c table	Schaper (1987)
	3.5×10^4	15	4.2	Ti addition	Sharma (1987)
	4.0×10^5	11	4.2	CVD tape	Zhou (1983)
	1.7×10^5	15	4.2	Diffusion processed tape	Zhou (1983)
	2.7×10^4	21	4.2	Tape prepared from Nb_6Sn_5; see B_c table; adding Ge improves T_c, J_c	Tachikawa (1996, 1997)
	1×10^4	17	4.2	Bronze processed multifilamentary wire	Watanabe (1991)
Cu–Nb_3Sn	10^4	12		Multifilamentary composites	Flukiger (1979)
$Ti_{0.45}Nb_{0.40}Si_{0.15}$	1.2×10^6		4.2	Composition range studied, $T_c = 9.9$ K	Inoue (1980)
	1.5×10^4		4.2	Amorphous alloy after crystallization	Inoue (1981)
Nb–Ti–Si alloy	10^5	5		Effects of aging studied	Ishida (1981)
Oxidized polypropylene	10^8			Material has conducting channels	Demicheva (1990)
K_3C_{60}, fullerene	1.3×10^5	1	7		Holczer (1991)
Rb_3C_{60}, fullerene	4×10^6	1	7		Politis (1992)
$Nd_{1.85}Ce_{0.15}CuO_{4-\delta}$	8×10^5	0	4.2	Thin film, $T_c = 22.4$ K	Mao (1993)
$YBa_2Cu_3O_{7-\delta}$	10^8–10^9	0	4.2	Below depairing limit	Tsuei (1988)
	10^7–10^8	0	77	Below depairing limit	Tsuei (1988)
	4×10^6	0	77.3	*c*-axis oriented films	Hitotsuyanagi (1989)
	10^4	20	77.3	*c*-axis oriented films	Hitotsuyanagi (1989)
	3.5×10^7	0	4.2	Epitaxial films	Lensink (1989)
	1.3×10^6	0	77	Epitaxial films	Lensink (1989)

	1.2×10^6	0	53	Primarily c-axis oriented film	Singh (1991)
	3×10^5	0	77	Primarily c-axis oriented film	Singh (1991)
	1.6×10^7	0	4.2	Thin film on several substrates	Gorbenko (1993)
	2×10^7	0	5	Thin film, tetragonal phase, $T_c = 87\,K$	Garcia Lopez (1997)
	2.7×10^6		44	10 wt% Ag doped thin films on MgO	Kim (1997)
	1.2×10^6		44	20 wt% Ag doped thin films on MgO	Kim (1997)
	3×10^5	0	77.3	Angular and field dependence studied	Watanabe (1991)
	2.4×10^4	2	77	J_c measured for different B_{app} and a, b plane orientations	Ren (1990)
	1.4×10^5			$B \perp c$, $J = J_0 \exp(-T/T_0)$, $T_0 = 27\,K$, monocrystal	Moshchalkov (1991)
	8.1×10^5			$B \| c$, $J = J_0 \exp(-T/T_0)$, $T_0 = 40\,K$ monocrystal	Moshchalkov (1991)
	5.8×10^6		77	Thin film with Ag doping	Clausen (1996)
	2.7×10^6	0	77	Film prepared by MOCVD	Matsuno (1991)
	2.5×10^4	30	77	Film prepared by MOCVD	Matsuno (1991)
	3.25×10^7		10	Thin film unirradiated, $T_c = 89\,K$	Agarwal (1991)
	0.9×10^7		10	Thin film after He^+ irradiation	Agarwal (1991)
	4.9×10^6	0	77	$J_c(B, T) \sim J_c(B, 0)[1 - \alpha(T/T_c) - \beta(T/T_c)^2]$; thin film	Cui (1992)
				$J_c = J_{c0}(1 + t)^2(1 - t)^{1.75} \times [1 - (B/B_{c2})]$	Kes (1988)
	1.2×10^6	0.3	4.2	Electron spin resonance (ESR) method	Meshcheryakov (1992)
	2×10^4	0		SNS; many Josephson junctions reported	Akoh (1991)
$DyBa_2Cu_3O_{7-\delta}$	$> 10^5$			With Dy_2BaCuO_5 pinning centers, intergrain J_c is given	Cloots (1995)
$EuBa_2Cu_3O_{7-\delta}$	1.4×10^6		90	Sputtered film, $T_c = 93\,K$, microwave measurement	Asano (1991)
$LuBa_2Cu_3O_{7-\delta}$	4.5×10^6		77	Thin film grown on $LaAlO_3$	Pinto (1994)

(*continued*)

Table 9.6. (*continued*)

Material	J_c (A/cm^2)	B_{app} (tesla)	T_{meas} (K)	Comments	Reference
$NdBa_2Cu_3O_{7-\delta}$	3.7×10^5	5	20	Polycrystalline	Fujihara (1997)
	4.5×10^4	1	77	$B \| c$, $Nb_4Ba_2Cu_2O_{10}$ particles added	Takagi (1995)
	7.1×10^4	1	77	Monocrystal, Ba site doped 10% with Nd	Egi (1995)
$TmBa_2Cu_3O_{7-\delta}$	2.5×10^6		0	Exponential temperature dependence	Moshchalkov (1990)
$CuBa_2Ca_3Cu_4O_x$	10^6	1	5	$T_c = 117$ K, polycrystal, $J_c \sim B^{-m}$; $J_c \sim [1 - (T/T_c)]^n$, $n = 5.24$	Iyo (1997)
	10^4	1	77	$T_c = 117$ K, polycrystal, $J_c \sim B^{-m}$; $J_c \sim [1 - (T/T_c)]^n$, $n = 5.24$	Iyo (1997)
BiSrCaCuO with Pb	1.26×10^4	0	77.3	Ag sheathed tapes	Hitotsuyanagi (1989)
$Bi_2Sr_2CaCu_2O_y$ (Bi-2212)	1.2×10^5	1	4.2	Ag-sheathed tape, B_{app} parallel to tape	Enomoto (1990)
	5×10^4	10–23	4.2	Ag-sheathed tape, B_{app} parallel to tape	Enomoto (1990)
	10^4		78	Anisotropy approx 10^3 near T_c; $J_c \sim [1 - (T/T_c)]^m$ near T_c where $m = 0.7$ longitudinal, $m = 1.0$ transverse	Bulyshev (1991)
	2.4×10^5	12	4.2	Ag tape	Shimoyama (1993)
	$> 10^5$	10	4.2	Ag tape; effect of O_2 pressure studied	Inoue (1997)
	$> 10^5$	Self field	77	Ag-clad tape	Balachandran (1997)
	8×10^3	0	77	Multilayer tape	Hasegawa (1996)
	10^6	12	4.2	Multilayer tape	Hasegawa (1996)
	3×10^4		4	Superconducting fraction 18% yields wire $J_c = 1.7 \times 10^5$	Herrmann (1997)
	3.6×10^4			At edge of core of Ag-sheathed tape	Pan (1997)
	1.8×10^4			In central region of Ag-sheathed tape	Pan (1997)

	1.4×10^4	0	77	Tape; column 2 gives average J_c; local values were found up to 7.6×10^4	Larbalestier (1994)
	10^6		4.4	Monocrystals, doping with Pb, Ba, Li; J_c enhanced by Pb substitution for Bi	Fujii (1991)
	250	0	71	Whisker composite	Funahashi (1994a, b)
$Bi_{2.0}Sr_{2.2}Ca_{0.8}Cu_{1.9}O_x$	1.13×10^5	4	4.2	Thick film	Hasegawa (1995)
$Bi_2Sr_2Ca_2Cu_3O_y$ (Bi-2223)	3×10^7		20	Pb doped thin film on MgO, $T_c = 83$ K	Kuroda (1990)
	4×10^5		77	Pb doped thin film on MgO, $T_c = 83$ K	Kuroda (1990)
	$> 2 \times 10^5$	0	4.2	Ag tapes	Flukiger (1992)
	4×10^4	0	77	Ag tapes	Flukiger (1992)
	1.8×10^5	0	4.2	> 1 m long monofilamentary tapes	Grasso *et al.* (1995)
	3×10^4	0	77	> 1 m long monofilamentary tapes	Grasso *et al.* (1995)
	10^4	0.5	77	> 1 m long monofilamentary tapes; $B_{app} \parallel$ tape surface	Grasso *et al.* (1995)
	5.5×10^3	1	77	> 1 m long monofilamentary tapes; $B_{app} \parallel$ tape surface	Grasso *et al.* (1995)
	7×10^4	15	4.2	> 1 m long monofilamentary tapes; $B_{app} \parallel$ tape surface	Grasso *et al.* (1995)
	1.2×10^4	0	77	17 m long 19 filament Ag tape	Fischer (1995)
	5×10^3	0	77	100 m long 19 filament Ag tape	Fischer (1995)
	2.3×10^4	0	77	Pb doped, almost single phase tape; $J_c = 140$ A/cm^2 for corresp. cermaic	Babic (1995)
	4×10^3	1	81	Bapp $\parallel$ plane of tape	
	8×10^2	1	81	Bapp $\perp$ plane of tape	
	2×10^4	0	77	Pressed and cold rolled Ag-sheathed tapes compared	Grasso (1993)
	4×10^3	1	77	Pressed and cold rolled Ag-sheathed tapes compared	Grasso (1993)

(*continued*)

Table 9.6. (*continued*)

Material	J_c (A/cm^2)	B_{app} (tesla)	T_{meas} (K)	Comments	Reference
	4.7×10^4	15	4.2	Pressed and cold rolled Ag-sheathed tapes compared	Grasso (1993)
	2×10^5	Self field	77	Current flows adjacent to Ag sheath of the tape	Lelovic (1996)
	2.8×10^4	2 mT		Average J_c is given in column 2; $J_c = 2.0 \times 10^4$ at center, 5.3×10^4 at sides	Grasso and Flukiger (1995)
	4.5×10^4	28	4.2	$B \parallel$ surface, multifilament tape	Flukiger (1995)
	3.0×10^4	28	4.2	$B \perp$ surface, multifilament tape)	Flukiger (1995)
	3×10^4	0	77	Average J_c is given in column 2; $J_c = 1.7 \times 10^4$ at center, 4.6×10^4 at sides	Flukiger (1995), Grasso (1994)
	10^4	0.5	77	$B \parallel$surface, multifilament tape	Grasso (1994)
	5.4×10^3	1	77	$B \parallel$surface, multifilament tape	Grasso (1994)
	1.6×10^5	0	4.2	Multifilament tape	Grasso (1994)
	6×10^4	15	4.2	Multifilament tape	Grasso (1994)
	10^5	13	4.2	Ag–Mg(Ni)O-sheathed monocore tape	Yamada (1997)

	2.6×10^4	12	4.2	Ag–Mg(Ni)-sheathed multifilament tape	Yamada (1997)
$Tl_2Ba_2CaCu_2O_8$ (Tl-2212)	3.5×10^5	0	77	Epitaxial film, $T_c = 100.7$ K	Young (1991)
$Tl_2Ba_2Ca_2Cu_3O_y$ (Tl-2223)	10^4	5		Polycrystalline tape-shaped wire	Okada (1991)
	1.5×10^4		77	J_c in 150 μm thick diffusion layer	Kikuchi (1996)
Tl-2223 with Pb	5.5×10^3	0	77	Field dependence studied, Ag-sheathed wire	Takei (1990)
Tl-1234 with Pb	1.08×10^4	0	77	Field dependence studied, Ag-sheathed wire	Takei (1990)
$TlBa_2Ca_2Cu_3O_y$ (Tl-1223)	6.2×10^3	0	75	Ag-sheathed tape	Peterson (1992)
	250	1	75	Ag-sheathed tape	Peterson (1992)
	10^3	6	45	Ag-sheathed tape	Peterson (1992)
	1.5×10^5	0	77		Nabatame (1992)
	1.2×10^4	5	77	$B_{app} \parallel ab$ plane	Nabatame (1992)
	1.5×10^3	16	77	$B_{app} \parallel ab$ plane	Nabatame (1992)
	1.3×10^3	0.7	77	$B_{app} \perp ab$ plane	Nabatame (1992)
	9×10^4	0	77	Textured Ag tape	Doi (1995)
	7×10^3	1	77	Textured Ag tape, $B \parallel c$	Doi (1995)
	1.1×10^5	0	77	Thin film, different Tl contents used	DeLuca (1993)
	$> 10^4$	2	60	Thin film, different Tl contents used, $B \parallel c$-axis	DeLuca (1993)
	5.9×10^6	0	10	Hg-doped polycrystal with	Chang (1996)
	1.1×10^4	1	77	Hg-doped polycrystal with	Chang (1996)

(*continued*)

Table 9.6. (*continued*)

Material	J_c (A/cm^2)	B_{app} (tesla)	T_{meas} (K)	Comments	Reference
$Tl_{0.5}Pb_{0.5}Sr_2Ca_2Cu_3O_9$	1.24×10^5	1	77		Liu (1992)
$Tl_{0.5}Pb_{0.5}Sr_{2-x}Ba_xCa_2Cu_3O_{9-\delta}$	2×10^5	1	80	Ceramic with $T_c \approx 120$ K	Pugnat (1996)
$Tl_{0.5}Pb_{0.5}Sr_{0.8}Ba_{0.2}Ca2Cu_3O_{9-\delta}$	2×10^4	1	77		Peng (1993)
$TlBi_{0.22}Sr_{1.6}Ba_{0.4}Ca_2Cu_3O_{9-\delta}$	2×10^4		77	J_c varies slightly with grain connectivity and c-axis alignment	Ren (1994)
$HgBa_2CuO_{4+\delta}$	7×10^4	0.8	20	Grain aligned, J_c est. by Bean model	Lewis (1993)
$Hg(Ba_{1-x}Sr_x)_2CaCu_2Re_yO_z$	$> 2 \times 10^3$	0	77	Mixed phase 1212 and 1223, max J_c for $x = 0.5$ and max $T_c = 130$ K for $x = 0.2$	Goto (1996)

F

Critical Currents

There are a number of ways to determine the critical current I_c in a wire, and a simple way to do so is to send more and more current through the wire until it goes normal. If the assumption is made that the density of current is uniform through the wire, then the critical current density J_c is obtained by simply dividing the critical current by the cross-sectional area of the wire, $J_c = I_c/A$. Actually, some workers have reported higher current densities at the outside part of the wire, as mentioned in Table 9.6 (Lelovic *et al.*, 1996; Grasso and Flukiger 1995, Flukiger *et al.*, 1995). A common way to estimate J_c is to measure a hysteresis loop in high field and make use of the Bean-model formula

$$J_c = 1.59 \times 10^6 \frac{\mu_0 \Delta M}{d} \qquad (\mathrm{A/m^2}), \tag{26}$$

where $\Delta M = M^+ - M_-$ is the difference in magnetization between the top and the bottom of the hysteresis loop, and d is the diameter of the sample grains in meters. This an MKS or SI formula; in the cgs system it becomes

$$J_c = \frac{30 \Delta M}{d} \qquad (\mathrm{A/cm^2}), \tag{27}$$

where d is now in centimeters. This constitutes one of the most important applications of the Bean model that is discussed in Section H of Chapter 4.

Table 9.6 lists critical current densities measured for a number of superconducting materials. Almost all measured values are far less than the theoretically attainable limits predicted by Eqs. (11) and (12). One of the most pressing technological challenges at the present time is the achievement of depairing current densities in superconducting wires and tapes.

References for Section F

S. K. Agarwal, O. Muller, J. Schubert, and C. Schlenker, *Physica C* **180**, 203 (1991).

H. Akoh, S. Kohjiro, C. Camerlingo, R. Yuosa, and S. Takada, *Physica C* **180**, 227 (1991).

N. E. Alekseevskii, N. M. Dobrovolskii, D. Ekkert, and V. I. Tsebro, *Zhurnal Eksperimental'noi i Teoreticheskoi Fiziki* **72**, 1145 (1977).

N. E. Alekseevskii, A. V. Mitin, and E. P. Khlybov, *Zhurnal Eksperimental'noi i Teoreticheskoi Fiziki* **82**, 927 (1982).

H. Asano, M. Satoh, and T. Konaka, *Appl. Phys. Lett.* **58**, 2981 (1991).

N. Ayai, A. Mikumo, Y. Yamada, K. Takahashi, K. Sato, N. Koizumi, T. Ando, M. Sugimoto, H. Tsuji, K. Okuno, and N. Mitchell, *IEEE Trans. Appl. Supercond.* **7**, 1564 (1997).

E. Babic *et al.*, *Fizika* **4**, 549 (1995).

U. Balachandran, A. N. Iyer, R. Jammy, M. Chudzik, M. Lelovic, P. Krishnaraj, N. G. Eror, and P. Haldar, *IEEE Trans. Appl. Supercond.* **7**, 2207 (1997).

V. Boffa, U. Gambardella, V. Marotta, A. Morone, F. Murtas, S. Orlando, and G. P. Parisi, *Appl. Surf. Sci.* **106**, 361 (1996).

B. S. Brown, T. H. Blewitt, T. L. Scott, and D. G. Wozniak, *J. Appl. Phys.* **49**, 4144 (1978).

Y. Brunet, J. Mazuer, and M. Renard, *Cryogenics* **19**, 107 (1979).

Yu. S. Bulyshev, V. K. Kazantsev, A. I. Selyavko, S. V. Serykh, and A. G. Schneider, *Sverkhprovodimost': Fiziki, Khimiya, Tekhnika* **4**, 1422 (1991).

J. R. Cave, *Cryogenics* **29**(3A), suppl., 304 (1989).

I. C. Chang, J. Z. Liu, M. D. Lau, P. Klavins, and R. N. Shelton, *J. Supercond.* **9**, 53 (1996).

N. Cheggour, A. Gupra, M. Decroux, J. A. A. J. Perenboom, P. Langlois, H. Massat, R. Flukiger, and O. Fischer, *Applied Supercond. 1995. Proc. EUCAS 1995, Second European Conf. on Appl. Supercond.*, Vol. 1, p. 507. IOP, Bristol, UK, 1995.

N. Cheggour, M. Decroux, A. Gupta, O. Fischer, J. A. A. J. Perenboom, V. Bouquet, M. Sergent, and R. Chevrel, *J. Appl. Phys.* **81**, 6277 (1997).

N. A. Chernoplekov, *IEEE Trans. Magnetics* **28**, 121 (1992).

O. V. Chernyj, G. E. Storozhilov, L. G. Udov, G. F. Tikhinsky, N. F. Andrievskaya, E. Yu Klimenko, S. I. Novikov, V. L. Mette, Yu. A. Gulyaikin, A. K.-S. Tsoraev, E. A. Klyupa, G. A. Gaintsev, and L. A. Bogdanova, *Adv. Cryogenic Engrg. Materials* **42**, vol. 2, p. 1159. Plenum Press, New York, 1997.

T. Clausen, J. L. Skov, C. S. Jacobsen, K. R. Bukh, M. V. Bollinger, B. P. Tobiasen, M. P. Sager, I. Chorkendorff, and J. Larsen, *J. Appl. Phys.* **79**, 7062 (1996).

R. Cloots, A. Rulmont, H. Bougrine, and M. Ausloos, *Applied Supercond. 1995. Proc. EUCAS 1995, Second European Conf. on Appl. Supercond.*, Vol. 1, p. 95 IOP, Bristol, UK, 1995.

L. D. Cooley, P. D. Jablonski, P. J. Lee, and D. C. Larbalestier, *Appl. Phys. Lett.* **58**, 2984 (1991).

C. G. Cui, C. C. Lam, B. C. Yang, X. P. Wang, P. C. W. Fung, S. T. Tang, S. L. Li, and X. N. Jing, *Solid State Commun.* **81**, 75 (1992).

J. A. DeLuca, P. L. Karas, J. E. Tkaczyk, P. J. Bednarczyk, M. F. Garbauskas, C. L. Briant, and D. B. Sorensen, *Physica C* **205**, 21 (1993).

O. V. Demicheva, D. N. Rogachev, S. G. Smirnova, E. I. Shklyarova, M. Yu. Yablokov, V. M. Andreev, and L. N. Grigorov, *Pis'ma v Zhurnal Eksperimental' noi i Teoreticheskoi Fiziki* **51**, 228 (1990).

M. Dietrich, C.-H. Dustmann, F. Schmaderer, and G. Wahl, *IEEE Trans. on Magnetics* **MAG-19**, 406 (1983).

M. Dietrich, E. Fitzer, and T. Stumm, *High Temperatures — High Pressures* **19**, 89 (1987).

T. J. Doi, T. Yuasa, T. Ozawa, and K. Higashiyama, *Adv. in Supercond. VII. Proc. 7th Intern. Symp. on Supercond. (ISS' 94)*, Vol. 2, p. 817 (1995).

E. Drost, W. Specking, and R. Flukiger, *IEEE Trans. Magnetics* **MAG-21**, 281 (1985).

T. Egi, J. G. Wen, K. Kuroda, H. Unoki, and N. Koshizuka, *Appl. Phys. Lett.* **67**, 2406 (1995).

N. Enomoto, H. Kikuchi, N. Uno, H. Kumakura, K. Togano, and K. Watanabe, *Jpn. J. Appl. Phys. Lett.* **29**, L447 (1990).

K. Fischer, M. Schubert, C. Rodig, P. Verges, H.-W. Neumuller, M. Wilhelm, B. Roas, and A. Jenovelis, *IEEE Trans. Appl. Supercond.* **5**, 1259 (1995).

L. M. Fisher, I. F. Voloshin, V. S. Gorbachev, S. E. Savelev, and A. V. Kalinov, *Proc. 7th Intern. Workshop on Critical Currents in Supercond.*, p. 439. World Scientific, Singapore, 1994.

R. Flukiger, S. Foner, E. J. McNiff, Jr., B. B. Schwartz, J. Adams, S. Forman, T. W. Eager, and R. M. Rose, *IEEE Trans. Magnetics* **MAG-15**, 689 (1979).

R. Flukiger, W. Specking, and P. Turowski, *Proc. 9th Intern. Conf. Magnet Techn. MT-9 1985, Swiss Inst. Nucl. Res. Villigen, Switzerland*, p. 472 (1985).

R. Flukiger, B. Hensel, A. Jeremie, M. Decroux, H. Kupfer, W. Jahn, E. Seibt, W. Goldacker, Y. Yamada, and J. Q. Xu, *Supercond. Sci. Technol.* **5**, 561 (1992).

R. Flukiger, G. Grasso, B. Hensel, M. Daumling, A. Jeremie, A. Perin, J. C. Grivel, and R. Gladyshevskii, *IEEE Trans. Appl. Supercond.* **5**, 1150 (1995).

T. L. Francavilla and D. G. Howe, *Proc. Seventh Intern. Cryogenic Engrg. Conf.*, p. 723. IPC Sci. & Technol, Press. Guildford, UK, 1979.

S. Fujihara, N. Yoshida, and T. Kimura, *Physica C* **276**, 69 (1997).

T. Fujii, Y. Nagano, and J. Shirafuji, *Physica C* **185–189**, 2455 (1991).

K. Fukuda, G. Iwaki, F. Hosono, S. Sakai, Y. Iijima, T. Takeuchi, K. Inoue, N. Kobayashi, K. Watanabe, and S. Awaji, *IEEE Trans. Appl. Supercond.* **7**, pt. 2, 1572 (1997).
R. Funahashi, M. Konishi, L. Dimesso, I. Matsubara, M. Umeda, T. Ogura, S. Kosaka, N. Ohno, and H. Yamashita, *Bull. Electrotechnical Lab.* **58**, 188 (1994a).
R. Funahashi, I. Matsubara, S. Kusumi, T. Ogura, H. Yamashita, and L. Dimesso, *J. Appl. Phys.* **76**, 4891 (1994b).
J. R. Gavaler, J. Greggi, R. Wilmer, and J. W. Ekin, *IEEE Trans. Magnetics* **MAG-19**, 418 (1983).
O. Yu Gorbenko, A. R. Kaul, I. V. Pogosova, S. N. Polyakov, E. V. Kolosova, S. A. Pozigun, and V. I. Scritny, *Materials Sci. & Engrg. B Solid–State Materials for Adv. Technol.* **B17**, 157 (1993).
T. Goto and E. Sakai, *Czech. J. Phys.* **46**, suppl., 1455 (1996).
G. Grasso and R. Flukiger, *Physica C* **253**, 292 (1995).
G. Grasso, A. Perin, B. Hensel, and R. Flukiger, *Physica C* **217**, 335 (1993).
G. Grasso, B. Hensel, A. Jeremie, A. Perin, and R. Flukiger, *Nuovo Cimento D* **16D**, 2073 (1994).
G. Grasso, B. Hensel, A. Jeremie, and R. Flukiger, *IEEE Trans. Appl. Supercond.* **5**, 1255 (1995).
A. Gupta, N. Cheggour, M. Decroux, J. A. A. J. Perenboom, V. Bouquet, P. Langlois, H. Massat, R. Flukiger, and O. Fischer, *Phys. B* **211**, 272 (1995).
K. Hamasaki, T. Inoue, T. Yamashita, T. Komata, and T. Sasaki, *Appl. Phys. Lett.* **41**, 667 (1982).
K. Hamasaki, K. Hirata, T. Yamashita, T. Komata, K. Noto, and K. Watanabe, *IEEE Trans. Magnetics* **MAG-21**, 471 (1985).
K. Hamasaki, K. Noto, K. Watanabe, T. Yamashita, and T. Komata, *Proc. MRS Intern. Meeting Adv. Materials* Vol. 6, Supercond., p. 115. Mater. Res. Soc. Pittsburgh (1989).
T. Hasegawa, H. Kobayashi, and K. Togano, *IEEE Trans. Appl. Supercond.* **5**, 1845 (1995).
T. Hasegawa, Y. Hikichi, T. Koizumi, H. Kumakura, H. Kitaguchi, and K. Togano, *Showa Electric Wire and Cable Review* **46**, 82 (1996).
P. F. Herrmann, E. Beghin, G. Duperray, D. Legat, A. Leriche, D. Brouard, and P. Manuel, *IEEE Trans. Appl. Supercond.* **7**, 1679 (1997)
R. W. Heussner, J. D. Marquardt, P. J. Lee, and D. C. Larbalestier, *Appl. Phys. Lett.* **70**, 901 (1997).
H. Hitotsuyanagi, K.-I. Sato, S. Takano, and M. Nagata, *IEEE Trans. Components, Hybrids, and Manufacturing Technol.* **12**, 553 (1989).
K. Holczer, O. Klein, G. Grüner, J. D. Thompson, F. Deiderich, and R. I. Whetten, *Phys. Rev. Lett.* **67**, 271 (1991).
A. Inoue, C. Suryanarayana, T. Masumoto, and A. Hoshi, *Sci. Reports Research Inst. Tohoku Univ., Series A* **28**, 182 (1980).
A. Inoue, Y. Takahashi, C. Suryanarayana, A. Hoshi, and T. Masumoto, *J. Materials Sci.* **16**, 3077 (1981).
K. Inoue, T. Kuroda, and K. Tachikawa, *IEEE Trans. Magnetics* **MAG-21**, 467 (1985).
Y. Inoue, H. Kurahashi, Y. Fukumoto, and M. Shimada, *IEEE Trans. Appl. Supercond.* **5**, 1201 (1995).
N. Inoue, M. Okada, K. Higashiyama, K. Kato, H. Kitaguchi, H. Kumakura, and K. Togano, *Adv. Cryogenic Engrg. Materials* **42**, Vol. 2, p. 847. Plenum Press, New York, 1997.
F. Ishida, *J. Jpn. Inst. Metals* **45**, 525 (1981).
A. Iyo, K. Tokiwa, N. Terada, M. Tokumoto, M. Hirabayashi, and B. Ihara, *Adv. Cryogenic Engrg. Materials* **42**, vol. 2, 623 (1997).
H. C. Kanithi, C. G. King, B. A. Zeitlin, and R. M. Scanlan, *IEEE Trans. Magnetics* **25**, 1922 (1989).
P. H. Kes, *Physica C* **153–155**, 1121 (1988).
A. Kikuchi, T. Nakamura, and K. Tachikawa, *J. Jpn. Inst. Metals* **60**, 667 (1996).
Jeha Kim, Seok-Kil Han, and Kwang-Yong Kang, *IEEE Trans. Appl. Supercond.* **7**, 1490 (1997).
T. Kobayashi, T. Kimura, J. Shimoyama, K. Kishio, K. Kitazawa, and K. Yamafuji, *Physica C* **254**, 213 (1995).
Y. Kubo, K. Yoshizaki, F. Fujiwara, K. Noto, and K. Watanabe, *Proc. MRS Intern. Meeting on Advanced Materials* Vol. 6, *Supercond.*, p. 95. Mater. Res. Soc. Pittsburgh, 1989.

H. Kumakura, K. Togano, Y. Yamada, and S. Murase, *Materials and Manufacturing Processes* **5**, 549 (1990).

T. Kumano, M. Ichihara, E. Suzuki, E. Shimizu, D. Ito, I. Takano, H. Kasahara, S. Akita, and T. Tanaka, *11th Intern. Conf. on Magnet Technol.*, Vol. MT-11, p. 1045. Elsevier Appl. Sci., 1990.

K. Kuroda, K. Kojima, M. Tanioku, K. Yokoyama, and K. Hamanaka, *Adv. Supercond. II. Proc. 2nd Intern. Symp. Supercond. (ISS '89)*, p. 919 (1990).

Y. Kuwasawa, T. Tosaka, A. Uchiyama, S. Matuda, and S. Nakano, *Physica C* **175**, 187 (1991).

Y. Kuwasawa, T. Yamaguchi, T. Tosaka, S. Aoki, and S. Nakano, *Physica C* **169** 39 (1990).

D. C. Larbalestier, X. Y. Cai, Y. Feng, H. Edelman, A. Umezawa, G. N. Riley, Jr., and W. L. Carter, *Physica C* **221**, 299 (1994).

M. Lelovic, P. Krishnaraj, N. G. Eror, A. N. Iyer, and U. Balachandran, *Supercond. Sci. & Technol.* **9** (3) 201 (1996).

J. Lensink, C. F. J. Flipse, J. Roobeek, R. Griessen, and B. Dam, *Physica C* **162–164**, 663 (1989).

J. A. Lewis, C. E. Platt, M. Wagmann, M. Teepe, J. L. Wagner, and D. G. Hinks, *Phys. Rev. B* **48**, 7739 (1993).

C. R. Li, Xiao-zu Wu, and Nong Zhou, *IEEE Trans. Magnetics* **MAG-19**, 284 (1983).

R. S. Liu, D. NB. Zheng, J. W. Loram, K. A. Mirza, A. M. Campbell, and P. P. Edwards, *Appl. Phys. Lett.* **60**, 1019 (1992).

J. Garcia Lopez, J. Siejka, L. M. Mercandalli, R. Bisaro, M. G. Blanchin, and V. Teodorescu, *Physica C* **275**, 65 (1997).

S. N. Mao, X. X. Xi, S. Bhattacharya, Q. Li, J. L. Peng, J. Mao, D. H. Wu, S. M. Anlage, R. L. Greene, and T. Venkatesan, *IEEE Trans. Appl. Supercond.* **3**, 1552 (1993).

S. Matsuno, F. Uchikawa, K. Yoshizaki, N. Kobayashi, K. Watanabe, Y. Muto, and M. Tanaka, *IEEE Trans. Magnetics* **27**, 1398 (1991).

T. Matsushita, E. S. Otabe, and B. Ni, Supercond. Sci. Tech. **5**, S73 (1992).

V. F. Meshcheryakov and V. A. Murashov, *Zhurnal Eksperimental' noi i Teoreticheskoi Fiziki* **101**, 241 (1992).

O. Miura, K. Matsumoto, Y. Tanaka, K. Yamafuji, N. Harada, M. Iwakuma, K. Funaki, and T. Matsushita, *Cryogenics* **32**, 315 (1992).

V. V. Moshchalkov, A. A. Zhukov, D. K. Petrov, V. I. Voronkova, and V. K. Yanovskii, *Physica C* **166**, 185 (1990).

V. V. Moshchalkov, J. Y. Henry, C. Marin, J. Rossat-Mignod, and J. F. Jacquot, *Physica C* **175**, 407 (1991).

T. Nabatame, K. Watanabe, S. Awaji, Y. Saito, K. Aihara, T. Kamo, and S. P. Matsuda, *Jpn. J. Appl. Phys.* **31**, L1041 (1992).

T. Nabatame, Y. Saito, K. Aihara, T. Kamo, and S. P. Matsuda, *Supercond. Sci. Tech.* **9**, 17 (1996).

Y. Nakagawa, M. Umeda, and Y. Kimura, *Cryogenics* **27**, 558 (1987).

M. Okada, T. Nabatame, T. Yuasa, K. Aihara, M. Seido, and S. Matsuda, *Jpn. J. Appl. Phys.* **30**, 2747 (1991).

G. Oya and E. J. Saur, *J. Low Temp. Phys.* **34**, 569 (1979).

A. V. Pan, M. H. Ionescu, and S. X. Dou, *IEEE Trans. Appl. Supercond.* **7**, 1331 (1997).

Huo-Tian Peng, Qiu-Yun Peng, Xiang-Yun Lung, Si-Hai Zhou, Zhi-Wei Qi, Yu-Sheng Wu, Ji-Peng Chen, Yong Zhong, Bing-Sing Cui, Jun-Ren Fang, and Guo-Hui Cao, *Supercond. Sci. & Technol* **6**, 790 (1993).

D. E. Peterson, P. G. Wahlbeck, M. P. Maley, J. O. Willis, P. J. Kung, J. Y. Coulter, K. V. Salazar, D. S. Phillips, J. F. Bingert, E. J. Peterson, and W. L. Hults, *Physica C* **199**, 161 (1992).

R. Pinto, A. G. Chourey, and P. R. Apte, *Appl. Phys. Lett.* **64**, 2166 (1994).

C. Politis, V. Buntar, W. Krauss, and A. Gurevich, *Europhys. Lett.* **17**, 175 (1992).

P. Pugnat, K. Lebbou, M. T. Cohen-Adad, J. L. Jorda, M. Couach, and G. Fillion, *Czech. J. Phys.* **46**, suppl., 1711 (1996).

H. D. Ramsbottom and D. P. Hampshire, *Physica C* **274**, 295 (1997).

Y. S. Reddy, M. M. Krishna, and R. G. Sharma, *J. Low Temp. Phys.* **65**, 261 (1986).

Hontao Ren, Qing He, Ling Xiao, Ruikun Wang, Dingan Yu, Changgeng Cui, and Shanlin Li, *Cryogenics* **30**, suppl., 837 (1990).
Z. F. Ren, J. H. Wang, D. J. Miller, and K. C. Goretta, *Physica C* **229**, 137 (1994).
S. Saito, K. Ikeda, S. Ikeda, A. Nagata, and K. Noto, *11th Intern. Conf. Magnet Techn. (MT-11)*, Vol. 2, p. 974. Elsevier Appl. Sci., 1990.
W. Schaper, J. Wecker, K. Mrowiec, R. Bormann, and H. C. Freyhardt, *J. Appl. Phys.* 62, 1937 (1987).
R. G. Sharma, *Cryogenics* **27**, 361 (1987).
R. G. Sharma, Y. Tanaka, and K. Tachikawa, *Cryogenics* **21**, 165 (1981).
J.-I. Shimoyama, K. Kadowaki, H. Kitaguchi, H. Kumakura, K. Togano, H. Maeda, and K. Nomura, *Appl. Supercond.* **1**, 43 (1993).
R. Singh, S. Sinha, N. J. Hsu, J. T. C. Ng, P. Chou, R. P. S. Thakur, and J. Narayan, *J. Appl. Phys.* **69**, 2418 (1991).
M. Suenaga, K. Tsuchiya, and N. Higuchi, *Appl. Phys. Lett.* **44**, 919 (1984).
M. Suzuki, T. Kiboshi, T. Anayama, and A. Nagata, *Proc. MRS Intern. Meeting Adv. Materials*, Vol. 6, Supercond., p. 77. Mater. Res. Soc. Pittsburgh, 1989.
K. Tachikawa, T. Ansano, and T. Takeuchi, *Appl. Phys. Lett.* **39**, 766 (1981).
K. Tachikawa, M. Natsuume, Y. Kuroda, and H. Tomori, *Cryogenics* **36**, 113 (1996).
K. Tachikawa, Y. Kuroda, H. Tomori, and M. Ueda, *IEEE Trans. Appl. Supercond.* **7**, 1355 (1997).
A. Takagi, T. Yamazaki, T. Oka, Y. Yanagi, Y. Itoh, M. Yoshikawa, Y. Yamada, and U. Mizutani, *Physica C* **250**, 222 (1995).
Y. Takahashi, T. Ando, T. Hiyama, H. Tsuji, E. Tada, M. Nishi, K. Yoshida, K. Okuno, K. Koizumi, H. Nakajima, T. Kato, K. Kawanao, M. Oshikiri, Y. Hattori, R. Takahahi, S. Kamiya, Y. Ohgane, and S. Shimamoto, *IEEE Trans. Magnetics* **MAG-21**, 157 (1985).
H. Takei, Y. Torii, H. Kugai, T. Hikata, K. Sato, H. Hitotuyanagi, and K. Tada, *Adv. Supercond. II. Proc. 2nd Intern. Symp. Supercond. (ISS '89)* p. 359. Springer-Verlag, 1990.
Y. Tarutani, T. Nishino, Y. Hatano, and U. Kawabe, *Conference on Solid State State Devices and Materials, Business Centre for Acad. Sci., Tokyo, Japan*, p. 615 (1984).
C. C. Tsuei, J. Mannhart, and D. Dimos, *AIP Conf. Proc.* **182**, 194 (1988).
K. Watanabe, K. Noto, and Y. Muto, *IEEE Trans. Magnetics* **MAG-23**, 1428 (1987).
K. Watanabe, K. Noto, Y. Kamisada, E. Suzuki, and Y. Muto, *11th Intern. Conf. Magnet Techn. (MT-11)*, Vol. 2, p. 968. Elsevier Appl. Sci., 1990.
K. Watanabe, S. Awaji, N. Kobayashi, H. Yamane, T. Hirai, and Y. Muto, *J. Appl. Phys.* **69**, 1543 (1991).
K. Watanabe, K. Noto, and Y. Muto, *IEEE Trans. Magnetics* **MAG-27**, 1759 (1991).
Y. Yamada, H. Onoda, K. Yamamoto, S. Murase, O. Horigami, T. Koizumi, T. Hasegawa, and H. Kumakura, *Adv. Cryogenic Engrg. Materials*, Vol. 42, p. 811. Plenum Press, New York, 1997.
H. Yamasaki and Y. Kimura, *IEEE Trans. MAgnetics* **MAG-23**, 1756 (1987).
H. Yamasaki and Y. Kimura, *J. Appl. Phys.* **64**, 766 (1988).
H. Yamasaki, M. Umeda, and S. Kosaka, *J. Appl. Phys.* **72**, 1180 (1992).
Y. Yoshida, K. Togano, and K. Tachikawa, *Appl. Phys. Lett.* **43**, 1129 (1983).
K. H. Young, D. Arney, E. J. Smith, and D. Strother, *Jpn. J. Appl. Phys.* **30**, L710 (1991).
Wang Zhen, A. Kawakami, and Y. Uzawa, *Appl. Phys. Lett.* **70**, 114 (1997).
Lian Zhou, *IEEE Trans. Magnetics* **MAG-19**, 280 (1983).

G

Electron–Phonon Coupling Constants

Philip B. Allen

a. Theoretical Background

Grimvall (1981) has written a review of electron–phonon effects in metals. Prominent among these effects is superconductivity. The BCS theory gives a relation $T_c \approx \Theta_D \exp(-1/N(0)V)$ for the superconducting transition temperature T_c in terms of the Debye temperature Θ_D. Values of T_c are tabulated in Chapter 5, the most complete listing prior to the high T_c era being Roberts (1976). The electron–electron interaction V consists of the attractive electron–phonon-induced interaction minus the repulsive Coulomb interaction. The notation used is

$$\lambda = N(0)V_{\text{e-ph}} \tag{28}$$

and the Coulomb repulsion $N(0)V_c$ is called μ, so that $N(0)V = \lambda - \mu^*$, where μ^* is a "renormalized" Coulomb repulsion, reduced in value from μ to $\mu/[1 + \mu \ln(\omega_P/\omega_D)]$. This suppression of the Coulomb repulsion is a result of the fact that the electron–phonon attraction is retarded in time by an amount $\Delta t \approx 1/\omega_D$ whereas the repulsive screened Coulomb interaction is retarded by a much smaller time, $\Delta t \approx 1/\omega_P$, where ω_P is the electronic plasma frequency. Therefore, μ^* is bounded above by $1/\ln(\omega_P/\omega_D)$, which for conventional metals should be $\leqslant 0.2$.

Values of λ are known to range from $\leqslant 0.10$ to $\geqslant 2.0$. The same coupling constant λ appears in several other physical quantities, such as the electronic specific heat $C_{\text{el}}(T)$, which at low temperature equals

$$C_{\text{el}}(T) = \frac{\pi^2}{3} N(0)(1 + \lambda) k_B^2 T. \tag{29}$$

This relation enables a value for $(1 + \lambda)$ to be extracted if the bare density of states $N(0)$ is known from quasiparticle band theory. This procedure has large uncertainties, so the resulting values of λ are subject to substantial error and are not tabulated here.

When the BCS ideas are carefully worked out using the actual electron–phonon interactions (Migdal–Eliashberg theory[1]) then a quite complicated but in principle solvable relation occurs between electron–phonon coupling and T_c. If the anisotropy of the superconducting gap is ignored (or washed out by

[1]Reviews of Migdal–Eliashberg theory are: D. J. Scalapino, in *Superconductivity*, edited by R. D. Parks (Marcel Dekker, New York, 1969), Vol. 1, p. 449; P. B. Allen and B. Mitrovic, in *Solid State Physics* edited by F. Seitz, D. Turnbull, and H. Ehrenreich, (Academic Press, NY, 1982) v.37, p. 1; J. P. Carbotte, Rev. Mod. Phys. **62**, 1027 (1990).

nonmagnetic impurity scattering), then theory simplifies and T_c depends on μ^* and a single function $\alpha^2F(\Omega)$ which is similar to the phonon–density of states $F(\Omega)$, where α^2 contains an average square electron–phonon matrix element. Quasiparticle tunneling experiments in planar tunnel junction geometry (McMillan and Wolf 1969; Wolf 1985) in principle provide a way of measuring this function, which is related to λ by

$$\lambda = 2\int_0^\infty \frac{d\Omega}{\Omega}\alpha^2F(\Omega). \tag{30}$$

This provides perhaps the most reliable known values for λ. The techniques and the data are reviewed in Wolf (1985). However, there are still significant uncertainties in values of λ obtained this way, caused by difficulties in making good yet partially transparent barriers and ignorance of such details as the transmission coefficients for tunneling and inelastic effects in the barrier region. For a few metals (principally Pb, In, Tl, and alloys of these) the barriers seem particularly clean or else the complexities somehow cancel out; the accuracy of the resulting $\alpha^2F(\Omega)$ is well tested through various self-consistency checks. Tunneling in point contact geometry gives valuable information about $\alpha^2F(\Omega)$, especially in materials with weaker electron–phonon interactions where the planar junction techniques do not work. However, the absolute values of λ obtained this way are rather variable and are not listed here.

The Migdal–Eliashberg theory was solved numerically for T_c as a functional of $\alpha^2F(\Omega)$ and μ^* by McMillan (1968). He fitted his results to an approximate formula, generalizing the BCS result $T_c = \Theta_D \exp[-1/(\lambda - \mu^*)]$,

$$T_c = \frac{\Theta_D}{1.45}\exp\left[-\frac{1.04(1+\lambda)}{\lambda - \mu^*(1+0.62\lambda)}\right]. \tag{31}$$

The parameter μ^* is assigned a value in the range 0.10–0.15, consistent with tunneling and with theoretical guesses. The choice of μ^* is fairly arbitrary, but fortunately its precise value is not too important unless T_c is very low. Most of our knowledge of values of λ comes from using Eq. (31) to extract a value of λ from measured values of T_c and Θ_D. Values deduced in this fashion are denoted λ_{McM} in this article. Subsequent to McMillan's work, experiments and further numerical studies (Allen and Dynes, 1975) worked out the limits of applicability of Eq. (31). The "prefactor" $\Theta_D/1.45$ works well only for elements or materials whose phonon density-of-states is similar in shape to elements such as Nb. The correct (Allen and Dynes, 1975) prefactor $\omega_{\ln}/1.20$, is not measureable except by experiments such as tunneling. The definition of $\omega_{\ln}$ is

$$\omega_{\ln} = \exp\left[\frac{2}{\lambda}\int_0^\infty d\Omega \frac{\ln(\Omega)}{\Omega}\alpha^2F(\Omega)\right]. \tag{32}$$

Lack of knowledge of $\omega_{\ln}$ limits the accuracy of values of λ_{McM}, especially in compound materials with complicated phonon dispersion. When T_c becomes reasonably large (T_c greater than $\approx$ 5% of Θ_D or $\lambda \geqslant 1.2$), Eq. (31) under-

estimates T_c. Approximate correction factors were given in Allen and Dynes (1975). Unfortunately, additional parameters are required to give an accurate formula for T_c.

Calculations of μ or μ^* are computationally demanding and are not yet under theoretical control. Calculations of λ are slightly less demanding, are under somewhat better theoretical control, and have been attempted for many years. Prior to 1990, calculations of λ generally required knowing the phonon frequencies and eigenvectors as input information, and approximating the form of the electron–ion potential. Results of these calculations are not tabulated here. McMillan (1968) and Hopfield (1969) pointed out that one could define a simpler quantity,

$$\eta \equiv N(0)\langle I^2\rangle = M\langle\omega^2\rangle\lambda \tag{33}$$

$$\langle\omega^2\rangle \equiv \frac{2}{\lambda}\int_0^\infty d\Omega\Omega\alpha^2F(\Omega). \tag{34}$$

The advantage of this is that η and $\langle I^2\rangle$ are purely "electronic" quantities, requiring no input information about phonon frequencies or eigenvectors. Gaspari and Gyorffy (1972) then invented a simplified algorithm for calculating η, and many authors have used this. These calculations generally require a "rigid ion approximation" or some similar guess for the perturbing potential felt by electrons when an atom has moved. Given η, one can guess a value for $\langle\omega^2\rangle$ (for example, from Θ_D) and thereby produce an estimate for λ. Values produced this way are not tabulated in the present chapter. Instead the reader is referred to the following literature: Sigalas and Papaconstantopoulos (1994) have given a tabulation for d-band elements, and Skriver and co-workers have published calculations for rare earths (Skriver and Mertig, 1990) and lanthanides (Skriver *et al.*, 1988) that are particularly valuable since usually no other estimate of λ is available. Brorson *et al.* (1990) have extracted measured values of η from measured rates of thermal equilibration of hot electrons in various metals, using a theoretical relation (Allen, 1987a). Fairly recently, theory has progressed to the point where "first-principles" calculations (Baroni *et al.*, 1987) can be made of phonon dispersion curves using density functional theory, usually in the "local density approximation" (LDA) for quite complicated systems. It is not too hard to extend these calculations to give $\alpha^2F(\Omega)$ and λ; these values should be "reproducible" in the sense that most theorists would agree upon a unique recipe. Such calculations have been done by Savrasov and Savrasov (1996) and by Liu and Quong (1996). The results accord well with other methods of finding λ. Values of λ obtained this way will be denoted λ_{LDA}.

The T-dependence of the electrical resistivity sometimes offers an accurate way of evaluating the electron–phonon coupling. In clean metals (defined by a large resistance ratio $\rho(300K)/\rho(T = T_c + \varepsilon)$) the resistivity is normally dominated by electron–phonon interactions. Using the standard form $\sigma = 1/\rho = ne^2\tau/m$, the scattering rate $\hbar/\tau(T)$ at high temperatures is

$2\pi\lambda_{\rm tr}k_{\rm B}T$, which defines a coupling constant $\lambda_{\rm tr}$ that is very closely related to λ. Coulomb scattering of electrons with each other also contributes, but is smaller by the factor $(\mu^2/\lambda)N(0)k_{\rm B}T$, which is usually $\approx 10^{-2}$ at room temperature. The derivation of this result depends on Bloch–Boltzmann transport theory, which is closely analogous to the Migdal–Eliashberg theory of superconductivity. For both theories, the "Migdal theorem" shows that corrections (Feynman diagrams with phonon vertex corrections) should be smaller by a factor $N(0)\hbar\omega_D$. Both theories contain anisotropy corrections, which are almost always small. When anisotropy is ignored, superconductivity depends on the isotropic parameter λ and resistivity on the isotropic parameter $\lambda_{\rm tr}$. These two coupling constants are related to the electron–phonon matrix elements $M_{k,k'}$ and the phonon frequencies $\omega_{k-k'}$ by the formula

$$\lambda_{\rm w} = N(0)\frac{\sum_{k,k'} w(k,k')|M_{k,k'}|^2/\hbar\omega_{k-k'}\delta(\varepsilon_k)\delta(\varepsilon_{k'})}{\sum_{k,k'} w(k,k')\delta(\varepsilon_k)\delta(\varepsilon_{k'})}, \tag{35}$$

where ε_k is the quasiparticle energy of an electron constrained by the δ-function to be at the Fermi energy, the labels k, k' are short for the electron quantum numbers (wavevector, band index, spin), and $w(k,k')$ is a weight function to be specified. The superconducting λ uses $w = 1$ for the weight function, while the transport $\lambda_{\rm tr}$ uses $w(k,k') = (v_{kx} - v_{k'x})^2$, where $\hbar v_{k,x}$ is the group velocity $\partial\varepsilon_k/\partial k_x$. A review of the theory and the formulas is given by Allen (1996). Simultaneous calculations (Savrasov and Savrasov, 1996; Allen *et al.*, 1986) of these two parameters are available for a number of metals, shown in Table 9.7. From this it is known that the difference is typically no more than 15%, and never as much as a factor of 2. In principle there are separate coupling constants $\lambda_{{\rm tr},xx}$ and $\lambda_{{\rm tr},zz}$ in hexagonal or tetragonal metals, but the anisotropy of $\lambda_{\rm tr}$ is believed to be quite small. The explanation for the observed similarity between λ and $\lambda_{\rm tr}$ must be that the weight factor $(v_{kx} - v_{k'x})^2$ correlates only weakly with the matrix element $|M_{k,k'}|^2$. The same lack of correlation will also guarantee that the anisotropy of the resistivity tensor in noncubic materials will derive primarily from the anisotropy of the inverse effective mass tensor n/m rather than from anisotropy in $\lambda_{\rm tr}$.

To extract a value of $\lambda_{\rm tr}$ from $\rho(T)$ data, the safest procedure is a three-parameter fit to the data using the Bloch–Grüneisen formula,

$$\rho_{\rm BG} = \rho_0 + \frac{2\pi\lambda_{\rm tr}k_{\rm B}T/\hbar}{(n/m)e^2}\int_0^{\omega_D}\frac{d\Omega}{\Omega}\left(\frac{\Omega}{\omega_D}\right)^4\left[\frac{\hbar\Omega/k_{\rm B}T}{\sinh(\hbar\Omega/2k_{\rm B}T)}\right]^2. \tag{36}$$

At high T the factor $[\,]^2$ becomes 4 and thus the integral becomes 1. The three fitting parameters are ρ_0, ω_D, and the ratio $\lambda_{\rm tr}/(n/m)$. This equation assumes either an isotropic polycrystalline sample or else cubic symmetry, and also assumes that the phonon dispersion is adequately represented by a Debye model. It is easy to generalize to anisotropic or non-Debye cases, at the cost of

Table 9.7.

Comparison of theoretical values of λ and λ_{tr}.

Metal	λ_{theor}	$\lambda_{tr,theor}$
Al[a]	0.44	0.37
Pb[a]	1.68	1.19
V[a]	1.19	1.15
Nb[a]	1.26	1.17
Nb[b]	1.12	1.07
Ta[a]	0.86	0.83
Ta[b]	0.88	0.57
Mo[a]	0.42	0.35
Cu[a]	0.14	0.13
Cu[b]	0.111	0.116
Pd[a]	0.35	0.43
Pd[b]	0.41	0.46

[a]Full LDA theory (Savrasov and Savrasov, 1996). [b]LDA energy bands, rigid ion approximation, experimental phonons, (Allen *et al.*, 1986).

adding more fitting parameters. For example, the case of completely general phonon dispersion is handled simply by replacing the factor $2\lambda_{tr}(\Omega/\omega_D)^4$ by a function $\alpha^2_{tr}F(\Omega)$. Fortunately, except at low T, the form of ρ_{BG} is not very sensitive to the form of $\alpha^2_{tr}F(\Omega)$. One exception is ReO_3, where the acoustic vibrations are mainly Re-like and low in energy, while the optic vibrations are mainly O-like and very high in energy. For that material, it is adequate (Allen and Schulz, 1993) to represent $\alpha^2_{tr}F(\Omega)$ by a sum of a Debye and an Einstein part, $2\lambda_D(\Omega/\omega_D)^4 + (\lambda_E\omega_E/2)\delta(\Omega - \omega_E)$, where λ_{tr} is $\lambda_D + \lambda_E$. The remaining problem is that the tensor parameter n/m must also be known in order to get a value for λ_{tr}, and there is no firm experimental method. The theoretical formula is

$$\left(\frac{n}{m}\right)_{\alpha\beta} = \sum_k v_{k,\alpha}v_{k,\beta}\delta(\varepsilon_k). \tag{37}$$

For cubic symmetry, the tensor is a scalar, $(n/m)_{\alpha\beta} = (n/m)\delta_{\alpha\beta}$. It is usually not useful or even possible to make separate definitions of a scalar n (because it is unclear how many of the valence electrons should be counted) or of a tensor or scalar m or $1/m$. Another way to write Eq. (37) is $(n/m)_{\alpha\beta} = N(0)\langle v_\alpha v_\beta\rangle$, where the angular brackets denote a Fermi surface average. One can also define a "Drude plasma frequency" $\Omega^2_{\alpha\beta} = 4\pi e^2(n/m)_{\alpha\beta}$ that governs both dc and ac conductivity. Unfortunately it is not possible to get reliable values of the Drude plasma frequency from optical experiments, for a variety of reasons, outlined by Hopfield (1972). Surprisingly, it seems that LDA band theory gives for many

metals very reliable values of $(n/m)_{\alpha\beta}$, which therefore yield good values of $\lambda_{\rm tr}$. In quite a few metals, this provides the best available estimate of λ.

There are several other ways of getting values of parameters related to λ. Quasiparticles near the Fermi surface have energies and lifetimes given by poles of the Green's function or zeros of $G^{-1}(k,\omega)$ for small $|\omega|$ in the complex ω-plane,

$$\begin{aligned} G^{-1}(k,\omega) &= \omega - \varepsilon_k - \sum(k,\omega) \\ &= (1+\lambda_k(T))(\omega + i/2\tau_k(\omega,T)) - \varepsilon_k, \end{aligned} \tag{38}$$

where $\lambda_k(T)$ is defined as $-\partial\Sigma_1(k,\omega)/\partial\omega|_{\omega=0}$, $(1+\lambda_k)/2\tau_k$ is defined as $-\Sigma_2(k,\omega)$, and the zero of energy is shifted so that $\Sigma_1(k,\omega=0)$ is absorbed and disappears. Then $\lambda_k(T)$ is the mass enhancement parameter for the quasiparticle state k, and λ is the average of $\lambda_k(T=0)$ over the Fermi surface. The spectral weight function, $-\mathrm{Im}G^{-1}(k,\omega)$, then has a Lorentzian resonance centered at the renormalized quasiparticle energy $E_k = \varepsilon_k/(1+\lambda_k(T))$ with width equal to the lifetime broadening $1/\tau_k(E_k,T)$. If electron–phonon interactions dominate, then at $T \geqslant \Theta_D$, where $\lambda_k(T) \approx 0$, $\hbar/\tau_k(E_k,T) = 2\pi\lambda_k(T=0)k_{\rm B}T$. This also assumes that the state k being probed has a small enough $|\varepsilon_k|$ so that $|E_k| \leqslant k_{\rm B}\Theta_D$.

Various resonance methods can measure either $E_k(T)$ and $1/\tau_k(T)$. As an example, cyclotron resonance can do this for extremal orbits on the Fermi surface, but generally only at low temperatures where $E_k = \varepsilon_k/(1+\lambda_k(T=0))$. Under these conditions, $1/\tau_k(T)$ is small and does not contain complete information about λ_k; an orbit-averaged value of $(1+\lambda)$ can be extracted using theoretical values of the unrenormalized quasiparticle band structure ε_k. In principle, photoemission spectroscopy could measure $1/\tau_k(T)$ at high T, and thus directly measure λ_k with no need for theoretical input. The principal difficulty is that the perpendicular component $k_\perp$ of the wavevector $\mathbf{k}$ cannot be directly measured; a measured spectrum is a superposition of spectra for a range of values of $k_\perp$. One case where this is avoided is for a surface state. If there is no bulk state for some range of energy and some $\mathbf{k}_\parallel$, then a surface state may occur in that energy range with a sharp two-dimensional $\mathbf{k}$-vector. Then high-resolution photoemission can measure $1/\tau_k$ and thus λ_k for that state.

b. Commentary on λ Values

Tables 9.8 through 9.11 contain values of λ for selected materials. Values are only tabulated for those cases in which they are unlikely to change appreciably with time. Therefore, many interesting materials are omitted, such as the cuprate, bismuthate, and fullerene superconductors. Especially in the cuprates, properties of quasiparticles, including even whether they exist and what spin and charge they carry, are still mysterious. Electron–phonon coupling seems to affect some properties of cuprates, yet seems to be missing from other

properties. My opinion is that Migdal–Eliashberg theory and Eq. (31) do not apply to cuprates, but probably do apply to fullerenes and to the $BaBiO_3$ family of superconductors. Values of λ of order 1 probably apply to the latter two families, but firm numbers are hard to obtain.

Table 9.8 contains elements that are superconducting in crystalline form at atmospheric pressure, including two cases (Ga and La) where there is information about a metastable phase. The entries are taken from previously cited sources, as well as the following references: Allen (1987b); Sanborn *et al.* (1989); Garno (1978); Dynes (1970); Rowell *et al.* (1971); Hubin and Ginsberg (1969); McMillan and Rowell (1965); Zasadzinski *et al.* (1982); Wolf *et al.* (1980); Shen (1970); Wolf *et al.* (1981); and Lou and Tomasch (1972). The superconducting elements provide the best opportunity to compare λ values obtained by different methods. In particular, for Pb, V, Nb, and Ta there are transport, tunneling, and LDA values in addition to values from the McMillan equation, Eq. (31). In all cases, McMillan values are less than all other values, strongly suggesting that the McMillan equation underestimates λ. There are two main causes of this: (1) The McMillan prefactor $\Theta_D/1.45$ is often larger than the correct prefactor $\omega_{\ln}/1.2$, although probably not by much for the elements V, Nb, and Ta because the McMillan equation was based on the phonon spectrum of Nb; (2) knowledge of μ^* is still primitive; it is assumed to be $0.10 - 0.13$, but Table 9.8 suggests that it is often larger. In particular, in V it is suspected that spin-fluctuation effects may increase μ^* above the "renormalized" value $\mu/[1 + \mu \ln(\omega_P/\omega_D)]$ because the characteristic spin-fluctuation frequencies are lower than ω_P. For very strong-coupling materials such as Pb, the McMillan equation should overestimate λ because in this regime it is known to underestimate T_c. However, in Pb the other causes must dominate since λ_{McM} is an underestimate. I believe that theoretical LDA values are now more reliable than McMillan values. Tunneling values are excellent for the "simple" metals β-Ga, In, Sn, Hg, Tl, and Pb, but require more complicated junction preparation methods and more complicated theoretical analyses for d-band and exotic materials, which degrades the believability of the numbers. For most elements the transport values are good, but Tl and Re may have too high values of λ_{tr}.

Table 9.9 shows values for four elements where tunneling experiments (Chen *et al.*, 1969; Knorr and Barth, 1970) have been carried out on superconducting amorphous phases. Bi is semimetallic and not superconducting in its crystalline phase. The divergent experimental values of λ may reflect differences between samples of amorphous Bi made by different procedures, or may instead reflect difficulties in accurate measurement of tunneling characteristics, especially at bias voltages near the superconducting gap where λ can have important contributions due to soft mode vibrations that are hard to measure accurately. In Ga and Sn (but not in Pb) the amorphous phase has enhanced values of T_c. In all three elements, λ is enhanced. The reason is the softening of the vibrational spectrum in amorphous phases, which raises λ more than T_c.

Table 9.10 gives values for crystalline elements that are nonsuperconducting, using information from previously cited sources, as well as from Carlsson

Table 9.8.

Values of λ for superconducting crystalline elements.

Metal	T_c(K)	Θ_D(K)	λ^a_{McM}	λ_{tr}	λ_{tun}	λ_{LDA}
Be	0.026	1390	0.23			
Al	1.16	428	0.38	0.39[b]		0.44[c,d]
Zn	0.85	309	0.38	0.46[e]		
α-Ga	1.08	325	0.40			
β-Ga	5.9				0.97[f]	
Cd	0.52	209	0.38	0.37[e]		
In	3.40	112	0.69		0.834[g]	
Sn	3.72	200	0.60		0.72[h]	
Hg	4.16	72	1.00		1.60[i]	
Tl	2.38	79	0.71	1.11[e]	0.78[f]	
Pb	7.19	105	1.12	1.48[b]	1.55[j]	1.20[d],1.68[c]
Ti	0.39	425	0.38	0.50[k]		
V	5.30	399	0.60	1.09[b]	0.83[l]	1.19[c]
Zr	0.55	290	0.41	0.55[k]		
Nb	9.22	277	0.82	1.06[b]	1.05[m]	1.26[c]
Mo	0.92	460	0.41	0.32[b]		0.42[c]
Ru	0.49	550	0.38	0.45[e]		
Hf	0.09	252	0.34	0.42[k]		
Ta	4.48	258	0.65	0.87[b]	0.69[n], 0.73[o]	0.86[c]
W	0.012	390	0.28	0.26[b]		
Re	1.69	415	0.46	0.76[e]		
Os	0.65	500	0.39	0.54[e]		
Ir	0.14	420	0.34	0.50[b]		
α-La	4.88	151	0.81[p]		(0.77)[q]	
β-La	6.00	139	0.93[p]			
Th	1.38	165	0.56[b]	0.52[b]		

[a]Unless otherwise noted, from MacMillan (1968). [b]Allen (1987b). [c]Savrasov and Savrasov (1996). [d]Liu and Quong (1996). [e]Sanborn *et al.* (1989). [f]Garno (1978). [g]Dynes (1970). [h]Rowell *et al.* (1971). [i]Hubin and Ginsberg (1969). [j]McMillan and Rowell (1965). [k]Allen (1996). [l]Zasadzinski *et al.* (1982). [m]Wolf *et al.* (1980). [n]Shen (1970). [o]Wolf *et al.* (1981). [p]from Eqn. (31) using data from Roberts (1976). [q]Difficulties with the junction required *ad hoc* modifications in the analysis (Lou and Tomasch, 1972).

Table 9.9.

Values of λ for superconducting amorphous elements.

Metal	T_c	λ_{tun}
Ga	8.56	2.25[a]
Sn	4.5	0.84[b]
Pb	7.2	1.91[a]
Bi	6.1	2.46,[a] 1.84[b]

[a]Chen *et al.* (1969). [b]Knorr and Barth (1970).

et al. (1997); McDougall *et al.* (1995); and Hoyt and Mota (1976). Values from transport are known for many elements and appear consistent with other values when available. It would be very interesting to have reliable values for ferromagnetic elements. However, one expects that there should be quite different values of λ for the up and the down spin species, but two values ($\lambda_\uparrow$ and $\lambda_\downarrow$) cannot be extracted independently from transport measurements. Therefore, we must wait for theoretical values and measurements by spin-sensitive techniques. As an example, Gd is ferromagnetic with a Curie temperature of 292 K. Photoemission below this temperature has seen a surface state carrying the majority ($\uparrow$) spin, and its λ value is listed.

Table 9.11 lists most of the intermetallic compounds where there is reliable information (Dynes, 1972; Kihlstrom *et al.*, 1985; Kwo and Geballe, 1981; Rudman and Beasley, 1984; Schulz *et al.*, 1992; Glassford and Chelikowsky, 1994; Rathnayaka *et al.*, 1997; Pickett and Singh, 1994; Kim *et al.*, 1995; Singh, 1996; Michor *et al.*, 1996; Singh, and Pickett, 1995). Evaluating λ_{tr} for compounds is often risky. There are two main difficulties: (1) the measured $\rho(T)$ is sometimes sample dependent, especially in oxide materials where polycrystalline bulk, single crystal, and thin film samples give different results;

Table 9.10.

Values of λ for non-superconducting crystalline elements.

Metal	λ_{tr}^{a}	λ_{LDA}	λ_{other}
Li	0.35	0.45–0.51[b]	
Na	0.14		0.24[c]
K	0.11		
Rb	0.15		
Cs	0.16		
Cu	0.13	0.14[d]	0.14 ± 0.02[e]
Ag	0.12		
Au	0.15		0.2[f]
Mg	0.20[g]		
Ca	0.05		
Ba	0.27		
Sc	0.51[g]		
Y	0.62[g]		
Pd	0.47	0.35[d]	
Pt	0.66		
Gd			0.6[h]

[a]Unless otherwise noted, from Allen (1987b). [b]Liu and Quong (1996). [c]Surface quantum well state (Carlsson *et al.*, 1997). [d]Savrasov and Savrasov (1996). [e]Surface state on Cu(111) (McDougall *et al.*, 1995). [f]Extrapolation from superconducting alloys (Hoyt and Mota, 1976). [g]Sanborn *et al.* (1989). [h]Surface state with quantum numbers $5d(z^2, \uparrow)$ on Gd(0001), P. D. Johnson, private communication.

it is hard to know the "true" $\rho(T)$, but usually safe to assume that the smallest values are the best; (2) it is important to be sure that the transport mean free path is at least 10 Å; otherwise, wavevector **k** is not a good quantum number, Bloch–Boltzmann theory is not applicable, and λ_{tr} is ill-defined. In Eq. (35), the group velocity $\hbar v_{k,x} = \partial\varepsilon/\partial k_x$ is only well defined when wavevector **k** is a good quantum number. The superconducting λ, however, is still well defined from Eq. (35) provided the quantum numbers k, k' are reinterpreted as labels for the exact eigenstates of the disordered material.

RuO_2 is an interesting case where the transport value of λ suggests the possible occurrence of superconductivity at not too low a temperature, and this may not have been tested below helium temperature. The layered intermetallic borocarbides received a great deal of attention. In the case of $LuNi_2B_2C$, McMillan and transport values agree, which suggests (as does other evidence) conventional superconductivity. For the related material $La_3Ni_2B_2N_{3-\delta}$, transport and McMillan values badly disagree. My guess is that the transport value may change with better data, but usually the transport value goes down in time as samples improve, rather than up in time. An alternate possibility is the occurrence of unconventional superconductivity. A similar situation holds for cuprates, where transport values of λ of order 1 are found using LDA bands, whereas to account for T_c near 100 K, one needs λ of order 3 or higher. There are clear signs

Table 9.II.

Values of λ for crystalline compounds and ordered intermetallics.

Metal	T_c	λ_{tun}	λ_{tr}	λ_{McM}
In_2Bi	5.6	1.40[a]		
Bi_2Tl	6.4	1.63[a]		
Tl_7Sb_2	5.2	1.43[a]		
V_3Si	17.1	0.89[b]		
Nb_3Al	18.5	1.7[c]		
Nb_3Sn	17.8	1.75[d]		
Nb_3Ge	≈20	1.7[b]		
NbN	16.0	1.46[b]		
NbO	1.4		0.51[e]	0.41[e]
ReO_3	< 0.02		0.35[f]	
RuO_2	< 4.2		0.5±0.1[g]	
$CoSi_2$	1.22		0.44[f]	
Pd_2Si			0.15–0.20[f]	
$LuNi_2B_2C$	16.1		0.9,[h], 0.8[i]	1.0[h]
$La_3Ni_2B_2N_{3-\delta}$	12.25		0.29[j]	0.86[j]

[a]Dynes (1972). [b]Kihlstrom *et al.* (1985).[c]Kwo and Geballe (1981). [d]Wolf *et al.* (1980); Rudman and Beasley (1984). [e]Schulz *et al.* (1992).[f] Allen and Schulz (1993). [g]Glassford and Chelikowsky (1994). [h]Using data from Rathnayaka *et al.* (1997) and theory from Pickett and Singh (1994) and Kim *et al.* (1995). [i]Singh (1996). [j]Using data from Michor *et al.* (1996) and theory from Singh and Pickett (1995).

of unconventional behavior, which in my mind invalidates the transport analysis based on Bloch–Boltzmann theory. Another interesting intermetallic, Sr_2RuO_4, is also not listed. Nice-looking resistivity measurements are now being published, but do not accord well with the Bloch–Grüneisen formula, which is another sign of unconventional behavior. It is not clear whether the concept of an electron–phonon λ value can be retained in such cases. In most materials where the confusion is large, I have not tabulated any λ values, but $La_3Ni_2B_2N_{3-\delta}$ is included as a sign of the potential hazards.

Acknowledgements

I thank R. C. Dynes and W. E. Pickett for help with the manuscript. This work was supported in part by NSF Grant No. DMR-9725037.

References for Section G

P. B. Allen, *Phys. Rev. Lett.* **59**, 1460 (1987a).
P. B. Allen, *Phys. Rev.* **B36**, 2920 (1987b).
P. B. Allen, in *Quantum Theory of Real Materials* (J. R. Chelikowsky and S. G. Louie, Eds.), Chapter 17, pp. 219–250. Kluwer, Boston, 1996.
P. B. Allen and R. C. Dynes, *Phys. Rev. B* **12**, 905 (1975).
P. B. Allen and W. W. Schulz, *Phys. Rev. B* **47**, 14434 (1993).
P. B. Allen, T. P. Beaulac, F. S. Khan, W. H. Butler, F. J. Pinski, and J. C. Swihart, *Phys. Rev. B* **34**, 4331 (1986).
S. Baroni, P. Gianozzi, and A. Testa, *Phys. Rev. Lett.* **58**, 1861 (1987).
S. D. Brorson, A. Kazeroonian, J. S. Moodera, D. W. Face, T. K. Chenk, E. P. Ippen, M. S. Dresselhaus, and G. Dresselhaus, *Phys. Rev. Lett.* **64**, 2172 (1990).
A. Carlsson, B. Hellsing, S.-Å. Lindgren, and L. Walldén, *Phys. Rev. B* **56**, 1593 (1997).
T. T. Chen, J. T. Chen, J. T. Leslie, and H. J. T. Smith, *Phys. Rev. Lett.* **22**, 526 (1969).
R. C. Dynes, *Phys. Rev. B* **2**, 644 (1970).
R. C. Dynes, *Solid State Commun.* **10**, 615 (1972).
J. P. Garno, *Rev. Sci. Instrum.* **49**, 1218 (1978).
G. D. Gaspari and B. L. Gyorffy, *Phys. Rev. Letters.* **28**, 801 (1972)
K. M. Glassford and J. R. Chelikowsky, *Phys. Rev.* B**49**, 7107 (1994).
G. Grimvall, *The Electron-Phonon Interactim in Metals*, North-Holland, Amsterdam, 1981 (Vol. XVI of *Selected Topics in Solid State Physics*, edited by E. P. Wohlfurth.)
J. J. Hopfield, *Phys. Rev.* **186**, 443 (1969)
J. J. Hopfield, *Proceedings of the Rochester Conference on d- and f-Band Superconductors* (D.H. Douglass, Ed.) p. 354. AIP Conference Proceedings, 1972.
R. F. Hoyt and A. C. Mota, *Solid State Commun.* **18**, 139 (1976).
W. N. Hubin and D. M. Ginsberg, *Phys. Rev.* **188**, 716 (1969).
K. E. Kihlstrom, R. W. Simon, and S. A. Wolf, *Physica* **135B**, 198 (1985).
H. Kim, C. Hwang, and J. Ihm, *Phys. Rev. B* **52**, 4592 (1995).
K. Knorr and N. Barth, *Solid State Commun.* **8**, 1085 (1970).
J. Kwo and T. H. Geballe, *Phys. Rev. B* **23**, 3230 (1981).
A. Y. Liu and A. A. Quong, *Phys. Rev. B* **53**, R7575 (1996).
L. F. Lou and W. J. Tomasch, *Phys. Rev. Lett.* **29**, 858 (1972).
B. A. McDougall, T. Balasubramanian, and E. Jensen, *Phys. Rev. B* **51**, 13891 (1995).

W. L. McMillan, *Phys. Rev.* **167**, 331 (1968).
W. L. McMillan and J. M. Rowell, *Phys. Rev. Lett.* **19**, 108 (1965).
W. L. McMillan and J. M. Rowell, in *Superconductivity* (R. D. Parks, Ed., Vol. 1, p. 561. Marcel Dekker, New York, 1969.
H. Michor, R. Krendelsberger, G. Hilscher, E. Bauer, C. Dusek, R. Hauser, L. Naber, D. Werner, P. Rogl, and H. W. Zandbergen, *Phys. Rev. B* **54**, 9408 (1996).
W. E. Pickett and D. J. Singh, *Phys. Rev. Lett.* **72**, 3702 (1994).
K. D. D. Rathnayaka, A. K. Bhatnagar, A. Parasiris, D. G. Naugle, P. C. Canfield, and B. K. Cho, *Phys. Rev. B* **55**, 8506 (1997).
B. W. Roberts, *J. Phys. Chem. Ref. Data* **5**, 581 (1976).
J. M. Rowell, W. L. McMillan, and W. L. Feldmann, *Phys. Rev. B* **3**, 4065 (1971).
D. A. Rudman and M. R. Beasley, *Phys. Rev. B* **30**, 2590 (1984).
B. A. Sanborn, P. B. Allen, and D. A. Papaconstantopoulos, *Phys. Rev.* **B40**, 6037 (1989).
S. Y. Savrasov and D. Y. Savrasov, *Phys. Rev. B* **54**, 16487 (1996).
W. W. Schulz, L. Forro, C. Kendziora, R. Wentzcovitch, D. Mandrus, L. Mihaly, and P. B. Allen, *Phys. Rev. B* **46**, 14001 (1992).
L. Y. L. Shen, *Phys. Rev. Lett.* **24**, 1104 (1970).
M. M. Sigalas and D. A. Papaconstantopoulos, *Phys. Rev. B* **50**, 7255 (1994).
D. J. Singh, *Solid State Commun.* **98**, 899 (1996).
D. J. Singh and W. E. Pickett, *Phys. Rev. B* **51**, 8668 (1995).
H. L. Skriver and I. Mertig, *Phys. Rev. B* **41**, 6553 (1990).
H. L. Skriver, O. Eriksson, I. Mertig, and E. Mrosan, *Phys. Rev. B* **37**, 1706 (1988).
E. L. Wolf, *Principles of Electron Tunneling Spectroscopy.* Oxford University Press, New York, 1985.
E. L. Wolf, J. Zasadzinski, G. B. Arnold, D. F. Moore, J. M. Rowell, and M. R. Beasley, *Phys. Rev. B* **22**, 1214 (1980).
E. L. Wolf, D. M. Burnell, Z. G. Khim, and R. J. Noer, *J. Low Temp. Phys.* **44**, 89 (1981).
J. Zasadzinski, D. M. Burnell, E. L. Wolf, and G. B. Arnold, *Phys. Rev. B* **25**, 1622 (1982).

This Page Intentionally Left Blank

Chapter 10

Thermal Properties

Ctirad Uher
Physics Department, University of Michigan, Ann Arbor, Michigan

Charles P. Poole, Jr.
Department of Physics and Institute of Superconductivity, University of South Carolina, Columbia, South Carolina

Alan B. Kaiser
Physics Department, Victoria University, Wellington, New Zealand

ISBN: 0-12-561460-8
$30.00

HANDBOOK OF SUPERCONDUCTIVITY

A

Introduction

The present chapter deals with various thermal type properties of superconductors. It begins with the specific heat, which has been extensively studied for many superconductors. These data are of interest because the BCS theory makes explicit predictions about the behavior of the specific heat in the neighborhood of the transition temperature T_c. This chapter also contains more extensive sections on the thermal conductivity and various thermoelectric and thermomagnetic effects.

B

Specific Heat

a. Meaning of Specific Heat

The specific heat C of a material is the change in internal energy U brought about by a change in temperature,

$$C = \frac{dU}{dT}, \tag{1}$$

where the usual units for C are J/mol-K. We do not differentiate between the specific heat at constant volume, which is defined by Eq. (1), and that at constant pressure, which is the change in enthalpy brought about by a temperature change, because for solids the two are almost indistinguishable. Ordinarily the specific heat is measured as the heat input dQ that raises the temperature by a unit amount dT:

$$dQ = C\,dT. \tag{2}$$

In metals C is mainly the sum of an electronic term C_e due to the conduction electrons and a phonon contribution C_{ph} due to lattice vibrations:

$$C = C_e + C_{ph.} \tag{3}$$

The electronic term is only appreciable at low temperatures and changes dramatically at the superconducting transition, whereas the phonon contribution dominates at room temperature and is largely undisturbed by the transition at T_c. We will investigate these two contributions to the specific heat in the next two sections.

b. Electronic Specific Heat

In normal metals C contains a contribution from the conduction electrons C_e that increases linearly with temperature:

$$C_e = \gamma T \tag{4}$$

The so-called Sommerfeld constant γ,

$$\gamma = (\pi^2/3)D(E_F)k_B^2, \tag{5}$$

provides an experimental estimate of the density of states $D(E_F)$ at the Fermi level. Table 10.1 lists values of γ in the normal state for a number of superconductors. For many metallic elements γ is close to the free electron value γ_0,

$$\gamma_0 = \pi^2 R/2T_F = 4.93R/T_F, \tag{6}$$

where $R = N_A k_B$ is the gas constant and T_F is the Fermi temperature. The fact that T_F appears in the denominator of Eq. (6) makes it clear from Eq. (4) that $C_e \ll R$ for all temperatures of experimental interest. The ratio of the effective mass m^* to the free electron mass m is

$$m^*/m = \gamma/\gamma_0 = \gamma T_F/\tfrac{1}{2}\pi^2 R. \tag{7}$$

The free electron approximation also provides an expression for the ratio of γ_0 to the (Pauli) conduction electron susceptibility χ_e,

$$\gamma_0/\chi_e = \tfrac{1}{3}(\pi k_B/\mu_B)^2 \tag{8}$$

c. Phonon Specific Heat

The Debye model for the phonon contribution C_{ph} to the specific heat assumes that the sound velocity v is isotropic and independent of the frequency, and that there is a maximum vibrational frequency ω_D called the Debye frequency with an associated Debye temperature θ_D,

$$\hbar\omega_D = k_B\theta_D, \tag{9}$$

which gives for the phonon density of states per unit volume $D_{ph}(\omega)$

$$D_{ph}(\omega) = dn/d\omega = \frac{3\omega^2}{2\pi^2 v^3}. \tag{10}$$

Standard solid-state physics texts derive the following integral for the vibrational or phonon specific heat:

$$C_{ph} = 9R(T/\theta_D)^3 \int_0^{x_D} \frac{x^4 e^x\, dx}{(e^x - 1)^2}, \tag{11}$$

Table 10.1

Specific heat and related data for some selected superconductors. Data are from Table 4.1 of Poole *et al.* (1995); see also Junod (1990) and Vonsovsky *et al.* (1982).

Material	T_c (K)	Θ_D (K)	γ (mJ/mol-K^2)	$(C_s - C_n)/\gamma T_c$	A (mJ/mol-K^4)	$D(E_F)$ (states/eV)
Cd	0.55	252	0.67	1.36		
Al	1.2	423	1.36	1.45		
Sn, white	3.72	196	1.78	1.60		
Pb	7.19	102	3.14	2.71		1.55
Nb	9.26	277	7.66	1.93		2.0
$Zr_{0.7}Ni_{0.3}$	2.3	203	4.04	≈1.65	0.23	
V_3Ge *A*15	8.2		7.0			
V_3Si *A*15	17.1		17.0			
Nb_3Sn *A*15	18.0		13.0			
HfV_2 Laves	9.2	187	21.7			2.3
$(Hf_{0.5}Zr_{0.5})V_2$ Laves	10.1	197	28.3			3.0
ZrV_2 Laves	8.5	219	16.5			1.9
$PbMo_6S_8$ Chevrel	12.6		79.0			
$PbMo_6Se_8$ Chevrel	3.8		28.0			
$SnMo_6S_8$ Chevrel	11.8		105.0			
YMo_6S_7 Chevrel	6.3		34.0			
UPt_3 Hvy ferm	0.46		460.0	≈0.9	1525	
UCd_{11} Hvy ferm	5.	200	290.0		115	
URu_2Si_2 Hvy ferm	1.1		31.0	0.42		
$CeRu_2Si_2$ Hvy ferm	≈0.8		340.0	3.5		
$(TMTSF)_2ClO_4$ Org	1.2	213	10.5	1.67	11.4	
K-$(ET)_2Cu(NCS)_2$ Org	9.3		34.0			9.3
$BaPb_{1-x}Bi_xO_3$ Perovskite	10.0		0.6	8.0		0.24
$(La_{0.925}Sr_{0.075})_2CuO_4$	37.0	360	4.5	2.0		
$YBa_2Cu_3O_7$	92.0	410	20–35	1.3–2		1–3
$Bi_2Sr_2CaCu_2O_8$	95.0	250	0–10			
$Tl_2Ba_2CaCu_2O_8$	110.0	260	<6.8	>6		
$Tl_2Ba_2Ca_2Cu_3O_{10}$	125.0	280	~58	~1.4		

where $x_D = \theta_D/T$, and this expression is plotted in Fig. 10.1 using experimental data from Cu and Pb. The molar phonon specific heat has the following limiting behaviors:

$$C_{ph} = (12\pi^4/5)R(T/\theta_D)^3 = 234R(T/\theta_D)^3, \qquad T \ll \theta_D \tag{12a}$$

$$C_{ph} = 3R, \qquad T \gg \theta_D. \tag{12b}$$

The figure shows that at T_c the element Pb and LaSrCuO are in the T^3 region, while YBaCuO is significantly above it.

Fig. 10.1.

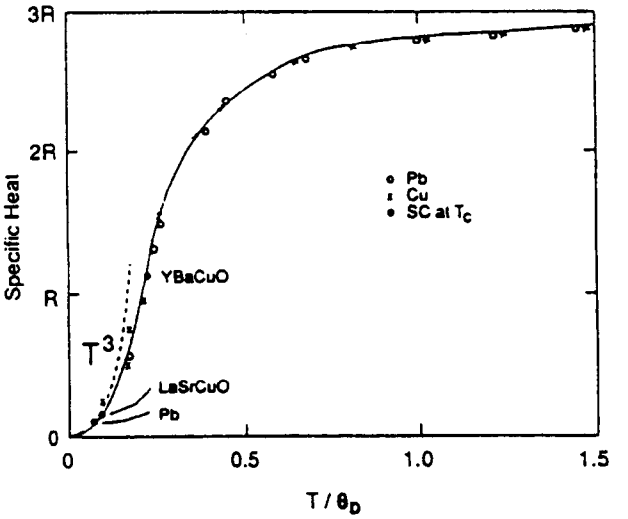

Debye model (solid curve) of the phonon specific heat with the T^3 low temperature approximation (dashed curve) indicated. Experimental data for the elements Cu and Pb are given. The specific heats of the three superconductors Pb, $(La_{0.925}Sr_{0.075})CuO_4$, and $YBa_2Cu_3O_{7-\delta}$ at their respective transition temperatures are indicated [From Poole *et al.* (1995 p.14).]

If C_{exp}/T is plotted vs T^2 at low temperature,

$$C_{exp}/T = \gamma + AT^2, \tag{13}$$

the slope gives the phonon part $A = 234R/\theta_D^3$ and the intercept at the origin, $T = 0$, gives the electronic coefficient γ. Sometimes other terms also contribute.

d. Discontinuity at T_c

The phase transition from the normal to the superconducting state in the absence of an applied magnetic field is second order, so the Gibbs free energy and its temperature derivative are continuous:

$$G_s(T_c) = G_n(T_c) \tag{14}$$

$$\frac{dG_s}{dT} = \frac{dG_n}{dT}. \tag{15}$$

There is no latent heat, but there is a discontinuity in the specific heat, and the BCS theory predicts a dimensionless jump in the normalized electronic specific heat at T_c given by

$$(C_{es} - \gamma T_c)/\gamma T_c = 1.43, \tag{16}$$

where here C_{es} is the electronic term immediately below T_c. This discontinuity has been observed, as shown in Fig. 10.2 and by the data presented in Table 10.1. The BCS theory predicts that far below T_c the specific heat depends exponentially on the temperature

$$C_{es}(T) \approx a \exp(-\Delta/k_B T), \tag{17}$$

where $E_g = 2\Delta$ is the energy gap in the superconducting density of states.

When a magnetic field is present there is still a discontinuity in the specific heat, but in addition there is a field-dependent latent heat given by

$$L(B) = (S_n - S_s)T_c(B), \tag{18}$$

so the transition is now first-order, where $T_c(B)$ is the transition temperature in the presence of the field. If the assumption is made that the critical field $B_c(T)$ has a parabolic dependence on the temperature,

$$B_c(T) = B_c(0)[1 - (T/T_c)^2], \tag{19}$$

then this expression can be inverted to give the magnetic field dependence of the critical temperature,

$$T_c(B) = T_c[1 - B/B_c(0)]^{1/2}, \tag{20}$$

where T_c is the transition temperature in the absence of the field, and of course $B < B_c(0)$ for the material to remain superconducting.

Fig. 10.2.

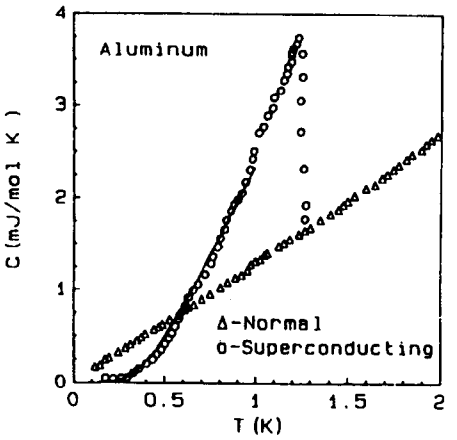

Specific heat of elemental aluminum in the normal and superconducting states showing the jump predicted by the BCS theory. [Phillips (1959); see Crow and Ong (1990), p. 225.]

References for Section B

J. E. Crow and N.-P. Ong, in *High Temperature Superconductivity* (J. W. Lynn, Ed.), Chapter 7. Springer-Verlag, Berlin, 1990.
A. Junod, in *Physical Properties of High Temperature Superconductors* (D. M. Ginsberg, Ed.), Vol. 2, Chapter 2. World Scientific, Singapore, 1990.
N. E. Phillips, *Phys. Rev.* **114**, 676 (1959).
C. P. Poole, Jr., H. A. Farach, and R. J. Creswick, *Superconductivity.* Academic Press, New York, 1995.
S. V. Vonsovsky, Yu. A. Izumov, and E. Z. Kumaev, *Superconductivity in Transition Metals.* Springer, New York, 1982.

C

Thermal Conductivity

Ctirad Uher

a. Introduction

Among the important properties of high-temperature superconductors (HTS) is their ability to conduct heat. There is not only an obvious technological interest in how efficiently and by what means the heat flows in these solids, but also a deep theoretical desire to understand the electronic and vibrational properties of these materials. In HTS, such information is especially valuable due to the fact that traditional galvanomagnetic probes such as resistivity, Hall effect, and thermopower are inoperative in the (now) wide temperature range below T_c. Detailed account of heat transport in HTS can be found in Jezowski and Klamut (1990) and Uher (1990, 1992).

For any isotropic solid, the thermal gradient ∇T imposed across the sample results in the rate of flow of heat across a unit cross-section perpendicular to the direction of heat flow governed by Fourier's law,

$$\mathbf{U} = -\kappa \nabla \mathbf{T}. \tag{21}$$

Here κ is the thermal conductivity and the negative sign implies that the heat flows down the thermal gradient, that is, from the warmer to the cooler end of the sample.

Measurements of the thermal conductivity can be accomplished by various experimental arrangements depending on the structural form of a sample, temperature interval of interest, and the desired accuracy of the data. One is mostly interested in the behavior of the thermal conductivity at and below room temperature and, for samples of bulk form, the most convenient and by far the most frequently used setup is the *longitudinal steady-state technique* illustrated in Fig. 10.3. One end of a sample with a uniform cross-sectional area A is attached to a cold tip of the cryostat while a small heater (typically a metal-film resistor) is

fastened to the other end of the sample. Electrical power Q dissipated in the heater provides a heat flow. The resulting temperature difference $\Delta T = T_h - T_c$ between two points separated by a distance L is measured by a pair of thermometers or a differential thermocouple. The thermal conductivity κ is then calculated from

$$\kappa = QL/(A\ \Delta T). \tag{22}$$

For not too large ΔT, the value of κ obtained from Eq. (22) will be that corresponding to the mean temperature between the thermometers. For very short samples, it is frequently preferable to use the so-called *two-heater/one thermometer technique*, wherein a thermometer is attached to the free end of the sample while the power is switched between two heaters spaced along the length of the sample. Since heaters can be made very small (e.g., by evaporating resistive strips), they can be easily accommodated on short samples. Thermal conductivity of samples in the form of thin films can be determined by the so-called *3-ω method* (Cahill, 1990). Experimental techniques of measuring thermal conductivity are discussed in several monographs and review articles, for example, Berman (1976) and Uher (1996).

Fig. 10.3.

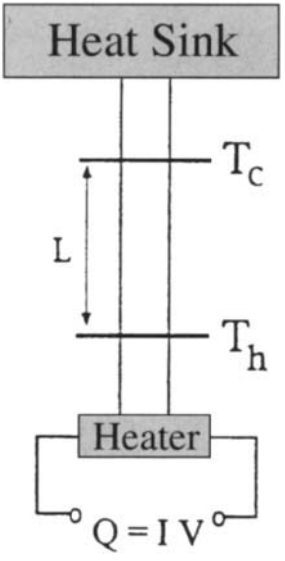

Experimental setup to measure thermal conductivity using the longitudinal steady-state method.

b. Normal State

Heat in a solid is carried by two distinct entities, free carriers, κ_e, and quantized lattice vibrations called phonons, κ_p. The total thermal conductivity, κ, is then

$$\kappa = \kappa_e + \kappa_p. \tag{23}$$

The relative magnitude of the two contributions in Eq. (23) can be used to classify solids in a way analogous to the magnitude of the electrical resistivity, Fig. 10.4. Each heat-conducting channel (carriers and phonons) is subject to relaxation mechanisms (scattering) that ensure the stationary nature of the heat-conducting process. Charge carriers are scattered by phonons yielding the thermal resistivity contribution W_{e-p}, by defects yielding W_{e-d}, and by other charge carriers, W_{e-e}. Phonons can scatter on free carriers, W_{p-e}, on defects, W_{p-d} and in interactions with other phonons, W_{p-p}. According to Matthiessen's rule, the scattering processes within each channel are additive, yielding

$$W_e \equiv 1/\kappa_e = W_{e-p} + W_{e-d} + W_{e-e} \tag{24}$$

$$W_p \equiv 1/\kappa_p = W_{p-e} + W_{p-d} + W_{p-p}. \tag{25}$$

Depending on the carrier density, the density of defects, and the temperature range, the magnitude and the temperature dependence of each term in Eqs. (24) and (25) can be evaluated (see, for example, Klemens, 1965). For instance, a

Fig. 10.4.

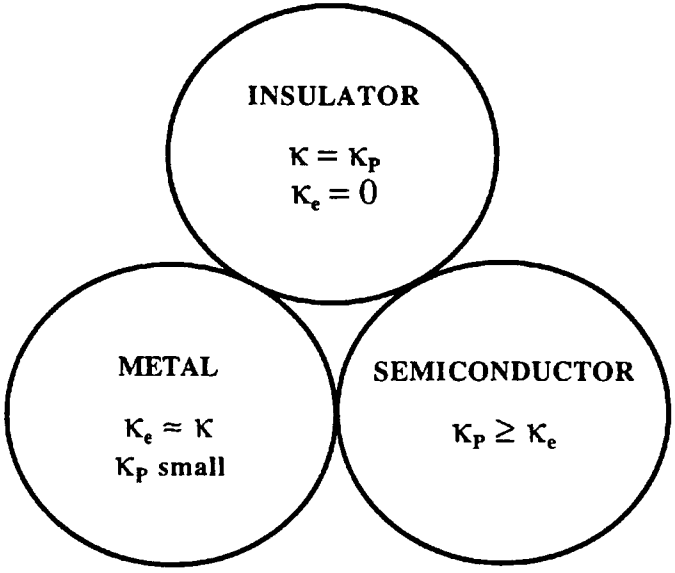

Main contributions to the thermal conductivity of various solids.

normal metal ($\kappa \approx \kappa_e$) can be modeled by the following expression with the temperature dependence

$$W_e \equiv 1/\kappa_e = aT^2 + b/T, \tag{26}$$

where the first term on the RHS stands for the carrier scattering by phonons and the second term represents the interaction of carriers with static lattice defects. Carrier-carrier interaction is usually small and is neglected in Eq. (26).

Assuming *elastic scattering*, the thermal conductivity associated with free carriers is related to the electrical resistivity via the *Wiedemann–Franz law*,

$$\kappa_e = L_0 T/\rho, \tag{27}$$

where $L_0 = \frac{\pi^2}{3}\left(\frac{k_B}{e}\right)^2 = 2.44 \times 10^{-8} V^2 K^{-2}$ is the Lorenz number.

Although pure metals are very good heat conductors, the highest values of the thermal conductivity are achieved in covalently bonded insulators with high Debye temperatures such as diamond and boron nitride. The thermal conductivity of isotopically pure diamond is so high that it is extremely difficult to determine accurately. Table 10.2 gives room-temperature values of the thermal conductivity of several selected materials.

Conventional superconductors are metals or alloys, and for $T > T_c$ their thermal conductivity has a substantially metallic character with a small contribution due to phonons that increases (as a percentage of the total thermal conductivity) as the metal becomes less pure and more disordered. HTS materials have a significantly reduced carrier density in comparison with typical metals and,

Table 10.2.

Thermal conductivity of several selected materials at a room temperature.

Material	κ(300 K) in W/m-K	Reference
Diamond	2200	1
Silver	420	1
Copper	390	1
Gold	320	1
Aluminum	240	1
Brass	120	1
MgO	60	1
Niobium	51	1
Lead	35	1
Constantan (55 Cu 45 Ni)	23	1
Stainless Steel	14	1
$YBa_2Cu_3O_7$ (ab-plane)	~10	2
Pyrex	1	1
Plexiglass	0.2	1
Styrofoam	0.04	3

References: 1, Childs *et al.* (1973); 2, Uher (1992); 3, Waite (1955).

as a consequence, phonons are the dominant heat conducting channel. For instance, in bulk sintered cuprates phonons account for 90–95% of the total thermal conductivity, and even in the best single crystal available phonons carry at least half of all heat in the normal state.

c. Superconducting State

The lowering of the temperature below the superconducting transition temperature T_c and the ensuing formation of the Cooper condensate lead to a sharp change in the electromagnetic and kinetic response of a material, and a consequent drastic modification of its heat flow pattern. Two properties of the condensate provide the overriding influence:

1. Cooper pairs carry no entropy
2. Cooper pairs do not scatter phonons

The first condition implies that the electronic thermal conductivity vanishes rapidly below T_c. In fact, the decrease is approximately exponential and has been justified by Bardeen, Rickayzen, and Tewordt (1959) in the so-called BRT Theory, and by Geilikman and Kresin (1958).

The effect of the second condition is more subtle. Provided that the mean free path of phonons at $T > T_c$ is limited by scattering on change carriers, on passing into the superconducting state the phonon thermal conductivity will rise because the number of normal carriers (more precisely, the density of quasiparticle excitations) rapidly decreases. The competition between the rapidly diminishing κ_e on the one hand and the increasing κ_p on the other will determine the overall dependence of the total thermal conductivity of any given superconductor. Because of the dominant contribution of charge carriers, a vast majority of conventional superconductors show a decrease in the ratio of the thermal conductivities in the superconducting and normal states, $\kappa^s(T)/\kappa^n(T)$, for $T < T_c$. In the case of elemental superconductors, the thermal conductivity may be reduced by 2–3 orders of magnitude in comparison to its normal-state value. On the other hand, in a few alloys, sufficiently disordered so that κ_e is relatively small and κ_p represents a significant fraction of the total thermal conductivity, and, at the same time, when the phonon–carrier interaction in the normal state is significant, the entry of such material into the superconducting domain may be accomplished by a rise in the thermal conductivity, Fig. 10.5. Such a rise is the consequence of an enhanced mean-free path of phonons as progressively fewer normal carriers are available to scatter them below T_c. Of course, at very low temperatures, all conventional superconductors will behave as ordinary dielectric solids, because phonons are the only entity that can carry heat.

Phonons carry the bulk of the heat in the normal state of HTS, and it is reasonable to assume that phonons also play a prominent role at temperatures

Fig. 10.5.

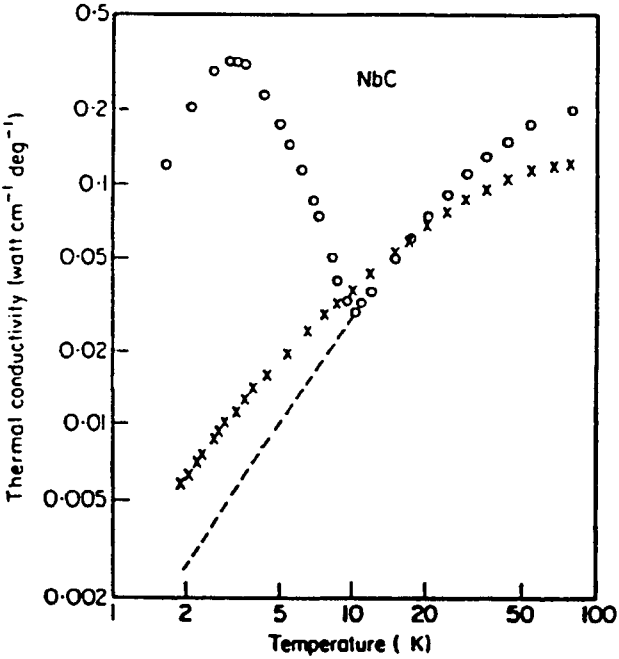

Thermal conductivity of niobium carbide. Open circles refer to a superconducting $NbC_{0.96}$ with $T_c \approx 10$ K. Crosses represent a nonsuperconducting $NbC_{0.76}$. [After Radosevich and Williams (1969).]

below T_c. The behavior of κ_p being limited by carrier scattering was originally treated in the BRT theory and supplemented by Tewordt and Wolkhausen (1989) to account for the relevant scattering processes and the anisotropy of the phonon–carrier interaction as appropriate to HTS cuprates. The in-plane phonon thermal conductivity becomes, Peacor *et al.* (1991a)

$$\kappa_{p,ab}(T) = (k_B/2\pi^2 v)(k_B/\hbar)^3 T^3 \int_0^{\theta_{D/T}} dx\, x^4 e^x/(e^x - 1)^2 \int_0^1 d\zeta\, 3/2(1 - \zeta^2)\mathscr{F}(T, x, \zeta), \tag{28}$$

where the overall scattering rate is given by

$$\mathscr{F}^{-1}(T, x, \zeta) = B + D_p t^4 x^4 + D_{sf} t^2 x^2 + Etxg(x, y)(1 - \zeta^2)^{3/2} + UT^4 x^2. \tag{29}$$

Coefficients B, D_p, D_{sf}, E, and U in Eq. (29), in turn, refer to phonon scattering by boundaries, point defects, sheetlike faults, charge carriers, and other phonons. The function $g(x, y)$ is the ratio of the phonon-carrier scattering times in the normal and superconducting states, and its exact form depends on the super-

conducting energy gap. The theory can accommodate the strong coupling limit for both the *s*-wave and *d*-wave pairing mechanisms, and provides a plausible explanation for the characteristic rise and the peak in the thermal conductivity of HTS below T_c, Fig. 10.6. The peak has been observed in samples of all major families of HTS except for BaKBiO and NdCeCuO structures. While excellent fits with perfectly reasonable parameters exist for both sintered and single crystal data (e.g., Peacor *et al.* 1991a), phonons may not be the sole entity responsible for the rising thermal conductivity and the peak below T_c.

Microwave surface resistance studies (Bonn *et al.*, 1992) and ultrafast laser pump-probe studies of carrier relaxation (Chwalek *et al.*, 1990) have clearly shown that the relaxation time of quasiparticles in HTS is dramatically enhanced below T_c. Such an unusually long quasiparticle lifetime provides and alternative explanation for the peak in the thermal conductivity (Yu *et al.*, 1992). In this case the fit to the experimental data is made with the aid of the formula for the carrier

Fig. 10.6.

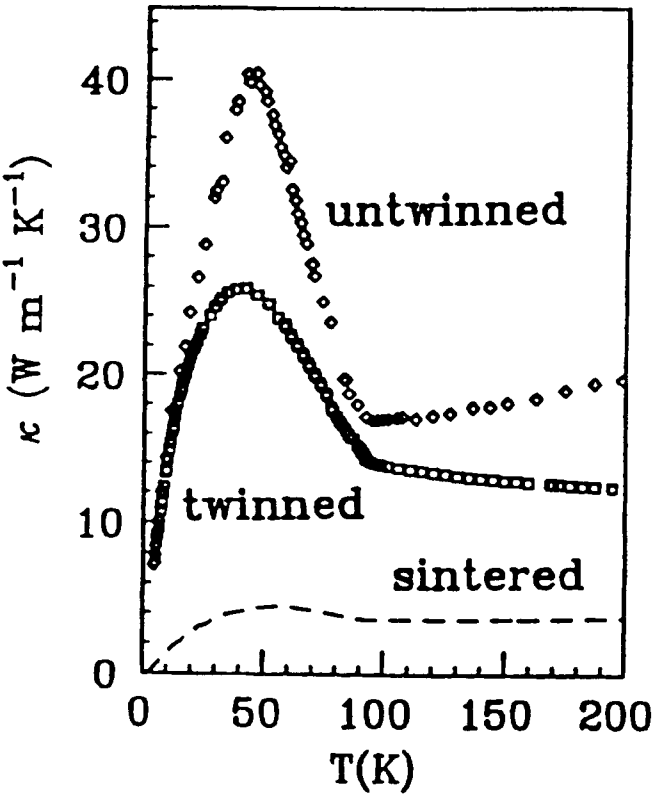

Thermal conductivity of sintered, twinned, and untwinned (*a*-direction) samples of $YBa_2Cu_3O_{7-\delta}$. [After Uher *et al.* (1994).]

contribution in the superconducting state derived by Kadanoff and Martin (1961) and independently by Tewordt (1962),

$$\kappa_e^s = 1/(2k_B T^2 m) \int d^3p (p_z^2 \varepsilon_p^2/\Gamma) \operatorname{sech}^2(E_p/2k_B T) \cong \Phi/\Gamma. \tag{30}$$

Here $E_p = (\varepsilon_p^2 + \Delta_p^2)^{1/2}$, where ε_p is the normal-state dispersion and Δ_p the superconducting gap. The scattering rate Γ is taken as $\Gamma \sim (T/T_c)^n + w_i$, implying a power law dependence augmented by a constant term w_i that stands for the residual scattering rate due to impurities. Yu *et al.* (1992) find that a *d*-wave pairing state fits best, and the relaxation rate varies as the fourth power of temperature.

The difficulty in making an unambiguous choice between the two competing interpretations rests in the fact that the charge carriers and phonons contribute roughly equally (in single crystals) to the heat transport in the normal state, and the physical processes that give rise to enhancements in either $\kappa_p(T)$ or $\kappa_e(T)$ below T_c have rather strong temperature dependences that lead to peaks in the thermal conductivity at virtually the same temperatures.

At very low temperatures, $T/T_c \ll 10^{-2}$, any anomalous behavior should cease and the only mode of heat transport should be via phonons, with grains and boundaries being the dominant scatterers, that is, $\kappa \sim T^3$. Although this is the case for insulating cuprates such as $YBa_2Cu_3O_6$ (Cohn *et al.*, 1988), the superconducting YBCO (Gottwick *et al.*, 1987) and LaSrCuO (Uher and Cohn, 1988) show a T-linear limiting dependence, Fig. 10.7, which is well approximated by

$$\kappa(T) = aT + bT^3. \tag{31}$$

Although various mechanisms were proposed to account for the linear term, the consensus converges on the presence of a small number (10–15%) of uncondensed carriers, and this provides support for the *d*-wave (nodes) symmetry of the superconducting state. BiSrCaCuO, on the other hand, displays a T^2-dependence below 2 K regardless of its structural form (Peacor and Uher, 1989; Zhu *et al.*, 1989; Sparn *et al.*, 1989). A correlation seems to exist between the T-linear limiting behavior and the magnitude of the γ-term in the specific heat.

HTS cuprates possess considerable structural anisotropy, which is reflected in the behavior of the thermal conductivity. Figure 10.8 provides the temperature dependence of the anisotropy ratio between the in-plane and the *c*-axis thermal conductivities, κ_{ab}/κ_c, for several cuprates.

d. Effect of a Magnetic Field

An external magnetic field $B > B_{c1}$ drives a superconductor into the mixed state characterized by the presence of Abrikosov vortices of core radius ξ that contain bound excitations not too different from normal electrons. Close to T_c the heat is

Fig. 10.7.

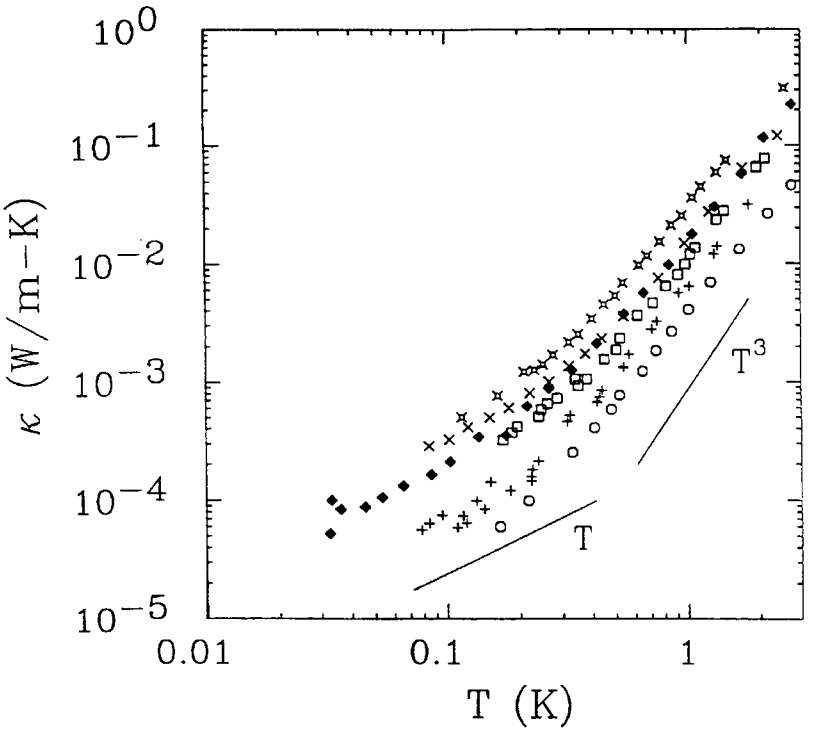

Thermal conductivity of several samples of sintered $YBa_2Cu_3O_{7-\delta}$ at very low temperatures. The slopes for linear (T) and cubic (T^3) temperature dependences are indicated. [After Uher (1992).]

carried by unbound excitations (uncondensed electrons), and they scatter on vortices, resulting in the thermal resistance

$$W_e(B) = W_e(0)[1 + (l_e a/\phi_0)B] \tag{32}$$

where l_e stands for mean free path (mfp) of quasiparticles and a is the effective vortex cross-section. There is no general theory to cover the entire range of magnetic fields, but beyond a certain field strength the scattering weakens as the vortices start to overlap. At the same time, tunneling between vortices drives the thermal conductivity toward its normal-state value κ_n as $B \to B_{c2}$. How the thermal conductivity actually attains its normal-state value depends critically on how large is l_e in relation to the coherence length ξ (Caroli and Cyrot, 1965; Maki, 1967). Unbound quasiparticles may also undergo the Andreev (1964) process, where an incoming electron-like quasiparticle scatters on the modulation of the order parameter $\Delta(\mathbf{r})$ and transforms into an outgoing hole-like

Fig. 10.8.

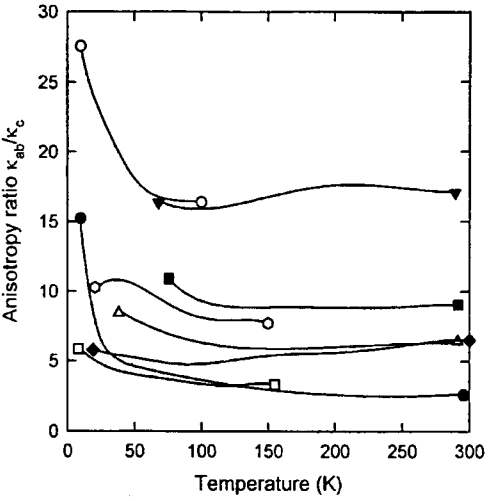

Anisotropy ratio κ_{ab}/κ_c temperature dependence for crystals of high-T_c superconductors: ○, $YBa_2Cu_3O_{6.7}$ (Sera *et al.*, 1990); ◆, $YBa_2Cu_3O_{7-\delta}$ (Hagen *et al.*, 1989); ▼, $YBa_2Cu_3O_7$ Cao *et al.*, 1991); □, $YBa_2Cu_3O_{7-\delta}$ (Efimov and Mezhov-Deglin, 1997); ◯, $Bi_2Sr_2CaCuO_{8-x}$ (Efimov and Mezhov-Deglin, 1997); △, $Bi_2Sr_2CaCuO_8$ (Crommie and Zettl, 1991); ■, $Tl_2Ba_2CaCu_2O_8$ (Cao *et al.*, 1991), ●, $La_{1.96}Sr_{0.04}CuO_4$ (Morelli *et al.*, 1990).

quasiparticle. This process may drastically alter the heat flow because of the near reversal of the group velocity.

Phonon–vortex scattering can be studied only at sufficiently low temperatures where the lattice carries most of the heat. For phonons to scatter, their wavelength must be comparable to the cross-section of the vortex. Phonon scattering intensifies with increasing vortex density as

$$W_p(B) = W_p(0)[1 + \alpha l_p(B/B_{c2})], \tag{33}$$

where α is the average scattering diameter of the vortex, and l_p is the phonon mfp. Again, as the vortices come close together, the electrons start to tunnel between them and the conductivity approaches the normal state as $B \to B_{c2}$. Typical behavior of the magnetothermal conductivity in conventional superconductors is sketched in Fig. 10.9. It is important to note that Eqs. (32) and (33) predict the same field dependence, and thus the magnetic field, on its own, cannot distinguish between the effects due to quasiparticles and those due to phonons.

A magnetic field has a strong influence on the heat transport in HTS single crystals and causes up to 30% reduction in the thermal conductivity (Palstra *et al.* 1990); Florentiev *et al.*, 1990; Zavaritski *et al.*, 1991; Peacor *et al.*, 1991b). The results show interesting hysteresis effects associated with the flux creep phenomenon, and this provides a way to study vortex dynamics via thermal transport measurements (Richardson *et al.*, 1991). Vortices scatter more effectively when

Fig. 10.9.

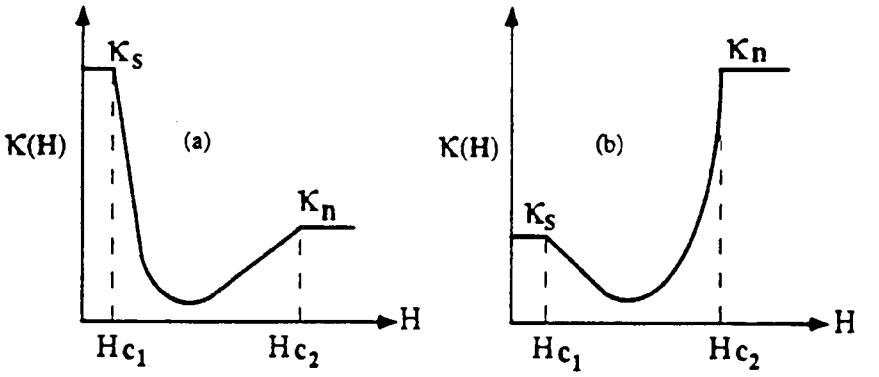

Effect of magnetic field on the thermal conductivity of conventional superconductors. (a) Behavior of a typical superconducting alloy. (b) Behavior of a "clean" superconductor.

they lie perpendicular to the CuO_2 planes than when they fit between the planes (see Fig. 10.10), and dimensionality of superconductivity has a considerable influence (Inyushkin *et al.*, 1994). In marked contrast to conventional superconductors, the field dependence of thermal conductivity in HTS is substantially sublinear, and stretched exponentials of the form

$$W_0(B) = cB \exp[-pB^{1/4}], \tag{34}$$

with c and p being fitting parameters, provide excellent fits to the data (Fig. 10.11; Richardson *et al.*, 1991). As yet, there is no consensus regarding the nature of this sublinear field dependence, (Richardson *et al.*, 1991; Bougrine *et al.*, 1993; Sergeenkov and Ausloos, 1995). Again, because of a similar functional dependence of the quasiparticle and phonon contributions on the magnetic field strength, one cannot assess the relative contributions of quasiparticles and phonons without some a priori information concerning the dominant carrier.

However, the nontraditional transport techniques that make use of the handedness in scattering of quasiparticles on vortices offer great hope for distinguishing between the contributions of quasiparticles and phonons. One such approach is the Righi–Leduc configuration used by Krishana *et al.* (1995); see Fig. 10.12. Although phonons are scattered symmetrically by the vortices, there is considerable asymmetry (handedness) as the quasiparticles encounter currents circling around the vortex core. Consequently, the transverse thermal conductivity κ_{xy} is given entirely by quasiparticles without any phonon background. The quasiparticle origin of this effect is easily confirmed simply by reversing the magnetic field, which causes a reversal of the transverse thermal current. Using this technique, Krishana *et al.* were able to estimate the in-plane quasiparticle component of the thermal conductivity, which turned out to be about

Fig. 10.10.

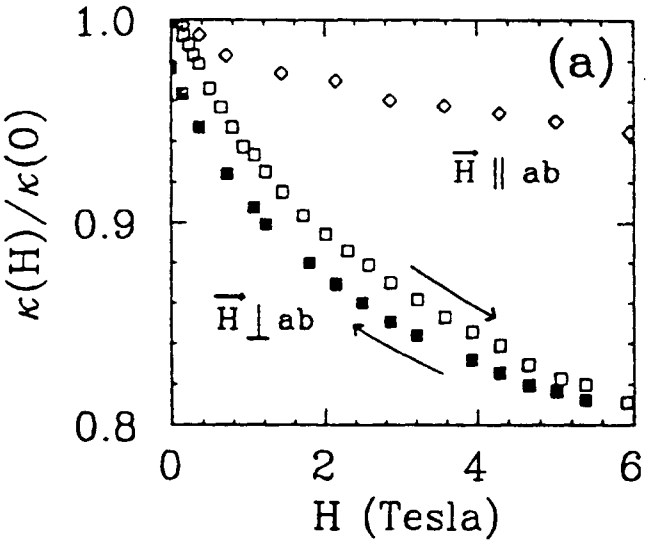

Field dependence of the thermal conductivity for an $YBa_2Cu_3O_7$ single crystal at 41 K. ◇, Magnetic field oriented parallel to the *a–b* plane. □, Magnetic field oriented perpendicular to the *a–b* plane and increasing in magnitude. ■ Field oriented perpendicular to the *a–b* plane and decreasing in magnitude. [After Peacor *et al.* (1991b).]

Fig. 10.11.

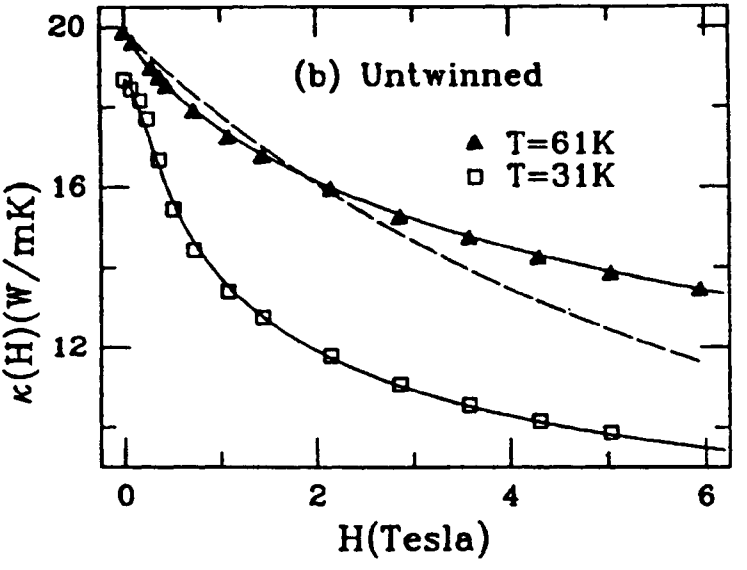

Field dependence of the thermal conductivity of an untwinned crystal of $YBa_2Cu_3O_{7-\delta}$. Solid lines are fits to Eq. 34. The dashed line is an unsuccessful fit assuming the functional dependence of Eq. 33. [After Richardson *et al.* (1991).]

Fig. 10.12.

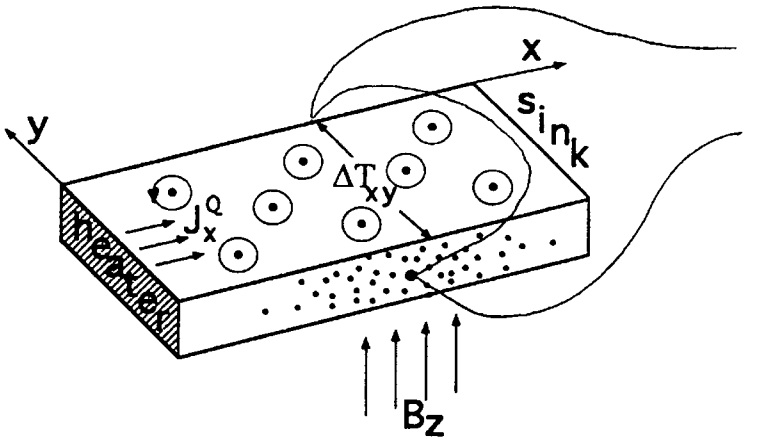

Experimental arrangement for the Righi–Leduc effect used to determine asymmetric scattering of quasiparticles in a crystal of $YBa_2Cu_3O_{7-\delta}$.

50% of the total thermal conductivity below T_c. The other 50% of heat current is then due to phonons.

References for Section C

A. F. Andreev, *Sov. Phys. JETP* **19**, 1228 (1964).

J. Bardeen, G. Rickayzen, and L. Tewordt, *Phys. Rev.* **113**, 982 (1959).

R. Berman, *Thermal Conduction in Solids*. Oxford University Press, 1976.

D. A. Bonn, P. Dosanjh, R. Liang, and W. N. Hardy, *Phys. Rev. Lett.* **68**, 2390 (1992).

H. Bougrine, S. Sergeenkov, and M. Ausloos, *Solid State Commun.* **86**, 513 (1993).

D. G. Cahill, *Rev. Sci. Instrum.* **61**, 802 (1990).

S.-C. Cao, D.-M. Zhang, D.-L. Zhang, H. M. Duan and A. M. Hermann, *Phys. Rev. B* **44**, 12571 (1991).

C. Caroli and M. Cyrot, *Phys. Kondens. Mater.* **4**, 285 (1965).

G. E. Childs, L. J. Ericks, and R. L. Powell, *NBS Monograph 131*. U.S. Government Printing Office, 1973.

J. M. Chwalek, C. Uher, J. F. Whitaker, G. A. Mourou, J. Agostinelli, and M. Lelental, *Appl. Phys. Lett.* **57**, 1696 (1990).

J. L. Cohn, S. D. Peacor, and C. Uher, *Phys. Rev. B* **38**, 2892 (1988).

M. F. Crommie and A. Zettl, *Phys. Rev. B* **43**, 408 (1991).

V. B. Efimov and L. P. Mezhov-Deglin, *Low Temp. Phys.* **23**, 204 (1997).

V. V. Florentiev, A. V. Inyushkin, A. N. Taldenkov, O. Melnikov, and A. Bykov, in *Progress in High Temperature Superconductivity* (R. Nikolsky, Ed.), Vol. 25, p. 462. World Scientific, Singapore, 1990.

B. T. Geilikman and V. Z. Kresin, *Sov. Phys. Doklady* **3**, 116 (1958).

U. Gottwick, R. Held, G. Sparn, F. Steglich, H. Rietschel, D. Ewert, B. Renker, W. Bauhoffr, S. von Molnar, M. Wilhelm, and H. E. Hoenig, *Europhys. Lett.* **4**, 1183 (1987).

S. J. Hagen, Z. Z. Wang and N. P. Ong, *Phys. Rev. B* **40**, 9389 (1989).

A. V. Inyushkin, A. N. Taldenkov, S. Yu. Shabanov, L. N. Demyanets, and T. G. Uvarova, *J. Supercond.* **7**, 331 (1994).

A. Jezowski and J. Klamut, in *Studies of High-Temperature Superconductors* (A. Narlikar, Ed.), Vol. 4, p. 263. Nova Science Publishers, New York, 1990.
L. P. Kadanoff and P. C. Martin, *Phys. Rev.* **124**, 670 (1961).
P. G. Klemens, in *Thermal Conductivity* (R. P. Tye, Ed.), Vol. 1. Academic Press, London, 1965.
K. Krishana, J. M. Harris, and N. P. Ong, *Phys. Rev. Lett.* **75**, 3529 (1995).
K. Maki, *Phys. Rev.* **158**, 397 (1967).
D. T. Morelli, G. L. Doll, J. Heremans, M. S. Dresselhaus, A. Cassanho, D. R. Gabbe and H. P. Jenssen, *Phys. Rev. B* **41**, 2520 (1990).
T. T. M. Palstra, B. Batlogg, L. F. Schneemeyer, and J. V. Waszczak, *Phys. Rev. Lett.* **64**, 3090 (1990).
S. D. Peacor and C. Uher, *Phys. Rev. B* **39**, 11559 (1989).
S. D. Peacor, R. A. Richardson, F. Nori, and C. Uher, *Phys. Rev. B* **44**, 9508 (1991a).
S. D. Peacor, J. L. Cohn, and C. Uher, *Phys. Rev. B* **43**, 8721 (1991b).
R. A. Richardson, S. D. Peacor, F. Nori, and C. Uher, *Phys. Rev. Lett.* **67**, 3856 (1991).
M. Sera, S. Shamoto and M. Sato, *Solid State Commun.* **74**, 951 (1990).
S. Sergeenkov and M. Ausloos, *Phys. Rev. B* **52**, 3614 (1995).
G. Sparn, M. Baenitz, S. Horn, F. Steglich, W. Assmus, T. Wolf, A. Kapitulnik, and Z. X. Zhao, *Physica C* **162–164**, 508 (1989).
L. Tewordt, *Phys. Rev.* **128**, 12 (1962).
L. Tewordt and Th. Wolkhausen, *Solid State Commun.* **70**, 839 (1989).
C. Uher, *J. Superconductivity* **3**, 337 (1990).
C. Uher, in *Physical Properties of High Temperature Superconductors*, (D. M. Ginsberg, Ed.), Vol. 3, p. 159. World Scientific, Singapore, 1992.
C. Uher, *Naval Research Reviews* **48**, 44 (1996).
C. Uher and J. L. Cohn, *J. Phys. C* **21**, L957 (1988).
C. Uher, Y. Liu, and J. F. Whitaker, *J. Supercond.* **7**, 323 (1994).
H. J. Waite, *NBS Report* No. 3527, p. 158 (1955).
R. C. Yu, M. B. Salamon, J. P. Lu, and W. C. Lee, *Phys. Rev. Lett.* **69**, 1431 (1992).
N. V. Zavaritsky, A. V. Samoilov, and A. A. Yurgens, *Physica C* **180**, 417 (1991).
D.-M. Zhu, A. C. Anderson, E. D. Bukowski, and D. M. Ginsberg, *Phys. Rev. B* **40**, 841 (1989).

D

Thermoelectric and Thermomagnetic Effects

Ctirad Uher and Alan B. Kaiser

a. Introduction

Thermoelectric and thermomagnetic phenomena are sensitive probes of the nature of electronic states and interaction processes within a conductor. As such they are useful tools to study the band structure and carrier dynamics of conducting solids. In superconductors, apart from providing valuable insight into the carrier transport above the superconducting transition temperature T_c, the thermoelectric and thermomagnetic effects are important in assessing the dynamics of vortices and quasiparticles. In this section we illustrate the spectrum of experiments and the physical parameters obtained from measurements of the

thermoelectric and thermomagnetic effects in superconductors. The terminology and designation of the effects is analogous to the thermoelectric and thermomagnetic effects in the normal metals and semiconductors; see Table 10.3. The reader may find useful and more in-depth treatment of the thermoelectric and thermomagnetic effects in superconductors in a monograph by Huebener (1979), and in the review articles by Kaiser and Uher (1991) and Freimuth (1992).

When discussing thermomagnetic effects at temperatures below T_c, one should keep in mind that the physics refers to the mixed state of a superconductor characterized by the presence of the flux lines or vortices. It is the dissipative motion of these vortices that gives rise to the transverse thermomagnetic effects. The vortex itself, to a first approximation, is viewed as a rigid tube of normal phase of radius ξ (coherence length) threading the superconducting phase. The core of the vortex is screened from the superconducting surrounding by the encircling screening supercurrent J_{sc} of magnitude

$$J_{sc} = (\phi_0/2\pi\mu_0\lambda^3)K_1(r/\lambda), \tag{35}$$

where $K_1(r/\lambda)$ is the first-order modified Bessel function, ϕ_0 is the flux quantum, λ stands for the penetration depth, and r is the distance from the center of the vortex. The functional form of J_{sc} together with its asymptotic behaviors for $r \ll \lambda$ and $r \gg \lambda$ are shown in Fig. 10.13. Although this description is quite adequate for the conventional superconductors, the vortices in the high-temperature superconductors (HTS) are much less rigid and may attain a partly two-

Table 10.3.

Galvanomagnetic and thermomagnetic effects.

Effect	Symbol	Electric field (E)	Electric current (I)	Temp. gradient (∇T)	Heat current (q)	Magnetic field (B)
Resistivity	ρ	Meas. x	Appl. x	0	—	0
Magnetores. longitudinal	$\rho(B_\parallel)$	Meas. x	Appl. x	0	—	Appl. x
Magnetores. transverse	$\rho(B_\perp)$	Meas. x	Appl. x	0	—	Appl. z
Thermal conductivity	κ	—	0	Meas. x	Appl. x	0
Hall effect	R_H	Meas. y	Appl. x	0	—	Appl. z
Seebeck	S	Meas. x	0	Appl. x	—	0
Magneto-Seebeck	$S(B)$	Meas. x	0	Appl. x	—	Appl. x, y, z
Peltier	Π	—	Appl. x	0	Meas. x	—
Ettingshausen	ε	—	Appl. x	Meas. y	—	Appl. z
Righi-Leduc	R_L	—	—	Meas. y	Appl. x	Appl. z
Nernst	Q	Meas. y	0	Appl. x	—	Appl. z

Fig. 10.13.

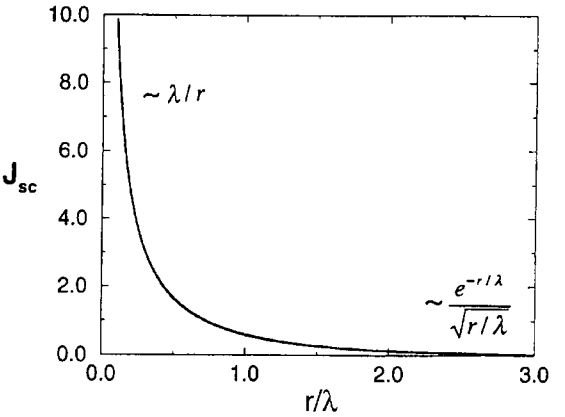

Radial dependence of the screening current J_{sc}. Asymptotic behavior for $r \ll \lambda$ and for $r \gg \lambda$ is indicated. The actual numerical value of J_{sc} is obtained by multiplying the vertical axis by $\phi_0/(2\pi\mu_0\lambda^3) = 2.62 \times 10^{-10}/\lambda^3$ A m, where λ is the penetration depth.

dimensional character, especially in the more anisotropic cuprates. Nonetheless, in describing the thermomagnetic effects, we adhere to the picture of vortices as rigid tubes. We first introduce the Lorentz force and the thermal force as the two driving forces responsible for the motion of vortices.

b. Lorentz and Thermal Forces

A flow of transport current density $\mathbf{J}$ exerts a Lorentz force $\mathbf{F}_L$ on a unit length of the vortex line given by

$$\mathbf{F}_L = \mathbf{J} \times \boldsymbol{\phi}_0, \tag{36}$$

where $\boldsymbol{\phi}_0$ is the flux quantum. In the configuration of Fig. 10.14 with the transport current density j_x along the x-axis and the vortex parallel to the z-axis, the Lorentz force points down along the negative y-axis. Assuming no pinning, vortices move in response to the Lorentz force but their motion is damped by the *viscous drag force* $\mathrm{f}_\eta = -\eta v_{L,y}$, where η is the viscous drag coefficient and $v_{L,y}$ is the steady-state vortex velocity. The motion of the free vortices, called *flux flow* or *viscous flow* of vortices, is thus governed by the equation

$$\mathbf{F}_L + \mathbf{f}_\eta = 0. \tag{37}$$

Fig. 10.14.

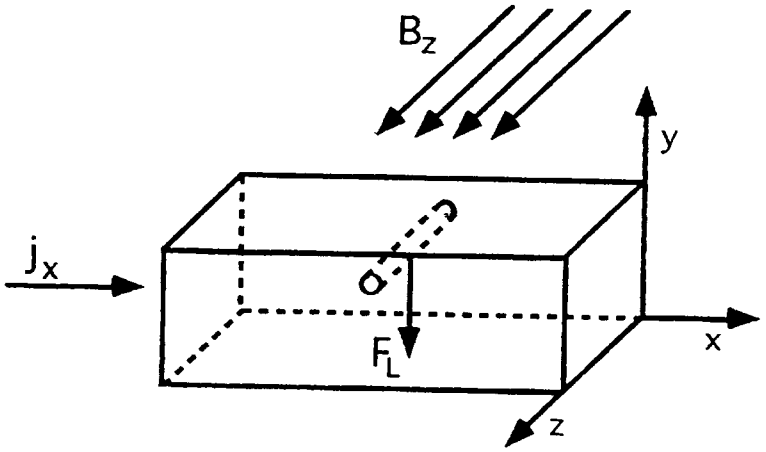

The Lorentz force $\mathbf{F}_L$ acting on a vortex oriented parallel to the z-axis arising from the presence of the transport current density along the x-axis.

According to Josephson, vortices moving with a velocity v_L generate the macroscopic electric field

$$\mathbf{E} = \mathbf{B} \times \mathbf{v}_L, \tag{38}$$

where B is the magnetic induction, $B = n\phi_0$ with n the density of vortices. Combining Eqs. (36)–(38), the electric field in the x-direction becomes

$$E_x = (\phi_0 B_z/\eta) j_x. \tag{39}$$

Equation (39) leads to the electrical resistivity called *flux flow resistivity* ρ_f, given by

$$\rho_f = E_x/j_x = \phi_0 B_z/\eta. \tag{40}$$

At the magnetic field equal to the upper critical field, B_{c2}, the material becomes normal,

$$\rho_n = \phi_0 B_{c2}/\eta. \tag{41}$$

Eliminating η between Eqs. (40) and (41) yields

$$\rho_f = \rho_n B_z/B_{c2} \propto \rho_n \xi^2/a_0^2. \tag{42}$$

The approximation on the RHS of Eq. (42) follows from a well-known relation $\xi = (\phi_0/2\pi B_{c2})^{1/2}$, and the expression for the vortex lattice parameter $a_0 = (\phi_0/B)^{1/2}$. Equation (42) basically states that the flux flow resistivity is proportional to the fraction of the normal volume occupied by the vortex cores in a unit cell of the vortex lattice.

If, instead of the external electric current, the vortex is subjected to a thermal gradient, then there is a *thermal force*, F_{th}, acting on the vortex. In reference to Fig. 10.15, the thermal force acts along the x-axis and is given by

$$\mathbf{F}_{\text{th}} = -\mathbf{S}_{\phi}\nabla_x\mathbf{T} \tag{43}$$

where $\mathbf{S}_{\phi}$ is the transport entropy per unit length of vortex. The origin of the thermal force is in the temperature dependence of the penetration length, which is larger at the hot end of the sample than at the cold end. This causes stronger repulsion of vortices near the hot end, which gives rise to their motion down the thermal gradient. The two forces, the Lorentz force and the thermal force, are at the heart of the thermomagnetic phenomena in the mixed-state of superconductors. We start with the so-called longitudinal effects, the Seebeck effect and the Peltier effect.

c. Seebeck Effect

A metal with no electric current flowing, and subjected to a longitudinal temperature gradient $\nabla_x\mathbf{T}$ in the x-direction, can develop a longitudinal electric field proportional to the temperature gradient

$$E_x = S\nabla_x T \tag{44}$$

a phenomenon called the Seebeck effect. The proportionality constant S is called the Seebeck coefficient or, equivalently, the thermopower. This coefficient should not be confused with the transport entropy S_{ϕ} of Eq. (43). Assuming the sample

Fig. 10.15.

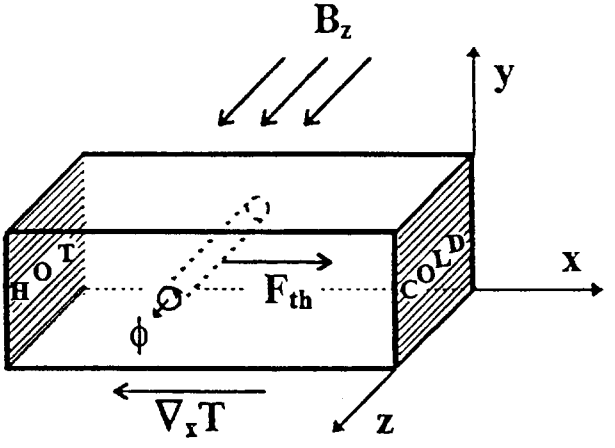

The thermal force $\mathbf{F}_{\text{th}}$ on a vortex oriented parallel to the z-axis arising from the presence of a temperature gradient $\nabla_x\mathbf{T}$.

geometry of a homogeneous bar with a temperature difference ΔT between its ends, the corresponding Seebeck voltage across the length of the sample is

$$\Delta V = S\,\Delta T. \tag{45}$$

The sign of the thermopower corresponds to the sign of the dominant charge carrier, positive for holes and negative for electrons.

1. Normal State

In metals, semiconductors, and in superconductors above T_c, the Seebeck effect arises as a consequence of the asymmetry in the diffusion of the electrons and holes along the temperature gradient. In metals, within the free-electron approximation, the thermopower becomes

$$S = (\pi^2/2)(k_B/e)(T/T_F) = 142(T/T_F) \qquad (\mu V/K). \tag{46}$$

Note a T-linear dependence and a very small magnitude of S due to a typical Fermi temperature $T_F \geq 10^4$ K. In semiconductors, a corresponding expression for the diffusion thermopower is

$$S = (k_B/e)(\varepsilon_c/k_B T) = 86(\varepsilon_c/k_B T) \qquad (\mu V/K). \tag{47}$$

Since the conduction band energy $\varepsilon_c \gg k_B T$, S is large and varies as T^{-1}. Exact quantitative evaluation of the thermopower is often difficult because other contributions such as the phonon-drag effect, more than one type of scatterer, and strong dependence on the particular electronic structure complicate the physical picture. In disordered solids where elastic disorder scattering dominates, the thermopower is approximately linear except for a characteristic change of slope near 50 K due to mass enhancement by a factor $(1 + \lambda)$, where λ stands for the dimensionless electron–phonon coupling constant.

Conventional superconductors are metals; hence, their thermopower at $T > T_c$ reflects the characteristic metallic features discussed earlier. Furthermore, because the electron–phonon interaction is the driving mechanism of superconductivity, large enhancement in the thermopower at low temperatures is expected. An example of such an enhancement in a Chevrel-phase superconductor is shown in Fig. 10.16.

In addition to their large structural anisotropy, high-temperature cuprates possess lower carrier density than typical metals and are very sensitive to doping and structural defects. Hence, one would expect the normal-state thermopower to be somewhat larger than the typical metallic value and perhaps more complex. In reality, the thermopower in HTS presents a surprisingly clear pattern, and this allows one to generalize the behavior across the spectrum of cuprates rather than to deal with idiosyncrasies of each perovskite family separately. The reader wishing to survey existing thermopower studies is referred to review articles dealing with the subject, such as that by Kaiser and Uher (1991).

Fig. 10.16.

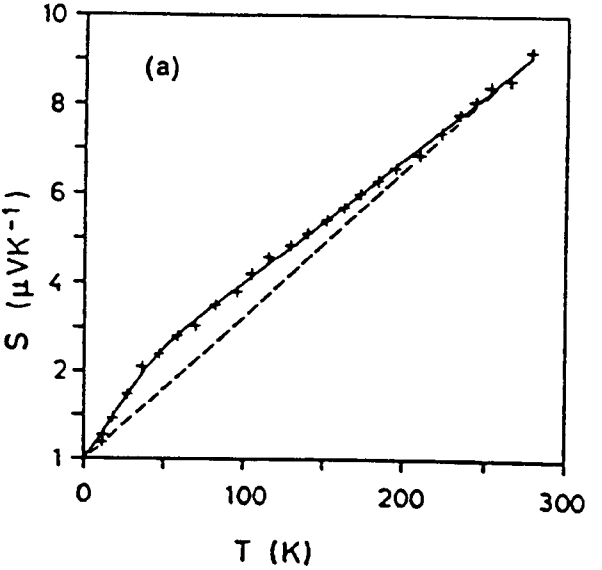

Thermopower (crosses) of the Chevrel-phase superconductor $Cu_{1.8}Mo_6S_5Te_3$. The solid line is a fit to the theoretical expression for the electron–phonon mass enhancement. [After Kaiser (1987).]

Perhaps the most striking feature of the thermopower in HTS is its strong dependence on doping, that is, on the hole concentration in CuO_2 planes, and its close tie with the doping trend in the transition temperature T_c. The superconducting domain of HTS cuprates is delineated by the minimum, p_{min}, and maximum, p_{max}, hole concentrations per planar Cu atom. Outside of these limits there is no superconductivity. The *overdoped* samples ($p \to p_{max}$) have reduced T_c, a metallic character, and a substantially linear and negative thermopower. As the hole density decreases (by means of nonisovalent substitutions or by lowering the amount of oxygen), one achieves a certain *optimal* level of doping, which yields the highest T_c and for which the thermopower is small, with a room-temperature value of practically zero. With a further decrease in the hole density ($p \to p_{min}$), in the so-called *underdoped* domain, the T_c decreases rapidly and the thermopower attains larger positive values, but with a temperature dependence that is essentially unchanged. Thus, as the material is brought from the overdoped to the underdoped regime, the thermopower undergoes a steady shift upward and toward more positive values. The slope of the thermopower, -3×10^{-8} V/K^2, is approximately the same for all cuprates, except the yttrium compound YBCO,[1]

[1]In the text and in Tables 10.4 and 10.5 we use the following usual designations for the various families of high-temperature superconductors: YBCO stands for $YBa_2Cu_3O_{7-\delta}$, BSCCO represents $Bi_2Sr_2Ca_{n-1}Cu_nO_{2n+4}$, TBCCO designates $Tl_mBa_2Ca_{n-1}Cu_nO_{2(n+1)+m}$, LSCO represents $La_{2-x}Sr_xCuO_4$, and NCCO stands for $Nd_{2-x}Ce_xCuO_4$.

which is only weakly dependent on the doping, and insensitive to the spacer layers. Furthermore, high structural anisotropy and, specifically, orders of magnitude higher in-plane electrical conductivity over the c-axis conductivity ensure that meaningful measurements that reveal the behavior of the in-plane thermopower can be made on sintered samples where stoichiometry is easier to control than in single crystals. A canonical example of the trend in the thermopower is shown in Fig. 10.17. In fact, the common thermopower pattern led Obertelli *et al.* (1992) to consider a correlation between the room temperature thermopower, S (290 K), and the T_c for a wide range of cuprates; see Fig. 10.18. The vanishing of the room-temperature thermopower that coincides with the maximum in T_c is actually being used as a measure of optimal sample doping.

We have already pointed out that YBCO departs from the general trend followed by all other HTS cuprates. The reason is the presence of CuO chains running along the *b*-axis of the structure that provide, in addition to the CuO_2 planes, a substantial contribution to the overall charge carrier transport and are responsible for the in-plane transport anisotropy. Thus, while there is considerable discord between the few existing measurements (see Fig. 10.19), the thermopower data nevertheless clearly reflect the inequality of the *a* and *b* crystallographic directions in this orthorhombic material. The *a*-axis thermopower resembles that of the other cuprates but with a considerably weaker temperature dependence. The *b*-axis thermopower, that is, where the chains make their strongest presence, shows a weak and positive slope. By reducing the oxygen level and thus introducting vacancy disorder in the chains, both thermopower components shift to positive values and both display weak negative slopes.

Fig. 10.17.

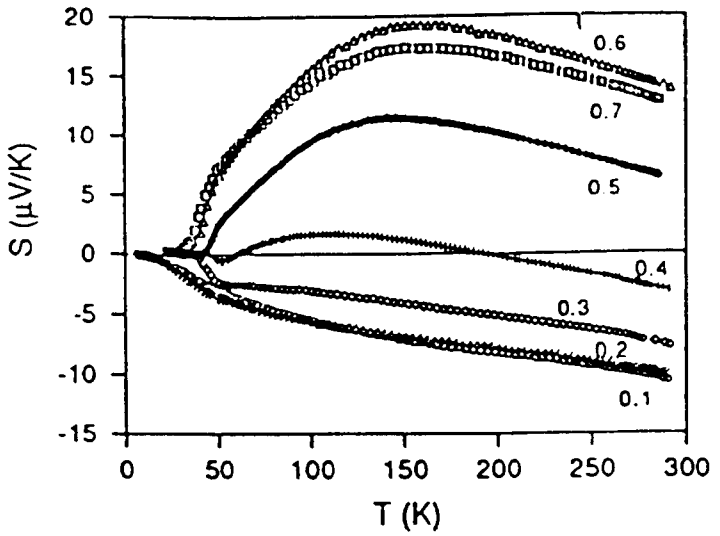

Thermopower temperature dependence of $Tl_{0.5}Pb_{0.5}Sr_{2-x}La_xCuO_5$ as a function of the indicated lanthanum doping $0.1 < x < 0.7$. [Subramaniam *et al.* (1994).]

Fig. 10.18.

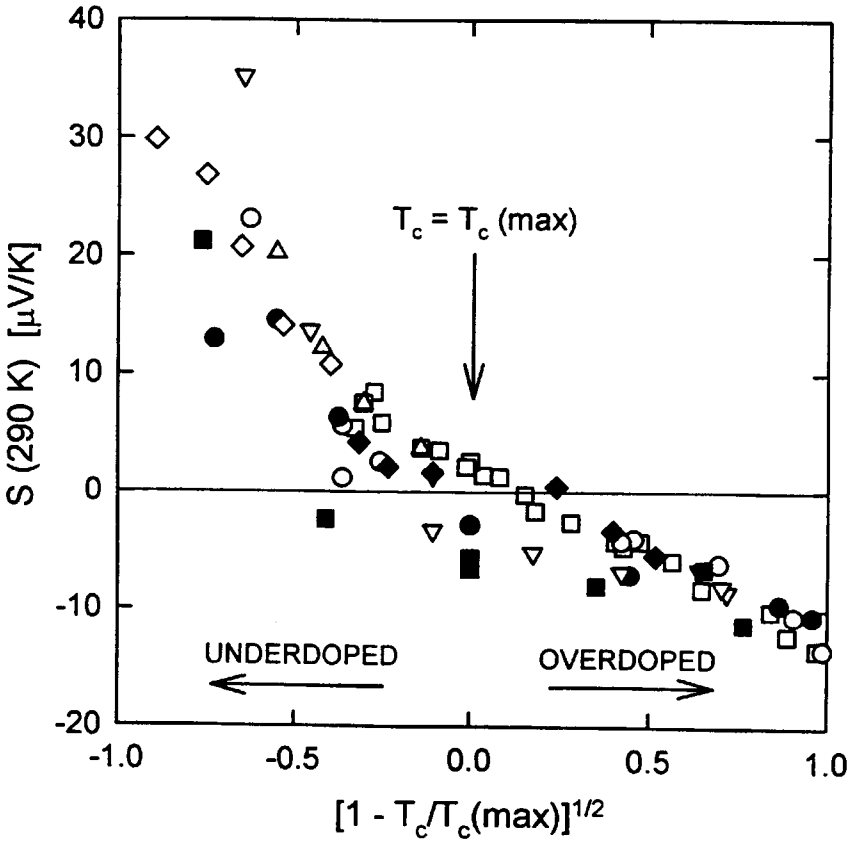

Room temperature thermopower for a variety of cuprate superconductors displaying the $[1 - T_c/T_c(\text{max})]^{1/2}$ correlation. See original article for symbol identification. [Obertelli *et al.* (1992).]

For completeness, Fig. 10.20 shows thermopower data on YBCO measured perpendicular to the CuO_2 planes, that is, along the *c*-axis. This configuration is experimentally quite challenging and the existing measurements are sparse. Nevertheless, the data clearly indicate a relatively large and positive thermopower.

2. Superconducting State

We stated in the previous section that the diffusion of charge carriers down the thermal gradient gives rise to an electric field that opposes the flow of the carriers. In the superconducting phase there is no need for such an electric field because

Fig. 10.19.

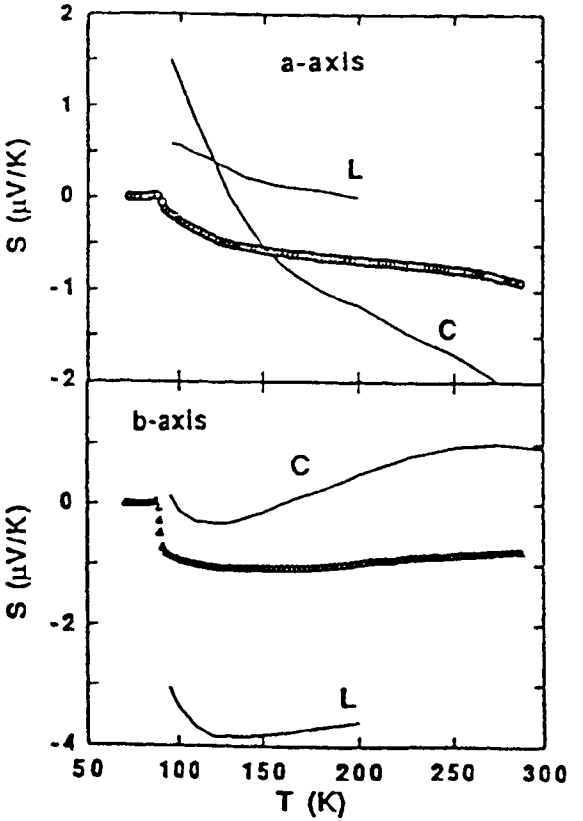

Thermopower of untwinned $YBa_2Cu_3O_{7-\delta}$ crystals in the a and b directions. Symbols are the data of Subramaniam *et al.* (1995); the line labeled L stands for the data of Lowe *et al.* (1991), and the line labeled C represents the data of Cohn *et al.* (1992). [Subramaniam *et al.* (1995).]

any normal current density j_n can be balanced by the counterflow of supercurrent j_s. Thus, thermopower of a superconductor is zero. All experimental data, including those in Figs. 10.17 to 10.19, are fully consistent with this hypothesis. The fact that the thermopower of a superconductor is zero (in zero magnetic field) can be used for determination of the absolute thermopower of individual materials such as wires intended for construction of thermocouples, (Uher, 1987).

Although thermopower is zero in the superconducting state, the circulating current pattern comprising the flow of the normal component j_n and the counterflow of the supercurrent j_s results in a quasiparticle imbalance near the ends of the sample and may give rise to very weak thermoelectric effects. For details we refer the reader to the original literature, for example, Ginzburg (1991).

Fig. 10.20.

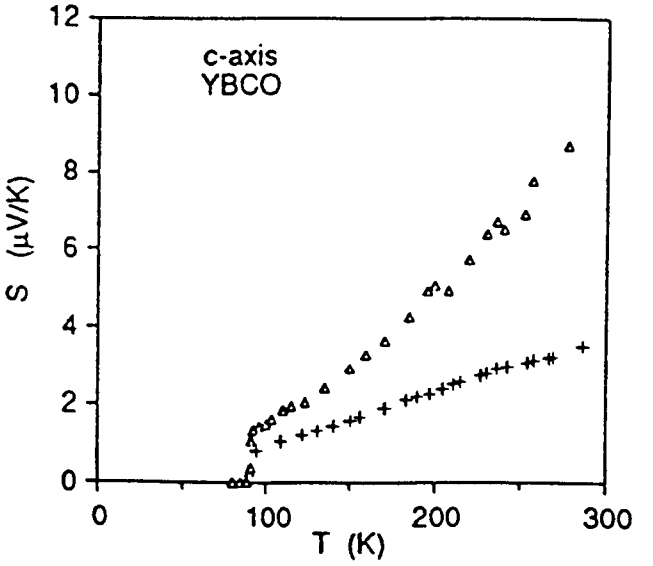

Thermopower of $YBa_2Cu_3O_{7-\delta}$ measured perpendicular to the CuO_2 planes. Crosses represent the data of Sera *et al.* (1988); triangles stand for the measurements of Wang and Ong (1988).

3. Mixed State

From the form of Eq. (47) the Seebeck effect is frequently interpreted as the entropy transport per unit electric charge. In the mixed state of a superconductor there are two distinct entities that can transport entropy across the sample: vortices that transport magnetic flux, and unbound quasiparticles outside of the vortex cores that transport electric charge. As we shall show, vortex transport is essential for the occurrence of the transverse thermomagnetic effects (Nernst and Ettingshausen), whereas quasiparticle transport gives rise to the longitudinal thermomagnetic effects (Seebeck and Peltier).

Consider a thermal force F_{th} acting on a vortex in the geometry of Fig. 10.15. If pinning is absent, the vortex moves down the thermal gradient and it is obvious that unless there is some mechanism that deflects the vortex sideways (e.g., a twin plane oriented away from the x-axis that "guides" the vortex, or by invoking a very large Hall angle) the vortex motion cannot produce a longitudinal (Seebeck) field. This follows immediately from the relation in Eq. (38). Thus, a vortex moving subject to the thermal force of Fig. 10.15 generates an electric field transverse to the thermal gradient (the Nernst field) but contributes nothing to the longitudinal field. The Seebeck effect thus cannot arise as a consequence of thermally driven flux of vortices and, indeed, has never been observed in the

conventional superconductors. In HTS cuprates, thanks to a fortuitous confluence of a large region of reversibility and a power-law rather than exponential dependence of the quasiparticle density that ensures the presence of quasiparticles at temperatures well below T_c, the Seebeck effect is robust, can easily be measured, and rivals the transverse thermomagnetic effects. The Seebeck effect in this case stems from the quasiparticle transport or, more precisely, from quasiparticles interacting with vortices.

A physical interpretation was first proposed by Huebener *et al.* (1990) and subsequently refined by a number of authors (e.g., Ri *et al.*, 1993; Meilikhov and Farzetdinova, 1994). The essential physics is an extension of the two-fluid counterflow model of Ginzburg to a regime where $B \neq 0$. Taking into account Hall angles of both vortices (θ_v) and quasiparticles (θ_{qp}), the Seebeck effect for the mixed state of a superconductor is

$$S = S_n(\rho_f/\rho_n)[1 + \tan\theta_v \tan\theta_{qp}] + (S_\phi \rho_f/\phi_0)\tan\theta_v, \tag{48}$$

where S_n and ρ_n are the normal-state Seebeck coefficient and resistivity, and ρ_f is the flux flow resistivity. Later, we shall recognize the second term of Eq. (48) as related to the Nernst coefficient multiplied by the tangent of the Hall angle.

If the sample contains any extended structural defects that could serve as "guide rails" and guide the motion of vortices under angle φ away from the direction of $-\nabla_x T$, Ghamlouch and Aubin (1996) have shown that Eq. (48) becomes

$$S = S_n(\rho_f/\rho_n)\{[1 + \tan\theta_v \tan\theta_{qp}\cos\varphi] + (S_\phi \rho_f/\phi_0)[\tan\theta_v + \tan\varphi]\}\cos\varphi. \tag{49}$$

Since both Hall angles are typically very small, the dominant term in Eqs. (48) and (49) is the first term and to a good approximation

$$S = S_n(\rho_f/\rho_n). \tag{50}$$

The Seebeck coefficient (thermopower) in the mixed state is thus closely related to the flux-flow resistivity, Eq. (42). Just as the flux-flow resistivity reflects the anisotropy of the structure (broader transition range for more anisotropic materials), so does the Seebeck coefficient: More two-dimensional cuprates have a more extended temperature range where the Seebeck effect is finite (compare Figs. 10.21a and 10.21b).

d. Peltier Effect

The Peltier effect arises as a consequence of the heat current density being carried by the electric current density along an applied electric field in zero temperature gradient. Assume that a battery is applied to the terminals A and B to drive a current clockwise around the circuit consisting of a thermocouple (elements a and b initially at the same temperature) as shown in Fig. 10.22. The presence of the

Fig. 10.21.

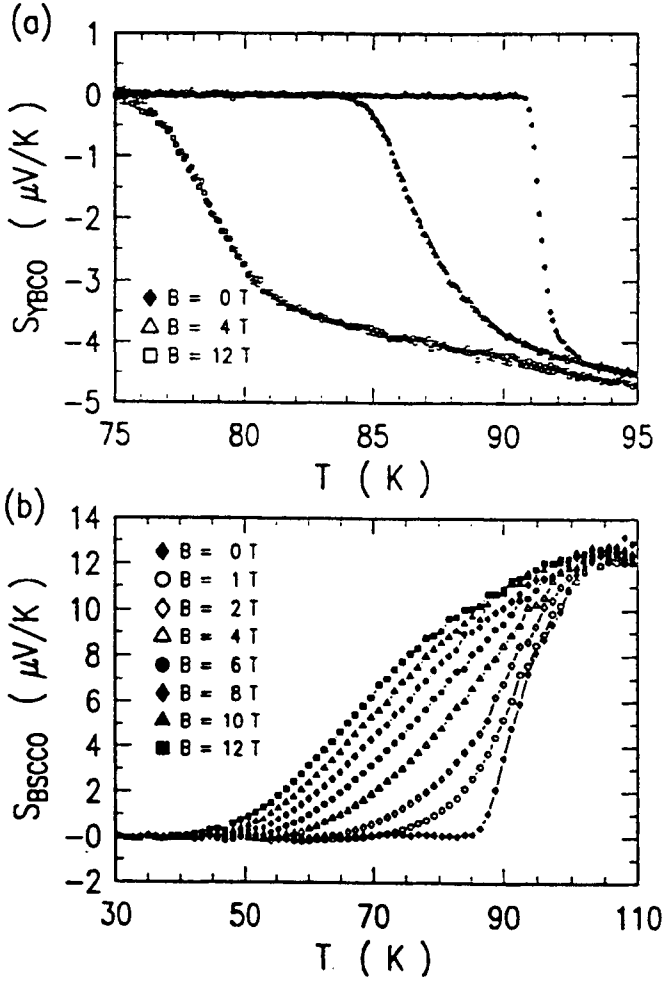

Seebeck coefficient in the mixed state of a supeconductor. (a) Data for $YBa_2Cu_3O_{7-\delta}$; (b) for $Bi_2Sr_2CaCu_2O_8$. Note a much broader transition range for the more anisotropic sample of BSCCO. [Ri *et al.* (1994).]

current density J gives rise to a rate of heating $+q$ at one junction, say at the junction H, and the rate of cooling $-q$ at the other junction C. Reversing the current flow leads to a reversal of the effect: the junection H cools while the junction C warms up. The *differential Peltier coefficient* Π_{ab} is defined as the heat generated per second per unit current flow through the junction between metals a and b,

$$\Pi_{ab} = q/J. \tag{51}$$

Fig. 10.22.

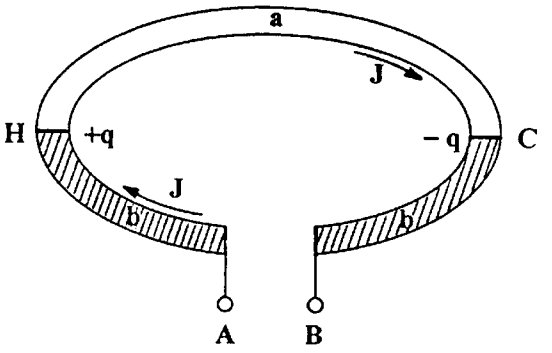

Origin of the Peltier effect in a circuit consisting of two dissimilar semiconductors.

By convention, Π_{ab} is taken as positive if the clockwise current in Fig. 10.22 makes the junction H warm and the junction C cold. Although the Peltier effect can be observed only when one joins together dissimilar conductors (the same is true for the Seebeck effect where the measuring probes play the role of the second conductor), the effect is a bulk one and one can write the differential Peltier coefficient as

$$\Pi_{ab} = \Pi_a - \Pi_b, \tag{52}$$

where Π_a and Π_b are the *absolute Peltier coefficients* of the two individual materials comprising the thermocouple. From now on we drop the subscripts and will consider the Peltier coefficient of a single conductor.

Although the Peltier effect is the essence of thermoelectric refrigeration (e.g., Goldsmid, 1986), the effect itself is rarely measured directly even in the thermoelectric materials. Rather, one makes use of the Kelvin relation

$$\Pi = TS, \tag{53}$$

which allows determination of the Peltier coefficient knowing the behavior of the Seebeck coefficient S and the absolute temperature T. Equation (53) in conjunction with any one of Eqs. (48)–(50) allows the Peltier coefficient to be assessed in the mixed state of a superconductor. For example, the dominant contribution to the Seebeck coefficient, Eq. (50), immediately yields the Peltier coefficient.

$$\Pi = \Pi_n(\rho_f/\rho_n), \tag{54}$$

where Π_n is the normal-state Peltier coefficient, ρ_n is the normal-state resistivity, and ρ_f is the flux flow resistivity. Thus, one expects a similar kind of broadening transition for $T < T_c$ as observed for the Seebeck effect and the flux flow resistivity.

Fig. 10.23.

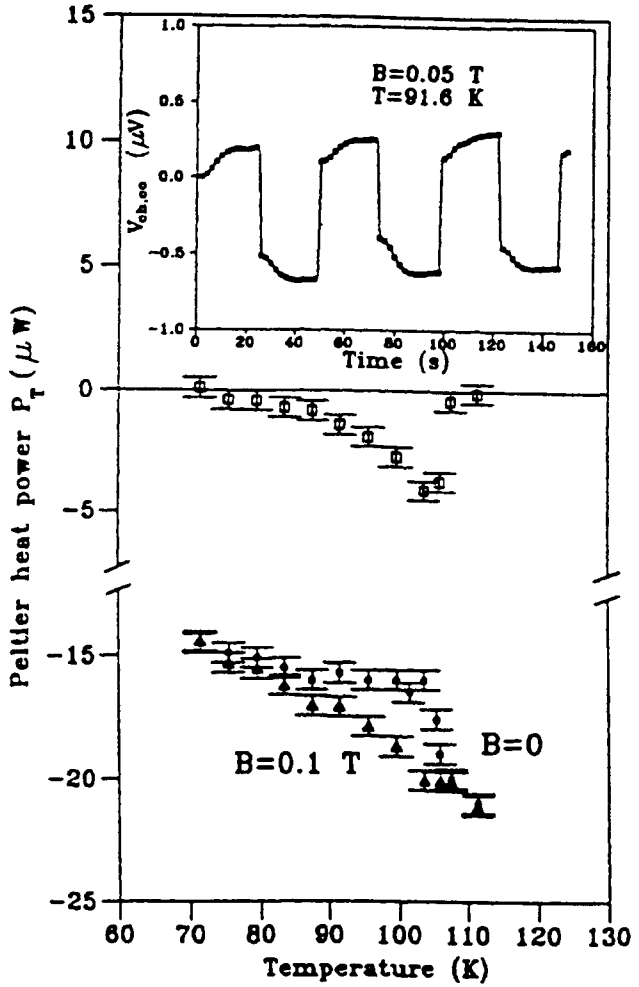

Peltier heat power measured in zero field (solid circles) and in the field of 0.1 T (solid triangles). The small difference between the two is shown by open squares. The inset shows the chromel–constantan thermocouple voltage during one measurement. [Logvenov *et al.* (1992).]

So far, only one direct measurement of the Peltier coefficient in the mixed state of HTS has been reported (Logvenov *et al.*, 1992), and the results confirm the expected behavior (Fig. 10.23). This paper also provides an alternative physical picture of the Peltier effect in the mixed state that does not rely on the use of the Kelvin relation.

e. Ettingshausen Effect

The Ettingshausen effect is the transverse equivalent of the Peltier effect except that the coefficient itself is defined in terms of the transverse temperature gradient rather than the transverse heat flow. With the electric current in the x-direction and the magnetic field along the z-axis, the Ettingshausen coefficient is defined as

$$\varepsilon = \nabla_y T/(j_x B_z), \quad \text{with } j_y = q_y = \nabla_x T = 0. \tag{55}$$

Just as the Peltier effect is the basis of the thermoelectric refrigerator, the Ettingshausen effect serves as the means for thermomagnetic cooling (Goldsmid, 1986).

It is easy to apply the Ettingshausen effect to the mixed state of a superconductor. The essential point is that the core of a vortex is normal, that is, it has higher entropy than the surrounding superconducting phase. Thus, a vortex in motion represents the transport of entropy. Referring to Fig. 10.14 where the transport current j_x exerts the Lorentz force on the vortex given by Eq. (36), the vortex will move in the negative y-direction. The flow of vortices is sustained by their generation at the upper edge of the specimen and their annihilation at the opposite edge. Since vortices carry entropy, there is absorption of heat at the upper edge and liberation of heat at the other edge. Consequently, a thermal gradient $\nabla_y T$ is set up. Moving vortices represent heat current density q_y that is balanced by ordinary heat conduction once the steady state is established.

$$q_q \equiv nTS_\phi v_{L,y} = -\kappa_y \Delta_y T. \tag{56}$$

Here n is the density of vortices, S_ϕ is the transport entropy per unit length of vortex, and κ_y is the thermal conductivity in the direction of the vortex motion. According to Eq. (38), this same vortex flow generates the longitudinal (x-axis) electric field $E_x = -v_{L,y} B_z$, which, upon substitution into Eq. (56) and writing $B_z = n\phi_0$, yields

$$\nabla_y T = (TS_\phi \kappa_y/\phi_0) E_x. \tag{57}$$

Proportionality of $\nabla_y T$ and E_x is a manifestation of the Ettingshausen effect. Substituting for E_x from Eq. (39), one obtains the Ettingshausen coefficient

$$\varepsilon \equiv \nabla_y T/(j_x B_z) = TS_\phi \kappa_y/\eta. \tag{58}$$

Thermodynamics requires the transport entropy S_ϕ to vanish at $T = 0$. This is no problem since at and near absolute zero, no quasiparticle excitations exist within the vortex core because of a gap in the excitation spectrum. The transport entropy also vanishes at T_c because vortices have filled the entire sample volume and the sample has become normal. Thus, one expects a maximum for the transport entropy (and for the measured transverse thermal gradient $\nabla_y T$) somewhere between the absolute zero and T_c.

Fig. 10.24.

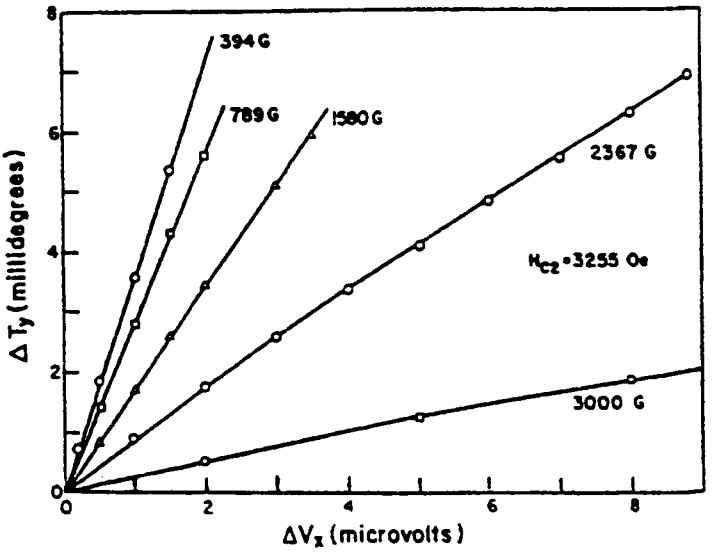

Ettingshausen temperature difference vs. longitudinal potential difference for a type-II alloy In + 40 at.% Pb in magnetic fields ranging from 39.4 to 300 mT. [Solomon and Otter (1967).]

Fig. 10.25.

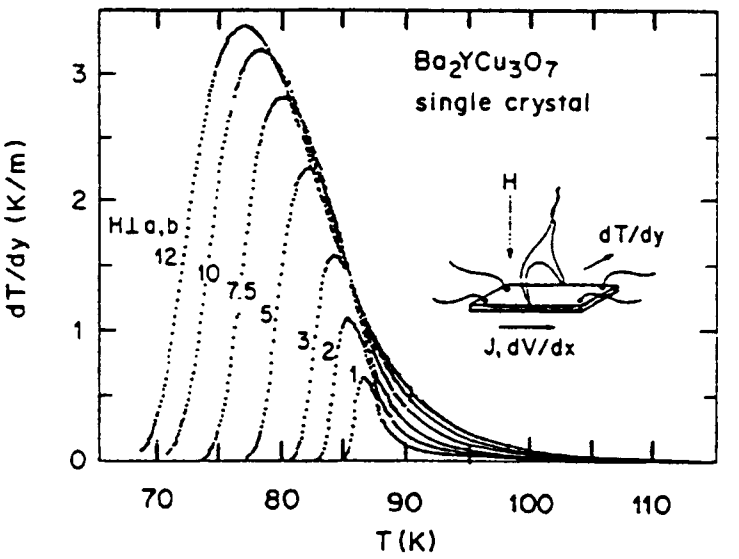

The transverse (Ettingshausen) temperature gradient induced in a single crystal of $YBa_2Cu_3O_7$ by the electric current in the presence of a magnetic field. The inset shows the probe arrangement. [Palstra *et al.* (1990).]

Very few measurements of the Ettingshausen effect exist in either the conventional superconductors or HTS cuprates. Figure 10.24 shows the data on $In_{0.6}Pb_{0.4}$ alloy (Solomon and Otter, 1967), while the behavior of the transverse thermal gradient $\nabla_y T$ in YBCO is shown in Fig. 10.25 (Palstra *et al.*, 1990). Note persistence of the transverse thermal gradient at temperatures some 15 K above T_c, which, according to the authors, may be due to a pronounced fluctuation effect.

f. Righi–Leduc Effect

The Righi–Leduc effect is the thermal analogue of the Hall effect. A heat current q_x arising because of the applied thermal gradient $-\nabla_x T$ in the presence of magnetic field in the z-direction gives rise to a transverse temperature gradient $\nabla_y T$ given by

$$\nabla_y T = R_L B_z q_x, \tag{59}$$

where R_L is the Righi-Leduc coefficient. Provided the carriers scatter elastically, that is, within the regime of validity of the Wiedemann–Franz law, the Righi–Leduc coefficient relates directly to the Hall coefficient R_H as

$$R_H = L_0 T R_L, \tag{60}$$

where L_0 is the free-electron Lorenz number $L_0 = 2.44 \times 10^{-8}\ V^2\ K^{-2}$. In analogy to the Hall effect, one defines the Righi–Leduc angle θ as

$$\tan\theta = \nabla_y T / \nabla_x T. \tag{61}$$

In a normal metal the transverse thermal gradient $\nabla_y T$ results from the asymmetric scattering of the hot and cold carriers and the sign of the Righi–Leduc effect, that is, whether the upper edge of the sample (along the y-axis) is hotter or colder than the lower edge, is determined by the sign of the carriers.

The formalism of the Righi–Leduc effect can be applied to the mixed state of a superconductor. However, although it is necessary for the vortices to move in order to observe the Hall effect, the Righi–Leduc effect does not require any motion of vortices. In fact, essentially all studies ever made of the Righi–Leduc effect were performed with a stationary vortex lattice. The reason is simple: Unlike an electric field, a temperature gradient can be sustained in a superconductor with a static vortex structure. Figure 10.26 shows the transverse thermal gradient $\nabla_y T$ as a function of magnetic field obtained on pure niobium (Stephan and Maxfield, 1973). The behavior in the mixed state is rather dramatic but not well understood, and the signal may even change sign as in some alloys of conventional superconductors (Sichel and Serin, 1976).

Only two reports mention attempts to measure the Righi–Leduc effect in HTS cuprates, both noting that the effect is very small (Galffy *et al.*, 1990; Zavaritsky *et al.*, 1991). A successful use of the Righi–Leduc sample geometry to

Fig. 10.26.

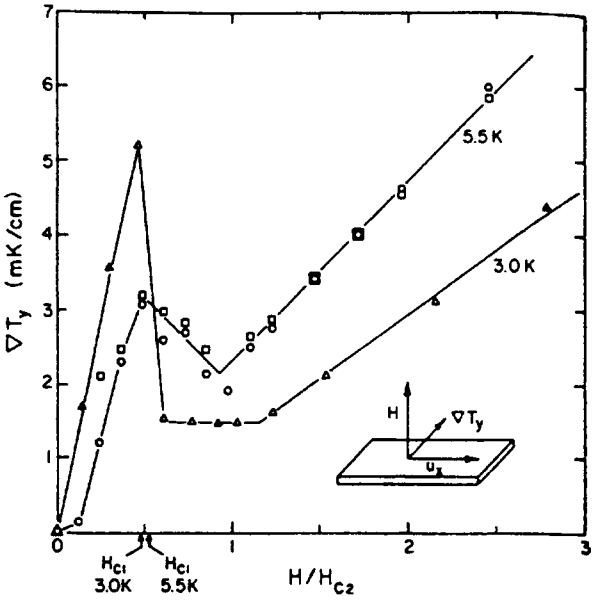

The transverse thermal gradient arising as a consequence of the longitudinal heat flow in the presence of a magnetic field (Righi–Leduc effect) for pure niobium. [Stephan and Maxfield (1973).]

study quasiparticle scattering on a pinned vortex structure and its relevance to the issue of heat transport in HTS below T_c (Krishana *et al.*, 1995) is discussed in Section C,d on thermal conductivity in a magnetic field.

g. Nernst Effect

The Nernst effect refers to generation of the transverse electric field that results from a longitudinal thermal gradient in a perpendicular magnetic field and with no electric current in any direction. Referring to Fig. 10.27, the Nernst coefficient Q is defined as

$$Q = E_y/(\nabla_x T B_z), \quad \text{with } \mathbf{j} = 0. \tag{62}$$

The effect is rather small in normal conductors. In contrast, the Nernst signal becomes quite significant and is easily detected in the mixed state of superconductors, and this is perhaps the main reason why the Nernst effect is the most frequently studied thermomagnetic coefficient. The Nernst effect is significant for

Fig. 10.27.

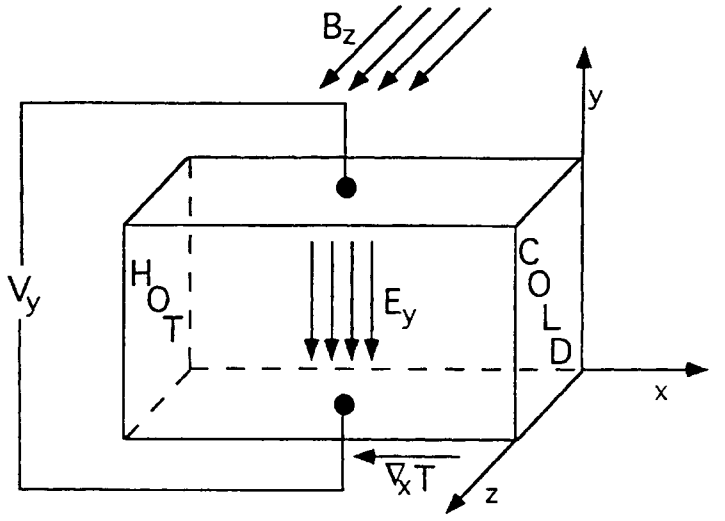

Sample and probe configuration for measuring the Nernst effect.

its unequivocal tie with the motion of vortices. It marks the field and temperature range where pinning is absent or very weak and vortices move freely.

Assuming pinning is absent, $\nabla_x T$ exerts the thermal force $F_{\text{th}} = -S_\phi \nabla_x T$ on the vortex which moves down the thermal gradient with velocity $v_{\phi,x}$. The motion is hindered by a viscous drag force $f_\eta = -\eta v_{\phi,x}$, and the equation of motion for the vortex is

$$F_{\text{th}} + f_\eta = 0. \tag{63}$$

The motion of the vortex (along the x-axis) gives rise to the electric field $E_y = -v_{\phi,x} B_z$ and, upon substitution into Eq. (63), one obtains

$$S_\phi \nabla_x T = \eta E_y / B_z. \tag{64}$$

The appearance of the transverse electric field E_y is an unmistakable sign of the Nernst effect. The actual Nernst coefficient, see Eq. (62), becomes

$$Q \equiv S_\phi / \eta = \rho_f S_\phi / (\phi_0 B_z). \tag{65}$$

The RHS of Eq. (65) follows upon substitution for the viscous drag coefficient η from Eq. (40) and one assumes that the viscous drag is isotropic in the x–y plane, that is, the viscous drag in Eq. (63) that refers to vortex motion along the x-axis is identical with the viscous drag in Eq. (40), which applies to the y-axis vortex motion. Equations (64) and (65) allow determination of the transport entropy as

$$S_\phi = E_y \phi_0 / (\nabla_x T \rho_f). \tag{66}$$

For completeness, we include here the expression for the transport entropy derived by Maki (1971) using the time-dependent Ginzburg–Landau theory,

$$S_\phi = (\phi_0/4\pi T)[B_{c2}(T) - B]L(T)/\{1.16(2\kappa_{GL}^2 - 1) + 1\} = (\phi_0/T)\langle M\rangle L(T). \tag{67}$$

Here $\langle M\rangle$ is the spatially averaged magnetization and $L(T)$ is a numerical function close to 1 near T_c. Equation (67) is valid only near B_{c2}, and in the intermediate field range where most of the experiments are conducted it is less reliable.

As already noted, the Nernst effect has been measured frequently in both the conventional superconductors and in many HTS cuprates. An example of the Nernst effect behavior in cuprates is presented in Fig. 10.28, which shows the data of Ri *et al.* (1994) for *c*-axis oriented films of $YBa_2Cu_3O_{7-\delta}$ and $Bi_2Sr_2CaCu_2O_{8+x}$ together with the respective flux-flow resistivities. Note a significant Nernst signal extending to temperatures some 10–15 K above T_c, suggesting the important role fluctuations play in these highly anisotropic superconductors. Furthermore, we point out a much broader regime of flux flow resistivity and a correspondingly wider temperature range of the Nernst effect in the more anisotropic $Bi_2Sr_2CaCu_2O_{8+x}$.

Two important points need to be kept in mind when measuring the Nernst effect in highly anisotropic superconductors: (a) The concept of rigid, tubelike vortices needs to be replaced by that of two-dimensional pancake-like vortices centered on individual superconducting planes and connected by Josephson vortices. Since Josephson vortices lack the normal core, the thermal force on such a vortex is zero and the Josephson vortices do not contribute to the Nernst effect. (b) Even if realized, the vortex–antivortex unbinding above the Kosterlitz–Thouless temperature is not going to contribute to the Nernst effect in spite of the fact that it is an important resistive mechanism. Very simply, under the action of the Lorentz force the vortex and the antivortex move in opposite directions, and, having opposite vorticities, they will generate resistive voltage. In contrast, under the influence of the thermal force the vortex and the antivortex both move down the thermal gradient, and the electric fields they generate cancel each other.

With a stronger driving force in excess of the pinning force, one should be able to extend the domain over which the thermomagnetic effects are observed. Although it is easy to increase the Lorentz force by increasing the transport current, the small heaters typically used in the thermal force-driven experiments do not supply enough power to create the large thermal gradients needed to overcome strong pinning forces. With the use of focused laser light one may overcome this limitation, as shown by Lengfellner *et al.* (1990) and, more recently, by Zeuner *et al.* (1994), who were able to explore all three regimes of flux motion: thermally assisted flux flow, flux creep, and viscous flux flow.

Table 10.4 gives values of the transport entropy collected from various experiments on conventional superconductors and HTS cuprates. In general, the

Fig. 10.28.

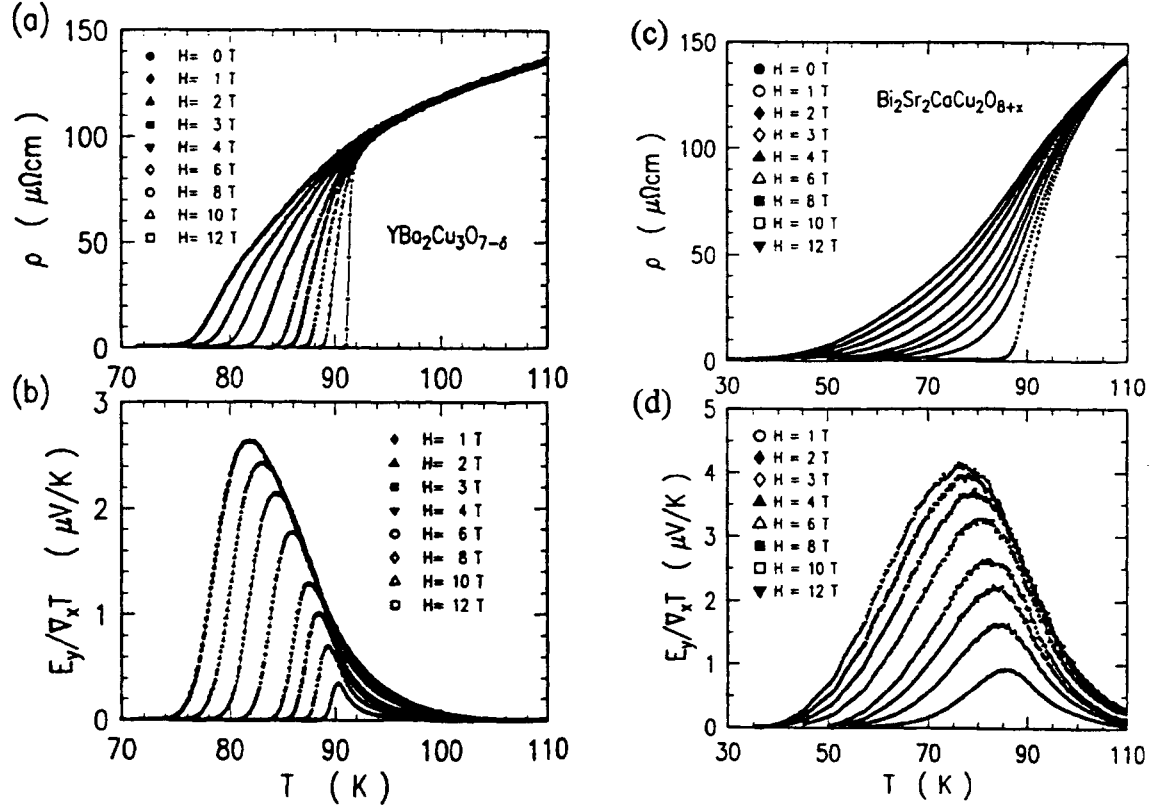

The Nernst effect data and the associated flux-flow resistivities for c-axis oriented films of $YBa_2Cu_3O_{7-\delta}$ and $Bi_2Sr_2CaCu_2O_8$. [Ri *et al.* (1994).]

Table 10.4.

Experimental values of the transport entropy S_ϕ.

S_ϕ[J/m-K]	T[K]	B[T]	Material	Reference
1.6×10^{-12}	3.0	0.1	In+40% Pb	Solomon and Otter (1967)
6.0×10^{-12}	1.6	0.15	Pb+4.56% In	Vidal (1973)
4.4×10^{-17}	87	0.54	YBCO, c-axis oriented film	Zeh *et al.* (1990)
3.0×10^{-14}	87	4	YBCO, c-axis oriented film	Hagen *et al.* (1990)
4.3×10^{-16}	77	4	YBCO, polycrystalline slab	Kober *et al.* (1991)
1.1×10^{-16}	87	4	YBCO, polycrystalline film	Kober *et al.* (1991)
2.6×10^{-15}	87	4	YBCO, epitaxial film	Kober *et al.* (1991)
5.0×10^{-16}	87	5	YBCO, epitaxial film	Hohn *et al.* (1991)
6.5×10^{-13}	87	4	YBCO, epitaxial film	Ri *et al.* (1994)
1.0×10^{-15}	87	4	BSCCO, 2212 single crystal	Zavaritsky *et al.* (1991)
3.7×10^{-13}	81	4	BSCCO, 2212 c-axis film	Ri *et al.* (1994)
6.0×10^{-16}	87	5	BSCCO, 2223 polycrystal	Dascoulidou *et al.* (1992)
9.5×10^{-13}	87	4	TBCCO, epitaxial film	Hagen *et al.* (1991)
3.0×10^{-16}	80	1	TBCCO, 2212 single crystal	Logvenov *et al.* (1992)
1.0×10^{-16}	87	5	TBCCO, 2212 polycrystal	Dascoulidou *et al.* (1992)
1.0×10^{-16}	70	5	TBCCO, 2223 polycryst. film	Zeuner *et al.* (1994)
1.6×10^{-15}	34	3	LSCO, bulk polycrystal	Hohn *et al.* (1994)
1.6×10^{-14}	18	0.5	NCCO, c-axis oriented film	Haensel *et al.* (1995)
5.0×10^{-16}	16.8	1.5	NCCO, epitaxial film	Jiang *et al.* (1995)

Table 10.5.

Transport entropy obtained from the slope of the transport energy.

$-dU_\phi/dT$ [J/m-K]	B[T]	Material	Reference
8.9×10^{-13}	4	YBCO, epitaxial film	Hagen *et al.* (1990)
6.6×10^{-13}	3	YBCO, single crystal	Palstra *et al.* (1990)
4.0×10^{-13}	3	YBCO, single crystal	Hao *et al.* (1991)
2.2×10^{-13}	3	YBCO, epitaxial film	Kober *et al.* (1991)
1.4×10^{-14}	3.5	YBCO, epitax film, $\delta < 7$	Huebener *et al.* (1991)
6.7×10^{-14}	3	YBCO, single crystal	Oussena *et al.* (1992)
2.0×10^{-13}	4	YBCO, epitaxial film	Ri *et al.* (1993)
2.5×10^{-13}	4	YBCO, epitaxial film	Ri *et al.* (1994)
2.5×10^{-13}	1	YBCO, thin film	Haensel *et al.* (1995)
1.2×10^{-12}	4	YBCO, melt grown	Sasaki et al. (1996)
4.8×10^{-17}	5	BSCCO, 2223 bulk polycr.	Dascoulidou *et al.* (1992)
4.2×10^{-12}	4	TBCCO, 2212 epitax film	Hagen *et al.* (1991)
8.3×10^{-16}	1	TBCCO, 2212 single crystal	Logvenov *et al.* (1992)
1.4×10^{-14}	3	LSCO, granular bulk	Hohn *et al.* (1994)
2.4×10^{-13}	0.5	NCCO film	Haensel *et al.* (1995)

transport entropy of conventional superconductors is 2–3 orders of magnitude larger than the transport entropy in HTS materials. Among the cuprates, the data frequently differ by a wide margin, and it is important to understand why such large discrepancies may arise. First of all, the transport entropy is sensitive to the temperature and magnetic field, and because the superconducting transition temperature may differ by several degrees even among the same family of cuprates, a direct comparison of the respective transport entropies at a particular fixed temperature is not very revealing or meaningful. It is more practical to make use of the transport energy per unit vortex length, $U_\phi = TS_\phi$, and specifically its temperature derivative, dU_ϕ/dT, at a fixed value of the magnetic field. This approach tends to suppress the influence of different T_c's among the family of cuprates. The values of the transport entropy obtained by this procedure are collected in Table 10.5.

References for Section D

J. L. Cohn, E. F. Skelton, S. A. Wolf, and J. Z. Liu, *Phys. Rev. B* **45** 13140 (1992).

A. Dascoulidou, M. Galffy, C. Hohn, N. Knauf, and A. Freimuth, *Physica C* **201**, 202 (1992).

A. Freimuth, in *Selected Topics in Superconductivity, Frontiers of Solid State Science*, Vol. 1 (L. C. Gupta and M. S. Multani, Eds.). World Scientific, Singapore, 1992.

M. Galffy, A. Freimuth, and U. Murek, *Phys. Rev. B* **41**, 11029 (1990).

H. Ghamlouch and M. Aubin M, *Physica C*, **269**, 163 (1996).

V. L. Ginzburg, *Sov. Phys. Usp.* **34**, 101 (1991).

H. J. Goldsmid, *Electronic Refrigeration*. Pion Limited, 1986.

H. Haensel, A. Beck, F. Gollnik, R. Gross, R. P. Huebener, and K. Knorr, *Physica C* **244**, 389 (1995).

S. J. Hagen, C. J. Lobb, R. L. Greene, M. G. Forrester, and J. Talvacchio, *Phys. Rev. B* **42**, 6777 (1990).

S. J. Hagen, C. J. Lobb, R. L. Greene, and M. Eddy, *Physica C* **185**, 1769 (1991).

Z. Hao, J. R. Clem, M. W. McElfresh, L. Civale, A. P. Malozemoff, and F. Holtzberg, *Phys. Rev. B* **43** 2844 (1991).

C. Hohn, M. Galffy, A. Dascoulidou, A., Freimuth, H. Soltner, and U. Poppe, *Z. Phys. B--Condensed Matter* **85**, 161 (1991).

C. Hohn, M. Galffy, and A. Freimuth, *Phys. Rev. B* **50**, 15875 (1994).

R. P. Huebener, *Magnetic Flux Structures in Superconductors*. Springer-Verlag, Berlin, 1979.

R. P. Huebener, A. V. Ustinov, and V. K. Kaplunenko, *Phys. Rev. B* **42**, 4831 (1990).

R. P. Huebener, F. Kober, H.-C. Ri, K. Knorr, C. C. Tsuei, C. C. Chi, and M. R. Scheuermann, *Physica C* **181**, 345 (1991).

X. Jiang, W. Jiang, S. N. Mao, R. L. Greene, T. Venkatesan, and C. J. Lobb, *Physica C* **254**, 175 (1995).

A. B. Kaiser, *Phys. Rev. B* **35**, 4677 (1987).

A. B. Kaiser and C. Uher, in *Studies of High Temperature Superconductors*, Vol. 7 (A. V. Narlikar, Ed.), p. 353. Nova Science, New York, 1991.

F. Kober, H.-C. Ri, R. Gross, D. Foelle, R. P. Huebener, and A. Gupta, *Phys. Rev. B* **44**, 11951 (1991).

K. Krishana, J. M. Harris, and N. P. Ong, *Phys. Rev. Lett.* **75**, 3529 (1995).

H. Lengfellner, A. Schnellbogl, J. Betz, W. Prettl, and K. F. Renk, *Phys. Rev. B* **42**, 6264 (1990).

G. Yu. Logvenov, M. Hartmann, and R. P. Huebener, *Phys. Rev. B* **46**, 11102 (1992).

K. Maki, *Physica* **55**, 124 (1971).

E. A. Meilikhov and R. M. Farzetdinova, *J. Supercond.* **7**, 897 (1994).

S. D. Obertelli, J. R. Cooper, and J. L. Tallon, *Phys. Rev. B* **46**, 14928 1992).

M. Oussena, R., Gagnon, Y. Wang, and M. Aubin, *Phys. Rev. B* **46**, 528 (1992).

T. T. M. Palstra, B. Batlogg, L. F. Schneemeyer, and J. V. Waszczak, *Phys. Rev. Lett.* **64**, 3090 (1990).

H.-C. Ri, A. Kober, A. Beck, L. Alff, R. Gross, and R. P. Huebener, *Phys. Rev. B* **47**, 12312 (1993).

H.-C. Ri, R. Gross, F. Gollnik, A. Beck, R. P. Huebener, P. Wagner, and H. Adrian, *Phys. Rev. B* **50**, 3312 (1994).
T. Sasaki, M. Sawamura, S., Awaji, K. Watanabe, N. Kobayashi, K. Kimura, K. Miyamoto, and M. Hashimoto, *Jpn. J. Appl. Phys.* **35**, 82 (1996).
M. Sera, S. Shamoto, and M. Sato, *Solid State Commun.* **68**, 649 (1988).
E. K. Sichel and B. Serin, *J. Low Temp. Phys.* **24**, 145 (1976).
P. R. Solomon and F. A. Otter, *Phys. Rev.* **164**, 608 (1967).
C. H. Stephan and B. W. Maxfield, *J. Low Temp. Phys.* **10**, 185 (1973).
C. K. Subramaniam, C. V. N. Rao, A. B. Kaiser, H. J. Trodahl, A. Mowdsley, N. E. Flower, and J. L. Tallon, *Supercond. Sci. Technol.* **7**, 30 (1994).
C. K. Subramaniam, H. J. Trodahl, A. B. Kaiser, and B. J. Ruck, *Phys. Rev. B* **51**, 3116 (1995).
Uher, *J. Appl. Phys.* **62**, 4636 (1987).
F. Vidal, *Phys. Rev. B* **8**, 1982 (1973).
Z. Z. Wang and N. P. Ong, *Phys. Rev. B* **38**, 7160 (1988).
N. V. Zavaritsky, A. V. Samoilov, and A. A. Yurgens, *Physica C* **180**, 417 (1991).
M. Zeh, H.-C, Ri, F. Kober, R. P. Huebener, J. Fischer, R. Gross, H. Muller, T. Sermet, A. V. Ustinov, and H.-G. Wener, *Physica C* **167**, 6 (1990).
S. Zeuner, W. Prettl, K. F. Renk, and H. Lengfellner, *Phys. Rev. B* **49**, 9080 (1994).

Chapter 11

Electrical Properties

Charles P. Poole, Jr.
Department of Physics and Institute of Superconductivity,
University of South Carolina, Columbia, South Carolina

A Introduction

This chapter deals with some of the electrical properties of superconducting materials. One of the most important of these is the critical current density J_c, and measured values are tabulated for many superconductors in Section F. of Chap. 9. It was mentioned there that experimentally determined critical current densities seldom come close to theoretically predicted limits such as the depairing value. Researchers around the world are presently spending a great deal of time and effort trying to increase attainable critical currents in wires and tapes. We now proceed to examine some specific electrical properties such as the Hall effect, tunneling, Josephson junctions, and Superconducting QUantum Interference Devices, commonly referred to as SQUIDs.

ISBN: 0-12-561460-8
$30.00
HANDBOOK OF SUPERCONDUCTIVITY

B

Hall Effect

The Hall effect employs crossed electric and magnetic fields to provide information on the sign, concentration, and mobility of charge carriers. The experimental arrangement illustrated in Fig. 11.1 shows a magnetic field B_0 applied in the z direction perpendicular to a slab, and a battery that establishes an electric field E_y that causes the current $I = JA$ of density $J = nev_d$ to flow along y. The Lorentz force $q\mathbf{v} \times \mathbf{B}_0$ on each moving charge q causes a buildup of charge on the sides of the plate, which produces an electric field E_x and establishes a Hall voltage $\Delta V_x = E_x d$ perpendicular to the directions of I and B_0. In the superconducting state a Hall voltage can arise from the transverse electric field E_x induced by flux motion. At equilibrium after the buildup of the charge the electric force $q\mathbf{E}_x$ balances the magnetic force $q\mathbf{v} \times \mathbf{B}_0$, and the Hall coefficient R_H, defined as the ratio

$$R_H = E_x/JB_z = \pm 1/ne, \tag{1}$$

is positive when the majority carriers are holes, as with most cuprates, and negative for electrons.

Fig. 11.1.

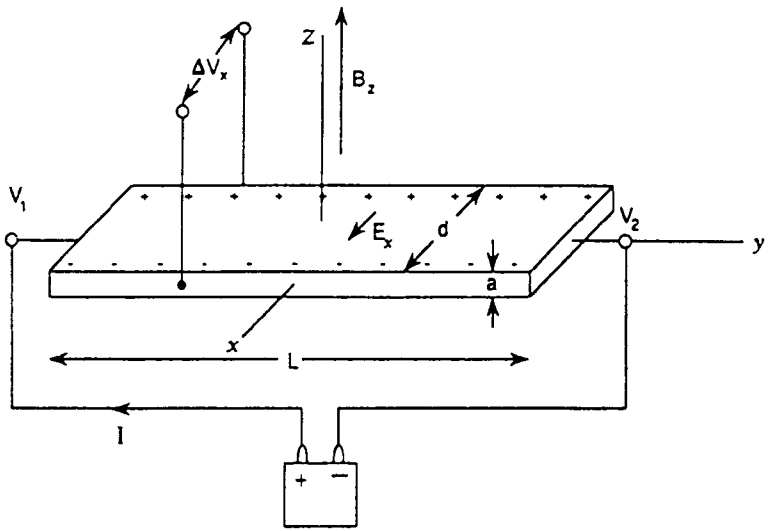

Experimental arrangement for Hall effect measurement showing an electrical current I flowing through a plate of width d and thickness a in the presence of a uniform, transverse magnetic field B_z. The voltage drop $V_2 - V_1$ along the plate, the drop ΔV_x across the plate, and the electric field E_x across the plate are indicated. The figure is drawn for the case of negative charge carriers, that is, electrons. [From Poole *et al.* (1995), p. 18.]

We can define the dimensionless Hall number, the Hall effect resistivity ρ_{xy}, the Hall mobility μ_H (charge carrier drift velocity per unit electric field), and the Hall angle Θ_H as follows:

$$\text{Hall number} = V_0/R_H e \tag{2}$$

$$\rho_{xy} = E_x/J \tag{3}$$

$$\mu_H = |v|/E_y = R_H/\rho \tag{4}$$

$$\tan\Theta_H = E_x/E_y, \tag{5}$$

where V_0 is the volume per formula unit. Thus, the Hall effect distinguishes electrons from holes, and when all charge carriers have the same sign Eq. (1) provides the charge density n. When both positive and negative charge carriers are present, their Hall effects partially (or totally) cancel.

C

Tunneling

Tunneling or barrier penetration is a process whereby an electron confined to a region by an energy barrier can penetrate the barrier through a quantum mechanical process and emerge on the other side. Tunneling is carried out through an insulating layer, I, between two normal materials (N–I–N) such as semiconductors, between a normal metal and a superconductor (N–I–S), and between two superconductors (S–I–S). Tunneling through the barrier proceeds to energy states that are empty so the Pauli exclusion principle is not violated, and the total energy of the system is conserved in the process. Therefore, single-electron tunneling occurs between levels with the same energy, and in two-electron tunneling, involving for example the breakup of a Cooper pair, one electron gains as much energy as the other loses. A positive bias $+V$ on the material lowers the Fermi energy level by eV, and electrons tunnel toward the positive bias, with the tunneling current I flowing in the opposite direction.

Figures 11.2 and 11.3 depict tunneling at absolute zero when a normal metal has its conduction band full below the Fermi level E_F and empty above it, and a superconductor has its energy states full below its energy gap $E_g = 2\Delta$ and empty above. Figure 11.2 shows the N–I–S case in which electrons tunnel from the superconductor to the normal metal for a negative bias $V < -\Delta/e$, and from the normal metal to the empty superconductor levels above the gap for a positive bias $V > \Delta/e$. At absolute zero no tunneling occurs for the intermediate range of bias voltages $-\Delta e < V < \Delta/e$, as indicated at the bottom of the figure. Figure

Fig. 11.2.

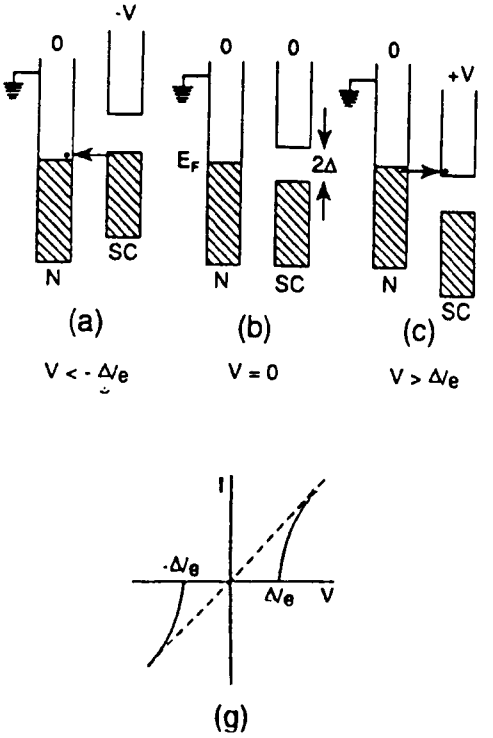

Normal metal to superconductor (N–I–S) tunneling at 0 K showing (a) super electron tunneling (SC $\Rightarrow$ N) for $V < -V/e$, (b) the absence of tunneling when the Fermi level is in the gap ($-\Delta/e < V < \Delta/e$), and (c) normal electron tunneling (N $\Rightarrow$ SC) for $V > \Delta/e$. Arrows indicate electron tunneling directions, which are opposite to current flow directions. The current–voltage characteristic is given in (d). [From Poole *et al.* (1995), p. 407.]

11.3 shows the S–I–S case in which tunneling occurs in one direction for $V < -2\Delta/e$, in the reverse direction for $V > 2\Delta/e$, and at absolute zero it does not occur at all for the range $-2\Delta/e < V < 2\Delta/e$. At finite temperatures a few electrons of a normal metal are found above E_F, and some electrons of superconductor are excited to levels above the gap, with the result that a weak tunneling current flows for the range of biases where it is forbidden at 0 K. If the gap has a different value for the each material in the S–I–S case, then the weak tunneling current above absolute zero will exhibit a peak at the bias $|\Delta_2 - \Delta_1|/e$, and a sharp rise at $(\Delta_2 + \Delta_1)/e$, as indicated in Fig. 11.4.

The thickness of the insulating layer is a critical factor in the operation of the junction. If a superconducting rod is cut at some point, and then joined through an intervening insulating section, there are three cases to consider: (1)

Fig. 11.3.

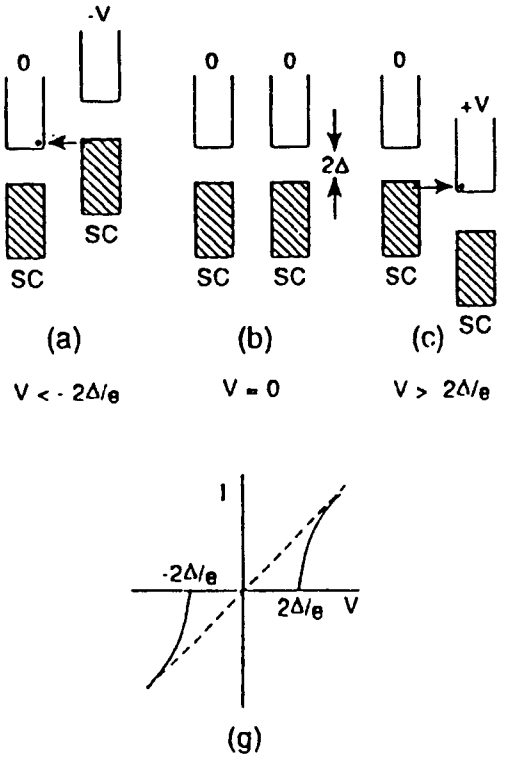

Superconductor to superconductor (S–I–S) tunneling at 0 K showing (a) super electron tunneling (SC $\Rightarrow$ N) for $V < -2\Delta/e$, (b) the absence of tunneling for bias voltages in the range ($-2\Delta/e < V < 2\Delta/e$), and (c) reverse direction superelectron tunneling for $V > 2\Delta/e$. Arrows show tunneling directions. The current–voltage characteristic is given in (d). [From Poole *et al.* (1995), p. 408.]

The insulating region can be so thick that the two separated superconducting sections lose contact, and no tunneling occurs. (2) The insulating section, called a weak link, can be intermediate in thickness so that the superconductors are weakly coupled and electrons can tunnel. (3) There can be close to direct touching, or perhaps with an intervening monolayer of foreign atoms, so that strong contact is maintained across the interface. When two superconductors that differ in T_c are in strong contact, electron pairs leak back and forth and can cause the two materials to exhibit one intermediate T_c, a phenomenon called the proximity effect.

Fig. II.4.

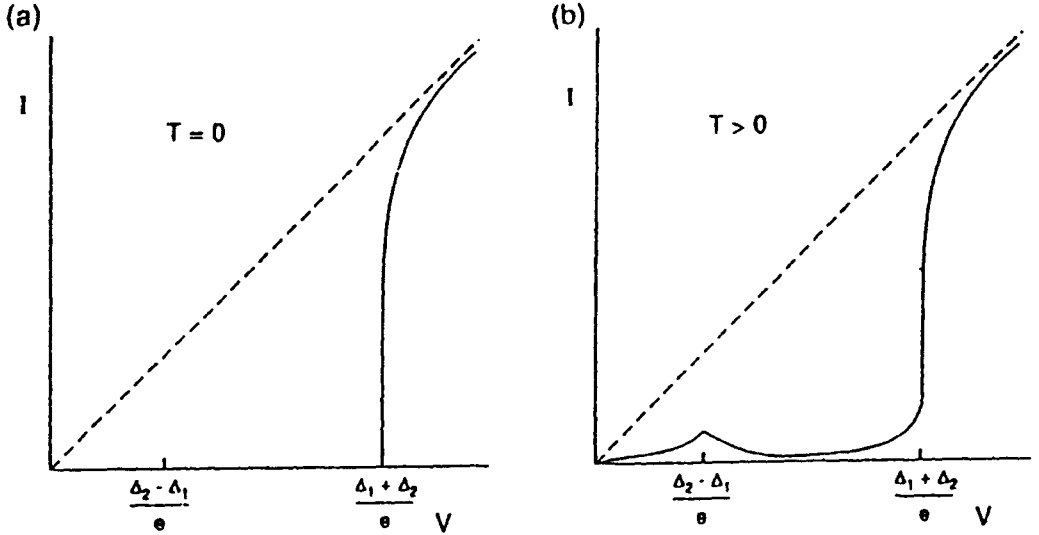

Tunneling current vs bias voltage for S–I–S case involving two superconductors with the energy gaps $\Delta_2 > \Delta_1$. No tunneling occurs for $T = 0$ until the bias $V = (\Delta_2 + \Delta_1)/e$ is reached, and weak tunneling appears at the bias $V = (\Delta_2 - \Delta_1)/e$ for $T > 0$, with the onset of strong tunneling at $V = (\Delta_1 + \Delta_2)/e$. [From Poole *et al.* (1995), p. 416.]

D

Josephson Effect

The dc Josephson effect involves Cooper pair tunneling from one superconductor to another across an insulating barrier at zero bias ($V = 0$) (see Likharev, 1986; Van Duzer and Turner, 1981). The wavefunctions for the two sides of the junction can be written in the form

$$\Psi_1 = (n_{s1})^{1/2} e^{i\theta_1} \tag{6}$$

$$\Psi_2 = (n_{s2})^{1/2} e^{i\theta_2} \tag{7}$$

$$\phi = \theta_2 - \theta_1, \tag{8}$$

where n_{s1} and n_{s2} are the densities of super electrons in the two superconductors, and ϕ is the phase difference across the barrier. The Josephson expressions

$$\frac{d}{dt}\phi = \frac{2e}{\hbar} V \tag{9}$$

$$J = J_c \sin\phi \tag{10}$$

relate ϕ to the current density J through the junction and to the voltage V across it. The super electron densities determine the magnitude of the critical current density J_c,

$$J_c \propto (n_{s1} n_{s2})^{1/2} \tag{11}$$

Thus, the presence of a phase difference (8) across the junction causes dc current to flow spontaneously at zero voltage.

When a constant voltage is applied across the junction, Eq. (9) can be integrated directly to give

$$\phi(t) = \phi_0 + 2\pi\nu_J t, \tag{12}$$

where ν_J is known as the Josephson frequency

$$\nu_J = 2eV/h = V/\Phi_0. \tag{13}$$

$\Phi_0 = h/2e$ is the quantum of flux, and the ratio ν_J/V has the value

$$\nu_J/V = 2e/h = 483.6\ \text{MHz}/\mu\text{V} \tag{14}$$

This ac Josephson effect has the following expression for the oscillations of the critical current density:

$$J = J_c \sin(2\pi\nu_J t + \phi_0). \tag{15}$$

These oscillations occur for a constant applied voltage. The current density amplitude J_c reaches a maximum value when the applied voltage is the gap voltage, $V = 2\Delta/e$. There is also an inverse ac Josephson effect whereby the dc voltage is induced across the junction when an ac current is caused to flow through it, or when an electromagnetic field, as from microwaves, is incident on it.

A practical Josephson junction can be represented as driven by a current source $I_c \sin\phi$ from Eq. (10) in parallel with a conductance G to account for quasiparticle tunneling and a capacitor C to take into account displacement current, as illustrated in Fig. 11.5. The current flow in this equivalent circuit is described by the differential equation

$$I(\mathrm{t}) = I_c \sin\phi + GV + C\frac{dV}{dt}. \tag{16}$$

With the aid of the Josephson relation (9) this becomes

$$I = \frac{\hbar C}{2e}\frac{d^2\phi}{dt^2} + \frac{\hbar G}{2e}\frac{d\phi}{dt} + I_c \sin\phi. \tag{17}$$

We can define a critical voltage $V_c = I_c/G$, an associated Josephson frequency ω_c from Eq. (14),

$$\omega_c = (2e/\hbar)V_c, \tag{18}$$

and a dimensionless admittance ratio β_c,

$$\beta_c = \omega_c C/G. \tag{19}$$

Fig. 11.5

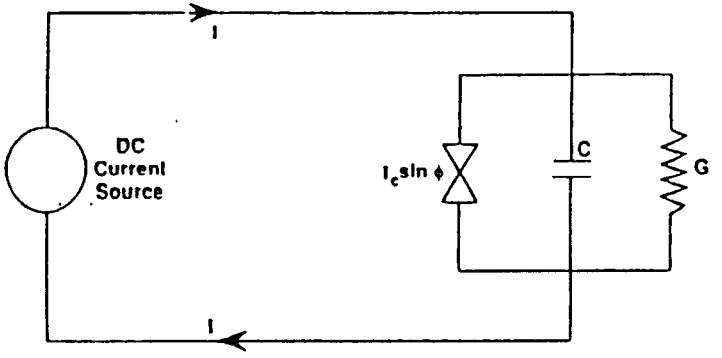

Parallel circuit representing a Josephson junction driven by the dc current source $I(t)$ on the left. The right-hand side shows the junction current source $I_c \sin\phi$ in parallel with a capacitor C and a conducatance G. [From Poole *et al.* (1995), p. 430.]

Fig. 11.6.

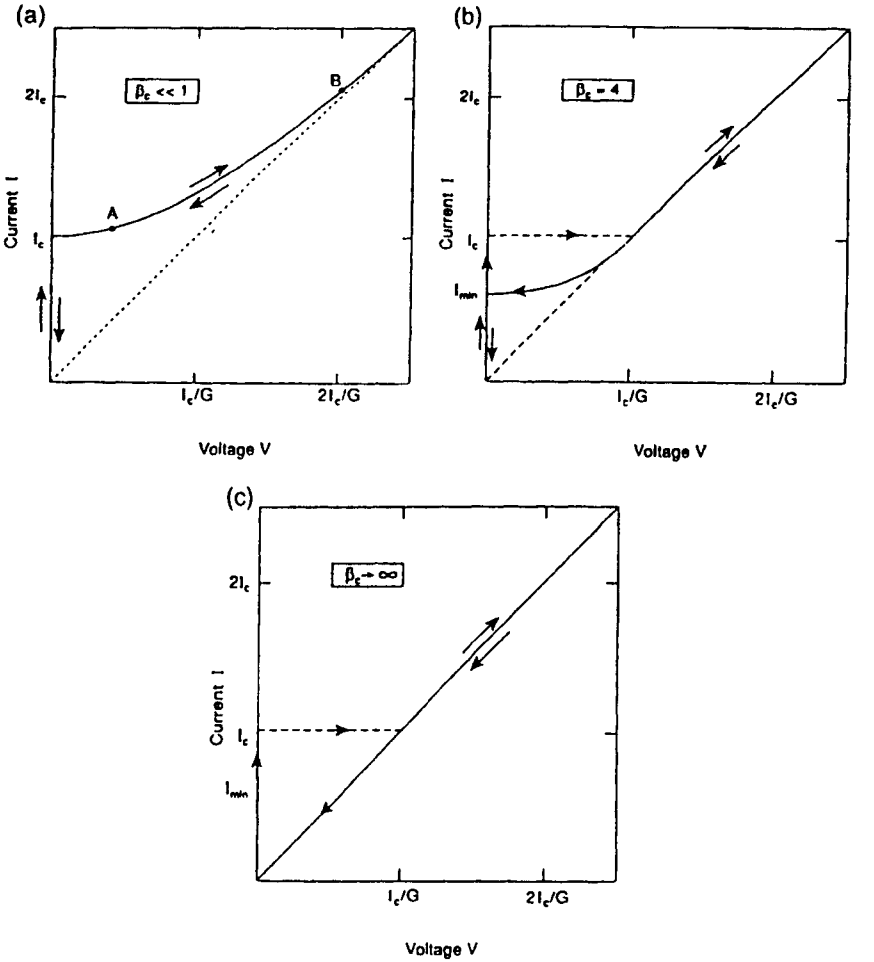

Normalized current–voltage characteristics, I vs V, where $V = \langle V \rangle$ is the average voltage, for the Josephson junction circuit of Fig. 11.5 with (a) negligible capacitance, $\beta_c \ll 1$, (b) appreciable capacitance, $\beta_c = 4$, and (c) dominating capacitance, $\beta_c \Rightarrow \infty$, where the admittance ratio is defined by $\beta_c = \omega_c C/G$. [From Poole *et al.* (1995), p. 432.]

Solutions to this second-order differential equation (17) are plotted in Fig. 11.6 for small ($\beta_c \ll 1$), medium ($\beta_c = 4$), and large ($\beta_c \gg 1$) values of the admittance ratio. This figure is a plot of current vs the average voltage $V = \langle V \rangle$, and Fig. 11.7 shows the oscillations of the voltage at points A and B of Fig. 11.6a. Note the presence of hysteresis in the plots of Fig. 11.6.

Fig. 11.7.

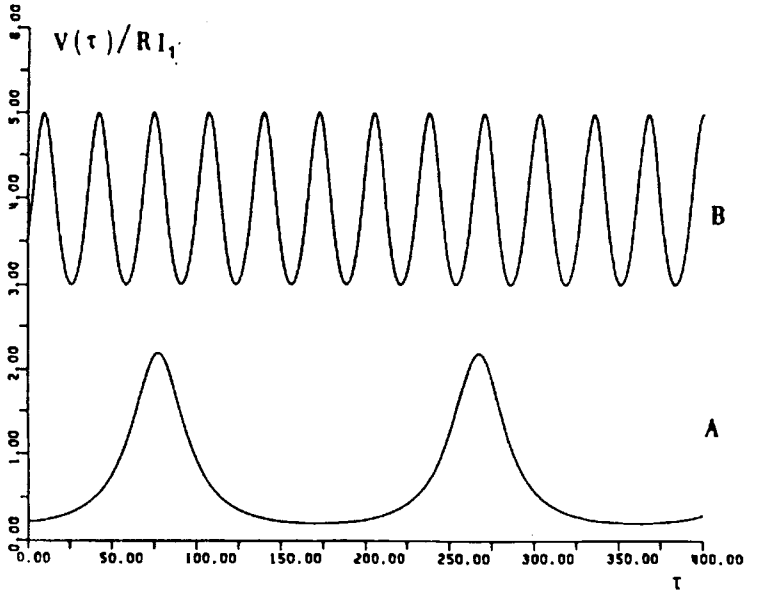

Voltage oscillations across the Josephson junction of Fig. 11.5 for the negligible capacitance case $\beta_c \ll 1$, and small and large dc bias voltages as marked at points A and B, respectively, of Fig. 11.6a. [From Barone and Paterno (1982), p. 128.]

E

Magnetic Field and Size Effects

When a magnetic field is applied to a Josephson junction, the behavior of the junction will depend on its size relative to the Josephson penetration depth λ_J defined by

$$\lambda_J = (\Phi_0/2\pi\mu_o J_c d_{eff})^{1/2}, \tag{20}$$

where d_{eff} is the effective thickness of the junction. This penetration depth is approximately equal to the length L of a Josephson junction when the stored magnetic field energy U_B equals the energy U_J associated with the current flow.

A long Josephson junction, with $L \gg \lambda_J$, has its phase ϕ determined by the sine Gordon equation, which has solitary wave (soliton) solutions. A short Josephson junction, with $L \ll \lambda_J$, can exhibit the current oscillations shown in Fig. 11.8 arising from the Josephson junction (Fraunhofer) diffraction expression

$$I = I_c \sin\phi_0 \frac{\sin(\pi\Phi/\Phi_0)}{\pi\Phi/\Phi_0}, \tag{21}$$

Fig. 11.8.

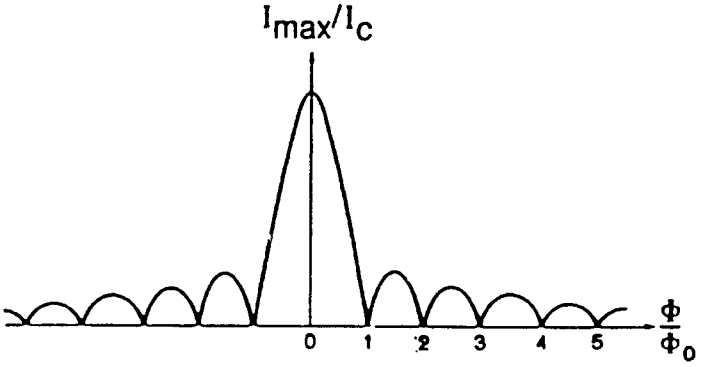

Josephson Fraunhofer diffraction pattern showing the dependence of the maximum zero-voltage current I_{max}/I_c on the normalized flux $\Phi/\Delta\Phi_0$ through the junction. [From Van Duzer and Turner (1981), p. 155.]

where $I_c = AJ_c$ is the critical current and I has a maximum value for the phase difference $\phi_0 = \pi/2$. The figure shows how the tunneling current varies with increasing magnetic flux Φ through the junction. Extremely small Josephson junctions called nanojunctions exhibit new phenomena. The change in voltage $\Delta V = e/C$ arising from single-electron tunneling can become comparable with a typical junction voltage and produce a blockage of current flow (Coulomb blockade). Fluctuations can appear that produce a so-called Coulomb staircase on an I vs V characteristic plot. A dc current biased ultrasmall Josephson junction can exhibit correlated tunneling of Cooper pairs leading to what are called Bloch oscillations at the frequency $\nu_B = I/2e$.

F

Superconducting QUantum Interference Device (SQUID)

A Superconducting QUantum Interference Device or SQUID measures flux changes in a loop containing weak links to determine the strength of an applied magnetic field. In one arrangement, called a dc SQUID, the current change through a pair of two weak links is detected as a voltage and amplified. Another type, called an rf SQUID, consists of a loop with one weak link coupled to an LC tuned circuit driven by an rf current source. A change of flux in the loop changes the loading of the tuned circuit, and this is detected by measuring the change in rf voltage across the circuit. Since a SQUID easily detects a change in one quantum of flux in an area with dimensions in the centimeter range, it is said to measure a macroscopic quantum phenomenon (vide Poole *et al.* (1995), p. 451).

References

A. Barone and G. Paterno, *Physics and Applications of the Josephson Effect*. Wiley. New York, 1982.
K. K. Likharev, *Dynamics of Josephson Junctions and Circuits*. Gordon and Breach, New York, 1986.
C. P. Poole, Jr., H. A. Farach, and R. J. Creswick, *Superconductivity*. Academic Press, New York, 1995.
T. van Duzer and C. W. Turner, *Principles of Superconductive Devices and Circuits*. Elsevier, New York, 1981.

Chapter 12

Magnetic Properties

Charles P. Poole, Jr.
Department of Physics and Institute of Superconductivity, University of South Carolina, Columbia, South Carolina

A Introduction

One of the main characteristics of a superconductor is its magnetic behavior, and this behavior arises from its vortex structure. The present chapter surveys the configurations and interactions of vortices and discusses the macroscopic magnetic properties that result from them. The role that they play in influencing electric current flow and their dependence on the sample shape are examined. Most of the chapter is devoted to Type II superconductivity, but toward the end the intermediate state of a Type I superconductor is treated.

ISBN: 0-12-561460-8
$30.00
HANDBOOK OF SUPERCONDUCTIVITY

B

Internal Fields and Magnetization

The general expressions for the B and H fields,

$$B = \mu_0(H + M) = \mu H = \mu_0 H(1 + \chi), \tag{1}$$

are valid both inside and outside a superconducting sample. Here M is the magnetization or magnetic moment per unit volume, χ is the dimensionless magnetic susceptibility, μ_0 is the permeability of free space where $M = 0$ and $\chi = 0$, and $\mu = \mu_0(1 + \chi)$ is the permeability of a medium. When an external magnetic field $B_{\text{app}} = H_{\text{app}}/\mu_0$ is applied, the magnetization $M = 0$ in the free space outside the sample. Inside the B and H fields are related to the magnetization M through Eq. (1), so we have

$$B_{\text{in}} = \mu_0 H_{\text{in}}(1 + \chi), \tag{2}$$

where the dimensionless susceptibility χ

$$\chi = M/H_{\text{in}} \tag{3}$$

is an intrinsic property of the medium. If the medium is anisotropic, then the susceptibility will have different values, χ_a, χ_b, and χ_c, along the three principal directions, with $\chi_a = \chi_b \neq \chi_c$ for axial symmetry.

For an ideal Type I superconductor $\chi = -1$, and assuming that there are no demagnetization effects, we have the formulae

$$\begin{aligned} B_{\text{in}} &= 0 \\ M &= -H_{\text{in}} = -B_{\text{app}}/\mu_0, \end{aligned} \tag{4}$$

which are plotted in Fig. 12.1. For a Type II superconductor, which has two critical fields B_{c1} and B_{c2}, the analogous expressions have the form

$$\begin{aligned} B_{\text{in}} &= 0 \\ 0 \leq B_{\text{app}} &\leq B_{\text{c1}} \\ M &= -H_{\text{in}} = -B_{\text{app}}/\mu_0 \end{aligned} \tag{5a}$$

$$\begin{aligned} B_{\text{c1}} \leq B_{\text{app}} &\leq B_{\text{c2}} \\ \mu_0 M &= -(B_{\text{app}} - B_{\text{in}}); \end{aligned} \tag{5b}$$

shown plotted in Fig. 12.2. In practice the actual magnetization and internal field curves are more rounded than indicated by the figure.

Also shown in these two figures is the thermodynamic critical field B_{c}, defined geometrically for a Type II material by the equal area criterion corresponding to the integrals

$$\int_{B_{\text{c1}}}^{B_{\text{c}}} (B_{\text{app}} + \mu_0 M)\mathrm{d}B_{\text{app}} = \mu_0 \int_{B_{\text{c}}}^{B_{\text{c2}}} (-M)\mathrm{d}B_{\text{app}}, \tag{6}$$

Fig. 12.1.

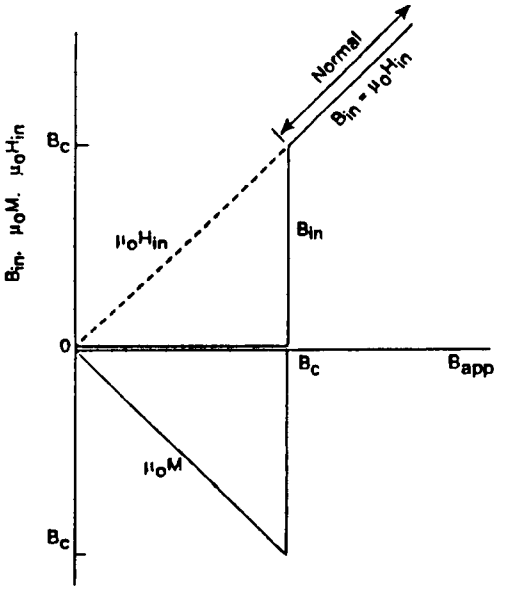

Internal fields B_{in}, H_{in}, and magentization M for an ideal Type I superconductor. [From Poole *et al.* (1995), p. 267.]

Fig. 12.2.

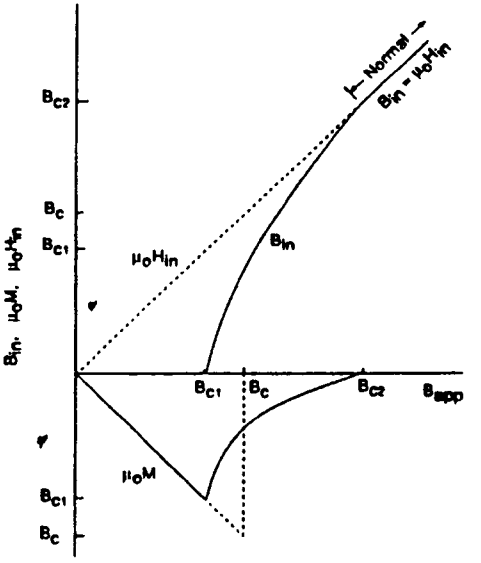

Internal fields B_{in}, H_{in}, and magnetization M for an ideal Type II superconductor. [From Poole *et al.* (1995), p. 267.]

Fig. 12.3.

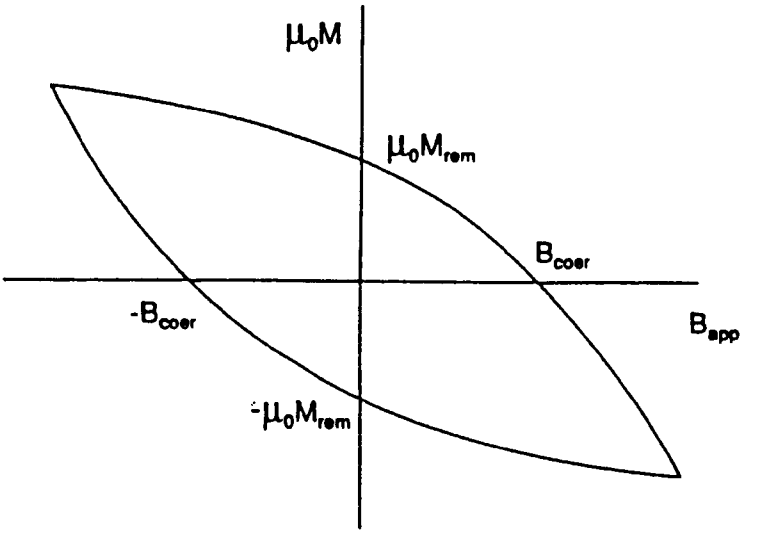

Representative low-field hysteresis loop showing the coercive field B_{coer} where the magnetization is zero, and the remnant magnetization M_{rem} that remains when the applied field has been reduced to zero. [From Poole *et al.* (1995), p. 317.]

(where M is a negative quantity), and energetically B_c involves the difference between the Gibbs free energies of the normal and superconducting states,

$$G_n - G_s = B_c^2/2\mu_0. \tag{7}$$

where $B_c^2/2\mu_0$ is the condensation energy. All three quantities in this expression (7) are temperature dependent, and it is valid for both Type I and Type II superconductors.

The magnetization often exhibits hysteresis, that is, it depends on the previous history of how the external field was applied. Figure 12.3 sketches a representative hysteresis loop showing the coercive field B_{coer}, which is the value of the applied field that reduces the magnetization to zero, and the remanent magnetization M_{rem}, which is the magnitude of the magnetization when the applied field passes through zero. The temperature and field dependences of some typical low-field and high-field hysteresis loops are presented in Figs. 12.4 and 12.5, respectively.

C

Critical Fields

The lower and upper critical fields for the isotropic Type II case are given by

$$B_{c1} = \frac{\Phi_0 \ln \kappa}{4\pi\lambda^2} \tag{8}$$

Fig. 12.4.

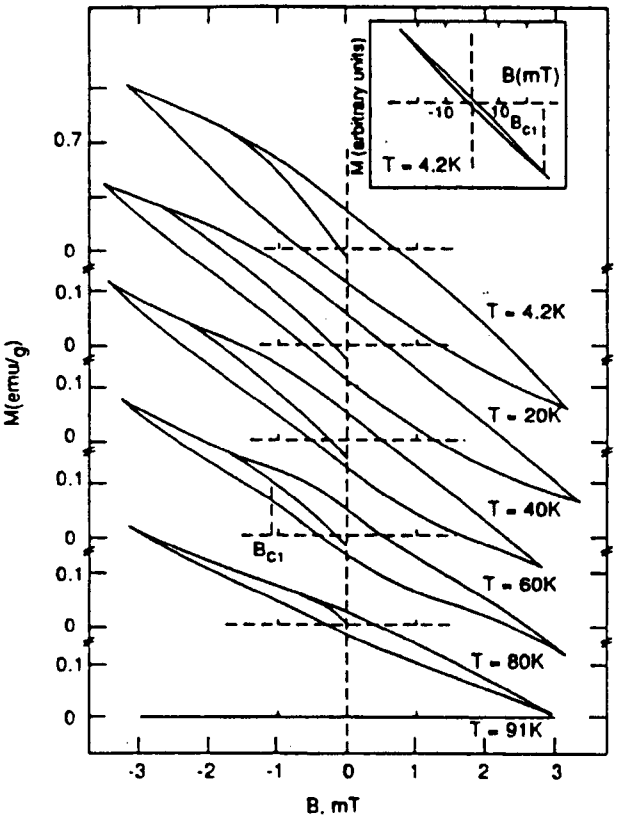

Low-field hysteresis loops of $YBa_2Cu_3O_7$ cycled over the same field scan, -3 mT $\leq B_{app} \leq 3$ mT, for several temperatures. The loops gradually collapse as the temperature increases. The virgin curve for the initial rise in magnetization is given for each loop. [Senoussi *et al.* (1988).]

$$B_{c2} = \frac{\Phi_0}{2\pi\xi^2}, \tag{9}$$

where λ is the penetration depth and ξ is the coherence length. These two fields can be expressed in terms of the thermodynamic critical field,

$$B_c = \frac{\Phi_0}{2\sqrt{2}\pi\lambda\xi}, \tag{10}$$

as follows:

$$B_{c1} = \frac{B_c \ln \kappa}{\sqrt{2}\kappa} \tag{11}$$

$$B_{c2} = \sqrt{2}\kappa B_c. \tag{12}$$

Fig. 12.5.

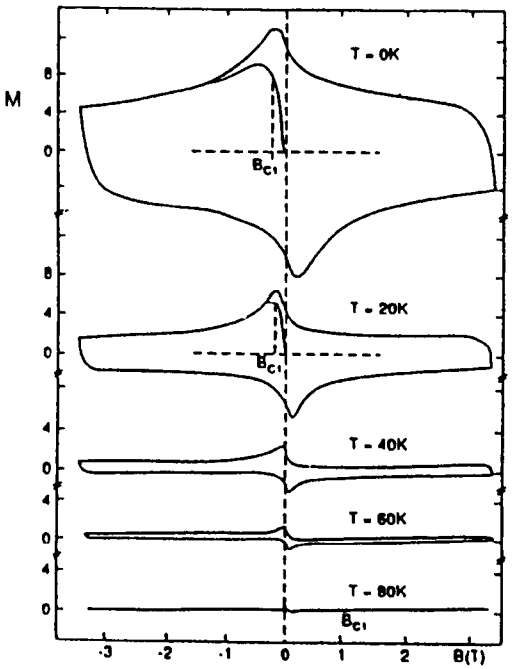

High-field hysteresis loops of $YBa_2Cu_3O_7$ cycled over the same field scan, $-3T \leq B_{app} \leq 3T$, for several temperatures. The loops gradually collapse as the temperature increases. The deviation of the virgin curve from linearity occurs near the lower critical field B_{c1}, which increases as the temperature is lowered. [Senoussi *et al.* (1988).]

$\kappa = \lambda/\xi$ is called the Ginzburg–Landau parameter. Figure 12.2 shows the position of the lower and upper as well as the thermodynamic critical field on the magnetization curve, and Tables 9.1, 9.2, 9.4, and 9.5 respectively, lists the isotropic length parameters and critical fields of some Type II superconductors. The bulk of the material goes normal when B_{app} reaches B_{c2}, but the superconducting state can persist in a thin surface sheath for B_{app} up to the higher applied field value $B_{c3} = 1.7\, B_{c2}$.

The thermodynamic critical field B_c is related to the depairing current density J_{depair} through the expression

$$J_{depair} = \alpha B_c/\mu_0\lambda, \tag{13}$$

where the dimensionless coefficient α is of the order of unity.

D

Vortices

The magnetic flux of an individual (isolated) vortex is determined by integrating its magnetic field over its area,

$$\int \mathbf{B} \cdot d\mathbf{A} = \Phi_0, \tag{14}$$

and it equals the flux quantum Φ_0,

$$\Phi_0 = h/2e = 2.0678 \times 10^{-15}\ \mathrm{Tm}^2. \tag{15}$$

This flux quantum Φ_0 is associated with the Hall effect quantum of resistance R_H,

$$R_H = h/e^2 = 2\Phi_0/e = 25{,}813\Omega. \tag{16}$$

Some superconductivity researchers use $R_0 = h/4e^2 = 6.45\ \mathrm{K}\Omega$ as the quantum of resistance since the charge of a Cooper pair is $2e$.

For the high κ limit of the cuprates, $\lambda \gg \xi$, the vortex magnetic field $B(r)$ and shielding current density $J_s(r)$ outside the core, $r > \xi$, have the radial dependences

$$B(r) = \frac{\Phi_0}{2\pi\lambda^2} K_0(r/\lambda) \tag{17}$$

$$J_s(r) = \frac{\Phi_0}{2\pi\mu_0\lambda^3} K_1(r/\lambda), \tag{18}$$

where $K_0(r/\lambda)$ and $K_1(r/\lambda)$ are the zero-order and first-order modified Bessel functions, respectively, with the properties that $K_1(r) \gg K_0(r)$ for small $r \ll \lambda$, and $K_1(r) \approx K_0(r)$ for large $r \gg \lambda$. Inside the core, $r \leq \xi$, we have $J_s(r) = 0$, and $B(r)$ may be approximated as having the constant value

$$B(r) = \frac{\Phi_0}{2\pi\lambda^2} K_0(\xi/\lambda). \tag{19}$$

Equations (17) and (18) have the following asymptotic behaviors near the core:

$$B(r) = \frac{\Phi_0}{2\pi\lambda^2} \ln(1.123\lambda/r), \qquad r \ll \lambda \tag{20}$$

$$J_s(r) = \frac{\Phi_0}{2\pi\mu_0\lambda^3} \lambda/r, \qquad r \ll \lambda, \tag{21}$$

Fig. 12.6.

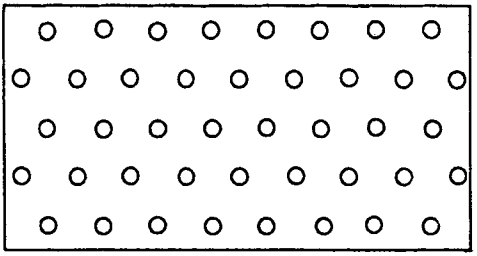

Hexagonal vortex lattice. [From Poole *et al.* (1995), p. 277.]

and far away from the core

$$B(r) = \frac{\Phi_0}{2(2\pi)^{1/2}\lambda^2}\frac{\exp(-r/\lambda)}{(r/\lambda)^{1/2}}, \qquad r \gg \lambda \tag{22}$$

$$J_s(r) = \frac{\Phi_0}{2(2\pi)^{1/2}\mu_0\lambda^3}\frac{\exp(-r/\lambda)}{(r/\lambda)^{1/2}}, \qquad r \gg \lambda. \tag{23}$$

where the numerical factor 1.123 in Eq. (20) is $2e^{-\gamma}$ and $\gamma = 0.57721566\ldots$ is the dimensionless Euler–Mascheroni constant.

Ordinarily, vortices arrange themselves in the hexadic pattern of Fig. 12.6 separated by the distance d, where $\frac{1}{2}\sqrt{3}d^2$ is the area occupied per vortex. Near the lower critical field $d \approx 2\lambda$ and near the upper critical field $d \approx 2\xi$. For large κ the amount of flux Φ_{core} in the core of an isolated vortex is much less than the flux quantum Φ_0. Near the upper critical field B_{c2} the vortex cores almost overlap and the flux in each core approaches Φ_0. The average field B_{in} inside the superconductor is given by

$$B_{\text{in}} = \frac{\Phi_0}{\frac{1}{2}\sqrt{3}d^2} = N_A\Phi_0, \tag{24}$$

where N_A is the number of vortices per unit area.

E

Vortex Anisotropies

The characteristic length relationship of anisotropic superconductors is

$$\xi_a\lambda_a = \xi_b\lambda_b = \xi_c\lambda_c, \tag{25}$$

and the GL parameter κ_i in the ith principal direction is

$$\kappa_i = \frac{|\lambda_j\lambda_k|^{1/2}}{|\xi_j\xi_k|^{1/2}}. \tag{26}$$

The critical fields for the ith direction are obtained by generalizing Eqs. (11) and (12), respectively:

$$B_{c1} = \frac{\ln \kappa_i}{\sqrt{2}\kappa_i} B_c \tag{27}$$

$$B_{c2} = \sqrt{2}\kappa_i B_c. \tag{28}$$

Comparing Eqs. (10) and (25), we see that the thermodynamic critical field,

$$B_c = \frac{\Phi_0}{2\sqrt{2}\pi\xi_i\lambda_i}, \tag{29}$$

is independent of the direction.

Axially symmetric superconductors with in-plane ($m_a^* = m_b^*$) and axial direction (m_c^*) effective masses are characterized by the anisotropy ratio Γ,

$$\Gamma^2 = m_c^*/m_{ab}^* = (\xi_{ab}/\xi_c)^2 = (\lambda_c/\lambda_{ab})^2, \tag{30}$$

where for the cuprates $m_c^* > m_{ab}^*$ and we have

$$\xi_c \ll \xi_{ab} \ll \lambda_{ab} \ll \lambda_c. \tag{31}$$

Some reported values of these quantities are listed in Table 9.2. For the cuprates with the applied field in the ab plane (κ_{ab}) and along the c direction (κ_c), respectively, we have

$$\kappa_{ab} = \frac{|\lambda_{ab}\lambda_c|^{1/2}}{|\xi_{ab}\xi_c|^{1/2}} \tag{32}$$

$$\kappa_c = \lambda_{ab}/\xi_{ab}, \tag{33}$$

and Eqs. (27)–(29) provide the critical fields for axial symmetry in the ab plane,

$$B_{c1}(ab) = \frac{\Phi_0 \ln \kappa_{ab}}{4\pi\lambda_{ab}\lambda_c} \tag{34}$$

$$B_{c2}(ab) = \frac{\Phi_0}{2\pi\xi_{ab}\xi_c} \tag{35}$$

and along the c direction,

$$B_{c1}(c) = \frac{\Phi_0 \ln \kappa_c}{4\pi\lambda_{ab}^2} \tag{36}$$

$$B_{c2}(c) = \frac{\Phi_0}{2\pi\xi_{ab}^2}. \tag{37}$$

Table 9.5 provides some experimentally determined values of these critical field anisotropies.

When the applied magnetic field is in the z direction, along the c axis, the vortex has axial symmetry, its cross-section is a circle, and it has a distance dependence

$$B_z(x, y) = \frac{\Phi_0}{2\pi\lambda_{ab}^2} K_0[(x^2 + y^2)^{1/2}/\lambda_{ab}]. \tag{38}$$

When the applied field is in the x direction, along the a axis, there is no longer axial symmetry, the cross-section is elliptical, and the distance dependence is more complicated (Poole *et al.*, 1995, Chap. 9).

Figure 12.7 shows vortex cross-sections for the two applied field directions. When the applied magnetic field is aligned at an oblique angle relative to the c direction, the expressions for the magnetic field and current density become very complicated, with neither the internal magnetic field nor the magnetization oriented in the same direction as B_{app}.

In the cuprates the coherence length ξ_c along the c axis is less than the average spacing between layers of copper oxide planes, and following the Lawrence–Doniach model (1971), the Josephson coupling between layers is weak. A vortex perpendicular to these layers is looked upon as a stacking of two-dimensional (2D) pancake-shaped vortices, as shown in Fig. 12.8.

F

Individual Vortex Motion

The repulsive force per unit length F/L between two vortices arises from the Lorentz force interaction $\mathbf{F} = \mathbf{J}_1 \times \mathbf{B}_2$ between the current density $\mathbf{J}_1$ from one vortex and the magnetic field $\mathbf{B}_2$ of the other:

$$\mathbf{F}/L = \int \mathbf{J}_1 \times \mathbf{B}_2 r_2 \, dr_2 \, d\phi_2. \tag{39}$$

For the hypothetical case of vortices that are far apart, $d \gg \lambda$, the current density of one vortex is fairly uniform in the neighborhood of the other, and we can make the approximation

$$\mathbf{F}/L \sim \mathbf{J}_1(d) \times \int \mathbf{B}_2 r_2 \, dr_2 \, d\phi_2, \tag{40}$$

where the integral is equal to the flux quantum Φ_0, and in the high κ approximation $\mathbf{J}_1(d)$ is given by Eq. (23). For applied fields far above the lower critical field, $B_{\text{app}} \gg B_{c1}$, nearest-neighbor vortices overlap, i.e. are much closer to each other than the penetration depth λ, and Eq. (40) does not apply.

Fig. 12.7.

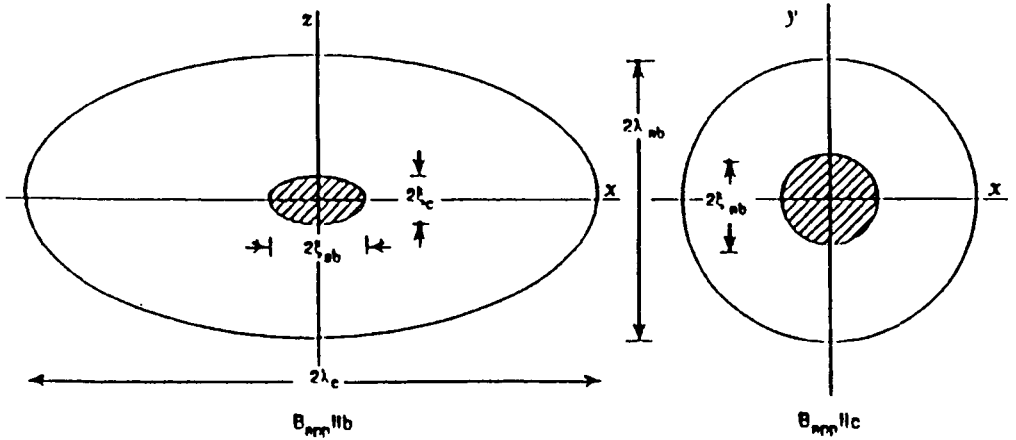

Shape of the core (shaded) and the perimeter one penetration length from the center of a vortex for the applied magnetic field along b (left) and c (right) crystallographic directions, respectively. The magnetic field is constant along each ellipse and along each circle. The figure is drawn for the condition $\lambda_c = 2\lambda_{ab} = 6\xi_{ab} = 12\xi_c$. [From Poole *et al.* (1995), p. 285.]

Fig. 12.8.

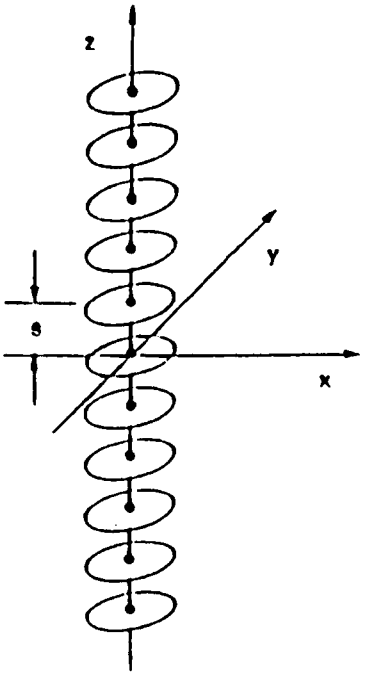

Stack of two-dimensional pancake vortices along the c direction. [From Clem (1991).]

The Lorentz force required to depin a single vortex equals the pinning force, and the force per unit length needed to produce this depinning, F_p, was found to have the temperature dependence

$$F_p(T) = F_{po}[1 - (T/T_c)]^n, \tag{41}$$

with F_{po} varying from 10^{-12} to 4×10^{-4} N/m, and n ranging from 1.5 to 3.5.

An isolated vortex $\mathbf{\Phi}_0$ in a region of constant current density $\mathbf{J}$ has its steady-state motion governed by the equation

$$\mathbf{J} \times \mathbf{\Phi}_0 - \alpha n_s e(\mathbf{v} \times \mathbf{\Phi}_0) - \beta \mathbf{v} = 0, \tag{42}$$

with the Lorentz force $\mathbf{J} \times \mathbf{\Phi}_0$ balanced by the two velocity-dependent forces, a dissipative force $\beta\mathbf{v}$ and the sideways-acting Magnus force $\alpha n_s e(\mathbf{v} \times \mathbf{\Phi}_0)$. The Magnus coefficient α has different values for different theoretical models.

G

Transport Current in a Magnetic Field

Consider a transport current of uniform density J_x flowing along a superconducting wire located in a transverse magnetic field B_z. The superconductor is considered soft, that is, the pinning forces are not strong enough to prevent flux motion, so three things can happen:

1. The current exerts the force $\mathbf{J} \times \mathbf{\Phi}_0$ on the vortices, causing them to move from one side of the wire to the other. The viscous drag $\beta \mathbf{v}$ limits this motion to a constant velocity v_ϕ, and the Magnus force causes it to occur at the angle Θ_ϕ defined by the ratio of the Magnus force to the drag force,

$$\tan \Theta_\phi = \alpha n_s e \Phi_0 / \beta. \tag{43}$$

2. Through Maxwell's equation $\nabla \times \mathbf{B} = \mu_0 \mathbf{J}$, a magnetic field gradient is established across the sample given by

$$\frac{d}{dy} B_z = \mu_0 J_x, \tag{44}$$

as depicted in Fig. 12.9.

3. By flux flow a magnetic field B moves across the sample at the constant speed v_ϕ and generates an electric field

$$\mathbf{E} = \mathbf{v}_\phi \times \mathbf{B} \tag{45}$$

Fig. 12.9.

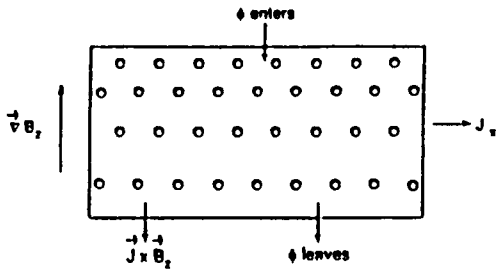

Hexagonal lattice of vortices with a gradient $\nabla B_z = dB_z(y)/dy$ in the y direction due to the application of a transport current density J_x in addition to the magnetic field B_z. The Lorentz force $\mathbf{J} \times \mathbf{B_z}$ exerted by the current on a vortex is shown. In the absence of pinning forces, the current density causes the vortices to move downward at a constant velocity, with new ones entering at the top and old ones leaving at the bottom. Strong pinning forces can prevent this motion and provide dissipationless current flow. [From Poole *et al.* (1995), p. 303.]

perpendicular to both $\mathbf{v}_\phi$ and $\mathbf{B}$ that gives rise to the ohmic loss $\mathbf{J} \cdot \mathbf{E}$,

$$\mathbf{J} \cdot \mathbf{E} = \mathbf{J} \cdot (\mathbf{v}_\phi \times \mathbf{B}), \tag{46}$$

and heat dissipation.

H

Magnetic Phase Diagram

A simplified phase diagram of the magnetic states of a Type II superconductor consists of a Meissner phase of perfect dimagnetism (absence of vortices) at the lowest temperatures, and a mixed (vortex lattice) phase at higher temperatures. The situation is actually much more complicated than this, and Fig. 12.10 presents one of the many more realistic phase diagrams that have been proposed (Yeh, 1989). This shows, in addition to the Meissner phase, a flux solid phase with vortices pinned or otherwise held in place, and flux liquid phase where many vortices are unpinned or free to move, but with dissipation. These two phases are separated by a melting line that is also called the irreversibility line T_{irr}. Flux creep can occur to its left and flux flow to its right. In the narrow region called the

Fig. 12.10.

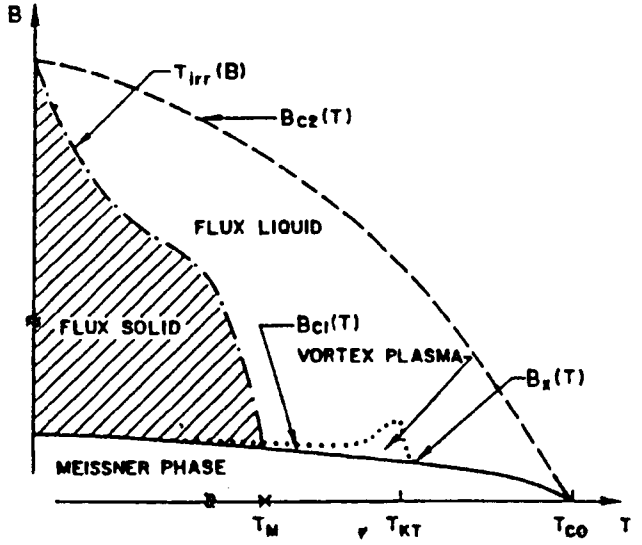

Magnetic phase diagram showing the Meissner phase, the flux solid and flux liquid regions separated by the irreversibility line (T_{irr}), the plasma phase, the lower ($B_{c1}(T)$) and upper ($B_{c2}(T)$) critical field curves, and the melting (T_M) and Kosterlitz–Thouless (T_{KT}) temperatures. [Yeh *et al.* (1989).]

plasma phase, thermal fluctuations create short-lived positively and negatively oriented vortices that are called intrinsic.

I Ellipsoids in Magnetic Fields

Until now we have ignored demagnetization effects. We have implicitly treated the case of a long cylindrical superconductor in an external magnetic field applied along its axis.

When an ellipsoid with a susceptibility χ is placed in a uniform magnetic field $\mathbf{B}_{\mathbf{app}}$ oriented along one of its principal directions, then its internal fields $\mathbf{B}_{\mathbf{in}}$ and $\mathbf{H}_{\mathbf{in}}$ are parallel to the applied field. Their values can be obtained from Eqs. (1) to (3) with the aid of the demagnetization expression

$$NB_{\text{in}} + (1 - N)\mu_0 H_{\text{in}} = B_{\text{app}}, \tag{47}$$

which relates the internal and applied fields, where N is the demagnetization factor that satisfies the normalization condition

$$N_{\text{a}} + N_{\text{b}} + N_{\text{c}} = 1 \tag{48}$$

for the three principal directions a, b, c. The largest value of N_i is for field alignment along the shortest principal axis, etc. For the common case of an ellipsoid of revolution with the c direction selected as the symmetry axis, the semimajor axes are $a = b \neq c$, and the demagnetization factors are

$$N_{\parallel} = N_{\text{c}}, \qquad N_{\perp} = N_{\text{a}} = N_{\text{b}}, \tag{49}$$

subject to the normalization condition

$$N_{\parallel} + 2N_{\perp} = 1. \tag{50}$$

Combining Eqs. (2), (3), and (47) gives

$$B_{\text{in}} = B_{\text{app}} \frac{1 + \chi}{1 + \chi N} \tag{51}$$

$$H_{\text{in}} = \frac{B_{\text{app}}/\mu_0}{1 + \chi N} \tag{52}$$

$$M = \frac{B_{\text{app}}}{\mu_0} \cdot \frac{\chi}{1 + \chi N} \tag{53}$$

for the internal fields and the magnetization expressed in terms of the applied field. We should bear in mind that the susceptibility χ is negative for a superconductor, so the denominators in these expressions become small when χ approaches -1 and N approaches 1.

Experimentalists often express the measured susceptibility χ_{exp} in terms of the applied field

$$\chi_{exp} = \mu_0 M / B_{app}, \tag{54}$$

and this is related to the true susceptibility $\chi = M/H_{in}$ as follows:

$$\chi_{exp} = \chi/(1 + N\chi), \qquad \chi = \chi_{exp}/(1 - N\chi_{exp}). \tag{55}$$

An oblate ellipsoid, that is, one flattened in the a, b plane, has $c < a$ with $N_\parallel > N_\perp$, and von Hippel (1954) gives

$$N_\parallel = \frac{1}{\varepsilon^2} - \frac{[1 - \varepsilon^2]^{1/2}}{\varepsilon^3} \sin^{-1} \varepsilon, \qquad c < a, \tag{56}$$

where the oblate eccentricity ε is

$$\varepsilon = [1 - (c^2/a^2)]^{1/2}, \qquad c < a. \tag{57}$$

For a prolate ellipsoid, that is, one elongated along its symmetry axis so $c > a$ and $N_\parallel < N_\perp$, we have

$$N_\parallel = \frac{1 - \varepsilon^2}{\varepsilon^2} \left[\frac{1}{2\varepsilon} \ln\left(\frac{1 + \varepsilon}{1 - \varepsilon} \right) - 1 \right], \qquad c > a, \tag{58}$$

where the prolate eccentricity ε is

$$\varepsilon = [1 - (a^2/c^2)]^{1/2}, \qquad c > a. \tag{59}$$

Figure 12.11 shows how the demagnetization factor depends on the c/a ratio, and Table 12.1 gives expressions for several special cases. The four small correction factors, $\delta_i \ll 1$, included in this table may be deduced from power series expansions of Eqs. (56) and (58).

J

Intermediate State of Type I Superconductor

Until now we have been discussing Type II superconductors. Let us now consider a Type I superconducting ellipsoid with a demagnetization factor N. It will exist

Fig. 12.11.

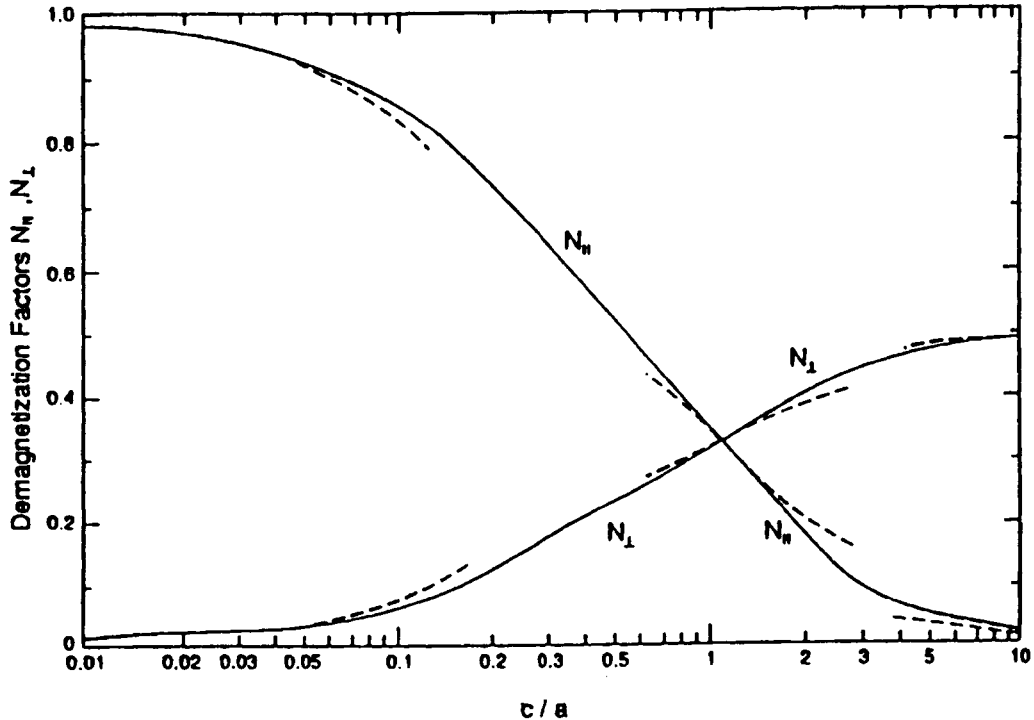

Dependence on the ratio c/a of the demagnetization factors $N_{\perp} = N_x = N_y$ perpendicular to the axis, and $N_{\parallel} = N_z$ along the axis of an ellipsoid with semimajor axes $a = b \neq c$. [From Poole *et al.* (1995), p. 327.]

Table 12.1

Demagnetizatin factors for ellipsoids of revolution with semiaxes $a = b$ and c for the cases of a disk (oblate, $c < a$), sphere ($c = a$), and rod (prolate, $c > a$) (Poole *et al.*, 1995 p. 326).

Shape	Condition	$N_\perp$	$N_\parallel$
Disk limit	$c \to 0$	0	1
Flat disk	$c \ll a$	$\frac{1}{2}\delta_1$	$1 - \delta_1$
Oblate	$c < a$	$\frac{1}{3} - \frac{1}{2}\delta_2$	$\frac{1}{3} + \delta_2$
Sphere	$c = a$	$\frac{1}{3}$	$\frac{1}{3}$
Prolate	$c > a$	$\frac{1}{3} + \frac{1}{2}\delta_3$	$\frac{1}{3} - \delta_3$
Long rod	$c \gg a$	$\frac{1}{2} - \frac{1}{2}\delta_4$	δ_4
Rod limit	$c \to \infty$	$\frac{1}{2}$	0

$\delta_1 = \pi c/2a$
$\delta_2 = (4/15)[1 - c/a]$
$\delta_3 = (4/15)[1 - a/c]$
$\delta_4 = [\frac{1}{2}\ln(2c^2/a^2) - 1](a^2/c^2)$.

in a true Meissner state excluding magnetic flux for applied fields less than $(1 - N)B_c$ with the characteristics (vide Eqs. (51) to (53))

$$B_{app} < (1 - N)B_c \tag{60}$$

$$B_{in} = 0 \tag{61}$$

$$H_{in} = B_{app}/(1 - N)\mu_0 \tag{62}$$

$$\mu_0 M = -B_{app}/(1 - N) \tag{63}$$

$$\chi = -1. \tag{64}$$

At higher applied fields, namely, $(1 - N)B_c \leq B_{app} \leq B_c$, the material is in the intermediate state in which it splits into domains of normal material with $\chi \approx 0$ embedded in pure superconducting regions with $\chi = -1$. The boundary separating normal from superconducting regions has the approximate thickness

$$d_{bound} \approx (\xi - \lambda), \tag{65}$$

and the overall energy density per unit area of this boundary layer is

$$E_{bound} = (B_c^2/2\mu_0)d_{bound}. \tag{66}$$

The domains of normal material have dimensions and separations that are much greater than d_{bound}. The fields averaged over these regions of normal, boundary

Fig. 12.12.

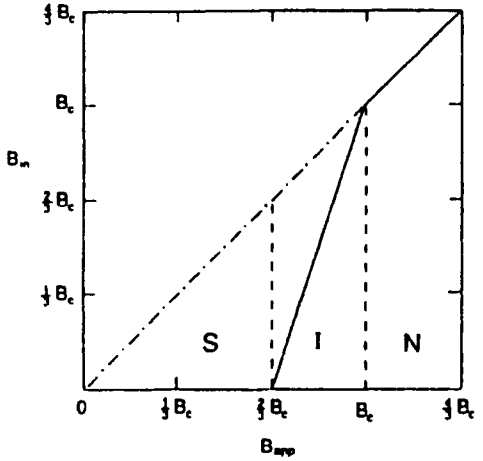

Internal magnetic field B_{in} in the Meissner (S) and intermediate (I) states of a Type I superconducting sphere ($N = 1/3$) as a function the applied field B_{app} [Eqs. (61) and (68)]. Solid lines represent the function being plotted; vertical dashed lines indicate the boundaries of the Meissner, intermediate, and normal regions. [From Poole *et al.* (1995), p. 347.]

layer, and superconducting material in the intermediate state of an ellipsoid are given by

$$(1 - N)B_c < B_{app} < B_c \tag{67}$$

$$B_{in} = \frac{1}{N}[B_{app} - (1 - N)B_c] \tag{68}$$

$$H_{in} = B_c/\mu_0 \tag{69}$$

$$\mu_0 M = -\frac{1}{N}(B_c - B_{app}) \tag{70}$$

$$\chi = -\frac{1}{N}\left(1 - \frac{B_{app}}{B_c}\right). \tag{71}$$

The internal field B_{in} (61) and (68) is plotted vs the applied field B_{app} in Fig. 12.12 for the case of a sphere ($N = 1/3$).

K

Ac Susceptibility

An ac field $B_{ac}(t) = B_0 \cos \omega t$ applied to a superconductor causes the magnetization $M(t)$ to trace out a magnetic hysterisis loop during every cycle of the applied field. During the cycle $M(t)$ does not follow $B_{ac}(t)$ directly, but tends to lag, to distort in shape, and to shift in phase relative to the applied $B_{ac}(t)$, so it acquires an out-of-phase component that varies as $\sin \omega t$. To account for this we define in-phase dispersion χ' and out-of-phase (quadrature) absorption χ'' susceptibilities (Matsumoto *et al.*, 1991):

$$\chi' = \frac{\mu_0}{\pi B_0} \int M(t) \cos \omega t \, d\omega t \tag{72}$$

$$\chi'' = \frac{\mu_0}{\pi B_0} \int M(t) \sin \omega t \, d\omega t. \tag{73}$$

Figure 12.13 presents the temperature dependences of χ' and χ'' determined for several values of the ac field amplitude applied at the frequency $\omega/2\pi = 73$ Hz

Fig. 12.13.

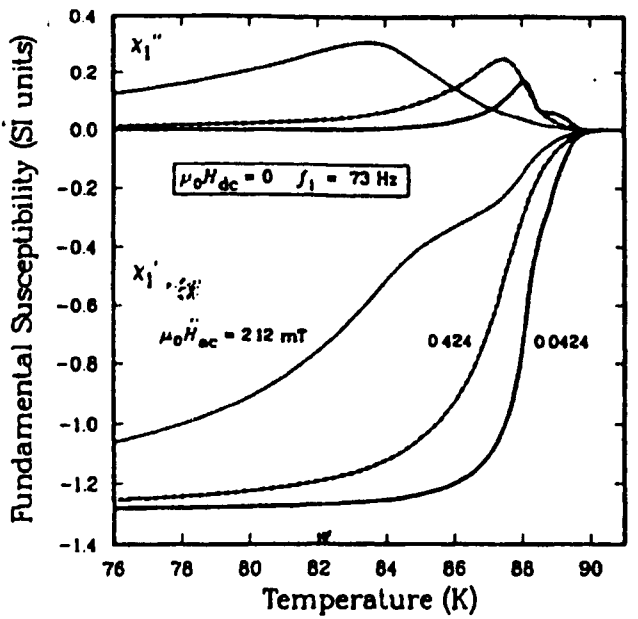

Real (χ') and imaginary (χ'') components of the susceptibility of $YBa_2Cu_3O_{7-\delta}$ measured in the applied ac magnetic fields $\mu_0 H_{ac} = 0.0424$, 0.424, and 2.12 mT as a function of the temperature below T_c for the frequency 73 Hz. For this experiment no dc field was present, and the data were not corrected for the demagnetization factor. [Ishida and Goldfarb (1990).]

with no dc field present. A simultaneously applied dc field affects the temperature dependence of χ' and χ''.

References

J. R. Chem, *Phys. Rev. B* **43**, 7837 (1991).
T. Ishida and R. B. Goldfarb, *Phys. Rev. B* **41**, 8937 (1990).
W. E. Lawrence and S. Doniach, in *Proc. 12th Int. Conf. Low Temp. Phys. Kyoto, 1970* (E. Kanda, Ed.), p. 361. Keigaku, Tokyo, 1971.
Y. Matsumoto, M. Katada, and T. Nishida, *Physica C* **185**, 1229 (1991).
C. P. Poole, Jr., H. A. Farach, and R. J. Creswick, *Superconductivity.* Academic Press, New York, 1995; vide Chapters 9–12.
S. Senoussi, M. Oussena, and S. Hadjoudi, *J. Appl. Phys.* **63**, 4176 (1988).
A. R. von Hippel, *Dielectrics and Waves*, p. 255. MIT Press, Cambridge, MA, 1954.
N.-C. Yeh, *Phys. Rev. B.* **40**, 4566 (1989); see also *ibid.* **39**, 9708 (1989).

This Page Intentionally Left Blank

Chapter 13

Mechanical Properties

Ronald G. Munro
Ceramics Division, National Institute of Standards and Technology, Gaithersburg, Maryland

ISBN: 0-12-561460-8
$30.00

HANDBOOK OF SUPERCONDUCTIVITY

A

Introduction

Mechanical properties are important to the study and application of superconductors in three respects: (1) scientifically through the electron–phonon interaction; (2) technologically through processing conditions and product design parameters; and (3) economically through the durability and reliability of the manufactured products. In all cases, superconductors require cryogenic environments within which the material may be required to survive long-term exposure to significant electromagnetic and thermomechanical stresses. Poor mechanical properties or low structural reliability can result in premature failure of these materials during normal service conditions. If the material is fragile, stresses that arise from handling during routine production operations can introduce deleterious cracks in the material. Knowledge of the mechanical properties of the material can be particularly helpful in considering safeguards against the occurrence of such situations. More beneficially, it may be possible to exploit that same knowledge to produce an improved material, even, perhaps, with tailored properties. For example, the elastic–plastic deformation properties can be exploited during the material processing stages to produce more highly textured (grain aligned) materials that tend to achieve higher critical current densities.

In the following text, the elastic properties are discussed first, followed by discussions of flexural and tensile strengths, hardness, and fracture toughness. In each case, basic terminology, critical issues, measurement methods, and tables of property data are presented. To facilitate comparisons of results, all of the data tables have a similar structure, although some variation occurs in the column headers to emphasize the variables and measurement features that are important to the determination of specific property values. The first column in each table identifies the material using the abbreviations defined by Table 13.1. The structure of each table is otherwise self-explanatory.

B

Elastic Properties

The elastic properties of superconducting materials are important to the theoretical understanding of the phenomenon of superconductivity, as well as being important to its practical application. In the BCS theory (Bardeen *et al.*, 1957) of superconductivity, the electron–lattice interaction is crucial to the formation of superconducting states. Since the long-wavelength phonon spectrum is intimately related to the elastic properties of the material, it follows that the superconducting characteristics also must be related to the elastic properties of the material. In the

Table 13.I.

Material abbreviations.

Phase	Nominal formula
Bi : 2212	$Bi_2Sr_2CaCu_2O_{8+x}$
Bi(Pb) : 2223	$Bi_{2-y}Pb_ySr_2Ca_2Cu_3O_{10+x}$
Dy : 123	$DyBa_2Cu_3O_{7-x}$
Eu : 123	$EuBa_2Cu_3O_{7-x}$
Gd : 123	$GdBa_2Cu_3O_{7-x}$
Ho : 123	$HoBa_2Cu_3O_{7-x}$
La(Sr) : 21	$La_{2-y}Sr_yCuO_4$
Nd(Ce) : 21	$Nd_{2-y}Ce_yCuO_{4-x}$
Sm : 123	$SmBa_2Cu_3O_{7-x}$
Tl : 2212	$Tl_2Ba_2CaCu_2O_{8+x}$
Tm : 123	$TmBa_2Cu_3O_{7-x}$
Y : 123	$YBa_2Cu_3O_{7-x}$

BCS theory, the critical temperature, T_c, is related to the Debye temperature, Θ_D, of the lattice and the electron–phonon interaction parameter (Poole *et al.*, 1988), λ:

$$T_c \approx 1.134\Theta_D \exp\left(-\frac{1}{\lambda}\right). \tag{1}$$

Anderson (1965) showed that the Debye temperature can be expressed as

$$\Theta_D = V_m\left(\frac{h}{k_B}\right)\left(\frac{3qN_A\rho}{4\pi M}\right)^{1/3}, \tag{2}$$

where h is Planck's constant, k_B is Boltzmann's constant, q is the number of atoms per molecule, N_A is Avogadro's number, ρ is the density, M is the molar mass, and V_m is a mean sound velocity computed as

$$\frac{1}{V_m} = \left[\frac{1}{3}\left(\frac{2}{V_S^3} + \frac{1}{V_L^3}\right)\right]^{1/3}, \tag{3}$$

where V_S and V_L are the shear and longitudinal sound velocities, respectively. For high-T_c mateirals, $V_L \approx 2V_S$; hence, $V_m \approx V_S$. Given that $V_S = (G/\rho)^{1/2}$, where G is the shear modulus, it follows approximately that

$$\Theta_D \approx \left(\frac{h}{k_B}\right)\left(\frac{3qN_A}{4\pi\Omega_{mol}}\right)^{1/3}\left(\frac{G}{\rho}\right)^{1/2}, \tag{4}$$

where Ω_{mol} is the molar volume; hence, the critical temperature should vary as the square root of the shear modulus,

$$T_c \propto G^{1/2}. \tag{5}$$

a. Terms and Basic Relations

When a material is subjected to a stress, σ (force per unit area), the material undergoes a deformation. For a given direction in a solid material, the engineering tensile strain, ε, of the material is defined (Timoshenko, 1940) as the relative change of a linear dimension in that direction:

$$\varepsilon = \frac{L_\sigma - L_0}{L_0}, \tag{6}$$

where L_σ is the length of a linear dimension of a material segment after the application of the stress, and L_0 is the length of that material segment before deformation.

The elastic deformation of a material refers to a limited domain of stress and strain in which the material behaves reversibly. In this domain, Fig. 13.1, the elastic response of the material is described by Hooke's law, that is, the tensile stress, σ, is proportional to the strain:

$$\sigma = E\varepsilon. \tag{7}$$

The proportionality constant, E, is known as the elastic modulus (also known as Young's modulus, modulus of elasticity, coefficient of elasticity, modulus of

Fig. 13.1.

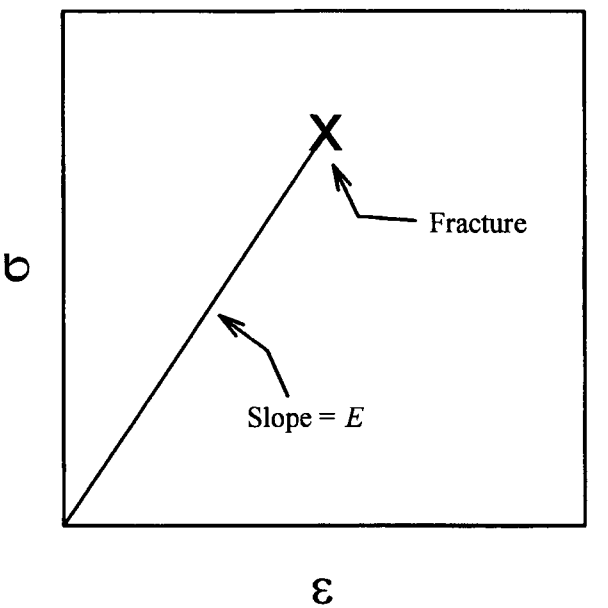

Schematic illustration of the relation between stress σ and strain ε for a brittle material. Such materials are said to be linearly elastic up to the point of failure (yield point) where the material fractures.

extensibility, stretch modulus, tensile modulus, and numerous other less common terms).

In general, when a tensile or normal stress is applied, the deformation of the material involves a strain that is transverse to the direction of the applied stress (called variously the transverse or lateral strain), as well as the strain in the direction that is parallel to the applied stress (called variously the tensile, axial, or longitudinal strain). For example, the diameter of a cylindrical rod tends to decrease as the rod is stretched along its length, as illustrated in Fig. 13.2. The negative of the ratio of the lateral strain to the axial strain is called Poisson's ratio, v:

$$v = -\frac{\varepsilon_{\text{lateral}}}{\varepsilon_{\text{axial}}}. \tag{8}$$

Taking Poisson's ratio into account, the strain, ε_x, in the x direction depends on the stress components in the x, y, and z directions. Hence, the generalized Hooke's law for ε_x becomes

$$\varepsilon_x = \frac{1}{E}[\sigma_x - v(\sigma_y + \sigma_z)], \tag{9}$$

and similarly for ε_y and ε_z with appropriate permutations of the indices.

For a homogeneous, isotropic material, E and v completely describe its elastic properties. However, it is sometimes convenient to consider another elastic property called the bulk modulus, $B = -V(dP/dV)$, where V is the volume and P is an applied hydrostatic pressure. For this case, the volumetric strain is $dV/V = \varepsilon_x + \varepsilon_y + \varepsilon_z$ to first order in the strain, and the stresses are $\sigma_x = \sigma_y = \sigma_z = -P$. Hence,

$$B = \frac{E}{3(1-2v)}. \tag{10}$$

Fig. 13.2.

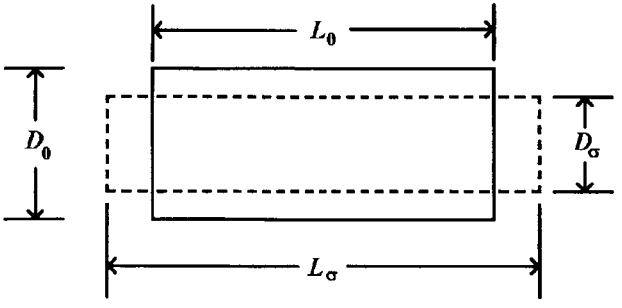

An illustration of tensile strain with lateral contraction.

Comparable quantities can be defined for conditions of shear stress, τ, which results in a shear deformation, γ. Hooke's law for shear conditions is

$$\tau = G\gamma, \tag{11}$$

where G is called the shear modulus (also called the rigidity modulus). For a homogeneous, isotropic material, G is related to E and ν according to

$$G = \frac{E}{2(1+\nu)}. \tag{12}$$

Within the realm of linear elasticity, $E > 0$ and $G > 0$. The definition of the bulk modulus also requires $B > 0$. Hence, from Eqs. (10) and (12), the bounds of Poisson's ratio are readily seen to be $-1 \leq \nu \leq 1/2$. In practice, $0 < \nu < 1/2$ for most materials.

In some cases, it is more convenient to express E and ν in terms of B and G:

$$E = \frac{9BG}{3B+G} \tag{13}$$

$$\nu = \frac{3B-2G}{6B+2G}. \tag{14}$$

b. Measurement Methods

Several different types of measurement methods are used to determine the elastic properties of solid materials: direct stress–strain measurements in tensile tests (ASTM D3379), static pressure–volume measurements using crystallographic techniques, ultrasonic techniques (Krautkrämer and Krautkrämer, 1990), and resonance measurements (ASTM C 1198). The tensile tests use strain gauges, extensometers, and calibrated loads to determine the elastic properties via direct applications of Hooke's law. The crystallographic methods use X-ray or neutron diffraction to determine the change in the lattice parameters as a function of an applied stress and then calculate the bulk modulus from the pressure and volume relation, often using a model isothermal equation of state (Munro *et al.*, 1984). The most widely used methods involve ultrasonic techniques that can provide a complete determination of the elastic properties in nondestructive measurements.

Ultrasonic techniques commonly measure the longitudinal and shear sound velocities, V_L and V_S, from which the elastic properties may be calculated if the mass density, ρ, is also known. The quantities most simply related to the sound velocities are the shear modulus and the bulk modulus:

$$G = \rho V_S^2 \tag{15}$$

$$B = \rho\left[V_L^2 - \tfrac{4}{3}V_S^2\right]. \tag{16}$$

Given G and B, Eqs. (13) and (14) can be used to evaluate E and ν.

c. Corrections for Porosity

Porosity in the range of 15 to 40% is quite common for ceramic superconductors. A considerable effort has been made in the literature to normalize the measured results to the limiting condition of zero porosity. Both empirical models and computations based on elasticity theory have been used. The empirical methods generally are extrapolations based on trend analyses and least squares fitting techniques. Early investigations suggested that the elastic and shear moduli of ceramics decreased exponentially with increasing porosity (Spriggs and Brissette, 1962),

$$X = X_0 e^{-a_X p}, \tag{17}$$

where X is either E or G; X_0 is the modulus at zero porosity; $p = 1 - \rho/\rho_{\max}$ is the volume fraction of porosity for a material whose density, ρ, is less than the theoretical maximum density, $\rho_{\max}$; and a_X is an empirical fitting parameter. When comparable trends are found for the elastic and shear moduli, it follows from Eqs. (12) and (17) that Poisson's ratio should vary approximately linearly with the porosity,

$$\nu = \nu_0 - \eta p; \tag{18}$$

where $\eta \approx (1 + \nu_0)(a_E - a_G)$.

Other studies have reported linear (Hasselman and Fulrath, 1964),

$$X = X_0 - b_X p, \tag{19}$$

and power-law results (Ishani and Cohen, 1967; Wagh *et al.*, 1993),

$$X = X_0(1 - p^{2/3}) \tag{20}$$

$$X = X_0(1 - p)^q, \tag{21}$$

where b_X and q are fitting parameters.

Applications of elasticity theory have generally assumed spherical voids or inclusions dispersed in an otherwise homogeneous, isotropic medium. Differences among the various models have resulted from the specific approximations that are invoked to obtain useful solutions. Mackenzie (1950) applied elasticity theory to a spherical void surrounded by a spherical shell of matrix material that was, in turn, surrounded by a self-consistent bulk medium representing the macroscopic ensemble of matrix material and voids; estimates for the bulk modulus and the shear modulus were found in the forms

$$\frac{1}{B} = \frac{1}{B_0(1-p)} + \frac{3p}{4G_0(1-p)} \tag{22}$$

$$\frac{G_0 - G}{G_0} = 5p\frac{(3B_0 + 4G_0)}{(9B_0 + 8G_0)}, \tag{23}$$

in which higher order terms in p were neglected.

Uemura and Takayanagi (1966) developed expressions for the shear modulus and Poisson's ratio in an elastic two-phase system; Reddy *et al.* (1995), taking the inclusions to be voids, applied those expressions and found

$$\frac{G}{G_0} = \frac{(7 - 5\nu_0)(1 - p)}{15(1 - \nu_0)p + (7 - 5\nu_0)(1 - p)} \tag{24}$$

$$\frac{B}{B_0} = \frac{4G_0(1 - p)}{4G_0 + 3B_0 p}. \tag{25}$$

Ledbetter *et al.* (Ledbetter and Datta, 1986; Ledbetter *et al.*, 1994) applied scattering theory to a homogeneous composite material consisting of a random distribution of spheroidal particles in a continuum matrix. By considering the inclusions to be massless voids with zero elastic resistance to shear and dilatation, the shear and bulk moduli were expressed as

$$G_0 = \frac{1}{2A_1}[-A_2 + (A_2^2 - 4A_1A_3)^{1/2}] \tag{26}$$

$$B_0 = \frac{4G_0B}{4(1 - p)G_0 - 3pB} \tag{27}$$

$$A_1 = \tfrac{8}{3}(1 - p), \qquad A_2 = (3 - 2p)B - \left(\tfrac{8}{3} + 4p\right)G, A_3 = -3(1 + p)BG. \tag{28}$$

d. Property Data

Data for elastic properties are given in Tables 13.2 to 13.5. The elastic modulus did not exceed 200 GPa for any material in Table 13.2, and the typical value was on the order of only 100 GPa. The Bi : 2212 and Bi(Pb) : 2223 materials tended to have an elastic modulus of less than 50 GPa, with the exception of one study (Chang *et al.*, 1993) that found highly anisotropic results for highly textured Bi : 2212 (nearly 120 GPa in the *ab*-plane and about 45 GPa along the *c*-axis). Values of Poisson's ratio, Table13.5, were in the range from 0.1 to 0.3.

C

Strength

High-T_c superconductors are predominantly brittle materials; that is, in a plot of tensile stress vs strain, as illustrated schematically in Fig. 13.1, there is a critical strain at which the material fractures. This situation is distinct from the behavior of metals that deform plastically prior to the occurrence of material failure. Conceptually, brittle fracture is the catastrophic propagation of a crack through continguous regions of a material body resulting in the rupture of that body into

Table 13.2.

Elastic modulus (E).

Phase	Relative Density (%)	T [K]	Elastic modulus (GPa)	Measurement method	Notes	Ref.
Bi : 2212	74	4.2	40	Ultrasound		Dominec *et al.* (1992)
Bi : 2212	82	300	38.8	Ultrasound		Yusheng *et al.* (1990)
Bi : 2212	95	296	44.2	Ultrasound	$P = 0$ MPa; c-axis; highly textured, grain aligned ceramic	Chang *et al.* (1993)
			45.7		$P = 50$ MPa; c-axis	
			46.6		$P = 100$ MPa; c-axis	
			47.5		$P = 140$ MPa; c-axis	
			118.2		$P = 0$ MPa; ab-plane	
			118.9		$P = 50$ MPa; ab-plane	
			119.6		$P = 100$ MPa; ab-plane	
			120		$P = 140$ MPa; ab-plane	
Bi : 2212		270	20	Bend test	Described as porous	Tritt *et al.* (1991)
Bi(Pb) : 2223		296	185	Three-point bend	$Bi_{1.2}Pb_{0.8}Sr_2Ca_2Cu_3O_{10+x}$	Alford *et al.* (1990)
Bi(Pb) : 2223	59	296	14	Ultrasound	$Bi_{1.7}Pb_{0.3}Sr_2Ca_2Cu_3O_{10+x}$, $\rho = 3.73$ g/cm^3, $\rho_{th} = 6.27$ g/cm^3	Topare *et al.* (1995)
	100		32.2		Corrected to zero porosity	
Bi(Pb) : 2223		296	40	Three-point bend	$Bi_{1.7}Pb_{0.3}Sr_2Ca_2Cu_3O_{10+x}$	Low *et al.* (1995)
Bi(Pb) : 2223	91	296	63.7	Ultrasound	$Bi_{1.7}Pb_{0.3}Sr_2Ca_2Cu_3O_{10+x}$, $\rho = 4.989$ g/cm^3	Muralidhar *et al.* (1992)
Bi(Pb) : 2223		296	124	Tensile	$Bi_{1.8}Pb_{0.3}Sr_2Ca_{1.9}Cu_3O_{10+x}$	Yuan *et al.* (1996)
Bi(Pb) : 2223	69	13	35.5	Ultrasound	$\rho = 4.35$ g/cm^3	Yusheng *et al.* (1990)
		77	35.2			
		134	35.1			
		201	34.7			
		205	34.6			
		275	34.1			
		290	34			

(*continued*)

Table 13.2. (*continued*)

Phase	Relative Density (%)	T [K]	Elastic modulus (GPa)	Measurement method	Notes	Ref.
Dy : 123	74	296	48.2	Ultrasound		Reddy *et al.* (1994)
	100		95.5		Corrected to zero porosity	
Eu : 123	69	295	52.6	Ultrasound	$\rho = 4.793$ g/cm^3; $\rho_{th} = 6.97$ g/cm^3	Al-Kheffaji *et al.* (1989)
Gd : 123	83	296	68.2	Ultrasound	$\rho = 5.8$ g/cm^3; $\rho_{th} = 7.014$ g/cm^3; $GdBa_2Cu_3O_{6.758}$	Reddy *et al.* (1994)
	100		102.3		Corrected to zero porosity	
Gd : 123	79	295	73.3	Ultrasound		Al-Kheffaji *et al.* (1989)
Gd : 123	78	4.2	154	Ultrasound	$\rho_{th} = 7.138$ g/cm^3	Almond *et al.* (1989)
Gd : 123	78	295	73.4	Ultrasound	$P = 0$ MPa	Cankurtaran *et al.* (1989)
			73.7		$P = 50$ MPa	
			74		$P = 100$ MPa	
			74.3		$P = 150$ MPa	
La(Sr) : 21		295	121	Ultrasound	$\rho = 6.000$ g/cm^3	Fanggao *et al.* (1991)
La(Sr) : 21		19	109	Ultrasound	$\rho = 6.22$ g/cm^3	Yusheng *et al.* (1990)
		37	109			
		56	111			
		78	116			
		98	121			
		126	125			
		151	126			
		188	126			
		227	125			
		261	125			
		270	125			
Nd(Ce) : 21	88	295	128	Ultrasound	$\rho = 6.481$ g/cm^3	Fanggao *et al.* (1991)
Sm : 123	77	296	52	Ultrasound		Reddy *et al.* (1994)
	100		91.8		Corrected to zero porosity	
Tm : 123	81	296	48.5	Ultrasound		Reddy *et al.* (1994)
	100		76		Corrected to zero porosity	

Y:123	89	11	95.8	Ultrasound	$\rho = 5.69$ g/cm^3; $\rho_{th} = 6.37$ g/cm^3	Yusheng *et al.* (1990)
		87	95.1			
		150	94			
		200	93			
		252	92.4			
		288	92.4			
Y:123	87	296	142	Three-point bend		Alford *et al.* (1988)
	97		165			
Y:123	60	296	5	Three-point bend		Low *et al.* (1994)
Y:123	100	296	151	Model analysis		Bridge (1990)
Y:123	94	5	94	Ultrasound	$\rho = 5.985$ g/cm^3	Almond *et al.* (1987)
		36	92.9			
		50	92.3			
		73	91.4			
		90	91.6			
		110	91.6			
		126	91.5			
		144	91.2			
		164	90.4			
		186	89.1			
		205	88.5			
Y:123	62	296	31.2	Ultrasound	$\rho = 4.1$ g/cm^3	Reddy *et al.* (1994)
	100		91.5		Corrected to zero porosity	
Y:123	79	296	85.5	Ultrasound	Specimen Y1	Reddy *et al.* (1993)
	100		143		Corrected to zero porosity	
	84		92.2		Specimen Y2	
	100		134		Corrected to zero porosity	
Y:123	82	295	78	Ultrasound	Y1, $\rho = 5.199$ g/cm^3	Al-Kheffaji *et al.* (1989)
	94		116		Y2, $\rho = 5.985$ g/cm^3	
Y:123	88	295	95.2	Ultrasound	$\rho = 5.56$ g/cm^3	Wang *et al.* (1995)
	100		125.5		Corrected to zero porosity	

(*continued*)

Table 13.2. (*continued*)

Phase	Relative Density (%)	T [K]	Elastic modulus (GPa)	Measurement method	Notes	Ref.
Y:123	87	295	114	Ultrasound		Ledbetter *et al.* (1994)
	100		148		Corrected to zero porosity	
Y:123	90	296	221	Indentation	Nanoindentations of single grains	Martinez *et al.* (1992)
Y:123	100	296	190	Three-point bend	$T_c = 92$ K	Alford *et al.* (1990)
Y:123	88	295	95.2	Ultrasound	$YBa_2Cu_3O_{6.94}$; $\rho = 5.56$ g/cm^3	Cankurtaran *et al.* (1994)
	100		125		Corrected to zero porosity	
Y:123	100	296	151	Analysis (ultrasound)	Single crystal	Martinez *et al.* (1992)
Y:123		296	154	Vickers' indentation		Lucas *et al.* (1991)
Y:123	85	296	106	Ultrasound	Grain size = 2 μm	Suasmoro *et al.* (1992)
	86		101		Grain size = 5 μm	
	93		60		Grain size = 13 μm	
Y:123	96	296	104	Ultrasound		Cankurtaran *et al.* (1992)
	100		113		Corrected to zero porosity	
Y:123	95	296	104	Ultrasound	$\rho = 6.070$ g/cm^3	Cankurtaran and Saunders (1992a)
Y:123	100	296	143	Indentation	Direction= (001); single crystal	Goyal *et al.* (1991)
	100		182		Direction= (010)	
Y:123	72	5	51.2	Ultrasound	$\rho = 4.433$ g/cm^3; $\rho_{th} = 6.171$ g/cm^3, $YBa_2Cu_3O_{6.2}$	Lin *et al.* (1993)
	100		91.3		Corrected to zero porosity	
	72		56.6		$\rho = 4.523$ g/cm^3; $\rho_{th} = 6.304$ g/cm^3; $YBa_2Cu_3O_{6.7}$	
	100		101.1		Corrected to zero porosity	
	71		57.8		$\rho = 4.528$ g/cm^3; $\rho_{th} = 6.339$ g/cm^3, $YBa_2Cu_3O_{6.8}$	
	100		103.9		Corrected to zero porosity	
	72		57.4		$\rho = 4.553$ g/cm^3; $\rho_{th} = 6.363$ g/cm^3, $YBa_2Cu_3O_{6.9}$	
	100		102.9		Corrected to zero porosity	
Y:123	77	296	78.4	Ultrasound	$\rho = 4.9$ g/cm^3	Pal-Val *et al.* (1992)

Table 13.3.

Shear modulus (G).

Phase	Relative Density (%)	T [K]	Shear modulus (GPa)	Measurement method	Notes	Ref.
Bi : 2212	82	300	16.1	Ultrasound		Yusheng *et al.* (1990)
Bi(Pb) : 2223	59	296	5	Ultrasound	$Bi_{1.7}Pb_{0.3}$, $\rho = 3.73$ g/cm^3, $\rho_{th} = 6.27\ g/cm^3$	Topare *et al.* (1995)
	100		10.7		Corrected to zero porosity	
Bi(Pb) : 2223	69	9	15.3	Ultrasound	$\rho = 4.35$ g/cm^3	Yusheng *et al.* (1990)
		67	15.2			
		134	15			
		201	14.8			
		241	14.7			
		272	14.5			
		290	14.4			
Dy : 123	74	296	18.9	Ultrasound		Reddy *et al.* (1994)
	100		38.4		Correced to zero porosity	
Eu : 123	69	295	21.7	Ultrasound	$\rho = 4.793$ g/cm^3; $\rho_{th} = 6.97$ g/cm^3	Al-Kheffaji *et al.* (1989)
Gd : 123	83	296	26.6	Ultrasound	$\rho = 5.8$ g/cm^3, $\rho_{th} = 7.014$ g/cm^3, $O_{6.758}$	Reddy *et al.* (1994)
	100		39.9		Corrected to zero porosity	
Gd : 123	79	295	29.5	Ultrasound		Al-Kheffaji *et al.* (1989)
Gd : 123	78	4.2	64.5	Ultrasound	$\rho_{th} = 7.138$ g/cm^3	Almond *et al.* (1989)
Gd: 123	78	295	29.52	Ultrasound	$P = 0$ MPa	Corkurtaron *et al.* (1989)
			29.58		$P = 50$ MPa	
			29.63		$P = 100$ MPa	
			29.68		$P = 150$ MPa	
La(Sr) : 21		295	75.3	Ultrasound	$\rho = 6.000$ g/cm^3	Fanggao *et al.* (1991)
La(Sr) : 21		16	43.5	Ultrasound	$\rho = 6.22$ g/cm^3	Yusheng *et al.* (1990)
		34	43.3			
		53	44.1			

(*continued*)

Table 13.3. (*continued*)

Phase	Relative Density (%)	T [K]	Shear modulus (GPa)	Measurement method	Notes	Ref.
		75	46			
		88	48.1			
		114	49.7			
		142	50.6			
		185	50.7			
		233	50.4			
		261	50.3			
		270	50.4			
Nd(Ce):21	88	295	68	Ultrasound	$\rho = 6.481$ g/cm^3	Farggao *et al.* (1991)
Sm:123	77	296	20	Ultrasound		Reddy *et al.* (1994)
	100		35.3		Corrected to zero porosity	
Tm:123	81	296	19.1	Ultrasound		Reddy *et al.* (1994)
	100		30		Corrected to zero porosity	
Y:123	89	15	40.2	Ultrasound	$\rho = 5.69$ g/cm^3	Yusheng *et al.* (1990)
		79	39.9			
		139	39.5			
		207	38.9			
		252	38.5			
		291	38.5			
Y:123	100	296	58.5	Model analysis		Bridge (1990)
Y:123	94	5	40	Ultrasound	$\rho = 5.985$ g/cm^3	Almond *et al.* (1987)
		36	39.5			
		50	39.3			
		73	39			
		90	39			
		110	39			
		126	38.9			

		144	38.7			
		164	38.2			
		186	37.5			
		205	37.4			
Y: 123	62	296	8.6	Ultrasound	$\rho = 4.1$ g/cm^3	Reddy *et al.* (1994)
	100		41.6		Corrected to zero porosity	
Y: 123	79	296	34.2	Ultrasound	Specimen Y1	Reddy *et al.* (1993)
	100		58.6		Corrected to zero porosity	
	84		38.1		Specimen Y2	
	100		57.1		Corrected to zero porosity	
Y: 123	82	295	32.7	Ultrasound	Y1, $\rho = 5.199$ g/cm^3	Al-Kheffaji *et al.* (1989)
	94		50.1		Y_2, $\rho = 5.985$ c/cm^3	
Y: 123	88	295	37.3	Ultrasound	$\rho = 5.56$ g/cm^3	Wang *et al.* (1995)
	100		48.6		Corrected to zero porosity	
Y: 123	87	295	45.6	Ultrasound		Ledbetter *et al.* (1994)
	100		59		Corrected to zero porosity	
Y: 123	96	280	46.2	Ultrasound	$T_c = 92$ K; $\rho = 6.07$ g/cm^3;	Cankurtaran and Saunders (1992b)
		265	46.4		hysteresis with respect to temperature	
		251	46.4			
		232	46.6			
		214	47			
		204	47.4			
		200	48.8			
		197	51.4			
		195	53.4			
		191	57.1			
		187	58.9			
		186	59.7			
		170	60.7			
		148	61.5			
		121	62.5			

(*continued*)

Table 13.3. (*continued*)

Phase	Relative Density (%)	T [K]	Shear modulus (GPa)	Measurement method	Notes	Ref.
		100	62.9			
		74	63.4			
		51	63.6			
		29	63.8			
		13	63.8			
		19	63.8			
		49	63.6			
		70	63.4			
		100	62.9			
		121	62.3			
		148	61.5			
		174	60.1			
		189	59.3			
		209	57.9			
		224	56.5			
		228	54.7			
		230	50.6			
		234	48.4			
		235	47.2			
		239	46.6			
		251	46.6			
		263	46.4			
		281	46.4			
Y:123	88	295	37.3	Ultrasound	$O_{6.94}$; $\rho = 5.56$ g/cm^3	Cankurtaran *et al.* (1994)
	100		48.5		Corrected to zero porosity	
Y:123	100	296	59	Analysis (ultrasound)	Single crystal	Ledbetter and Lei (1991)
Y:123	90	296	68.5	Ultrasound	$\rho = 5.72$ g/cm^3	Fanggao *et al.* (1991)

Y:123	96	296	45	Ultrasound		Cankurtaran *et al.* (1992)
	100		49		Corrected to zero porosity	
Y:123	72	5	21.5	Ultrasound	$\rho = 4.433$ g/cm^3; $\rho_{th} = 6.171$ g/cm^3, $YBa_2Cu_3O_{6.2}$	Lin *et al.* (1993)
	100		38.4		Corrected to zero porosity	
	72		23.6		$\rho = 4.523$ g/cm^3; $\rho_{th} = 6.304$ g/cm^3, $YBa_2Cu_3O_{6.7}$	
	100		42.2		Corrected to zero porosity	
	71		24.2		$\rho = 4.528$ g/cm^3; $\rho_{th} = 6.339$ g/cm^3, $YBa_2Cu_3O_{6.8}$	
	100		43.5		Corrected to zero porosity	
	72		24.2		$\rho = 4.553$ g/cm^3; $\rho_{th} = 6.363$ g/cm^3, $YBa_2Cu_3O_{6.9}$	
	100		43.6		Corrected to zero porosity	
Y:123	77	296	28.5	Ultrasound	$\rho = 4.9$ g/cm^3, grain size= 10 μm	Pal-Val *et al.* (1992)

Table 13.4.

Bulk modulus (B).

Phase	Relative Density (%)	T [K]	Bulk modulus (GPa)	Measurement method	Notes	Ref.
Bi : 2212	82	300	21.9	Ultrasound		Yusheng *et al.* (1990)
Bi(Pb) : 2223	91	296	33.2	Ultrasound	$Bi_{1.7}Pb_{0.3}$, $\rho = 4.989$ g/cm^3	Muralidhar *et al.* (1992)
Bi(Pb) : 2223	69	25	17.2	Ultrasound	$\rho = 4.35$ g/cm^3	Yusheng *et al.* (1990)
		50	17.2			
		100	17.2			
		150	17.2			
		175	17.3			
		200	17.4			
		225	17.3			
		250	17.3			
		270	17.4			
		290	17.4			
Dy : 123	100	296	61.5	Ultrasound	Corrected to zero porosity	Reddy *et al. (1994)*
Eu : 123	69	295	30.4	Ultrasound	$\rho = 4.793$ g/cm^3; $\rho_{th} = 6.97$ g/cm^3	Al-Kheffaji *et al.* (1989)
Gd : 123	83	296	51.7	Ultrasound	$\rho = 5.8$ g/cm^3, $\rho_{th} = 7.014$ g/cm^3, $O_{6.758}$	Reddy *et al.* (1994)
	100	296	78.2		Corrected to zero porosity	
Gd : 123	79	295	47.4	Ultrasound		Al-Kheffaji *et al.* (1989)
Gd : 123	78	4.2	84.6	Ultrasound	$\rho_{th} = 7.138$ g/cm^3	Almond *et al.* (1989)
Gd : 123	78	295	47.5	Ultrasound	$P = 0$ MPa	Cankurtaran *et al.* (1989)
			48.3		$P = 50$ MPa	
			49.1		$P = 100$ MPa	
			49.8		$P = 150$ MPa	
La(Sr) : 21		295	93	Ultrasound	$\rho = 6.000$ g/cm^3; $dB/dP = 36$ at $p = 0$ GPa	Farggao *et al.* (1991)

La(Sr) : 21		25	73.8	Ultrasound	$\rho = 6.22$ g/cm^3	Yusheng *et al.* (1990)
		44	74.3			
		66	75.4			
		82	76.7			
		98	78.4			
		119	79.4			
		144	80.4			
		185	80.5			
		222	80.1			
		240	79.4			
		259	79.2			
		271	79.4			
Nd(Ce) : 21	88	295	93.2	Ultrasound	$\rho = 6.481$ g/cm^3	Fanggao *et al.* (1991)
Sm : 123	100	296	76.8	Ultrasound	Corrected to zero porosity	Reddy *et al.* 1994)
Tm : 123	100	296	54.2	Ultrasound	Corrected to zero porosity	Reddy *et al.* (1994)
Y : 123	89	8	51.6	Ultrasound	$\rho = 5.69$ g/cm^3	Yusheng *et al.* (1990)
		17	51.6			
		36	51.6			
		39	51.6			
		42	51.5			
		70	51.4			
		94	51.3			
		107	51.2			
		119	51.2			
		125	51.1			
		134	51.1			
		215	51.1			
		234	51.2			
		243	51.2			
		252	51.4			

(*continued*)

Table 13.4. (*continued*)

Phase	Relative Density (%)	T [K]	Bulk modulus (GPa)	Measurement method	Notes	Ref.
Y:123		4.2	87	Ultrasound		Lemmens *et al.* (1990)
Y:123	100	296	120	Model analysis		Bridge (1990)
Y:123	94	5	48.4	Ultrasound	$\rho = 5.985$ g/cm^3	Almond *et al.* (1987)
		36	48.0			
		50	47.3			
		73	46.4			
		90	46.6			
		110	46.8			
		126	47.0			
		144	47.2			
		164	47.7			
		186	47.4			
		205	46.3			
Y:123	100	296	38.1	Ultrasound	$\rho = 4.1$ g/cm^3, corrected to zero porosity	Reddy *et al.* (1994)
Y:123	79	296	57.0	Ultrasound	Specimen Y1	Reddy *et al.* (1993)
	100		89.8		Corrected to zero porosity	
	84		50.9		Specimen Y2	
	100		70.3		Corrected to zero porosity	
Y:123	82	295	42.4	Ultrasound	Y1, $\rho = 5.199$ g/cm^3	Al-Kheffaji *et al.* (1989)
	94		56.4		Y2, $\rho = 5.985$ c/cm^3	
Y:123	88	295	70.8	Ultrasound	$\rho = 5.56$ g/cm^3	Wang *et al.* (1995)
	100		99.9		Corrected to zero porosity	
Y:123	87	295	75.1	Ultrasound		Ledbetter *et al.* (1994)
	100		101		Corrected to zero porosity	
Y:123	96	273	47.6	Ultrasound	$T_c = 92$ K; $\rho = 6.07$ g/cm^3;	Cankurtaran and Saunders (1992b)

251	48.2
248	48.4
246	48.4
232	49
220	49.9
201	50.9
197	50.9
195	52.1
192	56.8
190	58
172	58.6
161	59.6
155	59.8
135	60.3
106	60.9
90	61.3
77	61.5
59	61.6
39	61.8
16	62
22	61.8
36	61.8
57	61.6
79	61.3
100	60.9
124	60.3
139	59.9
149	59.5
155	59.4
161	59.2
174	58.6

hysteresis with respect to temperature

(*continued*)

Table 13.4. (*continued*)

Phase	Relative Density (%)	T [K]	Bulk modulus (GPa)	Measurement method	Notes	Ref.
		184	58			
		190	58			
		204	56.8			
		217	56.2			
		225	55			
		227	52.8			
		228	50.6			
		232	50.8			
		232	51.2			
		242	51.6			
		248	51.4			
		261	50.2			
		271	49.2			
		279	48.4			
		296	47.2			
Y:123	88	295	70.8	Ultrasound	$\rho = 5.56$ g/cm^3; $O_{6.94}$	Cankurtaran *et al.* (1994)
	100		98.7		Corrected to zero porosity	

Y: 123	96	296	52	Ultrasound		Almond *et al.* (1989)
	100		56		Corrected to zero porosity	
Y: 123	72	5	27.5	Ultrasound	$\rho = 4.433$ g/cm^3; $\rho_{th} = 6.171$ g/cm^3; $YBa_2Cu_3O_{6.2}$	Lin *et al.* (1993)
	100		48.6		Corrected to zero porosity	
	72		31.3		$\rho = 4.523$ g/cm^3; $\rho_{th} = 6.304$ g/cm^3; $YBa_2Cu_3O_{6.7}$	
	100		55.9		Corrrected to zero porosity	
	71		31.6		$\rho = 4.528$ g/cm^3; $\rho_{th} = 6.339$ g/cm^3; $YBa_2Cu_3O_{6.8}$	
	100		56.6		Corrrected to zero porosity	
	72		30.4		$\rho = 4.553$ g/cm^3; $\rho_{th} = 6.363$ g/cm^3; $YBa_2Cu_3O_{6.9}$	
	100		53.6		Corrected to zero porosity	

Table 13.5.

Poisson's ratio (ν).

Phase	Relative Density (%)	T [K]	Poisson's Ratio	Measurement method	Notes	Ref.
Bi : 2212	82	300	0.2	Ultrasound		Yusheng *et al.* (1990)
Bi(Pb) : 2223	91	296	0.18	Ultrasound	$Bi_{1.7}Pb_{0.3}$; $\rho = 4.989$ g/cm^3	Muralidhar *et al.* (1992)
Bi(Pb) : 2223		296	0.169	Tensile	$Bi_{1.8}Pb_{0.3}Sr_2Ca_{1.9}Cu_3O_{10+x}$	Yuan *et al.* (1996)
Bi(Pb) : 2223	69	10	0.16	Ultrasound	$\rho = 4.35$ g/cm^3	Yusheng *et al.* (1990)
		50	0.16			
		100	0.16			
		150	0.16			
		200	0.17			
		250	0.17			
		290	0.18			
		300	0.18			
Dy : 123	74	296	0.27	Ultrasound		Reddy *et al.* (1994)
	100		0.24		Corrected to zero porosity	
Eu : 123	69	295	0.212	Ultrasound	$\rho = 4.793$ g/cm^3; $\rho_{th} = 6.97$ g/cm^3	Al-Kheffaji *et al.* (1989)
Gd : 123	83	296	0.28	Ultrasound	$\rho = 5.8$ g/cm^3; $\rho_{th} = 7.014$ g/cm^3; $O_{6.758}$	Reddy *et al.* (1994)
	100		0.28		Corrected to zero porosity	
Gd : 123	79	295	0.242	Ultrasound		Al-Kheffaji *et al.* (1989)
Gd : 123	78	4.2	0.196	Ultrasound	$\rho_{th} = 7.138$ g/cm^3	Almond *et al.* (1989)
Gd : 123	78	295	0.242	Ultrasound	$P = 0$ MPa	Cankurtaran *et al.* (1989)
			0.246		$P = 50$ MPa	
			0.249		$P = 100$ MPa	
			0.251		$P = 150$ MPa	
La(Sr) : 21		295	0.188	Ultrasound	$\rho = 6.000$ g/cm^3; $dB/dP = 36$ at $p = 0$ GPa	Fanggao *et al.* (1991)

La(Sr) : 21		12	0.26	Ultrasound	$\rho = 6.22$ g/cm^3	Yusheng *et al.* (1990)
		33	0.26			
		72	0.25			
		110	0.24			
		150	0.24			
		200	0.24			
		270	0.24			
Nd(Ce) : 21	88	295	0.207	Ultrasound	$\rho = 6.481$ g/cm^3	Fanggao *et al.* (1991)
Sm : 123	77	296	0.3	Ultrasound		Reddy *et al.* (1994)
	100		0.3		Corrected to zero porosity	
Tm : 123	81	296	0.27	Ultrasound		Reddy *et al.* (1994)
	100		0.26		Corrected to zero porosity	
Y : 123	89	20	0.19	Ultrasound	$\rho = 5.69$ g/cm^3	Yusheng *et al.* (1990)
		100	0.19			
		215	0.2			
		290	0.2			
Y : 123		4.2	0.24	Ultrasound		Lemmens *et al.* (1990)
Y : 123	100	296	0.29	Model analysis		Bridge (1990)
Y : 123	94	5	0.176	Ultrasound	$\rho = 5.985$ g/cm^3	Almond *et al.* (1987)
		36	0.177			
		50	0.175			
		73	0.172			
		90	0.173			
		110	0.174			
		126	0.175			
		144	0.178			
		164	0.184			
		186	0.187			
		205	0.182			

(*continued*)

Table 13.5. (*continued*)

Phase	Relative Density (%)	T [K]	Poisson's Ratio	Measurement method	Notes	Ref.
Y:123	62	296	0.3	Ultrasound	$\rho = 4.1$ g/cm^3	Reddy *et al.* (1994)
	100		0.1		Corrected to zero porosity	
Y:123	79	296	0.25	Ultrasound	Specimen Y1	Reddy *et al.* (1993)
	100		0.22		Corrected to zero porosity	
	84		0.2		Specimen Y2	
	100		0.17		Corrrected to zero porosity	
Y:123	82	295	0.194	Ultrasound	Y1; $\rho = 5.199$ g/cm^3	Al-Kheffaji *et al.* (1989)
	94		0.157		Y2; $\rho = 5.985$ g/cm^3	
Y:123	88	295	0.276	Ultrasound	$\rho = 5.56$ g/cm^3	Wang *et al.* (1995)
	100		0.291		Corrrected to zero porosity	
Y:123	87	295	0.248	Ultrasound		Ledbetter *et al.* (1994)
	100		0.255		Corrrected to zero porosity	
Y:123	88	295	0.276	Ultrasound	$O_{6.94}$; $\rho = 5.56$ g/cm^3	Cankurtaran *et al.* (1994)
	100		0.288		Corrected to zero porosity	
Y:123	100	296	0.281	Analysis (ultrasound)	Single crystal	Ledbetter and Lei (1991)

Y:123	96	296	0.163	Ultrasound		Cankurtaran *et al.* (1992)
	100		0.162		Corrected to zero porosity	
Y:123	95	296	0.163	Ultrasound	$\rho = 6.070$ g/cm^3	Cankurtaran and Saunders (1992a)
Y:123	72	5	0.19	Ultrasound	$\rho = 4.433$ g/cm^3; $\rho_{th} = 6.171$ g/cm^3, $YBa_2Cu_3O_{6.2}$	Lin *et al.* (1993)
	100		0.187		Corrected to zero porosity	
	72		0.199		$\rho = 4.523$ g/cm^3; $\rho_{th} = 6.304$ g/cm^3, $YBa_2Cu_3O_{6.7}$	
	100		0.199		Corrected to zero porosity	
	71		0.196		$\rho = 4.528$ g/cm^3; $\rho_{th} = 6.339$ g/cm^3, $YBa_2Cu_3O_{6.8}$	
	100		0.194		Corrected to zero porosity	
	72		0.185		$\rho = 4.553$ g/cm^3; $\rho_{th} = 6.363$ g/cm^3, $YBa_2Cu_3O_{6.9}$	
	100		0.18		Corrected to zero porosity	

two or more pieces. In this context, the term "strength" is used to indicate the level of stress that can be sustained without catastrophic cracking. In practice, the "strength" of a ceramic material is determined as the value of the stress, σ_f, attained at fracture.

a. Terms and Basic Relations

The value of the stress that is required to produce fracture depends, in part, on the type of stress system that is applied to the material. Thus, the terminology for fracture strength is refined somewhat according to the particular design of the apparatus that is used to measure the fracture stress. When fracture is produced in a specimen subjected to purely tensile stress, the result is called the tensile strength. The fracture stress deduced from a specimen subjected to bending is called the flexural strength (also called the bending strength and the modulus of rupture).

For a given production lot of a ceramic material, the fracture stress is not an invariant quantity across all specimens drawn from that lot. Rather, the strength of a brittle material is controlled by the distribution of defects, inclusions, and microscopic inhomogeneities that are known collectively as flaws. The measured strength of two specific test specimens can be significantly different because the specific flaws in two specimens are different. Thus, brittle fracture strength is best understood in a statistical context (Davies, 1973; Batdorf, 1978; Hild and Marquis, 1992).

The basic understanding of brittle fracture was established by Griffith (1921). By assuming that crack extension (i.e., fracture for an ideally brittle material) occurs when the elastic energy (which is released during crack extension) is just sufficient to form the new surfaces, Griffith found that a flaw will be the origin of fracture when

$$\sigma_G = \left[\frac{4E'\gamma}{\pi c_0}\right]^{1/2}, \tag{29}$$

where $E' = E$ for plane stress and $E' = E/(1 - \nu^2)$ for plane strain; E is the elastic modulus; ν is Poisson's ratio; γ is the fracture energy per unit area; and $2c_0$ is the initial crack size.

Since the production lot of any ceramic material, in general, possesses a distribution of flaw sizes over the specimens drawn from the lot, there must be a corresponding distribution of fracture strengths. Weibull (1939; 1951) showed that the statistics of fracture could be described quite effectively by assuming a weakest link model for the flaws. In this model, each volume element has a local

value of fracture strength, and the probability of failure, P_f, of the whole specimen is given by integrating over the stressed volume:

$$P_f = 1 - \exp\left[-\int_V (\sigma/\sigma_0)^m \, dV/V_0\right], \tag{30}$$

where σ_0 and m are parameters known respectively as the Weibull characteristic strength and the Weibull modulus, and V_0 is a volume scale parameter. For uniform stress, this expression simplifies to

$$P_f = 1 - \exp[-(V_s/V_0)(\sigma/\sigma_0)^m], \tag{31}$$

where V_s is the volume of the test specimen.

Given P_f, the mean fracture strength can be calculated formally from the defining relation

$$\bar{\sigma} = \frac{1}{N}\sum n_f(\sigma) \cdot \sigma, \tag{32}$$

where $n_f(\sigma)$ is the number of specimens that fail at stress σ and $N = \sum n_f(\sigma)$. Noting that the number of specimens that fail at stress σ is the difference between the number of specimens surviving at $\sigma - d\sigma/2$ and the number surviving at $\sigma + d\sigma/2$,

$$\frac{n_f(\sigma)}{N} = [1 - P_f(\sigma - d\sigma/2)] - [1 - P_f(\sigma + d\sigma/2)], \tag{33}$$

means that Eq. (32) can be recast in the form

$$\bar{\sigma} = \int_0^\infty P_f' \cdot \sigma \, d\sigma, \tag{34}$$

where $P_f' = dP_f/d\sigma$. Using Eq. (31) in this latter relation, one can obtain a critically important result for the strength of ceramic materials: specifically, that two sets of geometrically similar specimens having the same flaw system will have different measured fracture strengths if the volumes of the specimens are different. Explicitly,

$$\frac{\bar{\sigma}_1}{\bar{\sigma}_2} = \left(\frac{V_2}{V_1}\right)^{1/m}, \tag{35}$$

which expresses the reasonable result that a larger volume will contain more flaws by which fracture may be initiated.

b. Measurement Methods

In view of Eq. (35), meaningful comparisons of strength data across independent studies require careful attention to the specifications of the specimens and the strength test configurations. Consequently, there has been a considerable effort worldwide to develop and standardize appropriate test methods.

Fig. 13.3.

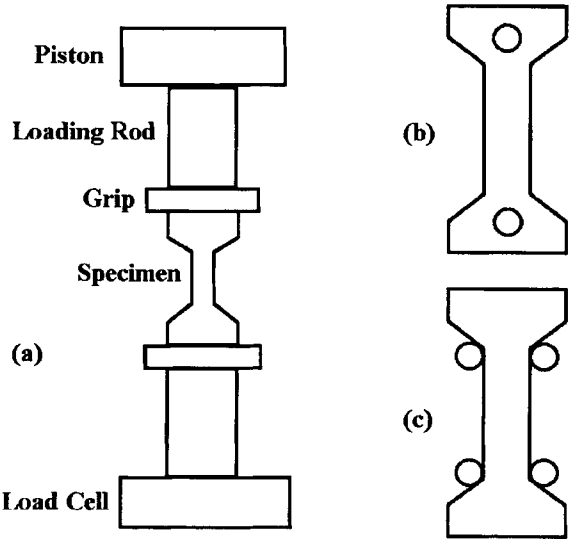

Schematic of a tensile test: (a) apparatus, (b) specimen with a pin-loaded grip, (c) specimen with a shoulder-loaded grip.

The simplest test, conceptually, is the tensile test, Fig. 13.3, in which a specimen is uniformly loaded in tension (Ohji, 1988). The fracture stress of the specimen is then simply the ratio of the loading force, F, applied to the specimen at the time of fracture, to the initial cross-sectional area of the specimen, A_0; i.e., $\sigma_t = F/A_0$. The simplicity of this test is encumbered somewhat by the necessity of gripping the specimen so that the tensile load can be applied to it (French and Wiederhorn, 1996). Because of the difficulty in machining ceramics, it is desirable to keep the shape of the specimen as simple as possible. Furthermore, screw threads and other features with high stress concentration also need to be avoided because of the possible fracture at the specimen grip. Two designs that have met with some success are illustrated in Fig. 13.3. A further concern in the tensile test is the alignment of the specimen along the tensile axis. Any misalignment can introduce a bending moment in the specimen and thereby affect the measured value of the fracture stress.

Another test method for determining the tensile strength is the diametral compression test (Rudnick *et al.*, 1963), Fig. 13.4. The specimen is a cylinder with a circular cross-section. The load is applied along the length of the cylinder and directed along a diameter of the cross-section. While a large compressive stress exists along the load contact line, tensile stress develops in the direction normal to the load axis in the central region of the specimen. A method of distributed loading must be used to avoid high compressive and shear stresses at the ends of the cylinder such that the maximum tensile stress dominates the

Fig. 13.4.

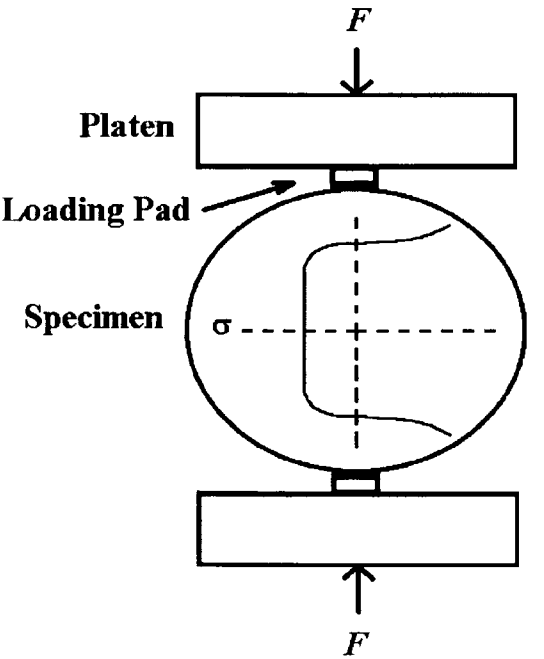

Schematic of a diametral compression test. A schematic of the stress profile along the load axis is shown superimposed on the specimen.

fracture results. The fracture stress is calculated as the maximum tensile stress in the specimen which, for ideal line loading, is $\sigma_t = 2F/\pi DL$, where F is the applied loading force, D is the specimen diameter, and L is the length of the specimen.

The most widely used type of test for measuring the strength of ceramics is a bend test (Quinn and Morrell, 1991), Fig. 13.5. There are two primary versions of the bend test, known, respectively, as the three-point bend test and the four-point bend test. In the three-point bend test, the load is applied to the specimen at a point midway between the two support bearings. In the four-point bend test, the load is applied at two positions located symmetrically between the support bearings. In recent years, the 1/4-point loading design, $s_i = s_o/2$, has become the more prominent four-point configuration. (ASTM C 1161; C 1211). In both versions of the bend test, the specimen is subjected to a large stress gradient through the cross-section. Upon bending, tensile strain occurs on the convex surface of the specimen, and compressive strain occurs on the concave surface. As a result, the effective volume of the specimen, that is, that portion experiencing the maximum tensile stress, is significantly less than would occur in the direct tension test. However, this disadvantage of the bend test is offset by the

Fig. 13.5.

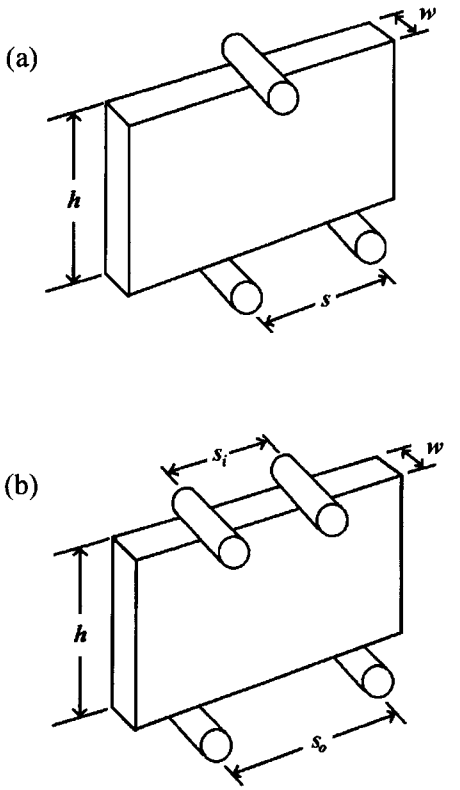

Schematics of two flexural tests: (a) three-point bend test, (b) four-point bend test.

relative ease of preparing the specimens. Most of the standardized bend test methods in use today specify uncomplicated rectangular bars on which the tensile surface is polished and the long edges of the specimen are chamfered at 45°. The primary concerns about this method involve alignment of the load train and the potential for friction at the loading points. The fracture stress, calculated from beam theory for linearly elastic materials, is given by

$$\sigma_f = \frac{3Fs}{2wh^2} \text{ (three-point test)} \tag{36}$$

$$\sigma_f = \frac{3Fs_o}{4wh^2} \text{ (four-point test, 1/4-point loading)} \tag{37}$$

where F is the load at fracture, L is the distance between the support bearings, w is the width of the specimen, and h is the thickness of the specimen.

c. Property Data

Strength data are given in Tables 13.6 and 13.7. Although there is only a small amount of flexural strength data in Table 13.6, the results are sufficient to indicate a strong dependence on both the density and the grain size. The largest flexural strength in this table is a relatively low 216 MPa for Y: 123, and the largest tensile strength in Table 13.7 is only 103 MPa for Bi(Pb): 2223.

D

Hardness

Hardness is a property that is widely used for quality control and as a relative performance parameter, but that is considered to have little merit as an intrinsic material property. This situation stems from the empirical nature of its definition. Hardness is an engineering property that is used to quantify the resistance of a material to irreversible deformation (McColm; 1990). Because of its empirical definition, measurement of the property requires that an irreversible deformation be produced as an integral part of the measurement process. How the deformation is produced determines what particular definition of hardness is being used. As a result, there are numerous hardness values that may be quoted, and there is no established method of converting one hardness scale to another. Nevertheless, hardness has evolved as an important property in homogeneity studies, process control, and material selection. The popularity of hardness testing may be due in part to the relative ease of conducting the test, its relatively low cost, and its basically nondestructive nature.

a. Terms and Basic Relations

Two hardness tests, the Vickers hardness test and the Knoop hardness test, have become widely used for advanced ceramics. These tests belong to the subclass referred to as indentation hardness tests. In both tests, an object, called an indenter, is pressed into a locally flat, polished surface of the specimen. The applied load and the residual impression of the indenter, Fig. 13.6, determine the hardness.

In the Vickers hardness test (ASTM E 92; E384), the indenter is a pyramid with a square base and with an included angle between opposite faces of $\alpha = 136°$. The Vickers hardness is calculated as the ratio of the applied load, F, and the actual surface area of the residual impression;

$$H_V = \frac{2F\sin(\alpha/2)}{d^2} = 1.8544\frac{F}{d^2}, \tag{38}$$

Table 13.6.

Flexural strength (σ_f).

Phase	Relative Density (%)	T [K]	Flexural strength (MPa)	Measurement method	Notes	Ref.
Bi : 2212	90	296	84	Four-point bend	3 mm × 3 mm cross-section; $S_i = 9.6$ mm, $S_o = 19.2$ mm; 2.54 mm/min	Goretta *et al.* (1993)
Bi : 2212	90	296	57	Four-point bend	3.7 mm × 7.5 mm × 43 mm; $S_i = 9.5$ mm, $S_o = 19.1$ mm; 1.27 mm/min	Joo *et al.* (1994)
Bi : 2212	77	296	84	Four-point bend	2 mm × 3 mm × 22 mm; $S_i = 9.6$ mm; $S_o = 19.2$ mm; 1.27 mm/min	Martin *et al.* (1993)
	90		112			
	99		144			
Bi(Pb) : 2223		296	174	Three-point bend	$Bi_{1.2}Pb_{0.8}$; 1.0 mm diameter; $S = 20$ mm; 5 mm/min	Alford *et al.* (1990)
Bi(Pb) : 2223		296	7.6	Three-Point bend	$Bi_{1.7}Pb_{0.3}$; 3 mm × 12 mm × 60 mm; S = ?; 0.5 mm/min	Low *et al.* (1995)
Bi(Pb) : 2223	91	80	113	Three-point bend	$Bi_{1.8}Pb_{0.3}Sr_2Ca_{1.9}Cu_{3.1}O_{10+x}$ $\rho = 5.7$ g/cm^3 3 mm × 4 mm × 20 mm $S = 16$ mm; 0.5 mm/min	Murayama *et al.* (1992)
		100	119			
		120	116			
		180	113			
		240	109			
		292	105			

Y: 123	81	296	216	Three-point bend	0.9 mm diameter; $S = 20$ mm; 5 mm/min; observed range was 80 MPa $\leq \sigma_f \leq$ 250 MPa	Alford *et al.* (1988)
Y: 123	88	296	33.8	Four-point bend	Grain size= 16 μm 2 mm × 3 mm × 40 mm;	Ihm *et al.* (1990)
	83		23.7		Grain size= 45 μm $S_i = 10$ mm, $S_o = 20$ mm; 0.2 mm/min	
	76		57.6		Grain size = 11 μm	
	58		17.8		Grain size = 10 μm	
Y: 123	89	77	36	Three-Point bend	$\rho = 5.7$ g/cm^3; 2.8 mm × 5.6 mm × 22.4 mm; S = ?; 0.74 N/s	Siu and Teng (1993)
		300	27			
Y: 123	60	296	15	Three-point bend	3 mm × 12 mm × 60 mm; S = ?; 0.5 mm/min	Low *et al.* (1994)
Y: 123		296	110	Three-point bend	Varied with processing conditions, range: 73 MPa to 191 MPa; 1.14 mm diameter × 30 mm length; $S = 18.25$ mm; 1.27 mm/min	Sing *et al.* (1992)

Table 13.7.

Tensile strength (σ_t).

Phase	T [K]	Tensile strength (MPa)	Measurement method	Notes	Ref.
Bi(Pb) : 2223	296	26	Diametral compression	$Bi_{1.7}Pb_{0.3}$; 15 mm diameter, 3 mm thickness, 0.5 mm/min	Low *et al.* (1995)
Bi(Pb) : 2223	296	103	Tensile	$Bi_{1.8}Pb_{0.3}Sr_2Ca_{1.9}Cu_3O_{10+x}$; 1.52 mm × 5.6 mm × 12.7 mm; 0.254 mm/min	Yuan *et al.* (1996)
Y : 123	296	6.5	Diametral compression	12.5 mm diameter, 3 mm thickness, 0.5 mm/min; relative density = 62%	Low *et al.* (1994)

Fig. 13.6.

(a)

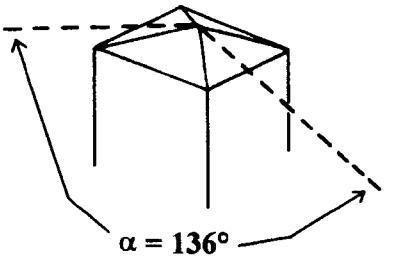

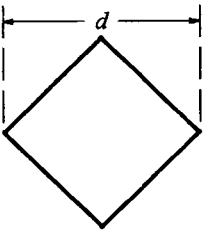

(b)

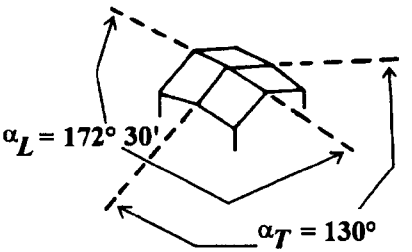

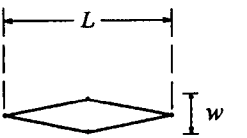

Schematics of two indenters and their indentation impressions: (a) Vickers indenter, (b) Knoop indenter.

where d is the mean diagonal length of the impression left by the indenter in the surface of the specimen.

The Knopp hardness test (Knoop *et al.*, 1939) is distinguished from the Vickers test both by the specification of the indenter and the specification of the hardness expression. The indenter is a pyramid with a rhombic base, and the included angles between the two pairs of opposite faces of the indenter are unequal; the larger angle is 172° 30′ and the smaller angle is 130°. The Knoop hardness is calculated as the ratio of the applied load and the projected surface area of the residual impression,

$$H_K = \frac{F}{\frac{1}{2}Lw} = \frac{2F}{L^2 \cot(\alpha_L/2)\tan(\alpha_T/2)} = 14.229\frac{F}{L^2}, \tag{39}$$

where L, w, α_L, and α_T are defined in Fig. 13.6b.

b. Measurement Methods

The empirical definition of indentation hardness has a strong intuitive appeal making hardness a useful comparative characteristic. Its application, however, must be approached with some caution. More direct empirical studies of the size of an indentation as a function of the applied load have found that the load and indentation size are often related by a power law, such that

$$F = \xi d^{\eta}, \tag{40}$$

where ξ and η are parameters for a given material (Mayer, 1908). Using this relation in the expressions for H_V and H_K, one can see that the indentation hardness will be a well-defined constant for a material only in the exceptional case that the value of η is exactly 2. This observation is very important to the measurement of hardness. In general, a reported value of hardness can be considered meaningful only when the load used to determine the hardness is also reported. It is fairly common for measurements of hardness to be conducted over a range of loads to provide an explicit accounting for the load dependence. At sufficiently high loads, significant cracks, subsurface damage zones, and fragmentation around the indentation site change the general nature of the deformation. At these higher loads, the hardness value, to the extent that it remains measurable, may become constant, i.e., independent of the load, but the interpretation of this constant value, even as a comparative statistic, is an open issue.

In both tests, the chosen load is applied along an axis that is normal to the surface of the specimen. Typically, the indenter is pressed into the specimen at a rate of 15 to 70 μm/s, and the maximum static load is sustained for 10 to 15 s. The lengths of the diagonals of the resulting impression commonly are measured using an optical microscope with a graduated ocular. Usually, multiple indentations are made on one specimen, and it is important that there be sufficient space between individual indentations so there is no overlap of any of the associated deformation features.

c. Property Data

Data from hardness measurements are given in Table 13.8. For most of the studies referenced in this table, indentation impressions began to form at very low loads on the order of 0.05 N. The largest value of hardness, 12.7 GPa, occurred for a single-crystal specimen of Y: 123. In contrast, the largest value for a Bi: 2212 or a Bi(Pb): 2223 material was less than 1 GPa.

Table 13.8.

Hardness (H).

Phase	Relative Density (%)	Crystal Face	Applied Load (N)	T [K]	Hardness (GPa)	Measurement method	Notes	Ref.
Bi : 2212			50 or 100	296	0.76	Vickers indentation	Hot isostatically pressed	Chu *et al.* (1992)
					0.66		Sinter forged	
Bi : 2212	100		0.6	77	0.62	Vickers indetation	Single crystal; load dependent below 0.4 N load	Muralidhar *et al.* (1991)
	100			296	0.33		Single crystal; load dependent below 0.4 N load	
				296	0.35		Polycrystal; load dependent below 0.4 N load	
Bi : 2212	100	(001)	0.02 to 0.75	296	0.95	Vickers indentation	Single crystal	Orlova *et al.* (1990)
Bi : 2212	90			296	0.85	Vickers indentation		Joo *et al.* (1994)
Bi(Pb) : 2223			2	296	0.6	Knoop indentation	$Bi_{1.7}Pb_{0.3}$	Low *et al.* (1995)
Bi(Pb) : 2223			10 to 50	296	0.35	Vickers indentation	Average for grain aligned specimens	Low *et al.* (1995)
Bi(Pb) : 2223	91		0.8 to 1.3	296	0.38	Vickers indentation	$Bi_{1.7}Pb_{0.3}$, $\rho = 4.989$ g/cm^3	Muralidhar *et al.* (1992)
Bi(Pb) : 2223	83		0.5 to 50	296	0.4	Vickers indentation	$\rho = 5.44$ g/cm^3	Lo *et al.* (1995)
Bi(Pb) : 2223			1.5	296	0.42	Vickers indentation		Luo *et al.* (1995)
Dy : 123	100		0.15	300	5.7	Vickers indentation	Single crystal	Bobrov (1993)
Ho : 123	100		0.15	300	5.9	Vickers indentation	Single crystal	Bobrov (1993)
La(Sr) : 21		(001)	0.02 to 0.8	296	6	Vickers indentation	Single Crystal	Orlova *et al.* (1990)
La(Sr) : 21			0.15	83	11.1	Vickers indentation	Single crystal	Bobrov (1993)
				84	11.7			
				109	11			
				110	10.6			

(*continued*)

Table 13.8. (*continued*)

Phase	Relative Density (%)	Crystal Face	Applied Load (N)	T [K]	Hardness (GPa)	Measurement method	Notes	Ref.
				136	11.1			
				140	10.9			
				161	10.6			
				167	10.3			
				188	10.3			
				192	10			
				200	10.1			
				207	10			
				217	9.3			
				230	9.9			
				233	9.6			
				265	9.3			
				292	9			
Tl:2212	100		0.15	300	2.8	Vickers indentation	Single crystal; Tl–Ba–Ca–Cu–O	Bobrov (1993)
Y:123	86		10 to 100	296	2	Vickers indentation	Grain size = 15 μm	Cook *et al.* (1987b)
Y:123	88		2	296	4.3	Knoop indentation	Grain size = 16 μm	Ihm *et al.* (1990)
	76				4.4		Grain size = 11 μm	
Y:123	100		0.25 to 2	296	7	Knoop indentation	Single crystal; varies with orientation	Fang *et al.* (1993)
Y:123	62		2	296	2.2	Knoop indentation		Low *et al.* (1994)
Y:123	100	(100)	0.2 to 0.4	296	10.1	Vickers indentation	Single crystal	Anderson (1989)
		(001)			8.4			

Y:123	100		5 to 20	296	5.3	Vickers indentation	Varies with load	Ni *et al.* (1993)
Y:123	90			296	11	Indentation	Single grains, 50 nm to 200 nm penetration	Marinez *et al.* (1992)
Y:123	100		0.05 to 0.5	296	9.7	Vickers indentation	Single crystal, $T_c = 65$ K	Demirskii *et al.* (1989)
Y:123	100	(001)	0.02 to 0.5	296	5	Vickers indentation	Single crystal; $T_c = 90$ K	Orlova *et al.* (1990)
Y:123	100		0.1 to 2	296	8.7	Vickers indentation	Single crystal	Cook *et al.* (1987a)
Y:123	100		0.25 to 0.5	296	9.6	Vickers indentation	Single crystal; twinned and untwinned	Raynes *et al.* (1991)
Y:123	100	(001)	0.1 to 2	296	6.7	Vickers indentation	Single crystal	Goyal *et al.* (1992)
		(100/010)			3.8			
Y:123				296	10.3	Vickers indentation		Lucas *et al.* (1991)
Y:123	100		0.15	87	13	Vickers indentation	Single crystal	Bobrov (1993)
				110	12.5			
				150	12.7			
				187	11.7			
				226	11			
				259	10.3			
				293	10			
Y:123	100	(001)	0.02	296	10	Indentation	Single crystal	Goyal *et al.* (1991)
		(010)			10.8			

E

Toughness

Fracture toughness refers to the resistance of a material to the extension of a crack. When a stress is applied to a brittle material, there is a maximum stress that can be sustained within the material before an existing crack begins to propagate. That stress, however, is not the same as the applied stress at fracture (which is the fracture strength discussed in Section C). Rather, propagation of a crack depends on the local stress that occurs at the tip of the crack. If one considers, for example, an idealized crack in the form of an elliptical hole in a semi-infinite plate, as shown in Fig. 13.7, with major axis $2a$ and minor axis $2b$, in a medium bearing an applied uniform tensile stress, σ, it can be shown (Inglis, 1913) that the maximum local tensile stress is

$$\sigma_{\max} = \left(1 + \frac{2a}{b}\right)\sigma, \tag{41}$$

which occurs at the tip of the ellipse along the major axis. The presence of the crack is said to intensify the stress. When $\sigma_{\max} = \sigma_G$, the specimen fractures. It is evident from Eq. (41) that $\sigma_{\max}$ depends on the geometric shape of the crack and, in particular, on the radius of curvature at the crack tip. As the ratio a/b increases, $\sigma_{\max}$ increases, indicating that sharper cracks produce a greater intensification of the stress. Thus, the extent to which a specimen can resist crack extension depends on the particular flaw distribution that is present in the material.

Fig. 13.7.

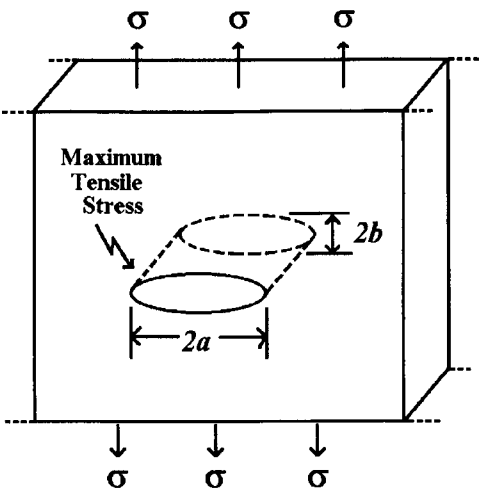

Schematic of an elliptical hole in a stressed medium.

a. Terms and Basic Relations

The development of linear elastic fracture mechanics has allowed the extension of a crack in a material body to be characterized using the methods of linear stress analysis. In this analysis, a parameter K, called the stress intensity factor, is introduced to represent the enhanced state of stress in the vicinity of the crack. The symbol K_I is used for tensile stress, which is formally classified as Mode I stress. The critical value of the stress intensity factor, K_{Ic}, commonly called the fracture toughness, is defined as the value for the onset of fast crack extension. Linear stress analysis leads to the relation

$$K_{Ic}^2 = \Gamma E' = 2\gamma E' \tag{42}$$

for tensile cracks. Recalling the Griffith criterion, Eq. (29), it is easy to see that a relation between the fracture toughness of the material and the measured fracture strength, σ_f, of the material should be expressible in the form

$$K_{Ic} = Y\sigma_f c_0^{1/2}, \tag{43}$$

where Y is a dimensionless numeric factor that depends on the test configuration and the shape of the initial crack. Numerous test methods for measuring K_{Ic} exploit this relation using an initial crack that has a measurable shape and size.

b. Measurement Methods

Designs for fracture toughness test methods may be grouped rather broadly into two basic types (Anderson; 1989). In one type, an initial flaw is created in the surface of the specimen, and then the specimen is fractured, usually in a bend test. In the other type, an indenter is used in the manner of a hardness test, but with sufficient load to create an indentation flaw with radial cracks extending from the corners of the impression. Both approaches have advantages and disadvantages that add or detract from their use, and numerous variations of these basic ideas have been pursued to enhance or minimize specific features. For high-T_c materials, the predominant methods of determining K_{Ic} have been the single-edge notched-beam (SENB) method and the Vickers indentation toughness method.

In the basic SENB method (Rief and Kromp, 1988; Srinivasan and Seshadri, 1981; Quinn *et al.*, 1992), Fig. 13.8a an initial crack is cut into a bend test specimen using a saw blade or a wire. The specimen is then fractured in a three-point or a four-point bend test to determine σ_f, and the initial depth of the cut is taken as the initial crack size. The fracture toughness is evaluated as

$$K_{Ic} = Y_{SENB} \cdot \frac{3F \cdot \Delta_s}{2wh^2} \cdot c_0^{1/2}, \tag{44}$$

Fig. 13.8.

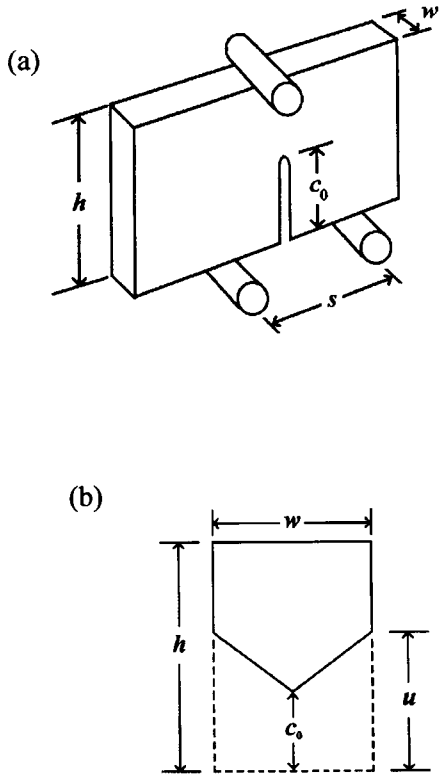

Schematic of (a) the SENB (single-edge notched-beam) test in the three-point bend configuration, and (b) a chevron notch.

where Δ_s is s in the three-point test and $s_o - s_i$ in the four-point test. In the three-point test when $s/h = 4$, Y_{SENB} is

$$Y_{SENB,3} = 1.93 - 3.07\left(\frac{c_0}{h}\right) + 13.66\left(\frac{c_0}{h}\right)^2 - 23.98\left(\frac{c_0}{h}\right)^3 + 25.22\left(\frac{c_0}{h}\right)^4 \quad (45)$$

and in the four-point test

$$Y_{SENB,4} = 1.99 - 2.47\left(\frac{c_0}{h}\right) + 12.97\left(\frac{c_0}{h}\right)^2 - 23.17\left(\frac{c_0}{h}\right)^3 + 24.8\left(\frac{c_0}{h}\right)^4, \quad (46)$$

where the geometric parameters are defined in Figs. 13.5 and 13.8a. Although the simplicity of the SENB method is highly desirable, it is sometimes argued that the notch produced in this manner is relatively blunt. Since the result may vary with the radius of the notch tip, the measured values can be somewhat unreliable and typically too high. To correct that situation, a sharp crack at the notch tip may be induced by a mechanical procedure (Nose and Fujii, 1988). Use of such

precracked specimens, however, leads to other concerns, such as a greater uncertainty in the value of the initial crack size.

A modification of the SENB method that retains the simplicity of the test while providing a sharp tip within the notch is the chevron notch method (Munz *et al.*, 1980), Fig. 13.8b. In this method, the straight notch is replaced with a notch in the shape of a chevron. The point of the chevron provides a deliberate stress concentration and serves as the primary origin for fracture. In the four-point test configuration, K_{Ic} is evaluated as

$$K_{Ic} = Y_{CN,4} \cdot \frac{F \cdot (s_o - s_i)}{wh^{3/2}} \tag{47}$$

$$Y_{CN,4} = \left[3.08 + 5.00\left(\frac{c_0}{h}\right) + 8.33\left(\frac{c_0}{h}\right)^2\right] \cdot \left[1 + 0.007\left(\frac{s_i s_o}{h^2}\right)\right] \cdot \left[\frac{u - c_0}{h - c_0}\right], \tag{48}$$

where the geometric parameters are defined in Figs. 13.5 and 13.8b.

An alternative to the notch methods is the surface crack in flexure method (Tracy and Quinn, 1994). This method uses a Vickers hardness indenter with sufficient load to create a crack under the indentation impression. The impression and the stress damage zone immediately below the impression, however, are removed by mechanical lapping so that only the crack remains. Then, the specimen is fractured in a four-point bend test. Subsequently, scanning electron microscopy is used to examine the fracture surface and to determine the initial crack depth. The fracture tougness is evaluted directly as

$$K_{Ic} = Y_{SCF}\sigma_f c_0^{1/2}, \tag{49}$$

where Y_{SCF} is an empirical factor discussed extensively by Newman and Raju (1981). Although this method is not yet widely used for high-T_c materials, it has become recognized as one of the more reliable methods, and substantial progress has been made toward standardizing the test procedure (Quinn *et al.*, 1994).

Fracture toughness tests using bend test configurations require relatively large specimens. A useful alternative method that requires only a small amount of material is provided by the indentation method. (Evans and Charles, 1976). In this approach Fig. 13.9 a Vickers indenter is pressed into the surface of the specimen until cracks develop radially from the corners of the impression. The analysis of the method by Anstis *et al.* (1981) found that K_{Ic} could be evaluated as

$$K_{Ic} = \zeta\left(\frac{E}{H}\right)^{1/2}\left(\frac{F}{c_0^{3/2}}\right), \tag{50}$$

where E is the elastic modulus, H is the indentation hardness, and ζ is a numeric factor determined empirically to be $\zeta = 0.016 \pm 0.004$ based on the average and standard deviation of values for a wide range of ceramics. The analysis assumes that a well-defined crack morphology, known as median cracks, develops around the impression. At sufficiently low loads, only shallow cracks, known as

Fig. 13.9.

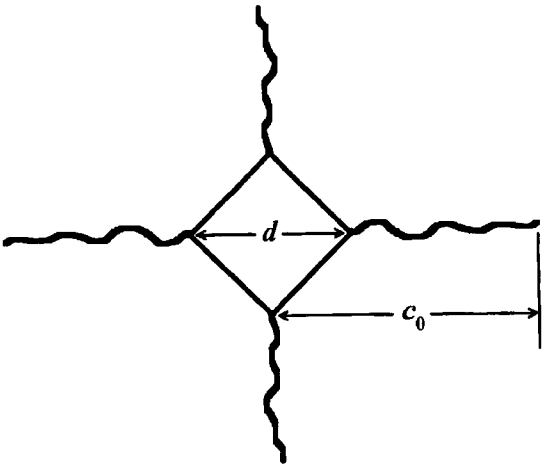

Schematic of the Vickers indenter impression in the indentation toughness test.

Plamqvist cracks, develop, and a different analysis is required for determining K_{Ic}. Various studies of the indentation method have found that average values computed across laboratories are consistent with average results from other methods, but the variance of the values among laboratories is greater for the indentation method than for other methods. Often, the advantages of the simplicity of the method and the need for only a small specimen outweigh the concerns for interlaboratory consistency, with the result that the method is widely used for high-T_c materials (Ponton and Rawlings, 1989a,b).

c. Property Data

Fracture toughness data are given in Table 13.9. Three-point bend SENB tests and Vickers indentation toughness tests account for all of the data in this table. The largest value, 3.9 MPa · $m^{1/2}$ for Bi : 2212, is comparable to the fracture toughness values found for structural ceramics such as sintered alumina or silicon carbide. However, most of the reported values were less than 2 MPa · $m^{1/2}$ and often less than 1 MPa · $m^{1/2}$.

F Conclusion

The mechanical properties of high-T_c superconductors are important to the development of commercial applications of these material, particularly for

Table 13.9.

Fracture toughness (K_{Ic}).

Phase	Relative Density (%)	T [K]	K_{Ic} (MPa $m^{1/2}$)	Measurement method	Notes	Ref.
Bi:2212		296	3.2	SENB[a]	Hot isostatically pressed; notch perpendicular to pressing direction	Chu *et al.* (1992)
			3.9		Hot isostatically pressed; notch parallel to pressing direction	
			2.7		Sinter forged; notch perpendicular to pressing direction	
			3.2		Sinter forged; notch parallel to pressing direction	
Bi:2212	90	296	1.9	SENB[a]		Joo *et al.* (1994)
Bi:2212	77	296	1.2	SENB[a]	2 mm × 3 mm × 22 mm	Martin *et al.* (1993)
	77		1.8			
	90		1.4			
	90		1.8			
	99		2.9			
	99		2.8			
	99		2.4			
Bi(Pb):2223		296	1.3	SENB[b]	$Bi_{1.2}Pb_{0.8}$; 2 mm × 5 mm × 30 mm	Alford *et al.* (1990)
Bi(Pb):2223		296	0.3	SENB[c]	$Bi_{1.7}Pb_{0.3}$; 3 mm × 12 mm × 60 mm	Low *et al.* (1995)
Bi(Pb):2223		77	3	SENB[d]	$Bi_{1.8}Pb_{0.3}Sr_2Ca_{1.9}Cu_3O_{10+x}$; 2 mm × 6.4 mm × 31.75 mm	Yuan *et al.* (1996)
		293	2.6			
Y:123	86	296	1.3	Vickers indentation	Assumes $E/H = 40$; 2 N to 100 N; 10 s	Cook *et al.* (1987b)

(*continued*)

Table 13.9. (*continued*)

Phase	Relative Density (%)	T [K]	K_{Ic} (MPa $m^{1/2}$)	Measurement method	Notes	Ref.
Y:123	67	296	1.05	Chevron notch[e]	8 mm × 10 mm × 60 mm	Yeh and White (1991)
	73		1.13			
	87		1.4			
Y:123	81	296	0.7	Vickers indentation	Grain size = 1.5 μm; uses E = 180 GPa, H_v = 8.7 GPa	Osterstock *et al.* (1996)
	81		0.84		Grain size = 3.5 μm	
	78		1.64		Grain size = 5.5 μm	
	84		0.24		Grain size = 10 μm	
Y:123	80	296	1.07	SENB[b]		Alford *et al.* (1988)
Y:123	89	77	1.21	SENB[f]	Grain size = 7 μm; ρ = 5.7 g/cm^3	Siu and Zeng (1993)
		300	0.94			
Y:123	60	296	0.5	SENB[c]	3 mm × 12 mm × 60 mm	Low *et al.* (1994)
Y:123	100	296	1.85	Vickers indentation	Assumes E = 97.1 GPa; 5 N, 10 s	Ni *et al.* (1993)
Y:123	100	296	0.43	Vickers indentation	Single crystal, T_c = 65 K	Demirskii *et al.* (1989)
Y:123	100	296	1.1	Vickers indentation	Single crystal; 0.1 N to 2 N, 5 s	Cook *et al.* (1987a)
Y:123	81	296	0.7	Vickers indentation	Very fine grains; 10 N to 100 N, 10 s; assumes E = 180 GPa, H_v = 8.7 GPa	Osterstock *et al.* (1993)
	81		0.84		Fine grains	
	78		1.64		Medium grains	
	84		0.24		Coarse grains	

Y:123	100	296	0.8	Vickers indentation	Single crystal; twinned; cracks parallel to c; $E = 157$ GPa; 0.25 N to 0.5 N	Raynes *et al.* (1991)
			0.3		Single crystal; twinned; cracks perpendicular to c; $E = 89$ GPa, 0.25 N to 0.5 N	
Y:123	100	296	0.67	Vickers indentation	Single crystal, (001) face; 0.1 N to 2 N, 10 s; uses $E/H = 27$	Goyal *et al.* (1992)
Y:123	85	296	1.2	SENB[a]	3 mm × 7 mm × 50 mm; 3 mm notch depth	Goretta *et al.* (1991)
	90		1.5			
	93		3.1			

[a] Three-point bend, 14 mm to 19 mm span, 1.27 mm/min loading rate.
[b] Three-point bend, 20 mm span, 5 mm/min loading rate, 0.2 mm notch width.
[c] Three-point bend, 0.5 mm/min loading rate, 2 mm notch depth.
[d] Three-point bend, 25.4 mm span, 0.254 mm/min loading rate, 0.25 mm notch width.
[e] Three-point bend, 40 mm span, 0.254 mm notch width, notch depth/specimen height = 0.44.
[f] Three-point bend, 0.74 N/s stressing rate, 1.5 mm to 2.2 mm notch depth, 0.08 mm notch width, ASTM E 399-83 cited.

Table 13.10.

Means and standard deviations of property values given in Tables 13.2–13.9, absorbing all variations due to material and measurement differences into the standard deviation. Values for other types of materials are given for comparison.

Phase	Elastic modulus (GPa)	Shear modulus (GPa)	Bulk modulus (GPa)	Poisson's ratio	Flexural strength (MPa)	Tensile strength (MPa)	Hardness (GPa)	Fracture toughness ($MPa \cdot m^{1/2}$)
Bi : 2212	69 ± 40	16	22	0.2	95 ± 30		0.6 ± 0.2	2.4 ± 0.8
Bi(Pb) : 2223	54 ± 47	13 ± 3	19 ± 5	0.17 ± 0.01	107 ± 46	64 ± 54	0.4 ± 0.1	1.8 ± 1.2
Dy : 123	72 ± 33	29 ± 14	62	0.26 ± 0.02			5.7	
Eu : 123	53	22	30	0.212				
Gd : 123	87 ± 29	35 ± 13	57 ± 15	0.25 ± 0.03				
Ho : 123							5.9	
La(Sr) : 21	120 ± 7	50 ± 8	79 ± 5	0.24 ± 0.02			10 ± 1	
Nd(Ce) : 21	128	68	93	0.207				
Sm : 123	72 ± 28	28 ± 11	77	0.3				
Tl : 2212							2.8	
Tm : 123	62 ± 19	25 ± 8		0.26 ± 0.01				
Y : 123	104 ± 38	47 ± 12	56 ± 14	0.20 ± 0.05	60 ± 65	6.5	8 ± 3	1.1 ± 0.6
Aluminum alloys[a,b]	65–75	20–25	70–80	0.345		100–600		15–100
Ferrous alloys[c]	70–220	27–87	50–117	0.25–0.30	75–2250	90–2240	0.9–7.6	9–150
Brass[b]	101	37.3	112	0.350		280–730		
Hardened steel[b]	210	79	165	0.295		1800–2300		30–160
Alumina ceramic[d]	416 ± 30	169 ± 5	257 ± 50	0.231 ± 0.001	380 ± 50	267 ± 30	15 ± 2	3.5 ± 0.5
Natural diamond[e]	700–1200		440–590	0.07–0.2	1050	16–33	80–150	4.8–11

[a] Felbeck and Atkins (1984).
[b] Smith (1994).
[c] Ashby (1993).
[d] Munro (1997).
[e] Ownby and Stewart (1991).

wires and tapes. Currently, for example, the most prominent method for the production of wires is a powder-in-tube method (Dou and Liu, 1993) in which a composite, consisting of a superconductor and a metal sheathing, is produced. The composite may be subjected to several mechanical deformation processes as the material is drawn, rolled, or pressed, and further deformation may occur as the final product is shaped or coiled. Optimization of the process and minimization of the generation of deleterious microcracks requires a substantial knowledge of the mechanical behavior of the ceramic superconductors.

The mechanical properties of high-T_c superconductors exhibit significant and complex variations with processing conditions, as well with temperature, pressure, microstructure, and the specific measurement procedures. However, a highly simplified overview of the mechanical characteristics of these materials can be constructed, Table 13.10, in terms of the means and standard deviations of the respective properties for each material. In making such an overview, variations arising from the material and procedural factors are effectively absorbed as contributions to the standard deviation. While much detailed information is necessarily suppressed in this construction, a reasonable relative view of the high-T_c materials emerges. According to Table 13.10, the Bi : 2212 and Bi(Pb) : 2223 materials are softer (lower bulk modulus and hardness), stronger (higher flexural and tensile strengths), and more resistant to cracks (higher fracture toughness) than Y : 123 specimens. Such characteristics imply a lower degree of brittleness (a greater tolerance of imperfections) and make the Bi : 2212 and Bi(Pb) : 2223 materials more amenable to being adapted to such applications as tapes and wires.

Acknowledgement

The data sets included in this review were compiled as part of the effort at NIST to develop a computerized materials property database on high-temperature superconductors (NIST, 1995; 1997).

References

A. Al-Kheffaji, M. Cankurtaran, G. A. Saunders, D. P. Almond, E. F. Lambson, and R. C. J. Draper, "Elastic Behaviour under Pressure of High-T_c Superconductors $RBa_2Cu_3O_{7-x}$ (R=Y, Gd and Eu)," *Phil. Mag. B* **59**, 487–497 (1989).

N. M. Alford, J. D. Birchall, W. J. Clegg, M. A. Harmer, K. Kendall, and D. H. Jones, "Physical and Mechanical Properties of $YBa_2Cu_3O_{7-\delta}$ Superconductors," *J. Mater. Sci.* **23**, 761–768 (1988).

N. M. Alford, T. W. Button, and J. D. Birchall, "Processing, Properties and Devices in High-T_c Superconductors," *Supercond. Sci. Technol.* **3**, 1–7 (1990).

D. P. Almond, E. Lambson, G. A. Saunders, and W. Hong, "An Ultrasonic Study of the Elastic Properties of the Normal and Superconducting States of $YBa_2Cu_3O_{7-\delta}$," *J. Phys. F: Metal Phys.* **17**, L221–L224 (1987).

D. P. Almond, Qingxian Wang, J. Freestone, E. P. Lambson, B. Chapman, and G. A. Saunders, "An Ultrasonic Study of Superconducting and Non-Superconducting $GdBa_2Cu_3O_{7-x}$," *J. Phys. Condensed Matt.* **1**, 6853–6864 (1989).

American Society for Testing and Materials, C 1161, "Standard Test Method for Flexural Strength of Advanced Ceramics at Ambient Temperature."

American Society for Testing and Materials. C 1198, "Standard Test Method for Dynamic Young's Modulus, Shear Modulus, and Poisson's Ratio for Advanced Ceramics by Sonic Resonance."

American Society for Testing and Materials, C 1211, "Standard Test Method for Flexural Strength of Advanced Ceramics at Elevated Temperature."

American Society for Testing and Materials D 3379, "Standard Test Method for Tensile Strength and Young's Modulus for High-Modulus Single-Filament Materials".

American Society for Testing and Materials, E 92, "Standard Test Method for Vickers Hardness of Metallic Materials."

American Society for Testing and Materials, E 384, "Standard Test Method for Microhardness of Materials."

O. L. Anderson, "Determination and Some Uses of Isotropic Elastic Constants of Polycrystalline Aggregates Using Single-Crystal Data," in *Physical Acoustics*, Vol. 3B (W. P. Manson, ed.), Academic Press, Boston, pp. 43–95 (1965).

R. M. Anderson, "Testing Advanced Ceramics," *Adv. Mater. Proc.* **135**, 31–36 (1989).

G. R. Anstis, P. Chantikul, B. R. Lawn, and D. B. Marshall, "A Critical Evaluation of Indentation Techniques for Measuring Fracture Toughness: I, Direct Crack Measurements," Journal of the American Ceramic Society, Vol. 64, pp. 533–538 (1981).

M. F. Ashby, "Criteria for Selecting the Components of Composites," *Acta Metallurgica et Materialia* **41**, 1313–1335 (1993).

J. Barden, L. N. Cooper, and J. R. Schrieffer, "Theory of Superconductivity," *Phys. Rev.* **108**, 1175–1204 (1957).

S. Batdorf, "Fundamentals of the Statistical Theory of Fracture," *Fracture Mechanics of Ceramics* **3**, 1–30 (1978).

V. S. Bobrov, "Deformation, Structure and Properties of Ceramics and Crystals of High-T_c Superconductors," *Mater. Sci. Eng. A* **164**, 146–152 (1993).

B. Bridge, "Confirmation of and Discussion of a Previous Model of the Elastic Constants of the Metal-Oxide Superconductor $YBa_2Cu_3O_{7-x}$, *J. Mater. Sci. Lett.* **9**, 1184–1186 (1990).

M. Cankurtaran and G. A. Saunders, "Ultrasonic Determination of the Elastic Moduli and Their Temperature and Pressure Dependences in $YBa_2Cu_3O_{7-x}$/Ag(15 vol.%) Composite," *Supercond. Sci. and Technol.* **5**, pp. 210–215 (1992a).

M. Cankurtaran and G. A. Saunders, "Correlation between Anomalous Elastic Behaviour Under Pressure and with Temperature near 220 K in $YBa_2Cu_3O_{7-x}$," *Supercond. Sci. Technol.* **5**, 529–533 (1992b).

M. Cankurtan, G. A. Saunders, D. P. Almond, A. Al-Kheffaji, E. F. Lambson, and R. C. J. Draper, "The Effect of Hydrostatic Pressure on the Elastic Behavior of $GdBa_2Cu_3O_{7-x}$," *J. Phys. Condensed Matt.* **1**, 9067–9076 (1989).

M. Cankurtaran, G. A. Saunders, K. C. Goretta, and R. B. Poeppel, "Ultrasonic Determination of the Elastic Properties and Their Pressure and Temperature Dependences in Very Dense $YBa_2Cu_3O_{7-x}$," *Phys. Rev. B.* **46**, 1157–1165 (1992).

M. Cankurtaran, G. A. Saunders, and K. C. Goretta, "Ultrasonic Study of the Temperature and Pressure Dependences of the Elastic Properties of Fully Oxygenated $YBa_2Cu_3O_{6.94}$," *Supercond. Sci. Technol.* **7**, 4–9 (1994).

F. Chang, P. J. Ford, G. A. Saunders, L. Jiaqiang, D. P. Almond, B. Chapman, M. Cankurtaran, R. B. Poeppel, and K. C. Goretta, "Anisotropic Elastic and Nonlinear Acoustic Properties of Very Dense Textured $Bi_2Sr_2CaCu_2O_{8+y}$," *Supercond. Sci. Technol.* **6**, 484–489 (1993).

C. Y. Chu, J. L. Routbort, N. Chen, A. C. Biondo, D. S. Kupperman, and K. C. Goretta, "Mechanical Properties and Texture of Dense Polycrystalline $Bi_2Sr_2CaCu_2O_x$," *Supercond. Sci. Technol.* **5**, 306–312 (1992).

R. F. Cook, T. R. Dinger, and D. R. Clarke, "Fracture Toughness Measurements of $YBa_2Cu_3O_x$ Single Crystals," *Appl. Phys. Lett.* **51**, 454–456 (1987a).

R. F. Cook, T. M. Shaw, and P. R. Duncombe, "Fracture Properties of Polycrystalline $YBa_2Cu_3O_x$," *Adv. Ceram. Mater.* **2**, 606–614 (1987b).

E. Cruceanu, J. Deutz, H. Klein, W. Schmitz, and H. Ullmaier, "Mechanical Anisotropy of $YBa_2Cu_3O_x$ Single Crystals," *Mater. Sci. Eng. A* **160**, L9–L11 (1993).

D. G. S. Davies, "The Statistical Approach to Engineering Design in Ceramics," *Proc. Brit. Ceram. Soc.* **22**, 429–452 (1973).

V. V. Demirskii, H. J. Kaufmann, S. V. Lubenets, V. D. Natsik, and L. S. Fomenko, "Microhardness and Microbrittleness of Single Crystals of the High-Temperature Superconductor YBaCuO," *Sov. Phys. Solid State* **31**, 1065–1066 (1989).

J. Dominec, P. Vasek, P. Svoboda, V. Plechacek, and C. Laermans, "Elastic Moduli for Three Superconducting Phases of Bi–Sr–Ca–Cu–O," *Mod. Phys. Lett. B* **6**, 1049–1054 (1992).

S. X. Dou and H. K. Liu, "Ag sheathed Bi(Pb)SrCaCuO Superconducting Tapes" *Supercond. Sci. Technol.* **6**, 297–314 (1993).

A. G. Evans and E. A. Charles, "Fracture Toughness Determinations by Indentations," *J. Am. Ceram. Soc.* **59**, 371–372 (1976).

Y. Fang, S. Danyluk, Z. Li, and D. Lam, "Knoop Microhardness Anistropy of $YBa_2Cu_3O_{7-\delta}$ Single Crystals," *J. Mater. Sci. Lett.* **12**, 1070–1072 (1993).

C. Fanggao, M. Cankurtaran, G. A. Saunders, A. Al-Kheffaji, D. P. Almond, P. J. Ford, and D. A. Ladds, "Ultrasonic Evidence of Strong Vibrational Anharmonicity in High-T_c Superconductors and Its Effect on Determination of their Elastic Properties," *Phys. Rev. B* **43**, 5526–5537 (1991).

D. K. Felbeck and A. G. Atkins, *Strength and Fracture of Engineering Solids*. Prentice-Hall, Englewood Cliffs, NJ (1984).

J. D. French and S. M. Wiederhorn, "Tensile Specimens from Ceramic Components," *J. Am. Ceram. Soc.* **79**, 550–552 (1996).

K. C. Goretta, M. L. Kullberg, D. Bar, G. A. Risch, and J. L. Routbort, "Fracture Toughness of $YBa_2Cu_3O_x$ Containing Y_2BaCuO_5 and ZrO_2," *Supercond. Sci. Technol.* **4**, 544–547 (1991).

K. C. Goretta, M. E. Loomans, L. J. Martin, J. Joo, R. B. Poeppel, and N. Chen, "Fracture of Dense, Textured $Bi_2Sr_2CaCu_2O_x$," *Supercond. Sci. Technol.* **6**, 282–286 (1993).

A Goyal, W. C. Oliver, P. D. Funkenbusch, D. M. Kroeger, and S. J. Burns, "Mechanical Properties of Highly Aligned $YBa_2CU_3O_{7-\delta}$, Effect of Y_2BaCuO_x Particles," *Physica C* **183**, 221–233 (1991).

A. Goyal, P. D. Funkenbusch, D. M. Kroeger, and S. J. Burns, "Anisotropic Hardness and Fracture Toughness of Highly Aligned $YBa_2Cu_3O_{7-\delta}$," *J. Appl. Phys.* **71**, 2363–2367 (1992).

A. A. Griffith, "Phenomena of Rupture and Flow in Solids," *Phil. Trans. Roy. Soc. Lon.*, **221**, 163–198 (1921).

D. P. H. Hasselman and R. M. Fulrath, "Effect of Small Fraction of Spherical Porosity on Elastic Moduli of Glass," *J. Am. Ceram. Soc.* **47**, 52–53 (1964).

F. Hild and D. Marquis, "A Statistical Approach to the Rupture of Brittle Materials," *Eur. J. Mechan. A* **11**, 753–765 (1992).

M. K. Ihm, B. R. Powell, and R. L. Bloink, "The Flexural Strength and Microhardness of $YBa_2Cu_3O_{6+\delta}$, *J. Mater. Sci.* **25**, 1664–1674 (1990).

C. E. Inglis, "Stresses in a Plate due to the Presence of Cracks and Sharp Corners," *Transactions of the Institute of Naval Architects* **55**, 219–241 (1913).

O. Ishani and L. J. Cohen, "Elastic Properties of Filled and Porous Epoxy Composites," *Int. J. Mech. Sci.* **9**, 539–546 (1967).

J. Joo, J. P. Singh, T. Warzynski, A. Grow, and R. B. Poeppel, "Role of Silver Addition on Mechanical and Superconducting Properties of High-T_c Superconductors," *Appl. Supercond.* **2**, 401–410 (1994).

F. Knoop, C. G. Peters, and W. B. Emerson, "A Sensitive Pyramidal-Diamond Tool for Indentation Measurements," *J. Res. Nat. Bur. Stand.* **23**, 39–78 (1939).

J. Krautkrämer and H. Krautkrämer, *Ultrasonic Testing of Materials*. Springer-Verlag, New York, 1990.

H. M. Ledbetter and S. K. Datta, "Effective Wave Speeds in an SiC-Particle-Reinforced Al Composite," *J. Acoust. Soc. Am.* **79**, 239–248 (1986).

H. Ledbetter and M. Lei, "Monocrystal Elastic Constants of Orthotropic $Y_1Ba_2Cu_3O_7$: An Estimate," *J. Mater. Res.* **6**, 2253–2255 (1991).

H. Ledbetter, M. Lei, A. Hermann, and Z. Sheng, "Low-Temperature Elastic Constants of $Y_1Ba_2Cu_3O_7$," *Physica C* **225**, 397–403 (1994).

P. Lemmens, C. Hunnekes, P. Froning, S. Ewert, H. Passing, G. Marbach, and A. Comberg, "Elastic Properties of $YBa_2Cu_3O_x$, $(Y_{1-y}Pr_y)Ba_2Cu_2Cu_3O_7$ and $(BiPb)_2Sr_2Ca_2Cu_3O_{10}$ Studied by Ultrasound," *J. Less-Common Met.* **164 & 165**, 1129–1135 (1990).

S. Lin, M. Lei, and H. Ledbetter, "Elastic Constants and Debye Temperature of $Y_1Ba_2Cu_3O_x$: Effect of Oxygen Content," *Mater. Lett.* **16**, 165–168 (1993).

W. Lo, A. M. Campbell, J. Luo, and R. Stevens, "Indentation-Induced Deformation and Microcracking of Highly Textured Superconducting $(Bi, Pb)_2Sr_2Ca_2Cu_3O_x$ Ceramics," *J. Mater. Res.* **10**, 568–577 (1995).

I. M. Low, R. D. Skala, and G. Mohazzab-H, "Mechanical and Fracture Properties of Epoxy-Modified YBaCuO (123) Superconductors," *J. Mater. Sci. Lett.* **13**, 1340–1342 (1994).

I. M. Low, H. Wang, and R. D. Skala, "Epoxy-Modified Bi(Pb)SrCaCuO Superconductors with Improved Mechanical Properties," *J. Mater. Sci. Lett.* **14**, 384–386 (1995).

B. N. Lucas, W. C. Oliver, R. K. Williams, J. Brynestad, and M. E. O'Hern, "The Hardness and Young's Modulus of Bulk $YBa_2Cu_3O_{7-x}$ (1 : 2 : 3) and $YBa_2Cu_4O_8$ (1 : 2 : 4) as Determined by Ultra Low Load Indentation," *J. Mater. Res.* **6**, 2519–2522 (1991).

J. Luo, R. Stevens, W. Lo, and A. Campbell, "Anisotropic Plastic and Elastic Deformation in Highly Textured Superconducting $(Bi, Pb)_2Sr_2Ca_2Cu_3O_x$ Ceramics," *J. Mater. Sci.* **30**, 3050–3056 (1995).

J. K. Mackenzie, "The Elastic Constants of a Solid Containing Spherical Holes," *Proc. Phys. Soc. B*, **63**, 2–11 (1950).

L. J. Martin, K. C. Goretta, J. Joo, J. P. Sing, S. R. Olson, S. Wasylenko, R. B. Poeppel, and N. Chen, "Mechanical Properties of BiSrCaCuO/Ag Superconductors," *Mater. Lett.* **17**, 232–236 (1993).

L. Martinez, W. C. Oliver, and R. K. Williams, "Characterization of $YBa_2Cu_3O_{7-x}$ in a Mechanical Properties Microprobe," *Scripta Metallurgica et Materialia* **26**, 7–12 (1992).

I. J. McColm, *Ceramic Hardness*. Plenum Press, New York, 1990.

E. Meyer, "Untersuchungen über Härteprüfung und Härte," *Vereines Deutscher Ingenieure* **52**, 645–654 (1908).

R. G. Munro, "Evaluated Material Properties for a Sintered α-Alumina," *J. Am. Ceram. Soc.* **80**, 1919–1928 (1997).

R. G. Munro, S. Block, and G. J. Piermarini, "Reliability of the Isothermal Bulk Modulus Deduced from Model Equations of State," *J. Appl. Phys.* **56**, 2174–2176 (1984).

D. G. Munz, J. L. Shannon, Jr., and R. T. Bubsey, "Fracture Toughness Calculation from Maximum Load in Four Point Bend Tests of Chevron Notch Specimens," *Int. J. Fracture* **16**, R137–R141 (1980).

M. Muralidhar, K. N. Reddy, and V. H. Babu, "Microhardness Studies on BiCaSrCuO (2122) Superconducting Single Crystals and Pellets," *Physica Stat. Solid (a)* **126**, 115–120 (1991).

M. Muralidhar, K. N. Kishore, Y. V. Ramana, and V. H. Babu, "Elastic and Plastic Behavior of Lead and Silver Doped Bi–Sr–Ca–Cu–O Superconductors," *Mater. Sci. Eng. B* **13**, 215–219 (1992).

N. Murayama, Y. Kodama, S. Sakaguchi, and F. Wakai, "Mechanical Strengths of Hot-Pressed Bi–Pb–Sr–Ca–Cu–O Superconductor," *J. Mater. Res.* **7**, 34–37 (1992).

National Institute of Standards and Technology, Maryland, Gaithersburg, Standard Reference Database No. 62: High Temperature Superconductors, Standard Reference Data Program, Version 1 (1995) and Version 2 (1997).

J. C. Newman, Jr. and I. S. Raju, "An Empirical Stress-Intensity Factor Equation for the Surface Crack," *Eng. Fracture Mechan.* **15**, 185–192 (1981).

Q. H. Ni, D. L. Wang, and Q. P. Kong, "Mechanical Properties of YBCO Superconductors Prepared by the Melt-Textures Growth Method," *Physica Stat. Solidi (a)* **138**, K29–K33 (1993).

T. Nose and T. Fujii, "Evaluation of Fracture Toughness for Ceramic Materials by a Single-Edge-Precracked-Beam Method," *J. Am. Ceram. Soc.* **71**, 328–333 (1988).

T. Ohji, "Towards Routine Tensile Testing," *Int. J. High Technol. Ceram.* **4**, 211–225 (1988).

T. S. Orlova, B. I. Smirnov, and V. V. Shpeizman, "Microhardness of Single Crystals of Various High-Temperature Superconductors," *Sov. Phys. Solid State* **32**, 1838–1839 (1990).

F. Osterstock, S. Strauss, B. L. Mordike, and G. Desgardin, "Toughness and Thermoshock Resistance of Polycrystalline $YBa_2Cu_3O_{7-\delta}$," *J. Alloys Compounds* **195**, 679–682 (1993).

F. Osterstock, I. Monot, G. Desgardin, and B. L. Mordike, "Influence of Grain Size on the Toughness and Thermal Shock Resistance of Polycrystalline $YBa_2Cu_3O_{7-\delta}$," *J. Eur. Ceram. Soc.* **16**, 687–694 (1996).

P. D. Ownby and R. W. Stewart, "Engineering Properties of Diamond and Graphite," in *Engineered Materials Handbook*, Vol. 4, pp. 821–834. ASM International, 1991.

L. N. Pal-Val, P. P. Pal-Val, V. D. Natsik, and V. I. Dotsenko, "Comparative Study of the Low-Temperature Acoustic Properties of CuO and $YBa_2Cu_3O_x$ Ceramics," *Solid State Commun.* **81**, 761–765 (1992).

C. B. Ponton and R. D. Rawlings, "Vickers Indentation Fracture Toughness Test, part 1, Review of Literature and Formulation of Standardised Indentation Toughness Equations," Materials Science and Technology, Vol. 5, pp. 865–872 (1989a).

C. B. Ponton and R. D. Rawlings, "Vickers Indentation Fracture Toughness Test, Part 2, Application and Critical Evaluation of Standardised Indentation Toughness Equations," *Mater. Sci. Technol.* **5**, 961–976 (1989b).

C. P. Poole, Jr., T. Datta, and H. A. Farach, *Copper Oxide Superconductors*. John Wiley and Sons, New York, 1988, p. 44.

G. D. Quinn and R. Morrell, "Design Data for Engineering Ceramics: A Review of the Flexure Test," *J. Am. Ceram. Soc.* **74**, 2037–2066 (1991).

G. D. Quinn, J. Salem, I. Bar-on, K. Cho, M. Foley, and H. Fang, "Fracture Toughness of Advanced Ceramics at Room Temperature," *J. Nat. Inst. Stand. Technol.* **97**, 579–607 (1992).

G. D. Quinn, R. J. Gettings, and J. J. Kubler, "Fracture Toughness by the Surface Crack in Flexure (SCF) Method: Results of the VAMAS Round Robin," *Ceram. Eng. Sci. Proc.* **15**, 846–855 (1994).

A. S. Raynes, S. W. Freiman, F. W. Gayle, and D. L. Kaiser, "Fracture Toughness of $YBa_2Cu_3O_{7-\delta}$ Single Crystals: Anisotrpy and Twinning Effects," *J. Appl. Phys.* **70**, 5254–5257 (1991).

P. V. Reddy, R. R. Reddy, K. B. Reddy, and V. N. Mulay, "Ultrasonic Anomalies in Y–Ba–Cu–O High-T_c Superconducting Materials," *Mod. Phys. Lett. B* **7**, 1457–1465 (1993).

P. V. Reddy, S. Shekar, and K. Somaiah, "Elasticity Studies of RE–Ba–Cu–O High-T_c Superconductors," *Mater. Lett.* **21**, 21–29 (1994).

R. R. Reddy, M. Muralidhar, V. H. Babu, and P. V. Reddy, "The Relationship between the Porosity and Elastic Moduli of the Bi–Pb–2212 High-T_c Superconductor," *Supercond. Sci. Techol.* **8**, 101–107 (1995).

C. Rief and K. Kromp, "Fracture Toughness Testing," *Int. J. High Technol. Ceram.* **4**, 301–317 (1988).

A. Rudnick, A. R. Hunter, and F. C. Holden, "An Analysis of the Diametral-Compression Test," *Mater. Res. Stand.* **3**, 283–289 (1963).

J. P. Singh, R. A. Guttschow, J. T. Dusek, and R. B. Poeppel, "Role of p_{O_2} in Microstructural Development and Properties of $YBa_2Cu_3O_x$ Superconductors," *J. Mater. Res.* **7**, 2324–2332 (1992).

G. G. Siu and W. G. Zeng, "Phase-Transition Toughening of High-T_c Superconducting Ceramics," *J. Mater. Sci.* **28**, 5875–5879 (1993).

E. H. Smith, *Mechanical Engineer's Reference Book*, 12th ed. Society of Automotive Engineers, Inc., Butterworth-Heimemann Ltd, Oxford, 1994.

R. M. Spriggs and L. A. Brissette, "Expressions for Shear Modulus and Poisson's Ratio of Porous Refractory Oxides," *J. Am. Ceram. Soc.* **45**, 198–199 (1962).

M. Srinivasan and S. J. G. Seshadri, "Application of Single Edge Notched Beam and Indentation Techniques to Determine Fracture Toughness of Alpha Silicon Carbide," (in Fracture Mechanics Methods for Ceramics, Rocks and Concrete, ASTM STP 745, S. W. Freiman and E. R. Fuller, Jr., Eds.). American Society for Testing and Materials, 1981, pp. 46–68.

S. Suasmoro, D. S. Smith, M. Lejeune, M. Huger, and C. Gault, "High Temperature Ultrasonic Characterization of Intrinsic and Microstructural Changes in Ceramic $YBa_2Cu_3O_{7-\delta}$," *J. Mater. Res.* **7**, 1629–1635 (1992).

S. Timoshenko, *Strength of Materials*, Part I. Van Nostrand, New York, 1940, p. 4.

R. J. Topare, K. Ganesh, N. K. Sahuji, S. S. Shah, and P. V. Reddy, "Elastic Anomalies in Bi–Pb–2223/Ag Superconducting Composite Materials," *Physica C* **253**, 89–96 (1995).

C. A. Tracy and G. D. Quinn, "Fracture Toughness by the Surface Crack in Flexure (SCF) Method," *Ceram. Eng. Sci. Proc.* **15**, 837–845 (1994).

T. M. Tritt, M. Marone, X. Chen, M. J. Skove, A. C. Ehrlich, G. X. Tessema, D. J. Gillespie, J. P. Franck, and J. Jung, "Measure of the Magnitude of Young's Modulus in Whisker-Like Samples of the Bi-based High-T_c Materials $Bi_2Sr_2CaCu_2O_x$ and $Bi_2Sr_2Ca_2Cu_3O_x$," *Physica C* **178**, 296–300 (1991).

S. Uemura and M. Takayanagi, "Application of the Theory of Elasticity and Viscosity of Two-Phase Systems to Polymer Blends," *J. Appl. Polymer Sci.* **10**, 113–125 (1966).

A. S. Wagh, J. P. Singh, and R. B. Poeppel, "Dependence of Ceramic Fracture Properties on Porosity," *J. Mater. Sci.* **28**, 3589–3593 (1993).

Q. Wang, G. A. Saunders, D. P. Almond, M. Cankurtaran, and K. C. Goretta, "Elastic and Nonlinear Acoustic Properties of $YBa_2Cu_3O_{7-x}$ Ceramics with Different Oxygen Contents," *Phys. Rev. B* **52**, 3711–3726 (1995).

W. Weibull, "Statistical Theory of Strength of Materials," *Proc. Swed. Inst. Eng. Res.* **151**, 1–45 (1939).

W. Weibull, "A Statistical Distribution Function of Wide Applicability," *J. Appl. Mechan.* **18**, 293–297 (1951).

F. Yeh and K. W. White, "Fracture Toughness Behavior of the $YBa_2Cu_3O_{7-x}$ Superconducting Ceramic with Silver Oxide Additions," *J. Appl. Phys.* **70**, 4989–4994 (1991).

Y. S. Yuan, M. S. Wong, and S. S. Wang, "Mechanical Behavior of Mg-whisker Reinforced $(Bi, Pb)_2Sr_{22}Ca_2Cu_3O_y$ High-Temperature Superconducting Composite," *J. Mater. Res.* **11**, 1645–1652 (1996).

H. Yusheng, X. Jiong, J. Sheng, H. Aisheng, and Z. Jincang, "Ultrasonic Investigations of the Layered Perovskite Ceramic Superconducting Systems," *Physica B* **165**, 1283–1284 (1990).

Chapter 14

Phase Diagrams

Winnie Wong-Ng
Ceramics Division, National Institute of Standards and Technology, Gaithersburg, MD

ISBN: 0-12-561460-8
$30.00

HANDBOOK OF SUPERCONDUCTIVITY

A

Introduction

Investigation of high-temperature superconductor materials has become an exciting and extensive research area in the past 10 years. Since the initial report of the 30 K superconductor by Bednorz and Müller (1986), a large number of multicomponent oxide materials have been discovered (Cava, 1995); most of these compounds exhibit complex chemistry, including nonstoichiometry, defects, and incommensuracy. International efforts in superconductivity research have led to many alternative methods of processing as well as novel applications. The developments of coated conductors utilizing the $Ba_2YCu_3O_{6+x}$ and $Ba_2RCu_3O_{6+x}$ (R = lanthanides) phases with ion beam assisted deposition (IBAD) and rolling assisted biaxially textured substrate (RABiTS) techniques have prompted the intensive investigations of these systems in thin- and thick-film forms (Goyal *et al.*, 1996; Wu *et al.*, 1995; Paranthaman *et al.*, 1997). In the Bi_2O_3–PbO–SrO–CaO–CuO systems (BSCCO), the Bi-containing materials were found to show promising superconducting and other properties that are appropriate for wire and tape applications using the powder-in-tube (PIT) techniques (Balachandran *et al.*, 1994; Sandhage *et al.*, 1991; Sato *et al.*, 1991; Malosemoff *et al.*, 1997; Zhou *et al.*, 1995) for fabrication. These novel processes have brought superconducting technology closer to reality. Presently, high-quality high-temperature superconducting materials are still relatively difficult to prepare. Challenging problems have to be overcome for large-scale commercial processing to be successful (Wong-Ng, 1999). At a more basic level, the underlying principles governing the superconducting properties are not totally understood.

Phase diagrams are critical research tools for many scientific disciplines, including materials science, ceramics, geology, physics, metallurgy, chemical engineering, and chemistry. These diagrams contain important information for the development of new materials, control of structure and composition of critical phases, and improvement of properties of technologically important materials. Phase diagrams can be thought of as "road maps" for processing; they provide the theoretical basis for synthesis of high-T_c materials. Applications of phase diagrams range from preparation of high-quality single crystals and single-phase bulk materials to deliberate precipitation of second phases as flux pinning sites (Majewski, 1996; Majewski *et al.*, 1995a; Tiefel *et al.*, 1990) and the formation of melts. The presence of melts can have a beneficial effect on superconductor processing. For example, melts were found to be essential during PIT processing of Bi-2223 and 2212 wires, and during the production of textured or crystallographically aligned material in tapes or thin films (Aksenova *et al.*, 1993; Zhang and Hellstrom, 1993).

The aim of this chapter is to provide experimental phase diagrams of high-T_c superconductors representative of systems undergoing research. Among

current systems, the $BaO–Y_2O_3–CuO$ (BYC), $BaO–R_2O_3–CuO$ (BRC), and BSCCO systems have been studied most extensively. A brief description of some of the frequently encountered terms used in phase equilibrium work, as well as a few experimental techniques involved in determining some of these diagrams, are also presented prior to the discussion of the diagrams.

In the following description of the multicomponent systems, a numerical code is used to indicate the stoichiometry of compounds in the order in which the cations are listed. For example, the symbol 213 (or 2 : 1 : 3) is used to represent the compound $Ba_2YCu_3O_{6+x}$, and the symbol 2212 (or 2 : 2 : 1 : 2) is used to represent the compound $Bi_2Sr_2CaCu_2O_x$ and its solid solution.

B

General Discussion and Scope

a. Information Provided

Before any research and development is conducted on material synthesis or processing, it is logical to first study the relevant phase diagrams to obtain information about the phase relationships and other characteristics of the material. Phase diagrams can be used to depict a wide range of information, such as (1) identity of compounds formed from specific end members, (2) stability range, composition, and temperature range of a specific phase, (3) the optimum conditions for synthesis, (4) the impurities likely to be present with a phase prepared under specific conditions, (5) the region of homogeneity of solid solutions, (6) polymorphism of a phase, (7) temperature and composition range suitable for glass formation, (8) melting temperature (or temperature range) of a compound, (9) primary phase field (crystallization composition field) of a phase, (10) effect of admixture on the melting point or stability of a phase, (11) effect of temperature and pressure on processing, and (12) prediction of properties of the final products, based on the phase assemblage.

b. Key Terms Used

The frequently encountered nomenclature and the general terms discussed in the following sections are briefly described next. For a more complete set of definitions and a glossary, refer to Volume 1 of *Phase Diagrams for Ceramists* (Levin *et al.*, 1964).

A *solidus* is the locus of temperature–composition points in a system at temperatures above which solid and liquid are in equilibrium and below which the system is completely solid. In binary diagrams without solid solutions, it is a straight line, or a combination of straight lines representing constant tempera-

tures, and with solid solutions, it is a curved line or a combination of curved and straight lines. Likewise, in ternary systems, the solidus is represented by flat planes or by curved surfaces.

A *phase* is any portion, including the whole, of a system that is physically homogeneous within itself and bounded by a surface that mechanically separates it from any other portions.

The *components* (of a system) are the smallest number of independently variable chemical constituents necessary and sufficient to express the composition of each phase present in any state of equilibrium. Zero and negative quantities of the components are permissible in expressing the composition of a phase.

The *phase rule* states that, for a system in equilibrium, the sum of the number of phases (P) plus a number of degress of freedom (F) must equal the sum of the number of components (C) plus 2, or $P + F = C + 2$.

The number of *degrees of freedom* of a system is the number of intensive variables that can be altered independently or arbitrarily without bringing about the disappearance of a phase or the formation of a new one. Intensive variables are those that are independent of mass, such as pressure, temperature, and composition.

A *join* (tie-line) is the region of a phase diagram representing all mixtures that can be formed from a given number of selected compositions. A join may be a line (binary), a surface (ternary), etc., depending on the number of selected compositions, which need not be compounds. Each selected composition, however, must be incapable of formation from the others.

The *lever rule* (or center of gravity principle) states that when a particular composition separates into only two phases, the given composition and that of the two phases are colinear; furthermore, the amounts of the two separated phases are inversely proportional to their distances from the given composition. Thus, if A and B represent the compositions of two phases formed from composition C, then the amount of A times the length AC equals the amount of B times the length BC, or $A/B = BC/AC$:

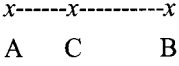

The *composition (or compatibility) triangle* in the phase diagram of a condensed ternary system is the area bounded by three tie-lines (joins) connecting the composition points of three phases that are in equilibrium within the triangle.

The *composition (or compatibility) tetrahedron* in the phase diagram of a condensed quaternary system constitutes the four triangular planes connecting the compositions of four solid phases that can coexist in equilibrium with liquid. The composition of the liquid is represented by a *quaternary invariant point*, which may be either a eutectic point within the composition tetrahedron or a peritectic or reaction point outside the tetrahedron.

A *solid solution* is a single crystalline phase that may be varied in composition within finite limits without the appearance of an additional phase.

A *liquidus* is the locus of temperature–composition points representing the maximum solubility (saturation) of a solid phase in the liquid phase. In a binary system, it is a line; in a ternary system, it is a surface, usually curved. At temperatures above the liquidus, the system is completely liquid. A point on the liquidus represents equilibrium between liquid and, in general, one crystalline phase (the primary phase).

The primary phase is the only crystalline phase in equilibrium with a liquid of a given composition. It is the first crystalline phase to appear on cooling a composition from the liquid; or conversely, it is the last crystalline phase to disappear on heating a composition to melting.

The *primary phase region* (or primary phase field) is the locus of all compositions in a phase diagram having a common primary phase.

The *invariant points* are the particular conditions within a system, in terms of pressure, temperature, and composition, for which the system possesses no degrees of freedom. An example is the triple point of a gas.

A *eutectic* represents an invariant (unique temperature, pressure, composition) point for a system at which the phase reaction on the addition or removal of heat results in an increase or decrease of the proportion of liquid to solid phases, without change of temperature. At a eutectic point the composition of the liquid phase in equilibrium with the solid phases can always be expressed in terms of positive quantitatives of the solid phases.

The *eutectic composition* is that combination of components in a simple system having the lowest melting temperature at any ratio of the components and is located at the intersection of the two solubility curves in a binary system and of the three solubility surfaces in a ternary system.

A *peritectic point* is an invariant point at which the composition of the liquid phase in equilibrium with the solid phases cannot be expressed in terms of positive quantities of the solid phases. Whereas the composition of a eutectic point always lies between or within the composition limits of the solid phases in equilibrium with the liquid, the composition of a peritectic point always lies outside the composition limits.

A *congruent melting point* is a specified pressure and temperature at which a solid subtance changes to a liquid of identical chemical composition.

An *incongruently melting point* is a specified pressure and temperature at which one solid phase transforms into another solid phase plus a liquid phase, both of different chemical compositions than the original substance.

A *boundary line* is the intersection of adjoining liquidus surfaces in a ternary phase diagram. The area enclosed by a series of boundary lines is termed a primary phase area.

An *isothermal section* is a phase equilibrium diagram constructed at a given specific temperature.

Liquid immiscibility refers to two or more distinct liquid phases coexisting in equilibrium.

c. Phase Diagram Compilations

Various sources of information are needed for users for pursuing phase diagram studies. For more than 60 years, a long-standing cooperative effort between NIST and the American Ceramics Society (ACerS) has resulted in an extensive set of compilations of Phase Diagrams for Ceramists (PDFC) (NIST, *Phase Diagrams for Ceramists*. To date, these compilations include 12 volumes of oxides, salts, and refractory materials, three annual volumes of diagrams published in 1991, 1992 and 1993. In addition, two volumes containing high-temperature superconductor data, including diagrams, write-ups and biblographic information, were also published in 1991 and 1997 (*Superconductors*, Vol. I and II) (Whitler and Roth, 1991; Vanderah *et al.*, 1991). These phase diagrams are mostly from the literature, and the data have been edited by experts in the field. Under this NIST/ACerS phase diagram effort, technical expertise in the compilation of phase diagrams is provided by NIST researchers and by various university, industry, and government collaborations. The ACerS assumes the responsibility for the production aspects of the work and for all means of data dissemination.

The PDFC series have also been computerized and published in the form of a CD-ROM database (version 2.1). This database contains more than 13,000 diagrams published in the *Phase Diagrams for Ceramists*, Vol. I through X, Annuals 1991, 1992, and 1993, and *High-T_c Superconductors*, Vol. I. Future supplements will also include *High-T_c Superconductors*, Vol. II. Computer search capabilities include authors, system components, year of publication, bibliographic reference, and location in the PDFC series. On-screen manipulations of the diagrams are also possible, which include plotting of the diagrams, magnification of selected regions, conversion from mole fraction (%) to weight % (or vice versa), lever rule calculations, overlay of related diagrams, display of the cursor position in real units, reverse function for binary diagrams (permits switching of left and right end members), and a curve follow feature to track curve coordinates.

Computer and software developments have prompted increased applications of databases for materials analysis. If the phase diagram information of a specific system is not complete, one can search through other sources of databases in conjunction with the phase diagram database for providing additional phase information. These databases include the Powder Diffraction file (PDF) produced by ICDD,[1] the Crystal Data database (NIST), the Crystal Structure Series (Wyckoff), the Inorganic Crystal Structural Database (ICSD),

[1]ICDD, International Center for Diffraction Data, Newton Square; 12 Campus Blvd, Newton Squares, PA 19073–3273.

Structural Data on Intermetallic Phases (CRYSTMET) (Toth Information Systems), and the NIST/Sandia/ICDD Electron Diffraction Database (NIST). ICDD has identified a subfile of high-T_c superconductors and related phases (such as those found in phase diagrams, products of reaction with container materials, with thin film substrates and conventional superconductors) (Wong-Ng *et al.*, 1996).

C

Experimental Methods

A phase diagram is usually constructed using a combination of methods. For subsolidus phase diagrams, a number of compositions are prepared in the region of interest, followed by the determination of the phase assemblages present. Tie-lines connecting phases in equilibrium are determined in this way. When a new phase is discovered, the structure can be studied either by using single crystals, or by *ab initio* structural determination using the powder sample. The experimental methods for determining phase diagrams are generally divided into two types: static and dynamic. In the static methods, the temperature of the sample is held constant until equilibrium is attained. The most widely used of these is the quenching method (air quench or quench into a medium such as water bath, oil, liquid nitrogen cooled helium). Quenching studies in combination with powder X-ray diffraction and petrographic microscopy for phase identification are essential for obtaining subsolidus phase diagrams. Liquidus phase diagrams require further experiments for determining the melting temperatures of phases or assemblages, and the estimation of liquid compositions. Dynamic techniques, including differential thermal analysis (DTA) and thermogravimetric analysis (TGA), are needed to obtain an indication of phase transitions, reactions, and associated loss of volatiles, such as oxygen. Scanning electron microscopy (SEM) techniques are used to study the microstructures of the experimental products, particularly of the primary crystals. Quantitative microanalysis techniques, including energy dispersive x-ray analysis (EDX) or wavelength dispersive methods, are used for the determination of the compositions of the residual grains (primary crystals) and of the quenched liquid.

a. Quenching Methods

For relatively fast quenching, experiments are generally carried out using a vertical tube furnace. Upon achieving equilibrium, the sample is dropped into the quenching medium (Wong-Ng and Cook, 1995). The goal of this type of experiment is to capture the phase assemblages and microstructure by cooling from high temperature to room temperature in a few seconds. The sample is

contained in a small crucible suspended from the thermocouple assembly by thin wires (such as Pt). After insertion of the sample, the vertical-tube furnace is valved off and flushed with desired gas. The sample is then equilibrated in the hot zone of the furnace in the presence of flowing gas of the desired atmosphere. At the conclusion of the experiment, current is passed through the thin suspension wires, causing them to melt. For controlled atmospheric quenching, the sample drops into a liquid nitrogen (LN_2)-cooled copper cold well, with helium flowing at a rapid rate. This prevents reaction of the sample with atmospheric constituents during the quench.

b. X-ray Powder Diffraction

X-ray diffraction is a very convenient and nondestructive method for phase identification. Results can show if the composition is a single phase, a mixture of phases that correspond to the compositional tie-line of a two-phase system, or an aggregate of higher component regions. In order to study lattice parameters for establishing or confirming the formation of solid solution, the powder x-ray diffraction method can also be used. In these methods instrumental (external) and internal calibrations can be achieved by using standard reference materials (SRM) produced by NIST (Hubbard *et al.*, 1987; Hubbard, 1982). For atmospherically sensitive materials, a special cell with an O-ring seal can be employed to avoid reaction with atmospheric CO_2 and H_2O during analysis (Ritter, 1988). Signal absorption can be minimized by employing an X-ray transparent window.

c. Differentiation Thermal Analysis and Thermogravimetric Analysis

Thermal analysis is a technique that measures a physical property of a substance as a function of temperature, generally under a controlled temperature program. In the case of the TGA experiment, the weight of a specimen is measured as a function of time (or temperature). The changes of the weight before and after the experiment can be determined. In a DTA experiment, a sample and a reference material (usually alumina in the high-T_c superconductor experiments) are heated (or cooled) at a uniform rate and the difference in temperature between the two is plotted as a function of the temperature of the reference sample or furnace temperature. From the characteristic of the peak observed along the DTA curve, an exothermic or endothermic event involving the sample can be determined.

d. Scanning Electron Microscopy

During the SEM experiment, a focused electron beam is swept over the surface of a specimen in a raster pattern, and various resulting emissions from the sample (backscattered electrons, secondary electrons, or X-rays) are detected. An image is formed on a cathode ray screen by mapping the intensity of the detected signal as a function of position. Combining this technique with an X-ray spectrometer allows chemical analysis of a microvolume of the sample.

e. Determination of Liquid Compositions

In general, after a sample is melted and solidified, the liquid will assume the form of an amorphous state and one can easily distinguish the amorphous regions from the primary crystals after melting. In the case of high-temperature superconducting oxides, often the melts recrystallize instantaneously as crystals. This is particularly true in Ba–Cu–O and related systems, where relatively large barium cuprates form and it is difficult to distinguish between primary crystals and crystals crystallized from liquid. In this situation a wicking technique can be used (Wong-Ng and Cook, 1995). To capture liquid free of any primary crystalline phases for SEM/EDX analysis, a sintered ceramic wick with open porosity (i.e., MgO) can be placed in the crucible with the appropriate sample. During the heat treatment, liquid is drawn into the wick by capillary action. Because of the filtering action of the small (<5–$10\,\mu m$) openings in the wick, primary solid phases do not enter the capillary. During the quench, the liquid is retained in the wick, thus making a representative sample of the melt available for analysis.

The liquid composition can be obtained most directly by using electron probe microanalysis. This method measures the intensity of characteristic X-rays emitted from a specimen and relates this intensity to the concentration of the elements involved. Standardization using samples of known composition is essential. Corrections for the atomic number Z, the absorption A, and the fluorescence F (ZAF method) must be applied to the intensity ratios. A detailed description of quantitative microanalysis is given by Heinrich and Newbury (1991). Modern software such as DTSA (Fiori *et al.*, 1991) facilitates the application of these methods.

f. Vapor Pressure Measurements

For the equilibrium study of vapor pressure of Tl_2O in the Tl-containing superconducting systems, an efficient method is the two-zone technique (Aselege

et al., 1994), which utilizes a condensed thallium oxide source to supply a constant partial pressure of Tl_2O vapor through the vaporization reaction

$$2\,Tl_2O_x(c) \longleftrightarrow 2\,Tl_2O(v) + (x-1)O_2(v). \quad (1)$$

Using this procedure, the sample, which is in powder form, and the condensed thallium oxide (Tl_2O_3) are each held typically in high-purity Al_2O_3 boats, and in turn are held within an Al_2O_3 tube. The source boat is held in the closed end and the sample boat in the open end. The open end is then wrapped tightly with several layers of thin gold foil.

The equilibrium constant $K(T)$ for reaction (1) is expressed by

$$K(T) = p(Tl_2O)^2 2p(O_2)^{(x-1)}/a(Tl_2O_x)^2. \quad (2)$$

The activity of Tl_2O_x in the denominator of Eq. (2) is unity if the condensed thallium oxide exists as a pure phase. With source temperature and $p(O_2)$ fixed, $p(Tl_2O)$ may be determined from the equilibrium constant $K(T)$.

D

Representative Phase Diagrams

In the two volumes of *Phase Diagrams for High-T_c Superconductors* (Whittler and Roth, 1991; Vanderah *et al.*, 1991), a total of 542 diagrams have been collected and edited. As superconductor research is a highly active field, many systems have been investigated extensively in various laboratories. Inevitably, there are repetitions and inconsistencies. The following is a group of selected diagrams that represent either the major industrial activities of high-T_c systems today, or systems that have attracted considerable attention. This compilation emphasizes the BYC, BRC, and the BSCCO systems that contain the actual high-temperature superconductors, and not the subsystems or systems containing only related phases.

a. Ba–Y–Cu–O Systems

Extensive international research efforts since 1987 have led to the accumulation of a large body of information concerning the crystal chemistry and phase equilibria of the BYC system; this is particularly true for the subsolidus relationships, as they are essential for the preparation of the high-T_c compound $Ba_2YCu_3O_{6+x}$ in single-phase, crystalline form. Phase diagrams of this high-T_c system vary significantly depending on the annealing atmosphere (and the presence of CO_2).

1. Prepared in Air

Roth *et al.*, (1988) were among the first to determine a complete phase diagram of the $BaO(BaCO_3)$–$\frac{1}{2}Y_2O_3$–CuO system, at ≈950°C, and it is shown in Fig. 14.1. $Y_2Cu_2O_5$ is the only binary oxide reported in the $\frac{1}{2}(Y_2O_3)$–CuO system. Four phases were observed in the $BaO(BaCO_3)$–$\frac{1}{2}(Y_2O_3)$ subsystem. Barium rich $Ba_4Y_2O_7$ and $Ba_2Y_2O_5$ have been reported to be oxycarbonates, with formulas of $Ba_4Y_2O_7{\cdot}CO_2$ and $Ba_2Y_2O_5{\cdot}2CO_2$. When pure BaO is used instead of $BaCO_3$, the $Ba_4Y_2O_7$ and $Ba_2Y_2O_5$ compounds cannot be prepared. There are a total of three ternary oxides, including the high-temperature superconductor $Ba_2YCu_3O_{6+x}$ (2 : 1 : 3) and an ubiquitous impurity phase BaY_2CuO_5 (1 : 2 : 1) that is known as the "green phase." Another barium-rich oxycarbonate solid solution region is known as "the other perovskite phase," and is bounded by the 4 : 1 : 2, 5 : 1 : 3, and 3 : 1 : 2 compositions. The $Ba_2YCu_3O_{6+x}$ phase is known to

Fig. 14.1.

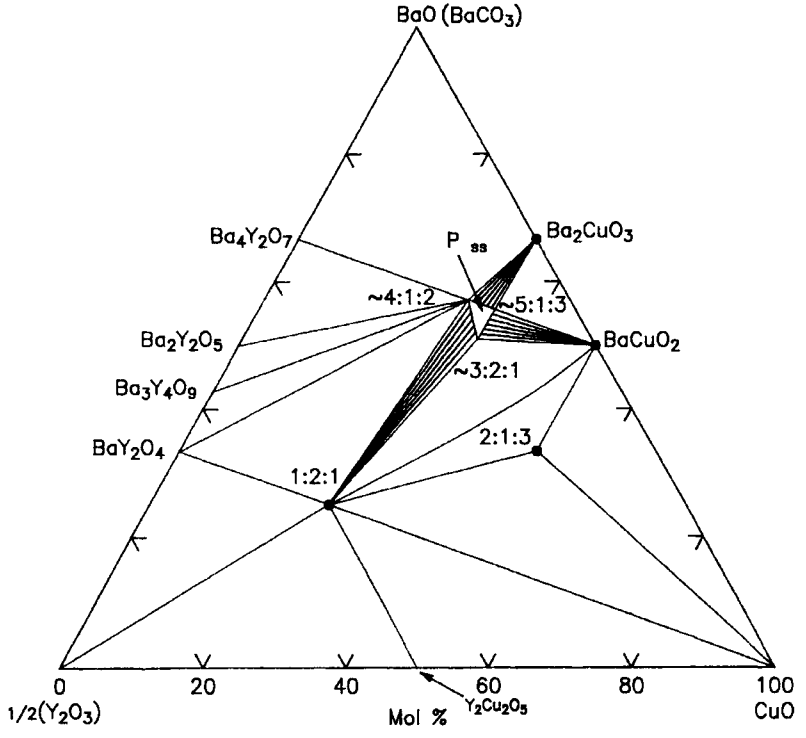

Phase diagram of the ternary system $BaO(BaCO_3)$–$\frac{1}{2}Y_2O_3$–CuO at ≈950°C (Roth *et al.*, 1988). The positions of the $Ba_2YCu_3O_{6+x}$ (2 : 1 : 3) superconductor and the green phase BaY_2CuO_5 (1 : 2 : 1) are shown.

exhibit an orthothomic-tetragonal phase transition depending on the oxygen content (Wong-Ng *et al.*, 1988; Jorgenson *et al.*, 1987).

The high-temperature reaction of CO_2 with $Ba_2YCu_3O_{6+x}$ is known to lead, upon completion, to $BaCO_3$ and copper and yttrium oxides (Gao *et al.*, 1990); however, oxycarbonates may form prior to complete carbonatization (Karen and Kjekshus, 1991). Phase diagrams of the $Ba(O/CO_3)$–$Y(O/CO_3)$-$Cu(O/CO_3)$ pseudoternary system, as determined by powder X-ray diffraction after repeated firings of samples at (a) 800°C and (b) 900°C in 1 atm oxygen containing ≈40 ppm CO_2, are shown in Figs. 14.2 and 14.3. In these two diagrams, the envelopes of oxycarbonate stability are shown bounded by dotted curves. The carbonate stability regions are near the $BaO(BaCO_3)$ region and are bounded by the broken curves. The Ba-rich oxides in the Ba(O)–Y(O)–Cu(O) system have a high affinity for CO_2, leading to the formation of oxycarbonates. Three oxycarbonates were identified: (1) The first phase is near the "other perovskite phase" composition (8 : 1 : 4; Roth *et al.*, 1988), with a homogeneity region extending toward Y, and has a formula of $Ba_8Y_{1+x}Cu_{4+z}(CO_3)_uO_{11+w}$, with $u \approx 2$,

Fig. 14.2.

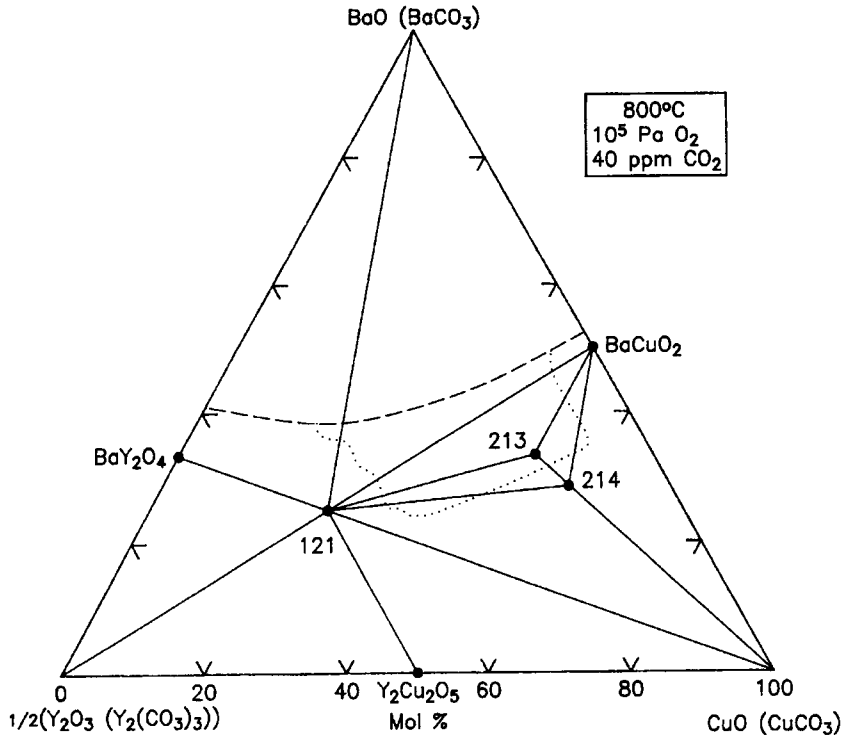

Phase diagram of the system $BaO(BaCO_3)$–$\frac{1}{2}Y_2O_3(Y_2(CO_3)_3)$–CuO at 800°C, 10^5 Pa O_2, and 40 ppm CO_2 (Karen and Kjekshus, 1991).

Fig. 14.3.

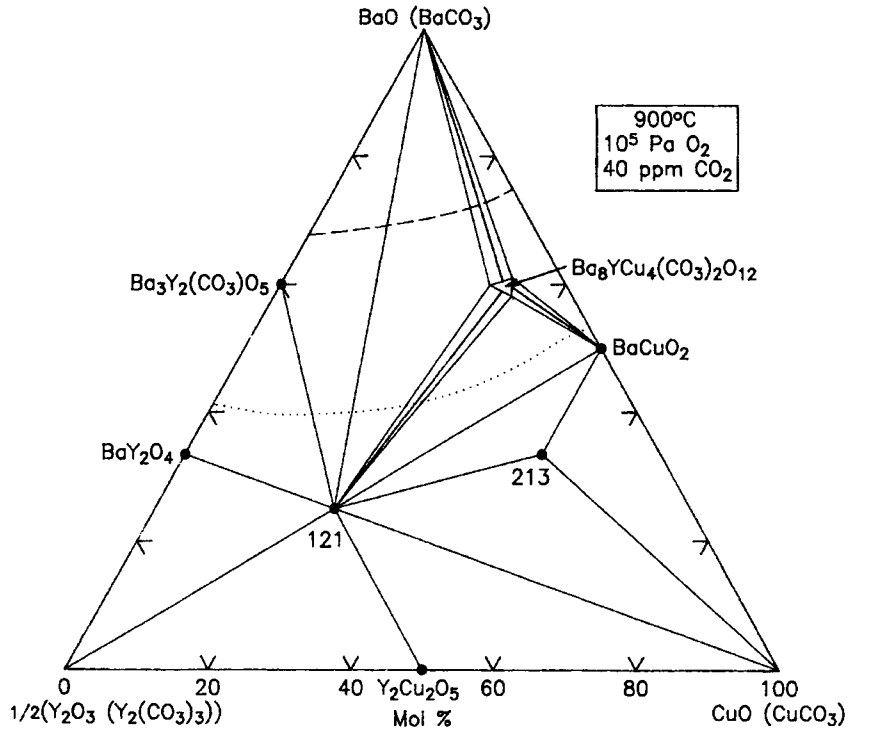

Phase diagram of the system $BaO(BaCO_3)$–$\frac{1}{2}Y_2O_3(Y_2(CO_3)_3)$–CuO at 900°C, 10^5 Pa O_2, and 40 ppm CO_2 (Karen and Kjekshus, 1991).

$0x < 0.03$, $0 < z < 0.04$. There is a pressure–temperature equilibrium between oxygen gas and vacancies in the solid; for $0.05 < w < 0.08$, $x = z = 0$. (2) The tetragonal $Ba_3Y_2(CO_3)_uO_{6-u}$, $u \approx 1$, phase is stable up to 960°C in purified oxygen. (3) The third carbonized phase is the important 2 : 1 : 3 phase. It appears that accommodation of the rather small "size" of cation at the the Ba site is promoted by the carbonization. An extended solid solution $(Ba_{1-y}Y_y)_2YCu_3(CO_3)_{0.2}O_{6.7+y}$, $0 < y < 0.2$, was obtained. For $u \approx 0.2$, $v \approx 0.1$, the $Ba_2YCu_3(CO_3)_uO_{7-u-v}$ phase is tetragonal, with unit cell $a = 3.877(2)$ Å and $c = 11.573(3)$ Å. The structure of $Ba_2YCu_3(CO_3)_uO_{7-u-v}$ is basically derived from $Ba_2YCu_3O_7$ by replacing some of the oxygens by carbonate groups (Karen *et al.*, 1999).

2. Prepared in Air in the Absence of CO_2

The diagram of the CO_2-free system prepared at ≈950°C is shown in Fig. 14.4 [42]. BaO_2 or $Ba(NO_3)_2$ was used as one of starting reagents. Instead of three

ternary oxide phases as found in Fig. 14.2, five were found. The $Ba_2YCu_3O_{6+x}$ (2 : 1 : 3) and BaY_2CuO_5 (1 : 2 : 1) phases are the same as those prepared in pure air, but the perovskite solid solution discussed previously (Ritter, 1988) has become two point compounds with compostion $Ba_4YCu_3O_{8\cdot5}$ (4 : 1 : 3) and $Ba_8Y_3Cu_5O_{17.5}$ (8 : 3 : 5). Another phase with composition $Ba_5Y_1Cu_2O_x$ (5 : 1 : 2) was also found. The $Ba_4Y_2O_7{\cdot}CO_2$ and $Ba_2Y_2O_5{\cdot}2CO_2$ compounds are absent in this diagram. A comparison of this diagram to Fig. 14.2 (prepared with $BaCO_3$) reveals that the tie-lines connecting the 2 : 1 : 3, 1 : 2 : 1, $BaCuO_2$, and perovskite phases are different. There are still uncertainties involved these tie-lines due to the hampered kinetics at 950°C.

3. Prepared in Oxygen

The phase relations of the BYC system at lower temperatures of 800°C ($p(O_2) = 1$, 10^5 Pa $\leq P_{total} \leq 5 \times 10^5$ Pa, $p(CO_2) \approx 0.000$), and at 700°C, 10^5 Pa O_2 are schematically shown in Figs. 14.5 and 14.6 (Roth, 1990). In these two diagrams, the 2 : 1 : 4 and 4 : 2 : 7 phases were indicated as stable at 10^5 Pa O_2 at

Fig. 14.4.

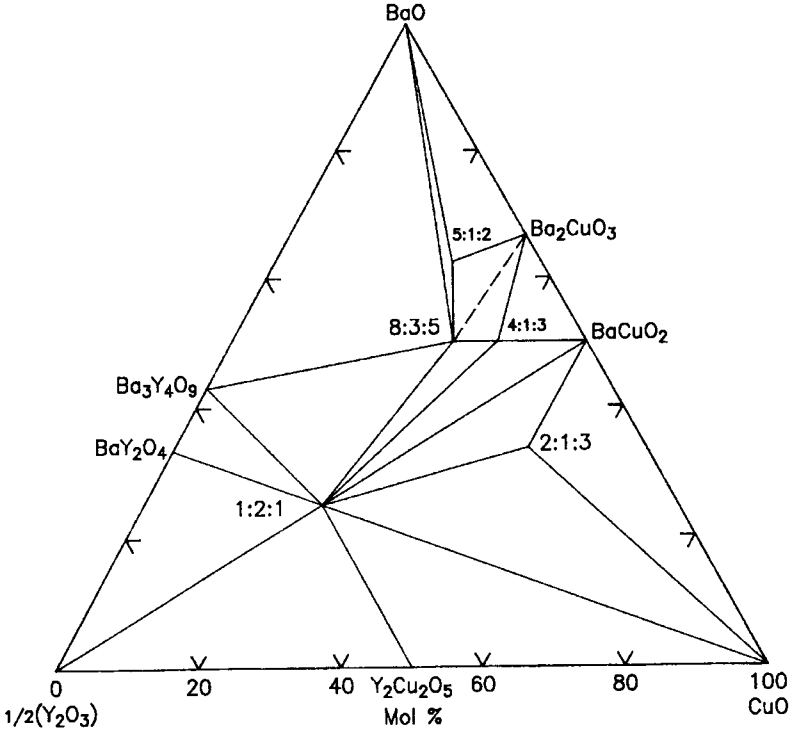

Phase diagram of the system BaO-$\frac{1}{2}Y_2O_3$-CuO at ≈ 950°C in (Deleeuw *et al.*, 1988).

Fig. 14.5.

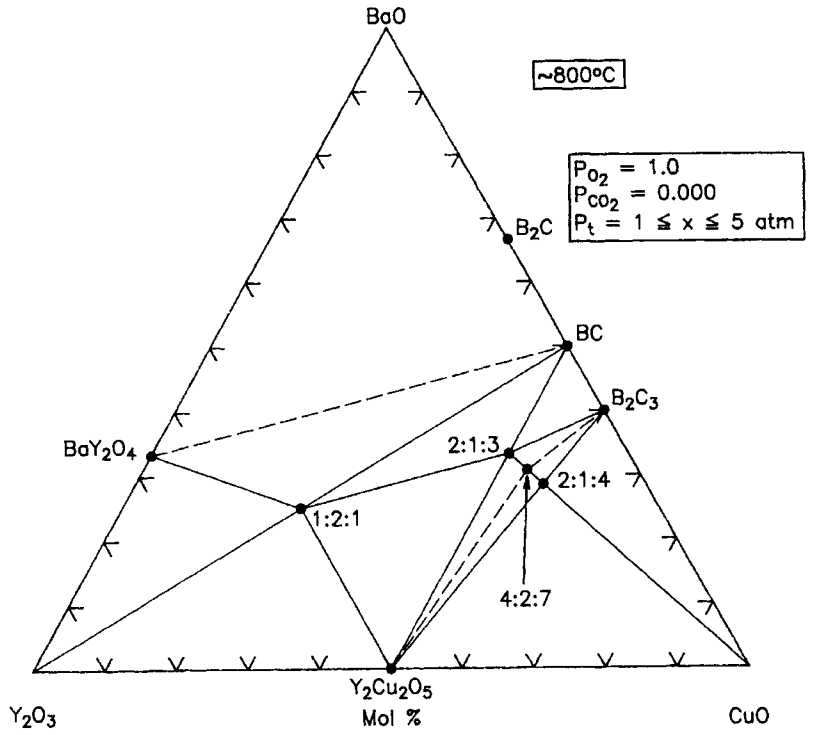

Phase diagram of the system BaO–$\frac{1}{2}Y_2O_3$–CuO. Schematic phase relations in O_2 at ≈800°C ($pO_2 = 1.0$ and 1 atm $\leq P_{Total} \leq 5$ atm, $P_{CO_2} \leq 0.000$) (Roth, 1990).

800°C. The 2 : 1 : 4 phase decomposes at ≥850°C. However, at lower temperature, such as ≈700°C, neither the 2 : 1 : 3 nor the 4 : 2 : 7 phase can formed, and a tie-line exists between Y_2O_3-$Ba_2Cu_3O_{5+x}$. The $Ba_2Cu_3O_{5+x}$ phase only forms in the absence of CO_2. This phase is only stable at $pO_2 \approx 0.2$ if the CO_2 content is well below that of the ambient atmosphere. It decomposes after formation if heated in air.

4. Effect of Oxygen Partial Pressure

Figure 14.7 shows for the 213, 214, and 427 phase regions of the BYC system vs. the oxygen partial pressure plotted vs inverse temperature over the range between 500 and 1000°C and 10^{-2} Pa $< p(O_2) < 10^7$ Pa (Morris, 1990). The approximate boundaries between the phases are indicated by the dotted curves. Included in this plot for the 213 system, the decomposition line (thick solid line [Bormann and Noelting: 1989), and the orthorhombic–tetragonal transition line (bold dashed line) (Lindermer and Sutter, 1988; Specht *et al.*, 1989), lines of constant oxygen

Fig. 14.6.

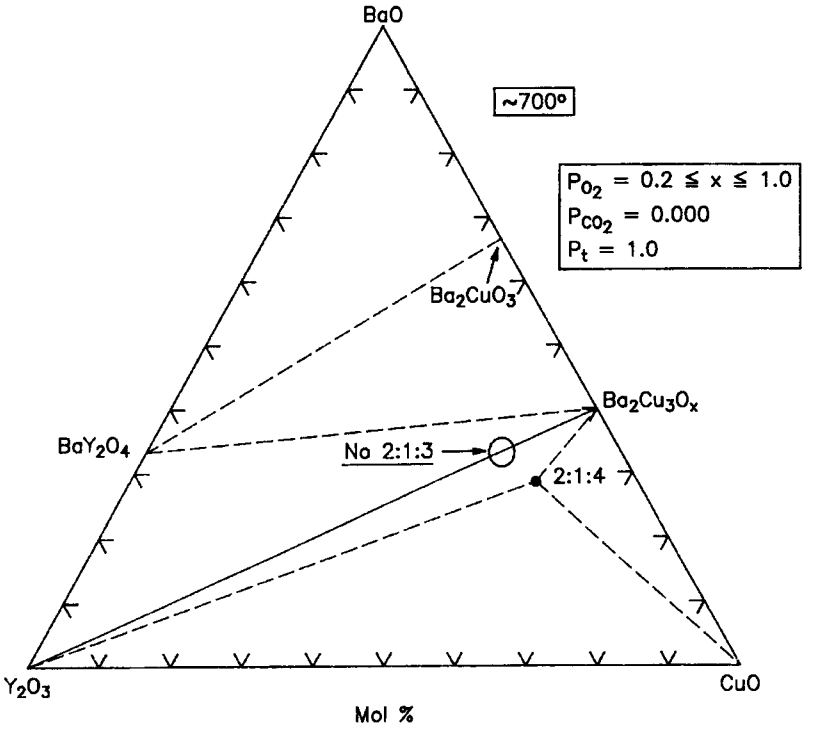

Phase diagram of the system BaO–$\frac{1}{2}Y_2O_3$–CuO. Schematic phase relations in O_2 at ≈700°C and 1 atm O_2 (Roth, 1990).

content (full lines) in the 213 stability region, and dashed lines where 123 is metastable. The $2CuO \rightarrow Cu_2O + \frac{1}{2}O_2$ phase boundary above 900°C (alternating dots and dashes) lies close to the 123 decomposition boundary. The stability boundary between 213 and 214 phases continues to decrease to lower oxygen partial pressure as temperature decreases. This 213/214 phase boundary occurs at considerably higher temperatures than that of the 213 tetragonal/orthorhombic transition, indicating that the fully oxidized orthorhombic 213 superconductor is not thermodynamically stable at any temperature or pressure. The slope of the 213/214 phase boundary is so large that at lower temperatures (< 600°C) the 213/214 boundary will intersect the 213 decomposition line. The oxygen-depleted tetragonal 213 phase is unstable at all oxygen pressures below 600°C.

5. Liquidus Diagrams

Melt processing investigations of this high-T_c material for viable commercial applications constitute a major activity within the high-T_c superconductor

Fig. 14.7.

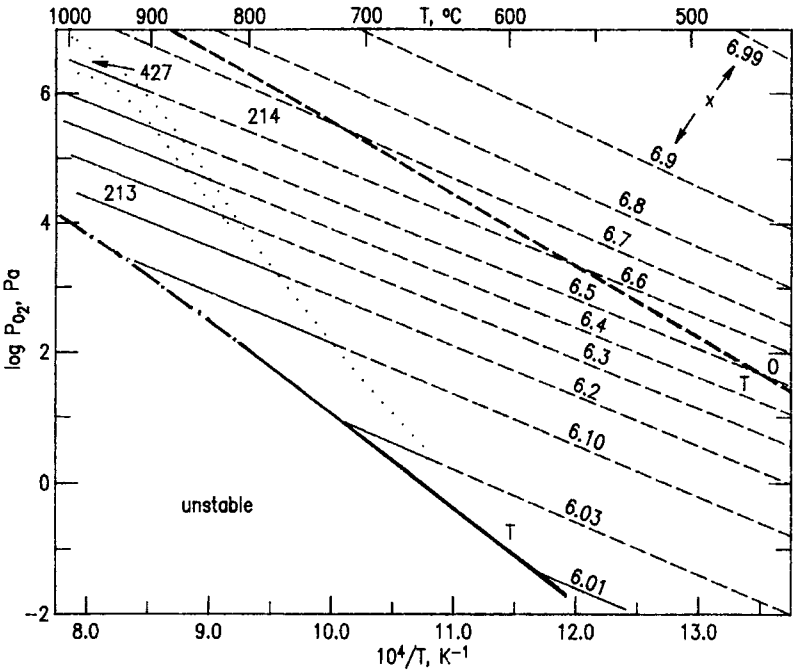

Oxygen pressure pO_2 vs $1/T$ for oxygen contents x in the range 6.01 to 6.99 near 2 : 1 : 3 (—) and 2 : 1 : 4 (- - -) compositions in the BaO–$\frac{1}{2}Y_2O_3$–CuO system (Morris, 1990). The decomposition (——) and orthorhombic-to-tetragonal transition (– – –) lines are shown as well as the phase transition boundaries (· · · ·). The orthorhombic phase exists above the (– – –) line. Lines of constant oxygen content are shown by solid lines in the 2 : 1 : 3 stability region, and dashed lines in the 2 : 1 : 4 region where 1 : 2 : 3 is metastable.

research community. The liquidus information for the Ba–Y–Cu–O system is critical for crystal growth and melt processing. The primary phase field for $Ba_2YCu_3O_{6+x}$, and univariant reactions in the phase diagram near the CuO-rich corner have been reported (Aselege and Keefer, 1988; Krabbes *et al.*, 1993; 1994; Zhang and Osamura, 1991). The most referenced schematic liquidus based on a reaction melting sequence (Table 14.1) is shown in Fig. 14.8. (Aselege and Keefer; 1988). According to Table 14.1, the eutectic melting of the system took place at 890°C (e1). Other eutectics (e), melting (m), and peritectic (p) events are also listed.

The liquidus diagram of Fig. 14.8 is in general a good approximate model for bulk material processing. More detailed studies, however, provide evidence that the liquid field of the BYC phase has a miscibility gap, as shown in Fig. 14.9 (Wong-Ng and Cook, 1998). This diagram is presented by "stretching" the customary ternary composition triangle in order to magnify the yttrium oxide contents of the liquids, all of which were below 4 mole fraction (%). The phase

Table 14.1.

The melting reactions of the BYC system (Aselege and Keefer, 1988) that are identified as eutectic (e), peritectic (p), or peritectic melting (m) (Ullman *et al.*, 1989) (see Fig. 14.8). The symbol L is used to represent liquid.

Type	Temp (°C)	Phases involved
e1	890	$Ba_2YCu_3O_{6+x} + BaCuO_2 + CuO \rightarrow L$
e2	920	$BaCuO_2 + CuO \rightarrow L$
p1	940	$Ba_2YCu_3O_{6+x} + CuO \rightarrow BaY_2CuO_5 + L$
p2	975	$BaY_2CuO_5 + CuO \rightarrow Y_2Cu_2O_5 + L$
e3	1000	$BaCuO_2 + BaY_2CuO_5 \rightarrow L$
p3	1000	$BaCuO_2 + Ba_2YCu_3O_{6+x} \rightarrow BaY_2CuO_5 + L$
m1	1015	$Ba_2YCu_3O_{6+x} \rightarrow BaY_2CuO_5 + L$
m2	1015	$BaCuO_2 \rightarrow L$
—	1026	$CuO \rightarrow Cu_2O$
e4	1110	$Y_2Cu_2O_5 + Cu_2O \rightarrow L$
m3	1122	$Y_2Cu_2O_5 \rightarrow Y_2O_3 + L$
m4	1270	$BaY_2CuO_5 \rightarrow Y_2O_3 + L$

Fig. 14.8.

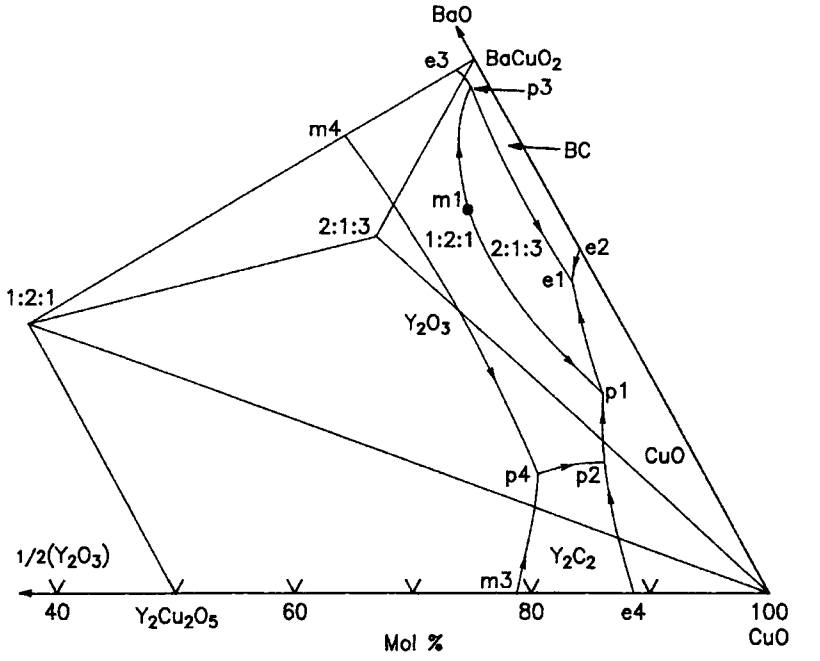

Liquidus surface and subsolidus relationships in the BaO–Y_2O_3-CuO system (see Fig. 14.4) in air (Aselege and Keefer, 1998). Table 14.1 provides the temperatures and involved phases for the eutectic (e), melting (m), and peritectic (p) points, and Table 14.2 provides corresponding DTA onset temperatures.

Fig. 14.9.

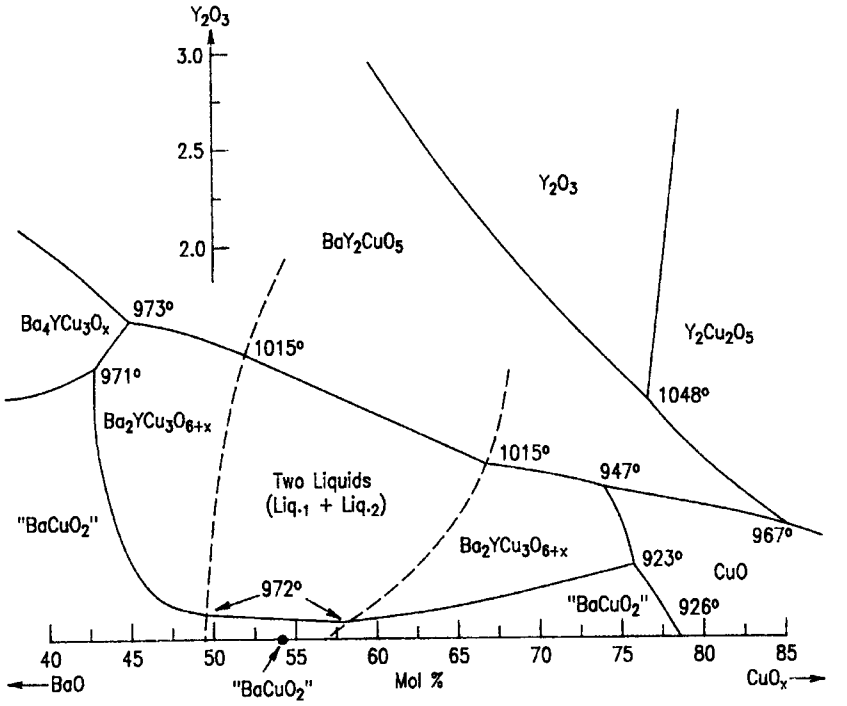

Liquidus surface in the BaO–Y_2O_3–CuO system in air, showing the liquid immiscibility field of the $Ba_2YCu_3O_{6+x}$ phase (Wong-Ng and Cook, 1998).

fields of BaY_2O_4, Y_2O_3, BaY_2CuO_5, $Ba_4YCu_3O_x$, $Y_2Cu_2O_5$, Cu_2O, nominal $BaCuO_2$, and CuO are also shown. The $Ba_2YCu_3O_{6+x}$ superconductor, which contains 16.7 mol fraction (%) $\frac{1}{2}Y_2O_3$, would plot off the top of the diagram at a height more than four times that of the diagram. The crystallization field of the $Ba_2YCu_3O_{6+x}$ phase occurs in two segments. Both segments of the field are entirely below the 2.0 mol fraction (%) $\frac{1}{2}Y_2O_3$ level. The right-hand segment of the $Ba_2YCu_3O_{6+x}$ field is bounded by the crystallization fields of BaY_2CuO_5, "$BaCuO_2$," $Y_2Cu_2O_5$, and CuO, and the left-hand segment was bounded by the $Ba_4YCu_3O_x$, BaY_2CuO_5, and "$BaCuO_2$" primary phase fields.

A sequence of isothermal reactions that describe the melting sequence are found in Fig. 14.10, (a) to (i). In these isothermal sections, a split scale is used as indicated by the break in the side axes in order to give a more comprehensive view of the solids participating in the equilibria, and simultaneously present the schematic details of the participating liquids near the base in expanded form. L1 and L2 represent two immiscible liquids. The dominant reaction at each temperature is as follows:

Fig. 14.10.

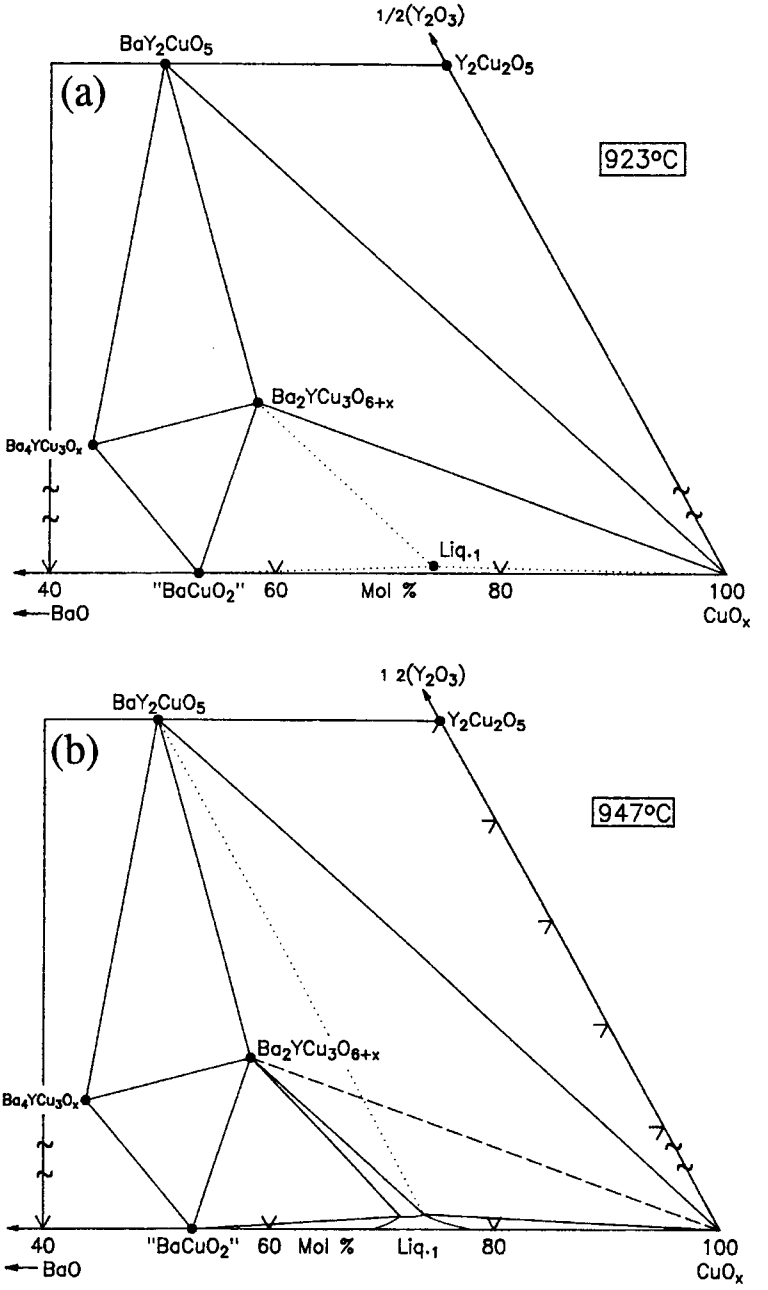

Topological sequence of the melting events in the BaO–$\frac{1}{2}Y_2O_3$-CuO system (Wong-Ng and Cook, 1998), from 923 to 1274°C. The main overall reaction for each temperature is given in the text.

(*continued*)

Fig. 14.10. (*continued*)

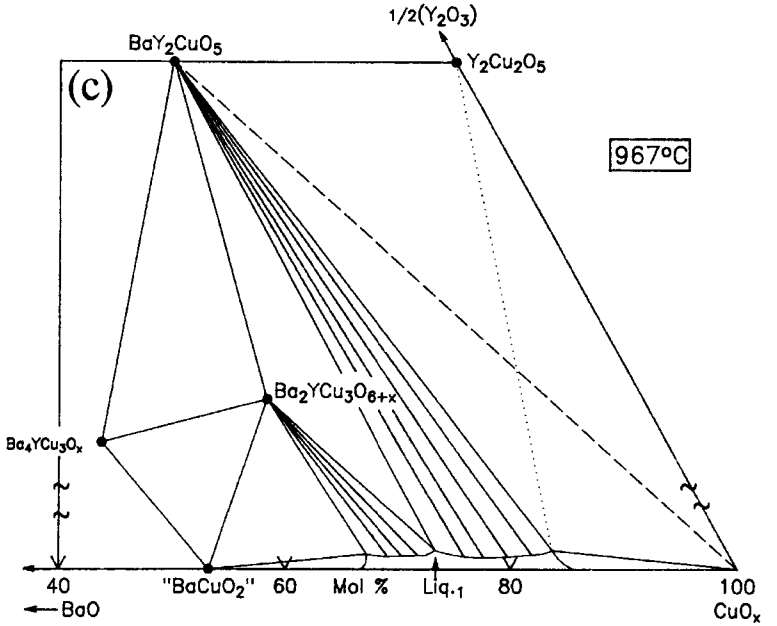

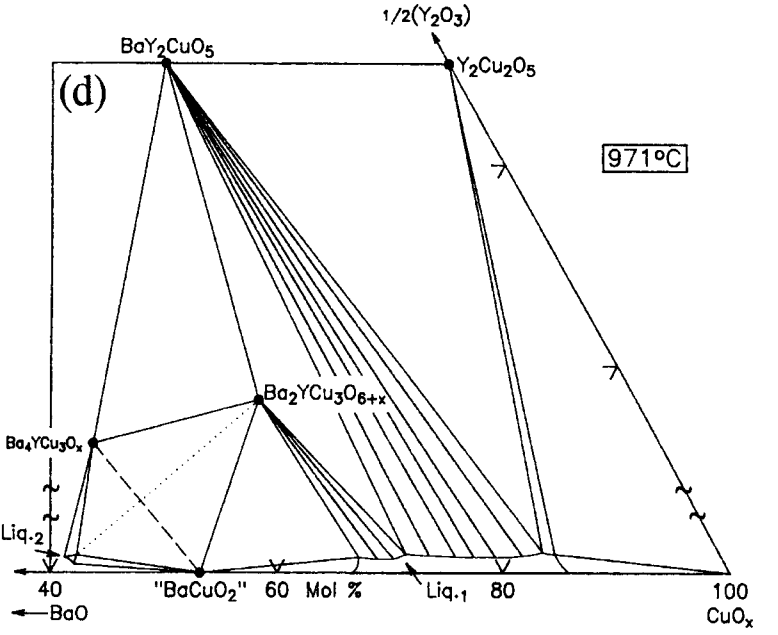

(*continued*)

Fig. 14.10. (*continued*)

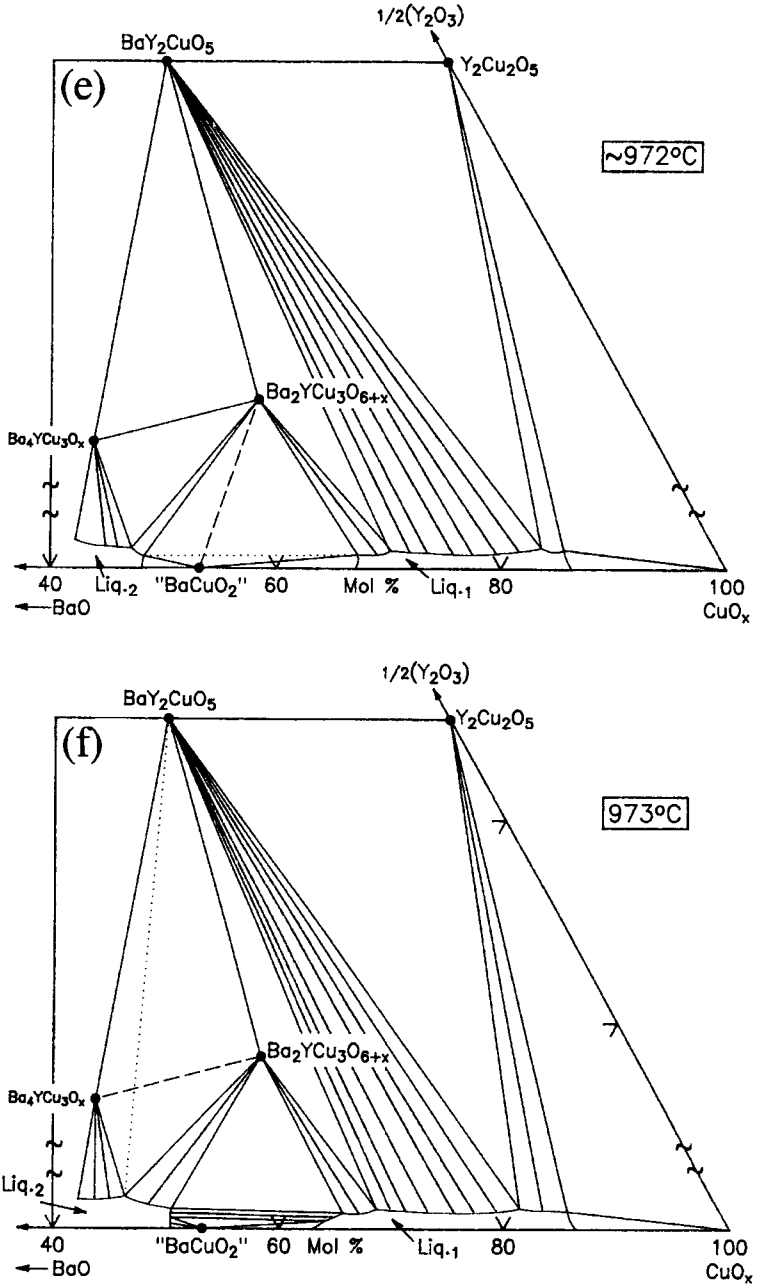

(*continued*)

Fig. 14.10. (*continued*)

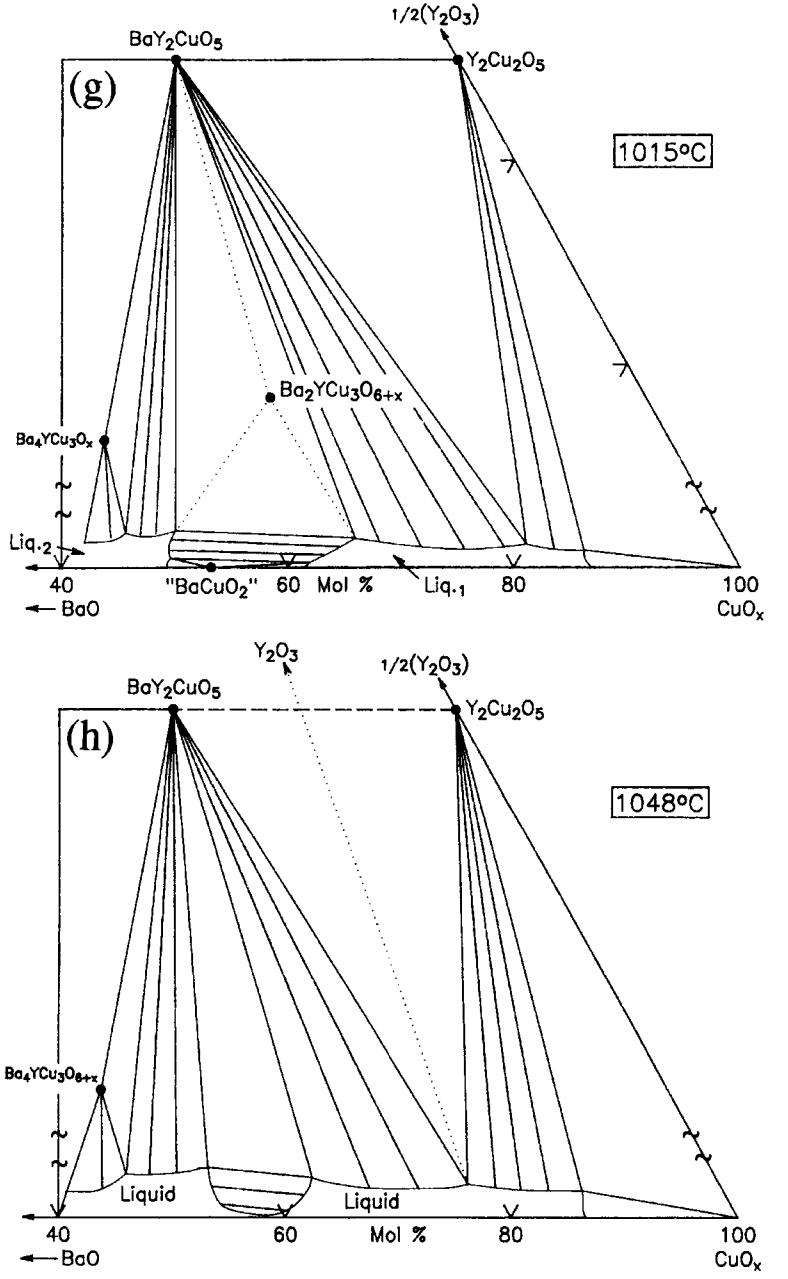

(*continued*)

Fig. 14.10. (*continued*)

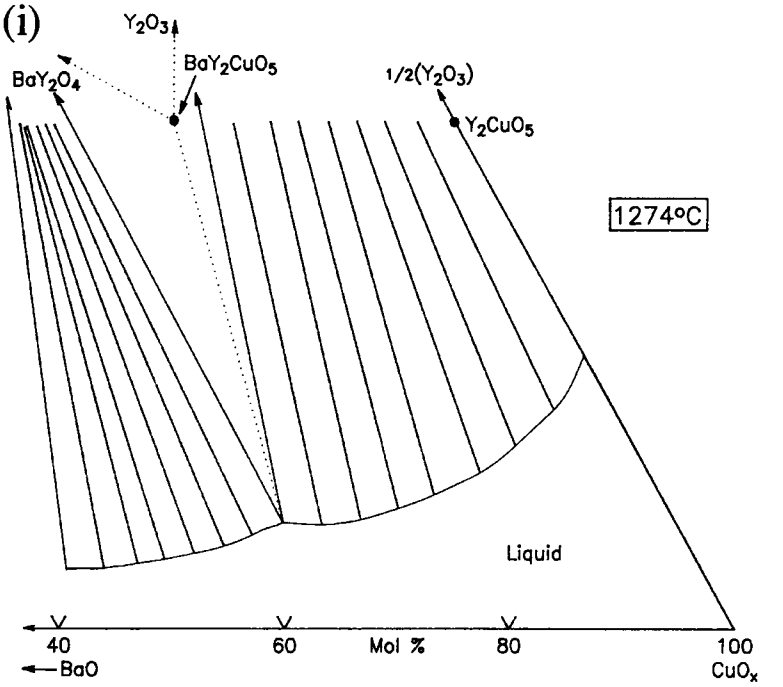

(a) 923°C: "$BaCuO_2$" + CuO + $Ba_2YCu_3O_{6+x}$ → L_1 + O_2
(b) 947°C: $Ba_2YCu_3O_{6+x}$ + CuO → BaY_2CuO_5 + L_1 + O_2
(c) 967°C: BaY_2CuO_5 + CuO → $Y_2Cu_2O_5$ + L_1 + O_2
(d) 971°C: $Ba_4YCu_3O_x$ + "$BaCuO_2$" → $Ba_2YCu_3O_{6+x}$ + L_2 + O_2
(e) 972°C: "$BaCuO_2$" + $Ba_2YCu_3O_{6+x}$ → L_1 + L_2 + O_2
(f) 973°C: $Ba_4YCu_3O_x$ + $Ba_2YCu_3O_{6+x}$ → BaY_2CuO_5 + L_2 + O_2
(g) 1015°C: $Ba_2YCu_3O_{6+x}$ → BaY_2CuO_5 + L_1 + L_2 + O_2
(h) 1048°C: BaY_2CuO_5 + $Y_2Cu_2O_5$ → Y_2O_3 + L_1 + O_2
(i) 1274°C: BaY_2CuO_5 → BaY_2O_4 + Y_2O_3 + L + O_2

b. Ba–R–Cu–O Systems (R = Lanthanide)

The discovery that the substitution of the most of lanthanide (3+) ions, R, for Y also produced a superconductor with a transition temperature of ≈90 K has provided numerous alternative materials for investigations of possible desirable properties (Le Page *et al.*, 1987). Proceeding from the La system, which has the largest ionic size of R, toward the Er system with a smaller ionic size, a general

trend of phase formation, solid solution formation, and phase relationship was found to be correlated with the ionic size of R. The ternary phase compatibility diagrams of the systems $BaO(BaCO_3)-\frac{1}{2}Y_2O_3-CuO$ and $BaO(BaCO_3)-\frac{1}{2}R_2O_3-CuO$ in the vicinity of the CuO corners (most relevant to the processing of the high-T_c materials), where R = La, Nd, Sm, Eu, Gd, Er, are shown schematically in Fig. 14.11 (a) to (f) (Wong-Ng *et al.*, 1990). Features of the progressive changes in the appearance of these ternary diagrams near the CuO corner include the following: (1) The La system has the largest number of ternary compounds and solid-solution series; this number decreases as the size of R decreases. (2) The superconductor phase, $Ba_2RCu_3O_{6+x}$, for the first half of the lanthanide family, that is, R = La, Nd, Sm, Eu, and Gd, which are relatively larger in size, exhibit a solid solution of $Ba_{2-z}R_{1+z}Cu_3O_{6+x}$ with a range of formation that decreases as the size of R decreases; this solid-solution region terminates at Dy and beyond, where the superconductor phase assumes a point stoichiometry. The size compatibility between Ba^{2+} and R^{3+} is a predominant factor governing the formation of this solid solution. As the mismatch between R^{3+} and Ba^{2+} increases, the range of substitution decreases.The approximate upper limit of the solid solution range of z of $Ba_{2-z}R_{1+z}Cu_3O_{6+x}$ are La : 0.7, Nd : 0.7, Sm : 0.7, Eu : 0.5, and Gd : 0.2, (3) A trend is observed regarding the tie-line connections between BaR_2CuO_5, CuO, the superconductor phases $Ba_{2-z}R_{1+z}Cu_3O_{6+x}$, and the binary phase R_2CuO_4, or $R_2Cu_2O_5$; note that the binary phase R_2CuO_4 is replaced by the binary phase $R_2Cu_2O_5$ after the tie-line connection changes.

More complete diagrams of the systems with R = La, Nd are shown in Figs. 14.12 and 14.13, respectively. It is within the Ba–La–Cu–O system that the first 30 K high-T_c phase in polycrystalline form, $Ba_xLa_{5-x}Cu_5O_{5(3-y)}$, was discovered by Bednorz and Müller (1986). The isothermal section of the Ba–La–Cu–O system (Klibanow *et al.*, 1988) shows a total of five solid solutions: $Ba_{2+x}La_{4-2x}Cu_{2-x}O_{10-2x}$ (242), $BaLa_4Cu_5O_{13+x}$ (145), $Ba_xLa_{2-x}CuO_{4-(x/2)+\delta}$ (021), and $Ba_{1+x}La_{2-x}Cu_2O_{6-(x/2)}$ (122), and a solid solution $Ba_{3+x}La_{3-x}Cu_6O_{14\pm x}$ that spans from the 213 composition to the 336 composition. The limits of most of these solid solutions have not been quantified. The solubility limits for $Ba_{2+x}La_{4-2x}Cu_{2-x}O_{10-2x}$ were reported to be $0.15 \leq x \leq 0.25$ [54]. The tie-line connectivity of the figure is schematic.

The ternary diagram of the Ba–Nd–Cu–O system at 890°C in air [56] is reported in Fig. 14.13. In the barium-rich region, samples were annealed in air with $CO_2 < 3$ ppm. A total of three phases were found in this system. In addition to the solid solution of the superconductor (213), $Ba_{2-x}Nd_{1-x}Cu_3O_{7-\delta}$ ($0.04 \leq x \leq 0.6$) and $Ba_{2+x}Nd_{4-2x}Cu_{2-x}O_{10-2x}$ (242) (x is negligible), a 6 : 1 : 3 phase (orthorhombic: $a = 3.886(2)$, $b = 3.984(2)$ and $c = 13.001(5)$ Å) is also found. The existence of the $Ba_{2-x}Nd_{1+x}Cu_3O_z$–$Ba_{2+x}Nd_{4-2x}Cu_{2-x}O_{10-2x}$ two-phase field enables one to select a starting composition that leads to composite superconductors of these two phases that are completely devoid of the minor second phases that segregate at $Ba_{2-x}Nd_{1+x}Cu_3O_z$ grain boundaries after a solid-state sintering.

Fig. 14.11.

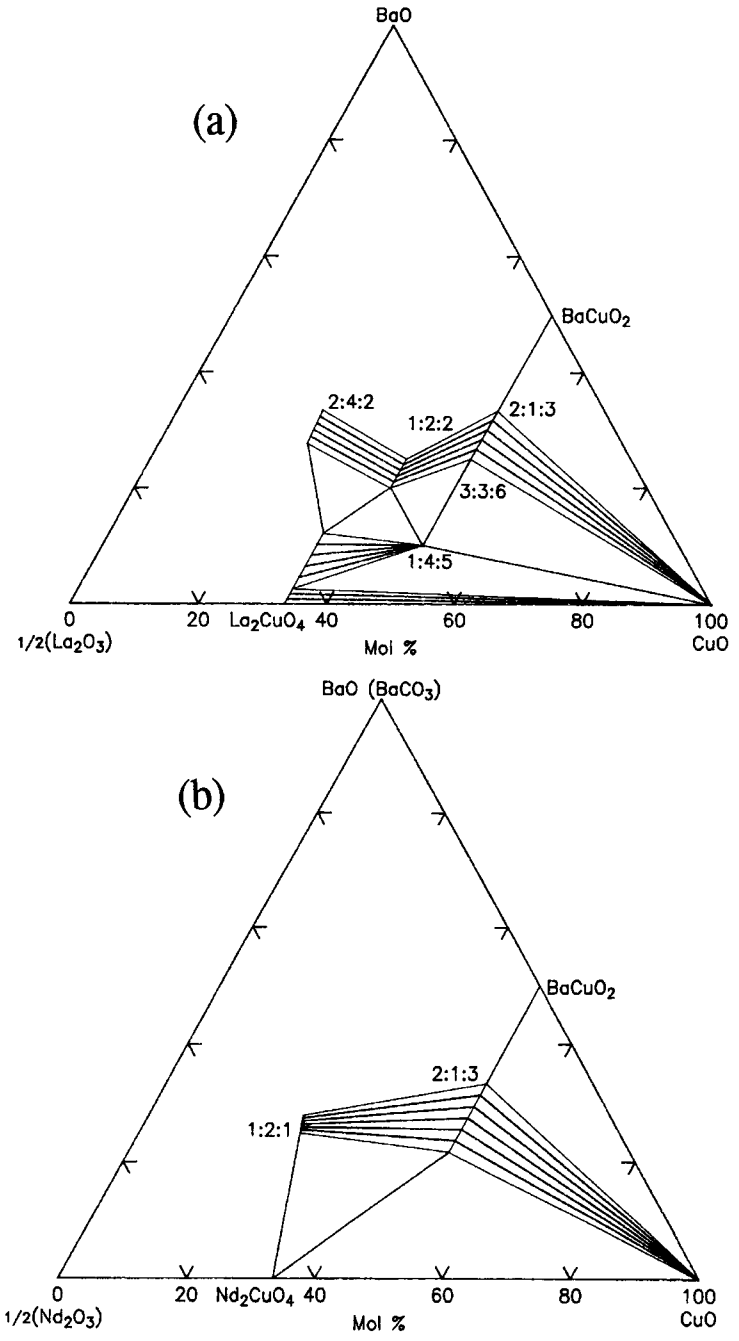

Subsolidus phase equilibira of the $BaO–\frac{1}{2}R_2O_3–CuO$ system near the CuO corner. (a) R = La, (b) R = Nd (Wong-Ng *et al.*, 1990).

(*continued*)

Fig. 14.11. (*continued*)

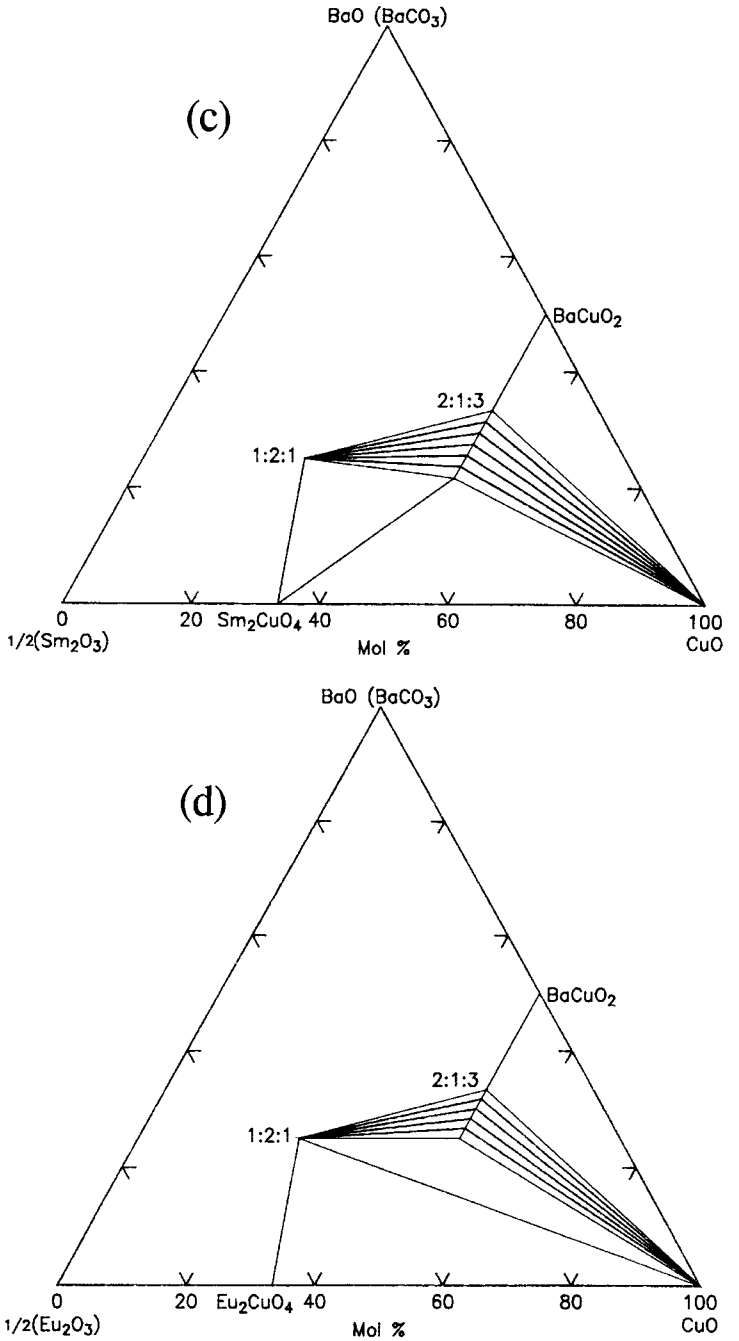

Subsolidus phase equilibira of the BaO–$\frac{1}{2}R_2O_3$–CuO system near the CuO corner. (c) R = Sm, (d) R = Eu (Wong-Ng *et al.*, 1990).

(continued)

Fig. 14.11. (*continued*)

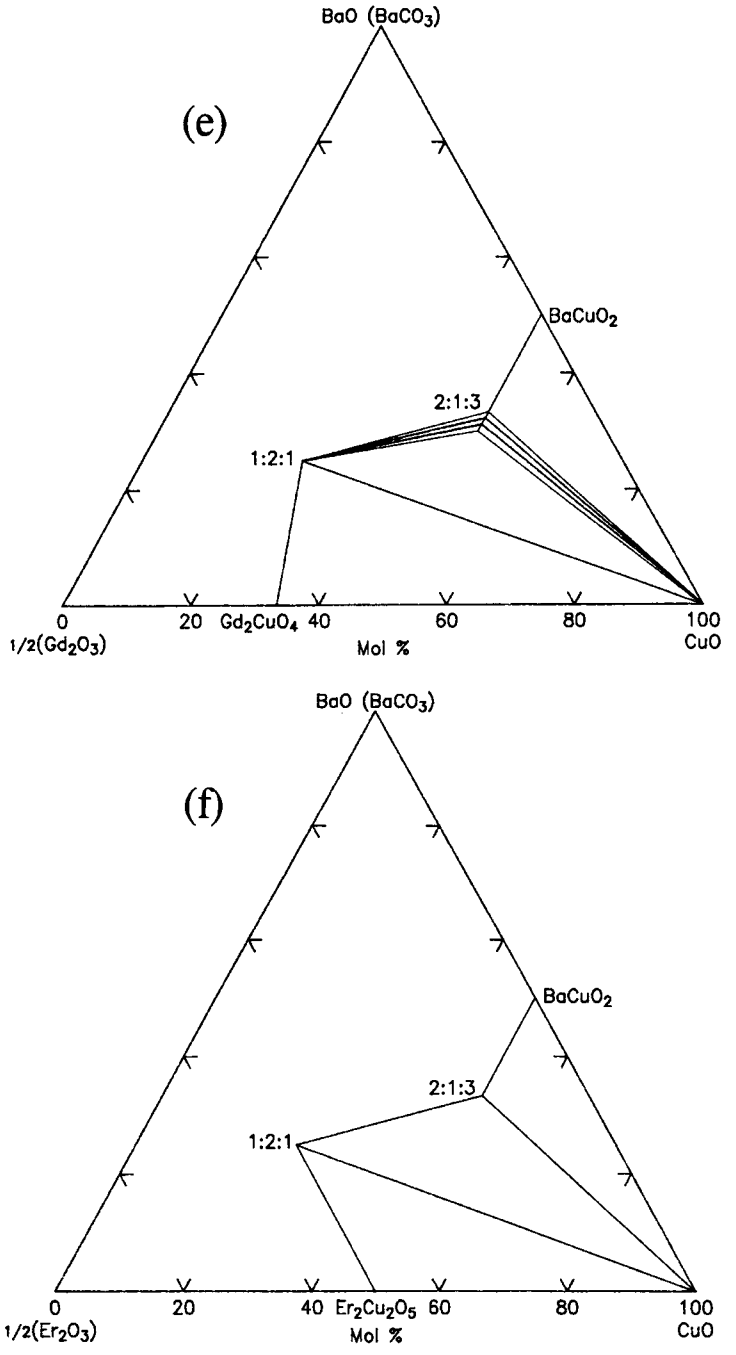

Subsolidus phase equilibria of the BaO–$\frac{1}{2}R_2O_3$–CuO system near the CuO corner. (e) R = Gd, and (f) R = Er (Wong-Ng *et al.*, 1990).

Fig. 14.12.

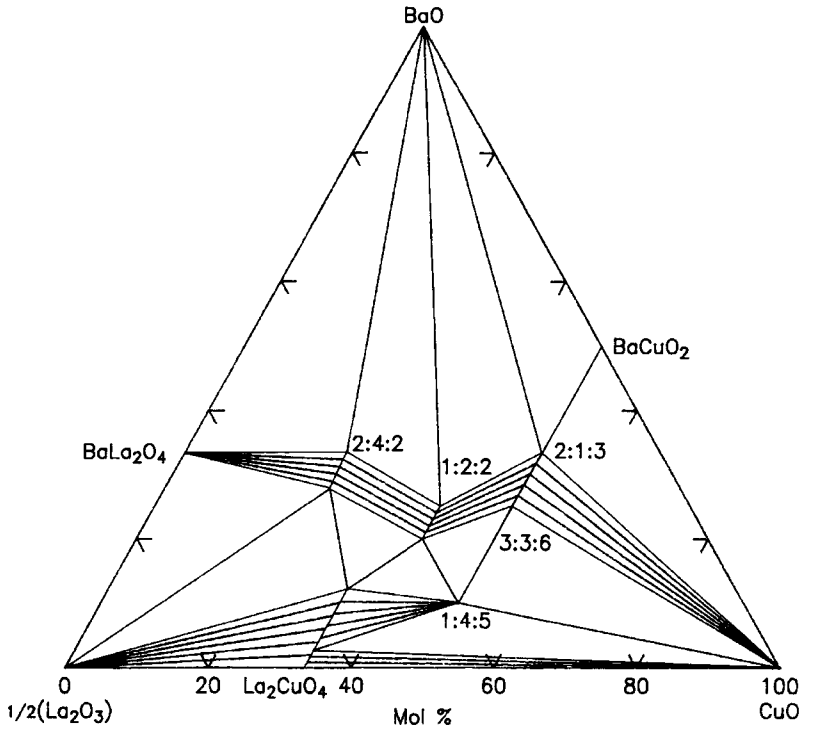

Phase diagram for the system BaO–$\frac{1}{2}La_2O_3$–CuO at 950°C in air (Klibanow *et al.*, 1988).

A melting study of the $Ba_{2-x}Nd_{1+x}Cu_3O_z$ solid solution has been conducted by Goodilin *et al.*, (1997). A sequence of schematic quasiternary sections of the Cu-rich corner of the BaO–$\frac{1}{2}Nd_2O_3$–CuO system between 970 and 1060°C in air is shown in Fig. 14.14, (a), (g). Figure 14.14a shows the phase relationships below liquid formation, and at the bottom Fig. 14.14b shows the onset of liquid formation in the system. From Fig. 14.14c to 14f, the stability region of $Ba_{2-x}Nd_{1+x}Cu_3O_z$ is extensive and its maximum range was found in air at 995°C ($0 \leq x \leq 1$). At 995–1045°C, the $Ba_{2-x}Nd_{1+x}Cu_3O_z$ phase with the maximum x value co-exists in the copper-rich corner with the Ba-free Nd_2CuO_4 phase and Cu-rich liquid. At 1060°C (Fig. 14.14g); the simultaneous presence of the $Ba_{2+x}Nd_{4-2x}Cu_{2-x}O_{10-2x}$ and Nd_2CuO_4 phases was found, and only the $Ba_{2+x}Nd_{4-2x}Cu_{2-x}O_{10-2x}$ phase was detected in equilibrium with Nd-poor $Ba_{2-x}Nd_{1+x}Cu_3O_z$ solid solution.

Examples of the effect of atmosphere and different lanthanide ions on the various invariant points on the liquidus surface for the BYC and BRC (R = Er, Gd, and Nd) systems in oxygen, air, and argon are given in Table 14.2. The reactions of the Y system were used as a model (Table 14.1) (Le Page *et al.*,

Fig. 14.13.

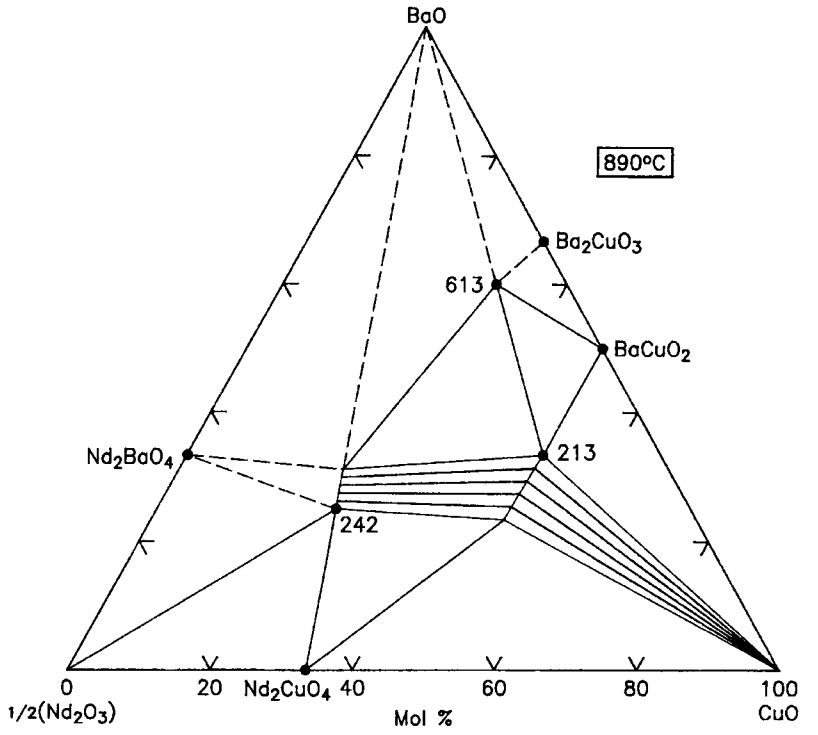

The subsolidus phase diagram of the BaO–$\frac{1}{2}Nd_2O_3$–CuO system around the $Ba_{2-x}Nd_{1+x}Cu_3O_z$ compound in air at 890°C (Yoo and McCallum; 1993).

1957). In this table, while the temperatures of the low-melting reactions are almost independent of the rare earth species, they are strongly dependent on oxgyen partial pressure. The peritectic decomposition temperature of the $Ba_2RCu_3O_7$ phase (ml) was found to be a function of rare earth with a significantly higher value for the Nd compound than for the other rare earths.

c. (La, Sr)–Cu–O Systems

In this system, the composition, $La_{2-x}Sr_xCuO_{4-y}$ in polycrystalline form was found to exhibit onset T_c temperatures in the 20 K range. Figure 14.15 shows the dependence of the tetragonal-to-orthorhombic phase transition temperature on the hole concentration of oxygen-deficient $La_{2-x}Sr_xCuO_{4-y}$ (Birgeneau and Shirane, 1989). Figure 14.16 shows a schematic phase diagram of the SrO–La_2O_3–CuO system at 980°C in air (Hahn *et al.*, 1989). The precise solid solution limit has not been determined. Extensive solid solutions were observed for quite a few phases.

Fig. 14.14.

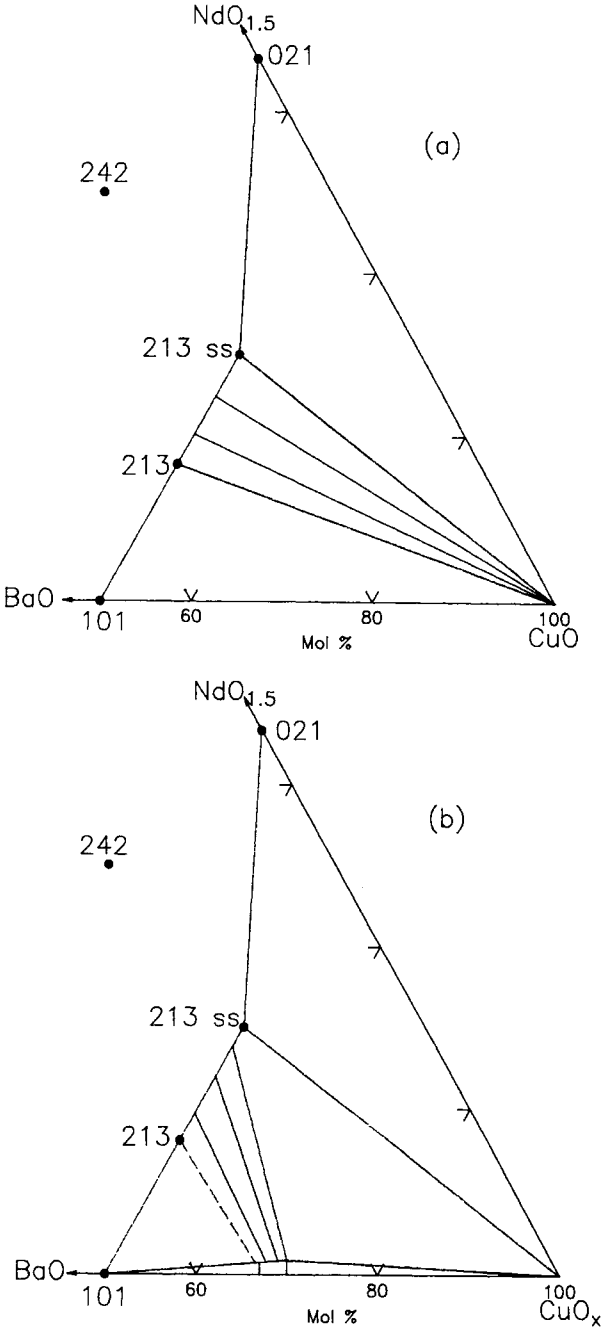

Schematic quasiternary sections of the Cu-rich corner of the $BaO–\frac{1}{2}Nd_2O_3–CuO$ system phase diagram in air at different temperatures: (a) phase relations below melting, (b) beginning of liquid formation in the system.

(continued)

Fig. 14.14. (*continued*)

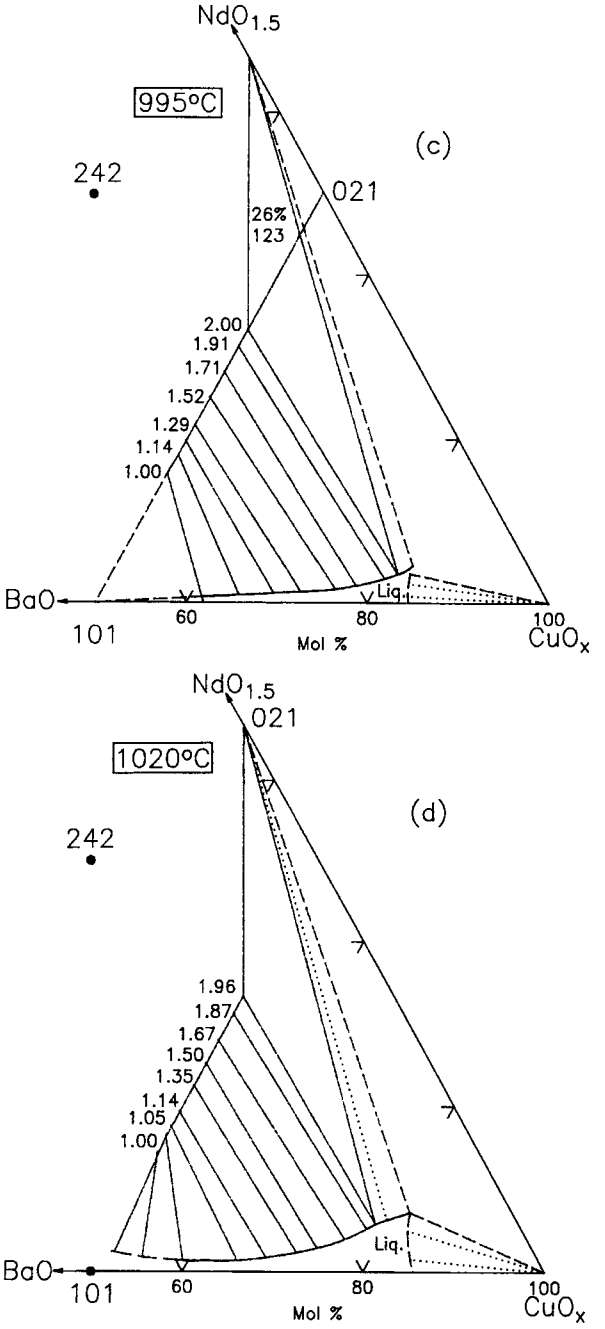

Schematic quasiternary sections of the Cu-rich corner of the BaO–$\frac{1}{2}Nd_2O_3$–CuO system phase diagram in air at different temperatures: (c) 995°C, (d) 1020°C.

(*continued*)

Fig. 14.14. (*continued*)

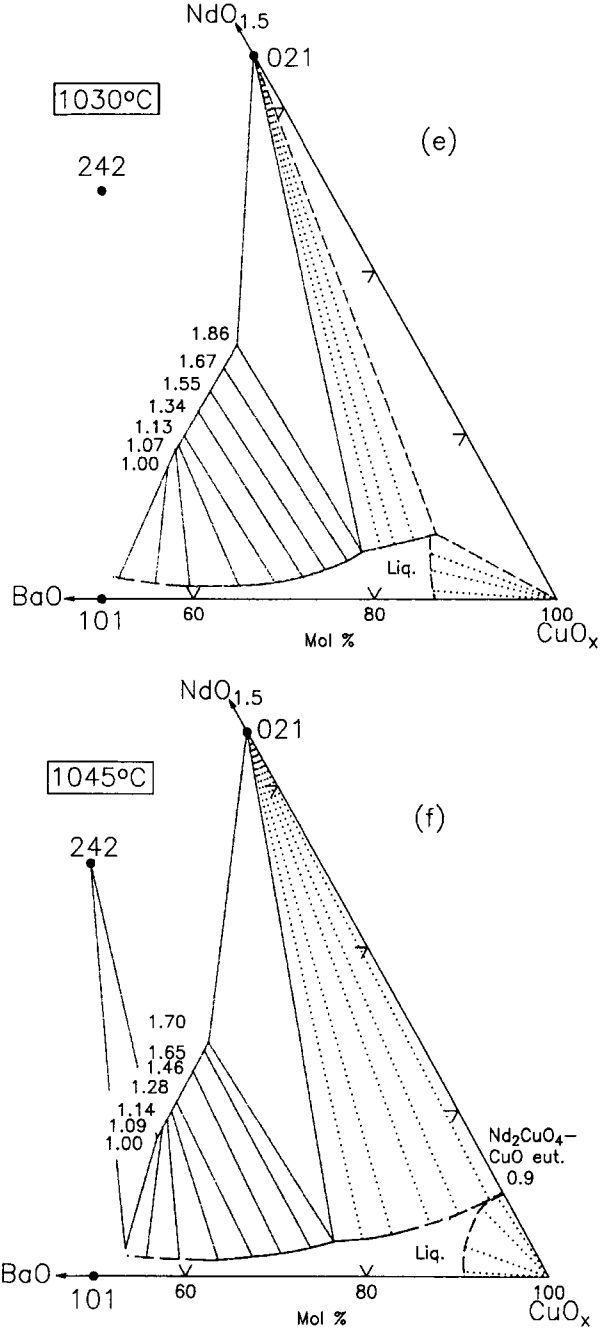

Schematic quasiternary sections of the Cu-rich corner of the BaO–$\frac{1}{2}Nd_2O_3$–CuO system phase diagram in air at different temperatures: (e) 1030°C, (f) 1045°C.

(*continued*)

Fig. 14.14. (*continued*)

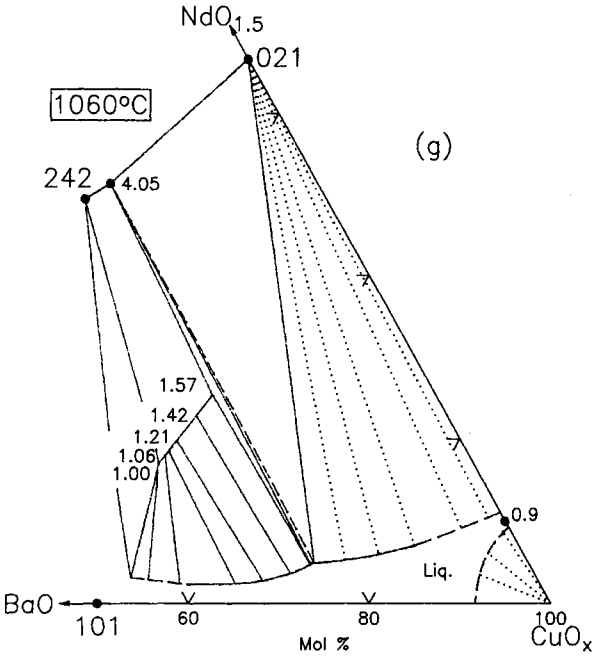

Schematic quasiternary sections of the Cu-rich corner of the BaO–$\frac{1}{2}Nd_2O_3$–CuO system phase diagram in air at different temperatures: (g) 1060°C (Goodilin *et al.*, 1997). The numbers on (e), (f), and (g) correspond to the x value in the solid solution $Ba_{2-x}Nd_{1+x}Cu_3O_z$.

The superconducting solid solution series $La_{2-x}Sr_xCuO_4$ that crystallized with the K_2NiF_4 structure was confirmed to exist with complete substitution of $0 \leq x \leq 1$. This solid solution is in equilibrium with all the three end members of this ternary oxide system, the 1 : 4 : 5 phase and another solid solution series, $La_{2-x}Sr_{1+x}Cu_2O_{6-x/2+\delta}$ (1 : 2 : 2). The 1 : 2 : 2 phase is an end member of the $La_{2-x}Sr_{1+x}Cu_2O_{6-x/2+\delta}$ series, which has the $Sr_3Ti_2O_7$ structure, and has a smaller solid solution range of $0 \leq x \leq 0.14$.

d. (Bi, Pb)–Sr–Ca–Cu–O Systems

In 1987, the ability of bismuth to form lamellar oxides was recognized, and the single-layer Bi–Sr–Cu–O compound having a critical superconducting temperature ranging from 9 to 22 K was discovered (Michel *et al.*, 1987). Superconducting bismuth cuprates were later reported to form a family of layered-structure phases with ideal formulas $Bi_2Sr_2Ca_{n-1}Cu_nO_{4+2n}$ with $n = 1, 2$ and 3, depending on the number of $(CuO_2)_n$ layers. These phases exhibit variations of cation ratio.

Table 14.2.

DTA onset temperatures (°C) for various reactions identified as eutectic (e), peritectic (p), or peritectic melting (m) (Ullman *et al.*, 1989) (see Fig. 14.8). Approximate uncertainties are indicated in parentheses next to the selected temperature values.

	Reaction	Argon	Air	Oxygen
Yttrium	e1	...	898(5)	925(3)
	e2	816(17)	902(2)	938(2)
	p1	862(7)	933(2)	962(3)
	p2	897(5)	956(5)	990(5)
	p3	...	...	1010(5)
	e3	...	...	1015(1)
	m1	...	999(3)	1028(3)
Erbium	e1	...	898(5)	923(3)
	e2	...	902(2)	943(1)
	p1	860(5)	928(5)	957(2)
	p2	...	...	999(1)
	p3	...	...	1000(5)
	e3	...	...	1018(5)
	m1	...	...	1012(3)
Gadolinium	e1	...	...	923(2)
	e2	815(5)	907(5)	936(3)
	p1	870(10)	949(5)	927(5)
	p2	...	...	1007(1)
	p3	...	...	1020(5)
	e3	...	...	1017(5)
	m1	...	...	1063(5)
Neodymium	e1	...	...	923(2)
	e2	...	...	945(5)
	p1	...	...	963(3)
	p2	...	...	1014(1)
	m1	...	...	1108(5)
	e3 and p3: ≈1005 to ≈1020°C			

To date, the three well known superconductor phases in the BSCCO system are commonly referred to as the single-layered 2201 (Bi : Sr : Ca : Cu) phase, the two-layered 2212 (Bi : Sr : Ca : Cu) phase, and the three-layered 2223 (Bi : Sr : Ca : Cu) phase. Among them, the two most widely investigated are the 80 K Pb-free two-layered 2212 phase (MacManus-Driscoll and Bravman, 1994; Majewski *et al.*, 1993; Sung and Hellstrom, 1995) and the 110 K Pb-doped 3-layered 2223 ((Bi, Pb) : Sr : Ca : Cu) phase (Merchant *et al.*, 1995; Hu *et al.*, 1995; Jiang and Abell, 1996). Because of the small temperature range and sluggish kinetics of formation of the Pb-free phase, little has been reported on the phase equilibria or processing of this phase. Pb substitution was found to increase the processing window and to stabilize the 2223 structure.

Fig. 14.15.

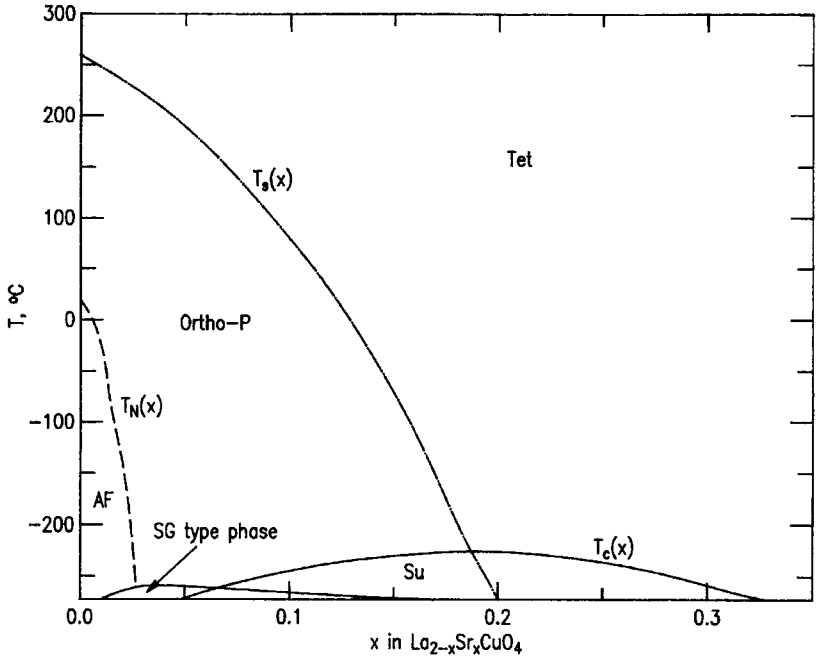

Temperature diagram of the system SrO–La_2O_3–CuO, section of $La_{2-x}Sr_xCuO_4$ (Birgeneau and Shirane; 1989). T_c refers to the superconducting transition temperatures of the orthorhombic paramagnetic phase and the tetragonal phase, and T_N represents the Néel temperature between the orthorhombic antiferromagnetic phase and the paramagnetic phase; Ortho-P = orthorhombic paramagnetic phase; AF = orthorhombic antiferromagnetic phase; Tet = tetragonal phase; SG = spin glass type phase; Su = superconductor phase; T_s = temperature of the orthorhombic-P and the tetragonal phases.

The interpretations of phase relations in a quaternary system is the same as those in the binary and ternary systems. In the quaternary system, however, it is more difficult to present the relations in a simple form because of the many variables present. When detailed knowledge of data is available, it is common practice to build a tetrahedral model of the system to portray the phase relationships. Figure 14.17 shows the tetrahedral system used to illustrate the position of the three superconductors in the Pb-free BSCCO system. (Hettrich *et al.*, 1991).

1. Phase Diagrams for One CuO_2 Layer

Figure 14.18 shows the phase equilibria of the Bi–Sr–Cu–O system reported by Roth *et al.*, at 875–925°C. Four ternary oxide compounds were found. Note the

Fig. 14.16.

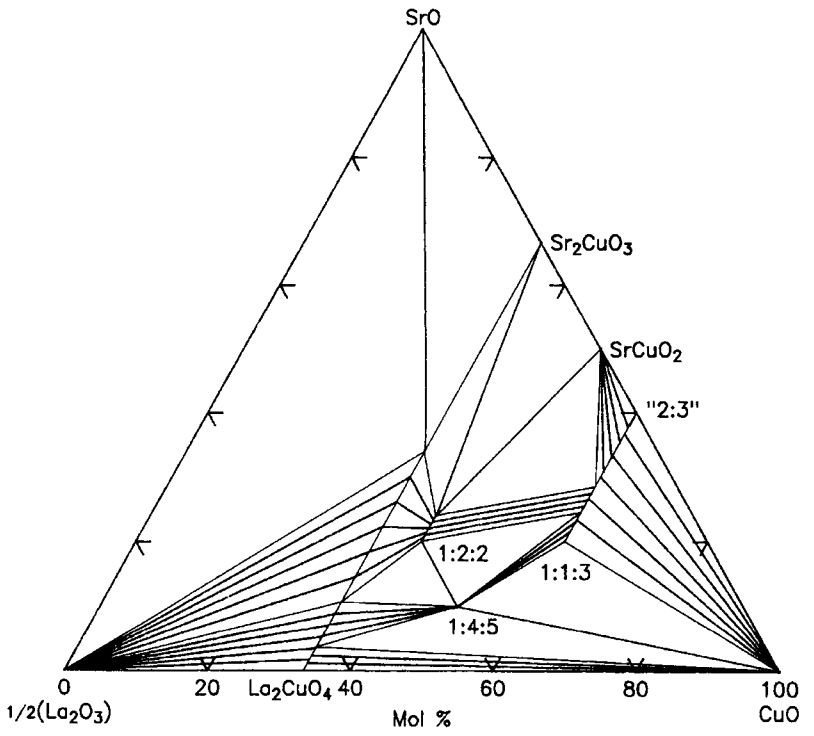

Phase diagram of the system SrO–La_2O_3–CuO at 980°C in (Hohn *et al.*, 1989).

coexistence of the solid solution $Bi_{2.2-x}Sr_{1.8+x}CuO_z$ (commonly referred to as the Raveau 11905 phase) and the $Bi_2Sr_2CuO_6$ (2201) phase. It is this 11905 that is the single-layered 9–20 K superconductor, whereas the 2201 phase does not superconduct. The Raveau phase and the 2201 phase are in equilibrium with each other. The Raveau solid solution was found for the approximate range $0 \leq x \leq 0.15$ for $Sr_{1.8-x}Bi_{2.2+x}Cu_{1\pm x/2}O_z$. This phase is structurally similar to the $n = 1$ member of $Sr_2Bi_2Ca_{n-1}Cu_nO_{2n+4}$. The 2201 phase was found to be monoclinic and CuO-deficient (<1 mol%) and only has a small homogeneity region. The observed X-ray diffraction of this phase does not match that of the Raveau phase. Thoughout the literature, the 2201 symbol is commonly used in place of the Raveau phase and may be interpreted as a part of the extended single-phase region of the Raveau phase (Fig. 14.17). The Raveau phase was found to melt at 870°C (Nevřiva *et al.*, 1993). The other two ternary compounds ($Bi_4Sr_8Cu_5O_x$ and $Bi_2Sr_3Cu_2O_x$) are not superconductors.

Fig. 14.17.

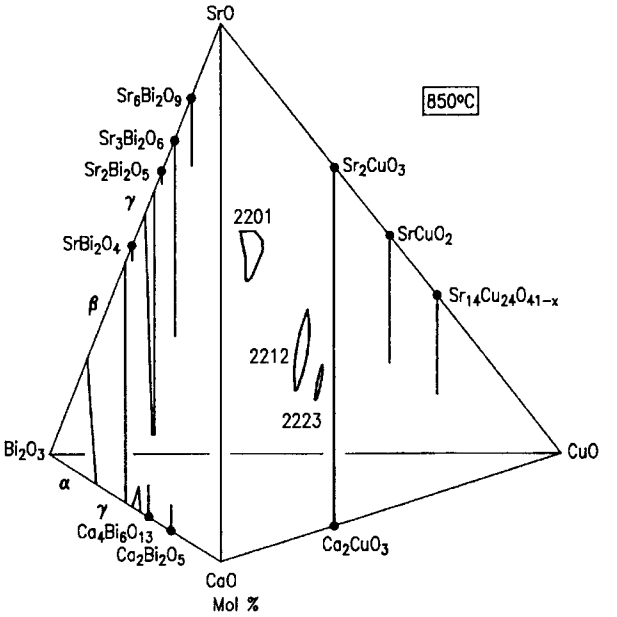

Tetrahedral phase diagram of the Bi_2O_3–SrO–CaO–CuO system at 850°C showing the presence of various phases and the locations of the 2201, 2212, and 2223 phases (Hettrich *et al.*, 1991).

2. Phase Diagrams for Two CuO_2 Layers

Solid solution region. Various investigations of the solid solution boundaries of the 2212 phase have been published. Figure 14.19 summarizes some of the literature data and indicates the range in size and shape reported for the solid solution field up to 1993 (Krizek *et al.*, 1993; Holesinger *et al.*, 1993; Majewski, 1994; Hong and Mason, 1991; Golden *et al.*, 1991; Muller *et al.*, 1992). Disagreements among the reported solid solution regions indicate the complicated nature of the equilibria in this system. Many factors influence the experimental results, including the sensitivity of the phase assemblages to processing conditions, the sluggish kinetics of phase formation, and the very closely spaced phase stability fields of the high-T_c phases.

Figure 14.20 shows the temperature stoichiometry dependence of the $Bi_{2.18}Sr_{3-y}Ca_yCu_2O_{8+x}$ composition (Majewski *et al.*, 1995b). In this projection, the 2212 phase exhibits an extended single-phase region with variable Sr, Ca, Bi, and oxygen content. This single-phase region approximates a half-moon shape, with the greatest width of y at about 800°C. With increasing temperature the extension of the single-phase region shrinks and is shifted to Sr-richer compositions. The four-phase regions outside the single-phase area vary depending on the

Fig. 14.18.

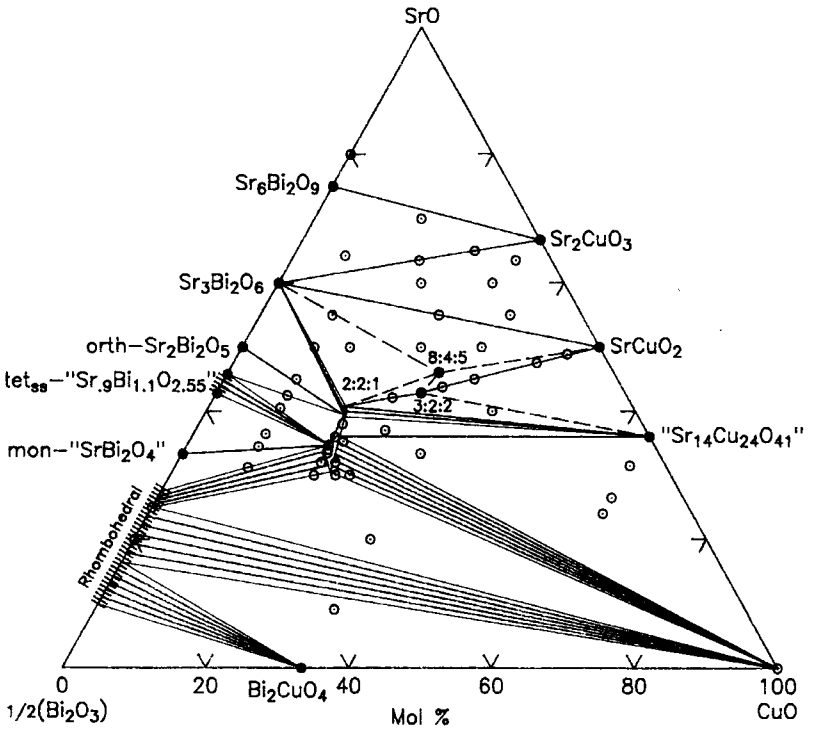

Phase diagram of the system Bi_2O_3–SrO–CuO at 875-925°C in air (Roth *et al.*, 1990).

y value of the formula. The high-temperature annealing of the Ca-rich 2212 phase leads to precipitation of Ca_2CuO_3 and a liquid, whereas annealing of the Sr-rich 2212 phase leads to the formation of $Bi_2Sr_3Cu_2O_{88}$, cuprates, and liquid. At temperatures above 870°C the Sr-rich 2212 phase decomposes. The ratio Sr : Ca of the critical composition of the 2212 phase was determined to be about 2 : 1 ($Bi_{2.18}Sr_2CaCu_2O_{8+d}$). At the maximum melting temperature, the 2212 phase melts to 2201 + cuprates + L.

Subsolidus four-phase compatibilities. The 2212 solid solution was found to be in equilibrium with 10 phases at 830°C (Wong-Ng *et al.*, 1998). The equilibrium phases were $0x21$ {[(Ca, Sr)$_2$CuO$_3$], x is used to represent the solid solution concentration of the lesser component}, 119×5 [(Bi,Pb)$_{2.2}$Sr$_{1.8-x}$Ca$_x$CuO$_z$], 2110 [Bi$_{16}$(Sr, Ca)$_{14}$O$_z$], 014×24 [(Sr, Ca)$_{14}$Cu$_{24}$O$_{41}$], 2310 [Bi$_2$(Sr,Ca)$_4$O$_z$], 4805 [Bi$_4$Sr$_8$Cu$_5$O$_z$), 2201 [(Bi, Pb)$_2$Sr$_{2-x}$Ca$_x$CuO$_z$], (Ca, Sr)O, CuO, and $0x11$ [(Sr$_{1-x}$Ca$_x$)CuO$_2$, Ca-rich]. Because of the presence of extensive ternary and quaternary solid solutions, the 2212 phase compatibilities include a number of relatively "flat," or shallow, four-phase equilibrium volumes. The implication is that a small variation of composition, or temperature, can lead to a

Fig. 14.19.

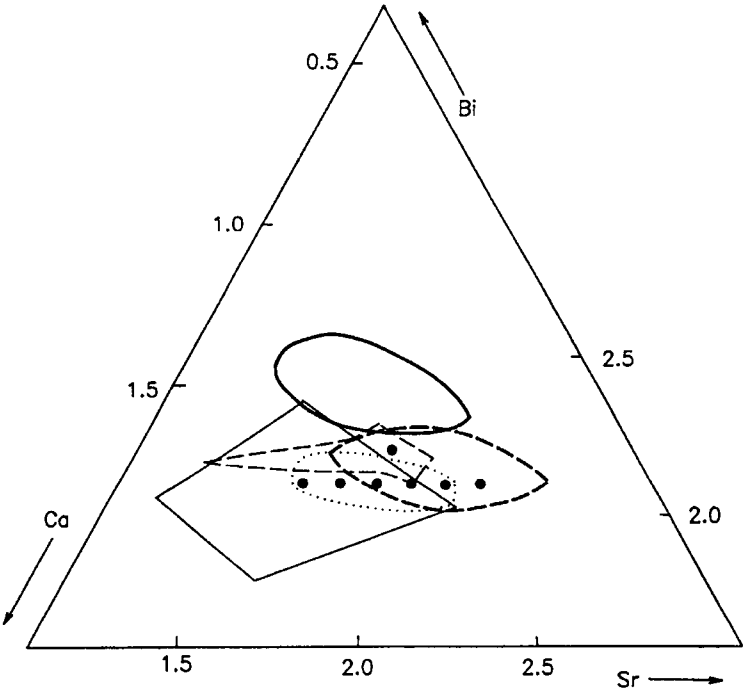

Summary of various determinations of the single-phase solid solution region of the 2212 phase in the Bi_2O_3–SrO–CaO–CuO system (Knizek *et al.*, 1993). The cross-section shown corresponds to the formula $Bi_{2+y}Sr_{3-y-x}Ca_xCu_2O_{8+\delta}$. Knizek *et al.* (1993), (• • •) 850°C, air; Holesinger *et al.* (1993), (· · · ·) 865°C, oxygen; Majewski (1994), (– – – –) 850°C, air; Hong and Mason (1991) (— — —) 860°C, air; Golden *et al.* (1991), (——) varying temperature; Muller *et al.* (1992), (–·–) 830°C, air.

dramatic change in the phase equilibrium assemblage. Table 14.3 lists a series of 16 four-phase equilibrium volumes arranged according to the initial melting temperatures obtained from the DTA events (Wong-Ng *et al.*, 1998). They are mutually stable in a topologically consistent manner (i.e., no compositional overlaps with each other), and they form a close-packed arrangement. The eutectic temperature ($\approx$825°C), or the lowest temperature at which the 2212 phase is in equilibrium with liquid, was found to involve a liquid near the strontium-poor part of the Bi–Sr–Ca–Cu oxide system: 2110 + 119x5 + 2212 + CuO → L.

Primary crystallization field of the 2212 phase. Table 14.3 also shows the initial melt compositions for the 16 four-phase volumes involving the 2212 phase. The Bi concentration was found to cover a range from 24 to 42%, Sr from 7 to 33%, Ca from 2 to 27%, and Cu from 19 to 43%. The three-dimensional pictorialization of the 2212 crystallization volume is shown via the two views in

Fig. 14.20.

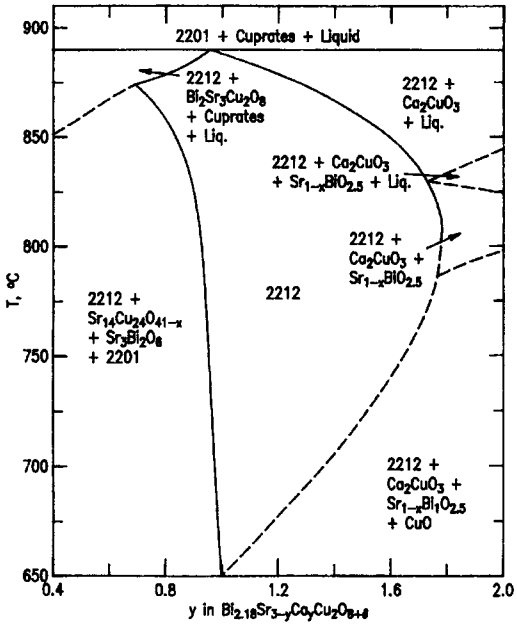

Temperature–(Sr, Ca) stoichiometry phase relations for the 2212 phase with composition $Bi_{2.18}Sr_{3-y}Ca_yCu_2O_{8+\delta}$. The designation 2201 is used to represent the Raveau superconducting phase (Majewski *et al.*, 1995b) Table 14.3 gives initial melts of four-phase equilibrium volumes containing the 2212 phase.

Figs. 14.21 and 14.22, where approximate temperatures of the four-phase initial melting equilibria are also indicated. In these diagrams the volumes are expressed in Cartesian coordinates. The polygonal areas on the surface of the crystallization volume have been labeled according to the presence of a second solid in equilibrium with 2212. The maximum melting temperature in Fig. 14.21 is 889°C, corresponding to the initial melting equilibrium for the four-phase volume 2212–2310–0*x*21–CaO. The overall wedgelike shape of the volume is apparent in Fig. 14.22. In the lower-melting region (low SrO), the volume is very thin and terminates along a sharp edge. The higher SrO end of the volume is much wider and is terminated by the 2201 crystallization surface. Inside the volume, the 2212 phase is in equilibrium with liquid. At the corners, it is in equilibrium with three phases and with L. At the edges, 2212 is in equilibrium with two phases plus L, and on each face 2212 is in equilibrium with L and the labeled phase.

Effect of Ag addition. The use of silver as an additive is widespread in BSCCO tape and wire processing. Except at very high temperaures, the presence of Ag does not affect the stability of the 2212 phase (Driscoll *et al.*, 1993). Figure 14.23 shows a schematic temperature–composition phase relations of the

Table 14.3.

Initial melts of four-phase equilibrium volumes containing the 2212 phase of BSCCO, see Fig. 14.20.

Sample		DTA	Melt Composition			
ID	Four-phase equilibria	T(°C)	Bi	Sr	Ca	Cu
1	2212–2110–119*x*5–CuO	25	41.7	16.1	22.3	19.9
2	2212–0*x*21–2110–CuO	830	30.4	7.4	26.6	35.6
3	2212–0*x*21–CaO–2110	838	35.2	20.8	24.6	19.4
4	2212–014*x*24–CuO–119*x*5	856	27.6	25.1	8.8	38.5
5	2212–2110–119*x*5–CaO	856	37.8	18.0	19.6	24.6
6	2212–014*x*24–0*x*11–CuO	861	26.2	24.2	22.3	27.3
7	2212–014*x*24–0*x*11–0*x*21	863	25.3	23.6	18.9	32.2
8	2212–119*x*5–2310–CaO	873	29.8	23.2	21.9	25.1
9	2212–4805–0*x*21–CuO	875	25.9	21.8	14.2	38.1
10	2212–2201–2310–014*x*24	877	23.9	32.8	11.7	31.6
11	2212–4805–0*x*11–CuO	877	26.4	26.3	12.7	34.6
12	2212–119*x*5–2201–2310	877	32.8	30.7	4.5	32.0
13	2212–119*x*5–014*x*24–2201	878	27.7	26.9	2.5	42.9
14	2212–0*x*21–014*x*24–2310	885	28.7	21.4	20.8	29.1
15	2212–4805–0*x*11–0*x*21	887	29.9	24.7	14.9	30.5
16	2212–2310–0*x*21–CaO	889	26.9	24.7	17.6	30.8

Fig. 14.21.

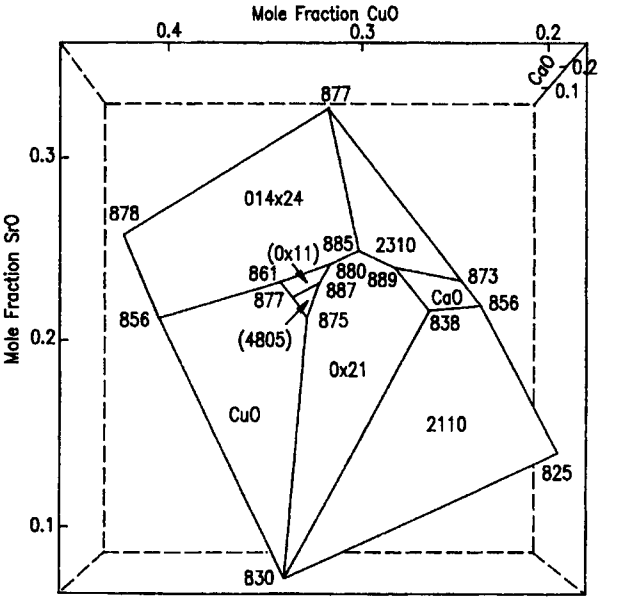

Primary crystallization field of the Bi–Sr–Ca–Cu–O2212 phase using orthogonal coordinates (Wong-Ng *et al.*, 1998).

Fig. 14.22.

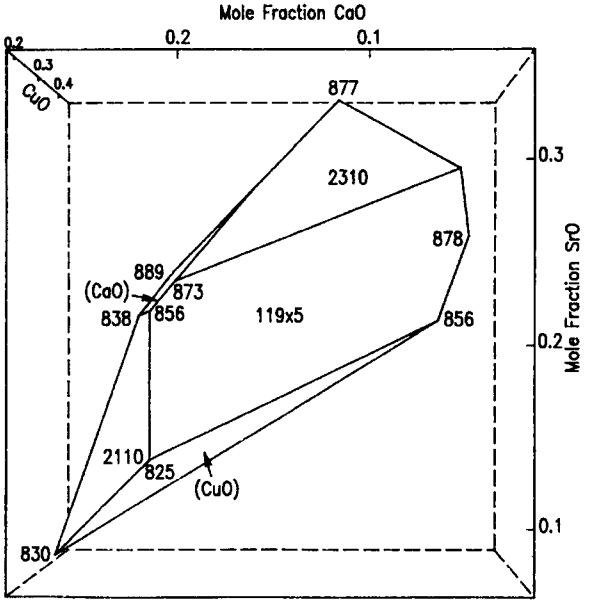

View of the primary crystallization field of the Bi–Sr–Ca–Cu–O 2212 phase approximately orthogonal to the view shown in Fig. 21 (Wong-Ng *et al.*, 1998).

$Bi_2Sr_2CaCu_2O_x$ composition and Ag. Liquid immiscibility between oxide and Ag liquids in 8–98 at.% Ag range at all temperature is found (McCallum *et al.*, 1994). The solubility of Ag in the specific 2212 composition was less than detection limits, but that Ag depressed the melting temperature of mixtures with the $Bi_2Sr_2CaCu_2O_x$ composition through the formation of a eutectic with $\approx 4\%$ Ag.

With the addition of excess silver ($\approx$30 wt%), the initial melting temperatures of the 2212 four-phase equilibrium volumes were all lowered, by amounts ranging from 4 to 22°C (Wong-Ng *et al.*, 1998) Silver entered the melt, with a mole fraction of 6 to 8%. In Fig. 14.24, the outline of the Ag-free and Ag-containing melts are shown as projections (normalized in terms of the CaO, CuO, and Bi_2O_3 contents). Ag addition is manifested in a reduced copper content of the melts.

3. Phase Diagrams fir Three CuO_2 Layers

Phase equilibrium investigations of the Pb-free high-T_c three-layered superconductors are much less numerous than those of the Pb-containing system. One such study in air is represented in Fig. 14.25 (Majewski *et al.*, 1991),

Fig. 14.23.

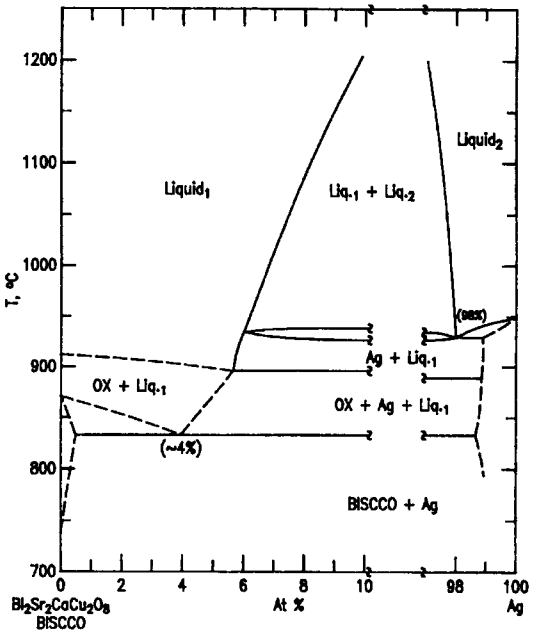

Temperature–compostion phase relations in the system of $Bi_2Sr_2CaCu_2O_8$–Ag (McCallum *et al.*, 1994). The symbol OX is used to represent oxygen.

showing the section of Bi_2O_3–$\frac{1}{2}$(SrO + CaO)–CuO at 850°C through the quaternary system Bi_2O_3–SrO–CaO–CuO. The 2223 phase is also surrounded by very flat two-, three-, and four-phase equilibria. Therefore, a small deficiency of CuO and/or Bi_2O_3 during the preparation of the 2223-phase sample results in a significant decrease of the volume content of the 2223 phase. On the other hand, an excess of Bi_2O_3 and CuO results in the formation of the 2223 phase in addition to CuO and liquid. At 850°C, the 2212 and the 2223 Pb-free superconductors are in equilibrium with a liquid of composition close to a Ca-rich 2201 phase. The 2223 phase only exists above 840°C.

Figure 14.26 shows the schematic projection diagram of the solid solution region of the Pb-2223 phase of composition $Bi_{2.27-x}Pb_xSr_2Ca_2Cu_3O_{10+d}$ as a function of temperature (Kaesche *et al.*, 1995). A single phase region was identified between $x = 0.18$ and $x = 0.36$. This schematic diagram is intended to illustrate phase existence regions only. There is a relatively narrow temperature range within which a single phase can form (about 838–860°C). Below and above this temperature range with x values of $0.1 > x > 0.36$, a multiple phase region is observed. For $x > 0.36$, 2223 was found in equilibrium with numerous phases, including $Pb_4(Sr, Ca)_5CuO_x$, indicating that the maximum Pb solubility was exceeded. For $x < 0.18$, only small amounts of 2223 were detected with the 2212

Fig. 14.24.

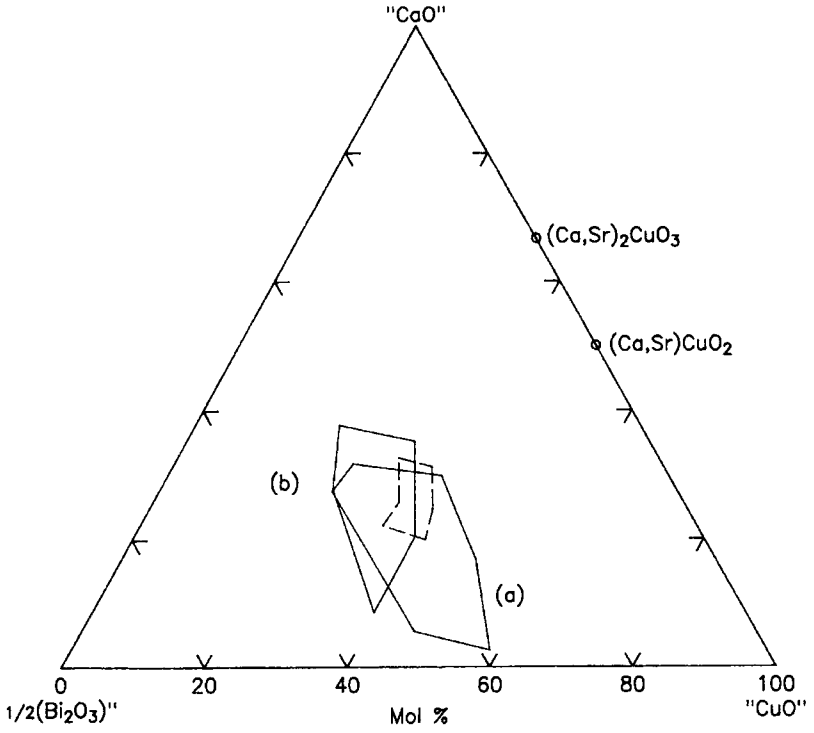

Primary crystallization field of the Bi–Sr–Ca–Cu–O 2212 phase projected onto the ternary plane and shown in broken lines, (a) without the addition of Ag and (b) with Ag added (Wong-Ng *et al.*, 1998). The projection of the 2212 solid solution is also shown in broken lines.

phase predominant over the entire temperature range. Figure 14.27 illustrates the solid solution region of a composition $Bi_yPb_xSr_2Ca_2Cu_3O_{10+d}$ at 850°C and the surrounding phase fields as a function of the x and y values. The solid solution has a triangular shape, and Pb substitution has widened the homogeneity range of the 2223 phase.

In another subsolidus equilibrium study (Wong-Ng *et al.*, 1997), the Pb-2223 phase was found to be in equilibrium with 11 phases: 1x20 [$(Ca,Sr)_2PbO_4$], 0x21, CaO, CuO, 3221 [$(Pb, Bi)_3(Sr, Ca)_5O_x$]), 0x11 [Ca-rich], 0x11′ [Ca-poor], 2310, 119x5, and 2212. Equilibria involving the complete 29 subsolidus five-phase volumes and their initial melting temperatures of the Pb2223 phase in the (Bi,Pb)–Sr–Ca–Cu–O system are shown in Table 14.4. Because of the large number of phases and closely spaced phase compositions, the Pb-2223 phase compatibilities, similar to those of the 2212 and Pb-free 2223 phases, include a number of relatively "flat," or shallow, five-phase equilibrium volumes. Among the 29 five-phase volumes, 16 involve the 2223–2212 phases that are mutually

Fig. 14.25.

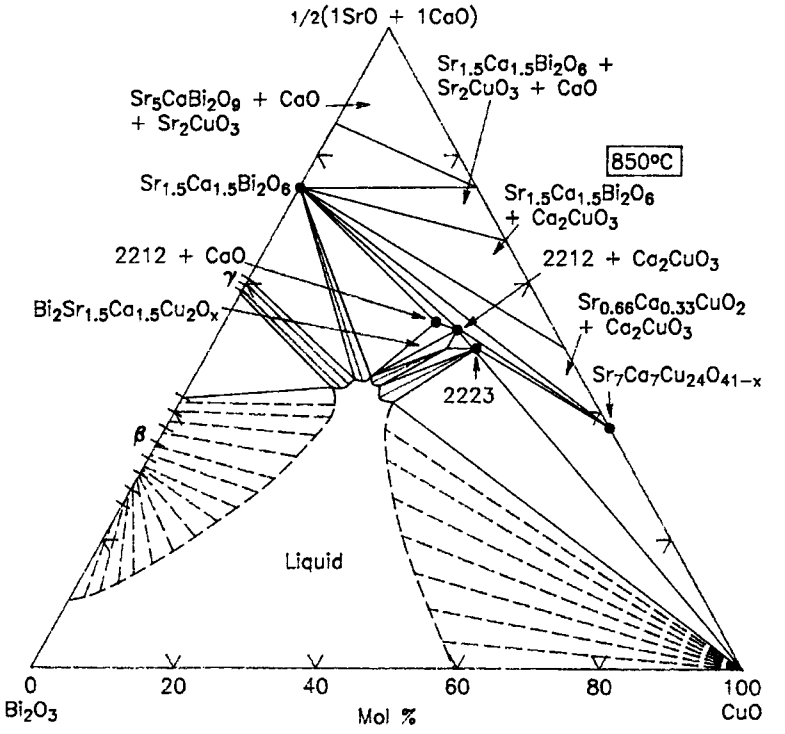

Section Bi_2O_3–$\frac{1}{2}$(SrO + CaO)–CuO through the quaternary phase diagram of the system Bi_2O_3–SrO–CaO–CuO at 850°C in air, showing the equilibrium of 2212 and 2223 with liquid (Majewski *et al.*, 1991).

stable in a topologically consistent manner. Because the 2212 and 2223 phases have similar structures (being members of the same homologous series), and the 2212 phase is a precursor for the formation of the 2223 phase, their mutual solid-state compatibilities are extensive.

e. Tl–Ba–Ca–Cu–O Systems

Phase equilibrium studies in the Tl–Ba–Ca–Cu–O system are not as extensive as those in the BYC, BRC, or the BSCCO systems, partly because of the additional processing parameters of vapor pressure, and also because of the toxicity of Tl-containing compounds. Figure 14.28 shows the four-component composition tetrahedron for the TlO_x–BaO–CaO–CuO system (Siegal *et al.*, 1997). The nominal compositions of the presently known and confirmed superconducting phases were found to lie in the plane determined by TlO_x, 2BaO·CuO, and

Fig. 14.26.

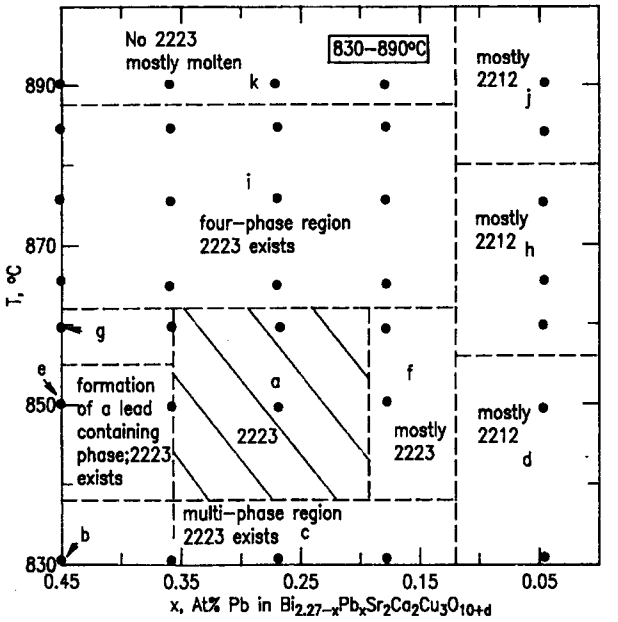

Plot of temperature vs lead content x showing phase regions for $Bi_{2.27-x}Pb_xSr_2Ca_2Cu_3O_{10+d}$ (Kaesche *et al.*, 1995).

CaO·CuO (Fig. 14.29). Furthermore, the nominal composition of each quaternary superconductor phase lies at the intersection of one of the two lines originating at the component CaO·CuO and terminating at the Tl-1201 and Tl-2201 compositions. A second set of lines originates at TlO_x and terminates at the Tl-free compositions 0212, 0223, and 0234. Therefore, traveling along any one of the second family of lines corresponds to adding or deleting thallium from the previous compound.

The phase diagram of the system containing the 20 K superconductor $Tl_2Ba_2CuO_6$ (2201) is shown in Fig. 14.30 (Jondo *et al.*, 1993). The $Tl_2Ba_2CuO_6$ phase exists in both tetragonal and orthorhombic forms, and is in equilibrium with Tl_2BaO_4, $Tl_6Ba_4O_{13}$, $Tl_2Ba_2O_5$, $BaCuO_2$, and CuO. The pseudobinary cut of the system $Tl_2Ba_2O_5$–CuO is shown in Fig. 14.31. The $Tl_2Ba_2CuO_6$ phase melts incongruently into $Tl_2Ba_2O_5$ and L.

The solid solution extent of the Tl-2212 phase is illustrated in the $Ba_2CaCu_2O_x$–Tl_2O_3 system as a function of temperature (Fig. 14.32) (Cook *et al.*, 1990). A single phase region around the 2212 composition at higher temperatures has been confirmed. It was also found that a sample with maximum T_c occurred with less Tl_2O_3 than the 2212 stoichiometry.

Fig. 14.27.

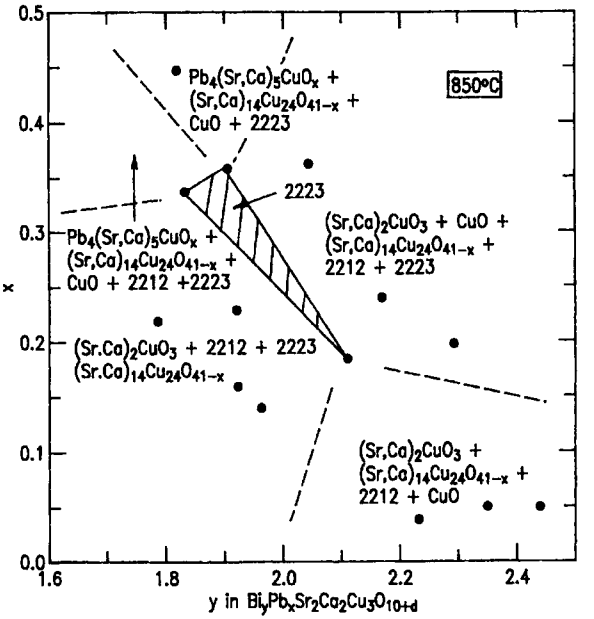

Phase fields surrounding the 2223 phase ($Bi_yPb_xSr_2Ca_2Cu_3O_{10+d}$) as a function of lead content x vs bismuth content y at 850°C (Kaesche *et al.*, 1995). Table 14.4 provides a set of 20 five-phase volumes of Pb-2223.

The phase equilibria in the Tl_2O–BaO–CaO–CuO system that are slightly below the onset of melting (two-zone furnace) are shown in Fig. 14.33 (Aselege *et al.*, 1994). The stable ranges of $p(Tl_2O)$, $p(O_2)$, and sample composition for individual Tl superconductors, including the 1122, 2122, 1223, and 2223 phases, are shown in Figs. 14.33a to 14.33c. In these diagrams, the partial $p(Tl_2O)$–$p(O_2)$ subsolidus phase relationships with the BaO : CaO : CuO ratios of 2 : 1 : 2, 2 : 2 : 3,

Table 14.4.

Set of 29 Pb-2223 five-phase volumes (7.5 vol% O_2/92.5 vol% Ar) of the (Bi, Pb)–Si–Ca–Cu–O system. See Fig. 14.27.

2223–2212–1x20–119x5–2310	2223–2212–014x24–1x20–119x5	2223–2212–0x11–2310–119x5
2223–2212–1x20–2310–CaO	2223–2212–2310–0x11–3221	2223–2212–119x5–0x11–CuO
2223–2212–0x21–1x20–CuO	2223–2212–014x24–119x5–CuO	2223–2212–0x21–014x24–CuO
2223–2212–1x20–0x11–3221	2223–2212–014x24–0x21–1x20	2223–2212–0x11–0x11′–CuO
2223–2212–1x20–CuO–0x11	2223–2212–3221–CaO–1x20	2223–2212–0x11–0x11′–2310
2223–2212–3221–CaO–2310	2223–0x11′–2310–0x11–119x5	2223–0x11′–CaO–2310–0x11
2223–1x20–0x11′–CuO–0x11	2223–0x11′–014x24–119x5–CuO	2223–0x11′–CaO–0x11–3221
2223–1x20–CuO–0x21–014x24	2223–1x20–CuO–0x11′–01424	2223–2310–3221–CaO–0x11
2223–1x20–CaO–0x11′–2310	2223–1x20–2310–014x24–0x11′	2223–1x20–0x11′–3221–0x11
2223–1x20–CaO–0x11′–3221	2223–0x11′–2310–119x5–014x24	

Fig. 14.28.

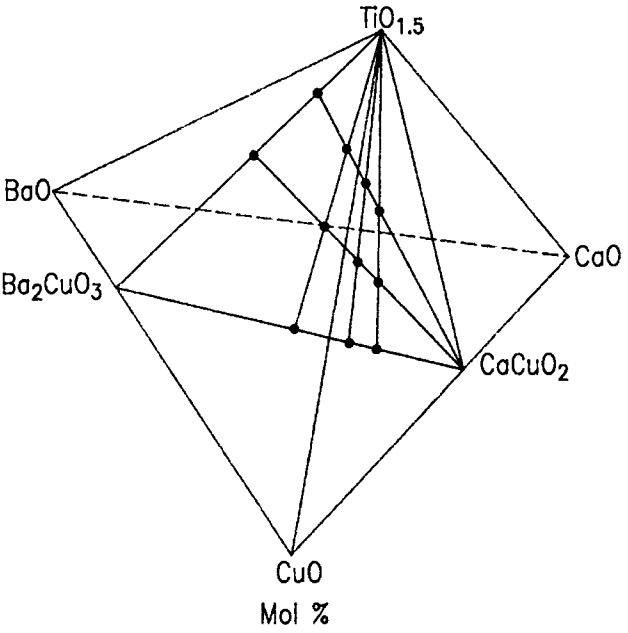

Four-component composition tetrahedron for the TlO_x-BaO–CaO–CuO system. The nominal compositions of the superconducting phases in the system all lie in the plane determined by TlO_x, 2BaO·CuO, and CaO·CuO [84]. (Siegal *et al.*, 1997)

and 2 : 3 : 4, are illustrated. It was found that $p(O_2)$ is not a critical variable controlling the relative thermodynamic stabilities of 2223 and 2212, and their stabilities are controlled by $p(Tl_2O)$. The 2212 phase is the stable superconductor phase, independent of batch stoichiometry and $p(O_2)$ within the highest range of $p(Tl_2O)$ (Fig. 14.33a). Higher values of $p(Tl_2O)$ produced Tl-rich, nonsuperconducting phases. The 2223 phase is stable on both the 2 : 2 : 3 and 3 : 2 : 4 tie-lines over a narrow, lower range of $p(Tl_2O)$, independent of $p(O_2)$ between at least 8×10^3 Pa and 8×10^4 Pa (Fig. 14.33c). An excess of Ca and/or Cu is required to prepare single-phase 2223. As $p(Tl_2O)$ is reduced below about 5×10^2 Pa, the m = 1 phases ($Tl_mCa_{n-1}Ba_2Cu_nO_{2(n+1)+m}$) become more stable (Fig. 14.33b). On the 2 : 2 : 3 and 3 : 2 : 4 tie-lines, 1223 intergrowth with 2223 is observed (the amount of intergrowth ranges from 50 to 90%). The 1324 phase (also present as an intergrowth) is stable at lower $p(Tl_2O)$ than 1223 on both the 2 : 2 : 3 and 3 : 2 : 4-tie lines. The 1122 phase is observed on the 1 : 2 : 2 tie-line in 100% O_2 with $p(Tl_2O) < 5 \times 10^2$ Pa.

Fig. 14.29.

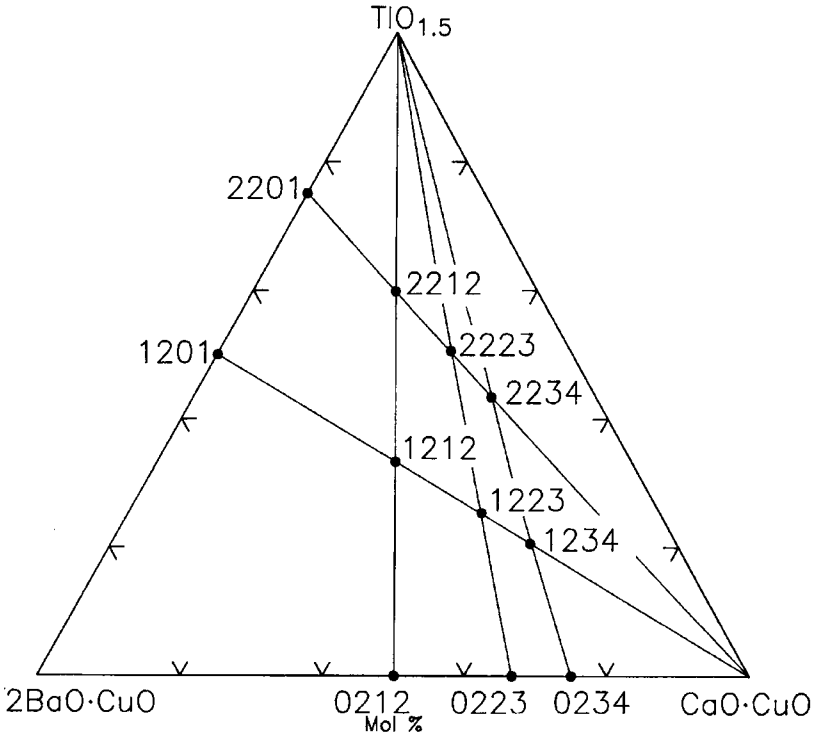

Pseudoternary composition diagram for triangular plane of Fig. 14.28 of the TlO_x–BaO–CaO–CuO system, illustrating the location of the superconducting phases (Siegal *et al.*, 1997).

f. (Nd, Ce)-CuO_4 Systems

In 1989, a family of superconductors in which the carriers of the superconducting current are electrons themselves rather than electron vacancies, or "holes," was discovered (Tokura *et al.*, 1989). These superconductors are Ce^4-doped compounds, with the formula $R_{2-x}Ce_xCuO_{4-y}$, where R stands for Pr, Nd, or Sm. The compounds have the Nd_2CuO_4 (T′-phase) type structure, which is composed of sheets of Cu–O squares.

An isothermal section at 1000°C of the phase diagram of the Nd–Ce–Cu–O system is shown in Fig. 14.34 (Pieczulewski *et al.*, 1990). The only ternary compound in this system is the solid solution $(Nd_{2-x}Ce_x)CuO_4$, which extends from $x = 0$ to 0.2. Three sets of solid solution tie-lines were observed that connected the (Ce, Nd)O_x solid solution, Nd_2O_3, and CuO to $(Nd_{2-x}Ce_x)CuO_4$. Superconductivity was only observed in the range of solid solution of $(Nd_{2-x}Ce_x)CuO_4$, with $0.14 < x < 0.18$. The absence of superconductivity from

Fig. 14.30.

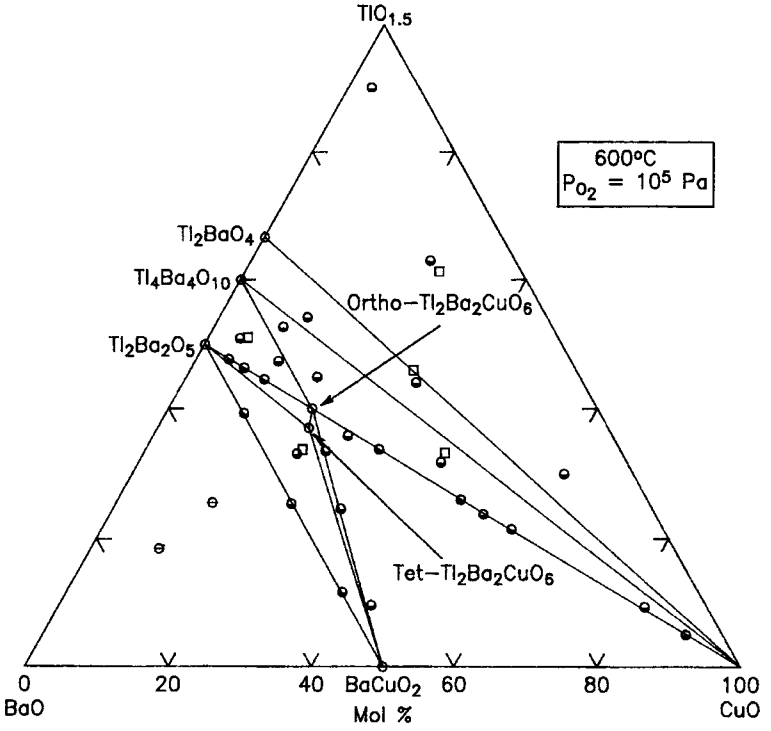

Phase diagram showing the subsolidus relationships at 600°C and 10^5 Pa O_2 of the system of BaO–CuO–Tl_2O_3. Ortho = orthorhombic; Tet = tetragonal (Jondo *et al.*, 1993).

the greater part of the diagram is a significant feature of this system, which is a direct result of the narrow composition range in $Nd_{2-x}Ce_xCuO_4$ that is superconducting.

The dependence of the degrees of oxygen nonstoichiometry in $Nd_{1.85}Ce_{0.15}CuO_{4-x}$ on temperature and oxygen pressure have been reported in the range of temperature 350–950°C and of oxygen pressure 10^{-5} to 1 atm (Kim and Gaskell, 1993). The stability field (Fig. 14.35) of $Nd_{1.85}Ce_{0.15}CuO_{4-x}$ contains subfields with and without superconducting properties. The two subfields meet at the Cu_2O–CuO transition line (dashed line). The variance of the value x within the $Nd_{1.85}Ce_{0.15}CuO_{4-x}$ stability field is between 0.0 and 0.045. This is a very small value in comparison with the variance of $x = 0.0$–1.0 that occurs in the $Ba_2YCu_3O_{6+x}$ compound. The maximum value of $(4 - x)$ in $Nd_{1.85}Ce_{0.15}CuO_{4-x}$ was determined to be 3.995. $Nd_{1.85}Ce_{0.15}CuO_{4-x}$ melts incongruently above 1150°C and decomposes to $Nd_2O_3 + NdCeO_{3.5} + Cu_2O$. The value of T_c in the superconducting phase increases from 5 to 24 K as x increases from 0.008 to 0.05.

Fig. 14.31.

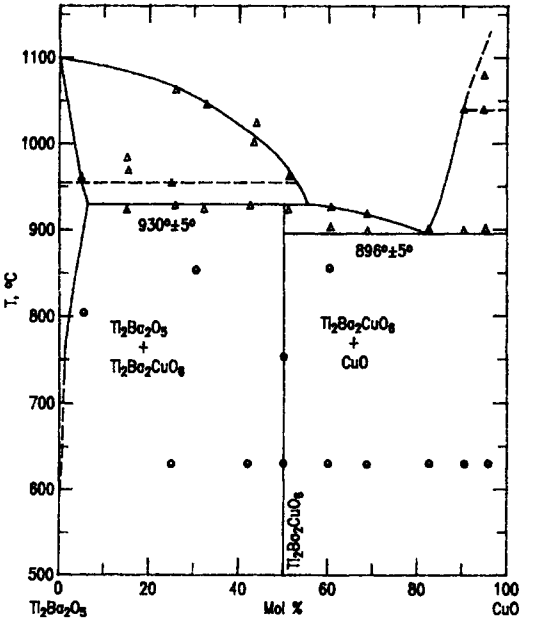

Temperature vs composition plot for the binary system of $Tl_2Ba_2O_5$–CuO (Jondo *et al.*, 1993).

g. Hg–Ba–Ca–Cu–O Systems

The mercury-containing high-T_c superconductor oxides $HgBa_2Ca_{n-1}Cu_nO_{2n+2+\delta}$, where $n = 1, 2, 3 \ldots$, have fascinated scientists in recent years. Not only does this family of compounds exhibit the highest T_c among the systems known to date (Antipov *et al.*, 1990), but also, under high pressure, these materials show many unusual properties, including pressure-induced T_c enhancements (Chou, 1996). In general, a parabolic variation of T_c with δ and with pressure has been observed over a wide range of superconductivity values (Loureiro, 1997; Akesenov and Antipov, 1977; Fukuoka *et al.*, 1996; Chu *et al.*, 1993; Nuñez-Regueiro *et al.*, 1993; Gao *et al.*, 1994; Takahashi *et al.*, 1993; Jover *et al.*, 1996; Ihara *et al.*, 1993). Pressure-induced T_c enhancement is still under intense investigation.

Because of the experimental difficulties involving the determination of Hg vapor pressure, and the toxicity of Hg, very little activity has occurred on phase equilibrium studies. In this system, the 1201, 1212, 1223, and 1234 phases have been characterized rather extensively. In Fig. 14.36 the maximum value of the T_c as a function of pressure of various Hg-containing compounds 1201, 1212, 1223, and 1234 up to 15 GPa is shown (Loureiro; 1997). The initial rate of increase of T_c under pressure appears to be similar for these compounds, indicating that up to the pressure of 15 GPa, there is a strong intrinsic term controlling T_c and charge

Fig. 14.32.

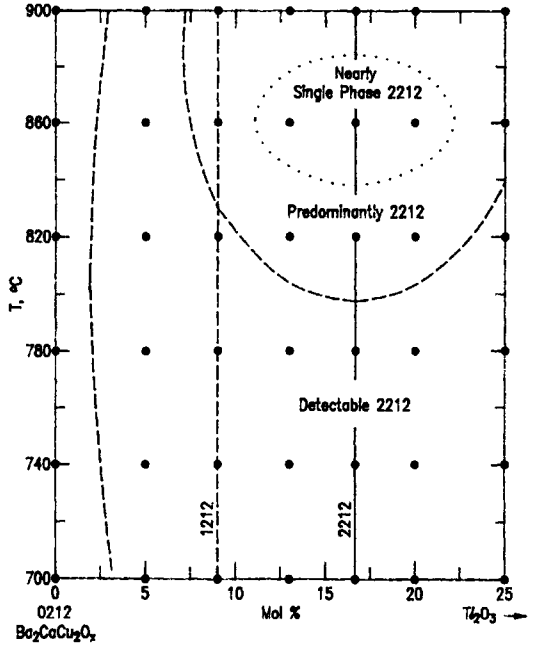

Temperature vs composition plot showing the solid solution extent of the Tl-2212 phase as a function of temperature (Cook *et al.*, 1990).

transfer is not relevant in this region (Chou, 1996). The slopes at the origin for the shown fits are Hg-1201: 2.02 K/GPa, Hg-1212: 2.2 K/GPa, Hg-1223: 2.07 K GPa, and Hg-1234: 1.7 K/GPa. A substantial study of P vs T_c has been reported for the Hg-1223 phase (Louvero, 1997). Figure 14.37 shows a summary of results from various groups; the T_c increased under pressure at a rather strong rate. The highest pressures reached the onset value of 164 K at around 30 GPa.

E

Summary and Future Needs

Representative systems of the high-T_c superconductors have been summarized. Special attention was given to the BYC and BRC systems, followed by the BSCCO systems. These systems have currently been studied most extensively because of their viable industrial applications in the coated-conductor and wire/tape development areas. A large number of these diagrams, however, were by no means complete. For example, a complete series of phase diagrams

Fig. 14.33.

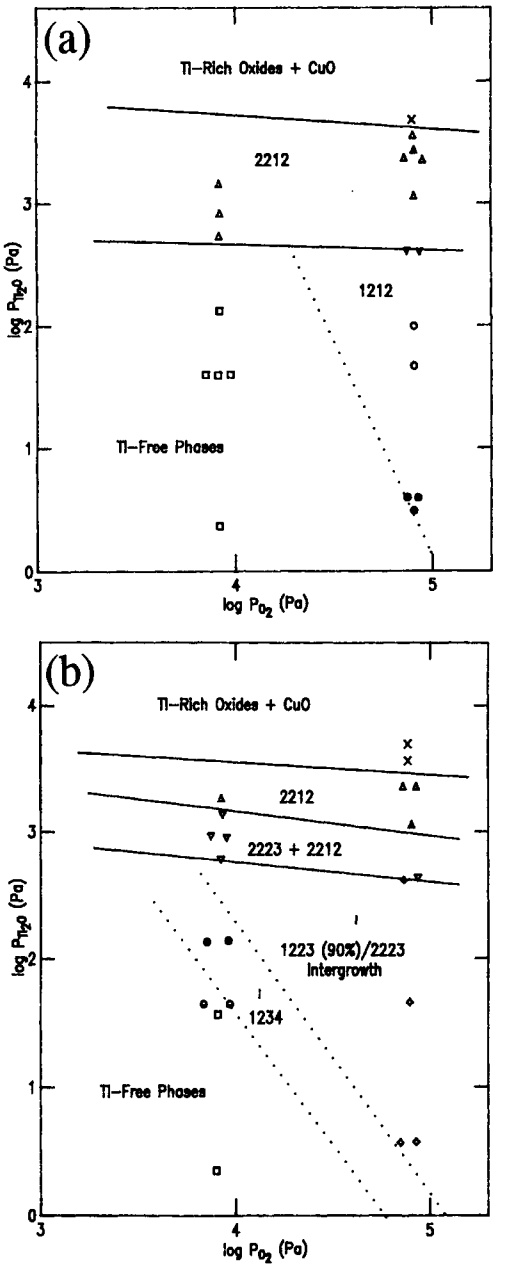

Partial $p(Tl_2O)$–$p(O_2)$ subsolidus phase diagrams of the system Tl_2O–BaO–CaO–CuO with BaO : CaO : CuO ratios of (a) 2 : 1 : 2, and (b) 2 : 2 : 3. Compounds formed are: $2212 = Tl_2Ba_2CaCu_2O_x$; $1212 = TlBa_2CaCu_2O_x$; $2223 = Tl_2Ba_2Ca_2Cu_2O_x$; $1234 = TlBa_2Ca_3Cu_4O_x$; $1223 = TlBa_2Ca_2Cu_3O_x$ (Tokura *et al.*, 1989).

(*continued*)

Fig. 14.33. (*continued*)

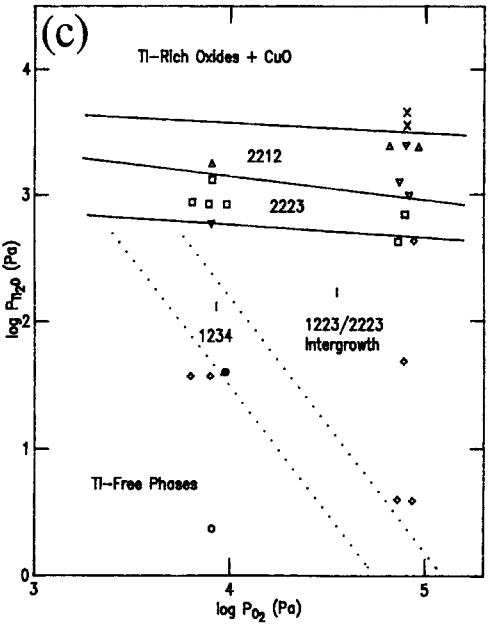

Partial $p(Tl_2O)$–$p(O_2)$ subsolidus phase diagrams of the system Tl_2O–BaO–CaO–CuO with BaO : CaO : CuO ratios of (c) 2 : 3 : 4. Compounds formed are: $2212 = Tl_2Ba_2CaCu_2O_x$; $1212 = TlBa_2CaCu_2O_x$; $2223 = Tl_2Ba_2Ca_2Cu_2O_x$; $1234 = TlBa_2Ca_3Cu_4O_x$; $1223 = TlBa_2Ca_2Cu_3O_x$ (Tokura *et al.*, 1989).

of the BRC systems as a function of oxygen partial pressure and their corresponding liquidus diagrams are not available. Furthermore, for the coated conductor research, materials compatibility is an important issue. Therefore, information on interactions of high-T_c superconductor films with substrates and other buffer layers is essential. It will be important to have phase equilibrium data that include the high-T_c phases and the buffer materials. In the complicated multicomponent BSCCO system, complete phase equilibria including Ag are needed in order to understand Ag's influence on processing by using the PIT technique. In the other multicomponent systems, only very limited information on the Tl-containing and Hg-containing systems has been reported.

Besides the systems that have been discussed, other systems of interest to the high-temperature superconductor research community are Ni–R–C–B, Pb–Sr–R–Cu–O, Sr–R–Nb–Cu–O, Sr–R–Ga–Cu–O, and the (Tl, Pb)Sr–Ca–Cu–O variants (Cavam 1995). Although these systems are not of immediate industrial interest, knowledge of the phase relationships of a collection of systems will contribute substantially to further understanding of the crystal chemistry and phase equilibria of the high-temperature superconductor oxide family as a whole.

Fig. 14.34.

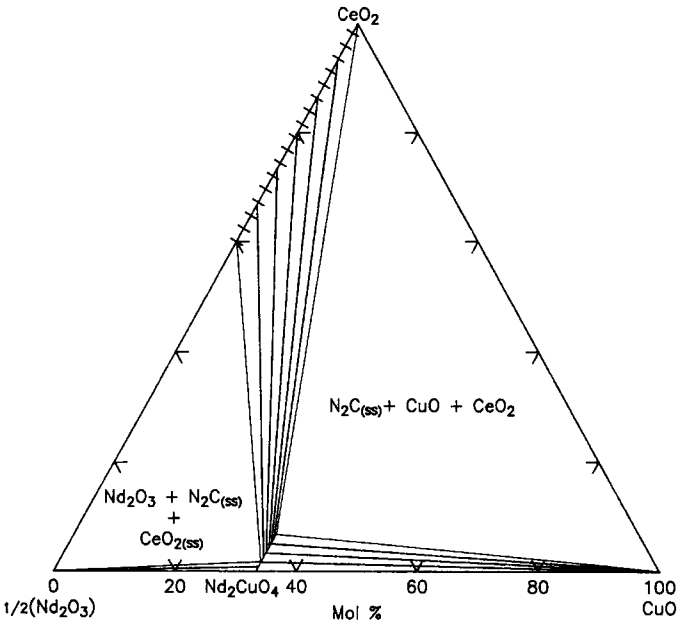

Phase diagram of the (Nd, Ce)CuO_4 system at 1000°C (Kim and Gaskell, 1993).

Fig. 14.35.

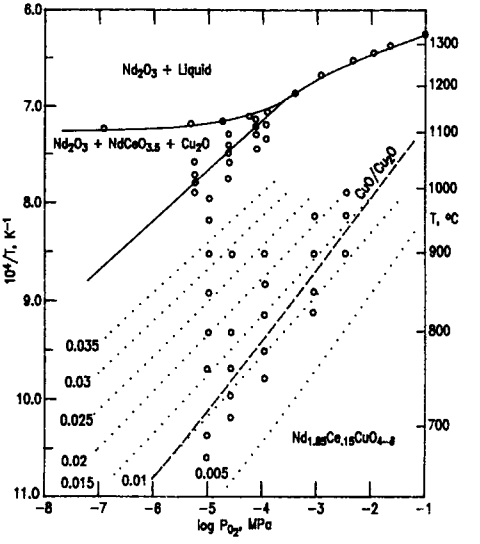

Temperature vs pressure plot showing the effect of oxygen partial pressure on the stability field of (Nd,Ce)CuO_4. The dotted lines are isocomposition lines (Antipov *et al.*, 1993).

Fig. 14.36.

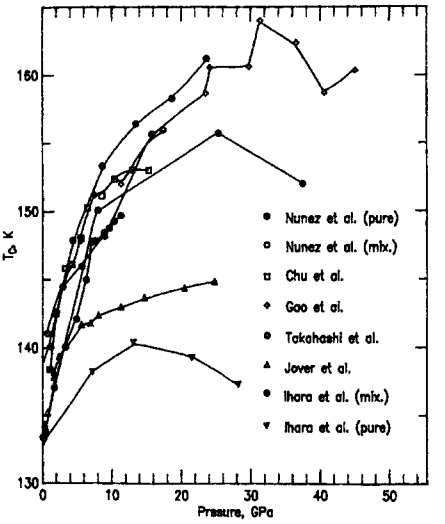

Pressure dependence of T_c for the first four members of the mercury cuprates in the HgO–BaO–CaO–CuO system (Loureiro, 1997).

Fig. 14.37.

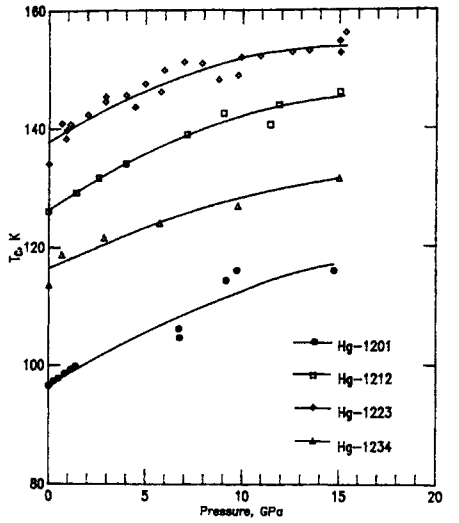

The superconducting transition temperature T_c of Hg-1223 vs pressure P in the HgO–BaO–CaO–CuO system (Loureiro, 1997; Akesenov and Antipov, 1977; Fuikuoka *et al.*, 1996; Chu *et al.*, 1993; Nuñez-Regueiro *et al.*, 1993; Gao *et al.*, 1994; Takahashi *et al.*, 1993; Jover *et al.*, 1996; Ihara *et al.*, 1993).

References

V. L. Akesenov and E. V. Antipov, *Phys. Rev. B* **55**, 3966 (1977).

T. D. Aksenova, P. V. Bratukhin, S. V. Shavkin, V. L. Melnikov, E. V. Antipova, N. E. Khlebova, and A. K. Shikov, *Physica C* **205**, 271 (1993).

E. V. Antipov, S. M. Loureiro, C. Chaillout, J. J. Capponi, P. Bordet, J. L. Tholence, S. N. Putlin, and M. Marezio, *Physica C* **215**, 1 (1993).

T. Aselege and K. Keefer, *J. Mater. Res.* **3**, 1279 (1988).

T. L. Aselege, E. L. Venturini, and S. B. Van Deusen, *J. Appl. Phys.* **75** 1023 (1994).

U. Balachandran, A. N. Iyer, P. Haldar, J. G. Hoden, Jr., and L. R. Motowidlo, in K. Kristen and C. Burnham, eds, *Proceedings 4th World Congress on Superconductivity, Orlando, FL, June 27–July 1, 1994.* Vol. 2, pp. 639–649.

J. G. Bednorz and K. A. Müller, *Z. Phys. B* **64**, pp. 189–193 (1986).

R. J. Birgeneau and G. Shirane, in *Neutron Scattering Studies of Structural and Magnetic Excitations in Lamellar Copper Oxides—A Review, Prog. High Temp. Superconduct.* (D. M. Ginsberg, Ed.), pp. 151–211. World Scientific Publishing, Singapore, 1989.

R. Bormann and J. Noelting, *Appl. Phys. Lett.* **54**, 2148 (1989).

R. J. Cava, *Amer. Ceram. Soc. Bull.* **74**, 85 (1995).

C. W. Chu, in *Proceedings of Quantum Theory of Real Materials*, Festschrift to Honor Marvin Cohen, (J. R. Chelikowsky and S. G. Louie, Eds.), p. 411. Kluwer Academic, Norwell, MA, 1996.

C. W. Chu, L. Gao, F. Chen, Z. J. Huang, R. L. Meng, and Y. Y. Xue, *Nature* **365**, 323 (1993).

L. P. Cook, W. Wong-Ng, C. K. Chiang, and L. H. Bennett, in *Superconductivity and Ceramic Superconductors*, (K. M. Nair and E. A. Geiss, Eds.), *Ceramics Trans.* **13**. American Ceramics Society, Westerville, OH, 1990.

D. M. DeLeeuw, C. A. H. A. Mutsaers, C. Langereis, H. C. A. Smoorenburg, and P. J. Rommers, *Physica C* **152**, 39 (1988).

J. L. Driscoll, J. C. Bravman, and R. B. Beyers, in *Appl. Supercond. 1st*, Goettingen, Germany, October 4–9, 1992, Vol. 1 (H. C. Freyhardt, Ed.), p. 325. DGM Informationsges., Oberursel, Germany, 1993.

C. E. Fiori, C. R. Swyt, and R. L. Myklebust, "DTSA-NIST/NIH Desktop Spectrum Analyzer Program and X-ray Database," NIST Standard Reference Database No. 36 (1991).

A. Fukuoka, A. Tokiwa-Yamamoto, M. Itoh, R. Usami, S. Adachi, H. Yamauchi, and K. Tanabe, *Physica C* **265**, 13 (1996).

Y. Gao, K. L. Merkle, C. Zhang, U. Balachandran, and R. B. Poeppel, *J. Mater. Res.* **5**, 1363 (1990).

L. Gao, Y. Y. Xue, F. Chen, Q. Xiong, R. L. Meng, D. Ramirez, C. W. Chu, J. H. Eggert, and H. K. Mao, *Phy. Rev. B.* **50**, 4260 (1994).

S. J. Golden, T. E. Bloomer, F. F. Lange, A. M. Segadaes, K. J. Vaidya, and A. K. Cheetham, *J. Am. Ceram. Soc.* **74**, 123 (1991).

E. Goodilin, M. Kambara, T. Umeda, and Y. Shiohara, *Physica C* **289**, 251 (1997).

A. Goyal, D. P. Norton, J. Budai, E. D. Paranthaman, D. M. Specht, D. M. Kroeger, D. K. Christen, Q. He, B. Saffian, F. A. List, D. F. Lee, P. M. Matrin, C. E. Klabunde, E. Hatfield, and V. K. Sikka, *Appl. Phys. Lett.* **69**, 1795 (1996).

J. Hahn, T. O. Mason, S.-J. Hwu, and K. R. Poeppelmeier, *Chemtronics* **2**, 126 (1987).

F. J. Heinrich and D. E. Newbury, Eds., *Electron Probe Quantitation*, Plenum, New York, 1991.

B. Hettich, B. Freilinger, P. Majewski, T. Popp, and K. Schulze, in *High Temp. Superconduct. Proc. ICMC '90 Conference, Mater. Aspects High-Temp. Supercond.*, Garmisch-Partenkirchen, Germany, 1990, Vol. 1, (H. C. Freyhardt, R. Fluckiger, and M. Peuckert, Eds.), p. 399. DGM Informationsges., Oberursel, Germany, 1991.

T. G. Holesinger, D. J. Miller, and L. S. Chumbley, *Physica C* **217**, 85 (1993).

B. Hong and T. O. Mason, *J. Am. Ceram. Soc.* **74**, 1045 (1991).

Q. Y. Hu, H. K. Liu, and S. X. Dou, *Physica C* **250**, 7 (1995).

C. R. Hubbard, "Standard Reference Material 675, Fluorophlogopite Powder X-ray Diffraction Standard" (1982). To obtain, see procedure below for Hubbard *et al.*, (1987).

C. R. Hubbard, C. Robbins, and W. Wong-Ng, "Standard Reference Material 640b, Silicon Powder X-ray Diffraction Standard" (1987). Obtainable from the NIST, Office of Standard Reference Materials, Gaithersburg, MD 20899. Current price will be quoted on request.

ICSD, The Inorganic Crystal Structure Database, Structural Data on Inorganic Phases. Fachinformationszentrum Karlsruhe, D-76344 Eggenstein-Leopoldshafen, Germany.

H. Ihara, M. Hirabayashi, H. Tanini, K. Tokiwa, H. Ozawa, Y. Akahama, and H. Kawamura, *Jpn. J. Appl. Phys.* **32**, L1732 (1993).

J. Jiang and J. S. Abell, in *High Temperature Superconductor: Synthesis, Processing and Large Scale Applications* (U. Balachandran, P. J. McGinn and J. S. Abell, Eds.), p. 13. The Minerals, Metals & Materials Society, 1996.

T. K. Jondo, C. Opagiste, J. L. Jorda, M. T. Cohen-Adad, F. Sibieude, M. Couach, and A. F. Khoder, *J. Alloys Compd.*, **195**(1–2), (1993).

J. D. Jorgenson, M. A. Beno, D. G. Hinks, L. Soderholm, K. J. Volin, R. L. Hitterman, J. D. Grace, I. K. Schuller, C. U. Segre, K. Zhang, and N. S. Kleefische, *Phys. Rev. B* **36**, 3608 (1987).

D. T. Jover, R. J. Wijngarrden, H. Wilhelm, R. Griessen, S. M. Loureiro, J.-J. Capponi, A. Schilling, and H. R. Ott, *Phys. Rev. B.* **54**, 4265 (1996).

S. Kaesche, P. Majewski, and F. Aldinger, *J. Electron. Mater.* **24**(12) 1829 (1995).

P. Karen and A. Kjekshus, *J. Solid State Chem.* **94**, 298 (1991).

P. Karen, A. Kjekshus, Q. Huang, V. Karen, A. D. Mighell and A. Santoro, submitted to *Physica C* (1999).

J. S. Kim and D. R. Gaskell, *Physica C* **209**, 381 (1993).

D. Klibanow, K. Sujata, and T. O. Mason, *J. Am. Ceram. Soc.* **71**, C-267 (1988).

K. Knizek, E. Pollert, D. Sedmidubsky, J. Hejtmanek, and J. Pracharova, *Physica C* **216**, 211 (1993).

G. Krabbes, W. Bieger, U. Wiesner, M. Ritschel, and A. Teresiak, *J. Solid State Chem.* **103**, 420 (1993).

G. Krabbes, W. Bieger, and U. Wiesner, *Trans. Mater. Res. Soc. Jpn.* **19A**, 463 (1994).

Y. Le Page, T. Siegrist, S. A. Sunshine, L. T. Schneemeyer, D. W. Murphy, S. M. Zahurah, J. V. Waszczak, W. R. McKinnon, J. M. Tatscon, G. W. Hull, and L. H. Green, *Phys. Rev. B* **36**, 3617 (1987).

E. M. Levin, C. R. Robbins, and H. F. McMurdie, *Phase Diagrams for Ceramists*, Vol. I. American Ceramic Society, 1964.

T. B. Lindermer and A. L. Sutter, Jr., Oak Ridge Natl. Lab. Report ORNL/TM-10827 (1988).

S. M. Loureiro, "The Synthesis and Structures of Superconductors of Mercury", Ph.D. thesis, CNRS, Grenobles, France, 1997.

J. I. MacManus-Driscoll and J. C. Bravman, *J. Am. Ceram. Soc.* **77**, 2305 (1994).

P. Majewski, *Adv. Mater.* **4**, 508 (1992); Adv. Mater. **6**, 460 (1994).

P. Majewski, in *High Temperature Superconducting Compounds: Processing and Related Properties*, (S. H. Whang and A. DasGupta, Eds.), p. 61. The Minerals, Metals & Materials Society, 1996.

P. Majewski, B. Hettich, H. Jaeger, and K. Schulze, *Adv. Mater.* **3**(1) 67 (1991).

P. Majewski, B. Hettich, N. Ruffer, and F. Aldinger, *J. Electronic Mater.* **22**, 1259 (1993).

P. Majewski, S. Elschner, and F. Aldinger, *Physica C* **249**, 234 (1995a).

P. Majewski, S. Elschner, and F. Aldinger, *Physica C* **249** [34] 234–240 (1995).

A. P. Malozemoff, W. Carter, S. Fleshler, L. Fritzeneier, O. Li, L. Masui, P. Miles, D. Parker, R. Parrella, E. Podtburg, G. N. Riley, Jr., M. Rupich, J. Scudiere, and W. Zang, Proc. Applied Superconductivity Conf., Palm Desert, CA, Sept., 13–18, 1988; in press.

R. W. McCallum, K. W. Dennis, L. Margulies, and K. J. Kramer, in *Processing of Long Lengths Superocnd. Proc. Symp.*, Pittsburgh, Pennsylvania, October 17–21, 1993. (U. Balachandran, E. W. Collings and A. Goyal, Eds.), p. 195. Minerals, Metals & Materials Society, Warrendale, PA, 1994.

N. Merchant, J. S. Luo, V. A. Maroni, G. N. Riley, and W. L. Carter, *Appl. Phys. Lett.* **65**(8), 1039 (1994).

C. Michel, M. Hervieu, M. M. Borel, A. Grandin, F. Deslandes, J. Provot, and B. Raveau, *Z. Phys. B* **68**, 421 (1987).

D. E. Morris, A. G. Markelz, B. Fayn, and J. H. Nickel, *Physica C* **168**, 153 (1990).

R. Muller, T. Schweizer, P. Bohac, R. O. Suzuki, and L. J. Gauckler, *Physica C* **203**, 299 (1992).
National Institute of Standards and Technology, NIST Crystal Data (a database with chemical and crystallographic information compiled and evaluated by the NIST Crystallographic Data Center). National Institute of Standards and Technology, Gaithersburg, MD 20899.
National Institute of Standards and Technology, NIST/Sandia/ICDD Electron Diffraction Database, NIST Crystallographic Data Center. National Institute of Standards and Technology, Gaithersburg, MD 20899.
National Institute of Standards and Technology, *Phase Diagrams for Ceramists*, CD-ROM version. American Ceramic society, Westerville, OH 43081–8720.
M. Neveřiva, E. Pollert, and P. Honskus, *Physica C* **199**, 328 (1992).
M. Nuñez-Reguiero, J.-L. Tholence, E. V. Antipov, J.-J. Capponi, and M. Marezio, *Science* **262**, 97 (1993).
M. Paranthaman, A. Goyal, F. A. List, E. D. Specht, D. F. Lee, P. M. Martin, Q. He, D. K. Christen, D. P. Norton, J. D. Budai, and D. M. Kroeger, *Physica C* **275**, 266 (1997).
Phase Diagrams for Ceramists. American Ceramic Society, Westerville, OH 43081–8720.
C. N. Pieczulewski, K. S. Kirkpatrick, and T. O. Mason, *J. Am. Ceram. Soc.* **73**(7) 2141 (1990).
J. Ritter, *Powder Diff.* **3**, 30 (1988).
R. S. Roth, *Proc. User Aspects of Phase Equilibria*, Joint Research Centre, Petten, The Netherlands, June 25–27, 1990. Institute of Metals, London, 1990.
R. S. Roth, C. J. Rawn, F. Beech, J. D. Whitler, and J. O. Anderson, in *Ceramic Superconductors II* (M. F. Yan, Ed.), Publ. American Ceramic Society. 13 1988.
R. S. Roth, C. J. Rawn, B. P. Burton, and F. Beech, *J. Res. Natl. Inst. Stand. Technol. (USA)* **95**, 291 (1990).
K. H. Sandhage, G. N. Riley, Jr., and W. Carter, *J. Metals* **43**, 21 (1991).
K. Sato, T. Hikata, H. Mukai, M. Ueyama, N. Shibata, T. Kato, T. Masuda, M. Nagata, K. Iwata, and T. Mitsui, *IEEE Trans Mag.* **27** 1231 (1991).
M. P. Siegal, E. L. Venturini, B. Moroin, and T. L. Aselege, *J. Mater. Res.* **12**(11), 2825 (1997).
E. D. Specht, C. J. Sparks, A. G. Dhere, J. Brynestad, O. B. Cavin, D. M. Kroeger, and H. A. Oye, *Phys. Rev. B: Condens. Matt*, **37**, 7426 (1989).
Y. S. Sung and E. E. Hellstrom, *Physica C* **255**, 266 (1995).
H. Takahashi, A. Tokiwa-Yamamoto, N. Môri, S. Adachi, H. Yamauchi, and S. Tanaka, *Physica C* **218**, 1 (1993).
T. H. Tiefel, S. Nakahara, J. E. Graebner, H. M. O'Bryan, R. A. Fastnacht, and G. W. Kammlott, *Appl. Phys. Lett.* **56**, 1287 (1990).
Y. Tokura, H. Takag, and S. Uchida, *Nature* **337**(26), 345 (1989).
Toth Information Systems, CRYSMET—Structural Data on Intermetallic Phases. Developed and maintained by Toth Information Systems, Inc., Ottawa, Canada, K1J 6B2.
J. E. Ullman, R. W. McCallum, and J. D. Veroeven, *J. Mater. Res.* **4**, 752 (1989).
T. A. Vanderah, R. S. Roth, and H. F. McMurdie, *Phase Diagrams for High T_c Superconductors II*, American Ceramic Society, 1991.
J. D. Whitler and R. S. Roth, *Phase Diagrams for High T_c Superconductors I*. The American Ceramic Society, 1991.
W. Wong-Ng, "XRD Industrial Application to High T_c superconductors", in *Industrial Applications of X-ray Diffraction*, (D. K. Smith and F. Chung, Eds.). Marcel Dekker, New York, 1999, in press.
W. Wong-Ng and L. P. Cook, *J. Amer. Ceram. Soc.* **77**, 1883 (1995).
W. Wong-Ng and L. P. Cook, *J. Natl. Inst. Stand Tech. Res.* **103**, 379 (1998).
W. Wong-Ng, L. P. Cook, C. K. Chiang, L. Swartzendruber, L. H. Bennett and J. E. Blendell, and D. Minor, *J. Mater. Res. Soc.*, **3**, 832 (1988).
W. Wong-Ng, B. Paretzkin, and E. R. Fuller, Jr., *J. Solid State Chem.*, **84**, 117 (1990)
W. Wong-Ng, R. L. Snyder, C. Park, E. Antipov, and W. F. McClune, *Powd Diff.* **12**, 13 (1996).
W. Wong-Ng, L. P. Cook, F. Jiang, W. Greenwood, U. Balachrandran, and M. Lanagan, *J. Mater. Res.* **12**(11), 2855–2865 (1997).

W. Wong-Ng, L. P. Cook, and J. Feng, *J. Amer. Ceram. Soc.*, **81**, 1829 (1998).
X. D. Wu, S. R. Foltyn, P. N. Arendt, W. R. Blumenthal, I. H. Campbell, J. D. Cotton, J. Y. Coulter, W. L. Hults, M. P. Maley, H. F. Safar, and J. L. Smith, *Appl. Phys. Lett.* **67**, 237 (1995).
R. G. W. Wyckoff, *Crystal Structures Series*. John Wiley & Sons, New York, London, Sydney.
S. I. Yoo and R. W. McCallum, *Physica C* **210**, 147 (1993).
W. Zhang and E. E. Hellstrom, *Physica C* **218**, 141 (1993).
W. Zhang and K. Osamura, pp. 437–440 in *Adv. Supercond. III, Proc. 3rd Int. Symp. Supercond.* International Superconductivity Technology Center, Sendai, Japan, November 6–9, 1990 (K. Kajimura and H. Hayakawa, Eds.). Springer-Verlag, Tokyo, 1991.
R. Zhou, W. L. Hults, J. F. Bingert, J. Y. Coulter, E. J. Peterson, and J. L. Smith, *Physica C* **249**, 166 (1995).

This Page Intentionally Left Blank

Index

This Page Intentionally Left Blank